Science and Art: A Future for Stone

Hughes, John; Howind, Torsten

Published: 01/01/2016

Document Version
Publisher's PDF, also known as Version of record

SCIENCE and ART: A Future for Stone

Proceedings of the 13th International Congress on the Deterioration and Conservation of Stone – Volume I

SC16

Edited by
John Hughes & Torsten Howind

SCIENCE AND ART: A FUTURE FOR STONE

PROCEEDINGS OF THE 13TH INTERNATIONAL CONGRESS ON THE DETERIORATION AND CONSERVATION OF STONE

6th to 10th September 2016, Paisley, Scotland

VOLUME I

Edited by
John J. Hughes and Torsten Howind

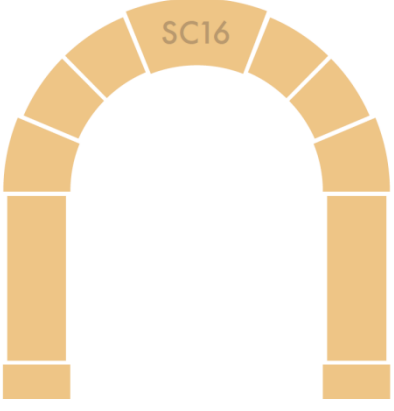

UNIVERSITY OF THE WEST of SCOTLAND
UWS

ISBN: 978-1-903978-57-3
ISBN: 978-1-903978-54-2 (eBook)

ISBN: 978-1-903978-59-7 (Set: Volume 1&2)
ISBN: 978-1-903978-56-6 (eBook-Set: Volume 1&2)

Hughes J.J. and Howind T. (Editors), "Science and Art: A Future for Stone. Proceedings of the 13th International Congress on the Deterioration and Conservation of Stone", University of the West of Scotland, Paisley, September 6th to 10th, 2016.

Cover image: The front door of the Paisley Technical College building, now University of the West of Scotland. T.G. Abercrombie, architect 1898. Photograph and cover design by T. Howind.

PREFACE

Standing under the portico of the Paisley Town Hall, completed in 1882, and looking south east towards the West Façade of Paisley Abbey, built in the 13th to 15th Century, it is possible to compare two historical periods in Scottish building where the use of stone was unavoidable. Walking further into the historic centre of Paisley, or any other town or city in Scotland, reveals the ubiquitous use of uncovered natural stone in our architecture, and also the problems that it faces. The challenge in maintaining the essential integral character of our towns for the future, and to recognise and enhance their values is a complex one, but not our challenge alone. Much hard work is still needed to characterise, assess and propose conservation approaches that are compatible with the existing fabric and prevailing philosophies, in Scotland and around the world.

We sought to bring the 13th Congress to a damp Scotland of decaying stone structures, to share our stone-built heritage with the conservation community and also to focus on the needs of stone conservation for our built heritage in Scotland. We hope that by bringing some global attention to the issue, in the country were, arguably, modern geology began, we demonstrate the sharing of our common heritage and our values in seeking its understanding and protection.

In these volumes you will find the proceeds of the work of many people, the conservators, practitioners and even academics and researchers whose concern is the protection of our stone-made cultural heritage. The Permanent Scientific Committee (PSC) of the Stone Congresses worked to review each contribution followed by revision by the authors. The editing effort by ourselves involved direct improvements to text, in many cases, and by one of us in particular to the formatting. However, beyond the title pages and abstracts, after review by the PSC and revision by the authors, proof correction was limited. The contents and accuracy of the papers are therefore the responsibility of the authors.

John J. Hughes and Torsten Howind

Paisley, Scotland, August 2016

Permanent scientific committee

ACKNOWLEDGEMENTS

Historic Environment Scotland, for their assistance and support in the hosting of the Congress Dinner at the Kelvingrove Art Gallery and Museum, Glasgow. Ewan Hyslop, Maureen Young and Christa Gerdwilker are thanked for their voluntary input to the organisation of technical visits to Largs and Glasgow.

The British Geological Survey.

Our commercial sponsors: SINT Technologies, Surface Measurement Systems, GC Laser Systems, Fokus GmbH Leipzig and Remmers.

Renfrewshire Council and the staff of the Town Hall.

The community at Paisley Abbey.

Alexander Collins, excursion guide.

Drew Wilson, Richard Potts and Stuart Johnson of UWS's Corporate Marketing for design and layout of the Congress Logo, programmes and other printed matter.

Finally, thanks must go to Alison Wright (formerly of Glasgow University), who bravely bore our application to host the Congress to New York in 2012, without complaint. On this occasion we must also thank the team at the University of the West of Scotland; Georgia Adam, Irene Edmiston, Gaia Frola, Matt Gilmour and Emma Paterson, without whose efforts the Congress could not have been held.

This page has been left intentionally blank.

CONTENTS

Volume I

Volume II

This page has been left intentionally blank.

DAMAGE

This page has been left intentionally blank.

TRAFFIC-INDUCED EMISSIONS ON STONE BUILDINGS

M. Auras[1*], P. Bundschuh[1], J. Eichhorn[2], D. Kirchner[3], M. Mach[4], B. Seewald[4], D. Scheuvens[5] and R. Snethlage[6]

Abstract

Despite enormous enhancements in air quality in the past many cities still have serious problems to comply with the legal limits of air pollution. Nitrogen oxides and fine particulate matter still are at high concentrations, originating in relevant proportions from urban traffic. Current threshold values are based on health considerations, but the impact on our built heritage cannot be neglected. At five German cities of different size and different traffic load the proportion of historic buildings exposed to elevated traffic emissions was recorded. Less than 100 up to more than 1000 historic buildings per city are exposed to increased traffic emissions. For five buildings at heavy-trafficked roads of the near-field air flow and the deposition rate of air pollutants were modelled. Passive samplers were exposed at these buildings to determine the composition and amount of particulate matter, the concentrations of NO_2 and HNO_3 as well as the soiling and the mass loss of stone samples. The results clearly demonstrate the input of nitrates and chlorides as well as the soiling of stone samples as a consequence of road traffic.

Keywords: air pollution, traffic-induced emissions, stone, soiling, nitrates, chlorides

1. Introduction

Air pollution in Germany has been reduced strongly over the last decades. Especially the concentrations of sulphur dioxide and its secondary products are reduced to a fraction of the values reached in the seventies. The *pH* value of rain has increased and is now at a level being inherent by the saturation with carbon dioxide. Nevertheless, nitrogen oxides and particulate matter remain at problematic levels and high proportions of them originate from

[1] M. Auras*
Institut für Steinkonservierung e.V., Mainz, Germany,
auras@ifs-mainz.de

[2] J. Eichhorn
Institut für Physik der Atmosphäre, Universität Mainz, Germany

[3] D. Kirchner
Deutsches Bergbaumuseum, Bochum, Germany

[4] M. Mach
Bayerisches Landesamt für Denkmalpflege, München, Germany

[5] D. Scheuvens
Umweltmineralogie, Institut für Angewandte Geowissenschaften,
Technische Universität, Darmstadt, Germany

[6] R. Snethlage
Bamberg, Germany

*corresponding author

road traffic. Besides their negative health effects, their impact on materials has to be considered. This is particularly true for historic buildings, because they were exposed to air pollutants for decades or even centuries and they will also suffer from future emissions.

Up to the eighties, most of the scientific researches on the effects of pollutants on materials has been focused on sulphur-rich emissions. Later, other pollutants were equally considered, for example in the research project MULTI ASSESS in the framework of the program UN-ECE (amongst others Kucera 2005). In the project presented here, the situation in several German cities was studied by means of various techniques. More details of the project's results are given in a specific conference paper (IFS 2015).

2. Methods

To evaluate the air pollution in German cities and their consequences for stone buildings data of air quality stations, meteorological conditions, traffic volume, and others were analysed, combined and interpreted. The cities of Bamberg, Würzburg, Mainz, Essen, and Munich were selected to obtain an overview of the situation in cities with different climate and traffic volume (Tab. 1, data referring to the year 2011).

Tab. 1: Size, inhabitants and number of registered motor vehicles of the selected cities.

City	Area, km^2	Inhabitants	Motor vehicles
Bamberg	54.62	70,863	44,168
Würzburg	87.63	124,577	71,342
Mainz	97.74	202,756	107,004
Essen	210.30	566,862	307,943
Munich	310.70	1,388,308	771,625

Maps of traffic volume were drawn and superimposed with data on the monument stock to estimate the portion of historic buildings exposed to elevated traffic volume.

In each city one historic building at a heavy-trafficked road was chosen for the exposure of several passive samplers (Tab. 2). Exposure racks were constructed and fixed at the facades in traffic-near positions. Slabs of three stone varieties (Portland limestone, Baumberger sandstone, Carrara marble) were exposed in sheltered and unsheltered positions.

Horizontally oriented rain-sheltered passive samplers made of a boron substrate were used to collect particulate matter for ESEM studies and EDS-analyses. The collected particles were characterised chemically by semi-automated individual-particle analysis with a Scanning Electron Microscope (FEI Quanta 200 Feg) combined with energy-dispersive microanalysis (EDS). Pictures of each particle were taken and their morphological features were evaluated visually. Image analysis showed that the coverage of the substrates was mainly due to the deposition of particles of a size > 3 µm. Therefore so far only the fraction > 3 µm is evaluated and smaller particles are neglected. About 31,000 particles were evaluated and - based on chemical composition and morphology - classified into 14 groups. The relative particle number and the relative area abundance (area coverage) of each group were calculated. Additionally, the absolute surface coverage by particles was determined.

Additionally, bi-monthly replaced glass platelets were used as particle samplers. By means of microscope pictures and image analysis using the program RADIUS by Seelos and Sirocko (2005), the amount and size of the deposited particles was calculated. Polished marble slabs were used for colour measurements (Konica-Minolta cm-600d) before and after exposition. According to Rumpel (1984) Surface Active Monitors (SAM) are filter papers impregnated with a solution of alkali carbonate. They were used to collect sulphate, nitrate and chloride. The contents of chloride, sulphate and nitrate of SAM filters and of the stone slabs (rain sheltered) were analysed by ion chromatography (Dionex ICS 1000). NO_2 and HNO_3 diffusive samplers (Ferm and Svanberg 1998, Ferm *et al.* 2005) were provided and analysed by the IVL Swedish Environmental Research Institute.

Tab. 2: Exposure sites (2 racks at Mainz and Würzburg: UP upper rack, LO lower rack).

Rack code	City	Building	Average traffic volume (vehicles/d)	Rack: Horizontal distance from street	Rack: Height above street
BA	Bamberg	Nonnenbrücke 1	15,000	1 m	5 m
WÜ,up WÜ,low	Würzburg	Residence Castle	15,000	4 m	up: 23 m low: 4 m
MZ,up MZ,low	Mainz	Christuskirche	27,000	up: 35 m low: 24 m	up: 31 m low: 13 m
E	Essen	Wasserturm	30,000	2 m	6 m
M	Munich	Bayer. National Museum	52,000	5 m	3 m

For the five buildings the prevailing wind fields and the dispersion of traffic emissions were modelled, using the 3-dimensional non-hydrostatic flow and dispersion model MISKAM. The model solves prognostic equations for the wind vector as well as turbulence energy and dissipation. Once the flow field has been computed, a transport equation for pollutants can be solved. The performance of the flow and turbulence model was evaluated according to the VDI guideline 3783/9 (VDI 2005; Eichhorn and Kniffka 2010).

3. Results

3.1. Traffic volume and stock of cultural heritage

In a former study the dispersion of traffic emissions along the main roads of Munich and Mainz was modelled (Schorling 2011, see also Auras *et al.*2013). The study showed that peak concentrations of traffic pollutants decrease strongly with increasing distance from their emission source along the roads. According to this, very high concentration can be expected on facades directly facing the main roads, while on side roads the concentrations correspond to the urban background level. In the study presented here traffic volume maps were used instead of the comprehensive modelling along all main roads. The spectrum of traffic volume in the different cities is quite broad. It reaches from less than 5,000 motor vehicles per day to more than 100,000 vehicles per day (>50.000 only in Munich).

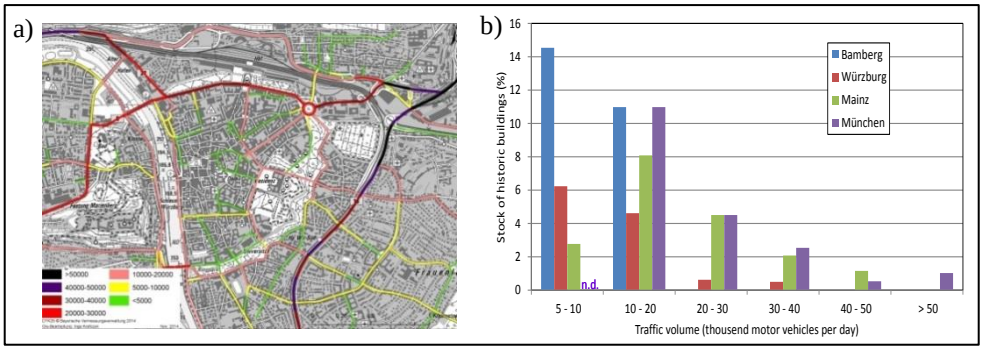

Fig. 1: a) Traffic volume map of Würzburg (in vehicles per day); b) Historic building stock and traffic volume (ADT) for the cities of Bamberg, Würzburg, Mainz and Munich.

The traffic volume maps depicting the average daily traffic (ADT) as shown in Fig. 1a were superimposed by maps of the stock of historic buildings and monuments, thus allowing to roughly estimating their exposure to road traffic emissions. The proportion of historic buildings affected by high traffic volumes was evaluated. At Bamberg, Würzburg and Mainz proportions between 12 and 26 % of the stock of historic buildings are exposed to an ADT of more than 5,000 vehicles per day (Fig 1b). At Munich about 20 % are exposed to an ADT of more than 10,000.

3.2. Modelling of wind fields and deposition rates

As an example of the numerical modelling with MISKAM, the flow pattern and the local variation of a pollutant concentration at the Residence Castle of Würzburg are displayed in Fig. 2a. At Würzburg, the prevailing wind direction is WSW (240°). This direction was assumed for the detailed modelling of the wind field in the proximity of the Residence Castle. As the graph shows, the diagonal inflow into the central entrance area leads to the formation of a major stationary swirl. At the northern facade, the airflow is forced into a narrow road where a distinct swirl forms at the northwestern corner. The first, major swirl has only little effect on the concentration of a pollutant because the emissions are diluted during their transport across the empty space in front of the building. However, along the narrow road at the north side, the concentration significantly increases as shown in Fig. 2b. At the lee side of the strong swirl a zone of low wind flow enhances deposition of particulate matter on the facade. The passive samplers were exposed at this side as shown by the blue arrow in Fig. 2b.

A comparison of the modelling results from different sites shows that the highest emission rates (Munich) do not necessarily result in the highest particle concentrations. Small-scale ventilations can lead to high pollutant concentrations even at relatively low emission rates (Bamberg) where the local wind fields transports the emissions directly to the exposition rack. Calculated for the prevailing wind directions of Bamberg and Munich, the numerical model results in deposition rates at the Bamberg rack that are several times higher than the ones calculated for of the Munich rack. For Munich the model predicts a transport of the main portion of particles away from the rack.

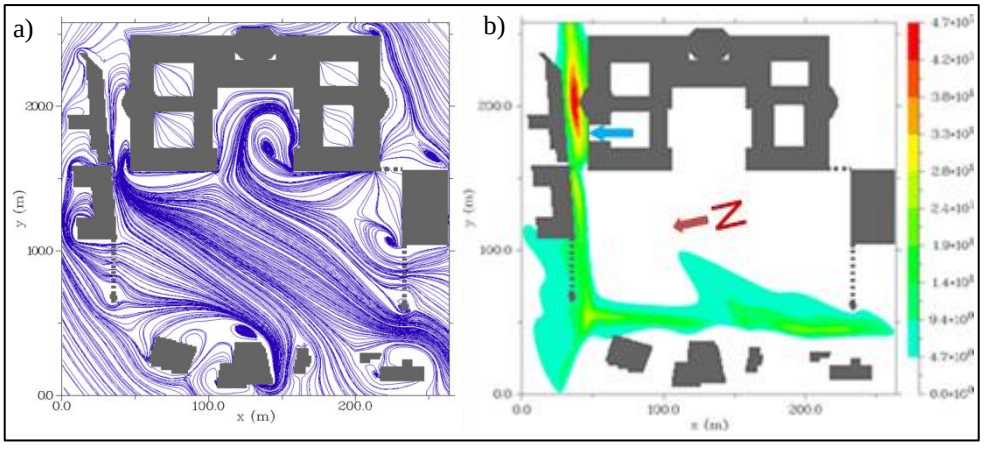

Fig. 2: a) Modelling of the airstream at the Residence of Würzburg; b): Corresponding pollutant concentration. The red zone indicates high pollutant concentration in the air directly in front of the façade. The blue arrow indicates the position of the exposure rack, the red one the northern direction.

3.3. Exposure program

The results from bi-monthly replaced SAM filters were used to calculate the annual average deposition rates as given in Fig. 3a. Maximum deposition rates are determined for nitrate, reaching to more than 1 g/m^{2}a. Sulphate rates vary between 0.1 and 1 g/m^{2}a, whereupon the maximum value is from Essen, characterised by industrial influence. Chloride rates are all less than 0.1 g/m^{2}a. Deposition rates from stone samples show a large spread, depending on stone type and exposure site. As an example, the values for Munich are given in Fig. 3b.

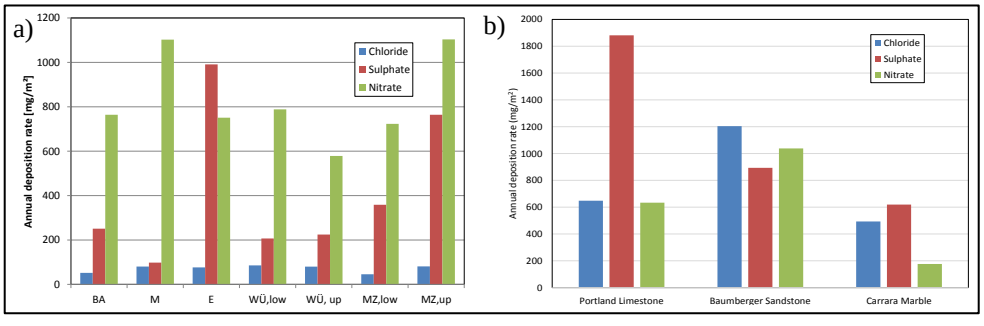

Fig. 3: a) Annual deposition rates from SAM filters, calculated from 2-month data. Nitrate values are sums of (very small) nitrite and (dominating) nitrate concentrations; b) Annual deposition rates from stone slabs at Munich.

On rain-sheltered passive samplers with horizontal surfaces, the surface coverage was calculated from images taken through an optical microscope on glass slabs and by SEM on boron substrate. Both methods lead to consisting results. In Fig. 4a data from the optical microscope show the results from the seven exposure sites. Each dot represents the surface coverage after exposure times of two months. The exposure sites are arranged by their distance from the road, showing a negative correlation between surface coverage and

distance. The exposure sites at Munich with about 52,000 vehicles per day and Bamberg with only 15,000 v/d show very similar values, indicating that not the absolute vehicle number, but the distance and the wind field (see above) are the dominant parameters.

The increase in mass of marble samples (6-months and 12-months exposure) and of glass platelets (2-months exposure) was used to calculate annual deposition rates. The values shown in Fig. 4b plot around 6 g/m^2 per year with a minimum of 3 and a maximum of 15 g/m^2 per year. At the sites close to the road, i.e. Munich, Bamberg and Würzburg (lower rack), the highest values were found, thus again indicating a correlation between distance from the road and the intensity of the traffic impact.

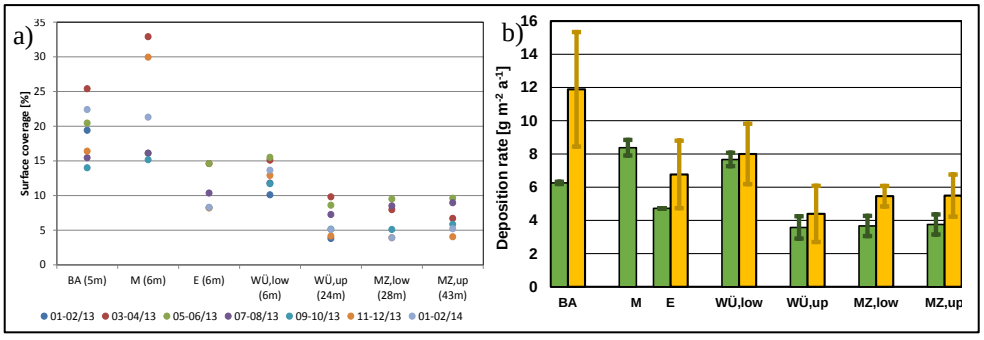

Fig. 4: a) Surface coverage of horizontally exposed rain-sheltered glass platelets. Exposure sites in order of increasing distance (in meter) from the road. Each dot represents an exposure period of two months; b) Rate of annual dry deposition, calculated from mass increase of marble samples (green) and glass platelets (orange).

Passive sampling of aerosol particles on horizontally oriented boron substrates under sheltered conditions provides some insight into the amount and chemical composition of dry-deposited particles on a building facade at heavily trafficked sites. Some conspicuous compositional features were detected in the samples and these and their probable impacts on facades are discussed briefly in the following.

The soiling of facades is influenced by microbiological growth and particularly by the deposition of opaque or coloured particles (amongst others Grossi *et al.* 2003, Brimblecombe and Grossi 2005, Urosevic *et al.* 2012). Noteworthy, opaque particles include anthropogenic particles, such as soot and abrasive wear (for example Nord and Holenyi 1999). Other coloured particles are Fe-oxides and -hydroxides, which may be of anthropogenic (brake wear, fly ash) or geogenic origin. The soiling and weathering of stone on facades depends amongst others on the amount and on the composition of the deposited particles. The chemical composition of all two-months samples have been investigated by automated single-particle analysis. Afterwards, the particles > 3µm were classified due to their chemical and morphological properties in 14 classes (compare Fig. 5). Please note that percentage rates given in Fig. 5 were calculated for one year of exposure on the base of data collected in bi-monthly experiments. The relevant classes referring to traffic were tire wear particles, Fe-rich particles, metal-bearing particles (Pb, Sc, V, Cr, Mn, Co, Ni, Zn, and Sb), chloride-bearing particles, secondary aerosol (N- and S-bearing), internal mixtures of silicates and C-bearing particles (re-suspended material after Weinbruch *et al.* 2014).

The coverage data from bimonthly replaced samples were used to calculate annual surface coverage (Fig. 5). Besides silicates and carbonates (probably associated both with a geogenic origin and a re-suspension source), tire wear plays an important role. At Munich and Bamberg Cl-particles from de-icing salt are present in large proportions. Nitrates as a part of the secondary aerosol is found only in minor amounts, probably due to low detection by EDS and to the limitation on the particle fraction > 3 µm in this study. It is likely that a substantial part of the nitrate particles lie below this limit (e.g. Weinbruch *et al.* 2014).

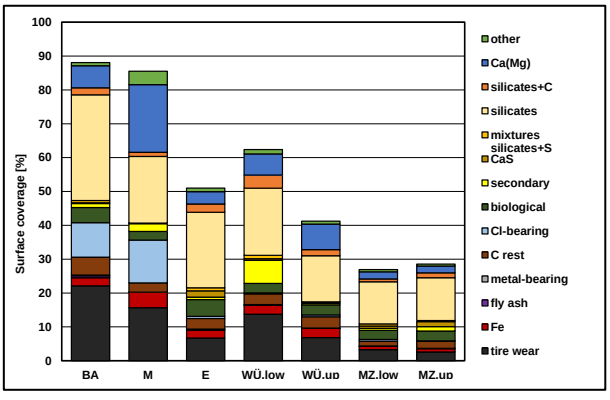

Fig. 5: Absolute surface coverage of the particle classes at different exposure sites (horizontal orientation, sheltered conditions, calculated for one year exposure).

4. Discussion

The concentration of PM_{10} and $PM_{2.5}$ decreases since the beginning of measurement in the late 1970's. Nevertheless, high deposition rates of particles are found especially at the exposure sites in Munich and Bamberg. The difference between urban background and traffic 'hot-spots' is of interest, if the impact of road traffic has to be regarded. Amongst others, Boogaard *et al.* (2011) showed that the concentrations of black carbon and NO_x are significantly higher in the main roads compared to the urban background. The evaluation of public air quality data in this study lead to comparable factors for NO_2 and PM_{10} (Tab. 3).

Tab. 3: Relation of concentrations in heavy-trafficked roads to urban background.

City	PM10	PM2.5	BC	NO_2	NOx	Source
Amsterdam	1.2	1.2	1.9	1.5	1.8	Boogaard *et al.* 2011
Munich	1.2			2.3	2.9	This study
Mainz	1.3			1.7	2.3	This study
Würzburg				1.3	1.8	This study

Regarding the impact of road traffic on historic buildings, the soiling by deposition of particles and the deterioration processes induced by soluble salts have to be considered. Contributing factors for soiling are the amount of deposited material and its proportion of dark particles. The major part of dark particles consists of abrasive wear from tires, brakes

and road cover. Minor parts are either soot or iron-rich particles (brake wear or geogenic). In contrast to the dark particles, the water-soluble salts do not remain on the stone surface. In dissolved state, they can penetrate into the stone and cause damage by crystallization – dissolution cycles. Concerning road traffic, especially the nitrates originating from nitrogen oxides as well as chlorides from re-suspended de-icing salts have to be taken into account. The evaluation of the traffic volume maps allows to roughly estimate that in the model cities about 20 % of the stock of historic buildings is exposed to increased traffic emissions. Modelling the wind fields at monuments clearly indicates where wind speed increases or decreases and where the wind flow hits the facades. They inform about the segments being exposed to high pollutant concentrations and deposition rates. Exposure experiments provide evidence that the distance from the road and the prevailing wind field are the most important parameters concerning deposition rate, surface coverage and soiling intensity. The concentrations of PM_{10} do not necessarily match with soiling intensities, because the soiling is mainly caused by particles bigger than PM_{10}. The difference between fine particulate matter and total suspended matter therefore has to be taken into account when the endangering of monuments by traffic pollutants is discussed. The high proportions of chloride particles found in the winter months in the cities with colder winter climate should give reason to further attention. Especially, buildings very close to main roads are at elevated risk. The role of nitrogen oxides is not very clear yet. Of course they can react to nitrates and those are found as secondary aerosol. But the amount of those particles detected by single particle analysis is rather small, which is also true for the concentrations of nitrates found in most of the stone samples. In contrast, the SAM filters show relatively high nitrate contents, which in part may be attributed to their ability to fix the nitrates on the substrate and to prevent them from solution and penetration into the stone, as well as from transformation by microbiological processes.

Acknowledgements

Many thanks to Silvia Beer, Stefan Brüggerhoff, Thomas Dirsch, Martin Ferm, Anette Hornschuch, Inga Kraftczyk, Karin Kraus, Wolfgang Mühlschwein, Clemens Seelos, Roger Thamm, Stefan Weinbruch and Tim Yates for their assistance. We also wish to express our gratitude to the involved authorities for the supply of data. Financial support by the Deutsche Bundesstiftung Umwelt is gratefully acknowledged.

References

Auras, M., Beer, S., Bundschuh, P., Eichhorn, J., Mach, M., Scheuvens, D., Schorling, D., v. Schuhmann, J., Snethlage, R. & Weinbruch, S. (2013): Traffic-related immissions and their impact on historic buildings: implications from a pilot study at two German cities. Environmental Earth Sciences 69: 1135 – 1147.

Boogaard, H., Kos, G.P.A., Weijers, E.P., Janssen, A.H., Fischer, P.H., van der Zee, S.C., de Hartog, J.J., and Hoek, G., 2011, Contrast in air pollution components between major streets and background locations: Particulate matter mass, black carbon, elemental composition, nitrogen oxide and ultrafine particle number. Atmospheric Environment 45: 560-658.

Brimblecombe, P., Grossi, C.M., 2005: Aesthetic thresholds and blackening of stone buildings. Science of the Total Environment 349: 175–89.

Eichhorn, J., Kniffka, A. (2010): The numerical flow model MISKAM: State of development and evaluation of the basic version. Meteorol. Zeitschrift 19: 81-90.

Ferm, M., Svanberg, P.-A., 1998, Cost-efficient techniques for urban- and background measurements of SO_2 and NO_2. Atmospheric Environment 32, 1377-1381.

Ferm, M., De Santis, F. Varotsos, C. 2005, Nitric acid measurements in connection with corrosion studies. Atmospheric Environment 39, 6664-6672.

Grossi, C.M., Esbert, R.M., Diaz-Pache, F. & Alonso, F.J. (2003): Soiling of building stones in urban environments.- Building and Environment 38: 147–159.

IFS, 2015, Baudenkmäler unter dem Einfluss verkehrsbedingter Immissionen. Institut für Steinkonservierung e.V., Mainz, IFS-Bericht 49, 163pp.

Kucera, V. (2005): Model for multi-pollutant impact and assessment of threshold levels for cultural heritage. Project period 1 January 2002 to 30 April 2005, Publishable Final report, www.corr-institute.se, 52 pp.

Nord, A.G., Holenyi, K., 1999, Sulphur deposition and damage on limestone and sandstone in Stockholm city buildings.- Water, Air, and Soil Pollution 109: 147–162.

Rumpel, K. (1984): Ein Verfahren zur Feststellung potentieller Immissionsraten: Oberflächenaktive Monitore SAM (Surface active monitoring); Monatsberichte aus dem Messstellennetz des Umweltbundesamtes 7; 2-15.

Schorling, M. (2011): Modellierung der innerstädtischen Ausbreitung verkehrsbedingter Immissionen. In: Wirkung verkehrsbedingter Immissionen auf Baudenkmäler - Eine Pilotstudie zu den Innenstädten von Mainz und München. Institut für Steinkonservierung e.V., Mainz, IFS-Bericht 37: 87-113.

Seelos, C., Sirocko, F. (2005): RADIUS - Rapid Particle Analysis of digital images by ultra-high-resolution scanning of thin sections; Sedimentology; 52; 669-681.

UBA, 2014, Umweltbundesamt: Emissionsentwicklung 1990-2012 für klassische Luftschadstoffe http://www.umweltbundesamt.de/themen/luft/emissionen-von-luftschadstoffen (downloaded 16.09.2014)

Urosevic, M., Yebra-Rodriguez, A., Sebastian-Pardo, E. & Cardell, C. (2012): Black soiling of an architectural limestone during two-year term exposure to urban air in the city of Granada (S Spain).- Science of the Total Environment 414: 564–75.

VDI Guideline 3783/9, 2005: Umweltmeteorologie – Prognostische mikro-skalige Windfeldmodelle — Evaluation für Gebäude- und Hindernisumströmung. Beuth-Verlag, Berlin, 53 pp.

Weinbruch, S., Worringen, A., Ebert, M., Scheuvens, D., Kandler, K., Pfeffer, U., Bruckmann, P., 2014, A quantitative estimation of the exhaust, abrasion and resuspension components of particulate traffic emissions using electron microscopy.- Atmospheric Environment 99: 175–182.

This page has been left intentionally blank.

WEATHERING PATTERNS OF THE CARVED STONE AND CONSERVATION CHALLENGES - WORLD HERITAGE SITE OF QUTB COMPLEX, NEW DELHI

S.S. Bais[1*] and S.C. Pandey[2]

Abstract

The *Qutb Minar* and its monuments, a World Heritage Site, is one of the earliest heritage sites located in New Delhi. Although, the site demonstrates the various stages of development between 12th to18th century in terms of architecture, building construction and most importantly, the stone decorative patterns, some of the most significant monuments of the complex such as *Quwwat-ul Islam* Mosque (1191 A.D.), *Qutb Minar* (1202 A.D.), the Tomb of *Ittutmish*(1235 A.D.) and *Alai Darwaza*(1311 A.D.) depict the earliest stone craftsmanship that existed in 12-13th century. The most attractive features of the carved stone master pieces include finest arabesque patterns, *Quranic* inscriptions in *Kufi* and *Naskh* script, Hindu motifs, and intricate geometrical and floral patterns craved beautifully in red and pink sandstones and marble, symbolises the combination of Hindu-Islamic Architecture. These masterpieces depict the existence of rich appreciation of aesthetics, supreme craftsmanship and amalgamation of two different cultures, which marks a significant era of Indian history. Monuments of *Qutb* complex have already undergone weathering cycles for over 800 years due to extreme variations in climatic conditions, which has lead to severe structural and material deterioration. The conservation decisions for such architectural decorative members are very crucial, as it has to embrace the intrinsic values and significance along with the peculiar construction systems and continuous exposure to the weathering conditions. Conservation decisions have to ensure the structural stability and architectural integrity, which is very challenging. Severe deterioration of carved stone has not only resulted in loss of the decorative surfaces but has also affected the structural stability of the monument. This paper aims to investigate the processes of weathering of the carved stone of *Qutb* monuments and discuss the conservation challenges, considering its multifaceted values and architectural/construction complexity.

Keywords: Qutb Minar, Alai Darwaza, carved stone, stone weathering, decay assessment, conservation issues

[1] S.S. Bais*
Dharohar, New Delhi, India
sangeeta.s.bais@gmail.com

[2] S.C. Pandey
Department of Art Conservation, National Museum Institute, New Delhi, India

*corresponding author

1. Introduction

Qutb complex, located in *Aravali* Mountain range, is one of the oldest walled cities of Delhi. The construction of the *Qutb* complex was started by the first slave ruler *Qutb-ud-din Aibak* with the construction of Delhi's first Jami Masjid, which had laid the foundation stone for the advent of Islamic civilization and architecture in India. The complex has several monuments representing the history and the evolution stages of the architecture. Considering its unique historical and architectural significance, the complex was designated as UNESCO World Heritage Site in 1993. This paper focuses on the study of the deterioration pattern of stones used in the carved stone of screen of *Quwwat-ul Islam* Mosque, *Qutb Minar*, Tomb of *Sultan Iltutmish* and *Alai Darwaza.* Out of these monuments, *Alai Darwaja* was documented and studied in detailed to establish the desired parameters for the conservation.

2. Study of Alai Darwaza

Alai Darwaza is a gateway from the southern side of the *Quwwat-ul Islam* Mosque and an example of early Islamic architecture in northern India. It is the only surviving gate of the four gates added to the *Qutb* Complex by *Ala-ud-din Khilji.* The gate is square in plan measuring 17.2×17.2 m, constructed with 3.35 m thick walls and cladded with carved red sand stones on an octagonal base, achieving the first successful transition from an octagonal base to a circular dome through a careful use of squinches (Fig. 1). The external and internal wall surfaces are cladded with red sandstone and marble fixed using 10 to 15 cm long, U shaped iron dowels to the core masonry. Visual documentation of individual stone was carried out to understand the type and extent of deterioration, which are explained further in the paper.

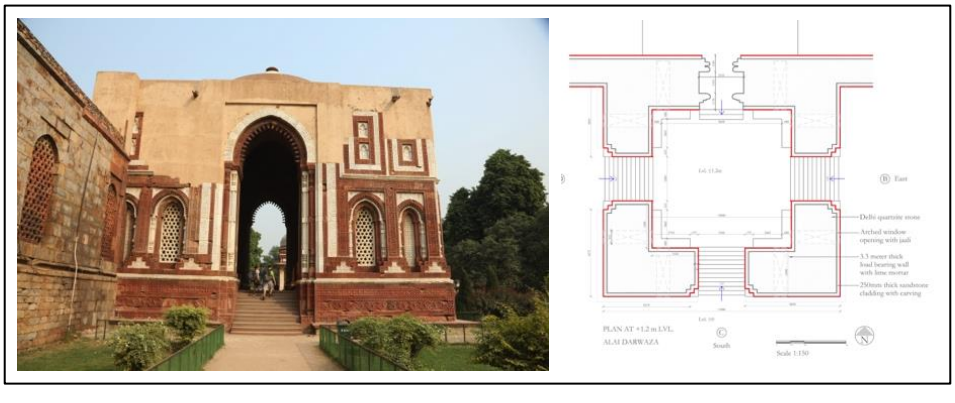

Fig. 1: A view of Alai Darwaza (left) and floor plan (right).

3. Stone mineralogy

The red sandstone samples collected from fallen fragments at the site were used for mineralogical analysis. The minerals were identified using a CENSICO POL-TN-O-CXL polarizing microscope. The microphotographs and images of different minerals were analysed for modal percentage analysis using Image Analyser (MICROCAM-CAP-I). The red sandstone used in *Alai Darwaza* is geologically identified as fine-grained

(0.25 - 0.50 mm) clastic sedimentary rock. It mainly consists of quartz, feldspar (microcline and plagioclase), muscovite, chalcedony, iron oxide, iron oxide cement and matrix. The mineralogical examination of the red sandstone under polarised light microscopy indicates it to be composed of moderately sorted and moderately compacted grains. Monocrystalline quartz grains are angular to subrounded and are set in iron oxide cement and clay matrix. The feldspars are mainly plagioclase & microcline and sub rounded to sub angular in shape. Muscovite is found to occur as very small flakes. Iron oxide in the form of ilmenite is also present in the rock. Iron oxide cement forms 7% to 10% of the rock. The matrix is composed of very fine-grained muscovite, clay and silt size quartz grains (Tab. 1; Fig. 3a& b). The porosity of the sandstone is rather low with an average of 5.6%. Overall the stone can be classified as feldspathicarenite and presence of plagioclase in abundance indicates an igneous origin. The pale/buff coloured minerals present in the sandstone as discrete layers, sandwiched between the red sandstone layers, were also analysed. These discrete layers are composed of fine-grained minerals from clastic origin. The mineralogical study was aimed at understanding the mineral composition of the sandstone used in the monument, however it may not be representative as individual stone blocks may have different source of origin.

Tab. 1. Mineralogical composition of red sandstone in Alai Darwaza.

Sample No.	Quartz (%)	Feldspar (%)	Muscovite (%)	Chalcedony (%)	Iron oxide (%)	Iron oxide cement (%)	Matrix (%)
1	60-65	7-8	2-3	1	4-5	8-10	5-8
2	64-69	6-7	2-3	1	3-4	7-9	4-7
3	62-67	6-7	2-3	1	4-5	8-10	5-8

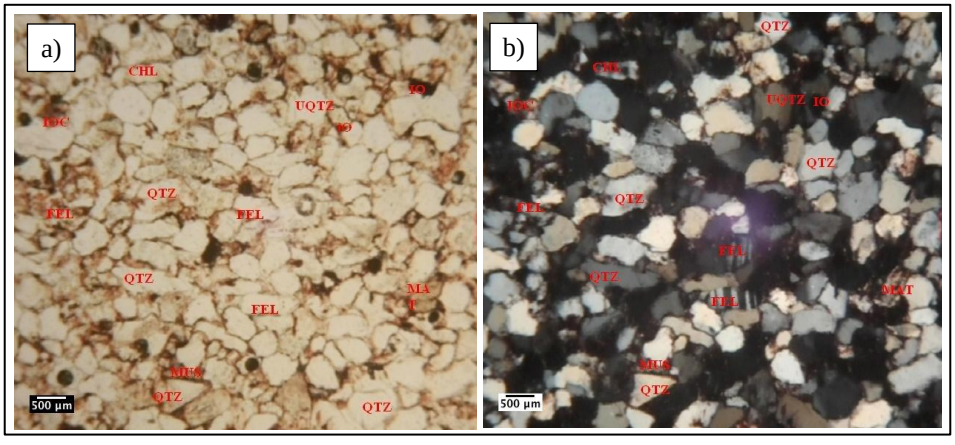

Fig. 2: Photomicrographshowing quartz (QTZ), feldspar (FEL), iron oxide (IO), iron oxide cement (IOC), undulosequartz (UQTZ), chalcedony (CHL) andmuscovite (MUS) under plane polarized light.

4. Weathering of Sandstone in *Alai Darwaza*

It is evident from the mineralogy that the red sandstone used in the monument is submature and exhibits a significantly lower porosity. Submature sandstones are less resistant to weathering as compared to well-sorted, mature sandstones. A visual survey of the red sandstone in the monument revealed a variety of deterioration patterns due to action of various internal and external factors. Among the external factors the ingress of moisture due to seepage of rainwater and condensation from the environment is most important. The cyclic penetration and evaporation of moisture has not only caused deformation due to dimensional changes in the sandstone but has also led to mobilisation and crystallisation of salts and biological growth. The exterior surfaces show visible salt crystallisation (efflorescence) at many places; however, the possibility of sub florescence (sub-surface crystallisation or cryptoflorescence) cannot be eliminated. The red sandstone may contain a high quantity of oxyhydroxides and 2:1 clays with high ion exchange capacities. Research has shown that stones with high exchange capacities preferentially retain ions of dissolved salts in order of their affinity to the exchange sites (Pandey*et al.,* 2014). This preferential retention may favour sub-surface crystallisation of salts leading to massive damage. The weathering forms in this monument are not uniform on all stone blocks and many of them are in fairly sound state of preservation. This indicates that the sandstone blocks with active decay have different mineralogical and mechanical properties. It may be possible that some of the sandstone blocks are immature, soft bed stones with very poor resistance to weathering. The most prominent weathering forms identified in the monument can be classified under four main categories following the ICOMOS illustrated stone glossary on stone deterioration patterns:

4.1. Detachment of stones

4.1.1. Delamination

It corresponds to a physical separation into one or several layers following the stone laminae (ICOMOS- ISCS stone glossary). The thickness and the shape of the layers are variable. In case of *Alai Darwaja*, separation of layers of red sandstone occurred along the bedding plane particularly when the stone is laid vertically as a cladding material exposing the carved face of stone to weathering. There are several carved sandstone blocks that have incorrect orientation of bedding plane (parallel to exposed face), which is a fault in the building craftsmanship, probably carried out to maximise the available surface area for carving(such stones show considerably less surface area across the bedding plane available for carving). Visual inspections had depicted that such stone blocks have deteriorated faster than those with the correct orientation of bedding plane. The thickness of detachment varies to a great extent and in *Alai Darwaza* the delamination measures from a few millimetres to several centimetres in thickness leading to exfoliation (Fig. 3a and Fig. 3b). There may be several factors responsible for delamination in sandstone – the most common being ingress of moisture and crystallisation of salts. The water penetration results in swelling of clay matrix and dimensional changes across the layers. It has been noticed that presence of certain salts in solution enhances the swelling behaviour of clays. Clay minerals are all subjected to osmotic swelling when a concentration gradient is provoked by the presence of an electrolyte and NaCl is one of the most effective electrolytes for osmotic swelling of clays (Rodriguez-Navarro *et al.*, 1997; Sebastian *et al.*, 2008). Accumulation and crystallisation of salts may take place at the interface of various layers due to inherent variations in hydraulic properties generating sufficient pressure for detachment of layers

(Fig. 3a). The presence of mica increases the potential for delamination because they reduce the grain interlock and most micaceous sandstones do not achieve the level of strength as compared to quartz sandstones (Hunt, 2008). The mineralogy of red sandstone used in *Alai Darwaza* indicates presence of significant amount of mica (Tab. 1), which can favour detachment of layers. In several stone blocks it can be noticed that the superficial layer is fairly sound but the decay of underlying layers where moisture movement is severe, is causing massive detachment.

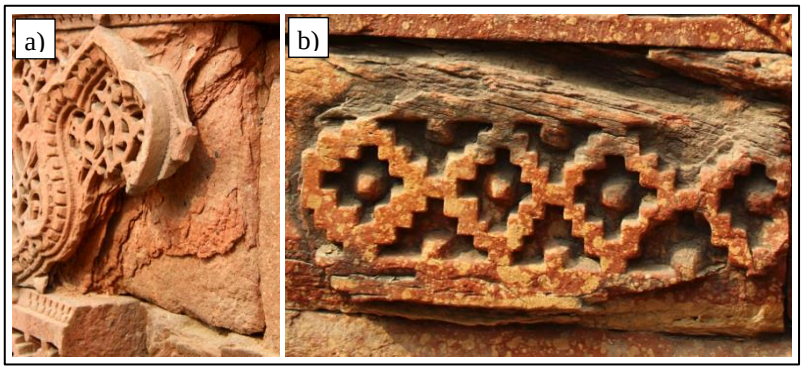

Fig. 3: Delamination of carved sand stone.

4.1.2. Exfoliation

This subtype of delamination is characterised by a detachment of multiple thin stone layers sub-parallel to the stone surface.Exfoliation develops in the form of separation of layers, typically at a depth of a few millimetres to a few centimetres. Exfoliation detaches large and thin layers of stone surface in *Alai Darwaza* at several locations (Fig. 4a). At some places it is combined with powder disintegration, of very thin layers that fall off from the surface (Fig. 4b).

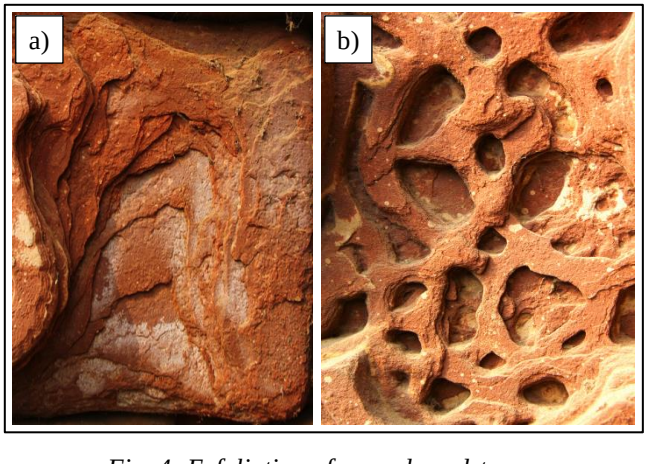

Fig. 4: Exfoliation of carved sandstones.

The primary mechanism for exfoliation of sandstone is considered to be the dissolution of silica and other cementing materials during wetting cycles and the leaching out of the dissolved constituents in the surface layers in the course of drying (Robinson and Williams 1992). Sub-surface crystallisation of salt during wetting-drying cycles has also been reported to cause spalling (GoudieandViles 1997; Holmer 1998). Most of exfoliation, that is taking place at a lower level in this monument, appears to be due to moisture and salt action (Fig. 4a and Fig.4 b).

4.1.3. Scaling

Scaling is the detachment of stone as a scale or a stack of scales, not following any stone structure and detaching like fish scales or parallel to the stone surface. The thickness of a scale is generally of millimetric to centimetric scale, and is negligeable compared to its surface dimension (ICOMOS- ISCS stone glossary). In case of *Alai Darwaja*, contour scaling also had developed as thin detachments along the the face of carved surfaces (Fig. 5a). Scales on a sandstone surface is varying from a few millimetres to a few centimetres in thickness. At most places in this monument the thickness of the single scale were found to be more than 3-5 mm (Fig. 5b).

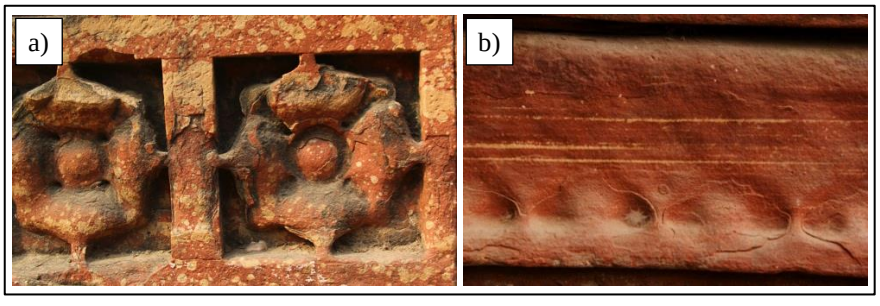

Fig. 5: Contour scaling in sandstone.

Although, the reasons for contour scaling are still debated, it has previously been linked to sub-surface crystallisation of salts (Smith and McGreevy, 1988). Recent studies have shown that mechanical stresses generated due to cycles of wetting of drying (Sebastián *et al.*, 2008) and shear forces during wetting of the surface lead to contour scaling (Jiménez-González *et al.*, 2008). However, the action of salts during the wetting and drying cycles cannot be omitted. Crystallisation and kinetic transformation of salts in the course of wetting and drying within the superficial layers of the stone can contribute to generation of stresses. Since the porosity of this sandstone is significantly low, absorption of moisture due to seepage and/or condensation is restricted to the superficial layers resulting in thinner scales. Repeated wetting and drying cycles probably combined with crystallisation of salts at the wetting-drying boundaries weaken the stone at the points of average infiltration and the entire surface detaches in the form of scales. Flaking, another related phenomenon, has also been attributed to frost action or a combination of frost and salt weathering (Thomachot and Jeannette 2002; Thomachot and Matsuoka 2007).

4.2. Material loss

4.2.1. Erosion

Loss of original surface, leading to smoothed shapes is known as erosion (ICOMOS- ISCS stone glossary).In case of *Alai Darwaja*, surface erosion, characterised by the breakdown of the intergranular clays or other minerals that bind together the grains of silica, is one of the most abundant forms of deterioration visible on both internal and external facades of the monument. Erosion of the surface can take place due to a variety of natural and/or anthropogenic causes and the actual mechanism can be due to chemical and/or physical processes. The erosion is not uniform in all the carved stone blocks and some of them show more severe form of erosion than the others, which indicates that it may be the result of inherent material properties and their response to external environmental factors. The most important reason for surface erosion in this monument is ingress of large amount of rainwater and cycles of wetting and drying. The wetting of sandstones leads to volume increases of the material and to heterogeneous stress accumulation within the stone, which leads to disintegration (Ruedrich *et al.*, 2011; Siegesmund and Snethlage, 2014). The combined effects of hygric and hydric swelling, thermal dialation and the crystallisation of salts have lead to erosion of carved details from the surfaces of several stone blocks (Fig. 6a and Fig. 6b).

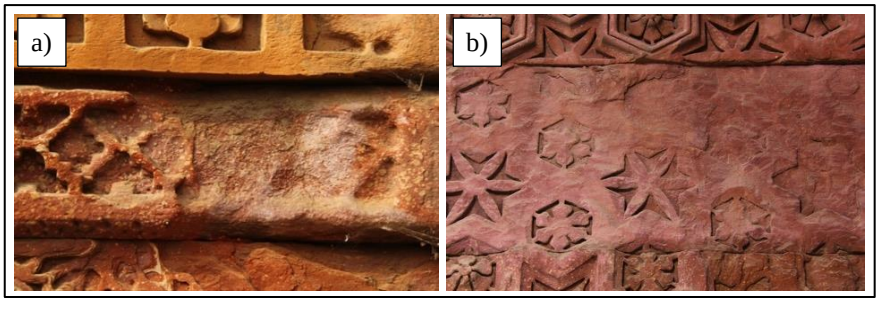

Fig. 6: Material loss due to surface erosion.

4.2.2. Bursting and fracturingof sand stone

Bursting is the local loss of the stone surface from internal pressure usually manifesting in the form of an irregularly-sided crater (ICOMOS- ISCS stone glossary). Fracturing of sandstone is caused by the cracks that cross the stone completely. In case of *Alai Darwaza*, the fracturing and bursting of sandstone both are caused by a multitude of factors and the most common factor is expansion of ferrous fixings within the stone. The use of ferrous fixings, such as dowels and clamps, in the construction of stone monuments was common practice in the monuments of *Sultanate* period. The volume expansion of ferrous dowels and clamps due to rusting generates a force sufficient to cause fracturing and bursting/dislocation of stone elements, and this is a commonly observed phenomenon in this monument (Fig. 7a and Fig. 7b). Corroding 'U' shape iron clamps, used to join the massive carved stone blocks, appears to be made of wrought iron and show a significant amount of rusting and cracking due to expansion (Fig. 7a and b).

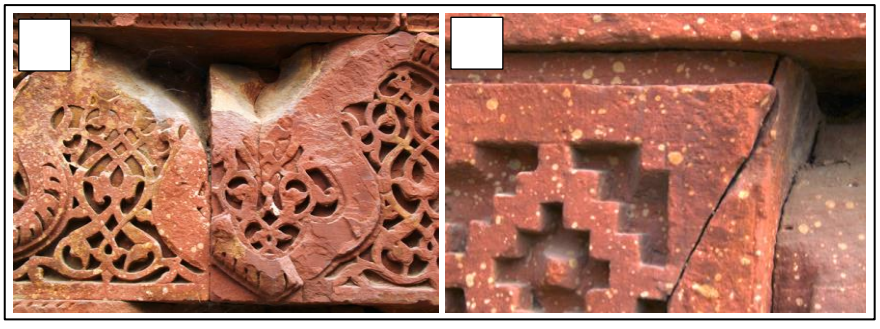

Fig. 7: Bursting (a) and fracturing of sandstone (b).

4.3. Disintegration

4.3.1. Sugaring

Calcareous stones including marbles have a characteristic pattern of weathering by granular disintegration, which is known as 'sugaring'. The marble cladding used in the monument is exposed to urban pollutants and deterioration of the surface layers has resulted in a granular, sugary texture because of dissolution along the calcite grain edges (McGee, 1991). The original, smooth surface finish is lost due to dissolution around the edges of individual grains of calcite in the stone and minerals, that are more resistant than the calcite, protrude above the dissolved calcite surface. Sharp edges and carved details have become rounded as the exposed surface of the stone is dissolved by polluted rainwater. The overall surface of marble has accumulated a brownish accretion particularly in the areas that are hidden from washing effect of the rainwater (Fig. 8). This accretion may be formation of gypsum crust from the chemical transformation of calcitic minerals from the stone.

Fig. 8: Sugaring of carved marble.

4.4. Biological colonization - Algal growth

Algal growth can be noticed as dry crust in the areas where prolonged moisture accumulation takes place. Although, identification of types of microbial growth on the monument was not carried out, presence of fungal and bacterial growth cannot be ruled out.

Algae growth encourages retention of moisture that may lead to further deterioration of the stone. Due to their phototrophic nature, they easily grow on the stone forming coloured patinas and incrustations as a result of formation of biofilm. Biofilms facilitate attachment and serve as a mechanism for resisting adverse abiotic conditions. Biofilm act as a precursor for the physical damage to the stone leading to its biodeterioration and discoloration (Crispim *et al.*, 2003; Dakal and Cameotra 2012). Microbial growth on stone surface can also lead to mineral dissolution, secondary mineral formation, encrustation and mobilisation of ions from the mineral lattice, which in turn, can weaken and discolour the substrate (Dakal and Cameotra 2012).

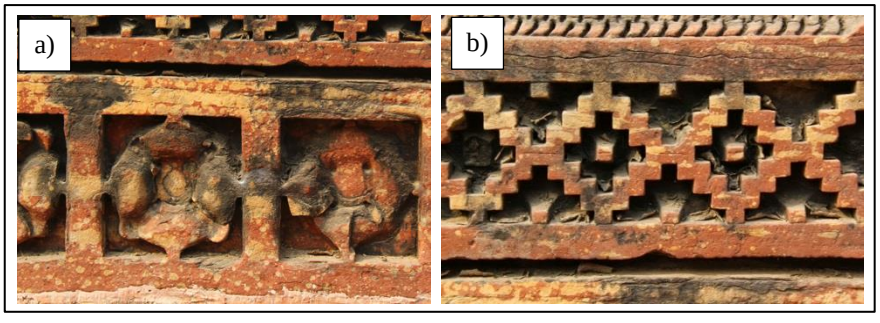

Fig. 9: Biological growth on sandstone surface.

5. Architectural stone mapping of the deterioration pattern

A detailed architectural drawing is prepared and condition of individual stone has been mapped over the external and internal elevations. Mapping of the stone deterioration pattern over the drawings has given an idea about the extent of each architectural stone members and its overall impact (Fig. 10). Detailed condition mapping has revealed alarming results of deterioration of historic carved stone, which can affect the architectural character of the monument. The number of deteriorated stones has been calculated by counting and numbering the existing cladding stones on the facade and following observations were made:

- Stone bursting has affected the loss of stone most over the façade. It had happened mostly at the places where iron dowels were originally inserted to anchor the stone members. The study revealed that stone bursting is approximately 16% of the stones and results in partial loss of the carved stones.
- Approximately 7% of stones have been eroded through the process of delamination, mostly due to an incorrect placing with bedding planes perpendicular to the façade. Erosion has caused the loss of the original carved layers of the stones leaving behind the plain stone surfaces.
- Other deterioration problems include algae deposition (3.5%), salt efflorescence (3%), discolouration (1%) and fracturing (0.5%).
- Nearly 69% of the total stones still contain the original shape and carving patterns but showing sign of initial stages of deterioration. These are the stones, which are prone to further deterioration in similar pattern, which could cause a great loss of historic carved stones.

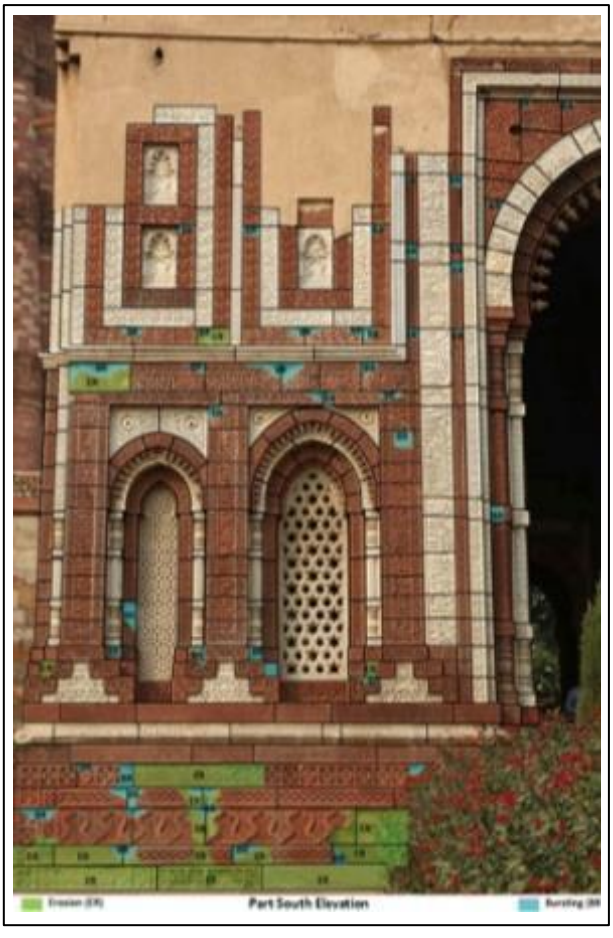

Figure10: Condition mapping of deteriorated stone in Alai Darwaza.

6. Conclusion

Considering the historical values and significance of monuments in the *Qutb*complex, the conservation of the historic carved stone is really a challenging work. The architectural, structural and material complexity of the monuments along with varying environmental conditions have led to intricate problems of deterioration. Many carved stones (approximately 25%) have already decayed considerably and only 69% carved stone still retain the original profiles however, there are signs of initial deterioration on these stones as well. In such as complex situation, the conservation requirement of the monument include following challenges:

- Consolidation of the weak and fragile stones showing severe deterioration would be difficult task considering these are all structural and architectural members and therefore cannot be taken out for the conservation works.

- Minimising the rate of decay of the carved stone in open environment, where stones are exposed to adverse climatic conditions. Carved stone where bedding planes are placed vertically (with bedding plane parallel to the exposed face) have already deteriorated severely. More than 50 % of the carved stones of *Alai Darwaza* are laid with bedding planes facing the surface and are prone to further deterioration, which needs to be controlled to minimize the future decay of these masterpieces.
- Stone bursting had left behind severe losses and cracks in the walls, which is allowing water penetration, vegetation growth and therefore accelerating the structural deterioration as well as deterioration of the carved stone.16 % of the stones are already affected due to partial loss of the stone. Other carved stones too are prone to be get affected by similar bursting due to presence of original iron dowels. It would be essential to find the existing locations of the iron dowels and work out appropriate conservation solutions to stop the future decay of the stones.
- Above all, the most challenging conservation task is to control the deterioration process in open environment where carved fragile stones are exposed to the extreme climatic condition and seasonal variations.
- The original craftsmanship does not exist anymore and it would be difficult to carry out the minor repair works especially when stone pieces would need to be inserted for partially repair works wherever stones are broken or partially lost and affect the structural stability of the monument.

The study of the *Alai Darwaza* had revealed the alarming results of the deterioration of the carved stones, which are the integral part of the architecture of the complex. Similarly other monuments of the complex such as *Qutb Minar*, screen of *Quwwat-ul Islam* Mosque and tomb of *Ittutmish* are also depicting similar decay patterns. Multifaceted cultural values and significance and complexity of the issues, therefore, would need to be addressed together to preserve and retain the architectural and historical character of the monuments.

Acknowledgement

The authors would like to thank the Archaeological Survey of India for providing required assistant for the site work.

References

Crispim, C.A., Gaylarde, P.M., Gaylarde, C.C., 2003. Algal and cyanobacterial biofilms on calcareous historic buildings, Curr. Microbiol.46:79-82.

Dakal, T.C., Cameotra, S.S., 2012.Microbially induced deterioration of architectural heritages: routes and mechanisms involved,Environ. Sci. Eur. 24, 36.

Goudie, A.S. &Viles, H.A., 1997, Salt Weathering Hazards, John Wiley & Sons, Chichester.

Holmer, B., 1998, 'Flaking by insolation drying and salt weathering on the Swedish west coast', ZeitschriftfrGeomorphologie 42, 39−55.

Hunt, B.J., 2008. Sandstone, Geol.Today 24, 33–38.

Jiménez-González, I., Rodríguez-Navarro, C., Scherer, G.W., 2008.Role of clay minerals in the physic-mechanical deterioration of sandstone. J. Geophys. Res. Earth Surf. 113,F02021.

McGee, E.S., 1991. Influence of Microclimate on the Deterioration of Historic Marble Buildings. APT Bull. 23, 37–42.

Pandey, S.C., Pollard, A.M., Viles, H.A., Tellam, J.H., 2014. Influence of ion exchange processes on salt transport and distribution in historic sandstone buildings. Appl. Geochem. 48, 176–183.

Robinson, D.A. & Williams, R.B.G., 1992, 'Sandstone weathering in the High Atlas, Morocco', ZeitschriftfrGeomorphologie, 36, 413−429.

Rodriguez-Navarro, C., Hansen, E., Sebastian, E., Ginell, W.S., 1997.The Role of Clays in the Decay of Ancient Egyptian Limestone Sculptures. J. Am. Inst. Conserv. 36, 151–163.

Ruedrich, J., Bartelsen, T., Dohrmann, R., Siegesmund, S., 2011. Moisture expansion as a deterioration factor for sandstone used in buildings, Environ. EarthSci. 63, 1545–1564.

Sebastián, E., Cultrone, G., Benavente, D., Linares Fernandez, L., Elert, K., Rodriguez-Navarro, C., 2008. Swelling damage in clay-rich sandstones used in the church of San Mateo in Tarifa (Spain). J. Cult. Herit. 9, 66–76.

Siegesmund, S., Snethlage, R., 2014.Stone in Architecture: Properties, Durability. Springer, pp 162.

Smith, B. and McGreevy, J. (1988) Contour Scaling of Sandstone by Salt Weathering under Simulated Hot Desert Conditions.Earth Surface Processes and Landforms, 13, 697-705.

Thomachot, C., Jeannette, D., 2002. Evolution of the petrophysical properties of two types of Alsatian sandstone subjected to simulated freeze-thaw conditions, in Siegesmund, S., Weiss, T., and Vollbrecht, A. (eds.) Natural Stone, Weathering Phenomena, Conservation Strategies and Case Studies, Geol. Soc. Lond. Spec. Publ. 205, 19–32.

Thomachot, C., Matsuoka, N., 2007. Dilation of building materials subjected to frost action, in Přikryl, R., Smith, B.J., (eds.) Building Stone Decay: From Diagnosis to Conservation, Geol. Soc. Lond. Spec. Publ. 271, 167-177.

Vergès-Belmin, V., (ed.) 2008. Illustrated Glossary on Stone Deterioration, ICOMOS (International Council on Monuments and Sites) and ISCS (International Scientific Committee for Stone). (http://www.icomos.org/publications/monuments_and_sites/15/pdf/Monuments_and_Sites_15_ISCS_Glossary_Stone.pdf).

EFFECT OF MICROORGANISM ACTIVITIES IN A POLLUTED AREA ON THE ALTERATION OF LIMESTONE USED IN HISTORICAL BUILDINGS

C. Balland-Bolou-Bi[1], M. Saheb[2], N. Bousserrhine[1], S. Abbad-Andaloussi[1], V. Alphonse[1], S. Nowak[3], A. Chabas[2], K. Desboeufs[2] and A. Verney-Carron[2]

Abstract

We have studied the alteration of limestone exposed to microbial activities in a polluted environment. Our work focuses on the Père-Lachaise Cemetery, a garden located in the Parisian urban area (France) that contains many unrestored monuments out of limestone from the 19th century. We have selected one tomb representative of the buildings, in terms of material (Lutetian limestone from the Parisian basin), location (exposed to pollution and vegetated environment) and alteration patterns. The mineralogical composition was determined using XRD and the bacterial communities were studied using pyrosequencing. Results indicate a significantly higher diversity of bacteria in the horizontal part of monument than in the vertical one linked to local environmental conditions. Horizontal zones contain potassium nitrate which formation has been linked to the presence of nitrogen fixator alphaproteobacteria. Vertical illuminated and dry zones contain a black crust out of gypsum and soot which formation may be induced by gaseous pollutants.

Keywords: limestone, microbial alteration, polluted environment, pyrosequencing

1. Introduction

During their lifetime, buildings out of stone are exposed to chemical and biological actions that cause different alteration patterns, such as loss of materials, chemical transformations and deposits. In addition to climatic factors (rainfall, thermal variations and relative humidity), pollution (as gas and particulate matter) and biological activity influence the alteration processes, depending on the nature of the environment (rural, industrial, and urban). Beyond the aesthetic inconvenience that could affect the cultural value of the building, these changes modify its sustainability. Therefore one needs to understand the involved mechanisms and the impact of the different environmental factors to propose suitable conservation and restoration treatments. Since 52% of historical buildings in France are built from limestone, we decided to focus on the alteration of this kind of stone.

[1] C. Balland-Bolou-Bi, N. Bousserrhine, S. Abbad-Andaloussi, V. Alphonse
IEES, UMR 113 CNRS/UPEC, France

[2] M. Saheb*, A. Chabas, K. Desboeufs and A. Verney-Carron
LISA, UMR 7583 CNRS/UPEC/UPD, France
mandana.saheb@lisa.u-pec.fr

[3] S. Nowak
Plateforme Rayons X, UFR de Chimie, UPD, France

*corresponding author

Gaseous pollutants (CO_2, SO_2, NOx, HNO_3) increase the stone dissolution as they are responsible of the acidification of water (Kirkitsos and Sikiotis, 1995). This phenomenon generally leads to the formation of crusts, mainly composed of gypsum (Sabbioni, 2003). Particulate matter can also deposit on the limestone surface and cause soiling and contribute to the blackening of crusts. In 1933, Paine *et al.* showed that decaying limestone houses a sizeable bacterial flora, including gram variable and gram-negative rods and cocci, whereas spore formers are rare or absent. From a biochemical point of view, the limestone alteration results from the instability of carbonates in an acid solution. Although low molecular weight organic acids and CO_2 from heterotrophic metabolisms were described as the principal cause of the limestone decay, autotrophic nitrifying and sulfur-oxidizing bacteria were also shown to promote this decay. These alterations are mediated by nitric and sulfuric acids from ammonia and reduced sulfur. Krumbein (1968) also found a variable number of fungi, algae and ammonifying, nitrifying and sulfur-oxidizing bacteria on the surface of limestone. Moreover, microorganisms can increase stone dissolution rate by keeping a high surface humidity, inducing chemical perturbations and producing metabolites such as organic acids, which increases the lixiviation of cations from the minerals (Bousserrhine *et al.*, 1999). However on limestone from historical buildings, the action mechanisms of microorganisms are still unknown. Furthermore, pollution can influence the development of some microbial species aggressive for the limestone (Mihajlovski *et al.*, 2014). Sulfur-oxidizing, nitrifier and ammonifier bacteria are more numerous and active in urban environments, where the atmosphere contains more nutrients. In addition, microorganisms can catalyze the fixation of atmospheric pollutants. Consequently, studies on limestone alteration need to take into account the chemical and the biological actions as they can have a synergetic effect.

To perform this interdisciplinary study between materials and biological sciences, we have selected the Père-Lachaise Cemetery (1804) located in Paris where most of the tombs dated from the 19th century are out of limestone from the Parisian basin. The preservation of this historical listed site is crucial. Most of the mausoleums have not been restored which gives the opportunity to observe old and dated alteration patterns. Last, the cemetery is located in Paris City center, in a polluted environment and close to important vegetation. Thus the alteration is caused by both chemical and biological actions. Limestone samples were collected and analyzed to identify the microorganisms and characterise the alterations.

2. Materials and methods

2.1. Studied area and sample collection

A tomb located in the Romantic area of the Cemetery (division 25, n°66) was selected. This area is a green zone with the presence of numerous plants and trees. The monument is out of a Lutetian limestone and presents a sole, a bedrock, a horizontal tombstone and a vertical stele (Fig. 1). The back of the stele is South-East oriented. Two zones were sampled on September 11th 2015. The temperature mean and pluviometry of this month in Paris were 19.6°C and 72.2 mm, respectively. For the biological sampling, three samples were collected using a sterile scalpel and placed into a 2 mL sterile tube (Eppendorf ®) before freezing until analysis: one in the green vertical part (BT 66 V) and two in the horizontal part under two different genus of mosses: *Grimmia* (BT 66 H) and *Pleurochaete* (AT 66 H) (Fig. 1). For the mineralogical characterization, the sampling was performed on the vertical (CT 66 V) and the horizontal part (CT 66 H).

Fig. 1: Photography of the tomb 66 located in the 25th division of the Père-Lachaise Cemetery (a), of the sampled zone CT 66 V in the vertical part (b) and zone CT 66 H in the horizontal part (c); Dimensions: 1.8m long, 0.8m wide and 1.8m high.

2.2. Materials characterization

The mineralogical composition of the alteration phases (samples CT 66 H and CT 66 V) was identified using XRD on an Empyrean diffractometer from Panalytical equipped with a multichannel PIXcel 3D detector and a filtered-copper X-ray source (1.5418 Å). Each pattern was recorded in the 10°-60° 2θ range (0.013° for 150 s). Therefore samples were crushed into powder. The phases were identified using the Inorganic Crystal Structure Database (ICSD) with a selection of the best correlation.

2.3. Biological analyses

2.3.1. Bacterial DNA extraction, pyrosequencing and data analysis

DNA was extracted from approximately 0.1 g of each sample by employing the Fast DNA spin kit for soil (MP Bio®). The concentration and purification of the extracted DNA (2 µL) were determined by agarose gel electrophoresis (1%) and microspectrophotometry (absorbance at 260 nm). A high-throughput sequencing method (pyrosequencing) was used to characterise bacterial communities and examine their relative abundance and diversity. Extracted DNA was sent to the Research and Testing Laboratory (Lubbock, TX, US) for bacterial 16S rRNA gene tag-encoded FLX amplicon pyrosequencing (bTEFAP). PCR amplification was performed using the primers Gray28F and Gray388r (Callaway *et al.*, 2010). Sequencing reactions used a Roche 454 FLX instrument (Roche, Indianapolis, IN) with titanium reagents, titanium procedures, a one-step PCR reaction (35 cycles), and 1 U of Hot Star High fidelity Polymerase was added to each reaction. 16S rRNA gene

sequences analyses were carried out by Research and Testing Laboratory to obtain taxonomical assignments from sequences reads. For the taxonomy assignments from 16S rRNA sequences reads, low quality sequence ends, tags and primers were removed and sequences depleted of any non-bacterial ribosome sequences and chimeras using Black Box Chimera Check software (B2C2) (Gontcharova *et al.*, 2010). To identify the bacteria, sequences were denoised, assembled into clusters and queried using a distributed BLASTn.NET algorithm against a database of 16S bacterial sequences derived from the National Centre for Biotechnology Information (NCBI). Database sequences were characterised as high quality based upon similar criteria used by the Ribosomal Database Project (RDP) ver 9 (Cole *et al.*, 2009). Using a .NET and C# analysis pipeline the resulting BLASTn (Nucleotide Basic Local Alignment Search Tool) outputs were compiled, validated using taxonomic distance methods, and data reduction analysis performed as described previously (Callaway *et al.*, 2010).

2.3.2. Microorganisms extraction, isolation and acidification test

0.1 g of sample was aseptically homogenized in 1.2 mL of physiological water in a sterile tube (Eppendorf®) for 120 minutes. 1 mL of the resulting mixture was tenfold serially diluted in sterile saline solution (NaCl 0.9 $w.v^{-1}$). Microbial suspensions were plated incubated as follows: total mesophilic counts on R2A agar (R2A agar plates double wrapping; VWR chemicals) incubated aerobically at 30°C for 72h. For each sample, several bacterial colonies representing different morphologies were randomly picked from plates and sub-cultured on the corresponding medium. The ability of each strain to acidify the medium was tested. 10 mL of medium (containing $5g{\cdot}L^{-1}$ Glucose (VWR), $1g{\cdot}L^{-1}$ Yeast extract (Prolabo), $5g{\cdot}L^{-1}$ NaCl (Rectapur) and $1g{\cdot}L^{-1}$ NH_4Cl (Rectapur)) was used for cultivation. The *pH* was measured after 2 days of incubation at 30°C.

3. Results and discussion

XRD on the horizontal (CT 66 H) and vertical (CT 66 V) parts revealed two different alteration patterns depending on the location on the tomb (Fig. 2). On the vertical part (CT 66 V), the new-formed phases are mainly gypsum $CaSO_4{\cdot}2H_2O$ and graphite. Graphite is the crystallized part of soot, so that the presence of these both phases corresponds to the formation of a black crust on the limestone. On the horizontal part (CT 66 H), the presence of calcite and quartz is linked to the underlying substrate. The presence of clay as potassium aluminum silicate may be induced by the soil located close to this part. The main alteration phase is potassium nitrate KNO_3, which was not found on the vertical part. No gypsum has been found on this horizontal part.

From a biological point of view, the results indicate a significantly higher diversity of bacteria in the horizontal part of the monument than in the vertical part (Fig. 3). A total of 850 sequences were retrieved. Bacteroidetes (28-31%), Acidobacteria (1-8%) and Proteobacteria (25-33%) are important phyla on the horizontal zone whereas Cyanobacteria (51%), Actinobacteria (27%) and Proteobacteria (17%) are on the vertical zone. These phyla are commonly found on historic monuments (i.e. Scheerer *et al.*, 2009). The samples collected under different mosses on the horizontal part (AT 66 H and BT 66 H) are similar as far as pyrosequencing analysis is concerned. The proportion of the main phyla Bacteroidetes, Acidobacteria, Proteobacteria, Actinobacteria and Cyanobacteria do not significantly vary as well as the subgroup and species (Fig. 3). However, after isolation of several bacterial strains, the proportion of acidifying bacteria changes according to

sampling. 33 strains were isolated from horizontal and vertical parts of monument. The acidification test showed that 12 strains of bacteria can acidify medium from pH 6.5 to 4.0. On the vertical part, 5 strains were isolated; among them, only one acidified the medium. For the horizontal part, 13 and 12 strains were isolated from BT 66 H and AT 66 H, respectively. Two strains acidified the medium for BT 66 H and 7 strains acidified the medium for AT 66 H. These results indicated that production of organic acids take part in the alteration mechanisms.

Whatever the sample (Fig. 4), in the actinomycete phylum, the genus *Pseudonocardia* was found in high quantity (5-6%). These bacteria are frequently associated to hydrocarbons pollution (Mahendra and Alvarez-Cohen, 2005). Although this genus is known to produce H_2S (Zhang *et al.*, 2014), gypsum was only detected on the vertical part of the stele (Fig. 2). The presence of this category of bacteria is thus not sufficient to explain gypsum formation which could be induced by other parameters such as gaseous pollutants.

Specific organisms (Cytophagales subgroup) are particularly associated to environments characterised by low light and high water availability. Indeed, Bacteroidetes phylum was almost exclusively present on the horizontal part where these conditions are favored. Most of these bacteria and especially the Cytophagales subgroup are known to have a central role in the global carbon cycle as organic carbon demineralizers (Buchan *et al.*, 2003). It is consistent with their presence in the horizontal part where the monument was colonized by moss and lichen and received dead leafs from trees. The vertical dry and illuminated zone (BT 66 V) was exclusively colonized by desiccation-tolerant Cyanobacteria (51%) and more precisely by *Chroococcidiopsis* sp. These cyanobacteria are photolithoautotrophic organisms that can survive to dry periods. Several studies (i.e. Scheerer *et al.*, 2009) concluded that Cyanobacteria are the first colonizers in the microbial succession of stone. Associated to these Cyanobacteria, Actinobacteria, especially *Microlunatus* sp. (13%) have been preferentially detected on this vertical part. These bacteria produce polyphosphates involved in the adaptation to extreme arid environment by modulating microbial stress response (Seufferheld *et al.*, 2008) comforting that the exposition induced by the geometry of the tomb is a major factor controlling the ecology of bacteria. Concerning the horizontal zone, *Microlunatus* sp. accounts for only 8%. Actinobacteria phylum is represented by Nocardioides subgroup (7%), gram positive, non-acid fast, aerobic and was isolated from a variety of habitat (Yoon and Park, 2006). Proteobacteria phylum represented 18% for the vertical sample (BT 66 V), 28% (BT 66 H) and 31% (AT 66 H) for the horizontal samples. The proportion of alphaproteobacteria was significantly higher for horizontal samples than vertical ones, especially with the subgroup Rhizobiales (20%) that are nitrogen fixators. This result is consistent with the significant amount of KNO_3 identified on the horizontal zone CT 66 H (Fig. 2). On the vertical sample, these bacteria only represented 3%, which could explain why no potassium nitrate was observed on this part.

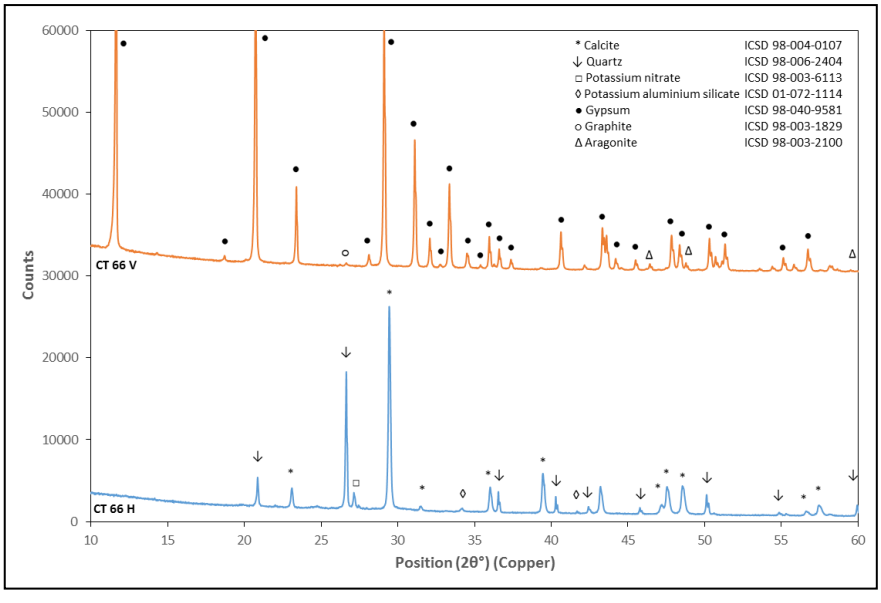

Fig. 2: XRD analyses on powder sampled from the vertical (CT 66 V) and the horizontal (CT 66 H) part.

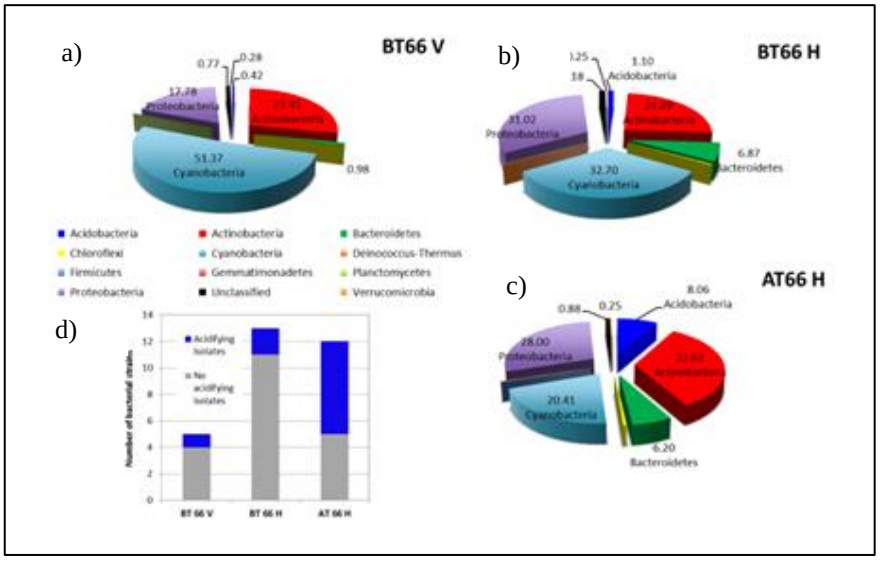

Fig. 3: Bacterial composition at the phylum level of: a) BT 66 V, vertical part; b) BT 66 H, horizontal part 1; c) AT 66 H, horizontal part 2 and d) Percentage of each phylum (number of cultivable acidifying bacteria).

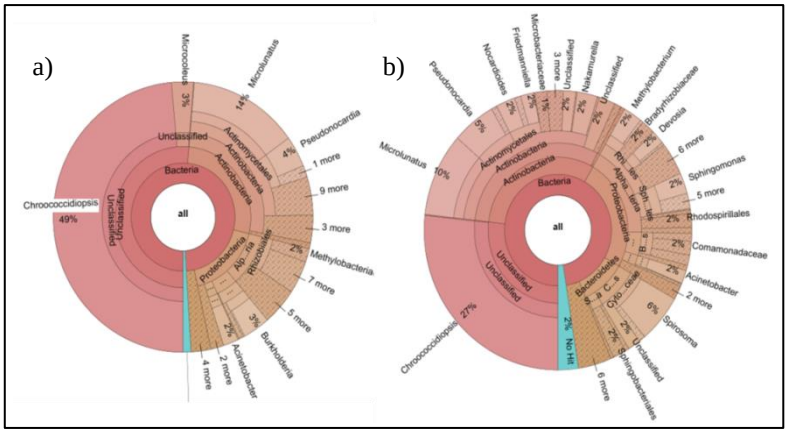

Fig. 4: Bacterial composition at phylum to genus level of BT 66 V (a) and BT 66 H (b).

4. Conclusion

This work is part of an ongoing study aiming at understanding the joint effects of biological activity and pollution on the alteration mechanisms on limestone. It allowed confronting the alteration patterns and the microorganisms present on real limestone blocks exposed during a long period to an urban and vegetated environment. The results indicate a significantly higher diversity of bacteria in the horizontal part of the monument than in the vertical one linked to the environmental conditions. Horizontal zones contain potassium nitrate which formation has been linked to the presence of nitrogen fixators. Vertical zones colonized by desiccation-tolerant Cyanobacteria present a black crust out of gypsum and soot whose formation may be induced by gaseous pollutants. To complete this study and validate the hypotheses, other experiments are in progress. Firstly pristine limestone samples are exposed close to the monuments to identify the first microbial populations that colonize the stone. At the same time, rainwater is collected to study its contribution via its microbial and chemical composition. Secondly laboratory experiments are carried out to expose limestone samples to site representative micro-organisms in a controlled environment. The comparison of their activities on pristine and on weathered samples will allow determining the impact of the microorganisms on the biodeterioration of limestone under pollution.

Acknowlegements

The authors thank M. Faudot, M. Lecuyer and G. Groud for the authorization to collect samples at the Père-Lachaise Cemetery and OSU-EFLUVE for its financial support.

References

Balland C., Poszwa A., Leyval C., Mustin C., 2010, Dissolution of phyllosilicate as a function of bacterial metabolic diversity. Geochim. Cosmochim. Acta, 74, 5478-5493.

Bousserrhine N., Gasser U., Jeanroy E., Berthelin J., 1999a, Bacterial and chemical reductive dissolution of Mn, Co, Cr and Al substituted goethites. Geomicrobiol. J., 16, 245-258.

Buchan, A., Newell, S., Butler, M., Biers, E., Hollibaugh, J., Moran M., 2003, Dynamics of Bacterial and Fungal Communities on Decaying Salt Marsh Grass. Appl. Environ. Microbiol., 69, 6676-6687.

Callaway S.E., Dowd T.S., Edrington R.C., Anderson N., Krueger N., Bauer P.J., Kononoff D.J., 2010, Evaluation of bacterial diversity in the rumen and feces of cattle fed different levels of dried distillers grains plus solubles using bacterial tag-encoded FLX amplicon pyrosequencing. J. Anim. Sci., 88, 3977-3983.

Cole J.R., Wang Q., Cardenas E., Fish J., Chai B., Farris R.J., Kulam-Syed-Mohideen A.S., McGarrell D.M., Marsh T., Garrity G.M., Tiedje J.M., 2009, The Ribosomal Database Project: improved alignments and new tools for rRNA analysis. Nucleic Acids Res., 37, 12 p.

Gontcharova, E. Youn, R.D. Wolcott, E.B. Hollister, T.J. Gentry, S.E. Dowd, 2010, Black box chimera check (B2C2): a windows-based software for batch depletion of chimeras from bacterial 16S rRNA gene datasets. Open Microbiol. J., 4, 47-52.

Kirkitsos P., Sikiotis D., 1995, Deterioration of pentelic marble, Portland limestone and baumberger sandstone in laboratory exposures to gaseous nitric acid. Atmos. Envir., 29, 77-86.

Krumbein WE., 1968. Zur Frage der biologischen Verwitterung: Einfluss der Mikroflora auf die Bausteinverwitterung und ihre Abhangigkeit von adaphischen Faktoren. Z. Allg. Microbiol.; 8, 107-117.

Mahendra, S., and Alvarez-Cohen, L., 2005, Pseudonocardia dioxanivorans sp. nov., a novel actinomycete that grows on 1,4-dioxane. Int. J. Syst. Evol. Micr., 55, 593-598.

Mihajlovski A., Seyer D., Benamara H., Bousta F., Di Martino P., 2014, An overview of techniques for the characterization and quantification of microbial colonization on stone monuments. Anal. Microbiol., 65, 1243-1255

Paine SG, Lingood FV, Schimmer F, Thrupp TC. 1933, IV. The relationship of microorganisms to decay of stone. Roy. Soc. Phil. Trans., 222B, 97-127.

Sabbioni C., 2003, Mechanisms of air pollution damage to stone, The Effects of Air Pollution on the Built Environment. Air Poll. Rev., 2, 63-106.

Scheerer S., Ortega-Morales O, Gaylarde C., 2009, Microbial deterioration of stone monuments: an updated overview. Adv. Appl. Microbiol., 66, 97-139.

Seufferheld, M. J., Alvarez, H. M. Farias, M. E., 2008, Role of polyphosphate in microbial adaptation to extreme environments. Appl. Environ. Microb., 74, 5867-5874.

Yoon, J., Park Y., 2006, The Genus Nocardioides. In: The Prokaryotes, 3, 1099-1113.

Zhang, D., Jiang, Z., Li, L., Liu, B., Zhang, X., Tian, X., Zhang, S., Li, W., 2014, Pseudonocardia sediminis sp. nov. isolated from marine sediment. Int. J. Syst. Evol. Micr., 64, 745-750.

GRANITE AND MARINE SALT WEATHERING ANOMALIES FROM SUBMERGED AND INTER-TIDAL AND COASTAL ARCHAEOLOGICAL MONUMENTS IN IRELAND

J. Bolton[1*]

Abstract

The phenomenon of severe stone decay in coastal areas is well documented as a significant threat to stone cultural heritage in both Mediterranean and Atlantic Europe, and previous research has consistently shown that the action of salts of marine origin play a significant role in the deterioration of these stone surfaces. However, in an Irish context, a monument located on the coastline does not necessarily or even normally experience any greater degradation than a similar monument of the same stone type located in a non-polluted inland environment. Outside the harsh inter-tidal zone and the special deterioration processes found in shallow marine environments, there is often negligible difference in the rate or severity of stone decay on a granite monument built 2 metres from the high water mark, with a comparable granite monument located 50 metres or 50 kilometres inland. Why then would coastal buildings in Ireland survive in better condition than their counterparts elsewhere in Europe? This paper presents a synthesis of field- and laboratory studies of 88 archaeological monuments built of granite located in three of the four granite batholiths in Ireland on the east, west and south coasts of the country from submerged, inter-tidal, coastal and unpolluted inland environments. The research detected particular patterns of salt deposition on granite building stones, and developed a hypothesis to explore the anomalies of salt-related granite weathering in Ireland and the significance of local distinctiveness in building conservation studies.

Keywords: Granite, marine salts, weathering, coastal, Ireland

1. Introduction

The coast is often characterised as an aggressive environment where natural and artificial pollutants enter a system based on rapid change. It is generally accepted that rock degradation proceeds faster in a wet environment (Kühnel 2000), and that the salt-induced decay derived from the marine environment accelerates decay mechanisms (Zezza 2002). However, investigations into the deterioration of archaeological monuments and historic buildings in Ireland (Pavía and Bolton 2001, Bolton 2007) noted little contrast between the levels of decay encountered in buildings located on the coast and comparable building located up to 120 km inland. To address this research question, 88 granitic stone monuments were examined - 33 sites located on or adjacent to the shoreline on the east,

[1] J. Bolton*
Dublin, Ireland
jboltonconservation@gmail.com

*corresponding author

west and south coasts of Ireland, and 55 monuments located in inland unpolluted environments.

2. The problem of salts of marine origin

The formation, transport, and crystallisation of salts in rocks and other porous building materials has been widely recognised as one of the primary causes of the deterioration of historical architecture, archaeological monuments and archaeological objects (Winkler 1994, Rodriguez-Navarro and Doehne 1999, Charola 2000, Doehne and Price 2010). The crystallisation of salts within a granitic rock can be a complex and very destructive weathering process as a result of thermal, hydration and/or crystallisation stresses leading to decay forms such as scaling, flaking, effloresence and granular disintegration. Salts may not always be the original cause of deterioration and often act synergistically with other processes, but their presence in conjunction with water and/or moisture significantly increases the deterioration rate of a stone. Sources for salts in building materials include atmospheric pollution, other building materials, groundwater, biological organisms and salts of marine origin. The degree of damage to building stones associated with marine salts is generally considered to be severe (Alves and Sequeira Braga 1996, Silva *et al.* 1996, Zezza 1996, Rodriguez-Navarro and Doehne 1999, Charola 2000, Chabas and Jeanette 2001, Doehne 2002). Marine aerosol includes a range of particles termed according to their physical characteristics such as film drops, jet drops, sea-water drops, brine drops, hydroscopic salt drops, sea-salt nuclei and sea-salt particles. Sources of salts of marine origin on building stone include sea flooding, rising damp, contaminated building materials, and marine aerosol. Marine aerosol salts may accumulate through a three-stage process of deposition on the stone surface, accumulation, and penetration into the pore network of the stone. Previous studies in Europe note a high incidence of marine salt deposition on the surface of monuments located adjacent to the sea, while the transport and deposition of marine salts tends to gradually reduce moving inland. Silva *et al.* (2002) noted on a survey transect extending 166 km inland that the most intense deposition of salt was found within 0.15 km of the sea, and that proximity to the sea results in both greater deposition of marine salts and more intense weathering.

3. Field evaluations of granite stone monuments in Ireland

Fig. 1: a) The tenth century church of St. Begnet, Dalkey Island, Co. Dublin; b) Scaling of the granite masonry surface, St. Begnet's Church.

Field evaluations to evaluate and compare the current condition of granitic stone monuments in coastal and unpolluted inland environments were undertaken by rapid site

surveys examining visual indicators of stone decay, noting any variation[s] in the type(s), extent and severity of deterioration of granitic stone surfaces following an established methodology (Pavía and Bolton 2001). The monuments ranged from prehistoric monuments to medieval structures to post-medieval fortifications built of two types of granite. The key finding of these stone decay assessments was that despite the wide time range represented by these monuments, there was very little variation in the range of most common decay forms encountered in coastal and unpolluted inland environments in Ireland, and that scaling and granular disintegration which have been previously associated with salts of marine origin, are not especially prevalent in coastal locations (Tab. 1).

Tab. 1: Summary of Granite Stone Decay Assessments.

Type	**Total Population: 88**		**Coastal: 33**		**Inland: 55**	
	No.	%	No.	%	No.	%
Biological Colonisation	78	89%	27	82%	51	93%
Intense Biological Colonisation	11	12.5%	3	9%	8	15%
Brown Staining	39	44%	18	55%	21	38%
Dissolution	42	48%	16	49%	26	47%
Granular Disintegration	58	66%	22	67%	36	65%
Fracturing	28	32%	10	30%	18	33%
Scaling	31	35%	11	33%	20	37%
Dry Joints	20	23%	13	65%	7	35%
Spalling	17	19%	4	24%	13	76%
Oxidation	38	43%	11	33%	27	49%
Mild Stone Decay	75	85%	28	85%	47	85%
Strong Stone Decay	13	15%	5	15%	8	15%

All granite stone monuments showed some stone decay, classified (after Pavía and Bolton 2001) as either 'Mild' (85%) or 'Strong' (15%). Ratios of mild to strong stone decay remained equal regardless of location. The occurrence of strong stone decay found at coastal monuments could most often be attributed to a coast-specific factor with the inter-tidal and submerged zones such as abrasion and corrosion (Bolton 2007). There were some minor variations in the frequency of decay forms found at inland and coastal locations. For example, dry joints (mortar no longer present) were found to be more common on coastal buildings than inland buildings. However, this may be due to the greater amount of water present on the coast and coast-specific processes such as abrasion and corrosion acting on the joints. Strong stone decay in unpolluted inland environments was often associated with incompatible repair materials, spalling due to visitor pressure or animal abrasion, or another well-understood stone decay processes. The key decay forms of granular disintegration, fracturing, scaling, biological colonisation and dissolution were found to occur equally in both coastal and unpolluted inland environments. This contrasted strongly with the general findings from the existing literature which almost universally noted more severe weathering and significant salt-related decay of coastal stone surfaces and an associated correlation between proximity to the coast and severity of decay (Silva *et al.* 2002, Zezza 2002);

4. Laboratory analyses

4.1. Petrography

The purpose of the petrography was to assess the characteristics of the granitic stone types found in the sample population, and note the type and severity of decay forms found. Thirteen stone monuments were selected from coastal areas in counties Dublin, Wicklow, Wexford and Galway. All granites evaluated shared some weathering characteristics. The key macroscopic decay forms were granular disintegration and biological colonisation, with lesser amounts of oxidation, scaling and dissolution. Microscopic weathering forms focused on alterations to the weaker feldspar and mica components. These decay forms are common physical expressions of a number of deterioration processes including water-based dissolution and salt-related decay processes. Overall, the level of deterioration found to all granites is consistent with that observed during field evaluations. The stone surfaces were generally sound showing relatively poorly-developed decay forms, and therefore contrasting with the condition of granite in coastal environments reported in the literature.

Tab. 2: Key macro- and microscopic decay forms noted during petrographic analysis.

		Macroscopic		**Microscopic**	
Most Severe Observed Decay		• Granular Disintegration (G) • Biological Colonisation (B)		• Alteration of Feldspar (aF) • Alteration of Mica (aM)	
Other Decay Forms		• Scaling (S) • Surface Roughening (R) • Fracturing (F) • Oxidation (O)		• Micro-fracturing (MF) • Oxidation (O)	
No.	**Monument**	**Macroscopic Decay**		**Microscopic Decay**	
		Form	**Severity**	**Form**	**Severity**
1.	Kilternan Church	(G), (B)	Mild-Strong	(aF), (aM)	Mild
2.	Kilternan Portal Tomb	(B), (S), (F), (R)	Mild	(aF)	Mild
3.	Goreen Church	(G), (F), (S), (O)	Strong	(aF), (aM), (MF)	Strong
4.	St. MacDara's Church	(O), (G)	Mild	(aF), (aM), (O)	Mild
5.	Lady's Island Church	(B), (G)	Mild	(aF)	Mild
6.	Lady's Island Mural Tower	(G), (R), (S), (B)	Mild	(aF)	Mild
7.	Lady's Island Tower House	(G), (S)	Mild	(aM), (aF)	Mild
8.	Rathshillane Castle	(G), (O), (B)	Mild	(aF), (O), (aM)	Mild
9.	St. Margaret's Church	(B), (G)	Mild-Strong	(aF), (aM)	Mild
10.	Fassaroe Castle	(O),(B),(F),(S),(G)	Mild	(O), (aF), (aM)	Mild
11.	Old Conna Church	(G), (O), (F), (B)	Mild-Strong	(aF), (aM)	Mild-Strong
12.	Oldcourt Castle	(G), (O), (D)	Mild	(aF), (O)	Mild
13.	St. Crispin's Cell	(G),(F),(O),(S),(B)	Mild-Strong	(aF), (O)	Mild-Strong

4.2. Ion chromatography

Ion chromatography was used to investigate whether salts, if any, were present from surface samples of 11 granite monuments on a transect of submerged, littoral zones and the landward and seaward elevations of coastal monuments, to three inland monuments located with increasing distance (500 m, 1.5 km, 70 km) from the high water mark. (Na and Cl) were detected on granitic stone surfaces showing granular disintegration and scaling at all sites, regardless of location in coastal or unpolluted rural environment. The highest salt levels were found below the high-water mark in the inter-tidal zone, and gradually

decreasing as distance from the shore increased. The highest values for salts were found on elements of monuments located either at the high water mark or partially submerged. However, high salt levels were not accompanied by increasing occurrence of, or severity of, scaling, granular disintegration or other decay forms in these areas. Conversely, stone surfaces in these salt-laden areas appeared reasonably sound on close visual inspection with no obvious signs of surface disruption, though showing signs of surface recession.

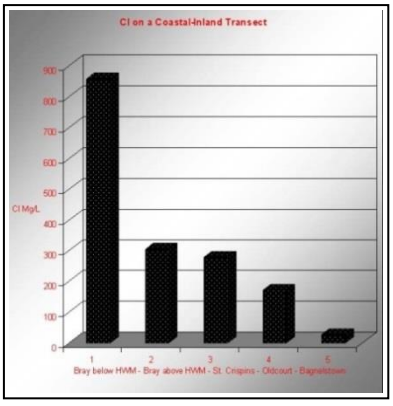

Fig. 2: Cl Levels from above below and the high water mark (Bray, 8 structures) to 500m (St.Crispins Church) to 1500m (Oldcourt Castle) to 70 km inland (Bagnelstown Court) showing a decrease in Cl levels with increasing distance from the coast.

4.3. Scanning Electron Microscopy

Stone fragments from archaeological monuments located on the east and west coasts of Ireland were sampled on transects of buildings which were fully submerged, inter-tidal, within the spray zone, and within 300 metres of the high water mark. These samples were prepared for electron microscopy analysis and were analysed with a Scanning Electron Microscope (SEM) incorporating an EDS (Energy Dispersive Spectrometry) attachment. Each analysis consisted of two parts. Firstly, scanning electron microscopy was used to evaluate the condition of the deteriorating stone surfaces under very high magnification, and note the presence of any salt crystals or other matter which could contribute to stone decay. Secondly, EDS analysis was carried out simultaneously to determine the mineral composition of the stone surface – a process which should identify any salts of marine origin which may be present. Granite surfaces above the high water mark showed no observable anomalies and often commonly showed a relatively clean 'washed' surface. Salt were detected in samples from sub-tidal and inter-tidal areas, while salts of marine origin were present at low levels above the high water mark. Samples from submerged and inter-tidal zones were coated by marine organisms, and these may play a more significant factor in deterioration processes than salt crystallisation in these areas.

4.4. XRF Analysis

A portable XRF (Niton XL700) was used to examine the type(s) and amount of salt found *in situ* on 206 stone surfaces from 39 archaeological monuments and historic quarries. Sample locations comprised horizontal transects from sub-tidal through inter-tidal zones to

the high water mark, into the supra-tidal and then at increasing distance from the sea. Vertical transects of individual building walls comprising landward and seaward elevations allowed investigation of possible vertical zonation of salt deposition on a stone wall surface. Chloride (Cl), a key salt of marine origin, was detected on all stone surfaces (Tab. 3). However, the average salt level found on granite samples was less than half that of average The average salt levels on Irish granite monuments of 4744 ppm is a small fraction (4.9%) of the control sample of pure sea salt crystals. There was a common tendency for a slight salt peak to be found at the 1 metre level, regardless of orientation, and salt levels tended to be greater on the landward elevations of all monuments, regardless of vertical height. However, there was no corresponding greater tendency for stone deterioration at the 1 metre level. XRF analysis indicated relatively low levels of salts of marine origin on granite monuments from both coastal and inland unpolluted environments, with a decrease in salt levels detected on a horizontal transect from sub-tidal to inter-tidal and progressively away from the sea. This finding was consistent with the results of ion chromatography and electron microscopy. Salt levels also tended to decrease with an increase in building height, with a slight peak at the 1 metre level. The highest salt levels tended to occur in the inter-tidal and sub-tidal zones - a zone showing the greatest wetting and drying and the greatest amount of salt action and mobilisation. However, in this area the impact of the decay processes specific to the coastal edge (Bolton 2007) are likely to far out-weigh any impact salts of marine origin may have had on a stone surface.

Tab. 3: Cl levels on Irish granite surfaces.

Sample Averages	**Cl [ppm]**
Control – pure sea salt crystals	122,382.94
Average salt level found in Venice	10,357.41
Average salt level from Irish granite samples	4,743.84
Average salt level - Intertidal area	4,848.21
Average salt level - High Water Mark (HWM)	4,674.76
Average salt level - Ground level (1m from HWM)	3,665.04
Average salt level - 1m height	4,116.86
Average salt level - 2m height	3,942.13
Average salt level - 3m height	4,077.14

5. Discussion

Salts of marine origin are found on granite building stones in Ireland, with Na and Cl consistently found through electron microscopy, ion chromatography and XRF on the surface of granitic stone, and in areas showing granular disintegration and scaling. Salt deposition was highest in sub-tidal and inter-tidal areas, with salt levels gradually decreasing with increasing distance from the sea until reaching trace levels comparable to those found in groundwater deposits, but without a corresponding variation in the levels of stone decay observed. Why then do these stones not show the severe levels of stone decay which would be expected from previous studies from elsewhere in Europe?

A possible solution to this anomaly can be found by comparing the process of salt-related stone deterioration with Irish climatic conditions. The process of damage by salts of marine origin is well understood occurring as a three-stage process of deposition, accumulation on the stone surface, and penetration into the porous network of the stone where salts can crystallise and move. In the case of Irish granites, the accessible porous network is typically confined to the surface of the stone, and salt-related decay of granite results in scaling or granular disintegration of the stone surface and tends not to penetrate deeply within the stone. As Irish granite is susceptible to surface decay (Pavía and Bolton 2001), and salts of marine origin have been shown to be present, it is reasonable to suggest that a possible reason why salt-related weathering forms do not develop as expected from European studies, is an interruption or deviation in the process of deterioration.

Salts are depositing on Irish granite surfaces and were detected through a number of analytical methods, though decreasing both with building height and with increasing distance from the high water mark. Salts of marine origin appear to be depositing, but not accumulating on exposed granite stone surfaces, thus interrupting the process of salt-related decay, and resulting in a lack of severe salt-related stone decay forms on historic granite surfaces. The deposited salts are either not adhering well to the granite surface, or are being removed by wind, water or other means. However, the low porosity of granite also plays a role as accumulation and deposition within the stone is also reduced. Irish climatic conditions provide an environment with strong winds and more frequent precipitation events than would be experienced on the European mainland and the Mediterranean where the majority of previous studies have been undertaken. The most likely process which could be responsible for the ongoing removal of salts of marine origin is cyclical precipitation events in the form of natural rainfall.

An argument could be made that Irish granite surfaces are constantly being washed by rainfall, removing deposited soluble salts of marine origin before they can accumulate to damaging levels. Natural washing of rainfall would ‘clean’ the granite stone surfaces of soluble salt deposits, interrupting the deposition-accumulation-damage cycle common to historic stone surfaces in regions which do not experience the high levels of wind and rainfall characteristic of the Irish climate. In contrast, European historic stone surfaces typically experience a long, hot summer with infrequent precipitation events, but with significant fluctuations in relative humidity (*RH*). *RH* fluctuations allow salts contained within and on the surface of a building to penetrate the stone, crystallise, re-solubilise, and re-crystallise in an ongoing cycle which can effectively disintegrate a stone. The findings of the research reflect the difficulties in drawing on stone decay studies from other regions, and that even the most generally accepted findings cannot be drawn on blindly without due consideration and a critical understanding of the types of local stone, local stresses and local environmental parameters which underlie stone deterioration problems.

References

Alves, C. and Sequeira Braga, M.A.,1996, Salts Systems on Granitic Monuments (Braga - NW Portugal) in Degradation and Conservation of Granitic Rocks in Monuments, Vicente, M.A., Delgado-Rodrigues, J. and Acevado, J. (eds) Brussels. European Commission, 109-114.

Bolton, J., 2007, Submerged Ruins in Conservation of Ruins, Ashurst, J. (ed). Oxford, England. Elsevier, 212-234.

Chabas, A. and Jeannette, D., 2001, Weathering of Marbles and Granites in Marine Environment: Petrophysical Properties and Special Role of Atmospheric Salts in Environmental Geology 40 (3), January 2001. Springer-Verlag.

Charola, A.E., 2000, Salts in the Deterioration of Porous Materials: an Overview, Journal of the American Institute for Conservation, Volume 39, Number 3, Article 2, pp327-343.

Doehne, E., 2002, Salt Weathering: a Selective Review" in Natural Stone, Weathering Phenomena, Conservation Strategies and Case Studies, Siegesmund, S., Weiss, T. & Vollebrecht, A. (eds) Geological Society, London. Special Publications No. 205, 51-64.

Doehne, E. And Price, C.A., 2010, Stone conservation – an overview of current practice. The Getty Conservation Institute. Los Angeles, USA.

Kühnel, R., 2002, Driving forces of Rock degradation, in Protection and Conservation of the Cultural Heritage of the Mediterranean cities, Galán, E. and Zezza, F. (eds) Swets & Zeitlinger B.V. Lisse, The Netherlands, 11-17.

Pavía, S. and Bolton, J. 2001 Stone Monuments Decay Study 2000: an Assessment of the Degree of Erosion and Degradation of a Sample of Stone Monuments in the Republic of Ireland. The Heritage Council. Kilkenny, Ireland.

Rodriguez-Navarro, C. and Doehne, E., 1999, Salt Weathering: Influence of Evaporation Rate, Supersaturation and Crystallisation Pattern. Earth Surface Processes and Landforms, 24, 191-209.

Silva, B., Rivas, T. Prieto, B. and Delgado-Rodriguez, J., 1996, A Comparison of the Mechanisms of Plaque Formation and Sand Disintegration in Granite in Historical Buildings" in Degradation and Conservation of Granitic Rocks in Monuments, Vicente, M.A., Delgado-Rodrigues, J. and Acevado, J. (eds) Brussels. European Commission, 269-274.

Silva, B., Rivas, T. Prieto, B. and Pallares, O., 2002, A Methodological Approach to Evaluate the Decay of Granitic Monuments Affected by Marine Aerosol in Protection and Conservation of the Cultural Heritage of the Mediterranean cities, Galán, E. and Zezza, F. (eds) Swets & Zeitlinger B.V. Lisse, The Netherlands, 365-370.

Winkler, E.M., 1994, Stone in architecture, properties and durability. Springer-Verlag. Berlin, Germany.

Zezza, F.,1996, The EC Project Marine spray and Polluted Atmosphere as Factors of Damage to Monuments in the Mediterranean Coastal Environment: Objectives and Results, in Origin, Mechanisms and Effects of Salts on Degradation of Monuments in Marine and Continental Environments, Zezza, F. [ed] Bari. European Commission, 3-19.

Zezza, F., 2002, Inland Dispersion of Marine Spray and Its Effects on Monument Stone in Protection and Conservation of the Cultural Heritage of the Mediterranean cities, Galán, E. and Zezza, F. (eds) Swets & Zeitlinger B.V. Lisse, The Netherlands, 23-39.

DECAY OF MESOZOIC SALTRIO AND VIGGIÙ LIMESTONES: RELATIONSHIP BETWEEN MICRO-STRUCTURAL, COMPOSITIONAL AND ENVIRONMENTAL CHARACTERISTICS

G. Cavallo[1*], R. Bugini[2], D. Biondelli[2] and S. Franscella[3]

Abstract

Saltrio and Viggiù limestones were exploited in the Southern pre-Alpine region (Western Lombard Pre-Alps) along Italian and Swiss border. The use of Saltrio facies is documented since the Roman age whilst Viggiù since the 12th century. In the Insubric region - i.e. Northern Lombardy (Italy) and Southern Tessin (Switzerland) - the use reached the peak during 16th-18th century. for the execution of arches, portals, windows and sculptures. The two stones belong to the bottom of the formation called "Calcari Selciferi Lombardi" (Lombardic Siliceous limestones) of the Lower Jurassic. They are formed by calcarenites and conglomerates (about 10 m thick) linked to the Lower Jurassic marine transgression.

Saltrio stone is a bioclastic calcarenite with calcite cement and Viggiù stone is a (dolomitic) calcarenite with calcite cement; the allochemical are composed by fragmented ooids and fragments of limestones and dolostones.

Visual and microscopic analysis by means of optical (PLM) and electron (SEM/EDS) microscopy allowed the distinction of the two varieties and the causes of the deterioration to be recognized. The decay phenomena of Saltrio limestone are independent from the exposure of the architectural surface and are strongly influenced by the presence of micro-laminations which act as preferential planes for the action of aggressive aqueous solutions. Another issue is related to the chromatic alteration due to the presence of pyrite and its oxidation forming Fe-oxi-hydroxides. Decay of Viggiù limestone is due to inter-granular disintegration of the calcite cement and the formation of cavities; in addition, the removal of the cement causes the loss of the allochemical constituents (ooids). The constant presence of biological patina and deposits is the consequence of the higher porosity with respect to the Saltrio limestone and to textural characteristics.

Keywords: Saltrio stone, Viggiù stone, decay, exfoliation, granular disintegration

[1] G. Cavallo*
Institute of Materials and Constructions, University of Applied Sciences and Arts of Southern Switzerland, Deptartment of Earth and Environmental Sciences, University of Pavia, Italy
giovanni.cavallo@supsi.ch

[2] R. Bugini and D. Biondelli
Institute for the Conservation and Valorisation of Cultural Heritage, CNR, Unit of Milan, Italy

[3] S. Franscella
Museo della Pesca, Switzerland.

*corresponding author

1. Introduction

The use of Saltrio and Viggiù limestone is widespread in the Insubric region corresponding geographically to the actual Northern Lombardy (NW Italy) and Southern sector of the Tessin Canton (Southern Switzerland).

Both materials were used as block, ashlar or dressed stone; artefacts as column shaft (monolith or drums), capital, base, carved element, bas-relief, sculpture. The final dressing of the true surface of stone was almost always made using a plain chisel.

The begin of the exploitation is unknown, but the use of the stone is witnessed by some Roman stelae. Several monuments notice a widespread use in the 12th century; these buildings are close to the quarry area: church of *Santo Stefano* (Viggiù), church of *San Materno* (Clivio) and the cloister of *San Michele* (Voltorre). The stone of Viggiù, Brenno and Saltrio was described by Vincenzo Scamozzi (Scamozzi 1615) as better than Roman Travertine; the Author also reports the use of carriages to transport the dressed stone from the quarries to Milan and surroundings (about 50 km): this kind of transport was uncommon in Lombardy, a region where a vast network of artificial waterways eased the transportation of goods since the Middle-Ages. The use of stone involved dozen of quarries at the same time and now is almost always difficult to distinguish the proper quarry of each building. The stone was also employed according to the colour, as evident in the small cloister of *Santa Maria delle Grazie* (Milan, late 15th century): a grey shaft is put together with a brown capital and a brown base and vice versa. During the 16th century, the main achievements in Milan are the columns of the *Villa of Ferrante Gonzaga* (now called *Villa Simonetta*, 1547) and the columns of *Palazzo dei Giureconsulti* (1561). Other important achievements of 16th century were the façade with fine carved decorations of the cathedral of *San Lorenzo* (Lugano, early 16th century) (Fig. 1a), the façade of the church of *Certosa* (Pavia, first half 16th century), the colonnaded façade of *Santuario della Madonna dei Miracoli* (Saronno, late 16th century) (Fig. 1b). In the main hospital of Milano (called *Ca' Granda* or Big House, first half 17th century), the brown limestone was employed to make the carved capitals of the colonnaded portico and loggia in the great court, planned by Francesco Maria Ricchino. In the church of *San Paolo Converso* (Milan, 1613) the limestone was employed for the columns and for the ornamental elements together with granite and marble.

The use of Viggiù and Saltrio limestones was revitalized in Milan at the turn of the 18th century: the façades showed a stone frame (pilasters, cornices, entablatures, mouldings, windows) together with masonries coated with layers of plaster (*palazzo Reale*, *palazzo Litta*, *palazzo Mellerio*, *teatro alla Scala*). During the 19th century the use increased according to the broad expansion of private buildings, but the most important achievements in Milan are: veneering and ornamental elements on *Galleria Vittorio Emanuele II* (1865-78), veneering of the side buildings of *Arco della Pace* (1838), columns made of superimposed drums at *Porta Garibaldi* and, in other regions, the colonnaded chapel of the main cemetery of Staglieno (Genoa, 1840) or some elements of *Mole Antonelliana* (Turin, 1862-78).

When exposed to the external environments, Saltrio and Viggiù stones exhibit characteristic decay patterns. The former is prone to exfoliation, delamination, pelage and scaling whilst the latter to granular disintegration and biological colonization (Vergès-Belmin 2008).

In this work the microstructural and compositional characteristics will be highlighted and a relationship to the decay patterns discussed, focusing mainly on Saltrio stone as the main cause of deterioration of Viggiù stone was already discussed by Bugini and Folli (1998).

Fig. 1: Use of Saltrio stone. a) Carved decorations of the cathedral of San Lorenzo (Lugano, early 16th century) b) Colonnaded façade of Santuario della Madonna dei Miracoli (Saronno, late 16th century)

2. Experimental

2.1. Geological setting

Mesozoic sedimentary formations outcrop in the area of Val Ceresio north of Varese (Lombardy, Northern Italy) across the southern Swiss border, near Lugano lake (Tessin Canton). Marine sedimentation began in the Lower Triassic with a breccia, conglomerate and sandstone formation ("Servino") lying on the Permian volcanic rocks ("Granofiro"). Mesozoic formations contain limestone and dolomite: grey dolomites ("Dolomia del San Salvatore" formation, "Hauptdolomit") represent the Middle Triassic; light dolomites ("Dolomia principale" formation, Norian) followed by black limestones, marls, calcarenites and massive dolomites with ooids (Rhaetian), represent the Upper Triassic. The whole region emerged between Triassic and Jurassic causing erosion phenomena on Rhetian formations. The Jurassic period began with a marine transgression: grey and brown cherty limestones ("Calcari selciferi lombardi" formation, "Lombardischer Kieselkalk") represent the lower Jurassic (Sinemurian to Pliensbachian); this formation is followed by grey limestones ("Calcare a Cefalopodi" formation, "Cephalopodenkalke") and by thin-bedded red marly limestones ("Rosso Ammonitico Lombardo" formation) pertaining to middle Jurassic, massive white cherty limestones ("Majolica" formation) represent the Upper Jurassic - Lower Cretaceous and conclude the Mesozoic sedimentary series. The Val Ceresio area features an intense syngenetic tectonic with one swell (Lugano) and two basins (monte Nudo, westward; monte Generoso, eastward) evolving from Norian to Domerian.

The regional palaeogeographic setting of the Val Ceresio refers to the marginal area of the Lugano swell, close to the Lugano - Monte Grona fault scarp separating a higher foot-wall block from the hanging-wall block of the strongly subsiding Generoso basin: this area is marked by syn-sedimentary tectonic fragmentation along the eastern margin of the Lugano swell: this tectonic activity resulted in the formation of breccias, actively quarried in the past ("Macchiavecchia").

Calcari Selciferi Lombardi. The formation reaches a thickness of 250 metres in Val Ceresio; the thickness is 3000-4000 metres in the Monte Generoso basin and about 1500 metres in the Monte Nudo basin. The bottom of the formation features 10 metres thick detrital limestones containing ooids reworked from Rhaetian formations; the beds are about 1.0 metre thick together with very thin marly layers. Detrital limestones evidence the marine transgression in the early Jurassic; they are rapidly substituted by calcilutites featuring nodular cherts on irregular beds (thickness from few centimetres to 1.0 metre) with thin laminations. Ancient Authors classified dozen of fossils pertaining to different phyla: echinodermata (Crinoidea), brachiopoda (Articulata), mollusca (Bivalvia, Gastropoda, Cephalopoda): some molluscs as Aretites Bucklandi, Asteroceras obtusum (ammonites) and Gryphaea arcuata (bivalve) are typical of Sinemurian (Wiedenmayer 1963; Bernoulli 1964; Neuweiler and Bernoulli 2005).

2.2. Materials and Methods

Samples were collected both from the abandoned quarries and monuments and analysed using light (PLM) and electronic (SEM/ESD) microscopy. A Zeiss Axioskop 40 polarizing microscope was used and micrographs captured using a digital camera. A Jeol JSM-5910LV electron microscope was used operating at the following conditions: 20 kV, low vacuum mode LV (28Pa), working distance 9 mm. In addition, accurate photographic documentation of the studied buildings was carried out taking into account the exposure, the weather (rainy, sunny, cloudy, snowy) and the time of the day. This to understand if a correlation between inherent characteristics and external variables existed.

2.3. Petrographic features (PLM)

Different quarries were opened in this limestone formation and they are named according to the closest village (Viggiù, Saltrio, Brenno); the stone characteristics show some variations in each quarry.

Viggiù: Medium grained calcarenite, the colour ranges from brown to dark grey tending to pale grey when exposed to the atmosphere, grain size varies from 0.2 mm to 2.5 mm. Microscopic observations point out calcareous micritic intraclasts (size 0.2 - 2.5 mm) and dolomitic clasts containing broken ooids (size 0.2 - 0.9 mm) with concentric structure and micritic nuclei. A drusy calcite spar cement fills the pore space; irregularly shaped voids are also present. Classification: intraoosparite (Folk 1962), rudstone (Dunham 1962). Macroscopic observations allow for distinguishing between three different varieties: i) detrital (called Granitello); ii) grey (called Pietra grigia); iii) brown (called Rossetto).

Brenno: Coarse grained calcarenite, the colour varies from brown to grey, conchoidal fracture. Microscopic features, except for grain-size, are comparable to those described for Viggiù stone.

Saltrio: Bioclastic calcarenite, the colour ranges from brown to grey-black; the grain size ranges from 0.2 mm to 1.0 mm. Microscopic observations show the presence of intraclasts (predominant) and bioclasts (subordinate). Intraclasts are micritic, equant shape and rounded corners, bioclasts are Echinodermata, Mollusca and calcareous algae with regular cellular structure; ooids are scarce. The cement is calcite with sintaxial overgrowth; concentrations of opal are sometimes present. A thin lamination accompanied by glauconite, quartz and iron oxides is almost always present; irregular cracks follow the

laminations (Fig. 2a and Fig. 2b). Classification: intrabiosparite (Folk 1962), grainstone (Dunham 1962).

Macroscopic observations allow to distinguish four different varieties, from the bottom to the top of the formation: i) yellowish, thin laminations; ii) black (called *Piombino*); iii) brown, compact (called *Rossetto*); iv) grey, thin laminations (called *Grigio*). Above this variety the sedimentary deposition includes nodular cherts containing sub-spherical nodules.

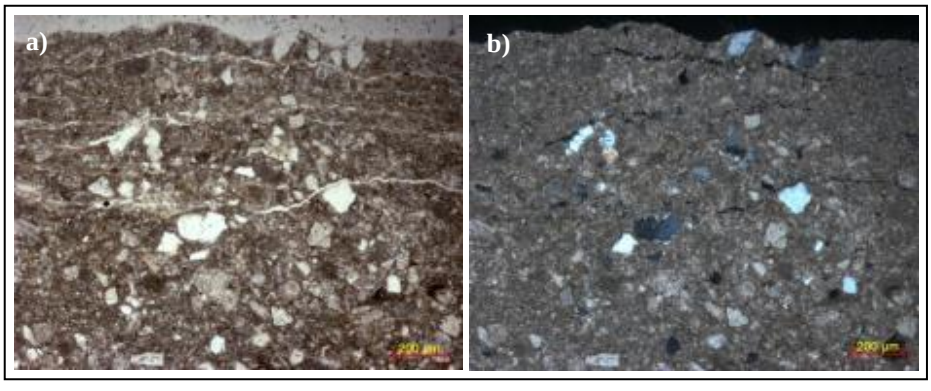

Fig. 2: Saltrio stone; a) micro-cracks following the original microlaminations (PPL); b) as in Fig. 2a but XPOL.

2.4. Micro-structural features of the Saltrio stone (SEM/ESD)

SEM/EDS analysis was carried out for understanding the morphology and composition of the material that fills the micro-laminations. The following characteristics were highlighted. Most of the samples corresponding to the black variety of the Saltrio stone exhibit black micro-laminations 5-20 µm width (medium width 10 µm) rich in C-based material. The inner side of each micro-lamination shows the loss of continuity of the calcite grains and intergranular solutions of continuity. In a few cases, the presence of cluster of pyrite was detected as well even if it is not directly correlated with the micro-laminations (Fig. 3a and 3b). In other cases, Si-based compounds containing Fe, Al, Mg and Na referable to clay minerals fill the micro-laminations. Finally, micas containing Si, Al, Mg, K, Ti where detected within the micro-cracks. They are euhedral and disposed along the micro-laminations, are altered along cleavage planes giving intra-crystal discontinuity (Fig. 4). We cannot exclude alteration into other clay minerals.

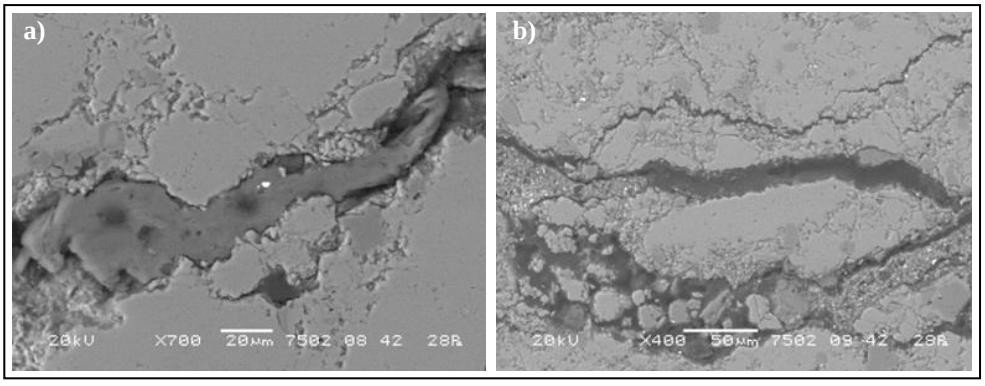

Fig. 3: BSE images of the Saltrio stone. a) micro-crack filled with C-based material. b) loss of continuity of calcite crystals.

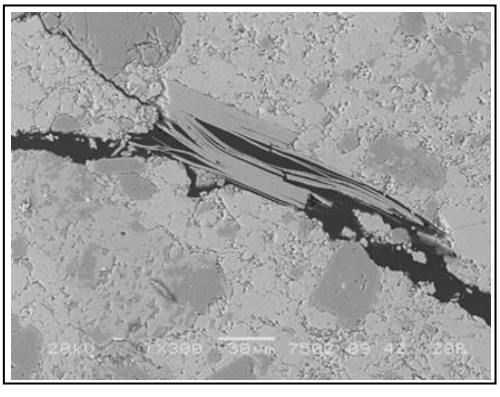

Fig. 4: BSE images of the Saltrio stone.
Altered mica along the cleavage plane (section ⊥ 001).

3. Discussion and conclusions

Accurate observations carried out on several monuments in Tessin Canton where Saltrio stone was used allowed to state that most of the decay phenomena can be ascribed to delamination, exfoliation, scaling and pelage using the terminology of Vergès-Belmin (2008). The development of these phenomena was not depending on the exposure; in addition, they were active both on elements having micro-laminations disposed horizontally and vertically. These surfaces are responsible of the detachment of small laminae whose thickness is in the range 0.1-0.3 cm. In other cases, fragments 0.6-2.0 cm thick detached from the stone causing partial or total loss of the decoration. Another important decay process affecting Saltrio stone is pelage observed both on monuments and in the quarry in areas where water can percolate. It was evident for those stones with micro-laminations disposed vertically.

All of the observed decay processes are strictly tied with the microstructural characteristic of the stone. The micro-laminations are surfaces generated by dissolution under pressure

and filled with C-based material, micas and clay minerals. In other cases, the infilling material is composed by Fe-oxy-hydroxides deriving from the alteration of pyrite. The decay processes are active along these preferential surfaces as water and aqueous solutions can easily have access determining the mechanical elimination of the infilling material. This is particularly evident whereas the geometric disposition of the stones facilitates the run off. In addition, we cannot exclude the possibility that water can be adsorbed by Fe-oxy-hydroxides and clay minerals and be responsible of volume change determined by thaw-freeze cycles as also reported elsewhere (Dreesen et al., 2006). BSE pictures show that calcite crystals close to the micro-laminations and micro-cracks have inter-crystal porosity due to chemical dissolution. Micro-cracks are an adequate environment for biological colonization; micro-organisms can release CO_2 during the cellular respiration and activate the chemical dissolution of carbonates (Urzì and De Leo, 2000).

The action of static load acting in the same direction of the micro-lamination planes is an additional argument to explain the deterioration along these surfaces. The exfoliation, scaling and pelage phenomena are strongly connected with the action of meteoric water and rising damp. Processes of salt crystallization can cause or help the development of detachments. The main decay patterns observed on Viggiù stone are the granular disintegration and the presence of biological patinas. The granular disintegration is active at the contact of the sparry calcite crystals of the cement resulting in the formation of macro-cavities (Fig. 5). The consequence is that the loss of contact between the cement, the intraclasts and the allochemical determine their separation. According to Lindqvist (2007) a positive correlation exists between the crystal size and the effects of the cyclic action of the water and of the thermal radiation. Finally, the major total porosity of the Viggiù stone (12%) respect to Saltrio one (3%) (Bugini and Folli 1998), combined with the roughness of the surface due to the working process, determines a major retention of water and the development of biological patinas.

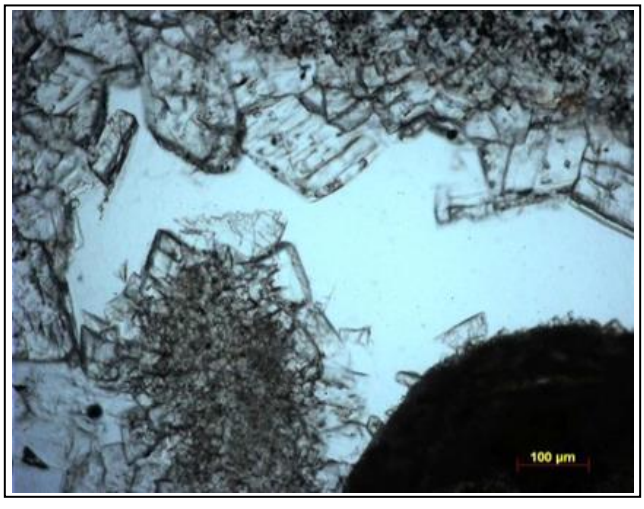

Fig. 5: Viggiù stone. Micrograph shows a cavity formed after granular disintegration of the calcite crystals of the cement (PPL).

References

Bernoulli D., 1964, Zur Geologie des Monte Generoso (Lombardische alpen), Beitrage Geologische Karte der Schweiz NF 118, 1-134.

Bugini, R., Folli L., 1998, I calcari di Viggiù e Saltrio, Recuperare l'edilizia - Arkos, Milano 22-27.

Dreesen, R., Nielsen, P., Lagrou D., 2006, Provenance, durability and damage analysis of natural building stones by means of petrographical techniques, in S. K. Kourkoulis (ed) Fracture and failure of natural building stones, Springer, , pp. 471-485.

Dunham, R., J., 1962, Classification of carbonate rocks according to depositional texture. In: Classification of carbonate rocks (W.E. Ham ed.), Mem. American Association Petroleum Geologists, 1, 108-121.

Folk, R, .L., 1962, Spectral subdivision of limestone types. In: Classification of carbonate rocks (W.E. Ham ed.), Mem. American Association Petroleum Geologists, 1, 62-84.

Lindqvist, J. E., Akesson, U., Malaga, K., 2007, Microstructure and functional properties of rock materials, Materials characterization, 58, 1183-88.

Neuweiler F., Bernoulli D., 2005, Mesozoic (Lower Jurassic) red stromatactis limestones from the Southern Alps (Arzo, Switzerland), Journal Earth Science, 94, 130-146.

Scamozzi, V., 1615, L'idea dell'architettura universale, Venice, Part 2, Book 7, Chap. 5.

Stoppani, A., 1857, Studi geologici e paleontologici sulla Lombardia, Milan.

Vergès-Belmin, V., 2008, Illustrated glossary on stone deterioration patterns. Champigny/Marne, France

Wiedenmayer F., 1963, Obere Trias bis mittlerer Lias zwischen Saltrio und Tremona (Lombardische Alpen), Eclogae Geologicae Helvetiae, 56, 2, 529-640.

Urzì, C., De Leo, F., 2000, Biodeterioration of Cultural Heritage in Italy: State of Art. Dept. of Microbiological, Genetic and Molecular Sciences.

ROLE OF HYDRO-MECHANICAL COUPLING IN THE DAMAGE PROCESS OF LIMESTONES USED IN HISTORICAL BUILDINGS

F. Cherblanc[1*], J. Berthonneau[2] and P. Bromblet[3]

Abstract

Historical monuments of the Provence region display different sensitivities to spalling decay. Even if some phenomenological scenario have been proposed, the physical processes that govern this kind of damage have not been clearly identified and quantified. The more reliable hypothesis involves the hydro-mechanical behaviour of such limestones triggered by naturally occurring expandable clay minerals (smectite). In order to sense the internal factors involved, a characterization campaign has been carried out. Clay mineral quantification was performed based on a recent methodology coupling transmission electron microscopy, X-ray spectrometry, X-ray diffraction. The relevant mechanical properties were characterised with a particular attention paid on their dependencies on the water content. Then, permeability, capillary pressure, vapour diffusion, sorption isotherm, and hydric dilation of these stones were measured. This set of experimental characteristics was introduced in a numerical model of a block inside a masonry structure to simulate water transport and mechanical behaviour. Simple climatic scenarios have been imposed to simulate alternating wetting and drying boundary conditions. Numerical simulations showed that the mechanical stresses generated by hydric dilation or shrinking are not large enough to lead to a direct damage. Nevertheless, in a case study, numerical simulations highlighted some tendencies in agreement with observations.

Keywords: limestone, spalling decay, clay minerals, hydro-mechanical behaviour, numerical simulation

1. Introduction

Roman and medieval historical monuments of the Provence region (South East of France) erected with limestones are affected by particular stone deterioration patterns called “spalling” and “splintering” (Vergès-Belmin 2008). Spalling corresponds to the progressive loss of plates from surfaces exposed to rain and/or runoff whatever their position in the building. The plane of detachment is located near the stone surface and develops perpendicularly to the bedding so that it cannot result from mechanical weaknesses linked to the anisotropy of these sedimentary stones (Berthonneau *et al.*, 2014, 2015). Splintering

[1] F. Cherblanc*
Laboratory of Mechanics and Civil Engineering, CNRS, University of Montpellier, France
fabien.cherblanc@umontpellier.fr

[2] J. Berthonneau
CNRS-MIT Joint Laboratory, Massachusetts Institute of Technology, Civil and Environmental Engineering Department, USA

[3] P. Bromblet
CICRP, Marseille, France

*corresponding author

corresponds to the detachment of sharp and slender pieces of stone broken off from the main body.

Even if several phenomenological scenario have been proposed, the physical processes that govern this kind of damage have not been clearly identified. One reliable hypothesis involves the hydro-mechanical behaviour of such limestones triggered by naturally occurring expandable clay minerals (smectite). Indeed, among clay minerals, the smectite group is very sensitive to water and is subject to a significant tendency to swell. Under cyclic conditions of wetting and drying, swelling and shrinkage phenomena can play a major role in the deterioration processes (Jiménez-González *et al.*, 2008; Ruedrich *et al.*, 2011; Berthonneau *et al.*, 2014). Numerous studies on stone conservation point out the swelling clay content to be a key factor in durability evaluation of sedimentary stones (Weiss *et al.*, 2004; Franzini *et al.*, 2007; Sebastián *et al.*, 2008; Berthonneau *et al.*, 2014).

While this description of stone damage seems to be well accepted, the relative roles of underlying physical phenomena need to be quantified. In particular, several studies refer to mechanical interpretation such as "differential stress" (Doehne and Price 2010) or "buckling of wetted surface" (Jiménez-González *et al.*, 2008; Wangler *et al.*, 2011) without being supported by unambiguous results. At this point, the objectives are to investigate this hypothetical process of degradation from a physical approach by proposing a numerical modelling. In the framework of this work, the focus has been put on two historical monuments: the Roman amphitheatre in Nîmes and the church St Maurice in Caromb.

2. Experimental characterization of limestone

Five different types of limestone are under investigation (ES: Estaillades, BM: Modern Barutel, BA: Antique Barutel, CY: Yellow Caromb, CG: Grey Caromb) all coming from the south region of France. While Barutel stone is a fine grained limestone of Barremian age (129 -125 Ma), Caromb and Estaillades stones belong to the "Pierre du Midi" type, a Burdigalian (20-16 Ma) deposit extensively used for building since antiquity. Materials (BA, CG, CY) were sampled on deposits of ancient stones coming from dismantling of old buildings (Nîmes amphitheatre, Caromb church) and BM, ES were taken from active quarries. Additional details can be found in Berthonneau *et al.* (2014, 2015), Cherblanc *et al.* (2016).

2.1. Clay content quantification

Mineralogical characterization was conducted by calcimetry (NF X 31-105) and X-ray diffraction (XRD) on total and acid (acetic acid 0.2 N) insoluble powders. Diffractograms were recorded on a Bruker D8 Focus diffractometer (CoKα radiation) equipped with a Lynx'Eye detector operating with an aperture of 1°2θ.

Clay mineral identification and quantification were done on the clay fraction (<4 μm) through the combination of transmission electron microscopy (TEM, JEOL JEM 2011) coupled with an energy-dispersive X-ray spectrometer (EDS, X-Flash Silicon Drift Detector 5030, Bruker) and profile modelling of XRD patterns of oriented preparations. Details on the elemental quantification and structural formula calculation from TEM microanalysis can be found in Berthonneau *et al.* (2014). XRD patterns were collected on oriented preparations saturated with calcium (Ca) at 0.01426°2θ step intervals from 2.5 to 60°2θ, using a 4 seconds counting time per step. A first set of XRD patterns was acquired after drying at room temperature (Ca + AD), then the same preparations were exposed to

ethylene glycol (Ca + EG) vapour for at least 24 hours and re-analysed. All the experimental XRD patterns were fitted over the 4.5 - 60°2θ CoKα range using the ASN program.

Eventually, the quality of the simulation was estimated using the unweighted goodness of fit parameter R_p. This parameter was calculated over the 5 - 60°2θ range, excluding the hkl reflections, and was used as an estimation of the error associated to the final quantitative values. The quality of the fits was mainly influenced by the low crystallinity of the phyllosilicates structures and the presence of strong hkl reflections of quartz. These mismatches explained the relatively high values of the goodness of the fit parameters (R_p), especially for the Barutel stones (BA, BM). In order to account for it within the proposed quantitative models, the evolution of the diffracted intensity of the 101 reflections of quartz was studied as a function of its weight fraction in a mixture with pure Na-Montmorillonite (Swy-2). The results showed a linear trend which slope was used to provide a precise estimation of the quartz content of the analysed clay fractions. These results varied from 0.21 (CY) to 6.02 wt.% (BA) with an error of about 5%.

The total contents of each clay mineral can be found in Cherblanc *et al.* (2016). ES is a pure calcite rock, while the clay content varied from 1.7% to 2.6% in Caromb stones. One can note the significant amount of quartz in the clay fraction of Barutel stones. Since the smectite group (Beidellite and Montmorillonite) presents the larger specific area, it will have the more significant impact on the sorption behaviour this work will focus on it.

2.2. Hygric/hydric properties

Water transport inside block occurs in both gaseous and liquid phases. Thus, the characterization of stone/water interactions includes the measurement of water permeability at saturation, vapour diffusivity, sorption isotherm curve, water retention curve.

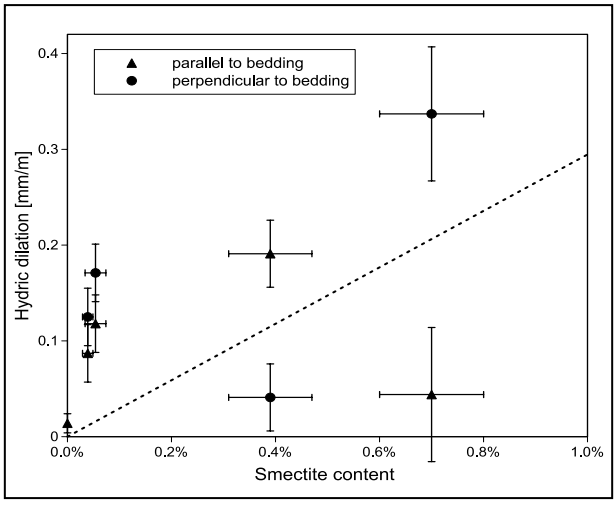

Fig. 1: Hydric dilation as a function of smectite content.

One major issue concerns the determination of hydric dilation coefficient. The principle relies on the measurement of the length variation during a capillary imbibition experiment. Since this property was only measured at saturation, it is supposed to depend linearly on the

water content. Regarding the 5 limestones under investigation, the hydric dilation measured at saturation is represented as a function of the smectite content in Fig. 1. Despite the weak correlation shown in this case, smectite content seems to be a key factor that governs swelling mechanisms.

2.3. Mechanical properties

Main mechanical characteristics of samples were identified experimentally, including Young's modulus, Poisson's ratio, tensile and compressive strength. Each property was measured on several samples prepared at imposed water content to cover the full range of hydric state from dryness to water saturation. While plotted for CY limestone in Fig. 2, further data can be found in Cherblanc *et al.* (2016).

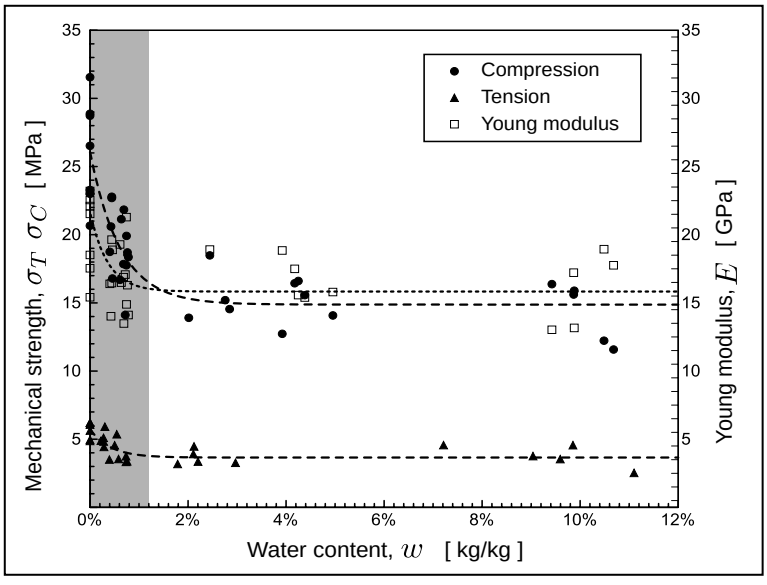

Fig. 2: Mechanical characteristics of CY limestone as functions of the water content.

As already evidenced, the mechanical properties of sedimentary rocks highly depend on the water content. It usually shows a strong decrease from dry condition to low water content and almost constant values for larger water content that can be described by a simple exponential representation based on 3 material parameters (Vásárhelyi and Ván 2006). It is worth noting that the range of water content where the decrease of mechanical strengths is observed (grey zone in Fig. 2) corresponds to the hygroscopic domain defined in sorption isotherm curves (Cherblanc *et al.*, 2016). It means that it is not necessary to undergo rain or flooding to observe the softening behaviour, a 97% *RH* atmosphere is sufficient to lead to a significant loss of mechanical properties.

3. Numerical modelling

The state variables chosen to describe the phenomena are the water content and the solid phase strains. To describe water transport inside stone block in both gaseous and liquid phases, local equilibrium is assumed at liquid/gas interface (Ouedraogo *et al.*, 2013). Modelling is based on classical diffusive equations involving capillary phenomena in liquid

phase and vapour diffusion in gas phase. Using the small perturbations framework, the mechanical behaviour is considered elastic relying on Young modulus and Poisson ratio. A linear swelling term is added to represent hydric dilation phenomena. This theoretical description is fully coupled through the hydric dilation term that describes the influence of water transport on stress, and by means of the dependence of stone mechanical properties on water content (Fig. 2).

Numerical modelling is developed using the open source software LMGC90. Based on finite elements method, it allows simulating multi-physics processes. For physical consistency purposes, 2nd order discretization is used for mechanical phenomena and 2nd order for water transport. Temporal integration is performed using a fully implicit scheme to get numerical stability. To handle with non-linearities, a Newton–Raphson method ensures an accurate convergence for a moderate time step. Since we focus on the external part of stone blocks, a finely discretized mesh is taken in the first 10 cm from the outer surface while a coarser mesh is imposed elsewhere.

Since one block is embedded in a masonry wall, rigid boundary conditions is imposed on 5 faces. The outer face is free and subjected to climatic conditions, wetting or drying. To represent the gravity load from above building, a vertical background stress of about σ_b = 1 MPa is imposed over the block. Finally, the damage level is analysed based on the failure criterion proposed by Hoek&Brown (Eberhardt 2012).

4. Case study

Two case studies have been carried out, the 1st one relates to the Roman amphitheatre of Nîmes (Gard, France) while the 2nd one deals with the church St Maurice of Caromb (Vaucluse, France). Only this last case is presented below.

4.1. The Caromb church

The church Saint Maurice of Caromb displays a good example of the different degrees of spalling. In particular, the grey Caromb limestone CG is much more sensitive to this type of decay mechanism than the yellow one CY, independently of any preferential cardinal orientation (Berthonneau *et al.*, 2014). While both materials are subjected to the same climatic conditions, some intrinsic stone properties should play a major role in the decay pattern. As proposed by Jiménez-González *et al.* (2008), hydric dilation can generate overstresses during wetting or drying processes. Thus, a simple climatic scenario is considered comprising 2 successive stages: first, a 2 hour wetting phase by imposing 95% of the water content at saturation over the outer face of the block, second, a 10 days drying phase by imposing a 20% *RH* atmosphere.

4.2. Evolution of water content

Regarding CG material, simulated water content profiles inside a block are plotted in Fig. 3 for different time steps. In the first phase of wetting ($0 < t < 7200$ s), a water content front penetrates perpendicularly to the outer surface. After 2 hours of rain, a few centimetres are saturated by water. Then, during the second phase of drying ($7200 < t < 100\,000$ s), the water content near the outer surface decreases quickly while a slow diffusion process takes place inside the block. At low water content and in particular in the hygroscopic domain (grey zone in Fig. 2), unsaturated permeability lowers drastically and vapour diffusion becomes the dominant transport mechanism. Therefore, the drying condition imposed on the surface takes several days to spread through the block. These alternating wetting and

drying phases maintain an average water content above the hygroscopic state. Indeed, in situ mechanical characteristics are closer to water saturated values rather than dry ones (Fig. 2).

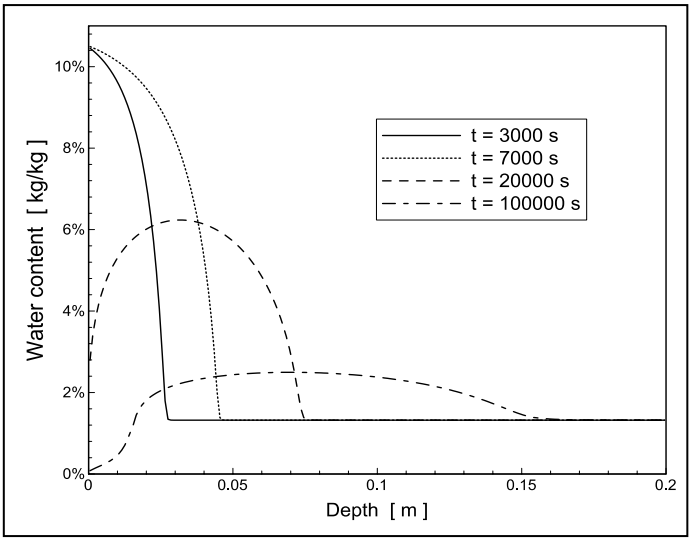

Fig. 3: Water content profiles inside CG block at different time steps.

4.3. Development of mechanical stresses

Based on the climatic scenario simulated above, the most critical situation is encountered during the wetting phase. Since the block under investigation is embedded in the masonry wall, vertical strains are prevented. Thus, the swelling driven by water imbibition generates mechanical stresses perpendicular to the outer face in the thin layer saturated by water. To account for the triaxial stress state, the evolution of Hoek & Brown failure criterion is represented in Fig. 4. The grey spread of these curves represent the variability in mechanical characteristics that can be observed in Fig. 2. Indeed, CG limestone is more heterogeneous and a larger scattering of measures was obtained with CG samples than with CY ones.

Obviously, swelling stresses are not large enough to lead to the direct rupture of blocks and the risk level does not exceed 50% in the worst case (Fig. 4). Thus, the spalling decay should rather be associated with a progressive phenomenon. The variations in climatic conditions generate hydro-mechanical cycles that would lead to a slow damaging process occurring over years. Anyway, the swelling stresses that develops parallel to the outer surface are compatible with the failure mode observed where crack planes are perpendicular to the bedding plane and parallel to the outer face. This case study evidences that CG material is more sensitive to spalling decay than CY in agreement with in situ observations (Berthonneau *et al.*, 2014).

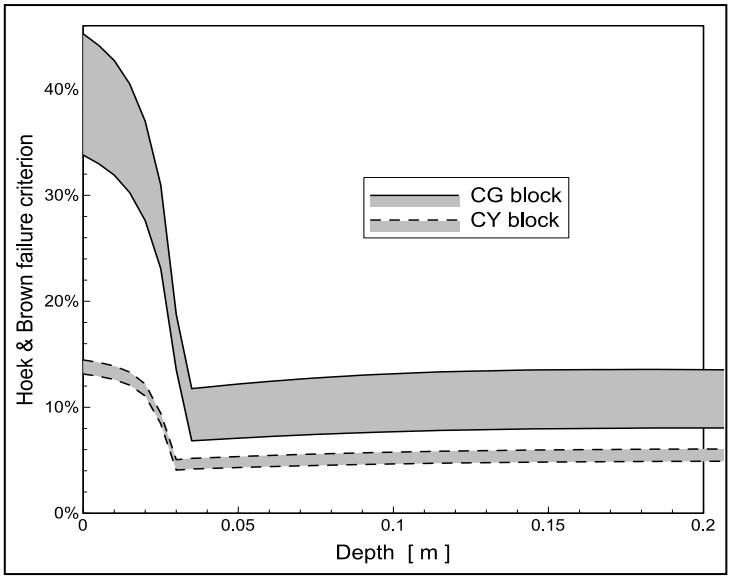

Fig. 4: Hoek & Brown failure criterion along the depth of stone blocks at t = 4000 s.

5. Conclusions

Numerical simulations showed that the mechanical stresses generated by hydric dilation or shrinking are not large enough to directly lead to damage. Obviously, the spalling decay phenomenon takes place over a very long time representing many wetting / drying cycles and should rather be associated with a progressive fatigue process. Furthermore, several factors can act simultaneously (freezing, salt crystallization) and hydro-mechanical effects would be a speed up process. Nevertheless, in a case study on Caromb church where two kinds of stone are used, numerical simulations highlighted some tendencies in agreement with observations. These results constitute an encouraging first step toward a predictive approach for stone replacement campaign aimed at limiting the impact of spalling of historical building facades.

Acknowledgements

This work was done within the framework of a collaboration between the CICRP and the LMGC supported by the French Ministry of Culture and Communication through the PNRCC program (Programme National de Recherche sur la Connaissance et la Conservation du patrimoine culturel matériel).

References

Berthonneau, J., Grauby, O., Ferrage, E., Vallet, J.-M., Bromblet, P., Dessandier, D., Chaudanson, D. and Baronnet, A., 2014, Impact of swelling clays on the spalling decay of building limestones: Insights from X-ray diffraction profile modelling, European Journal of Mineralogy, 26, 643 – 656.

Berthonneau, J,. Bromblet, P., Cherblanc, F., Ferrage, E., Vallet, J.-M. and Grauby, O., 2015, The spalling decay of building bioclastic limestones of Provence (south east of France): from clay minerals swelling to hydric dilation, Journal of Cultural Heritage, In Press.

Cherblanc, F., Berthonneau, J,. Bromblet, P. and Huon, V., 2016, Influence of water content on the mechanical behaviour of limestone: Role of the clay minerals content, Rock Mechanics and Rock Engineering, In Press.

Doehne, E.F. and Price, C.A., 2010, Stone Conservation : An Overview of Current Research (2nd ed.), Getty Publications , Los Angeles, ISBN 978-1-60606-046-9, 175pp.

Eberhardt, E., 2012, The Hoek–Brown Failure Criterion, Rock Mechanics and Rock Engineering, 45, 981 – 988.

Franzini, M., Leoni, L., Lezzerini, M. and Cardelli, R., 2007, Relationships between mineralogical composition, water absorption and hydric dilatation in the macigno sandstones from lunigiana (Massa, Tuscany), European Journal of Mineralogy, 19, 113 – 123.

Jiménez-González, I., Rodríguez-Navarro, C. and Scherer, G.W., 2008, Role of clay minerals in the physicomechanical deterioration of sandstone, Journal of Geophysical Research, 113, F02021.

Ouedraogo, F., Cherblanc, F., Naon, B. and Bénet, J.-C., 2013, Water transfer in soil at low water content. Is the local equilibrium assumption still appropriate?, Journal of Hydrology, 492, 117 – 124.

Ruedrich, J., Bartelsen, T., Dohrmann, R. and Siegesmund, S., 2011, Moisture expansion as a deterioration factor for sandstone used in buildings. Environmental Earth Science, 63, 1545 – 1564.

Sebastián, E., Cultrone, G., Benavente, D., Fernandez, L.L., Elert, K. and Rodríguez-Navarro, C., 2008, Swelling damage in clay-rich sandstone used in the church of san mateo in tarifa (Spain), Journal of Cultural Heritage, 9, 66 – 76.

Vásárhelyi, B. and Ván, P., 2006, Influence of water content on the strength of rock. Engineering Geology, 84, 70 – 74.

Vergès-Belmin, V., 2008, Illustrated glossary on stone deterioration patterns. ICOMOS, International Scientific Committee for Monuments and Sites (www.icomos.org).

Wangler, T.P., Stratulat, A., Duffus, P., Prévost, J.H. and Scherer, G.W., 2011, Flaw propagation and buckling in clay-bearing sandstones, Environmental Earth Science, 63, 1565 – 1572.

Weiss, T., Siegesmund, S., Kirchner, D. and Sippel, J., 2004, Insolation weathering and hygric dilatation: two competitive factors in stone degradation. Environmental Geology, 46, 402 – 413.

THE CONTRIBUTION OF TRADITIONAL TECHNIQUES TO NEW TECHNOLOGY TO EVALUATE THE POTENTIAL RISK OF STONE DETERIORATION BY MICROORGANISMS

E. Sirt-Ciplak[1*], A. Cetin-Gozen[2] and E.N. Caner-Saltık[1]

Abstract

Stones used in cultural objects are affected from weathering actions resulting in different types of deterioration in the long run. Biodeterioration is one of them which is usually observed following an initial state of deterioration of the stone. There are few investigations based on a joint interpretation of data that are obtained from various quantification methods of microorganisms present on stone material, to conduct diagnostic and monitoring studies. Hence, there is a necessity for developing new techniques in the light of traditional ones. In this study stones of Nemrut Mount Monument (Adiyaman, Turkey), and Temple of Augustus (Ankara, Turkey) were selected as cases to develop different types of methods as FDA hydrolysis; total microflora; MPN, and ATP bioluminescence for the determination of microbial activity on stones of the monuments. The results showed that the stones of Temple of Augustus had higher microbial activity than the stones of Nemrut Mount Monuments. Furthermore, sandstone and limestone of Nemrut Mount Monuments revealed that only stones having visible biological layers i.e. lichens gave values closer to intermediate level. Considerable quantity of FDA hydrolyses has revealed the importance of alga population, however, bacterial and fungal activity was low in the stones of the two studied historical sites. Although they have different measuring units, applicability and accuracy of methodologies of these techniques for evaluation of biodeterioration in historic stones were scientifically proved when results are compared and interpreted together.

Keywords: microbial activity, microorganisms, quantification techniques, biodeterioration, historic stones

1. Introduction

Different biodeterioration types eventuate in materials by the activity of microorganisms (Caneva *et al.*, 1991). Solar radiation, humidity and temperature are the environmental factors that affect habitation, growing and expansion of these microorganisms on rock surfaces (Gorbushina, 2007). Therefore there is a need for a practical method to determine the level of microbial activity and to assess if this microbial activity is a potential risk to the integrity of stone. This paper describes how to develop a standardized procedure of high precision for counting microorganisms growing on stones of historical monuments and at

[1] E. Sirt-Ciplak* and E.N. Caner-Saltık
Faculty of Architecture, Middle East Technical University, Ankara, Turkey
elif.sirt@metu.edu.tr

[2] A. Cetin-Gozen
Department of Biological Sciences, Middle East Technical University, Ankara, Turkey

*corresponding authors

the same time initiates a database establishment for interpretation of FDA measurement unit (μg fluorescein/g of stone) in the light of traditional techniques.

2. Material and methods

2.1. Description of studied sites

Two sites were selected as case studies namely, Nemrut Mount Monument (NMM), located in the town of Kahta, Adiyaman (Sahin-Guchan, 2011) and Temple of Augustus (TA), which is also known as "Momentum Ancyranum", located next to the Hacı Bayram Mosque in Ulus which was the centre of Ankara in older times (Caner-Saltık, 2005).

2.2. Sampling

Biodeteriorated sandstone and limestone (having visible, slightly visible coverings, the samples were also taken from stones that might have microbiofilm coverings although it is not evident by naked eye) were sampled from NMM. Biodeteriorated marble and andesite were sampled from TA. Samples were collected aseptically by using disposable gloves and 70% alcohol washed equipment from field. Samples were crushed to a fine powder in a sterile agate mortar and then stored in sterile caps at +5°C until the day of the experiment.

2.3. Qualitative analyses of soluble salts by spot tests

Spot tests were done for the salt detection on stones of monuments since water-soluble salts as nitrites, nitrates and sulphates may be present as a result of the activity of some microorganisms such as nitrosomonas, nitrobacter and thiobacillus. For detection of sulphate ions (SO_4^{2}) few drops of test solution were put in a tube. Then 1-2 drops dilute hydrochloric acid solution (HCl 2N) and 1-2 drops of barium chloride solution (BaCl2 10%) were added, respectively. Finally, white precipitate as an indicator of sulphate ions were investigated in those samples. In the case of nitrite ion (NO_2^{-}) determination, few drops of test solution were put on a spot plate and 1 drop of sulfanilic acid solution and α naphthylamine solution were added, respectively. If nitrite ions are present, solution turns to pink. Lastly, for determination the presence of nitrate ions (NO_3^{-}), few drops of test solution were put on a spot plate as first stage. Then one drop of acetic acid solution (2N), sulfanilic acid, α naphthylamine solution and a few mg of zinc dust were added in turn. If nitrate ions are present, *solution turns to pink.* Then, MPN (Most Probable Number) method was conducted for the samples with the positive results in order to understand if the origin of the existed salt formations is microbial.

2.4. Determination of biological activity

2.4.1. FDA (Fluorescein Diacetate) Hydrolysis Method

Fluorescence that is formed as a result of hydrolysis of FDA, is measured by spectrophotometers. Since there is a direct correlation between the enzymatic activity and the amount of fluorescence formed, it is possible to determine the biological activity of samples taken on site by the measurement of fluorescence formed. Being adapted from the studies of Gillian and Harry (2001), this method was conducted on powdered limestone and sandstone of NMM and marble and andesite of TA in order to determine the total microbial activity of bacteria, fungi, and algae. Samples prepared for FDA analyses were placed in glass flasks to which 15 ml of phosphate buffer (pH 7.5) was added. Then, FDA stock solution was added to initiate the reaction. The samples were shaken thoroughly and placed in an oven at 30°C for 30 minutes. After that, the powdered samples were centrifuged at

4000 rpm for 3 minutes. The supernatant was filtered with Whatman No 40 filter paper and the filtrate was measured at 490 nm in a spectrophotometer (Optima SP-3000 Plus UV/VIS spectrophotometer).

2.4.2. TMF (Total Microflora) Method

In this method, 1 g of powdered stone sample were placed in glass tubes and diluted from 10^{-1} to 10^{-6} using sterile distilled water. Nutrient agar medium, czapek dox agar medium, and malt extract agar medium were prepared and poured into plates for the growth and counting bacterial and fungal species accordingly. Inoculations to these plates from each dilution were conducted until the bacteria reached optimum concentration for counting accurately. Nutrient agar medium and czapek dox agar medium were incubated at 30°C for 1 week and malt extract agar medium was incubated at 24°C for 4 days. After incubation period, petri dishes having colonies between 30 and 300 were counted and the colony-forming unit (CFU) in 1 g of the original sample was calculated.

2.4.3. Measurement of the Global Microbial Activity with ATP (Adenosine 5'-triphosphate)

ATP is a compound existing in all living cells as a viability marker; its determination in stones gives an idea about the global microbial activity. ATP is tracked specifically by reaction with a Luciferin/Luciferase mixture in a buffered solution. The quantification of ATP is based on the measurement of the light emitted during the ATP's reaction with the enzymes. In this method, the amount of light emitted was measured in which the values are between 0-99,999 as RLU (Relative Light Unit) (Lundin *et al*, 1986). Surface samples were taken with cotton swabs from selected areas of historical monument by making small movements parallel to each other. The contaminated cotton swabs were submerged into the buffer solution of the kit, of which the cap of the bottom part was removed afterwards. The long-thin-pen like part was pushed through the solution containing luciferin/luciferase enzyme. Finally, the pen was put inside the device and measured immediately.

2.4.4. MPN (Most Probable Number Method) and Biochemical tests

2.4.4.1. Nitrification

The activity of nitrous and nitric ferments was investigated separately in two different types of medium. For the determination of nitrous ferments, a nitrogen source, ammonium sulphate was added and after the incubation period diphenylamine included sulphuric acid solutionwas used as well for the detection of nitrites and nitrates. The investigation of produced nitrates was conducted using the same reactive, after the elimination of nitrites, and by using sodium nitrite in the medium as nitrogen source.

Same soil suspension-dilutions as the ones prepared in the total micro flora method (section 2.4.2) were used for the inoculation of media in an amount of 0.5 ml for each tube of the dilution series ranging from 10^{-1} to 10^{-6} as triplicates and then placed in an incubator at 28°C for 20 days. After 3 week of incubation period, for nitrous fermenters; the presence of nitrite and nitrate formations were investigated by adding 10 drops of diphenylamine ($C_{12}H_{11}N$) sulphuric acid solution and the reactive to each tube. The presence of nitrites and nitrates were determined by observing blue colour formations. Dilutions showing blue colour formations were counted as positive result. For nitric fermenters; the existence of nitrate formations were identified after approximately 50 mg urea addition to each tube just after incubation period to deplete nitrite formations. Then 10 drops of sulphuric acid and diphenylamine reactive were added in turn. The tubes that have blue color formations due

to nitrate presence were counted as positive result. The positive tube results in each dilution of nitrous and nitric series were counted and then the number of bacteria/g of powdered stone were calculated by using Mc Grady table (Sutton, 2010).

2.4.4.2. The oxidation of sulphur

The same soil suspension-dilutions prepared in the total micro flora method (part 2.4.2) were used for the inoculation of media in an amount of 1 ml for each tube from the dilution series ranging from 10^{-1} to 10^{-4} as triplicates and 50 mg sublimed sulphur was added aseptically. Then all these tubes were placed in an incubator at 28°C for 21 days. After 3 week of incubation period, 1 or 2 ml of sample were taken from the top brilliant part of the solution without shaking and transferred to empty tube and this process was applied to all tubes. Following this step, 2 drops of hydrochloric acid (HCl^-) solution and 5 drops of aqueous barium chloride solution were added in turn. The presence of sulfates was determined by observing white precipitate formations. Dilutions showing white precipitates were counted as positive result then the number of sulphur oxidising bacteria per gram of powdered stone was calculated by Mc Grady table. After that, positive tube results were counted and then the number of sulphur oxidizing bacteria per gram of powdered stone was calculated by using Mc Grady table (Sutton, 2010).

3. Results and discussion

3.1. Spectrophotometric measurements

Spectrophotometric measurements are performed systematically on stones characterised by different surface textures, mineral components, and microbial activity levels at different times of the year, more specific in June (2010), October (2010) and May (2011). Stones of the NMM, having slightly visible biological coverings, showed enzymatic activity values in the range of 4.34-9.32 μg fluorescein/g of stone, whereas the ones having visible biological coverings, resulted in values in the range of 11.35-50.02. The lowest biological activity was measured on samples showing visible no biological coverings on theirsurface as 2.52 μg fluorescein/g of stone. High values obtained on lichened zones of stones were considered as normal (Swisher and Carroll, 1980) because lichens show considerable enzymatic activity owing to their symbiotic partners as alga and fungus (Deborah and Sharon, 1987). The highest biological activity was obtained on an east oriented interior wall built in andesite stone and lowest one on a west interior of a marble wall, both related to the TA, respectively 23.25 and 1.19 μg fluorescein/g of stone . East exterior of marble wall having black discoloration on its surface showed 7.24 μg fluorescein/g of stone. Obtaining high values of fluorescein on andesite and marble having discolorations could be related with algae existence on the surfaces of those stones. A variety of studies has used fluorescein diacetate to measure microbial activity in soils (Gillian and Harry, 2001; Schnürer and Rosswall, 1982) and stone surfaces (Prieto *et al.*, 2004). Moreover, fungal activity in fungal batch cultures (Ingham and Klein, 1982) and algal activity in lichens (Deborah and Sharon, 1987) were determined by the fluorescence formed as a result of enzymatic conversion of FDA to fluorescein, measured by means of a spectrophotometer or an optical microscope. When the results of FDA analysis are compared with the soil fluorescein concentrations found in aforementioned studies, an evaluation can be done according to studies of Gillian and Harry (2001), revealing that most stones of NMM and TA had a high biological activity. However when this comparison is done according to the studies of Diack and Stott (2001), both above-mentioned monuments had low biological activity. This brings the fact

that the results of FDA analyses should be evaluated according to variable environmental conditions because soil ecology has a rich biological population, unlike stone; even some microorganisms have the ability to grow both on stone and soil. As a traditional technique TMF helped us to interpret the spectrophotometric measurement data when stone is the subject of the study. Hence it can be concluded that "samplingsfrom stones of both NMM and TA, having non biological coverings, showed low fluorescein concentrations" based on microbial count of the sample in TMF method while lichen species growing on stones seem to be majorly responsible for the biodeterioration in NMM.

3.2. TMF method

The method of total microflora has been widely used for counting the aerobic heterotrophic bacteria and fungi since 1933 (Eckhardt, 1988; Gorbushina *et al.*, 2002; May and Lewis, 1988; Paine *et al.*, 1933; Wilimzig and Bock, 1992; Wilimzig *et al.*, 1992). The method proposed in this study was adapted from the study of Jaton (1972). According to the studies of Jaton (1972), a cell number of 10^6 CFU/g of stone is considered as normal microflora for bacteria living on stones. Also in the studies of Wilimzig *et al.*, (1992), a cell number of 10^3 CFU/g of stone is low for bacteria and fungi to play a role in the decay process of stones. Bacterial counts ranged between 10^2 and 10^6 CFU/g in June 2010, was 10^4 CFU/g in October 2010 and 10^4 to 10^6 CFU/g in May 2011 in limestone and sandstone of NMM. Besides, the number of fungi counted on Czapeks dox (June and October, 2010) and Malt Extract Agar (May 2011) was slightly similarin the range of 10^2-10^3 CFU/g. On the other hand, marble and andesite of TA in May2011 showed colony counts in the range of 10^3-10^7 CFU/g for bacteria and 10^3-10^5 CFU/g for fungi. When all obtained results of total microflora are compared with the colony counts as detected in the studies of Caneva *et al.*, (1991), Wilimzig *et al.*, (1992) and Jaton (1972), various interpretations could be done. To begin with, according to the study of Jaton (1972), the stones of NMM showed low bacterial and low fungal activity which could be underestimated in terms of normal microflora on stones. However, when the microbial activity of stone surfaces is interpreted in relation to the seasons, the highest bacterial activity is obtained in summer and spring in comparison to autumn. According to Caneva *et al.*, (1991), the level of bacterial activity analysed in the stones of TA, were closer to the limit of risk in terms of their contribution to stone decay processes than that analysed on those of NMM. Nevertheless, based on the study of Wilimzig *et al.*(1992), considering the mean value of the colony counts, the activity of fungi and bacteria, being slightly higher than 10^3 CFU/g, was considered at an intermediate level. Concerning the relationship of biological coverings (lichens) on stones and microbial activity, there was no significant correlation between them. Eventually, the method of total microflora showed that stones of NMM and TA had low bacterial and fungal activity most probably due to harsh weather conditions, where the wind speed reaches to 220 km/h, severe temperature differences is existed between day and night during summer and the stones are under the snow during winter. Considering biodeterioration in the case of NMM, lichens on the surface of limestone and sandstone play a great part in the decay process either by physical or chemical actions. In addition, according to the recent researches, the main factor causing and/or accelerating decay processes of these stones are wet-dry cycles and thermal fluctuations (Akoğlu and Caner-Saltık, 2015; Topal *et al.*, 2015).

3.3. ATP analyses

The ATP bioluminescence method has been used commonly in the field of hygiene monitoring to assess the degree of microbial contamination (Kašková *et al.*, 2007; Sigler *et al.*, 2003; Vilar *et al.*, 2008). In recent years, this technique has been used to measure the global metabolic activity with Adenosine Triphosphate (ATP) of historical stone surfaces (Orial *et al.*, 2009). This method was adapted from the studies of Orial *et al.* (2009) in order to detect the global microbial activity degree of stones of NMM and TA. In this study "2-3000 RLU" (Relative Light Unit) was considered as very low for microbial activity to provoke stone decay. When results obtained on stones having visible, slightly visible and invisible biological covering are compared with those presented in (Sigler *et al.*, 2003; Kaskova *et al.*, 2007; Vilar *et al.*, 2008 and Orial *et al.*, 2009), very low values in the range of 4-25 RLU/cm^2 are obtained. Although the the method m has advantages in terms of being practical and giving results in a short time, sampling method and protocol were not efficient to measure the global microbial activity of stones belonging to NMM and TA depending on low porosity (NMM and low moisture content of the stone surfaces of two studied historical sites.

3.4. MPN and biochemical tests

Together with biochemical tests, the MPN method has been widely used in the past both to asses microbial biomass of soils (Belser and Mays, 1982; Molina and Rovira, 1964; Papen and Von Berg, 1998) and to understand if the microbial activity is responsible for salt deposit on stones (Gorbushina *et al.*, 2002; Leite-Magalhaes and Sequeira-Braga, 2000; Reiner and Eberhard, 1998; Wilimzig and Bock, 1992; Wilimzig *et al.*, 1992) Protocols of nitrification and sulphur oxidation were adapted from the studies of Pochon and Tardieux (1962) where the quantity of microbial cells was obtained by the MPN method as microorganism per gram of stone. According to the studies of Leite-Magalhaes and Sequeira-Braga (2000), 1×10^3 cells nitrifying and sulphur oxidizing bacteria/g of stone was considered low. At the same time, based on the studies of Gorbushina *et al.*, (2002), the amount of bacterial activity on several monuments, in the range of 1-10^4 cells/g of stone, confirms a low microbial activity. On the other hand, as stated in the report of Wilimzig *et al.*, (1991), the average cell number of nitrite oxidizing bacteria was 1×10^5cells/g of stone, out of which bacteria related stone decay was suggested.

In the present study, in July 2011, stone samples of TA were tested in order to understand if the salt deposit was originating from the activities of bacteria. Concerning sulphur oxidizing bacteria, an average of 1×10^2 cells/g of stone was obtained. Regarding nitrifying bacteria, nitric ferments were counted as 1×10^2cells/g of stone, and nitrous ferments as 10^2-10^3 cells/g of stone. When all obtained results were compared with the cell numbers detected in the studies of Leite-Magalhaes and Sequeira Braga (2000), Gorbushina *et al.*, (2001) and Wilimzig *et al.*, (1991), stone samples of TA showed a low autotrophic bacteria activity on their surfaces. Existence of ammonia and nitrite oxidizers in low cell numbers could be related with the reverse reaction between these bacteria and ammonia (Leite-Magalhaes and Sequeira-Braga, 2000) Even sulphur oxidizing bacteria existed in low cell numbers in stones of TA, the results of qualitative soluble salt test detected the presence of sulfate, precisely. This case could be explained by potential salt sources such as anthropogenic air pollution (Reiner and Eberhard, 1998), rain water, underground waters (Leite-Magalhaes and Sequeira-Braga, 2000), and pigeon's fecal matter (Caner *et al.*, 1988)

4. Conclusions

In this study, historic marble, andesite, sandstone and limestone, exposed to atmospheric conditions, were analysed by means of different techniques such as FDA hydrolysis, TMF and MPN Method in order to show the level of biological activity based on different types of microorganisms. From the results of TMF method and FDA hydrolysis, no biodeterioration due to aerobic heterotrophic bacteria and fungi on the stone surfaces of two studied historical sites is concluded. On the other hand, considerable fluorescein levels detected by FDA hydrolyses and the presence of biominerals as calcium oxalates determined by (Üstünkaya, 2008) indicated the importance of algal activity in biodeterioration of those stones. Hence the presence of algae and its critical concentrations at the surface layers and cracks of stone has to be studied by measurable parameters, e.g. amount of Chlorophyll a / g of stone. Moreover, conducting experiments regarding organic acid production would be useful for detecting the existence of bacteria and fungi having the ability to solubilize minerals. During field survey in TA, samples were only lifted at the surface of marble and andesite. However, according to the findings of Reiner and Eberhard, (1998), nitrifying bacteria commonly colonize in deeper layers of stones. Therefore, in future studies, sampling from deeper decay zones should be made in order to prevent underestimations of bacterial colonization. Consequently, even the MPN method underestimates the cell numbers of nitrifying bacteria, (Belser and Mays, 1982), it seems to be appropriate in terms of determining the cell numbers of ammonia, nitrite and sulphur oxidising bacteria. In other words, liquid media enables bacteria to grow efficiently in the absence of heterotrophs (Berg, 1986). This study has shown that microbial activity of stones could be measured practically through enzymatic activity of microorganisms habiting in and/on stones. Hence, further studies are needed to use FDA analysis as a practical method for the measurement of microbial activity levels that are further integrated in a database, including TMF and MPN data, in order to minimise the risk of errors and increase reliability of the method.

Acknowledgements

I would like to express my deepest gratitude to Eng. Orial for always guiding me through critical discussions, and giving opportunity to work in her laboratory and also I would like to thank to François for his valuable assistance in this laboratory. Lastly, I wish to express my sincere thanks to Dr. Akoğlu for her continued advice, and constant encouragement.

References

Akoğlu, K.G., and Caner-Saltık, E.N. (2015). Hydric dilation of Mount Nemrut sandstones and its control by surfactants. J. Cult. Herit. 16, 276–283.

Belser, L.W., and Mays, E.L. (1982). Use of nitrifier activity measurements to estimate the efficiency of viable nitrifier counts in soils and sediments. Appl. Environ. Microbiol. 43, 945–948.

Berg, P. (1986). Nitrifier populations and nitrification rates in agricultural soil.Rapport-Sveriges lantbruksuniversitet, Institutionen for mikrobiologi.

Caner, E.N., Göktürk, E.H., Türkmenoğlu, A.G., and Eseller, G. (1988). Effects of Air Pollution on the Monuments in Ankara-Case Study: Temple of Augustus. Durab. Build. Mater. 463–473.

Caner-Saltık, E.N. (2005). TÜBİTAK Research Project İçtag-1684/PIA Progress Report "Development of new methods bu using biomineralisation and nanoparticle technologies in the preservation and conservation of historic marbles."

Caneva, G., Salvadori, O., and Nugari, M.P. (1991). Biology in the conservation of works of art (Rome : ICCROM, 1991).

Deborah, B., and Sharon, E. (1987). Flow Cytometric Measurement of Pollutant Stresses on Algal Cells.

Diack, M., and Stott, D., E. (2001). Development of a soil quality index for the Chalmers Silty Clay Loam from the Midwest USA: International Soil Conservation Organization Meeting held (10) Purdue University–USDA-ARS National Soil Erosion Research Laboratory. pp. 550-555.

Eckhardt, F.E.W. (1988). Influence of culture media employed in studying microbial weathering of building stones and monuments by heterotrophic bacteria and fungi. pp. 71–81.

Gillian, A., and Harry, D. (2001). Development of a sensitive and rapid method for the measurement of total microbial activity using fluorescein diacetate (FDA) in a range of soils.

Gorbushina, A.A. (2007). Life on the rocks: Life on the rocks. Environ. Microbiol. 9, 1613–1631.

Gorbushina, A.A., Lyalikova, N.N., Vlasov, D.Y., and Khizhnyak, T.V. (2002). Microbial communities on the monuments of Moscow and St. Petersburg: biodiversity and trophic relations. Microbiology 71, 350–356.

Ingham, E.R., and Klein, D.A. (1982). Relationship between fluorescein diacetate-stained hyphae and oxygen utilization, glucose utilization, and biomass of submerged fungal batch cultures. Appl. Environ. Microbiol. 44, 363–370.

Jaton, C. (1972). Aspects microbiologiques des alterations des pierres de monuments. 1er Coll.Int. sur la deterioration des pierres en oeuvre. La Rochelle. 149-154.

Kašková, A., Ondrašovičová, O., Vargová, M., Ondrašovič, M., and Venglovskỳ, J. (2007). Application of Peracetic Acid and Quarternary Ammonium Disinfectants as a Part of Sanitary Treatment in a Poultry House and Poultry Processing Plant. Zoonoses Public Health 54, 125–130.

Leite-Magalhaes, S., and Sequeira-Braga, M.A. (2000). Biological colonization features on a granite monument from Braga (NW, Portugal). pp. 521–529.

Lundin, A., Hasenson, M., Persson, J., and Pousette, A. (1986). Estimation of biomass in growing cell lines by adenosine triphosphate assay.

May, E., and Lewis, F.J. (1988). Strategies and techniques for the study of bacterial populations on decaying stonework. pp. 60–70.

Molina, J.A., and Rovira, A.D. (1964). The influence of plant roots on autotrophic nitrifying bacteria. Can J Microbiol 249–257.

Orial, G., Bousta, F., and Francois, A. (2009). Lascaux cave : monitoring of microbiological activities.

Paine, S.G., Lingood, F.V., Schimmer, F., and Thrupp, T.C. (1933). The relation of micro-organisms to the decay of building stones. Phil Trans Roy Soc 97–127.

Papen, H., and Von Berg, R. (1998). A most probable number method (MPN) for the estimation of cell numbers of heterotrophic nitrifying bacteria in soil. Plant Soil 199, 123–130.

Pochon, J., Tardieux, P. (1962). Techniques d'analyse en microbiologie du sol. service de microbiologie du sol de I'Institut Pasteur, p. 59-62, 83-84.

Prieto, B., Silva, B., and Lantes, O. (2004). Biofilm quantification on stone surfaces: comparison of various methods. Sci. Total Environ. 333, 1–7.

Reiner, M., and Eberhard, B. (1998). Biodeterioration of natural stone with special reference to nitrifying bacteria. 47–64.

Sahin-Guchan, N. (2011). The Commagene Nemrut Conservation and Development Program. An Approach to the Conservation Problem of Nemrut DaĞ Tumulus.

Schnürer, J., and Rosswall, T. (1982). Fluorescein diacetate hydrolysis as a measure of total microbial activity in soil and litter. Appl. Environ. Microbiol. 43, 1256–1261.

Sigler, K., Gášková, D., Chládková, K., Knebl, R., Wimmer, T., Vacata, V., and Gebel, J. (2003). Standardized system for quantifying residual dirt on medical appliances cleansed in hospital washers-disinfectors: Dirt detection by different methods. Folia Microbiol. (Praha) 48, 95–102.

Sutton, S. (2010). The most probable number method and its use in QC microbiology. J. GXP Compliance 14, 28.

Swisher, R., and Carroll, G. (1980). Fluorescein diacetate hydrolysis as an estimator of microbial biomass on coniferous needle surfaces.

Topal, T., Deniz, B.E., and Güçhan, N.Ş. (2015). Decay of Limestone Statues at Mount Nemrut (Adiyaman, Turkey). Int. J. Archit. Herit. 9, 244–264.

Vilar, M.J., Rodríguez-Otero, J.L., Diéguez, F.J., Sanjuán, M.L., and Yus, E. (2008). Application of ATP bioluminescence for evaluation of surface cleanliness of milking equipment. Int. J. Food Microbiol. 125, 357–361.

Wilimzig, M., and Bock, E. (1992). Microbial investigation of selected marble sample from the Gustav II Adolph statue in Goteborg. -. pp. 123–124.

Wilimzig, M., Jozsa, P., Lin, L., Sand, W., and Bock, E. (1992). The determination of microbes on the surface of marble figures on the old cemetery in Munich. pp. 63–72.

This page has been left intentionally blank.

POROSIMETRIC CHANGES AND CONSEQUENCES FOR DAMAGE PHENOMENA INDUCED BY ORGANIC AND INORGANIC CONSOLIDATION TREATMENTS ON HIGHLY POROUS LIMESTONE

P. Croveri[1*], L. Dei[2], J. Cassar[3] and O. Chiantore[4]

Abstract

Surface consolidation treatments on stone materials induce relevant modifications in the porous substrates that can potentially trigger deterioration phenomena not active in the same untreated materials. Unlike most protective products that form films on stone surfaces, consolidants must penetrate the first layers of the substrate in order to function, partially filling the voids of the porous network. Meso- and macro-porosities of Globigerina Limestone (Malta's highly porous sedimentary stone), before and after treatments with several organic and inorganic consolidants were investigated by means of N_2-BET (Brunauer–Emmett–Teller) analysis. BET total inner superficial area together with pore size distribution data gave interesting information on preferential distribution of different products inside the open porosity network. The treatment can produce in some cases small changes in total superficial area (inorganic treatment), in some others cases a dramatic reduction (organic) and also an unexpected relevant increase (ethylsilicate). Pore size distribution shows shifts towards lower pore diameters turning a predominantly macro-porous system into a meso-porous one. These porosimetric changes have a direct relationship with the physical properties of porous building materials. In relation to the environmental context and the direct exposure to deterioration agents, the consolidation treatment can also have a negative impact for the conservation of works of art.

Keywords: BET, calcareous stone, consolidation treatment, porous materials, Malta Globigerina limestone

1. Introduction

Deterioration mechanisms on natural porous stones were widely investigated during the last decades, the main decay processes usually sought in chemical weathering, mechanical

[1] P. Croveri*
Chemistry Department, University of Turin, Via P. Giuria 7, Torino, Italy, Centro Conservazione e Restauro "La Venaria Reale", Via XX Settembre 18, Venaria Reale Italy
paola.croveri@unito.it

[2] L. Dei
Chemistry Department, University of Florence, Sesto Fiorentino, Italy

[3] J. Cassar
Department of Conservation and Built Heritage, Faculty for the Built Environment, University of Malta, Msida, MSD 2080, Malta

[4] O. Chiantore Chemistry Department, University of Turin, Via P. Giuria 7, Torino, Italy

*corresponding author

degradation and biodeterioration caused by extrinsic agents like air pollutants, soluble salts, fungal growth (Winkler, 2013). In order to slow down deterioration, to restore the original physical, chemical and mechanical properties of damaged materials and to combat the action of aggressive agents several methods of conservation interventions were developed. A part of them makes use of chemical products that, applied to buildings surfaces, act as a barrier to external deterioration causes with the aim of strengthening the intrinsic defences of historical works of art. From a general point of view it is possible to assert that the application of protective and consolidating products has an impact mainly on *surface* physical properties as colour, hydrophobicity, cohesion but the highly porous materials are deeply affected not only on their "external interface" but also on their "*internal interface",* in other words in their porosity structure. And also if the protective products should exert their action only on the external surfaces, while consolidant must enter inside the materials by definition, literature data supports, without any doubt, evidence of substantial penetration of conservation materials inside highly porous substrates (Doehne E. and Cliffort C.A., 2010). Despite the limited thickness of the impregnated layer compared to the bulk, a very small quantity of product can induce dramatic changes in physical properties of the entire artefact, like water uptake and vapour water permeability, and consequently in its durability (Ferreira Pinto A.P. and Delgado Rodrigues J., 2008).

Several studies and investigations have focussed on the evaluation of macroscopic physical property changes as a result of stone conservation treatments (colour, water absorbance and water vapour permeability, hardness etc.). These laboratory tests on stone samples or on experimental in situ-tests on building materials were often performed according to international standard methods (EN, ISO, UNI, UNI-NORMAL, ASTM, RILEM) with different non-invasive or quite simple procedures. Changes in macroscopic properties are strongly linked to changes in the microscopic structure of materials, nevertheless very few authors elaborate on changes induced by treatments in the microscopic properties of substrates by direct investigation of porosity. In fact, the analysis of porosity by optical methods (areal porosity determined on polished sections of samples), by mercury injection or gas expansion methods are invasive techniques and require a minimum quantity of material often of the order of some grams, not always easily sampled on artefacts.

The aim of the present research was the investigation of changes induced by organic and inorganic consolidant products after their application on a highly porous natural stone, the Globigerina Limestone, widely used as building material in the Maltese Islands. Modifications in the porosity network was investigated and some considerations on the correlations between these data and water sorption properties were discussed, being aware that a difficult goal is the interpretation and prediction of macroscopic properties of porous media with the help of microscopic pore structure models.

2. Materials and methods

2.1. Globigerina limestone

Samples of stone of *Globigerina Limestone* (Glob1, acquired as *Franka* type according macroscopic evaluation but discovered to be, after specific chemical characterization, a *Soll* type (Cassar J., Vella A. 2010)) were cut from a local quarry in Malta (n°44, near Mqabba) and previously characterised by SEM/EDS (cross-sections analysis with a LEO 1430, Oxford Link spectrometer with an ATW2 window for the detection of light elements) and calcimetric analysis (Dietrich-Frühling method) (Croveri *et al.* 2004). Glob1 is characterised by a $CaCO_3$

content of 91% (σ = 0.5). EDS microanalysis results are shown in Tab. 1 (5 areas, mean values expressed as percentage of oxides, standard deviation in brackets)

Tab. 1: EDS microanalysis of Glob1 substrates.

	CaO	**SiO_2**	**Al_2O_3**	**MgO**	**FeO**
Glob 1	91.0 (1.5)	4.8 (0.6)	1.9 (0.3)	0.9 (0.1)	1.7 (0.4)

2.2. Consolidant products and treatment methodologies

Samples (5×5×2 cm, 5×5×1 cm) were first conditioned following the UNI 10921 standard and then treated on one surface only. Inorganic treatments were carried out with aqueous saturated solutions of $Ba(OH)_2 \cdot 8H_2O$ and $(COONH_4)_2 \cdot H_2O$ (AmOx) in cellulose poultice (Arbocel BC1000) with a contact time of 5 and 6 hours, respectively. A 2-propanol dispersion [0.06 M] of nanosized calcium hydroxide particles (Salvadori B. and Dei L., 2001) was applied by brush (350 ml/m^2). An ethyl silicate (Estel 1000, CTS, 500g/m^2, SiEt), an acryl-silicon based polymer (Acrisil 201/O.N. 0,5 l/m^2, CTS, Acrisil), a fluoelastomer (Akeogard CO, 50g/m^2, Syremont S.p.A., AkCO), a perfluoropolyurethanic pre-polymer (Akeogard Z1074 –Edilgard® Wall, 50g/m^2, Syremont S.p.A., Ak74) and a functionalised fluorinated polyurethane (Akeogard PU, 50g/m^2, Syremont S.p.A., AkPU) were applied by brush.

2.3. Porosimetric analysis

Analyses of superficial areas and pore-size distributions were carried out with a surface analyzer Coulter SA3100 according to the BET model and BJH calculation using N_2 gas. The material analyzed was sampled from the treated surface taking the first 0,5 cm thickness. About 3-5 g of stone material was used for each analysis, replicated twice for each treatment. In order to compare the results of pore size distribution, the experimental data were normalized using the following equation:

$$V\%_N = V\% * (BJH\ tot_{TR} * W_{TR}) / (BJH\ tot_{NT} * W_{NT}) \qquad (Eq.\ 1)$$

where BJH_{tot}: Total volume of pores (mm^3/g)
W: weight of the sample (g)
TR: treated sample
NT: not treated sample

3. Results and discussion

3.1. Porosimetric analysis

The physical properties of natural stones such as total effective porosity, surface area, pore size, pore geometry and pore size distribution influence the weathering phenomena and related effects. The open interconnected pore network gives a measure of the "receptivity" of a lithotype with respect to external aggressive agents but the pore size and geometry, the surface area and the pore size distribution are the really significant parameters that drive the deterioration processes due to change of state phenomena. For this reason, the mere total effective porosity of a stone and its mean pore size are only indicative but not sufficient to understand the sorption, transport, permeability, capillarity, crystallization and diffusion

processes occurring inside porous building materials that are strictly linked to the other above-mentioned parameters. The classification of porous systems following pore size and related water phenomena are reported on Fig. 1, together with pore size detection ranges covered by analytical techniques (Fitzner, B., 1994).

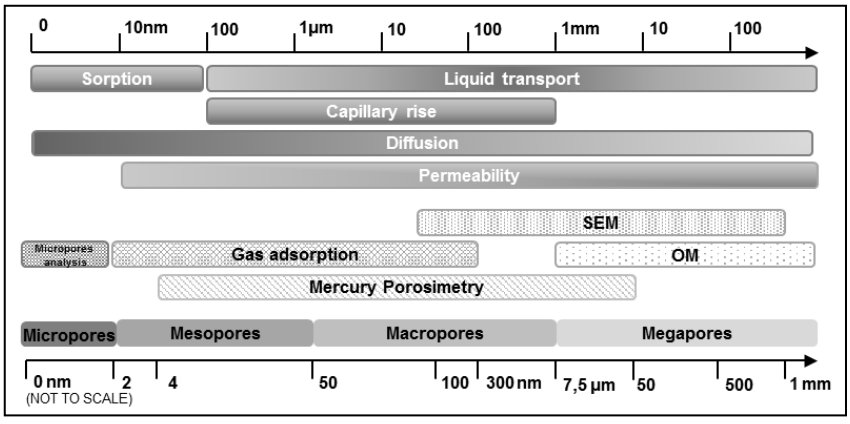

Fig. 1: Pore classification, detection analytical ranges and related water phenomena.

For this research the N_2-BET (Branauer, Emmett and Teller) technique was used in order to investigate aspects related to total surface area and pore size distribution, with a focus on much fine mesopores, a range not completely covered by mercury porosimetry, in which physical sorption phenomena play a relevant role. Untreated Globigerina samples exhibit a surface area of 6.2 m^2/g and type II isotherm-like, typical of macroporous systems, but with a weak hysteresis loop characteristic of type IV isotherm, associated with capillary condensation taking place in mesopores. The hysteresis loop is Type H3 indicating the presence of cylindrical pores or agglomerates of uniform spherical particles. Moreover, the extrapolation to a positive intercept on the adsorption axis of V_a/t plot (not reported here) indicates the presence of a microporous volume (Sing K.S.W. *et al.*, 1985). Inorganic treatments induce a reduction of about 2 m^2/g in the internal surface area (Tab. 2) and no significant modification in the hysteresis curves (Fig. 2). Organic treatments (with acrylic and fluorinated products) induce more dramatic changes in the internal surface area with a decrease down to around 2 m^2/g (AkPU down only to 3.2 m^2/g) showing a relevant occlusion of the total open porosity. The surface area after the application of ethyl silicate shows a sharp rise (up to 8.5 m^2/g, about +40%) indicating the creation, by the consolidant, of a secondary porosity inside the cavities of the stone (Fig. 3). Moreover the isotherm form changes to a clear Type IV, with Type I hysteresis loop, indicating the transformation of the stone matrix into a prevalently mesoporous system. The transformation of the hysteresis loop from Type H3 to Type H1 could suggest a modification in the shape of interconnected porous network due to the deposition of the alkoxysilane gel. Mineralogy can influence the deposition mechanism by promoting acid or basic hydrolysis, the alkaline nature of the stone substrate should give rise to a soft gels film filling intergranular spaces (Wheeler, G. 2005).

Pore size distribution of treated samples in comparison with untreated ones are reported in Figures 4 and 5. $Ba(OH)_2$ and AmOx treatments cause a slight increase in all pore classes above 6 nm, a larger one in pores greater than 20 nm, suggesting a homogeneous deposition

of consolidant agglomerates reducing part of macropores into mesopores or macropores with a smaller diameter. $Ca(OH)_2$ consolidation treatment induces a small reduction in all the pore size distribution that could be explained by a better penetration capacity and deposition of nanoparticles inside the mesoporosity of stone porous network. Porosimetric distribution is completely modified by the application of SiEt on Globigerina showing a monomodal distribution with a maximum centred on the 10-12 nm pore diameter and a relevant reduction of pores between 20 nm and 80 nm. This modification can be explained by secondary porosity creation. A shift of the porosimetric distribution towards lower pore diameters was already noticed on bricks treated with SiEt: a monomodal distribution centred at 0,4<r<0,5 µm was shifted to a new one centred at 0,1<∅<0,2 µm (Croveri P. and Appolonia L., 2002). Acrisil, Ak74 and AkCO treatments lead to similar pore distribution changes, with a decrease in all pore classes below 80 nm and a slight increase above, while for AkPU there is an evident increase of pores bigger than 20 nm, resulting from of a deposition of the product in larger macropores.

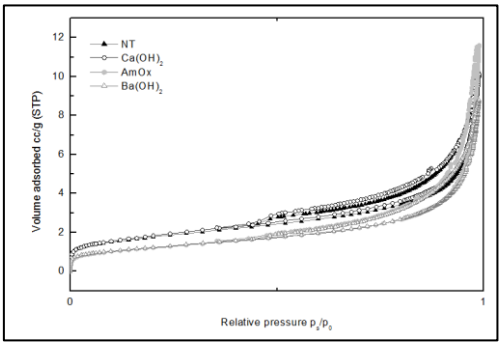

Fig. 2: Nitrogen adsorption/desorption isotherms for Globigerina Limestone.

Tab. 2: BET surface area results (σ=0.1 estimated error 1.2%) expressed in m^2/g.

	NT	**$Ca(OH)_2$**	**$Ba(OH)_2$**	**AmOx**	**SiEt**	**Acrisil**	**Ak74**	**AkCO**	**AkPU**
BET	6.2	4.2	4.4	4.3	8.5	1.9	1.7	2.1	3.2

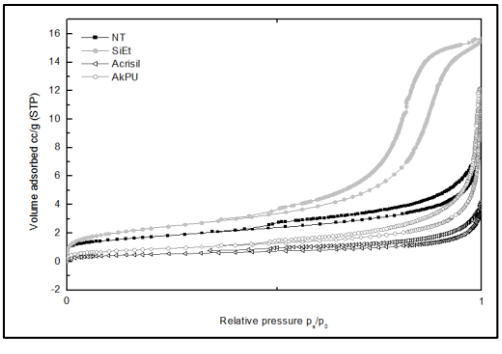

Fig. 3: Nitrogen adsorption/desorption isotherms for Globigerina Limestone.

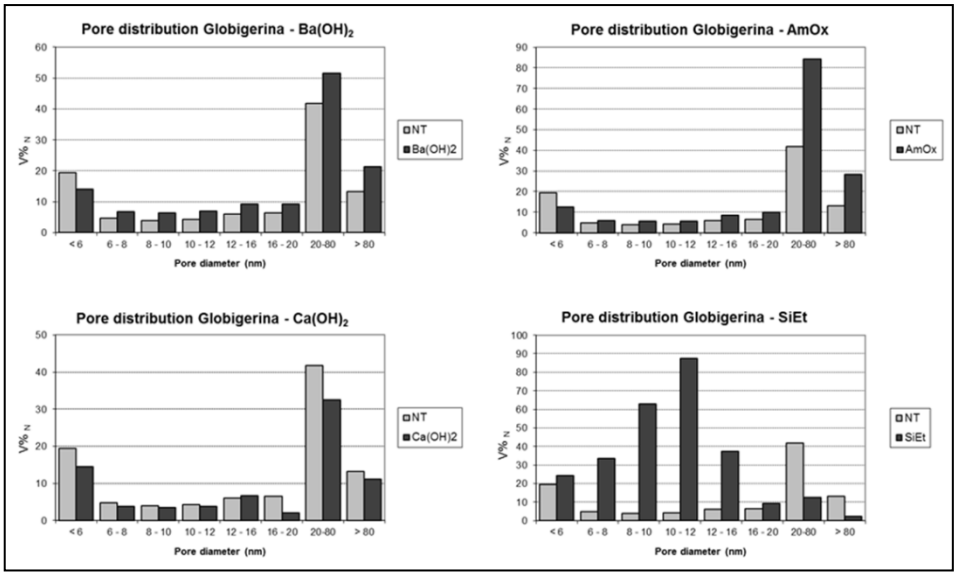

Fig. 4: Pore distribution in inorganic, SiEt treated and untreated samples of Globigerina Limestone.

3.2. Impact on deterioration phenomena

Changes in mesopores and small macropores (the range under investigation) potentially affect all water transport phenomena (Fig. 1). A decrease in the surface area of Globigerina Limestone can develop in parallel a dramatic change in capillarity water absorption, as in the case of organic treatments, where however the chemistry of products also plays a relevant role in the change of surface tension properties, or has slight effects as in the case of inorganic conservation treatments (Croveri *et al.* 2004). SiEt treatment impacts deserve a specific discussion since in this case the stone matrix changed from a prevalent macroporous system (∅>50nm) to a prevalent mesoporous system (2<∅<50 nm). This substantial modification of the pore network could activate, under equal environmental conditions, deterioration processes not active in the same material, when not treated. For example, a stone that does not suffer frost damage could be transformed into a freeze-thawing susceptible material. In the Maltese Islands this latter phenomenon is irrelevant, since temperatures under 0°C are generally not registered, but considering the peculiarity of the local environment it is significant to take into account aspects related to water vapour condensation and salt crystallization (Franzen and Mirwald, 2009). After treatment of Globigerina Limestone with SiEt we are moving from a system where capillary condensation occurs in most of the pores (mainly 20<∅<200 nm) only when *RH*%≥90%, to a system where capillarity condensation takes place in most of pores (predominance of pores between 8 and 12 nm) at *RH*%≥70% (Collepardi and Coppola, 1996). When environmental conditions exceed 70% *RH*, quite often in the Islands, the impact of treatment by SiEt is that of remarkably enhancing the quantity of water inside the porous network, potentially inducing internal stresses due to hydration - dehydration of the stone that lead to shrinking - swelling of clay components.

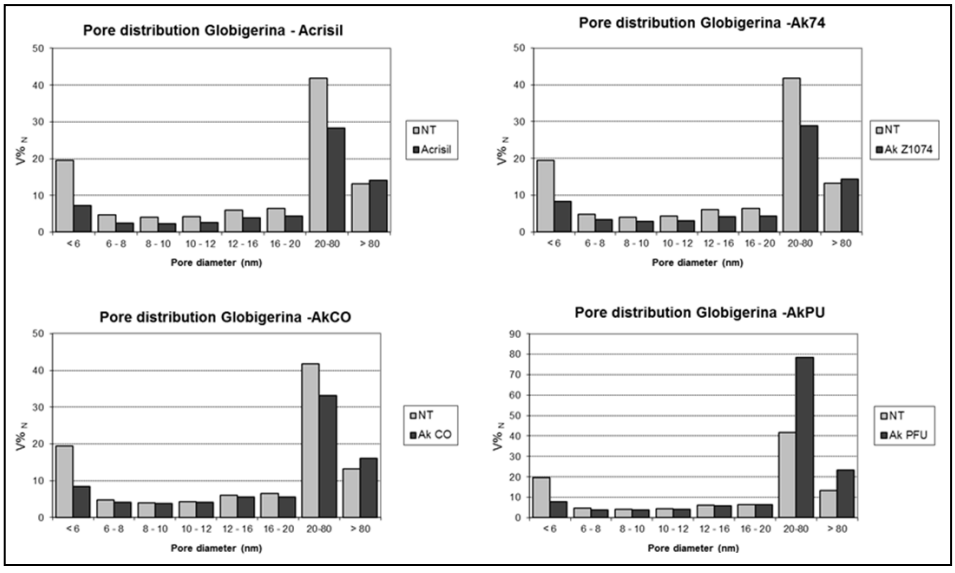

Fig. 5: Pore distribution in organic treated and untreated samples of Globigerina Limestone.

Water retention is associated not only with a physical factor (pore size reduction) but also with a chemical one, being the SiEt an hygroscopic material able to adsorb and retain significant water as a function of environmental thermodynamic equilibria. Moreover, in the marine environment, condensation phenomena can involve marine aerosol, inducing the transport of soluble salts inside the porosity of building materials. The enhancement of total surface area could be a negative aspect since the system offer a more extensive exchange interface to external aggressive agents (e.g. pollutant gases). The role of pore size distribution is significant also in the damage caused by salt crystallization, materials with small pores suffer from higher crystallization pressure than materials with larger pores and mineral precipitation takes place deeper beneath the stone's surface, forming subflorescences (Benavente D. *et al.*, 2004). A shift of the stone network distribution towards smaller pore diameters leads to an increase in stone decay and less resistance against salt crystallization.

4. Conclusions

The main aim of conservation interventions is to change some properties of the original materials to make them more resistant towards external aggressive agents and less susceptible to decay, slowing down deterioration processes. The application of consolidant and protective products on the one part can have positive impacts on the durability of porous stone, strengthening the substrate, limiting water related phenomena (liquid transport and permeability) and mitigating the effects of physical pressure (salt crystallization, frost), but can induce modifications in the porous structure that potentially move in the opposite direction. The modification of the internal surface area and the pore size distribution of highly porous materials are relevant parameters to be investigated in order to be able to give a meaningful assessment of the effectiveness of the intervention and

to foresee and prevent any potentially dangerous effects generated by the conservation treatment itself.

References

Benavente D *et al.*, 2004, Role of pore structure in salt crystallisation in unsaturated porous stone, Journal of Crystal Growth, 260, 532–544

Cassar J., Vella A., 2003, Methodology to identify badly weathering limestone using geochemistry: case study on the Lower Globigerina Limestone of the Maltese Island, Quarterly Journal of Engineering Geology and Hydrogeology, 36, 85-96

Collepardi M , Coppola, L., 1996 Materiali negli edifici storici: degrado e restauro, Enco ed.

Croveri P., Appolonia L., 2002, Il silicato di etile a confronto con consolidanti fluorurati: distribuzione all'interno di substrati porosi e cinetiche di reazione in Proceedings of International Congress "The silicates in conservative treatments, test improvements and evaluation of consolidating performance", Torino 13-15/2/2002, Associazione Villa dell'Arte onlus ed., 83-92

Croveri *et al.*, 2004, Consolidation of Globigerina Limestone (Malta) by means of inorganic treatments: preliminary results, Proceedings of the 10th International Congress on Deterioration and Conservation of Stone, Kwiatkowski & Löfvendahl eds, Stockholm, vol.1, 463-470

Doehne E., Cliffort C.A., 2010, Stone Conservation: An overview of Current Research, 2nd Ed. J.P. Getty Trust

Ferreira Pinto, A.P, Delgado Rodrigues, J., 2008, Stone consolidation: The role of treatment procedures Journal of Cultural Heritage, 9, 38-53

Fitzner B., 1994, Porosity properties and weathering behaviour of natural stones – methodologies and examples, Proceedings of the C.U.M. 2nd Course "Stone materials in monuments: diagnosis and conservation", Crete (Greece)

Franzen C. and Mirwald P.W., 2009, Moisture sorption behaviour of salt mixtures in porous stone, Chemie der Erde, 69, 91-98

Salvadori B., Dei L., 2001, Synthesis of $Ca(OH)_2$ nanoparticles from diols, Langmuir, 17, 2371-2374

Sing K.S.W. *et al.*, 1985, Reporting physisorption data for gas/solid systems with special reference to the determination of surface area and porosity (Recommendations 1984), IUPAC, Pure & Appl. Chem., Vol. 57, No. 4, 603-619.

Wheeler, G., 2005, Alkoxysilanes and the consolidation of stone, Getty Publications

Winkler, E.M., 2013, Stone in Architecture, Properties, Durability, 3rd Edition, Springer

ALTERATION OF MARBLE STONES BY RED DISCOLORATION PHENOMENA

O.A. Cuzman[1*], S. Vettori[1], F. Fratini[1], E. Cantisani[1], S. Ciattini[2], L. Chelazzi[2], M. Ricci[3] and C.A. Garzonio[4]

Abstract

Red discoloration on marble showed particular interest between 1980-2000, when red stain phenomena were investigated on different monuments such as the façade of the Certosa di Pavia, the Siena Cathedral, the Orvieto Cathedral, the marble Cenotaph in the Monumental Cemetery of Pisa, the Labyrinth Fountain in the Garden of Villa di Castello in Florence, the Fountain of Galatea in Villa Litta (Lainate-Milan), the Pretoria Fountain in Palermo. New examples of red stains were recently observed in Genoa (columns of Carlo Felice Theatre , Basilica of Santa Maria Assunta in Carignano, cloister of Genoa University in Balbi Street, etc.) and Florence Cathedral of Santa Maria del Fiore, the Baptistery, basement of the statuary complex of Ratto delle Sabine by Giambologna, the statue of Giovanni delle Bande Nere, etc.). Comparative macroscopic observations on these new case studies are presented, showing that water plays an essential role in the formation of red stains, together with the presence of microorganisms and a source of lead. This work was therefore focused on the characterization of such red discolorations observed on the marble cladding of the apse side of the Florence cathedral. A multi-analytical approach was chosen for the red stain investigations, using the following techniques: microscopic analysis (OM), Raman spectroscopy, X-ray microtomography and XRF. The red stains display heterogeneous aspect, the wideness of the covered area and their chromaticity being variable. They were observed both on horizontal and vertical slabs, and often the presence of microorganisms was detected (mainly chasmolitic cyanobacteria and chromogenic bacteria). The results revealed the presence of lead as well. The Raman spectra showed the presence of minium (lead oxide) in both phases - crystalline and amorphous. The possible source of lead is located in the joins between the marble slabs and/or the traffic pollution, while the experiential microorganisms, lead-resistant, join in the process of red stain formation.

Keywords: red stain, marble, biodeterioration, lead oxide, red chromatic alteration, microorganisms

[1] O.A. Cuzman*, S. Vettori, F. Fratini and, E. Cantisani
Institute for the Conservation and Valorisation of Cultural Heritage (ICVBC-CNR), Sesto Fiorentino (FI), Italy
cuzman@icvbc.cnr.it

[2] S. Ciattini and L. Chelazzi,
Structural Cristallography Center (CRIST), Sesto Fiorentino (FI), Italy

[3] M. Ricci
Department of Chemistry, University of Florence, Florence, Italy

[4] C.A.Garzonio
Department of Earth Sciences, University of Florence, Florence, Italy

*corresponding author

1. Introduction

The study of red discoloration on marble showed particularly interest for two decades between 1980-2000, when many papers dealt with the investigation of red stains phenomena observed on different monuments. The façade of the Certosa di Pavia was the first documented case study (Realini and Sorlini, 1988; Bruni *et al.*, 1995; Zanardini *et al.*, 2003) but other red discolorations were reported in Italy in the same period on different monuments, such as the Siena Cathedral (Tiano and Tomaselli, 2004), the Orvieto Cathedral (Zanardini *et al.*, 1994), the Marble Cenotaph in the Monumental Cemetery of Pisa (Tiano and Tomaselli, 2004), the Labyrinth Fountain from Garden of Villa di Castello in Florence (Matteini *et al.*, 1986), Fountain of Galatea in Villa Litta (Lainate-Milan; Sorlini *et al.* 1994) and the Pretoria Fountain from Palermo (Palla and Tartamella, 2007). The red alteration phenomena on marble were observed in other countries as well (Konkol *et al.* 2009, Grissom *et al.* 2010).

Recently, red alterations were observed especially in Genoa, Florence and Siena (Fig. 1), as follows:

- Santa Maria del Fiore Cathedral, Florence (in the Apuan marble cladding of the apse side);
- Baptistery of Florence (observed mainly in the upper part, where the marble slabs are mostly all original. Different typologies (spotted or continuous morphology) are present on both vertical and horizontally placed slabs);
- In the statuary complex of Ratto delle Sabine realized by Giambologna in 1574-1580 and sited in Loggia dei Lanzi, Florence (observed on the vertical surface of the basement, made of Apuan marble, exposed to rain, with a dark red hue and homogenous aspect);
- Basement of the monument to Giovanni delle Bande Nere, realized in Apuan marble by Baccio Bandinelli in 1540 and placed in front of San Lorenzo Church, Florence);
- A statue inside the Park of Villa Demidoff in Pratolino, near Florence, made of Apuan marble;
- Columns of the neoclassic pronaos of Carlo Felice Theatre, Genoa, realized by Carlo Barabino (first half of XIXth century), made of Apuan marble (little red areas especially in the basement of the columns, both on the side exposed to rain and on the side protected);
- Columns of the portal in the main façade of S. Maria Assunta Basilica in Carignano Genoa (second half of XVIth century), made of Apuan marble;
- Volumns of the cloister of the University Palace (former Jesuit College), sited in via Balbi,Genoa, realized by Bartolomeo Bianco (first half of XVIIth century), made of Apuan marble;
- Columns of the courtyard of Palazzo Doria Tursi, sited in via Garibaldi, realized by Domenico and Giovanni Ponzello (second half of XVIth century), made of Apuan marble;
- Parapet of the terrace of Villa Durazzo Pallavicini, Pegli-Genoa(first half of XIXth century), made of Apuan marble;
- Façade of the church of S. Raimondo al Refugio, Siena (second half of XVIth century), made of Montagnola Senese marble.

Fig. 1: Some red chromatic alterations on monuments in Genova (a-d) and Florence (e-j), such as: the columns of cloister of the University of Genoa, Balbi Street (a-b), Villa DurazzoPallavicini, Pegli (c), Villa DurazzoPallavicini, Pegli (d), monument to Giovanni delleBandeNere (e-f), Santa Maria del Fiore Cathedral (g-h), statuary complex of Rattodelle Sabine by Giambologna (i) and a statue in the park of Villa Demidof in Pratolino, near Florence (j).

It was observed that in Italy the red alteration on marble occurs on different types of marbles (like Apuan marble, Montagnola Senese marble.etc.) and its presence is not related with the closeness to the sea, being observed both in Genoa, Palermo, Florence, Siena, Milan, Pavia, Orvieto.

Considering Genoa and Florence, taken into account in this study, Genoa is little warmer than Florence and with more precipitations in the autumn and winter seasons (http://www.ilmeteo.it/portale/archivio-meteo/Genova;http://www.ilmeteo.it/portale/ archivio- meteo/Firenze).

The presence of the red alterations was observed in the areas affected by rain, and this fact can be correlated to both, the presence of possible microorganisms and to dissolution and migration of possible presence of lead. It seems that the internal microstructure of the marble substrate could influence the wideness of the red phenomena. As a matter of fact in Fig. 1c little white areas not affected by redness can be observed in a wide alteration area. In the case of the Florence Cathedral the red stains are diffused from the bottom up to many tens of metres in height without any particular relation to the exposition. Nevertheless, it seems that these phenomena only occur on marble slabs with a certain oldness being exposed for a long time, thus suggesting the alteration process is slow requiring a long time to pass before it becomes noticeable by naked eyes. Grissom *et al.* (2010) for example observed the migration of red stains over a period of five years on one of the investigated surfaces of the Memorial Amphitheatre in Washington D.C. made of Mountain White marble from the Danby quarries of Vermont. Furthermore, the authors also mention the presence of lead red stains on theTripoli Monument made of Carrara marble at the U.S. Naval Academy in Annapolis.

This paper focuses on the red stains alteration observed on marble slabs on Santa Maria del Fiore Cathedral in Florence. Different investigation techniques such as optical microscopy, X-ray microtomography, XRF mapping and Raman spectroscopy were used. The results confirmed the presence of microorganisms and lead in different oxidation states.

2. Materials and methods

The samples analyzed in this paper comes from the apse side of Santa Maria del Fiore Cathedral (Fig. 1h).

2.1. Optical microscopy

The marble samples were observed with a Nikon Eclipse 600 microscope in reflection mode using optical fibres. The presence of the microorganisms was analyzed in transmission mode with the same microscope. The images were recorded using a Nikon DXM1200F digital CCD camera. Moreover, the characterization of marble was performed through XRD and petrographic observation in thin section under the optical microscope in polarized transmitted light (Zeiss Scope A1 microscope).

2.2. Micro-Raman spectroscopy

All micro-Raman measurements were carried out by means of a RenishawRM2000 single grating (1200 g/mm) spectrometer and charge-coupled device (CCD) air cooled (577×400 pixels) detector. A near infrared diode laser (785 nm) was employed as excitation source. Spectra were acquired using a 50 (N.A. = 0.75) magnification objective, providing a spatial resolution of about 2 mm. The spectral range investigated was comprised between 200 and 1800 cm^{-1}.Acquisition times were on the order of 60 s and the laser power on the order of a few milliwatts on the samples.

2.3. X-ray micro-tomography

One little fragments were used as such using a Skyscan 1172 high resolution microCT. This system has a sealed, micro-focus tungsten X-ray tube with a 5µm focal spotsize. The X-rays were produced by exposing the anode to an electron beam at 100 kV and 100mA. The beam was filtered by an Aluminum (0.5 mm) or Aluminum and Copper filter. Each sample was placed on the pedestal between the X-ray source and the CCD detector. The 2D X-ray images were captured over 180°, rotating the sample with a slice-to-slice rotation angle of

0.3° or 0.2°. Each 2D image represents one slice. The spatial resolution time was kept in the range 11-12 µm in terms of pixel size. The 3D images of the objects have been reconstructed using a modified Feldkamp algorithm for cone-beam acquisition geometry realized in Nrecon 1.6.9.4 software. The alignment, beam hardening and ring artifacts were corrected before starting the reconstruction process. CTan software was used for the image clean up and CVol or CVox for the 3D visualization.

2.4. XRF mapping

A little fragment was analyzed using a wavelength dispersive X-ray fluorescence spectrometer Rigaku ZSX Primus II equipped with an end-window 4 kW Rh X-ray tube and device for macro-mapping the elements (1 mm per point). The detectors were a scintillation counter and a gas flow proportional counter in which P-10 gas (argon 90% and methane 10%) flowed at 50 cm3 min−1.An elemental mapping analysis of Pb, Fe and Ca was performed on three different samples in order to correlate different colours to different compositions.

3. Results and discussions

The marble of the Florence Cathedral which suffered the development of the red stain comes from the Apuan Alps (as testified by archive data) and it is characterised by an homeoblastic-polygonal microfabric with straight boundaries among the constitutive calcite crystals (Fig. 2a). The mean grain size of the crystals is 350-400 µm. The red chromatic alteration was mainly concentrated on the exposed surface (Fig. 2b) and the presence of phototrophic microorganisms was observed as well (Fig. 2b and Fig. 2c).

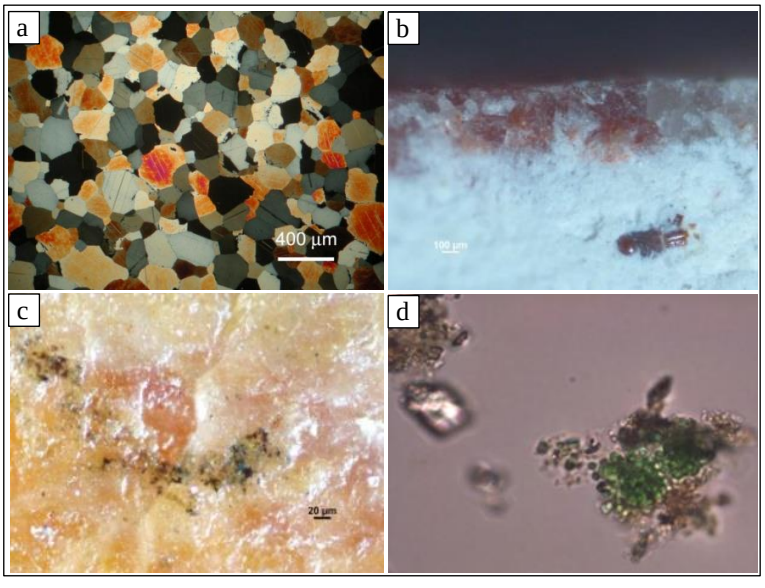

Fig. 2: Petrographic section of Apuan marble (a) and microscopic observations in reflection (b and c) and transmission mode (d)of the sample coming from Florence Cathedral Santa Maria del Fiore.

XRF mapping makes it possible to evaluate the different composition of the sample surface and, thanks to the X-ray capability to penetrate the matter, also of a small volume under the surface. With the micro-CT analysis, it is possible to reconstruct completely the sample volume distinguishing different part of the sample with different mass absorption coefficient.

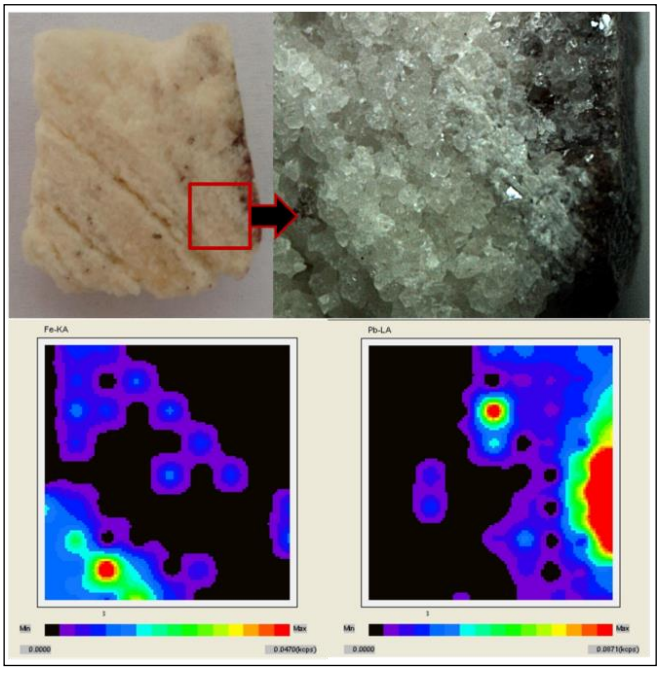

Fig. 3: XRF mapping of Fe (left) and Pb (right). A square of DF sample (in red) was analyzed.

The different colour in the 3D reconstruction of the analysed sample (Fig. 4a) shows clearly the red chromatic alterations in the surface exposed to air (lead) but only little points of red alteration can be observed in the longitudinal section of the marble core sample.

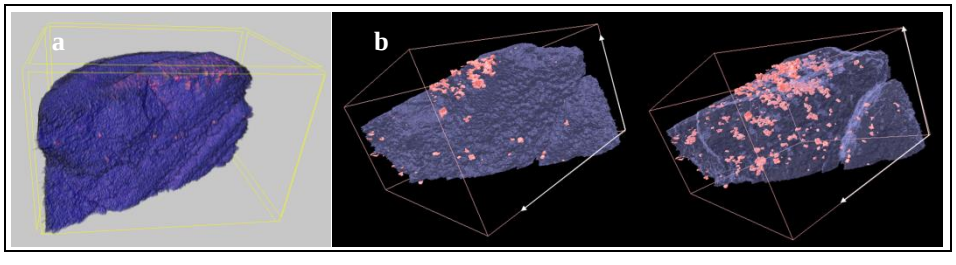

Fig. 4: 3D reconstruction of the analyzed sample showing the red chromatic alteration on the surface of the sample (a) and the 3D reconstruction in the same orientation with the CVol software (b).

Thanks to the microCT, the internal volume of the analyzed sample was exposed and studied. Surprisingly the alteration is found in abundance within the sample and concentrated in some agglomerates (Fig. 4b). Fig. 4b (on the right) shows the distribution of the red alterations inside the sample. From the 3D reconstruction it is clear that the red altered parts are concentrated in regions located deeply in the sample.

Raman spectra obtained on the sample at different positions are reported in Fig. 5. In both spectra the most intense bands are situated at 1085 (s), 711 (w), 547 (s), 389 (s), 313 (m), 280 (m) cm^{-1}. The bands at 1085, 711 and 280 cm^{-1}, are assigned to calcium carbonate and are, respectively, due to ν_1 (CO_3^{2-}) vibrational mode, ν_4(CO_3^{2-}) vibrational mode, whereas the band at 280 cm-^{1} is due to cooperative lattice modes of calcium carbonate. Instead, the bands 547 cm^{-1},389 cm^{-1} and 313 cm^{-1}, can be assigned to lead oxide, minium, (Pb_3O_4), which is red in colour. Although Raman technique is capable of distinguishing among different oxides of lead, and no other oxides are identified on the sample.

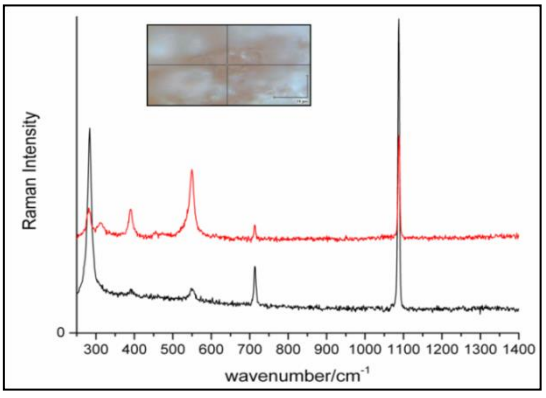

Fig. 5: Raman spectra of the red stained marble.

4. Conclusions

The red stains on marble monuments are quite frequent in Italy. From the new case studies observed in Genoa, Florence and Siena, it seems this phenomenon occurred especially on Apuan marbles, but they have been observed also on Montagnola Senese marble and on Mountain White marble from the Danby quarries of Vermont as well. The red color is associated with the presence of lead oxide, minium, (Pb_3O_4), which was identified by Raman spectroscopy. The red alterations seem to be concentrated as a layer on the stone surface exposed to open air, but with the help of microCT it was possible to observe the 3D arrangement of the lead inside the stone. The lead inside the analyzed stone sample was distributed in concentrated regions located deeply in the sample, and not always connected among them. The cause of these red alterations is definitely a result of the jointed action of chemical and microbiological processes, as microorganisms (coccoid cyanobacteria) were observed as well. The presence of a lead source is often correlated with the red stains, but it cannot always explain the occurrence of this type of red stains (Fig. 1j). The fact that the Apuan marble is the stone type most affected by red alterations containing lead leads to the

conclusion that more investigation is required especially on the marble's impurities and accessory minerals. Furthermore, it would be beneficial to attempt the reproduction of such stains under laboratory conditions.

Acknowledgements

Thanks to the Opera of Santa Maria del Fiore in the person of Marcello Del Colle for giving us the possibility to take a sample from the marble covering of the Cathedral.

References

Bruni, S. and Cariati, F., 1995, Spectroscopic investigation of red stains affecting the Carrara marble façade of the Certosa di Pavia, Archeometry, 37, 249-255.

Grissom, C.A., Gervais, C., Little, N.C., Bieniosek, G., Speakman, R.J., 2010, Red "staining" on marble: biological or inorganic origin?, APT Bulletin, J. Preservation Technology 41, 11-20.

Konkol, N., McNamara, C., Sembrat, J., Rabinowitz, M., Mitchell, R., 2009, Enzymatic decolorization of bacterial pigments from culturally significant marble, J. Cultural Heritage 10, 362-366.

Matteini, M., Moles, A., Manganelli,C., Fratini, F., Lazzarini, L., Pecoraro, M., 1986, Fonte del Labirinto o de Fiorenze: indagini scientifiche, Schede di restauro: Fonte del Labirinto o di Fiorenza, OPD Restauro 1, 184-186.

Palla, F. and Tartamella, E., 2007,Chromatic alteration on marble surfaces analyzed by molecular biology tools, Conservation Science in Cultural Heritage, 7, 111-127.

Realini, M. and Sorlini, C., 1988, Le macchie rosse del marmo Apuano. In: La Cerosa di Pavia: passato e presente nella facciata della chiesa, ed. C. Sorlini (Rome, CNR), pp. 198-199, 253-255.

Sorlini, C., Zanardini, E., Albo, S., Praderio, G., 1994, Research on Chromatic alteration of marbles from the fountain of Villa Litta (Lainate, Milan). Int. Biodet.& Biodegrad., 33, 153-164.

Tiano, P., Tomaselli, L., 2004, Red staining and heterotrophic bacteria, Coalition, 8, 2-4

Zanardini, E., Bruni, S., Cariati, F., Ranalli, G., Sorlini, C., 1994, Investigation on the red spots present on the Carrara marble façade of Orvieto Cathedral, In: Proceedings of 3rd International Symposium on the Conservation of Monuments in the Mediterranean Basin, Venice, pp. 349-352.

Zanardini, E., Abbruscato, P., Scaramelli, L., Onelli, E., Realini, M., Patrignani, G., Sorlini, C., 2003, Red stains on Carrara: a case study of the Certosa of Pavia, Italy. In: Art, Biology and Conservation marble: Biodeterioration of works of art, ed. RJ Koestler, VH Koestler, AE Charola and FE Nieto-Fernandez (New-York, Metropolitan Museum of Art), pp. 226-247.

QUANTIFYING SALT CRYSTALLIZATION DYNAMICS IN SANDSTONE USING 4D LABORATORY X-RAY MICRO-CT

H. Derluyn[1*], M.A. Boone[2], J. Desarnaud[3], L. Grementieri[4], L. Molari[4], S. de Miranda[4], N. Shahidzadeh[3] and V. Cnudde[1]

Abstract

We present data on the kinetics of drying and deliquescence, and on the precipitation and distribution of salt crystals within the pore space of Mšené (Prague) sandstone, as derived from quantitative image analysis on laboratory X-ray micro-computed tomography (µCT) scans. For that purpose, climatic chambers were developed at the Ghent University Centre for X-ray Tomography (UGCT), compatible with the centre's high-resolution X-ray micro-tomography scanners. This allows for inducing crystallisation under controlled temperature and relative humidity, and for dynamically visualizing salt weathering phenomena in building materials, by simultaneously imaging the transport and crystallisation process during consecutive scanning. Mšené sandstone samples of 8 mm in diameter were initially capillary saturated with a saturated NaCl-solution and subsequently dried at 20% *RH* and at 50% *RH*, at room temperature. During drying, the samples were scanned at defined moments in time. At 20% *RH*, the dynamics of the formation of a salt skin were quantified, partially closing the pores and causing a slower drying during the continuation of the process. At 50% *RH*, a constant drying rate and a constant salt growth rate was found during the full drying period. Furthermore, X-ray µCT scans were acquired during subsequent cycles of deliquescence, i.e. exposure to high *RH*, and drying at 20% *RH*. During the deliquescence, the salt efflorescence dissolves first, followed by the subflorescence dissolution and the pore space filling with saline fluid at a constant rate. The X-ray µCT datasets reveal the direct coupling between the transport and crystallisation dynamics through quantitative image analysis of the simultaneous visualization of both processes in 4D.

Keywords: Mšené sandstone, 4D X-ray micro-CT, salt weathering, crystallisation dynamics, drying and deliquescence kinetics

[1] H. Derluyn* and V. Cnudde
UGCT-PProGRess, Department of Geology and Soil Science, Ghent University, Belgium
hannelore.derluyn@ugent.be

[2] M.A. Boone
UGCT-PProGRess, Department of Geology and Soil Science, Ghent University and
XRE – X-ray Engineering bvba, Belgium

[3] J. Desarnaud and N. Shahidzadeh
Van der Waals-Zeeman Institute, Institute of Physics, University of Amsterdam, The Netherlands

[4] L. Grimentieri, L. Molari, S. de Miranda
DICAM, University of Bologna, Italy

*corresponding author

1. Introduction

Salt crystallisation causes major weathering of building stones. Numerical models have been developed to predict salt damage risks, but direct experimental studies of the governing processes at the pore scale in building stones are however limited. Experimental data at this scale would aid the advancement of the current models, and consequently improve the damage risk prediction. The system we study in the framework of the JPICH-JHEP project KISADAMA (de Miranda *et al.*, 2013), is the crystallisation of NaCl in Mšené sandstone. In a previous study (Desarnaud *et al.*, 2015), we showed that during drying-induced crystallisation, the distribution of salt crystals in the pore space (subflorescence) and on the material's surface (efflorescence) strongly influences the drying rate. We described the effect of the crystal growth on the drying behaviour of Mšené sandstone initially saturated with NaCl solution, by comparing drying at 20% *RH* and 50% *RH*, at room temperature. These *RH*-values are representative for winter and summer conditions for the salt NaCl, which is not temperature sensitive. Primary drying at 20% *RH* was found to take longer than at 50% *RH*, on account of the formation of a salt skin on the surface at 20% *RH*. Further deliquescence-drying cycles at 20% *RH* induce a movement of the salt precipitation, i.e. the salt skin partly disappears, salt precipitates in the pores and the drying is faster than the first drying. At 50% *RH*, deliquescence-drying cycling does not cause any changes with respect to the first drying. The drying during different cycles was monitored by measuring the weight change of the sample, while the salt precipitation was characterised by SEM images and X-ray µCT after the samples had dried out. The dynamics of the salt growth/dissolution during evaporation/deliquescence were however not measured. Experimental data of the simultaneous measurement of drying/deliquescence and salt precipitation/dissolution would however strongly aid the advancement of the understanding of coupled drying- crystallisation, or deliquescence-dissolution dynamics. This kind of data is also essential for numerical models that predict salt damage risks in building materials, as model parameters for the transport and crystallisation kinetics need to be defined, as well as for the distribution of crystals within the pore space.

Here, we describe the coupling between the drying- crystallisation and deliquescence-dissolution dynamics in Mšené sandstone as revealed by 4D X-ray µCT datasets. Two custom-designed climatic chambers were built adapted to the CT scanners of the UGCT in order to control the environmental conditions surrounding the sample. One is dedicated for the HECTOR scanner (Masschaele *et al.*, 2013), and was used to perform drying experiments. This setup and the results are discussed in section 2. The dynamics during deliquescence, studied in a second setup compatible with the EMCT scanner (Dierick *et al.*, 2014), are discussed in section 3.

2. Drying- crystallisation dynamics

2.1. Experimental work at the HECTOR scanner

Two cylindrical samples of 8 mm in diameter and 10 mm in height were cored from a Mšené sandstone plate. This sandstone has a unimodal pore system with an average pore size of 30 µm (Shahidzadeh-Bonn *et al.*, 2010). The samples were initially scanned in their dry state at the X-ray µCT scanner HECTOR of the UGCT. Next, the samples were capillary saturated by immersing them in a saturated NaCl solution for 30 minutes. The samples were then scanned in their wet state, and subsequently during their drying, by scanning them every 30 minutes during the first 3 hours, and every hour during the

succeeding 12 hours. Drying was controlled by placing the sample in a custom-built climatic chamber, compatible with the µCT setup, depicted in Fig. 1. Conditioned air is produced by the Gen*RH*-T generator (Surface Measurement Systems Ltd) and blown in the plexi-glass test chamber at a slow rate (3.3 ml/s). The inner volume of the test chamber is 4×4×3 cm³. The outlet of the chamber is connected to a separate *RH*-T sensor. Polyimide windows of 2×2 cm², which are quasi transparent to X-rays, are present at the front and the backside of the chamber. The chamber is clamped at its upper rod and has a hole in the bottom of 2 cm diameter that allows for the sample's rotation while scanning. The sample is attached to a 1 cm diameter plastic rod fixed on the rotation stage, and the flow loss was found to be minimal. This setup ensured that the samples were dried at a constant temperature of 19.2°C and a *RH* of 20% and 50% for the first and the second sample, respectively.

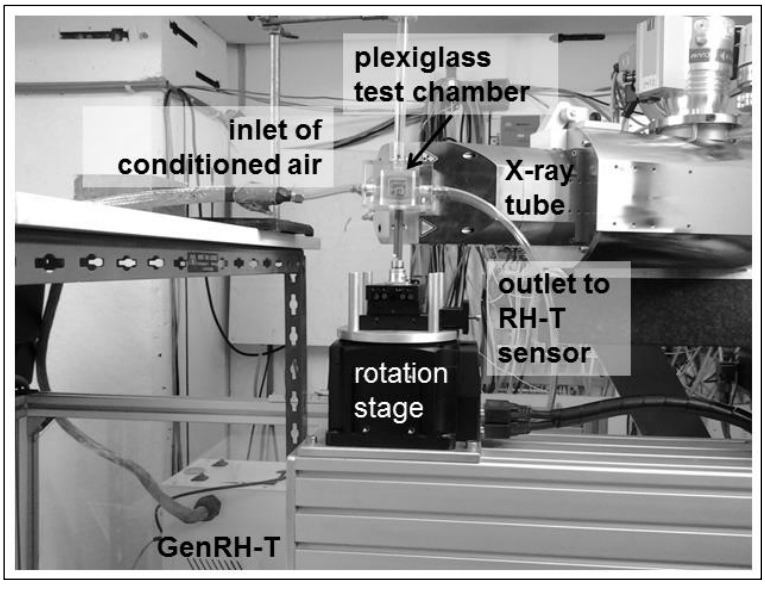

Fig. 1: Experimental setup at the X-ray µCT scanner HECTOR of the UGCT for performing dynamic scans of salt weathering cycles.

For each scan a total of 1351 projections was acquired over an angle of 360°, with an exposure time of 400 ms per projection. A thin aluminium filter (1 mm) was used to block low-energetic X-rays at the source to reduce beam hardening. In order to correct for inhomogeneities of the detector and beam, 32 dark-field and 200 flat-field images were acquired before the initial scan. The X-ray tube provided a voltage of 100 kV with a target power of 10 W. The source-detector distance was 1530.7 mm and the source-object distance 38.3 mm. The projections were binned by a factor 2×2 in order to increase the signal-to-noise ratio, resulting in a reconstructed voxel size of 10 µm. The raw data were reconstructed using the software Octopus Reconstruction (Inside Matters bvba (Vlassenbroeck *et al.*, 2007)). The same set of parameters for ring and spot removal, tilt and skew of the detector and beam hardening were adopted for all scans. Small shifts in the reconstructed volumes with respect to the reference volume were corrected by aligning all

volumes to the reference scan using the software DataViewer (Bruker microCT). This ensured the same positioning in 3D space for all datasets.

The datasets were further analysed with the software Avizo (FEI). As it was not possible to directly segment the salt crystals and the salt solution based on the image histogram, due to an overlap of the grey values of crystals and solution, the following procedure was applied: the wet scan was subtracted from the series of scans taken while drying, resulting in differential images (Boone *et al.*, 2014), where all negative values correspond to the solution that has dried-out, and all positive values correspond to salt crystals that precipitated. Two volumes-of-interest (VOI's) were defined, one including only the sample's volume and one including the sample's volume and the salt efflorescence at the end of drying. The evolution of the volume fractions of the salt solution, the total amount of precipitated salt, the salt efflorescence and salt subflorescence were then calculated with respect to the volume of the second VOI.

2.2. Results and discussion

The drying of the two samples is given in Fig. 2a. We can observe that drying at 20% *RH* is initially faster than at 50% *RH*, due to the higher difference in *RH* between the sample's surface and the environment. This first drying stage is characterised by a constant rate, due to the capillary action which induces a hydraulic connection between the surface and the inner pore space. Subsequently, the evaporation at the surface mainly results in salt efflorescence. At 50% *RH*, this constant rate period lasts until the sample is almost completely dried out. After about 1 hour at *RH* of 20% the drying process changes to a slower, exponential regime, i.e. after approximately half of the initial salt solution has dried out.

The differences in drying kinetics are caused by the differences in salt precipitation dynamics, which are presented in Fig. 2b and Fig. 2c. As the initial amount of salt is equal for both samples, the resulting total amount of salt precipitation is the same (Fig. 2b). The crystal precipitation develops however slower at 50% *RH*, where the salt crystals forming on the surface (efflorescence) and the salt crystals precipitating in the pores close to the surface, develop at the same relative rate during the whole duration of drying (with respect to their respective total amounts, Fig. 2c). No salt crystals were found deep inside the volume. While drying at 20% *RH*, the crystal growth at the surface develops first, and much faster than at 50% *RH*, mainly during the first hour of the experiment and then reaches a plateau. The salt crystals precipitating just below the surface at this lower *RH* develop more gradually, during the whole duration of the drying. The period of the formation of efflorescence at 20% *RH* is congruent with the period of the constant drying rate in the drying curve. The second exponential drying stage at 20% *RH* must thus be resulting from this salt efflorescence, corroborating the statement that a salt skin is forming on the surface during the first stage of drying (Desarnaud *et al.*, 2015), partially closing the pores and causing a slower drying during the continuation of the process. The salt skin still grows slightly during this second period, but most of the salt crystals precipitate just below this layer. Typical snapshots of the sample drying at 20% *RH* are given in Fig. 3.

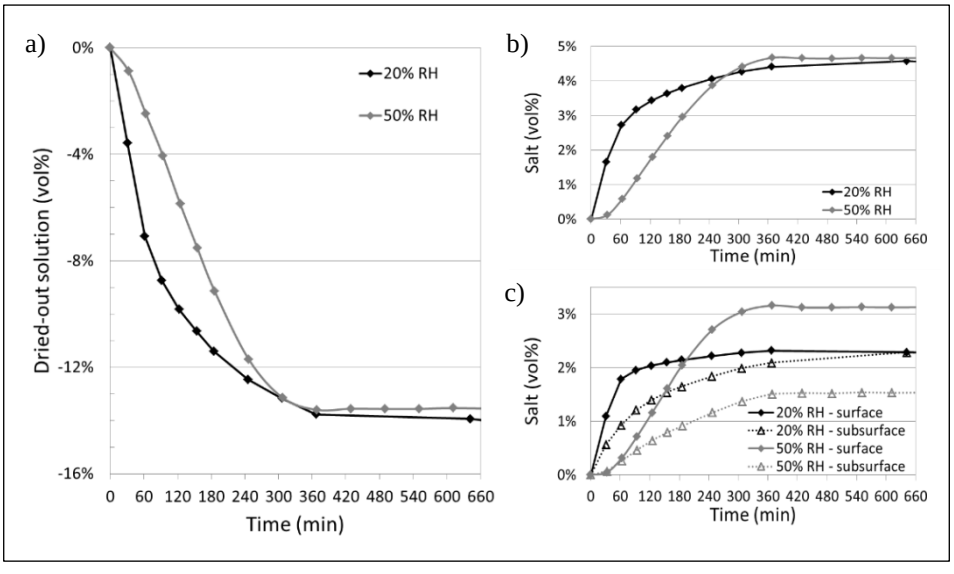

Fig. 2: The drying (a) and crystallisation dynamics (b and c) of Mšené sandstone at 20% RH and 50% RH. Fig 2c distinguishes between the salt crystals forming on the outer surface (efflorescence) and the salt crystals precipitating just below, in the pores of the subsurface.

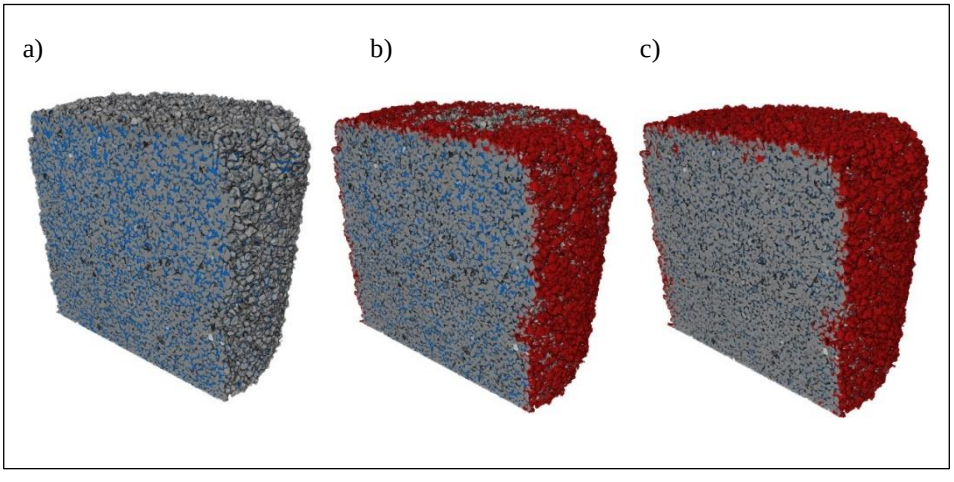

Fig. 3: Typical snapshots of the Mšené sandstone sample while drying at 20% RH: at the wet state (a), after 1 hour (b) and after 6 hours (c). Blue: salt solution – red: salt crystals. (For interpretation of the references to color in this figure legend, the reader is referred to the digital version of the article.)

3. Deliquescence dynamics

3.1. Experimental work at the EMCT scanner

In order to study the deliquescence dynamics, a setup was developed for the EMCT scanner. The EMCT scanner consists of a rotating gantry system (Fig. 4a), i.e. the source and detector rotate around the sample, and the sample remains fixed. This has the advantage that a closed test chamber could be made as no hole is needed for the sample to rotate. Consequently, there is no risk of water leakage at high *RH*, and additional sensors can be easily connected as their wiring does not need to rotate. The setup is depicted in Figures 4b-c. The Gen*RH*-T generator (Fig. 4b) is connected to a cylindrical plastic test chamber in which the sample is positioned on a plastic holder (Fig. 4c). A Sensirion SHT75 *RH*-T sensor is placed in the upper lid of the chamber, to measure the climate independently from the inlet conditions. The workflow is further similar to the one discussed in section 2.1.

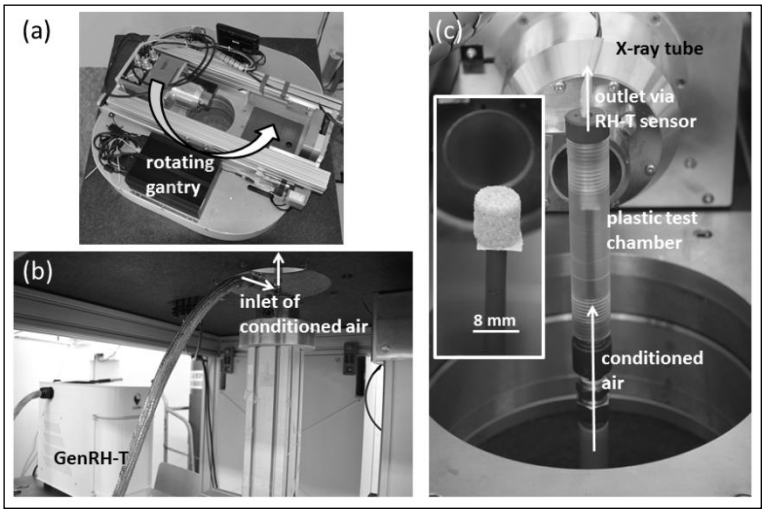

Fig. 4: The climatic chamber setup at the EMCT scanner.

A Mšené sandstone sample of 8 mm diameter and saturated with a 6.1 molal NaCl-solution was placed in the climatic chamber. The sample was first dried at 20% *RH*, and subsequently exposed to two deliquescence-drying cycles by alternating between an *RH* of 100% and 20%, respectively. Scans were taken during the drying and the deliquescence process. During the first 2 hours, scans were taken every 15 minutes, during the next 2 hours every half an hour, and subsequently every hour. The scans were acquired at a tube voltage of 80 kV, each scan taking 11 minutes for 1501 projections. The reconstructions were performed using the 4D suite from XRE (X-Ray Engineering bvba), resulting in datasets with a voxel size of 10.2 µm. The image analysis was performed with the software Avizo, as described in section 2.1.

3.2. Results and discussion

Some preliminary results are depicted in Fig. 5. Fig. 5a shows a cross section after the second drying of the sample. The pores are emptied, and salt crystals are predominantly present at the surface. Fig. 5b shows the cross section after the deliquescence process. The

salt crystals have dissolved, and the pore space is filled by salt solution. The dynamics of the process are represented in Fig. 5c. The image analysis indicates that the salt crystals on the surface dissolve first, after which the salt crystals located in the subsurface get dissolved, and the pores fill up with brine. The decrease of the total amount of salt shows a linear behaviour with time, as well as the deliquescence process itself, i.e. the increase in saline solution in the pore space.

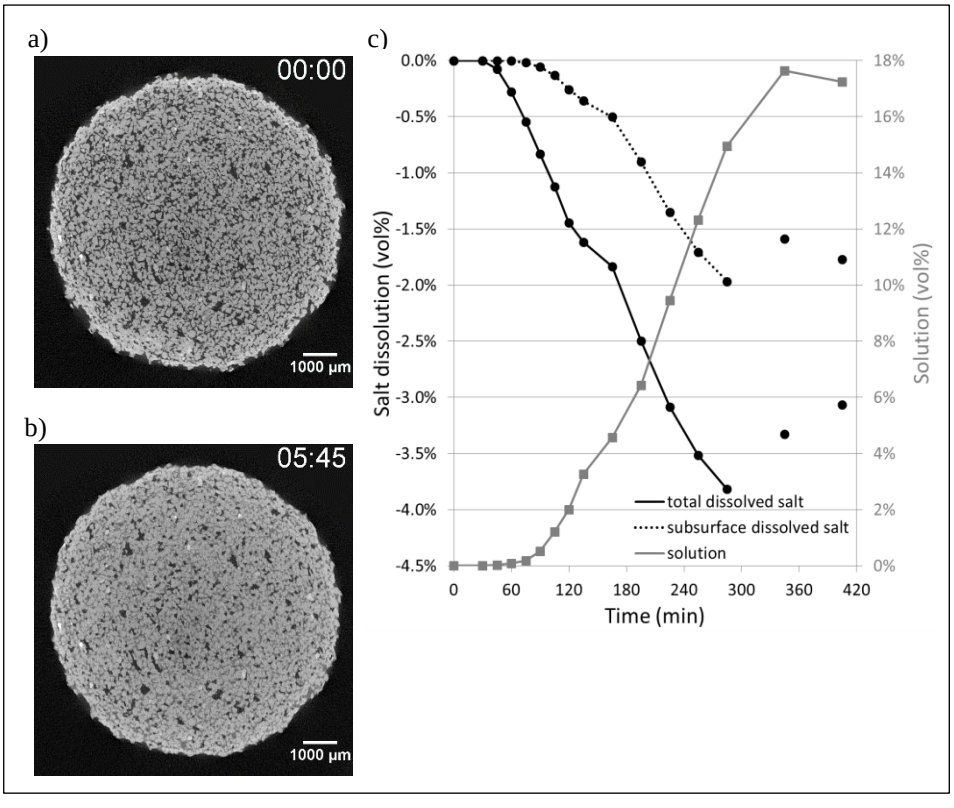

Fig. 5: The deliquescence process in a Mšené sandstone sample containing NaCl: (a) cross section after the second drying and (b) after subsequent 5h 45min exposure to high RH. (c) Quantitative analysis of the deliquescence.

4. Conclusions

We have demonstrated that we can monitor crystallisation and deliquescence processes dynamically in 4D by means of X-ray µCT in a porous sandstone, by combining the µCT scanners at the Ghent University Centre for X-ray Tomography with dedicated peripheral equipment to control relative humidity conditions. We quantified the simultaneous drying-crystallisation kinetics of NaCl-saturated sandstone, as well as the deliquescence-dissolution kinetics. The developed experimental setup is however generic, and could be used for drying-deliquescence studies on other porous media, and with pure water or different saline liquids.

In the specific experiment described in the paper, the results showed linear drying and crystallisation kinetics when drying at 50% *RH*, with mainly the development of salt efflorescence on the surface. When drying at 20% *RH*, the initial linear drying slows down with time, which is congruent with the initial fast formation of a salt skin on the surface. This salt skin subsequently reduces the further development of efflorescence, slows down the drying, and promotes subsurface precipitation. During deliquescence, a linear rate is found for the dissolution of the salt and the filling of the pores by the salt solution.

Acknowledgements

H. Derluyn acknowledges the support from the Research Foundation – Flanders (FWO) for her postdoctoral fellowship. J. Desarnaud is a postdoctoral fellow of Fom/f grants – (NWO) and acknowledges its support. The work reported in this paper has been supported by the KISADAMA project, funded by JPI Cultural Heritage within the Joint Heritage European Programme JHEP and by BOF research fund 01B00512 entitled 'Systems for controlling temperature and relative humidity' and by FWO research grant 1521815N.

References

Boone, M.A., De Kock T., Bultreys T., De Schutter G., Vontobel P., Van Hoorebeke L. & Cnudde V., 2014, 3D mapping of water in oolithic limestone at atmospheric and vacuum saturation using X-ray micro-CT differential imaging. Materials Characterization, 97, 150-160.

de Miranda, S., Molari, L., Cnudde, V., Shahidzadeh, N., Favaro, F., 2013, Joint Heritage European Programme grant JPI-JHEP: Kinetics of salt crystallization and mechanical damage in historic masonry (KISADAMA), 2y. project, November 2013-October 2015, www.kisadama.eu.

Desarnaud, J., Derluyn, H., Molari, L., de Miranda, S., Cnudde, V., Shahidzadeh, N., 2015, Drying of salt contaminated porous media: effect of primary and secondary nucleation. Journal of Applied Physics, 118, 114901.

Dierick, M., Van Loo, D., Masschaele, B., Van den Bulcke, J., Van Acker, J., Cnudde, V., Van Hoorebeke, L., 2014, Recent micro-CT scanner developments at UGCT, Nuclear Instruments and Methods in Physics Research B, 324, 35-40.

Masschaele, B., Dierick, M., Van Loo, D., Boone, M.N., Brabant, L., Pauwels, E., Cnudde, V., Van Hoorebeke, L., 2013, HECTOR: A 240kV micro-CT setup optimized for research, Journal of Physics: Conference Series, 463, 012012.

Shahidzadeh-Bonn, N., Desarnaud, J., Betrand, F., Chateau, X., Bonn, D., 2010, Damage in porous media due to salt crystallization, Physical Review E, 81, 066110.

Vlassenbroeck J., Dierick M., Masschaele B., Cnudde V., Van Hoorebeke L. & Jacobs P., 2007, Software tools for quantification of X-ray microtomography. Nuclear Instruments & Methods In Physics Research Section A-Accelerators Spectrometers Detectors And Associated Equipment, 580, 442-445.

INVESTIGATION OF SALT SOLUTION BEHAVIOUR IN BUILDING STONES USING PAPER PULP POULTICES UNDER LABORATORY CONDITIONS

I. Egartner[1*] and O. Sass[1]

Abstract

The behaviour of moisture and salt solution during the drying process in porous stone material and their distribution inside the substrate are investigated under laboratory condititions. Blocks of two porous limestones (Cotswold limestone, Oxfordshire, UK and Aflenzer stone, Austria) were cut into stone cubes (5×5×5 and 5×5×20 cm) and soaked first with ultrapure H_2O and second with different concentration of saline solutions (0.1 mol/l, 0.5 mol/l and 1 mol/l solutions) of NaCl and Na_2SO_4 to determine their behaviour during the dehydration process under different conditions. Based on the analysis of the capillary absorption coefficient and the capillary rise behaviour of the samples, a multi-method approach including sampling by drilling, paper pulp poultices, handheld moisture sensor, conductivity sensor, Ion Chromatography (IC) and X-ray diffractometry (XRD) were applied to detect the moisture and salt (ion) content. The laboratory analyses were carried out at the department of applied geoscience of the Technical University of Graz, Austria. The main aim of the laboratory analysis was to investigate the effectivity of the paper pulp poultices in comparison with drilling profiles into the stone cubes. Furthermore, the laboratory work supports a field work investigation at a College wall in Oxford, UK.

Keywords: salt weathering, paper pulp poultices, building stone, laboratory investigation

[1] I. Egartner* and O. Sass
Department of Geography and Regional Science, University of Graz, Austria
isabel.egartner@uni-graz.at

*corresponding author

1. Introduction

The presented laboratory investigation is part of a longer-term project which deals with salt and moisture dynamics in weathered limestone walls. The main investigation object in the field is a part of the 300 hundred year old boundary wall of the Worchester College in Oxford, UK. The motivation for the lab work is based on two points:

1. To investigate the behaviour and distribution of water and salt solution of known concentration in a porous material during the dehydration process at different saturation states by applying different approaches on limestone cube samples.
2. To verify the mechanism, reliability and effectivity of salt sampling by paper pulp poultices. This method (which is described later) is frequently used as a desalination treatment in view of building conservation. Here it is used to evaluate salt contamination in a diagnostic phase and in this context published systematical investigations are not common.

The behaviour of moisture and salt ions during the drying process inside a porous substrate and during the interaction of two porous substrates, like a poultice and a porous stone material are described in the following.

1.1. Interaction of two substrates (Poultices – porous material)

The poultices/substrate system describes an interaction between two porous materials in hydraulic contact. There are processes, like dissolution, diffusion and crystallisation involved (Verges-Belmin and Siedel 2005). The mode of operation depends on environmental conditions (*RH*, *T*, wind speed), properties of the materials (like composition, porosity and pore-size distribution) and the degree of present liquid and vapor phases inside the substances (Sawdy *et al.*, 2008; Van Hees *et al.*, 2006). The pore-size distribution is of importance for the moisture and ion transport during a drying period of a wet porous material (Van Hees *et al.*, 2006; Sawdy *et al.*, 2008). If the relative humidity is rising inside an interconnected pore system of a material, micropores are going to be water-filled first. If drying sets in, macropores start to empty of water, while micropores remain water-filled (Voronina 2013; Sawdy *et al.*, 2008; Asmussen 2007)

1.2. Moisture and ion transport between poultice and substrate

The "wetting phase" represents the movement of moisture from a wet poultice into the substrate, where the extra water causes the solution of the present salts. In the second phase, the "salt extraction", the dissolved ions move as saline solution from the substrate into the poultice. This transport is able to take place in two different ways. "Advection" forces the salt transport from the substrate to the poultice through a capillary water flow. It is a relative quick process in comparison to diffusion. The other process is called "diffusion" and transports salt ions from the substrate into the poultice due to an unbalanced salt ion concentration gradient (Fig. 1). To maintain this process the poultice has to stay wet (Voronina 2013; Voronina 2011). To force capillary moisture flow during the drying process, the substrate has to consist of larger pores than the poultices, because the direction of water movement by advection is align from coarser to finer pores. Large pores provide water, while small pores extract salts during drying (Pel *et al.*, 2010; Sawdy *et al.*, 2010; Voronina 2013). Cellulose poultices possess mainly large pores. The pore size distribution of the cellulose poultices type "Arbocell BC1000" amount to 10-30 µm (Lubelli and van Hees 2010).

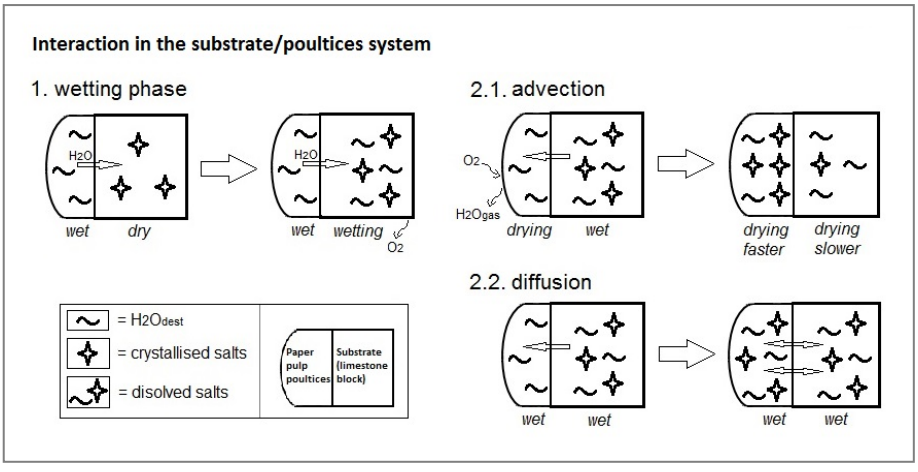

Fig. 1: Interaction of moisture and salt ions in the substrate/poultices system (own draft inspired by Van Hees et al., 2006; Gupta 2013; Voronina 2011; Sawdy et al., 2008).

2. Material

The samples consist of limestone, the so-called Aflenzer stone (Austria). It is porous, rich in fossils and has a high percentage of calcium carbonate (>90%). For most of the experiments the samples were cut into 5×5×5 cm cubes and for one of the applications (capillary rise) we used stone samples which measured 5×5×20 cm. The Aflenzer stone block, which was cutted into the cuboid samples, originated from a subterranean quarry, so it is a fresh, non-weathered stone.

3. Methods

To form the basis for the following approaches, the water (EN 1925) and salt solution absorption coefficient by capillarity [kg m^{-2} $s^{-0.5}$] and the capillary rise behaviour of the limestone cubes were analysed. Then, the cubes were immersed in two passes, first into ultrapure H_2O and second into a mixture of saline solutions under air pressure for 24 hours. During the ensuing dehydration process samples were analysed at different states of saturation. Saturation levels were approximately 100%, 75%, 50%, 25% 10% and 0%. Several samples were used in each run to get more significant results for each saturation level. The first sampling session started after 24 hours of immersion treatment. At this point, the stone cubes were almost fully saturated. On the next day, after approximatly 24 to 36 hours (depending on different stone characteristics) the 75% saturation level was reached (and so on). Weighing of the stone cubes was carried out to find out the actual saturation level. Salts were sampled by drilling as well as by non-destructive application of paper poultices on the stone surfaces of the cubes. Immediately before the sampling the moisture content of the stone surface was measured with a handheld moisture sensor. The sampling resultants (drill dust and poultice, respectively) were analysed with a conductivity sensor and by means of Ion Chromatography (IC).

3.1. Sampling by paper pulp poultices

Paper pulp poultices (PPP) were used as salt sampling method for non-destructive application. They consist of cellulose fibers and we used the so called "Arbocell BC1000" fibers. PPP (3 g of cellulose fibers) were soaked in de-ionized water with a pulp-to-water weight ratio of about 1/20 and applied to the sampling points for 60 minutes. The poultices were then removed, soaked in 50 ml deionized water and filtered to remove the paper poultice (Backbier and Rousseau 1993; Martinho *et al.*, 2012; Dionisio *et al.*, 2012). The investigated stone cubes were immersed with saline solutions of different concentration (0.1 mol/l, 0.5 mol/l and 1 mol/l) of NaCl and Na_2SO_4. The conductivity of the resultant saline solutions were analysed by using a conductivity sensor. In a second step the anions and cations of the samples were investigated by a Ion Chromatograph (IC).

3.2. Sampling by drilling

Prior to this sampling method stone cubes were treated just with ultrapure H_2O and with 0.5 M saline solutions of NaCl and Na_2SO_4. Drilling profiles inside the stone cubes up to a depth of 2 cm were done to detect the distribution of the salt solution within the stone. The drilling material was collected across assembly levels of 0.5 cm from the stone surface up to 2 cm in depth. A certain amount of the stone powder was resolved with ultrapure water (1:10), shaked for 1h, filtered (45 µm filter size) and measured by a conductivity sensor and further be analysed by Ion Chromatography (IC). The (destructive) method allows to verify the quality and reliability of the sampling by PPP.

3.3. Conductivity sensor

After sampling (drill dust or poultice), immersion and filtering, the conductivity of the saline solutions was measured by a "WTW Cond 315i" sensor.

3.4. Ion Chromatography (IC)

After sampling by means of PPP the filtered samples were prepared for the ion chromatograph (Dionex IC DX500 Chromatograph) at the Department of Applied Geoscience, Technical University of Graz. Ion chromatography is a type of fluid chromatography and is used to separate inorganic anions and cations.

4. Results

The water (standard EN 1925) and salt solution absorption coefficient by capillarity [$kg/m^2s^{1/2}$] were done for six samples and show a good accordance between the samples. The maximum fluid uptake of the stone cubes ranges from 35.8 to 41.0 g/cm² within 96 hours. The heights of capillary rise in the 5×5×20 cm stone cubes fluctuate from 19.2 to 21.5 cm in 3.5 hours. This result illustrates that the stone cubes used are well comparable to each other (with only a small variability).

4.1. Paper pulp poultices

Stone cubes were treated with different concentrations of NaCl and Na_2SO_4 saline solutions. The amount of substance [mol/l] is well mirrored by the range of the measured conductivity values [µS/cm]. The conductivity measurement of the resultant saline solutions sampled by PPP shows an increasing trend from stone cubes with a low saturation level to the fully saturated examples. The highest conductivity was measured at the approximately 100% saturated samples, strongly decreases at 50% saturation, and then follows a slightly falling curve down to 0% saturation of the stone cubes. Samples

immersed by ultrapure H_2O can be used as a base level because the conductivity values are very low and show almost no range between different saturation levels (Fig. 2).

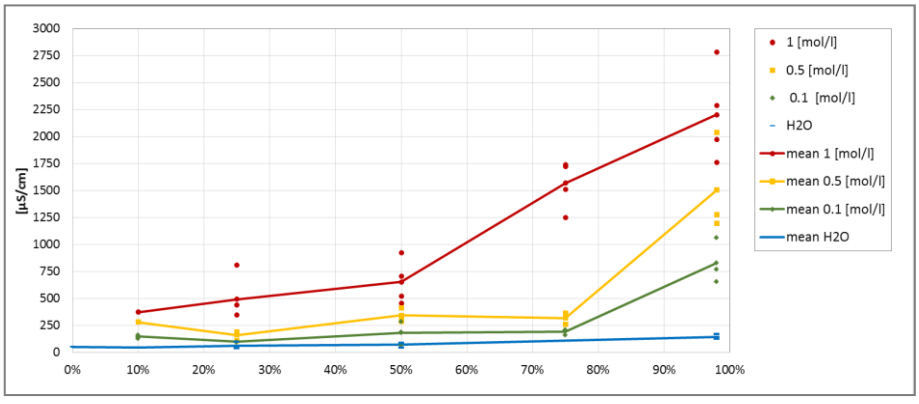

Fig. 2: Conductivity [µS/cm] of resultant saline solutions of varied amount of substance [mol/l] sampled by poultices at different saturation levels [%].

4.2. Drill dust

The conductivity values [µS/cm] shown in Fig. 3 relate to the immersed drill dust from different depth intervals (0 – 2 cm), obtained from a stone cube soaked in 0.5 mol/l NaCl and 0.5 mol/l Na_2SO_4 solution. The conductivity of the samples and their relationship to the saturation degree are shown in Fig. 3. A steady increase from 0 to approx. 100% saturation is visible: At saturated conditions as well as at very low saturation, conductivity are relatively uniform at the different drilling levels. At intermediate saturation, instead, the range between the saline solutions collected near to the stone surface and those from deeper drilling levels is remarkable, with salts being concentrated in the outermost 0.5 cm near the surface.

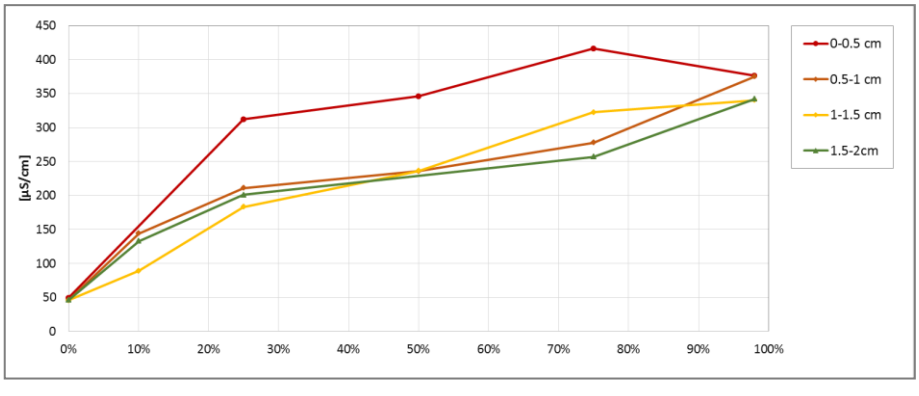

Fig. 3: Conductivity [µS/cm] of the resultant saline solution (0.5 mol/l) obtained by different assembly drilling levels at different saturation levels [%].

A notable decrease of conductivity values is visible from the stone surface to 2 cm depth (Fig. 4). The biggest gradient in conductivity decrease happens from the surface layer (0-0.5 cm) to the deeper subsurface (0.5-1 cm).

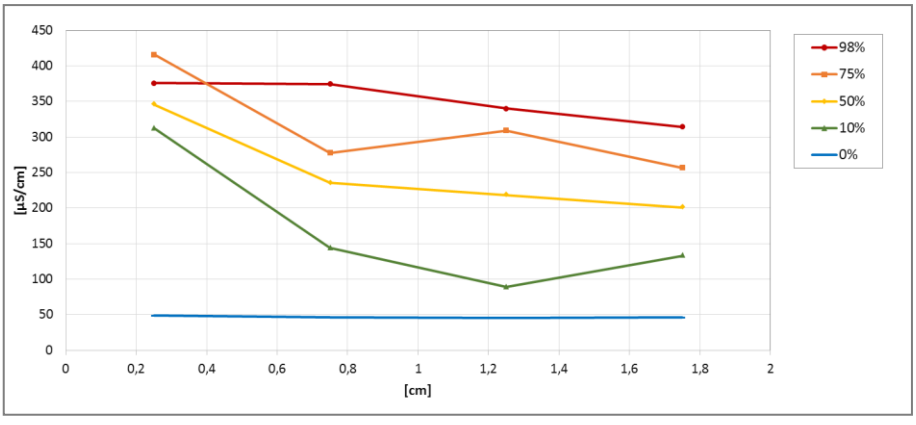

Fig. 4: Conductivity [µs/cm] of saturation levels at varied depths of drilling (0 to 2 cm).

4.3. Salt ion concentrations measured by Ion Chromatography (IC)

Selected examples were measured by Ion Chromatography to receive the mass concentration [mg/cm³] of the resultant saline solution. The results correlate quite well with the conductivity [µS/cm] measured by the conductivity sensor. This means that cheaper conductivity measurements can be applied without losing significant accuracy, and the measured values can be converted into salt concentration using the calibration function. This correlation is plotted in relation to the drilling depth in Fig. 5. The differentiation between the different ions applied is still under investigation.

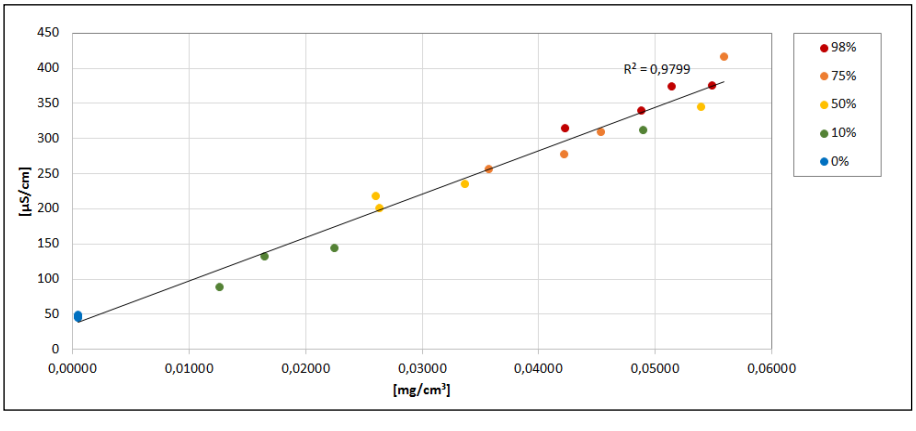

Fig. 5: Conductivity [µs/cm] versus mass concentration [mg/cm³] of different saturation degrees at varied depth of drilling (0-2 cm).

5. Discussion

5.1. Moisture and salt solution behaviour during the dehydration process

The most significant result of both sampling methods is that the conductivity [µS/cm] increases with rising saturation gradients. The highest conductivity is measured at c. 100% saturation, but the area with the strongest gradients is different between the methods. The conductivities of the PPP samples strongly decrease down to 50%, following then by a slightly falling curve down to 0% saturation of the stone cubes. This progression may emerge because salt ions are much better mobilised in an almost fully saturated stone than under partially saturated conditions. The poultice insert water into the stone which enables capillary transport to a certain depth. Low saturated stones have a less interconnected pore system and so a lot of large air-filled pores remain (Gupta 2013; Sawdy *et al.*, 2008). Saturated stones have well interconnected pores, so the range of the transport induced by the poultice may reach deeper regions of the stone and more salt ions can be activated. Conversely, at the sampling method by drilling the strongest decrease in saturation is found near to the lowest saturation levels. From about 25% down to 0% the conductivity of all sample curves are strongly declining. The same result was measured by the IC, thus the amounts of salt ions decrease with decreasing saturation degree of the stone. From the drilling profiles we can see that the amount of salt ions are almost uniform at low saturation degrees. This results are in contrast to intermediate saturation, where a well visible difference between the drilling level near to the stone surface and all deeper located occur. In all samples, decreasing conductivity values with increasing depth were found. This result demonstrates that salt ions favour to crystallise near to the surface in the course of the dehydration process.

5.2. Effectivity of salt sampling by paper pulp poultices

Two of the motivations of this paper are the questions ‘how much salt ions can a poultice extract compared to the total amount of salt ions inside the stone?’ and ‘how deep does the influence of the poultice reach during its application to attract salt ions?’. Both questions will be further investigated in our project. To answer the first question, salt concentrations of the PPP samples and the drilling samples have to be correlated. Although samples collected by poultices as well as by drilling show a similar spectrum of results, the absolute conductivity values are different. The saline solutions received by immersion of the poultices reach much higher values (up to 2800 µS/cm) than those of immersed drill dust (up to 430 µS/cm) at approximately 100% of saturation. This is not surprising considering the wholly different mode of sampling. The poultices have a contact area to the stone surface of 13.7 cm² while the stone powder derives from a drilling area of 0.79 cm². Thus, the poultice can suck much more ions by capillary flow from inside the stone cube.

To correct for this fundamental difference, the values of drilling method were corrected by area and volume to make them comparable to the PPP samples. The results of the drilling samples were extrapolated in a calculative way to the salt concentration [mg/cm³] of the entire stone cube. The resultant amount of salts which are present in the stone cube match quite well the total amount of salts deriving from the initial saline solution (deviation of 4 – 15%). These values were finally compared to the amounts of salt extracted by the respective poultices. The result of this comparison is that the salt concentration a poultice is able to take up [mg/cm³] depends mainly on the saturation degree of the stone cube. Approximately 24% of the salts within a 100% saturated stone cube are able to move into

the poultice. At 75% and lower saturation degrees, only 14 to 11% of the salts are moving into the poultices. But these values should be treated with caution, because other parameters are acting a role too. So, we do not know how much salts might have been pushed deeper in the substrate in the course of poulticing.

References

Backbier, L. and Rousseau, J., 1993, Analytical study of salt migration and efflorescence in a mediaeval cathedral, Analytica Chimica Acta, 283, 855-867.

Gupta, S., 2013, Sodium chloride crystallization in drying porous media: influence of inhibitor. Disseration.

Lubelli, B. and van Hees, R.P.J., 2010, Desalination of mansonry structures: fine tuning of pore size distribution of poultices to substrate proberties, Journal of Cultural Heritage 11, 10-18.

Martinho, E., Alegria, F., Dionisio, A., Grangeia, C. and Almeida, F., 2012, 3D-resistivity imaging and distribution of water soluble salts in Portuguese Renaissance stone bas-reliefs, Engineering Geology 141-142, 33-44.

Pel, L., Sawdy, A. and Voronina, V., 2010, Physical principles and efficiency of salt extraction by poulticing, Journal of Cultural Heritage, 11, 59-67.

Sawdy, A., Heritage, A. and Pel, L., 2008, A review of salt transport in porous media, assessment methods and salt reduction treatments, Salt Weathering on Buildings and Stone Sculptures, Proceedings from the International Conference 22–24 October 2008, Ottosen, L.M., Rörig-Dalgaard, I., Larsen, P.K., Brajer, I., Bøllingtoft, P., Marciniak, M. and Svane, M. (eds.), National Museum Copenhagen, Denmark, Technical University of Denmark, Lyngby 1-28.

Sawdy, A., Lubelli, B., Voronina and V. Pel, L., 2010, Optiminzing the extraction of soluble salts from pourous materials by poultices, Studies in Conservation, 55, 26-40.

Van Hees, R.P.J., Lubelli, B., Vergès-Belmin, V., Bourgés, A., Zezza, F., Di Sipio, E., Heritage, A. and Sawdy, A., (2006), "Guideline for desalination of porous substrates", Desalination - Assessment of Desalination Mortars and Poultices for Historic Masonry, Contract no.: 022714, 26pp.

Voronina, V., 2011, Salt extraction by poulticing: an NMR study. Dissertation.

Voronina, V., Pel, L., Sawdy, A. and Kopinga, K., 2013, The influence of osmotic pressure on poulticing treatments for cultural heritage objects, Materials and Structures 46, 221–231.

EXPERIMENTAL STUDY OF THE AGEING OF BUILDING STONES EXPOSED TO SULFUROUS AND NITRIC ACID ATMOSPHERES

S. Gibeaux[1*], C. Thomachot-Schneider[1], A. Schneider[2], V. Cnudde[3], T. De Kock[3], V. Barbin[1] and P. Vazquez[1]

Abstract

During the last few decades, due to remediation procedures, SO_2 emissions in the atmosphere have decreased, unlike NOx. Air pollution has changed. Indeed, the aim of this research is to assess the effect of NOx and their interactions with SO_2 on stones, particularly on limestones used in Champagne-Ardenne (France) during the restoration processes. Three French building limestones (Courville, Dom and Savonnières) and one reconstituted stone were exposed during 28 days to four strong acid atmospheres i.e. two H_2SO_3 solutions with different concentrations and two mixed atmospheres with different proportions of HNO_3 and H_2SO_3. These tests produced an intensive acid attack on the stone, allowing the observation of short-term salt precipitation and the evolution of stone properties. Each day, one sample was removed from the acid atmosphere to measure the concentration of SO_4^{2-} and NO_3^- by ion-chromatography. The surface changes were assessed before and after the tests by 3D scanning and observations with electron microscopy. X-ray microtomography has been performed in the Centre for X-ray Tomography (UGCT) and the Department of Geology at Ghent University (Belgium) in order to observe the penetration of salts and the consequences in stones porosity. First observations showed that exposure to acid atmosphere, led to gypsum efflorescences. Obvious colour changes occurred in all tests. Salt crystallization entailed a change in the porous system, which was evidenced by 3D, mercury porosimetry and X-ray microtomography. Difference between weathered and fresh stone was highlighted by Ion chromatography analyses.

Keywords: acid atmosphere ageing tests, limestone, non-destructive testing (NDT), sulphates, nitrates

[1] S. Gibeaux* ,C. Thomachot-Schneider V. Barbin and P. Vazquez
GEGENAA, University of Reims, France
soizic.gibeaux@univ-reims.fr

[2] A. Schneider
IFTS, University of Reims, France

[3] V. Cnudde and T. De Kock
Dept. Geology and Soil Science, Ghent University, Belgium

*corresponding author

1. Introduction

The 21st century is known as a financial crisis period and an air pollution evolution era (CITEPA 2015). In this context we have to respect sustainability of our monuments choosing the best restoration processes while finding the cheapest solution. The two determining factors to take into account are the choice of the material and the type of environment. One of the most important weathering agent is the dry deposition of gaseous pollutants on stones which results in salt weathering (Török *et al.*, 2004; Charola *et al.*, 2007; Grossi *et al.*, 2007; Monna *et al.*, 2008). Crust formation, blackening, yellowing and carbonate dissolution are the consequences of this phenomenon (Grossi *et al.*, 2007; Monna *et al.*, 2008). Sulphur dioxide is particularly known as the main gaseous pollutant responsible for salt weathering but last decades, ratios in emissions of pollutants have changed with a SO_2 decrease and an increase in NOx). The consequences of these changes in atmospheric composition on the type of salt crystallization are scarcely investigated (Sikiotis and Kirkitsos, 1995; Camaiti *et al.*, 2007; Vazquez *et al.*, 2016) unlike the effects of NOx as catalysts for the SO_2 oxidation (Massey 1999).The alteration processes of the stones also depend on the material characteristics like chemical composition, porosity and texture (Massey 1999; Grossi *et al.*, 1995; Vazquez *et al.*, 2015). The goal of this study is to compare, quantitatively and qualitatively, the reactivity of fresh and weathered stones exposed to different acid atmospheres.

2. Material

2.1. Samples

Three natural stones and one artificial stone were tested. Samples of reconstituted stone and Savonnières limestone are not fresh because they stem from historical buildings, respectively from Orval Abbey (Belgium) and Saint-André Church (Reims, France), unlike the Courville and Dom samples which are fresh stones particularly used in the North of France and the South of Belgium (Fronteau 2000; Thomachot *et al.*, 2011; 2015). These stones present different composition and porosity detailed in Tab. 1.

Tab. 1: Characteristics and composition of the four studied stones.

Stone	**Limestone type**	**Colour**	**$CaCO_3$** wt.%	**SiO_2** wt.%	**Porosity** %	**Named as**
Reconstituted Stone	Lithoclastic	Orange	94.6	1.09	23	RS
Savonnières	Oolitic vacuolar	Grey	90.3	4.90	30	S
Courville	Micritic fine	Russet	86.9	6.64	16	C
Dom	Oolitic to bioclastic	Yellow ochre	96.3	0.68	20	D

2.2. Ageing tests

The dry deposition process was evaluated by means of accelerated ageing tests, based on the standard UNE-EN 13919:2003 procedures (CEN, 2002). They were performed with the atmospheres created by four solutions using nitric and/or sulphurous acids in different proportions (Vazquez *et al.*, 2016) as described in Tab. 2.

Tab. 2: Ageing tests solutions concentrations.

	HNO_3, mol l^{-1}	**H_2SO_3**, mol l^{-1}	**HNO_3/H_2SO_3 ratio**	**Named as**
Solution 1	$4.8\ 10^{-1}$	$1.7\ 10^{-1}$	3/1	$H_2SO_3 < HNO_3$
Solution 2	$1.4\ 10^{-1}$	$5.6\ 10^{-1}$	1/4	$H_2SO_3 > HNO_3$
Solution 3	-	$5.6\ 10^{-1}$	-	H_2SO_3 HC
Solution 4	-	$1.7\ 10^{-1}$	-	H_2SO_3 LC

The stock solution for nitric acid was Panreac 69% w/w M = 14.4 g mol^{-1}, and for sulphurous acid was Panreac 6% w/w M = 6 g mol^{-1}.

Tab. 3: Samples type in function of analysis.

Number of samples	**Size**	**Analysis**	**Analysis frequency**
28		Ion chromatography	One per day
7	1×1×0.4 cm	SEM/EDS	After 1, 3, 5, 8, 15, 22 and 28 days
1	 1×1×2 cm	Hg porosimetry	At the end of the experiment
1	 5×5×1 cm	Macroscopic evaluation Weight 3D scanning	At the end of the experiment
1	 Ø 0.4 cm	X-ray Microtomography	After 1, 10 and 28 days

3. Analytical methods

Dry deposition on stones lead to salt precipitation and stone dissolution. Different technics were used to assess change of the samples (Tab. 2). Photos and images of the upper face were taken with a Nikon Coolpix 4500 and a SEM Hitachi TM-1000 Tab. Top equiped with an EDS. The roughness change was assessed with the ZScan 700Cx device for the 3D scanning and the 3D Reshaper software for the processing of the point cloud with an accuracy of 0.05 mm and a resolution of 0.1 mm. Quantity of NO_3^- and SO_4^{2-} was determined by Ion Chromatography (IC) (Dionex ICS 2000). The high resolution X-ray Computed Microtomography was performed for RS and S tested with $H_2SO_3 < HNO_3$ using the in-house scanner HECTOR (Masschaele *et al.*, 2013) developed in the Centre for X-ray Tomography of Ghent University (UGCT). The tomographs were reconstructed with the Octopus Reconstruction software (Inside Matters, Belgium; Vlassenbroeck *et al.*, 2007), while the reconstructed images were subsequently analyzed using Octopus Analysis, formerly called Morpho+ (Brabant *et al.*, 2011). Porosity characterization was obtained using an Hg intrusion porosimeter (MIP) Micromeritics Autopore IV 9500.

4. Results

4.1. Visual and SEM observations

The observation showed a yellowing of every stone for every test. Only a located blackening of RS and D appeared in the H_2SO_3 < HNO_3 test and slightly in the H_2SO_3 LC test. In the former, white spots arise on C sample. The SEM images highlighted different salt crystal habits (Fig. 1) independently of the time of exposure. Moreover no evolution in the crystals shape or size was detected between the tests or the samples.

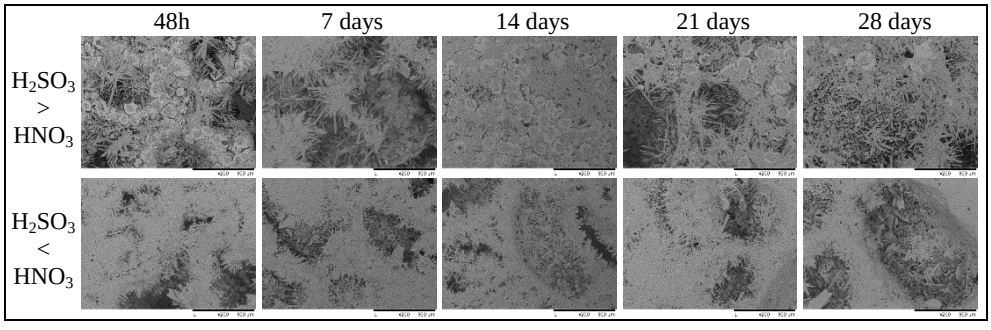

Fig. 1: SEM images of Savonnières sample during the mixed atmospheres tests.

4.2. Weight changes

After the H_2SO_3 < HNO_3 and H_2SO_3 LC tests, the weight gain did not exceed 0.5% with few differences between the stones. The weight gain was notable after the H_2SO_3 > HNO_3 and H_2SO_3 HC tests (from more than 0.5 to 2.0%), the latter with the highest values for all the stones except for S.

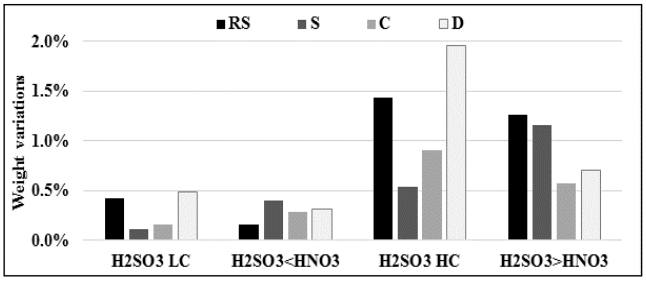

Fig. 2: Weight variations between initial and final states.

4.3. Roughness

Dry deposition created a new surface roughness. No spatial differences were observed among the tests. Fig. 3a showed the numerical subtraction of the surface before and after the tests. Green colour indicated that no change took place on the surface. Salt crystallized mainly in the sample's limits and in preexistent defects and pores (red colour). Dissolution occurred in carbonate grains in the case of RS (blue colour). In other stones, dissolution could be observed disseminated through the surface without a defined pattern.

4.4. X-ray Computed Micro tomography (µCT)

After solely one day of exposure to the H_2SO_3 < HNO_3 test, a homogeneous crust and some areas showing dissolution process appeared on RS and S. After 10 and 28 days, the growth crust was negligible. The fine crust large of around 50µm for RS and 100µm for S seemed to be mainly composed of needle-like crystals (Fig.3b).

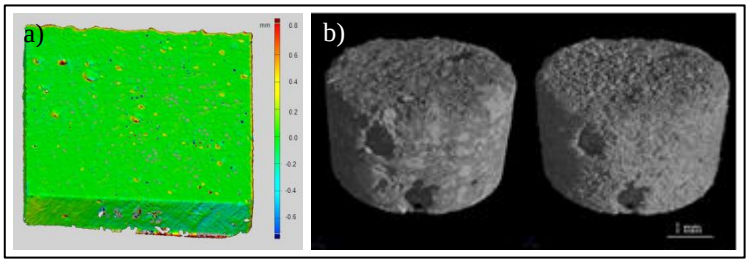

Fig. 3: a) Roughness measurements (subtractions between initial and after test states) on RS after H_2SO_3<HNO_3; b) 3D reconstruction of RS µCT scans before (left) and after 28 days (right) exposed to the H_2SO_3 < HNO_3 test.

4.5. Pore access radii

The total porosity varied slightly, between 0 and 6%, unlike the pore radius access (Fig.4). The volume of pore access radii could increase according to the stone and the test: C for every test except H_2SO_3 > HNO_3, S for H_2SO_3 > HNO_3 and H_2SO_3 HC tests, D for H_2SO_3 < HNO_3 tests. Some pore access radii could also disappear like the macropores of RS and S submitted to H_2SO_3 LC test and those of D submitted to H_2SO_3 LC and HC tests. The H_2SO_3 LC led to the closing of pore access radii of all stones except the Courville stone for which the pore access radii widened (H_2SO_3 > HNO_3).

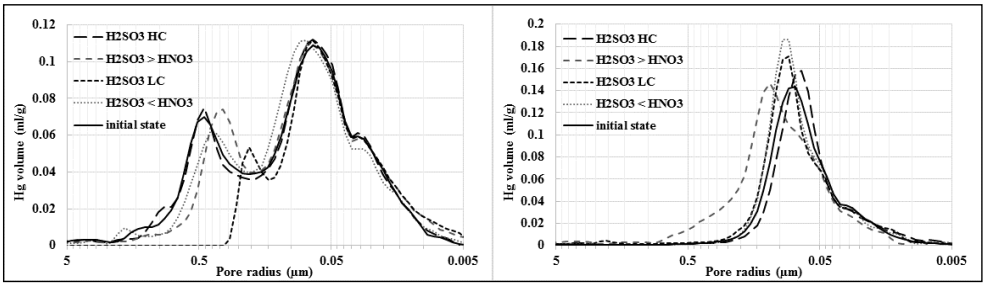

Fig. 4: Pore distribution of RS (left) and C (right) samples before and at the end of the tests.

4.6. Ion chromatography

S and RS were initially S-rich, because they were not fresh stones (from 5000 to 6000 mg/g, Fig. 5). In all tests, the NO_3^- concentration was less than 250 mg/g, therefore negligible if compared to SO_4^{2-} concentration which could reach up to 8000 mg/g. For C and D samples, there was a remarkable increase of the SO_4^{2-} concentration after the first

day, after which the concentration stabilized. The SO_4^{2-} concentration did not change during mixed atmospheres exposures for RS and S samples.

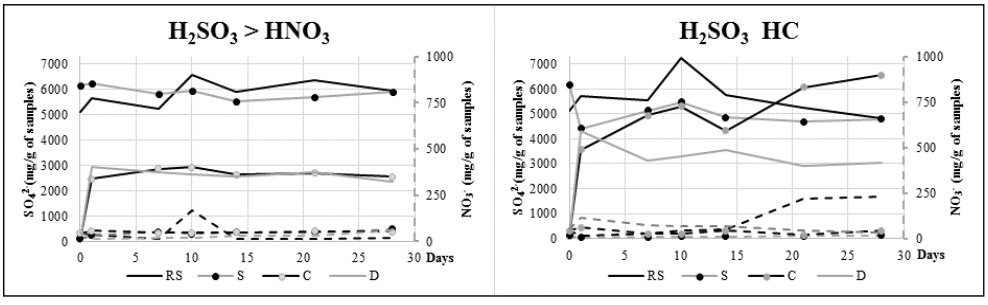

Fig. 5: SO_4^{2-}(solid lines) and NO_3^-(dotted lines) concentrations.

5. Discussion and conclusion

5.1. Type of atmosphere

Every test led to salt efflorescence growth on each stone. It formed a fine and homogeneous crust highlighted by the X-ray computed microtomography. Additionally, 3D measurements revealed the location of crystallization in the stone defects while dissolution occurred mainly at the contact with calcite elements. Weight variations showed the reactivity between stones and acid atmospheres seemed directly linked to the quantity of H_2SO_3 regardless pure or mixed with HNO_3. MIP showed that pure H_2SO_3 atmospheres led to the closing of pore access radii while the mixed atmospheres (H_2SO_3 combined with HNO_3) led to the widening of the pore access radii. The ion chromatography showed the maximum production of sulfates during the first day of exposure regardless the test and the stone. A low quantity of nitrates was measured in both mixed test because of their high instability in water and their hygroscopicity (Cheng *et al.*, 1987). Or nitrates play a catalytic role in the oxidation of sulfur compounds. The variations of SO_4^{2-} concentrations were similar from on test to another for each stone except for Courville limestone. The bad correlation between the weight variations and salts quantity can be due to the difference in size scale of samples.

5.2. Behaviour *of fresh stone and exposed stone*

The presence of sulphates in the initial state of the tested weathered samples did not differ in the degree or type of decay to the fresh ones. The only difference was found in ion chromatography analyses. The initial concentration of sulphates in the initially weathered stones (RS and S) is much higher than in the fresh ones (C, D). However, this high concentration in RS and S remained constant through the whole test, while in C and D sometimes an increase was observed after the first day, and then the concentration kept almost constant.

5.3. Suitable techniques in the study of stone decay by exposure to acid atmosphere

The exposure to an acid atmosphere enriched in SO_2 entailed the formation of a gypsum crust from the very first day of test. The different techniques to assess the evolution of the decay gave rich but varied information about the process. Visual observation gave

information about the general changes on the stone surface, such as colour changes or crystal formation. On one hand, visual observation resulted fast and suitable techniques to evaluate the decay (Vazquez *et al.*, 2015). On the other hand, SEM observations only showed the crystal shapes since the salt crust was formed during the first day. Weight variations give information about the new precipitated crystals. However, this information should be taken with care. Dry deposition in controlled atmosphere involves precipitation and dissolution, two processes that depend strongly on stone properties. A weight gain reflects that salt precipitation was more important than dissolution. To have detailed information about where precipitation or dissolution occurs, 3D measurements is an optimal technique to study the sample's surface (Vazquez *et al.*, 2016), MIP to assess the variation in the pore radii access and the µCT to observe exactly in which grain or pore the process took place (Dewanckele *et al.*, 2012). Ion chromatography gives a general idea about the anion quantity, however, only the strong changes in concentration must be taken into account due to the heterogeneous reactivity of each sample.

References

Brabant, L., Vlassenbroeck, J., De Witte, Y., Cnudde, V., Boone, M.N. and Dewanckele, J., 2011, Three-dimensional analysis of high-resolution X-ray computed tomography data with Morpho+, Microscopy and Microanalysis, 17, 252–263.

Camaiti, M., Bugani, S., Bernardi, E., Morselli, L. and Matteini, M., 2007, Effects of atmospheric NOx on biocalcarenite coated with different conservation products, Applied Geochemistry, 22, 1248–1254.

CEN (EUROPEAN COMMITTEE FOR STANDARDISATION), (2002), "EN 13919: Natural stone test methods. Determination of resistance to ageing by SO_2 action in the presence of humidity", CEN, Brussels.

Cheng, R.J., Hwe Ru, J., Kim, T.J. and Leu, S-M., 1987, Deterioration of marble structures - the role of acid rain, Analitical Chemistry, 59, 104A-106A.

Charola, A.E., Pühringer, J. and Steiger, M., 2007, Gypsum: a review of its role in the deterioration of building materials, Environmental Geology, 52, 339–352.

CITEPA, (2015), "Inventaire des émissions de polluants atmosphériques et de gaz à effet de serre en France", Ministère de l'Écologie, du Développement durable et de l'Énergie. http://www.citepa.org/fr/activites/inventaires-des-emissions/secten.

Dewanckele, J., De Kock, T., Boone, M.A., Cnudde, V., Brabant, L., Boone, M.N., Fronteau, G., Van Hoorebeke, L. and Jacobs, P., 2012, 4D imaging and quantification of pore structure modifications inside natural building stones by means of high resolution X-ray CT, Science of The Total Environment, 416, 436–448.

Fronteau, G., 2000, Comportements télogénétiques des principaux calcaires de champagne-ardenne, en relation avec leur faciès de dépôt et leur séquençage diagénétique, Ph.D. thesis, University of Reims Champagne-Ardenne, France.

Grossi, C. M., Murray, M. and Butlin, R. N., 1995, Response of porous building stones to acid deposition, Water, Air, and Soil Pollution, 85, 2713–2718.

Grossi, C.M., Brimblecombe, P., Esbert, R.M., Alonso, F.J., 2007, Color changes in architectural limestones from pollution and cleaning, Color Research & Application, 32, 320–331.

Masschaele, B., Dierick, M., Loo, D.V., Boone, M.N., Brabant, L., Pauwels, E., Cnudde, V. and Hoorebeke, L.V., HECTOR: A 240kV micro-CT setup optimized for research, Journal of Physics: Conference Series, 463, 1-4.

Massey, S.W., 1999. The effects of ozone and NOx on the deterioration of calcareous stone. Science of the total environment 227, 109–121.

Monna, F., Puertas, A., Lévêque, F., Losno, R., Fronteau, G., Marin, B., Dominik, J., Petit, C., Forel, B. and Chateau, C., 2008, Geochemical records of limestone façades exposed to urban atmospheric contamination as monitoring tools? Atmospheric Environment, 42, 999–1011.

Reddy M.M., 1988, Acid rain damage to carbonate stone: a quantitative assessment based on the aqueous geochemistry of rainfall runoff from stone, Earth Surface Processes and Landforms, 13, 335-354.

Sikiotis, D. and Kirkitsos, P., 1995, The adverse effects of nitrates on stone monuments. Science of the Total Environment, 171, 173–182.

Thomachot-Schneider, C., Gommeaux, M., Fronteau, G., Oguchi, C.T., Eyssautier, S. and Kartheuser, B., 2011, A comparison of the properties and salt weathering susceptibility of natural and reconstituted stones of the Orval Abbey (Belgium), Environmental Earth Sciences, 63, 1447–1461.

Thomachot, C., Gommeaux, M., Vazquez, P., Lelarge, N., Conreux, A., Mouhoubi, K. and Bodnar, J.-L., 7-11 September, 2015, Relationship between Na_2SO_4 concentration and thermal response of reconstituted stone in the laboratory and on site, Proceedings of The WORLD Multidisciplinary Earth Sciences Symposium, Prague, Czech Republic, 456.

Török, A. and Rozgonyi, N., 2004, Morphology and mineralogy of weathering crusts on highly porous oolitic limestones, a case study from Budapest, Environmental Geology, 46, 333-349.

Vazquez, P., Carrizo, L., Thomachot-Schneider, C., Gibeaux, S. and Alonso, F.J., 2016, Influence of surface finish and composition on the deterioration of building stones exposed to acid atmospheres, Construction and Building Materials, 106, 392-403.

Vázquez, P., Menéndez, B., Denecker, M.F.C. and Thomachot-Schneider, C., 2015, Comparison between petrophysical properties, durability and utilisation of two limestones of Paris region, Geological Society of London, Special Issue, 416.

Vlassenbroeck, J., Dierick, M., Masschaele, B., Cnudde, V., Van Hoorebeke, L., Jacobs, P., 2007, Software tools for quantification of X-ray microtomography, Nuclear Instruments and Methods in Physics Research A, 580, 442-445.

GEOLOGICAL STUDIES ON VOLCANIC TUFFS USED AS NATURAL BUILDING STONES IN THE HISTORICAL CENTER OF SAN LUIS POTOSI, MEXICO

R.A. López Doncel[1*], W. Wedekind[2], N. Cardona-Velázquez[3], P.S. González-Sámano[1], R. Dohrmann[4], S. Siegesmund[2] and C. Pötzl[2].

Abstract

The use of volcanic tuffs as building elements in historical monuments built during the 17th, 18th and 19th century are an important part of the cultural heritage in the city of San Luis Potosi, Mexico. For the constructions of the historical buildings pink-colored volcanic tuff rocks of the region were used, geologically defined as units of the "Cantera Ignimbrite". This rock, locally also known as "Cantera Rosa" shows very different appearances and colors which can vary from pink to dark pink, grey, brown and orange. However these building rocks have significant variations in texture, compositions and mechanical properties and these properties determine the resistance to weathering and deterioration, because they show a wide range of deterioration types, e.g. scaling, flacking, sanding, back weathering and coloration/discoloration. Geological, petrophysical, geochemical and mechanical studies were realized on these rocks to understand the causes of their weathering and deterioration.

Keywords: tuff, Mexico, deterioration, porosity, pore distribution

[1] R.A. López-Doncel* and P.S. González-Sámano
Instituto de Geología, Universidad Autónoma de San Luis Potosí, Mexico
rlopez@uaslp.mx

[2] W. Wedekind, S. Siegesmund and C. Pötzl
Geoscience Centre of the University of Göttingen, Germany

[3] N. Cardona-Velázquez
Facultad del Habitat, UASLP, Mexico

[4] R. Dohrmann
Bundesanstalt für Geowissenschaften und Rohstoffe, Hannover, Germany

*corresponding author

1. Introduction

The old mining city of San Luis Potosí in middle Mexico was founded in the year 1592 (Villar Rubio, 2000). Due its important mining activities San Luis Potosí was one of the richest cities of the Nueva España, which was clearly demonstrated in the impressive colonial (Baroque) architecture of the old downtown. For the constructions of these buildings were used volcanic tuff rocks of the surroundings. These tuff rocks are utilized until today for the construction of modern buildings in the city. The uses of the volcanic tuff rock as building element in royal houses, government buildings and religious settlements as chapels and temples build in the 17th, 18th and 19th century are an important part of the cultural heritage in the city of San Luis Potosi, Mexico (Fig. 1).

Fig. 1: Some of the principal buildings and monuments build with the Cantera Rosa. Left to right: Tower and facade of the San Agustín Church, facade of the El Carmen Church, fountain in the Santuario and Santuario del Desierto Church.

For the construction of the historical buildings in San Luis Potosi were used impressive pink-like colored volcanic tuff rocks of the region, geologically defined as units of the "Cantera Ignimbrite", which belongs to the Tertiary acid volcanism of the San Luis Potosí-Volcanic Field (SLPVF) (Labarthe *et al.* 1982). These rocks locally grouped and known as "Cantera Rosa" show some variations in color from pink to dark pink, grey, brown and orange (Fig. 2). Although physical appearance of the rocks seems to be not very different, observing nearly and in detail, these building rocks have significant variations in texture, compositions and mechanical properties and these properties determine the resistance to weathering and deterioration, because they show a wide range of deterioration types, that include scaling (Fig. 3c), flacking (Fig. 3d), sanding, back weathering and coloration/discoloration (Fig. 3a and Fig. 3b; González-Sámano, 2012). Geological, petrophysical, geochemical, physical and mechanical studies were realized to know the causes of their weathering and deterioration and thereby to contribute to the care, preservation and if necessary restoration of buildings constructed with these rocks.

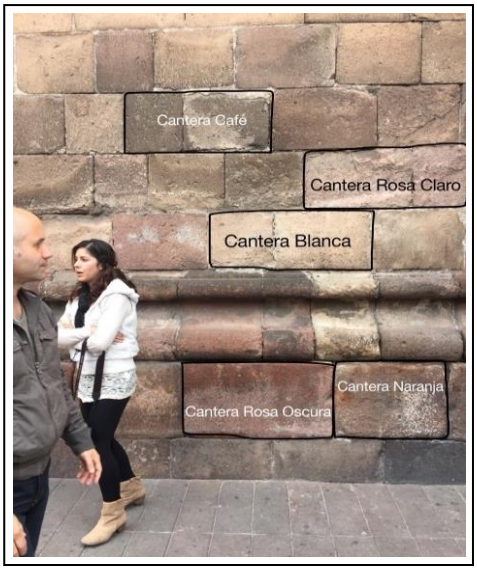

Fig. 2: North wall of the Templo del Carmen. Five variations of the Cantera Rosa can be distinguished here. Cantera Café (brown), Cantera Rosa Claro (light pink), Cantera Rosa Oscura (dark pink), Cantera Naranja (orange) Cantera Blanca (white).

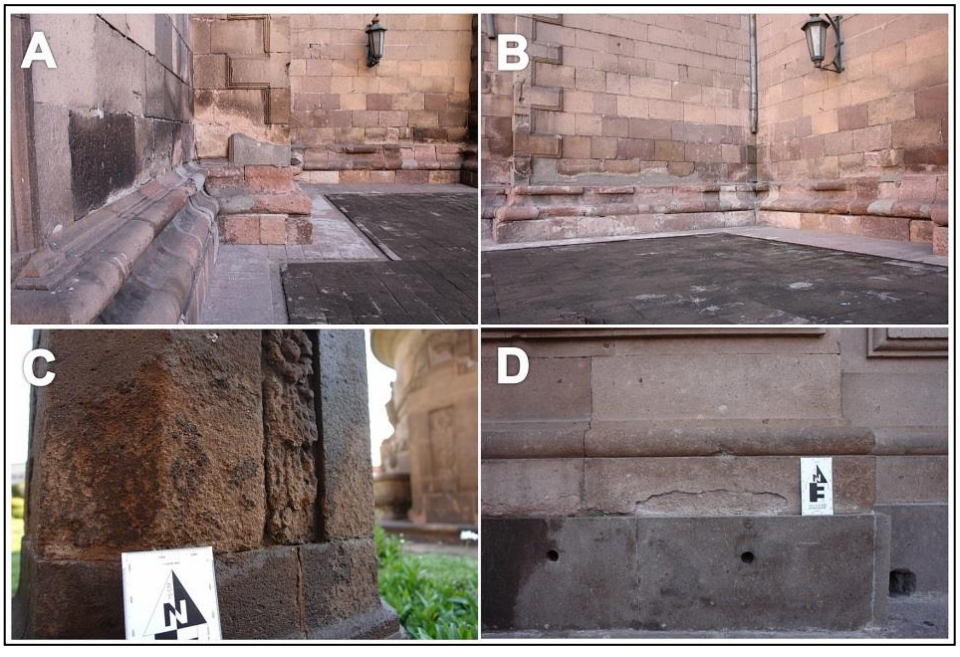

Fig. 3: Appearance of the different damage and deterioration types observed in the Cantera Tuff; a and b) Sanding, back weathering and coloration/discoloration in the San Carmen Church; c) Scaling and lost material in the Caja de Agua monument; d) Extensive flacking in lower parts of the south wall of the cathedral of San Luis Potosí.

2. Materials and methods

Five different types of Cantera tuff rocks of San Luis Potosí were analyzed petrographically, geochemically and geomechanically in laboratory. The analyzed tuff rocks are (Fig. 4): Cantera Rosa Clara, Cantera Rosa Oscura, Cantera Blanca, Cantera Café and Cantera Naranja. The petrographic analyses were performed on oriented thin sections and studied under a polarizing microscope. The percentage of minerals and matrix was measured using the point counting method. Mineralogical and geochemical analyses were performed using XRD, elemental carbon and sulphur analysis, and CEC analyses. Hydrostatic weighing was carried out to acquire the absolute and apparent density as well as the porosity of each Cantera of San Luis Potosí. The pore radii distribution was determined using mercury injection porosimetry. The hydric and hygric expansion of each rock was measured on cylindrical samples (diameter 15 mm, length 100 mm). For hydric expansion measurements the cylinders were completely immersed in distilled water. The compressive strength load was realized on cylinders with 40 mm in diameter and 20 mm in length using a servo-hydraulic testing machine with a stiff testing frame (3,000 kN/mm^2) and a load range up to 300 kN. The tensile strength measurements were determined by means of the ‘‘Brazilian test’. Finally to assess the salt weathering resistance of the five investigated tuffs, a salt-crystallization test was performed. For this test the samples were cut into cubes (6.5×6.5 cm) and were soaked in a 10% Na_2SO_4 solution. The samples stayed about 4 hours in the salt solution and then they were dried in an oven at 60°C - 70°C for 48 hours. This process was repeated as often as the sample allows. After each cycle, the samples are weighed to determine the loss of material. Photos documented the result of each cycle.

3. Results

3.1. Petrography

The Cantera Rosa in all their types has rhyolitic composition. The percentage of crystals and matrix vary of 35% - 65% in Cantera Rosa Clara, and Cantera Naranja, 30% - 70% in Cantera Rosa Oscura and Cantera Café and < 30% - >70% in Cantera Blanca respectively (Fig. 4). The main crystals are quartz with 45% in the Cantera Rosa Claro and Cantera Naranja, 35% - 40% in the Cantera Rosa Oscura and 30% in the Cantera Café. Alkali feldspar (mostly sanidine) is present in some samples but their amount vary of 35% - 40% in the Cantera Blanca, 30% in the Cantera Café (most as orthoclase) and < 30% in the Cantera Naranja Rosa Oscura and Rosa Claro. Cantera Naranja shows the highest content on plagioclase (microcline and anortite) crystals with more than 30%. The types Cantera Rosa Clara and Oscura show euhedral crystals (Fig. 4a and b) and Cantera Blanca, Café and Naranja have mostly anhedral crystals (Fig. 4c, 4d and 4e). Cantera Rosa Clara, Cantera Café and Cantera Naranja show a porphyritic hypocrystalline texture and Cantera Rosa Clara and Cantera Blanca have a vitrophyric texture (Fig. 4).

XRD analysis (Fig. 5) demonstrates that most of the samples are quartz-rich and they show in general a clearly acid composition. Cantera Naranja is the only sample containing additionally microcline and Cantera Rosa Oscura is the only having halloysite. Alkali feldspar (sanidine) is almost exclusively in the Cantera Blanca and the Cantera Café has practically only orthoclase (Fig. 4).

3.2. Petrophysical and moisture properties

Analyses for the five studied volcanic rocks were performed, in order to determine their density and porosity. The results of the determination of the porosity and density are presented in Tab. 1. As shown in the Tab. 1, the Cantera Café has a greater density than the others tuffs with an average of 2.611 and the lightest is the Cantera Rosa Oscura with 2.331 g/cm^3 respectively.

Tab. 1: Porosity, density and average pore radius of the studied rocks (López Doncel et al. 2016).

Sample	**Porosity** (%)	**Density** (g/cm^3)	**Average pore radius** (µm)
Cantera Rosa Clara	21.14	2.500	0.148
Cantera Rosa Oscura	17.88	2.331	0.476
Cantera Blanca	36.14	2.447	1.080
Cantera Café	25.45	2.611	4.029
Cantera Naranja	23.8	2.500	0.275

The Cantera Blanca has the highest porosity with 36.14% and the Cantera Rosa Oscura shows only 17.88% of porosity. A very interesting result is that the heaviest tuff (Cantera Café) has the biggest pore radius with an average of 4.029 µm

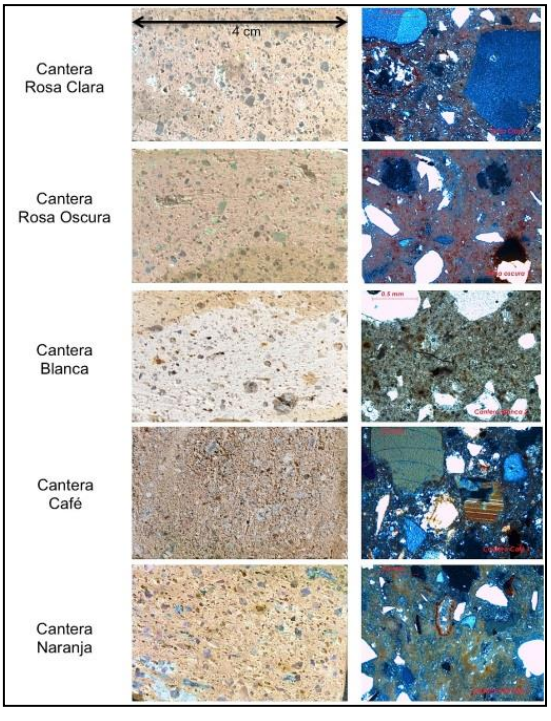

Fig. 4: Macroscopical photographs and thin section photomicrographs of the studied rocks (explanation in Text, obj. ×5, crossed nicols, except Cantera Blanca parallel nicols)

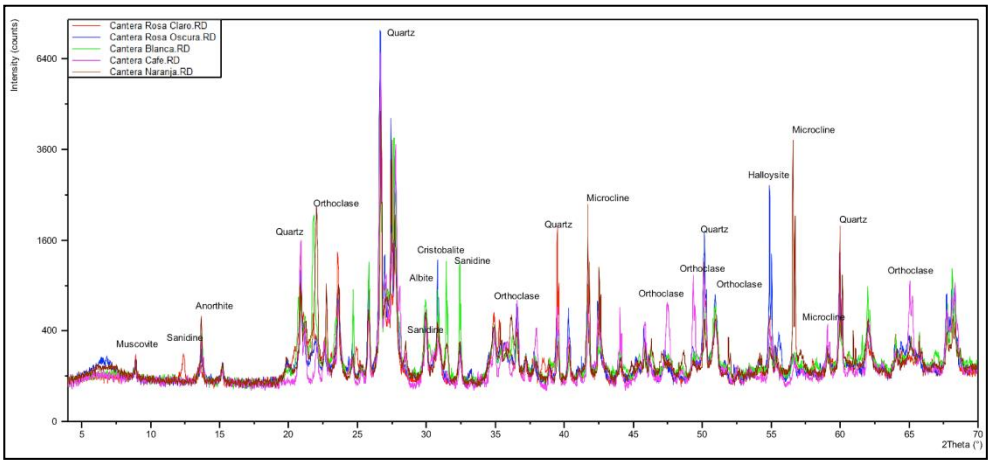

Fig. 5: XRD-diffractograms of the five analyzed volcanic tuff rocks of San Luis Potosí.

The distribution of the pore size in the analyzed volcanic rocks is unimodal by the Cantera Rosa Oscura, Cantera Blanca and Cantera Café (Fig. 6). These three samples rocks are dominated by macropores with pore sizes ranging from 1.0 to 10 µm (Fig. 6). As seen in Tab. 1 the Cantera Café has the biggest pores and it consists practically only of macropores. Cantera Rosa Clara and Cantera Naranja show a bimodal pore size distribution with a very similar porosity (Fig. 6, compare with Tab. 1).

All five samples were tested about the hydric expansion and all of them did not show any expansion and by the Cantera Rosa Claro and Cantera Naranja occur even contraction with values around -0,03 mm/m. The practically non-existent hydric expansion is securely associated to the poor content on clay mineral with average values of 0.3 meq/100 gr after CEC-analysis.

Tensile strength tests under dry and wet conditions were realized on four of the five selected samples and they show values that range from 1.28 MPa (wet) by the Cantera Blanca to 7.05 MPa (dry) by the Cantera Rosa Clara (Tab. 2). The results show that the Cantera Café with a tensile strength average value of 1.83 MPa under dry conditions and the Cantera Blanca with an average value of 1.44 MPa under wet conditions are the less resistant to the strength (Tab. 2). Under dry and wet conditions Cantera Rosa Clara was with values around the 5 MPa the hardest tuff.

Tab. 2: Tensile strength under dry and water-saturated conditions

Dry samples	**Tensile strength**, MPa			**Average**
Direction	X-axis	Y-axis	Z-axis	
Cantera Rosa Clara	7.05	4.86	4.13	5.34
Cantera Rosa Oscura	2.94	4.16	3.93	3.67
Cantera Blanca	2.51	2.11	2.16	2.26
Cantera Café	1.43	1.58	2.48	1.83
Wet samples	**Tensile strength**, MPa			**Average**
Direction	X-axis	Y-axis	Z-axis	
Cantera Rosa Clara	4.31	5.71	5.62	5.21
Cantera Rosa Oscura	1.97	1.79	2.72	2.16
Cantera Blanca	1.52	1.28	1.54	1.44
Cantera Café	1.62	1.33	1.99	1.64

The conducted salt bursting tests (Fig. 7) show that after 7 cycles Cantera Blanca lost 20% of its weight and Cantera Café and Cantera Rosa Oscura lost 10 % of their weight. After 14 cycles Cantera Blanca tuff was total destroyed and Cantera Café and Cantera Rosa Oscura had lost around 30% of their weight. Cantera Rosa Clara and Cantera Naranja showed after 14 cycles less than 5% of lost material and have resisted at the end of the test 47 and 48 cycles respectively (Fig. 7).

4. Discussion

The data from the conducted experiments on the natural building rocks show that the tuff with the highest absolute density is the Cantera Café (2.611 g/cm^3), and it has also the largest pore radii (4.029 µm with 78% of the pores between 1-10 µm), but contrary to expected. it is the rock with the lowest tensile strength (1.83 MPa by dry conditions), therefore the large pores may be the cause that this rock has a poor cohesion and likely poor resistance against weathering.

The tuff rock with the greatest porosity is the Cantera Blanca tuff (36.14%) and it was the less resistant against salt bursting. Laboratory experiments realized with rocks with similar values of porosity showed that these conditions favoured the water uptake by capillarity and with that increase the deterioration (López-Doncel *et al.* 2012, 2013).

The Cantera Rosa Clara tuff with a density of 2.5 g/cm^3, porosity of 21.14%, tensile strength values of 5.3 MPa and with the smallest pores (0.148 µm with 94% micropores) is the least-damaged rock under our test (salt bursting and strength). Under wet conditions all the samples were less resistant against strength and e.g. Cantera Café and Cantera Blanca reached values comparable to very soft rocks. As our experiments and tests show, Cantera Café and Cantera Blanca are the most sensitive rocks against salt bursting and tensile strength and under wet conditions both tuff rocks reach critical values of resistance. However, the moderate annual rain fall in this area of Mexico, located in a semi-arid region, seems to be the cause for just an incipient deterioration of this tuff rock after more than 400 years exposure. Recently, the historic center of San Luis Potosi was declared

world heritage site and plans to carry out extensive restoration work in different buildings and historical monuments have been initiated. It is precisely for this reason that the study of geological, geochemical and geomechanical properties of the rocks used play a predominant role in the care and restoration works.

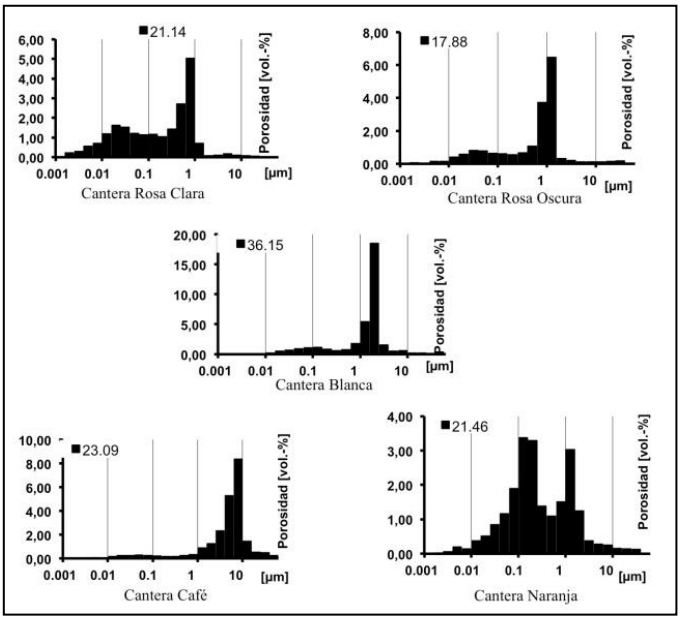

Fig. 6: Pore size distribution (MIP) of the five studied tuffs (López Doncel et al. 2016).

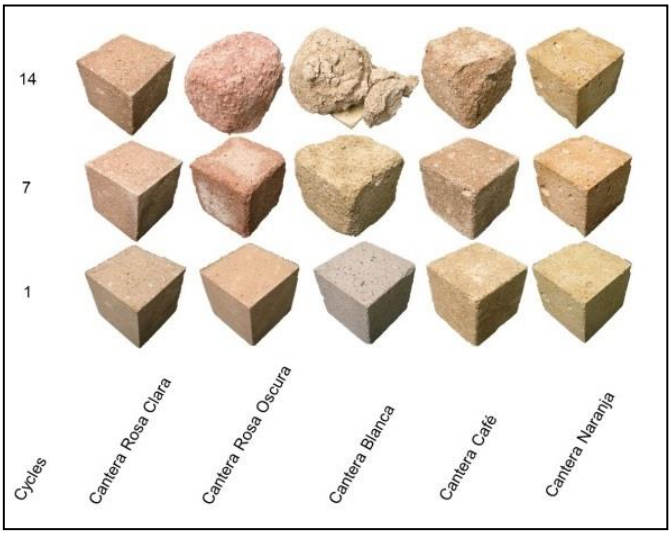

Fig. 7: Salt bursting test conducted on the analyzed tuff rocks of San Luis Potosí. Comparison between the five selected samples after 1. 7 and 14 cycles (López Doncel et al. 2016).

Acknowledgments

The authors want to thank for the financial support of the CONACyT (BC 191044 and CB 130282). DFG (Si-438/44-1) and the DAAD.

References

González Sámano, P.S., 2012, La Formación Cantera; su utilización, durabilidad y deterioro como roca natural de construcción. Ejemplos en edificios históricos de la ciudad de San Luis Potosí. Tesis de Licenciatura, Fac. de Ing – Inst. de Geología, UASLP, 131 P.

Labarthe-Hernández, G., Tristán-González, M.Y. and Aranda-Gómez, J.J., 1982, Revisión Estratigráfica del Cenozoico de la parte central del estado de San Luis Potosí, Instituto de geología y metalurgia, Universidad Autónoma de San Luis Potosí, Folleto Técnico No. 85, p.208.

López-Doncel, R., Wedekind, W; Dohrmann, R. and Siegesmund, S., 2012, Historical building stones of Guanajuato, Mexico: weathering, properties and restoration. - 12th International Conference on the deterioriation and conservation of Stones, Extend abstracts book.

López-Doncel, R., Wedekind, W; Dohrmann, R. and Siegesmund, S., 2013, Moisture expansion associated to secondary porosity. An example of the Loseros Tuff of Guanajuato, Mexico. Environmental Earth Science. 69:1189–1201. DOI 10.1007/s12665-012-1781-1.

López-Doncel, R., Cardona-Velázquez, N. and Wedekind, W., 2016, El rescate del patrimonio cultural pétreo de San Luis Potosí. Revista Universitarios Potosinos. 194:6-12.

Villar Rubio, J.V., 2000, El centro histórico de la ciudad de San Luis Potosí y la obra del ingeniero Octaviano Cabrera Hernández. Facultad del Hábitat, UASLP, 373 P.

Wedekind, W; López-Doncel, R.; Dohrmann, R. and Siegesmund, S., 2012, Hygric and hydric expansion of tuffs exclusively caused by clay minerals? - 12th International Conference on the deterioration and conservation of Stones, Extend abstracts book.

Wedekind W., López-Doncel R., Dohrmann R., Kocher M. andSiegesmund S., 2013, Weathering and deterioration of volcanic tuff rocks used as building stone causes by moisture expansion. Environmental Earth Science. 69:1203–1224. DOI 10.1007/s12665-012-2158-1.

This page has been left intentionally blank.

WEATHERING AND DETERIORATION OF BUILDING STONES IN TEMPLO MAYOR, MEXICO CITY

G. Mora Navarro[1*], R.A. López Doncel[2], M. Espinosa Pesqueira[3] and W. Wedekind[4]

Abstract

Templo Mayor Archaeological Site, the remains of the ancient ceremonial precinct of Tenochtitlan, the Aztec city constructed between the 14th and the 15th century, partially destroyed and buried after the Spanish Conquest, is located in the Historical Center of Mexico City. Because of its geological setting in the center of the Trans-Mexican Volcanic Belt, the city was built mainly from volcanic stones. Systematic excavations in the site have been carried on since late 1970s and the extreme pollution of the metropolitan area, the subtropical climate, hydrological conditions, and frequent seismic activity of the region, have accelerated degradation process of the stone structures exposed. In this paper, different aspects of weathering and stone deterioration of the Edificio B "Altar de cráneos", a remarkable structure because of the carved stones in its facades and the variety of lithic material types, are discussed. Geochemical characterization by XRF onsite, ICP-MS, ICP-OES, XRD SEM/EDS, salts identification; petrophysical properties investigated by means of thermographic analysis and previous studies of density, porosity, pore radii distribution and environmental data supported the diagnosis. A relationship, between lithic varieties, water transport properties, swelling, shrinking pressure, salt crystallization, specific weathering forms, orientation and previous conservation treatments was deduced. The obtained results help in the understanding of the different weathering process to support adequate conservation methods and materials.

Keywords: stone weathering, petrophysical properties, environmental conditions

1. Introduction

The ceremonial precinct of the Postclassical Aztec city, Mexico-Tenochtitlan, now Templo Mayor Archaeological Site, is located in the Historical Center of Mexico City which was declared by UNESCO a World Heritage Site in 1987. The site was named after the 'Great Temple' a pyramid with 100-80 meters at its base and according to the historical records, approximately 45 meters high, with two sanctuaries on top dedicated to Huitzilopochtli,

[1] G. Mora Navarro*
National Coordination of Conservation of Cultural Heritage (CNCPC), Mexico City, Mexico
gabrielamoranavarro@gmail.com

[2] R.A. López-Doncel
Geological Institute, Autonomous University of San Luis Potosí, San Luis Potosí, Mexico

[3] M. Espinosa Pesqueira
National Institute of Nuclear Research (ININ), Estado de México, Mexico

[4] W. Wedekind
Geoscience Centre of the University of Göttingen, Germany

*corresponding author

god of war and Tlaloc, god of rain and agriculture. Archaeological studies point that it was first built as an earthen and wooden structure, when the city was founded in 1325, and enlarged six times, a common practice in pre-Columbian architecture by which buildings were periodically modified, according on political changes and ceremonial traditions (Matos Moctezuma 2014). The precinct of Tenochtitlan was destroyed after the Spanish Conquest in 1521, and remained buried until the second half of the 20th century. Although some archaeological surveys were conducted at the end of the 19th century and early 20th century, the systematic excavations at the site began in 1978 with the fortuitous discovery of the monolith of the deity Coyolxauhqui.

The Edificio B, a rectangular platform of approximately 7.8 meters E-W, 5.48 meters N-S, and 2.4 meters high, with a distinctive decoration of carved skulls in its façades, was excavated in the early 1980s (Fig. 1). Because of its location at the Northwest side of the Great Temple and its decoration, the Edificio B has been interpreted as representative of the *Mictlampa*, the land of the dead in the Mexican cosmovision. The construction presents different stages, the last one being temporarily associated with the sixth construction stage of the Templo Mayor, during the ruling of the *tlatoani* Ahuízotl (1486-1502 AD; Matos Moctezuma 2003).

Fig. 1: Edificio B, Templo Mayor Archaeological Site.

As a result of more than three decades of exposure to environmental conditions of Mexico City, different weathering effects are visible in the Edificio B. In alteration processes Geochemical and petrophysical properties of the stones, interaction within constituent materials, and the building orientation have played a crucial role in the alteration processes.

2. Properties of building materials

The main building materials used in Templo Mayor Architecture were *tezontle*, an extrusive volcanic basaltic andesite scoria, basalt, andesite, limestone, adobe, wood, and lime mortar (López Luján *et al.*, 2003). *Tezontle* was also the main building stone used in the Edificio B, the core, the blocks of the walls, the staircase that leads to the top of the structure, and most of the carvings were made of it. Macroscopically its voids are predominantly 10 millimetres in diameter, microscopically the walls of the cellular rock fabric show acicular plagioclase crystals and isolated pyroxene and amphibole crystals. Geochemically it contains approximately 60% SiO_2, 12% Al_20_3, 8% MgO, 5% Fe_2O_3, 4% CaO and 3% Na_2O. Petrophysical properties reported for this material are 35 to 66% porosity in non-

weathered conditions due to its heterogeneous cellular structure, very low bulk density (1.4 g/cm^3), no measurable hydric swelling but a relatively high thermal dilatation coefficient (7.0×10^{-6} K^{-1}), and compressive strength ranges from 12 to 32 N/mm^2 under dry conditions (Acevedo-Dávila *et al.*, 2007, Wedekind *et al.*, 2011).

Tuff stones were also used in the carvings, mostly in the North façade, and rarely basalt. The variety of pyroxene andesite tuffs of intermediate composition and dacite tuffs of acid composition show high hydric swelling and thermal dilatation coefficients that increase in weathered surfaces. Through petrographic observation and XRD, SEM/EDS analysis it was possible to characterise alteration of feldspars and some degradation products.

The Edificio B was originally covered with lime render, which is better conserved in the South façade where carvings still show several layers with traces of polychrome decoration. The loss of this finish that protected the stone from weathering is higher in the North façade. In addition, the loss of architectural elements and irregular excavation in the inside part of the structure favour water accumulation.

3. Weathering and stone decay

3.1. Environmental conditions

Systematic excavations in Templo Mayor during the 1980s suddenly exposed the structures to a highly polluted atmosphere. In the mid-1970s Mexico City was considered one of the most polluted cities of the world, and at the end of the 1980s emissions exceeded the recommendations contained in the Air Quality Guidelines of the World Health Organization (WHO). Even though a significant reduction of pollution levels has been achieved since 1990, when environmental pollution control policies were implemented, current levels of sulphates, nitrate, carbon monoxide, pollutant particulates, and ozone in México City metropolitan area, remain high. Mexico City has a temperate highland tropical climate with dry winters and summer rains. Downtown area average annual temperature varies from 12 to 18ºC, with total annual rainfall between 600 and 950 millimetres. This area exhibits the urban heat island phenomenon (UHI), induced by the concentration of ozone and aerosol particles, transported by the main wind flows that follow a north-south direction. Wet deposits in downtown Mexico City are predominantly acide (*pH* = 5-6.4), total deposition of the most abundant anions in the last two years reached 5.93 g/m^2 for sulphates, followed by a deposition of 4.85 g/m^2 of nitrates and 0.97 g/m^2 of chlorides (Secretaría del Medio Ambiente, 2015).

It is well known that areas that remain wet for long periods promote adhesion of particles. Deposition of transition metal oxides particles promotes oxidation reactions and favours the adhesion of pollutants that once fixed in the surface react with moisture and acid rain. The presence of sulphates and nitrates in regions of high humidity increases the solubility of metals and their potential reaction (McAlister *et al.*, 2008). These conditions also generate nucleation areas with predominant growth of sulphates that show particularly aggressive crystallization (Charola and Ware 2002, Sabbioni 2003, Charola *et al.*, 2007, Graue *et al.*, 2013, Wiese *et al.*, 2013).

In addition, ground subsidence that affects Mexico City as the result of the decreasing underground aquifer water level and the behaviour of the highly compressible lake basin sediments (compression index up to 10, with water content up to 400%, and plasticity index over 300%), has led to a rate of -92 to -115 millimetres per year (Cabral Cano *et al.*, 2011),

causing severe structural problems in buildings. Subsidence has caused an inclination of 4 degrees north of the Edificio B, and consequently, compressive stress on the North façade of the building has produced cracks. Inclination also reduces insolation which slows water evaporation and contributes to the accumulation of polluting particles in the lower zone. Moreover, constant seismic activity increases significantly structural stress, considering that waves are accelerated and amplified in lacustrine soils (Díaz Rodríguez 2006).

3.2. Weathering effects on stone materials

Weathering effects observed on the façades of the Edificio B are the result of complex decay phenomena that affect volcanic stones by different mechanisms. As a result of the environmental exposure, tuff stones are less preserved than vesicular basalts or *tezontle* that shows significant resistance to weathering. Interaction of pollutants with stone materials is higher on the North façade due to the direction of prevailing winds and low insolation that leads to high humidity conditions. In this façade only 18% of lime renders are preserved, 12% of the surface remained wet by October when rainy season was already over, and 9% showed contour scaling, weathering form frequently associated with salt efflorescence. In the East façade lime renders are preserved on 20% of the surface, while the areas affected by weathering processes represent less than 1%. The South facade shows the best condition, 51% of the surface preserve lime renders and remains of polychrome decoration, only 0.3% of the surface is affected by weathering processes (Fig. 2).

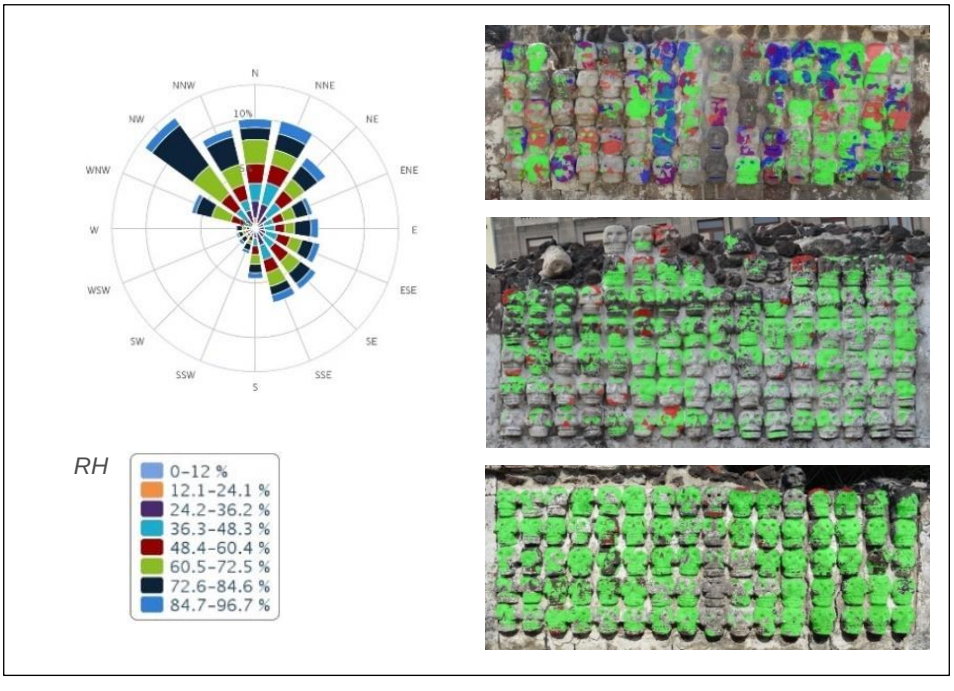

Fig. 2: RH values according to the direction of prevailing winds, weathering (red), wet areas (blue), and lime renders preserved (green), on the North, East and South façades.

Exposure and critical property values as thermal dilatation, hydric swelling, anisotropic behaviour or compressive strength, as well as cementation also define building stones resistance to weathering and weathering forms (Wedekind *et al.*, 2011). Within tuff stones while exposure to wet-dry conditions increases weathering effects by salts crystallization and erosion, prolonged wetness accelerates decay by the presence of soluble salts and pollutants that promotes an acidic medium causing the chemical decomposition of feldspars and oxidation. On the other hand, ion migration by dissociation of alkaline components of mortars and the dragging of calcite particles promote concentration of high *pH* solutions into the tuff stones pores. These alkaline mediums are particularly aggressive for acidic tuffs causing the dissolution of silica and plagioclase.

Hygroscopic behaviour significantly determines the resistance of building stones to weathering conditions because it prevents or promotes water, soluble salts and contaminants transport, leading to the mentioned degradation mechanisms. Such behaviour is controlled by the amount of swelling clay minerals and the size and distribution of active capillary pores (micropores of 0.1 to > 100 μm) (Ruedrich *et al.*, 2011, López-Doncel *et al.*, 2013, Wedekind *et al.*, 2013). The concentration of capillary pores in the weathered zones of stones increases and thus the penetration and retention of water, while hardness decreases. Therefore, interaction between materials with marked differences in thermal and hygroscopic behaviour accelerates decay of the more hygroscopic and less resistant ones, as can be observed in tuffs surrounded by vesicular basalts in the North façade, under prolonged wetness conditions. Through thermographic analysis it was possible to confirm that the loss of lime render finish increases significantly differential thermal stress in the most exposed carvings (Fig. 3).

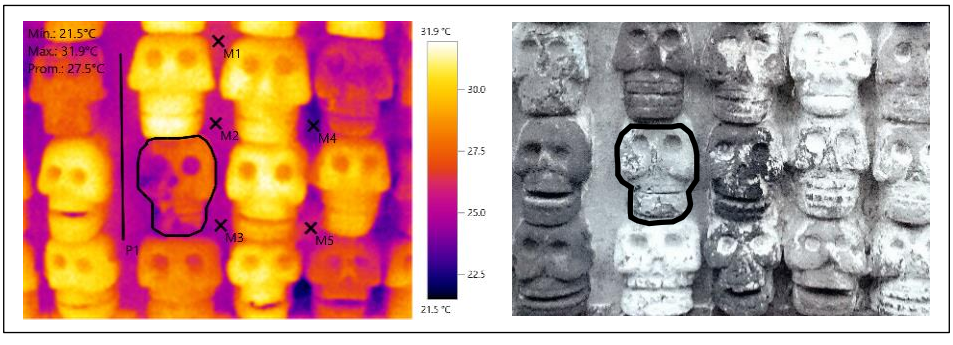

Fig. 3: Thermal image showing differences in lime mortar junctions, tuff and basalt carvings behaviour.

Since erosive process affects dacitic and andesitic tuffs in the East façade, scaling, detachment and disintegration are the weathering forms observed on similar varieties in the North façade. Poor welded andesitic tuffs in the North façade are highly affected by salt crystallization which causes granular disintegration of the matrix, hornblende phenocrysts loss and the consequent collapse of the surrounding material. Instead pyroxene dacitic tuffs in the North façade show a typical weathering form starting with crust formation and scaling approximately 0.5 cm from the surface, combined with back-weathering, microcracks and salt crystallization (Fig. 4a/I). In contrast same type of tuff stones in the East façade shows erosive weathering effects like sanding (Fig. 4b/II).

On the other hand, *tezontle* shows significant resistance to both wet-dry conditions and prolonged wetness because it almost does not show hydric swelling due to the fact that linked pore space areas are sporadic within the material. Nevertheless, microscopically alteration processes of the plagioclase in the rock fabric cell walls could be observed, as well as salt crystallization on the surface. Macroscopically the most common deterioration observed in this volcanic rock type is due to fractures and cracks because of its moderate hardness and high thermal dilatation (Fig. 4c/III).

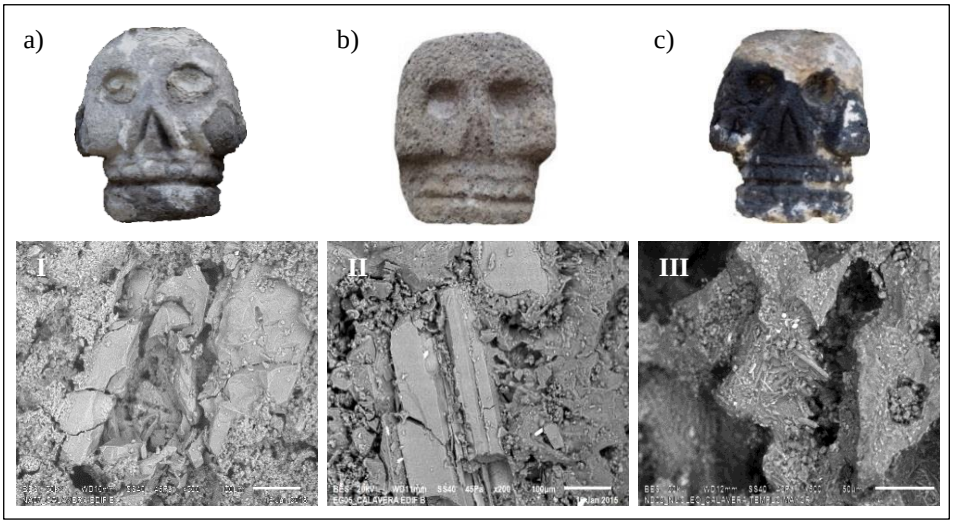

Fig. 4: Different weathering effects macroscopically and microscopically. SEM images; a/I) dacitic tuff skull in the North façade (200×100 µm); b/II) dacitic tuff skull in the East façade (200×100 µm); c/III) tezontle skull in the North façade (500×50 µm).

4. Previous treatments and future perspectives

Some materials used in previous conservation treatments in the Edificio B, have proven to have long-term negative effects, particularly the application of consolidating and water-repellent products during the 1980s and 1990s, such as Curasol, Mowilith DM4, Primal AC33, Wacker 19OL, among others (Matos Moctezuma 1993, Franco Brizuela 1990). Some negative effects of these products are related with their limited penetration and surface hardening, which has reduced the evaporation and solutions transfer capacity of the stones, favouring salts cryptocrystallization and detachment of the hardened layers.

Future interventions should consider that conservation of the structure will not be achieved through isolated treatments applied on the building materials. For instance, it is a priority to stop the transport of water salts and contaminants into the structure, a challenging task taking into account the environmental and underground conditions. Solutions should look up for balancing the system attending structural and water conduction problems, as well as reducing the negative effects of building materials interaction and exposure, considering differences in their proprieties and condition.

5. Conclusions

The exposure conditions and the distribution of building materials in the Edificio B has led to the accelerated decay of the North facade. In the alteration process a relationship between lithic varieties properties such as water transport, hydric swelling, shrinking pressure, thermal dilatation, and specific weathering forms, can be deduced. In addition to the intrinsic properties of the materials, exposure and previous conservation treatments play an important role in accelerating the deterioration processes. The obtained results help in the understanding of the different factors involved in the weathering process and to recommend conservation methods and materials. To slowdown deterioration of building stones in challenging environments such as Templo Mayor Archaeological Site, a multifactorial and interdisciplinary approach to conservation problems is needed considering that structures are dynamic systems that require constant evaluation of their response to changing environmental conditions.

Acknowledgements

We would like to thank Maria Barajas Rocha, Conservator at Templo Mayor Archaeological Site, Irlanda Fragoso Calderas, Chairperson at Department of Archaeological Conservation at the National Coordination of Conservation of Cultural Heritage, and Consejo Nacional de Ciencia y Tecnología (CONACyT) Bilateral Cooperation Project 191044 and Science Project 130282 to support this research.

References

Acevedo Dávila, J., Torres Treviño, L. M. and Gómez, L. Y. Z., 2007, Tezontle aggregate substitute optimization in building blocks mixture, Electronics, Robotics and Automotive Mechanics Conference (CERMA), Cuernavaca, IEEE, 307–311.

Cabral Cano, E., Díaz Molina, O. and Delgado Granados, H., 2011, Subsidencia y sus mapas de peligro : Un ejemplo en el área nororiental de la Zona Metropolitana de la Ciudad de México, Boletín de la Sociedad Geológica Mexicana, 63 (1), 53-60.

Charola A. E. and Ware, R., 2002, Acid deposition and the deterioration of stone: a brief review of a broad topic, in Natural stone, weathering phenomena, conservation strategies and cases studies, Siegesmund, S., and Vollbrecht, A., (eds.), Geological Society of London, Special Publications, 205, ISBN-13 978-1862391239, 393–406.

Charola, A. E, Pühringer, J. and Steiger, M., 2007, Gypsum: a review of its role in the deterioration of building materials, Environmental Geology, 52, 339–352.

Díaz Rodríguez, J. A., 2006, Los suelos lacustres de la Ciudad de México, Revista Internacional de Desastres Naturales, Accidentes e Infraestructura Civil, 6 (2), 111-129.

Franco Brizuela M. L., 1990, Conservación del Templo Mayor de Tenochtitlán, Asociación de Amigos del Templo Mayor, ISBN 9789684980679, 169pp.

Graue, B., Siegesmund, S., Oyhantcabal, P., Naumann, R., Licha, T. and Simon, K., 2013, The effect of air pollution on stone decay: the decay of the Drachenfels trachyte in industrial, urban, and rural environments a case study of the Cologne, Altenberg and Xanten cathedrals, Environmental Earth Sciences, 69, 1095-1124.

López-Doncel, R., Wedekind, W., Dohrmann, R. and Siegesmund, S., 2013, Moisture expasion associated to secondary porosity: an example of the Loseros Tuff of Guanajuato, México, Environmental and Earth Sciences, 69 (4), 1189-1201.

López Luján, L., Torres, J., and Montúfar, A., 2003, Los materiales constructivos del Templo Mayor de Tenochtitlán, Estudios de Cultura Nahuatl, 34, 137-167.

Matos Moctezuma, E., 1993, Arqueología y Conservación en el Templo Mayor de Tenochtitlan, Actas de la Reunión 6-13 Abril 1986, Hodges, H., (ed), Mexico, Santa Monica, Getty Publications, Instituto Nacional de Antropología e Historia, ISBN 978089236216, 162-184.

Matos Moctezuma, E., 2003, Vida y Muerte en el Templo Mayor, Fondo de Cultura Económica, ISBN 9681657128, 160pp.

Matos Moctezuma, E., 2014, A un siglo del descubrimiento del Templo Mayor, Arqueología Mexicana, 56, 8-32.

McAlister, J. J., Smith, B. J., and Török, A., 2008, Transition metals and water-soluble ions in deposits on a building and their potential catalysis of stone decay, Atmospheric Environment, 42 (33), 7657-7668.

Ruedrich J., Bartelsen, T. Dohrmann, R. and Siegesmund, S., 2011, Moisture expansion as a deterioration factor for sandstone used in buildings, Environmental and Earth Sciences, 63, 1545-1564.

Sabbioni, C., 2003, Mechanism of air pollution damage to stone, in The effects of air pollution on the built environment, Brimblecombe, P., (ed.), Air Pollution Reviews 2, 63–88.

Secretaría del Medio Ambiente (SEDEMA), 2015, Data Base - Red de Depósitos Atmosféricos Ciudad de México, updated December 2014, (www.aire.df.gob.mx/default.php?ops=”aKBk”, accessed 15th May, 2015).

Wedekind, W., Ruedrich, J. and Siegesmund, S., 2011, Natural building stones of Mexico-Tenochtitlán: their use, weathering and rock properties at the Templo Mayor, Palace Heras Soto and the Metropolitan Cathedral, Environmental and Earth Sciences, 63, 1787-1798.

Wedekind, W., López-Doncel, R, Dohrmann R, Kocher, M., and Siegesmund, S., 2013, Weathering of volcanic tuff rocks caused by moisture expansion, Environmental and Earth Sciences, 69 (4), 1203-1224.

Wiese, U., Behlen, A. and Steiger, M., 2013, The influence of relative humidity on the SO2 deposition velocity to building stones: a chamber study at very low SO2 concentration, Environmental and Earth Sciences, 69 (4), 1125-1134.

DECAY PRODUCTS OF THE KERSANTITE BUILDING STONE IN THE MONUMENT OF THE SMALL STAIRCASE AT THE KALEMEGDAN PARK (BELGRADE, SERBIA)

N. Novaković[1], M. Franković[2*], V. Matović[3], K. Šarić[3] and S. Erić[3]

Abstract

The monument named Small Staircase at the Kalemegdan Park in Belgrade was built in 1903 in the Baroque style. It is the first and unique architectural structure made of kersantite stone. The monument is located in the central and oldest part of Belgrade, in one of the most polluted parts of the city. Although this rock type belongs to the category of resistant stones, after decades of exposure to environmental conditions it has started to show signs of deterioration. This study presents and discusses optical microscopy and SEM-EDS analyses of both the built stone and its decay products all in order to explain decay processes. Visual observation of the built stone shows the presence of the following decay forms: scaling, flaking to sanding, and, as most dominant, "red weathering crust". The results of our study suggest that the most significant components of the brown-reddish crust are Fe-oxide/hydroxide and spheroidal particles. The Fe-rich decay products are the result of interaction between the rock forming minerals and environmental factors, especially atmospheric pollutants.

Keywords: Kersantite, decay, scaling, discoloration, Iron oxide/hydroxide, spheroidal particles

1. Introduction

1.1. General words

Stone is an important building material of culture heritage worldwide. Although limestone and sandstone are the most commonly used building stone types, igneous rocks that include a wide range of siliceous and crystalline lithological types (e.g. granites, gabbros, kersantite, basalt etc), known in literature as "granites", are also often used, mostly because they are more durable to weathering, especially in urban polluted atmospheric conditions. However, despite the fact that igneous rocks are highly resistant to aggressive action of different agents in the environment, these hard and low porosity rocks may show signs of decomposition after installation in buildings, as it is reported for granitic rocks (Schiavon

[1] N. Novaković
Cultural Heritage Preservation Institute of Belgrade, Belgrade, Serbia

[2] M. Franković*
Central Institute for Conservation in Belgrade, Serbia
maja.frankovic@cik.org.rs

[3] V. Matović, K. Šarić, S. Erić,
Department of Mineralogy, Crystallography, Petrology and Geochemistry, University of Belgrade and Faculty of Mining and Geology, Belgrade, Serbia

*corresponding author

1993; Smith *et al.*, 1993; Schiavon *et al.*, 1994). These transformations are related to intrinsic characteristics of rocks (mineral composition, fabric and soundness) and extrinsic such as conditions of application, kind of surface finish, and environmental conditions. For this reason, the assessment of decay of a built element should be considered from the aspect of intensity and distribution of alteration features (Fitzner and Heinrichs 2002), and with respect to the exposure age of the element (Alves and Sanjurjo-Sánchez 2011).

Frequent decay forms of granitic and other igneous rocks used for monument constructions are scaling of stone surface and sanding and discoloration, but "red weathering crust" is considered as one of the most aggressive forms of deterioration (e.g. El-Gohary 2009). Taking into consideration that the colour of "granites" is one of the most important characteristics that define their aesthetic value. It is known that the formation of superficial deterioration crusts is a consequence of interaction between the polluted environment and stone (Sabbioni 1995). When "granitic" monuments are exposed to the aggressive environment, especially when the stone contains Fe-minerals, such as pyrite, magnetite, ilmenite, the colour of built stone elements can be changed. This discoloration is commonly caused by deposition of atmospheric pollutants and oxidation reactions that occur during weathering (Benavente *et al.*, 2003; Del Lama *et al.*, 2015).

Kersantite is an igneous rock green in colour, siliceous in composition and granular in texture, and due to these characteristics it belongs to the "granitic" group of rocks. It was extensively used for building prominent Belgrade edifices in the first half of the 20th century. After more than 100 years of exposure to environmental conditions, deterioration forms can be observed on the most important kersantite monument, the Small Staircase. In order to determine the state, morphology and cause of the kersantite decay, this study investigates the petrographic properties of pristine rocks taken from the quarry and the composition of surface crusts of the stone built in the monument. Using these data, the relationship between the compositions of rocks and decay products is considered in an attempt to clarify the factors of degradation of the kersantite built in the monument.

1.2. The monument Small Staircase

The monument Small Staircase, built in 1903, is located in the Kalemegdan park on the Belgrade fortress, in the city center. It was constructed in the Neo-baroque style, according to the plan drawn by Jelisaveta Načić, the first woman-architect in Serbia. The monument has two semi-circular sections and a rest platform from which one enters the promenade plateau of the Kalemegdan park. The frontal part of the object is represented by shallow blind arcade with a fountain and a central ornament in the form of a bronze lion's head (Fig. 1a). The monument is made entirely of stone elements and panels of kersantite interconnected with cement mortar. The visible surfaces of stone (total of 392 visible elements) are rustically processed, bush-hammered or carved with chisel, whereas elements of the tread have visible sawn surfaces. The shape and dimensions of the stone elements are adapted to the slope and to the angle of the stairway.

The kersantite originates from the quarry called Tešića Majdan (Fig. 1b), which is located in the Ripanj village, near Belgrade. In geological terms, the rock mass appears in the form of an NW-SE oriented elongated lens that crops out in the length of 200 m and along a maximum width of approximately 50 m (Pavlović *et al.*, 1977). The rock mass is intersected in blocks by a system of faults, parallel fissures and cracks, which facilitated the decade-long exploitation of stone.

Fig. 1: a) Small Staircase monument; b) Tešića Majdan quarry.

2. Methodology

In terms of petrographic characterization of primary (geological) characteristics of the kersantite built stone, five different samples were taken from the Tešića Majdan quarry. Petrographic analyses were performed by studying thin sections under a transmitted-light polarized microscope (type Leica DMLSP). The morphology and chemical compositions of the phases from the surface decay crust of the studied kersantite were analyzed by a JEOL JSM-6610LV scanning electron microscope (SEM) with an X-Max EDS. The samples were covered with gold using a BALTEC-SCD-005 sputter coating device. In order to examine the nature of stone damage, the classification and registration was done by mapping of the existed decay forms of the monument. According to morphological criteria and internationally accepted classification scheme developed by the Aachen working group "Natural Stones and Weathering" (Fitzner *et al.* 1995), all decay forms are located on a mm–cm scale. Determination of the weathering forms types were harmonized with the ICOMOS-ISCS glossary on stone deterioration patterns (Vergès-Belmin 2008).

3. Results and discussion

3.1. Petrographical properties of the Tešića Majdan kersantite

The studied kersantite has different texture and variable contents of the main mineral phases. It is a green rock with the texture that varies from fine- to coarse ophitic, whereas its fabric is massive (Fig. 2a). The main minerals are plagioclase, biotite, augite, and the secondary phases are chlorite, calcite and epidote. Accessories are apatite, zircon, opaque minerals and sphene. Plagioclase (albite) is the most abundand mineral. It appears as idiomorphic to allotriomorphic laths which are intersected and make an ophitic network. Their sizes range from 0.5 mm to 3 mm in lenght. The plagioclase grains are rarely fresh, and are often transformed to calcite and epidote. Biotite is developed as sheets up to 10 mm in length (Fig. 2b). Augite is allotriomorphic and is situated within the interstitial space between plagioclases. Both femic minerals, biotite and augite, are altered into chlorite and epidote, mostly along their rimes. Chlorite is developed along the cleavage planes or it attacks the entire grains of both mentioned primary minerals, whereas calcite appears along the twinning lamellae of albite and fills microcracks within the rock ground mass.

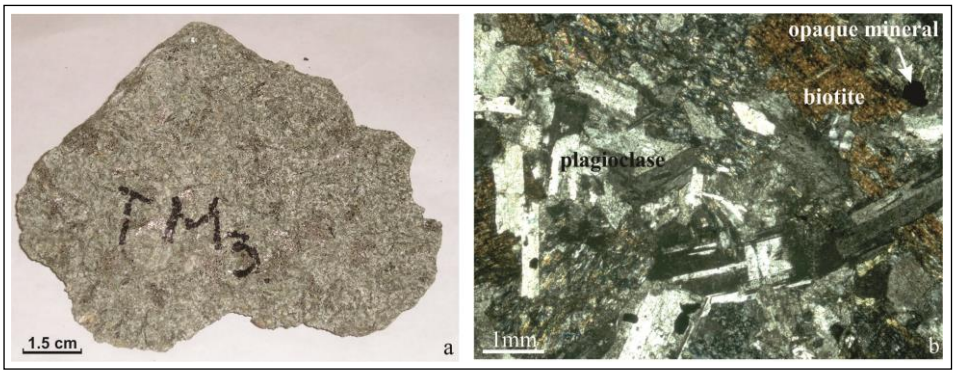

Fig. 2: Macroscopic (a) and microscopic (b) appearance of the studied kersantite.

3.2. SEM-EDS analyses of decay stone surface crusts

The SEM-EDS analyses of the surface crusts confirmed that this sample contains the same mineral association as the sample from the quarry: chloritized biotite (Fig. 3a), sodic plagioclase - albite, pyroxene, epidote, as well as minor quantities (up to 1 vol.%) of pyrite, titanite (Figures 3b) and apatite.

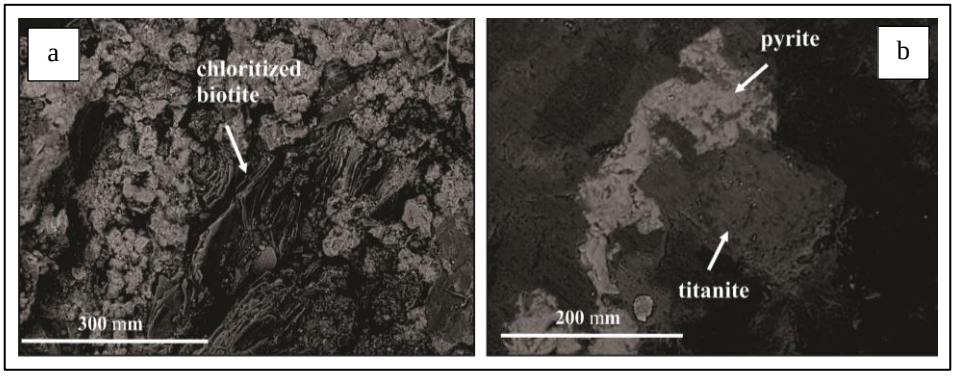

Fig. 3: SEM images of the analysed particles: a) sheets of chloritized biotite; b) accessory and secondary mineral phases: titanite, pyrite and Fe oxide/hydroxide.

Iron oxides and/or hydroxides are developed as granular aggregates with the size of individual grains of up to 30 μm and may represent the primary magnetite, or they appear as dendritic aggregates (Fig. 4a) which are probably the products of pyrite or magnetite alteration. Beside the mentioned constituents, two types of spheroidal particles are found, too. The first one is homogeneous and aluminosilicate in composition, whereas the second represents Fe-oxides and/or hydroxides with a puzzle like surface (Fig. 4b).

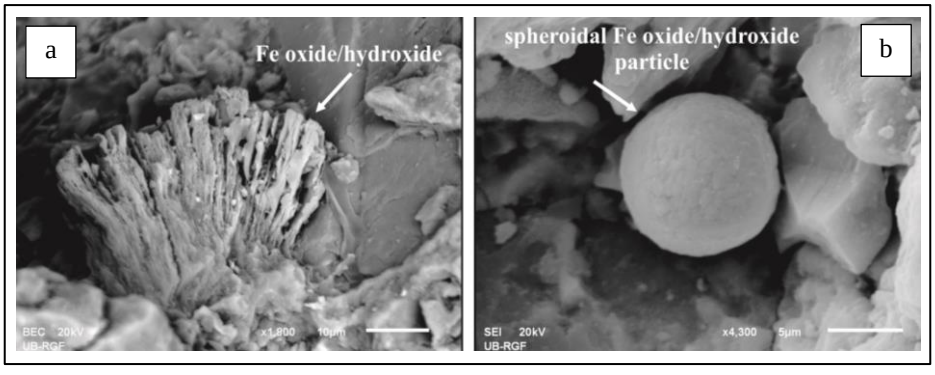

Fig. 4: SEM images of the analysed particles: a) accessory and secondary mineral phases: titanite, pyrite and Fe oxide/hydroxide; b) spheroidal Fe oxide/hydroxide particle probably of artificial origin.

According to Król and Fiałkiewicz-Kozeil (2014), the spheroidal inorganic particles (aluminosilicate particles and Fe spherules) probably originate from industrial activities, mainly from coal combustion. From the petrological standpoint, there are no substantial differences in mineral composition of the damaged crusts and the pristine rock samples taken from the quarry. Additionally, the surface crust contains spheroidal Fe-particles and morphologically specific Fe oxides/hydroxides.

3.3. Decay forms

Weathering forms on the kersantite blocks/elements show a wide range of types and intensity of damages. The main weathering forms were classified into the following groups: loss of stone material, discolouration and detachment (Fig. 4).

Loss of stone material is generally presented as surface recession and relief as well as missing parts. It is manifested by loosening and separation of small or large pieces of stone, mostly found in the stairs and the angular columns (Fig. 5). Detachment is a dominant form of decay. It appears in the form of contour scaling, flaking, granular disintegration and crust detachments (Fig. 5). Contour scaling occurs in the form of parallel surface crusts up to 10 mm in thickness. On numerous stone elements, original surfaces, preserved in whole or in part, are substantially physically separated from the substrate. Flaking and granular disintegration are supporting forms of the contour scaling decay. After delamination of the surface crust, the re-opened surface undergoes flaking and granular disintegration up to 2 cm in depth (Fig. 5a). Flakes size varies in mm-cm scale, whereas granular disintegration is manifested in the sanding form. The last decay form causes rounding of originally sharp corners and edges of the stone elements, especially on stair treads.

Almost all visible bush-hammered finish surfaces are characterised by the decay forms mentioned above. It is known that bush-hammering alters the physical properties of natural stone (porosity and water absorption), and causes decreasing in resistance to the aggressive action of water/moisture and frost. Besides their rustic appearance, bush-hammering forms a weakened surface layer and increases the natural porosity of a rock. After construction, this artificially created weakened zone turns into surface crusts that have a tendency to separate from the stone very quickly. Detachment of stone surface crusts is absent on chiselled stone surface (central part of the monument, Fig. 5).

Fig. 5: Decay forms of the kersantite stone elements: loss of stone mass as missing corner part, scaling and detachment of the surface crust, discoloration; a) detail of flaking and sanding of stone surface.

On the other side, the remarkable form of the kersantite degradation is discoloration or "red weathering crust" (Fig. 5). Whereas the natural colour of kersantite is green, the colour of the decayed stone surface of the built stone is intensive reddish-brown. The rock colour is affected by the presence of iron minerals contained therein (Nakashima *et al.*, 1992), what suggests that the studied kersantite becomes reddish-brown due to alteration and weathering of its iron minerals. It is probably caused by the abundance of oxygen, water (rain, snow, moisture) and because of other physical and chemical factors in the urban environment that had strong influence over time. Chemical decay of some Fe-mineral phases from the studied surface crusts is not complete. Thus, coarser grains of pyrite (Fig. 3b) are relatively fresh (SEM-EDS analysis shows the presence of oxygen), whereas the presence of Fe oxides/hydroxides in forms of dendritic or fan-like aggregates (Fig. 4a), which are not typical for the natural rocks, confirm the role of significant chemical alteration. Nevertheless, the Fe-spheroidal particles are engaged in this chromatic modification of the kersantite, too.

4. Conclusions

Changes in the state of conservation of the kersantite stone used for the Small Staircase monument in Belgrade due to degradation have been investigated and the decay forms and mineral composition have been determined. The following conclusions can be drawn from this study:

- Chloritization and calcitization as alteration processes that affected the pristine samples from the quarry most likely accelerate the weathering (oxidation, hydration) and facilitate decomposition of the stone in the urban environment.
- The alteration and weathering contribute to increasing the primary porosity of the studied kersantite and decreasing its durability.
- Bush-hammered finish of surface additionally increases inter- and intra-crystalline porosity of the kersantite; it causes its faster scaling, flaking and granular disintegration.
- The discoloration ("red weathering crust") of the kersantite is caused by oxidation/hydration of Fe mineral phases and their accumulation along the stone surface; Fe-spheroidal particles, originating from environmental pollution, also contribute to the stone discoloration.

References

Benavente, D., Martınez-Verdu, E., Bernabeu, A., Viqueira, V., Fort, R., Garcıa del Cura, M.A., Illueca, C. and Ordonez, S., 2003, Influence of Surface Roughness on Color Changes in Building Stones, Color Research and Application, 28(5), 343-351.

Alves, C. and Sanjurjo-Sánchez J., 2011, Geoscience of the Built Environment: Pollutants and Materials Surfaces, Geosciences, 1, 26-43.

El-Gohary, M., 2009, Experimental tests used for treatment of red weathering crusts in disintegrated granite – Egypt, Journal of Cultural Heritage 10, 471–479.

Del Lama, E.A., Dehira, L.K., Grossi, D. and Kuzmickas, L., 2015, The Colour of the Granite That Built the City of Sao Paulo, Brazil, Color Research and Application, in press.

Fitzner, B., Heinrichs, K. and Kownatzki, R., 1995, Weathering forms classification and mapping, in: Verwitterungsformen – Klassifizierung und Kartierung. - Denkmalpflege und Naturwissenschaft, Natursteinkonservierung I: 41-88, Forderprojekt des Bundesministeriums fur Bildung, Wissenschaft, Forschung und Technologie, Verlag Ernst & Sohn, Berlin, 41-88.

Fitzner, B. and Heinrichs, K., 2002, Damage diagnosis on stone monuments - weathering forms, damage categories and damage indices, in: Understanding and managing stone decay, Proceeding of the international conference ''Stone weathering and atmospheric pollution network (SWAPNET)'', Prikryl, R., Viles, H. (eds.), Charles University, The Karolinum press, Prague, 11–56.

Król, B.B. and Fiałkiewicz-Koziel, B., 2014, Quantitative determination of minerals and anthropogenic particles in some Polish peat occurrences using a novel SEM point-counting method, Environmental Monitoring and Assessment, 186, 2573–2587.

Nakashima, S., Miyagi, I., Nakata, E., Sasaki, H., Nittono, S., Hirano, T., Sato, T. and Hayashi, H., 1992, Color measurement of some natural and synthetic minerals: Rep. Res. Inst. Natural Resources, Mining College, Akita Univ., 57, 57-76.

Pavlović, Z., Marković, B. and Atin, B., 1977, Explanatory booklet for the Sheet Smederevo (Basic Geological map of SFR Yugoslavia 1:100000), Federal Geological Survey, Belgrade.

Sabbioni, C., 1995, Contribution of atmospheric deposition to the formation of damage layers, The Science of the Total Environment 167, 49-55.

Schiavon, N., 1993, Microfabrics of weathered granite in urban monuments, in: Conservation of Stone and Other Materials, Thiel, M.J. (ed.), Spon, London, 271-278.

Schiavon, N., Chiavari, G., Fabbri, D. and Schiavon, G., 1994, Microscopical and chemical analysis of black patinas on granite, in: Stone and Monuments: Methodologies for the Analyses of Weathering and Conservation, Proceedings of the IIIrd International Symposium on the Conservation of Monuments in the Mediterranean Basin, Fassina, V., (ed.), 93-99.

Smith, B.J., Magee, R.W. and Whalley, W.B., 1993, Weathering of granite in a polluted environment: Budapest, in: Alteration of Granites and Similar Rocks used as Building Materials, Vicente-Hemandez, A., Molino Ballesteros, E. and RivesAmau, V. (eds.), C.S.I.C. Madrid, 159-162.

Vergès-Belmin, V., ed., 2008, Illustrated Glossary on Stone Deterioration Patterns = Glossaire illustré sur les formes d'altération de la pierre. English-French ed. Monuments & Sites 15. Paris: ICOMOS (International Council on Monuments and Sites) and ISCS (International Scientific Committee for Stone), Ateliers 30 Impression, Champigny/Marne, ISBN : 978-2-918086-00-0, p.78.

RELATIONSHIP BETWEEN THE DURABILITY AND FABRIC OF PASARGADAE CARBONATE STONES (ARCHAELOGICAL SITE FROM ACHAEMENID PERIOD, SOUTH OF IRAN)

A. Shekofteh[1], H. Ahmadi[1] and M. Yazdi[2*]

Abstract

Pasargadae is an Achaemenid archaeological site in south of Iran. There are some remains of stone monuments in this site such as Cyrus Tomb, Tomb of Cyrus' son and successor (Cambyses II), two royal palaces, and the fortress of Toll-e Takht. The monuments have been made out of three different types of carbonate stones in beige, green gray and dark gray colours. Despite of the same climate, deteriorations of three stone types are different in appearance; meanwhile, the beige type is in better conditions than the others in respect of deterioration. Also, some decay morphologies such as exfoliation and scaling have occurred on the dark gray stone. The aim of this research is to determine the reasons of deteriorations related to the nature of stones that caused different decay ratio and morphological deformation of stones in the same conditions. To clarify the nature of related factors of decay and deformation reasons, we prepared high resolution photos from thin sections and SEM images. The results of this research revealed that, the microfabric of beige stones are a low rate of metamorphism (marble like) of grain-to-grain pressure-solution and inequigranular hypiodiotopic fabric as well as the dolomitization phenomenon in one sample. The dark gray is a biomicrite (microbial micrite) with some stylolites and micro cracking. The lower part of the palaces' floor made of sandstone in two sizes of grains (fine and medium). The presence of calcite, opal, bioclast particles and clay cement whereby different resistance between grains of sandstone caused a high percentage of decays during the long time. In SEM micrographs, calcite dehydration, dehydration channels, sugaring phenomenon, and some bio-mineralized pitting are visible in stones. Hence, the presence of porosity (stylolite, interparticle and microporosity), recrystallized calcite, and difference of resistance between different grains in the sandstone and the biomicrite stone as well as the chemical nature of them caused the high ratio of decay by comparing to other used stones in the Pasargadae site during the time.

Keywords: Pasargadae, carbonate stone, fabric, nature factors, deterioration, SEM/EDS analysis

[1] A. Shekofteh and H. Ahmadi
Faculty of Conservation, Art University of Isfahan, Iran

[2] M. Yazdi*
Department of Geology, Faculty of science, University of Isfahan, Iran
meh.yazdi@gmail.com

*corresponding author

1. Introduction

Pasargadae is a historical site from Achaemenid (550-330 BC) in south of Iran. It is the capital of *Cyrus the Great* and also thereafter was a city in ancient Persia (Stronach 1985); it has located near the city of Shiraz in Fars province and is today an archaeological site and one of Iran's UNESCO World Heritage Sites (Fig. 1). Pasargadae was first studied by *Ernst Herzfeld* in 1905. After *Herzfeld*, *Sir Aurel Stein* completed a site plan for Pasargadae in 1934 (Stein 1936). From 1949 to 1955 an Iranian team under supervision of *Ali Sami* worked on conservation operations of the site. A British Institute of Persian Studies team led by *David Stronach* continued archaeological excavations from 1961 to 1963 (Stronach 1963). The archaeological site covers 1.6 square kilometers and includes a structure commonly believed to be the tomb of Cyrus the great, the fortress of *Toll-e Takht* sitting on top of a nearby hill, and the remains of three royal palaces as well as gardens (Sami 1971). All of the monuments are made of stone blocks. The stones are different in type and also different in the decay situations. Some of the stone that are in beige color are in a better condition than the others regarding to their physical stability and appearance. In general, three types of stones exist based on the color; beige, green gray and dark gray (Fig. 1). The aim of this research is identify the relationship between the durability and fabric of different types of stones. In order to identifying the nature reasons of deterioration some experiments were done including petrography and SEM (scanning electron microscope) in order to microstructure observation.

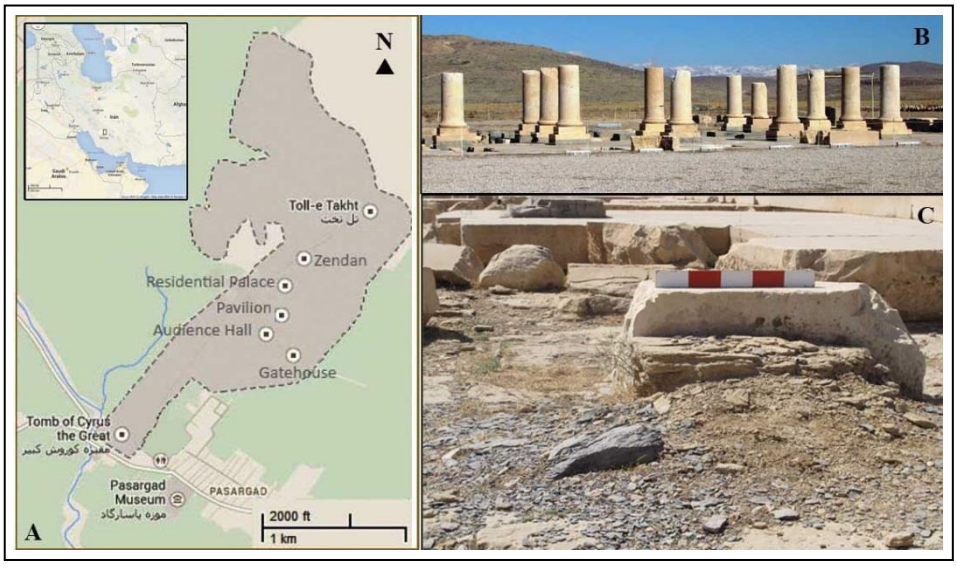

Fig. 1: a) The location of Pasargadae in Iran map is specified by rectangle, the Pasargadae area is separated in gray colour and the location of each important monument is defined in point (www.maps.google.com); b) Residential Palace, each three different kind of stone is used in this place; c) Three types of stones are used in residential palace, shows the different ratio of deterioration in the same situation.

2. Experimental

Totally, 12 samples from three stone types were selected. One thin section was prepared from each sample and another part of each sample was prepared to study and examination by SEM microscopy. The texture and microstructure of stone samples were observed by optical microscopy and electron scanning microscopy methods. In the case of optical microscopy, a polarized light microscope BK-POL/BKPOLR model manufactured by Alltion Company was used. Also stone samples were observed and analyzed in high magnification by TESCAN model MIRA III FE-SEM instrument in low vacuum, with a RONTEC backscattered electrons detector (BSE) and an energy dispersive spectrometer (EDS) (FE-SEM).

3. Result and discussion

According to the OM observation, Dark Gray stone has made of fine grains of Biomicrite that is moderately-sorted. Some stylolites and growth of micrite into the sprites indicate that recrystallizing was occurred, but it seems that it is controlled by some percentages of clay (Bausch 1968). The matrix is a kind of mudstone and the existence of some clay and iron veins may cause secondary porosity. SEM observation shows degradation particles and some channels between particles that may have been caused by dehydration or removal of clay, and the veins or fractures filled by secondary calcite (Fig. 2).

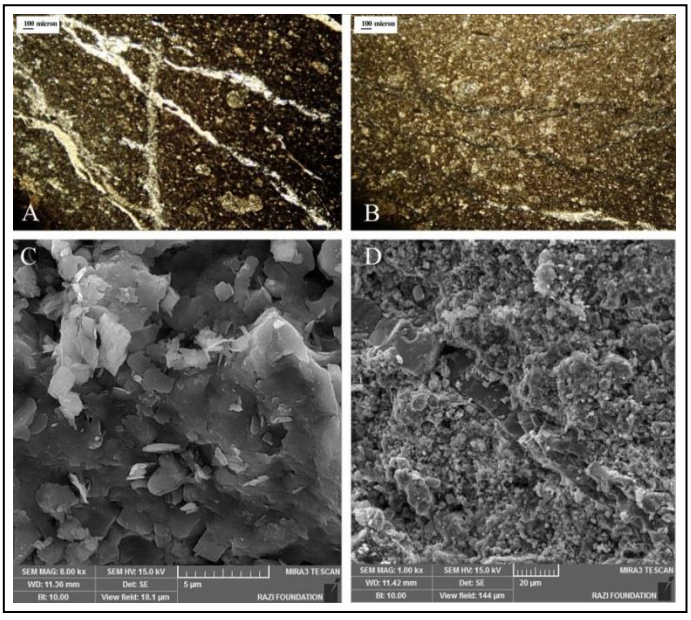

Fig. 2: a) OM of Dark Gray stone, magnification 4X, micrite stone that the including some stylolites are filled by secondary calcite; b) OM of Dark Gray stone, magnification ×4, pressure solution seams filled by secondary iron; c) SEM image of Dark Gray stone shows particles of clays; d) SEM image of Dark Gray stone, shows a vein is filled by secondary calcite.

The petrography of beige stone showed the xenotopic and hypiodiotopic and some rhombohedral dolomite crystals that exhibits indications of low rate of metamorphic processes (Flugel and Munnecke 2010). The dolomites are replaced by secondary calcite. Different texture on beige stone are indicated; a kind of biosparite in poor sorted grains including ooid, clast, and some quartz particle (Fig. 3).

SEM observations revealed the dislocation and the separation of the grains and the formation of residual pores as well as calcite dehydration. The interesting point in SEM picture is the presence of a layer that covered surface of the stone. This layer is obvious in naked eye that is so-called Patina and generally is attributed to Oxalate (Vergès-Belmin et al 2008). The present of microorganisms such as lichen and fungal are obvious on the patina layer that is made a hole around each of them. The holes are detectable by naked eye (Fig. 3).

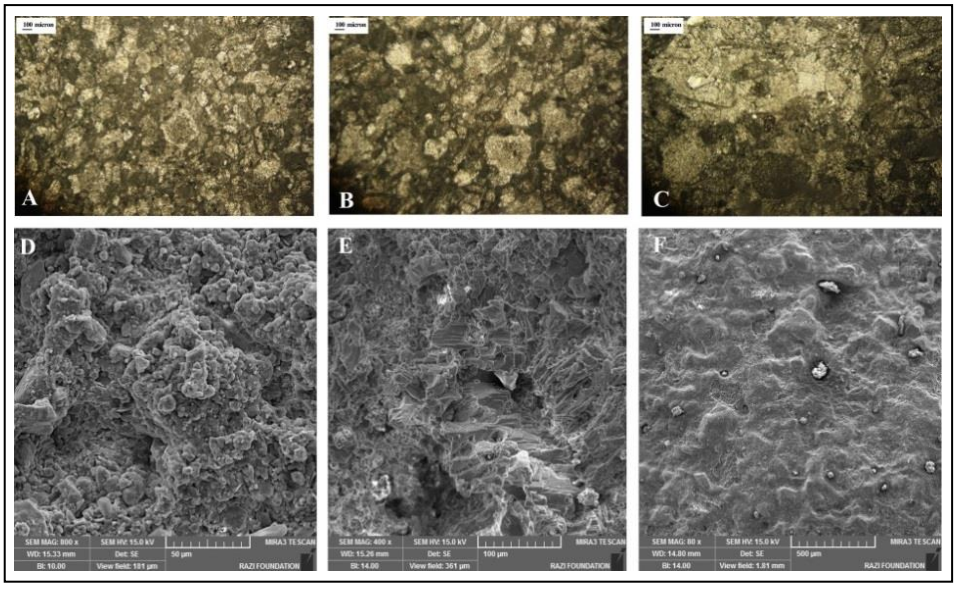

Fig. 3:a and b) OM of Biege stone, magnification 4X, calcite-dolomite stone, the crystals of mosaic dolomites formed by replacement of calcite; c) OM of Biege stone, magnification ×4, Biosparite composed; d) SEM image of Beige stone shows compactness of particles; e) SEM image of Beige stone, shows calcite dehydration; f) SEM image of Beige stone, shows a cover on the surface of the stones that may related to the Oxalate patina, the Bright spots related to the microorganism that cause some pits on the surface of stones.

The samples of green gray stone have similar texture but difference in the grain size. The stones are composed of different grains such as calcite, dolomite, quartz, opal, and clay. They are well-sorted, but the interparticle porosity is about 25-30 percentages. In the SEM images some channels between the particles are obvious that may relate to the calcite dehydration. Also, the sugaring as a deterioration phenomenon even in the high magnification is the main features of this kind of stone (Fig. 4). The biomicrite (dark gray) stone has a large amount channels filled by clay and iron as well as calcite. The calcite channels and vein are easily dissolved by water. And the joint of the layers is broken by

solubility of this kind of material. Subsequent, it causes more porosity in stone that finally reduces the Compressive strength of stone. The green gray stone made from some different grains with respect to the mineralogy, the more different ingredients the more difference in behaviour. The differential hygric stress, differential thermal stress, and stress from differential expansion rates of material are done. In addition, clay is the most important factor of deterioration in the petrology of this kind of stone because of clay swelling phenomenon. Also the porosity makes the important role for the water penetration in the stone structure causing the channeling, dissolution and crystallization of salts, because of its mobility in the porous system. The calcite-dolomite stone and biosparite (beige) stone are in better condition rather than other because they have less porosity and they are more compact. Also the formation patina layer on the surface of stone is an advantage against the further weathering, except the biological factors that limestone is much more vulnerable than other types.

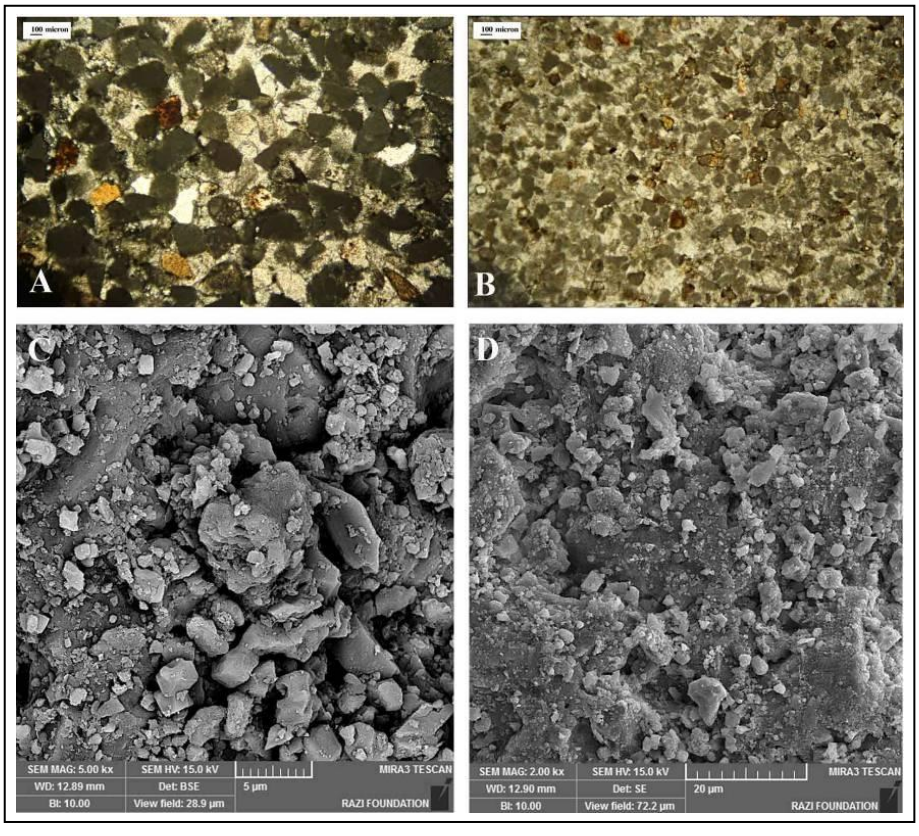

Fig. 4: a) OM of Green Gray stone, magnification 4X, different grain such as calcite, dolomite, quartz and also bioclast; b) OM of Green Gray stone, magnification ×4, size of grain is smaller than the other one, but they are similar in ingredients; c) SEM image of Green Gray stone, shows interspaces between the grain boundaries that caused by calcite dehydration; d) SEM image of Green Gray stone, shows sugaring phenomenon.

4. Conclusion

By means of Petrography and SEM observation appeared the relationships between the facias and the weak point of the stones and the reason of different decay ratio and morphological deformation of stones in the same conditions. The most important mineralogy characters of dark gray stones that cause degradation are veins of clay and the stylolite and fractures filled by secondary calcite. The main natural reason of deterioration the green gray stone is Non-homogeneity particles. Videlicet, the presence of calcite, opal, bioclast particles and clay cement whereby different resistance between grains of sandstone caused a high percentage of decays during the long time. The strength point of the beige stone petrology is the compactness and the layers of patina that formed because of chemical nature.

References

Bausch, W.M. 1968, Clay content and calcite crystal size of limestones, Sedimentology, 10 (1), 71-75.

Flugel, E., Munnecke, A., 2010, "Microfacies of carbonate rocks: analysis, interpretation and application", Springer-Verlag, Berlin, ISBN: 978-3-642-03795-5.

Sami, A., 1971, "Pasargadae. The Oldest Imperial", Capital of Iran 4, Rev. RN Sharp transl (2nd ed.), Learned Society of Pars, Musavi Print Office, Shiraz.

Stein, A., 1936, An Archaeological Tour in Ancient Persis, Iraq, 3,217-20.

Stronach, D., 1963, "First Preliminary Report", Excavations at Pasargadae, Iran, 1,19-42.

Stronach, D., 1985, "Pasargadae", in The Cambridge History of Iran, vol. II: The Median and Achaemenian Periods, Ilya Gershevitch (ed.), Cambridge University Press, Cambridge, 838-855.

Verges Belmin et al, (Eds.), 2008, Illustrated glossary on stone deterioration patterns, Monuments and Sites XV, ICOMOS, Paris.

BIODETERIORATION OF LIMESTONE BUILT HERITAGE: A MULTIDISCIPLINARY CHALLENGE

P.J.A. Skipper[1*], H. Schulze[2], D.R. Williams[1] and R.A. Dixon[1]

Abstract

Built heritage is at risk from the effects of bacterial species within biofilms (a microbial community encapsulated in a matrix of complex sugars, protein and DNA). Some microbes in biofilms can damage stone surfaces and cause discolouration. Although biofilm research has been carried out in Mediterranean regions, few studies cover temperate Northern Europe climates, or the UK oceanic climate. In a previous study we recorded environmental conditions of damaged, with deterioration of the worked surface to greater than 10mm depth, and undamaged limestone at fifteen sites across two locations in Lincoln, UK, and sampled surfaces to detect biofilm associated bacterial species. A correlation between low surface *pH* and damage was observed, and bacterial species were isolated from the samples using media which would select for species which could survive in a wide range of conditions and identified at the genetic level. The isolated bacteria from that study have been tested for their ability to dissolve limestone, as well as resistance to commonly used biocides. We have identified species which, within our dataset, are solely or predominantly associated with damaged limestone and also tested positive for dissolution of limestone. Many of these species have been previously associated with biodeterioration in studies from Tropical and Mediterranean climates. Our present study has also identified them as being able to rapidly recolonise biocide treated areas (within 48 hours). As well as increasing our knowledge in a currently under-researched area of environmental microbiology, this study provides valuable information for the conservation of historic buildings.

Keywords: biocide, biodeterioration, bacteria, limestone, building conservation

[1] P.J.A. Skipper*, D.R. Williams and R.A. Dixon
School of Life Sciences, University of Lincoln, United Kingdom
pskipper@lincoln.ac.uk

[2] H. Schulze
School of History and Heritage, University of Lincoln, United Kingdom

*corresponding author

1. Introduction

Historically limestone, and its metamorphic relative marble, have been used as a building material on a global scale for both aesthetic and practical reasons. Global examples range from the pyramids of Giza, Nummulite limestone with a Tura limestone casing (Park and Shin 2009), the Diocletian's Palace in Split built from Brač Limestone (Marasović *et al*, 1976), to the Gothic Cathedrals of Europe. Limestone is a sedimentary rock composed largely of different crystalline forms of calcium carbonate, and as such is soluble in the presence of weakly acidic solutions (Stanley, 1983). As one of the potential mechanisms of bacterial deterioration of stone is the production of acids, colonization by acid producing bacteria would be likely to have a detrimental effect on this stone. The present study focuses on bacterial colonisation in an oceanic climate, and considers their potential effects on the stonework, with the current work focusing on buildings made from limestone in Lincolnshire.

It has long been acknowledged that the deterioration seen on stone surfaces results from chemical, physical and biological processes (Doehne and Price, 2010). Biological processes of decay range from the macroscopic such as plants, lichens and bird droppings, but can also be due to the microscopic such as the colonisation of the stone surface by microorganisms, such as bacteria, fungi and algae, in the form of biofilms. A biofilm is a community of microorganisms which excrete protective materials, usually proteins and sugar polymers, to produce an extracellular polysaccharide matrix (EPS) (Lewis, 2001). The EPS protects the microorganisms from desiccation and physical damage while providing a greater surface area for them to occupy. It is gradually becoming recognised that many bacterial species will spend at least part of their life cycle in a biofilm. Recent studies have identified biofilms containing bacteria and fungi from many sources of historically relevant stonework including Mediterranean statuary (Miller *et al*, 2012; Dakal and Cameotra, 2012).

The growth of biofilms on surfaces can produce discoloration, chemical deterioration and promote physical deterioration. Discoloration can be caused by excreted bacterial by-products staining or chemically changing surfaces, as well as the natural pigmentations of the bacteria or other microorganisms (Urzi, 1992; Urzi, 1993). Bacterial metabolism often results in acidic by-products which can result in chemical damage, as can the scavenging of minerals essential for bacterial growth and excretion of salts and EPS. The damage caused by these mechanisms can seed physical deterioration processes by producing the initial disruption of the stone surface. In addition, the EPS may affect the pores within the stonework through a physical process, as the biofilm swells and shrinks within the pore network which can cause microfractures (Dornieden et al, 2000). The alteration of moisture circulation through the pores of the stone may also impact on stability of the stone itself (Warscheid and Braams, 2000). Furthermore, evidence suggests that biofilms may encourage the build-up of pollutants from the atmosphere on the stonework, thus accelerating the deterioration rates (Young, 1996; Mansch and Bock, 1998).

In a previous study (Skipper and Skipper, 2012) we took a comparative approach to sampling which allows the breakdown of the microbial community into those associated solely with damaged stone, those associated with undamaged stone and the species which overlap the two. The 43 previous studies by other groups reviewed in Dakal and Cameotra (2012), only sampled damaged stone, and so included species which were generally found

in the environmental microbiome as opposed to those specific to the damaged environment. In collaboration with The Cathedral Church of the Blessed Virgin Mary of Lincoln (Lincoln Cathedral) and the Diocese of Lincoln we carried out sampling of bacterial biofilms present on the external walls of Lincoln Cathedral (8 sampling sites), an exposed structure close to the edge of the Lincoln Cliff at 72.8m above sea level, and Saint Peter at Gowts in Lincoln (7 sampling sites), located in the valley below the cliff at 20.4m above sea level.

For this study we have taken a panel of 54 species previously isolated from both damaged and undamaged environments to test for biocide efficacy and the ability to cause chemically mediated biodeterioration. The homogeneity of limestone chemistry and environmental flexibility of bacterial species means that it will be applicable to all but extreme environments.

2. Methodology

2.1. Biocide testing

Microtech Biocide by Wykamol was selected for testing as it is the principal biocide in use at both sites sampled. Biocide testing was performed using the agar spot test as per Hernández *et al*, 2005, with the following modifications. Strains were cultured in nutrient broth and agar and plated onto nutrient agar plates in a 50% nutrient top agar. 10µl aliquots of biocide concentrations which were equivalent to the manufacturers recommended dose range (2-5m^2 coverage of a 1:24 dilution of the stock biocide: water as per manufacturer's instructions) were spotted onto the plates which were incubated aerobically at 25°C for 48 hours. Inhibition was scored as positive if the zone was greater than 10 mm. The plates were then incubated for a further 48 hours at 25°C to test for breakthrough, i.e. colonies forming within the zone of inhibition. In order to determine the mechanism of breakthrough, bacterial colonies from within the zone were subcultured from the plates, and re-tested against the biocide. When the breakthrough colony showed the same response as the original test this identified habituation, i.e. the cells were utilizing a previously evolved mechanism. When the colony showed higher resistance than the original test this identified mutation to adapt to the biocide environment.

2.2. Testing for active dissolution of calcium carbonate

Effects of bacterial metabolism on the dissolution of limestone were tested for on a solid agar medium as per Del Gallo *et al*, 1999, with the following modifications. Calcium carbonate in the enriched medium was reduced from 50 g/L to 20 g/L which resulted in a more homogenous dispersion of calcium carbonate through the medium. The additional supplementation of $CaCO_3$ for the carbonate solubilisation test was shown to be unnecessary. Glucose in the enriched medium was reduced from 67 g/L to 1 g/L, in line with more commonly used growth media, after it was shown to inhibit growth of many species at the original concentration. Single isolates were streaked onto the agar using sterile technique and incubated for 28 days at 25°C being monitored every seven days. Solubilisation was determined by the formation of a clear halo around the colonies.

3. Results

3.1. Biocide testing

Of the 54 species tested for resistance to Microtech biocide forty seven were inhibited by the biocide. The remaining seven were identified as showing resistance at commercially

recommended concentrations and ten were identified as showing breakthrough within 48 hours (Tab. 1). Of the species resistant to the biocide *Pseudomonas fluorescens, putida* and *sp. HZ06* were only resistant to the lowest recommended concentration. *Pseudomonas PAG3U3b* and *Streptomyces LCA3A4* were resistant up to the middle of the recommended concentration range (2.5 m^2 and 3.5m^2 coverage, respectively) but showed breakthrough above the recommended range within 48 hours. The remaining species were completely resistant to the biocide.Species which showed breakthrough, (see Fig. 1 for an example) other than *B. licheniformis* and *M. luteus* broke through across the entire range of recommended concentrations. *B. licheniformis* and *M. luteus* broke through at the equivalent to 4.5m^2 biocide coverage. Only *B. muralis* showed adaption by mutation as the cause for breakthrough, all the other species that broke through did so by habituation.

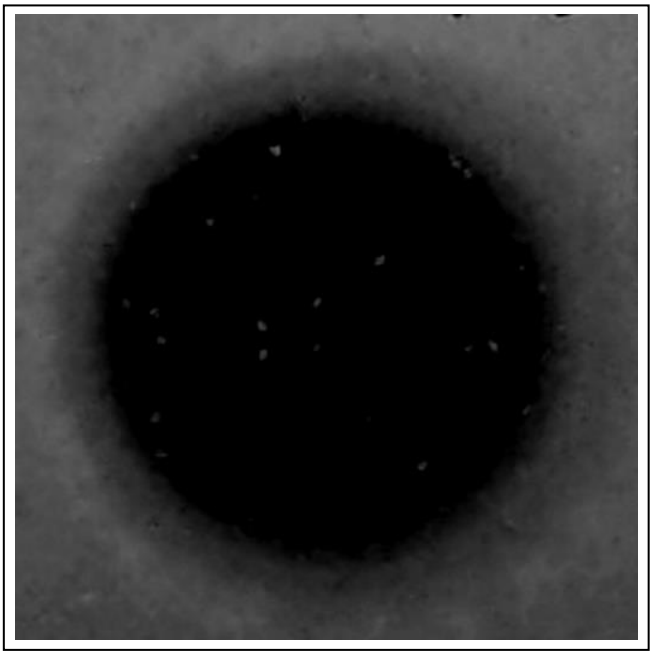

Fig. 1: Bacillus muralis breakthrough at the lowest recommended dose of Microtech biocide after 24 hours. The black disc is the zone of clearance shown by the biocide, white spots are individual bacterial colonies which have broken through. The surrounding grey regions are confluent, uninhibited, bacterial growth.

Tab. 1: Species identified as showing resistance to or breakthrough at commercially recommended levels of Microtech Biocide. The building they were isolated from and condition of the stonework is identified in the isolation column with both used when either the species was found at both locations or on damaged and undamaged stonework.

Species	**Isolation**	**Biocide resistant**	**Break-through**
Advenella kashmirensis	Cathedral - undamaged	+ve	-ve
Stentrophomonas rhizophila	Cathedral - undamaged	+ve	-ve
Streptomyces LCA3A4	Cathedral - damaged	+ve	+ve
Pseudomonas fluorescens	St. Peters - undamaged	+ve	-ve
Pseudomonas putida	St. Peters - damaged	+ve	-ve
Pseudomonas sp. HZ06	St. Peters - damaged	+ve	-ve
Pseudomonas PAG3U3b	St. Peters - undamaged	+ve	+ve
Bacillus licheniformis	Both - damaged	-ve	+ve
Bacillus muralis	Cathedral - damaged	-ve	+ve
Bacillus pumilis	St. Peters - damaged	-ve	+ve
Isocoptera variabilis	Cathedral - damaged	-ve	+ve
Micrococcus luteus	Both - both	-ve	+ve
Psychrobacter LCATB	Cathedral - undamaged	-ve	+ve
Solibacillus silvestris	Cathedral - undamaged	-ve	+ve
Staphylococcus xylosus	Both - both	-ve	+ve
Stentrophomonas maltophilia	Cathedral - undamaged	-ve	+ve
Arthrobacter LCA1U	Cathedral - undamaged	-ve	+ve

3.2. Calcium carbonate dissolution

Twelve species out of the fifty four tested were positively identified as being capable of dissolving calcium carbonate (Tab. 2). Four of the species were solely isolated from damaged stone, four from undamaged stone and the remainder being found on both surfaces. In all cases where a species was found on both damaged and undamaged stone it was twice as likely to be isolated from damaged stone (data not shown).

Tab. 2: Species associated with chemical dissolution of calcium carbonate together with the building they were isolated from and the condition of the stone surface.

Species	**Isolation**
Bacillus sporothermodurans	Cathedral - damaged
Acinetobacter calcoaceticus	St. Peters - damaged
Micrococcus luteus	Both - both
Stentrophomonas maltophilia	Cathedral - undamaged
Arthrobacter agilis	Cathedral - damaged
Bacillus cereus	Both - both
Micrococcus roseus	Both - both
Pseudomonas PAG3U3b	St. Peters - undamaged
Pseudomonas putida	St. Peters - damaged
Solibacillus silvestris	Cathedral - undamaged
Psychrobacter LCATB	Cathedral - undamaged
Staphylococcus xylosus	Both - both

4. Discussion

With a third of the species isolated from St. Peters-at-Gowt and Lincoln Cathedral showing either resistance to, or breakthrough of Microtech biocide within 48 hours, rapid regrowth on the treated surfaces is a likely outcome. Of those species only *M. luteus, S. xylosus, S. maltophilia* and *S. rhizophilia* are strongly pigmented and as the pigments are yellows and browns regrowth will not be as visually obvious as the recolonization by algae and cyanobacteria (Berdoulay and Salvado, 2009). The current policy of biocide usage at both buildings is to use the minimum recommended concentration (personal communication, 2015) which means that all species identified will be actively growing within 48 hours.

Of greater concern however is that seven of the seventeen species identified as showing resistance or breakthrough have also been identified as chemically dissolving calcium carbonate. *M. luteus, S. maltophilia, P. PAG3U3b, P. putida, S. silvestris, P. LCATB* and *S. xylosus* are all capable of resisting the effects of Microtech biocide. Of these species only *P. putida* is solely associated with damaged stone, therefore generic cleaning of stonework could result in an environment where recolonization of undamaged limestone is driven by species which actively dissolve calcium carbonate. Of the entire undamaged microbiome identified in our previous study, only *A. LCA1U, A. kashmirensis* and *P. fluorescens* are resistant to biocide and showed no sign of active dissolution of calcium carbonate. While the effect of their presence in the microbiome of undamaged limestone may be to suppress damage such as biocorrosion by maintaining an alkaline environment (*A. LCA1U* may well fulfil this role, authors own data, unpublished) there is no guarantee that they would be capable of suppressing damage in the biocide treated environment.

5. Conclusion

It is clear from the results of this study that a better understanding of the microbiome of stonework is needed to ensure that conservation treatments designed to stabilise our built heritage and prevent further deterioration are not creating an environment which will enhance deterioration. With this in mind the authors are currently expanding the number of biocides investigated to see whether a combination of treatments will diminish the likelihood of damaging species being left on the surface. Also under investigation are the mechanisms behind bacterial limestone dissolution for the species identified in the hopes of identifying alternatives to biocide treatment.

Acknowledgements

The authors would like to acknowledge their gratitude to the Masters committee of The Cathedral Church of the Blessed Virgin Mary of Lincoln and the Reverend Jeremy Cullimore of Saint Peters-at-Gowt Church, Lincoln, for their kind permission to sample their buildings.

References

Berdoulay, M., and Salvado, J. C. (2009). Genetic characterization of microbial communities living at the surface of building stones. Letters in Applied Microbiology, 49(3), 311–316.

Dakal, T.C. and Cameotra, S.S. (2012) Microbially induced deterioration of architectural heritages: routes and mechanisms involved. *Environmental Sciences Europe*, 24 36-49.

Del Gallo, M., Cacchio, P., Ercole, C., and Lepidi, A., with Maria Pia Di Bonaventura (1999). Microbial Formation of Oxalate Films on Monument Surfaces: Bioprotection or Biodeterioration? *Geomicrobiology Journal*, 16, 55-64.

Doehne, E. and Price, C.A. (2010). *Stone Conservation An Overview of Current Research.* Los Angeles: The Getty Conservation Institute. Available from: http://www.getty.edu/conservation/publications_resources/pdf_publications/pdf/stoneconservation.pdf [Accessed 10/12/2013].

Dornieden T., Gorbushina, A.A., Krumbein W.E. (2000), Patina. In: Orio Ciferri, Piero Tiano, and Giorgio Mastromei (eds). *Of microbes and art : the role of microbial communities in the degradation and protection of cultural heritage*. New York London: Kluwer Academic/Plenum, 105-119.

Hernández, D., Cardell, E., and Zárate, V. (2005). Antimicrobial activity of lactic acid bacteria isolated from Tenerife cheese: initial characterization of plantaricin TF711, a bacteriocin-like substance produced by Lactobacillus plantarum TF711. Journal of Applied Microbiology, 99(1), 77–84.

Lewis K. (2001). Riddle of Biofilm Resistance. *Antimicrobial Agents and Chemotherapy*, 45 (4) 999-1007.

Mansch, R. and E. Bock. (1998). Biodeterioration of natural stone with special reference to nitrifying bacteria. *Biodegradation* 9 (1) 47–64.

Marasović, J., Marasović, T., McNally, S., and Wilkes, J. (1976). Diocletian's Palace: Report on Joint Excavations in South-East Quarter. The Classical Review (New Series) 26 (2) 255-256.

Miller, A.Z., Sanmartin, P., Pereira-Pardo, L., Dionísio, A., Saiz-Jimenez, C., Macedo, M.F. and Prieto, B. (2012). Bioreceptivity of building stones: A review. *Science of the Total Environment*, 426 1-12.

Park, H. D., and Shin, G. H. (2009). Geotechnical and geological properties of Mokattam limestones: Implications for conservation strategies for ancient Egyptian stone monuments. Engineering Geology, 104(3-4), 190–199.

Skipper, P.J.A and Skipper L.K. (2014). A survey of bacterial colonisation of historic limestone buildings: Lincoln Cathedral and St. Peter at Gowts, United Kingdom. In: Rogério Amoêda, Sérgio Lira and Cristina Pinheiro (eds). *Rehab 2014 – Proceedings of the International Conference on Preservation, Maintenance and Rehabilitation of Historic Buildings and Structures*. Green Lines Institute ISBN: 978-989-8734-02-0.

Stanley, J.L. (1983). Industrial minerals and rocks, 5th ed. Society of Mining Engineers, ISBN 0895204029, 1446.

Urzi, C.E., Krumbein, W.E. and Warscheid, T. (1992). On the question of biogenic colour changes of mediterranean monuments. In: D. Decrouez, J. Chamay and F. Zezza. (eds.), *Proceedings of the Second International Symposium on: The Conservation of Monuments in the Mediterranean Basins.* Geneva: Ville de Gèneve, 397–420.

Urzi, C.E., Criseo, G., Krumbein, W.E., Wollenzien, U. and Gorbushina A.A. (1993). Are colour changes of rocks caused by climate, pollution, biological growth, or by interactions of the three? In: M.-J. Thiel (Ed.), *Conservation of Stone and Other Materials, Vol. 1.*, London: EandFN Spon, 279–286.

Warscheid, T. and Braams, J. (2000). Biodeterioration of stone: a review. *International Biodeterioration and Biodegradation*, 46 (4) 343-368.

Young, P. (1996). Pollution-fueled "biodeterioration" threatens historic stone. *Environmental Science and Technology* 30 (5) 206–208.

CHARACTERISATION OF A PINK DISCOLORATION ON STONE IN THE PNOM KROM TEMPLE (ANGKOR, CAMBODIA)

M. Tescari[1*], F. Bartoli[1], A. Casanova Municchia[1], T. Boun Suy[2] and G. Caneva[1]

Abstract

The formation of pigmented patinas and encrustations on stone monuments, connected to chemical or biological deterioration, can give rise to aesthetic alterations. Pink patinas related to biodeterioration phenomena have been widely observed throughout Europe and in tropical climates, like on the Khmer temple of Bayon (Angkor, Cambodia) or Mayan monuments in Uxmal (Mexico). They generally occur under specific environmental conditions, such as interior or semi-confined areas with specific lighting conditions, a high saline content and substantial variations in humidity and temperature. Other pink discolorations can be observed in the morphology of hard encrustations on the sandstone of one of the buildings of Phnom Krom temple. They occur on exterior surfaces characterised by different conditions than those of the pink alterations at Bayon. Considering their unclear origin and unusual morphology, this paper aims to characterise them and define their chemical or biological origin. The observation of fresh slides, fracture samples and cross-sections with optical and SEM/EDS microscopes shows the presence of very small coccoid cells (0.5 µm) surrounded by an extracellular matrix. SEM-EDS analysis highlighted the presence of Si, Fe, Mg, Ca, Na, K associated with the substrate. Phosphorus, aluminium and a small amount of silicon were detected in correspondence with the body of the patina. The high level of P at the Phnom Krom temple can be traced to salts efflorescence originating in bat guano deposits. It seems necessary to hypothesize the simultaneous presence of other phenomena in order to explain the origin of these encrustations. Microscopic observations have shown a microbiological colonization corresponding to P accumulation, arising, at first, from the guano and then mobilised by wet-dry cycles in areas exposed to direct sunlight. The presence of microorganisms seems able to explain this peculiar coloration, but biomolecular analysis will be needed to understand the precise taxonomy of such bacteria.

Keywords: bacteria, biodeterioration, sandstone, SEM/EDS analysis, rosy alteration

[1] M. Tescari*, F. Bartoli, A. Casanova Municchia and G. Caneva
Department of Science, Roma Tre University, Roma, Italy
marco.tescari@uniroma3.it

[2] T. Boun Suy
Authority for the Protection and Management of Angkor and the Region of Siem Reap (APSARA), Cambodia

*corresponding author

1. Introduction

The formation of pigmented patinas and encrustations on stone monuments can be related to chemical or biological deterioration. In either case, they constitute an aesthetical alteration of the surface and in some cases they can contribute to physicochemical damage to the stone. In the case of a chemical origin, they are caused by the interaction of salts, or of some other treatment, with the stone, leading to physical-chemical reactions (Siedel *et al.*, 2010). In the case of a biological origin, several studies attributed this phenomenon to the colonization of different taxa: actinobacteria, such as *Rubrobacter radiotolerans*, *R. xylanophilus*, *Kocuria* sp., Firmicutes such as *Halobacillus herbersteinensis*, *H. naozhouensis*, and Archaea, such as *Halococcus* sp. and *Haloferax* sp. were detected in different studies (Giacobini *et al.*, 1979; Imperi *et al.*, 2007; Cappitelli *et al.*, 2009; Kusumi *et al.*, 2013; Ettenauer *et al.*, 2014). The environmental conditions in which they were detected show the simultaneous occurrence of certain conditions, like high saline content in the stone, an interior space or semi-confined area with specific lighting conditions, and in some cases with substantial variations in humidity and temperature (Imperi *et al.*, 2007; Laiz *et al.*, 2009). Similar pink patinas were also detected on stone monuments in tropical climates, including limited areas of Mayan monuments in Uxmal (Mexico) and Bayon Temple in the Angkor archaeological area (Cambodia). Here too, they were seen to appear only in semi-confined areas and on walls characterised by specific illumination conditions, low water and high saline content (Ortega-Morales *et al.*, 2004; Kusumi *et al.*, 2013). Unexpectedly, during our study of the Angkor archaeological area, we recently observed a pink alteration of the stone at Phnom Krom temple, in the shape of thick and hard layers on the surface, like an encrustation. This phenomenon, whose origin was unclear, seemed to be quite different from the pink patinas described above, which mainly appear as thin and soft layers (Normal UNI 1/88). Moreover, it was only present on external surfaces exposed to direct sunlight and winds and protected from incident rainfall by wooden scaffolding. Interpreting this phenomenon seemed interesting both for the differing morphology of the alteration, and for the different environmental conditions under which it occurs. This work aims to characterise, through microscopic and spectroscopic analysis, the nature of these pink discolorations, and to identify their chemical or biological origin, and their association with particular environmental conditions.

2. Study area and environmental setting

The Angkor monuments in Cambodia, included in UNESCO's World Heritage List in 1992, numbers about forty temples, in area of 400 km^2, built between the 9th and 15th centuries. These temples, abandoned from the 15th century were reclaimed by the tropical forest until the 20th century, when several restoration campaigns were performed. The monsoon climate of the Angkor region consists of a short rainy season, a prolonged dry season, and irregular but generally plentiful rainfall (between May and mid-October) (Caneva *et al.*, 2015). During the dry season, monthly mean relative humidity is about 75% and temperature about 20°C, whereas in the rainy season *RH* is about 80% and the temperature reach up to 30°C (Siedel *et al.*, 2010). Phnom Krom temple, built in early 10th century on a hill (137 m a.s.l.), in the south of ancient Angkor city (Uchida *et al.*, 1999), is one of most deteriorated temples in the park (Delvert, 1963). It stands close to a modern inhabited and functioning Buddhist temple, and consists of three sanctuary towers (*prasat*) built on a terrace and another four annexed buildings, placed in a line in front of the *prasat* (Fig. 1). In 1938,

Phnom Krom Temple was freed from vegetation and topsoil and rubble was removed from the area (Glaize, 1940).

The three *prasat*, the terrace and the two annexed buildings closest to the east entrance of Phnom Krom were constructed with grey to yellowish brown sandstone consisting mainly of quartz, plagioclase, K-feldspar, biotite, muscovite and rock fragments. The range of major chemical components are: SiO_2 66-72%; Al_2O_3 12-14%; Fe_2O_3 3,8-5,2%; MgO 1.6-2.6%; CaO 0,9-3,3%; Na_2O 2,5-3,1% and K_2O 1,8-2.3% (Delvert, 1963; Uchida *et al.*, 1999). The other two annexed buildings were built with clay bricks, and the wall that surrounds the area was built with laterite (Daigoro *et al.*, 1992) (Fig. 1). The lack of forest canopy around the ruins and their location on a hilltop expose them to high ventilation, high solar radiation and substantial rainfall, giving rise to recurrent wet-dry cycles typical of tropical climates, and increasing the weathering processes (Andrè *et al.*, 2014; Bartoli *et al.*, 2014, Caneva *et al.*, 2015). The effects of weathering are widespread, such as the flaking of sandstone, the presence of salt efflorescence, and the colonization of several biodeterioration patterns on surfaces subject to pouring rain. Moreover, the specific environmental conditions of the site, with its position on the top of a hill and surrounded by agricultural fields and humid areas, have attracted a large bat colony, which is the cause of the plentiful guano deposits inside the buildings (Uchida *et al.*, 1999).

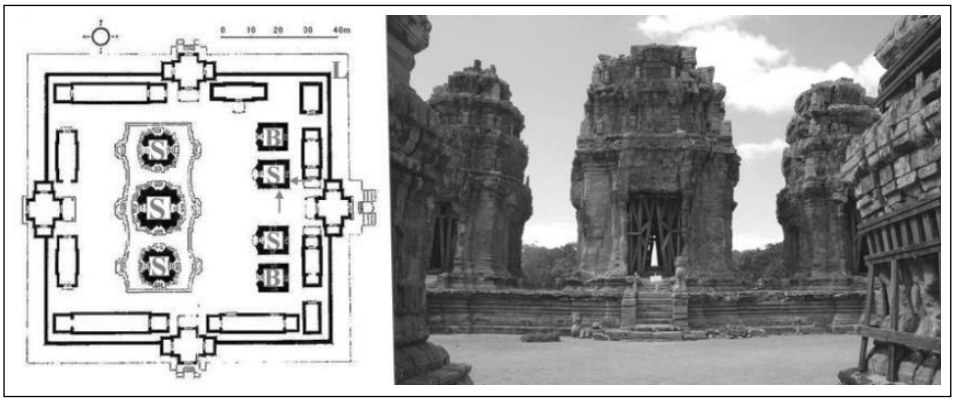

Fig. 1: Map of Phnom Krom Temple (grey arrows indicate the sampling walls, letters indicate materials: B, bricks; L, laterite; S, sandstone) and view of the complex from the east entrance.

3. Materials and methods

Five samples of stones with pink incrustation were collected from one of the secondary temple buildings (Fig. 1) using sterile scalpels and then stored in tubes. Three samples were collected from the southern wall (C1; C2; C3) and two from the eastern wall (C4, C5) (Fig. 2). All areas were also partially protected by a wooden scaffold structure that provides partial cover from external environmental factors.

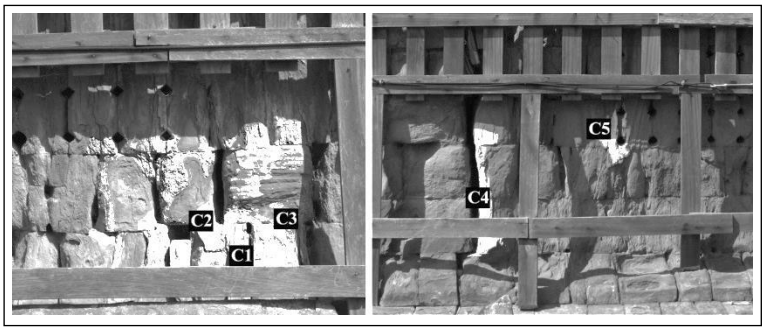

Fig. 2: Sampling plan - C1, C2 and C3 have a southern exposure, C4 and C5 are exposed to the east.

3.1. Sample preparation and optical microscopy

Fractured samples and polished cross-sections were performed in order to investigate the fragment in depth. These were obtained after inclusion in a polyester resin in accordance with UNI 10922. In order to characterise the samples and prepare the polished cross-sections, pictures of all samples were taken with an Olympus SZX16 stereomicroscope, digital images were taken with a Color View II (Soft Imaging System GmbH, Münster, Germany) digital camera using Cell^B software. The polished cross-sections were observed with a Leitz Orthoplan microscope and digital photographs were taken with a Leica DC300 digital camera and processed with the IM100 software. Fresh slides of the scraped material were also observed through an optical microscope with a 100x magnification immersion objective (Olympus BX41) following the procedures set out in UNI 10923.

3.2. Scanning Electronic Microscopy/Energy Dispersive Spectrometery (SEM/EDS)

All samples were placed on an aluminium SEM stub and coated with gold using a K550 sputter coater (Emitech Technologies Ltd., Kent, England). They were then observed with a XL30 SEM microscope (FEI Company, Eindhoven, The Netherlands) with back-scattered electron detectors equipped with an energy dispersive spectrometer (EDS analysis). Backscattered electron (BSE) images were acquired in order to obtain information on the elemental distribution of the samples, using an accelerating voltage of 20 kV and a working distance of 11 mm. In order to identify the elemental distribution of the points of interest, an EDS energy dispersive X-ray spectrometer was used to perform microanalysis on single spots or small areas using an accelerating voltage of 20kV; filament current: 1.80A; emission current: 20μA; aperture current: 300nA; working distance: 11 mm.

4. Results and discussion

The stereomicroscopic examination confirmed the presence of a hard and thick layer on the stone, resulting in pink discolorations in the form of an encrustation (Fig. 3a). Microscopic observation of fresh slides failed to show any biological traces, but a SEM image of the fracture sample showed a well-defined crust-like layer (Fig. 3b). This layer appears as a solid matrix covering the sandstone (Fig. 3c) and the presence of microorganisms was detected in the fracture surface (Fig. 3d). This colonization was characterised by the presence of coccoid shaped cells, approximately 0.5 μm in diameter, coherent with the size

of a small prokaryote, surrounded by an extracellular matrix that is responsible for producing the encrustation.

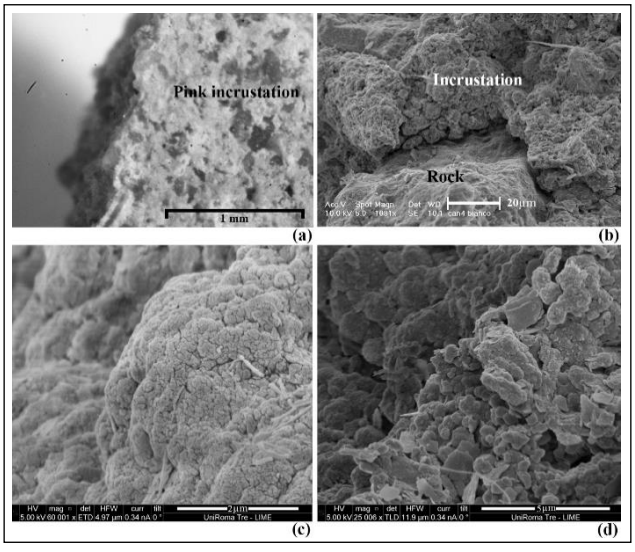

Fig. 3: Fractured sample: stereomicroscopic image (a); SEM images at different magnifications (b), (c), (d).

It is plausible that the pink discolorations at Phnom Krom were caused by the colonization of pigmented microorganisms. The size of the coccoid shape cells and the presence of an extracellular matrix do indeed suggest a biological origin for the pink discolorations and are consistent with the presence of bacteria (Imperi *et al.*, 2007; Laiz *et al.*, 2009). Furthermore, the observation of a cross section through optical microscopy revealed the thickness of the external pink layer. It confirms a strong association between the salt efflorescence, a thin white layer below the pink exterior, and the encrustation (Fig. 4a). Microanalysis with EDS on a single spot of the pink surface layer showed the abundant presence of P, and to a lesser extent of Si, Al, K, Mg, Mn and Fe. The SEM/EDS maps highlighted the presence of Si (Fig. 4d), Al (Fig. 4e) and K (Fig. 4f) associated with the substrate. Instead, in correspondence with the thickness of the encrustation was detected P, Al and small amount of Si (Fig. 4c, 4d, 4e). The presence of P was related to bat excrement (Delvert, 1963; Fusey, 1991; Uchida *et al.*, 1999). In fact, P can be leached from bat guano by rainwater and filter into the sandstone through a capillary process, and the water evaporation causes the crystallization of phosphate minerals onto the surface of the sandstone (Fusey, 1991; Uchida *et al.*, 1999). Moreover, Al into the pink layer, was chemically correlated to a phosphate mineral identified as taranakite, a potassium aluminium phosphate hydrate (Uchida *et al.*, 1999).

We believe, therefore, that the high level of P at the Phnom Krom temple can be traced back to salts efflorescence arising from the bat guano deposits, but we would also like to stress that the presence of guano alone produces blackish deposits and encrustations. The simultaneous presence of other phenomena seems necessary to explain the origin of the pink encrustations. Microscopic observations have, in fact, revealed a microbiological

colonization corresponding to P accumulation related to guano deposits, so the presence of microorganisms can explain this peculiar coloration. These findings suggested that the pink discoloration in presence of salt efflorescences may be connected to halophilic and xerotolerant bacteria colonizing niches suffering periods of drought (Imperi *et al.*, 2007; Laiz *.et al.*, 2009) caused by intense sunlight and/or seasonal rain cycles.

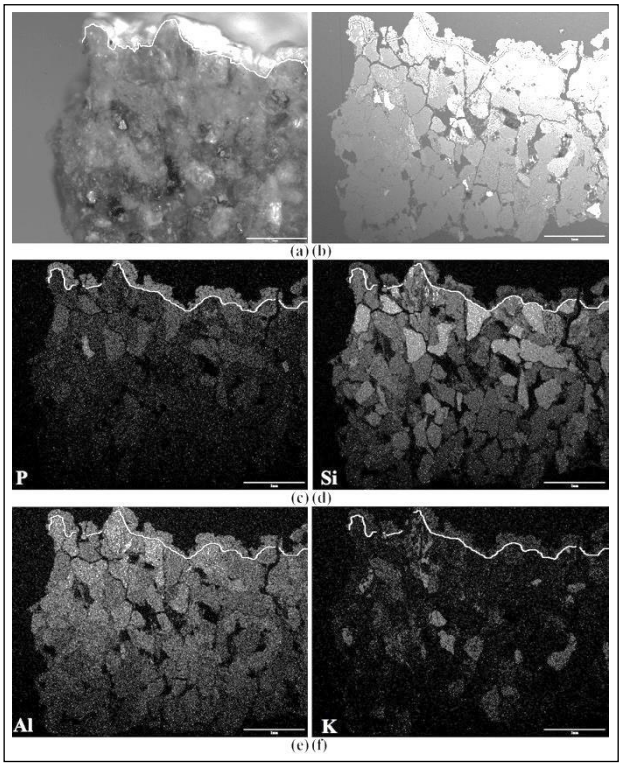

Fig. 4: Cross section analysis: (a) optical microscopy image; (b) SEM image; EDS maps of (c) Phosphorous; (d) Silicon; (e) Aluminium; (f) Potassium. The bar is 1mm. [The white line indicates the interface between encrustation and rock].

This particular weathering pattern was observed on only one building in the temple area, and this can be explained both by stone composition, by location and exposure of the building in temple context. Lacking of reciprocal covering between buildings affects the colonized area to highest thermic stresses on the south and east facing sides, due to higher solar radiation (Donegani 1982, unpublished work). Furthermore, the wooden scaffold structures provide partial cover which protects the surfaces from pouring rain but not from direct sunlight, and salt efflorescences as a result of evaporation are widespread.

5. Conclusion

The appearance of pink discoloration on monuments is a worldwide issue in the field of cultural heritage conservation. In this study we report, for the first time, the detection of pink discolorations on Phnom Krom temple (Cambodia). The biological nature of this phenomenon has been proved through a morphological analysis that identifies bacteria as

the main agents of the development of the pink encrustations. The phenomenon is related to the presence of guano deposits inside the temple and to evaporation cycles, which transport P and other chemical elements to the surface of external walls, especially in areas exposed to direct sunlight and protected from pouring rain. The simultaneous occurrence of several different conditions explains the limited distribution of such alterations, which involve the presence of halophilic microorganisms as a final cause of the phenomenon. Its development can be traced to a complex ecosystem which involves the nature of the stone, physical and microclimatic conditions, and biological components (bats and the chemical composition of their excrement, and finally microorganisms).

Information on the structure of microbial communities in the biofilms is indispensable in order to understand the microbial community in question and control biofilm colonization on the historic bas-reliefs. Therefore, further analysis is needed to identify the biological composition of the pink encrustation though taxonomic characterization using genetic tools, and to understand whether, in such a deteriorated situation, the formation of this patina can be protective or deteriorative for the sandstone surface.

References

André, M.F., Vautier, F., Voldoire, O., and Roussel, E., 2014, Accelerated stone deterioration induced by forest clearance around the Angkor temples, Science of the Total Environment, 493, 98 - 108.

Bartoli, F., Municchia, A.C., Futagami, Y., Kashiwadani, H., Moon, K.H., and Caneva, G., 2014, Biological colonization patterns on the ruins of Angkor temples (Cambodia) in the biodeterioration vs bioprotection debate, International Biodeterioration & Biodegradation, 96, 157 - 165.

Caneva, G., Bartoli, F., Ceschin, S., Salvadori, O., Futagami, Y., and Salvati, L., 2015, Exploring ecological relationships in the biodeterioration patterns of Angkor temples (Cambodia) along a forest canopy gradient, Journal of Cultural Heritage, 16 (2), 728 - 735.

Caneva, G., Danin, A., Ricci, S., and Conti, C., 1994, The pitting of Trajan's column, Rome: an ecological model of its origin. in Conservazione del Patrimonio culturale II. Contributi Centro Linceo Interdisciplinare Beniamino Segrè, Accademia Nazionale dei Lincei, 88, 77 - 102.

Cappitelli, F., Abbruscato, P., Foladori, P., Zanardini, E., Ranalli, G., Principi, P., Villa, F., Polo, A., and Sorlini, C., 2009, Detection and elimination of Cyanobacteria from Frescoes: The case of the St. Brizio Chapel (Orvieto Cathedral, Italy), Microbial Ecol., 57, 633 – 639.

Daigoro, C., Yasushi, K., Yoshiaki, I., Endo, N., Launay, J., and Yamada, S., 1992, "Considerations for the conservation and preservation of the historic city of Angkor", World Monuments Fund Report I, Overview, New York.

Delvert, J., 1963, Recherches sur l'érosion des grès des monuments d'Angkor, Bull. École Française d'Extrême-Orient, 2, 453 – 534.

Ettenauer, J.D., Jurado, V., Piñar, G., Miller, A.Z., Santner, M., Saiz-Jimenez, C., and Sterflinger, K., 2014, Halophilic Microorganisms Are Responsible for the Rosy Discolouration of Saline Environments in Three Historical Buildings with Mural Paintings, PLoS ONE, 9 (8), e103844.

Fusey, P., 1991, Altération biologiques des grés Cambodgiens et recherche de moyens de protection, École Française d'Extrême-Orient, Paris, France, ISBN 285539550X, 91 pp.

Giacobini, C., Andreoli, C., Casadoro, G., Fumanti, B., Lanzara, P., and Rascio, N., 1979, Una caratteristica alterazione delle murature e degli intonaci, Atti del 3° Congresso Internazionale sul Deterioramento e la Conservazione della Pietra (Venezia, 24-27/10/1979), Badan B. (eds.), Padova, 289 – 299.

Glaize, M.V., 1940, Le dégagement du Phnom Krôm, précédé de quelques remarques sur les fondations de Yaçovarman, Bull. de l'Ecole française d'Extrême-Orient, Tome 40 N°2, 371 - 381.

Hosono, T., Uchida, E., Suda, C., Ueno, A., and Nakagawa, T., 2006, Salt weathering of sandstone at the Angkor monuments, Cambodia: identification of the origin of salts using sulphur and strontium isotopes, J. Archaeol. Sci., 33, 1541 – 1551.

Imperi, F., Caneva, G., Cancellieri, L., Ricci, M., Sodo, A. and Visca, P., 2007, The bacterial aetiology of rosy discoloration of ancient wall paintings, Environ. Microbiol., 9, 2894 – 2902.

Kusumi, A., Li, X., Osuga, Y., Kawashima, A., Gu, J.D., Nasu, M., and Katayama, Y., 2013, Bacterial Communities in Pigmented Biofilms Formed on the Sandstone Bas-Relief Walls of the Bayon Temple, Angkor Thom, Cambodia, Microbes and Environments, 28 (4), 422 - 431.

Laiz, L., Miller, A.Z., Jurado, V., Akatova, E., Sanchez-Moral, S., Gonzalez, J.M., Dionísio, A., Macedo, M.F., Saiz-Jimenez, C., 2009, Isolation of five *Rubrobacter* strains from biodeteriorated monuments, Naturwissenschaften, 96 (1), 71 - 79.

Normal-1/88, 1990, Alterazioni Macroscopiche dei Materiali: Lessico, Roma, C.N.R.-I.C.R.

Ortega-Morales, B.O., Narváez-Zapata, J.A., Schmalenberger, A., Sosa-López, A., and Tebbe, C.C., 2004, Biofilms fouling ancient limestone Mayan monuments in Uxmal, Mexico: a cultivation-independent analysis, Biofilms, 1, 79 - 90.

Siedel, H., Pfefferkorn, S., von Plehwe-Leisen, and E., Leisen, H., 2010, Sandstone weathering in tropical climate: results of low-destructive investigations at the temple of Angkor Wat, Cambodia, Eng. Geol., 115, 182 – 192.

Uchida, E., Ogawa, Y., Maeda, N., and Nakagawa, T., 1999, Deterioration of stone materials in the Angkor monuments, Cambodia, Eng. Geol., 55, 101 – 112.

UNI 10922, 2001, Beni culturali: Materiali lapidei ed artificiali. Allestimento sezioni sottili e sezioni lucide di materiali lapidei colonizzati da biodeteriogeni, Milano, UNI.

UNI 10923, 2001, Beni culturali: Materiali lapidei naturali ed artificiali. Allestimento di preparati biologici per l'osservazione al microscopio ottico, Milano, UNI.

INFLUENCE OF THE VILLARLOD MOLASSE ANISOTROPY ON CRACKING ADVANCES IN THE COMPREHENSION OF THE DESQUAMATION MECHANISMS

M. Tiennot[1*], A. Bourgès[1] and J.-D. Mertz[1]

Abstract

Mineralogical characteristics as well as natural structural anisotropy have a huge impact on sustainability, fatigue resistance and alteration processes of monumental stone heritage. This research studies the Villarlod molasse alteration, especially due to swelling mechanisms at the surface. As previous researches have shown that clay minerals are involved in this phenomenon, the impact of these phases on the dimensional variations and on the mechanical behaviour of the stone is considered to understand such weathering processes. Macroscopic mechanical properties are measured with respect to the bedding, and an innovative approach based on fracture mechanics was carried out. Results indicate the lower resistance and lower stiffness of the stone after water saturation. During hygric cycles, free swelling strains are measured twice higher in the direction normal to the bedding planes. Relative humidity variations induced an anisotropic mechanical damage. This indicates that the microcracking generated by the swelling of the stone is oriented. Moreover, observations of fracture surfaces illustrate that clay minerals are located on the weakness planes of the stone and that the specific orientation of these swelling phases created an anisotropic damage involved in decay phenomena.

Keywords: clay minerals, swelling, fracture mechanics, damage, microcracking

1. Introduction

Natural weathering processes are involved in the deterioration of the monumental stone. Mechanisms related to thermal effects, salts crystallization or biocolonization, to freeze-thaw cycles and especially to water effect are essential factors for the alteration of the monumental stone (Siegesmund and Snethlage 2011, Bourgès 2012, Fontaine *et al.* 2015). A large number of studies on these alteration processes pointed out the influence of water, inducing repeated dimensional variations that may become irreversible. Water also specially affects the mechanical properties, as strength, elasticity and ability to withstand initiation of cracking phenomenon (Erguler and Ulusay 2009, Morales *et al.* 2007). Various stone deterioration patterns are observed, as material loss or cracking and detachment alteration (ICOMOS-ISCS 2008). This research focuses on desquamation, a detachment alteration widely observed on our monumental stone heritage and especially on Villarlod molasse (Fig. 1). Subsurfaces of the exposed stone are affected and contour scaling develops parallel to the surface. Such alteration pattern is related to swelling mechanisms in

[1] M. Tiennot*, A. Bourgès and J.-D. Mertz
Laboratoire de Recherche des Monuments Historiques, CRC-LRMH USR 3224, France
mathilde.tiennot@culture.gouv.fr

*corresponding author

close correlation with water saturation and relative humidity (*RH*) variations repeated over natural cycles (Doehne and Price 2010). Such dimensional behaviour is governed by the mineralogical composition and the microstructural properties of the stones. Impact of the clay minerals on the stone dilatation was studied over the past few years (Scherer and Jimenez-Gonzalez 2005, Ruedrich *et al.* 2011, Reyes-Zamudio *et al.* 2011). The role of the clay phases on the anisotropic swelling and on the mechanical properties is discussed. Moreover, as desquamation results from damage and initiation of cracking a few millimetres within the monumental stone, a fracture mechanics approach is proposed to understand the mechanisms involved. The influence of the surrounding environment is also evaluated to improve the comprehension of stone deterioration mechanisms under water effects.

Fig. 1: Desquamation pattern developing on Villarlod molasse at the Fribourg city hall.

2. Materials and methods

2.1. Villarlod molasse sampling

Villarlod molasse (Burdigalien formation 16-20 My) is a clay-bearing sandstone rich in glauconite from the region of Fribourg in Switzerland, used as a traditional building material in this country (Felix 1983). Typical decay of this stone is related to small scales around 1 cm thick without any relation with the position of the ashlar block in the building monument. As a result, environmental conditions seem to be a secondary factor by contrast with the stone intrinsic parameters conditioning the swelling-shrinking mechanisms (Fig. 1). Cylindrical plugs of 40 mm in diameter and 80 mm in length are cored on blocks on the two principle directions of this molasse, perpendicular and parallel to the natural bedding planes.

2.2. Characterisation methods

2.2.1. Mineralogical and structural properties

Observations of the mineral phases and the porous network are performed by optical microscopy (OM) using thin sections and scanning electron microscopy (SEM) on gold-coated fresh fractures. Mineralogical identification is investigated by X-ray diffraction (XRD) on a Bruker D8 Advance® Bragg-Brentano diffractometer. The clay fraction (< 2 µm) of the stone is extracted and three different analyses are performed: on natural clay, after heating at 490°C during 4 hours and after a conditioning in a ethylene glycol saturated atmosphere, in order to identify the clay minerals present within the stone.

2.2.2. Mechanical characterisation

Macroscopic mechanical properties of this stone are determined. The non-destructive system GrindoSonic® based on the resonance frequencies of the material is used to characterise the dynamic elastic properties, Young E modulus and Poisson ratio ν. Samples cored perpendicular and parallel to the bedding plane are tested, allowing to identify and quantify the anisotropy of the parameters. All mechanical testing are performed using an Instron® machine at a displacement rate of 0.2 mm·min^{-1}. Indirect tensile testing using Brazilian discs of 20 mm in radius R and 20 mm in thickness t, so that $t/R = 1$, are prepared to measure the tensile strength (Fig. 2). These measurements are performed under three configurations, to verify the influence of the stone's natural heterogeneity on the tensile strength. A specific fracture mechanics approach is proposed to study this scaling alteration. Several methods have been tested and developed over the past few years to evaluate the fracture properties of geomaterials. To study cracking initiation and propagation for stone as a building material, and in the specific field of cultural heritage, feasibility of toughness measurement methods using small cores of 40 mm in diameter was verified (Tiennot and Bourgès 2016). Semi-Circular Bending (SCB) method is adapted for these cultural heritage researches, for adequate parameters. SCB uses a semi-circular specimen, loaded under a three-point bending. The pre-existing notch required for fracture mechanics samples is here straight aligned with the loading direction (Fig. 2).

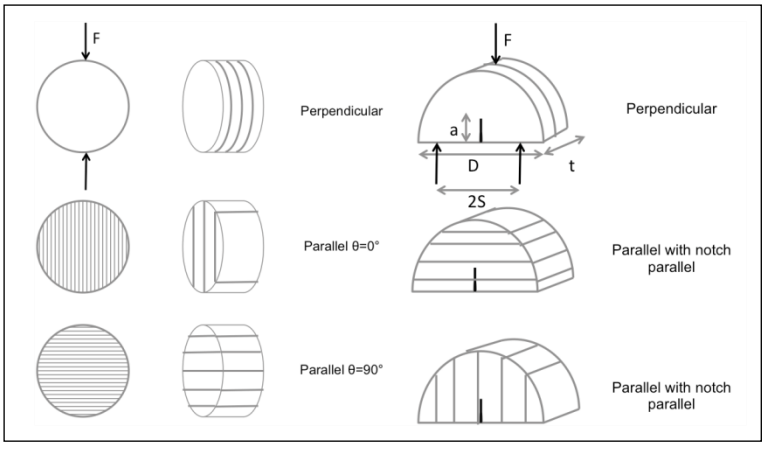

Fig. 2: Semi-Circular Bending geometry and parameters for the three configurations tested with respect to the natural bedding.

As usual thickness *t* and radius *R* for SCB samples are such as *t/R* = 1, thickness of the samples is 20 mm. Based on our previous researches, the straight initial notch *a* is cut with a width of 1 mm and a length of 4 mm, such as the ratio *a/R* = 0.2. For sedimentary stones as Villarlod molasse, fracture properties have to be studied with respect to the stratigraphic bedding and to the planes of isotropy. Three configurations are proposed for this research, and eight samples for each configuration are tested (Fig. 2). Anisotropy of cracking properties can be estimated.

2.2.3. Saturation at 48 hours, hygric behaviour and dimensional variations

Influence of water saturation on the molasse is studied following the 48h saturation protocol (Hirschwald 1908), where samples are progressively immerged into water. Hygric dimensional behaviour is measured by LVDT sensor TWK® (accuracy 0.3 µm), placed on a dilatometric system adapted at the laboratory (Mertz *et al*. 2012). Cores are subjected to three isothermal cycles (T=20°C) of humidification from 25 % to 97 % *RH* during 96 hours and drying to 25 % *RH* during 48 hours. Free swelling strains of the molasse $\varepsilon_{s\perp}$ and $\varepsilon_{s//}$, perpendicular and parallel to the natural stratigraphy, are measured.

3. Results and discussion

3.1. Mineralogical and structural properties

The identified mineralogical phases are coarse-grains of quartz, feldspars, biotite and clay phases included in a compacted calcitic matrix. Large spots of glauconite dispersed particles provide the global green colour of this stone (Fig. 3). Clay minerals are identified by XRD analyses as kaolinite, illite, vermiculite and glauconite. Furthermore several mineral phases, especially vermiculite and glauconite, present well-known swelling properties and may induce damage when submitted to water saturation and *RH* change. Their organisation, along the bedding as observed in the thin section, induces natural anisotropy of the stone.

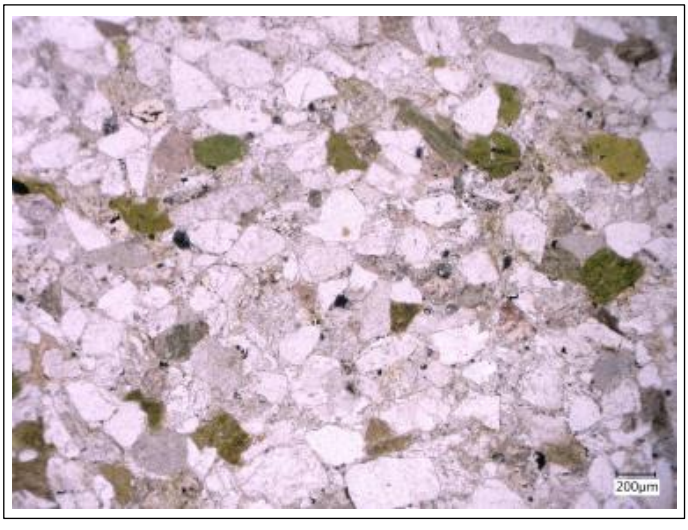

Fig. 3: Petrographic observation on thin section of the Villarlod molasse.

3.2. Dimensional behaviour under relative humidity variations

Uniaxial dimensional behaviour is measured during three cycles of *RH* humidification and drying. Anisotropy of this stone dilatation is pointed out. Free swelling in the direction perpendicular to the bedding is twice higher than parallel to it, with the respective measured dilatations of $\varepsilon_{s\perp}$ = 0.48 mm.m^{-1} and $\varepsilon_{s//}$ = 0.27 mm.m^{-1} (Fig. 4). We assume that the measured dimensional variations are related to the oriented swelling of the clay minerals sensitive to *RH* change.

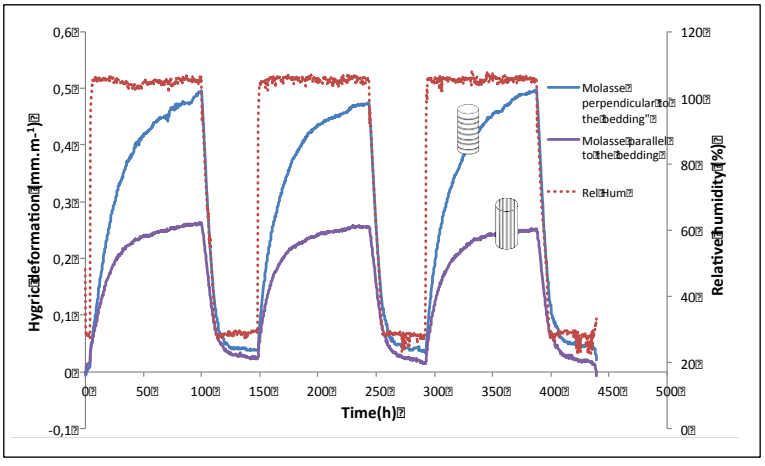

Fig. 4: Dimensional behaviour of Villarlod molasse in the directions perpendicular and parallel to the bedding subjected to three cycles of RH variations.

3.3. Mechanical characterization of the Villarlod molasse

3.3.1. Mechanical properties at the initial dry state

Young modulus and Poisson ratio are measured on the two directions, perpendicular and parallel to the bedding (Tab. 1). The Young moduli are higher in the direction parallel to the bedding. Anisotropy parameter is measured a $\alpha = E_{//}/E_{\perp}$s = 1.27 at the dry state. The evolution of this parameter after hydric and hygric solicitations is evaluated in the following sections. The tensile strength depends on the orientation of the applied load with respect to the orientation of the stone phases (Tab. 2). Indeed, $\sigma_{max-tens}$ is lower when the load is applied on the direction of the natural orientation of the stone (configuration parallel θ=0°). Fracture toughness K_{IC} under mode I is measured with respect to the natural bedding of the stone (Tab. 2). Fracture properties and especially cracking initiation also depend on the natural anisotropy of the stone. The lower value is measured when the initial notch is parallel to the natural orientation of the minerals. A crack is more difficult to initiate in the perpendicular configuration and when the notch is perpendicular to the bedding, as it requires more energy to progress.

Tab. 1: Measured values of the Young modulus and the Poisson ratio perpendicular and parallel to the bedding of the stone, and calculated anisotropy parameter, under dry, saturated and cyclic RH conditions. Standard deviation is in brackets.

Young modulus (GPa)	**Dry**	**Saturated**	**After 3 *RH* cycles**
$E_{\perp}$	8.4 (± 0,4)	6.6 (± 0,3)	7.1 (± 0,1)
$E_{//}$	10.7 (± 0,2)	6.5 (± 0,4)	9.8 (± 0,1)
$\boldsymbol{\nu}_{\perp}$	0.40 (± 0,01)	0.30 (± 0,0)	0.38 (± 0,01)
$\boldsymbol{\nu}_{//}$	0.30 (± 0,10)	0.30 (± 0,0)	0.35 (± 0,0)
Anisotropy parameter α	1.27	0.98	1.38

Tab. 2: Measured values of the tensile strength and of the fracture toughness in mode I with respect to the natural anisotropy of the Villarlod molasses.

		Dry	**Saturated**
$\sigma_{max-tens}$ (MPa)	Perpendicular	1,97 (± 0,06)	0,43 (± 0,07)
	Parallel θ=0°	1,5 (± 0,09)	0,40 (± 0,05)
	Parallel θ=90°	1,85 (± 0,3)	0,45 (± 0,12)
K_{IC} (MPa.√m)	Perpendicular	0,097 (± 0,04)	0,034 (± 0,02)
	Parallel notch ⊥	0,104 (± 0,03)	0,033 (± 0,02)
	Parallel notch //	0,080 (± 0,02)	0,028 (± 0,02)

3.3.2. Influence of water saturation on mechanical properties

Young moduli in the two directions are measured after saturation. $E_{\perp}$ and $E_{//}$ are lower for the saturated molasse (Tab. 1). Anisotropy parameter is close to one: the anisotropy of the stone is lower when the porous network is saturated. The tensile strength decreases significantly for the wet samples (Tab. 2). The ability to resist to the initiation of a crack is also affected when water fills the porous network, as fracture toughness K_{IC} decreases after saturation with liquid water. Such decreasing of the resistance and fracture properties of the stone induces decay alteration by cracking and desquamation of the affected surfaces.

3.3.3. Influence of hygric variations on Villarlod molasse

Evaluation of the Young moduli after the three cycles of swelling under *RH* variations indicates a decrease of the stiffness of the stone. As a matter of fact, $E_{\perp}$ as well as $E_{//}$ are lower after hygric solicitations. This is due to the creation of microcracks within the stone. The anisotropy of this isotropic transverse material is also influenced by such cycles. Indeed, results show an increase of the anisotropy parameter, calculated as α = 1.38 after the *RH* variations. Samples used for these dilatometric measurements are then oven-dried, in order to compare the Young modulus before and after the hygric cycles. The influence of such *RH* variations on stiffness and on the mechanical damage induced within the material can be estimated using the damage variable D. It quantifies the degradation of the cohesion

of a material under solicitations, leading to the initiation of cracking. This variable is determined considering the variations of the Young's modulus as $\tilde{E} = E(1 - D)$, where E is the Young's modulus at the initial state, and $\tilde{E}$ after solicitation. Two damage variables are defined: $D_{\perp}$ and $D_{//}$. After three cycles of variations from 25 % to 97 % *RH*, $D_{\perp}$= 0.15 and $D_{//}$= 0.08. These values indicate that repeated swelling of molasse induces damage, and that this damage is anisotropic, twice higher in the direction perpendicular to the bedding. Microcracking network created is oriented, and stiffness is not affected in the same way by such dimensional variations. The natural anisotropy of the stone influences the evolution of the mechanical properties under such *RH* variations.

3.4. Influence of clay minerals on fracture behaviour

Fracture surfaces of samples used for the tensile Brazilin tests are observed by SEM. The two directions, perpendicular and parallel to the planes of the molasse are studied. Clay minerals aggregates can be noticed on the fracture surfaces, in both directions (Fig. 5 and 6).

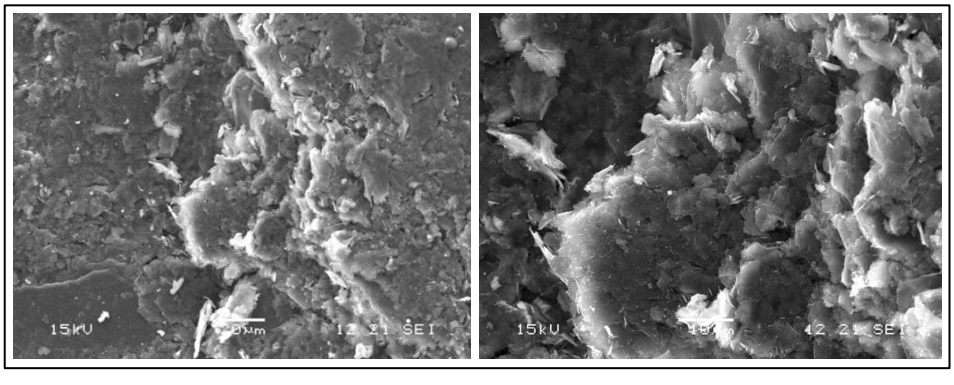

Fig. 5: SEM observations of the fracture surface for a specimen tested in the configuration parallel θ=0°, a) ×650 b) ×1500, with detachment of the clay aggregates.

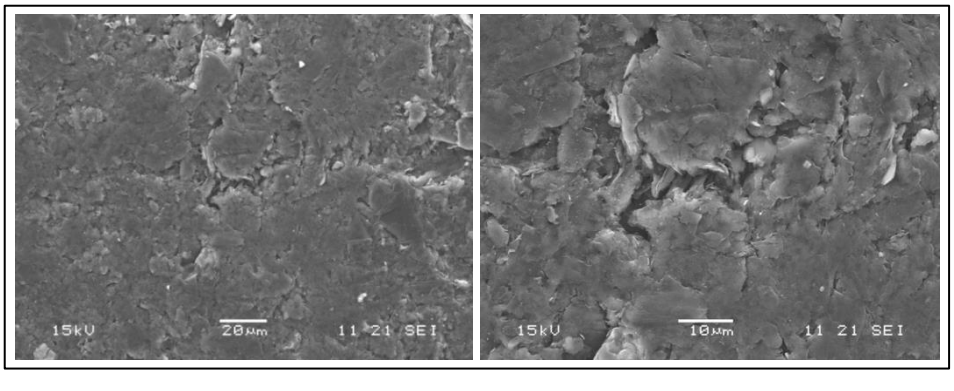

Fig. 6: SEM observations of the fracture surface for a specimen tested in the configuration parallel θ=90°, a) ×650 b) ×1500.

Failure occurs in a plane where clays are located and fracture patterns followed these platy minerals orientation. Moreover, tensile strength measurements in the different configurations point out the weakness planes of this sedimentary stone when the load is applied in the direction parallel to the minerals (Tab. 2). For these crack paths on configuration parallel θ=0° samples, detachment and scaling can be seen on the whole fracture surfaces, while such patterns cannot be observed perpendicular to the bedding. We assume that the clay platelets divergence due to the particles exfoliation can explain the lower resistance of these fracture planes. Such distribution of clay particles and the delamination of aggregates also illustrate the orientation of the microcracking network demonstrated by the difference between the $D_{\perp}$ and $D_{//}$ variables.

4. Conclusion and perspectives

This research focuses on the weathering phenomena of the Villarlod molasse, especially due to swelling mechanisms. First of all, tensile resistance and toughness measurements demonstrated the anisotropic behaviour of this stone with respect to the natural bedding. Decay observed under natural environment conditions are due to the decreasing of the mechanical properties with water saturation and *RH* variations. Moreover, under such hygric swelling, mechanical damage induced is higher perpendicular to the bedding planes of the stone. Observations of the fracture surfaces on the two directions illustrate the difference in the microcracking network created within the stone. Weakness planes of the Villarlod molasse correspond to clay minerals phases and the swelling on a specific orientation of these platy minerals created anisotropic damage involved in decay phenomena. Further indications on the real distribution of the mineral phases sensitive to humidity will be investigated.

Acknowledgments

This work was supported by French state funds managed by the ANR within the Investissements d'Avenir program under reference ANR-11-IDEX-0004-02, and more specifically within the framework of the Cluster of Excellence MATISSE led by Sorbonne Universités.

References

Bourgès, A., 2012, Fracture mechanic : a new approach to tackle stone conservation, in proceedings of 12th International congress on the deterioration and conservation of stone, New-York.

Doehne, E. and Price, C.A., 2010, Stone Conservation: An Overview of Current Research, CA: The Guetty Conservation Institut, Los Angeles.

Erguler, Z.A. and Ulusay, R., 2009, Water-induced variations in mechanical properties of clay-bearing rocks, International Journal of Rock Mechanics and Mining Sciences, 46, 355-370.

Felix, C., 1983, Sandstone linear swelling due to isothermal water sorption, Materials Science and Restoration, Ed. by F.H. Wittmann, Tech. Akademie Esslingen, Ostfildern, 305-310.

Fontaine, L., Hendrickx, R. and De Clercq, H., 2015, Deterioration mechanisms of the compact clay-bearing limestone of Tournai used in the Romanesque portals of the Tournai Cathedral (Belgium), Environmental Earth Science, 74, 3207-3221.

Hirschwald, J., 1908, Die Prüfung der natürlichen Bausteine auf ihre Wetterbeständigkeit. Berlin: Verlag von Wilhelm Ernst and Sohn, p. 675.

ICOMOS-ISCS, 2008, Illustrated glossary on stone deterioration, Conseil scientifique international "Pierre" de l'ICOMOS. Monuments & Sites 15. Paris: ICOMOS and ISCS, 78pp.

Mertz, J.-D., Guiavarc'h, M. and Pagnin, P., 2012, Dilation behaviour of lime mortars for restoration work : application to the compatibility of cracked stones reassembling, European Journal of Environmental and Civil Engineering, Special Issue Built Heritage, 16, 527-542.

Morales, D.M., Jahns, E. and Ruedrich, J., 2007, The impact of partial water saturation in rock strength: and expe.rimental study on sandstone, Z dtsch GesGeowiss, 158, 869-882.

Scherer, G.W. and Jimenez-Gonzalez, I., 2005, Characterization of swelling in clay-bearing stone, Edited by Turkington, Geological Society Am, 51-61.

Siegesmund, S. and Snethlage, R., 2011, Stone in Architecture, Heidelberg: Springer.

Ruedrich, J., Bartelsen, R., Dohrmann, R., and Siegesmund, S., 2011, Moisture expansion as a deterioration factor for sandstone used in buildings, Environmental Earth Science 63, 1545-1564.

Reyes-Zamudio, V., Angeles-Chaves, C. and Cervantes, J., 2011, Clay minerals in historic buildings, Journal of thermal Anal Calorim 104, 405-413.

Tiennot, M. and Bourgès, A., 2016, Evaluation of small core-based specimens for characterization of stone deterioration, International Journal of Rock Mechanics & Mining Sciences, 84, 69-73.

This page has been left intentionally blank.

DECAY PHENOMENA OF MARBLES IN THE ARCHAEOLOGICAL SITE OF HIERAPOLIS OF PHRYGIAE (DENIZLI, TURKEY)

S. Vettori[1*], S. Bracci[1], P. Caggia[2], E. Cantisani[1], O.A. Cuzman[1], T. Ismaelli[2], C. Riminesi[1], B. Sacchi[1], G. Scardozzi[2] and F. D'Andria[3]

Abstract

The paper describes the state of conservation and the decay phenomena of marble elements of the ancient Phrygian city of Hierapolis in the Denizli district in Turkey. The archaeological site presents some peculiarities that make it unique in terms of conservation and decay phenomena of marbles and travertines. Environmental factors (i.e. thermal springs, high thermal stress, seismic faults) together with the microstructural characteristics of the typologies of marble play a fundamental role on the durability and the state of conservation of the materials. A lot of architectonic elements, belonging to several monuments (e.g. Civil *Agorà*, Sanctuary of *Apollo*, *Ploutonion*, Marble *Stoà*, Gymnasium, North *Agorà*, *Stoà near the Springs*, *Bouleuterion*) were selected and investigated. A monitoring network in the areas of the *Ploutonion* (positioned close to the major fault) and the Sanctuary of *Apollo* was installed in August 2013. The network consists of several sensors measuring ~~e~~nvironmental parameters (T and *RH*%), both in external and in confined environments and gases (CO_2, CO, O_2, H_2S). Stone sampling was carried out for laboratory analyses (XRD, FT-IR, OM, SEM-EDS). In parallel, the geochemical characterisation of waters circulating in the site and dissolved gases was carried out. Furthermore, the biological characterisation of patinas affecting some architectonic elements, was performed.

Keywords: decay, marble, archaeological site, thermal waters, gases

[1] S. Vettori* S. Bracci, E. Cantisani, O.A. Cuzman, C. Riminesi and B. Sacchi
Institute for the Conservation and Valorisation of Cultural Heritage, Sesto Fiorentino (FI), Italy
vettori@icvbc.cnr.it

[2] P. Caggia, T. Ismaelli G. Scardozzi
Institute for the Archaeological and Monumental Heritage, Lecce, Italy

[3] F. D'Andria
University of Salento, Lecce, Italy

*corresponding author

1. Introduction

1.1. Historical setting

The city of Hierapolis, founded in the Hellenistic age on high ground overlooking the valley of the Lykos, a tributary of the Meander, near the modern village of Pamukkale (Turkey), contains monumental remains (Fig. 1) from the Imperial and Byzantine epochs, situated in a regular road network arranged around a *plateia* about 1.5 km long that constitutes a stretch of the ancient road between Pergamum and Laodikeia on the Lykos, an important axis of communication between the Aegean coast and central Anatolia.

Fig. 1: The archaeological site of Hierapolis: Sanctuary of Apollo and the Theatre in the back.

The presence of thermal springs and the huge precipitation of $CaCO_3$ forming travertine, together with the fact that the town of Hierapolis is cut longitudinally by several parallel fractures of the Pamukkale fault, thus being subjected to an intense seismic activities, determine specific decay phenomena. The monumental remains were selected on the basis of some parameters: different distance from the fault system, greater or lesser exposition to the gases, different times from the excavation (started in 1957 by an Italian Archaeological Mission), exposition to the touristic flow or not.

The ruins of Civil *Agorà* are located in an area currently occupied by a lake probably developed in XIV century A.D., following a seismic event that strongly modified the hydrology of the area. Now the marble blocks belonging to the porticos are included in the structure of Pamukkale Thermal. These structures are one of the most significant touristic destinations. More than 1 million and half tourists visit the site every year. The stones are subjected to all the alteration phenomena typical of submerged environment, to which the problems created by touristic flow are added. The so-called *Stoà near the Springs* was selected because is considered representative of a typical decay phenomenon of Hierapolis site: it is located on a seismic fault, where gaseous mixtures come out being responsible of heavy phenomena of granular disintegration of marbles. The so-called *Building A* of Sanctuary of *Apollo*, built in III century A.D., is the best preserved temple of the site. The monument was excavated in the sixties of XX century and was selected as representative of several decay and alteration phenomena due to the characteristics of material and exposure conditions.

The Marble *Stoà*, realized in the I century A.D., along the main road of the city, has been recently excavated (2005-2006) and some thick deposits of travertine have been removed. The travertine blocks were formed in Medieval Age due to prolonged contact with thermal waters. The monument is an example of decay phenomena due to the extreme conditions of conservation of lapideous material, submerged by a swampy environment and subsequently included in the travertine strata.

During the antiquity Hierapolis was a famous pilgrimage centre because of the *Ploutonion*, the sanctuary dedicated to Hades-Pluto and his wife Kore-Persephone, visited also by Cicero and Strabo. The sanctuary was constructed during the early Imperial period (I century B.C. – I century A.D.) exactly above the entrance of a natural cave, from which thermal waters and poisonous gases emerge. A monumental facade with ionic half-columns framed the entrance to the sacred cave, while a huge rectilinear theatre, in travertine blocks, housed the spectators participating to the sacred rituals. Bulls were sacrificed in front of the grotto by asphyxiation while the *Galli*, the eunuch priests of the goddess Cybele, miraculously entered the cave remaining inside without any harm. In front of the cave a marble circular building (*tholos*) was flanked by two rectangular pools for the warm thermal water flowing from the grotto.

During the last years the excavation conducted by the Italian Archaeological Mission, headed by Francesco D'Andria, brought to light the entire sanctuary of Pluto, discovering the grotto and the theatre, described by the literary sources. The grotto is opened along the eastern side of a large fissure of the ground that was produced by the seismic fault that crossed all the urban area of Hierapolis. The natural agents characterizing the site (carbonatic hot-thermal waters and gases rich in CO_2), important for the ancient cult rituals, are responsible for critical conservation of the architectural structure of the *Ploutonion*.

2. Materials and methods

The evaluation of decay, the definition of the chemical-physical processes involved, are inescapable parameters that must be considered for the definition of protocols for the conservation. On each monument a sampling campaign was realized and the following analytical methodologies were applied:

- X-ray diffractometry (X-ray diffractometer X' Pert PRO- PANalytical, anticathode Cu equipped with an X'Celerator multidetector. Data were processed using HighScore software and the ICDD database was used) and Fourier Transform Infrared Spectroscopy (System 2000 FTIR spectrometer (Perkin-Elmer) with Spectrum software) for the identification of new developed phases;

- Optical (OM Zeiss Axio Scope A1) and electronic (SEM Quanta 200 (FEI) environmental scanning electron microscope equipped with an EDS microprobe) microscopy for the assessment of the state of conservation and evaluation of the thickness and composition of the alteration phases;

- IR thermography survey of the earthly and of areas and buildings close to the faults was performed using a FLIR B425 IR camera. The target of this investigation was firstly to find a correlation between the decay/alteration phenomena and exposure to warm air, rich of gases due to the closeness at faults, secondly to establish the location of the monitoring points and the correct

positioning of sensors. The choice of the positioning of sensors was also established through preliminary investigation using portable devices (thermos-hygrometers, and CO_2 and CO loggers);

- Environmental parameters (T and *RH*%), both in external and in confined environment, were measured by commercial data logger with a customized sensors based on micro-thermocouple for the measurement of the surface temperature on marble;
- Commercial gas sensors devoted to the measurement and control of particular environment as well as for the combustion gas monitoring were used. For this target solid state sensors produced by Alphasense, in particular sensors to measure CO_2, CO, O_2, and H_2S, were adapted to the peculiar situation (very high concentration of gases).

Preliminary measurements in the *Ploutonion* showed a peak of CO_2, at values over 90% close to the cave access: such concentration decreases with the increasing of the distance from the cave access. Fig. 2 shows the localization of the monitoring points. In order to evaluate the maximum concentration of gases a monitoring point was placed inside the cave, and the other monitoring point was positioned at the entry passage for the sacrificial animal.

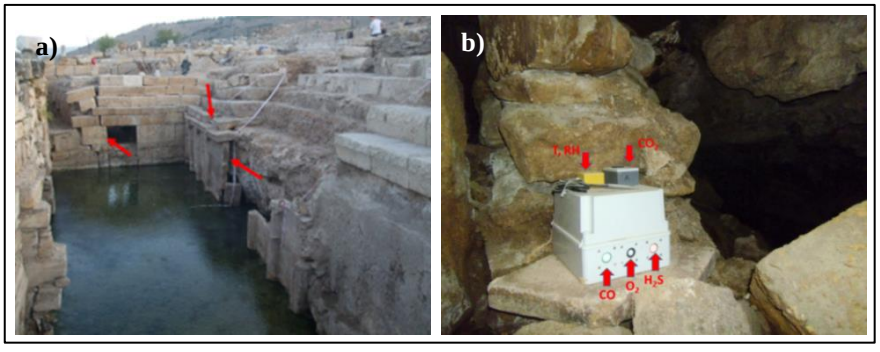

Fig. 2: a) Localization of the monitoring points in the Ploutonion; b) Positioning of the monitoring station inside the cave of the Ploutonion.

In Fig. 2b is shown the positioning of the monitoring station inside the cave. The monitoring station consists of three parts: the data logger for the environmental measurements of temperature (*T*) and relative humidity (*RH*), the data logger for the measurement of CO_2, and a third part, white case, containing gas sensors for the measurement of CO, O_2, and H_2S concentration.

The extreme climatic conditions in the open area of the archeological site impose the need to control the weathering exposition of the stone surfaces, in particular of marble surfaces. For the marble can be critical the fast variations of surface temperature respect to the internal temperature of the substrate. In order to establish the maximum temperature gradient the monitoring of the temperatures of the surface and inside the marble blocks was performed in selected areas. The selected areas were the marble statue at the theatre and a marble block at the Sanctuary of *Apollo*.

Samples of water and dissolved gas were collected inside the archaeological site, where the underground springs of Hierapolis, characterised by an intense circulation, are close to the surface. Filtered aliquots of water were transferred in 125 mL polyethylene bottles for the analysis of anions and in 50 mL for the cations (acidified with ultrapure HCl). An aliquot (8 mL) of water was collected in plastic tubes filled with 2 mL of an ammonia-cadmium (Cd-NH_4) solution for the determination of the reduced sulfur species (H_2S, HS^- and S^{2-}, expressed as ΣS^{2-}) according to Montegrossi *et al.* (2006). Dissolved gases were sampled using pre-evacuated 250 mL glass vials equipped with a Teflon stopcock that were connected to the Rilsan tube and filled with water up to about three fourths of their inner volume (Chiodini, 1996; Tassi *et al.*, 2008).

Temperature, *pH* value, and electrical conductivity (EC in $mS \cdot cm^{-1}$) were measured directly on site using a multiparameter PCE-PHD 1 probe. Little pieces of thermal samples were immersed in BG11-M nutrient medium (C3061 SIGMA) for the development of possible phototrophic microorganisms. The tubes were kept under controlled conditions of light (low and continuous white fluorescent light of 10 µmolphoton $m^{-2} \cdot s^{-1}$) and temperature (28°C), and controlled after 3-4 weeks using an optical microscope Zeiss AxioPlan.

3. Results and discussion

3.1. Main decay phenomena

The description of phenomena was done according to ICOMOS glossary (2008). The main decay phenomena observed in the monument are strictly linked to exposition of environmental conditions. The granular disintegration is particularly evident in the area subjected to relevant thermic excursion (Sanctuary of *Apollo*, *Ploutonion*, *Stoà* near the Springs) and was also influenced by grain size distribution and microfabric of marbles. In some cases it is particularly intense creating a strong and deep detachment of aggregates of grains from the substrate (Fig. 3).

Fig. 3: Blocks of marbles with granular disintegration at Civil Agorà.

The blocks extracted, since 2013 during the excavation campaign, from water between the entrance of the grotto and the byzantine wall, are affected by thick manganese-based crusts and deposits (Fig. 4a). Rancieite $(Ca,Mn^{2+})Mn^{4+}{}_4O_9 \cdot 3(H_2O)$ was detected by XRD analyses. Very diffuse were also the phenomena of encrustations resulting from water infiltration followed by precipitation of different calcium carbonatic phases (i.e. calcite, aragonite and vaterite as polymorphs of calcium carbonate and huntite ($CaMg_3(CO_3)$ identified by XRD and FT-IR analyses) (Fig. 4b) and the formation of efflorescences constituted by Ca and Mg sulphate in Sanctuary of *Apollo* and *Ploutonion*.

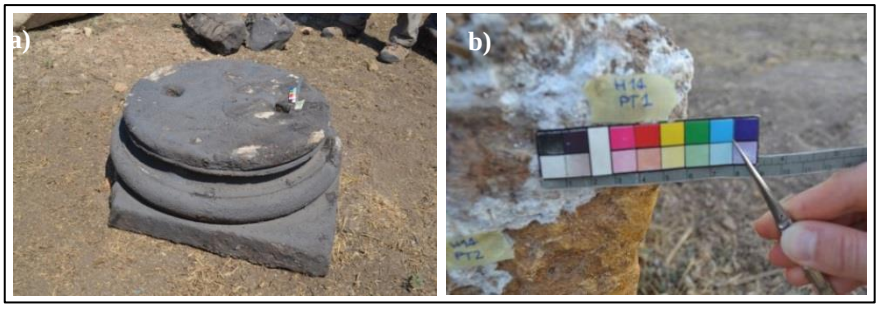

Fig. 4: a) blocks with black Mn crusts and b) white encrustation of huntite.

3.2. Composition of water

The thermal spring waters present on the archaeological site are calcium bicarbonate-sulfate (Ca-HCO_3-SO_4): Ca^{2+}, HCO_3^- and $SO4^{2-}$ concentrations were up to 524, 1296 and 713 mg L^{-1}, respectively. The temperature ranges from 33.1°C to 34.8°C, the EC values from 2.22 to 2.45 mS·cm^{-1} and the *pH* is weakly acid (6.04-6.57). The dissolved gases are mainly constituted by CO_2 (up to 97.5%) and H_2S, determined as the total reduce S species), is within the compositional range of the common Italian thermal waters (Montegrossi *et al.*, 2006).

3.3. Environmental monitoring

Environmental measurements were acquired since August 2013 until August 2015 at the Sanctuary of *Apollo*, the *Ploutonion* and the Theatre with a sampling rate of 15 minutes. The temperatures of the marble surface and inner were measured to detect the temperature gradient on a statue of the Theatre and on a block at the Sanctuary of *Apollo*. The inner temperature was measured inserting a thermocouple in a fissure up to 2-3 cm in depth. Fig. 5a shows the surface temperature versus the inner one at the Sanctuary of *Apollo*. The results of the monitoring of CO_2 inside the cave of the *Ploutonion* are shown on Fig. 5b from August 2014 to August 2015.

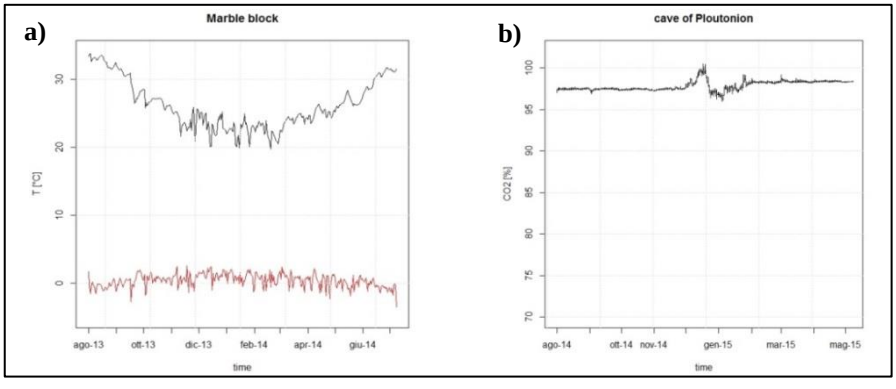

Fig. 5: a) plot of the difference between the surface temperature and inner temperature in a marble block at the Sanctuary of Apollo (bottom/red line) respect to the environmental temperature (top/black line); b) concentrations of CO_2 inside of the Ploutonion cave.

3.4. Biological investigation

The black patinas were dominant in the *Gymnasium*, North *Agorà* and Marble *Stoà*. This patina is associated with the presence of cyanobacteria and/or lichens. In fact, some lichens (*Verrucaria* sp. and *Lecanora* sp.) and cyanobacteria (Cya 2 and Cya 3) were common for all monuments. The highest biodiversity was observed on North *Agorà* (4 species of green algae, 7 species of cyanobacteria, 9 species of lichens and 1 type of bryophyte), followed by *Gymnasium* (2 species of green algae, 6 species of cyanobacteria, 7 species of lichens and 1 type of bryophyte) and Marble *Stoà* (3 species of cyanobacteria, 7 species of lichens and 1 type of bryophyte). The morphological aspect of some isolated organisms is shown in the Fig. 6. The red patinas present in the marble blocks of Civil *Agorà* consist of filamentous cyanobacteria (*Pseudoanabaena pseudoterminata*) and *Leptolyngbya sp.* Spherical unicellular cyanobacteria belonging to the Chroococcales group and two types of diatoms such as *Navicula* sp. and *Suriella* sp. were also observed. The *Surirella* sp. is noted as epipelic microorganism, which means it grows on the surface of sediments or silt, residing at the water/sediment interface.

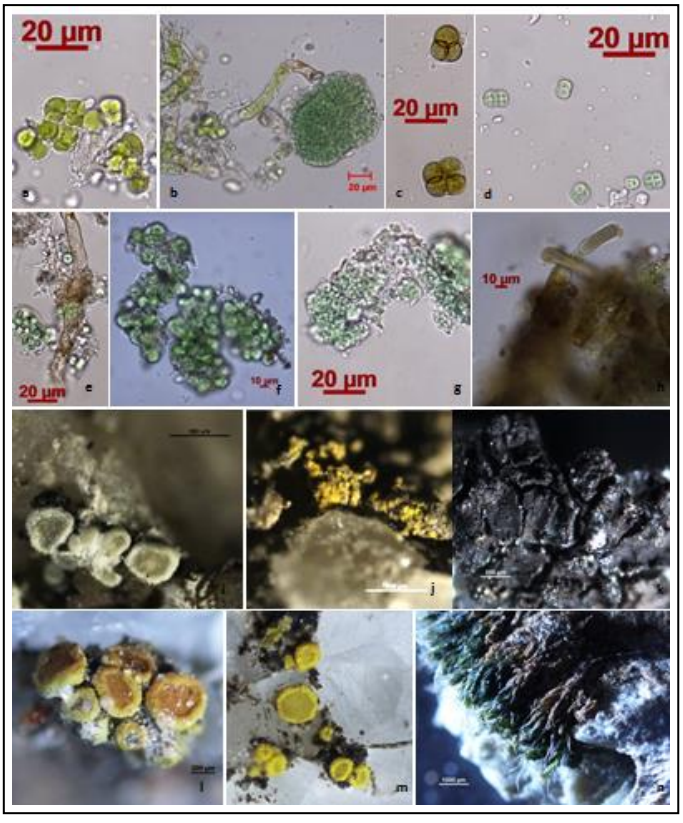

Fig. 6: The biological diversity found in samples of Hierapolis, represented by green algae (a and b), cyanobacteria (c to h), lichens (i-m) and bryophytes (n).

4. Conclusion

An exhaustive investigation of the state of conservation and the decay phenomena on marble artefacts in the archeological site of Hierapolis (Phrygia) was carried out between the August 2013 and August 2015 during the Archaeological Italian Mission. In this site, environmental factors together with the microstructural characteristics of the typologies of marble play a fundamental role on the durability and the state of conservation of the materials. The main decay phenomena observed at Hierapolis are efflorescences on the surface of marbles and travertines, carbonatic encrustations, granular disintegration of marbles, typical crusts rich of Mn, as well as the biological colonization of the surfaces. The hardness of the environmental factors is due to the closeness of the monuments with respect to the seismic faults and thermal waters. The monitoring data confirm the high thermal stress on the surface, particularly relevant on marble artifacts, due to the strong solar radiation, and the presence of high concentration of CO_2 inside and near the *Ploutonion* area. The role of thermal waters was also investigated. Geochemical analyses of water were performed and the composition of thermal spring waters present on the archaeological site are calcium bicarbonate-sulfate.

Acknowledgements

All these activities are co-founded by the Ministry of Education Universities and Research (MIUR) of Itlay in the framework of the FIRB project “Marmora Phrigiae”.
A special thanks to Prof. Francesco D’Andria, head of the Italian Archaeological Mission in Hierapolis.

References

Chiodini, G., 1996, Gases dissolved in groundwaters: analytical methods and examples of applications in central Italy, Proceeding Symp. Environmental Geochemistry, Castelnuovo di Porto, Rome, Italy, pp. 135-148.

Illustrated glossary on stone deterioration patterns, International Council On Monuments and Sites (ICOMOS), 2008, International Scientific Committee for Stone (ISCS) publication.

Montegrossi, G., Tassi, F., Vaselli, O., Bidini, E., Minissale, A., 2006, A new, rapid and reliable method for the determination of reduced sulphur (ΣS^{2-}) species in natural discharges, Appl. Geochem., 21, 849-857.

Tassi, F., Vaselli, O., Luchetti, G., Montegrossi, G., Minissale, A., 2008, Metodo per la determinazione dei gas disciolti in acque naturali, Int. Rep. CNRIGG Florence n° 10450-11, pp. 1-12.

FREEZING-THAWING PHENOMENA IN LIMESTONES AND CONSEQUENCES FOR THEIR PHYSICAL AND MECHANICAL PROPERTIES

C. Walbert[1*], J. Eslami[1], A.-L. Beaucour[1], A. Bourgès[2] and A. Noumowe[1]

Abstract

The frost weathering of five French limestones with different physical-mechanical properties, during freeze-thaw cycles was studied. Considering, all the results, two mechanisms of damage evolution depending on the physical-mechanical properties of stones, during freeze-thaw cycles are been proposed.

Keywords: frost weathering, limestone, elastic modulus, saturation degree

1. Introduction

Building materials of historical monuments, such as natural stones, are subjected to aggressive environmental conditions which are responsible for alteration in their microstructure and this can eventually lead to macro scale decay as spalling, granular disintegration, fragmentation. Among the different environmental weathering of building materials, we are interested in freeze-thaw cycles of different types of limestone. The objective of this research is to correlate the microstructural as well as physical and mechanical properties of limestones before weathering with their evolution under freeze-thaw cycles. Indeed, during the transformation of water into ice, two types of stresses are exerted on the material (Powers, 1953; Everett, 1961; Litvan 1978). The first is due to the volume expansion of the ice, which has a volume 9% higher than liquid water. The second source of stress is due to the migration of unfrozen water in the stone where that cause overpressure in the pores (Prick, 1997; Chen, 2004). Some stone intrinsic parameters influence the frost within the stone. The porous network is a critical factor, it determines the amount and distribution of fluid present in the stone. The pore size affects the crystallization temperature; smaller pores induce a freezing temperature below 0°C (Tourenq, 1970). The state of saturation of the natural stone also plays an important role. Some authors (Hirschwald, 1908; Chen, 2004) proposed a critical degree of saturation of 80% beyond what the stone is damaged by freezing but this value is contested by other authors. Other parameters such as elastic properties, mechanical strength, water transport, pre-existing defect are important to assess the frost sensitivity of stone.

The main focus of this work is to understand and quantify the damage of porous oolitic limestone during the freeze-thaw cycles. The weathering evolution in stones samples

[1] C. Walbert*, J. Eslami, A.-L. Beaucour and A. Noumowe
L2MGC, Université de Cergy-Pontoise, 5, Mail Gay-Lussac 95031 Neuville-sur-Oise, France
charlotte.walbert@u-cergy.fr

[2] A. Bourges
LRMH, CRC USR 3224, 29, rue de Paris 77420 Champs-sur-Marne, France

*corresponding author

undergoing the freeze-thaw cycles was studied through the measurement of total porosity, P-wave velocity, static elastic moduli, uniaxial compressive strength and toughness. The thermo-mechanical behaviour of rocks is also studied with strain and temperature monitoring during the freeze-thaw cycles.

2. Properties of fresh stones

The selected limestone rocks are Massangis (MA), Lens (LS), Migné (MI), Savonnières (SA) and Saint-Maximin (MX). They come from French quarries, used in the construction and replacement of stone for historic monuments. These five oolitic limestones are made up of over 99 % of calcite and 1 % impurities but they exhibit a wide range of porosity, different microstructure and mechanical properties.

2.1. Petrophysical properties

The total porosity under vacuum, Nt, is determined according to the standard (NF EN 1936) for each type of stone intact on cylindrical samples of 4 cm in diameter and 8 cm high, cored perpendicular to bedding. The porosity determined after 48h of immersion under atmospheric pressure, N48, is measured on the same samples according to standard (NF B 10-504). With these measures, the coefficient of saturation at 48h, S48, is determined. The distribution of the pore diameter and the access type of porous network are determined by mercury porosimetry on stone fragments of about 1 cm^3.The water transport properties of a material are controlled by the permeability of the material which is an important parameter in frost action. The values of intrinsic permeability are determined in triaxial cell. Tab. 1 summarizes the results obtained and shows various properties for different stones.

Tab. 1: Petrophysical properties of fresh stones.

Limestone		Total porosity, N_t (Vol.%)	Porosity at 48 h, N_{48} (Vol.%)	Saturation coefficient S_{48}	Porous networks	Pore size (µm)	Permeability (m^2)
Massangis	MA	**10.7** ± 1.2	**4.4** ± 0.8	**40.8** ± 3.4	Hetero-geneous	0.4	$\mathbf{2.43 \cdot 10^{-18}}$
Lens	LS	**14.3** ± 0.9	**12.7** ± 0.9	**89.4** ± 3.9	Bimodal	0.5/0.9	$\mathbf{4.34 \cdot 10^{-16}}$
Migné	MI	**28.8** ± 0.8	**27.5** ± 0.7	**95.3** ± 1.3	Unimodal	0.9	$\mathbf{1.36 \cdot 10^{-14}}$*
Savonnières	SA	**31.5** ± 1.7	**18.6** ± 0.8	**59.1** ± 4.1	Bimodal	0.3/13.0	$\mathbf{6.37 \cdot 10^{-13}}$*
Saint-Maximin	MX	**35.5** ± 1.8	**26.6** ± 1.6	**80.8** ± 0.03	Bimodal	0.3/22.5	$\mathbf{6.44 \cdot 10^{-12}}$*

*data from literature (De Witte, 2001)

The investigated stones show a wide range of porosity. Massangis and Lens stones have a relatively low total porosity compared to Savonnières, Migné and Saint-Maximin stones. The porous spectrum, obtained from the mercury injection of the Purcell test on two samples per limestone, represents a unimodal distribution of the entrance radius of pores (throats) for Migné, a bimodal distribution for Lens, Savonnières and Saint-Maximin which thereby defines two kinds of pores: intra-oolite and inter-oolite pores, and a heterogeneous distribution for Massangis. It should be noted that Savonnières and Saint-Maximin stones have two distinct pore sizes, but the Lens stone has two very similar pore sizes. The results show different natural saturation coefficient for studied stones. The saturation coefficient,

as mentioned by different authors (Hirschwald 1908; Chen, 2004), is dependent of microstructure and, therefore, of porous network and the pore size. The highest and lowest natural saturation coefficients were obtained, respectively, for Migné (95.3%) and Massangis (40.8%). These results could be explained by a unimodal and sharp pore size distribution for Migné and a heterogeneous distribution for Massangis. The saturation coefficient of Lens, Migné and Saint-Maximin stones are higher than the critical value of 70 % proposed by Chen (2004); but it is lower than the critical value for Massangis and Savonnières. The values of intrinsic permeability shows Massangis and Lens have a low permeability in comparison with Migné, Savonnières and Saint-Maximin stones (De Witte, 2001).

For velocity measurement, the classical ultrasonic pulse transmission technique was used according to standard NF EN 14579. P-wave velocities in the axial and lateral direction were measured for the twenty-five samples per limestone. The results of P-wave velocity measurement of studied stones are summarized in Tab. 2. In the case of Massangis and Lens, the values of P-wave velocities are identical in axial and lateral directions, meaning that these stones are quasi-isotopic. The comparison between lateral and axial P-wave velocities shows the anisotropy due to horizontal bedding for Migné, Savonnières and Saint-Maximin stone.

Tab. 2: P-wave velocity and Mechanical properties of fresh stones.

Limestone		**P-wave velocity (m/s)**		**Mechanical properties**		
		Axial measurement (saturated, 48h)	Lateral measurement (saturated, 48h)	Static elastic modulus (GPa)	Comp. strength (MPa)	Fracture toughness K_{IC} (MPa·√m)
Massangis	MA	**5342.0** ± 169.6	**5286.6** ± 144.5	**50.8** ± 1.2	**65.2** ± 1.2	**0.59** ± 0.12
Lens	LS	**4236.2** ± 99.6	**4282.7** ± 172.4	**33.4** ± 2.2	**35.5** ± 2.1	**0.41** ± 0.18
Migné	MI	**2560.9** ± 129.7	**2715.9** ± 157.3	**12.1** ± 0.8	**13.1** ±1.0	**0.11** ± 0.02
Savonnières	SA	**3141.0** ± 88.7	**3272.2** ± 187.0	**15.3** ± 1.3	**13.5** ± 3.6	**0.17** ± 0.03
Saint-Maximin	MX	**2672.0 ±** 152.9	**2405.8 ±** 129.4	**10.9** ± 0.6	**9.7** ±1.1	**0.17** ± 0.04

2.2. Mechanical properties

The cyclic uniaxial compression test (standard NF EN 1926) is used to characterise the elastic behaviour of the material and its compression strength. The test is performed on cylindrical specimen of 4 cm diameter and 8 cm in height, instrumented with strain gauges and allows obtaining the static modulus of elasticity and the compressive strength (Tab. 2). The elastic modulus and compressive strengths of Massangis and Lens stones are much higher than Migné, Savonnières and Saint-Maximin stones, where the lasts have closed mechanical properties. These results are in accordance with the values of P-wave velocities obtained.

The analysis of the critical stress intensity factor is used to evaluate the stone's resistance to initiation and propagation of cracks and is connected to the pre-existing defect size in the microstructure. The toughness K_{IC} is determined with Semi-Circular Bending test (Tutluoglu, 2011) wherein the defect in the structure is simulated with a notch, whose length depends on the sample geometry. Massangis stone exhibits (Tab. 2) the highest toughness; flowed by Lens stone, and Migné, Savonnières and Saint-Maximin stones have similar toughnesses.

3. Frost weathering

3.1. Freeze-thaw cycle

The freeze–thaw test is applied by adapting the standard NF EN 1237. Freezing and thawing stages take place in the air in a temperature-controlled chamber. Each stage of freezing or thawing lasts six hours. The air temperature ranges from 10 to -10°C and vice versa at a rate of 4°C/h followed by a stage, where the temperature is maintained constant for 1 h at -10 or 10°C. The samples were saturated in natural condition (saturation at 48h). Saturated samples, they were sealed using plastic bags to prevent any weight change during the test.

The freeze–thaw tests were carried out on cylindrical specimen of 4 cm diameter and 8 cm length, cored perpendicular to the bedding plane. Twenty-five intact core samples were prepared from each stone for freeze–thaw tests and divided into several groups to identify changes in physico-mechanical properties. Before breaking, stones samples underwent different numbers of cycles, 30 cycles for Migné and Saint-Maximin, 150 cycles for Savonnières and 320 cycles for Massangis and Lens stones. At the end of each stage, P-wave velocity measurements were carried out on all saturated samples. After each step, three or four samples of each stone were dried in an oven at 60 ± 5°C for porosity measurement and mechanical tests.

3.2. Temperature and strain monitoring during freeze–thaw cycle

A dummy specimen from each stone was specially prepared for the measurement of temperature. Two thermocouples were installed to measure the temperature at the surface and the centre of the dummy specimen. Another specimen from each stone was prepared for the measurement of strain during freeze–thaw cycle. Strains are measured by four strain gauges, two in axial direction and two in lateral direction.

4. Results and discussion

4.1. Thermal behaviour *of stones during freeze-thaw cycle*

The strains and temperature variations during one freeze-thaw cycle are presented in Fig. 1. During the initial phase of heat loss, when the temperature drops below the freezing point of water without ice forming, the liquid phase in the pores is said to be supercooled. As the temperature drops further, ice forms in the pore spaces, and heat energy is released as a result of the latent heat of fusion of water. As a result, when ice first forms, the temperature rises rapidly and it remains at that level until the entire pore water is frozen (solidification phase). When that point is reached, heat release stops, and the temperature begins to fall again. Supercooling processes were observed for all stones, the end of which is between -3 and -6°C depending on the stone. The solidification phase is instantaneous for Massangis and Lens' stone and is about 1 h for Savonnières, Migné and Saint-Maximin stones. This

difference is probably due to the amount of water contained in the stone. In fact Savonnières, Migné and Saint-Maximin stones have water contents higher than that in Massangis and Lens stones.

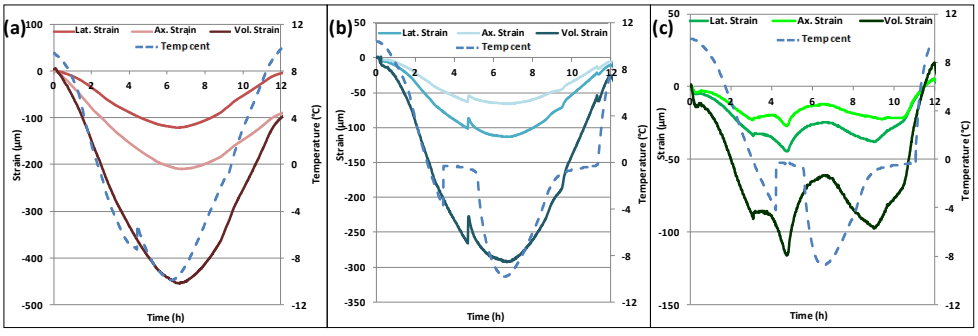

Fig. 1: Strain and temperature versus time for (a) Massangis and Lens; (b) Savonnières; (c) Migné and Saint-Maximin stone.

In the case of Massangis and Lens (Fig. 1a), the strain curve reveals the existence of two phases of contraction and dilatancy of sample corresponding to the freeze and thaw periods, respectively. The contraction is mainly thermal between 0 and -10°C. The variation of the strain for Savonnière (Fig. 1b) during the freeze–thaw is similar to that observed for Massangis and Lens stones. However, during the freezing period an instantaneous dilatancy occurs during solidification phase. In the case of Migné and Saint-Maximin (Fig. 1c), the behaviour is more complex, and different phase are visible. The first step corresponds to a thermal contraction due to temperature reduction from, 10°C until the end of the super-cooling phase. It can be noted that the contraction is almost stabilized during the super-cooling phase. At the beginning of the freezing process, (solidification phase) the material continues to shrink, despite the temperature increase. The shrinkage in this state is due to, the water which remains unfrozen in the micro-porosity, and the migration of part of this water away from the tiny pores towards larger cavities where ice was already formed. The shrinkage, at the beginning of solidification phase, is followed by a volume expansion, which can be attributed, on the one hand, to the rise in pressure coming from the water flows towards the ice front and, on other hand, to the relatively important quantity of ice formation during the solidification phase. It should be noted that, the thermal contraction, and the contraction due to migration also occur during this state, but is masked by the volume expansion. In other words, the volume expansion due to pore pressure effect dominates the thermal contraction. This dilatancy continues until the minimum temperature of -10°C is reached (Walbert, 2015). Inverse behaviour is observed during thawing.

4.2. Physical properties variations

Fig. 2 shows the changes in the relative P-wave velocity (Fig. 2a) and the relative porosity of the stone (Fig. 2b) when being repeatably exposed to freeze-thaw cycles. In comparison to the initial values all stones show a reduction in the P-wave velocity. This decrease reflects a change in the microstructure with the formation of microcracks or growing of existing microcracks in the material. However, the loss in P-wave velocity differs between the different stone types.

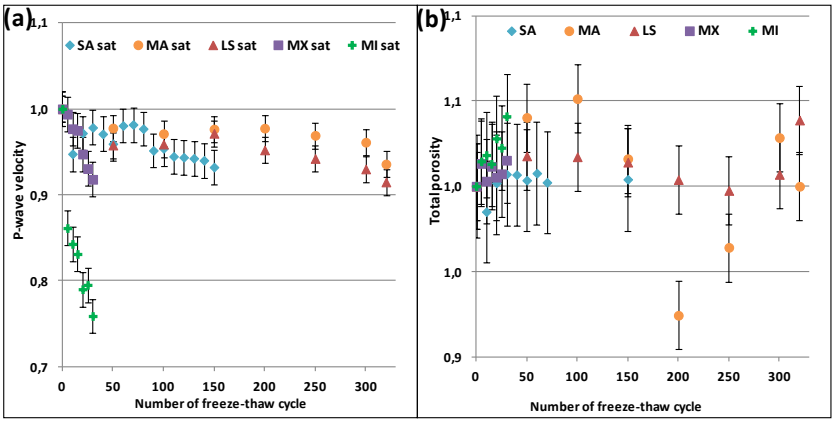

Fig. 2: Evolution of (a) the relative P wave velocity and of (b) the relative total porosity as a function of the number of freeze–thaw cycles.

The relative P-wave velocity for Migné stone decreases the most, with a loss about 25 % after 35 cycles, followed by Saint-Maximin and Savonnières stone, with a loss of 10 % after 30 and 150 cycles, respectively, and finally Massangis and Lens stones, with a failing lower than 10 % after 320 cycles. It is should be noted that, in the cases of Migné and Saint-Maximin stones, the reduction of the P-wave velocity starts with the the first freeze-thaw cycle, and continues until the failure of specimens. In the cases of Massangis and Lens stones, the P-wave velocity only decreases significantly after 200 cycles. After 30 freeze–thaw cycles, the total porosity increased by approximately 5 % and 3% for Migné and Saint-Maximin, respectively. For Massangis, Lens and Savonnières stones, the total porosity can be regarded as constant during frost damage.

4.3. Mechanical properties variations

Fig. 3 shows the evolution of the relative uniaxial compressive strength (Fig. 3a) and of the relative toughness (Fig. 3b) as a function of the number of freeze–thaw cycles.

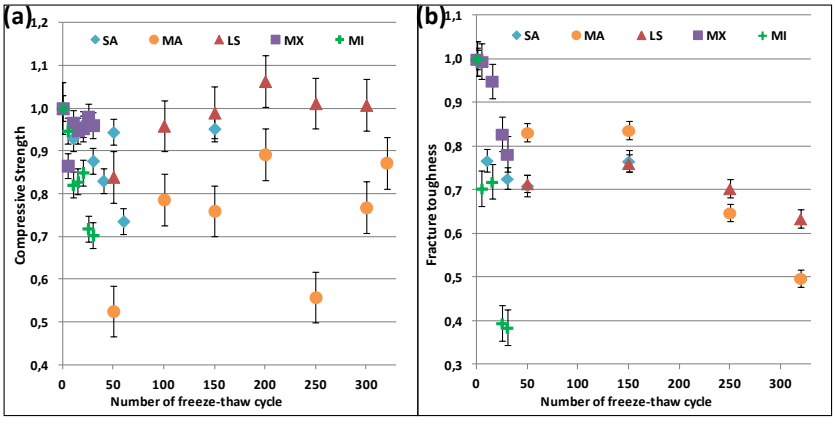

Fig. 3: Evolution of (a) the relative compressive strength and of (b) the relative fracture toughness as a function of the number of freeze–thaw cycles.

The uniaxial compressive strength decreases with the number of freeze–thaw cycles for Migné and Saint-Maximin stone, but does not show a clear trend for Savonnières, Massangis and Lens stones. For all the stones, a drop in toughness is observed. Migné stone shows the maximum reduction in toughness with a 60 % drop. Massangis and Lens stones have a loss of 50% and 40 % respectively. Savonnières and Saint-Maximin stones have the least toughness with a loss of 30 %. The evolution of toughness of stones reveals that stones show microcracking processes which are not detectable with the other parameters such as the porosity and the compressive strength. This can be highly dangerous as mentioned by Marco Castaño *et al.* (2010) for the material's long-term physicochemical stability and it should be taken into account to guarantee the correct use of these materials.

5. Conclusion

Considering all the results, physical and mechanical damages can be explained by two mechanisms. During the first freeze-thaw cycles both, Massangis and Lens Stones suffer slight damage linked to the action of frost in the absence of the expansion phenomenon. At higher numbers of freeze-thaw cycles a greater damage due to thermal fatigue becomes observable (evidenced by the decrease of the P-wave velocity after 200 cycles). For stones of Migné and Saint-Maximin, damage is caused by crystallization pressures related to volume expansion of the ice, and mainly by the migration of water to the ice front which increases the pressure of unfrozen water in the pores. This mechanism is highlighted, by volume expansion observed during freezing at the first freeze-thaw cycle thus resulting in an increased porosity and a significant drop in the P-wave velocity. In many past works, the coefficient of saturation is considered as one of the most important parameters for the frost sensitivity of a stone. However, the results show that it is difficult to define a single critical degree of saturation for all of the stones as freeze-thaw resistance depends on the pore size distribution, pore connectivity, the total porosity and mechanical properties. The results show that the critical coefficient of saturation for the stones with a bimodal pore distribution is lower than for stones with a unimodal distribution. A bimodal pore network and the presence of macro-porosity promote the migration of unfrozen water to the ice front, thus increasing the pressure within the stone and thereby the damage. Furthermore, the water transfer capability also depends on the permeability of the stone, with higher permeability facilitating the migration of unfrozen water thus increasing the extent of damage in the material.

Acknowledgments

This research was carried out thanks to subsidies from the ‘‘Fondation des sciences du Patrimoine, Labex PATRIMA’’ and to Rocamat and France Pierre. The authors express their gratitude to these organizations.

References

Chen, T.C., Yeung, M.R. and Mori, N., 2004, Effect of water saturation on deterioration of welded tuff due to freeze-thaw action. Cold Reg Sci Technol 38, 127–136.

De Witte, E., Vergès Belmin, V., De Clercq, H., Van Hees, R., Miquel, A., Bromblet, P., Brocken, H., Cardani, G., Tedeschi, C., Binda, L., Baronio, G., Lubelli, B. and Garavaglia, E., 2001, Salt Compatibility of Surface Treatments (SCOST): Final Report. European Contract ENV4-CT98-0710. Brussels: KIK-IRPA.

Everett, D.H., 1961, The thermodynamics of frost damage to porous solids. Trans Faraday Soc 57:1541–1551.

Hirschwald, J.,1908, Die Prüfung der Natürlichen Bausteine auf Ihre Wetterbestandigkeit. Verlag von Wilhelm Ernst & Sohn, Berlin, p 675.

Litvan, G.G., 1978, Freeze–Thaw durability of porous building materials, in Durability of building materials and components. Special Technical Publication STP 691. American Society for Testing and Materials, 455–463.

Marco Castaño, L.D., Martinez-Martinez, J., Benavente, D. and Garcia-del-Cura, M.A., 2010, Failures in the standard characterization of carbonate dimension stone durability during freeze-thaw testing. Global Stone Congress.

NF EN 12371 (2010), Natural stone test methods - determination of frost resistance.

NF EN 14579 (2005), Natural stone test methods - determination of sound speed propagation.

NF EN 1926 (2007), Natural stone test methods - determination of uniaxial compressive strength.

NF EN 1936 (2007), Natural stone test methods - determination of real density and apparent density, and total and open porosity.

NF B 10-504 (1973), Quarry products – limestone - measuring the water absorption coefficient.

Powers, T.C. and Helmuth, R.A., 1953, Theory of volume changes in hardened Portland cement paste during freezing. Proceedings of the Highway Rese. Board, N_32, 285–297.

Tourenq, C., 1970, La gélivité des roches, application aux granulats. Rapport de Recherche N°6 LCPC.

Tutluoglu, L., Keles, C. (2011), Mode I fracture toughness determination with straight notched disk bending method. Int J Rock Mech Min Sci 48, 1248–1261.

Walbert, C., Eslami, J., Beaucour, A.-L., Bourgès, A., Noumowé, A., 2015, Evolution of the mechanical behaviour of limestone subjected to freeze–thaw cycles. Environ Earth Sci Volume 74, Issue 7, 6339–6351.

RAPID DEGRADATION OF STYLOLITIC LIMESTONES USED IN BUILDING CLADDING PANELS

T. Wangler[1*], A. Aguilar Sanchez[1] and T. Peri[2]

Abstract

Two types of limestone, one cream coloured and one light gray coloured, have been used in building cladding in Israel and have been observed to degrade within the space of just a few years, with material loss occurring at boundaries defined by stylolites within the limestones. Panels exposed to the sun tend to show the highest level of degradation, suggesting that wetting and drying cycles of the clay minerals in the stylolites is the primary reason for the degradation, but the cream type showed no moisture expansion. Petrographic analysis suggests that the thickness and openness of the stylolites control the moisture uptake and moisture expansion properties of the two types. Oxidation of pyrite in the stylolites may also play a role in the deterioration of these panels. A clay swelling inhibitor can significantly reduce the moisture expansion in the type that swells.

Keywords: limestone, swelling clay, stylolites, swelling inhibitor

1. Introduction

Limestone is a frequently used building stone both in historical buildings and in new buildings, especially as a cladding material. In Israel, carbonate stones form 75% of the natural outcrops in the country, and are the main source of the domestic natural stone market, with cladding tile domestic production estimated to be up to 600,000 m^2 (Calvó and Reguiero 2010). Among these stones are the famous "Jerusalem stone", a limestone used historically to build Solomon's temple, and required by law to be used for the old city of Jerusalem since 1918. In general, the abundance of carbonate stones in Israel means that they are used widely in new structures as well as historic structures.

This case study focuses on two types of limestone used as building cladding for new buildings in Israel. The two types that are used are described as follows: one cream coloured, and one light gray coloured. Pictures of both types of limestone and close ups of the typical damage observed are seen in Figures 1a-d. The limestone has been observed to degrade quite quickly, particularly on the side of buildings with the highest exposure to the sun. The damage can be described as surface detachment of pieces several mm to cm in size, with boundaries defined by stylolites occurring within the stone.

[1] T. Wangler* and A. Aguilar Sanchez
Postdoctoral Researcher, ETH Zürich Institute for Building Materials, Zürich, Switzerland
wangler@ifb.baug.ethz.ch

[2] T. Peri
Nanotechnology Solutions Israel, 6 Hamatechet St. QADIMA 60920, Israel

*corresponding author

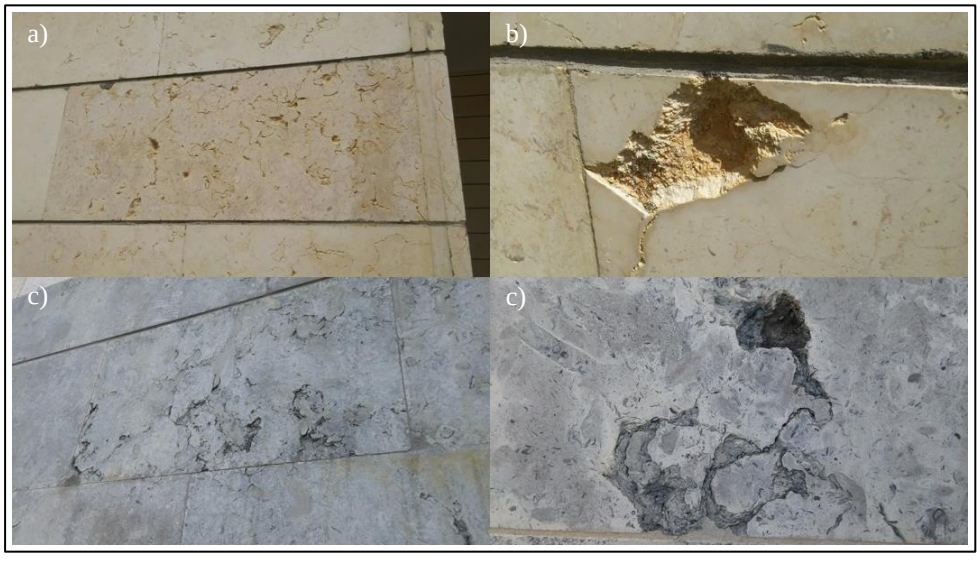

Fig. 1a-d: Cream coloured limestone (top) and light gray coloured limestone (bottom) showing typical damage. Blocks are approximately 15 cm in width and 40 cm in length.

Stylolites are features often observed in limestones, defined as material boundaries with an often tooth-like or jagged appearance cutting across the rock. Their exact formation mechanism is debated, but most agree that they are dissolution boundaries, where host rock mineral dissolves and reprecipitates elsewhere to reduce the primary host rock porosity (Aharonov and Katsman 2009). Clays, pyrite, organic matter, and other less soluble materials then are concentrated at these boundaries. Stylolites are often found in well consolidated carbonate rocks, and are often considered aesthetically pleasing features in building stones such as marbles, limestones, and travertines. They typically are oriented parallel with the bedding planes of the host rock, but their orientations can vary.

2. Materials and Methods

2.1. Stone and swelling inhibitor

Pieces of two variants of limestones used as building cladding were obtained from NTSI Solutions in Israel, one variant being cream coloured and one being light gray coloured. Samples were cut with a precision diamond saw to dimensions of approximately 4×4×3 cm for moisture uptake and 3×1×1 cm for moisture expansion experiments. It was ensured that stylolites were captured in all cut samples. The swelling inhibitor tested in this study was 1,6 diaminohexane at 5 wt% aqueous solution. Samples were treated by saturation at ambient conditions in the solution for 3 hours, then drying at ambient conditions for 1 hour, followed by drying at 105°C overnight.

2.2. Microscopy: thin section and SEM/EDS

Thin sections were prepared and petrographically examined under transmitted light microscopy with polarized light mode, as well as by scanning electron microscopy (SEM) with electron dispersive x-ray analysis (EDS) under low vacuum with a FEI Quanta 200 3D

microscope (FEI, North America NanoPort, Hillsboro, OR, USA). Images were obtained in backscattered electron (BSE) mode.

2.3. Moisture absorption and porosity

Moisture absorption was carried out by suspending stone samples from a balance and touching one surface to a water bath at ambient conditions. The moisture uptake through this surface was monitored vs. time with the balance. The uptake surface was selected to allow uptake through stylolites. The porosity of the same samples was obtained by vacuum impregnation with water.

2.4. Moisture expansion

Moisture expansion experiments were carried out with a linear voltage differential transducer (LVDT) obtained from TESAgroup (France) with a precision of +/- 0.2 μm. After drying overnight at 105°C, the samples were placed in a stainless steel cup held within a stainless steel frame to hold the LVDT and thermally equilibrated. Wetting was accomplished by pouring demineralized water until only the top of the sample was unsaturated.

3. Results

3.1. Petrographic analysis: cream limestone

The specific lithotype is a bio-calcirudite-calcarenite. The main components are fossils or bioclasts, with sizes ranging from 0.2-70 mm. Open stylolites are abundant. Microscopically, the limestone is a fossiliferous grainstone (Dunham 1962). The bioclasts are included within a crystalline, sparry calcite cement, but also some of the original micritic matrix is remaining. Stylolites are filled partially with clay and organic matter. The primary porosity is intergranular, partially closed by sparry cement, as well as intercrystalline porosity. The open stylolites form the secondary porosity.

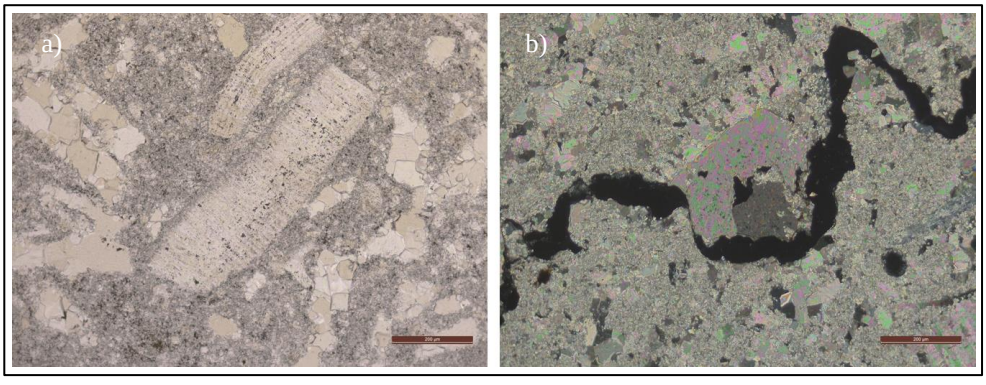

Fig. 2: Thin section images of cream limestone. Bioclasts held in a sparry cement seen in the image on the left. Right image shows an open stylolite in crossed polarized light. Scale bar on both images is 200 μm.

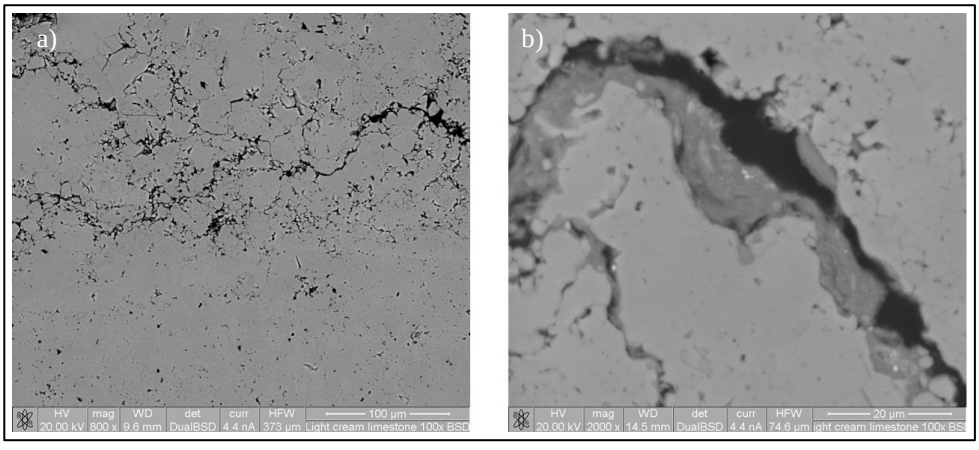

Fig. 3: BSE SEM images of cream limestone, showing uniform calcite with stylolites running through (scale bar at 100 µm). Closeup of stylolite on the right (scale bar at 20 µm) shows clay filling.

3.2. Petrographic analysis: light gray limestone

The lithotype of the light gray limestone is similar to the cream, a bio-calcirudite-calcarenite, with bioclasts of similar size range and many open stylolites. Thin section analysis showed what is classified as a fossiliferous packstone-grainstone (Dunham 1962). Dolomite crystals are also abundant, scattered throughout a micritic, recrystallized matrix. Organic matter and pyrite are dispersed throughout the stone, and are more concentrated within the abundant stylolites along with clay and dolomite crystals. The primary porosity is intergranular and intercrystalline, with the stylolites forming the secondary porosity.

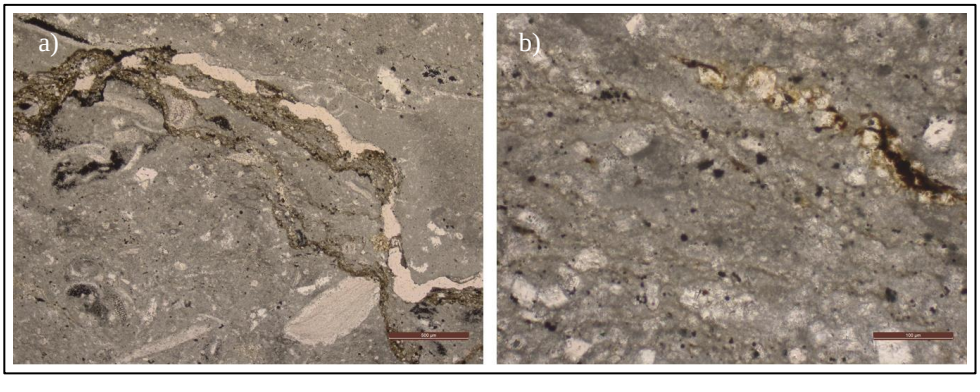

Fig. 4: Thin section images of light gray limestone. Left image (scale bar 500 µm) shows large stylolites, with dolomite and clay, and surrounding micritic matrix. Right image (scale bar 100 µm) shows closer view of a stylolite, with pyrite and oxidation products seen.

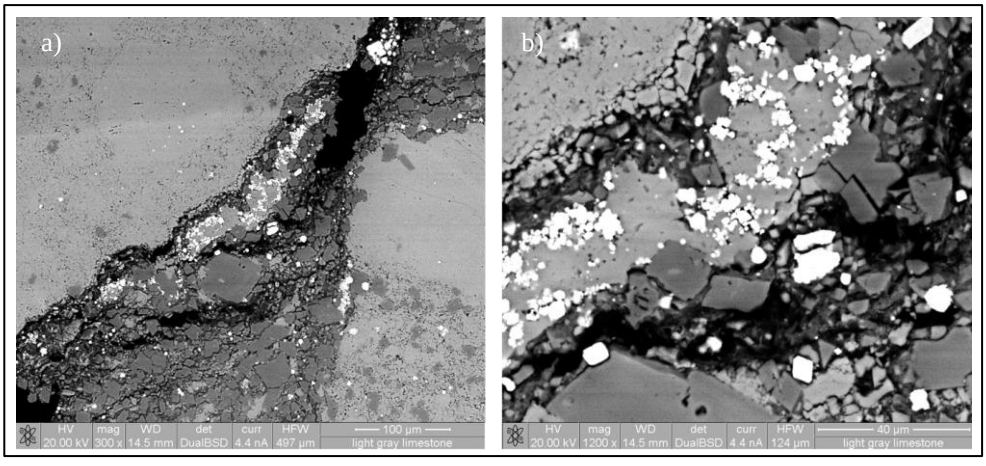

Fig. 5: BSE SEM images of light gray limestone. Left image (scale bar 100 μm) shows dispersed pyrite (white) and dolomite (dark gray) seen throughout whole stone as well as the stylolites. Right image (scale bar 40 μm) shows closeup of pyrite and dolomite in the stylolites. Phase identification was confirmed with EDS analysis.

3.3. Moisture uptake and porosity

The moisture uptake properties of the two limestone types are summarized in Tab. 1.

Tab. 1: Moisture absorption properties.

Type	**Porosity** (%)	**Moisture uptake coefficient** ($kg / m^2 s^{0.5}$)
Cream	2.1	0.0065
Light gray	5.2	0.0096

3.4. Moisture expansion

Results of moisture expansion experiments are seen in Fig. 6. The figure shows moisture expansion only for two samples of light gray coloured limestone, as the cream coloured limestone showed zero moisture expansion. The figure shows that the two samples showed an expansion of 4.9 mm/m with one, and about 1.9 mm/m with the other. In the figure, one can also see the moisture expansion curves following treatment, where the swelling has been reduced by approximately 50%.

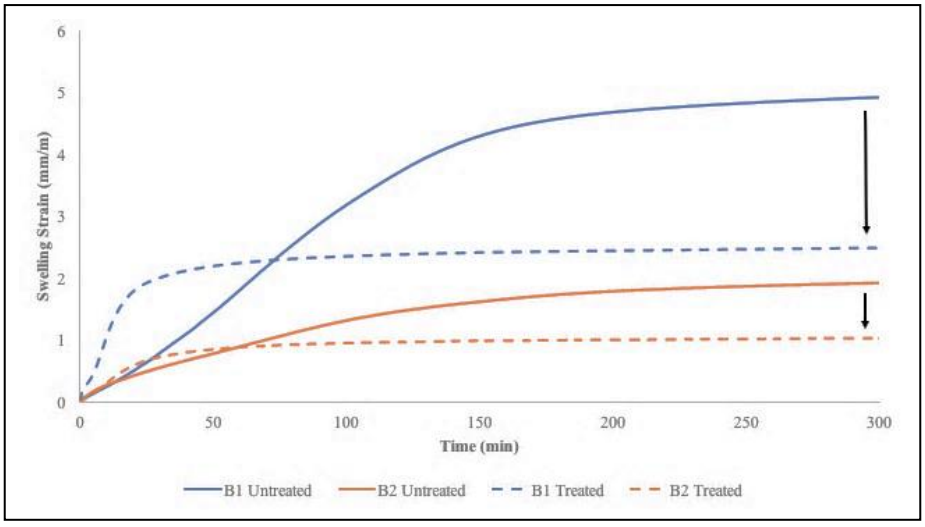

Fig. 6: Moisture expansion experiments for two samples of the light gray coloured limestone, pre- and post-treatment with swelling inhibitor (solid and dashed lines, respectively). Reduction in swelling indicated by arrows. Cream coloured limestone showed no moisture expansion.

4. Discussion

Much of the evidence behind the damage observed in these limestone cladding panels points to the stylolites, and the swelling clays within them. The role of swelling clays in the deterioration of stones has been well documented by numerous authors, with the damage mechanism described as similar to a thermal stress, in that a uniform wetting or drying gradient leads to a differential strain and therefore either a compressive or a tensile stress in a stone block (González and Scherer 2004). However, this presupposes a uniformly distributed swelling clay fraction throughout the stone, which is not the case in these stones, where the swelling clays are concentrated within the stylolites. Only a few studies have examined possible damage mechanisms for building stones containing stylolites (Winkler 1990, Larbi 2003, Pires *et al.* 2010). In these studies, the role of the swelling clays has been central, with wetting and drying cycles as well as freezing and thawing cycles suspected to lead to weakening of the stylolitic layers locally, but not leading to the sort of stresses believed to believe to damage in stones with uniformly distributed swelling clay. Additionally, it has been suspected that oxidation of minerals such as pyrite and dissolution of other materials within the stylolites leads to damage (Dreesen *et al.* 2007). Oxidation of pyrite could certainly play a role in the deterioration of the light gray limestone, as abundant pyrite was found in the stylolites.

The stylolites vary between the two different stones in terms of their thickness and openness. The stylolites of the cream coloured limestone are much thinner, usually on the order of 10-20 μm or less, and more closed than the light gray. The stylolites of the light gray limestone are usually much thicker, on the order of hundreds of μm to mm in thickness, and they are also much more open. This difference in stylolite thickness and

openness probably accounts for the large difference in moisture uptake between the two types of limestone, and also for the difference in moisture expansion. In fact, the light gray limestone, as a packstone, should have a smaller primary porosity (qualitatively observed in thin section and SEM analysis), but overall has more than double the porosity of the cream limestone, suggesting the important role of the stylolites in moisture transport. The larger and more open stylolites certainly contribute to faster moisture uptake, and facilitate moisture expansion. The difference in swelling may also be attributed to the type of clays in the stylolites, however. X-ray diffraction data should be collected to determine the clay type within the stylolites of both limestones, to confirm that swelling clays are present. In the case of the light gray limestone, however, swelling clays are almost certainly present, and their impact is also determined by their thickness and distribution. Fig. 6 shows swelling for two samples, and the difference in magnitude between the two samples is likely due to the fact that there were more and thicker stylolites in sample B2 compared to sample B1. Additionally, the presence of swelling clays in the light gray limestone can be confirmed because the swelling inhibitor was so effective.

It is not known if the swelling inhibitor would lead to an increase in durability of the limestones, however. First of all, their usage depends on the assumption that swelling clays are the issue, and this is not confirmed in the case of the cream coloured limestone, which showed zero moisture expansion. Secondly, their use is also predicated on the idea of uniform wetting and drying cycles leading to stresses as explained earlier. In the light gray limestone, certainly swelling clays are creating very high local stresses, and the swelling strains generated there could lead to local damage, especially as it has been demonstrated that swelling clays also become very soft when wetted (González and Scherer 2004). In the same study, the swelling inhibitor improved the mechanical properties as well, stiffening the stone. It is telling that the swelling inhibitor reduced swelling in this study by half, which suggests it is operating similarly to previous studies (Wangler and Scherer 2009), so the mechanical properties benefit could also apply here. In this case, the swelling inhibitor, possibly applied as a pretreatment before installation of the panel, could lead to an increase in durability. Further investigations should focus on determining if a useful accelerated weathering test can be devised to test their effectiveness in improving durability.

5. Conclusions

This study examined stylolitic limestone building cladding for two types of limestone that were showing damage defined by the stylolite boundaries. The results of this case study show that the stylolites contain swelling clays which could be responsible for the damage observed, at least in the gray limestone. Swelling clays in the gray limestone can lead to expansion of the whole stone that is controlled by the amount and thickness of stylolites in a cross section, and this swelling can be controlled by a clay swelling inhibitor. However, macroscopic swelling of a panel cannot explain the damage to both stone types, as the cream coloured variant displayed no macroscopic swelling. More investigation is needed to determine the exact damage mechanism, especially in the case of the cream coloured limestone, as it may be different from the gray coloured limestone, even if it visually decays in a similar fashion. It is possible that a local weakening is occurring at the stylolites, which causes them to erode preferentially, leading to the losses, and this can be attributed also to the swelling clay, as well as other mechanisms such as pyrite oxidation. Further investigation can also determine if swelling inhibitors will contribute to the durability of the stone.

References

Aharonov, E., and Katsman, R., 2009, Interaction between pressure solution and clays in stylolite development: Insights from modeling, Amer. Jour. of Sci. 309 (7) 607-632.

Calvo, J.P. and Regueiro, M., 2010, Carbonate rocks in the Mediterranean region – from classical to innovative uses of building stone, from Limestone in the Built Environment: Present-Day Challenges for the Preservation of the Past, Smith, B.J., Gomez-Heras, M., Viles, H.A. and Cassar, J. (eds), Geological Society of London Special Publications, 331 27-35.

Dreesen, R., Nielsen, P. and D. Lagrou, 2007, The staining of blue stone limestones petrographically unraveled, Mat. Charac. 58 1070-1081.

Dunham, R.J., 1962, Classification of carbonate rocks according to depositional texture, In Classification of carbonate rocks, Ham, W.E. (ed.), Amer. Assoc. of Petr. Geol. Mem., 1 108–121.

González, I. J., Scherer, G.W., 2004, Effect of swelling inhibitors on the swelling and stress relaxation of clay bearing stones, Env. Geo. 46 (3-4) 364-377.

Larbi, J.A., 2003, Effect of stylolites on durability of building stones: Two case studies, HERON 48 (3), 231-247.

Pires, V., Silva, Z.S.G., Simão, J.A.R., Galhano, C., and Amaral, P.M., 2010, "Bianco di Asiago" limestone pavement – Degradation and alteration study, Const. and Build. Mat., 24 (5) 686-694.

Wangler, T. and Scherer, G.W., 2009, Clay swelling inhibition mechanism of α, ω diaminoalkanes in Portland brownstone, Jour. Mat. Res. 24 (5) 1646-1652.

Winkler, E., 1990, Deep weathering of stylolites in limestone on the columns of the temple of Apollo Epicurios, Greece, in Proceedings of the Conservation of Monuments in the Mediterranean Basin: International Symposium, Bari, Italy, Zezza, F. (ed.), Grafo Edizionio, Brescia, Italy, 185-187.

SWELLING CLAY AND ITS INHIBITION IN THE VILLARLOD MOLASSE

T. Wangler[1*]

Abstract

Villarlod molasse, a Swiss subarkosic sandstone with a calcareous cement, has been used in numerous historic buildings throughout Switzerland, such as the Fribourg Cathedral. The stone is notoriously lacking in durability, particularly due to the high moisture expansion of the swelling clay fraction, which also precludes its treatment with ethylsilicate consolidants. Diaminoalkane swelling inhibitors can reduce swelling strains due to swelling clays, and can potentially provide a benefit to consolidation of these types of stones. In this study, dilatometric measurements are performed that indicate that damage can occur in Villarlod molasse via extended wetting cycles, and this damage can be mitigated with a swelling inhibitor. The swelling inhibitor functions via reduced rehydration upon treatment, but also produces what could be a "pre-stressing" effect by dehydration of the initial hydration state of the clay layers.

Keywords: molasse, moisture expansion, swelling clay, swelling damage

1. Introduction

The sandstones of the Swiss Molasse Basin have been used as a building material for many centuries, finding widespread usage in various culturally significant buildings such as the Cathedrals of Fribourg and Lausanne. These sandstones (termed "molasses" from here) are subarkose sandstones rich in clays and with a calcitic cement. The Villarlod molasse, extracted in the canton of Fribourg, has been studied for decades (Félix 1977, González and Scherer, 2004). The swelling clays as well as the calcareous cement make the stone particularly susceptible to damage, with the former leading to damaging swelling strains and the latter leading to accelerated dissolution damage as well as gypsum salt formation. Additionally, the swelling clays make the stone difficult to conserve via the use of ethylsilicate consolidants, as just a few wetting and drying cycles post consolidation lead to almost complete loss of the consolidation benefit (Félix 1994, Caruso *et al.* 2012). Moisture expansion due to swelling clays is an issue common to many clay-bearing sandstones, as noted by many authors (Wendler *et al.* 1990, González and Scherer 2004, Sebastián *et al.* 2008, Wedekind *et al.* 2013). In swelling clay minerals, swelling occurs via hydration of the counterbalancing cations in the clay interlayer in the intracrystalline regime before proceeding to the weaker, electrostatic repulsion of the osmotic regime (van Olphen), although the possibility of other swelling mechanisms unrelated to clays has been proposed (Rüdrich *et al.* 2011). Swelling can lead to damage via the development of differential strains during wet and dry cycles, as well as uneven wetting patterns leading to internal

[1] T. Wangler*
ETH Zürich Institute for Building Materials, Zürich, Switzerland
wangler@ifb.baug.ethz.ch

*corresponding author

stresses sufficient to propagate a flaw (González *et al.* 2008, Wangler *et al.* 2011). Typically, this damage manifests itself as buckling in the case of wetting, and mud cracking in the case of drying. This swelling can be reduced via α,ω alkyldiamines, also called diaminoalkanes (DAA) (Wendler *et al.* 1990, Wendler *et al.* 1996, González and Scherer 2004). It has been demonstrated that that these molecules function via substitution of the amine groups for the counterbalancing cations in the interlayer and subsequently reducing the rehydration, although they leave a residual strain after treatment due to their intercalation (Wangler and Scherer 2009). This study examines the microstructure of Villarlod molasse, as well as its behaviour during extended wetting and drying cycles. The effect of a swelling inhibitor on this behaviour is also examined.

2. Materials and Methods

2.1. Stone and swelling inhibitor

Villarlod molasse was obtained from Molasse de Villarlod SA, Farvagny, Switzerland. Prismatic samples of approximately 1 cm × 1 cm × 3 cm were cut with a precision diamond saw. The porosity as determined by vacuum saturation was 16%. The swelling inhibitor tested in this study was 1,4 diaminobutane at 5 wt% aqueous solution, a swelling inhibitor widely tested in past studies (Wendler *et al.* 1996, González and Scherer 2004, Wangler and Scherer 2009).

2.2. Rietveld analysis

The XRD patterns were obtained using a Bruker AXS D8 ADVANCE diffractometer with CoKα (λ = 1.7902 Å) radiation. The qualitative analysis of powders was conducted using DiFFPlus EVA software, and AutoQuan software was used for Rietveld analyses.

2.3. Scanning electron microscopy

Fractured surfaces of Villarlod molasse were studied by Scanning Electron Microscopy (SEM) using a FEI Quanta 200 3D microscope (FEI, North America NanoPort, Hillsboro, OR, USA). Backscattered-electron (BSE) images were taken in low vacuum mode.

2.4. Moisture expansion experiments

Moisture expansion experiments were carried out with a linear voltage differential transducer (LVDT) obtained from TESAgroup (France) with a precision of +/- 0.2 μm. After drying overnight at 105°C, the samples were placed in a stainless steel cup held within a stainless steel frame to hold the LVDT and thermally equilibrated. Wetting was accomplished by pouring demineralized water (or treatment solution) until only the top of the sample was unsaturated, and drying was accomplished by suctioning out as much water (or solution) as possible before turning on a compressed air gun held above the sample.

3. Results

3.1. Rietveld analysis

Tab. 1 gives the result of the Rietveld analysis of the molasse used in this study.

Tab. 1: Rietveld analysis of Villarlod molasse.

Phase	% by mass	Error
Quartz	43.55	0.72
Calcite	17.10	0.36
Plagioclase albite	14.64	0.69
Microcline	6.63	0.42
Dolomite	3.19	0.45
Hematite	0.20	0.11
Muscovite	4.13	0.45
Chlorite	4.82	0.57
Smectite	5.75	1.17

3.2. SEM Images

Figures 1a and 1b show backscattered scanning electron microscope images of a fractured Villarlod molasse surface. The microstructure of the molasse, where the clays are both coating the grains and filling the porosity of the rock, is easily observed.

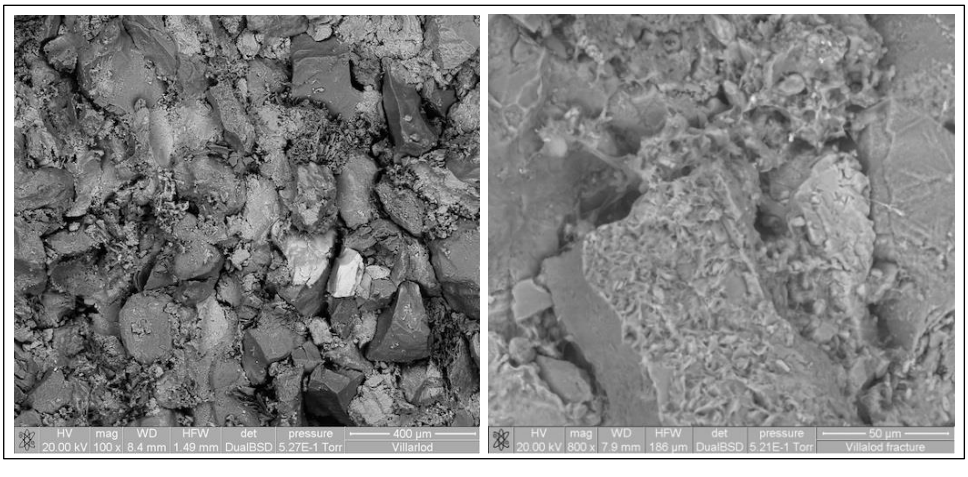

Fig. 1: BSE image of fracture surface of Villarlod molasses (a); BSE Image of fracture surface, with closer view of grain coating clays (b).

3.3. Moisture expansion and treatment experiments

Fig. 2 shows the results of wetting and drying moisture expansion experiments on Villarlod molasse, showing damage demonstrated by a residual strain of about 0.6 mm/m. This result was repeatable. The swelling strain of the Villarlod molasse, untreated, is taken to be 2.0 mm/m.

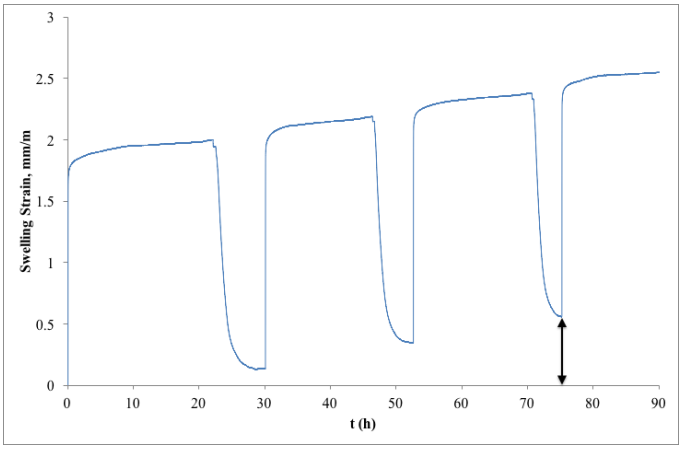

Fig. 2: Wetting and drying cycles of Villarlod molasse. After 3 wet/dry cycles, there is a residual strain of ~0.6 mm/m, marked on the figure.

Fig. 3 shows the results of a DAA treatment cycle on Villarlod molasse, showing the initial swelling with the treatment, shrinkage upon drying, and a subsequently reduced swelling strain. This curve continues with wetting and drying cycles in the next figure. The post-treatment swelling strain of the Villarlod molasse is taken to be 0.65 mm/m which is an approximately 70% reduction in the initial swelling strain.

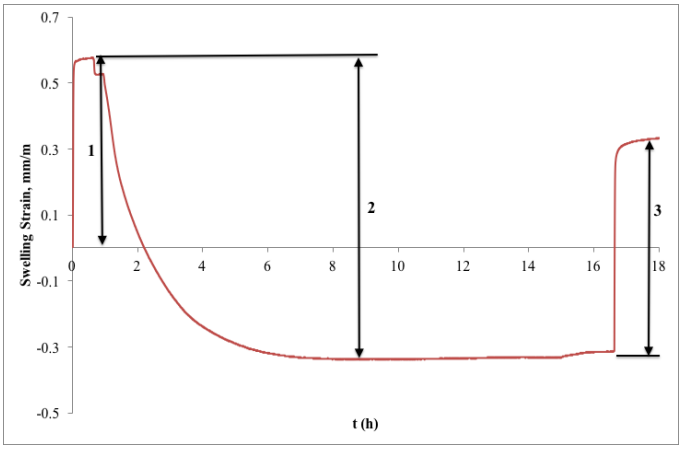

Fig. 3: DAA treatment cycle of Villarlod molasse. Direct treatment occurs at (1) on the figure, followed by drying (2), and then rewetting (3), which is the post-treatment swelling strain. Contraction from original dimension after treatment suggests a dehydration of the initial state of the clay layers.

Fig. 4 includes the wetting and drying cycles of the sample from Fig. 3, post treatment. No residual strain can be observed in the wetting and drying cycles. The results of Fig. 2 are overlaid in contrast.

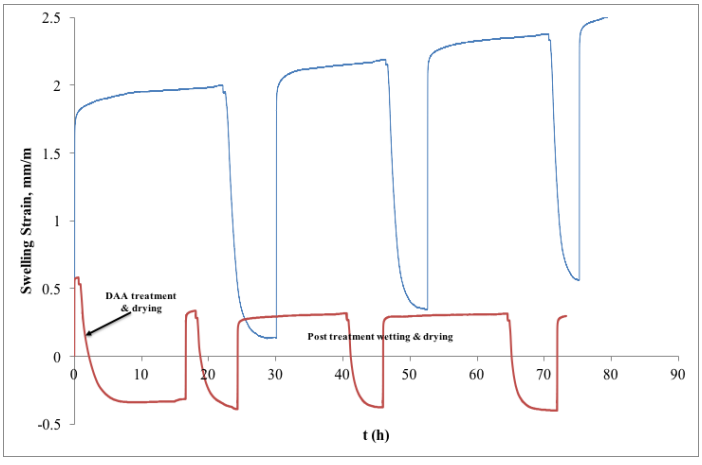

Fig. 4: Post DAA treatment wetting and drying cycles of Villarlod molasse (lower curve), showing no residual strain after initial treatment. Top curve is of wetting and drying cycles of untreated Villarlod molasse showing residual strain.

4. Discussion

The mineralogical makeup of the stone as determined by Rietveld analysis is similar to the summaries provided by previous petrographic analysis (Félix 1977), with a large emphasis on the clay, especially the swelling clay fraction, and the calcite cement. This particular sample contains 17% calcite and almost 6% swelling clays. An order of magnitude estimate for when strains can become damaging is approximately 0.1 mm/m, because elastic moduli of sandstones are on the order of GPa and strengths are on the order of MPa. Swelling clays in the intracrystalline regime can swell up to 100% of their original dimension, so only a volume fraction of 0.1% swelling clay can theoretically be the minimum for this much expansion. However, this hinges on the microstructure of the sandstone and the location of the clays within the sandstone, as noted by other authors (Rüdrich *et al.* 2011, Colas *et al.* 2011, Wangler *et al.* 2012). Clays within the pore space merely swell into the porosity, while clays at grain contacts can contribute to expansion of the entire composite structure of the stone. In the case of the Villarlod molasse it seems that both grain coated and pore filling clays exist, as seen in the SEM images.

The damage observed in Villarlod molasse during extended wetting and drying cycles is particularly interesting. The swelling strain never seems to reach a plateau during extended wetting, and upon drying, a residual strain remains. From the wetting cycles in Fig. 2, 14-18 hour wetting intervals seem to correspond to approximately 0.15-0.2 mm/m of residual strain. This damage is likely coming via internal strains in the stone dependent on the microstructure, as illustrated in Fig. 5. One can imagine that the stone contains many grain contacts, some with clay and some with calcite cement. As the clay minerals expand, they

stretch the calcitic grain contacts, which can lead to microcrack growth, especially under wet conditions, when stress corrosion would lower the fracture toughness of calcite and the other matrix minerals. Of course, however, the extreme conditions of extended wetting as well as fully unconfined wetting rarely exist in reality, so it would be instructive to see what partial wetting for variable amount of times, corresponding to actual field conditions, would produce. Nevertheless, this illustrates a conceivable micromechanical damage model, similar to that alluded to by González and Scherer (2006) in which increasing swelling strains after hundreds of wetting and drying cycles was interpreted as a decrease in the stone's stiffness due to fatigue cracking.

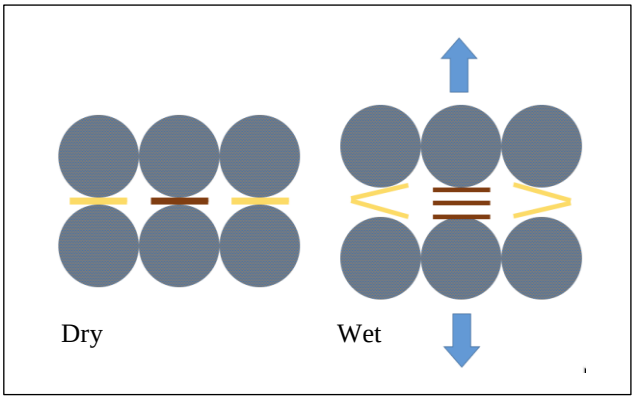

Fig. 5: Micromechanical conceptual model of Villarlod molasse, with swelling clays at some grain contacts (brown) and calcite at the others (yellow). Upon wetting, the clays swell, inducing microcrack growth in the calcite-containing grain contacts.

Also of interest is the behaviour of the Villarlod molasse upon treatment with the diaminoalkane swelling inhibitor. In a previous study, monitoring the length change of stone samples upon direct treatment with swelling inhibitor produced a permanent strain in the stone sample, corresponding to intercalation of the inhibitor into the clay galleries (Wangler and Scherer 2009). In this study, the introduction of the swelling inhibitor has actually produced a permanent contraction of the original clay layer spacing. This is likely due to hydration layers that exist in the clays before hydration, meaning that Villarlod molasse contains water layers even at ambient relative humidities, unlike in previous studies for other stones where it was shown that the clay layers were fully dehydrated (Wangler and Scherer 2008). This difference in behaviour from the stones of the previous study could be due to a layer charge density or distribution difference in the swelling clay layers. More extended studies utilizing both dilatometry and XRD are necessary to confirm this possibility.

The swelling inhibitor has also seemed to eliminate the permanent strain observed with extended wetting of untreated samples. Returning to the simple micromechanical model of Fig. 5, this can be due to the reduction of swelling strain at the clay-containing grain contacts as well as the contraction created by the seeming dehydration of the clay layers, which can produce a crack-closing effect, similar to pre-stressing. This "pre-stressing" effect could also conceivably be beneficial on the macroscopic scale according to the macroscopic damage mechanisms that have been proposed (Gonzalez and Scherer 2004,

Gonzalez *et al.* 2008, Wangler *et al.* 2011) where differential strains ultimately lead to damaging stresses. The effect of a permanent tensile strain, however, should be examined as well, although this effect could be mitigated by a gradient in the swelling inhibitor through the depth of the stone surface.

5. Conclusions

In this study, damage could be observed as a residual strain after long wetting cycles of Villarlod molasse, which could be potentially due to internal stresses generated at grain contacts leading to damage of the calcareous matrix. The swelling damage is mitigated by the application of an α,ω alkyldiamine swelling inhibitor. The inhibitor mitigates damage by an overall reduction of swelling in the interlayer of the clays, but could also function via a "pre-stressing" effect coming from contraction due to the dehydration of the clay layers. This contraction should be confirmed via XRD experiments in future studies.

Acknowledgments

The author would like to thank Gabriele Peschke (Institute for Building Materials, ETH Zürich) for her help in obtaining electron microscope images, and Dr. Michael Plötze (ClayLab, Institute for Geotechnical Engineering, ETH Zürich) for his help in the performance of the Rietveld analysis of the stone.

References

Caruso, F., Wangler, T., Aguilar, A.M., Richner, H., Melchior, J., and Flatt, R.J., 2012, Effect of swelling inhibitors and self-restraint on the durability of ethyl silicates applied to clay-bearing stones, in Proceedings of 12th International Congress on the Deterioration and Conservation of Stone, New York.

Colas, E., Mertz, J.D., Thomachot-Schneider, C., Barbin, V., and Rassineux, F., 2011, Influence of the clay coating properties on the dilation behaviour of sandstones, App. Clay Sci. 52 (3) 245-252.

Félix, C., 1977, Molasses et grès de Villarlod (Fribourg) (''Molasses and Sandstones of Villarlod (Fribourg)''), Technical Report from École polytechnique federale de Lausanne, Labarotoire des Materiaux Pierreux, Lausanne, Switzerland, 18 p.

Félix, C., 1994, Déformation des grès consecutive à leur consolidation avec un silicate d'ethyle (Deformation of sandstone following ethyl silicate consolidation), in Proceedings of the Congress of the International Association of Engineering Geology, Lisbon, Portugal, 3543-3550.

González, I. J., Scherer, G.W., 2004, Effect of swelling inhibitors on the swelling and stress relaxation of clay bearing stones, Env. Geo. 46 (3-4) 364-377.

González, I. J., Scherer, G.W., 2006, Evaluating the potential damage to stones from wetting and drying cycles, in Measuring, Monitoring and Modeling Concrete Properties, Konsta-Gdoutos, M. (ed.), Springer Netherlands, 978-1-4020-5104-3, 685-693.

Gonzalez, I. J., Rodriguez-Navarro, C., Scherer, G.W., 2008, Role of clay minerals in the physicomechanical deterioration of sandstone, Journal of Geophysical Research: Earth Surface 113 (F2).

Rüdrich, J., Bartelsen, T., Dohrmann, R., and Siegesmund, S., 2011, Moisture expansion as a deterioration factor for sandstone used in buildings, Env. Ear. Sci. 63 (7-8), 1545-1564.

Sebastián, E., Cultrone, G., Benavente, D., Fernandez L.L., Elert, K., and Rodriguez-Navarro, C., 2008, Swelling damage in clay-rich sandstones used in the church of San Mateo in Tarifa (Spain), Jour. Cult. Her. 9 (1) 66-76.

Van Olphen, H, An introduction to clay colloid chemistry, 1977, 2nd ed., Wiley, New York.

Wangler, T. and Scherer, G.W., 2008, Swelling mechanism in clay-bearing sandstones. Env. Geo. 56 (3-4) 529-534.

Wangler, T. and Scherer, G.W., 2009, Clay swelling inhibition mechanism of α, ω diaminoalkanes in Portland brownstone, Jour. Mat. Res. 24 (5) 1646-1652.

Wangler, T., Stratulat, A., Duffus, P., Prévost, J.H., and Scherer, G.W., 2011, Flaw propagation and buckling in clay-bearing sandstones, Env. Ear. Sci. 63 (7-8) 1565-1572.

Wangler, T., Ngo, E., and Scherer, G.W., 2012, Swelling pressure and stress development in clay-bearing sandstones, in Proceedings of the 12th International Congress on the Deterioration and Conservation of Stone, New York.

Wedekind, W., López-Doncel, R., Dohrmann, R., Kocher, M., and S. Siegesmund, 2013, Weathering of volcanic tuff rocks caused by moisture expansion, Env. Ear. Sci. 69 (4) 1203-1224.

Wendler, E., Charola, A.E., and Fitzner, B., 1996, Easter Island tuff: laboratory studies for its consolidation, in Proceedings of the 8th International Conference on the Deterioration and Conservation of Stone, Riederer, J. (ed.), Berlin, 1159-1170.

Wendler, E., Klemm, D.D., and Snethlage, R., 1990, Consolidation and hydrophobic treatment of natural stone, in Proceedings of the 5th International Conference on Durability of Building Materials and Components, Baker, J.M., Nixon, P.J., Majumdar, A.J., and Davies, H. (eds.), Chapman and Hall, London, 203-212.

FIRST INVESTIGATIONS OF THE WEATHERING AND DETERIORATION OF ROCK CUT MONUMENTS IN MYRA, LYCIA (TURKEY)

W. Wedekind[1*], R.A. López Doncel[2], B. Marié[3] and O. Salvadori[4]

Abstract

The rock cut architecture of the Lycian culture in Turkey, created from around 500 BC to 400 AC, is one of the most fascinating remains of humanity's ancient building heritage. The Lycian builders created monumental sarcophagi and tomb facades with unique forms and aesthetic styles which are never found twice in the Mediterranean world. Most of these magnificent monuments are cut into different limestone formations located in the area along the southern coast of Turkey, known as Lycia after its creators. The rocks as well as the monuments are affected by weathering and disasters, such as the dissolution and precipitation of calcite, biological growth and cracks due to earthquakes. To characterise the weathering forms and processes onsite investigations were done on rock cut monuments at the outstanding site known as Myra. Field investigations included quantitative mapping of damage phenomena, pointing surface hardness measurements utilizing a Schmidt pendulum hammer, water absorption using Karsten test pipes and closer surface observations using a digital microscope. The limestone varieties were characterised by petrophysical measurements and mineralogical analysis of thin sections.

Keywords: rock cut architecture, limestone, weathering, micro-climate, microbiology

1. Introduction

The historical landscape of Lycia lies on the Teke Peninsula in southwestern Anatolia in Turkey (Fig. 1a). Traveling overland to Lycia was difficult because of it being surrounded by massive mountain ranges rising over 3000 meters. The Lycian culture began around 3000 BC and lasted until 400 AC and was dominated by warfare. Lycian warriors were known all over the Mediterranean world. Homer (8^{th} or 7^{th} BC) described the Lycians as heroic warriors fighting for their allies the Trojans (between 1334 and 1135 BC). Lycian warriors armed with shields and lances as well as battle scenes are often depicted in the

[1] W. Wedekind*
Geoscience Centre of the University Göttingen, Germany,
Applied Conservation Science (ACS), Göttingen, Germany
wwedekind@gmx.de

[2] R.A. Lopéz-Doncel
Geological Institute, Autonomous University of San Luis Potosí, Mexico

[3] B. Marié
Inrap Centre de Recherches Archéologiques, Reims, France

[4] O. Salvadori
Polo museale del veneto, Venezia, Italy

*corresponding author

tombs and monuments (Fig. 2d). The Lycians were not only famous for their skills in battle, but also had a highly developed navy because they were masters in wooden ship construction (Kolb, Kalke 1992). They traveled in wooden ships and lived in wooden structures. The typical Lycian tomb copies the principles they used in their wooden architecture and transformed them into monuments that would last forever by carving them into the bedrock (Mühlbauer 2001, Fig. 1d and Fig.1e).

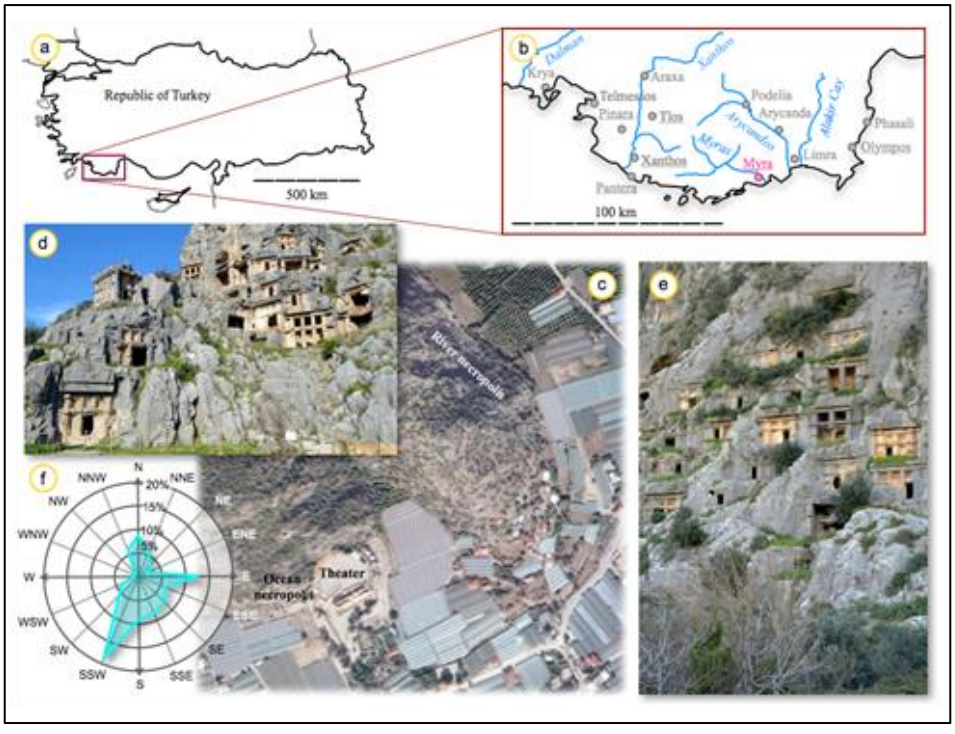

Fig. 1: a) Location of Lycia in the Republic of Turkey. b) Important Lycian cities. c) The ancient site of Myra (source: Google Earth). d) The ocean necropolis and e) the river necropolis. f) Annual wind and rain direction (source: www.windfinder.com).

The Lycian people had their own language, writing and from the 6th century to the 3th century BC different Lycian dynasties existed. Sometimes they were in conflict with each other and at other times they formed alliances. Due to its geographical location Lycia was politically and militarily vulnerable when confronted with the Persians and the Greeks. From 168 BC – 43 AD several Lycian cities created an alliance of independent dynastic city republics. In these city alliances, six major cities were established with the right to vote in the Lycian League based on their number of inhabitants: Tlos, Pinara, Xanthus and Pantara in western Lycia, Myra in central Lycia, and Olympos at the border to the east (Fig. 1b underlined). Only limited authentic written sources are known that talk about the Lycians. Most of their settlements are still awaiting excavation, investigation and conservation.

2. The site of Myra and its necropolis

The ancient town of Myra in Lycia is located where the small town of Kale (Demre) is situated today in the present day Antalya Province of Turkey. The ancient settlement was located on the river Myras near the Aegean Sea. There is no substantiated written reference for Myra before it was listed as a member of the Lycian alliance (168 BC – AD 43); according to the Greek chronicler Strabo (around 63 BC – 23 AC) it was one of the largest towns in the alliance.

There are two necropolises of rock-cut tombs in the form of house and temple fronts carved into the natural rocks at Myra: the ocean necropolis (Fig. 1c), which faces due south/south-south-east (168°) just northwest of the theatre and the river necropolis that faces north-east (45°) parallel to the river Myras (Fig. 1e). The remains of the Lycian and Roman town are mostly covered by alluvial silts. Only the acropolis, the Roman theatre and the Roman baths have been partly excavated. The semi-circular theatre and the necropolis were partly destroyed in an earthquake in 141 AC.

2.1. Geological setting

The study area is located in the Taurus Belt in southern Turkey. The Taurus Belt is separated into three different tectono-stratigraphic formations from north to south called Lycian Nappes in the north, Beydaglari Autochthonous in the middle and Antalya Nappes in the south (Özgül, 1976). The Lycian Nappes mainly represent Mesozoic platform carbonate sequences, which consist of dolomites, oncoidal limestones, intraformational limestone conglomerates, and cherty limestones. In recent studies, the Lycian Nappes are also named the Kütahya-Bolkardagi Belt (Göncüoglu, 2011).

2.2. Environmental and climatic conditions

The Myra region nowadays is dominated by agricultural production of vegetables (Fig. 1c). The Mediterranean Sea is located around 8 km southwards. The climate is warm and temperate and is classified as Csa according to the Köppen-Geiger climate classification system. Winter months are much rainier than the summer months. The average annual temperature is 18.4°C. In a year, the average rainfall is 920 mm. The driest month is August with only 2 mm of precipitation. Most of the precipitation falls in December and January, averaging 210 and 226 mm (www.clima-data.org). In November and February precipitation averages reach 110 and 145 mm. The three dominant average annual wind and rain directions are SSW with 17.2 %, N with 8.9 % and E with 12.5 % (Fig. 1f). During the month with much rainfall a different wind and rain direction occurs as well as in August (Tab. 1):

Tab. 1: The three main wind and rain directions related to different months.

Monthly Period	North	East	South-South-West
November & February	11.6%	13.6%	12.7%
December & January	17.6%	14.4%	7.8%
August	4.5%	10.2%	26.0%

2.3. Weathering forms

Deterioration of the tomb facades is due to tectonic movements (earthquakes) and to weathering. The damages due to the earthquakes in 141 AC are characterised by broken areas with a total loss of the decorated surface as well as fractures and cracks. Weathering phenomena in this case can be divided into different forms, colors and intensities. In contact with drainage rainwater the stone shows a gray to bluish color and two main forms of weathering intensities:

1.) A grayish discolouration forming a rough but closed surface (Fig. 2c);

2.) A gray to blue disintegrated surface by forming a visible relief (Fig. 3b and Fig. 3c). Different kinds of amorphous deposits white in color and sometimes also reddish, probably due to iron oxides precipitate on the surface.

2.4. Rock material and case studies

In this study the original rock material of the necropolis (NL) and a so-called Myra limestone (ML) was investigated. The Myra limestone is quarried around 15 km to the north of the ancient site and is sold on the international market. This stone material is also used for restoration of the ancient site. For this study two comparable monuments were chosen: one from the ocean necropolis and one from the river necropolis. Both monuments are similar in size and form. They have a size of around 4 by 4 meters and show the typical Lycian-stepped rectangular decoration on the façades (Fig. 2d and 3d).

3. Methods

Field investigations were done by quantitative mapping of the visible damage phenomena, surface hardness measurements by a Schmidt or pointing pendulum hammer, water absorption by Karsten test pipes and closer surface observations by using a digital microscope. Surface hardness was done on representative areas based on the mapped conditions by taking no less than 10 single measurements. Water uptake tests were done on several representative areas under different conditions. Laboratory tests were done by measuring the porosity and density using hydrostatic weighting (DIN 52 102), ultrasonic wave velocities using the pulse transmission technique and analysing thin sections.

4. Results

4.1. Mapping

4.1.1. The soldier tomb of the ocean necropolis

The soldier tomb of the ocean necropolis shows different forms of weathering (Fig. 2e). Large amounts of broken areas (15 %) mostly cover moderately weathered areas and form a gray discoloration that covers 37 % of the surface. These gray surfaces are connected to water stains and show a roughened surface (Fig. 2c). Only 1 % of the surface shows strong weathering. Sintered areas are found at well conserved surfaces (29 %). However, 18 % are still in a very good state of conservation even showing tool marks and only small forms of sintering (Fig. 2a). Sintered areas show reddish discolorations and amorphous precipitations (Fig. 2b).

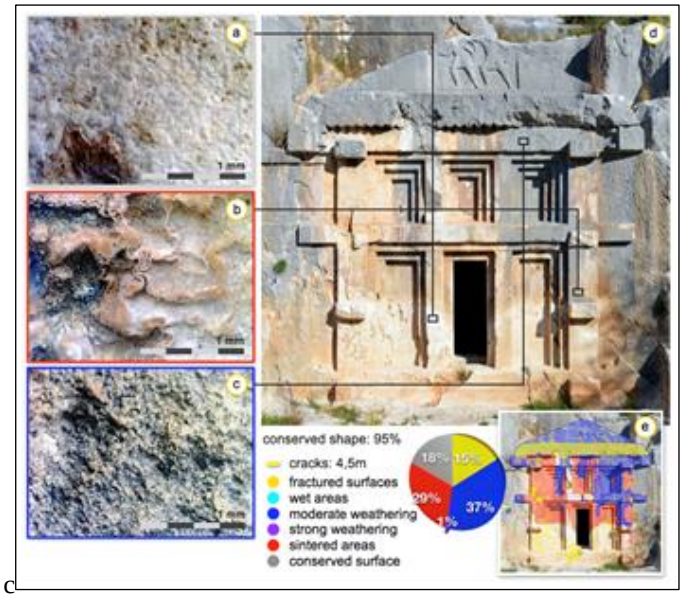

Fig. 2: The monument of the ocean necropolis (d); a) Well-conserved surface showing only partial sintering; b) Amorphous forms of sintering and reddish discolorations; c) Roughened surface with grayish discolorations on a moderately weathered area. e) Quantified mapping and results.

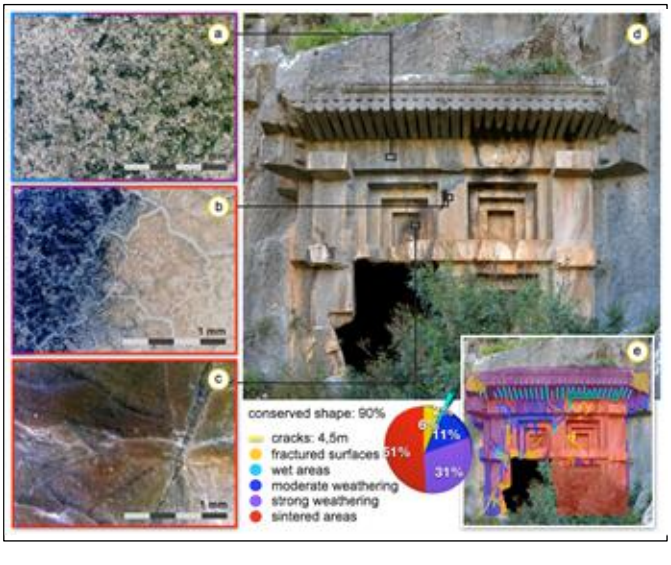

Fig. 3: The monument of the river necropolis (d); a) Moderate and strongly weathered surface; b) Strongly weathered and connected sintered area; c) Sintered area showing elephant skin-like forms, e) Quantified mapping and results.

4.1.2. The tomb of the river necropolis

The façade of the monument is protected by the still conserved stylized representation of the beam ceiling. Weathering phenomena are found all over the monument. Strongly weathered areas are connected with the water stains visible by the grayish discoloration**.** In contrast to the moderately weathered areas, they are showing the development of a micro-relief (Fig. 3a). Similar to the soldier monument different forms of sintered crusts are also found (Fig. 3b 6 c). Sintered areas (50%) and strong weathering (31 %) are the main forms of deterioration. In contrast to the tomb of the ocean necropolis wet areas could also be detected. These wet areas can be traced back to structural cracks and aquifer water transport mechanisms.

4.2. Surface hardness

Surface hardness measurements show that undamaged parts of the soldier monument (NL) reach the highest value with an averaged 90 pendulum surface hardness (Psh) (Fig. 4b). The moderately weathered area tested reached a value of 59 Psh by a clear spread of the single measurements. The monument of the river necropolis shows similar values in the non-weathered areas with an average value of 87 Psh (Fig. 4b). The moderate areas are also comparable with an average value of 61 Psh. The lowest values of all measurements are found in the strongly weathered areas. They reach an average value of 57.5 Psh and show the largest spreading (Fig. 4b). The rock material, according to Rilem (1997), can be defined as very hard, the weathered areas as hard.

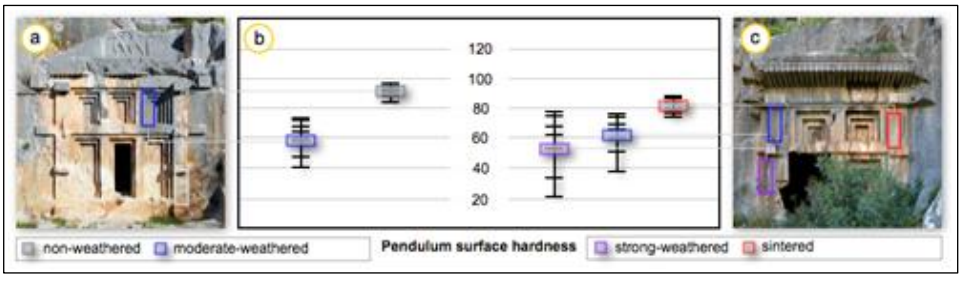

Fig. 4: a) Testing areas at the soldier monument of the ocean necropolis. b) Results of the measurements. c) Testing areas at the monument of the river necropolis.

4.3. Capillary water absorption

Capillary water absorption measured with Karsten test pipes show no water absorption at sintered surfaces and only a little water absorption at moderately weathered surfaces. This takes place only during the first minute of capillary suction. Strongly weathered areas clearly show water absorption with an A-value of around 0.4 kg/m^2 √1h. A nearly linear absorption is recognizable on freshly fractured surfaces with an A-value of around 1.4 kg/m^2 √1h (Fig. 5b).

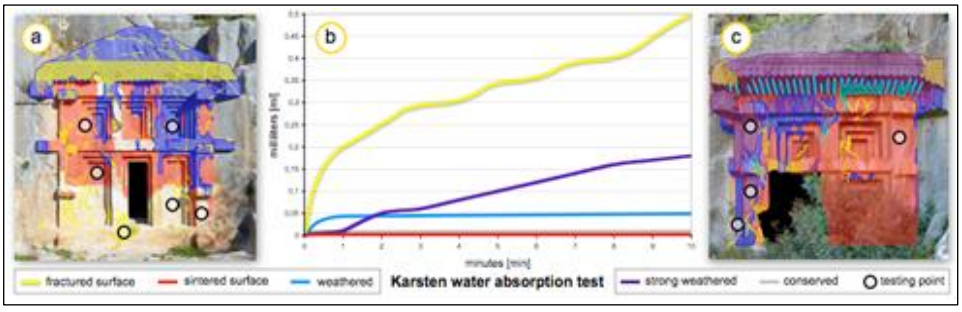

Fig. 5: a) The tomb of the ocean necropolis; b)Results of the Karsten absorption test; c) The tomb of the river necropolis.

4.4. Petrophysics and mineralogy

The necropolis limestone shows a micritic oolitic matrix (Fig. 6a). The Myra limestone contains many components like bioclasts and rudists fossils (Fig. 6c). Cathodoluminescence shows that both stone varieties are a very pure calcitic (calcareous) composition (Fig. 6b and Fig. 6d).

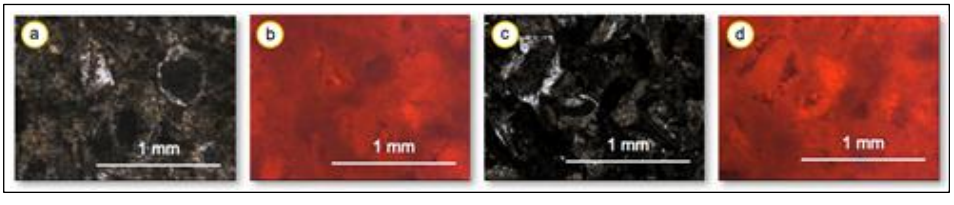

Fig. 6: a and b) Thin section of the necropolis limestone; c and d) Thin section of the Myra limestone; a and c) In transmitted light; b and d under cathodoluminescence.

Both stone varieties show a clear porosity, whereas the variety of the necropolis is less porous and also shows higher p-wave velocities (Tab. 2). In total the pendulum hammer hardness of the matrix in the necropolis limestone is harder, whereas rudists found in the Myra limestone show the highest values of all (Tab. 2).

Tab. 1: Summary of petrophysical results.

Specimen	**Porosity**	**Density**	**P-wave velocity**	**Pendulum hammer hardness**
	(%)	(kg/m³)	(km/s)	(-)
Necropolis Limestone (NL)	7.430	2.681	3.808 ± 33	75.5 - 83.7
Myra Limestone (ML)	10.832*	2.689*	3.524 ± 282*	76.77 / 105.8 (rudists)

*naturelmar madencilik company, www.naturelmer.com

5. Discussion and conclusions

Weathering mainly takes place due to chemical weathering by dissolution and precipitation. Relevant weathering only took place where the falling rainwater could reach the façade. Aquifer water leads to an intense form of damage because at affected parts of the facade infiltration takes place for a much longer time. Slightly dissolved and weathered areas develop a secondary porosity as was shown by surface hardness measurements and capillary water uptake. However, interaction with water and even light sintering effects leads to a protective sealing of the cut surface, where no water can penetrate. The investigations show that microclimatic conditions have a significant influence on the intensity of weathering of the limestone due to its exposition. After a rainfall the ocean necropolis exhibits a faster drying out, whereas the river necropolis, exposed to a north-easterly direction has a longer period of wetness. The most important factor for the different weathering intensities is the main wind and rain direction during periods with high precipitation rates in contrast to the dry summertime (Tab. 1). Based on the three annual main wind and rain directions, the river necropolis is confronted nearly two times stronger by direct rainfall than the ocean necropolis during February and November. In the months with the highest precipitation (December & January), the river necropolis is affected more than four times stronger than the ocean necropolis. In contrast drying winds in summer mainly affect the ocean necropolis. The presence of humidity is also a recognizable factor due to the settlement of higher plants. This is visible due to the growth of microbiology, which cannot be found in similar quantities at the ocean necropolis.

Acknowledgments

We would like to thank the persons responsible for the archaeological site of Myra Örenyeri for their friendly cooperation.

References

Göncüoglu, M.C., 2011, Geology of Kütahya-Bolkardag Belt (in Turkish). In Ergun Gökten (ed.), The Journal of mineral research and exploration, Ankara, 142, 227-282.

Rilem TC 127-MS, 1997, Tests for masonry materials and structures, Materials and Structures, vol. 30, July 1997, 323-328

Kolb, F., Kupke, B., 1992, Lykien. Geschichte Lykiens im Altertum, Antike Welt, special issue, Zaberns Bildbände zur Archäologie, vol. 2

Huelden, O., 2006, Gräber und Grabtypen im Bergland von Yavu. Studien zur antiken Grabkultur in Lykien Antiquitas issue 3, vol. 45. Habelt.

Mühlbauer, L., 2001, Lykische Grabarchitektur. Vom Holz zum Stein? PhD thesis, Technical University of Munich, Germany.

Özgül, N., 1976, Toroslar'ın bazı temel jeoloji özellikleri : TJK Bull., 19, 65 - 78.

CONTOUR SCALING AT THE ANGKOR TEMPLES: CAUSES, CONSQUENCES AND CONSERVATION

W. Wedekind[1*], C. Gross[1], A. van den Kerkhof[1] and S. Siegesmund[1]

Abstract

Contour scaling is the main weathering form observable at the Angkor monuments. In this study comparisons are made between the building stone and crust material from the Phnom Bakheng Temple and fresh stone material used for restoration. A significant difference in hydric and especially in thermal expansion of the crust and sandstone is shown in this study. This leads to an extensional effect and is a force for delamination (scale formation). By using an object-specific conservation treatment, the hydric and thermal expansion of the crust material was reduced.

Keywords: clay, moisture expansion, thermal expansion, mineralogy, conservation

1. Introduction

The temples and ruins of Angkor are located amid forests and farmland to the north of the Tonlé Sap and south of the Kulen Mountains, near Siem Reap City of Cambodia/Asia. The area was designated as a World Culture Heritage site in 1992. The legendary Angkor served as the seat of the Khmer Empire, which flourished from approximately the 9th to the 15th century and hosted the largest temples on earth (Fig. 1).

2. Site and conditions

2.1. Climate, rock material and weathering

2.1.1. Climate and environmental condition

The Angkor region is situated near two different types of climate, the tropical wet and dry climate and the tropical monsoon climate. The site has a wet tropical summer that is hot with dry, mild winters. The mean temperature is 28.5°C. Total annual precipitation averages 1425 mm. Precipitation takes place during the rainy season starting from March and ending in November. According to Waragai *et al.* (2012), the daily humidity during the dry season shows a minimum of 54 % in January and March. During the rainy season from May to October a high relative humidity of 80-90 % is measured.

[1] W. Wedekind*, C. Gross, A. van den Kerkhof and S. Siegesmund
Geoscience Centre of the University Göttingen, Germany,
Applied conservation Science (ACS), Göttingen, Germany
wwedekind@gmx.de

*corresponding author

2.1.2. Geological setting and stone material

The Angkor monuments in Cambodia are built of sandstone and can be classified into three types used for different temples and based on the color, texture, chemical composition and constituent mineral (Delvert 1963): gray to yellowish brown sandstone (Angkor Group), red sandstone (Banteay Srei) and greenish graywacke used for the Ta Keo Temple (Fig. 1e). Most natural building stones were brought from the Kulen Mountains by boat were different historical quarries could be identified (Carò 2009, Fig. 1). All stone types can be described as fine-grained porous sandstones. Recent petrographic investigations (Reucher *et al.* 2007) have shown that the building sandstones are feldspathic graywackes in the sense of Pettijohn *et al.* (1972). Graywackes are matrix-rich sandstones that are poorly sorted and derived from sediments, which were transported a relatively short distance before being deposited and contain chemically unstable minerals.

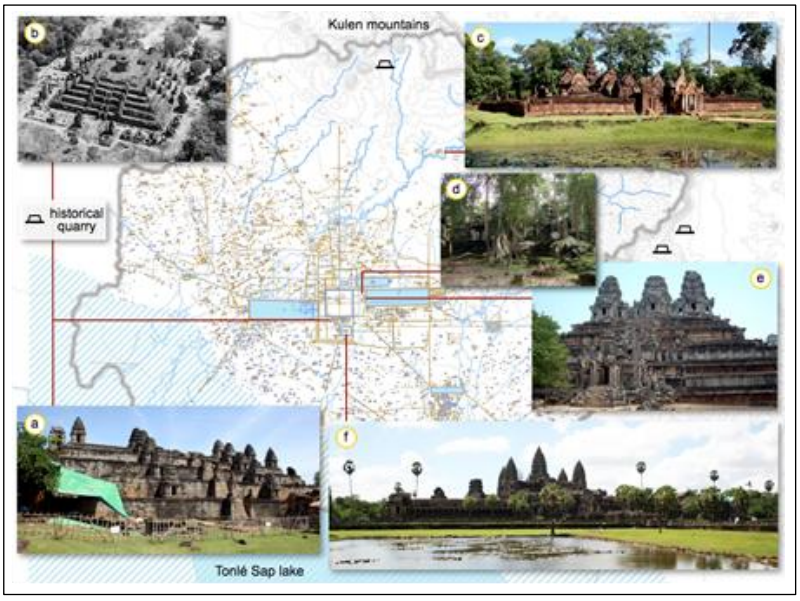

Fig. 1: Schematic map illustrating the historical Angkor complex and provinces with the major elevated temples indicated (source of the map: NASA); a) The Phnom Bakheng Temple made from gray sandstone that underwent restoration in 2009; b) The temple after being cleared of trees and plants in the 1920's; c) The Banteay Srei Temple constructed from red sandstone; d) The Ta Nei Temple surrounded by trees; e) The Ta Keo Temple made from green sandstone; f) The famous Angkor Wat temple made from gray sandstone.

2.1.3. Main weathering forms

Contour scaling is described as the main weathering forms observable in the Angkor buildings (Leisen 2002, André *et al.* 2008, UNESCO 2012). Contour scaling is defined as: "scaling in which the interface with the sound part of the stone is parallel to the stone surface. In the case of flat surfaces, contour scaling may be called spalling" (Vergés-Belmin 2008). This phenomenon is often related by crust formation and to the accumulation of

whitish efflorescences and crusts made of calcite ($CaCO_3$). Calcite within or underneath scales is most likely derived from the calcite cement in the sandstone, which creates crusts in the first few millimeters of the material (Fig. 2a, b). Small amounts of barite ($BaSO_4$) and gypsum can also be found (Hosono *et al.* 2006). In cross section the crust shows a distinct zonation where the first few millimeters display a brownish color followed by a bright discoloration (Fig. 2c). The bright discoloration was identified as calcite precipitation, which was also determined by cathodoluminescence microscopy (this study) and several other authors (e.g. Hosono *et al.* 2006 and André *et al.* 2008). This calcite mineralization results from the dissolution of calcite within the stone material due to chemical weathering and the remobilization near the drying surface as well as within cracks or weak zones within the stone material.

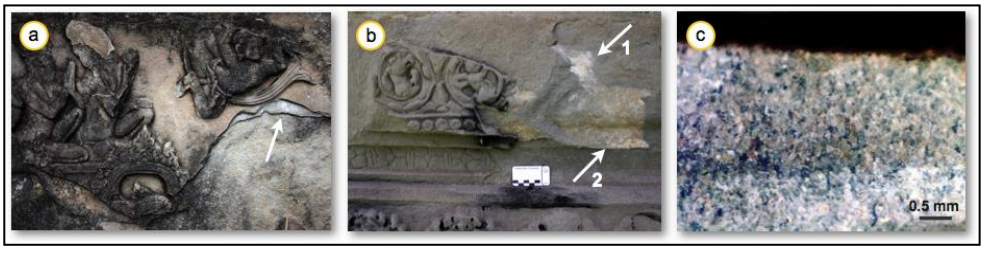

Fig. 2: a) Layered contour scaling with calcite precipitation underneath a recently lost scale (arrow); b) Calcite precipitation (arrow 1) and calcite and iron precipitation (arrow 2) between a recently lost scale; c) Cross section of the crust showing a distinct zoning - a brownish zone at the surface and a whitish one beneath.

3. Investigations

3.1. Methods and sample materials

The investigation included the determination of the pore space properties like porosity, density using hydrostatic weighting (DIN 52 102), mercury porosimetry measurements and hydric and thermal dilatation. Application of cathodoluminescence microscopy was used to give information on the alteration process and the distribution of calcite in the stones. This paper will focus on the weathering forms observed in the gray sandstone, the greenish graywacke type used for the Phnom Bakheng Temple as well as for the Angkor Wat Temple. They include the original building stone for the Phnom Bakheng Temple (PB), the weathering crust as well as the material that is now used for restoration (PBr). The sample material acquired in this study originates from the restoration team of the Phnom Bakheng Temple in 2009.

3.2. Mineralogical investigations

Cathodoluminescence microscopy (CL) was done on thin sections of the sandstone varieties to delineate alteration processes, to visualize possible microstructures and to determine what the differences are between the unaltered and altered building stones. Both sandstone varieties show evidence of alteration in minerals such as feldspar.

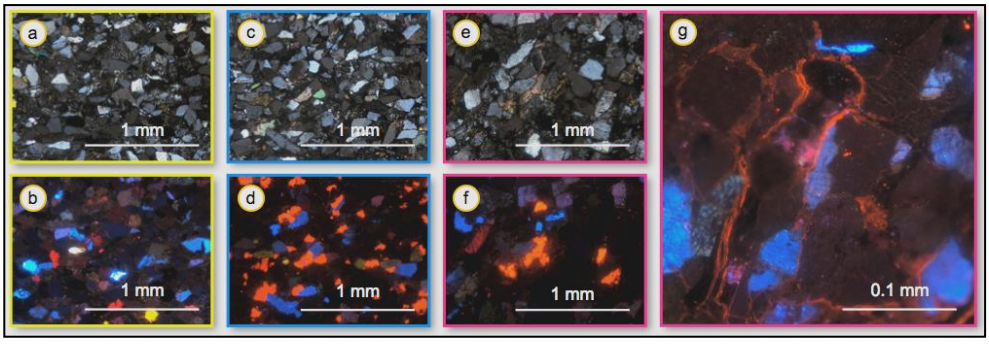

Fig. 3: a - b) Thin section of the Phnom Bakheng sandstone (PB) and c - d) of the restoration material (PBr.). e, f, g) Thin section of the weathering crust. a, c, e) Samples under polarized light and b, d, ,f, g) under cathodoluminescence. g) Detail of sample under CL showing the finely precipitated calcite within cracks and along the grain boundaries between grains of quartz (very low luminescence) and feldspar (blue). Coloured image frames correspond to the figures below.

The CL investigations clearly show the presence of calcite within the stone. Only a small amount of calcite, averaged around 2 % occurs in the PB variety (Fig. 3b), whereas the PBr variety has a calcite content of more than 7 % as is clearly visible by the orange CL color (Fig 3f). Alteration is also evident in the weathering crust (Fig. 3e). More calcite is observable in the crust of the Phnom Bakheng Temple than in the PB sample (Fig. 3f). A closer look shows that calcite precipitated along grain boundaries and microcrack formations (Fig. 3g).

Tab. 1: Pore size properties of the investigated stone material

Sample	**Porosity, %**	**Pore radii distribution [%]**				
		Micropores, µm		*Capillary pores, µm*		
		0.001– 0.01	0.01 – 0.1	0.1 - 1	1 - 10	>10
PB	12.3	44.02	39.37	10.92	14.45	1.75
crust	17.6	0	0	23.39	56.4	20.21
PBr	11.5	0	0	83.53	11.3	5.37

3.3. Petrophysical properties

The sandstones can be characterised as medium porous sandstone types with a porosity ranging between 11.5 % and 12.3 %. A porosity of 17.6 % however was measured in the crust (Tab. 1). The pore radii distribution of the crust and the PBr sample is dominated by macropores, whereas the PBr-sample shows a high amount of pores in the pore class of 0.1-1 with 83 % (Tab. 1). Microporosity in the case of the PB stone reaches 83 % and 0 % for the restoration material (PBr) and the crust. The main pore space properties of the sandstones are listed in Tab. 1.

3.4. Thermal dilatation experiment and hydric expansion

The crust sample has a dimension of around 2 by 2 centimeters and a thickness of around 4 mm. In order to compare the results with the stone material, the same or similar dimensions were used to perform the test on samples of the Phnom Bakheng sandstone as well as the restoration material (PBr). To test the thermal expansion of a thin and small piece of crust and stone material a simple but effective testing device was developed: The sample is placed on a massive cylinder of quartz glass. Another cylinder of quartz glass with thinner dimensions is put on the top of the sample. This cylinder is connected to an electronic dial gauge. Heat is applied by an infinitely variable fan heater concentrated on the sample. The temperature of the sample is measured by a digital contact thermometer placed directly at the back of the sample. Heating starts at 25°C (room temperature) and is continuously increased up to 100°C within 30 min. After reaching 100°C the heating is stopped and the cooling process starts until the sample reaches room temperature again. A length reduction occurs during the cooling process in all samples and in all directions. However, this length reduction shows a different behaviour. The thermal expansion measured at 60°C ranges between 1 mm/m and -0.2 mm/m with very high anisotropies (Fig. 4). The highest values were measured in the case of the PBr sample (0.227 mm/m, XY-direction) and the crust (1.036 mm/m, XY-direction), however the highest anisotropy was measured in the weathered crust. The gray sandstone of the Phnom Bakheng Temple has a hydric dilatation of nearly 2 mm/m in Z-direction, perpendicular to the bedding. Within the XY-direction an average dilatation of 1.165 mm/m is reached. Both values produce an anisotropic relation of 42 %. The weathered crust sample shows a dilatation of 1.55 mm/m in the Z-direction and 0.96 mm/m in XY-direction. Moisture expansion of the fresh quarry material (PBr) is comparably low, with values ranging between 0.2 to 0.4 mm/m.

4. Causes

The investigated samples differ in pore space radii distribution and mineral content. The gray sandstone of the Phnom Bakheng variety shows a pore radii distribution dominated by micropores probably due to high clay content.

4.1. Contour scaling due to hydric expansion?

Contour scaling of the sandstones of Angkor Wat can be explained by very high rates of hydric swelling of up to 4 mm per meter (Leisen 2002). Leisen assumed that the periodical processes of moisture expansion and shrinking by drying have weakened the structure of the stone. Hydric dilatation of the crust with 1.55 mm/m in the Z-direction is lower than the altered building stone (PB). The dilatation of the crust in the XY-direction with a value of 0.96 mm/m is quite similar to the XY-direction of the PB building stone (Fig. 4a). However, the process of dilatation differs in time and form in regards to the weathered crust or the building stone. During the first two and a half minutes of wetting the dilatation of the crust is faster than the dilatation of the building stone (Fig. 4b). This can be traced back to the higher porosity of the crust, which is only dominated by capillary pores and does not seem to contain many clay minerals. After that the dilatation of the crust takes much more time to reach the final value than the dilatation of the PB sample. This process can lead to a pull effect and is a force for delamination (Fig. 4b).

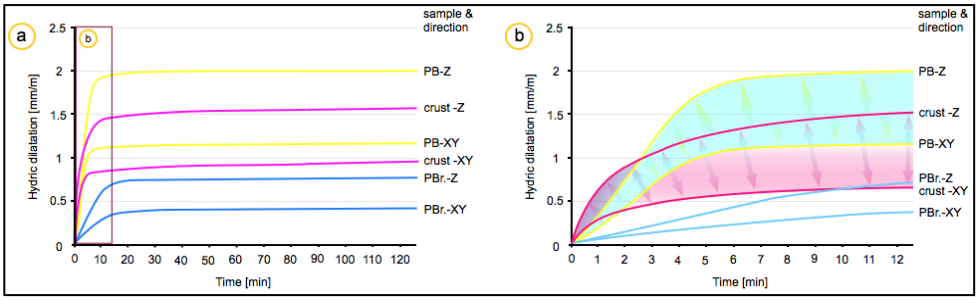

Fig. 4: a) Hydric dilatation of the PB sandstones. b) The dilatation of the PB sandstone within the first few minutes of water suction. The arrows indicate possible forces that may be responsible for the delamination of the crust from the building stone.

4.2. Contour scaling due to thermal expansion?

Thermal expansion of the various stone types and the crust shows considerable differences. The crust shows a maximum thermal expansion of 1.03 mm/m in XY-direction and 0.48 mm/m in Z-direction at 60°C with an anisotropy of 95%. However, the thermal expansion of the Phnom Bakheng building stone in the Z-direction with 0.049 mm/m is around ten times smaller than the crust (Fig. 5a). In the XY-direction a shrinking takes place that attains a value of - 0.2 mm/m at 60°C (Fig. 5b). This leads to an anisotropy greater than 100 %. The fresh quarry material attains a value of 0.14 mm/m in the Z-direction and 0.167 mm/m in XY-direction with a comparably low anisotropy of 15 % (Fig. 5b).

Thermal expansion of the crust is much higher than in the two building stones. The anisotropy of 95 % between the Z- and the XY-direction leads to shear stresses within the crust as well as between the crust and the stone material. A possible explanation of why the thermal dilatation within the XY-direction is much higher than in the Z-direction is that calcite precipitates in the cracks and empty spaces formed by the loss of clay minerals parallel to the bedding. The loss of clay minerals within the crust is also shown by the absence of any microporosity, whereas the building stone exhibits a microporosity of more than 80 % (Tab. 1).

In general, shrinking in the Phnom Bakheng sandstone is related to clay minerals during the cooling process. At around 60°C clay minerals begin to lose their crystal water. This sometimes leads to a depression of the thermal expansion during the heating process. On the other hand, the presence of clay minerals can reduce the thermal expansion of sandstone because the quartz grains expand, whereas the clay minerals show shrinkage at the same time. This decreases the expected thermal dilatation that is mainly related to the thermal expansion of quartz. Shrinking during cooling takes place because the thermal expansion of quartz decreases and the crystal water within the clay minerals is still lost. This leads to a collapse of the internal structure and a reduction in length, which has been observed in all sandstone varieties of the Phnom Bakheng Temple (Fig. 5b).

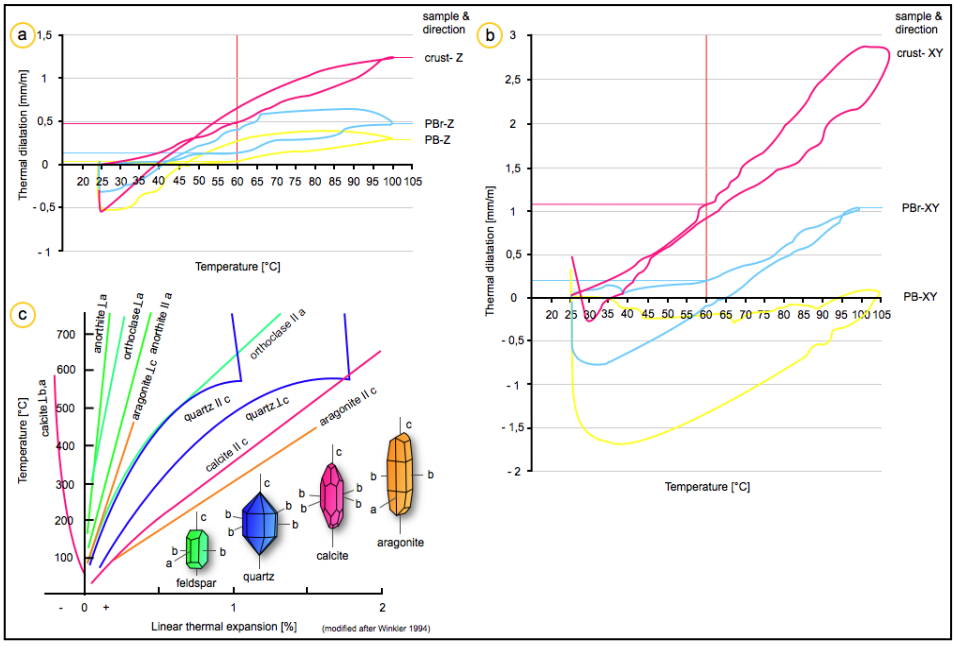

Fig. 5: Thermal dilatation of the crust, the PB building stone and the PBr stone in the Z-direction. b) Thermal dilatation of the crust, the BP stone and the stone used for restoration (PBr) in the XY-direction. c) Thermal expansion of different minerals.

5. Consequences

Consequently, all the investigations show that thermal dilatation seems to play a major role in the object specific deterioration form of contour scaling at Angkor. Furthermore, the CL investigations in this study have shown that an accumulation of calcite occurs in the crust. It is well known that calcite has a high coefficient of thermal expansion. The thermal coefficient of calcite is three times higher than quartz, the main mineral comprising sandstones (Fig. 5c).

6. Conservation

The investigations show that scaling is associated with the accumulation of calcite. Therefore, one option might be to reduce the calcite mineralizing out and to decrease the thermal expansion of the crust zone. To evaluate this hypothesis the tested crust sample was treated with a 5 % HCL solution. A small sample was placed in the solution for one hour and afterwards was washed with distilled water. The weight was reduced by 0.7 M-% after the treatment, probably due to the dissolution of calcite. However, as a result of the dissolution no loss of cohesion due to the separation of single grains could be detected.

The results of thermal expansion measurements show that only a slight change took place for the Z-direction in comparison to the thermal expansion before treatment. Both measurements show a thermal expansion of around 0.5 mm/m at 60°C, whereas the treated sample decreased to around 0.48 mm/m with a reduction of 13 % (Fig. 6a).

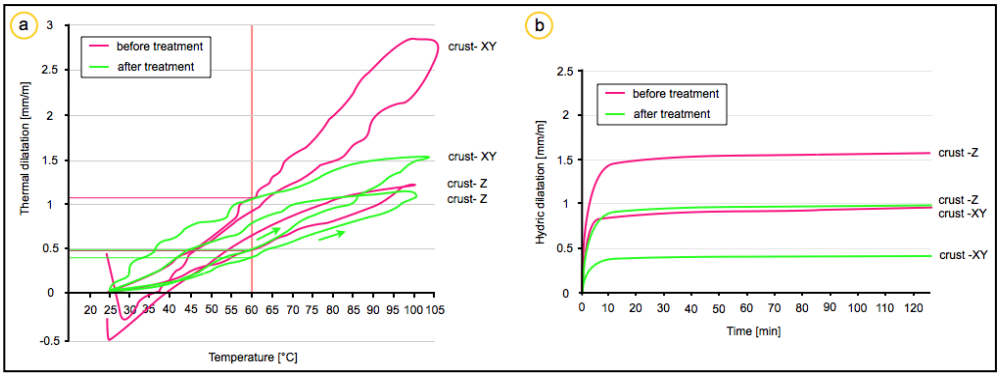

Fig. 6: a) Thermal dilatation before and after treatment and b) hydric dilatation before and after treatment of the crust.

In the case of the XY-direction of the crust a significant decrease of the thermal expansion was determined: The thermal expansion is still slightly higher than in the case of the Z-direction, but reached less than half at 60°C. The dilatation was reduced to 47 %. The anisotropy between the Z- and XY-direction was also reduced from 95 % to 15 %, which is significant in that we can expect the effect of scaling forces to become smaller. Hydric dilatation after the acid treatment also becomes smaller. A reduction of around 30 % takes place in the Z-as well as in the XY-direction (Fig. 6b). This can be explained by the increase of porosity because of the dissolution of calcite. Part of the clay cement can expand within this free pore space, and therefore does not have any influence on further expansion.

7. Final conclusions

Contrary to the assumption that hydric dilatation is the reason for contour scaling; the main causes of deterioration identified are chemical weathering by the precipitation of calcite at the surface combined with insolation-affected thermal dilatation. The recrystallization and precipitation of the case-hardening agent (calcite) throughout the surface rind is a probable formation mechanism for the crust. Insolation and the increase of thermal dilatation due to the accumulation of calcite, lead to shear stresses and scaling. Salt efflorescence and weathering related to bat guano and single mineral components of the stone material itself is a serious threat to the monument decorations (Siedel et al 2010). Both weathering factors can interact with each other and lead to an increase of weathering processes.

Our experimental investigations show that petrophysical properties can be measured even on small-dimensioned crust material. This leads to an understanding of the weathering processes involved in contour scaling. Acid treatment may be a promising approach to reducing the thermal expansion of the material and weathering due to contour scaling. The acid treatment is also an option for reducing the calcite accumulations within the weak zones and cracks behind the weathering crusts.

More onsite investigations as well as laboratory experiments are necessary to complete the picture and to add further knowledge in our understanding of the weathering mechanisms. The development of a suitable conservation treatment in combination with the up-to-date performed conservation techniques (UNESCO, APSARA 2012) has to be established in order to reduce the weathering from contour scaling, thus preventing further deterioration of the decorations at the Angkor temples.

Acknowledgments

We would like to thank the restoration team of the Phnom Bakheng Temple and the local authorities that safeguard Angkor (APSARA) and for their friendly cooperation. Our work was supported by the Hans-Boeckler-Foundation.

References

André, M.F., Etienne, S., Mercier, D., Vautier, F., Voldoire, O., 2008 Assessment of sandstone deterioration at Ta Keo temple (Angkor): first results and future prospects, Environ Geol 56, 677–688.

Caró, F., 2009, Khmer stone sculptures: a collection seen from a material point of view, Metropolitan Museum of Art Bulletin 67, no 5, 1455-1466.

Delvert, J., 1963, Recherches sur l'erosion des grès des monuments d'Angkor, *Bulletin de l'École française d'Extrême-Orient*, 51/2:453–534.

Hosono, T., Uchida E, Suda Ch, Ueno A, Nakagawa T (2006) Salt weathering of sandstone at the Angkor monuments, Cambodia: identification of the origins of salts using sulfur and strontium isotopes. Journal of Archaeological Science 33, 1541-1551

Leisen, H., 2002, Contour scaling: The disfiguring disease of Angkor Wat reliefs, Museum International 54 (1–2), 85–92.

Pettijohn, F.J., Potter P.E., Ever, R., 1972, Sand and sandstone, New York.

Reucher, R., Leisen, H., von Plehwe-Leisen E., Kleinschrodt, 2007 Petrographisch-geochemische Untersuchungen von Naturwerksteinen der Tempelanlagen des Angkor Parks/Kambodscha. Z. dt. Ges. Geowiss., 158/3, 617–629.

Siedel, H., Pfefferkorn, S., von Plehwe-Leisen, E., Leisen, H., 2010, Sandstone weathering in tropical climate: Results of low-destructive investigations at the temple of Angkor Wat, Cambodia. Engineering Geology 115, 182–192.

UNESCO, APSARA, 2012, Angkor Charter - Guidelines for Safeguarding the World Heritage Site of Angkor, Siem Reap, Cambodia, 5 December 2012.

Waragai, T., Morishima, W., Hada, A., 2012, Angkor Wat Meteorological Observation Station (AMOS):Installation of Monitoring System and Preliminary Results of Observation at Angkor Wat Temple, Cambodia. 日本大学文理学部自然科-学研究所研究紀要, no 48,35-48.

Vergés-Belmin, V. (ed.), 2008, ICOMOS-ISCS: Glossary on stone deterioration patterns. Champigny/Marne.

This page has been left intentionally blank.

GEORGIA MARBLE AT THE MINNESOTA STATE CAPITOL: EXAMINING THE CORRELATIONS BETWEEN MARBLE COMPOSITION, LOCAL CLIMATE, CLIMATE AND DURABILITY

P.G. Whitenack[1*] and M.J. Scheffler[1]

Abstract

Based on observations and tests of historic Georgia marble cladding at the Minnesota State Capitol, a field-discernible correlation exists between marble composition and weathering performance. Field studies noted over the course of a five-year restoration project of the capitol exterior were used to categorize the original marble cladding into four perceptible types. In situ chemical testing and comparison of repair assignments were then used to quantify the severity of weathering for each marble type, linking compositional differences within the marble to its long-term durability. This hypothesis was substantiated through detailed petrographic analysis in a laboratory setting that indicated marble that was more dolomitic than calcitic in its basic chemistry and with smaller, more interlocked grain structure consistently proved to be more durable in weathering performance over time. This information was used to guide the restoration process by selecting marble replacement units with the intent of maximizing anticipated service life.

Keywords: Georgia marble, calcitic, dolomitic, hysteresis, granoblastic, xenoblastic

1. Introduction

When selecting stone for architectural use, appearance of the material is often the primary consideration. Colour, texture, and visual uniformity of the finished stone surfaces are among the first attributes to be evaluated. Availability and cost of procuring, shipping and installing the stone are important early considerations as well. Following these initial criteria, the compositional characteristics of the stone, chiefly durability and weathering resistance, are often reviewed by the architect to differentiate among preliminary selections. The degree of analysis and the importance placed on these aspects of stone selection can differ widely according to the priorities of the individual designer, the anticipated service life of the stone, and other variables. Nevertheless, it has been clear from the very beginnings of its use as architectural cladding that some types of stone are more suitable to the task than others. This paper presents the findings of a study of Georgia marble masonry that has been in service for over a century at the Minnesota State Capitol in St. Paul. As the exterior stone restoration work progressed it became apparent that some portions of the marble cladding had weathered much more extensively than others, yet the specific origins and patterns of divergent durability were not immediately clear. This research was

[1] P. Whitenack* and M. Scheffler
Wiss, Janney, Elstner Associates, Inc., Minneapolis, Minnesota, United States of America
pwhitenack@WJE.com

*corresponding author

undertaken in an effort to determine how and why marble obtained from the same general quarry site, and even within the same masonry unit, could present such a varied response to weathering and atmospheric conditions. Ultimately, the results of the study proved to be a useful guide to the selection of replacement material.

2. Background

2.1. The Minnesota State Capitol

The Minnesota State Capitol was designed by Cass Gilbert, who began his career as a draftsman in his hometown of St. Paul and later enrolled in the architecture school of the Massachusetts Institute of Technology. Gilbert studied abroad in Europe, worked for two years at the New York City firm of McKim, Mead & White, and then returned to St. Paul where, in 1895, he won a design competition for the new state capitol. Undoubtedly influenced by his Beaux Arts training and travels in Europe where he studied prominent classical buildings including the Florence Cathedral and St. Peter's Basilica (upon which the Minnesota State Capitol dome is modelled), Gilbert selected marble as the primary exterior stone for cladding and carved ornamentation. Stating that the capitol "must last 500 years", Gilbert cited superior "durability in exposure to the atmosphere" as one reason for his selection of marble (Irish 1993). After considering several sources, including Vermont and Italy, Georgia marble was ultimately specified. The Amicalola quarry, located near the town of Tate, in Pickens County, supplied most of the stone for the capitol.

2.2. Georgia marble

When construction of the capitol began in 1896, the long-term durability of Georgia marble was not generally questioned. Architectural use of the stone had until that time been largely confined to interior finishes and monuments, with no substantial exterior use prior to the 1892 construction of the Equitable Building in Atlanta (McCallie 1907). Consequently, there was not a significant sample size of existing buildings clad in Georgia marble to evaluate for durability. As the industry of quarrying and marketing this stone for architectural use gained momentum, the Georgia State Geology Department published *A Preliminary Report on the Marbles of Georgia* in 1895 (2nd ed. 1907) describing the geology, history, and use of the stone. This publication, compiled by assistant state geologist, S. W. McCallie, included 15 chapters authored by various technical experts presenting evaluative tests and data that began to explore factors influencing the durability of Georgia marble. In a chapter on the chemical properties of Georgia marble, the report stated that the ideal objective would be to "trace the relations between strength, durability, colour, texture and chemical composition"; however, the author contended that insufficient information had been gathered and assessed to provide this level of comparison, noting that "scarcely anything has been done in studying the relations between the properties and the structure" of Georgia marble, such that "only a few isolated facts can be noted" (McCallie 1907). The restoration project at the Minnesota State Capitol presented a unique opportunity to test and build upon the findings presented in the Geological Survey report, over a century after the document was first published.

3. Methodology and results

3.1. Field study

3.1.1. Marble categorization

Because marble is a metamorphic rock, it can vary widely in composition; diverse patterns of multi-coloured material swirl randomly through the generally white stone, and the crystalline grain structure can vary in size and texture. In order to define visual and structural differences in the marble and to study the weathering response for each of these properties, a system of categorization was devised based on the colour, veining, grain texture, and accessory mineral content visible to the unaided eye. Four basic groupings of marble were established and designated as types 1 through 4: ***Type 1 marble***, estimated to comprise about 20 percent of the capitol's exterior cladding, is the most homogeneous, being uniformly white in colour, with virtually no veining or obvious accessory minerals. The grain structure of type 1 marble consists of large, lens-shaped crystals that are fairly consistent in size. ***Type 2 marble*** comprises about 30 percent of the exterior cladding, and is primarily white in colour, with moderate amounts of grey veining, but relatively few apparent accessory minerals. The grain structure of type 2 marble is similar to that of type 1, but with more textural variation, especially within the grey veins. ***Type 3 marble*** also accounts for around 30 percent of the exterior cladding. It is predominately grey in colour with occasional white veins, but more typically characterised by the presence of a variety of visible accessory minerals that give this type a darker, more variegated appearance than the others. The grain of type 3 marble is irregular and was often noted to be finer in texture than either type 1 or type 2 when exposed and weathered surfaces were viewed with a hand-held magnifying device. The remaining 20 percent of the cladding consists of ***Type 4 marble***, which is off-white or ivory coloured with visible accessory minerals that appear as tan bands, but with little to no grey veining. The grain of type 4 marble appears conspicuously finer than that of the other three types, even without magnification.

3.1.2. Modes and Patterns of Deterioration

After the existing marble on the capitol had been categorized into the four groups described above based on physical surface appearance, the weathering performance of each marble type was evaluated by in-situ visual assessment and laboratory microscopic examination of core samples extracted from a number of locations. Deterioration of the marble was observed to have progressed at differing rates and by diverse modes. These modes included delamination, normally associated with cleavage along mica veins; and the dissolution of the calcium carbonate by exposure to chemical and biological agents such as acid rain, by-products of industrial and automotive combustion, oxidization produced by algae growth, and pigeon waste. While the adverse effects of these chemical agents were conclusively present, petrographic analysis determined that the vast majority of marble deterioration was caused by internal distress that was more mechanical in nature: the unequal expansion of the marble crystals caused by cyclical heating and cooling at the exposed surfaces, referred to as thermal hysteresis (TEAM 2005). This progressive and irreversible process gradually created a network of micro cracking within the marble. When water entered this network of cracks and expanded during numerous freeze-thaw cycles, the marble progressively crumbled and sugared. This mode of disintegration was not fully understood at the time the capitol was constructed, and was not considered in the state geologist's report, which stated: "while marble is more rapidly attacked by chemical agents than other stones, its

ability to resist the mechanical agents of weathering, which are generally the most destructive, makes it a comparatively durable stone" (McCallie 1907).

3.1.3. Climatic Influences

The impact of localized environmental exposure was not significantly deliberated when marble was selected for use on the capitol exterior, yet arguably, there is no major city in the United States with a local climate that is more favourable to the deterioration of marble than St. Paul, Minnesota. Because the process of hysteresis is in part driven by temperature extremes, this may seem contradictory, given St. Paul's latitude at 46° N; however, the humid continental climate of Minnesota can deliver a wide range of ambient air temperatures: Minnesota's record high temperature is 45.5°C (114°F), and summertime average daily temperatures approach 28°C (82°F). While other cities with Georgia marble architecture can reach high temperatures in this range, few of these locations regularly experience the extremely cold wintertime temperatures that are common in St. Paul, where the lowest recorded temperature is -40.5°C (-41°F) (NCEI 2015). Further enhancing the effects of hysteresis, the Minnesota climate experiences frequent freeze-thaw cycling, where the daily high temperature rises above freezing and the nightly low temperature falls below. This cycling allows water to more frequently penetrate the micro cracks to a greater depth, hastening disaggregation by freezing and expanding. Consequently, for a building clad in Georgia marble, geographic location will have a profound effect on the durability of the stone over the life of the building. This point was demonstrated by a comparison of the marble cladding of the Candler Building in Atlanta, Georgia, to that of the Minnesota State Capitol. Both buildings were completed in 1905, and each features marble that was supplied by the Amicalola quarry. Close-up study of the exterior marble surfaces of the Candler building revealed the presence of hysteresis-induced micro cracks; but since Atlanta experiences a much narrower range of temperature extremes and far less freeze-thaw cycling when the stone is saturated than St. Paul, the marble of the Candler Building was in much better condition, with substantially less sugaring than what was observed at the Minnesota State Capitol.

3.1.4. Comparison of Repair Frequency by Marble Type

Disintegration produced by hysteresis and other factors was strikingly more commonplace and advanced in marble units characterised as types 1 and 2, many of which had crumbled so extensively that they no longer resembled their original form. Conversely, type 3 and particularly type 4 marble appeared to be more resistant to these effects, with minimal sugaring and the original tooling marks often still evident, even at locations directly exposed to weathering. This pattern emerged further when marble repairs were assigned by the architects and it was recognised that repairs were being allocated with greater frequency to marble that was whiter in colour, with less prominent veining and accessory minerals (types 1 and 2). Repair assignments for 350 of the original modillions at the main cornice of the capitol were tabulated and grouped by marble type to look for statistical support of the link between composition and durability. Modillions were selected for this part of the study because they are a repetitive element that occurs at the same location on all four primary orientations. Modillions were also well-suited for comparison because their small size made them more likely to consist of a single type of the four identified marble groups. Three repair options were available for modillions, based on the existing condition of the unit: (1) *No repair* - Modillions exhibiting little or no sugaring or other significant deterioration, as shown on the right in Fig. 1, were left intact with no repairs beyond

occasional cleaning with hot water; (2) *Light surface refinishing* - Modillions exhibiting moderate levels of disintegration, yet retaining the recognizable form and dimensions of the original unit were lightly redressed to restore visual consistency; and (3) *Replacement* - Modillions exhibiting an advanced degree of sugaring to the extent that the original form of the unit was no longer recognizable, as shown on the left in Fig. 1, were replaced with new units that matched the original profile and dimensions.

Figure1: The type 1 marble modillion on the left exhibits more extensive sugaring than the type 4 modillion on the right. Both units are located on the north facade of the capitol.

The 350 modillions selected for this study were grouped according to marble type and compared for frequency of repair assignments, revealing that the majority of modillions needing total replacement were originally fabricated of type 1 or type 2 marble, while exceedingly few of the modillions consisting of marble types 3 and 4 were replaced. The reverse was true for modillions that were left intact with no repairs; nearly all of which were originally fabricated of type 4 marble. The data gathered for this comparison is summarized in Tab. 1 below:

Tab. 1: Repair Assignments by Percentage for each Marble Type.

Marble Type	No Repair	Refinished	Replaced
Type 1	1.5	6.5	92
Type 2	1	41	58
Type 3	2.5	80.5	17
Type 4	50	47	3

3.2. Field testing

After the marble was categorized and a range of susceptibility to disintegration identified, field testing was conducted to more closely examine the reasons for this variation. Because it originated as predominately carbonate limestone, the basic component of Georgia marble is calcium carbonate, a soluble compound that is sensitive when exposed to stronger acid compounds. As with limestone, marble can exhibit elevated proportions of magnesium carbonate, which displaces the weaker calcium compounds, altering the marble's chemical composition from calcitic to dolomitic. A discussion of the chemistry of Georgia marble,

presented in the geological survey report of 1907, expanded on the significance of this variability, stating "calcium carbonate is easily dissolved… by cold dilute hydrochloric acid, as is evidenced by the brisk effervescence; while dolomite, under the same circumstances, dissolves so slowly as to produce a scarcely noticeable evolution of gas. In consequence of greater insolubility, when magnesium carbonate is present, we would expect those marbles, containing more of it, to weather more slowly than those containing less" (McCallie 1907). Based on visual assessments and the comparison of repair assignments by marble type at the capitol, it was suspected that magnesium content was lower in types 1 and 2, and elevated in types 3 and 4. To determine whether this was true, field chemical testing was conducted on a number of samples of each marble type using a mild acid solution and an alkaline reagent to qualitatively analyse the levels of calcium carbonate and magnesium carbonate present in each of the four identified types of marble (Mann 1955).

3.2.1. Calcium carbonate testing

The first phase of the test involved applying a 10 percent dilution of cold hydrochloric acid to the marble to determine the level of calcium carbonate present. This phase of testing was conducted on five samples of each marble type, including marble that remained intact on the building, as well as marble units that had been removed by the masonry contractor for replacement. When applied to samples that were identified as type 1 and type 2 marble, significant effervescence was observed due to the release of carbon dioxide. When the acidic solution was applied to samples identified as types 3 and type 4 marble, effervescence was minimal or non-existent. This phase of the field testing confirmed that types 1 and 2 were more calcitic than types 3 and 4.

3.2.2. Magnesium carbonate testing

The second phase of the field test was conducted by applying a violet-coloured alkaline reagent solution to the surface of the marble on the same units tested in phase 1. If the solution reacts with magnesium it turns blue in colour; the sooner conversion occurs, and the stronger the blue colour; the greater the presence of magnesium. When the reagent was placed on marble samples categorized as type 1, the solution remained mostly violet in colour until it evaporated or was absorbed into the stone after a few minutes. When placed on samples of type 4 marble the reagent changed to an intense blue colour within 10 seconds. Tests on samples identified as type 2 marble yielded similar results to those noted for type 1, while tests conducted on samples identified as type 3 marble yielded similar, though less conclusive, results to the type 4 samples. The reagent phase of field testing thus indicated that the type 4 marble contained a higher level of magnesium than the type 1 marble. When compared to the incidence of repair assignments per marble type, both phases of field tests confirmed the suggestion in the 1907 Georgia geologist's report correlating the presence of magnesium to increased weathering durability.

3.3. Laboratory testing

3.3.1. Grain size and texture

Petrographic evaluation was conducted in a laboratory setting on two samples for each of the four marble types collected from the capitol. Microscopic examination, X-ray diffraction, and other comparative measures were used to study basic chemistry, overall density, grain size and texture, and accessory mineral content. The results of this evaluation reinforced and expanded upon the differing compositional range from type 1 through type 4

marble that was first identified in the field. Chemical analysis of samples removed from the capitol confirmed field test results indicating that marble types 1 and 2 were more calcitic, while types 3 and 4 were increasingly dolomitic. Lab testing also reinforced contentions within the Georgia Geological Survey report pertaining to grain size. The 1907 report cited analysis of Georgia marble that indicated "dolomitic marbles were fine-grained, while the calcite marbles are coarse in texture." This assertion was confirmed by examination with a petrographic microscope of honed samples under polarized light that showed marble types 1 and 2 featured larger grain size, while the grain became increasingly finer through types 3 and 4 (Fig. 2). Magnification also showed that grain texture varied with the size of the crystals. The large grained marbles - types 1 and 2 - featured rational (granoblastic) crystals that were not well interlocked, whereas the smaller grained marbles - types 3 and 4 - exhibited irregular-shaped (xenoblastic) interlocking crystals.

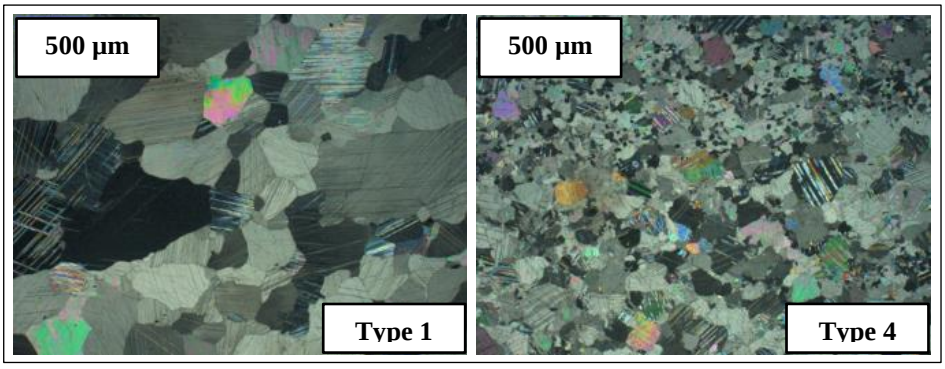

igure 2: Magnified views of type 1 marble on the left and type 4 marble on the right, show much larger grain size for type 1 when compared to type 4 at the same magnification scale.

3.3.2. Accessory mineral content

Accessory mineral content was briefly studied in the laboratory and it was noted that examined samples of type 1 and type 2 marble commonly contained veins and inclusions of white mica, a soft (2.8 on the Mohs hardness scale) accessory mineral that is prone to cleavage, while samples of type 3 and type 4 marble mostly contained discreet concentrations of corundum, a much harder mineral (9 on the Moh's hardness scale). While further study is needed to definitively evaluate the detrimental or beneficial effects of accessory minerals on the surrounding marble, it can be stated that the frequent presence of mica negatively affects the durability of marble types 1 and 2 and the incidence of corundum in types 3 and 4 marble further contributes to the surface hardness of units that contain significant concentrations.

4. Conclusions

Field observations, laboratory studies, and testing conducted on the exterior cladding of the Minnesota State Capitol have shown that compositional variations of marble from a single quarry are directly related to susceptibility to weathering-induced disintegration over time. Among influencing factors, the chemistry, grain size and texture, and accessory minerals contribute most directly to observed variations in long-term durability. These influencing

factors were recognized in the Georgia Geological Survey report of 1907 and confirmed by our testing: Marble with higher magnesium content (dolomitic marble) was observed to exhibit less severe sugaring than marble with little or no magnesium content (calcitic marble). Differences in grain texture and size were observed to contribute to variation in the levels of disintegration across the four basic marble types. The granoblastic crystals of types 1 and 2 more easily slip past each other during temperature cycling, amplifying the effects of hysteresis, while the xenoblastic crystal shapes of types 3 and 4 greatly reduce the ability of adjacent crystals to slide by one another during thermal cycling. Because the grain size is larger in types 1 and 2, the deformation caused by hysteresis becomes noticeable more quickly than with the smaller size crystals in types 3 and 4. Finally, all of the marble types featured some degree of accessory minerals of varying hardness and cohesiveness; types 3 and 4 marble generally contained higher concentrations of harder minerals than did types 1 and 2, likely contributing to increased durability.

What was not fully understood at the writing of the Georgia State Geologist's report in 1907 was the structural vulnerability of Georgia marble to hysteresis, and the true impact of the local climate where the stone will be used. Our study found that calcitic Georgia marble with a specific mineral composition was particularly susceptible to deterioration when used in the extreme climate of Minnesota. Comparisons of marble samples of the same vintage and quarry of origin demonstrated that the effects of micro cracking from thermal hysteresis are intensified when water enters those cracks and freezes. However, by selecting replacement marble that is not characterised by the detrimental qualities described in this paper, increased durability to this mode of disintegration is likely. Beyond simple aesthetic considerations, it is therefore desirable to select marble that is anticipated to have greater durability when intended for long-term exterior use on buildings; especially those located in climatic zones that experience frequent freeze-thaw cycling. For Georgia marble this may involve avoiding the traditional predilection for the purest, whitest marble available, in favor of marble with more visual character, including darker veins and minerals associated with dolomitic marble featuring finer, interlocked grain. When used to select replacement marble for the Minnesota State Capitol, this approach did not result in a noticeable change in the overall visual appearance of the marble cladding.

References

Irish, S., 1993, West hails east: Cass Gilbert in Minnesota, Minnesota History, 197-207.

Mann, V.I., 1955, A spot test for dolomitic limestones, Journal of Sedimentary Petrology, 25 (1), 58-59.

Mc Callie, S.W., 1907, A preliminary report on the marbles of Georgia, State of Georgia Printing Office, 58; 105-109

National Centers for Environmental Information (NCEI), State Climate Extremes Committee (SCEC): Records, (https://www.ncdc.noaa.gov/extremes/scec/records, accessed on September 9, 2015)

TEAM, "Testing and Assessment of Marble and Limestone," Final Technical Report, 2005, EC-Project: TEAM-G5RD-CT-2000-00233.

INVESTIGATION METHODS

This page has been left intentionally blank.

THE EFFECT OF SALT CRYSTALLISATION ON THE MECHANICAL PROPERTIES OF LIMESTONE: STATISTICAL CORRELATION BETWEEN NON-DESTRUCTIVE AND DESTRUCTIVE TECHNIQUES

N. Aly[1*], A. Hamed[1], M. Gomez-Heras[2], D. Benavente[3] and M. Alvarez de Buergo[4]

Abstract

Mokattam limestone is the most frequent building stone used in the cultural heritage buildings in Historic Cairo (Egypt) and it is susceptible to the ongoing effects of salt weathering. A purpose-made simulation chamber was used to test in the laboratory the salt weathering on limestone samples from an active quarry at Helwan area (30 km, south Cairo) at different temperature regimes (20, 30 and 40°C). To assess the extent of the resulted decay, mechanical properties of the fresh quarry and tested samples after different regimes were investigated with non-destructive techniques (P-wave velocity and Leeb rebound hardness) and destructive techniques (uniaxial compression strength). The different mechanical measurements of the tested samples were notably affected after the different temperature regimes. Uniaxial compressive strength is highly correlated with Leeb rebound hardness while P-wave velocity showed a low relevance for the prediction of the strength of the tested samples.

Keywords: stone decay, salt weathering, non-destructive testing (NDT), Mokattam limestone

1. Introduction

The mechanical properties can be used to indicate the degree of weathering of building stones (Sjöberg and Broadbent, 1991). Ultrasonic pulse velocity (UPV) measurement and rebound surface hardness (Leeb hardness) testing are simple non-destructive techniques to evaluate the mechanical properties and the extent of weathering of building stones in-situ and in laboratories (Vasconcelos *et al.*, 2008). The velocity of the UPV gives information about dynamic mechanical properties of the material, as well as, for example, porosity, degree of alteration, geometry of the pores, homogeneity of the material and the presence of discontinuities (Kahraman, 2002; Grinzato *et al.*, 2004; Benson *et al.*, 2005;

[1] N. Aly* and A. Hamed
Faculty of Petroleum and Mining Engineering, Suez University, Egypt
neven.ali@suezuniv.edu.eg

[2] M. Gomez-Heras
Geosciences Institute IGEO (CSIC, UCM) Madrid, Spain

[3] D. Benavente
Departamento de Ciencias de la Tierra y del Medio Ambiente. Universidad de Alicante, Spain

[4] M. Alvarez de Buergo
Laboratorio de Petrología Aplicada - Unidad Asociada CSIC-UA, Alicante, Spain

*corresponding author

Sousa *et al.,* 2005; Bourgès, 2006; Mateos *et al.,* 2006 and Martínez-Martínez *et al.,* 2007). Leeb rebound surface hardness is related to the energy loss of certain impact body after impacting on a sample. Although this test was primarily developed for metals, it is widely used now for other material, such as stones. The measurements of Leeb surface hardness are highly affected with surface irregularities; therefore it can be used to evaluate the surface weathering (McCaroll, 1991). The strength of stone material is affected by mineralogical composition, density, porosity and grainsize of the material (Hoek and Brown, 1980). In the Uniaxial Compressive Strength (UCS) test, the strain of a rock sample is measured under an increasing unconfined compressive force (Meulenkamp and Grima, 1999). The stress at which the sample fails is referred to as the peak strength**.** Many researchers have studied the correlation between UPV and Equotip hardness tester and the compressive strength and the reliability of using such NDT techniques to estimate the mechanical characteristics of the building stones (Meulenkamp and Grima, 1999; Kahraman 2001; Vasconcelos *et al.,* 2008; Sharma *et al.,* 2010 and Vasanelli *et al.,* 2013).

The main objective of this study is to assess the change of mechanical behaviour of limestone samples subjected to salt weathering test at different temperature regimes and to understand the statistical relationship between NDT (UPV and Equotip hardness) and UCS as the main methods for characterizing the mechanical properties of stones.

2. Materials and Methods

2.1. Materials

Limestone belonging to Middle Eocene Mokattam Group was extracted from Helwan area [30 km, south Cairo]. Mokattam group limestone is the most used construction material of Giza and Historic Cairo monumental sites. Cylindrical samples of 2 cm diameter and 4 cm height were prepared from this biomicritic limestone material (Fitzner *et al.,* 2003). During this work 10 % sodium chloride solution in distilled water was used as it is a common salt in building stones and in the groundwater water of Egypt (Gauri and Bandyopadhyay, 1999; Fitzner *et al.,* 2003). Limestone cores were subjected to different temperature regimes (20, 30 and 40ºC) in a purpose-made simulation chamber designed by Hamed *et al.,* (2015) based on continuous capillary imbibitions of samples (Aly *et al.,* 2015). Samples were tested for each temperature regime for 144 hours. Subsets of 15 samples were taken at 24, 48 and 72 h after the start of the experiments.

2.2. Methods

The effect of the different simulation regimes on the mechanical behaviour of the stone samples was evaluated non-destructively by means of a PUNDIT pulse tester with transducers of 1 MHz to measure the ultrasonic wave velocity (V_p). Five samples of each time interval were selected to measure the velocity of the ultrasonic propagation after different temperature regimes beside five quarry samples. The Leeb hardness number is a function of the velocity of the impact body as it rebounds from the surface, and this is dependent on the elastic properties and strength of the tested sample, which is electronically measured and converted to a Leeb number (Hack *et al.,* 1993; Verwaal and Mulder, 1993; Meulenkamp and Grima, 1999 and Aoki and Matsukura, 2007). The obtained values of Leeb number can be used to compare different rocks and structures in situ (Aoki and Matsukura, 2007 and Viles *et al.,* 2011). An Equotip3 (Proceq) shooting a 3 mm tungsten carbide ball with an impact energy of 1 N/mm² was used to determine the surface hardness (Leeb number) of sixty of the tested samples and of five quarry samples. The UCS test was

performed by means of universal testing machine Servosis® for small samples. The load rate was 0.53 MPa/s. Three quarry specimens plus six specimens after each temperature regime were selected for the UCS measurements. All the specimens were dried at 70°C before being used in different tests that were performed at room temperature.

3. Results

3.1. Ultrasonic P- wave velocity

The P-wave velocities for quarry cores and salt contaminated samples after different temperature regimes are shown in Fig. 1. The V_p average value for quarry cores equals (2450 ± 150 m/s) this value notably increased for all temperature regimes after 24 hours. Then P-wave velocity showed gradually a slight decrease with time at 20 and 30°C tests while it kept increasing continuously at 40°C test to 3300 (± 250) m/s after 144 hours. The salt was accumulated predominantly in the pore space of the tested sample after 24 hours and enables the waves to move faster within the stone material. However through time, the salt crystallization leads to the formation of cracks that reduce the P-wave velocity.

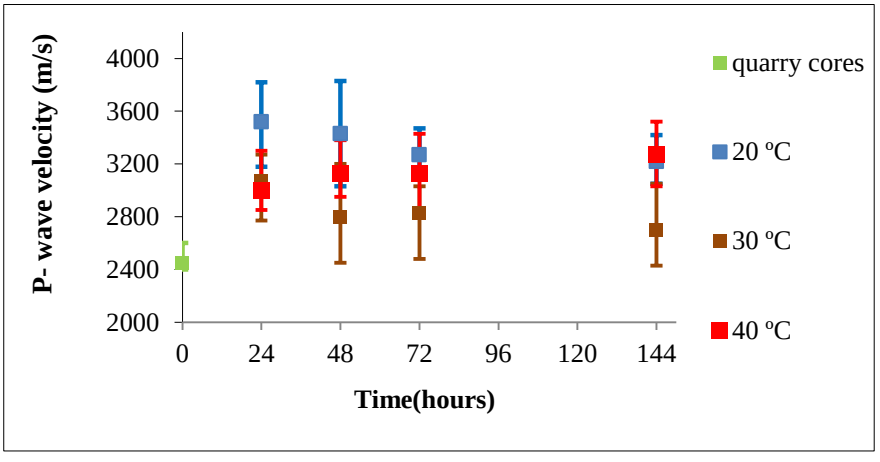

Fig. 1: P-wave velocity for limestone quarry cores and samples submitted to different temperature regimes.

3.2. Equotip surface hardness

Tab. 1 lists the average values of (Leeb) rebound hardness with the standard deviation for quarry cores and salt contaminated samples after different temperature regimes. The measurements indicated notable decrease through time after all regimes and reached to maximum decrease in the tested cores at 40°C to 70 (±20). The obtained results showed that the Leeb number describes properly the weathering evolution of tested samples which lead to an increase in surface roughness, and in turn to a decrease of the Leeb surface hardness (McCarroll, 1991). The rebound hardness seems unsensible to the deposition of salts within the stone material, which was not the case for the P-wave velocity.

Tab. 1: Equotip rebound (Leeb) number of quarry cores and samples submitted to different temperatures in the simulation chamber.

Surface Hardness (Leeb hardness)			
quarry cores = 210 ± 20			
Time	20°C	30ºC	40°C
24 hours	170 ± 20	150± 30	110 ±10
48 hours	160 ± 20	130 ± 10	80 ± 40
72 hours	130 ± 30	130 ± 20	80 ± 20
144 hours	130 ± 30	120 ± 20	70 ± 20

3.3. Unconfined Compression Strength (USC)

Fig. 2 shows the results of the compression strength of the used quarry limestone and of different simulation tests after 24 hours and 144 hours. The average value of UCS for quarry sample is 17.7 MPa which tends to decrease in all tests. A slight decrease was noticed after 24 hours, expect at 40°C (9.2 MPa), while a more important decrease is noticable after 144 hours.

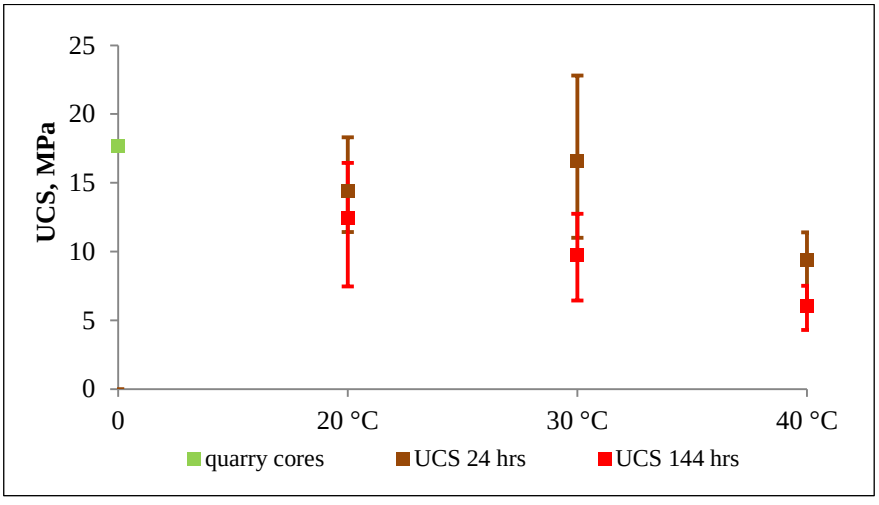

Fig. 2: Unconfined compression strength measurements for quarry limestone cores and samples submitted to different temperatures in the simulation chamber.

3.4. Statistical correlation of experimental results

Fig. 3 presents the results of P-wave velocity (V_p) versus compressive strength (UCS) as average values of the quarry and the salt contaminated samples submitted at different temperatures for 24 hours (Fig. 3a) and 144 hours (Fig. 3b).

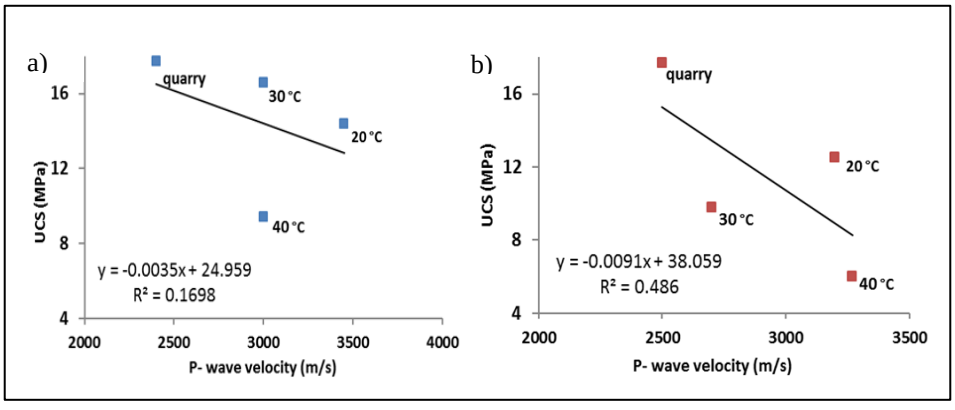

Fig. 3: Correlation between UCS and UPV of salt contaminated samples submitted to different temperatures for 24 hours (a) and 144 hours (b).

A moderate correlation factor (R^2 = 0.48) between the data of UCS and UPV after 144 hours exposure is obtained while after 24 hours the correlation factor was low (R^2 = 0.16). This indicates a low relevance of UPV results for the prediction of the strength of the samples.

A good correlation (R^2 = 0.73) was found between the compressive strength and equotip hardness (Leeb) in the samples that were put in the simulation chamber for 24 hours (Fig. 4a) that improved (R^2 = 0.97) for the ones that were aged during 144 hours (Fig. 4b). Hence, the Leeb hardness number appears to be a good approximation for the UCS.

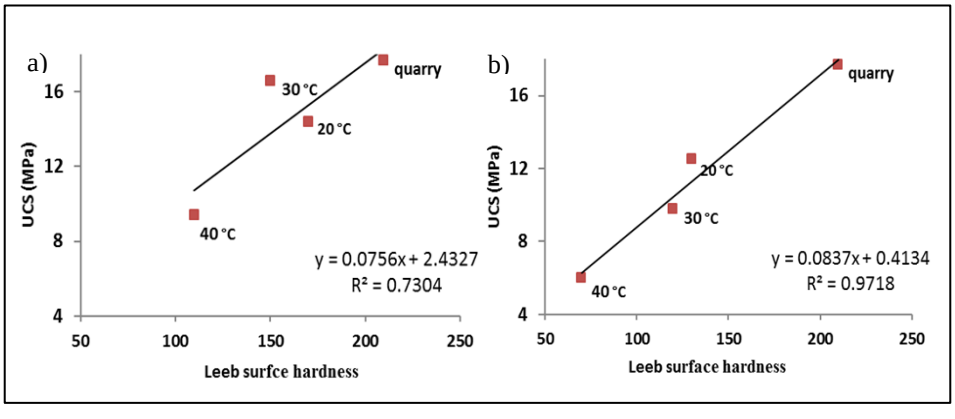

Fig. 4: Correlation between UCS and equotip hardness of the samples submitted to different temperatures for 24 hours (a) and 144 hours (b).

4. Discussion and conclusions

The mechanical properties of the tested samples were notably affected as a consequence of simulated salt weathering tests at different temperatures. The increase of P-wave velocity values after 24 hours at all tested temperatures can be explained by the salt crystallization within the pores of the limestone. Salt deposition leads to an increase of the UPV. As the simulation test progresses, there is a balance between evaporation and supply of water through the continuous flow of salt solution from below, that depends on the simulation temperature, as reported by Aly *et al.* (2015). These results in a more intense occurrence of efflorescences in the 30°C regime, while more subflorescences (and therefore salt-filled pores) are obtained in the samples tested at 20 and 40ºC. Hence, samples tested at 20 and 40ºC show a higher UPV than the ones tested at 30ºC. In any case, there is a trend towards a loss of strength at all the test temperature as confirmed with both equotip hardness (Leeb) and UCS values.

Because of the different rates of pore filling depending on the temperature at which the laboratory test is carried out, UPV is not a valid non-destructive method for the approximation of the UCS. In contrast, the values of the rebound hardness (Leeb number) are a good non-destructive alternative for UCS to determine the overall strength of samples.

The combined use of Non Destructive Testing and UCS in preliminary tests gave a good approximation to the understanding of how the of stone may be diminished by the action of salt weathering. Th preliminary testing is the first step to be able to go on to a historic building to carry our only Non Destructive Testing with a better accuracy.

Acknowledgements

This study was supported by the Mission Sector of the High Education Ministry, Egypt and the Regional Government of Madrid and the European Social Fund under the project entitled Geomateriales 2 S2013/MIT-2914. We would like to thank the Dr. V. Brotons of Department of Civil Engineering, University of Alicante where UCS tests were performed.

References

Aly, N., Hamed, A., Gomez-Heras, M., Alvarez de Buergo, M. and Soliman, F., 2015, The influence of temperature in a capillary imbibition salt weathering simulation test on Mokattam limestone, Materiales de Construccion, 65.

Aoki, H., and Matsukura, Y., 2007, A new technique for non-destructive measurement of rock-surface strength: an application of the Equotip hardness tester to weathering studies, Earth Surface Processes and Landforms, 32, 1759-1769.

Benson, P.M., Meredith, P.G., Platzman, E.S., and White, R.E., 2005, Pore fabric shape anisotropy in porous sandstones and its relation to elastic wave velocity and permeability anisotropy under hydrostatic pressure, Int J Rock Mech Min Sci , 42, 890-899.

Bourgès, A., 2006, Holistic correlation of physical and mechanical properties of selected natural stones for assessing durability and weathering in the natural environment, PhD Thesis, Fakultät für Geowissenschaften der Ludwigs-Maximilians-Universität, München.

Fitzner, B., Heinrichs, K. and La Bouchardiere, D., 2003, Limestone weathering of historical monuments in Cairo, Egypt. In: Siegesmund, S., Weiss, T. and Vollbrecht, A. (eds), Natural Stone, Weathering Phenomena, Conservation Strategies and Case Studies. Geological Society, London, Special Publications, 205, 217–239, http://doi.org/10.1144/GSL.SP.2002.205.01.17.

Gauri, K.L., and Bandyopadhyay, J.K., 1999, Carbonate Stone Chemical Behaviour, Durability and Conservation, Wiley, New York, ISBN 0471179779, 284pp.

Grinzato, E., Marinetti, S., Bison, P.G., Concas, M. and Fais, S., 2004, Comparison of ultrasonic velocity and IR thermography for the characterization of stones, Infrared Physics and Technology, 46, 63-68.

Hack, H.R., Hingira, J., and Verwaal, W., 1993, Determination of discontinuity wall strength by Equotip and ball rebound tests, Int J Rock Mech Min Sci, 30, 151–155.

Hamed, A., Aly, N., Gomez-Heras, M., and Álvarez de Buergo, M., 2015, New experimental method to study the combined effect of temperature and salt weathering. In Prikryl, R., Torok, A ., Gomez-Heras, M., Miskovsky, K. and Theodoridou, M. (eds), Sustainable Use of Traditional Geomaterials in Construction Practice. Geological Society, London, Special Publications, 416, http://doi.org/10.1144/SP416.

This page has been left intentionally blank.

COMPUTATIONAL SIMULATION: FOUR IMPORTANT STRUCTURAL ELEMENTS TO PROTECT THE BUILDINGS IN ANCIENT PERSIAN ENGINEERING

A. AmirShahkarami[1*], M. Mehdiabadi[2] and H. Ashooriha[3]

Abstract

The geological, topographic and environmental conditions of Iran impose a burden on the stability and durability of stone structures. Geotechnical engineering is perhaps the most important skill to protect the buildings. There are four key, smart structural elements, of ancient Iranian engineering, that are found in the temples and castles of Pasargad ancient city that provide structural protections against environmental stresses. The aim of this paper is to understand the physical properties of these details by using numerical simulation. The details considered here are: 1.) Slow-slip of contact surface between units for the hysteresis of energy dissipation during dynamic excitation (for seismic protection); 2.) Impermeable stone elements used as base isolation for columns and walls to protect against weathering; 3.) Curved section stone as base plate for stone columns to protect concentration of stress at the edge of column sections; 4.) Layered stone as a continuum-rigid mat foundation as a base isolation for dynamic, weathering and also differential settlement protection. ABAQUS and ANSYS software and Druger-Prager constitutive equation models are applied. First results on the computational assessment compare with visual inspections of structures in sites shows reasonable achievement (verifications).

Keywords: Pasargad and Persepolis monuments, important structural elements, earthquake response, weathering damages, settlement, stress concentration, numerical simulation

1. Introduction

The Fars region in the middle Zagros Mountains, Iran, is well-known for its famous rock monuments, such as Persepolis and Pasargad (530 BC; Fig. 1). These are collections of unique ancient stone monument engineering, registered as world heritage in 1979 and 2004. The monuments represent cultural identity and engineering abilities. Geological, topographic and environmental conditions, that are characterised by seismic, salt attack and differential settlements (also horizontal movement) are crucial influences on the structural stability of the sites.

[1] A. AmirShahkarami*
Civil Engineering Department, Amirkabir University of Technology, Tehran, Iran
Amirshah@aut.ac.ir

[2] M. Mehdiabadi
Cultural Heritage, Handicrafts and Tourism Organization Academic member, Iran

[3] H. Ashooriha
Cultural Heritage, Iran

*corresponding author

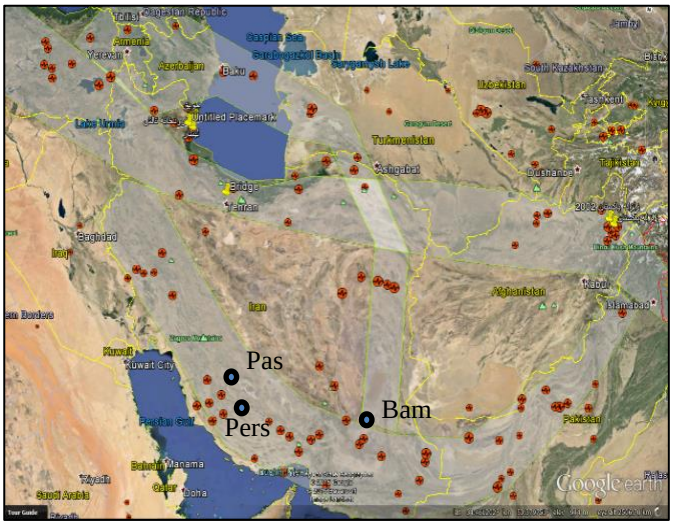

Fig. 1: Pasargad (Pas) and Persepolis (Per) are located in active seismic zone. Red dots show locations of earthquakes (Google Earth).

Weathering is complex and couples process that effect thermal (*T*), hydraulic (*H*), chemical (*C*), mechanical (m) and biological (*B*) effects on the structural properties and behaviours of monuments. Weathering and boundary condition changes effect of the structural properties and then increase the effects of earthquakes on the site buildings. The construction materials (stone, mud brick, ceramic brick and mortar) in the buildings and the natural ground materials are also affected by these environmental weathering processes. This is due to, chemical-biological as well as thermo-hydro-mechanical causes and coupled activities which affects the structural properties of materials as constitutive equations and structural behaviour of the building. From the structural point of view, the environmental conditions, composition of material (mineralogy), microstructure and stress-path (loading) are inter related to produce new states of the stresses and structural damage.

For understanding the four constructional details in this paper, it is necessary to define the following concepts and questions:

1.) What is happening to the structures we are dealing with, over time (stiffness matrix changes) as problems and solutions?
2.) What nature of impact have the loads (gravity and earthquake), are they operating as horizontal dynamic loading, boundary change effects and weathering phenomenon, effect on the structure?
3.) What are the existing stresses or the residual stresses in the present conditions ($\sigma_{t=0}$)?
4.) What stresses are the structural elements capable of carrying (bearing capacity, σ_y) at the end of construction, in the present situation and in the future (a defined time) after conservation?

The concepts of the specific constructional details are:

1.) Slow-slip of contact surface between units for the hysteresis of energy dissipation during dynamic excitation (seismic protection).
2.) The use of an impermeable stone element as base isolation for columns and walls to protect against weathering.
3.) Curved-section stone as a base plate for stone columns to protect concentration of stress in edge of column section.
4.) Layered stone as continuum rigid-mat foundation as base isolation for dynamic, weathering and also differential settlement protection.

2. Coupling systems: Damage combinations

Time and load-path dependency of K in $\Delta f = K \cdot \Delta \delta$, for deformation analysis is expressed in Figure 2. Earthquakes as well as conservation activities, introduce concentrated changes. Weathering and differential settlement also represent permanent and steady state changes. These inputs come together to produce the same effects as structural damage. Differential settlement caused by weathering or boundary condition changes, creates extra shear stress in the shear zone of a failure mechanism. Dilation occurs due to shear stresses, and therefore increases the potential damage arising from weathering phenomena. Dilation due to the stress concentration in lower part of columns deals with two causes of material properties change: a) softening and decreasing of shear resistance stress, b) smeared cracks and increasing weathering activities, e.g. salt crystallisation related decay. These problems are connected to the four stone constructional details seen at Pasargad.

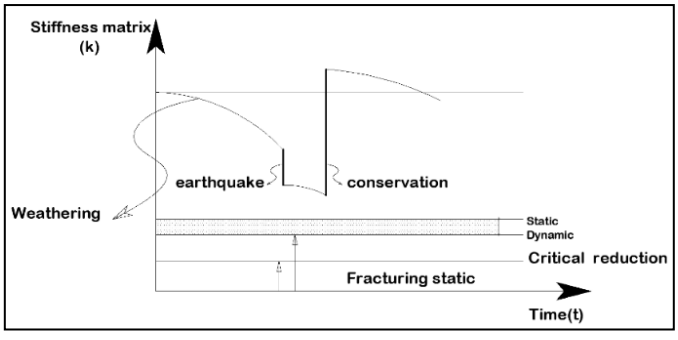

Fig. 2: Dependency of stiffness matrix (k) by time (weathering) and events/facts such as earthquake and conservation.

3. Problems and related solutions in historical structures

Earthquake, weathering and differential settlement are problems that affect the structural behaviours of historical buildings. With ageing, structures deal with three major excitations with a time dependency. These are classified with time dependency as:

1.) Dynamic causes by earthquake. $\Delta f_t = k\Delta\delta + c\dot{\delta} + M\ddot{\delta}$
2.) Transient causes by weathering $\Delta f_t = k\Delta\delta + c\dot{\delta}$
3.) Static causes as boundary changes $\Delta f_t = k\Delta\delta$

These three phases are related to each other as presented in Fig. 3:.

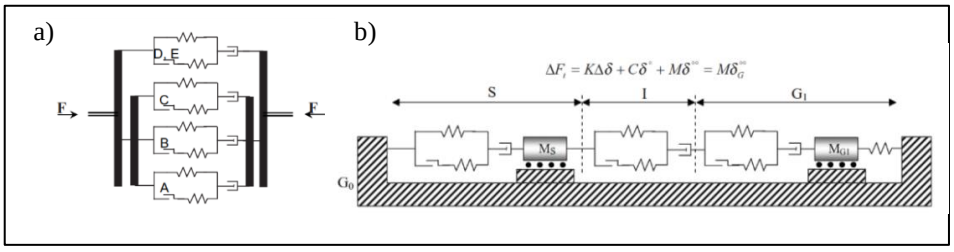

Fig. 3: Computational model, a) composite behaviour of different layers, b) soil-foundation/structure dynamic interaction.

Solutions to degradation mechanisms derived from experience and 'smart' engineering are understandable if we listen to what the structure is telling us from the structural point of view. With a sense of the continuity, ductility and unity of the structure as a whole, smart structural details were created by intelligent ancient engineers. Both Pasargad and Persepolis exhibit special and unique strategies to solve environmental problems during a long life time. These are seen in four important structural details, as engineering in three different elements of structures, for: 1.) Ground stabilization and foundations; 2.) Shear walls, piers, columns; 3.) Roof diaphragm.

4. Four important details:

4.1. Detail I: Slow-slip of contact surface between units for hysteresis of the energy of dissipation during dynamic excitation (seismic protection)

***A**: Dampers for earthquake hazard effects, by a slow-slip layer* (stone block diaphragm with no mortar in the foundation and retaining wall). The energy balance equation can be written as:

$$E_{kr} + E_d + E_a = E_{ir} \qquad \textit{(Eq. 1)}$$

Where $\boldsymbol{E_{kr}}$ is the relative kinetic energy, $\boldsymbol{E_d}$ is damping energy, $\boldsymbol{E_a}$ is the absorbed energy, and $\boldsymbol{E_{ir}}$ denotes the relative input energy. The absorbed energy could be divided between three different material responses as:

1.) Elastic energy,
2.) Plastic deformation,
3.) Frictional displacement energy between units (Fig. 4 and Fig. 5).

The first and third have no influence on material properties during the loading-unloading process, but the second one has a lasting influence on material properties. In Pasargad the details are prepared to use the third solution for energy distribution in the whole units of the structure.

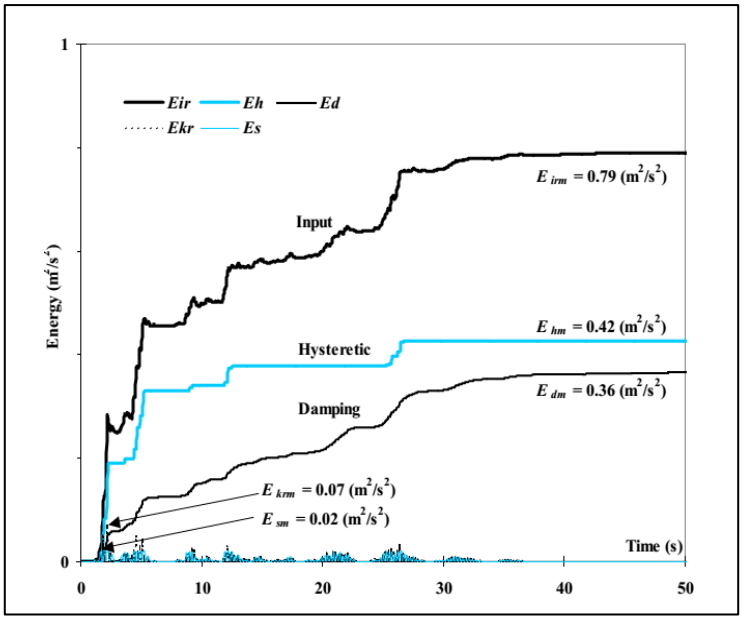

Fig. 4: Energy time-histories for bilinear SDOF structure with Tn=0.5 s, μ=3, α=0.02, and ζ=5% subjected to the S00E component of EI centro, the Imperial valley, CA earthquake of May 18,1940 (payam khashaee, Jan 2003).

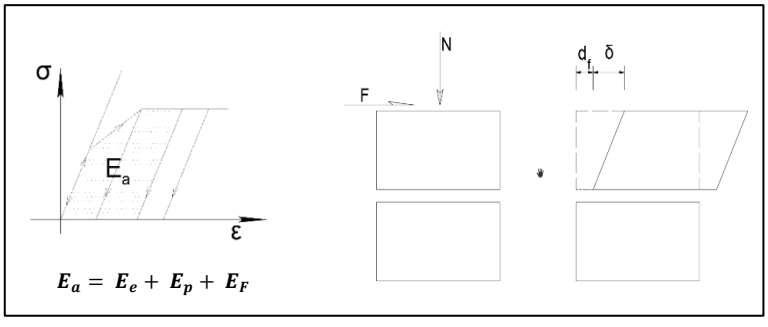

Fig. 5: Different types of energy distribution as elastio-plastic and frictional.

***B**: Columns, piers and shear walls designed for seismic responses*. Stone columns with rising damp protection are designed for only axial force. Piers and external shear walls bear both vertical and horizontal loads during earthquakes. The walls and piers are located external from the architectural and structural behaviour concepts.

Coupling system analyses considered the interaction of weathering and the stress-path which causes dilation (smeared cracks) in a shear zone, which is a geotechnical behavioural charactersitic of the materials. Numerical analyses show a good agreement with visual evidence. Continuum and ductile geotechnical structure is apparent in the ancient structures by intelligent design elements that solve the problems of weathering to provide durability

by inclusion of a ventilation channel network, the inclusion of an earthquake engineering frictional interface at the external edge of the stone blocks (with no mortar) and differential settlement overcome by a deep continuum-layered stone-mat foundation.

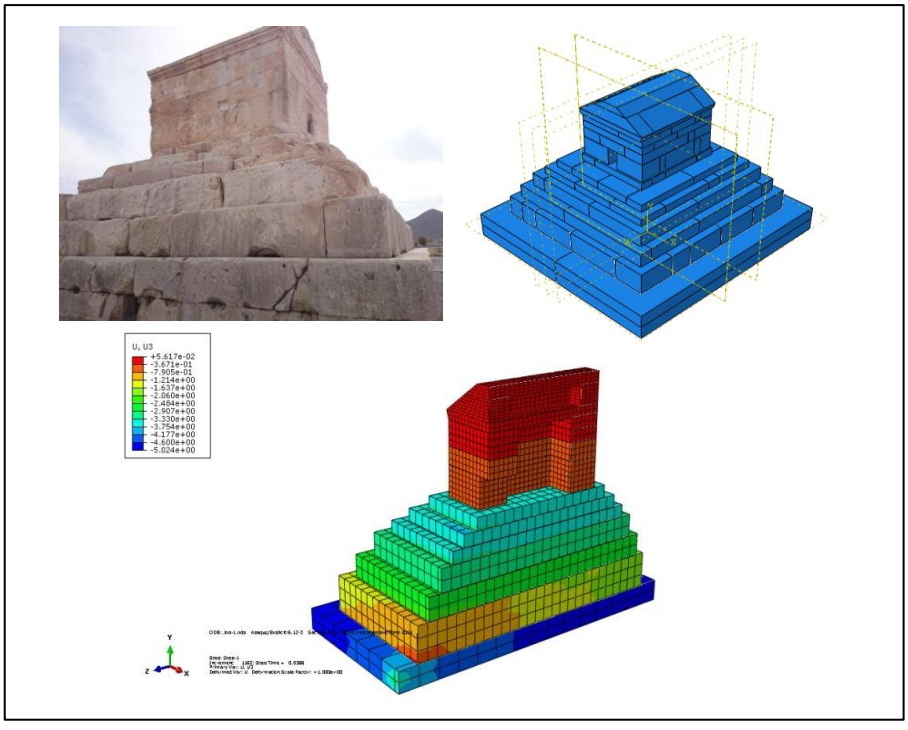

Fig. 6: a dynamic resistance able structure, Cyrus tomb with frictional interface dampers.

The ABAQUS software tool was used to simulate the Cyrus tomb with an explicit dynamic analysis which is a suitable approach for discrete rigid block structures. The above model (Fig. 6) contains 7 layers and a tomb at the top, and each part consist of blocks without any mortar. It means that the structure consists of stone-block units and structural interface joints (under compression and friction). For the representation of the material behaviour of stone we use Druger-Prager approach which can represent a reasonable behaviour of rock in ABAQUS software (Table 1).

Tab. 1: a) The Drucker-Praker (Yield surface) coefficient for stone, b) rock compression coefficient (stress-strain), material parameters.

a)

Angle of Friction	Flow Stress Ratio	Dilation Angle
30	0.8	3

b)

Yield Stress	Abs Plastic Strain
700	0
850	0.003

The BAM earthquake displacement record is used as an input in ABAQUS to assess the Cyrus tomb behaviour when the structure faced to real earthquake, Fig. 7.

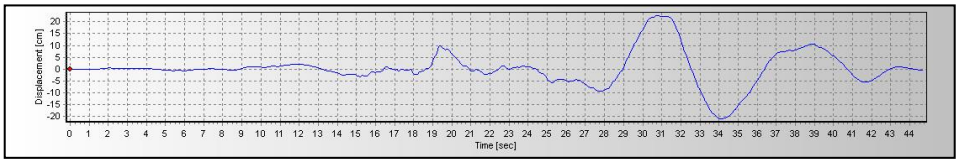

Fig. 7: BAM earthquake displacement record.

The output of the proper analyses indicates that during the earthquake, layers slow-slip on each other and dissipate the internal energy. It can be compared with the internal energy and the plastic dissipation energy in Fig. 8. Therefore, the result of simulating the Cyrus tomb indicates that intelligent engineers who designed and built these structures (Pasargad and Persepolis) may have had knowledge and foresight of the effects of seismic movements.

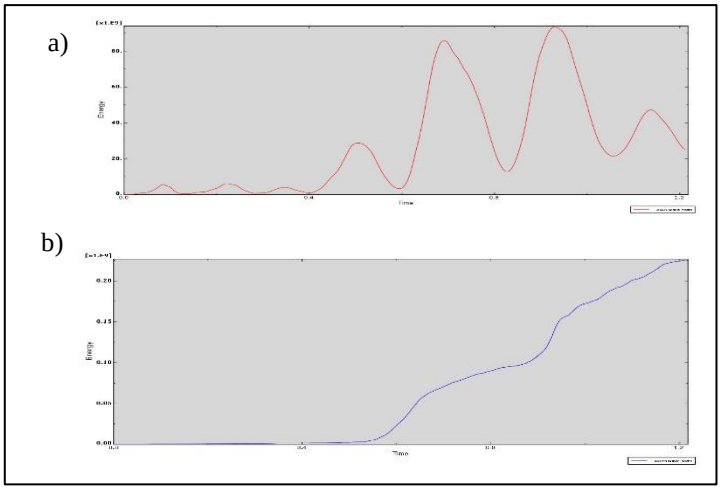

Fig. 8: a) Internal energy, b) Plastic dissipation energy.

4.2. Detail II: impermeable stone as base isolation for columns and walls to protect against weathering

Different properties and different applications for two types of stones (black and white, Fig. 9) were prepared in Pasargad and also Persepolis. The black stones are chosen as an 'isolator', they are hard to work and are not quarried any more. The white limestone, is relatively easy to work, has high permeability, is not stable to weathering. Protection against rising damp (and the weathering it causes) is achieved by the use of an impermeable, isolating black sandstone and also the use of ventilation channels between stone blocks in the finishing layer (the 3rd layer of the stone layered mat, Fig. 10).

Fig. 9: Comparison of white stone and black stone (with low permeability), showing the different the different behaviour for the height of rising damp and salinity in Pasargad monuments.

Fig. 10: Details of smart engineering at Pasargad, showing the combination of black and white stone with different physical properties.

4.3. Detail III: Curved section stone as base plate for stone columns to protect concentration of stress in edge of column section

Fig. 11: Frictional interface without any mortar (Damper), base isolation and also the curved stone base plate to prevent stress concentration.

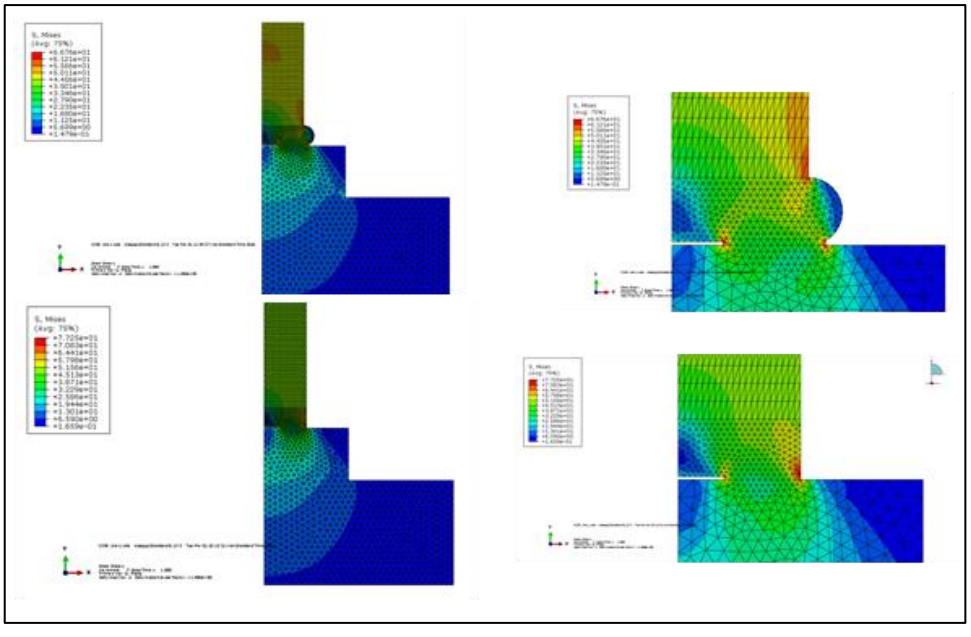

Fig. 12: Comparison of Von-Mises stress distribution with and without curved section stone base plate.

4.4. Detail IV: Layered stone as continuum rigid mat foundation as base isolation for dynamic conditions (damper and frictional energy absorption).

Weathering and also differential settlement protection are solved together with proper detail.

Fig. 13: Differential settlement protection, using more layers as a continuum layered isolator mat foundation.

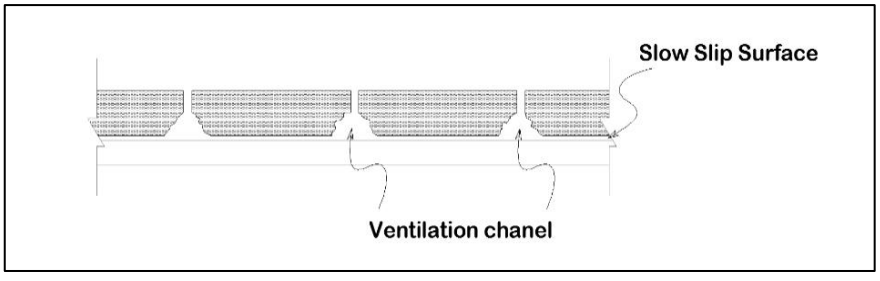

Fig.14: Slow-Slip phenomenon and Ventilation in foundation, to protect from earthquake effects and rising damp.

Bibliography

Khashaee P., Mohraz B., (2005), Distribution of Earthquake Input Energy in Structures, NISTIR 6903, United States Department of Commerce Technology Administration,

Anzani A., Binda, L., Mirabella Roberti G., (1995), A Numerical Interpretation of Long-term Behaviour of Masonry Materials under Persistent Loads", 4th STREMA, Architectural Studies, Materials & Analysis, computational Mechanics Publications.

Baronio, G., Binda , L. (1991), Experimental approach to a procedure for the investigation of historic mortars, 9th Int, Brick/Block Masonry Conf., Berlin.

Binda L., Anzani A.,Gioda G., (1991). An Analysis of the time- dependent behaviour of masonry walls.9th International Brick/Block Masonry conference, Berlin.

Karoglou, M., Krokida, A.K., Maroulis, Z.B., A power full simulator for moisture transfer in buildings, ELSEVIER, 17 October 2005.

Bucea, L., Sirivivatnanon, V.and Khatri R., Building Materials Deterioration due to Salts Attack Laboratory Experimental Program, Internal Technical report, cmIT 2005-165.

MATERIAL ANALYSIS OF TARSUS' (MERSÎN, TURKEY) TRADITIONAL BUILDINGS FOR THE DEVELOPMENT OF CONSERVATION STRATEGIES

M.C. Atikoğlu[1*], A. Tavukçuoğlu[1], B.A. Güney[1], E.N. Caner-Saltık[1], O. Doğan[1], M.K. Ardoğa[1] and M. Mayhar[1]

Abstract

The study deals with the determination of performance characteristics and compositional properties of original building materials forming the traditional stone masonry and timber-framed wall components of Tarsus' traditional houses. A preliminary study is needed for the development of conservation strategies, particularly to keep the inherent characteristics of traditional materials and buildings of the historic region. The results have shown the high breathing capability of traditional wall components which is essential for providing healthy boundary conditions for structural timber elements. The materials were found to be lime-based mortars and plasters with highly-pozzolanic additives. The main stone used is limestone. The presence of high amounts of soluble salts resulting in material deterioration at lower parts of stone masonry presented a continuous rising damp problem. The results indicate the priority strategies for the conservation of Tarsus' historical district and traditional houses. Urgent interventions are needed to eliminate the rising damp problem by establishing proper-functioning roof and surface water drainage systems. The properties of original stone and neighbouring lime based materials used in these structures should be taken into account as the specifications for repair materials. Further studies are needed to identify the natural resources of raw materials in the close vicinity of the Tarsus historical district for repair works.

Keywords: material conservation strategies, performance properties, compatibility properties, compositional properties, traditional timber-framed houses, Tarsus (Turkey) historic region

1. Introduction

Due to increasing awareness in cultural heritage issues and respect for the built heritage, conservation of traditional settlements/districts together with structures, building and material technologies become a highlighted and political concern. Development of conservation strategies requires comprehensive studies including extensive preliminary examinations to better understand the authentic architectural and technological features of historical buildings, to identify the main problems and their reasons and then to plan repair works and conservation treatments. Therefore, diagnostic and monitoring studies based on

[1] M.C. Atikoğlu*, A. Tavukçuoğlu, B.A Güney, E. Caner-Saltık, O. Doğan, M.K. Ardoğa and M. Mayhar
Middle East Technical University (METU), Ankara, Turkey
ceylinatikoglu@gmail.com

*corresponding author

performance and compatibility properties of materials have vital importance, particularly to keep the inherent characteristics of traditional materials and buildings of the historic region.

Considering that approach, a diagnostic study was conducted on timber-framed traditional dwellings in the historical district of Tarsus (Mersin) for development of conservation strategies. Those houses reflect the experience of the past on timber construction techniques and traditional building materials while now suffering from wrong repairs due to incompatible materials use and inappropriate construction detailing. The study, therefore, concerned to establish knowledge on performance and compatibility characteristics of building materials which forms the specifications for repair materials, therefore, contributes to the long-term durability of those houses.

2. Materials and methods

The building materials forming the timber-framed traditional houses in Tarsus (Mersin, Turkey) were examined in the study. Those houses are located in the multi-layered historic region of Tarsus and have survived more than a hundred years. There are mainly two types of traditional construction techniques observed in the houses (Fig. 1). Basically a masonry structure composed of cut stone and stone mortar was observed at the ground floor while a timber-framed structure composed of structural timber elements with rubble stone and mortar infill formed upper floors. The rubble stone infill between the timber structural elements has been covered with one layer of thick plaster and overall exterior surface of timber-framed walls have been plastered with two layers of lime-based coats. Samples were collected to represent the materials, such as cut stone, rubble stone infill and their mortars, exterior plasters in contact with rubble stone infill and structural timber elements, all of which forming the traditional masonry and timber-framed wall components of the houses (Fig. 1).

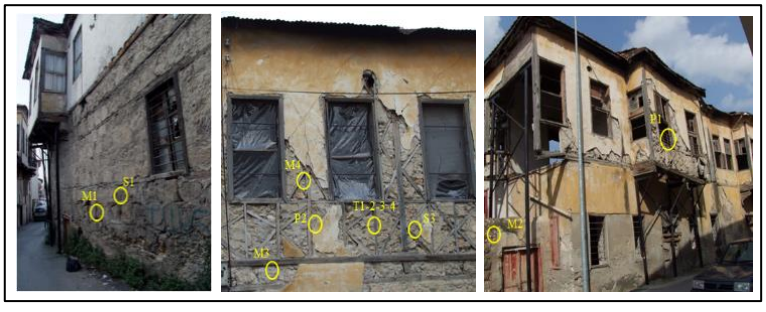

Fig. 1: Some traditional houses in Tarsus and the locations of some material samples where they were taken from.

Some basic physical properties of stone, stone mortar and plaster samples were examined in terms of bulk density, effective porosity, water absorption capacity and water vapour permeability (RILEM 1980; TS pr EN 7783-2 1999). Here, an emphasis was given to the breathing capability of the overall timber-framed wall section in terms of continuity of water vapour passage through its layers. The breathing capability of material layers was defined in terms of equivalent air thickness of water vapour permeability (SD) and water vapour diffusion factor (μ). SD values below 0.14 m indicate high water vapour permeability of a material while SD values above 1.4 m indicate low water vapour

permeability of a material. The SD values for the medium vapour permeability are defined in the range between 0.14-1.4 m (TS pr EN 7783-2 1999).

Some physicomechanical properties of stone, stone mortar, plaster and timber samples were determined in terms of ultrasonic pulse velocity (UPV) and modulus of elasticity (MoE) (ASTM Standard D 2845-08 2008; RILEM, 1980). The MoE value of the samples was calculated indirectly by using bulk density and UPV values of samples as an input in a specific equation defined in the standards (ASTM C 597 1999; RILEM, 1980). The uniaxial compressive strength (UCS) of stone, stone mortar and plaster samples was determined indirectly by measuring the point load strength of samples and using that data in relevant equations of UCS as defined in the literature (ISRM 1985; Winkler 1986).

The compositional and raw material characteristics of mortar and plaster samples were examined in terms of the binder aggregate ratio, particle size distribution, pozzolanic activity including the type and shape of aggregates. For the estimation of the binder-aggregate ratio of mortar and plaster samples, the samples were treated with 5% HCl (Hydrochloric acid with a distilled water solution) and weights of acid insoluble parts were determined, then the percentage of acid soluble and insoluble parts of the samples were calculated. Acid insoluble parts were sieved by using 4 mm, 2 mm, 1 mm, 0.500 mm, 0.250 mm and 0.125 mm diameter of sieves and the percentages of each grain size were calculated. The pozzolanic activity of the acid insoluble aggregates smaller than 0.125 mm (fine aggregates) was measured directly by measuring the amount of $Ca(OH)_2$ consumed by 1 g of aggregate. The X-Ray Diffraction (XRD) analyses were conducted on some stone, mortar and plaster samples for the identification of mineralogical compositions as well as the finest aggregates of mortar and plaster samples before and after treatment with saturated $Ca(OH)_2$ solution to investigate the possible pozzolanic reaction products. The presence of common types of soluble salts was examined by spot tests and total soluble salt content in the samples were determined as weight percentages based on electrical conductivity measurements (RILEM 1980; Black 1965).

3. Results and Discussion

The data obtained were evaluated in order to define some performance properties of materials used within the traditional wall section in terms of their basic physical and physicomechanical properties. The compatibility of the materials neighbouring each other was discussed in terms of their water vapour permeability characteristics. The compositional and raw material characteristics of mortar and plaster samples were discussed to better understand some specifications for production of repair materials. The interpretation of data on salt content gave the hints on the main sources of materials failures. The results on those topics were summarized under the respective headings.

3.1. Performance properties: Basic physical and physicomechanical properties

The bulk density, effective porosity and water absorption capacity of stone used as a cut stone block in masonry and rubble stone infill in timber-framed wall section was determined to be 2.05 g/cm^3, 26% by volume and 13% by weight, respectively. Those properties were found to be 1.62 g/cm^3, 36% by volume and 22% by weight for stone mortar used together with cut stone and infill stone, respectively, while those values were 1.57 g/cm^3, 40% by volume and 25% by weight of exterior plaster layers covering the infill and structural timber frame.

The resistances against water vapour permeation (water vapour diffusion factor – μ value) of stone and stone mortar were found to be 14.7 and 3.8, respectively. The average μ value of the exterior plaster layers and their total SD value were measured to be 7.1 and 0.11 m, respectively, while the finish coat had μ and SD values of 13.3 and 0.1 m, respectively. That data signalled that the exterior finishing system is highly breathable due to its SD value below 0.14 m. In addition, the data showed that the exterior finish coat may function as a water impermeable layer due to it μ value two times more than the sub layer while still having very high water vapour permeability with its SD value below 0.14 m. Considering the water vapour permeability characteristics of stone and stone mortar, the average μ value of the 60 cm-thick stone masonry wall and its total SD value were calculated as 9.45 and 5.67 m. Considering the water vapour permeability characteristics of infill stone, its mortar and exterior plaster layers, the 19.5 cm-thick timber-framed wall (composed of 15 cm-thick infill stone and its mortar, 3 cm-thick base plaster, 0.8 cm-thick undercoat and 0.7 cm-thick finish coat) was calculated to have average μ value of 8.4 and total SD value of 1.64 m. The results showed that the average μ values of stone masonry and timber-framed walls are similar to the μ value of timber, which is 8.0 (Akkuzugil 1997) and those results proved that healthier boundary conditions are provided for structural timber elements remained within those wall sections to keep them dry and sound. Such a breathing capability of traditional stone masonry and timber-framed walls is crucial for the long-term durability of structural timber elements.

The UPV values measured in direct transmission mode, the calculated MoE and UCS values of stone, stone mortar and the plaster sample in direct contact with the stone infill were given in Fig. 2a and Fig. 2b. The stone was found to have UPV value in the range of 1814-2696 m/s, while MoE and UCS values were found to be 6.2-13.4 GPa and 13.6-26.8 MPa, respectively. The physicomechanical strength of stone mortar and base plaster samples which were used in direct contact with the stone were found to be lower than stone with the UPV and MoE values of 1081-1783 m/s and 1.79-4.58 GPa, respectively. The UCS of the base plaster was found to be 2.9 MPa. The samples of stone and stone mortar which suffered from soluble salt content above 2% by weight, were found to have UCS of 2.9-3.0 MPa (See the salt content of the samples S1 and M1 in Tab. 1). The stone and stone mortar samples which were collected from the lower parts of the stone masonry wall, were determined to be severe-deteriorated due to their very low physicomechanical properties. The soluble salt content in many of these samples which were collected from the lower parts of the houses at street side (Tab. 1) and the presence of severe material loss in the same region signalled that the building walls suffer from continuous rising damp and salt attack problems for a certain period of time. The presence of soluble salts, mainly sulphates, nitrates and nitrites determined in the samples supported the continuous rising damp problem at street level.

In short, the infill stone mortar and exterior plasters seemed to have similar physical properties as well as a gradual decrease in their physicomechanical strength values was observed from the core to the outside of the wall section. In addition, continuity of water vapour passage seemed to be provided highly-enough through the layers of the wall section. Those features are compatibility properties that should be provided for neighbouring traditional materials contributing to the survival of historic structures long periods of time.

The UPV values of structural timber samples were found to be in the range 522 and 1845 m/s. The data showed that the parts of timber where their UPV values above 1000 m/s

were sound (Kandemir-Yucel *et al.*, 2007) and partial replacement of some structural timber elements may be needed according to their UPV values determined on site.

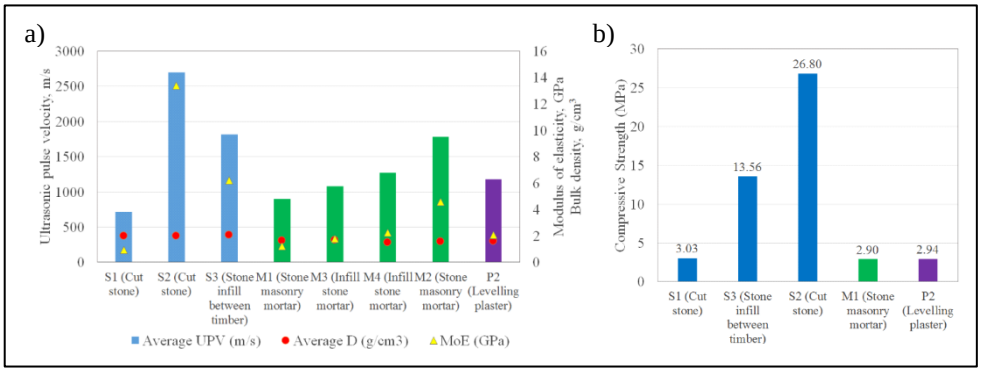

Fig. 2: a) Ultrasonic pulse velocity, modulus of elasticity and bulk density of samples; b) Compressive strength of stone, mortar and plaster samples.

Tab. 1: Contents of soluble salt in stone, stone mortar and plaster samples and salt types determined by means of conductometric analyses and soluble salt spot tests.

Name of sample	**PO_4^{2-}**	**SO_4^{2-}**	**Cl^-**	**NO_2^-**	**NO_3^-**	**CO_3^{2-}**	**Salt content %**
S1 (Cut stone)	(-)	(+)	(+)	(+)	(+)	(-)	1.99
S2 (Cut stone)	(-)	(+)	(+)	(-)	(-)	(-)	0.36
S3 (Stone infill between timber)	(-)	(-)	(+)	(-)	(+)	(-)	0.84
M1 (Stone mortar)	(-)	(+)	(+)	(+)	(+)	(-)	0.67
M2 (Stone mortar)	(-)	(-)	(+)	(-)	(+)	(-)	1.86
M3 (Stone mortar infill between timber)	(-)	(-)	(+)	(-)	(+)	(-)	0.63
P1 (Original plastet)	(-)	(-)	(-)	(+)	(-)	(-)	0.08
P2 (Levelling plaster)	(-)	(-)	(-)	(+)	(-)	(-)	0.05

4. Compositional characteristics

The data on acid soluble and insoluble percentages and particle size distribution were summarized in Fig. 3a and Fig. 3b, respectively. The binder (acid soluble part) percentage of jointing mortar used in the stone masonry was found to vary in the range of 68-71%, while that percentage is lower for the infill mortar used within the section of timber-framed wall varying in the range of 39-56% (Fig. 3b). Plaster layers in direct contact with the infill wall were found to have a binder percentage of 46-47%, which fall within the binder percentage range of the infill mortar. The results showed that the binder percentage of mortars used in the stone masonry were higher than those of mortars used in timber-framed infill wall. The mortars and plasters used in timber-framed wall section also were observed to have binder percentages in similar ranges (Fig. 3b). The higher binder percentage of stone masonry mortars can be attributed to the use of acid-soluble aggregates, such as limestone.

The particle size distribution of the aggregates (acid insoluble part) in mortar and plaster samples showed the dominance of medium and coarse grain sizes (between 0.25 mm and 1 mm) while the largest (above 1mm) and finest grain (below 0.25mm) sizes have lower percentages in acid insoluble part (Fig. 3a). The results can be summarized as follows:

- The medium and coarse sized grain percentage in the stone masonry mortar was found to be 53% on average, while that percentage for infill stone mortar and plasters used in timber-framed wall was 65% in average.
- The largest sized grain percentage was the lowest with the portion of 14% for infill stone mortar and plasters in timber-framed wall.
- The largest and finest sized grains have the lowest percentages in all of the mortar and plaster samples.

Since a certain portion of aggregates involving $CaCO_3$ might have been dissolved in acidic solution, further analyses of aggregate characteristics are needed to precisely determine the binder and aggregate ratio and particle size distribution.

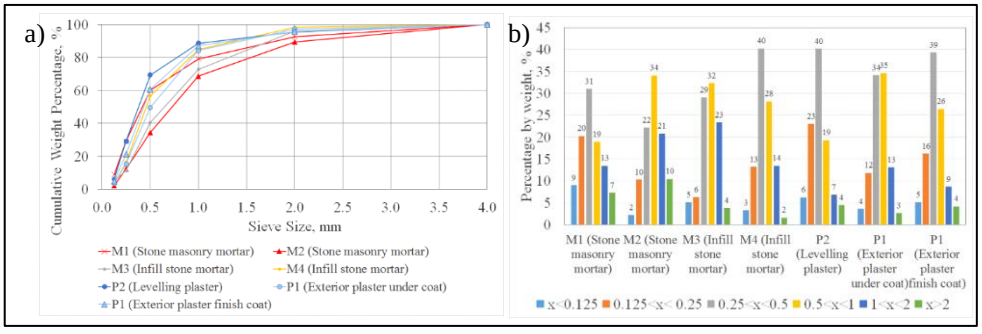

Fig. 3: a) Particle distribution according to the percentage of passed aggregate; b) Percentage of binders in different type of materials.

The mineralogical phases in the stone, stone mortar and plaster samples were examined by XRD analysis. In the XRD traces of stone, calcite was found to be the only mineralogical phase. For all mortar and plaster samples, the main mineralogical phases were found to be calcite (C) and quartz (Q) as can be seen in the XRD traces of stone masonry mortar samples of M1 and M2 (Fig. 5a and 6a). It can be concluded limestone has been used in the

stone masonry wall and lime was used as the binder in mortar and plasters. The comparison of XRD traces of the finest aggregates before and after treatment with $Ca(OH)_2$ solution (Fig. 5b and Fig. 6b) indicated that finest aggregates reacted with $Ca(OH)_2$ to form calcium silicate hydrates (C-S-H) as can be observed in the presence of C-S-H peak at around 30 2θ° (Nonat 2004) (Fig. 5c and 6c). The pozzolanic activity tests also showed the consumption of high amounts of $Ca(OH)_2$ by the finest aggregates of stone mortars and plasters and their high pozzolanicity (Fig. 4).

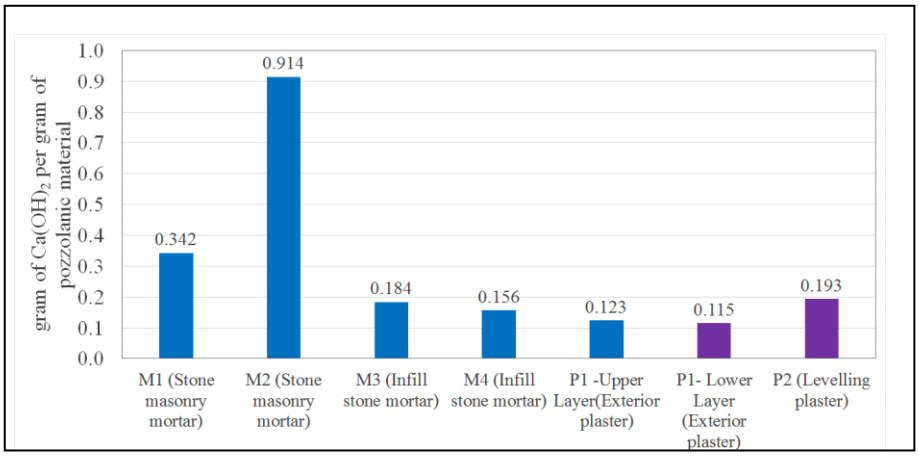

Fig. 4: Consumption of $Ca(OH)_2$ by 1g of aggregate (<0.125mm).

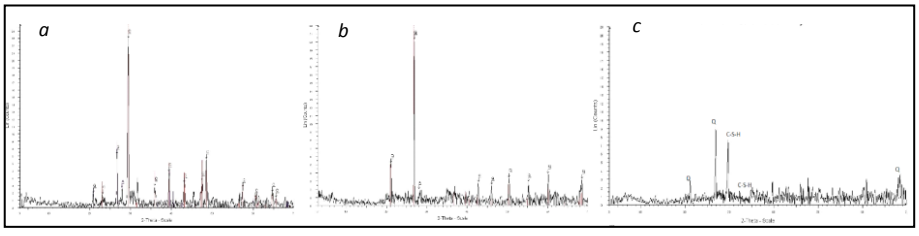

Fig. 5: XRD traces of stone mortar (M1) sample (a) and the aggregate (<0.125mm) before (b) and after treatment (c) with $Ca(OH)_2$.

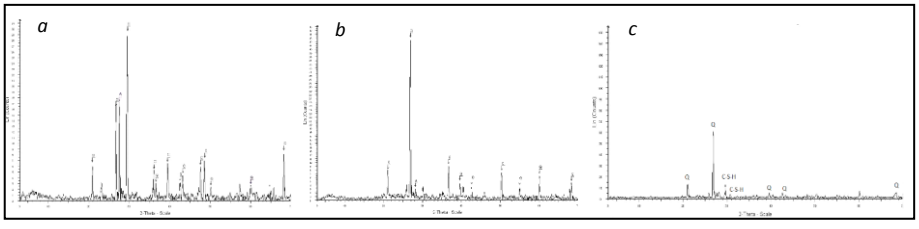

Fig. 6: XRD traces of stone mortar (M2) sample (a) and the aggregate (<0.125mm) before (b) and after treatment (c) with $Ca(OH)_2$.

5. Conclusion

The examination of the original stone, stone mortar and plaster forming the stone masonry and timber-framed wall components have shown the performance and compositional characteristics of these materials as well specifications expected from repair materials. Here, the infill stone mortar and exterior plasters seemed to have similar physical properties. A gradual decrease was also observed in their physicomechanical strength values from the core to the outside of the wall section. A continuity of high water vapour permeability was observed to be achieved through each layer of the wall section. These characteristics have vital importance for the health of structural timber elements hidden in the wall section and their survival for long periods of time. The compositional and raw material characteristics of mortar and plaster samples determined in the study should have been contributed to the long-term performance of mixed materials. These materials were found to be lime-based mortars and plasters with pozzolanic additives. The main stone used is the limestone of the region. The high pozzolanicity of the finest aggregates should have been contributed to the overall performance of wall components. The physicomechanical properties of the materials functioning more than 100 years were also determined to be still sufficient even though the lower parts of walls suffering from continuous rising damp problem for a certain period of time. These results indicated the conscious selection of raw materials in the construction of traditional houses. Further studies on the natural resources in the close vicinity of the Tarsus historical district are needed to better understand the sources of raw materials that were used in the studied buildings.

The presence of high amount of soluble salts and severely-deteriorated stone and mortar in some of the lower parts of stone masonry exhibited the continuous rising damp problem resulting in material deterioration. Properly-functioning roof and surface water drainage systems are needed to prevent further deterioration of materials.

This preliminary study has shown the priorities of a conservation strategy plan for the Tarsus historical district. Urgent interventions are needed to eliminate the rising damp problem due to improperly functioning rainwater drainage system. Comprehensive investigations are needed to examine the raw materials used in the construction of original Tarsus houses in detail, to identify their sources as well as to plan repair works.

Acknowledgement

The authors would like to thank the students of graduate course entitled ‘Laboratory Experiments in Conservation Science I’ given by the METU Material Conservation Laboratory, Department of Architecture, Middle East Technical University during 2014-2015 Spring Semester.

References

Akkuzugil, E., 1997, A Study of Historical Plasters. Ankara: METU: Unpublished MSc Thesis, Department of Architecture, METU.

ASTM D 2845, 2008: Standard Test Method for Laboratory Determination of Pulse Velocities and Ultrasonic Constants of Rock, American Society for Testing and Materials, Philadelphia.

ASTM C 597, 2009: Standard Test Method for Pulse Velocity through Concrete, American Society for Testing and Materials, Philadelphia.

Black, C.A., 1965, Methods of soil analysis. Madison, Wis., American Society of Agronomy, 1965.

ISRM Point Load Test, 1985, Suggested Method for Determining Point Load Strength, Int. J. Rock Mech. Min. Sci. & Geomech. Abstr., 22(2):51-70.

Kandemir-Yucel, A., Tavukcuoglu, A., and Caner-Saltık, E.N., 2007, In situ assessment of structural timber elements of a historic building by infrared thermography and ultrasonic velocity. Infrared Physics & Technology 49, 243-248.

Nonat, A., 2004, The structure and stoichiometry of C-S-H. Cement and Conrete Research 34, 1521-1528.

RILEM, 1980, Tentative Recommendations, Commission - 25 - PEM, Recommended Test to Measure the Deterioration of Stone and to Assess the Effectiveness of Treatment Methods. Materials and Structures, 13 No. 73, pp.173-253.

TS prEN 7783-2, 1999, Paints and varnishes-Coating Materials and Coating systems for exterior masonry-Part 2: determination and classification of water-vapor transmission rate permeability. TSE.

Winkler, E.M., 1986, Durability index of stone, Bulletin of Engineering Geologist, 23: 344.

This page has been left intentionally blank.

ARTIFICAL AGEING TECHNIQUES ON VARIOUS LITHOTYPES FOR TESTING OF STONE CONSOLIDANTS

M. Ban[1*], A.J. Baragona[2], E. Ghaffari[2], J. Weber[2] and A. Rohatsch[1]

Abstract

This paper focuses on a series of ageing tests performed in the frame of a wider study on the use of innovative consolidants for various architectural stone types. The tested lithotypes can generally be broken down into two categories: silicate (quartz sandstone with a clayey matrix) and carbonate (porous detrital limestone and marble). The predominant deterioration phenomenon of all these stones on-site is loss of grain cohesion and the formation of micro cracks. Thus, the emphasis lies on reproducing this key-deterioration effect in every lithotype. An additional effect to be studied for porous limestone is the formation of a gradient of compactness within the specimen, mimicking a crust on loose substratum. The ageing progress was evaluated by the methods of determining changes in ultrasound velocity and water absorption coefficient by capillarity. At critical stages the micro defects created are analysed by polarizing light and scanning electron microscopy on petrographic thin sections and mercury intrusion porosimetry. The methodologies for artificial ageing are as following: 1.) The samples were treated thermally by temperatures up to 600°C to induce various types of decay; 2.) All samples were additionally subjected to acid attack, freeze-thaw cycles and salt crystallization alone or in combination with thermal treatment. The approach of matching the ageing procedure for each lithotype to its predominant sensitivity and methods used to assess the effect of the ageing treatments are discussed in terms of relevance to the natural decay phenomena found in exterior environments of buildings. Thermal treatment proves to be a cost and time efficient method for assessing artificial ageing for testing of stone consolidants.

Keywords: artificial ageing, deterioration phenomena, consolidants, material testing

1. Introduction

Using sound stone to test the efficacy of consolidants in laboratory programs is likely to produce unrealistic results, due to the fact that these differ in their key properties from the weathered material. Unless a poorer quality of the same lithotype can be employed (Pápay and Török 2007, Ahmed 2015), ageing of the specimens prior to treatment is a prerequisite for such studies, though it must be kept in mind that artificial ageing will hardly result in a perfect mimic of true weathering states. While surface defects which could eventually be produced through salt or frost cycles causing, e.g. scaling or sanding, could in principle reflect true states of weathering usually associated with in-depth gradients, they don't

[1] M. Ban* and A. Rohatsch
Research Centre of Engineering Geology, Vienna University of Technology, Austria
matea.ban@tuwien.ac.at

[2] A.J. Baragona, E. Ghaffari and J. Weber
Institute of Art and Technology, Conservation Science, University of Applied Arts Vienna, Austria

*corresponding author

match the needs of modern test standards, most of which base on the assumption of properties evenly distributed over the full diameter of the test body, e.g. a cube of 5×5×5 cm³. Lubelli *et al.* (2015) designed a method where the stones were ground and sieved to a grain size approximate to that of the fresh stone with the particles then re-aggregated on top of the fresh stone by the addition of air lime. While this method seems appropriate to study prerequisites of consolidants and promises to create different decay profiles going from granular disintegration to the sound fabric, it still needs further investigation in terms of physical and mechanical characteristics. The literature reveals some possibilities of ageing different lithotypes but most of them are time consuming, costly and bear negative side effects, e.g. salt contamination (Labus and Bochen 2012). Moreover most standards for determining the resistance of building materials by applying artificial ageing techniques (e.g. EN 12371:2010) focus on describing the failure of a material rather than achieving the level of degradation necessary to study consolidation products. It is generally accepted that salt as well as ice crystallisation causes major deterioration phenomena in building materials. Even though it is certain that damage will occur with Mg- and Na-sulphate solutions, it is first likely that decay processes induced by the action of salt are limited to the surface of the test body, and second it may be very difficult to desalinate the samples to the extent that a novel consolidants can be applied in order to study its fundamental principles. On the other hand, freeze-thaw weathering often causes premature damage in certain lithotypes while others remain unaffected. Systematic observation of fabric decay by frost action is not often considered after a material collapses or shows cracks going through samples. Ruedich *et al.* (2011) describes that in most cases at least 50 cycles need to be accomplished in order to investigate clear deterioration patterns. An important decay process induced by the action of water is described within clay-containing stones, which can be damaged through the swelling and shrinkage of clay by wetting and drying cycles (Jiménez-González *et al.* 2008). Generally, the observation of these deterioration mechanisms is rather slow and can be obtained only in long-term studies. Clay minerals can be treated with different acids, with the aim of partly dissolving them. Concentrated hydrochloric-, nitric- and sulphuric acid may dissolve clay minerals but due to their reactivity they preferentially dissolve carbonate binding materials by destroying their grain boundaries and consequently causing sanding and granular disintegration. Sulphuric acid and sulphur dioxide are used to form gypsum by reproducing a gradient of compactness within the specimen mimicking a crust on loose substratum (Janvier-Badosa *et al.* 2015). However, a negative side effect of using acids to age stone is the formation of salts, which hinders the ability to study innovative consolidants. Thermal ageing is a widely studied technique for fissure formation in compact stones. In particular, various marbles but also limestones have been studied in terms of their anisotropic behaviour and main factors that influence deterioration caused by thermal stresses (Siegesmund *et al.* 2000, Andriani *et al.* 2014). Researchers Sassoni and Franzoni (2014) have systematically studied weathering levels induced by heating prior to test consolidants. However, Franzoni *et al.* (2013) summarises that the process of heating may differ between the stones significantly and thus necessitating a development of suitable heating procedures for every lithotypes. Of these, the method that shows the best performance in terms of reproducing damage as found in-situ will be applied on a large number of specimens prior to test stone consolidants.

2. Lithotypes selected and their typical deterioration phenomena

Samplings of small specimens were taken to study typical decay phenomena occurring on three cathedrals, namely the Cologne Cathedral (Germany), the Cathedral in Pisa (Italy) and the Cathedral in Vienna (Austria). The tested lithotypes were two silicate based sandstones with a clayey matrix from Cologne and two carbonate based stones, a porous detrital limestone from Vienna and a marble from Pisa. Two basic types of defects can be observed and need to be reproduced: (1) granular disintegration is a characteristic feature of clastic sedimentary and some types of volcanic rocks as well as granular metamorphic rocks like marbles; and (2) fissuring of various kinds, characteristic of compact rocks such as dense limestones, siliceous metamorphic and plutonic rocks. In addition to the described defects, shales and crusts that tend to detach from the surface can be found in all lithotypes.

The main materials from the 19th century reconstruction used for the load bearing structure of Cologne Cathedral were quartz arenites named after the towns in which they were quarried: Obernkirchen and Schlaitdorf. Obernkirchen is a fine-grained quartz dominated sandstone. It is composed mainly of quartz and few lithic siliceous fragments with sutured grain contacts between quartz grains and with a slight authigenic growth of quartz. Additional occurrence of kaolinite and dolomite can be observed. Schlaitdorf quartz arenite is a coarse grained sandstone without a visible sedimentary layering. The main components are quartz and few lithic siliceous fragments. Furthermore dolomite (coarse grained spar cement and microcrystalline binder), kaolinite and illite are present. The Carrara marble from the Apuan Alps was used for the construction of the Cathedral of Pisa. It is a more or less non-foliated low metamorphic carbonatic rock mainly consisting of calcite and traces of dolomite. The last stone which was investigated is a fine- to coarse-grained, rhodolite bearing, neogene calcareous arenite from the quarry in St. Margarethen (Austria, Burgenland). In thin sections it appears very porous and is composed mainly of small fragments of coralline red algae and foraminifera. The components are cemented with fine-grained dog-tooth calcite cement.

3. Artificial ageing techniques and evaluation methods

General aim of all ageing tests was to widen existing pore spaces, loosen grain contacts, or create micro fissures to an extent that the stone fabric could still be classified compact enough to be handed for test reasons. A wide variety of techniques were employed either individually or in combination. The predominate methods for checking the efficacy of the ageing treatments was by determining the ultrasonic pulse velocity (apparatus Labek, oscillation frequency 40 kHz) and rate of water absorption by capillarity after one hour, which was tested after each heat cycle or acid attack. Ultrasound pulse velocity was measured after every 5th cycle of wetting and drying, freeze-thaw and/or salt crystallisation. Mercury intrusion porosimetry (Porosimeter Porotec Pascal 140/440) were measured on 3 samples when the desired state of degradation was achieved in comparison to the sound material. Polished thin sections were produced from the latter stone samples, which were then examined by polarizing light microscopy and scanning electron microscopy. For every ageing method three 5×5×2.5 cm samples were investigated.

The sandstones were heated up in a muffle oven to 600°C to form a sudden volume exchange through the conversion from α to ß quartz, which occurs at ~573°C. Thermal expansion is known to form anisotropic deformation of calcite crystals, therefore temperatures from 300 to 400°C followed by "quenching" in water of 20±5°C were used

for marble. For the porous limestone higher temperatures were applied, from 400 to 600°C, to generate more stress and thus form micro cracks. The number of one-hour cycles used depended on whether the sample failed or had reached a "meta-stable" state; usually occurring between 3 and 5 cycles. The sandstones were additionally subjected to 80 wet/dry cycles (12 h water immersion by 20±5°C followed by 12 h drying at 75°C) as well as a 5% hydrochloride acid attack for partly dissolving the clayey matrix (12 h immersed and repeated 3 times). All lithotypes were aged by 25 cycles of freeze/thaw (12 h immersion in water by 20±5°C and 12 h freezing at -20°C). Another technique involved a two hour saturation of stones with a 14 % solutions of either magnesium or sodium sulphate, with a subsequent 16h drying out cycle at 75°C, which was repeated up to 25 times. With sodium sulphate, the specimens were dried at 100°C with addition of 350 ml water in the drying oven. Moreover the calcareous limestone was subjected to a 15 % sulphuric acid attack by a relative humidity of 50±5 %. The specimen was immersed edge-first into a 15 % sulphuric acid solution in order to draw the acid into its pore space till the top side is saturated. After ~24 hours of capillary absorption the side surfaces were sealed and the samples were put into water for one week so that a controlled evaporation only from the top side ensues. Nitric acid was additionally used for the limestone as it seems promising for stones with high porosity (Franzoni and Sassoni 2012). The samples were immersed in a 1.6 % solution for 24 h and afterwards washed for 3 days in an ultrasonic bath with constant change of the water. This ageing technique was repeated 3 times. A subsequent weathering effect was studied by immersing all samples into a 30 % hydrogen peroxide for the duration of 6 h and repeated 5 times. Finally the combination of heat treatment with freeze-thaw, hydrogen peroxide and acid attack was attempted, with the goal of forming susceptible damage.

4. Results and discussion

One concrete, reproducible result that could be attained quickly with thermal ageing was a reduction in ultrasound pulse velocity and an increase of water absorption capillarity, both of which correspond with a reduction in a stone sample's soundness by formation of new micro cracks and the opening of existing cracks. A general finding was that heating the stone is by far the most time efficient way for any lithotype to deteriorate and to reach a reduction of strength (Tab. 1 and Fig. 1). A suitable temperature to cause the desired effects for Carrara marble is 400°C while other lithotypes show the highest decrease in soundness at 600°C. Care in heating and cooling the samples must be taken as macro-cracking can occur, such as in the case of Obernkirchen which can crack after the first heat cycle unrelated to its original texture. Thermal conductivity of stones and resulting stresses formed through rapid or slow cooling play a crucial role in the failure of samples. The overall results of thermal treatment may vary drastically if specimens with different size and shape are subjected to the same conditions of thermal ageing.

Tab. 1: Mean values of water absorption by capillarity after 5 cycles of heat treatment

Difference	Carrara	Obernkirch.	Schlaitd.	St. Marga.	Units
Sound	0.058	2.641	3.031	10.846	$kg/(m^2h^{0.5})$
Aged	0.854	4.235	5.337	12.074	$kg/(m^2h^{0.5})$
Increase	1364.29	60.37	76.08	11.33	%

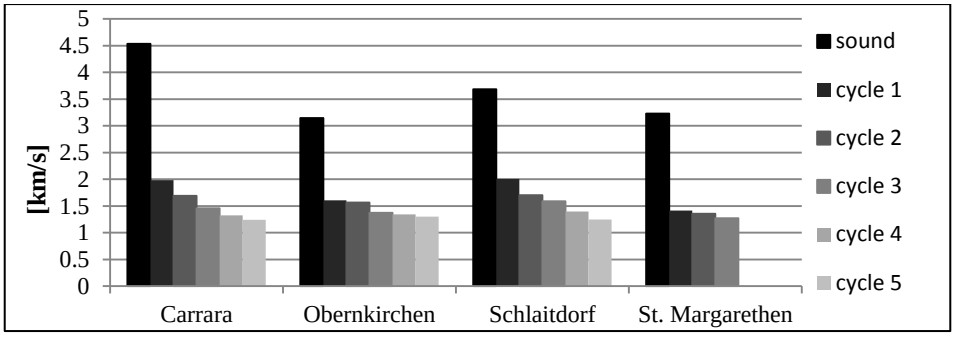

Fig. 1: Mean value of ultrasound pulse velocity after 5 cycles of heat treatment.

Following the measurement of water absorption by capillarity, the lowest increase can be seen in St. Margarethen limestone due to the high porosity of the stone that allows the calcite crystals more room for expansion without creating additional cracks. In this case, the rate of water uptake was constant after the 3rd cycle. As for the sandstones and the marble the relative increase of the capillary absorption is much higher due to the formation of inter- and intra-granular fractures, for example Obernkirchen shows an increase in water absorption after 3 cycles of approximately 25 % depending on its anisotropic orientation.

The evaluation of an aged stone's soundness by ultrasound pulse velocity shows the most significant drop after the first heat cycle but in the case of marble and the two silicates the velocity continues to decrease after additional cycles (Fig. 1). A stable state occurs after the 5th cycle. For St. Margarethen and very often also for Obernkirchen only 3 cycles are necessary to reach the lowest possible values. For the latter 3 cycles are likely to cause the failure of the sample. While some of the results may seem unrealistically low, for the testing of stone consolidants the lowest values should be taken even though in real life this condition indicates the danger of breakdown and the stones would either be replaced or put in a controlled environment (Siegesmund and Dürrast 2014). The highest possible deviation between sound and aged specimens make it possible to describe more accurately the difference of mechanical and physical properties of the stones and the performance of the consolidant.

The reasons for decay can be observed by scanning electron microscopy. The fissures created can be compared to the ones found in-situ (Fig. 2). The only difference is that the artificially induced cracks range through the whole specimens and are quite homogenous while the naturally developed occur only in exposed surfaces. While inter- and intra-granular fractures can be observed in the whole specimen, the natural decay phenomena show cracks parallel to the surface and thus contour scaling of different depths. Moreover the naturally decayed specimens show hollow spaces in a range of 10 µm up to 1 mm and the same effect can be achieved through thermal treatment. These effects are created due to the reduction of kaolin cement, some of which has been converted to meta-kaolin and re-deposited away from the grain boundaries and the formation of fissures within the silica grains (Fig. 2). On St. Margarethen calcareous arenite it is observable that the first heating results in the increase in porosity while re-heating the stone shows only minimal changes. This is due to the formation of micro-cracks that can accommodate more calcite crystals

deformation and therefore a less significant drop is observed after this cycle, a phenomenon observed also by Sassoni and Franzoni (2014). It was observed that stones with smaller crystals size tend to crack faster during thermal ageing and depending on the shape large cracks and complete failures can ensue.

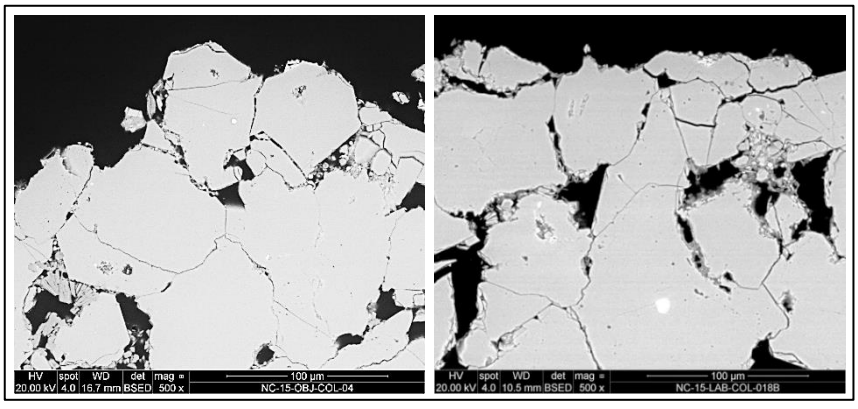

Fig. 2: Naturally (left) - compared to artificially aged (right) Obernkirchen Sandstone.

Tab. 2: Range of porometric parameters before and after thermal treatment.

	Carrara	**Obernkirchen**	**Schlaitdorf**	**St. Margarethen**
Total pore volume mm^3/g	2.79-3.90	74.77-79.79	62.26-72.96	119.02-130.90
	11.96-19.97	95.57-102.13	64.25-77.18	143.03-144.46
Total porosity Vol.%	0.76-1.05	16.66-17.29	14.65-16.11	23.65-26.17
	3.25-5.23	20.09-22.09	14.41-17.70	27.69-28.16
Average pore diameter µm	0.07-0.37	0.69-1.10	0.82-0.83	0.37-0.44
	0.53-2.38	0.59-0.67	0.25-1.09	0.42-0.54
Median pore diameter µm	0.20-3.28	6.14-6.28	20.88-29.96	48.92-49.81
	3.96-6.75	6.14-6.65	15.20-27.94	45.24-46.55

The changes in the pore structure can be determined by mercury intrusion porosimetry for all lithotypes. All lithotypes, in particular Carrara and Obernkirchen, show an apparent increase in total porosity. In the case of Carrara and Schlaitdorf this is accompanied by a shift in pore diameter, which should be investigated further through microscopy. However, the MIP results for St. Margarethen are of limited utility due to the heterogeneity of this lithotype.

The non-thermal ageing procedures gave very mixed results, which pointed to their marginal usefulness for the purposes of this study. However if the goal is the creation of surface or gradated phenomena to be evaluated by non-normative methods such as microscopy, a number of the following procedures may produce interesting results.

Hydrochloric acid was found to have the effect of reducing the soundness of sandstones when used in combination with heat-treatment due to a partial dissolution of the clayey matrix. Due to the formation of salt and the efficacy of the thermal treatment as a solely ageing method, ageing by hydrochloric acid will be omitted from future testing. In response to sodium sulphate crystallization only Obernkirchen fine-grained sandstone produced granular disintegration, sanding and flaking, which occurred as soon as after the 5th cycle. A rougher surface and light sanding could be observed on Schlaitdorf as well, while other lithotypes showed no damage that could be observed macroscopically. Magnesium sulphate showed no visible damage to any of the sample lithotypes after 25 cycles. With both sulphate solutions the evaluation methods did not show any significant difference despite the desalination. This, coupled with the difficulty of removing the salts before consolidation has led to the decision that this procedure be excluded from the future test program, but is of interest for additional research. The freeze-thaw ageing caused total failure of St. Margarethen limestone after as few as 3 cycles while other lithotypes remained sound after 25 cycles. Due to the complete failure of St. Margarethen and the different life cycles of the stones this method was aborted. Drying and wetting didn't cause any measurable changes after 80 cycles except colour changes due to the iron-containing components. While a gypsum crust was formed on the St. Margarethen limestone following partial immersion in weak acid, it was found to have a consolidating rather than degrading effect, at least in the short term. Since naturally weathered samples of all lithotypes show the formation of gypsum inside the fabric, the consolidation efficiency on a gypsum-contaminated substrate will be topic for further investigation. No significant changes could be observed with the ageing with nitric acid after 3 cycles.

Combining the above methods did not show a significant change in the degradation process. Thus even with a wide variety of treatments it was determined that thermal ageing is by far the most time efficient technique with reliably reproducible results.

5. Conclusion and Outlook

The degree of degradation is of major importance when studying stone consolidants; thus a systematic approach to age the substrate is required. Heat treatment allows a cost and time efficient reduction of soundness reflective of the degradation processes observed in-situ. Moreover the decay level can be specifically tailored and a systematic investigation of the efficacy is possible for every lithotype. Therefore the large scale production of samples on which to test consolidants will be mainly achieved through thermal treatments. Nevertheless, the results may vary drastically if specimens with different size are subjected to the same conditions of thermal ageing. Laboratory observations alone cannot always provide insight into understanding these interacting phenomena, but used in combination with numerical modelling these phenomena can be understood with greater precision, with the caveat that even these data are only roughly comparable with what occurs naturally. The influences of gypsum, salt and biological colonisation will be studied separately in advanced stage of this project. The most important conclusion of our research is that a set of standards for the artificial ageing of stone by lithotype is desirable.

Acknowledgments

This research was conducted in the framework of the European program Horizon 2020 Call NMP21-AC 646178 "Nanomaterials for conservation of European architectural heritage developed by research on characteristic lithotypes (NANO-CATHEDRAL)". The authors wish to express their gratitude towards Verena Hammerschmidt and Karin Fussenegger.

References

Ahmed, H.T., 2015, Physical and Mechanical Characteristics of Helwan Limestone: For Conservation Treatment of Ancient Egyptian Limestone Monuments, Journal of American Science, 11 (2), 136-151.

Andriani, F.G. and Germinario, L., 2014, Thermal decay of carbonate dimension stones: fabric, physical and mechanical changes, Environ. Earth Sci., 72, 2523-2539

Franzoni, E., Sassoni, E., Scherer, G.W. and Naidu S., 2013, Artificial weathering of stone by heating, Journal of Cultural heritage, 14S, 85-93.

Franzoni, E. and Sassoni, E., 2012, Comparison between different methodologies for artificial deterioration of stone aimed at consolidants testing, in proceedings of the 12th International Congress on the Deterioration and Conservation of Stone, Columbia University, New York, ICOM-CC.

Jiménez-González, I., Rodríguez-Navarro, C. and Scherer, G.W., 2008, Role of clay minerals in the physicomechanical deterioration of sandstone, J. Geophys. Res., 113, F02021, 1-17.

Janvier-Badosa. S., Beck. K., Brunetaud. X., Guirimand-Dufour, A. and Al-Mukhtar, M., 2015, Gypsum and spalling decay mechanism of tuffeau limestone, Environl. Earth Sci., 74 (3), 2209-2223.

Lubelli, B., Van Hees, R.P.J., Nijland, T.G. and Bolhuis, J., 2015, A new method for making artificially weathered stone specimens for testing of conservation treatments, Journal of Cultural heritage, 16, 698-704.

Labus, M. and Bochen, J., 2012, Sandstone degradation: an experimental study of accelerated weathering, Environ. Earth Sci., 67, 2027-2042.

Pápay, Z. and Török, Á., 2007, Evaluation of the efficiency of consolidants on Hungarian porous limestone by non-destructive test methods, Central European Geology, 50 (4), 299-312.

Ruedrich, J., Kirchner, D. and Siegesmund, S., 2011, Physical weathering of building stones induced by freeze-thaw action: a laboratory long-term study, Environ. Earth Sci., 63, 1573-1586.

Siegesmund, S., Ullemeyer, K., Weiss, T. and Tschegg, E.G., 2000, Physical weathering of marbles caused by anisotropic thermal expansion, Int. J. Earth Sci., 89, 170-182.

Sassoni, E. and Franzoni, E., 2014, Influence of porosity on artificial deterioration of marble and limestone by heating, Applied Physics A, 115, 809-816.

Siegesmund, S. and Dürrast, H., 2014, Physical and Mechanical Properties of Rock, in Stone in Architecture: Properties, Durability, Siegesmund, S. and Snethlage, R. (eds.), Springer-Verlag Berlin Heidelberg, ISBN 978-3-642-45155-3, 97-225.

APPLICATIONS OF IMAGE ANALYSIS TO MARBLE SAMPLES

R. Bellopede[1*], E. Castelletto[1], N. Marcone[1] and P. Marini[1]

Abstract

The study of natural stone decay is useful in the field of modern building, but also for the protection and recovery of artistic and architectural heritage. The presence of voids in compact rock is one of the main features that drive the processes of decay of stone materials. In particular, the pore characteristics, such as their volume, their network connectivity and their distribution inside the stone are key parameters to better study and understand the weathering of natural stone. For this reason, image analysis (jPOR for ImageJ) on thin sections cut from different portion of ten kinds of marble specimens have been performed. The results obtained show that different crystal habits and the presence of subgrains are correlated with mechanical strength and durability of the stone. Also a correlation between Total Optical Porosity (TOP) and water absorption for marbles in natural state have been found. The analysis of TOP of marble artificially and naturally weathered has given the explanation of the different variations in water absorption obtained from natural to artificial ageing. In particular it seems that the naturally decay is more aggressive that the artificial one (performed according to EN 16306: 2013). In fact, for marble with polygonal contour and no subgrains, it seems to be a different distribution of porosity on the specimens naturally aged respect those artificially aged.

Keywords: total optical porosity, decay, artificial ageing, natural ageing

1. Introduction

Bowing is one of the marble weathering phenomena that attracted much attention in the last decade and consequently many authors (Siegesmund *et al.*, 2000, Grelk *et al.* 2007, Schouenborg *et al.* 2007) and recent European Projects as MARA (2001) and TEAM (2005) focused on this issue suggesting technologic methods to evaluate the decay that, with the time, have been endorsed as standardized test methods by CEN Technical Committee (TC). There are European Standards on natural stones than recommend test methods to evaluate both the naturally deteriorated stone (EN 16515: 2015 by CEN TC 346 "Conservation of Cultural Heritage") and artificial aged ones (such as EN 16306: 2013 by CEN TC 246 "). Among the standardized test methods there are the petrographic examination, the water absorption coefficient and the open porosity, the measure of mechanical resistance and non-destructive test such as ultrasonic pulse velocity measurements. The Image analysis, at difference of these techniques, is not standardized and is therefore little known and probably of limited use for the evaluation of the stone decay. Only the authors Grove and Jerram (2011) used the image analysis for limestone to

[1] R. Bellopede*, E. Castelletto, N. Marcone and P. Marini
Politecnico di Torino - Department of Environment, Land and Infrastructure Engineering,
C.so Duca degli Abruzzi 24, 10129 Torino, Italy
rossana.bellopede@polito.it

*corresponding author

evaluate the effectiveness and accuracy of method, which was assumed to be satisfactory for that kind of porous rocks. In this work, the Image analysis is, instead, applied to different types of marbles and compared with the other conventional techniques, in order to evaluate the reliability of this method for the study of the decay of this kind of stone. Marble, in fact, is a low porous stone but it is most affected by the decay, showing an increasing in porosity often connected with the decreasing in mechanical strength (Marini and Bellopede 2009, Åkesson *et al.* 2006).

2. Materials and Methods

2.1. Petrographic characteristics of marbles

Ten kinds of marble have been studied and their main characteristics are reported as follows:

- GI - Italian marble (Fig. 1a): totally calcitic composition with polygonal and equigranular grains (size from 0.1 to 0.5 mm) and no presence of subgrains;
- CO – Italian marble (Fig. 1b): mainly calcitic composition with opaque minerals, mica and quartz in the grey veins. Seriate polygonal/interlobate grains (size from 0.07mm to 0.5mm) and presence of subgrains;
- CA – Italian marble (Fig. 1c): mainly calcitic composition with pyrite, magnetite, dolomite and quartz as accessories minerals. Seriate/interlobate grains (size <0.6mm with rare 4mm grains) and presence of subgrains;
- BU – Italian marble (Fig. 1d): mainly calcitic composition with opaque minerals, quartz and feldspar. Seriate interlobate/polygonal grains (size from 0.03mm to 0.6mm) and presence of subgrains;
- SG – Portoguese marble (Fig. 1e): totally calcitic composition with seriate polygonal/interlobate grains (size from 0.2 mm to 1.8 mm) and presence of few subgrains;
- PS – Portoguese marble (Fig. 1f): totally calcitic composition with seriate interlobate grains (size from 1.2 mm to 3 mm) and presence of subgrains;
- MK - Portoguese marble (Fig. 1g): totally calcitic composition with seriate interlobate grains (size from 0.2 mm to 2 mm) and presence of few subgrains;
- RU - Portoguese marble (Fig. 1h): mainly calcitic composition with seriate interlobate medium and polygonal fine grains (size from 0.15mm to 1mm) with presence of subgrains;
- IK - Greek marble (Fig. 1i): composition is 96% dolomitic and 4% calcitic with interlobate/polygonal and inequigranular grains (size from 0.07mm to 0.3mm) and presence of few subgrains;
- EK - Swedish marble (Fig. 1l): mainly dolomitic composition with 9% of calcite, quartz and amphibole as accessory minerals. Interlobate microstructure, allotriomorphic and sometimes lobated grains (size from 0.15mm to 1mm).

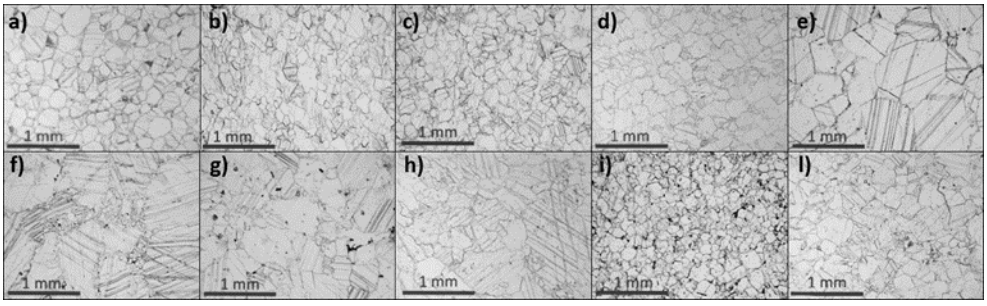

Fig. 1: Marbles studied and their mineralogical and textural characteristics.

Two slabs of the dimension 500×400×30mm of marbles CA, GI, BU, CO, RU and EK were exposed to natural ageing for about ten years - from 2003 to 2013 - on the terrace of the third floor of the Politecnico di Torino DIATI Department (Turin, Italy). Specimens of the dimension of 400×100×30mm of marbles GI, BU, IK, MK, SG and PS were subjected to artificial accelerated ageing according to the European Standard EN 16306 (2013) "Natural stone test methods - Determination of resistance of marble to thermal and moisture cycles". Meanwhile, other specimens of the same marbles were kept indoors not subjected to decay and in order to represent the original physical and mechanical properties of the materials. All the slabs subjected to thermal and moisture cycles have sawn surface finishes except PS, SG and MK.

The artificial ageing test reproduces in a laboratory the effects caused by the presence of water and temperature variations on stone. The specimens were positioned on a layer of wet sponge and soaked in water to one third of their thickness while their upper side was heated by infrared lamps. During each cycle, the temperature increased from 20°C to 80°C in four hours; it was kept constant for three hours, and then it decreased to 20°C in 18 hours. Different from the procedure described in the standard, in order to monitor the artificial decay process for three marbles, the heating-cooling cycle was repeated 60 times.

2.2. Methods

For each kind of stone naturally or artificially weathered, as well as those in natural condition, the following determinations were executed: water absorption by contact sponge (UNI 11432), water absorption at atmospheric pressure (EN 13755) , flexural strength under concentrated load (EN 12372), bowing (EN 16306 par. 8.2) and Total Optical Porosity by the Image analysis. The determination of Total Optical Porosity (TOP) has been performed using the free software IrfanView 4.40 and the macro file jPOR.txt (Grove and Jerram, 2011) for ImageJ. For each kind of the ten marbles, six thin sections soaked with epoxy resin and methylene blue have been made as illustrated in Fig. 2. In order to better analyse the increase of decay, the five thin sections obtained from the weathered marble has been cut respectively, three along the upper (P1), medium (P2) and lower (P3) sections parallel to exposed surface and two along a transversal section (the external T1 and the internal T2). The impregnation process was repeatedly performed under vacuum in order to obtain a smooth surface when viewed against light.

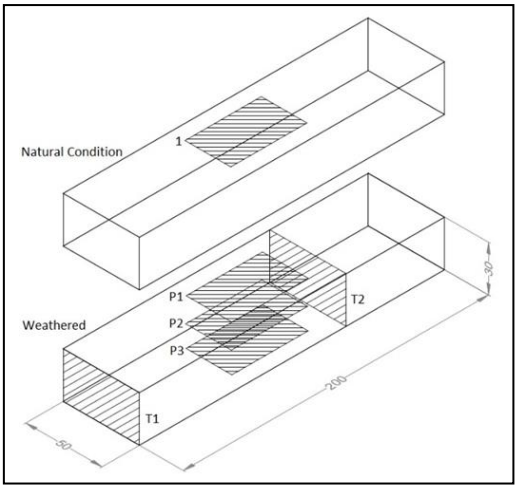

Fig. 2: Cutted areas from the specimens to obtain thin sections.

All the thin sections have been analysed using the optical macroscope LEICA MZ6 and the PANASONIC LUMIX DMC-GF6 digital camera. For each thin section, ten photos have been made uniformly spaced among its surface (Fig. 3) and then pre-processed using IrfanView. Each 24-bit image has been converted to an 8-bit palette .bmp file using the custom palette of jPOR created in order to use a colour thresholding that requires less pre-processing and removal of noise, thereby reducing inter-operator variability. The conversion creates an indexed 256 colour image which is not sorted according to hue, but instead forces the grouping of all the feature blues classes. The threshold values used to determine the porosity were left as constant as possible (lower threshold = 0 and upper threshold = 69/70) in order to find representative and comparable results between different marbles. At the end of this process, the average porosity value has been calculated and compared for each thin section.

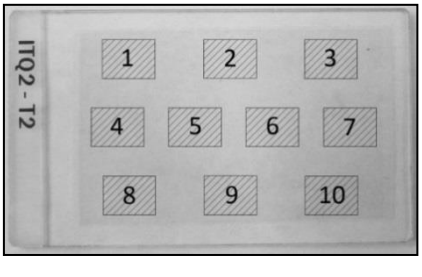

Fig. 3: Position of pictures taken from thin section for image analysis.

3. Results

In the table 1 the changes in percentage of measurements performed by means the standardized techniques on naturally aged and artificially aged specimens respect the measurements taken on specimens in natural conditions are reported. Values of bowing both after artificial ageing and after 10 years of exposition are shown in table 1, too.

Tab. 1: Change in percentage of conventional measurements recommended from the standard and bowing for the different types of marbles studied.

	AA Flex. Str.	**NA Flex. Str.**	**AA UPV**	**NA UPV**	**AA Water abs**	**NA Water abs**	**AA Sponge**	**NA Sponge**	**AA Bow**	**NA Bow**
	%	%	%	%	%	%	%	%	mm/m	mm/m
CA	-21	-4	-10	-3	168	50	78	28	0.85	0.18
GI	-40	-45	-55	-68	46	186	109	203	0.89	6.00
BU	-25	-25	-3	3	12	13	267	254	0.14	0.15
CO	-25	-26	-31	-19	28	179	73	124	0.93	0.92
EK	10	9	-	0	-	12	-	3	0.01	0.02
RU	0	-7	0	-40	0	-	23	19	0,04	0.08
SG	-19	-	-19	n.a.	12	-	-13	-	0.04	-
PS	-21	-	-8	n.a.	-6	-	0	-	0.06	-
MK	-13	-	–8	n.a.	15	-	-9	-	0.02	-
IK	12	-	-14	n.a.	-0.9	-	-	-	0.05	-

From the Tab. 1 it is possible to note how the surface finish of the slabs can affect the results of measurements of superficial water absorption by means of contact sponge: in particular the change of water absorption of PS, SG and MK are near to zero and negative because of their polished (with polishing additives) surface. For certain kind of marble such as CA and GI there is a different answer to artificial and natural ageing especially in term of bowing and water absorption measurements. In Tab. 2 and Tab. 3 the results of Image Analysis (TOP in %) by means jPOR on the marbles studied respectively after natural ageing and after artificial ageing have been reported with the related standard deviations and compared with the Total Optical Porosity in the natural condition (1). Despite the 10 different pictures from which the TOP has been evaluated, the image analysis gives very high uncertainty values. The marbles GI and BU have been studied by means of Image analysis both after natural and artificial ageing: on the base of these results in the following paragraph some conclusions can be drawn.

Tab. 2: Mean values of Total Optical Porosity for each thin section in natural state and after 10 years of natural weathering.

	NAT.CONDITION		NATURALLY AGED							
	1		P1		P2		P3		T1	
	Mean value	St. dev.	Mean value	St. dev.	Mean value	St. dev.	Mean value	St. dev.	Mean value	St. dev.
	%	%	%	%	%	%	%	%	%	%
CA	0.16	0.10	0.52	0.27	0.14	0.11	1.09	0.64	0.23	0.10
GI	0.34	0.52	16.69	6.86	0.57	0.27	7.08	2.87	12.85	5.34
BU	0.33	0.32	0.30	0.24	0.30	0.23	0.13	0.19	0.46	0.45
CO	2.72	2.35	12.97	8.83	9.49	3.54	12.30	3.35	12.33	4.33
EK	0.96	0.63	1.95	0.81	1.11	0.72	0.80	0.94	0.76	0.39
RU	0.24	0.14	2.08	0.86	1.35	0.68	2.25	0.74	2.37	1.32

Tab. 3: Mean values of Total Optical Porosity for each thin section in natural state and after 50 thermal and moisture cycles.

	NAT.CONDITION		ARTIFICIALLY AGED									
	1		P1		P2		P3		T1		T2	
	Mean value	St. dev.	Mean value	St. dev.	Mean value	St. dev.	Mean value	St. dev.	Mean value	St. dev.	Mean value	St. dev.
	%	%	%	%	%	%	%	%	%	%	%	%
GI	0.34	0.52	0.66	0.32	0.77	0.33	0.29	0.11	1.84	0.77	0.42	0.51
BU	0.33	0.32	0.02	0.02	0.11	0.08	0.42	0.18	0.08	0.05	0.13	0.07
SG	0.16	0.09	0.40	0.28	0.07	0.08	0.21	0.10	0.18	0.11	0.16	0.10
PS	0.20	0.16	0.04	0.03	0.11	0.13	0.03	0.02	0.02	0.02	0.07	0.05
MK	0.08	0.07	0.03	0.02	0.02	0.03	0.02	0.02	0.01	0.01	0.01	0.02
IK	6.29	2.50	15.50	3.94	5.89	2.08	13.02	6.05	4.57	2.00	8.13	4.44

4. Discussions and Conclusions

This research is the first application of Image Analysis method, by the script jPOR used within the program ImageJ, on methylene blue stained thin section on marble in the field of durability investigations on stone. With this technique it was possible to analyse the Total Optical Porosity of test specimens not altered and altered, and especially to compare between them the values of the thin sections obtained from the superficial part of the

specimen (P1) and those of the sections formed by the central part (P2). For example, for GI naturally aged the TOP measured in the superficial thin section is higher than the one cut in the central part of specimen: showing a high superficial decay (Tab. 2).

From the analysis of the results in Tab. 2 and Tab. 3 it is possible to note a correspondence between the values obtained by Image Analysis and the values of water absorption of the marble tested. As, shown in Fig. 4, where a correlation between Total Optical Porosity and water absorption in % for the marbles in natural state is shown, it is possible to assert that the marbles with higher values of water absorption have high values of TOP: GI is those with the highest values of TOP and WA. There is no correlation between TOP and water absorption by means contact sponge, surely because of different surface finishes of marbles that affected the results (see Tab. 1).

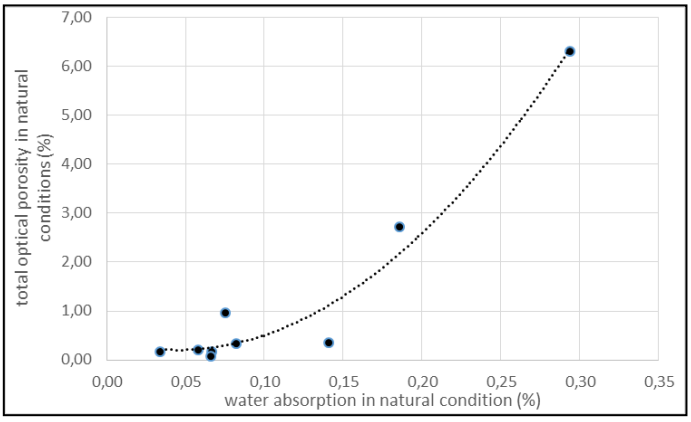

Fig. 4: jPOR porosity values vs water absorption in natural conditions.

The study of the ten marbles with the standardized techniques has shown that the thermal and moisture cycles do not given the same decay effect of the natural weathering. : From the Tab. 1 in fact the change in values of water absorption after natural and artificial ageing are different: for example the case of GI, CA and CO. To further investigate the reason of these different results, Image Analysis have been performed on marble GI and BU. These kinds of marble are characterised by different crystal habits and presence of subgrain (respectively polygonal–non subgrains and interlobate/polygonal with subgrain: Fig. 1a and Fig. 1d) that are correlated with the mechanical strength and durability of the stone. In particular GI marble, characterised by different values of water absorption (total and superficial) is characterised very different values of optical porosity by Image Analysis after natural and artificial ageing (from 0.34% to 16.69% of TOP, Fig. 5). Indeed, in the case of GI marble, it seems that the naturally decay is more aggressive that the artificial one, concerning the evolution of porosity. In fact, for GI marble it seems to be a different distribution of porosity on the specimens naturally aged respect those artificially aged. This difference is not appreciable for BU marble, where the standard deviation are of the same order of measurements of Total Optical Porosity.

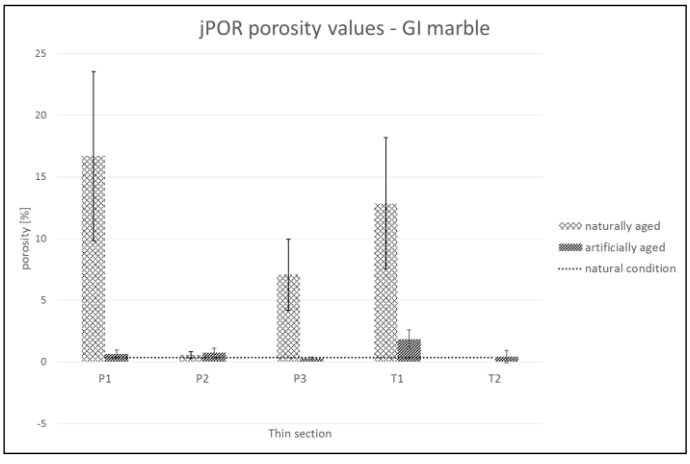

Fig. 5: jPOR porosity values in GI marble.

This new unconventional technique was used to verify if the marbles show different kind of weathering after being subjected both to natural ageing and to accelerated ageing tests. Even if the values of TOP are characterised by high uncertainty, for GI marble has been possible to detect the different answer in term of porosity distribution (Fig. 5) between artificial and natural weathering, giving an explanation to the different results obtained by means of conventional tests (with particular reference to water absorption and bowing values). .

References

Åkesson, U., Lindqvist, J.E., Schouenborg, B, Grelk, B., 2006, Relationship between microstructure and bowing properties of calcite marble claddings, Bull. Eng. Geol. Environ., Vol 65, No. 1, pp. 73-79.

Grove, C., Jerram, D.A., 2011, jPOR: An ImageJ macro to quantify total optical porosity from blue-steined sections, Computer & Geosciences", 37, 1850-1859.

EN 12372, 2007, Natural stone test methods – Determination of flexural strength under concentrated load. CEN Committee, Brussels, p 15.

EN 13755, 2008, Natural stone test methods – Determination of water absorption at atmospheric pressure. CEN Committee, Brussels, p 8.

EN 16515, 2015, Conservation of Cultural Heritage – Guidelines to characterise natural stone used in cultural heritage, 11p.

EN 16306, 2013, Natural stone test methods - Determination of resistance of marble to thermal and moisture cycles. CEN Committee, Brussels, p 18.

Grelk, B., Christiansen, C., Schouenborg, B., and Malaga, K., 2007, Durability of Marble Cladding - A Comprehensive Literature Review. Journal of ASTM International, Vol. 4, No. 4.

Marini, P., Bellopede, R., 2009, Bowing of marble slabs: evolution and correlation with mechanical decay, in "Construction and Building Materials", vol. 23, 2599-2605.

MARA EC Project, Final Report, 30.04.2001, unpublished.

Schouenborg, B., Grelk, B., and Malaga, K., 2007, Testing and Assessment of Marble and Limestone, TEAM — Important Results from a Large European Research Project on Cladding Panels. Journal of ASTM International, Vol. 4, No. 5.

Siegesmund, S., Ullemeyer, K., Weiss, T., Tschegg, E., 2000, Physical weathering of marbles caused by thermal anisotropic expansion, in "International Journal of Earth Science", vol 89: 1, 170-182.

TEAM EC Project, 2005, Testing and Assessment of Marble and Limestone – Final Technical Report TEAM-G5RD-CT-2000-00233.

UNI 11432 (2011) Cultural heritage – Natural and artificial stone – Determination of the water absorption by contact sponge.

This page has been left intentionally blank.

THE EFFECTS OF COMMERCIAL ETHYL SILICATE BASED CONSOLIDATION PRODUCTS ON LIMESTONE

T. Berto[1*], S. Godts[1] and H. De Clercq[1]

Abstract

The loss of cohesion of stone materials, mainly caused by weathering, is a common problem in the conservation of our cultural heritage. When granular disintegration occurs, a consolidation treatment with silicone compounds, specifically ethyl silicate (tetraethoxysilane, TEOS) is often chosen in order to improve cohesion between the material particles. Today there is a wide variety of TEOS-based products available on the market with different compositions and it is not at all clear which product(s) are more appropriate than others for a particular case. This paper describes the results of a laboratory research carried out at KIK-IRPA that aims to better understand the behaviour of eight different ethyl silicate products. The consolidation effect is related to three types of treatment applications, each time based on capillary absorption on two different types of limestone. The influence of product and application type is evaluated in terms of the quantity of absorbed product and amount of deposited gel (SiO_2). The consolidation effect is assessed by results of drilling resistance measurements (DRMS) and capillary water absorption. The results demonstrate that a major difference in consolidating effect can be distinguished and that there is a different influence of the product type on the final water absorption capacity. Furthermore a high amount of applied product is not always beneficial to the consolidation effect and reduces the water absorption capacity substantially.

Keywords: stone consolidation, TEOS, Tetraethoxysilane,
drilling resistance measurement (DRMS)

1. Introduction

The loss of cohesion of stone materials, mainly caused by weathering, is a common problem when dealing with the conservation of our cultural heritage. When granular disintegration occurs a consolidation treatment is often chosen in order to avoid further material loss by improving the cohesion between the material particles and thereby it's physical and mechanical proprieties. Commonly used products are silicone compounds, specifically ethyl silicate (tetraethoxysilane, TEOS). Today there are a wide variety of TEOS-based products available on the market, and it is not at all clear which products are more appropriate than others, and why. Furthermore there is no view on how much product should be applied on a weathered stone surface. Preliminary results of preceding research dealing with this subject have been described in Berto and De Clercq (2016). The present research is adapted to confirm and further the understanding of the properties of a variety of

[1] T. Berto*, S. Godts and H. De Clercq
Royal Institute for Cultural Heritage, Jubelpark 1, B-1000 Brussels, Belgium
tanaquil.berto@kikirpa.be

*corresponding author

commercially available consolidation products in terms of different application methods on two types of limestone.

2. Materials

2.1. Stones

Non-weathered Maastricht and Thénac limestones were selected for this research, both being representative for their use as building and replacement materials in Belgian monuments. Both limestones differ significantly in terms of pore structure. The Maastricht limestone has a high porosity accessible to water, 45 vol-%, and because of its greater share of macro pores it is characterised by a high sorption velocity. The Thénac limestone is also characterised by a high porosity (31 vol-%), of which 2/3 consists of micro pores explaining its much lower sorption velocity. This rather wide variety in absorption behaviour of the test materials allows for the extrapolation of the consolidation performance to the behaviours of quite a wide range of other frequently used historical stone types in Belgium and beyond. The characteristics of the stones are listed in Tab. 1.

Tab. 1: Characteristics of the stones used for the experiments.

Stone type	**$CaCO_3$**	**Density**	**Porosity accessible to water**	**Intergranular macro-porosity**	**Absorption coefficient**	**Water absorption capacity**
	wt-%	$kg \cdot m^{-3}$	vol-%	vol-%	$kg \cdot m^{-2}s^{-0.5}$	$kg \cdot m^{-3}$
Maas-tricht	98	1375	45	± 3/4	1.72	379 (2 min)
Thénac	99	1870	30,6	± 1/3	0.17	213 (60 min)

2.2. Consolidation products

Eight different commercially available ethyl silicate consolidation products are tested, specifically: KSE 100; KSE 300; KSE 300 HV; KSE 300 E; KSE 500 E; SH 75 eco (all Remmers) and Artisil SVS 75 and SVS 100 (from Rewah). Some characteristics of the products are listed in Tab. 2, including their codes used within this research. The selected TEOS-based products are generally different in terms of chemical structure of the active ingredient, dilution degree and additives.

The selection of a stone consolidant product in conservation practice is often made according to information received from the manufacturer or personal experience of a conservator, both principally based on the amount of active compound although the dry weight seems more relevant when considering the consolidating effect. In that respect, the commercial name of the product generally includes a number that refers to the content of the active compound, while to the dry weight in others, which makes a choice rather difficult for the end user who bears the final responsibility.

Tab. 2: Characteristics of the selected products.

Code	Product name	Content of active compound* (M-%)	Dry weight** (M-%)	Additive*
K100	KSE 100	20	12.9	not specified
K300	KSE 300	99	22.2	not specified
K300H	KSE 300 HV	95	26.3	coupling agent***
K300E	KSE 300 E	50	30.7	polyether
K500E	KSE 500 E	85	54.9	polyether
75eco	SH 75eco	75	44.8	not specified
S75	Artisil SVS 75	75	39.6	not specified
S100	Artisil SVS 100	100	57.0	not specified

* according to the manufacturer; **measured in laboratory; *** adhesive coupling agent specific for limestone.

3. Methods

3.1. Sample preparation, consolidation procedures and conditioning

The samples were cut into rectangular blocks of 4×5×5 cm, oven dried at 60°C for one week and coated with a poly-epoxy on four sides. A consolidation treatment is carried out on the front side of the sample with a surface area of 4×5 cm. Both stone types are treated by capillary absorption with the eight selected consolidation products, each according to the following procedures:

1. '*One Treatment*': the surface of the sample is put into contact with the product for 4 seconds at the start and again after 10 minutes. This procedure can be compared with an in situ treatment consisting of two applications of the product by means of spraying on the surface.
2. '*Two Treatments*': the treatment described in (1) is repeated after seven days. This procedure can be compared with two in situ consolidation treatments (with an interval of one week), each treatment consisting of two applications of the product by means of spraying on the surface.
3. '*Treatment of Three Hours*': the surface of the sample is put into contact with the product for 3 hours (in a closed container to avoid evaporation). This procedure can be compared with an in situ consolidation treatment consisting of repeated and extensively spraying the product on the surface. This procedure is included in this research, according to a proposal of an international test protocol as described in Ferreira Pinto and Delgado Rodrigues (2012).

Each type of treatment is duplicated, which brings the total number of specimen to 48; one set is used for the capillary absorption test while the other set for DRMS measurements. The treated samples, of which the back side is covered with aluminium foil, to avoid evaporation and unrepresentative product migration to the back of the sample, are conditioned in a climate chamber (T=20°C and RH= 65%), with the treated surface facing sideways.

3.2. Product absorption and gel deposit content

The consolidation properties are related to the amount of absorbed product as described by Ferreira Pinto and Delgado Rodrigues (2008). Before and after each consolidation treatment, the samples were weighed to determine the product uptake, expressed as $l \cdot m^{-3}$. The samples were weighed again one and three months after the last application to calculate the gel deposit content (SiO_2), expressed as $kg \cdot m^{-3}$.

3.3. Capillary water absorption

The capillary water absorption is determined according to the RILEM guidelines (1980). The capillary water absorption coefficient (A_{cap}) is derived from the slope of at least five points in the first linear part of the curve. The average A_{cap} of both non-treated stone types are determined from reference samples. The A_{cap} of the treated samples is determined one as well as three months after the last application. The drying properties have also been addressed but are not presented in this paper.

3.4. Hardness profiles (DRMS)

The effect of the consolidation treatments on the mechanical properties was assessed by drilling resistance measurements that were carried out one and three months after the last application. The drilling resistance was measured with a DRMS cordless device (SINT) with Diaber (polycrystalline diamond) drill bits. The graphical output indicates the drilling resistance in force (N) in function of the depth (mm). For each type of treatment, a minimum of four measurements were performed out of which the average curve was calculated and compared to the reference one obtained from the average of minimum two measurements on the same non-treated sample. The penetration rate and rotation speed were adapted according to the mechanical properties of the selected limestones, more precisely 80 $mm \cdot min^{-1}$ at 200 rpm for the softer Maastricht stone and 20 $mm \cdot min^{-1}$ at 300 rpm for the harder Thénac stone. Considering the data correction for the wear effect of the drill bits, as described by Delgado Rodrigues and Costa (2004), consecutive measurements on both stone types did not reveal a progressive increase of the drill resistance, therefore no modifications were required for the obtained profiles.

Due to the nature of both stone types, powder accumulated in the flutes of the drill caused a progressive increase of resistance with increasing depth of penetration (Pamplona *et al.* 2007). Since the measurement depth of the drill was set to 45 mm and the specimens have a depth of 50 mm, the accuracy of the drilling measurements was improved by carrying out similar measurements the other way round, starting from the back side. The profiles were corrected concerning the resistance increase due to the powder accumulation and graphically streamlined to improve readability.

4. Results

4.1. Product absorption and gel deposit content

The absorbed product ($l \cdot m^{-3}$) and the gel deposit content ($kg \cdot m^{-3}$) for each treatment method are shown in Tab. 3. The product uptake is characterised by greater variations in the two treatments for the Maastricht stone while for the Thénac stone this is the case for the treatment lasting 3 hours. The Maastricht limestone specimens treated for 3 hours are saturated, resulting in quite homogeneous product uptake values. Regardless of the number of treatments, both stone types show lower product absorption when treated with K500E

and S100 which is probably due to the higher viscosity of these products. The highest product absorption is achieved with K300.

The samples treated with products containing 75% active compound, that is, 75eco and S75, show an average of 24% higher product absorption compared to the samples treated with S100, excluding the 3h treatment on the Maastricht stone. All three products have on average almost the same gel deposit content (amorphous silica gel, SiO_2). The product which procures the highest gel deposit is K300H and S100 for the Maastricht and K300 for the Thénac limestone, after a 3 hour treatment.

Tab. 3: Product uptake ($l \cdot m^{-3}$) for the Maastricht (M) and the Thénac (T) according to the treatment procedures (1, 2 and 3) and gel deposit content (SiO_2) ($kg \cdot m^{-3}$).

	K100	***K300***	***K300H***	***K300E***	***K500E***	***75eco***	***S75***	***S100***
	Product uptake ($l \cdot m^{-3}$) / gel deposit content ($(kg \cdot m^{-3})$.)							
M1	131/10	127/27	114/35	108/24	89/36	112/36	114/35	84/39
M2	244/19	259/52	263/83	223/49	164/64	227/72	225/69	132/74
M3	394/34	423/92	384/124	394/85	398/163	403/126	361/114	393/202
T1	11/1	12/3	10/3	10/3	7/4	12/4	9/4	9/5
T2	22/2	28/7	17/5	19/5	15/7	17/6	19/6	16/7
T3	224/17	257/82	208/69	159/35	110/45	166/54	187/59	125/60

4.2. Capillary water absorption

The water absorption coefficient (A_{cap}) for the untreated Maastricht stone is 1.72 $kg \cdot m^{-2}s^{-0.5}$, the first linear slope reaches capillary saturation after approximately 2 minutes. The A_{cap} of the untreated Thénac stone is a tenth of that of the Maastricht limestone, 0.17 $kg \cdot m^{-2}s^{-0.5}$, and the first linear slope reaches capillary saturation after approximately 60 minutes. For the evaluation of the water absorption of treated samples, the A_{cap} was determined by considering the same time intervals of 2 and 60 min for respectively the Maastricht and Thénac stone. The results in Tab. 4 present the reduction of the A_{cap} in % compared to the reference (100%).

After three months the A_{cap} was reduced by 85% on average for both stone types treated according to the '3 hour treatment'. Low reductions of the A_{cap} were obtained for the Maastricht stone samples, 1 month and 3 months after one and two treatments with K300E, K500E and 75eco, with a maximum reduction of 25%. For the Thénac stone treated with the same products the results after 3 months are also relatively low with a maximum reduction of 28%, while after 1 month a much higher reduction with an average of 69% is measured. In contrast, the products K100, K300, S75 and S100 induce extreme reductions of the capillary absorption coefficient on both stone types, even after three months, with an average of 91%. The product K300H results in a reduction which ranks in between these two groups, where the A_{cap} after one treatment is reasonable for a non-water repellent product with maximum 19% after three months.

Tab. 4: Reduction of the Acap in % compared to the reference after 1 and 3 month.*

	K100	***K300***	***K300H***	***K300E***	***K500E***	***75eco***	***S75***	***S100***
	Reduction of the Acap in % of the reference after 1 / 3 month(s)							
M1	97/93	98/93	59/08	15/00	18/01	00/01	100/99	100/76
M2	100/95	96/86	69/34	07/04	25/08	09/13	100/96	100/88
M3	100/100	99/80	98/95	40/47	95/73	62/63	99/99	99/95
T1	99/99	99/u/**	24/19	89/00	91/15	95/03	88/51	99/98
T2	99/96	100/100	32/43	51/00	87/01	79/28	99/98	99/99
T3	100/**	100/99	98/93	86/86	72/68	90/80	94/95	98/99

* maximum standard deviation 11%
** unknown due to procedure fault.

4.3. DRMS measurements

The results of DRMS measurements performed one and three months after application did not reveal significant differences. All treatments, except for 'one treatment' with K300H for which the effect and thus de penetration capacity is limited to 30 mm depth, performed on the Maastricht limestone show a consolidation effect over the entire measurement depth (45 mm). The strengthening effect after one and two treatments of the Thénac samples is limited to a maximum depth of 10 mm and can be explained by significant lower absorption properties. Three different resistance profiles are distinguished. Each product results in one of the three following resistance profile types and is generally similar for both stone types:

1) A horizontal curve, which shows a consistent effect in the treated zone, for example, the products 75eco, S75 and S100 in the Maastricht stone after all 3 treatment methods (Figures 1, 2 and 3). 75eco shows a higher strengthening effect after all three treatment methods when compared to S75 and S100, while the highest effect is obtained with 75eco in the Maastricht stone after two treatments (Fig. 2).
2) A high strengthening effect at the surface that gradually decreases in depth of the treated matter, for example, in the Maastricht stone after 2 treatments for the products K300H and K300E (Fig. 2).
3) A pronounced high strengthening of the surface layer of a few mm followed by a rather sudden and much lower effect in the depth, for example, in both stone types after all treatments with the products K300 and K100 (Fig. 1, 2 and 3). The products K300 and K300E, both having a low dry weight, are most likely composed of low molecular weight compounds that tend to migrate back to the surface, a phenomenon known as back migration. The product K100, most probably composed of predominantly oligomers, also shows features concerning back migration, stimulated by the high solvent content (80%). The Thénac samples treated with K300E and K300H for three hours show a similar type of profile while in the case they are applied on the Maastricht limestone, a high force at the

surface which gradually decreases with depth is measured. The product KSE 300 HV (or K300H) in which the HV stands for "Hechtung Verbesserung" or bond improvement is considered to increase adhesion with calcite. The "E" in the product name KSE 300 E (or K300E) aims to increase the elasticity due to the addition of polyether (Snethlage and Sterflinger, 2011).

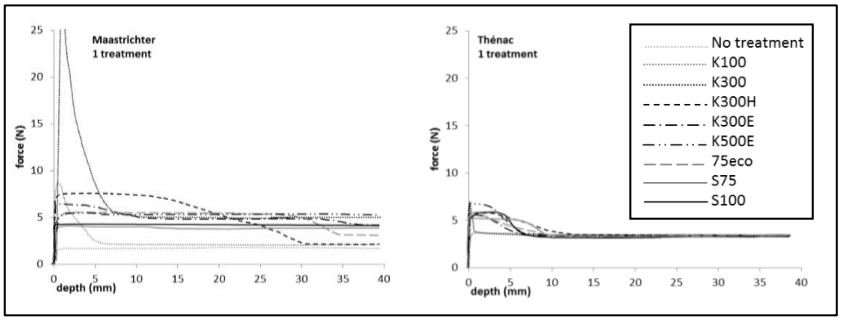

Fig. 1: Hardness profiles obtained by DRMS after 'one treatment' for each of the 8 different products (Maastricht (left) and Thénac (right)).

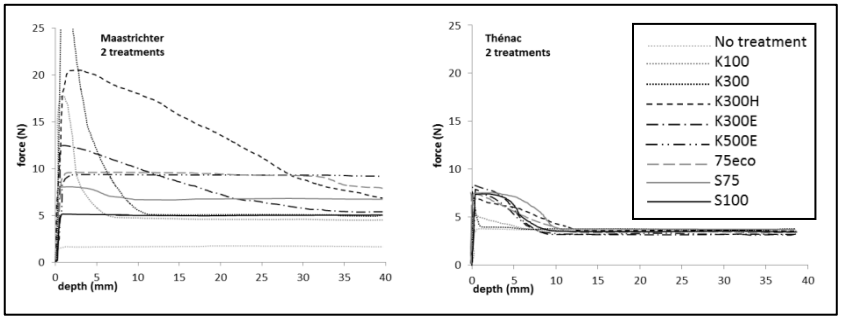

Fig. 2: Hardness profiles obtained by DRMS after 'two treatments' for each of the 8 different products (Maastricht (left) and Thénac (right)).

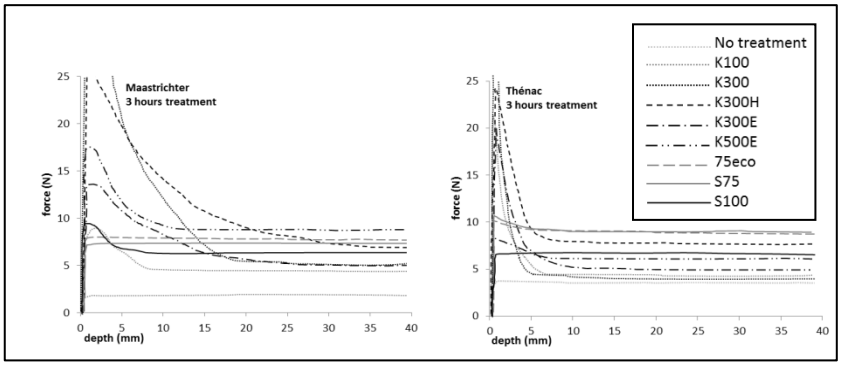

Fig. 3: Hardness profiles obtained by DRMS after '3 hours treatment' for each of the 8 different products (Maastricht (left) and Thénac (right)).

5. Conclusions

The measurements performed one and three months after the product application did not show significant differences in the resistance profiles, while the water absorption tests have shown a substantial change in the absorption capacity between one and three months for primarily the Thénac stone treated with the products K300E, K500E and 75eco.

The results of the research have shown that a long treatment such as the one of 3 hours results in higher amounts of absorbed product which is apparently not always related to a better degree of consolidation. Moreover it generally causes a disproportionate high strengthening effect at the surface. Since this effect stimulates pore filling, a significant reduction of the water absorption capacity is measured, continued up to a minimum of three months after the treatment. It is therefore clear that excessive product application is not recommended. Two products show the same noticeable strengthening effect also after 'one treatment' and 'two treatments'. It regards K100 for which this phenomenon is stimulated by the high solvent content in the product and K300 of which the potential cause lies in the active ingredient consisting mainly of low molecular weight compounds. A negative effect on the water absorption capacity, in the form of a high reduction, is also in these cases shown.

Over all the obtained hardness profiles from especially the Maastricht samples demonstrate that 'one treatment' and 'two treatments' result in an adequate increase in terms of strengthening degree. The products 75eco, S75 and S100 result in more favourable resistance profiles, that is, homogeneous curves with a rather constant increased hardness in the depth of the treated matter. However, a negative effect is measured for S75 and S100 concerning the water absorption capacity, while 75eco did not influence the absorption capacity one month after application on the Maastricht and three months after application on Thénac stone. Further favourable consolidating effects are noticed in the hardness profiles characterised by a high strengthening effect at the surface that gradually decreases in depth of the treated zone. This effect is obtained for both stone types after two treatments with K300E and K300H, the latter causing a decrease in the absorption coefficient by at least one-third. Both types of resistance profiles (homogeneous and decreasing) are favourable for porous stone types since a consolidation treatment with ethyl silicate is generally used for granular disintegration which take place in the first few centimetres of the material and not just at the surface.

The investigated products have shown a favourable consolidating effect, in terms of strengthening properties and a negligible influence on water absorption capacity, after three months are 75eco, K300E, K500E. In addition, for the Maastricht stone these products show a minimal influence on water absorption capacity after one month.

The results demonstrate significant differences amongst the variety of products, which can aid the decision-making process for the selection for practical use. Further research is required concerning these products on a wider range of samples and materials to verify the experimental effects described in this paper.

References

Berto T. and De Clercq H., 2016, Verstevigend effect van diverse commerciële ethylsilicaatproducten aangewend op kalksteen volgens drie verschillende behandelingsmethodes, Handboek Onderhoud Renovatie Restauratie, Kluwer, III, Afl. 64, 115-140.

Delgado Rodrigues J. and Costa D., 2004 A new method for data correction in drilling resistance. Tests for the effect of drill bit wear, Int. J. Restoration of Buildings and Monuments, Vol. 10, 1-18.

Ferreira Pinto A. P. and Delgado Rodriguez J., 2008, Stone consolidation: The role of treatment procedures, Journal of Cultural Heritage, Vol. 9, 38-53.

Ferreira Pinto A. P. and Delgado Rodriguez J., 2012, Consolidation of carbonate stones: influence of treatment procedures on the strengthening action of consolidants. Journal of Cultural Heritage, 13, 154-166.

Pamplona M., et al, 2007, Drilling resistance overview and outlook. Zeitschrift der Deutschen Gesellschaft für Geowissenschaften. Band 158 (3) 665-676.

RILEM TC 25-PEM, 1980, Recommended tests to measure the deterioration of stone and to assess the effectiveness of treatment methods. Materials and Structures 13(75), 175-253.

Snethlage R. and Sterflinger K., 2011, Consolidation of stone. Stone in Architecture: properties durability 4th edition, 473.

This page has been left intentionally blank.

FIELD EXPOSURE TESTS TO EVALUATE THE EFFICIENCY OF NANO-STRUCTURED CONSOLIDANTS ON CARRARA MARBLE

A. Bonazza[1], G. Vidorni[1*], I. Natali[1], C. Giosuè[2], F. Tittarelli[2] and C. Sabbioni[1]

Abstract

In the context of a changing environment, the preservation of outdoor built heritage is increasingly threatened. Furthermore the application of conservation products does not always achieve the expected results. Furthermore, preliminary tests aimed at evaluating the performance of new products often show them to be inappropriate. In such situations, the paper reports the outcomes of an innovative methodology adopted to assess the efficiency and durability of nano-based consolidating products utilized for the conservation of carbonate artworks, carrying out field exposure tests on Carrara Marble model samples in different sites. Surface properties, superficial cohesion, distribution and penetration of the conservation products and their interactions with substrates and environmental conditions were examined and compared with the features of undamaged samples and of artificially damaged samples.

Keywords: Carrara marble, field exposure tests, consolidating treatment, metal alkoxide, nano-based materials

1. Introduction

The intensification of climate changes in the last century is seriously affecting the conservation of outdoor built heritage (Sabbioni *et al.*, 2012). In particular, available projections have evidenced that temperate Europe will likely undergo an increase in loss of cohesion of carbonate stones (widely encountered in archaeological and historic built heritage) because of higher impact of (i) surface recession, (ii) thermal stress and (iii) salts crystallization (Grossi *et al.*, 2008, 2011; Bonazza *et al.*, 2009a, 2009b). Several consolidating as well as protective agents, both organic and inorganic, have been widely employed since the 20th century in order to reduce the impact of the environment on original substrates but unfortunately their performance and long-term efficiency often proved to be questionable (Amoroso, 2002; Favaro *et al.*, 2006, 2007; Doehne and Price, 2010; Giorgi *et al.*, 2000). The recent introduction of nanomaterials as consolidating agents for carbonate materials seems positively contributing to the conservation of cultural heritage (Giorgi *et al.*, 2000; Chelazzi *et al.*, 2013; Natali *et al.*, 2014) but further developments of appropriate preliminary tests aimed at evaluating the durability in real conditions of new products are necessary as pollutants and weathering factors may act on the new product as well as on the historic substrates.

[1] A. Bonazza, G. Vidorni* , I. Natali and C. Sabbioni
CNR-ISAC, Italy
g.vidorni@isac.cnr.it

[2] C. Giosuè and F. Tittarelli
SIMAU-UNIVPM, Italy

*corresponding author

This paper reports the results of an innovative methodological approach adopted to evaluate the efficiency, compatibility and durability of nano-based consolidating agents used for the conservation of cultural heritage, performing field exposure tests on Carrara Marble model samples exposed to different environmental conditions.

2. Materials and methods

The consolidating products trialled in this work are nano-based precursors for the deposition of calcium carbonate: calcium tetrahydrofurfuryloxide ($Ca(OTHF)_2$), hereafter indicated as NANOMATCH1, and CaLoSiL® (IBZ-Salzchemie GmbH & Co.KG) (Natali *et al.*, 2015). NANOMATCH1 is a nano-solution of calcium alkoxide in 1:1 ethanol:ligroin at 20 g/L of calcium, synthesized by EU NANOMATCH Project aimed at developing a family of innovative materials for the consolidation of historical substrates (Bernardi *et al.*, 2012; Favaro *et al.*, 2014). The performance of the new consolidating product is here compared with that of CaLoSiL®, nano-particles of calcium hydroxide dispersed in ethanol at 20 g/L of calcium, which is already widely employed for stone consolidation.

The efficiency and durability of NANOMATCH1 and CaLoSiL® were tested on quarried plaques of Carrara Marble (dimensions 10×10×5cm). Polished marble samples were exposed for eleven months outdoor to the direct action of rainwater on stainless metallic racks, perforated and tilted to allow the drainage of water (Natali *et al.*, 2015). Four European sites characterised by different environmental condition were selected to host the exposure of samples: Santa Croce Basilica in Florence (Italy), Cologne Cathedral (Germany), Oviedo Cathedral (Spain) and Stavropoleos Monastery in Bucharest (Romania). Some samples were previously artificially aged by thermal stress (600°C for 1 hour) in order to get the same compactness of exposed real samples since calcite crystals deform anisotropically upon heating (Bonazza *et al.*, 2009b; Sassoni and Franzoni, 2014; Andriani and Germinario, 2014). Field trials compare the performance of Carrara Marble samples (i) undamaged, (ii) artificially damaged by thermal stress, (iii) damaged and treated by brush with NANOMATCH1 and (iv) damaged and treated by brush with CaLoSiL®.

In order to evaluate and compare the features of different samples and to understand the possible influence of various environmental conditions, samples underwent the following analyses before treatment, after treatment/before exposure and after eleven months of exposure:

- Optical microscopy (OM) using a petrographic microscope Olympus BX 51 on thin and polished cross sections to analyse the microscopic features of marble samples before and after exposure and to verify the presence and the extent and condition of the tested consolidants;
- Scanning Electron Microscopy coupled with Energy Dispersive X-ray Spectroscopy (SEM/EDS) utilizing a ZEISS 1530 instrument on bulk samples and polished cross sections to better understand the microscopic features of samples and treatments;
- Colorimetric Analyses performed with a portable spectrophotometer Konica Minolta cm-700d/600d and according to the CIELAB system and the norm ISO 7724-1:1984 for quantitative colour evaluation of samples;
- Capillary Water Absorption (CWA) test in agreement with the Italian standard UNI EN 15801:2009;

- Scotch Tape Test (STT), following the procedure published by Drdácký *et al.* (2012) for the quantitative assessment of the cohesion of samples surface.

3. Results and discussion

OM and SEM analyses clearly show a reduction in cohesion of marble samples as consequence of thermal expansion. NANOMATCH1 is detectable as a microcrystalline layer rather homogeneously distributed on samples surface, with a thickness of about 20-30 µm, which increases in the hollowed areas of the surface (Fig. 1).

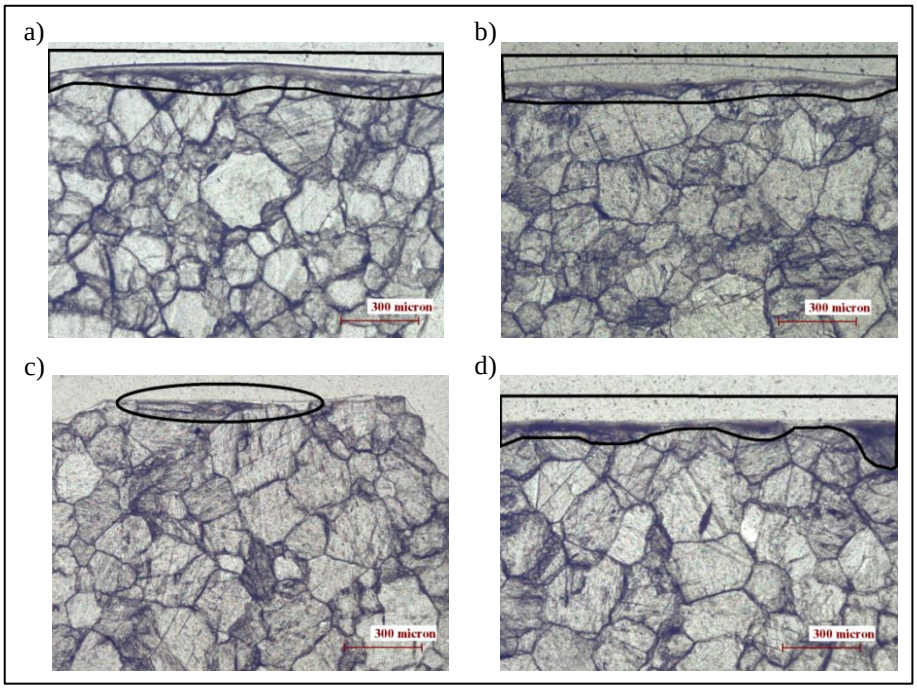

Fig. 1: Optical Micrographs (plane-polarized light) of sample treated with: a) NANOMATCH1 before exposure; b) CaLoSiL® before exposure; c)NANOMATCH1after the exposure in Florence; d) CaLoSiL® after exposure in Cologne. Black lines highlight the presence of the consolidating products.

Moreover, SEM results display that the new consolidating product has a cracked surface probably caused by too rapid evaporation of solvent, or improper environmental conditions under which the reaction happened. By contrast, the consolidation with CaLoSiL® leads to the formation of a more compact layer on the surface of all samples, distinguished by higher thickness values (Fig. 1). Anyway, both treatments remain mainly on surface or occasionally in the first micrometres of superficial chinks, as observable under OM and SEM. OM and SEM analyses carried out after exposure highlight a general increase in cracks and a loss of material on surface of all kinds of samples. It can be argued that the exposure to weather conditions and atmospheric pollutants may have weakened the stone substrate and solubilised the calcite by acid rain impact (Camuffo, 2013). In support of the hypothesis of chemical decay by precipitation, Fig. 2 shows the presence of rough and

pitted surface on treated samples. Additionally, the appearance of turbid, brownish portions in some cracks near the sample surface (observable by OM) may suggest the incomplete washout of the solubilised material and its partial penetration and re-precipitation inside chinks as microcrystals or in amorphous form. Results also show that the distribution and durability of the applied products after exposure were influenced by the kind of treatment and environmental conditions of each exposure site. In effect, NANOMATCH1 is present only in traces in all four European sites while generally the detectable amount of CaLoSiL® is higher. Furthermore the conservation products were more heavily detached and damaged in Florence and Oviedo than in Cologne and Bucharest: although the city of Florence and Oviedo are characterised by different climatic conditions, it was observed that both were affected by heavy rain events during the eleven months of exposure (Natali *et al.*, 2015). Therefore the mechanical erosion of intense rain may have enhanced the normal solubilisation of the applied consolidating products due to karst effect and acid rain. Nevertheless, where present, NANOMATCH1 and CaLoSiL® seem to be effective in preserving the stone substrate.

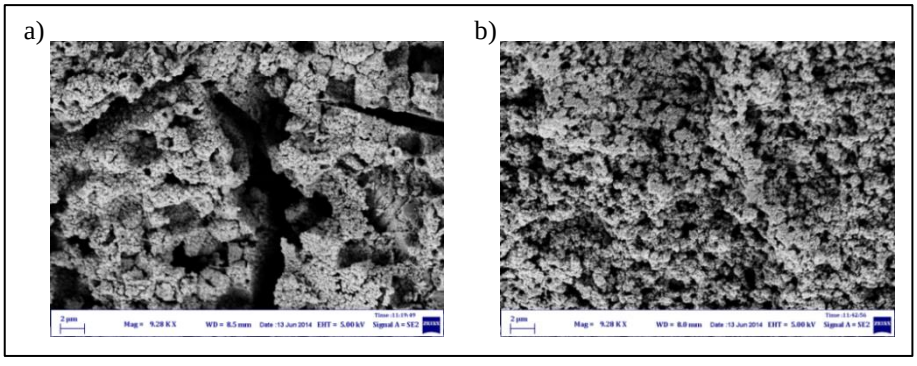

Fig. 1: SEM micrographs of marble samples treated with NANOMATCH1 (a) and CaLoSiL® (b) after exposure in Cologne.

The results of colorimetric analyses show that the application of NANOMATCH1 and CaLoSiL® caused a variation of total colour (ΔE^*) deemed not perceptible by human sight (i.e. $\Delta E^*<5$), according to indications given by Garcìa and Malaga (2012) (Fig. 3). Comparing colour measurements carried out before and after exposure, artificially damaged samples exposed in each site display the highest and visible change in total colour ($5<\Delta E^*<10$) while the application of consolidating products on marble samples sought to preserve a chromatic appearance of the substrate as much as possible similar to that of an exposed undamaged marble. Indeed, apart from samples treated with NANOMATCH1 and placed in Bucharest, the exposed treated samples did not exceed the threshold of perceptibility ($\Delta E^*=5$; Fig. 3).

Considering the results of capillary water absorption, an increase in open porosity is detectable as a consequence of thermal damage. However the treatments with NANOMATCH1 and CaLoSiL® do not influence the porosity of samples. Also, exposure at the different sites does not affect the capillary water absorption.

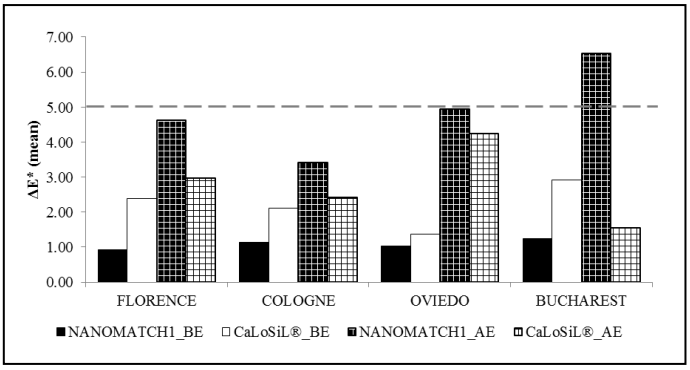

Fig. 3: Total colour variation (ΔE) before and after the application of treatments;and before (BE) and after (AE) exposure in each site. The dotted line indicates the threshold of perceptibility by human sight.*

The disintegration of marble grains induced by thermal stress and perceptible by microscopic investigations is confirmed by the peeling tests. The material released from the surface of artificially damaged samples is more than that removed from undamaged samples. After the application of NANOMATCH1 and CaLoSiL®, the amount of material peeled from treated samples is less than that removed before treatment, demonstrating the consolidating property of the products. In particular, NANOMATCH1 displays better cohesive performance than CaLoSiL®. The comparison between the amounts of material removed from the surface of exposed samples with those peeled from samples before exposure shows a general reduction, and is similar for each class of samples of all tested sites. Artificially damaged samples display the highest enhancement of cohesion, most probably due to the solubilisation and recrystallization inside cracks of $CaCO_3$ induced by rain. Concerning treated samples, good results emerged from samples treated with CaLoSiL®: an increase in cohesion is detectable in all peeling test steps, as shown in Fig. 4 for samples located in Florence.

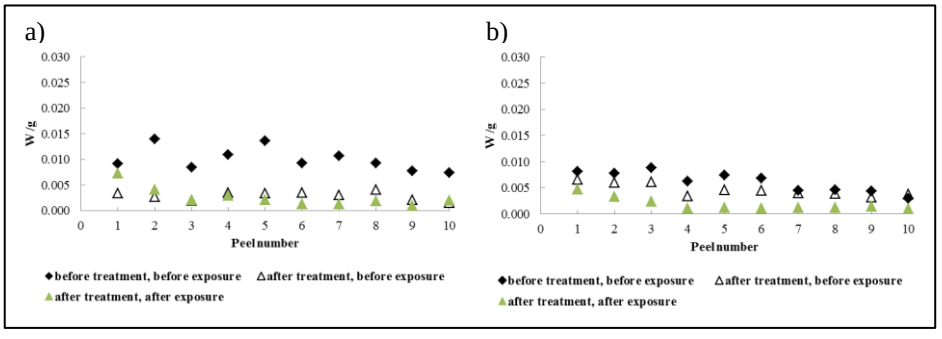

Fig. 4: Scotch tape test data referred to samples artificially damaged treated with NANOMATCH1 (a) and CaLoSiL® (b) and exposed in Florence.

Exposed samples treated with NANOMATCH1 underwent a slight reduction in cohesion in the most superficial part, with a gain in compactness in the inner portion of surface (Fig. 4). It can be supposed that the likely removal of parts of conservation products induced by

environmental factors should cause the exposure of marble damaged by thermal stress but not yet strengthened by the action of rain.

4. Conclusions

The paper has presented and discussed the outcomes of the study concerning the performance of consolidating products on marble samples before and after exposure in different sites. NANOMATCH1 and CaLoSiL® showed good chemical compatibility with the Carrara Marble on which were applied since both are precursors for calcium carbonate. Their application leads to the formation of microcrystalline layers rather homogeneously distributed on samples surface that occasionally penetrates in superficial cracks. Therefore NANOMATCH1 and CaLoSiL® increased the compactness of only samples surface as detected by scotch tape test, without acting as strong structural consolidants for low porosity material such as marble. The aesthetical appearance and the porosity of the marble samples were scarcely altered by the treatments.

The methodological approach utilized in this project proved to be useful in assessing the performance and durability of the products in different environmental conditions, characteristic of each selected site. Field exposure tests gave the possibility to evaluate the environmental impact on the studied substrate and the applied conservation actions. Results of analyses performed after exposure highlighted the importance of precipitations (in terms of acidity and pattern) in the deterioration of the applied conservative products. Acid rain as well as heavy rain events seems to be decisive in the increase of the natural dissolution of $CaCO_3$ induced by karst effect. Moreover the results of the scotch tape test confirmed that generally the exposure of samples resulted in a partial dissolution of $CaCO_3$ and recrystallization within the stone matrix. Nevertheless, colorimetric features of samples as well as their porosity were not significantly influenced by the exposure in different cities.

Testing using longer duration of exposure seems recommendable in order to provide conditions more similar to the real behaviour of conservation products applied on cultural heritage. Moreover improvements of the preparation procedure, penetration and strengthening effect of the new calcium alkoxide product are suggested to increase its performance as consolidant.

Acknowledgements

The NANOMATCH Project (Nano-systems for the conservation of immoveable and moveable polymaterial Cultural Heritage in a changing environment) has received funding from the European Union's Seventh Programme for research, technological development and demonstration under grant agreement No [283182]. Authors express their gratitude to all the partners and colleagues involved in the preparation of exposure field tests and analyses at SEM.

References

Amoroso, G.G., 2002, Trattato di scienza della conservazione dei monumenti: etica della conservazione, degrado dei monumenti, interventi conservativi, consolidanti e protettivi, ALINEA Editrice, Florence, ISBN: 8881254107, 415.

Andriani, G.F. and Germinario, L., 2014, Thermal decay of carbonate dimension stones: fabric, physical and mechanical changes, Environmental Earth Sciences, 72, 2523–2539.

Bernardi, A., Favaro, M., Nijland, T., García, O., Detalle, V., Wittstadt, K., Romero Sanchez, M.D., Pockelé, L., Kunday, B., Verhey, B., Brinkmann, U., De' Micheli, G., Labouré, M., Möller, B., Olteanu, I., 2012, NANOMATCH: a European project to develop consolidants through the synthesis of new inorganic nanomaterials for the conservation of built heritage, in proceedings of Euromed 2012 International Conference on Cultural Heritage, 29th October - 3rd November 2012, Lemesos (Cyprus), Ioannides M. *et al.* (eds.), 307-312.

Bonazza, A., Messina, P., Sabbioni, C., Grossi, C.M., Brimblecombe, P., 2009a, Mapping the impact of climate change on surface recession of carbonate buildings in Europe. Science of the Total Environment, 407 (6), 2039-2050.

Bonazza, A., Sabbioni, C., Messina, P., Guaraldi, C., De Nutiis, P., 2009b, Climate change impact: Mapping thermal stress on Carrara Marble in Europe, Science of the Total Environment, 407, 4506–4512.

Camuffo, D., 2013, Microclimate for Cultural Heritage, 2nd Edition, Elsevier Science, New York, ISBN: 9780444632968, 460.

Chelazzi, D., Poggi, G., Jaidar, Y., Toccafondi, N., Giorgi, R., Baglioni, P., 2013, Hydroxide nanoparticles for cultural heritage: Consolidation and protection of wall paintings and carbonate materials, Journal of Colloid and Interface Science, 392, 42–49.

Doehne, E. and Price, C.A., 2010, Stone Conservation: An Overview of Current research, 2nd Edition, Getty Conservation Institute, U.S.A., 158.

Drdácký, M., Lesák, J., Rescic, S., Slížková, Z., Tiano, P., Valach, J., 2012, Standardization of peeling tests for assessing the cohesion and consolidation characteristics of historic stone surfaces, Materials and Structures, 45 (4), 505-520.

Favaro, M., Mendichi, R., Ossola, F., Russo, U., Simon, S., Tomasin, P., Vigato, P. A., 2006, Evaluation of polymers for conservation treatments of outdoor exposed stone monuments, Part I: Photo-oxidative weathering, Polymer Degradation and Stability, 91 (12), 3083–3096.

Favaro, M., Mendichi, R., Ossola, F., Simon, S., Tomasin, P., Vigato, P. A., 2007, Evaluation of polymers for conservation treatments of outdoor exposed stone monuments, Part II: Photo-oxidative and salt-induced weathering of acrylic silicone mixtures, Polymer Degradation and Stability, 92 (3), 335–351.

Favaro, M., Chiurato, M., Tomasin, P., Ossola, F., El Habra, N., Brianese, N., Svensson, I., Beckers, E., Forrat Pérez, V.J., Romero Sánchez, M.D., Bernardi, A., 2014, Calcium and Magnesium Alkoxides for Conservation Treatment of Stone and Wood in Built Heritage, in Built Heritage: Monitoring Conservation Management, Toniolo, L., Boriani, M., Guidi, G. (eds.), Springer, Berlin, ISBN: 9783319085326, 413-422.

Garcìa, O. and Malaga, C., 2012, Definition of the procedure to determine the suitability and durability of an anti-graffiti product for application on cultural heritage porous materials, Journal of Cultural Heritage, 13 (1), 77-82.

Giorgi, R., Dei, L., Baglioni, P., 2000, A new method for consolidating wall paintings based on dispersions of lime in alcohol, Studies in conservation, 45, 154-161.

Grossi, C.M., Bonazza, A., Brinblecombe, P., Harris, I., Sabbioni, C., 2008, Predicting twenty-first century recession of architectural limestone in European cities, Environmental Geology, 56, 455-461.

Grossi, C.M., Brimblecombe, P., Menéndez, B., Benavente, D., Harris, I., Déqué, M., 2011, Climatology of salt transitions and implications for stone weathering, Science of the Total Environment, 409, 2577–2585.

ISO 7724/3, 1984, Paints and varnishes-Colorimetry-Part3: Calculation of colour differences.

Natali, I., Saladino, M.L., Andriulo, F., Chillura, Martino, D., Caponetti, E., Carretti, E., Dei, L., 2014, Consolidation and protection by nanolime: Recent advances for the conservation of the graffiti, Carceri dello Steri Palermo and of the 18th century lunettes, SS.Giuda e Simone Cloister, Corniola (Empoli), Journal of Cultural Heritage, 15, 151-158.

Natali, I., Tomasin, P., Becherini, F., Bernardi, A., Ciantelli, C., Favaro, M., Favoni, O., Forrat Pérez, V. J., Olteanu, I. D., Romero Sanchez, M. D., Vivarelli, A., Bonazza, A., 2015, Innovative consolidating products for stone materials: field exposure tests as a valid approach for assessing durability, Heritage science 3 (6), doi: 10.1186/s40494-015-0036-3.

Sabbioni, C., Brimblecombe, P., Cassar, M., 2012. The Atlas of Climate Change Impact on European Cultural Heritage. Scientific Analysis and Management Strategies. Anthem Press, London, ISBN 9780857282835, 160.

Sassoni, E. and Franzoni, E., 2014, Influence of porosity on artificial deterioration of marble and limestone by heating, Applied Physics A: Materials Science & Processing, 15, 809–816.

UNI EN 15801, 2009 Conservation of cultural property - test methods - determination of water absorption by capillarity.

ELECTROPHORESIS AS A TOOL TO REMOVE SALTS FROM STONE BUILDING MATERIALS – RESULTS FROM LAB EXPERIMENTS AND AN ON-SITE APPLICATION

H. De Clercq[1*], S. Godts[1], L. Debailleux[1], Y. Vanhellemont[2], N. Vanwynsberghe[3], L. Derammelaere[3] and V. De Swaef[3]

Abstract

Salt removal using poultices is a known and often applied technique for the extraction of salts in building materials, which in general is a rather time- and money-consuming process. Theoretically it should be possible to remove salts faster, by forcing the electrically charged salt ions in a solution to move towards the opposite charged electrode. The applicability of this technique is usually tested in laboratory conditions, while onsite applications are generally limited. This paper deals with results from lab experiments, set up to investigate the feasibility of and execution parameters for an application onsite. For that, lab tests were focused on parameters related to the feasible depth of salt extraction, the effect on combined materials consisting of mortar and brick besides the electrode configuration hereby using systematically a mixture of calcite and cellulose as contact material. The entire investigation has shown that positive results are obtained in terms of a deep salt extraction effect and the feasibility on combined materials, but that several questions remain related to the salt migration properties before and during the electrophoresis.

Keywords: salt contamination, electrophoresis, desalination, limestone, brickwork, conservation

1. Introduction

Moisture and salt contamination are major causes of degradation to historic building materials, in the form of aesthetic or mechanical damage. In Belgium, impermeable or salt resistant materials are quite often used in practice; interventions that have a tendency of hiding the salt problem instead of solving it and hence as such not contributing to a sustainable management of our built heritage. An alternative approach attempts to extract salts through poulticing or electrophoresis (Ottosen *et al.*, 2007; Ottosen and Christensen 2012).

[1] H. De Clercq*, S. Godts and L. Debailleux
Royal Institute for Cultural Heritage, Jubelpark 1, B-1000 Brussels, Belgium
hilde.declercq@kikirpa.be

[2] Y. Vanhellemont
Belgian Building Research Institute (BBRI), Avenue Pierre Holoffe 21, B-1342 Limelette, Belgium

[3] N. Vanwynsberghe, L. Derammelaere and V. De Swaef
KULeuven, Technologiecampus Ghent, Belgium

*corresponding author

During electrophoresis, a wet sample contaminated with salts is subjected to a direct current enabling ions to migrate to the oppositely charged electrode where they are stored in the contact material. In case of sodium salts, sodium hydroxide is formed at the cathode or negatively charged electrode (Herinckx *et al.*, 2011). An alkaline environment as such is not damaging a limestone. At the positively charged anode, water is transformed into oxygen and hydrogen ions. Chlorides form chlorine gas or combine with hydrogen ions to form hydrochloric acid. Sulphates present in the solution will similarly combine with the hydrogen ions and form sulfuric acid. An acidic environment can chemically attack the calcium carbonate of limestone and hence cause damage to it.

Previous investigation on lab samples using different contact materials, more specific cotton, cellulose and a mixture of cellulose and calcite, has shown that the last is the more suitable one and is capable of protecting the building materials against the acidic environment formed at the anode (De Clercq *et al.*, 2014). Extraction percentages up to 80% were obtained in ideal circumstances by which electrodes are positioned at opposite sides of a relatively thin salt laden substrate with a thickness of 4-5 cm.

This paper deals with results from lab experiments, set up to optimize and further work out an application on site. For that, lab tests were focused on parameters related to the feasible depth of salt extraction, the effect on combined materials consisting of mortar and brick besides the electrode configuration. The contact material consists of a mixture of calcite and recycled cellulose (De Clercq *et al.*, 2014).

Samples submitted to electrophoresis in lab conditions consist of limestone blocks with different sizes, bricks and so-called sandwiches consisting of a mortar layer in between two bricks, all contaminated with sodium chloride. In this paper, only the results obtained with the limestone blocks of 15×15×5 and 40×15×40 cm as well as those obtained on the sandwich are described. The effect of salt removal is controlled by ion chromatography on the aqueous extract of samples lifted at different positions. The tested zones for the onsite application, the first one in Belgium, consist of a brick wall of a barn, showing severe salt damage and highly contaminated with mainly sodium chloride, potassium nitrate and gypsum. The investigated parameters are related to the electrode configuration on one hand and pre-humidification (2 or 15 $l \cdot m^{-2}$) on the other hand. The choice of this onsite application was based on its conservation state, revealing the need for a durable intervention.

2. Experimental part

2.1. Substrates

The building materials used for the lab investigation are the French Savonnières limestone and a red brick (18×8×5 cm) characterised by porosity accessible to water, determined by immerging dry samples in demineralized water for 48 h, of about 10 %. The limestone blocks have different sizes (15×15×5 cm and 40×15×40 cm). The samples are previously dried at 105°C till constant weight.

The so-called sandwiches consist of two bricks having a mortar layer, composed of 1 volume part hydraulic lime (St. Astier, NHL 3.5) and two volume parts of sand 0-2, mixed with water to obtain a workable mortar. After 1 week of conditioning, during which they are daily wetted, sandwiches are put in a CO_2-chamber (27°C and 4 % CO_2) for 10 days to

accelerate the carbonation. The *pH* of the mortar decreased from 13 to between 11.5 and 10, respectively in the middle and at the surface.

2.2. Salts

Limestones and individual bricks are contaminated with a fixed amount of sodium chloride (1 wt%) and a water content of 3wt%, while the sandwiches are placed into an aqueous NaCl-solution (33 wt%).

2.3. Test setup

Graphite electrodes (15×15 cm) were selected for their good resistance in an acidic and alkaline environment, low cost and easy availability. They are linked to the power supply by means of a titanium nut. The electrophoresis is carried out during 1 week, with a voltage of 10 V, according to a test setup presented in (Herinckx, *et al.*, 2011 and De Clercq, *et al.*, 2014). In the cases when small limestone blocks (15×15×5 cm), bricks and sandwich structures, are used the electrodes are positioned at opposite sides. For the sandwich structure, both electrodes (5×5 cm) were also positioned at the front side (18×5 cm). In the case when larger limestone blocks (40×15×40 cm) are used, the electrophoresis process is carried out during 19 days, with a voltage of 30 V, and applies to a depth up to 40 cm. The electrodes are positioned in the middle and at opposite sides (40×15 cm) of the stone slab, on one hand and in the middle, at the left and the right and at the same side of the slab (40×15 cm) on the other hand. All tests are done in two or three fold. The contact material is a paste consisting of cellulose fibres, calcite powder and water, in a weight ratio of 50-250-450, which is applied in a thickness of 1 cm.

2.4. Onsite application

The onsite application concerns brick masonry of an inner façade, having a thickness of about 40 cm, in a barn of the old mill house at Hoksem-Hoegaarden. The choice for this onsite application was based on the severe damage in the form of powdering of especially the mortar as well as the quite uniform salt contamination, mainly consisting of a mixture of sodium chloride and potassium nitrate, with a total content up to 4 w%, and gypsum up to 2.3 w%. Four test zones are selected, half of them are pre-wetted with 2 $l \cdot m^{-2}$ and the other half with 15 $l \cdot m^{-2}$ of demineralized water. On each type of pre-wetted zone, the electrodes (15×15 cm) are positioned at the same (inner) side of the wall at a distance of 15 or 30 cm. Electrophoresis is carried out during 2 weeks with a constant voltage of 20 V. The last was selected for reasons of a feasible electrophoresis capacity while ensuring safety requirements.

2.5. Electrophoresis efficiency

After electrophoresis, drilled samples (5 mm diameter) are lifted of which the soluble salt content is measured according to De Clercq *et al.* (2014). Only in case of the slabs of 40×15×40 cm, the efficiency was controlled using chloride Test Strips (Merckoqukant®). The efficiency is calculated by comparing the content of Na^+ and Cl^- for the laboratory research while that of the sum of Na^+, K^+, Cl^- and NO_3^- for the onsite application, each time before and after electrophoresis.

3. Results and discussion

3.1. Stone slabs of 15×15×5 cm

The results of the electrophoresis efficiency of the 3 limestone slabs of 15×15×5 cm (Fig. 1) vary between 37 and 68 %, with an average of 56 %. The efficiency is based on the calculation of the sum of Na^+ and Cl^- of the sample drilled in the middle of the slab (15×15 cm) and through the entire depth (5 cm). Fig. 1 illustrates that, although the Savonnières is quite often used as a material for laboratory testing, its inhomogeneous pore structure is responsible for the important variation in electrophoresis efficiency, revealing the need for a sufficient number of testing to obtain representative results.

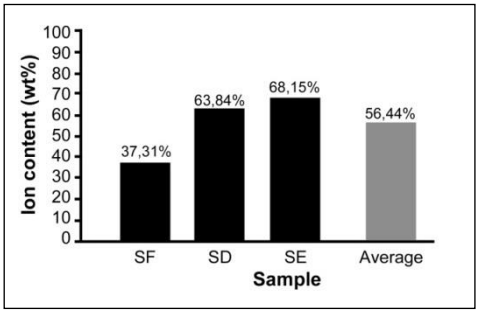

Fig. 1: electrophoresis efficiency of 3 limestone slabs (15×15×5 cm), contaminated with 1 w% of NaCl and 3 w% of moisture (10 V, 1 week).

3.2. Bricks

Sampling on individual bricks is performed as presented in Fig. 2. In this case, homogeneous results are obtained for the three tested samples, revealing an efficiency of about 80% on average for both sample types.

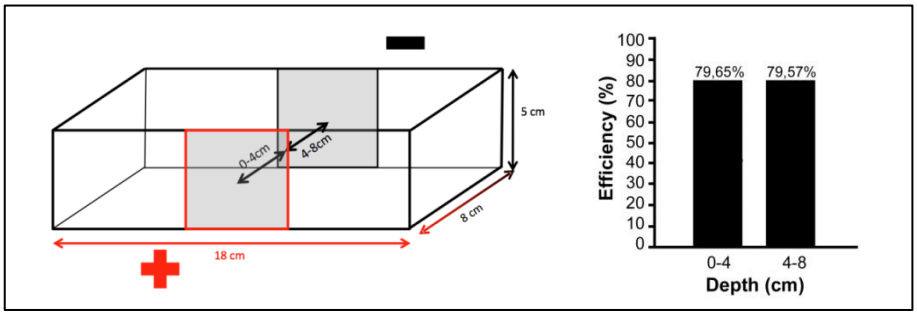

Fig. 2: scheme of sampling of bricks contaminated with 1 w% of NaCl and 3 w% of moisture submitted to electrophoresis (left) and resulting efficiency (right) (10 V, 1 week).

3.3. Sandwich structures

Figures 3 and 4 present the results obtained for the sandwich structure, consisting of 2 red bricks with 1 cm mortar in between them, tested according to different electrode positions. The results show that when the electrodes are positioned at opposite sides (Fig. 3), a similar efficiency is obtained for both bricks as for the one obtained in case the bricks are tested as a single material (Fig. 2). Although the physical properties of the mortar were not tested, the results show that the current passes through this interlayer. However, in case the electrodes are both positioned at the front side, a similar and high efficiency is obtained for the front brick while a lower one is obtained for the back brick, 65 % on average, and the mortar (Fig. 4). Of course, the higher distance towards the electrodes explains the difference in efficiency for the two electrode configurations.

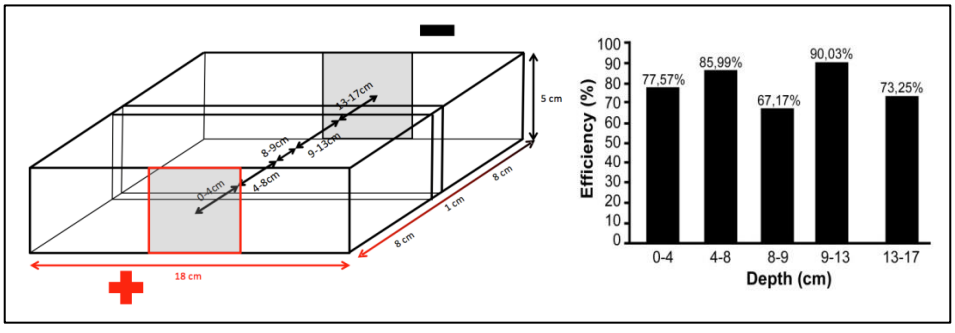

Fig. 3: sandwich structure saturated with an aqueous NaCl-solution (33 wt%) submitted to electrophoresis by positioning the electrodes on opposite sides (left) and efficiency (right) (10 V, 1 week). The sampling location is presented on the left scheme.

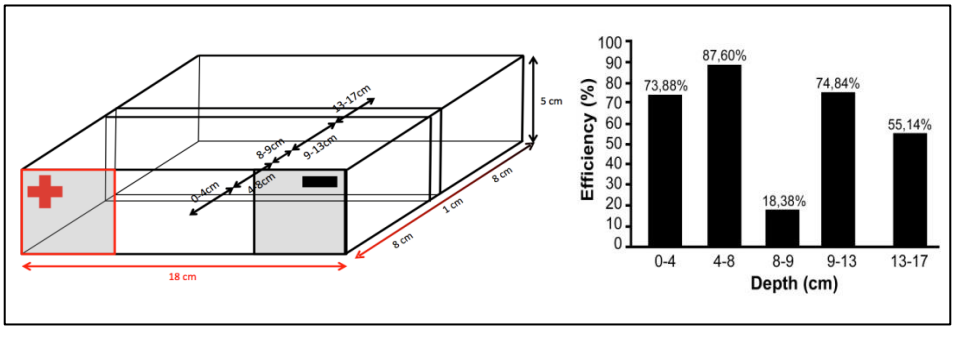

Fig. 4: sandwich structure saturated with an aqueous NaCl-solution (33 wt%) submitted to electrophoresis by positioning both electrodes on the front side (left) and efficiency (right) (10 V, 1 week). The sampling location is presented on the left scheme.

3.4. Limestone slabs of 40×15×40 cm

Larger stone blocks have been tested according to the schematic presentations given in Fig. 5 and Fig. 6 (left). This paper is limited to the results of the chloride profile obtained by means of chloride strip tests. In case the electrodes are positioned at opposite sides of the limestone slab, the results show that closer to the positive electrode, a higher content of

(migrated) chlorides is measured (Fig. 5 right). The efficiency, related to the initial content of chlorides of 0.6 wt%, goes from 25% for the stone layer up to 5 cm from the positive electrode, to 67% on average for the underlying layer up to 20 cm to further increase to 84 and 100% for respectively the layer 20-25 cm and the 25-40 cm. The last indicates that to a depth of 15 cm from the negative electrode, all chlorides have been migrated towards the positive charged one. In case both electrodes are positioned at the same side (Fig. 6 left), three chloride profiles have been set up. The corresponding results show that at a distance up to 15 cm from the negative electrode, no chlorides are detected, indicating an efficiency of 100%. In between both electrodes, corresponding to the central profile, the efficiency increases from 42 to 83% for respectively 0 to 5 and 5 to 10 cm, and remains quite constant around 65% to end up to almost 0%. The results of the profile at the positive electrode are quite similar compared to the central profile except for the first 15 cm characterised by a lower efficiency. At a distance of 40 cm from both electrodes, the average efficiency is 8 %. In case a minimum efficiency of 50% is set as criterion for success, this is obtained up to 30 cm from the surface where the electrodes are positioned.

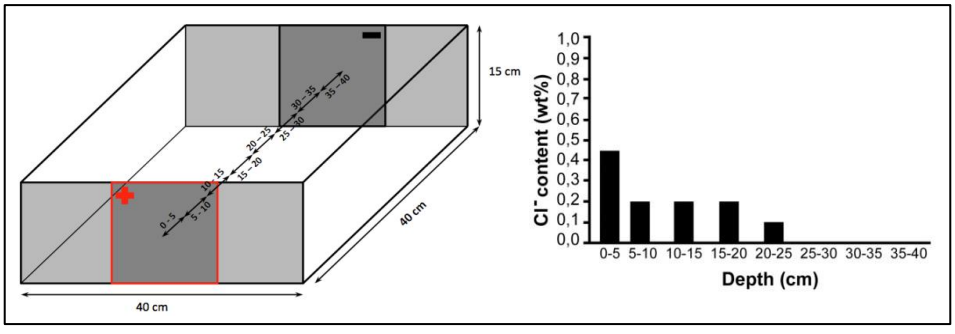

Fig. 5: limestone slabs (40×15×40 cm) contaminated with 1 w% of NaCl and 3 w% of moisture submitted to electrophoresis by positioning the electrodes on opposite sides (left) and resulting efficiency (right) (30 V, 19 days). The sampling location is presented on the left scheme.

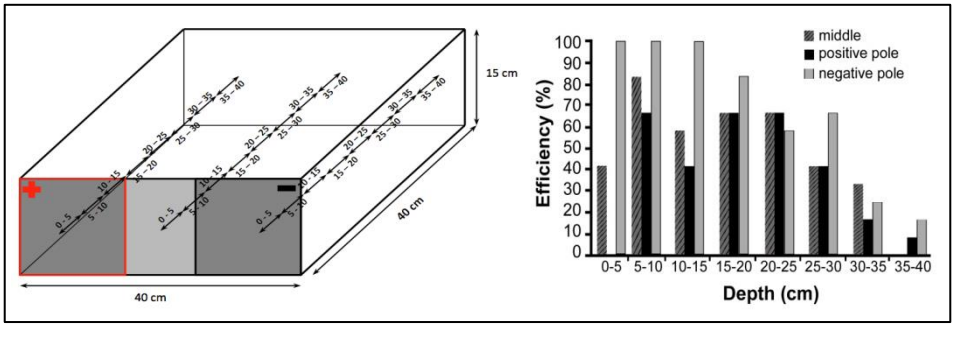

Fig. 6: limestone slabs (40×15×40 cm) contaminated with 1 w% of NaCl and 3 w% of moisture submitted to electrophoresis by positioning both electrodes on the front side (left) and resulting efficiency (right) (30 V, 19 days). The sampling location is presented on the left scheme.

3.5. Onsite application

Although the initial salt contamination was quite uniform, no systematic results were obtained after electrophoresis in a way that relevant data are obtained, for example, related to the distance from the surface onto which the electrodes were positioned. Therefore, the results, expressed as % reduction of the sum of Na^+, K^+, Cl^- and NO_3^-, have been averaged for the first 10 cm of brick and mortar (Tab. 1).

Tab. 1: average efficiency (%) of the first 10 cm of brick and mortar for the test zones according to the pre-wetting conditions and the distance between the electrodes.

Zone	Pre-wetting	Distance between the electrodes	Efficiency	
			Brick	Mortar
I	15 l/m^2	30 cm	76%	79%
II	15 l/m^2	15 cm	57%	81%
III	2 l/m^2	15 cm	62%	61%
IV	2 l/m^2	30 cm	44%	80%

From these results, a global high efficiency is concluded, which is generally higher for the mortar than for the brick; the last was also obtained from laboratory testing on the sandwich material. A further tendency of lower efficiency for lowering pre-wetting conditions is noticed. It should be mentioned that in case of an intensive high pre-wetting, one is confronted with the migration of salts deeper in the masonry. No systematic influence of the distance between the electrodes is noticed.

A further control of the electrophoresis was carried out by measuring the ion content, expressed as the "sum of Na^+ and K^+" and the "sum of Cl^- and NO_3^-", of the contact material lifted at the positive and the negative electrode (Fig. 7). As expected, the results illustrate that anions are principally detected on the positive electrode while cations on the negatively charged one. Electrophoresis performed at conditions where the electrodes are at a distance of 15 cm, seems to perform better, hence more ions are detected in the contact material, in case of pre-wetting with 15 l·m^{-2} (Zone II) than when only 2 l·m^{-2} is applied (Zone III). However, contradictory results apply in case the distance between the electrodes is 30 cm (respectively Zone I and IV).

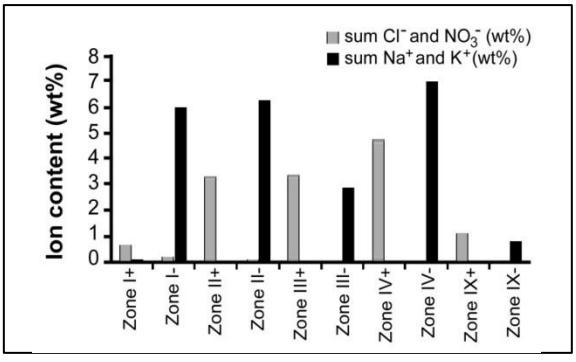

Fig. 7: Results of ion content (wt%) of the contact material lifted at the positive ("+") and the negative ("-") electrode of zones I to IV.

4. Conclusion

It has been shown that electrophoresis is a potential suitable method for the extraction of salts from a salt-laden building material. The results depend greatly on the setup of the laboratory test, including the type and size of building materials. Although a systematic salt and moisture content was applied for different types of small sized building materials that were in threefold submitted to a similar electrophoresis process, different results are obtained in terms of "representativeness" and "statistic relevance".

Further research in lab conditions that approach those onsite, hereby using a sandwich structure consisting of two bricks with a mortar layer in between, has shown that both bricks have a comparable efficiency of 80%, that is similar to the one obtained in case the brick is tested as a single material, in case the electrodes are positioned at opposite sides of both bricks of the sandwich structure. From this result it was concluded that the ion current indeed passes through the mortar layer. In case the electrodes were positioned both at the front side of the first brick of the sandwich structure, the last showed again an efficiency of about 80 % while that of the back brick was on average 65%. A much lower efficiency was also obtained for the mortar. The lower efficiency is explained by the higher distance to the electrodes compared to the configuration by which the electrodes are situated on opposite sides of the sandwich structure.

The general question: "how deep can salts be extracted out of building materials?", was approached using Savonnières limestone slabs of 40×15×40 cm enabling a maximum extraction depth of 40 cm. The voltage for this setup was increased to 30 V applied during 19 days instead of 10 V during 7 days, as was the case for the smaller slabs and the sandwich structures. A good efficiency was obtained in case the electrodes are positioned at opposite sides (40×15 cm) of the slabs: at a distance up to at least 15 cm from the negative charged pole, all chlorides were migrated towards the positive pole. For the setup by which the electrodes are both at the front side of the limestone slab, the efficiency decreases with depth. Nevertheless, if a minimum efficiency of 50% is set as a condition for success, this criterion is fulfilled until a depth of 30 cm from the front side.

Based on the above results, an onsite case for electrophoresis was finally selected. This implied a comprehensive thinking process to define the practical modalities to ensure a safe and secure execution. The brickwork showed severe damage in the form of powdering of

mainly the mortar and a high salt load, mainly consisting of gypsum, sodium chloride and potassium nitrate. The selected adjacent test zones are located on the inside of an eastern facade of a barn belonging to a mill site at Hoksem-Hoegaarden. The investigated test parameters were the amount of pre-wetting (2 or 15 $l \cdot m^{-2}$) on one hand and the distance between both electrodes (15-30 cm) on the other hand, while keeping the voltage constant at 20 V for 19 days. The electrophoresis effect, calculated by comparing the sum of Na^+, K^+, Cl^- and NO_3^- ions with the initial content, varied between 44 and 81 %, which is as such quite a positive result. However, despite the limited number of selected test parameters applied for these 4 test zones, a systematic influence on the extraction effect could not be observed and this despite the huge number of analyzed drilled samples. This is explained by the inhomogeneous properties of historical brickwork on one hand and the unknown real effect of pre-wetting on the salt migration deeper in the wall on the other hand. Further, the method for calculating the efficiency might not be completely representative for the real salt contamination, including gypsum. Gypsum was excluded from the calculations of the efficiency, for reasons of its low solubility, although it should influence the electrophoresis process, as mentioned by Paz-Garcia *et al.* (2011). The electrophoresis should effect the solubility and distribution of present gypsum through the migration of Ca^{2+} and SO_4^{2-} towards the oppositely charged electrode.

References

De Clercq, H, Vanhellemont, Y., De Swaef, V., 2014, Salt extraction of limestone by means of electrophoresis: some results on type of contact material and electrode position, in proceedings of 3rd. International Conference of Salt Weathering of Buildings and Stone Sculpture (SWBSS2014), De Clercq H. (ed.), Brussels, KIK-IRPA, ISBN 978-2-930054-24-7, 421-434.

Herinckx, S., Vanhellemont, Y., Hendrickx, R., Roels, S., De Clercq, H., 2011, Salt removal from stone building materials using an electric field, in proceedings of 2nd International Conference of Salt Weathering of Buildings and Stone Sculpture (SWBSS2011), Ioannou, I. and Theodoridou, M. (eds.), Limassol, ISBN 978-9963-7355-1-8, 357-364.

Ottosen, L.M., Pedersen, A.J., Rörig-Delgaard, I., 2007, Salt-related problems in brick masonry and electrokinetic removal of salts, Journal of Building Appraisal. (3), 181-194.

Ottosen, L.M., Christensen, I.V., 2012, Electrokinetic desalination of sandstone for NaCl removal: Test of different clay poultices at the electrodes, Elsevier, Electrochimical Acta, 86, 192-202.

Paz-Garcia, J.M., Johannesson, B., Ottosen, L.M., Ribeiro, A.B., Rodriguez-Maroto J.M., Influence of the chemical interactions on the removal rate of different salts in electrokinetic desalination processes, in proceedings of 2nd International Conference of Salt Weathering of Buildings and Stone Sculpture (SWBSS2011), Ioannou, I. and Theodoridou, M. (eds.), Limassol, ISBN 978-9963-7355-1-8, 373-380.

This page has been left intentionally blank.

SALT WEATHERING OF SANDSTONE DURING DRYING: EFFECT OF PRIMARY AND SECONDARY CRYSTALLISATION

J. Desarnaud[1*], H. Derluyn[2], L. Grementieri[3], L. Molari[3], S. de Miranda[3], V. Cnudde[2] and N. Shahidzadeh[4]

Abstract

In this study we show that the key to understanding why the same salt can cause damage in some conditions and not in others is the kinetics of recrystallisation. Salt-contaminated porous materials are known to deteriorate with environmental fluctuations. Salts can be naturally present in the materials used for construction or can be derived from external sources. With changes in climate, entrapped salt crystals can once again form a salt solution after contact with liquid water (dissolution) or with water vapour (deliquescence). The solution is mobilized in the porous network and then salts re-crystallize with drying. We present both macroscopic and microscopic experiments assessing the recrystallisation dynamics of NaCl in sandstone with wetting-drying and humidity cycling. Advanced techniques such as high resolution X-ray computed tomography and Scanning Electron Microscopy are used to study the recrystallisation process in the porous network in parallel with the drying kinetics. Our results show that recrystallisations following deliquescence and dissolution lead to very different crystallisation patterns. With humidity cycling, recrystallisation promotes the formation of localised bigger cubic crystals in the subsurface of the stone, whereas rewetting leads to efflorescence in the form of large localised 'cauliflowers' at the surface. The different growth dynamics have direct consequence on the drying behaviour of the sandstone and its deterioration.

Keywords: Mšené sandstone, salt weathering, drying and deliquescence kinetics, crystallisation pattern

1. Introduction

Salt crystallisation inside confined systems is one of the major causes of mechanical or physical weathering causing disintegration of porous rocks and building materials (Goudies and Viles, 1997; Shahidzadeh-Bonn *et al.*, 2010) It is also the most important forms of soil

[1] J.Desarnaud*
WZI-IoP-University of Amsterdam, The Netherlands
Julie.desarnaud@gmail.com

[2] H. Derluyn and V. Cnudde
UGCT-PProGRess, Department of Geology and Soil Science, Ghent University, Belgium

[3] L. Grimentieri, L. Molari and S. de Miranda
DICAM, University of Bologna, Italy

[4] N. Shahidzadeh
Van der Waals-Zeeman Institute, Institute of Physics, University of Amsterdam, The Netherlands

*corresponding author

degradation (Cook and Smalley, 1968) and problems for oil well productivity and CO_2 sequestration (Peysson, 2012).

With the variation of climatic conditions such as relative humidity, or rain followed by drying, the salts present in porous media crystallize either in the form of efflorescence (at the surface) or subflorescence (within the pore network) (Rodriguez-Navarro and Doehne, 1999). Once crystallized, salts can re-dissolve in two different ways: by contact with liquid water (dissolution) or by contact with water vapour (deliquescence). The latter is due to the hygroscopic properties of salts. The resulting salt solution is then mobilized in the porous network and salt subsequently re-crystallizes on drying.

The action of salts on weathering of porous media has attracted a lot of attention over the past decade, but remains incompletely understood. Most studies reported in the literature deal either with unidirectional (1D) evaporation of a porous material that is permanently supplied with the salt solution or with evaporation-wicking experiments (Eloukabi, *et al.*, 2013; Shokri, 2014).

These studies have revealed the impact of the pore size and the relative humidity on the type of crystallisation. Mainly efflorescence has been observed in different types: crusty or patchy (Verran-Tissoires and Prat, 2014) (also referred to as 'cauliflowers') (Shahidzadeh-Bonn *et al.*, 2008) and although it has been observed that the crystallisation affects the drying rate, there are still many aspects that need to be clarified in order to understand the interplay between salt crystallisation and evaporation. The dynamics of the crystallisation and recrystallisation processes (Mullin, 2001) have not been studied yet. In general, recrystallisation that results from cycling differs from the initial crystallisation (Desarnaud and Shahidzadeh-Bonn, 2010). Moreover if the nucleation is primary (directly from solution) high supersaturations can be achieved (Mullin, 2001; De Yoreo and Vekilov, 2003) which is the case for the evaporation of homogeneous salt solutions in confined systems (J. Desarnaud *et al.*, 2014). On the other hand, the secondary nucleation (from pre-existing crystallites present in the solution) typically happens around the saturation concentration (De Yoreo and Vekilov, 2003). It is clear from the above that the crystallisation dynamics in a porous medium depends on both thermodynamic and transport processes. These will have also a direct impact on the evaporation rate of the solvent (water) from the porous network.

In this paper we show that the dynamics of crystal growth is of paramount importance on both the evaporation rate and the possible damage generated by the salt crystallisation. When the same amount of water is used to dissolve the salt present in a stone, different recrystallisation patterns and evaporation kinetics can be found if this is done in different ways: by a rapid saturation with liquid water, or by a slow saturation using water vapour.

2. Experimental Section

We perform a multiscale study on the behaviour of sodium chloride contaminated sandstones. Solutions were prepared with Sigma Aldrich grade 99.9% NaCl and Ultrapure Millipore water. Macroscale experiments consist of studying the crystallisation pattern and the drying kinetics of saturated sandstones (porosity $\phi \sim 29\%$, and pore diameter $d_p \sim 30$ μm). We study the recrystallisation behaviour and the drying of the salt-contaminated sandstones once they were rewetted with liquid water or brought in contact with water vapour (RH~100%). The global drying kinetics (evaporation in 3D directions)

are followed on an automated balance with a precision of 0.001 g placed in a homemade, controlled climatic chamber at *T*=21°C, at *RH*~ 20% (Shahidzadeh and Desarnaud, 2012). We have investigated the crystallisation in the core of the stone and at the surface in more detail using high resolution X-ray computed tomography (μ-CT), optical and Scanning Electron Microscopy (SEM) combined with EDS. X-ray μ-CT was performed at the Centre for X-ray Tomography at the Ghent University (UGCT) using the scanner HECTOR (Desarnaud *et al.*, 2015). We also performed microscale experiment using square microcapillaries (100 μm) as simple model systems for a single pore within a porous medium, to investigate the kinetics of dissolution and deliquescence of crystals, followed by recrystallisation. Quantifying small-scale features is fundamental to improving our understanding of the underlying basis of macroscopic fluid and solute transport behaviour.

3. Results

3.1. Macroscale experiments

3.1.1. Crystallisation

During a first series of experiments, the sandstones samples are saturated by imbibition with NaCl solutions (at saturation: 6.1M). At *RH* ~ 20% the drying behaviour of the sample consists of three regimes: first a continuous constant drying rate period (CRP) until the residual saturation is roughly half of the initial saturation. In the second regime the saturation no longer decreases linearly in time, but follows an exponential decrease. The third regime is much slower: a $t^{1/2}$ dependence of the saturation as a function of time is found, characteristic of a mass transfer limited by diffusion that controls the evaporation (Prat, 2007) (Fig. 1).

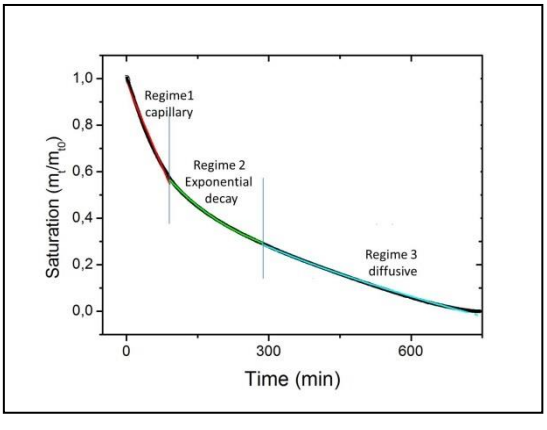

Fig. 1: Evaporation rates at RH ~20%. Three regimes are observed Regime 1(CRP):mt/mt0=-0,0049t+0,986; Regime 2: mt/mt0= 0,79e-0,003t; Regime3: mt/mt0=-0,026 t1/2+0,79.

This leaves the question what the origin is of the second (exponential decay) regime followed by a diffusive regime for drying at low relative humidity. Microscale analysis of the sample reveals the formation of salt crystals at the surface of the sample (Figures 2a and 2b) and no crystals in the core of the sample (Fig. 2c). The lateral rapid growth of salt crystals forms a skin on the outer surface of the sandstone that makes a barrier and prevents

the fluid from reaching the surface to evaporate (Figures 2d and 2e). In fact, the skin formation accounts for the exponential decrease of the drying rate with time: with the growth of the skin layer the evaporative surface rapidly becomes smaller, which slows down the evaporation. In fact, the drying rate is proportional to the surface of evaporation:

$$\frac{dm}{dt} = -cA \qquad \textit{(Eq. 1)}$$

As soon as crystals start to grow at the surface, the evaporative surface decreases according to:

$$\frac{dA}{dt} = \alpha \frac{dm}{dt} \qquad \textit{(Eq. 2)}$$

Consequently, the combination of these two differential equations for the evaporated mass gives:

$$\frac{d^2m}{dt^2} = -c\alpha \frac{dm}{dt} \qquad \textit{(Eq. 3)}$$

which has an exponential solution: $m = m_0 e^{-c\alpha t}$, as is observed in the experiments.

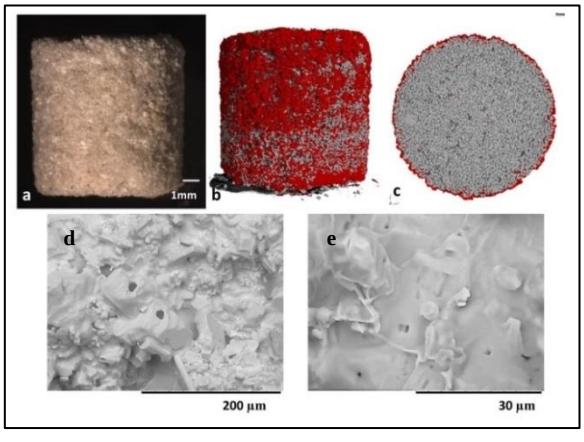

Fig. 2: Samples at RH 20%: a) Sample after drying; b and c) X-ray µ-CT analysis of NaCl at the surface and in the core (middle) of the samples. Below, SEM picture of the porous salt skin after evaporation of saturated salt solution in sandstone.

A more detailed investigation shows that the salt skin which covers the outer surface of the sandstone is in fact also porous with a mean pore size of about 3µm, i.e 10 times smaller than the pore radius of sandstone (Fig. 2d and 2e). The average thickness of the salt skin was estimated from micro-CT results and SEM images. Both methods give a maximum thickness of the salt skin around 250 µm ± 50 µm. According to Washburn's law (1921) reducing the pore diameter will reduce the speed of fluid transport through capillary suction. Here, the speed of the capillary flow through these small pores is found to be insufficient to overcome the evaporation rate at *RH* ~20%. This leads to rupture of the

wetting films at the outer surface; subsequently diffusive transport of vapour through the small pores controls the drying kinetics in the third regime.

3.1.2. Recrystallisation dynamics

After the initial drying described above, we bring the NaCl-contaminated sandstones in contact either with liquid water (dissolution) or with water vapour ($RH > RH_{eqNaCl,}$ deliquescence) until complete saturation. Once saturated, the sample is dried again at RH = 20%. We have repeated this cycling up to 3 times.

Dissolution-drying experiments In the case of saturation by rewetting with pure water which is a rapid process, we observe that independent of the relative humidity, not all salt crystals at the surface will have time to dissolve and distribute through the stone before the evaporation starts. Drying induces the secondary nucleation of new crystals on top of the existing, incompletely dissolved ones. In this situation, low supersaturations and small induction times are observed because the nucleation and growth take place on existing crystal surfaces. The rewetting is done with pure water so no additional salt is added. The observed precipitation of the new crystals at the surface thus implies the dissolution of crystals within the sample and the transport of material to the outer surface where the growth proceeds. Therefore, rewetting followed by drying cycles, tends to extract the salt from within the porous medium towards the outer surface by forming large cauliflower-like salt crystals assemblies at the surface (Figures 3a, 3b, 3c and 3d).

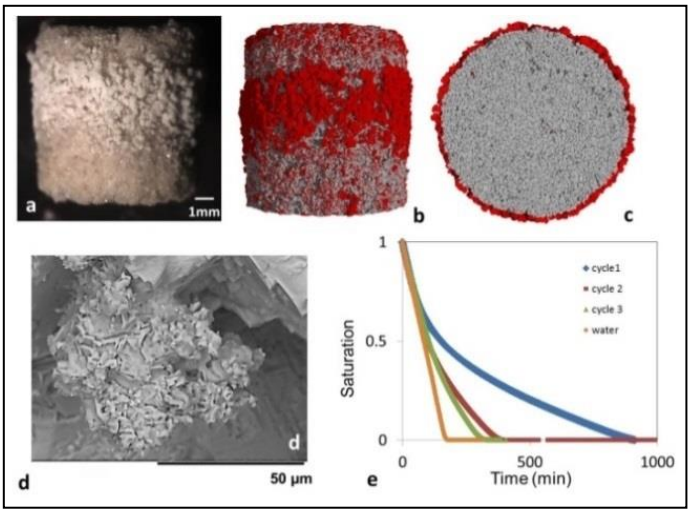

Fig. 3: Recrystallisation due to dissolution-drying cycles at RH~20%; a) crystallisation of cauliflower-like salt crystals; b and c) X-ray µ-CT analysis of NaCl at the surface and in the core of the samples; d) SEM of cauliflower structures; e) Drying kinetics with several dissolution-drying cycles.

The size increase of the 'cauliflowers' with increasing number of wetting/drying cycles leads to the disappearance of the skin at the surface of the sample (Fig. 3). This crystallisation dynamics has direct repercussions on the drying behaviour as can be seen in Fig. 3e. First, with increasing the number of cycles, the drying kinetics gets closer to the drying kinetics of water. Second, the exponential regime associated with the formation of a

salt 'skin' that slowed down the evaporation, disappears completely due to the fact that the skin layer disappears with cycling as discussed above. Third, because the skin layer is subsequently replaced by large cauliflowers, the constant rate period extends over a longer period with increasing the number of cycles. The drying dynamics can thus be described as a constant rate period due to the capillary transport to the surface followed by a diffusive regime. The transition between these two regimes becomes smaller and smaller with subsequent cycling.

Deliquescence-drying experiments: If water vapour is introduced into the porous medium, a very different recrystallisation dynamic is observed. The experiments show that the formation of large cauliflower crystals due to secondary nucleation upon recrystallisation is almost completely absent with increasing the number of cycles (Fig. 4a and Fig. 4b). The deliquescence of the salt crystals is a slow process which leads to the formation of a very homogeneous salt solution which gradually invades the porous network of the stone, thus transporting the salt to the interior of the stone. The subsequent recrystallisation (as a primary nucleation) of the homogeneous salt solution leads to the increase of the number of large cubic crystals (Fig. 4c); their formation is usual for recrystallisation because at each cycle impurities are expelled (Shahidzadeh and Desarnaud, 2012).

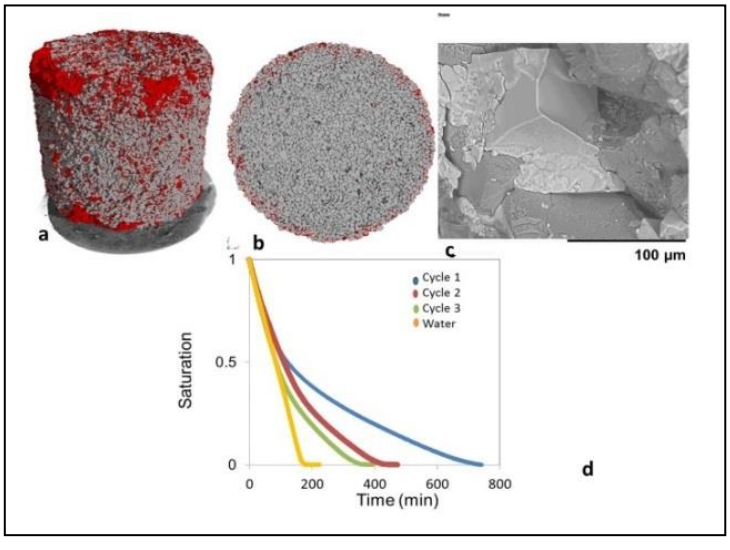

Fig. 4: Recrystallisation due to several deliquescence-drying cycles at RH~20%; a and b) X-ray µ-CT analysis, showing salt crystals (red) on and beneath the surface; c) SEM picture of large a cubic crystal in between the grains at the subsurface after 3 cycles of deliquescence-drying; d) Drying kinetics with several deliquescence-drying cycles.

The supersaturations is very high (Desarnaud and Shahidzadeh-Bonn, 2011) and the increase of salt concentration in the solution before recrystallisation reduces the wetting properties of the solution which in turn at high evaporation rates can be the cause of the retraction of the solution into the porous network and the crystallisation in the subsurface as is clearly visible in the microtomography images (Fig. 4b).

3.2. Microscale experiments

To confirm this hypothesis, we did some experiments in single square microcapillaries (100µm) to represent a single pore in a porous network. The results confirm that with an increasing number of cycles of deliquescence-drying, there is a retraction of the salt solution inside of the pore due to the increase of concentration and the formation of more cubic crystals. As it can be seen in Fig. 5, at the first cycle crystallisation occurs at the entrance of the capillary with the formation of a layer blocking the entrance. With two deliquescence-drying cycles, first the skin at the entrance is gradually replaced by well-shaped cubic crystals at the outer wall of the microcapillary and a second part of the salt solution retracts inside of the capillary leading to a deeper crystallisation in the microcapillary (Fig. 5b). In the dissolution-drying experiment, the salt crystallizes outside the microcapillary as efflorescence, and its quantity increases with the number of cycles (Fig. 5c) which is in good agreement with the bigger Cauliflowers efflorescence found in the sandstone experiments.

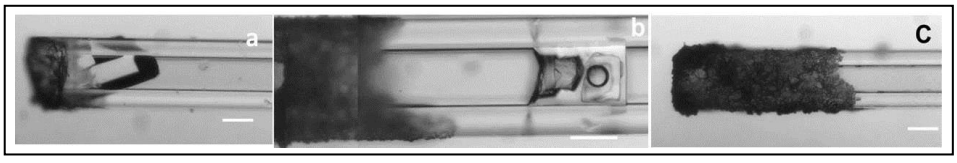

Fig. 5: a) crystallisation of NaCl after first drying; b) Crystallisation after 3 deliquescence-drying cycles; c) after3 dissolution-drying cycles, in 100µm square micro capillaries.

The way of salt crystallisation is a key factor for understanding the crystallisation not only for NaCl. In previous experiment we have shown that for Na_2SO_4, the deliquescence-drying cycles (long process) leads to the primary nucleation and growth of anhydrous crystals (thenardite) occurs (Desarnaud *et al.,* 2012) (Figures 6a and 6b). The homogeneous sodium sulfate solution can reach high concentration during long evaporation without any nucleation, favoring the formation of isolated thenardite crystals which leads to no damage. On the other hand, during rewetting of dissolution-drying experiment (very rapid process) in microscapillaries loaded with Na_2SO_4, anhydrous microcrystals dissolve only partially, giving rise to a heterogeneous salt solution that is supersaturated with respect to the hydrated phase. The remaining anhydrous crystals then act as seeds for the formation of large amounts of hydrated crystals, creating grape-like structures that expand rapidly (Figures 6a and 6c). These clusters can generate stresses larger than the tensile strength of the stone, leading to damage.

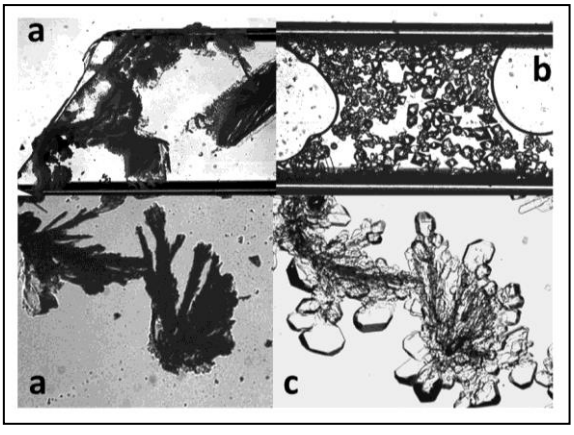

Fig. 6: a) After totale evaporation of Na2SO4 solution in capillary (C1) formation of anhydrous crystal (thenardite); b) Crystallisation primaire of thenardite after 3 deliquescence-drying cycles; c) rewetting of the dissolution-drying cycles: formation of clusters due to the growth of hydrated crystals on the remaining thenardite microcrystallites.

4. Conclusion

This paper summarized experimental studies showing the major role played by different salt crystallisation pathways on the drying behaviour of salt-containing sandstones subjected to several wetting-drying cycles. We show that the kinetics of crystal growth due to primary or secondary nucleation are of key factors for understanding the drying behaviour of salt contaminated porous materials and the possible physical weathering generated by salt crystallisation. We provide a clear identification of the different probable regimes that are possible, depending also on external parameters such as the relative humidity.

Acknowledgements

The authors would like to express theire gratitude to Netherlands organisation for *Scientific research–NOW* and *The Research Foundation – Flanders* (FWO). The work reported in this paper has been supported by the *KISADAMA project*, funded by *JPI Cultural Heritage* within the *Joint Heritage European Programme.*

References

Cook, R.U. and Smalley, I.J., 1968, Salt weathering in desert. Nature. 220, 1226-1227

Desarnaud, J., Derluyn, H., Molinari, L., De Miranda, S., Cnudde, V., Shahidzadeh N., 2015, Drying of salt contaminated porous media: Effect of primaty and secondary nucleation, J.Applied Physics. 18. 114901.

Desarnaud, J., Derluyn, H., Carmeliet, J., Bonn, D., Shahidzadeh, N., 2014, Metastability limit for the nucleation of NaCl crystals in confinement, J. Phys. Chem. Lett. 5 (5), 890-895.

Desarnaud, J., Shahidzadeh-Bonn, N., 2011, Salt crystal purification by deliquescence /crystallisation cycling, Euro. Phys. Lett. 95, 48002.

Desarnaud, J., Bertrand, F., Shahiodzadeh, N. 2012, Impact of the kinetics of salt crystallization on stone damage during rewetting/drying and humidity cycling. J.Appl. Mech

De Yoreo, J. J.,Vekilov, P., 2003, Principle in nucleation and growth, *Mineralogical Society of America*. 54, 57-93.

Eloukabi, N., Sghaier, S., Ben Nasrallah, S. B., Prat, M., 2013, Experimental study of the effect of sodium chloride on drying of porous media: The crusty–patchy efflorescence transition Int. J. Heat Mass. Transf. 56, 80-93.

Goudies, A. S., Viles, H. A., (1997), Salt Weathering Hazard (Salt Weathering Hazard John Wiley and Sons, Chichester).

Mullin, J. W., 2001, Crystallization (Butterwords-Heinemann, 4th edition).

Peysson, Y, 2012, Permeability alteration induced by drying of brines in porous media, Eur. Phys. J. Appl. Phys. 60, 24206.

Prat, M., 2007, On the influence of pore shape, contact angle and film flows on drying of capillary porous media. Int. J. Heat and Mass Tranfert. 50, 1455-1468.

Rodriguez-Navarro, C., Doehne, E., 1999, Salt weathering: influence of evaporation rate, supersaturation and crystallization pattern, Earth. Surf. Proc. Landforms. 24, 191-209.

Shahidzadeh, N., Desarnaud, J, 2012, Damage in porous media: Role of the kinetics of salt recrystallisation Eur. Phys. J. Appl. Phys. 60, 24205.

Shahidzadeh-Bonn, N., Desarnaud, J., Bertrand, F., Chateau, X., Bonn. D., 2010, Damage in porous media due to salt crystallization Phys. Rev. E, 81066110.

Shahidzadeh-Bonn, N., Rafai, S., Bonn, D., Wegdam, G., 2008, Salt crystallization during evaporation: Impact of interfacial properties, Langmuir 24, 8599-8605.

Shokri, N., 2014, Pore scale dynamics of salt transport and distribution on drying porous media, Phys. Fluids, 26 012106.

Verran-Tissoires, S., Prat, M., 2014, Evaporation of a sodium chloride solution from a saturated porous medium with efflorescence formation, J. Fluid Mech. 749, 701-749.

Washburn, E. W., 1921, The dynamic of capillary flow, Phys. Rev. 17, 273.

This page has been left intentionally blank.

HANDHELD X-RAY FLOURESCENCE ANALYSIS (HH-XRF): A NON-DESTRUCTIVE TOOL FOR DISTINGUISHING SANDSTONES IN HISTORIC STRUCTURES

P.A. Everett[1*] and M.R. Gillespie[1]

Abstract

Determining the provenance of building stone can be important when researching the history of historic structures or identifying suitable substitute stone to use in building repairs. Commonly, however, there is no written record of stone source, and a visual examination alone is inconclusive. In many such situations stone provenance can only be constrained with confidence if the stone has a distinctive property or character that allows it to be distinguished from, or matched with, other stones. A small proportion of stones have one or more genuinely distinctive visual characteristics that uniquely confirm their provenance, but for most stones such distinctive properties, if they exist at all, are cryptic and usually revealed only by microscope examination or bulk chemical analysis. However, collecting and analysing representative hand samples for this purpose can be difficult, time-consuming and damaging to historic structures. Handheld X-Ray Fluorescence analysis offers the potential to provide bulk composition data without the need to collect physical samples. HH-XRF instruments are lightweight, wireless and portable, and they provide a rapid, non-destructive means of analysing most materials in a wide range of settings. This study has examined the benefits and limitations of the instrument when applied to sandstone building stones from the UK. A programme of laboratory tests has been used to: develop a robust methodology for gathering, managing, displaying and interpreting data; determining the extent to which sample surface condition affects the analytical results; and assessing the degree to which different sandstones can be distinguished on the basis of their bulk composition. The results are promising: the data can be used to compare, distinguish and match visually indistinguishable sandstones (and potentially a wide range of other geological and man-made materials) quickly and easily, and as such the method should find widespread application in disciplines such as building conservation and archaeology.

Keywords: sandstone, composition, non-destructive, analysis, HH-XRF, provenance

1. Introduction

A means of gathering and comparing sandstone composition data from buildings and other stone structures without causing damage to the masonry would be of considerable benefit; for example, it may help to distinguish similar-looking sandstones, which may be of use in understanding the construction and repair history of buildings, and it could help to identify

[1] P.A. Everett* and M.R. Gillespie
British Geological Survey, The Lyell Centre, Edinburgh, United Kingdom
paer@bgs.ac.uk

*corresponding author

(or constrain) stone provenance which might be helpful when selecting stone to use in building repairs.

Handheld X-Ray Fluorescence (HH-XRF) analysis is a non-destructive means of obtaining bulk composition data, which potentially offers the means to differentiate geological (and other) materials, and in some cases could help to constrain or confirm their provenance.

HH-XRF analysis has been applied successfully in several studies of the provenance of archaeological artefacts, for which non-destructive analytical methods are essential; the analysed materials have included obsidian (Dyrdahl & Speakman 2013; Cecil *et al.* 2007) and pottery (Morgenstein & Redmount 2005) artefacts. Most HH-XRF instruments are designed by the manufacturers to provide optimised analytical sensitivity for elements of economic importance and/or potentially harmful elements, (e.g. Pb, Zn, Cu) because the mineral exploration industry and contaminated land sectors are the main customers. HH-XRF analysis has been applied to chemostratigraphy in borehole cores (oil and gas industry), rapid prospectivity analysis (mineral exploration industry; e.g. Fisher et.al. 2014) and contaminated land assessments. A brief literature review has revealed only one example of HH-XRF being used to analyse building stone (Historic Scotland 2012); however, the details and outcomes of that work have not been published.

This paper summarises the key findings of a study to develop a methodology for applying HH-XRF analysis to *in situ* testing of sandstone building stones, and to establish how the method can be used to distinguish or match sandstones using the results. The study is documented in more detail in Everett (2016).

2. The instrument

HH-XRF analyses were obtained using a Thermo Niton XLt 700 Series Environmental Analyser. The instrument is simply pressed against the sample surface and 'fired' using a trigger. The analysed volume corresponds to an area approximately 8mm wide and up to 5mm deep. An X-ray beam fired into the sample produces a spectrum of secondary X-rays, reflecting the bulk chemical composition of the analysed volume, that are measured by the detector inside the instrument. A calibration routine, which is built-in to the CPU of the instrument, was run before each analysis session. The routine measures the X-ray spectra and adjusts the internal electronics and sensors according to pre-loaded factory settings. This means that results should be internally consistent but may not be comparable to data produced using a different instrument. The instrument can measure the concentration (in parts per million (ppm)) of 22 elements; Sb, Sn, Cd, Ag, Sr, Rb, Pb, Se, As, Hg, Zn, Cu, Ni, Co, Fe, Mn, Cr, V, Ti, Sc, Ca, and K. However, the concentration of any of these elements is only reported by the instrument if it exceeds the Lower Limit of Detection (LLD), which is determined by the instrument for each individual analysis but is not recorded (i.e. the instrument reports the concentration of an element, or that it is below LLD, but does not record what the LLD value is). Broadly speaking, LLD values tend to be lower for elements with higher atomic numbers than for elements with lower atomic numbers.

3. Sample details

Sandstone building stones typically are comprised predominantly of detrital sand, primarily grains of quartz, feldspar and rock fragments in varying proportions. A range of other minerals, including mica, Fe (-Ti) oxide, apatite, tourmaline and zircon, are usually present

in minor to trace proportions. Secondary (authigenic) minerals, including calcite, dolomite, iron oxide (or oxyhydroxide), clay and quartz, are also commonly present in minor to trace proportions. Most building stone sandstones are porous (up to 25% pore volume). Quartz (SiO_2), which is usually the dominant constituent, will not produce a response from the HH-XRF instrument as neither Si nor O are measureable elements. This means that the compositional maturity of a sandstone (i.e. the proportion of quartz relative to other detrital components) has the potential to strongly influence the analytical results.

The programme of laboratory analysis was conducted on a suite of 26 hand samples of sandstone from 11 quarries in the UK. The samples were selected to represent much of the range of colour and mineral composition range displayed by UK sandstones, and some of the most important lithostratigraphic and chronostratigraphic associations. All the samples were obtained from the BGS Collection of UK Building Stones, and all consisted of fresh (unweathered) sandstone. Most of the samples are mineralogically and texturally uniform (not obviously bedded or laminated) when viewed at the hand specimen scale. The maximum grain-size in any sample is around 1.5 mm; this is much smaller than the volume of stone included in each analysis (section 2), so it is assumed that variations in grain size do not affect results significantly. For the sake of brevity only a subset of samples, all of which are uniform, are referred to in this paper (Tab. 1). The modal composition of each sample was estimated by visual assessment of thin sections under the microscope, and using this information each sample was classified according to its compositional maturity.

Tab. 1: Summary details of sandstones referred to in this paper.

Quarry name	**Location**	**Compositional maturity***	**Colour**	**Lithostratigraphic and chronostratigraphic association**
Craigleith	Edinburgh (Scotland)	very mature	white	Gullane Sandstone Formation, Strathclyde Group; Carboniferous
Cullalo	Burntisland, (Scotland)	very mature	white	Strathclyde Group; Carboniferous
Blaxter	Otterburn (England)	mature	buff	Tyne Limestone Formation; Carboniferous
Peakmoor	Matlock (England)	mature	buff	Ashover Grit, Millstone Grit Group; Carboniferous
Stanton Moor	Matlock (England)	mature	buff	Ashover Grit, Millstone Grit Group; Carboniferous
Crossland Hill	Huddersfield (England)	moderately mature	buff	Rossendale Formation, Carboniferous
Corsehill	Annan, (Scotland)	moderately mature	orange	St Bees Sandstone Formation; Triassic
St Bees	Ravensworth (England)	moderately mature	orange	St Bees Sandstone Formation; Triassic
Swinton	Kelso (Scotland)	moderately mature	buff	Ballagan Formation, Inverclyde Group; Carboniferous
Pennant	Forest of Dean (Wales)	immature	purplish grey	Pennant Sandstone Formation; Carboniferous

* Based on the proportion of thin section area occupied by quartz, where *very mature* = >70%, *mature* = 50-70%, *moderately mature* = 40-50% and *immature* = <40%.

4. The test programme

4.1. Plotting parameters

A key objective was to develop a means of gathering, assessing and interpreting analytical results quickly but with sufficient rigour to ensure they are meaningful. This is important because the method is likely to be useful only if it is quick and easy to use, without the need for the rigorous statistical evaluation that commonly is associated with other methods using bulk composition data. Ideally, a single set of elements or element ratios would be used to represent sandstone compositions, and the data would be evaluated using a simple, empirical method. With this in mind, the first test involved analysing each sample 10 times (on 10 different sites) to identify which elements are present in sufficient concentration to be useful.

Only Fe, Ti, Sr, Rb and K were consistently above the Lower Limit of Detection (LLD) in most (22) of the samples. Based on this result, plots of Fe/Ti vs Sr/Rb were identified as the optimum means of presenting data; in most sandstones these element ratios will be controlled mainly by Fe(-Ti) oxides and feldspar, respectively, though other minerals (notably carbonate minerals, mica and clay) will play a role. Mean values and coefficient of variance (CV) values for these elements are presented in Tab. 2.

Tab. 2: Average values and CV for elements measured in selected samples.

Sample	**Sr**		**Rb**		**Fe**		**Ti**		**K**	
	Mean ppm	CV %	Mean ppm	CV %	Mean ppm	CV %	Mean ppm	CV %	Mean ppm	CV %
Craigleith A	*	*	*	*	417.5	18.3	307.5	14.2	1702.8	14.8
Cullalo A	64.1	8.9	*	*	282.3	15.9	499.1	22.7	2009.2	14.9
Blaxter A	125.0	6.4	14.9	26.9	3807.9	5.5	1630.4	4.5	5719.1	6.4
Blaxter B	48.5	14.9	15.2	20.5	3063.8	3.4	668.4	5.7	6943.9	4.9
Blaxter C	31.5	13.5	22.1	24.0	5290.2	5.1	1927.0	4.3	7754.8	6.6
Peakmoor A	78.8	7.6	33.1	19.2	5706.3	5.6	2856.6	6.0	16076.6	8.1
Peakmoor B	91.5	6.9	33.6	15.4	4572.2	4.0	2419.6	3.7	17061.0	2.9
Peakmoor C	79.1	9.0	39.9	10.5	7431.8	5.5	2577.6	2.6	17222.6	3.0
S. Moor A	79.4	7.2	29.1	14.8	4073.8	6.3	2210.7	6.3	15685.9	2.8
C. Hill A	54.8	10.9	30.1	17.4	5504.3	3.7	1483.6	4.3	15320.9	3.2
C. Hill B	49.7	11.3	25.6	12.6	5097.9	3.5	1380.4	3.5	14301.2	5.2
Corsehill A	54.8	3.8	42.5	10.7	4175.5	5.9	1065.0	5.9	19556.7	2.3
St Bees A	65.4	8.2	82.1	10.6	8014.5	8.2	1931.9	11.6	28210.7	2.9
St Bees B	52.2	6.5	76.2	9.3	5639.5	3.0	1126.7	4.5	25578.3	2.1
St Bees C	62.9	6.5	84.8	8.5	8023.0	3.7	1137.5	5.4	29869.8	2.3
Swinton A	109.0	7.0	70.2	8.7	10787.2	4.1	2592.2	5.2	34044.3	3.0
Swinton B	100.7	9.3	63.0	9.7	4621.0	6.0	1847.3	3.3	30590.4	2.6
Swinton C	107.7	10.5	71.9	10.2	13514.4	4.4	2999.0	3.9	36958.6	1.9
Pennant A	43.2	15.2	53.1	11.8	13289.2	4.8	2428.4	6.0	21433.4	5.6

* indicates value below LLD. Coefficient of variation (CV) is a measure of the variation within a group of analyses; in this case it is the standard deviation of 10 analyses divided by their mean, expressed as a percentage.

Not surprisingly, the mean concentrations of these elements generally increase, and CV values correspondingly decrease, as compositional maturity decreases (Tab. 2). In samples of *very mature* sandstone only K, Fe and Ti were measured in concentrations above the LLD, and a different means of discriminating these sandstones will be required.

4.2. Comparison of sandstones

HH-XRF data for several sandstones that come from different geological formations and can readily be distinguished by eye in hand specimen, are plotted on Fig. 1. In each case, 3 samples from the same quarry (denoted -A, B, C) were used to represent each sandstone, and 10 analyses from different positions on the surface of each sample were obtained to represent the composition range of the stone at hand specimen scale. The following observations can be made.

- The data for two samples of Blaxter sandstone (A and B) display a much bigger range of Sr/Rb values than other samples and consequently do not form tight clusters. Blaxter sandstone is compositionally mature, and the Sr and Rb data have the highest CV values of any sandstone analysed in this study; this means that much of the range in Sr/Rb values is probably due to poor analytical reproducibility (due to low element concentrations) rather than natural compositional variation. The data for Blaxter sandstone therefore are considered unreliable. This result highlights the importance of taking CV values into account at an early stage, particularly for compositionally mature sandstones that don't produce tight clusters on scatterplots. Data displaying a significant degree of scatter but a low CV value are more likely to be a product of natural compositional variation on the scale of the analysed sample.

For the three remaining sandstones (Peakmoor, St Bees and Swinton):

- The data for individual samples typically form tight clusters, demonstrating that the instrument is capable of producing results which can be used to characterise and distinguish sandstones on an empirical basis.
- Data clusters for different samples of the same sandstone sometimes overlap on the scatterplot and sometimes do not; this probably reflects differences in the degree to which sandstones display real compositional variation on the bed or quarry scale.
- The data for all samples of each sandstone define a well constrained and largely distinct field; each field represents a compositional 'fingerprint' for the sandstone.

HH-XRF data for some sandstones that cannot be distinguished by eye are presented in Fig. 2 (Sr/Rb axis expanded to clarify cluster distributions). Two samples of orange sandstones come from different quarries in the same geological formation, while two buff sandstones (each represented by two samples from the same quarry) come from different geological formations. Each orange sandstone and each buff sandstone produces a distinct cluster on the plot, confirming that the method is able to distinguish sandstones that cannot be distinguished by eye.

4.3. Optimising analytical procedure

4.3.1. Number of analyses per sample

A test was carried out to determine how many analyses of a sample of uniform sandstone are typically required to define its compositional character. Two samples, one a compositionally mature sandstone (Peakmoor) and the other an immature sandstone (Pennant), were analysed 4, 10 and 20 times and the resulting data clusters were examined to determine the minimum number of analyses needed to adequately represent the sandstone composition. Both samples produced similar results: the 'spread' of the cluster on the X-Y plot expands up to 10 analyses, but thereafter does not change significantly (Fig. 3). On this basis it is concluded that a minimum of 10 repeat analyses is required to represent the composition of a typical sample.

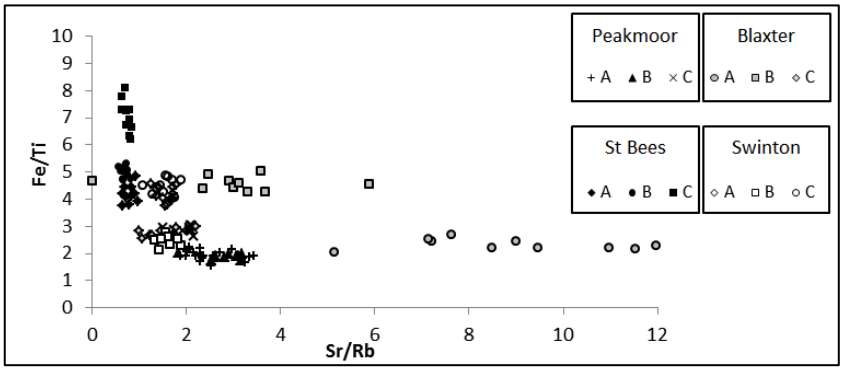

Fig. 1: HH-XRF data for sandstones that can be distinguished by eye.

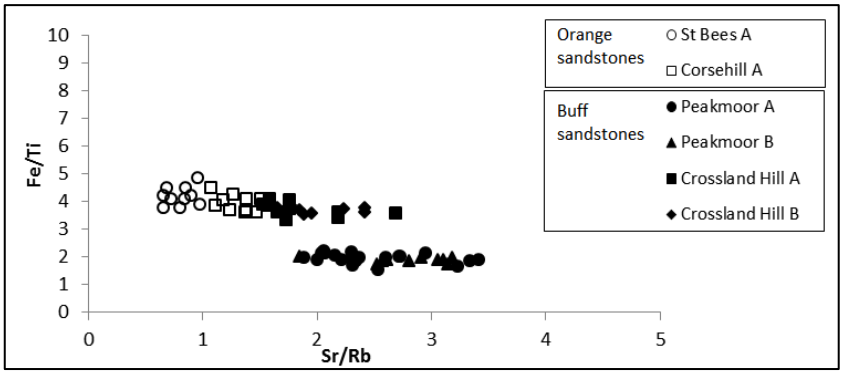

Fig. 2: HH-XRF data for sandstones that cannot be distinguished by eye.

4.3.2. Sample surface condition

Stone surfaces might be analysed in a range of settings, including in the laboratory, on exposed building facades, and in quarries, so two tests were conducted to compare the effects of different sample surface conditions.

Results from smooth (sawn; surfaces were cleaned to ensure pores were not blocked by rock powder produced by sawing) and rough (freshly broken) surfaces of the same samples generally are closely similar (Fig. 4); slight differences can be attributed to small sample-scale natural variations in bulk composition. An essentially similar pattern of results for moist and dry surfaces suggests variations in surface moistness also do not significantly affect results. However, to maximise the consistency of results it would be sensible in real-world applications to test samples of similar surface character (ideally smooth, dry surfaces) wherever possible.

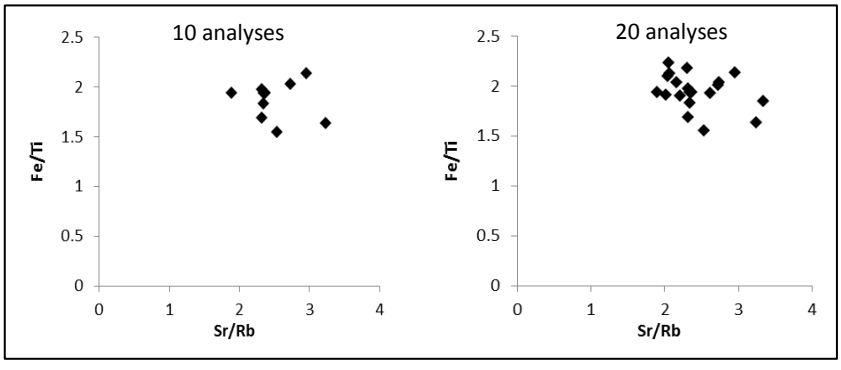

Fig. 3: Comparison of results for 10 and 20 repeat analyses of Peakmoor sandstone.

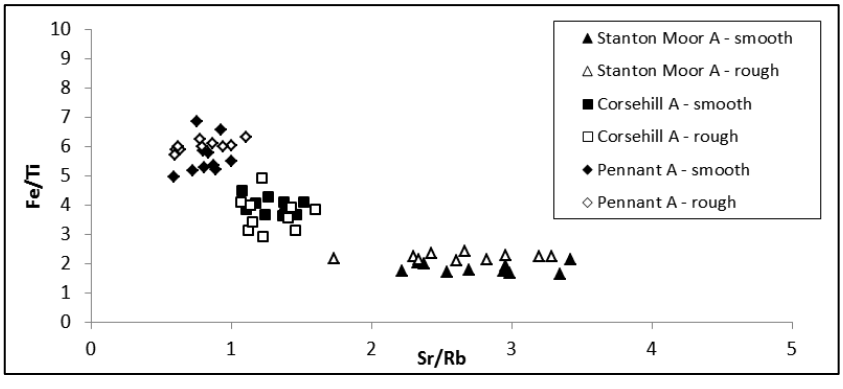

Fig. 4: Comparison of results for smooth and rough sample surfaces.

5. Conclusions

This study has shown that HH-XRF analysis, and evaluation of results on Fe/Ti vs Sr/Rb plots, can be used to distinguish building stone sandstones, including sandstones which are difficult to distinguish visually, quickly and easily, and without damaging the sample. Ideally, at least 10 analyses of visually uniform sandstone should be obtained to produce a robust cluster of data which could be considered to be a 'compositional fingerprint' for the stone. Surface moisture and roughness appear to have little effect on results; however, it would be sensible wherever possible to analyse dry, smooth surfaces.

The method clearly also has potential to help constrain the provenance of sandstone used in buildings, but this would require a reference dataset of values for sandstones from known sources. Combining the HH-XRF 'fingerprint' for a sandstone with one or more other discriminatory features (e.g. a distinctive mineral or textural property) could significantly increase the capacity of the method to constrain the provenance of sandstones.

Sandstones which are compositionally 'very mature', (and some that are classed here as 'mature') contain insufficient concentrations of key elements to produce reliable data; however, this problem is likely to diminish as manufacturers produce more sensitive instruments.

This study has concentrated on sandstones which are visually uniform on the hand sample scale. However, sandstones can be heterogeneous at a range of scales (e.g. due to lamination, bedding and facies variations) and further work will be needed to understand how best to deal with this. Further work will also be needed to evaluate the effect of weathering before the instrument is used in the field.

The accuracy of the instrument when testing sandstones could be better understood by comparing HH-XRF results from a sandstone sample, with high-precision laboratory-based XRF results from the same sample. In time, introducing a calibration routine that involves one or more suitable reference materials could lead to more consistent results, and a situation where results from different projects can be compared.

References

Cecil L. G., Moriarty M. D., Speakman R. J., and Glascock M. D., 2007, Feasibility of field-portable XRF to identify obsidian sources in Central Peten, Guatemala. In Archaeological Chemistry: Analytical Methods and Archaeological Interpretation, Glascock M. D., Speakman R. J., and Popelka-Filcoff R.S. (eds.) ACS Symposium Series 968, American Chemical Society, Washington DC, 506–521.

Dyrdahl E. and Speakman R.J., 2013, Investigating Obsidian Procurement at Integration Period (ca. AD 700-1500) Tola Sites in Highland Northern Ecuador via Portable X-ray Fluorescence (pXRF). In Archaeological Chemistry VIII, Armitage, R. A., Burton J. H. (eds.), American Chemical Society, Washington DC, ISBN9780841229242, Chapter 12, 211–232.

Everett P. A., 2016, Handheld X-Ray Fluorescence: a method for non-destructive compositional analysis of sandstone building stones. Open Report OR/16/008, British Geological Survey, Keyworth, UK.

Fisher, L., Gazley M. F., Baensch A., Barnes S. J., Cleverly J. and Duclaux G., 2014, Resolution of geochemical and lithostratigraphic complexity: a workflow for application of portable X-ray fluorescence to mineral exploration. Geochemistry: Exploration, Environment, Analysis. 14 (2), 149 - 159

Historic Scotland, 2012, Focus Magazine. Conservation Directorate of Historic Scotland, Edinburgh, UK.

Morgenstein, M., & Redmount, C. 2005. Using portable energy dispersive X-ray fluorescence (EDXRF) analysis for on-site study of ceramic sherds at El Hiba, Egypt. Journal of Archaeological Sciences, 32, 1613 - 162.

INTRINSIC PARAMETERS CONDITIONING THE FORMATION OF MN-RICH PATINAS ON LUNEVILLE SANDSTONES

L. Gatuingt[1*], S. Rossano[2], J.-D. Mertz[3], B. Lanson[4] and O. Rozenbaum[5]

Abstract

After a fire in 2003 and thus, after being submitted to a large quantity of water, part of the sandstones of the Luneville castle (XVIIIth century, France) developed a dark Mn-rich patina within a few weeks. This phenomenon is also observed on sandstones only subjected to rainwater but with a formation time of the order of several years. This project aims to better understand the formation mechanisms of dark Mn-patinas, especially in the Luneville castle case, focussing on the characteristics of the sandstones. In order to investigate intrinsic factors conditioning the formation of a patina, two pairs of representative stones (patinated/unpatinated) have been sampled on site, in the burnt and unburnt zones respectively. Macroscopic and microscopic observations and Inductively Coupled Plasma-Optical Emission Spectrometry (ICP-OES) were employed to obtain global, visual and chemical information on the bulk material. Optical and electronic microscopies, coupled with Energy-Dispersive X-ray Spectroscopy (EDS) establish a correlation between the visual aspect of an area and its Mn-content. Quantitative chemical data on selected regions of interest were obtained by Particle-Induced X-ray Emission (PIXE) method, to derive the Mn-chemical environment. Mercury intrusion porosimetry, capillary imbibition and permeability measurements have also been made to evaluate the impact of the rock transfer properties on the patina's development. Petrophysical properties of the sandstones facilitate water transport, but no significant differences have been underlined between patinated and unpatinated blocks. However, the sandstones which developed a patina contain a greater Mn-quantity than the others. Moreover, the chemical associations in Mn-rich areas are not the same, suggesting different original Mn-bearing phases.

Keywords: sandstone, manganese, patina

[1] L. Gatuingt*
Laboratoire de Recherche des Monuments Historiques CRC-LRMH-USR3224, Laboratoire Géomatériaux et Environnement, Université Paris-Est, France
laure.gatuingt@culture.gouv.fr

[2] S. Rossano
Laboratoire Géomatériaux et Environnement, Université Paris-Est, France

[3] J.-D. Mertz
Laboratoire de Recherche des Monuments Historiques CRC-LRMH-USR3224, France

[4] B. Lanson
ISTerre, CNRS, Université Grenoble Alpes, F-38041, France

[5] O. Rozenbaum
ISTO, Université d'Orléans CNRS BRGM, UMR7327, France

*corresponding author

1. Introduction

The Luneville castle, located in the North-East part of France, was built during the XVIIIth century with local Buntsandstein sandstones of various colourations. In January 2003, a violent fire affected the castle submitting building sandstones to an increase of their surface temperature and to an important volume of water (~21 m^3/min during ~10 hours). Several weeks later, black-brown patinas started developing on burnt parts of the castle (~8 % of the 1500 m² of exposed sandstones). Areas that have not been submitted to the accidental fire, may also present patinas formed over a long time range in natural environments as described for other buildings (Thomachot and Jeannette, 2004; Mertz, 2010). While it has been shown that the dark patinas contain iron oxides and sometimes manganese (oxihydr)oxides (Nord and Ericsson, 1993; Thomachot and Jeannette, 2004), the precise mineralogical compositions of these dark layers as well as their formation mechanisms remain to be determined. Besides, for given environmental solicitations (unburnt or burnt and watered area), and same period of implementation on the monument, the formation of dark stains is not systematic.

The main objective of this work is to characterise sandstone samples in order to identify intrinsic factors related to the development of the different patinas (short-time and long-time set-up). Chemical compositions of the rocks as well as storage and transfer properties of water in the sandstones have been measured, combining analytical techniques. Total rock chemical analyses have been obtained by Inductively Coupled Plasma-Optical Emission Spectrometry (ICP-OES). Optical microscopy (OM) and scanning electron microscopy coupled with Energy Dispersive Spectrosocopy (SEM-EDS) have been used to describe the samples and localize regions of specific interest which composition have been obtained by the Particle-Induced X-ray Emission (PIXE) method. The porous networks have been characterised by mercury intrusion porosimetry (MIP), capillary and permeability measurements.

2. Materials and methods

2.1. Materials

Buntsandstein sandstones (lower Triassic, ~250 My) are related with a deltaïc sedimentation environment (Perriaux, 1961 ; Colas 2011), and are mainly composed of quartz, K-feldspars, lithic fragments, micas, clay minerals and various oxides (Beyer, 1983; Soyk, 2015). The stone colouration is white for low Fe-content. For high Fe-content, colouration is yellow or red depending on the main Fe-bearing phase (goethite and hematite, respectively – Soyk, 2015). Most of the building stones of the castle are yellow.

Macroscopically similar (texture and grain size) pairs of yellow stones (patinated/unpatinated) have been sampled on site, in the burnt and highly watered (L2/L5) and unburnt (L1/L4) areas. The sampled volume is about 20×30×10 cm^3 for each block. Polished and unpolished sections, powders and cores had been prepared from the blocks. Information about the different preparations in terms of size, number of samples and performed analytical techniques are listed in table 1.

Tab. 1: Sample preparation and associated analytical techniques. N is the quantity per block.

Sample preparation	N	Analytical techniques
Polished section *(~15×15 mm²)*	1	OM, SEM-EDS
Unpolished section *(~15×15 mm²)*	1	OM, PIXE
Powder *(~2-3 g)*	1	ICP-OES
Core *(d=13 mm, h=9 mm)*	9	Mercury porosimetry
Core *(d=30 mm, h=60 mm)*	6 (4 for L1)	Capillarity, Permeability

2.2. Methods

OM pictures were obtained with a Keyence VHX-5000 microscope, with magnification ×20 or ×100. SEM-EDS observations were performed in backscattered electron mode, using a JEOL JSM 5600 LV SEM equipped with a tungsten filament operating at an accelerating voltage of 20 kV and using a low vacuum pressure (17 Pa) to avoid sample coating.

Bulk chemical compositions were determined from digested samples by ICP-OES at the Geochemical and Petrographic Research Center (CRPG, Nancy, F) following the procedure described in Carignan *et al.* (2001). PIXE analyses were performed on unpolished sections at the AGLAE facility using a proton energy of 3 MeV, and a 20 µm beam size. The detection system is detailed in Pichon *et al.* (2014).

The porous network of the four bulk samples was investigated by MIP using an Autopore IV Micrometrics® equipment. The applied pressures ranged 0.00226-206 MPa, corresponding to pore size radii of 270 µm and 0.003 µm, respectively. Three zones were selected for each block, and three measurements were made and averaged for each zone. Capillary imbibition measurements were conducted following the European standard procedure EN 1925. Cores were cut parallel to the bedding plans and their bases immersed in 3 mm of water. The kinetic coefficients of weight gain (A) and fringe's migration (B) were derived from Washburn equations. The average of the A and B coefficients have been calculated. Permeability values were acquired with a steady-state minipermeameter coupled with the software CYDAR™ (Cydarex Company, F). This is a non-destructive technique, which characterises the permeability until 21 mm depth in the sample. Air permeability measurements were averaged. For MIP, capillary and permeability measurements, error bars are equal to ± the standard deviation calculated for each analyzed zone.

3. Results and discussion

3.1. Visual description of the samples

Visual inspection of the four sandstone thin sections indicates great colour variability in patinated samples (L1 and L2 – Fig. 1). Yellow, orange and white stripes are observed in L1 parallel to the bedding and perpendicular to the exposed surface. Black dots, ~500 µm in diameter, are also distributed over the entire bulk. The coloured bands in L2 type are mostly brown and are combined with a series of different compaction zones. Consistent with the literature (Colas, 2011; Soyk, 2015) brown bands are likely related to Fe-oxihydroxides mixed with clay minerals. Non-patinated L4 and L5 are more homogeneous

than L1 and L2 and present uniform color and texture. However, small (~1 mm) over compacted zones and a mica-rich layer (~3 cm) are encountered in L4 and L5, respectively. The darker area observed on L5 (top left of the section – Fig. 1) is part of the mica-rich layer. For all samples, quartz grain size ranges 100-300 µm in diameter. The patina developed on L1 is ~350 µm thick while that on L2 is ~50 µm thick.

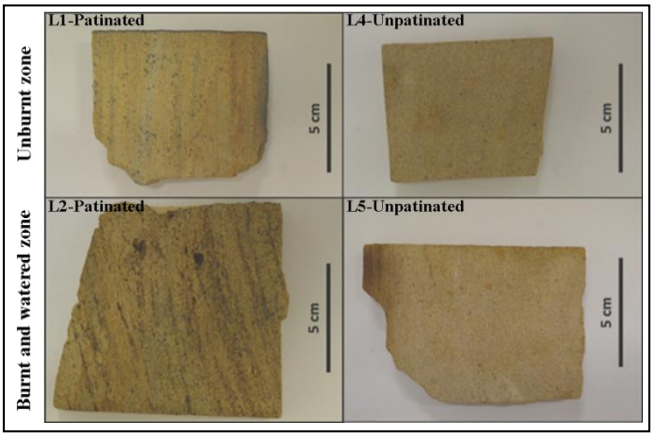

Fig. 1: Sample sections perpendicular to the bedding and to the surface. The exposed surfaces are positioned upward.

3.2. Storage and transfer properties

In order to obtain information on the properties of the porous networks and their variability in relation with texture, colour and compactness, porosity, capillary imbibition and permeability measurements have been performed for three areas of each block. The studied regions were chosen sufficiently far from the exposed surface, to ensure that the measurements are characteristic of the bulk sandstone. Core sizes for porosity measurements (13 mm in diameter) were chosen as small as possible to allow exploring millimetric heterogeneities in L1 and L4. By contrast, core size used for imbibition and permeability measurements (30 mm in diameter) is much greater than the size and the pattern of the heterogeneities. Measurements are reported in the Tab. 2 for the three zones.

MIP and capillary curves (not shown) are representative of unimodal pore size distributions and well-connected porous network. With total porosity values ranging from 18.5% to 26.1%, investigated samples rank among the most porous Buntsandstein sandstones (5%-25% - Thomachot and Jeannette, 2004; Colas, 2011). Permeability values from Luneville stones (87 to 880 mD) are typical for highly permeable quartzic sandstones (from 0.1 mD for not permeable to 1D for very permeable) (Gueguen and Palciaukas, 1992; Géraud, 2000). For all samples, capillary coefficients B lead to saturation times of a few hours for 60 mm sample length (2h56 for L1, 2h02 for L4, 1h00-1h34 for L2, and 1h09-2h38 for L5). Over 10 hours of continuous water flow such as long rainy episodes or during the 2003 fire extinction, at least 11 cm of rock may be invaded by water (considering the smallest B coefficient: 3.5 $cm \cdot h^{-1/2}$). Therefore, even if the cores were taken as far as possible from the surface, they may have been modified by the interaction with water and may not be representative of original sandstones.

*Tab. 2: MIP data (N_{Hg}=porosity), capillary (A and B) and permeability (K) coefficients. Grey lines correspond to patinated samples. UB (resp. B) corresponds to unburnt (resp. burnt) area. *****A, B and K values for L2 and L5 represent the average of measurements performed on 2 cores sampled in 3 different zones. A, B and K values for L1 (resp. L4) represent the average of measurements performed on 4 cores (resp. 6) sampled throughout the volume.*

	Sample	Zone	N_{Hg} (%)	A* ($g \cdot cm^{-2} \cdot h^{-1/2}$)	B* ($cm \cdot h^{-1/2}$)	K* (mD)
UB	L1	Orange	21.7 ±0.8	0.290 ±0.046	3.5 ±0.2	150 ±65
		white-yellow	21.6 ±0.3			
		Yellow	21.3 ±0.2			
	L4	White	21.6 ±0.9	0.388 ±0.019	4.2 ±0.2	118 ±41
		pale yellow	23.1 ±0.2			
		yellow	24.1 ±0.5			
B	L2	lightly uncompacted	23.9 ±0.1	0.433 ±0.001	4.8 ±0.2	759 ±34
		brown and uncompacted	26.1 ±1.7	0.549 ±0.028	5.3 ±0.4	880 ±245
		clearer	24.8 ±0.6	0.521 ±0.083	6.0 ±0.5	473 ±76
	L5	yellow	25.2 ±0.2	0.465 ±0.001	5.3 ±0.0	859 ±12
		yellow	24.8 ±0.2	0.490 ±0.041	5.6 ±0.2	632 ±1
		mica-rich layer	18.5 ±0.4	0.276 ±0.002	3.7 ±0.1	87 ±3

L1 shows important colour variability but the different coloured zones have similar porosity values. By contrast, for L4, porosity values are lower in the millimetric white over-compacted areas than in the yellow areas. In the L2 sample, the variability of all measured parameters from one zone to the other suggests a high heterogeneity. In L5, the two yellow areas studied have similar characteristics, whereas the mica-rich layer presents poorer storage and transfer properties. The unburnt blocks are more homogeneous than the burnt ones. Burnt blocks (L2 and L5) are more porous, more permeable, and have higher capillary properties than their unburnt counterparts. These characteristics are possibly related to the original block variability as the values are systematically consistent with those of Buntsandstein sandstones. But it could also be assumed that the amount of water used to drown the fire (~12720 m^3 i.e. ~2 l per block) was sufficient to saturate the porous network (1.1 l and 1.6 l for 18.5% and 26.1% porosity, respectively) thus inducing dissolution of mineral phases and porosity increase. Comparison of patinated samples (L1 and L2) with non-patinated samples (L4 and L5) does not lead to clear conclusions. L4 has slightly higher porous and capillary properties than L1, the two blocks having similar permeability. Except for the mica-rich zone in L5, which represents only a small part of its volume, L2 and L5 have similar macroscopic properties.

3.3. Chemical composition of the bulks and Mn content

Elemental bulk-rock analyses are given in Tab. 3. As for the other measurements, the powders have been produced from sandstone sampled as far as possible from the surface, to avoid its contribution. The concentrations of major elements are similar for all samples and lie in range known for Buntsandstein sandstones with high concentrations of oxides (Fe, Mn, Ti, P – Beyer, 1983; Thomachot et Jeannette, 2004; Colas, 2011). L2 is significantly enriched in Fe, which is consistent with the presence of numerous brown bands. The patinated blocks are also richer in Mn than the other ones (L1 is the richest and [Mn] is 10× larger in L2 than in L5).

Tab. 3: Sulphur content, ICP average chemical composition (oxide wt %) and loss of ignition (LOI) at 1000°C (in %) of the four bulks. Grey lines correspond to patinated samples. UB (resp. B) corresponds to unburnt (resp. burnt) area. Uncertainties are <20% for S, <15% for Ca, Na, and P, <10% for Mn, Mg, and Ti, <5% for K and LOI, <2% for Fe, <1% for Si, Al

Sample	SiO_2	Al_2O_3	Fe_2O_3	MnO	MgO	CaO	Na_2O	K_2O	TiO_2	P_2O_5	SO_3	LOI	Total
UB-L1	83.33	7.32	1.33	0.24	0.23	0.14	0.17	3.47	0.56	0.11	0.13	2.21	99.24
UB-L4	83.42	7.58	1.82	0.06	0.20	0.14	0.12	4.01	0.38	0.07	0.35	2.26	100.41
B-L2	81.56	7.02	3.64	0.10	0.14	0.16	0.14	4.36	0.23	0.12	0.08	1.80	99.35
B-L5	85.29	7.66	0.70	0.01	0.19	0.15	0.15	4.25	0.49	0.12	0.08	1.58	100.67

3.4. Mn-bearing phases in the bulk sandstones

Representative OM and SEM-EDS observations of the Mn-rich zones of L1 and L2 polished sections are shown in Fig. 2. Mn-rich zones in L5 and most Mn-rich zones in L4 are similar to those in L2. L4 presents a few zones similar to L1. Most Mn-rich zones in L1 appear as black dots distributed in the sandstone volume. In L2, Mn is mostly concentrated in very large stains (~500 μm) with red-brown and dark-brown colours. The Mn-rich areas are clearly more abundant in the patinated blocks. PIXE analyses were conducted on a Mn-rich area for each block (Tab. 4). For better clarity, only elements showing significant differences (i. e. Mn, Fe, Ba) are reported in the table. Mn concentrations in patinated samples (L1 and L2) are significantly higher than in their non-patinated counterparts (L4 and L5, respectively). Mn concentration is the highest in the L1 sample (between ×14 and ×54 as compared to Mn-rich areas in the other sandstones). By contrast with L2, L4 and L5, Mn-rich stains in L1 are characterised by a high Ba-content suggesting either the occurrence of Mn-Ba oxides, such as romanechite, hollandite, or todorokite, or the coexistence of Ba- and Mn-bearing phases. The absence of Ba in L4 black spots suggests the sole presence of Mn-bearing phases. No indication about the possible similarity between the phases can be deduced from chemical analyses. In L2, as in L5, Mn is less abundant as compared to unburnt sandstones, and is always associated with iron, which prevails over these areas. X-ray diffraction analyses (not shown) and morphological observations allowed identifying goethite as the main Fe-bearing mineral. It is known that Mn can be mixed with goethite, mainly as phyllomanganate (Manceau *et al.*, 2000), we can thus suspect such phases.

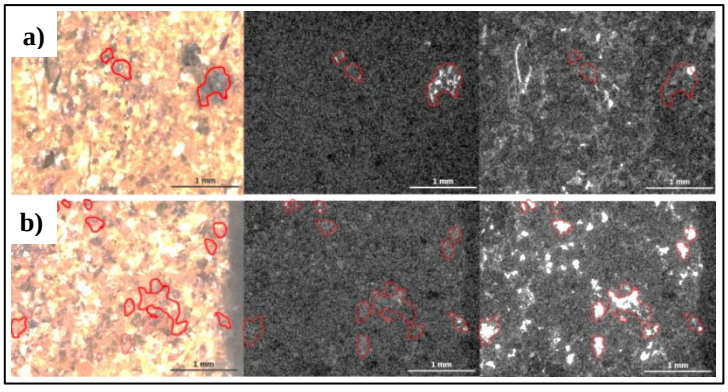

Fig. 2: Mn-bearing phases, circled in red, (a) in L1 and (b) in L2. Views on polished sections with, from left to right, optical microscopy, Mn and Fe maps obtained with EDS.

Tab. 4: PIXE analyses (oxide weight %) of Mn, Fe and Ba contained in Mn-rich areas (surfaces in µm²). Grey lines correspond to patinated samples.

Sample	Analysed surface	Fe_2O_3	MnO	BaO
L1	~500×300	3.16 ± 0.05	12.48 ± 0.06	11.91 ± 1.28
L4 *(L1-like)*	~200×200	2.37 ± 0.02	0.89 ± 0.01	0.00 ± 0.00
L2	~500×300	53.98 ± 0.51	0.69 ± 0.01	0.00 ± 0.00
L5	~200×400	24.89 ± 0.14	0.23 ± 0.01	0.00 ± 0.00

4. Conclusions and perspectives

Coupling analytical techniques allowed gaining information about the factors influencing the formation of a Mn-rich patina. A possible mechanism could be that Mn-compounds initially present in the sandstones might be dissolved by water (acid rains or water used to stop the 2003 fire) and transported through the porous network, from rock core towards their surface, to feed Mn-rich patina formation as it is assumed for Fe-rich patinas (Nord and Ericsson, 1993). Therefore, since the Luneville castle sandstones have good transfer properties, the main intrinsic parameter conditioning a patina development would be the quantity of Mn initially available in the stone volume impacted by the water, and the solubility of Mn-bearing phases initially present. Indeed, chemical analyses show that patinated blocks are enriched in Mn as compared non-patinated ones. Moreover, Mn appears to be located in specific zones, but in association to different chemical elements according to the sample considered. Determination of the nature of the Mn-bearing phases is thus needed to better constrain the Mn-rich patina formation mechanism. Getting information on Mn-bearing phases is however technically difficult. Laboratory X-ray Diffraction (XRD) experiments did not permit identifying the Mn-bearing phases due to their low content (0.1 and 0.24 weight % of MnO in patinated blocks L2 and L1, respectively) as compared to the total rock. µ-XRD and X-ray absorption spectroscopy at the synchrotron SOLEIL facility (Saint-Aubin, France) on Mn-rich areas will be conducted

in order to help identifying the minerals by coupling structural information with Mn oxidation states.

Acknowledgments

We thank the FLB Company for their financial support and their interest, with a special thanks to Recep Yildirim. We also thank the AGLAE team, especially Quentin Lemasson, for the PIXE analyses, and Mikaël Guiavarc'h for his help with the sample preparations.

References

Beyer, D., 1983, Evolution of reservoir properties in the Lower Triassic aquifer sandstones of the Thuringian Syncline in Central Germany, Dissertation, Friedrich Schiller University Jena, Germany.

Carignan, J., Hild, P., Mevelle, G., Morel, J., Yeghicheyan, D., 2001, Routine analyses of trace elements in geological samples using flow injection and low pressure on-line liquid chromatography coupled to ICP-MS: a study of geochemical reference materials BR, DR-N, UB-N, AN-G and GH, Geostandard Newsletter, 25, 187-198.

Colas, E., 2011, Impact de l'humidité et des solutions salines sur le comportement de grès du Buntsandstein: contribution à la sélection de faciès de restauration, Ph.D. thesis, Reims Champagne-Ardenne University, France.

Géraud,Y., 2000, Perméabilité des roches et loi de Darcy, Planet Terre ENS Lyon, http://planet-terre.ens-lyon.fr/article/permeabilite-des-roches.xml.

Gueguen, Y., Palciaukas, V., 1992, Introduction à la physique des roches, éd. Hermann, ISBN 2-7056-6138-0, 296.

Manceau, A., Schlegel, M. L., Musso, M., Sole, V. A., Gauthier, C., Petit, P. E., Trolard, F., 2000, Crystal chemistry of trace elements in natural and synthetic goethite, Geochimica et Cosmochimica Acta, 64, 3643-3661.

Mertz, J-D., 2010, Etat des lieux, diagnostic des pathologies et perspectives, in: Un chantier, restauration des façades des monuments urbains, Ministère de la Culture et de la Communication, OPPIC, ISBN 978-2-915755-27-5, 8-13.

Nord, A. G., Ericsson, T., 1993, Chemical analysis of thin black layers on building stone, Studies in conservation, 38, 25-35.

Perriaux, J., 1961, Contribution à la géologie des Vosges gréseuses, Mémoires du service de la carte géologique d'Alsace et de Lorraine N°18, Strasbourg University, 236.

Pichon, L., Moignard, B., Lemasson, Q., Pachero, C., Walter, P., 2014, Development of a multi-detector and a systematic imaging system on the AGLAE external beam, Nuclear Instruments and Methods in Physics Research B, 318, 27-31.

Soyk, D., 2015, Diagenesis and reservoir quality of the Lower and Middle Buntsandstein(Lower Triassic), SW Germany, Dissertation, Heidelberg University, Germany.

Thomachot, C., Jeannette, D., 2004, Effects of iron black varnish on petrophysical properties of building sandstone, Environmental Geology, 47, 199-131.

SMART HYDROPHOBIC TIO_2-NANOCOMPOSITES FOR THE PROTECTION OF STONE CULTURAL HERITAGE

F. Gherardi[1*], A. Colombo[2], S. Goidanich[1] and L. Toniolo[1]

Abstract

This study presents the set-up of photocatalytic hydrophobic TiO_2-nanocomposites and the assessment of their application in stone heritage conservation. TiO_2 nanoparticles were synthesized according to the non-aqueous route obtaining pure anatase phase nanoparticles with an opportune surface capping, which makes titania dispersible in aqueous systems and photo-active not only under UV radiation but also under solar light, thus enhancing its ability to degrade pollutants. Nanocomposite films were obtained by mixing different ratios of nanoparticle dispersions in commercial aqueous polymeric solutions. SEM analyses of the treated marble samples show crack-free coatings. The nanocomposites-based treatments do not affect the original colour of the specimens, which show a decrease in the water capillary absorption. By increasing the nanoparticles content, an enhancement of the static contact angles of the surfaces occurs, compared to both the untreated reference and the reference samples treated with the pristine polymers. The Rhodamine fading test after ageing in solar box with a Xenon lamp shows that the highest photocatalytic activity is achieved by specimens treated with the nanocomposites with the highest nanoparticles content. In order to evaluate the eventual degradation of the polymeric matrices due to the photoactive TiO_2 nanoparticles and the durability of the nanocomposites, accelerated ageing in a solar box were performed. The obtained results prove the effectiveness of the proposed TiO_2-based nanocomposites as protective coatings for stone surfaces of built heritage.

Keywords: self-cleaning, hydrophobic, TiO_2-nanocomposites, artificial ageing, marble

1. Introduction

In urban area, cultural heritage surfaces are soiled by the accumulation of pollutants, which can contribute to the formation of crusts, affecting the buildings from both the aesthetical and chemical point of view. In order to prevent the weathering of stone surfaces and protect them, water-repellent polymer coatings have been used, thanks to their ability to reduce the water-stone interface tension and to increase its water repellency. Different classes of polymeric coatings have been applied in the field of stone conservation (Tsakalof *et al.* 2007). Among them, acrylics have been used in the last decades even if the

[1] F. Gherardi*, S. Goidanich and L. Toniolo
Department of Chemistry, Materials and Chemical Engineering "Giulio Natta",
Politecnico di Milano, Italy
francesca.gherardi@polimi.it

[2] A. Colombo
Fondazione CIFE, Italy

*corresponding author

performances in terms of durability were not satisfactory (Favaro *et al.* 2006). Partially fluorinated and perfluoropolymers were developed with the aim to improve the water repellent behaviour and the resistance to photodegradation of nonfluorinated polymers (Ciardelli *et al.* 2000). Nowadays, alkyl-aryl-polysiloxanes products are the most used in the restoration field, since they show higher durability and stability than acrylics (Tesser *et al.* 2014), though they are not always appropriate for every lithotype (Tsakalof *et al.* 2007, Charola 2002).One of the strategy to enhance the hydrophobicity of the coatings is to increase the surface roughness, without changing the substrate morphology, by dispersing nanoparticles in polymeric films. If these surfaces are exposed to rainfall, water forms spherical droplets which roll away, removing dust and dirt. To achieve this goal, solutions of different polymer have been modified by adding different nanoparticles, increasing their protective efficiency, conferring super-hydrophobic (water contact angle > 150°) and self-cleaning properties (Manoudis *et al.* 2008). Different nanoparticles have been used for this aim and among them nano-TiO_2 are one of the most common, since their introduction into the polymeric matrix confers photocatalytic properties to the surface (Fujishima *et al.* 2008). Indeed, thanks to their photoactivity, nano-TiO_2 can lead to the breakdown both organic and inorganic compounds, which can be easily washed away by rainfall, with a reduction of time and costs for cleaning maintenance (Munafò *et al.* 2015). In the set-up of the proposed nanocoatings, TiO_2 nanoparticles have been selected because they contain pure phase anatase which are characterised by the presence of benzyl alcohol molecules anchored on their surfaces. This surface capping makes the nanocrystals photoactive even if exposed to solar irradiation, increasing their photoefficiency. Moreover, as reported in a previous study (Gherardi *et al.* 2015), the proposed nanoparticles allow to obtain highly stable dispersions in aqueous systems, preserving the aesthetic compatibility with stone substrates. The results obtained from the tests that are shown in this paper proved that the proposed nanocoatings present better effectiveness compared to pristine polymers commonly used as stone protective treatments as they demonstrate higher aesthetic compatibility, lower capillary water absorption and higher hydrophobicity of the stone surfaces.

2. Experimental procedure

2.1. Preparation of TiO_2-based nanocomposites and application on stone

TiO_2 nanoparticles have been synthetized according to a non-aqueous synthesis (Niederberger *et al.* 2002), by using benzyl alcohol and titanium (IV) tetrachloride, as solvent and precursor respectively, as reported in a previous paper (Colombo *et al.* 2012). This synthesis enables the formation of anatase primary nanocrystals of about 5–6 nm diameter which aggregate in elongated clusters whose the longest axis measures about 40 nm. Water dispersions of TiO_2 nanoparticles with a concentration of 3 % by weight were used for the preparation of nanocomposites. The pristine polymers used as references are commercial aqueous dispersion of fluoropolyethers (*Fluoline PE*, *CTS srl*, labelled as F REF) and aqueous dispersion of organosiloxanes (*Silo 112*, *CTS srl*, labelled as S REF). Nanocomposites were prepared by adding different ratios of the nanoparticles dispersion in the polymeric solutions. In particular, polysiloxane-based films were obtained with the following concentrations of nanoparticle in the polymer: 16 wt.%, 28 wt.% and 44 wt.% (labelled as S16, S28 and S44) whereas for fluoropolyethers-based only the nanoparticles concentration of 16 wt.% (labelled as F16) was used, since the use of higher concentrations did not allow the preparation of stable blends. Samples of Carrara marble with 50×50×10

mm and 50×50×20 mm sizes were washed with deionized water and dried at room temperature until a constant mass was achieved. Then, the nanocomposites were applied on their surfaces by brush. For comparison, untreated stone samples were analysed (named NT).

2.2. Evaluation of the effectiveness of TiO_2-based nanocomposites applied to stones specimens

The morphology of the stone surfaces before and after the application of the nanocoatings was analysed by Environmental Scanning Electron Microscopy (ESEM) and EDS analyses, using a Zeiss EVO 50 EP ESEM, equipped with an Oxford INCA 200 - Pentafet LZ4 spectrometer. The evaluation of the aesthetical compatibility with the stone was carried out by spectrophotometric measurements by a Konica Minolta cm-600D instrument, with a D65 illuminant at 8°, wavelength range between 360 nm and 740 nm. The data were elaborated according to the CIE *L*a*b** standard colour system and the average results of *L*a*b** were used to calculate the colour difference ΔE* between treated and untreated areas: $\Delta E^* = [(L_2^* - L_1^*)^2 + (a_2^* - a_1^*)^2 + (b_2^* - b_1^*)2]^{1/2}$ *[Eq.1]*. Static contact angle and capillary water absorption tests were performed in room conditions, without exposing the samples to solar lamps or UV light in order to evaluate the wettability changes and water absorption of the stone surfaces after the application of the nanocomposites. Static contact angle was evaluated on 15 points for each sample, using an OCA (Optical Contact Angle) 20 PLUS (DataPhysics, Germany), with a drop volume of 5 µl, after 10 seconds. The drop shape was recorded with a camera and the angle between the substrate surface and the tangent from the edge to the contour of the water drop (contact angle) was evaluated. The capillary water absorption of the stone samples was performed on 50×50×20 mm stone samples before and after the application of the dispersions in room conditions. The capillary water absorption value per unit area (Q_i,expressed in mg/cm^2) is defined with the expression: $Q_i = (m_i - m_0)/A*1000$ *[Eq.2]*, where m_i is the mass (g) of the wet sample at time t_i, m_0 is the mass (g) of the dried sample, A is the surface area (cm^2) in contact with the water. The samples were weighed at the following time intervals: 10 min, 20 min, 30 min, 60 min, 4 h, 6 h, 24 h, 48 h, 72 h, 96 h. The relative capillary index (CI rel) was calculated with the equation: $CI_{rel} = \int_{t0}^{tf} f(Q_i)_{tr}dt / \int_{t0}^{tf} f(Q_i)_{ntr}dt$ *[Eq.3]*, where $\int_{t0}^{tf} f(Q_i)_{tr}dt$ is the area under the absorption curve of the treated specimen (tr) and $\int_{t0}^{tf} f(Q_i)_{ntr}dt$ is the area under the absorption curve of the untreated specimen (utr). The photocatalytic activity of the stone surfaces treated with nanocomposites was assessed by decomposition tests of an organic colorant, which was applied as aqueous solution of rhodamine B (0.05 g/l ± 0.005 g/l) to the surface of both untreated and treated samples. The degradation of the applied organic dye was monitored by evaluating the colour change of the surface (using a VIS spectrophotometer, as previously described) exposed in a Suntest CPS$^+$ solar box, equipped with a Xenon arc lamp source and a cut off filter for wavelengths below 290 nm. The irradiance was 765 W/m^2, at the temperature of 35°C. In literature, other authors performed the test with the explosion of the samples to UV light, however, Xenon lamp was selected to simulate the real conditions of outside exposed treated stones because it emits radiations similar to those of solar light. The colorimetric measurements were performed after 15, 30, 60, 90 and 150 minutes of irradiation. The chromatic coordinate *a** was used to evaluate the photocatalytic discoloration of stain D* over time, by the equation: $D^* = (|a^*(t) - a^*(rB)|/|a^*(rB) - a^*(0)|*100$ *[Eq.4]*, where *a**(0) and *a**(rB) are the average values of the chromatic coordinate *a** before and after the application of the stained solution and *a**(t) is

the a^* value after t hours of light exposure. Finally, in order to evaluate the eventual degradation of the polymeric matrices due to the presence of photoactive of TiO_2 nanoparticles in the nanocomposites, accelerated ageing of the nanocomposites cast on glass slides in a solar box were performed as described above, for 750 h. The ageing of the films was followed by Fourier Transform Infrared Spectroscopy (FTIR) by using a Nicolet 6700 spectrophotometer coupled with a Nicolet Continuum FTIR microscope equipped with a MCT detector (acquired between 4000 and 600 cm^{-1} with 128 acquisitions and 4 cm^{-1} resolution). Spectra of micro samples were recorded using a micro compression diamond cell accessory and they were normalized on the intensity of the Si-O stretching (at 1100 cm^{-1}) for polysiloxane-based films and on F-C stretching (at 1200 cm^{-1}) for fluoropolymer-based films.

3. Results and discussion

ESEM/EDS analyses were performed on treated and untreated surfaces of Carrara marble. Fig. 1 reports the images of Carrara marble treated with the fluoropolyether (F REF) and the fluoropolyether-based nanocomposite (F16): darker areas on the surface represent the areas where the coatings accumulate. Both the pristine polymer and the nanocomposite are not homogeneously distributed on the stone specimens (Doehne and Price 2010). On the contrary, organosiloxanes-based coatings create crack-free films, with a homogenous distribution of TiO_2 nanoparticles in the blends cast on the stone (Fig. 2).

To verify the respect of the original aesthetic properties of the surface, colour measurements were performed on stone specimens before and after the application of the treatments. Tab. 1 summarizes the value of colorimetric coordinates L^*, a^*, b^* and ΔE^* of the stone before and after the application of the fluoropolymer (F REF), polysiloxane (S REF) and the coatings with nano-TiO_2 (F16, S16, S28 and S44).The values of ΔE^* were lower than 4 for every treatment but, in general, the application of the nanocoatings leads to lower ΔE^* values compared to the polymers (F REF and S REF). In particular, among surfaces treated with polysiloxane-based nanocoatings, ΔE^* values decrease with the increase of the nano-TiO_2concentration, since they present lower differences of L^* and b^* compared to those of the surface before the application of the treatments. This is due to the whitening effect of nano-TiO_2 towards the slight yellow colour of the polymer.

Static contact angle measurements were carried out on Carrara marble specimens in order to monitor the wettability change of the surface after the application of the treatments. As presented in Tab. 1, compared to the untreated specimen (NT), the treated specimens show higher value of contact angle θ, since the polymers reduce the wettability of the surface. Moreover, compared to the surfaces treated with the pristine polymers (F REF and S REF), the application of the nanocomposites (F16, S16, S28 and S44) increases the contact angle values, as the nanoparticles creates surface nanoroughness. Indeed, by increasing the nanoparticles concentration in the blends, higher values of contact angles were measured.

To study the change of water absorption by capilalrity, the relative capillary index (CI_{rel}) was selected as representative parameter. As shown in Tab. 1, the values of $CI_{rel,}$ obtained from specimens treated with the nanocomposites are lower compared to the pristine polymers, indicating that the addiction of nanoparticles further inhibit the water absorption by the stone surfaces. The reduction of water absorption is less evident in fluoropolymer-based nanocomposite (F16) compared to polysiloxane-based nanocomposites (S16, S28 and

S44), probably due to the poor distribution of the film on Carrara marble surface. Moreover, no relevant changes in CI_{rel} were obtained by increasing the concentration of TiO_2 nanoparticles in the blends.

Fig. 3 reports the trend of rhodamine B discoloration (*D**%) with time, after pre-fixed intervals of exposition to Xenon lamp irradiation, of stone specimens either untreated (NT) or treated with pristine polymers (F REF and S REF) and with the nanocomposites (F16, S16, S28 and S44). Compared to both the untreated specimen and the specimens with the pristine polymers, the *D** values are higher for nanocomposites, confirming the photocatalytic properties of nano-TiO_2. In addition, the photocatalytic activity of specimens increases with the increase of nano-TiO_2 in the blends. However, a less photo-efficiency is achieved by F16 compared to S16 as the maximum *D**% value obtained by specimen treated with F16 is 56% whereas for S16 is 81%. This is probably related to the lower amount of nanocomposite on the surface and able to confer photoactivity to the stone surface.

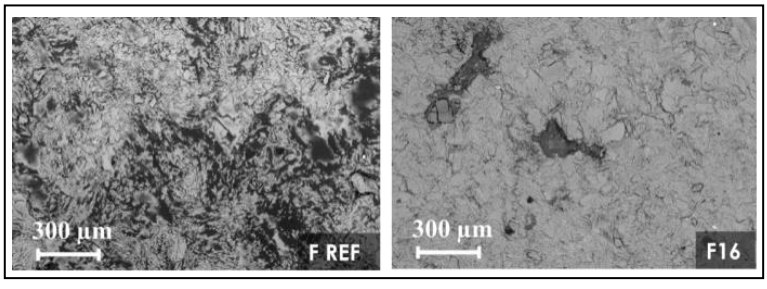

Fig. 1: ESEM/EDS characterization of Carrara marble surface treated with F REF (left) and F16 (right).

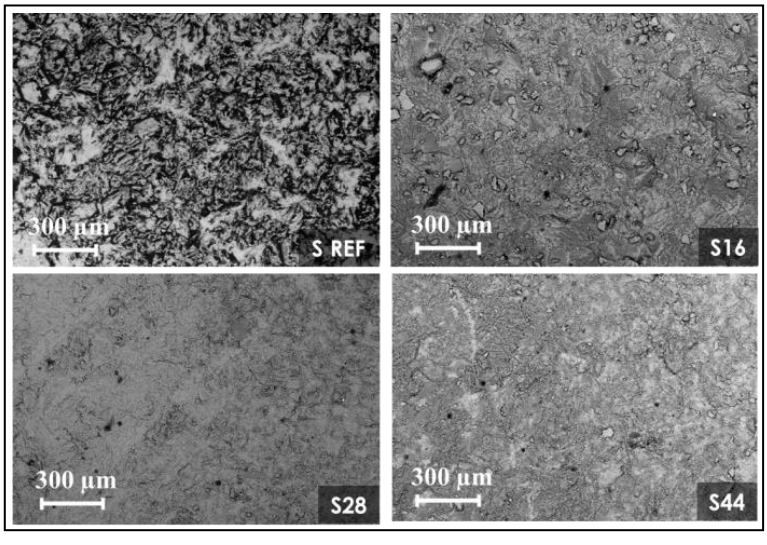

Fig. 2: ESEM/EDS characterization of Carrara marble surface treated with S REF, S16, S28 and S44, from left to right, from top to bottom.

Tab. 1: Colorimetric coordinates L, a*, b* and ΔE* of the stone before and after the application of fluoropolymer (F REF) and polysiloxane (S REF) and nanocoatings (F16, S16, S28 and S44) and average values of static contact angle (ϑ) and relative capillary index (CI_{rel}) of untreated and treated specimens.*

	Before the treatments			**After the treatments**					
	*L**	*a**	*b**	*L**	*a**	*b**	*ΔE**	*θ*	CI_{rel}
F REF	87.17	-0.77	0.35	85.39	-0.94	2.49	2.79	106.13	0.77
F16	89.24	-0.68	0.21	89.01	-0.68	0.33	0.26	135.68	0.73
S REF	86.90	-0.65	0.21	83.21	-0.77	1.20	3.82	95.34	0.78
S16	87.65	-0.74	0.45	85.09	-0.84	1.17	2.66	128.79	0.52
S28	87.27	-0.64	-0.14	85.37	-0.65	0.44	1.99	138.40	0.44
S44	86.21	-0.76	0.74	84.60	-0.83	1.41	1.75	142.49	0.48
NT								48.31	

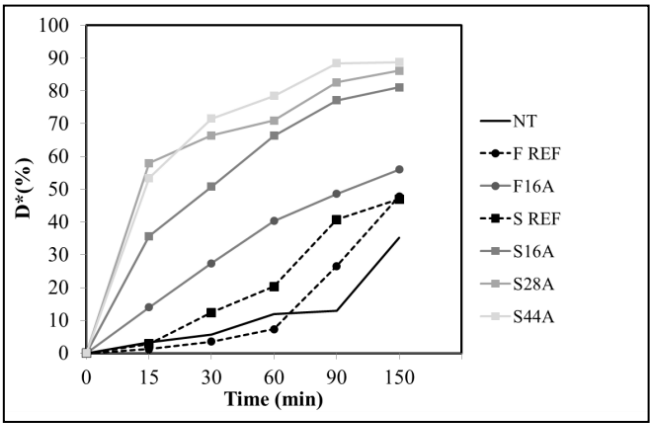

Fig. 3: Stain discoloration values D (%) as a function of time (min.) for untreated and treated Carrara marble after pre-fixed intervals of irradiation in solar box.*

Finally, both the pristine polymers and the nanocomposites were cast on glass slides and artificially aged in a irradiation chamber with a Xenon arc lamp source. The films were analysed by FTIR spectroscopy after 750 h of accelerated ageing. After the ageing, both siloxanes and fluorinated nanocomposites showed stability, due to the fact that no macroscopic defects (yellowing, cracks) were observed. As reported in Figures 4 and 5, compared to the spectra obtained from unaged film, the spectra from both aged pristine polymers (F REF and S REF) and aged nanocomposites (F16 and S16), show the presence of peaks at 1720 and 1740 cm^{-1} (C=O stretching) and the increase of the wide band between 3100-3400 cm^{-1} (OH stretching), due to the formation of new compounds (esthers). However, the chemical changes in nanocomposites are more evident compared to the aged pristine polymers.

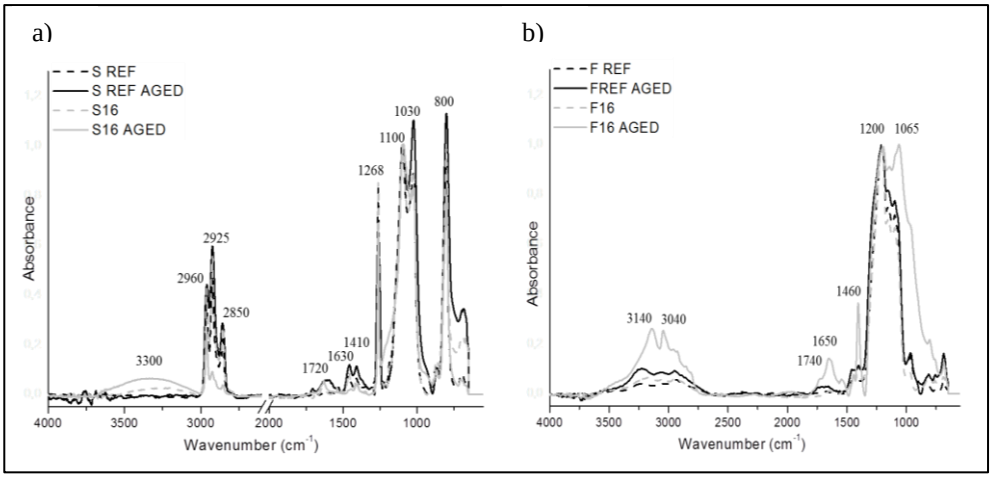

Fig. 4: FTIR spectra of F REF and F16 before and after 750 h of accelerated ageing in a Xenon solar irradiation chamber (a), FTIR spectra of S REF and S16 before and after 750 h of accelerated ageing i in a Xenon solar irradiation chamber (b).

4. Conclusions

The present study reports the development of formulations of nanocomposites, obtained by mixing different ratios of nano-TiO_2 dispersions in commercial aqueous polymeric solutions. According to ESEM/EDS analyses, both fluoropolymer (F REF) and fluoropolymer-based nanocomposite (F16) provide inadequate treatments from the morphological point of view, due to their poor distribution on the stone surfaces. On the contrary, polysiloxane-based nanocomposites are homogeneously distributed on the surfaces. Both the fluoropolyether and organosiloxanes-based nanocomposites do not affect the original colour of the specimens, which show also a decrease in the water capillary absorption. By increasing the nanoparticles content, an increase of the static contact angles of the surfaces occurs due to the increase of the surface roughness. Moreover, polysiloxane-based nanocoatings show higher photo-efficiency compared to the fluoropolymer-based coatings. Accelerated ageing prove that both siloxanes and fluorinated nanocomposites show stability, as no macroscopic defects are observed. However, FTIR spectra demonstrate that the presence of TiO_2 nanoparticle accelerate the degradation of the nanocomposites compared to the polymers, with the formation of new compounds. The results obtained from accelerated ageing of the nanocomposites will be compared with those obtained from nanocoatings applied on marble blocks in a pilot-areas on the façade of Duomo di Monza, where monitoring tests to assess their durability are currently underway. Nevertheless, the preliminary results prove the effectiveness of the proposed polysiloxane-based nanocomposites as self-cleaning and protective treatments for marble surfaces.

References

Charola, AE., 2001, Water Repellents and Other "Protective" Treatments: A Critical Review, in proceedings of Hydrophobe III - 3rd International Conference on Surface Technology with Water Repellent Agents, Aedificatio Publishers, Hannover, 3-19.

Ciardelli, F., Aglietto, M., Castelvetro, V., Chiantore, O., Toniolo, L., 2000, Fluorinated polymeric materials for the protection of monumental buildings, Macromolecular Symposia, 152(1), 211-222.

Colombo, A., Tassone, F., Mauri, M., Salerno, D., Delaney, J.K., Palmer, M.R., Rie. R.DL, Simonutti, R., 2012, Highly transparent nanocomposite films from water-based poly(2-ethyl-2-oxazoline)/TiO_2 dispersions, RSC Advances, 2(16), 6628-6636.

Doehne, E.F., Price, CA., Stone conservation: an overview of current research, 2010, Getty Conservation Institute, 16060604652010, 176.

Favaro, M., Mendichi, R., Ossola, F., Russo, U., Simon, S., Tomasin, P., Vigato, PA.,2006, Evaluation of polymers for conservation treatments of outdoor exposed stone monuments. Part I: Photo-oxidative weathering, Polymer Degradation and Stability, 91(12), 3083-3096.

Fujishima, A., Zhang, X., Tryk, D.A., TiO2 photocatalysis and related surface phenomena, 2008, Surface Science Reports, 63(12), 515-582.

Gherardi, F., Colombo, A., D'Arienzo, M., Di Credico, B., Goidanich, S., Morazzoni, F., Simonutti, R., Toniolo L., 2015, Efficient self-cleaning treatments for built heritage based on highly photo-active and well-dispersible TiO2 nanocrystals, Microchemical Journal, accepted

Manoudis, P.N., Karapanagiotis, I., Tsakalof, A., Zuburtikudis, I., Panayiotou, C., 2008, Superhydrophobic composite films produced on various substrates, Langmuir, 24(19), 11225-11232.

Munafò, P., Goffredo, G.B., Quagliarini, E., 2015, TiO_2-based nanocoatings for preserving architectural stone surfaces: An overview, Construction and Building Materials, 84, 201-218.

Niederberger, M., Bartl, M.H., Stucky, G.D., 2002, Benzyl alcohol and titanium tetrachloride - A versatile reaction system for the nonaqueous and low-temperature preparation of crystalline and luminescent titania nanoparticles,Chemistry of Materials, 14(10), 4364-4370.

Tesser, E. Antonelli, F., Sperni, L., Ganzerla, R., Maravelaki, N.P., 2014, Study of the stability of siloxane stone strengthening agents, Polymer Degradation and Stability, 110, 232-240.

Tsakalof, A., Manoudis, P., Karapanagiotis, I., Chryssoulakis, I., Panayiotou, C, 2007, Assessment of synthetic polymeric coatings for the protection and preservation of stone monuments, Journal of Cultural Heritage, 8(1), 69-72.

SALT EXTRACTION BY POULTICING UNRAVELLED?

S. Godts[1*], H. De Clercq[1] and L. Debailleux[1]

Abstract

A common applied method for the extraction of salt from contaminated building materials is the use of poultice materials. However, the application of a poultice in-situ is often random depending on the personal experience of the conservator or the manufacturer. The effect remains uncontrolled and insufficiently understood despite extensive research in this field. The prior evaluation of execution parameters is crucial for the success of a salt extraction, such as, the composition and application method of a poultice. Therefore the optimum conditions for a salt extraction can never be considered a copy-paste procedure. This paper describes the results of further investigation into some execution parameters, such as, the conditions of pre-wetting, the number and efficiency of poultice applications, and this in relation to the salt content and distribution within the depth of the materials. Moreover, the effect of climatic conditions is considered to support the evaluation of results. Experimental results are compared to theoretical approaches through computer modelling. The results indicate that the efficiency of a poultice is low and the water distribution within the depth of the substrate is an important factor to consider as salts are being evenly distributed up to the boundary where migration of water occurs. Results from laboratory tests and modelling indicate that the more water used the better the salt extraction effect. However, in practice, the humidification effect of pre-wetting and poultice application may also lead to redistribution of salts deeper within the material, towards dryer or less salt contaminated parts of the material. Furthermore, salts tend to accumulate in capillary active joint mortars behind the stones or bricks. Due to these complications, the assessment of the effect of a salt extraction is often misinterpreted. It seems that repeatedly wetting the surface can result in a similar outcome in terms of salt redistribution as poulticing.

Keywords: salt extraction, salt damage, poultice, water transport, case studies, building material

1. Introduction

The crystallization of salts is an important cause of damage to historic built heritage, murals and stone sculptures. Compared to new buildings, historic ones suffer more from salt damage due to their higher salt contamination accumulated over time. Mitigating of salt damage contributes to a sustainable preservation of our precious historical and architectural heritage. The occurrence of salt damage implies the presence of salts and moisture, in liquid

[1] S. Godts*, H. De Clercq and L. Debailleux
Monuments and monumental decoration laboratory - Royal Institute for Cultural Heritage (KIK-IRPA), Belgium
sebastiaan.godts@kikirpa.be

*corresponding author

or vapour form. Moisture can be regarded as the main catalyst for salt damage; without moisture transport processes and dissolution-crystallization cycles of the salts there would be no salt damage of porous material (Sawdy *et al.*, 2008).

While the removal of salts from movable stone objects by means of the water bath method is quite well known (Franzen *et al.*, 2008), salt extraction of masonry by means of poultices is often carried out on the basis of general assumptions, in most cases without control of the efficiency or the effect deeper in the masonry (Vergès-Belmin and Siedel, 2004; Heritage *et al.*, 2008) or a long term monitoring. In the framework of a European project "Desalination" (FP6, project number SSPI 22714) a modular system for poultices was developed (Lubelli and Van Hees, 2010, Lubelli *et al.*, 2011), by which the pore structure of the poultice was tailored towards that of the salt contaminated material. Promising results were obtained with salt extraction products based on a mixture of cellulose fibres, kaolin and sand. This paper goes deeper into the salt extraction technique using similar poultices and focuses on the influence of some of the experimental parameters on the salt extraction effect on natural stone and brickwork. The results of a laboratory test, computer simulations and case studies are described. The consecutive results of each case study contributed to the decisions and adaptations made for a following case. The results are compared and evaluated to further the understanding of extraction tests in laboratory and evaluate the effectiveness of poulticing in-situ. Furthermore the contribution of computer simulations is addressed for the assessment of the influence of the climate on the extraction process and for the validation of the model by comparing the theoretical with experimental results.

2. Methodology

2.1. General sampling and salt analysis

For all laboratory tests and case studies drilled samples are taken from the mortar and brick or stone at several locations and at different heights and depths. From each sample the actual moisture content is determined by comparing the initial weight to the weight reached after drying at 60°C. The hygroscopic moisture content is determined by conditioning the dried sample at RH = 95% until constant weight. The hygroscopic moisture content is calculated from the increase in weight. Demineralized water is added to the samples. The solution is mixed to dissolve ions followed by filtration. From the extract, sodium (Na^+), potassium (K^+), calcium (Ca^{2+}) and magnesium (Mg^{2+}) cations and chlorine (Cl^-), nitrate (NO_3^-) and sulphate (SO_4^{2-}) anions are quantitatively determined with Ion Chromatography (IC, Metrohm). From the excess of cations the amount of soluble carbonate (CO_3^{2-}) is calculated.

For the purpose of this paper the salt content in both stone/brick and mortar is averaged per case for the first 2 cm and for the total measured depths. Although a significantly higher salt content is noticed in the mortar compared to the stone/brick in all case studies.

2.2. Laboratory tests and simulations

For the laboratory tests a total of 6 brick samples are contaminated, by submersion, with a solution of sodium chloride, corresponding to 0.8 wt% in the brick. The samples are dried at 60°C, cut into cubes of 7×4×7 cm and covered with paraffin on five sides to allow evaporation from the top side (7×4 cm). Before applying a poultice the samples are pre-wetted with 5 ml of pure water applied on the top with a syringe, which corresponds to 1.8

$l.m^{-2}$. The poultice used for the laboratory tests is according to the paper by Lubelli and Van Hees (2010) (coded as CKS121_L) and contains cellulose fibres (BWW40: 200 μm), Kaolin Speswhite clay and calibrated sand (0.5-1 mm) (1-2-1 ratio by weight) and a water content of 0.8-1 (weight water- dry poultice). This poultice, when dry, has smaller pores then the tested bricks and theoretically favours advection rather than diffusion.

The poultice is applied on the top side of each sample with a thickness of 1.5 cm after which the setup is conditioned in a climatic chamber (T=20°C, RH=50%) until completely dry. The method of experimental salt extraction was designed by simulations using the porous media transport model Delphin 5.6 Salt-Beta (Nicolai, 2007). The parameters used as input for the simulations are, among others, the amount and distribution of salts, the physical properties of the materials and the environmental conditions. The simulations using this Beta software were only possible and reliable with the single salt potassium nitrate. The physical parameters include experimental results of mercury intrusion porosimetry (MIP), water absorption and drying tests of the related building materials and the poultice material. The control of the salt extraction effect is based on the determination of the salt content of drilled samples. After one poultice application an average salt content of the 6 tested samples is compared to the results of the simulation.

Additional simulations are carried out to assess the effect of climatic conditions and pre-wetting on the results of salt reduction. For that, a 2D model of brick masonry with a depth of 15 cm is used that is contaminated with a salt content that decreases continuously from 4 wt%, in the first two centimetres to 0.5 wt% between 10 and 15 cm. The salt reduction effect is simulated at four different climate conditions and systematically for two different amounts of pre-wetting with pure water: 0.5 and 2 $l.m^{-2}$, which brings the total number of simulations to 8 (see Tab. 1). The results of the salt reduction are compared after 20 days of simulated drying.

Tab. 1: Overview of set conditions used for the simulations to investigate the salt extraction process in different climatic conditions and with different pre-wetting amounts.

Temperature (°C)/ Relative Humidity (%)	20/40		20/80		10/40		10/80	
Amount of pre-wetting with distilled water ($l \cdot m^{-2}$)	0.5	2	0.5	2	0.5	2	0.5	2

2.3. Case studies

Six different case studies have been evaluated, for each case the locations and materials are coded in table 2 under point 4, Case studies. The *Case Code (Location)* in the table is followed by a number, which indicates the specific tested location. Except for Mp2, the test setup of one application consists of: 1) taking samples from the salt deteriorated substrate at different heights and depths, and analysed as described earlier; 2) pre-wetting (by spraying) the surface of the substrate with a known amount of pure water ($l \cdot m^{-2}$); 3) application of a poultice; 4) removal of the poultice after drying and taking drilled samples. The procedure is repeated entirely in case more applications are carried out. In the case of Mp2 the substrate is only wetted without applying a poultice. An overview of the parameters is presented in table 2.

3. Result of the laboratory tests versus the simulation

The average salt distribution of the samples after one poultice application and the results of the simulation are shown in Fig. 1. The results of the modelling showed a strong resemblance with the experimental ones. The salt distribution in the samples, after pre-wetting with 1.8 $l \cdot m^{-2}$ and a single extraction, fluctuates between 0.3 and 0.4 wt%. More than half of the initial salt content is extracted. It should be noticed that the promising results of the laboratory tests are explained by the unidirectional transport process of water and salts, during which drying is forced towards the poultice.

The simulations carried out in different climatic conditions (Fig. 2) have shown that a warmer climate (20°C) and a pre-wetting with 2 $l.m^{-2}$ are the most efficient to reduce the salt content in the first 5 cm, while an increases of the salt content is seen in the depth, especially in humid conditions (*RH*=80%). Between 5 and 15 cm, the efficiency is slightly better if a lower quantity of water is used for pre-wetting. In a colder environment (10°C), the effect of pre-wetting seems highly influenced by the conditions of relative humidity. At a low *RH* (40%) and by pre-wetting with less water it seems that a good reduction of the salt content is obtained in the first 5 cm without an important increasing in the depth of the wall. On the other hand, at higher *RH* values (80%), intensively wetting the wall seems to be the best way to lower the salt content in the first 5 cm, while the efficiency decreases in the depth.

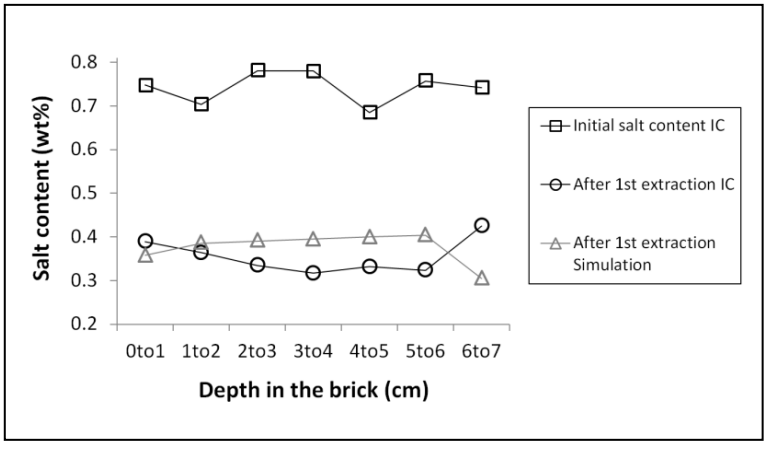

Fig. 1: Average salt content of six samples (wt%) in the depth of the brick (cm), after pre-wetting with 1.8 $l.m^{-2}$ of pure water and one poultice application.

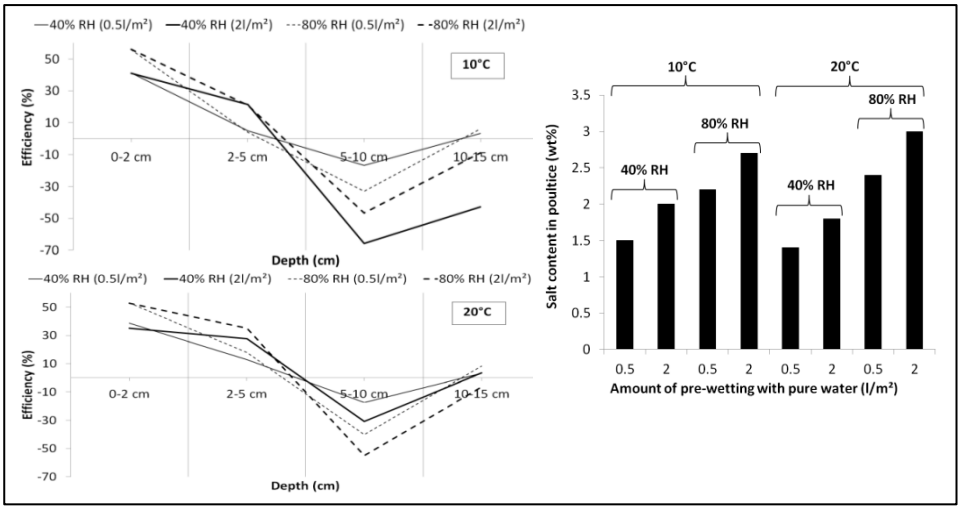

Fig. 2: Efficiency (%) of the extraction in the substrate (left) and salt content (wt%) poultice (right) 20 days after a poultice application, derived from the simulations carried out in different climatic conditions and with different amounts of water used for pre-wetting.

4. Results of the case studies

One of the main issues when comparing case studies is the differences between the material parameters that influence the salt extraction process (Tab. 2). Besides the deviation associated with the heterogeneous properties of building materials, other parameters also influence the physical process, such as, the type and content of detected salts, sampling depth, poultice material, amount of water used to pre-wet the test zone, amount and time of poultice application and the climatic conditions. Furthermore, the interpretation of the salt content found in a poultice in relation to that of the substrate is rather complicated (Fig. 3). It becomes even trickier when considering the amount of salts at different depths in the substrate and the different salt contents between stone/brick and mortar (the latter is not shown). Nevertheless, several assumptions and generalizations can be made to better understand the extraction process when using poultices.

The results of the poulticing procedure carried out in all cases are graphically represented in Fig. 3. According to the salt content in the first 2 cm of the substrate after one poultice application an average reduction of 69% is obtained. The salt content in the poultice only covers 8% of that (Fig. 3, top left). When considering the salt content averaged over the total measured depth a reduction of 20% is obtained, while the amount of salts detected in the poultice is on average 2% or less (Fig. 3, bottom left). Obviously there is a large discrepancy between the salt reductions in the walls compared to the salt content in the poultices. In general, based on the amount of salts deposited in the poultice, the efficiency of a poultice application can be considered low.

Tab. 2: Parameters of the case studies.

Case Code (Location)	Number of poultice applications	Total depth of sampling (cm)	Substrate material (Total porosity (%))	Av. salt content (wt%) in the first 2 cm, excluding $CaSO_4$ and Na_2CO_3	Main salt(s) in the mixture excluding $CaSO_4$	Poultice type (Total porosity (%))	Amount of H_2O ($l.m^{-2}$) used for pre-wetting	Time left to dry in days (min-max)	Location of the test	Av. climate conditions T(°C) - *RH*(%)
Tm1	3	5	LS(18)	4.0	Na_2SO_4	KL(50)	2	5-7	O	15-78
Tm2	3	5		1.8		CF	2	5-7	O	15-78
Gw1	4	5	BM	3.4	NaCl	CR1	0.5	4-4	I	20-U
Gw2	4	5		1.5		KL(50)	0.5	4-4	I	20-U
Gw3	4	5		5.1		CF	0.5	4-4	I	20-U
Ak1*	3	10	B(45) M(37)	2.8	$Ca(NO_3)$ Na_2CO_3	CR2(50)	2	7-17	I	13-65
Ak2*	3	10		3.5		CR3(44)	2	7-17	I	13-65
Gs1	3	30	AS(41)	1.7	Na_2SO_4	CR2(50)	12.55	4-4	C	20-50
Gs2	3	30		1.7		CR2(50)	0.88	4-4	C	20-50
Hb1*	2	15	BM	3.0	KCl Na_2CO_3	CR2(50)	0.5	6-10	E	13-65
Mp1	1	20	BM	1.2	$MgSO_4$	CR2(50)	2	8	E	14-78
Mp2	0	20		1.5		Non	2	8	E	14-78

Legend:

Tm: Tervuren, Royal Museum for Central Africa
Gw: Genk-Winterslag, C-Mine Industrial heritage
Ak: Antwerp, The Our Lady's Cathedral
Gs: Ghent, Our Lady of St Peter's Church
Hb: Hoegaarden, Farmhous
Mp: Mechelen, Preachers monastery

*test case includes several tested heights or locations, average results are presented.

LS: Luxembourg sandstone
B: Brick
M: Mortar
AS: Avender stone
O: Outdoor
I: Indoor
C: Climate chamber
E: Indoor with external climate
U: Unknown

KL: poultice contains cellulose fibres (BWW40), Kaolin Speswhite clay, calibrated sand (0.5-1mm) (1-2-1 ratio by weight) and a water content of 0.8-1 to 1-1 (weight water-weight dry poultice). **CR1**: is a discontinued commercial poultice produced by Rewah containing Sepiolite clay and cellulose fibres. **CR2** and **CR3** are experimental poultices produced by Rewah on the basis of **KL**, with **CR2** containing recycled cellulose fibres and **CR3** contains equal amounts of BWW40 and BC1000. CF: is a commercial poultice from Remmers (*Ontzoutingskompres - art. 1070*). Cases Ak and Gs are further described in De Clercq *et al.* (2013, De Clercq and Godts, 2014). Case Gs is a laboratory test on large limestone blocks conditioned in a climate chamber. For test case Mp1 one application was carried out, while Mp2 is a test case where the masonry was pre-wetted without applying a poultice.

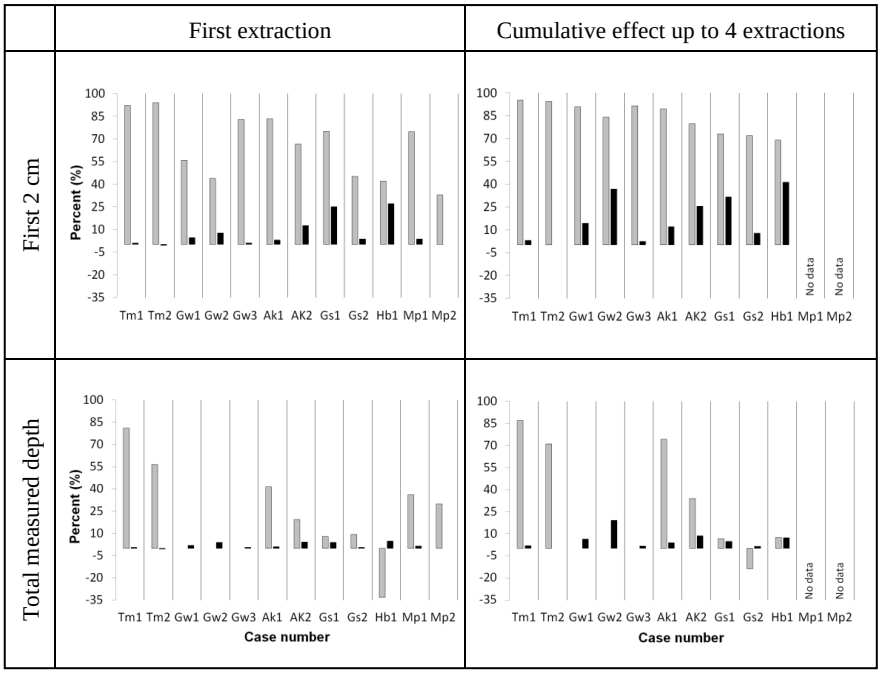

Fig. 3: Average reduction of the salt content (%) in the substrate (▒:grey) per case in the first 2 cm (top) or total measured depth (bottom) of the substrate and deposited salts (%) in the poultice (▒: black) related to the salt content initially present in the first 2 cm (top) or total measured depth (bottom) of the substrate. On the left side: after a first extraction and on the right side: the cumulative effect up to 4 extractions.

Considering the average number of additional poultice applications (av. 2.2) a similar efficiency is attained per poultice application, with an average amount of 8% of the salts initially present in the first 2 cm deposited in the poultice and 2% on average related to the initial salt content in the total measured depth. From the cumulated efficiency (Fig. 3, right) a same conclusion can be derived, that is, the efficiency of the extraction effect after additional poulticing can be considered low while the reduction of the salt content in the substrate reduces further up to 84% on average in the first 2 cm and 27% for the total measured depth.

Some exceptions can be noticed after all poultice applications in the cases Gw2, Gs1 and Hb1, where the salt content in the poultice is on average 37% compared to that initially present in the first 2 cm of the substrate. This seemingly better efficiency, might be true for the first centimetres of the substrate, however when considering the salt content in the depth of the substrate, the salt extraction efficiency of the poultice reduces to less than 10% on average. In all cases, salts are being redistributed in the depth of the substrate, diffused to lower salt contaminated areas and in joints behind the brick/stone (the latter is not shown) up to where water migrates by capillary action. These results are quite in contrast with the laboratory tests characterised by a unidirectional transport of water and salts. The different processes between laboratory tests and the case studies are schematically illustrated in Fig. 4.

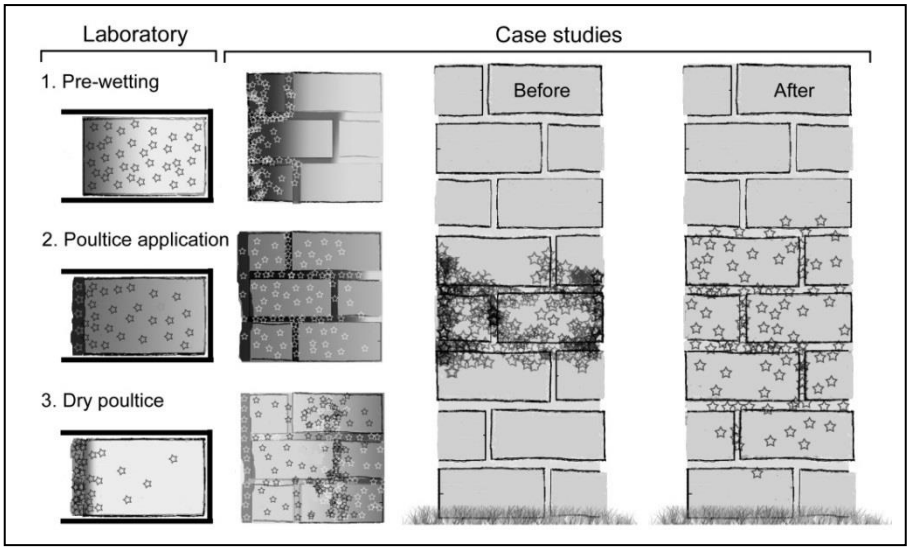

Fig. 4: Schematic representation of the salt distribution/migration during a poulticing procedure in laboratory (left) and case studies (right). Before: salts are concentrated at a certain height in the substrate as a result of decades of accumulation towards the drying front. After: redistribution of salts after pre-wetting and poultice application.

In the laboratory tests the salt distribution is often homogenous over the sample, while in reality salts are generally more heterogeneously distributed, concentrated in the joint mortar at the surface and at a certain height as a result of decades of accumulation towards the drying front (Fig. 4, Before). In laboratory and case studies pre-wetting saturates and dissolves salts in the first centimetres. Followed by the application of a poultice, in the lab samples advection/diffusion of salts will occur toward the poultice. In real cases this will also occur, however salts will also diffuse and migrate with water further to lesser salt contaminated areas, in joints behind stone/brick and in the depth of the substrate by capillary action (Fig. 4, "*After*"). The concentration of salts is lower and the efficiency of the poultice is easily misinterpreted.

At a certain moment of the drying process of the poultice, advection starts. In case small samples are used during laboratory tests water can only flow in one direction, hence most salts are logically deposited in the poultice. In the case studies, by the time a poultice is dry enough for advection to occur some salts that were initially present in the first centimetres end up in the poultice, while most of the salts have migrated in the wall to a depth where advection is no longer possible. The limits of advection are elaborately explained by Sawdy *et al.* (2010). However, due to the redistribution of salts the final concentration may be low enough to avoid further damage. Depending on the conditions, over time, salts might return to the surface. If the wall is completely saturated, which is generally not feasible, a high amount of salts is likely to migrate back to the surface and hence toward the poultice, mainly when the poultice has a longer drying period. If the wall is not pre-wetted or a small amount of water is used, salts are likely deposited in the depth of the substrate where water transport ends, which is more likely to occur when the poultice dries quickly. Seen that current research is based on the porosity of a completely dried poultice, it might

be interesting to investigate the changing porosity properties when a poultice is drying. One might find that the advection process starts too late, for example, when a poultice has lost most of its adhesion to the substrate or when water and salts have already spread due to capillary action of the dry substrate.

5. Conclusions

From the comparison of the laboratory tests and case studies it has been shown that the effect of a poultice tested on enclosed and small laboratory samples has little value when considering practical uses. Due to the large differences between the amounts of salts detected in the poultices compared to that of the substrate, it has become clear that it is seldom possible to methodically evaluate the efficiency of a poultice in situ. Furthermore, if the salt reduction is only evaluated in the first centimetres of the substrate, one might wrongfully conclude that the poultice was successful in extracting salts.

The results of the simulations indicated a strong resemblance with the experimental tests. This allowed for the use of simulations to model salt transport when pre-wetting with different amounts of water and poulticing in different climatic conditions. Independent of the temperature, in more humid conditions wetting the wall with a higher water content seems to increase the efficiency of salt transport toward the poultice and lowering the salt content in the first centimetres of the substrate. In dryer conditions pre-wetting with less water seems to result in a low to fair reduction of the salt content in the first centimetres without increasing the salt content greatly in the depth of the wall.

The evaluation of the case studies has shown that due to inconsistent salt distribution patterns in a substrate, salts generally migrate to lesser contaminated areas rather than toward the poultice. Consequently, when the effect of a salt extraction is based on the salt content in the substrate without comparing it to the poultice a skewed conclusion is probable. In general the results of the case studies have shown that the extraction effect of a poultice has a rather low efficiency in terms of reduction of the salt content and the use of water for pre-wetting the substrate promotes the migration of salts in the depth and to lesser salt contaminated areas. Additional pre-wetting and poulticing also promotes further redistribution of salts. It can be assumed that before a poultice is sufficiently dry, and has sufficiently small pores, the capillary action of the substrate surpasses the advection capacity of the poultice, thus pushing salts in the substrate rather than extracting them. More research is needed to fully understand the processes at hand.

The drying rate of a poultice and substrate will influence its performance, slower drying of the substrate seems to promote the extraction of salts. Hence, if the substrate could be completely saturated, which is generally not feasible, more salts will return to the surface and deposit in the poultice, and this to an extent depending on the drying characteristics of the substrate. Perhaps because the contact between poultice and substrate remains superior and the poultice is active longer, however the amount of extracted salts remains limited and the parameters for successful poulticing are yet to be defined. One could argue that the effect of wetting a salt contaminated surface, by applying sufficient amounts of water, waiting several days and repeating the process several times might have a similar effect as poulticing as the locally concentrated salts near the surface, whom have often gathered there over decades, will be re-distributed in the same manner. The application of a plastic sheet after wetting the surface might improve the redistribution and migration of the salts. However, this rather unconventional method might only be applicable in case problems

with water penetration can be completely excluded. Hence, it is unknown how long it will take before the salts return to the surface. Conductivity tests of the poultice material are typically carried out by conservators on site, the first poultice usually has a higher conductivity compared to that of additional applications. Although these tests might be useful, a decreasing conductivity of a poultice shouldn't be used as an indication that the salt content is decreasing substantially in the substrate but are rather being redistributed in the substrate.

References

De Clercq, H. and Godts, S., 2014, Salt extractions of brickwork a standard procedure? In: Hilde De Clercq (ed.): Proceedings of SWBSS 2014 3rd International Conference on Salt Weathering of Buildings and Stone Sculptures, KIK-IRPA, Royal Institute for Cultural Heritage Brussels 457-467.

De Clercq, H., Godts, S. and Hendrickx, R., 2013, Zoutbestrijding. Zoutextracties op metselwerk: een standaardprocedure? Handboek Onderhoud Renovatie Restauratie, Kluwer, III, 1-78.

Franzen, C., Hoferick, F., Laue, S. and Siedel, H., 2008, Water Bath desalination of sandstone objects, in proceedings 11th Int. Congress on Deterioration and Conservation of Stone, Torun, Vol II, 881-888.

Heritage, A., Sawdy, A., Funke, F., Vergès-Belmin, V., Bourgès, A., 2008, How do conservators tackle desalination? An international survey of current poulticing methods, in Postprints from the 8th European Conference on Research for Protection, Conservation and Enhancement of Cultural Heritage, Ljubeljana, Slovenia, 89-93.

Lubelli, B., van Hees, R.P.J. and De Clercq, H., 2011, Fine tuning of desalination poultices, try-outs in practice, in proceedings of the 2nd Int. Conference on Salt Weathering on Buildings and Stone Sculptures, Limassol, 381-388.

Lubelli, B. and van Hees, R.P.J, 2010, Desalination of masonry structures: Fine tuning of pore size distribution of poultices to substrate properties, Journal of Cultural Heritage, 11, 10-18.

Nicolai, A., 2007, Modelling and numerical simulations of salt transport and phase transitions in unsaturated porous building materials, dissertation, University of Dresden, Germany.

Sawdy, A., Heritage, A. and Pel, L., 2008, A review of salt transport in porous media, assessment methods and salt reduction treatments, in proceedings from the International Conference, Salt Weathering on building and Stone Sculptures, SWBSS, The National Museum, Copenhagen, 1-28.

Sawdy, A., Lubelli, B., Voronina, V. and Pel, L., 2010, Optimizing the extraction of soluble salts from porous materials by poultices, Studies in Conservation 55, 26-40.

Vergès-Belmin, V. and Siedel, H., 2004, Poultice desalination of masonries and monumental sculptures: a review, Restor. Build. Monum. 11 (6), 1-18.

QUANTIFYING THE DAMAGE AND DECAY FOR CONSERVATION PROJECTS: IDENTIFICATION, CLASSIFICATION AND ANALYSIS OF THE DECAY AND DETERIORATION IN STONE

P.T. Janbade[1*] N. Thakur[2] and B.N. Tandon[2]

Abstract

The process of identification of the material, including the stones used in construction, is the first step in any architectural conservation and restoration project. The process of identification and classification of stone involves many different techniques, like Physical examination, thin section analysis, chemical investigations, electron microscopy, X ray diffraction etc. These investigation forms the crucial backbone of information for deciding the strategy for conservation and restoration plan and further treatment (Larson, 1990). This information is also useful in understanding the cause and methods of decay and deterioration. The Trilokinath temple, a state listed monument of the mediaeval temple architecture in Nagari style was selected for understanding the nature of decay and deterioration and evolving an appropriate methodology. It is situated in Mandi, Himachal Pradesh, a northern Himalayan state of India. This temple was completely destroyed in major earthquake of 1905 and the restoration work was carried out at intermittent stages. As per the practice of the time, locally available stone of similar quality from the same live quarry were used as replacement and substitutes. Thus Trilokinath temple provides the opportunity to study the medieval stone against the stone from the restored work and fresh sample from the quarry. The thin sections, chemical analysis along with SEM analysis and X-ray diffraction analysis were used to understand the character and mineralogical composition of the stone along with various properties of the stones. An attempt has been made to quantify the surface decay of the stone by evolving a scale and assigning color coding for the same. A mechanism to streamline stone conservation process is suggested.

Keywords: architectural conservation and restoration, stone conservation, material conservation, stone characterisation, heritage management

1. Introduction

Natural stone deposits are found in abundance in the Indian sub-continent. These have been used as a building material from ancient times and have transformed India into a land of archaeological architectural wonder and world heritage. In India Stones belonging to all the systems known in the world are available but a few of the rocks from the geological

[1] P.T. Janbade*
Chandigarh college of architecture, Sector 12, Chandigarh 160012 India
prafullatj@gmail.com

[2] N. Thakur and B.N. Tandon
Department of Architectural Conservation, School of Planning and Architecture, New Delhi, India

*corresponding author

formation of India were chosen for use in the construction of buildings (Batra, 1996). Monuments and structures standing tall in various parts on its soil for centuries together bear testimony not only to skilled workmanship, artistry and architectural practices of their times but also to the excellent building material of which they have been fashioned from. The temples and monuments, the palaces and forts, built during varying ages are not just beautiful to behold; they also point to the durability of the stone as a building material (www.techno-preneur.net, 2008). While every endeavor was made to select the stones that possess the requisite strength, an attractive colour and appearance and those which can receive dressing whether ordinary or ornamental without much labour were selected. The stones selected were granite, charnockite, the limestone, khondolite, marble, sandstones, basalt, deccan trap, quartzite and laterite (Batra, 1996).The Taj Mahal at Agra, built of Makrana white marble from Rajasthan is a world famous architectural wonder. Sandstone has been widely used in erecting forts and palaces and these have been embellished with granite and marble. Use of natural stones as the mainstay of Indian architecture has continued till the present time. The designers of Rashtrapati and Sansad Bhavan and other government institutions have kept up the tradition by using sandstone as building material. Even today, facades, floors and other spaces of modern buildings, be they government institutions, public places, commercial establishments or private residences, use natural dimensional stones in some amount or the other.

Any undesirable change in the properties of a material is termed as deterioration (Arnold and Zehner, 1988). Deterioration of building stone begins immediately upon the completion of an artifact or structure and continues progressively for as they are in contact with any kind of environment. Deterioration of building stone begins immediately upon the completion of an artifact or structure and continues progressively for as long as they are in contact with any kind of environment (Cesari, 1982). The active components of the environment that influence the condition of building stones are: solar radiation, seasonal and daily temperature changes, wind, humidity from different origins, water soluble salts, atmospheric pollutants and particularly important in the primarily tropical climate of India, biological agents (both plants and animals) (Torraca, 1998). Thin section - Diagnosis of Stone Deterioration, briefly explores the mechanisms through which these active components of the external environment affect the internal properties and structure of stone subsequently determining the type and extant of stone deterioration (Arnold and Zehnder, 1988).

2. Conventional methods of documentation

Since it is not always possible to preserve the stone forever, it is necessary to use existing techniques and methods of forwarding the information and knowledge to future generation effectively and also evolve alternative methods by using the new technology. This makes a record (drawing and photography) creation and its preservation a vital stage. The specialized field of documentation has evolved with the field of stone conservation. Traditionally the architectural and allied field knowledge has been used as an application tool in conservation purpose. This included various types of record generation and record keeping like Inventory preparation, Sketching, Photography and drawing etc. As each of these fields in architecture including architectural drawings evolved, so the specialized record keeping techniques and drawings techniques were used for stone conservation purpose (Price, 1996).

3. Modern methods of documentation

All stone monuments are affected by stone deterioration, especially by weathering, which means physical disintegration or chemical decomposition is initiated and controlled by the interaction between stone and exogenic factors such as climate, biosphere or pollution. The increasing damage on stone monuments and the danger of irretrievable loss of cultural heritage has resulted in ever-increasing efforts world-wide for monument preservation. (Fitzner, 2004) Modern methods have come into vogues with the advent of modern technology and objective of record generation shifting from data creation to using it for application or intervention facilitated by the modern materials and techniques made available in digital computing and photography (Duran and Toz, 1991). This resulted in the creation of advancement in stereophotography, photogrammetry and 3D laser etc. (Stokin, 2002).

The modern method of monument mapping has evolved with the extensive usage of the modern computer technology for document creation and record keeping (Ogleby, 1999). The increase in the computation capabilities meant it was possible to integrate the various aspects of study and store it in similar format. This result into easy access and use of the information and data related to the materials used in monuments and physical condition as seen on the site and data provided by the lab tests and other sources of the information like research papers etc.

4. Introduction to modeling

The restoration processes require that stone used in the construction are identified in terms of their origin and constituents. This helps in the replacement, if any, required and deciding the strategy for the cleaning, treatment and consolidation.

Rationale for the modeling: This involves the visual inspection of the stone supported by the various tests at the lab, which include the thin section, X ray, SEM and chemical analysis. These analyses also helps in the broader classification of the stone in terms of its origin and major constituents and are important to understand the level or the extent of the damage and deterioration in the material, in this case stone. This process has remained subjective in early stages of the development of the field. This has resulted into the different assessment by the different agencies and expert resulting into piquant situation of the manager /fund raiser/ conservator etc. The first step in the direction of the quantification came from the ICOMOS in terms of formation of the group specially meant for the stone conservation treatment. This was further refined by Fitzner (2004) and developed as Damage index model for linear and progressive damage.

5. The Damage Classification

The intensity or the severity of the damage in the stone is difficult to classify but not an impossible task. As it can be started with two very broad groups of “no damage” and “full damage” which could also be further divided to get a distinct group of ten. This process has remained subjective in early stages of the development of the field. But with proper cataloguing it could be implemented. As shown in Tab. 10, the actual photograph of the site has been linked the categories of decay. Using this table, each surface of the monuments could be demarked with decay categories as shown in Fig. 6.

5.1. Identification

5.1.1. XRD analysis:

The samples were collected from the site consisting of the stone samples of the original stone used in 1520 and restored stone used during the restoration work. A fresh stone was also collected from the quarry in the vicinity claimed to the supplier of the original stone. All these samples were tested in the lab for their structural the mineralogical properties and compared for understanding the restoration work against the universally accepted principles of reversibility and minimum intervention. The thin section of the stone also used to understand the character of the stone and mineralogical composition. The stone of original construction time was labeled R1and the restored stone was labeled as R2. The fresh stone from the quarry was labeled as R3.

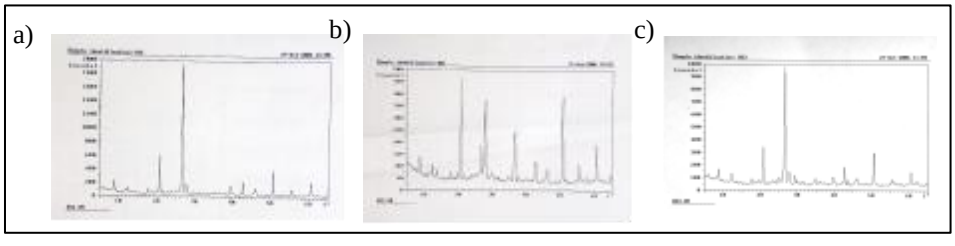

Fig. 1: SEM Analysis of antique stone (a), restored stone (b) and fresh quarry stone (c).

5.1.2. SEM Analysis of the sample

The stone samples were mounted on the aluminum cylindrical base (sample holder or stub) a day before the examination under the SEM. The size of the stone was reduced to fit the size of the holders and stubs and was fixed on the stubs by using s double coated carbon conductive adhesives tapes and allowed to dry up in an ionizer and then a coating provided for the closure examination.

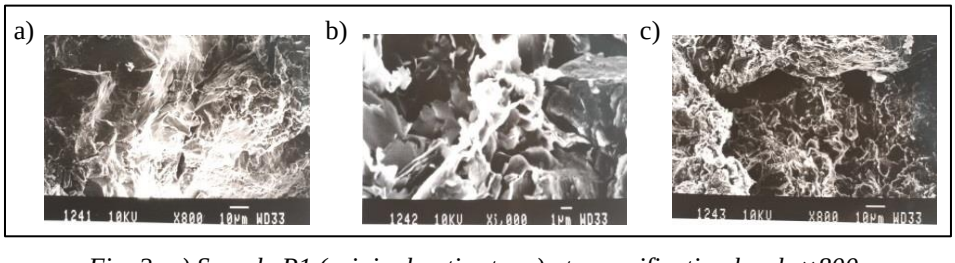

Fig. 2: a) Sample R1 (original antic stone) at magnification level: ×800;
b) Sample R1 at magnification level: ×5000;
c) Sample R2 (restored stone) at magnification level: ×800.

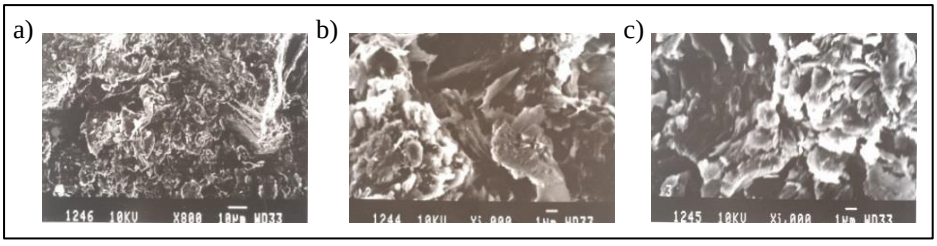

Fig. 3: a) Sample R2 (restored stone) at magnification level: ×5000;
b) Sample R3 (fresh stone) at magnification level: ×800;
c) Sample R3 (fresh stone) at magnification level: ×5000.

5.1.3. Analysis

The following can be inferred from the above photographs and information. The grain size is more compact in the restored stone compare to the original stone of the temple, but highest in the fresh sample from the nearby quarry. The stone of original construction of the temple and restored stone are similar in nature with few differences. Restored stone has higher number of Muscovite elements (white mica is a non-ferromagnesian rock-forming silicate mineral with tetrahedral arranged in sheets, sometimes called potassic mica.) Similarly plagioclases are higher in the restored stone.

5.2. Damage index, scale, multiplication factors and damage intensity

In Statistical science, various scale for measurement are available. These scales can be classified as "nominal", "ordinal", "interval" and "ratio".

Tab. 1: Rationale behind the damage scale and damage intensity

Scale	1	2	3	4	5	6	7	8	9	10
Damage Intensity	No Damage		Slight Damage		Visible decay		Moderate damage		Severe damage	Material loss

Tab. 2: Scale, damage intensity and multiplication factor along with color coding for each level of decay.

Scale	1	2	3	4	5	6	7	8	9	10
Factor	0.1	0.2	0.3	0.4	0.5	0.6	0.7	0.8	0.9	1.0
Damage Intensity	no damage		slight damage		visible decay		moderate damage		severe damage	material loss
Measures/Action required	**No action needed**		**Observation**		**Monitoring required**		**Assessment and treatment**		**Treatment**	

5.3. Illustrations

An example of plane area calculation can be taken to illustrate the calculation of the damage index. Imagine a wall area of '*d*' width and '*h*' height as shown in the example below. In this rectangular wall blue area is damaged in the scale of 5 and consists of area *d*/2 in width and *h*/2 in the height. The damage index for the said surface can be calculated accordingly as shown below. Its Damage Index, *DI*, came to be 0.125.

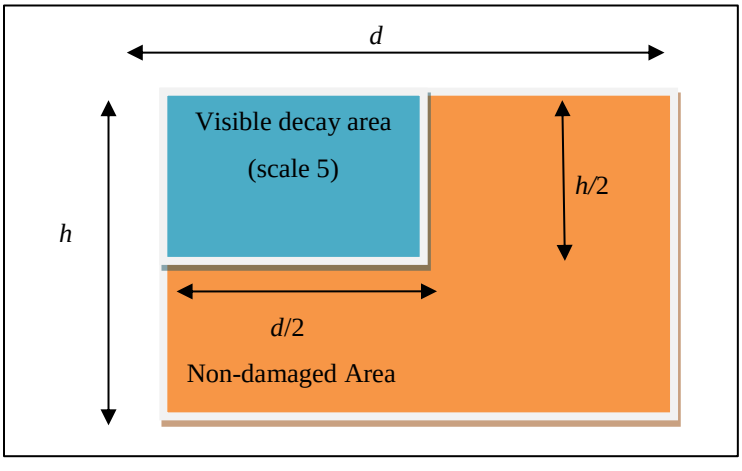

Figures 4: Damage index calculation scheme.

The damage index for the object:

$$DI = 1 - \frac{TAo - TAd}{TAo} \qquad (Eq.\ 1)$$

where the total surface area of the object is *Tao* and *Tad* is the total damaged surface area of the object.

- ***Total area of the object:***

  $TAo = h \times d$ and

- ***Total damaged area of the object:***

  $TAd = h/2 \times d/2 = hd/4 = 0.25\ hd$,

- ***Total damaged area of the object with severity of 2 (scale):***

  $Tad_{scale\ 2} = 0.5 \times 0.25\ hd = 0.125\ hd$,

- ***Damage Index:***

  $$DI = 1 - \frac{hd - 0.125\ hd}{hd} = 1 - \frac{(1 - 0.125)hd}{hd} = 1\text{-}0.875 = 0.125$$

The damage index for the various façades can be worked out in similar fashion and can be used for the quantification process.

5.4. The application case

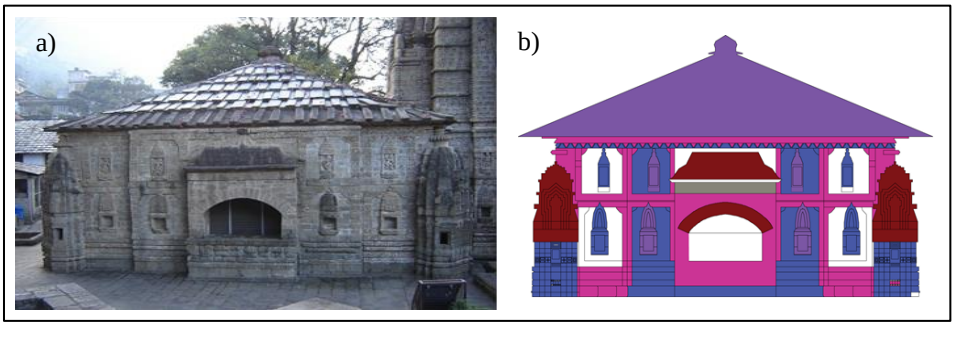

Fig. 5: a) North western façade of Trilokinath temple at Mandi, H P; b) Mapping of the damage index of north western façade (colour code is presented in Tab. 1).

Tab. 3: Scale, damage intensity, multiplication factor and color coding for each level of decay along with photographic example for each level.

Scale	Examples	Multiplication factor	Damage Intensity	Measures/
1		0.1	No Damage	No action needed
2		0.2		
3	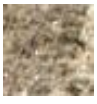	0.3	slight damage	Observation required
4		0.4		
5	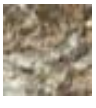	0.5	Visible decay	Monitoring required
6		0.6		
7	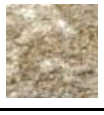	0.7	Moderate damage	Assessment and treatment required
8		0.8		
9	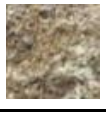	0.9	Severe damage	Treatment required
10	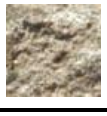	1.0	Material loss	

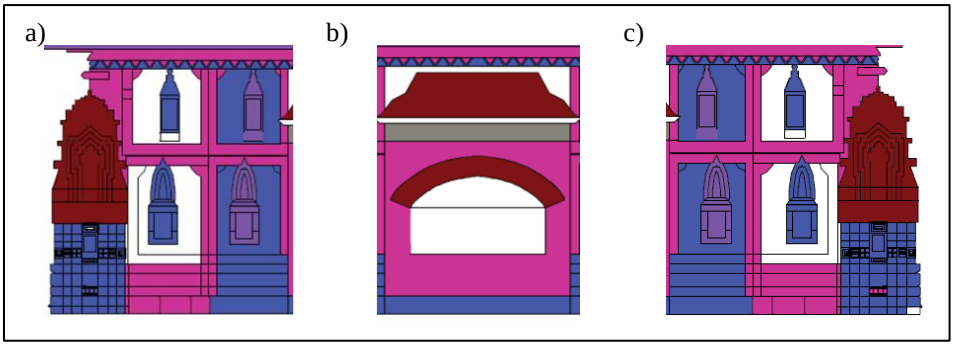

Fig. 6: Detailed mapping of the damage index of north western façade of Trilokinath temple at Mandi, H P according to the coding presented in Tab. 2 and Tab. 3.

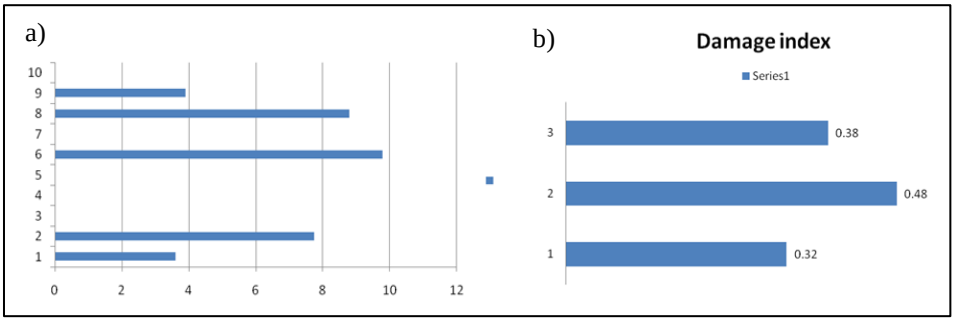

Fig. 7: a) Damage Index (extent of damage for each level of the scale from 1 to 10 in one part of the façade; b) Damage Index for each part of the façade (right).

6. Results

The deterioration of the stone is all too familiar to anyone who has looked closely at a historic stone building or monument. While there are few stones that seem to be little affected by centuries of exposure to the weather, the majority of stones are subject to gradual deterioration. We need to be able to describe the decay, and to measure the extent and severity of decay (Price, 1996). The damage index calculation helps us in this process. Only then can we hope to understand the behaviour of any particular stone in a given environment (Fitzner, 2004).

This type of damage index can provide a very good tool to conservator to arrive at quantified data which can be used for the decision making in a conservation project effectively. The Damage index for various parts of façade can be worked out in similar fashion and can be used for quantification processes. DI for part 1 and 2 (Fig. 6a and 6b) of the façade turns out to be much higher than for part 3 (Fig. 6c) of the façade helping us to understand the process of damage differently. This helps in quantifying the data relevant to the process of the conservation and restoration.

7. Conclusions

The damage index need to be integrated into overall conservation policy framework by Archaeological survey of India, Ministry of Culture or other decision making bodies to frame and achieve the quantified targets and its resource utilization.The damage index approach has the potential to strengthen the plan preparation process and provide useful input at different stages of the conservation process. The proposed Index based approach provides a framework to study and review the conservation process in the monuments and its part in India. The damage Index works as tool for prioritization of the issues at various levels in the conservation project and funds allocations. The damage Index measurement facilitates monitoring the impact of the policy intervention.

References:

Arnold, A. and Zehnder, K., 1988, Decay of stone materials by salts in humid atmosphere, Proc. 6th Int. Cong. On Deterioration and Conservation of Stone, Torun,138-148.

Batra, N.L., 1996, Heritage Conservation: Preservation and restoration of monuments, New Delhi:Aryan books International.

Cesari, C., 1999, Considerations on the problems of Integrated Conservation, Lecture notes, ICCROM Course in Architectural Conservation

Duran, Z., Toz, G., 2002. Using 3D GIS for documentation of historical monument. In: Close Range Imaging - Long Range Vision, Corfu, Greece

Fitzner, B., 2004, Documentation and Evaluation of Stone Damage on Monuments, 10th Int. Congress on Deterioration and Conservation of Stone Stockholm, pp. 680.

Larson, J., 1990, The conservation of stone sculpture in museums. In Conservation of Building and Decorative Stone, vol. 2, ed. J. Ashurst and F. G. Dimes, 197-207. London: Butterworth Heinemann,.

Ogleby, C. L., 1999. From rubble to virtual reality: Photogrammetry and the virtual world of ancient Ayutthaya, Photogrammetric Record, 16(94), pp. 651-670.

Price, C. A., 1996, The stone conservation: An Overview of Current Research. The J. Paul Getty Trust, Santa Monica, CA,

Stokin, M., 2002. Methodology and documentation techniques in conservation projects in Slovenia: Aims and reality. http://www.arcchip.cz/w05/w05_stokin.pdf (accessed 25 April 2003)

Torraca G., 1998, Porous materials building, materials science for architectural conservation, 3rd edition, ICCROM, Rome, Italy.

http://www.stone.rwth-aachen.de/index.php

THE POTENTIAL OF LASER SCANNING TO DESCRIBE STONE DEGRADATION

R. Janvier[1], X. Brunetaud[1*], K. Beck[1], S. Janvier-Badosa[1] and M. Al-Mukhtar[1]

Abstract

In the field of cultural heritage, the use of 3D acquisition tends to focus on the digitization of architecture or artefacts for conservation purposes. This research proposes to investigate the opportunity of using 3D acquisition as a non-destructive methodology to quantitatively describe stone degradation from the morphological point of view. To achieve this goal, a cubic stone sample (8 cm thick) was subjected to 10 cycles of artificial ageing in the laboratory and was monitored using laser scanning. The selected stone was tuffeau, which is white, soft and very porous limestone extensively used in the construction of the castles in the Loire Valley, France. The artificial ageing consisted in cycles of partial imbibitions (2 cm depth) of salt solution (14% of $Na_2SO_4 \cdot 10H_2O$) followed by drying at 105°C in an oven during one week. Laser scanning was performed with a triangulation-based Konica Minolta VI-910 3D digitizer. Along with the cycles, the weathering resulted in progressive efflorescence followed by flaking of lateral faces of the cube. The comparison of 3D models obtained by laser scanning at different stages of artificial weathering allows the computation of a distance map. By choosing the unaltered specimen as the reference, the distance map quantitatively describes the volume changes at the end of each cycle resulting from salt weathering. The discussion focuses on the optimization of the 3D processing pipeline, from laser scanning to distance map computation, with an emphasis on the quantification of errors generated at each step. From this quantification, an assessment of the overall standard deviation for the spatial location of points is proposed. The minimisation of standard deviation is found to be the key factor for allowing relevant morphological analysis, and subsequent description of degradation forms.

Keywords: 3D acquisition, non-destructive testing (NDT), stone degradation, salt weathering, laser scanning

1. Introduction

The use of 3D acquisition for cultural heritage digitization is now recognised as reliable, precise and affordable tool. The first application was the creation of digital replicas for conservation purposes. It has been applied to a wide variety of cultural heritage objects, from small artefacts (Spring and Peters, 2014; Ortiz Sanz *et al.*, 2010) to large archaeological sites (Lambers *et al.*, 2007), with the predominant objective of recording the digital model of the actual state of an object whose conservation is or could become an issue. To achieve the realization of 3D models, the most employed technologies are laser scanning and photogrammetry. Laser scanning is the reference technology for 3D

[1] R. Janvier, X. Brunetaud*, K. Beck, S. Janvier-Badosa and M. Al-Mukhtar
Univ. Orléans, INSA-CVL, PRISME - EA4229, 8 rue Léonard de Vinci, F-45072, Orléans, France
xavier.brunetaud@univ-orleans.fr

*corresponding author

acquisition. Photogrammetry can now be considered as a competitive alternative technology due to cutting-edge developments in its automation in the last decade.

Recent research investigated new strategies to use 3D models for conservation management with the aim of creating a 3D documentation platform (Pedeli 2013; Brunetaud *et al.*, 2012; Stefani *et al.*, 2013; Fiorini *et al.*, 2011; Campanaro *et al.*, 2015). More specifically, the development of the "digital health record" of a monument aspires to create a versatile tool able to visualize any heterogeneous data and to propose quantitative statistical analysis based on thematic map spatial correlation. The use of realistic 3D models allows the description of complex architecture; but a major added value of such a model is that it can be computed to extract quantitative features, such as mean plane, normal maps, ambient occlusion, depth maps, digital elevation map, differences map, etc.

To feed the database, an *in situ* survey can be performed. For example, it can consist in making local observations such as stone degradation maps. It may become difficult in the case of unreachable walls due to high elevation or moat. Moreover, a monitoring based on the repetition and comparison of such survey may not be affordable. Working on a high definition 3D model may constitute an alternative or at least a complementary technique for this survey. More specifically, it may allow the application of automatic processes to detect and segment stone degradation forms. The relevance of this alternative depends on how consistent is the model compared to reality. Some experiments based on 3D acquisition aimed at describing morphological changes due to stone weathering (Birginie and Rivas, 2005; López-Arce, 2010). Despite their promising concept, they were limited to statistical analysis because they could not compare the degraded surface to the original one due to impossibility of alignment between acquisitions. The objective of the present research is to test whether laser scanning could provide a relevant model for identifying stone degradation form, keeping in mind that alignment must not be lost.

2. Laboratory ageing test

2.1. Studied stone: Tuffeau

Tuffeau is the main building stone of historical monuments in the Loire Valley in France. It is a soft stone, easily workable, allowing the construction of buildings with elegant façades such as the famous Castle of Chambord. Tuffeau is a yellowish-white porous sedimentary limestone, plentiful in the Loire Valley. Its geological age is Middle Turonian, approximately 88-92 million years ago. Tuffeau is a fine-grained siliceous limestone with clayey minerals. The main crystalline phases are calcite, quartz, opal cristobalite-tridymite, glauconite, biotite, muscovite, and smectite. This limestone is a very lightweight building material with a bulk density of 1.3 in its dry state, a total porosity of about 45% and a very large range of pore sizes (from 0,003 µm to 20 µm for pore access diameter). With this high porosity, this building stone is a very soft stone with a compressive strength at the dry state of about 10 MPa (Dessandier *et al.*, 1997; Beck *et al.*, 2003). This stone is also very sensitive to environmental conditions and pollutants, and it is mainly degraded by scaling in two forms: spalling and flaking (Janvier-Badosa *et al.*, 2014). For this study, the fresh rock has been extracted from the quarry of Usseau in France.

2.2. Aging test protocol

For the study of durability of stones in laboratory, ageing tests based on the weathering caused by salt crystallization are commonly used (Flatt, 2002; Van *et al.*, 2007; Beck and

Al-Mukhtar, 2010a; Angeli *et al.*, 2010). The ageing test used in this study is based on the standard measurement of salt crystallization resistance of stones with the use of sodium sulphate solution (EN 12370 standard). However, partial imbibition was performed instead of full one. Performing partial imbibition allows a better assessment of the morphological changes induced by weathering thanks to comparison between the polluted part which will be weathered and the healthy one that can be used as a reference. Moreover, a partial imbibition with a capillary height of 2 cm reflects a more realistic process for degradation as the weathering on stones of monuments affects mainly the stone surface (Beck and Al-Mukhtar, 2010b).

In this test, a cubic sample (8×8×8 cm) of tuffeau was subjected to 10 wetting-drying cycles using the solution of $Na_2SO_4.10H_2O$ with 14% by weight. Each cycle consists of the following stages:

- wetting by partial imbibition with the salt solution of sodium sulphate at 20°C. The wetting is stopped when the capillary height reaches 2 cm.
- 7 days of drying at 105°C in the oven. The drying is complete for each cycle.
- 2 hours of cooling at room temperature (20°C, 40–50% *RH*) before the next wetting.

At the end of each cycle, the visual appearance was observed by photographs to assess the decay level of the stone sample, and the surface was digitized by laser scanning.

3. 3D acquisition

3.1. Laser scanning

For the acquisition step, a Konica Minolta VI-910 3D triangulation-based laser digitizer was used. The scanner is composed of a laser beam and CCD VGA (640×480) sensor. The laser beam is moved over the measured object by deflection on a mirror. The distortion of the beam induced by the object is recorder by the CCD. This process produces *range maps*, also called *depth maps* that are triangulated in the 2D sensor space and then converted to 3D space. The result for the end user is a 3D point cloud along with connectivity information (i.e. mesh). For this experimental procedure, the digitizer was equipped with a 14 mm lens. In this configuration, the constructor specifies an accuracy of ± 0.38 mm in X, ± 0.31 mm in Y, and ± 0.20 mm Z for a precision of 16 µm when working in the so called *high accuracy mode* at 0.6 m distance.

As it is impossible to digitize the whole cube by mean of only one scanning, we chose to perform 4 successive acquisitions around the sample thanks to a manual turntable, with a 90° angular step between each acquisition. The tuffeau sample is put on the center of this turntable. The face in contact with the turntable is the face opposite to the one subjected to salt solution imbibition**.** To minimize the number of scannings and also maximize the overlap between two scannings (needed for the subsequent registration step)**,** we avoided pure fronto-parallel acquisition of faces of the sample. Instead, the sensor is positioned at an oblique angle so as to digitize 3 faces simultaneously. The constructor software *Polygon Editing Tool* is used to export in an open format (Wavefront OBJ) for further processing.

3.2. Post-Processing

At the end of 3D acquisition, each scan is in its own coordinate frame. The alignment of the four scans of the same set is done by setting one of the scans as reference, and then manually picking 5 tie points on each pair of scans, knowing that 3 points are required to

compute the 6 degrees of freedom of the rigid transformation between two scans. This manual alignment is then refined by ICP (Iterative Closest Point, Besl and McKay, 1992). The resulting model contains the concatenation of the 4 disconnected aligned meshes with a lot of redundant information. To create a single surface, the Screened Poisson Surface Reconstruction – PSR – (Kazhdan and Hoppe, 2013) was used**.** This algorithm is known to be robust to noise and to provide an excellent hole interpolation. However, it tends to create some hallucinated surfaces on borders of the mesh. Therefore, an additional step consisting in manual cleaning is required before further processing. After the surface reconstruction, we register the scans corresponding to subsequent ageing cycles using point picking followed by ICP, incrementally comparing each cycle with the previous one, as two consecutive cycles share the most common information. Once the scans of all the cycles are correctly aligned together, the signed distance map can be computed between two scans. It is computed as the signed distance between a point in the compared point cloud to its closest triangle in the reference mesh. The first scan, corresponding to the healthy state, was chosen as the reference mesh. The signed distance map was computed for each cycle and then converted into a false colour map and mapped onto the compared mesh to visually enhance and quantify morphological changes. For the whole post processing pipeline we use the free and Open Source software CloudCompare (CloudCompare, 2015).

4. Results and Discussion

To present the results of this study, we chose to show the first mesh corresponding to the healthy state (Fig. 1a), the mesh of the sample after the 10^{th} cycle (Fig. 1b), the mesh of the sample after the 10^{th} cycle with the signed distance map as false colour mapped onto it (Fig. 1c), and for visual comparison, a photograph of the sample after 10 cycles (Fig. 1d) from a similar point of view.

In the previous studies (Birginie and Rivas, 2005; López-Arce, 2010) some degraded areas were compared to healthy surfaces based on calculation of morphological features. It was impossible to assess the actual influence of degradation in the estimated morphological changes compared to usual variations in stone surface morphology in the healthy state. Compared to these studies, the most significant contribution of this research is that we actually compare a degraded area to its original state thanks to a registration process. Hence, the data we can process is directly the evolution of morphology induced by weathering.

The main result is that this protocol of laser scanning can detect morphological changes induced by salt crystallization at the surface of the sample. The use of signed distance map as false colour allows the assessment of the amplitude of local changes, here up to 7 mm for the most opened flakes. Some parts in the corners of the sample appear as blue (negative changes of low amplitude), corresponding to loss of matter during the ageing test.

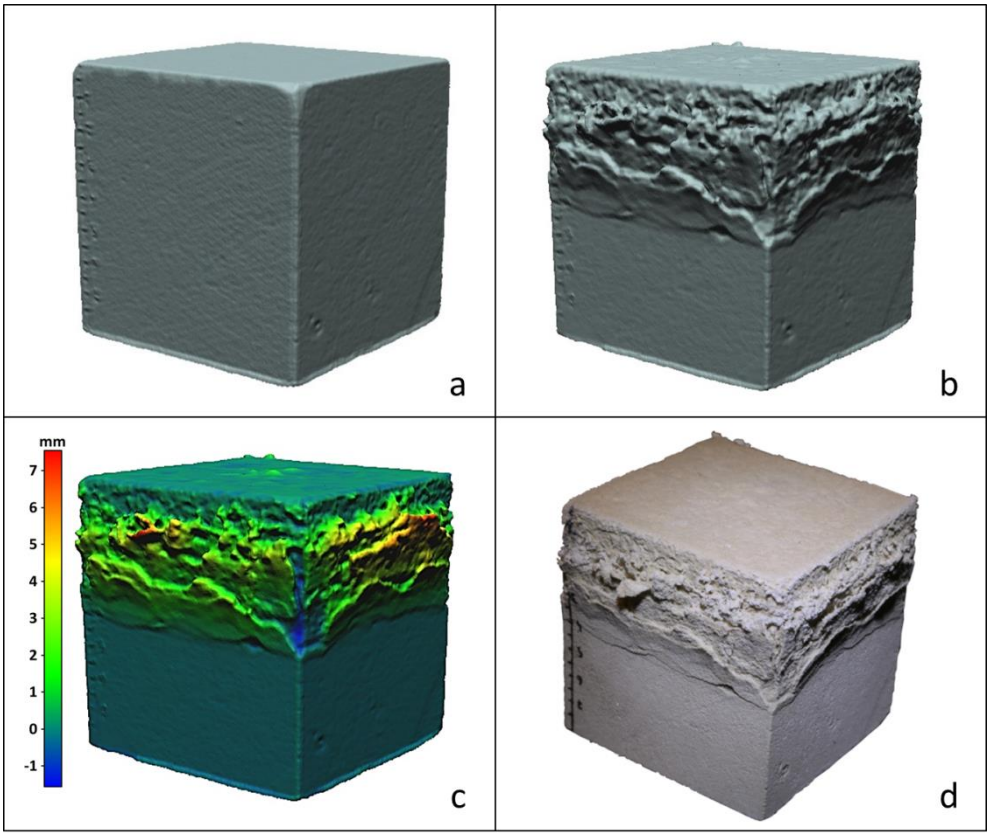

Fig. 1: a) 3D model of the original state; b) 3D model of the sample after 10 cycles of ageing; c) 3D model after 10 cycles enhanced with signed distance map [mm]; d) photograph of the sample after 10 cycles.

The cubic tuffeau sample suffers salt efflorescence combined with flaking, and all degraded surfaces are powdered. Compared to healthy surfaces, the colour of the powdered surfaces is a little yellowish and salt efflorescence is a little whitish. However, the overall colour variation is very low as it cannot be seen in Fig. 1d. Salt efflorescence results in small white deposits of salt while flaking generates millimetre-thick scales opened towards the surface submitted to imbibitions. Both processes contribute to the morphological changes, and any protocol based on morphological quantification at this scale is unable to distinguish them. Moreover, as laser scanning can only reflect external changes in the morphology of the sample, it can see the effect of a detached flake but it cannot see how wide the opening below the flake is. The authors chose not to brush the surfaces to avoid any impact on the degradation process. However, it could represent a relevant additional procedure to be included in the experimental plan in order to help the analysis of surface degradation process.

From the metrological point of view, two steps of post-processing can add supplementary uncertainty to native laser scanning inaccuracies: alignment and surface reconstruction. ICP

is the protocol used to refine alignment after manual point picking. Due to its local formulation, the ICP algorithm can be trapped in a local minimum. Moreover, the global minimum may not correspond to the true solution. Especially for healthy samples, smooth and featureless surfaces introduce a large amount of ambiguity. So it requires a very careful initialisation by point picking and a very fine tuning of parameters. That make the process particularly tedious and error prone, because point picking is a manual procedure. Moreover, we cannot really estimate precision of our registration in absence of an external ground truth. Surface reconstruction can also be a source of bias in our experiment. PSR builds a new point set that interpolates the whole point set; it can over smooth sharp details.

To assess the overall effect of post-processing on the topologic integrity of data, we compared the final mesh corresponding to the 10th cycle with each original mesh obtained directly by laser scanning. Each one of the 4 scans was aligned by point picking and ICP with final mesh, and the comparison was made in terms of distance computation taking the original scans as reference. The standard deviation reaches 0.1 mm. This value of deviation is considered admissible as it is less than the scanner accuracy, but higher than its precision. As a consequence, this protocol of morphological acquisition based on laser scanning is deemed relevant to assess morphological changes induced by salt weathering, as long as the changes are at least in the order of 0.1 mm.

5. Conclusion and prospect

This paper evaluates a protocol of 3D acquisition dedicated to morphological description of stone degradation forms, based on laser scanning and subsequent post-processing. In the present test, the degradation is induced by successive ageing cycles consisting in partial imbibition in a solution of $Na_2SO_4.10H_2O$ followed by full drying, applied to 8×8×8 cm tuffeau sample. After 10 cycles, the cubic stone sample showed powdered surfaces with salt efflorescence combined with flaking.

The digitization consisted in 4 consecutive laser scannings aligned by manual point picking followed by ICP. Surface reconstruction was obtained by PSR. The successive cycles were compared after their registration in the same coordinate frame by computing signed distance maps. The result can be presented as a mesh textured with a signed distance map in false colour. This allows to visually enhance and quantify morphological changes along with cycles. Such distance maps can then be processed to extract statistical morphological features able to represent the "3D fingerprint" of the degradation form. This measurement based on laser scanning acquisition constitutes a complementary characterization tool to be included in non-destructive testing panel.

The main sources of deviation come from registration and surface reconstruction. However, the overall assessment of additional standard deviation indicates that it is less than the accuracy, though higher than the precision, of native laser scanning specifications; that is why it was considered admissible. However, an option to minimise this additional deviation would be to segment the healthy areas that are most likely to be similar between two consecutive ageing cycles so as to constrain ICP to take into account a higher weight for healthy areas compared to degraded ones. It could be processed by means of calculation of features including ambient occlusion, curvature, roughness, etc.

The proposed protocol of laser scanning can detect and quantify morphological changes induced by salt crystallization if changes are at least in the order of 0.1 mm. However, as it

is based on morphology analysis without any colour information, it cannot dissociate salt efflorescence from flaking.

To benefit from colour information, an alternative to laser scanning is to use photogrammetry. Its advantages are its potentially low cost, its capability of recovering high quality colour information, and the fact it may not require any further alignment by point picking or ICP. However, the precision and accuracy of photogrammetry depends not only on camera and lens specifications, but also is sensitive to operating conditions (lighting, acquisition process, pipeline…) and on material appearance in terms of textural richness. Indeed, if the measured material locally lacks textural information, the resulting model will be noisy or of low accuracy. However, this opportunity of using photogrammetry must be tested to assess its relevance.

References

Angeli, M., Hébert, R., Menéndez, B., David, C., Bigas, J.-P., 2010, Influence of temperature and salt concentration on the salt weathering of a sedimentary stone with sodium sulphate, Engineering Geology, 115, 193-199.

Beck, K., Al-Mukhtar, M., Rozenbaum, O., Rautureau, M., 2003, Characterisation, water transfer properties and deterioration in tuffeau: Building material in the Loire Valley, France, Journal of Building and Environment, 38 (9), 1151-1162.

Beck, K. and Al-Mukhtar, M., 2010a, Evaluation of the compatibility of building limestones from salt crystallization experiments, Geological Society of London, SP333, 111-118.

Beck, K. and Al-Mukhtar, M., 2010b, Weathering effects in an urban environment: a case study of a French porous limestone, Geological Society of London, SP331, 103-111.

Besl, P.J., and McKay N.D., 1992. A Method for Registration of 3-D Shapes. IEEE Transactions on Pattern Analysis and Machine Intelligence, 14 (2), 239–56.

Birginie, J.M., Rivas T., 2005, Use of a laser camera scanner to highlight the surface degradation of stone samples subjected to artificial weathering, Building and Environment, 40 (8), 1011-1020.

Brunetaud, X., De Luca, L., Janvier-Badosa, S., Beck, K., Al-Mukhtar, 2012, M., Application of digital techniques in monument preservation, European Journal of Environmental and Civil Engineering, 16 (5), 543–556.

Campanaro, D.M., Landeschi, G., Dell'Unto, N., Leander Touati, A.M., 2015, 3D GIS for cultural heritage restoration: A 'white box' workflow, Journal of Cultural Heritage, doi:10.1016/j.culher.2015.09.006.

CloudCompare (version 2.6.2) [GPL software]. EDF R&D, Telecom ParisTech, 2015. Retrieved from http://www.cloudcompare.org/.

Dessandier, D., Antonelli, F., Rasplus, L., 1997, Relationships between mineralogy and porous medium of the crai tuffeau, Bulletin de la Société Géologique de France, 186 (6), 741-749.

EN 12370 Standard, 1999, Natural stone test methods – determination of resistance to salt crystallization.

Fiorini, A., Urcia, A., Archetti, V., 2011, The digital 3D survey as standard documentation of the archaeological stratigraphy, in The 12th International Symposium onVirtual Reality, Archaeology and Cultural Heritage VAST, 18th-21st October 2011, Prato, Italy.

Flatt, R.J., 2002, Salt damage in porous materials: how high supersaturations are generated, Journal of Crystal Growth, 242, 435-454

Janvier-Badosa, S., Beck, K., Brunetaud, X., Al-Mukhtar, M., 2014, The occurrence of gypsum in the scaling of stones at the Castle of Chambord (France), Environmental Earth Sciences, 71 (11), 4751-4759.

Lambers, K., Eisenbeiss, H., Sauerbier, M., Kupferschmidt, D., Gaisecker, T., Sotoodeh, S., Hanusch, T., 2007, Combining photogrammetry and laser scanning for the recording and modelling of the Late Intermediate Period site of Pinchango Alto, Palpa, Peru, Journal of Archaeological Science, 34 (10), 1702-1712.

Kazhdan, M. and Hoppe H. 2013. Screened Poisson Surface Reconstruction, ACM Transactions on Graphics, 32 (3), 1-12.

López-Arce, P., Varas-Muriel, M.J., Fernández-Revuelta, B., Álvarez de Buergo, M., Fort, R., Pérez-Soba, C., 2010, Artificial weathering of Spanish granites subjected to salt crystallization tests: Surface roughness quantification, CATENA, 83 (2-3), 170-185.

Ortiz Sanz, J., De la Luz Gil Docampo, M., Rodríguez, S.M., Rego Sanmartín, M.T., Cameselle, G.M., 2010, A simple methodology for recording petroglyphs using low-cost digital image correlation photogrammetry and consumer-grade digital cameras, Journal of Archaeological Science, 37 (12), 3158-3169.

Pedelì, C., 2013, An interdisciplinary conservation module for condition survey on cultural heritages with a 3D information system, international archives of the Photogrammetry, Remote Sensing and Spatial Information Sciences, VolumeXL-5/W2, in XXIV International CIPA Symposium, 2–6 September 2013, Strasbourg, France.

Spring, A. P., Peters, C., 2014, Developing a low cost 3D imaging solution for inscribed stone surface analysis, Journal of Archaeological Science, 52, 97-107.

Stefani, C., Janvier-Badosa, S., Beck, K., De Luca, L., Brunetaud, X., Al-Mukhtar, M., 2013, Developing a toolkit for mapping and displaying stone alteration on a web-based documentation platform, Journal of Cultural Heritage, 15 (1), 1–9.

Van, T. T., Beck, K., Al-Mukhtar, M., 2007, Accelerated weathering tests on two highly porous limestones, Environmental Geology, 52, 283-292.

APPLICATION OF COLORIMETRY FOR THE POST-FIRE DIAGNOSIS OF HISTORICAL MONUMENTS

S. Janvier-Badosa[1*], K. Beck[1], X. Brunetaud[1], Á. Török[2] and M. Al-Mukhtar[1]

Abstract

Building materials are subjected to high temperatures during fires and this can cause changes in their structural and aesthetic properties. In this paper, an *in situ* methodology is proposed to assess the state of degradation of stone materials subjected to fire by using their colour changes. Colorimetry is a non-destructive and indirect method for post-fire diagnosis. The principle of the method is to compare the colour of the stone of a monument having undergone a fire and the same material subjected to high temperatures in the laboratory for which the relationship between colour and mechanical properties can be established. This allows an estimation of the temperature level reached by the material on site during the fire, and hence its level of degradation. The present study was conducted on tuffeau, a limestone used in the construction or restoration of many built heritage monuments in the Loire valley in France such as the castle of Chambord. Laboratory tests were performed on stone samples heated at different temperatures, from 100°C to 900°C. Colorimetry measurement was coupled with P-wave velocity measurements. The data acquired are therefore a step in establishing a methodology for diagnosing the degradation state of stones after a fire, from colorimetric measurements. The validation of the colorimetric method of diagnosis was made on stones in a part of the castle of Chambord damaged by fire.

Keywords: colorimetry, non-destructive testing (NDT), post-fire diagnosis, limestone, high temperatures

1. Introduction

During a fire in a historic monument, building stones suffer damage. Some stones are completely destroyed and must be replaced, while others are subjected to significant changes, which can potentially have an impact on the sustainability of the monument. The replacement of these stones therefore needs to be considered: some stones may visually appear to be in good condition, although their properties may have been significantly altered; others may show significant chromatic changes and therefore be unaesthetic, but without their durability having been affected. Moreover, the curator's mission is to preserve the authenticity of the building, limiting restoration operations to a minimum, as long as the

[1] S. Janvier-Badosa, K. Beck*, X. Brunetaud and M. Al-Mukhtar
Univ. Orléans, INSA-CVL, PRISME - EA4229, 8 rue Léonard de Vinci, F-45072, Orléans, France
kevin.beck@univ-orleans.fr

[2] Á. Török
Department of Engineering Geology and Geotechnics, Budapest University of Technology and Economics, Hungary

*corresponding author

sustainability of the building and visitor safety are preserved (The Venice Charter, 1964). So it would be interesting to have a non-destructive *in situ* method for post-fire diagnosis, to characterise the level of damage of stones still in place in order to identify those that require replacement first.

Most studies on the sustainability of burned building materials concern concrete (Savva *et al.*, 2005; Cree *et al.*, 2013). A few studies focus on changes in stone properties as a function of the temperature rise (Török and Hajpal, 2005; Franzoni *et al.*, 2013; Ozguyen and Ozcelik, 2013), but these are laboratory studies that require destructive sampling to characterise the damage. No study focuses on non-destructive and *in situ* diagnosis methods. One of the main changes in the material, indicating a rise in temperature, is the colour change. Colorimetry, usually used for other conservation-restoration studies of built heritage (Duran-Suarez *et al.*, 1995; Rivas *et al.*, 2011), appears to be an interesting method of post-fire diagnosis. Its effectiveness has also been tested on concrete (Carré *et al.*, 2014). The present paper assessed the potential of this method, its advantages and its limitations, both in the laboratory and on monuments, as a simple and reliable *in situ* post-fire diagnosis tool.

The study was performed on a building stone frequently used throughout the Loire Valley: tuffeau. The method consisted in measuring the colour of the stone subjected to various temperatures in the laboratory, correlating these colour changes with the evolution of P-wave velocity measurements to evaluate the material damage. Once the "standard colorimetric curve" had been established in the laboratory, colorimetric measurements were made directly on a burned part of a monument built in tuffeau, in order to verify if it was possible to determine the temperature of heated stones, and therefore their state of deterioration.

2. Material and methods

2.1. Studied stone: Tuffeau

Tuffeau is the main building stone used in historical monuments in the Loire Valley in France, such as the famous castle of Chambord. It is a porous sedimentary limestone whose geological formation extends throughout the Loire Valley. Tuffeau is a whitish, fine-grained siliceous limestone with clayey minerals, formed in the Middle Turonian, approximately 88-92 million-years ago (Beck *et al.*, 2003). The composition and the main characteristics of this stone are shown in Tab. 1. For this study, the fresh rock was extracted from the tuffeau quarry at Usseau in France.

Tab. 1: Main characteristics of tuffeau limestone.

Mineralogical composition	**Solid density** (g/cm^3)	**Bulk density** (g/cm^3)	**Porosity** (%)	**P-wave velocity** (m/s)
Calcite : ≅ 50%, Quartz : ≅ 10%, Opal CT : ≅ 30%, Clay & Mica : ≅ 10%	2.5 ±*0.1*	1.3 ±*0.2*	45 ±*5*	1640 ±*78*

2.2. Fire test applied

The stones were submitted to a heating procedure at nine temperatures: 100°C, 200°C, 300°C, 400°C, 500°C, 600°C, 700°C, 800°C, and 900°C. The reference state was 100°C because the sample is considered to be dry without degradation of the material. The furnace used was a Carbolite ELF 11/6B. The heating rate was 2°C/min under air atmosphere up to the set temperature, this maximum temperature was kept constant for 3 hours, and then a slow natural cooling took place up to room temperature. A set of four cubic samples (50×50×50mm) was used for each set temperature. While the test conditions do not fully reflect the processes that take place during natural fire, this method makes it possible to compare the thermal behaviour of tuffeau at high temperatures (Beck *et al.*, 2015).

3. Results and discussion

3.1. Colour changes: Visual observation and colorimetry

The colorimetric measurements were performed by absorption spectrometry with diffuse reflection. After analysis of a white reference surface (magnesium oxide), the calibration of the wavelength was made with a sample of erbium oxide. The result of the analysis on stone samples is an absorption spectrum for diffuse reflection, located in the visible range (380 – 780 nm). From this spectrum, the chromatic coordinates (lightness L^*, green-red axis a^* and blue-yellow axis b^*) are derived and used in this paper (Sève, 2009; Beck *et al.*, 2015). Five measurements were performed on each sample, that is to say twenty measurements for each temperature. The measuring points were selected randomly on the surface of the set of 4 samples. The average and standard deviation of the coordinates of the twenty points were used to illustrate the results reported in this paper. The colours of the samples after exposure to different temperatures are presented visually and qualitatively in Fig. 1, and quantitatively by colorimetric measurements in Tab. 2.

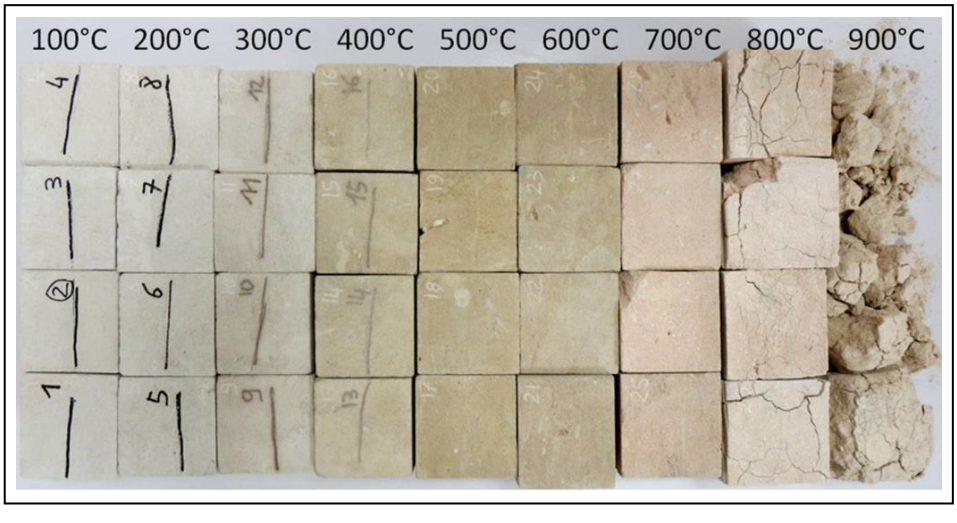

Fig. 1: Colour of samples after exposure to different temperatures.

Tab. 2: Results of colorimetric measurements (coordinates L, a*, b*) for tuffeau stone after exposure to different temperatures for the fire test applied.*

	100°C	200°C	300°C	400°C	500°C	600°C	700°C	800°C	900°C
L*	86.5 ±1.3	85.3 ±1.7	83.0 ±1.3	78.8 ±3.0	72.9 ±1.3	71.2 ±1.59	75.3 ±2.4	80.3 ±3.1	84.2 ±2.2
a*	-1.0 ±0.2	-1.1 ±0.2	-0.1 ±0.2	1.3 ±0.4	2.2 ±0.3	2.2 ±0.3	2.9 ±0.5	3.2 ±0.5	-0.3 ±0.4
b*	7.9 ±0.9	9.0 ±0.5	10.4 ±0.5	12.7 ±1.0	16.3 ±0.7	15.2 ±0.6	14.0 ±1.0	12.8 ±1.0	14.4 ±1.1

There was a gradual colour change of the stone with the temperature and a significant change in colour from 400°C, linked to a global browning of the stone. The coordinate *a** gradually increased toward the red up to 800°C, and decreased strongly at 900°C. The *L** coordinate gradually decreased up to 600°C (darkening) then increased from 700°C (lightening). This gradual browning was followed by an abrupt change close to 700°C where the stone became pinker and brighter (Fig. 1). This colour change can be explained by the transformation of glauconite grains with temperature. They are responsible for the slightly greenish colour typical for tuffeau. From 400°C, the green glauconite grains turned orange and became completely brown at 900°C (Török and Hajpal, 2005). From 700°C - 800°C, calcite started to decompose into the white coloured quicklime, and the colour pink became dominant on the samples. Once all the calcite had been converted into quicklime, the stone became very sensitive to moisture and the hydration reaction of the quicklime caused significant cracking of the stone in a few days.

3.2. Change in P-wave velocity

P-wave velocity measurements were performed at room temperature in the laboratory on the same samples before and after the heating procedure for each maximum temperature (Fig. 2). They highlight the damage of the material with the loss of mechanical properties.

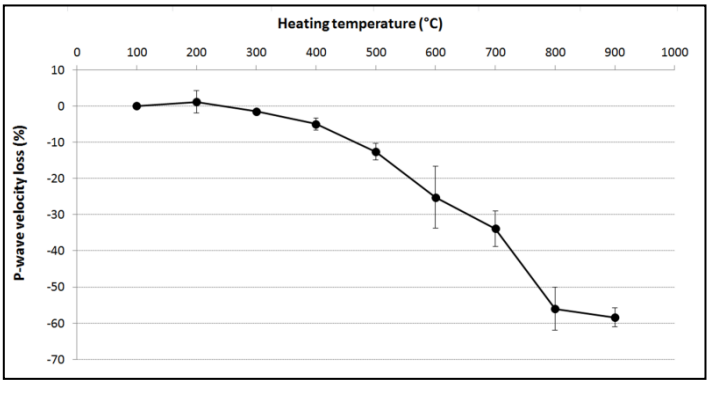

Fig. 2: Change in average P-wave velocity of the stone as a function of heating temperature for the fire test applied.

Before the heating procedure, the P-wave velocity measures were consistent from one sample to another with a value around 1640 m/s. The P-wave velocity of the sample after heating up to 300°C was similar to that of the unheated reference samples. The colorimetric measurements were also stable up to 300°C. However, from 400°C, the P-wave velocity steadily decreased with temperature, showing a gradual degradation of the elastic properties of the material with a loss around 60% at 800°C due to the appearance of micro-cracks. From 400°C, the colorimetric data also changed depending on the temperature with a gradual increase in coordinate a^* and a gradual decrease in coordinate L^*, causing browning and darkening of the stone. From 800°C, the link between P-wave velocity and colorimetric measurements was completely reversed because of the decarbonation reaction of calcite which led to a lightening in colour and great damage of stone.

In monument diagnosis, if a tuffeau stone does not appear to have undergone colour changes after a fire, it is conceivable that the surface temperature did not exceed 300°C, and therefore that the stone does not need be replaced, as lab results have shown that colour changes as well as changes of mechanical properties appear to be low up to 300°C. On the contrary, the parts of the stones which have undergone a heating to at least 800°C will be irreparably damaged and will therefore have to be replaced. For tuffeau, it is for temperatures between 300°C and 800°C that non-destructive diagnosis is most important to define a restoration strategy. Estimating the degree of alteration of a stone after a fire would be possible using colorimetry as a non-destructive test for post-fire diagnosis, since the results are well correlated to the P-wave velocity decrease resulting from damage to the stone. However, this technique requires both the initial colour of the stone and the evolution of its colour with temperature to be known.

4. *In situ* validation test of the methodology

The castle of Chambord, built in tuffeau stone in the early 16th century by Francis I, is the largest castle in the Loire Valley in France. The south tower of the donjon, called "Henry V tower", suffered a major fire on July 6th, 1945, which completely destroyed the frame and the roof. After the fire, only fireplaces and stone walls remained. During the restoration work most of the materials were replaced in the attic of this tower. The frames were rebuilt in wood and concrete. The roof was also rebuilt and some stones were replaced. But some of the stones having suffered the fire are still in place on the monument. The measurements were carried out in this attic, on an inside wall. Some stones have a fracture and a missing part revealing the internal part of the stone (Fig. 3). Thanks to this missing part, colorimetric measurements could be performed on the external surface of the stone and the internal part of the stone. Visually, the external surface of the stone was pink (zone 2), and this colour was uniform over approximately one centimetre depth. In the internal part of the stone (zone 1), the stone was white and resembled the normal colour of a healthy stone.

Tab. 3 shows the values of the coordinates L^*, a^*, b^* corresponding to the colorimetric measurements performed on zone 1 and zone 2. The values were averaged over a minimum of five measurements. The lightness L^* was nearly the same value (about 77) for both areas, but the external part (zone 2) appeared slightly darker than the internal part (zone 1) of this stone. Coordinate a^* was the most differing between the internal part (around -0.4) and the external part (around 3.3), highlighting the pinkish surface appearance (Fig. 3). By comparing the *in situ* and laboratory colour measurements, we can confirm that it is

coordinate *a** which is the most relevant to record the temperature reached during a fire in the case of tuffeau. From these measurements, we estimate that the stone on the site damaged by the fire experienced a rise in temperature up to 700°C to reach the pinkish colour and a coordinate *a** close to 3. At this temperature, the P-wave velocity decreased by almost 30%, showing deterioration in the mechanical properties of the affected stone.

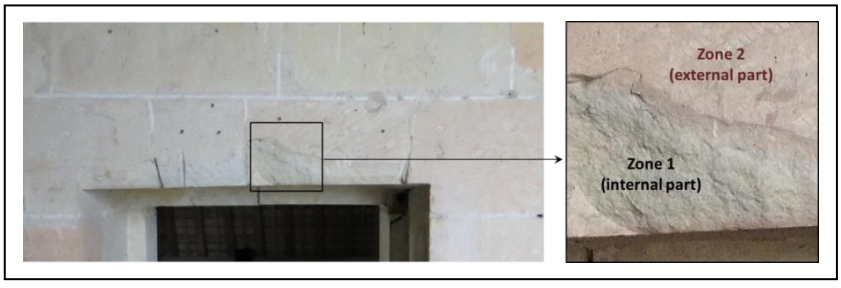

Fig. 3: Zones of the attic that suffered from a fire and that were submitted to colorimetric measurements (Castle of Chambord).

Tab. 3: Results of colorimetric measurements.

	Zone 1 (internal part)	**Zone 2 (external part)**
*L**	78.7 *±2.7*	76.6 *±2.2*
*a**	-0.4 *±0.3*	3.3 *±0.6*
*b**	15.2 *±1.1*	15.6 *±0.8*

Additional observations by optical microscopy were performed to confirm the diagnosis of temperature (Fig. 4) with colorimetry. Two samples were taken in zone 1 and zone 2 (Fig. 3). Zone 1 was considered healthy and was compared with the reference samples heated at 100°C in the laboratory. Zone 2 was considered to have been heated to 700°C during the fire, and was compared to the samples heated at the same temperature in the laboratory. Glauconite grains are an interesting marker to observe, as they are responsible for the gradual colour change of tuffeau from 400°C (Török and Hajpal, 2005). Green at 100°C, they were reddish-orange at 700°C (Fig. 4). However, between zone 1 and zone 2, in the samples taken at the Castle of Chambord in the part damaged by fire, the colour of glauconite had not changed and was still green. This calls into question the hypothesis of a heating temperature of 700°C and indicates that these stones were not heated to a temperature above 400°C during the fire that destroyed the attic of the tower and that their properties were therefore not changed. The origin of the pink colour on the surface of the stone is, however, unknown. Several hypotheses which would need to be checked in turn can be suggested in case a surface treatment was performed after the fire: consolidating or cleaning surface treatment, biological activity (algae, lichens), traces of glue, paint or other pollutants, colouring the stone to a depth of one centimetre. The historical archives on the castle of Chambord are incomplete because part was destroyed. The archives of the 20th century which could be consulted fail to provide answers. Colorimetry, which is non-

destructive and easy to implement, is therefore an interesting tool to diagnose degradation of a building after a fire, but it is not sufficient because it can be distorted by other types of deterioration or surface treatment that change the colour of the stone. It is therefore important for the expert making the post-fire diagnosis to cross-validate the data and methods of analysis.

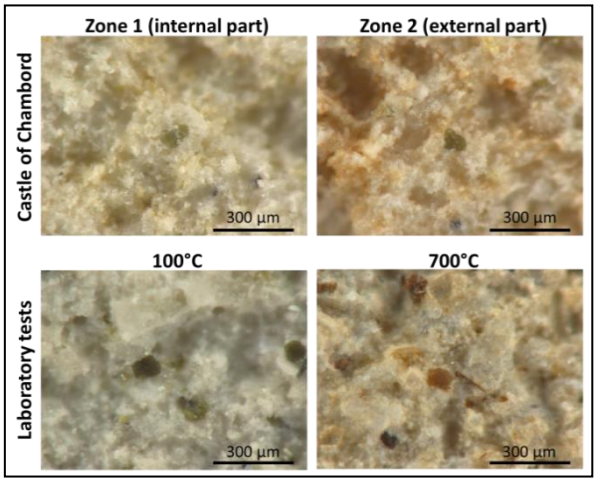

Fig. 4: Photographs (×300) showing the colour of glauconite in tuffeau sampling of the Chambord Castle (zones 1 and 2), and tuffeau exposed to fire tests (100°C and 700°C).

5. Conclusion

A reference curve of the colour change of tuffeau as function of the heating temperature has been established from colorimetric measurements on tuffeau stone subjected to temperatures ranging from 100°C to 900°C. P-wave velocity measurements were also performed on these samples, before and after the heating procedure, to measure the percentage of the mechanical properties reduction, and thus characterise the damage non-destructively. The results of colour measurements correlate well with P-wave velocity measurements, thereby rendering the use of colorimetry as a potential non-destructive method of post-fire diagnosis of damage to stone.

To further validate this method, colorimetric measurements were conducted for *in situ* post-fire diagnosis on tuffeau stones of the castle of Chambord, submitted to a fire and compared to those obtained in the laboratory. The coordinate a^* proved hereby to be the most relevant to a post-fire diagnosis by colorimetric measurements. Neglecting the impact of soot, smoke and a possible post-treatment, the observation of the surface colour with a quantitative measurement by colorimetry might be useful as a non-destructive test of the state of conservation of stones after a submission to high temperatures typical for a fire. Nevertheless, as shown in this paper, colorimetric measurements are indeed useful but they are not sufficient and need to be complemented by other analyses to characterise the textural and mineralogical properties of the stone (XRD, SEM, optical microscopy, mercury intrusion porosimetry) in order to assist the work of expertise for the post-fire diagnosis of historical monuments.

References

Beck, K., Al-Mukhtar, M., Rozenbaum, O., Rautureau, M., 2003, Characterisation, water transfer properties and deterioration in tuffeau: Building material in the Loire Valley, France, Journal of Building and Environment, 38 (9), 1151-1162

Beck, K., Janvier-Badosa, S., Brunetaud, X., Török, A., Al-Mukhtar, A., 2015, Non-destructive diagnosis by colorimetry of building stone subjected to high temperatures, European Journal of Environmental and Civil Engineering, available on line 28 May 2015 (doi:10.1080/19648189.2015.1035804).

Carré, H., Hager, I., Perlot, C., 2014, Contribution to the development of colorimetry as a method for the assessment of fire-damaged concrete, European Journal of Environmental and Civil Engineering, 18 (10), 1130-1144

Cree, D., Green, M., Noumowé, A., 2013, Residual Strength of Concrete Containing Recycled Materials After Exposure to Fire: A Review, Construction and Building Materials, 45, 208-223.

Duran-Suarez, J., Garcia-Beltran, A., Rodríguez-Gordillo, J., 1995, Colorimetric Cataloguing of Stone Materials (biocalcarenite) and Evaluation of the Chromatic Effects of Different Restoring Agents, Science of The Total Environment, 167, 171-180.

Franzoni, E., Sassoni, E., Scherer, G.W., Naidu, S., 2013, Artificial Weathering of Stone by Heating, Journal of Cultural Heritage, 14, 85-93.

Ozguven, A., Ozcelik, Y., 2013, Investigation of Some Property Changes of Natural Building Stones Exposed to Fire and High Heat, Construction and Building Materials, 38, 813-821.

Rivas, T., Matias, J.M., Taboada, J., Ordóñez, C., 2011, Functional Experiment Design for the Analysis of Colour Changes in Granite Using New L∗ a∗ B∗ Functional Colour Coordinates, Journal of Computational and Applied Mathematics, 235, 4701-4716.

Savva, A., Manita, P., Sideris, K.K., 2005, Influence of Elevated Temperatures on the Mechanical Properties of Blended Cement Concretes Prepared with Limestone and Siliceous Aggregates, Cement and Concrete Composites, 27, 239-248.

Sève, R., 2009, Science de la couleur: aspects physiques et perceptifs, ed. Chalagam, 374 p.

The Venice Charter, International charter for the conservation and restoration of monuments and sites, 2nd International Congress of Architects and Technicians of Historic Monuments, Venice, 1964.

Török, Á., Hajpal, M., 2005, Effect of Temperature Changes on the Mineralogy and Physical Proper- Ties of Sandstones. A Laboratory Study, Journal of Restoration of Buildings and Monuments, 11 (4), 211-218.

DEVELOPING APPLICATION TECHNOLOGY OF INFRARED THERMOGRAPHY FOR DOCUMENTATION OF BLISTERING ZONE

Y.H. Jo[1] and C.H. Lee[1*]

Abstract

This study focused on the quantitative modelling and documentation of blistering zones for deterioration evaluation of a Korean stone monument. To accomplish these goals, graduated heating thermography was carried out to obtain many thermographic images according to heating time and temperature rise of the blistering zones. Among these images, a representative blistering zone was selected for the quantitative modelling and documentation. As a result, the blistering zone gradually disclosed after sixty seconds, and the optimum thermographic image was acquired after 240 seconds. Then, for the documentation of the blistering zone, the following steps were performed; drawing the temperature distribution curve, establishing the critical temperature and transitional zone, making the contour map, transforming the monochrome image, converting the vector lines, and evaluating the deterioration degree. Through the completed blistering map, the total area and deterioration rate of the blistering zone were calculated at approximately 888 cm^2 and 25%, respectively. Infrared thermography served non-destructive detection of invisible defects and digital documentation for their evaluation and monitoring. In the future, cross-verification using a minimum of two non-destructive technologies will be needed to improve reliability.

Keywords: non-destructive detection, invisible defect, quantitative modelling, documentation, Korean stone monument

1. Introduction

Blistering is defined as separated, air-filled and raised hemispherical elevations on the face of stone that result from the detachment of an outer layer (ICOMOS-ISCS, 2008). This detachment is the most prevalent type of deterioration marking stone monument (Jo *et al.*, 2014). Because this blistering usually occurs at the stone's subsurface layer, it is not easily detectable with the naked eye unless it has expanded to the surface layer (Jo and Lee, 2014b).

Therefore, identifying a location and range of the blistering zones is very important for conserving the original forms of stone monuments. Currently, one of the most easily used methods around the world as a part of documentation and deterioration evaluation of the

[1] Y.H. Jo and C.H. Lee*
Department of Cultural Heritage Conservation Sciences, Kongju National University, Republic of Korea
joyh@kongju.ac.kr

*corresponding author

blistering zones is infrared thermography analysis (Moropoulou *et al.*, 2013; Bisegna *et al.*, 2014; Kylili *et al.*, 2014; Di Tuccio *et al.* 2015). This method quantitatively evaluates the degree of deterioration of a stone monument by thermal characteristics on the blistering zones. This study carried out non-destructive detection of blistering zones occurring at stone subsurface layers from a Korean monument using the active thermography and developed new application technology for documentation of the blistering zone.

2. Methodology

Graduated heating thermography, an active method, which creates abnormal temperature distributions between fresh and defected zones by an artificial external stimulus was used for blistering detection. In graduated heating thermography, various kinds of lamps are used as the artificial thermal source. Among these lamps, this study used is an infrared heater with a halogen lamp (Philips, 15021Z-2000W). This heater can radiate heat to a large area and supply a high amount of heat to an object by heating in a short time. Accordingly, the device has the advantage of quickly disclosing temperature differences between fresh and defected zones and it is suitable for large stone monuments in the open field.

The heating of the stone monument was observantly conducted to equally transfer heat to the measured area without saturating the heat capacity of blistering zones. Thermography shooting was then performed with a maximum surface temperature of 50℃ because excessive heating may lead to further damage of blistering zones by thermal shock (Jo and Lee, 2014a). The shooting distance was established between minimum 30 cm and maximum 300 cm.

The ThermaCAM SC660 camera, which is produced by FLIR Systems (SWEDEN), was used for acquisition of thermographic images. The camera performs remarkably well in terms of thermal sensitivity (0.045℃), measurable temperature range (-40 to 1500℃), and resolution (640 x 480 pixels). The temperature analysis of the acquired thermographic images was performed using the ThermaCAM Researcher 2.9 software provided by FLIR Systems. Additionally, AutoCAD (Autodesk, USA), Illustrator (Adobe Systems, USA) and vector transformation software were applied for mapping and documentation of the blistering zones.

3. Results

3.1. Analysis of thermographic images

Visual examination and percussion method were first performed in a Korean stone monument. As a result, the stone monument showed many blistering zones which have diverse layer thickness and crack widths. Particularly, the blistering zones were classified into two kinds based on the presence of blistering crack. They are open and enclosed styles. Then photograph and infrared thermography shootings were conducted in areas presumed to be blistering zones.

This study obtained many thermographic images according to heating time and temperature rise of the blistering zones. Thermographic images for representative blistering zones of Korean stone monuments are presented in Fig. 1. As shown in the Fig. 2, the location and range of the blistering zone was not detected by the passive method using the natural

temperature difference without artificial thermal source, because the stone surface is highly affected by direct sunlight.

Therefore, this study used the graduated heating thermography method with an infrared halogen heater based on energy transfer theory (Wirahadikusumah *et al.*, 1998). As a result, the blistering zone gradually disclosed after sixty seconds showing temperature increase. However, the exact shape of the blistering zone is not easily detected during short heating time because it has thick layer and enclosed style. Hence, the stone surface was continuously heated until heat conducted throughout the blistering zone. The optimum thermographic image was acquired after 240 seconds (Fig. 2).

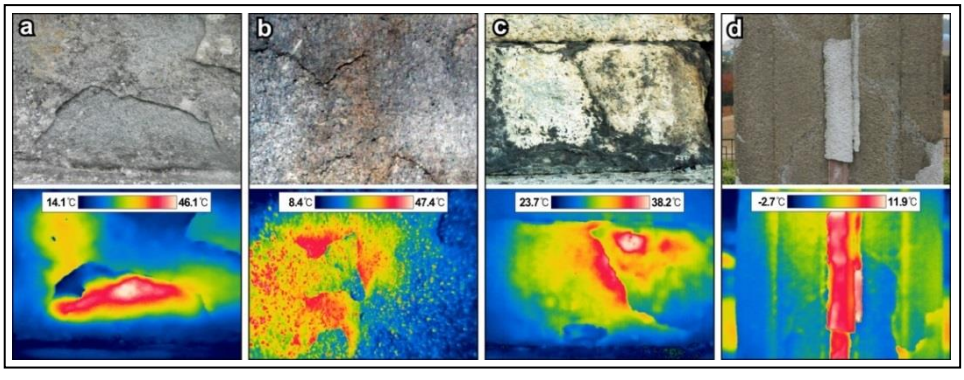

Fig. 1: Thermographic images for representative blistering zones of Korean stone monuments; a) Magoksa Temple Stone Pagoda; b) Sungnyemun Stone Block Foundation; c) Cheomseongdae Observatory; d) Flagpole Supports in Bankukdong.

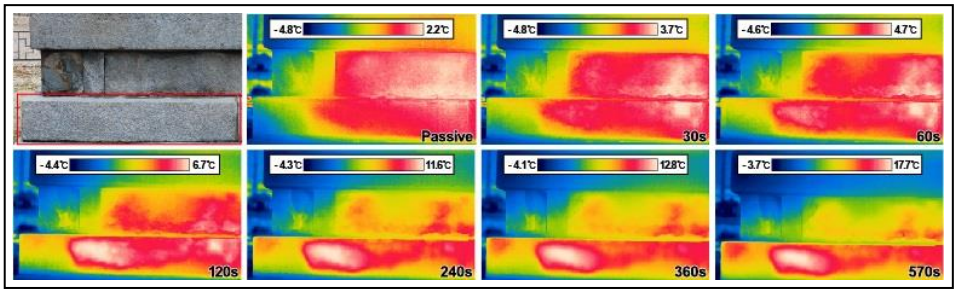

Fig. 2: Changes of thermographic images according to heating time and temperature rise of the blistering zone.

3.2. Quantitative modelling and documentation

This study carried out surface temperature analysis using the thermographic image of blistering zone showing enclosed style for its documentation and quantitative damage evaluation. A study on such quantitative modelling for blistering zones has already been reported by Jo and Lee (2014a; 2014b). Firstly, the critical temperature and transitional zone between fresh and blistering zone were established by forming the temperature

distribution curve on the thermographic image. As a result, the critical temperature is 8.2°C, and the transitional zone is maximum 9.2°C (Fig. 3a).

After the establishment of the transitional zone, its entire ranges were shown as a contour map based on the critical temperature (Fig. 3b). Then, the contour map was transformed into monochrome image of five grades and the monochrome images consisting of pixels were converted into vector lines (Fig. 3c). Through these processes, the quantitative area of the blistering zone was calculated. The completed blistering map is Fig. 3d, and the total area and deterioration rate of the blistering zone on the member were calculated at approximately 888 cm^2 and 25%, respectively.

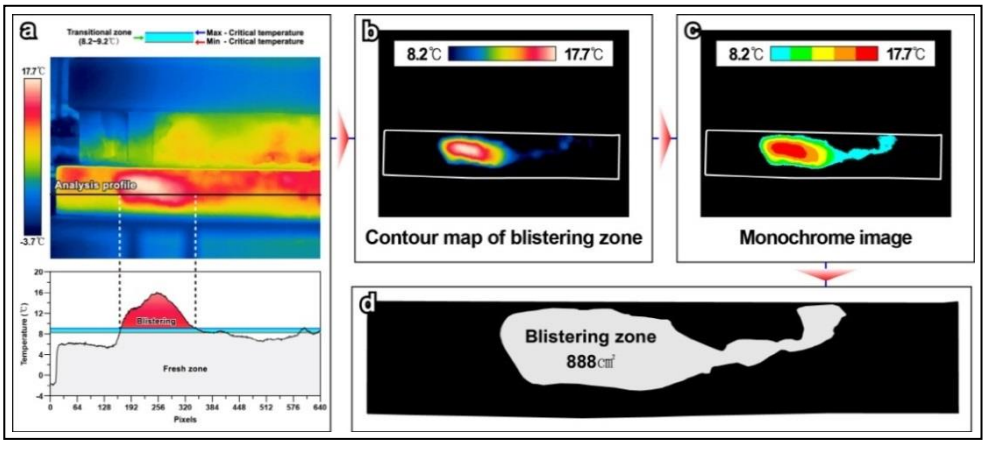

Fig. 3: Documentation processes of the blistering zone using quantitative modelling; a) Establishment of the critical temperature and transitional zone between fresh and blistering zone by forming the temperature distribution curve; b) Contour map of the blistering zone based on the critical temperature; c) Monochrome image of five grades; d) Completed blistering map and deterioration area.

4. Conclusion

This study focused on the documentation and deterioration evaluation of the blistering zone using quantitative modelling. To sum up, overall processes for quantitative modelling of the blistering zone were performed in the order of acquisition of the thermographic image using active method, drawing the temperature distribution curve, establishing the critical temperature and transitional zone, making the contour map, transforming the monochrome image, converting the vector lines and calculating deterioration rates. Infrared thermography served non-destructive detection of invisible defects and digital documentation for their evaluation and monitoring. In the future, cross-verification using a minimum of two non-destructive technologies will be needed to improve reliability.

References

Bisegna, F., Ambrosini, D., Paoletti, D., Sfarra, S. and Gugliermetti, F., 2014, A qualitative method for combining thermal imprints to emerging weak points of ancient wall structures by passive infrared thermography – A case study, Journal of Cultural Heritage, 15, 199-202.

Di Tuccio, M.C., Ludwig, N., Gargano, M. and Bernardi, A., 2015, Thermographic inspection of cracks in the mixed materials statue: Ratto delle Sabine, Heritage Science, 3, 1-8.

ICOMOS-ISCS, 2008, Illustrated glossary on stone deterioration patterns, ICOMOS, 978-2-918086-00-0, 14-15.

Jo, Y.H. and Lee, C.H., 2014a, Quantitative modeling and mapping of blistering zone of the Magoksa Temple stone pagoda (13th century, Republic of Korea) by graduated heating thermography. Infrared Physics & Technology, 65, 43-50.

Jo, Y.H. and Lee, C.H., 2014b, Quantitative modeling of blistering zones by active thermography for deterioration evaluation of stone monuments, Journal of Cultural Heritage, 15, 621-627.

Jo, Y.H., Lee, C.H. and Yoo, J.H., 2014, Application of infrared thermography for conservation treatment on the defect zone of stone monument, International Journal of Applied Engineering Research, 9 (21), 8663-8672.

Kylili, A., Fokaides, P.A., Christou, P. and Kalogirou, S.A., 2014, Infrared thermography (IRT) applications for building diagnostics: A review, Applied Energy, 134, 531-549.

Moropoulou, A., Labropoulos, K.C., Delegou, E.T., Karoglou, M. and Bakolas, A., 2013, Non-destructive techniques as a tool for the protection of built cultural heritage, Construction and Building Materials, 48, 1222-1239.

Wirahadikusumah, R., Abraham, D.M., Iseley, T. and Prasanth, R.K., 1998, Assessment technologies for sewer system rehabilitation, Automation in Construction, 7 (4), 259-270.

This page has been left intentionally blank.

STABILITY EVALUATION AND BEHAVIOUR MONITORING OF SONGSANRI ROYAL TOMB COMPLEX IN GONGJU, KOREA

S.H. Kim[1], C.H. Lee[1*], Y.H. Jo[1] and S.H. Yun[1]

Abstract

As Royal tomb of King Muryeong was firstly excavated in 1971, the Songsanri tomb complex had a great influence on the history of the unknown Baekje Kingdom. However, the stability of the Songsanri tomb complex has been undermined due to constant exposure to external environment since it was uncovered. Thus, this study involved monitoring of wall behaviour to diagnose structural stability of Songsanri tomb complex. The results showed very precise data on the deformed state of the structurally vulnerable walls and behaviour characteristics which varied, depending on environmental changes.

Keywords: wall movement monitoring, structural stability, Songsanri tomb complex

1. Introduction

The Songsanri tomb complex is the royal tomb of Ungjin Period in Baekje Kingdom from AD 475 to 538 in Korean Peninsula which is located at Geumseong-dong, Gongju City, Republic of Korea. Among the Songsanri tomb complex, the Royal tomb of King Muryeong was confirmed the identity of the dead and its construction period. Accordingly, Songsanri tomb complex became the basic point of the recording study of Baekje Kingdom and has been assessed as a precious cultural heritage.

But, since its excavation, it suffers from stability due to exposure to external environment, rainfall and poor drainage. Leakage, microorganism and wall movement were found and it was permanently closed in 1997. Currently, a thermo-hygrostat operation is stopped in the tomb and humid environment is kept. Therefore, it is vulnerable for secondary damage by dew and microorganism. Accordingly, this study performed conservation status survey and wall movement monitoring to examine structural stability of Songsanri tomb complex.

[1] S.H. Kim, C.H. Lee*, Y.H. Jo and S.H. Yun
Department of Cultural Heritage Conservation Sciences, Kongju National University, Republic of Korea
chanlee@kongju.ac.kr

*corresponding author

2. Conservation status

2.1. Songsanri tomb No.5

Structural cracks and shear fracture with members dislocated by vertical structural cracks in rock properties were found to be the primary cause of damage in Songsanri tomb No.5 (Fig. 1). Particularly, the swelling phenomenon of rock properties can be clearly observed in upper part on the northern wall and south-western wall, creating an impression of structural instability.

Fig. 1: Deterioration status of Songsanri tomb No.5. (A, B) Structural crack and fracture in rock properties. (C) Swelling phenomenon on west wall side.

2.2. Songsanri tomb No.6

The Songsanri tomb No.6 has mural paintings on the wall of bricks. However, the mural paintings have only the trace of dim white-coloured layer on the background layer surface, and are undergoing the powdering process due to the loss of bond in white pigment layer. Physical damage in Songsanri tomb No.6 is concentrated in ceilings of burial chamber and dromos, such as cracks, fracture and separation (Fig. 2).

Fig. 2: Deterioration status of Songsanri tomb No.6 - a) Powdering of white pigment layer on the wall painting, b) Crack, separation and distortion on ceiling; c) Vertical bricks arranged unevenly.

2.3. Royal tomb of King Muryeong

The physical and structural damages of Royal tomb of King Muryeong are more conspicuous, such as cracks, fracture, separation, exfoliation, twisting and etc., in overall way, compared to Songsanri tomb No.6 (Fig. 3). Particularly, bricks located at the center of ceiling of dromos are considered to have been moved downward.

Fig. 3: Deterioration status of Royal tomb of King Muryeong. (A) Crack, separation and distortion on ceiling of bricks. (B) Lack of dromos ceiling that looks to move downwardly. (C) Structural crack on floor of bricks.

3. Wall movement monitoring

3.1. Overview and methods

Behavioural measurement of architectural cultural heritage is carried out to identify the characteristics and cause of structural vulnerability and analyze the problems so as to present reinforcement plans and measures. By doing so, stable preservation and management can be ensured, as well as prevention of basic and structural problems of architectural cultural heritage (Inaudi *et al.*, 2001; Glisic *et al.*, 2007). In this study, we installed 7 single axis (x axis) tilt sensor and carried out monitoring for about 10 months from December 8, 2013 to October 8, 2014 (Tab. 1 and Fig. 4).

Tab. 1: Tilt sensor status installed in Songsanri tomb complex.

Specification	**T1**	**T2**	**T3**	**T4**	**T5**	**T6**	**T7**
Position	Songsanri tomb No.5		Songsanri tomb No.6			Royal tomb of King Muryeong	
	East	North	West	North	Ceiling	West	South

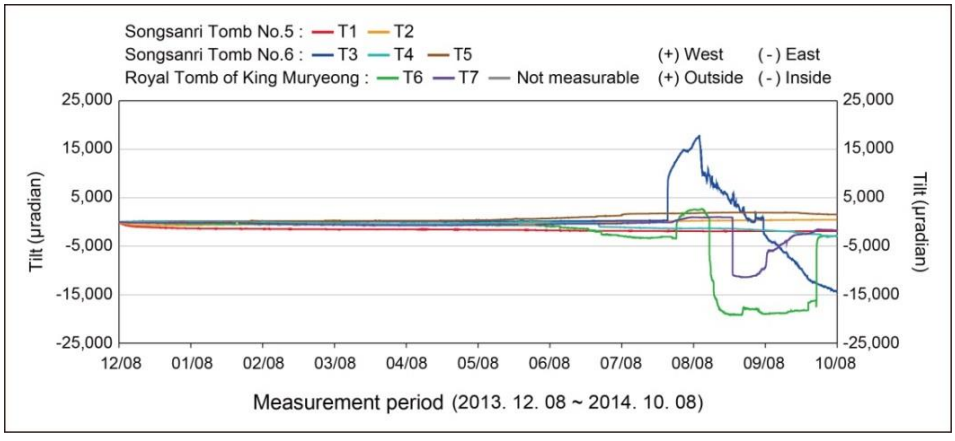

Fig. 4: Movement monitoring result of Songsanri tomb complex.

3.2. Movement characteristics

The slope of ground and structure are known to be affected significantly by temperature of atmosphere, pressure, precipitation, quantity of solar radiation and underground water level changes (Kumpel *et al.*, 1988; Lee, 1993; Suh *et al.*, 1997). The effects of such environmental changes always exist even inside the tomb. Therefore, we collected environmental data, such as temperature, humidity, precipitation and soil water content, for the duration of monitoring activities. Based on such data, we analyzed the effect of environmental changes in micro-behaviour of walls.

3.2.1. Change of rainfall and soil water contents

We analyzed the behaviour characteristics of walls inside the tomb based on variation of rainfall and soil water content. The unstable behaviour zone, shown in T1 to T7, was fully consistent with the zone where the soil water content changed fast due to the effect of rainfall. Particularly, very rapid behavioural changes in T3, T6, and T7 were observed in the intensive rainfall season in June to August. Maximum displacement variation quantity was found to be 32,250 μrad, 21,274 μrad and 11,959 μrad, respectively. Such displacement variation amount corresponded to approximately 1.8˚, 1.2˚, and 0.7˚ in terms of angle (Fig. 5).

Such phenomenon is considered attributable to an increase in soil water content ratio as a result of influx of rainwater into burial mound and an increase in the load on the inside of tomb, causing a change in external force such as compressive force, external soil pressure, etc. In addition, the behaviour of wall is considered to have been affected by the change in external force applied to the inside of tomb as the soil becomes dry after rainfall (Fig. 5).

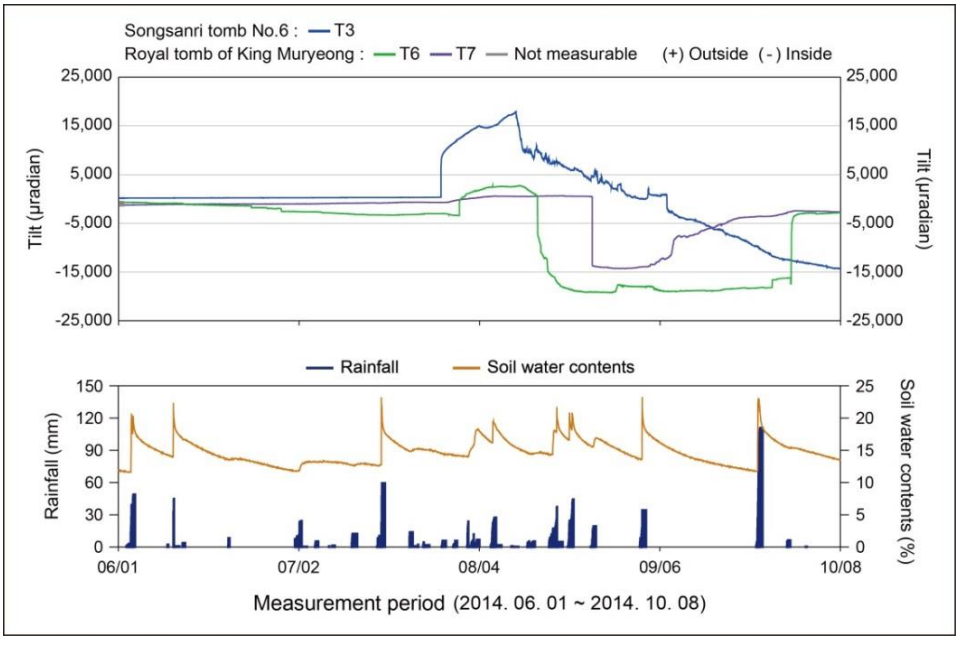

Fig. 5: Movement characteristics of T3, T6, T7 in the rainy season.

3.2.2. Visitors impact?

Although no significant change in indoor humidity was observed when two or three persons entered and exited(or went out from) the tomb, the temperature inside tended to increase temporarily. The internal temperature of tomb varied, depending on tombs, and rose by more than 2.0°C, the highest increase, in Songsanri tomb No.6. Thus, we analyzed the behaviour characteristic of wall based on artificial environmental changes induced by visitors inside tomb (Fig. 6).

The results showed that rapid behavioural change occurred in T1 to T7 instantly within a small range when we investigated the inside of tomb (Fig. 6). Such behavioural changes are considered attributable to the effect of temporary environmental changes and fine vibration caused by traffic of people entering and exiting the tomb. No internal temperature data was obtained from Songsanri tomb No.5 during the same period because of abnormality in temperature measurement sensor.

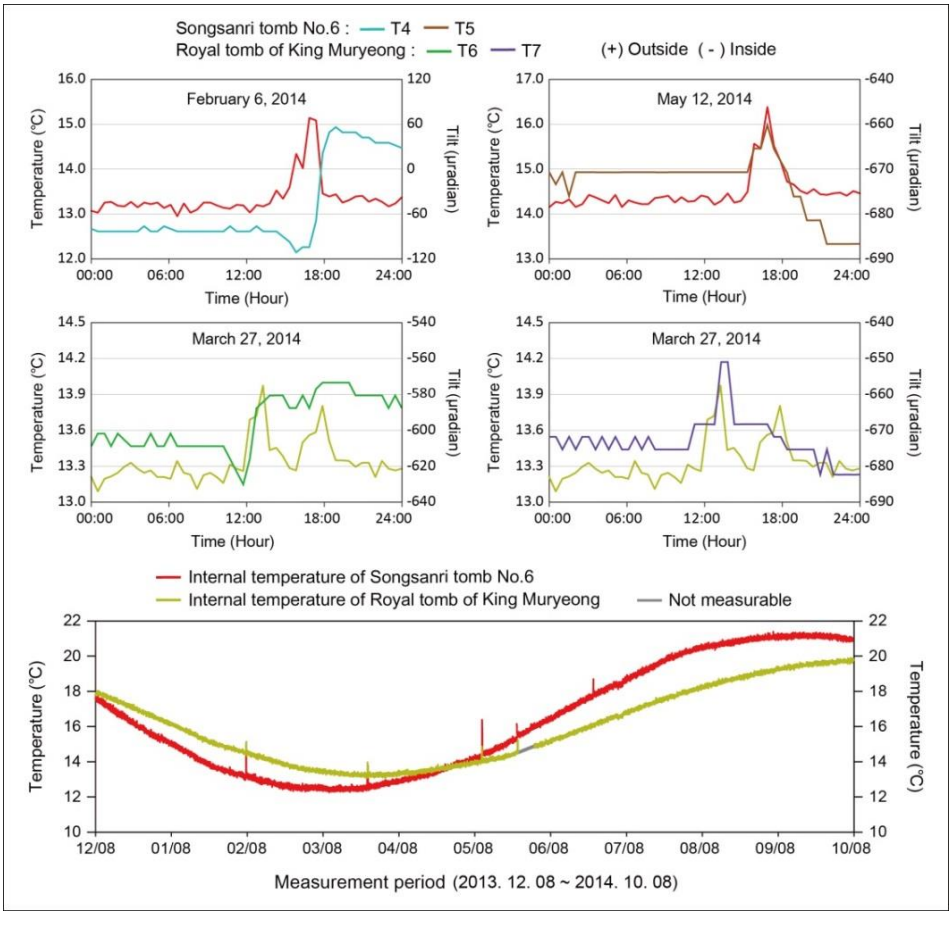

Fig. 6: Movement characteristics by artificial environmental change.

4. Conclusion

Based on comprehensive consideration of aforesaid results, relatively stable conditions were observed in Songsanri tomb No.5 which showed constant behavioural in walls despite various environmental changes. However, some walls of Royal tomb of King Muryeong and Songsanri tomb No.6 which exhibited unstable behaviour due to rainfall were found to be in a structurally vulnerable state and reacting easily to the changes in external forces. Moreover, extensive physical damage had been already caused to the bricks forming the Royal tomb of King Muryeong and Songsanri No.6 tomb, giving rise to partial problems of structural stability.

Thus, precise and in-depth investigation on structural engineering basis needs to be carried out to prevent damage to the bricks of Songsanri No.6 tomb and Royal tomb of King Muryeong and restore structural safety. Moreover, comprehensive maintenance plans need to be mapped out to ensure long-term preservation in the period ahead.

References

Kumpel, H.-J., Peters, J.A., Bower, D.R., 1988, Nontidal tilt and water table variations in a seismically active region in Quebec, Canada, Tectonophysics, 152, 253-265.

Lee, S.K., 1993, Shallow-depth Tilt Monitoring for Engineering Application, The journal of Engineering Geology, 3, 279-293.

Suh, M.C., Park, E.J., 1997, Characteristics of Subsurface Movement and Safety of the Songsanri Tomb Site of the Baekje Dynasty using Tiltmeter System, The Journal of Engineering Geology, 7, 191-205.

Inaudi, D., Casanova, N., Glisic, B., 2001, Long-term deformation monitoring of historical constructions with fiber optic sensors, Historical Construction, Guimaraes, 421-430.

Glisic, B., Inaudi, D., Posenato, D., Figini, A., Casanova, N., 2007, Monitoring of heritage structures and historical monuments using long-gage fiber optic interferometric sensor -an overview, The 3rd International Conference on Structural Health Monitoring of Intelligent Infrastructure, Vancouver, 13-16.

SIMULATED WEATHERING AND OTHER TESTING OF DIMENSION STONE

D. Kneezel[1*]

Abstract

Because stone is a natural material, its physical and mechanical properties vary significantly from quarry to quarry, and often even within a single quarry. Laboratory testing of dimension stone is thus necessary to evaluate a stone type prior to its use on a building, particularly for stone that does not have a significant history of use. This often includes simulated weathering testing to identify durability concerns for stone that will be exposed to severe weathering environments. Laboratory testing is also a useful tool in evaluating the effect of deterioration and strength loss on stone removed from the exterior of an existing structure. This paper will discuss the ASTM (and similar CEN) stone test methods that are routinely performed to evaluate dimension stone. Particular emphasis will be placed on laboratory simulated weathering testing that has been performed on various stone types by the author, and comparison with stone that has been exposed to real time weathering in Chicago's severe weathering environment.

Keywords: dimension stone testing, simulated weathering, ASTM, CEN, durability

1. Introduction

The characteristics that contribute to the appeal of stone as building cladding or paving, such as its natural aesthetic and its durability, are also the characteristics that necessitate testing and require specific attention. Being a natural material, no two stone panels have identical physical and mechanical properties. Testing should be performed to evaluate the strength, variability, and durability of stone, providing the designer necessary information to select appropriate stone spans and thicknesses and ultimately determine whether the stone selected is suitable for its intended use. The following summarizes standard ASTM and CEN test methods for evaluation of dimension stone, including a comparison of simulated weathering testing and real time weathering of various stone types to evaluate the effectiveness of the simulated weathering test.

2. Physical and mechanical testing

ASTM International publishes material specifications for granite (C615), limestone (C568), marble (C503), sandstone (C616), serpentine (C1526), slate (C406 and C629), and travertine (C1527). The material specifications list minimum requirements for absorption and density (C97), modulus of rupture (C99), compressive strength (C170), flexural strength (C880), and abrasion resistance (C241 or C1353). The minimum values listed in these standards are consensus values established by ASTM Committee C18 on Dimension

[1] D. Kneezel*
Wiss, Janney, Elstner Associates, Inc., United States
dkneezel@wje.com

*corresponding author

Stone, and are based on stone that has traditionally performed well in service for general building and structural purposes. Stone that does not meet these minimum values can still be used provided competent engineering has accounted for its material properties. While the minimum requirements for some stone types are less stringent than others, for example the maximum absorption for limestone and sandstone is significantly higher than for granite and marble, the application of different safety factors and differences in use between stone types account for the varying minimum requirements.

2.1. Tests for engineering properties

The tests for engineering properties are used to evaluate stone strength and variability, and include compressive strength, modulus of rupture, flexural strength testing, and anchorage strength testing (Fig. 1). Stone strength may be variable within a single block, or variable throughout a quarry (laterally and vertically). Depending on the size of the project, it may be appropriate to test specimens from several blocks throughout a quarry to obtain a representative test population or perform periodic testing during production to evaluate changes as stone extraction location varies. Test results greater than 2 years old are generally considered to be outdated, depending on the uniformity of the formation and amount of stone extracted since testing was performed, as test data from areas where stone is not currently being extracted is of limited use.

Fig. 1: Tests for engineering properties. Clockwise from upper left: compressive strength, modulus of rupture, flexural strength, anchorage strength.

The tests for engineering properties should also consider both the orientation (i.e., parallel, perpendicular, or fleuri) of the stone relative to bedding/foliation/rift, and wet or dry condition of the stone when tested. There may be significant strength differences due to specimen span relative to the orientation of the stone for vein cut and fleuri cut panels (Fig. 2). Strength testing should be performed on specimens that are oriented both parallel and perpendicular to loading, with up to three orientations for projects where both vein and fleuri cut panels are to be used. Where orientation of the stone on the project is unknown or random, it is common practice to perform testing of both vein cut specimens with load oriented parallel to rift and fleuri cut specimens, which provide representative low and high strength values, respectively.

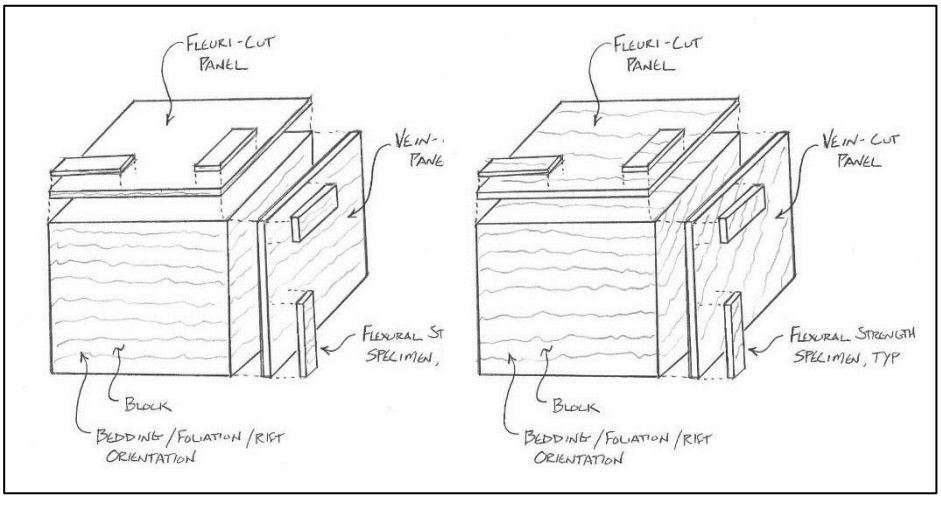

Fig. 2: Specimen orientation relative to slab and block orientations. Idealized block with bedding planes parallel orthogonal block edges shown on the left; more representative block with bedding planes running diagonally shown on right.

Wet (48 hour immersion in water) and dry (48 hour oven dry) conditioning can also affect strength, with wet conditioning typically resulting in similar or lower strength (e.g., due to the effect of water on the interlocking mineral structure of the stone or from softening of clay minerals). CEN and ASTM test methods differ slightly in oven dry temperature; however, both CEN and ASTM test methods require drying and wetting until an equilibrium weight is achieved, making the temperature difference of little significance as even the higher temperature is not likely sufficiently high to significantly affect the mineral structure of most stones.

For each orientation and condition to be tested, strength test methods require a minimum of five test specimens, typically resulting in twenty total test specimens (wet/dry, parallel/perpendicular). This quantity can be reduced if the panel span relative to stone orientation is consistent for a project, or if comparison between wet and dry testing is not necessary (e.g. - if petrography will be performed to identify deleterious materials, wet condition testing alone may be sufficient).

2.1.1. Compressive Strength

Compressive strength testing provides data for the structural design of bearing type masonry walls in which the stone is subjected to compressive stresses. While the test results are not applicable to structural design of thin stone veneers, this test is often specified even for these applications because it provides basic information on the stone strength for comparison with past data for the same stone (quarry uniformity), and comparison with minimum requirements listed in the stone specifications

The test procedures for compressive strength testing are summarized in ASTM C170, *Standard Test Method for Compressive Strength of Dimension Stone*, or EN 1926, *Determination of Uniaxial Compressive Strength*. The specimen size and procedure is very similar for both tests. The load at which the stone breaks is divided by the surface area of the stone to provide a failure stress in MPa or psi.

2.1.2. Modulus of Rupture

There are two test methods for flexural strength of dimension stone; flexural strength under concentrated load, also referred to as modulus of rupture testing, and flexural strength under constant moment. Flexural strength testing under constant moment is the preferred method for structural design of thin stone veneers in which the stone is subjected to flexural stresses, or for evaluation of strength loss of stone removed from a building where there is concern over its current strength. Test results for either method can also be compared with past data or minimum requirements listed in the stone specifications for a more general assessment. Flexural strength test results can also provide an indication of stone strength at anchors, particularly for kerf anchors, though stone strength at anchors is more accurately evaluated though anchorage strength testing.

Flexural strength testing under concentrated load is performed in accordance with ASTM C99, *Standard Test Method for Modulus of Rupture of Dimension Stone*, or EN 12372, *Determination of Flexural Strength under Concentrated Load*. The procedure for both the ASTM and EN tests is similar, utilizing mid-span loading of a specimen until failure, which typically occurs directly below the applied load at the maximum moment location. The EN procedure utilizes a greater span to thickness ratio of 5:1 than the ASTM procedure of approximately 3:1. This will generally result in slightly higher values for the ASTM method, as a shorter span will provide greater arching within specimens of similar thickness. Furthermore, it is our experience that thin specimens typically have lower average tested strength and greater variation than thicker specimens of the same material, likely because a small natural defect or difference in grain size will have a greater effect on a thin specimen. For both this test and the flexural strength test under constant moment (summarized below), the induced moment at which the stone breaks is divided by the section modulus of the rectangular cross-section to provide a failure stress in MPa or psi.

2.1.3. Flexural Strength

Flexural strength testing under constant moment is preferred to the concentrated load test because two load rollers are used to apply load to the specimen, resulting in a uniform maximum moment between the load rollers. Failure thus occurs at the weakest plane between load application rollers, as opposed to failure at a predetermined plane directly below the load, providing more representative strength and variability data for the stone.

Based on past experience, the ASTM constant moment test typically results in approximately 20 percent lower values than the ASTM concentrated load test.

Flexural strength testing under constant moment is performed in accordance with ASTM C880, *Standard Test Method for Flexural Strength of Dimension Stone,* or EN 13161, *Determination of Flexural Strength under Constant Moment*. The procedure for the ASTM and EN tests differs in that the EN test specifies loading at 1/3 span locations, while the ASTM test specifies loading at 1/4 span locations. The ASTM test also utilizes a greater span to thickness ratio of 10:1 compared to 5:1 for the EN procedure. Both of these factors will generally result in slightly lower values for the ASTM test, which subjects a greater length of the specimen to the maximum load and thus there is a greater potential for the presence of a weaker plane in this area.

2.1.4. Anchorage Strength

Anchorage strength testing is typically performed to evaluate the stone strength at the anchor type proposed for securing thin stone panels, or for evaluating stone strength at existing anchorages. The test procedures for anchorage strength testing are summarized in ASTM C1354, *Standard Test Method for Strength of Individual Stone Anchorages in Dimension Stone,* or EN 13364, *Determination of the Breaking Load at Dowel Hole*. The ASTM test method provides a procedure for testing of virtually any stone anchor type including dowel anchors, kerf anchors, or undercut anchors, while the EN procedure is limited to pullout testing of dowel anchors. The ASTM test is an inherently specialized test in which the specimen size, thickness, and anchor slot dimensions are variable and intended to replicate the anchorage to be used. The EN test lists a standard specimen size but allows thickness to be varied.

2.2. Durability tests

Stone loses strength when exposed to moisture, freezing and thawing cycles, temperature extremes, rain acidity, and crystallization of salts, or more typically a combination of these. While this may not be of significant concern in a bearing type masonry wall in which stone typically has excessive compressive strength capacity, it is often a critical consideration for thin stone veneers that inherently push the limits of a stone's strength (maximize the use of a stone's flexural strength), particularly for stone to be used in a severe weathering environment. It is not uncommon for a thin stone veneer that originally met code wind load requirements to lose enough strength to warrant intervention, including installation of repair anchors, isolated panel replacement, or even recladding. Test methods and evaluations that provide a better understanding of potential future weathering durability, as well as surface wear in paving or flooring applications, are therefore a critical part of the design process. These include petrographic evaluation, absorption and specific gravity, open porosity, abrasion resistance, salt crystallization, bow testing, and simulated weathering.

Durability tests are particularly useful for a stone with unknown or limited performance history, or for stone that does not meet the minimum specified physical properties for that stone type, to reduce the risk of using a poor durability stone on a project. While durability tests may not be of great value on a new project when using a stone that has an established history of use in the environment similar to that being considered, they may be appropriate for large or high profile projects where testing represents a small percentage of the total project cost regardless of the stone type. Even for projects of more limited scope, the minimal cost of absorption testing and petrographic evaluation warrant their use. The

primary drawback of durability testing, as with all testing, is that only a very small fraction of the material being used on a project can be evaluated, so testing may not identify an infrequent detrimental feature.

2.2.1. Petrographic Evaluation

Petrographic evaluation is a qualitative review of stone features or constituents that may affect stone strength and durability. Initial petrographic evaluation of a quarry provides a broad overview of the uniformity of the exposed stone or blocks within the quarry and presence of visible features or textures that may cause serviceability issues for use in establishing quality control measures. Quarry evaluation can also help to ensure that test specimens are representative of project material. Petrographic evaluation of representative individual specimens provides more detailed information on the stone mineralogy and structure of the stone for identification of minerals that may cause spalling, staining, or other serviceability issues (e.g. - iron inclusions or poor weathering minerals such as clay). Petrographic evaluation can also identify mineral sizes, grain structure, susceptibility to cleaving, orientation of bedding/foliation/rift, or other variations in the stone fabric that may contribute to strength variations, bowing, or low durability. It can also be used to help determine the cause of distress in an existing application.

The guides for petrographic evaluation are ASTM C1721, *Standard Guide for Petrographic Examination of Dimension Stone*, and EN 12407, *Petrographic Examination*. While the evaluation methods are generally similar, both are guides that are likely to be modified by the user depending on the stone type or specific intent of the evaluation.

2.2.2. Absorption and Specific Gravity

Absorption measures the amount of water retained by the stone when immersed, or the weight of water absorbed as percentage of the dried specimen weight, while specific gravity measures the density (mass per unit volume) of the stone relative to that of water. Absorption and density are indicators of durability, as water that is readily absorbed and retained within the stone can result in damage as it freezes and expands, producing tensile stresses in the stone structure to which stone is vulnerable. More dense stones are typically associated with lower absorption values. Stones with absorption or density values exceeding the ASTM requirements for that stone type are typically considered less durable, though the mineral composition and void structure may mitigate concern over stone with higher than normal absorption. Because of this, simulated weathering testing is more predictive of weathering durability; however, it is also significantly more expensive and time consuming than the absorption test. The test procedures for this testing are summarized in ASTM C97, *Standard Test Methods for Absorption and Bulk Specific Gravity of Dimension Stone*, EN 13755, *Determination of Water Absorption at Atmospheric Pressure*, and EN 1936, *Determination of Real Density and Apparent Density, and of Total and Open Porosity*. The primary difference between the ASTM and EN absorption test procedures is the specimen wetting technique. The EN procedure prescribes gradual immersion of specimens in water, while the ASTM procedure prescribes full immersion immediately. Round robin absorption testing was recently performed by the author on groups of approximately five specimens from each of fifteen stones (five granite types, four limestone types, and one type of marble, slate, sandstone, quartzite, travertine, and soapstone) using both the ASTM and EN test procedures to evaluate the effect of wetting technique and extreme specimen sizes on test results, finding that neither has a significant

effect. The ASTM and EN procedures are similar to one another for density testing, though EN also includes a test for open porosity in which the volume of open pores (or interconnected pores that may be occupied by water) is measured as a percentage of the volume of the sample. While these tests are indicators of durability, they do not evaluate the effect of freezing and thawing cycles, temperature extremes, acid rain, or salt crystallization, which can be evaluated through other durability tests.

2.2.3. Abrasion Resistance

Abrasion resistance testing is performed to evaluate resistance of stone to wear from pedestrian traffic. The test procedures for abrasion resistance testing are summarized in ASTM C1353, *Standard Test Method for Abrasion Resistance of Dimension Stone Subjected to Foot Traffic Using a Rotary Platform, Double-Head Abraser*[1], or EN 14157, *Determination of Abrasion Resistance*. For the ASTM procedure, test specimens are weighed before and after being subjected to 1,000 revolutions of a double-headed abrasive wheel, from which the weight loss is used to calculate an abrasive hardness value. Test results can be compared with minimum requirements listed in the stone specifications to determine suitability of the stone for paving or flooring applications. There is no correlation between ASTM and EN abrasion resistance test results.

2.2.4. Salt Crystallization

Salt crystallization testing is performed to evaluate resistance of a stone to crystallization of salts within its pore structure. The test procedure is summarized in EN 12370, *Determination of Resistance to Salt Crystallization*. There is currently no ASTM counterpart to this test. For this test, cube specimens are subjected to fifteen cycles of immersion in a sodium sulphate solution followed by oven drying to 105°C (220°F). The percentage change in average mass of specimens and presence of distress is used to determine the suitability of stone exposed to salt spray (e.g. coastal environments or near grade where deicing salts are used).

2.2.5. Bow Testing

Some varieties of marble bow when exposed to temperature extremes and moisture, particularly in thin stone veneer applications. To evaluate the potential for marble bowing, testing can be performed in accordance with EN 16306, *Determination of Resistance of Marble to Thermal and Moisture Cycles*. There is currently no ASTM counterpart to this test. For this test, specimens are exposed to heating from above and moisture from below while the temperature is cycled between 20°C and 80°C (68°F and 176°F). The change in bow of specimens after 50 one day cycles is compared to limit values provided by the standard for marble to be considered suitable for exterior cladding. Flexural strength testing is also performed on specimens not exposed and after exposure for evaluation of associated strength loss.

2.2.6. Simulated Weathering

Simulated weathering testing is performed to evaluate the effect of freezing and thawing cycles in the presence of moisture on stone durability. While there is no ASTM test method for simulated weathering of dimension stone, an “accelerated weathering” test method has

[1] Alternative test procedures are provided in ASTM C241, Standard Test Method for Abrasion Resistance of Stone Subjected to Foot Traffic.

been used to evaluate durability of stone proposed for use in severe weathering environments for more than 30 years and employs procedures similar to those outlined in ASTM C666, *Standard Test Method for Resistance of Concrete to Rapid Freezing and Thawing*. The corresponding CEN procedure is EN 12371, *Determination of Frost Resistance*.

For both tests, dynamic modulus of elasticity is typically performed at periodic intervals to non-destructively evaluate rate of deterioration in accordance with ASTM C215, *Test Method for Fundamental Transverse, Longitudinal, and Torsional Frequencies of Concrete Specimens*, or EN 14146, *Determination of the Dynamic Elastic Modulus of Elasticity*. Specimens are also visually examined concurrent with this periodic testing. For both methods, the tested strength of specimens after exposure is compared to companion specimens not exposed to evaluate the effect of freeze/thaw cycles on performance. The EN procedure allows flexural strength, compressive strength, or load at dowel hole specimens to be exposed, while the accelerated weathering testing is typically performed on flexural strength specimens. The EN test also provides specific failure criteria including limits on the degree of observed deterioration, decrease in dynamic modulus, or decrease in apparent volume, whereas results of accelerated weathering testing (change in strength, dynamic modulus, and visual appearance) are typically compared to past results for similar stone types.

The EN test procedure specifies temperature cycling from -12°C to 20°C (10°F to 68°F) with freezing in air and thawing in water, typically for a total of 12 cycles for stone to be used in exterior cladding applications or 48 cycles for stone to be used for paving. The accelerated weathering test subjects specimens to more severe temperature extremes of -23°C to 77°C (-10°F to 170°F), which are based on measured surface temperature extremes of stone in service, and a greater number of cycles (typically 100 cycles, or 300 cycles for more significant projects) and cycles per day (typically 4 versus 2), while specimens are partially immersed in a 4 *pH* acid solution to simulate acid rain exposure or water throughout testing. All of these factors result in the accelerated weathering test being more rigorous than the EN test, as greater temperature extremes are known to more greatly affect the mineral structure of some stone types, greater number of cycles per day result in more rapid temperature changes, exposure to acid solution may lead to dissolution of certain constituents (e.g. calcium carbonate), and exposure to water or acid solution during freezing temperatures results in expansive forces applied to the specimens as water expands within a confined space (typically a stainless steel pan) in which specimens are placed.

The accelerated weathering test is an intentionally aggressive test, as it is important that any weathering test be sufficiently severe to cause damage that may occur in service (assuming specimens are representative), as passing of the test followed by failure in service would warrant criticism. It is our experience that stone types that traditionally perform well in service also typically perform well in the test. This test may, however, be overly severe for regions where freeze/thaw cycles rarely occur. For environments where freezing rarely occurs, the minimum temperature extreme may be increased to 5°C (41°F). While this test is typically performed for severe weathering applications, simulated weathering testing is likely appropriate for any region that experiences regular freezing and thawing regardless of the actual number of cycles per year since stone construction is typically intended to have a long service life.

2.2.7. Real Time Weathering

While a direct correlation between simulated weathering cycles and real time weathering is often requested, the purpose of the simulated weathering test is not to identify a precise timeframe in which a stone will fail, but rather to evaluate a stone's potential susceptibility to weathering based on comparison with past testing of similar stone types. However, an ongoing study is in progress in which several groups of specimens representing various stone types have been exposed to up to 20 years of real time weathering on the roof of a building in Chicago's[1] severe weathering environment to provide a better understanding of how real time weathering relates to simulated weathering. The dynamic modulus of these specimens is typically monitored twice per year to approximate their strength loss over time. For several of these stone types, the difference in tested strength of specimens not exposed and companion specimens exposed to 100 cycles of accelerated weathering ("strength loss") are available from prior studies.[2] The following Tab. 1 lists the percent loss in dynamic modulus after approximately 20 years of real time exposure and "strength loss" of these stone types dues to 100 cycles of accelerated weathering exposure. The prior studies indicated that 12 to 15 cycles of accelerated weathering is equivalent to approximately one year of real time weathering in a temperate climate.

Tab. 1: Dynamic Modulus Loss, Real Time Weathering vs. Strength Loss, AW.

Stone Type	**Dynamic Modulus Loss**	**"Strength Loss" after 100 Cycles**
	%	%
White Granite	30.0	9.0 to 17.3
Marble 1	78.9	27 to 41
Marble 2	82.5	27 to 41
Medium Density Limestone - parallel	34.5	9.6
Medium Density Limestone - perpendicular	18.3	9.6

The table above shows that stone types that experienced greater "strength loss" due to accelerated weathering exposure have also experienced greater reduction in dynamic modulus (indicator of strength loss) when exposed to real time weathering. It also shows that the percent reduction in dynamic modulus over 20 years of real time weathering exposure is greater than the percent "strength loss" resulting from 100 cycles of accelerated weathering. For both accelerated weathering and real time weathering all specimen surfaces are exposed, whereas the temperature of cladding stone is often moderated by a heated building. Further study of this data is necessary to provide a more comprehensive

[1] More precisely, on WJE's campus at 330 Pfingsten Road, Northbrook, Illinois

[2] Values are taken from *Laboratory Evaluation of Building Stone Weathering*, see references. The table only includes stone types for which data was available in this report.

comparison of real time freeze/thaw cycles per year and extreme temperatures to which these specimens have been exposed.

3. Summary and conclusions

There is no single universal test for evaluation of dimension stone. While review of the same stone type in similar construction in a similar environment provides an indication of the suitability of a stone, it is also a natural material with variable (in some cases highly variable) properties throughout a quarry. Strength testing is performed for engineering evaluation or for comparison with past data, while durability evaluation and testing provide insight into the potential for deterioration and strength loss over time in exterior applications. A comprehensive test program is necessary to assess strength, uniformity, and durability of a particular stone type, particularly for high profile projects or where a significant amount of stone is used. The specifying authority must therefore have a thorough understanding of the purpose of each test to achieve the goals of a particular project with regard to the use of stone.

Acknowledgements

I would like to acknowledge Mr. Michael J. Scheffler, Principal with Wiss, Janney, Elstner Associates Inc. (WJE) for his helpful review in the preparation of this paper.

References

Bortz, S.A. and Wonneberger, B., October, 1997, Laboratory Evaluation of Building Stone Weathering, in proceedings of Degradation of Natural Building Stone, Labuz, J.F. (ed.), Minneapolis, Minnesota, ASCE American Society of Civil Engineers, Geotechnical Special Publication No. 72, 85-104.

IR THERMOGRAPHY IMAGING OF WATER CAPILLARY IMBIBTION INTO POUROUS STONES OF A GALLO-ROMAN SITE

J. Liu[1*], J. Wassermann[1], C.-D. Nguyen[1], J.-D. Mertz[2], D. Giovannacci[3], R. Hébert[3], B. Ledesert[3], V. Barriere[4], D. Vermeersch[4] and Y. Mélinge[1]

Abstract

The Gallo-Roman site of the Vaux-de-la-Celle in Genainville (France) is registered into French Historical Monuments since 1941. Studies on deteriorations caused by water and salts in masonry could be essential to the diagnosis and subsequent restoration. In the present work, we firstly characterised the limestone used in the site by describing its porosity, pore size distribution, volumetric mass and water permeability by means of hydrostatic weighing, mercury intrusion porosimetry and pressure applied. Infrared (IR) thermography was then employed as a monitoring technique during water capillary imbibition tests to study its kinetic. In results of this work, i) the withdrawn stones from the Gallo-Roman site have a high porosity and high water permeability; ii) the apparent front of capillary rise can be localized continuously during the test using the non-invasive infrared imaging.

Keywords: porous materials, capillary rise, monitoring, heritage buildings, infrared (IR) thermography, water content

1. Introduction

Water is a determining factor in the damaging processes of porous building materials, especially liquid water distribution in pores and flow. Liquid water flow in porous media may cause internal erosion (Vardoulakis *et al.*, 2001) or dissolution of the solid material resulting in porosity and permeability changes (e.g. Hoefner and Fogler, 1988). Solute (like salts) concentration variation results from external supply, liquid water influxes (like capillary supply by the water table, etc.), outfluxes (such as evaporation, etc.); dependant of environmental conditions such as atmospheric temperature, barometric pressure, air humidity, precipitation (snow, rain), winds, soil water transport. Cyclic drying-wetting

[1] J. Liu*, J. Wassermann, C.-D. Nguyen and Y. Mélinge
Laboratoire de Mécanique et Matériaux du Génie Civil (L2MGC),
University of Cergy-Pontoise, France
jun.liu@u-cergy.fr

[2] J.D. Mertz
CRC-LRMH USR3224, Sorbonne University, France

[3] R. Hébert and B. Ledesert
Laboratoire Géosciences et Environnement (GEC), University of Cergy-Pontoise, France

[4] V. Barriere and D. Vermeersch
Departement of Geography and History, University of Cergy-Pontoise, France

*corresponding author

processes act on solute or salt concentration and then may involve cyclic crystallization-dissolution processes. The latter may induce mechanical damage, cracking, cohesion loss, resulting from stress concentration between salt crystals and pore walls (Scherer, 1999); it can also combine with ice crystal action (Coussy, 2005). Damage due to salt, named salt weathering, involves several mechanisms (Doehne, 2002) and features from nanometer scale (swelling of clay minerals) to centimeter and meter scales (e.g. crack and fracture growth).

This research deals with *in situ* characterization and monitoring — using non-invasive methods such as IR imaging and electrical resistivity tomography — of water content distribution and diurnal to seasonal evolution into the masonry of a Gallo-Roman temple. In the valley of Vaux-de-la-Celle (Genainville, North West of Paris basin, France), the building stony materials are subject to degradation and their basement to water capillary rise from the shallow water table. Hence, a variation of water content within the masonry (conditioning salt weathering and consequent damages) could be induced by seasonal variations of the water table or barometric pumping due to atmospheric pressure oscillations (Turk, 1975).

This paper focuses on experiments of spontaneous capillary imbibition into limestone samples coming from the archeological site of Genainville. The capillary rise phenomenon was characterised using an InfraRed (IR) camera. The study consists in: first, a description of the archeological site and concerned material properties; second, the experimental procedure details; third, results and discussion, in particular from the IRT data preliminary analysis. Finally, perspectives of this study concern additional experiments and future data analysis.

2. Site description and characterization of the studied materials

The archaeological site of Vaux-de-la-Celle, dating from the second half of the second century, includes a square temple 28 meters wide with 2 cella rooms, a theatre of about 100 meters in diameter, plus a town revealed by last century excavation. It was built due to the presence of very shallow underground water, allowing erecting a shrine with nymphaeum (3 basins). It is now accepted that the rise of the water table over the centuries has forced the population to move out the temple to a higher area of the site and then to abandon it (Mitard, 1993). The soil drainage has recently been strengthened to prevent damages induced by water-table fluctuations. Nevertheless, the latter is still near the surface and continues to impact the conservation of the temple through capillary imbibition process into the masonry and drying-wetting cycles affecting the clay-rich soil formation.

Our research focuses on the masonry walls (1 m thick, maximum 5 m tall) of a cella. The walls are composed by carved limestone ashlar jointed by lime mortar and an intern structure filled with rubbles and lime. Layers of bricks placed every 70 cm throughout the wall thickness distribute the load and avoid the capillary rise from below. Every pieces of limestone into the external masonry have a length of about 10 cm to 15 cm, 10 cm for height and 15 cm for depth. For the present preliminary study, different blocks have been collected from a pile of rubbles (but not directly from the building, as the sampling in the walls are not allowed) into the laboratory for sampling of cylindrical samples (8 cm long and 4 cm diameter) cut perpendicular to the bedding planes. Ashlars were prepared by the Romans from Lutetian limestone outcrops and underground quarries located close to the shrine. Petrophysical characterization was performed at LRMH and L2MGC Laboratories

using classical methods on 4 samples to determine the water porosity, mercury porosity, density, and water permeability (Tab. 1).

Tab. 1: Petrophysical properties of the limestone samples.

Total Water Porosity	Total Hg Porosity	Equivalent access radius	Density	Water Permeability
%	%	µm	kg/m^3	m^2
45±1	43.56±1.49	0.01 to 200	1460.4±13.09	$2.11 \cdot 10^{-16} \pm 0.03 \cdot 10^{-16}$

3. Experimental procedure

Two cylindrical samples were used for the capillary imbibition test. They were all dried at 60°C until a stable mass. The mass variations after several 24h duration periods were lower than 0.1%. One of the sample was then dipped into the convex meniscus of distilled water in the container for certain depth (around 2 mm) when the other specimen was the reference sample (Fig. 1).

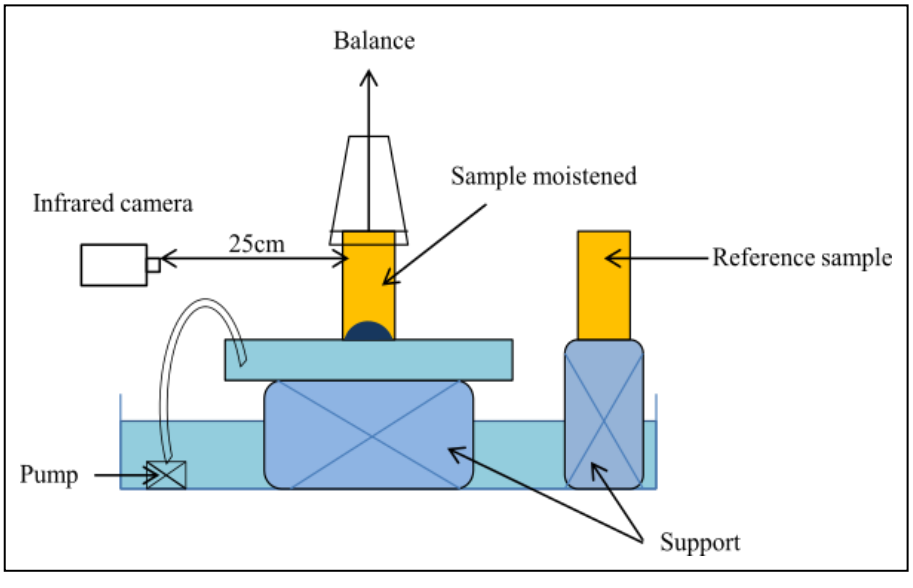

Fig. 1: Experimental set-up. Mass evolution of the sample was monitored with a balance. Environmental parameters (air temperature, barometric pressure and relative humidity) were also monitored.

Our test was carried out using an automatic data-recorder balance (accuracy of ±0.1 g) to follow the mass variation. The sample to be moistened was hung under the balance with its bottom touching distilled water in a container below. The level of water in the container was maintained constant by pumping water into it. The reference sample was put on a

support to keep more or less a same height for the two samples during the imaging process. The IR camera of FLIR® SC655 (thermal sensitivity <0.03°C, 640×480 pixels, 25°×19° field of view) was placed at the shortest distance (of 0.25 m) from the forefront of the two parallel samples in order to reduce the atmosphere thickness between the samples and IR radiation sensors. Reflection phenomena due to the environment were limited by putting a cardboard at the background of the experiment. The temperature of the air and the water in container were measured by type K thermocouples (accuracy of 0.1°C). The barometric pressure was also measured (accuracy of ±0.2 microbar), as well as the relative humidity (± 5 % accuracy). A photo was taken every 10 s by IR camera and the mass of the moistened sample was recorded every second by the balance connected to a computer. All of the environmental properties were recorded with the same sampling time of 1 s. The pump was stopped at 1240 s after noticing a plateau in the mass variation curve with time (Fig. 2d).

4. Results and preliminary analysis

During the test, environmental parameters remained more or less constant (Fig. 2e). The IR images, with no observation of clear changes of the reference sample, confirm the stability of these parameters (Fig. 2). A sequence of temperature distribution images (without any filtering or geometric correction) obtained during the test shows the two specimens at time t=10 s, 200 s and 1500 s (Fig. 2a to Fig. 2c). At t=10s, the specimen surface appears at more or less the same temperature as the background, in orange (Fig. 2a), which represents a warmer temperature than the distilled water (in blue). Reflection phenomenon on the surface of the water could explain the slightly warmer temperatures (in purple and pink). During the capillary rise, more and more "blue zones" raised from the bottom of the sample. The apparent front of capillary rise appears as a band which color (temperature equivalent) gradually varies from blue to purple and pink (Fig. 2b). The corresponding variations of mass with time are presented in Fig. 2d. At the beginning of the test (about first 18 minutes) water capillary imbibition proceeds, the measured mass increases, until reaching a plateau where mass appeared constant. The pump was then stopped; a very sudden increase-decrease (rebound, Fig. 2d) of the mass was observed when the sample was no more in contact with water; no more buoyant force was then exerted on the hanged specimen. Finally the measured force (via the balance) remains constant after this quick variation. Imbibed water rate is then deduced as well as the water absorption coefficient (Tab. 2) from (EN 1925, 1999):

$$C = \frac{m_i - m_d}{A\sqrt{t_i}} \qquad \textit{(Eq. 1)}$$

with m_i (g) is the successive mass of the sample during test; m_d (g) the mass of dry sample, A the section of the side immersed in water (cm^2) and t_i (s) the time of the absorption.

Tab. 2: Parameters of the capillary rise test.

Imbibed water	Water absorption coefficient
%	g/(cm^2·s½)
16.8	0.0565

Preliminary analysis of the IR images consists in selecting representative profiles along central axis of the tested specimen and the reference (Profile 1 and Profile 2, Fig. 3 left). The two profiles are both made of 239 pixels with a whole length of 7cm. Profile 1 (Fig. 3 left) crosses here the apparent rising front. Indeed, the IR image is the radiation response at the surface of the specimen to phenomena related to water rising. The apparent front presents a curvy shape with convexity upward. Both profiles present major trends, i.e. large band variations (Fig. 3 right), and short bands or noisy-like variations. The temperature of the reference specimen appears slightly and gradually warmer from the bottom (pixel 0) to the top (pixel 250). The temperature variation along the Profile 1 (wet sample, Fig. 3 right) includes a major step corresponding to the apparent transition (in surface radiation) from dry specimen zone (with temperature profile corresponding to the reference one) to wet zone (in blue on the corresponding image).

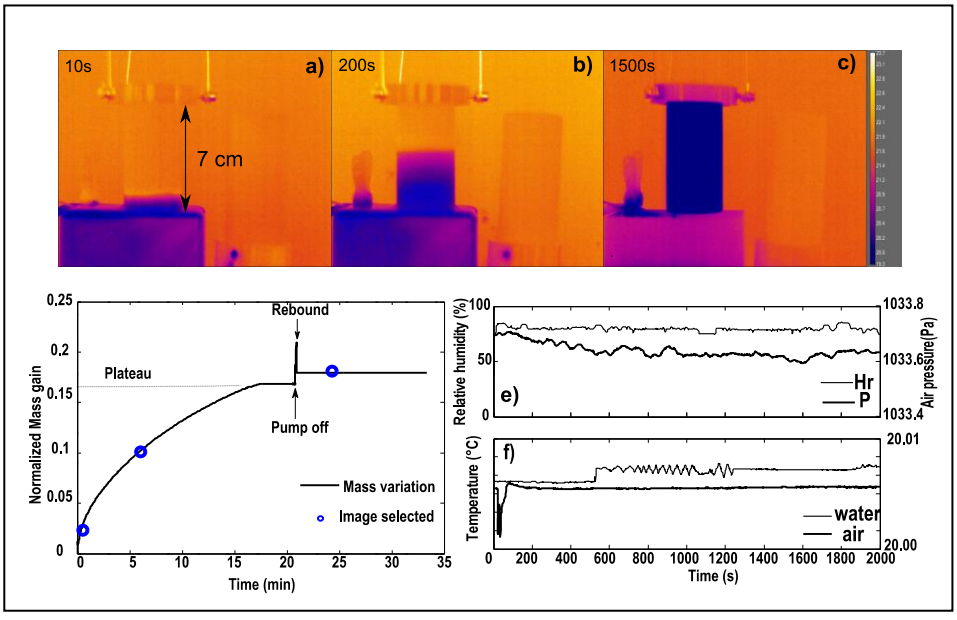

Fig. 2: a), b), c) IR images of temperature distribution at test time t=10 s, 200 s and 1500 s respectively; d) Variation of mass water absorption during the test, with dots corresponding to the time of the images a), b), c); e) The variations of air pressure, relative humidity; f)The variations of reservoir water and air temperature.

The major trend and step along profiles of the tested specimen are observed during the water imbibition rise. The raw profiles start from an average temperature of 20°C, then decrease slightly; show a subsequent increase until an almost constant temperature more or less equal to the reference specimen temperature profile. In order to identify the apparent position of rising front along these profiles, the short band variations are filtered using a Savitzky-Golay filter (Savitzky and Golay, 1964). The noisy short band variations are then smoothed and the major trends appear clearly (Fig. 4). Derivation (i.e. temperature variation for each gap pixel) along these smoothed profiles and then smoothing of the obtained derivation curves, provide a quantitative identification of the major step position at any time of the test along temperature profiles (examples on 5 profiles are presented Fig. 5). A derivative curve presents a maximum value which is supposed to correspond to the position of the apparent water imbibition front.

During the capillary rise test, distilled water rises in sample. The estimated capillary front height increases in proportion to the square root of the time (Fig. 6) until the capillary front reaches the top of the sample (Washburn, 1921; Zinszner and Pellerin, 2007). The deduced kinetic from IR imagery appears faster than the kinetic obtained from classical measurements (Fig. 6) manually performed with direct measurements on sample surface implying gap-time in the rising test.

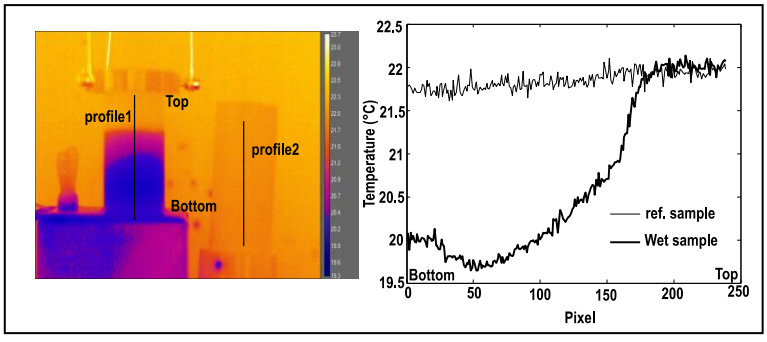

Fig. 3: Left, IR image of radiance at t=300 s; right, corresponding radiance profiles of tested sample and reference sample along their central axis.

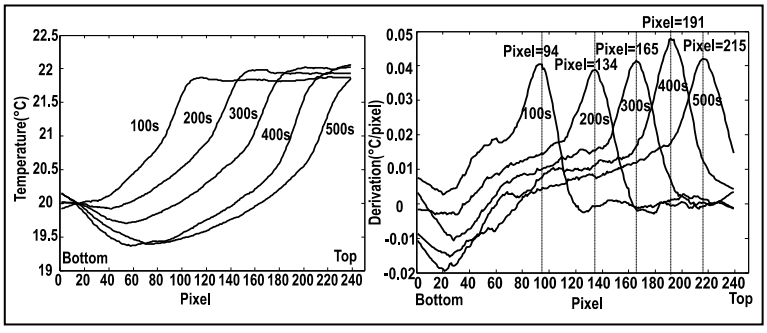

Fig. 4: Left, major trends deduced from a filtering of the short band temperature variations along the central axis profile at t= 100 s, 200 s, 300 s, 400 s and 500 s; right, derivative curves of filtered profiles.

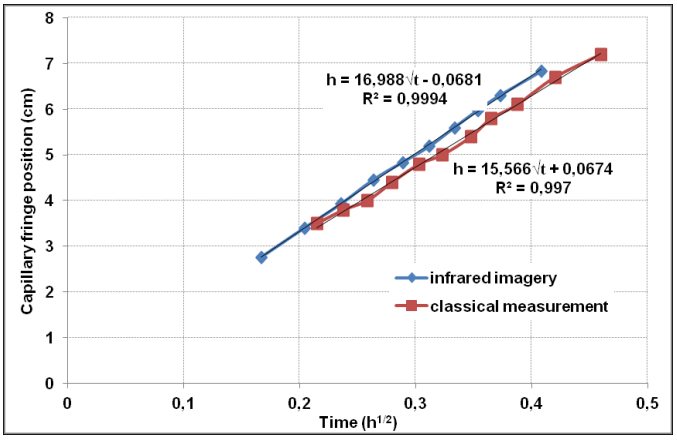

Fig. 5: Capillary imbibition front position versus squared time, deduced from IR imaging (blue diamonds) and from classical imbibition testing (red squares).

5. Discussion

Due to different emissivity of water and the specimen, the cooling effect of water evaporation and the different specific heats for water and specimen (Jenkins *et al.*, 2000), the radiation flux received by the IR camera sensors varied during the capillary rise test. Different temperature distributions along profiles in the central axis of specimens are observed. The IR images provide contrasting specimen emissions with strong color (temperature or emission correspondence) gradients. The latter, from the top of the sample dry zone in orange and progressively turning from red to pink, purple and blue at the bottom of the sample in the wet zone (Fig. 3). The pink purple zone could be related to a partially saturated zone corresponding to the front of capillary rise.

Once the plateau observed during the kinetic (weight evolution with time, Fig. 2d) is reached, the sample cannot absorb any more water by capillary imbibition. A more accurate weighting system could be able to monitor slight increase due to trapped air dissolution and diffusion (Zinszner and Pellerin, 2007). The apparent weight measured by the balance consists of the Archimedes force and the bonding strength between the water contained in the sample and water on the surface at its bottom. Noises or short band emission variations were observed all along the central axis not only in the wet sample, but also in the reference sample (Fig. 3). These noises could be probably due to diffusion phenomenon from the surface of the sample occurring at small scale.

6. Conclusion and perspectives

Porous media characterization and water transport characterization were accomplished from a stone taken from rubbles in Vaux-de-la-Celle. IR imaging camera was used during capillary rise tests. The main results of this study are: (i) the withdrawn stone from the Gallo-Roman site have a relative high storage and transfer properties which were corroborated by coupling hydrostatic weighing method and intrusion porosimetry and water permeability; (ii) the apparent front of capillary rise can be localized continuously during the test using the non-invasive IR imaging.

Petrographic description using optical and scanning electrons microscopy coupled with X-ray tomography is required to enhance the characterization of the material structure and composition (pores distribution, locations and geometry). Mineralogy could be investigated by X ray diffraction. It should provide the clay mineral content and nature which swelling could have an effect on imbibition kinetics. In addition, an isothermal and black room should be constructed for IR imaging enhancement. Moreover, observation angle compensation (e.g. Vázquez *et al.* 2015) should be performed. All these enhancements should provide a better mean to study the IR response of the media to water capillary imbibition. It should be completed by in depth signal analysis (Fourier and Singular Vector Decomposition) of the emission profiles and images in order to provide accurate signature of the capillary imbibition front.

References

Coussy, O., 2005, Poromechanics of freezing materials, Journal of the Mechanics and Physics of Solids, 53(8), 1689-1718.

Doehne, E., 2002, Salt weathering: a selective review, Geological society, London, special publications, 205(1), 51-64.

EN-1925, 1999, Natural stone test methods, Determination of water absorption coefficient by capillarity, 1999-03, 1999.

Hoefner, M.L., and Fogler, H.S., 1988, Pore evolution and channel formation during flow and reaction in porous media, AIChE Journal, 34(1), 45-54.

Jenkins, D.R., Knab, L.I., Mathey, R.G., 2000, Laboratory Studies of Infrared Thermography in Roofing Moisture Detection, Moisture Migration in Buildings (00) 207-220.

Mitard, P-H., 1993, Le sanctuaire Gallo-romain des Vaux-de-la-Celle à Genainville, ouvrage du centre de recherches archéologiques du Vexin français.

Savitzky, A., and Golay, M.J.E., 1964, Smoothing and differentiation of data with simplified least squares procedures, Anal. Chem. 36, 1627–1639.

Scherer, G.W., 1999, Crystallization in pores, Cement and Concrete research, 29(8), 1347-1358.

Turk, L.J., 1975, Diurnal fluctuations of water tables induced by atmospheric pressure changes, Journal of Hydrology, 26(1), 1-16.

Vardoulakis, I., Papanastasiou, P. and Stravropoulou, M., 2001, Sand erosion in axial flow conditions, Transport in Porous Media, 45(2): 267-281.

Vázquez, P., Schneider-Thomachot, C., Mouhoubi, K., Fronteau, G., Gommeaux, M, Benavente, D., Barbin, V, Bodnar, Jean-Luc., 2015, Infrared Thermography monitoring of the NaCl crystallisation process, Infrared Physics & Technology, 71, 198-207.

Washburn, E.W., 1921, The dynamics of capillary flow, Phys. Rev. 17, 273-283.

Zinszner, B., and Pellerin, F.M., 2007, A Geoscientist's Guide to Petrophysics, Editions Technip, Paris. ISBN 978-2-7108-0899-2.

INVESTIGATION OF URBAN ROCK VARNISH ON THE SANDSTONE OF THE SMITHONIAN CASTLE

R.A. Livingston[1*], C.A. Grissom[2], E.P. Vicenzi[2], Z.A. Weldon-Yochim[3], N.C. Little[2], J.G. Douglas[2], A.J. Fowler[4], C.M. Santelli[5], D.S. Macholdt[6], D.L. Ortiz-Montalvo[7] and S.S. Watson[7]

Abstract

Bluish black, highly adherent patches have been observed growing on the Seneca sandstone of the Smithsonian Castle in Washington, DC. They are enriched in Mn compared to the underlying sandstone, by a factor of 100, which suggests that microbial activity plays a role. The mineralogy is likely a mixture of birnessite and todorokite. Estimated thickness is on the order of 250 nm, 3 orders of magnitude thinner than typical desert varnish, and the patches lack the significant clay component found in desert varnish. However, the rate of growth, 9 nm/a, falls within the range of 1-40 nm/a measured for desert varnish. Trace amounts of Mn are found in Seneca sandstone, but they do not appear to be the major contributor to the varnish, which implies that airborne particulate matter would be a significant source. Ambient air concentrations of Mn have been measured at 4 ng/m^3 in the District of Columbia.

Keywords: manganese, varnish, Smithsonian Castle, elemental analysis, particulate matter

1. Introduction

The Smithsonian Castle on the National Mall in Washington, DC, designed by James Renwick, Jr., was built in 1847-55. Fig. 1 shows its distinctive Neo-Romanesque architecture constructed with dark red Seneca sandstone quarried in nearby Maryland

[1] R.A. Livingston*
Materials Science and Engineering Department., University of Maryland, United States of America
rliving1@umd.edu

[2] C.A. Grissom, E.P. Vicenzi, N.C. Little and J.G. Douglas
Museum Conservation Institute (MCI), Smithsonian Institution, United States of America

[3] Z.A. Weldon-Yochim
Art History Department, University of Maryland, United States of America

[4] A.J. Fowler
Smithsonian National Museum of Natural History, United States of America

[5] C.M Santelli
Department. of Earth Sciences, University of Minnesota, United States of America

[6] D.S. Macholdt, Graduate
Max Planck Institute for Chemistry, Germany

[7] D.L. Ortiz-Montalvo and S.S. Watson
National Institute of Standards and Technology, United States of America

*corresponding author

(Livingston *et al.*, 2015). Gateposts made out of the sandstone according to Renwick's design were added in 1987 to enclose the Enid A. Haupt Garden.

Fig. 1: South facade of the Smithsonian,' Castle and Enid A. Haupt Garden with the Gateposts in the foreground.

Fig. 2: Patches of rock, varnish on the southwest corner of the Smithsonian Castle.

Recently, visual inspection of the exterior of both the Castle and Gateposts identified patches of very thin adherent layers of bluish black material on the sandstone (see Fig. 2). Its distinctive appearance resembles desert varnish, which is thought to be associated with microbial action (Broecker and Liu, 2001). Nondestructive measurement of the set of patches in Fig. 2 using portable X-ray fluorescence (pXRF) showed a high enrichment in manganese (Mn) (Livingston *et al.*, 2014a), which is also a sign of rock varnish. This has led to further research using an array of analytical techniques to characterise the varnish, the sandstone and the environment around the Castle (Tab. 1).

Tab. 1: Summary of analytical techniques

Topic	**Methods**
Varnish characterization	
Elemental composition	pXRF, LA-ICP-MS
Mineralogy	XRD, EPR
Thickness	SEM, hyperspectral XRF
Biology	DNA sequencing
Sandstone characterization	
Elemental composition	pXRF, INAA, PGAA
Microstructure	X-ray microanalysis
Varnish spatial distribution	Photogrammetry
Airborne particulate matter	High-volume air sampler

2. Varnish Characterization

2.1. Mn Enrichment

Nondestructive measurements made with pXRF at a number of points on the varnish as well as bare stone were used to calculate Mn enrichment. In order to compensate for variations in standoff, surface roughness, etc., results for locations on the Castle and a gatepost are reported as the ratio of the Mn peak to the adjacent Fe peak in Tab. 2. It can be seen that the ratios for the varnish are 50 to 100 times greater than the bare sandstone, indicating significant enrichment. The mean value for the Castle locations is roughly double that of the gatepost; this may be related to the greater age of the former, which would have provided more time to grow a thicker layer. On the other hand, the Mn/Fe for the bare stone is the same for both structures within experimental uncertainties, which indicates the uniformity of the underlying sandstone and is consistent with the ratio of 0.01-0.02 measured for the sandstone by instrumental neutron activation analysis (INAA) (Livingston *et al.*, 2015).

Tab. 2: Mn/Fe ratios measured by pXRF.

Location	Varnish	Bare Stone
Castle	1.04 ± 0.5 (9)*	0.011 ± 0.02 (10)
Gatepost	0.55 ± 0.03 (5)	0.016 ± 0.003(5)

*Values in parentheses are number of data points

In addition to pXRF, laser ablation ion-coupled mass spectrometry (LA-ICP-MS) and X-ray microanalysis were applied to measure Mn and Fe on chips taken from the sandstone surface. The former method gave a mean Mn/Fe ratio of 4.1 and the latter, 4.5 ± 1.8 (Vicenzi *et al.*, 2016). Some of the differences are probably because of the inherent variability of the varnish, as shown by the large standard deviation for the Castle samples in Tab. 2. Also, the three methods sampled different patches. Finally, the sampled depth varied with the method and hence may have included more or less of the bulk sandstone. Nevertheless, the ratios all fall within a range of about 0.5-6.0, which is two orders of magnitude greater than the range of 0.01-0.02 in the bulk sandstone.

2.2. Mn Mineralogy

X-ray diffraction (XRD) of the varnish did not yield a usable diffractogram because of poor crystallinity or limited sensitivity given the sample thickness. An electron para-magnetic resonance (EPR) spectrum was obtained from a gatepost sample to constrain the chemical state of the Mn. This was compared to a set of standards of candidate Mn-bearing minerals including pyrolusite, manganite, lithiophorite, manganosite, birnessite and todorokite. Fig. 3 presents a plot of the first derivative of absorption versus magnetic field strength for the Smithsonian sample compared to spectra the most likely Mn minerals, birnessite and todorokite. With X-ray microanalysis, it is possible to sample directly individual Mn-rich patches, as shown in Fig. 4. The mean composition suggests a mixture of a Mn and silicate phase. Extrapolation to a Si-free end-member yields a composition consistent with birnessite (Fig. 5), which is the main Mn phase typically found in desert varnishes (Vicenzi *et al.*, 2016).

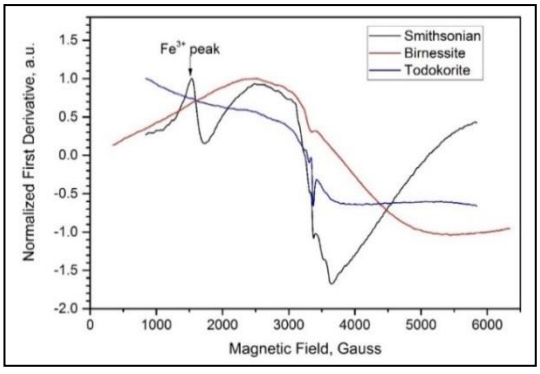

Fig. 3: Comparison of the Smithsonian varnish EPR spectrum to Mn oxide mineral standards.

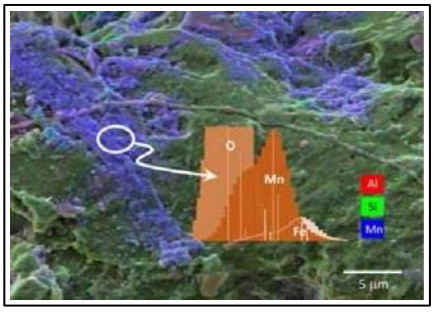

Fig. 4: SEM image of a Mn-rich surface patch investigated by X-ray microanalysis.

Mean composition:

$Na_{0.2}Ca_{0.1}Mg_{0.1}Al_{0.1}Si_{0.5}Mn_{1.9}Fe_{0.5}O_{6.7}$

(Vicenzi et al., 2016)

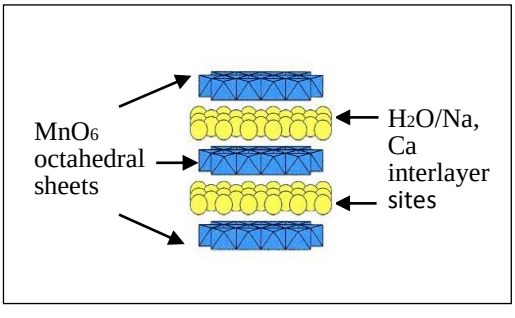

Fig. 5: Birnessite structure: $(Na,Ca)_{0.5}(Mn^{4+}, Mn^{3+})_2O_4 \cdot 1.5H_2O$ *(Post, 1999).*

2.3. Thickness

An SEM image of a cross-section of a chip taken from a gatepost is presented in Fig. 6 overlain with an element map of Mn. It shows that the varnish layer is very thin and discontinuous on a microscopic scale on the surface and to a greater extent at depth along cracks and grain boundaries. Higher magnification images indicate that the varnish consists of fine particles of Mn between 20 to 200 nm in size. Unlike in desert varnish (see Fig. 7), clay minerals are largely absent in the layer. An estimate of a nominal or effective varnish layer thickness of 250 nm was obtained from the X-ray microanalytical data (Fig. 4) by modeling the attenuation of Si X-rays generated in the sandstone substrate by a layer of pure MnO_2 (Vicenzi *et al.*, 2016). This is three orders of magnitude smaller than the thicknesses of desert varnish layers. However, the rate of growth of the layer for the young age (28 years) of the Gateposts at 9 nm/a falls within the range of 1-40 nm/a measured for desert varnish.

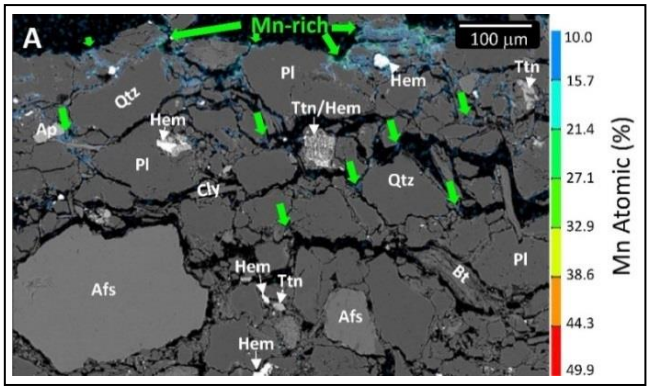

Fig. 6: SEM image and elemental map of a polished cross-section of the varnish and sandstone from a gatepost (Vicenzi et al., 2016). Key: Afs =Alkali feldspar; Ap =Apatite; Bt =Biotite; Cly = Clay; Hem = Hematite; Pl = Plagioclase; Qtz = Quartz; Ttn = Titanite.

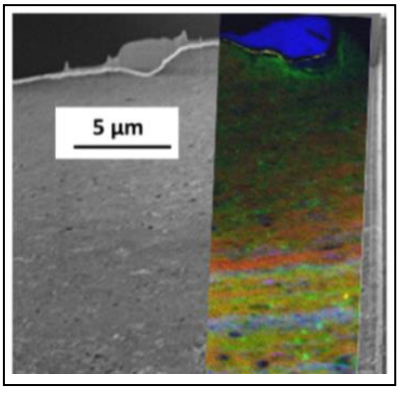

Fig. 7: Optical (left) and (STXM) scanning transmission X-ray map (right) of desert varnish cross-section from the Mojave Desert in California (Macholdt et al., 2015). Key: red = Mn; green = Fe: blue = C; yellow = Ca.

2.4. Biology

In order to determine the species of the Mn-oxidizing microbes responsible for growth of the varnish, swabs were taken at several locations on the Castle and Gateposts. The swabs were then applied to growth media on petri dishes to develop cultures. From these initial plates, active Mn-oxidizing microbes were isolated to produce the next generation of cultures. Fig. 8 is an image of the end result of several generations of this isolation process for a swabbed patch on the southwest corner of the Castle shown in Fig. 2. The colony has been identified as a fungus. The closest relative in the Genbank DNA database is *Leotiomycetes sp*. (accession #JQ761063.1). The identification as a fungus is consistent with SEM imaging of the varnish from the gatepost, which shows hyphae that are characteristic of fungal growth (Fig. 9) which shows hyphae that are characteristic of fungal growth (Fig. 9).

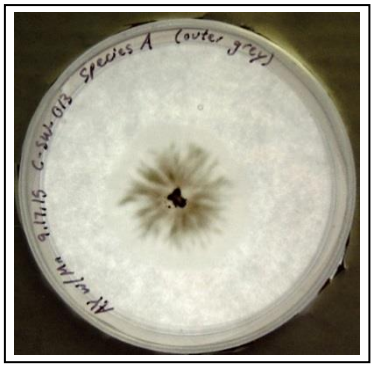

Fig. 8: Colony of Mn-oxidizing fungus isolated from a Castle sample.

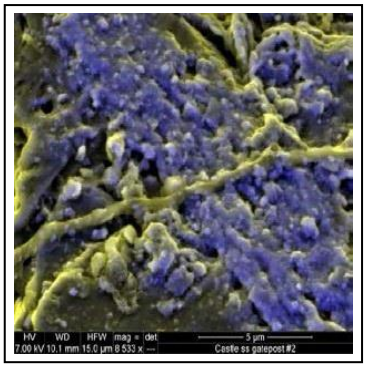

Fig. 9: False coloured SEM secondary electron (yellow) and backscattered (purple) image of possible fungal hyphae on surface of gatepost sample.

3. Sandstone Petrography

The Seneca sandstone used to build the Smithsonian Castle is formally known as the Poolesville Member of the Manassas Formation, which is in turn a member of the Newark Supergroup (Livingston *et al.*, 2015). The bulk chemical composition of the sandstone as determined by elemental analysis is given in Tab. 3. The elements were measured by INAA (Livingston *et al.*, 2014a), except for bound water, H_2O^+, which was measured by prompt gamma neutron activation (PGAA) (Livingston *et al.*, 2014b). Silicon was calculated by difference. The composition is consistent with the classification of the sandstone as arkosic and micaceous.

Tab. 3: Chemical composition of Seneca sandstone.

SiO_2	Al_2O_3	CaO	MgO	Fe_2O_3	K_2O	Na_2O	TiO	MnO	H_2O^+
55.99	23.53	0.44	0.09	5.44	3.20	10.13	0.69	0.05	0.44

This composition is confirmed by the mineral assemblage identified in the SEM image in Fig. 6. The most abundant detrital grains are quartz, plagioclase feldspar, alkali feldspar, and micas. Accessory minerals hematite (Fe_2O_3), titanite ($CaTiSiO_5$) and rutile (TiO_2) are present at minor to trace volumes. While these minerals typically contain minor Mn, the SEM-based compositional imaging reveals no pattern of Mn migration from these interior grains to the rock surface.

4. Airborne Particulate Matter

Since the source of Mn for the varnish does not appear to be the Seneca sandstone itself, another possibility is airborne particulate matter, either natural or anthropogenic. Analysis of twelve years of PM_{10} air pollution monitoring data from a District of Columbia-operated site located 3.38 km northeast from the Castle found an average ambient air concentration of roughly 4 ng/m^3. However, the site is relatively remote from heavy vehicular traffic, which

may be a source of Mn. In contrast, the Castle is located next to a major roadway, Independence Avenue. Therefore, during the summer of 2015, an air pollution monitoring site was operated on the grounds of the Arthur M. Sackler Gallery of Art, located next to the Castle and Gateposts. This used a high-volume air sampler to collect particulate matter on 47 mm polycarbonate filters, which are now being analyzed.

5. Spatial Distribution of Varnish

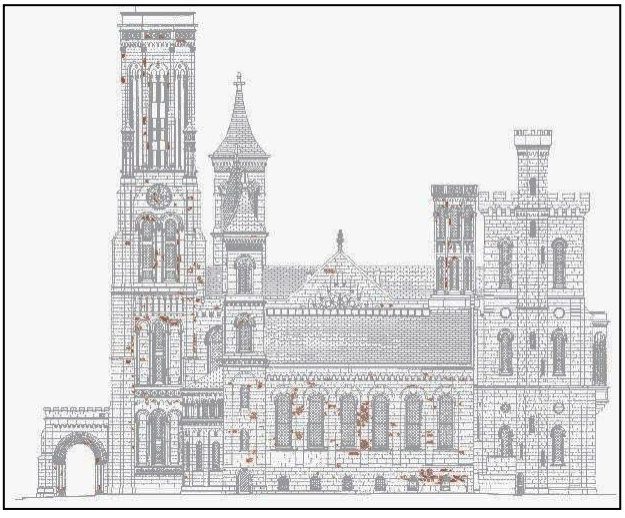

Fig. 10: West elevation of the Castle modified from the Smithsonian's 2002 Master Plan Survey. Varnish patches are highlighted in red.

In order to better understand the environmental factors influencing the development of the patches, their distribution was mapped by taking a comprehensive series of digital photographic images covering the entire building. Each identified patch was then manually mapped onto digital scale drawings of the elevations of the Castle using Adobe Photoshop, as illustrated in Fig. 10. The area of each patch will be quantified, and the resulting data set will be used to investigate possible correlations with solar heating, prevailing wind direction, exposure to vehicular traffic, etc.

6. Conclusions

Elemental analysis of the varnish on the Castle and Gateposts has shown that it is significantly enriched in Mn compared to the underlying sandstone, by a factor of 100. This suggests that microbial activity may play a role. The mineralogy is likely a mixture of birnessite and todorokite, which is also consistent with microbial activity. The varnish thickness is estimated to be on the order of 250 nm, three orders of magnitude thinner than typical desert varnish; in addition, the varnish lacks a significant clay component found in desert varnish. However, the rate of growth of the layer is 9 nm/a, which falls within the range of 1-40 nm/a measured for desert varnish. The trace amounts of Mn in the Seneca sandstone do not appear to be the major contributor to the varnish, which implies that airborne particulate matter would be significant. Ambient air concentrations of Mn have

been measured at 4 ng/m^3 in the District of Columbia, but they may be higher at the Castle because its proximity to a major roadway. Future research includes obtaining more information on the biological aspects of the varnish; analyzing the ambient air concentration of Mn particulate matter; quantifying the distribution of the varnish around the Castle; and mapping the occurrence of the varnish on other sandstone structures in the Washington area.

Acknowledgements

Due to lack of space not all of the participants in this research could be listed as co- authors. These include: Emily Aloiz, Mohamad Al-Sheikhly, Elena Charola, Paula DePriest, Willa Freedman, Jennifer Giaccai, Klaus Jochum, Gwénaëlle Kavich, Robert Koestler, Florence Ling and John Ondov. The research has been supported by the Smithsonian's Museum Conservation Institute (MCI# 6453.2).

References

Broecker, W.S. and Liu, T., 2001, Rock varnish: Recorder of desert wetness? GSA Today 11(8), 4-10.

Livingston, R.A., Grissom, C. and Aloiz, E., 2015, Building stones of the National Mall, in Tripping from the Fall Line: Field Excursions for the GSA Annual Meeting, Baltimore, Brezinski, D.K., Halka, J.P., and Ortt, R.A., Jr. (eds.), Denver, CO, Geological Society of America, 40, 543–571.

Livingston, R.A., Grissom, C., Giaccai, J., Little, N., Vicenzi, E., Freedman, W. and Aloiz, E., 2014a, Dark crusts on urban sandstone: Natural or anthropogenic? in 2014 Goldschmidt Conference, Sacramento, CA, Geochemical Society, 1501.

Livingston, R.A., Al-Sheikhly, M., Grissom, C., Aloiz, E., and Paul, R., 2014b, Feasibility study of prompt gamma neutron activation for NDT measurement of moisture in stone and brick, 40th Annual Review of Progress in Quantitative NDE, Chiment, D.E., Bond, L.J. and Thompson, D.O. (eds.), American Institute of Physics, 1581, 828-835.

Macholdt, D.S., Jochum, K.P., Stoll, B., Pöhlker, C., Weis, U., Weber, B., Müller, M., Kappl, M., Buhre, S., Kilcoyne, A.L.D., Weigand, M., Scholz, D., Al-Amri, A.M., An-dreae, M.O., 2015, Microanalytical methods for in-situ high-resolution analysis of rock varnish at the micrometer to nanometer scale, Chemical Geology 411, 57-68.

Post, J.E., 1999, Manganese oxide minerals: Crystal structures and economic and environmental significance, in Proceedings of the National Academy of Science, USA, 96, 3447-3454.

Vicenzi, E.P., Grissom, C.A., Livingston, R.A. and Weldon-Yochim, Z., 2016, Rock varnish on architectural sandstone: Microscopy and analysis of nanoscale manganese oxide deposits on the Smithsonian Castle, Washington, DC, Heritage Science, in press.

PETROPHYSICAL CHARACTERIZATION OF BOTH ORIGINAL AND REPLACMENT STONE USED IN ARCHTECTURAL HERRITAGE OF MORELIO (MEXICO)

J. Martinez-Martinez[1*], A. Pola Villaseñor[2], L. García-Sánchez[2], G. Reyes-Agustín[3], L.S. Osorio Ocampo[2], J.L. Macías Vazquez[2] and J. Robles-Camacho[4]

Abstract

One of the requirements for the construction of new buildings and restoration of historic ones in the centre of the Morelia city (Michoacán state, México) should be the aesthetical homogeneity of the used materials. Color of new rocks must be similar to the pink original stone used. Currently, three rock varieties have been employed for building restoration: Cointzio, Jamaica and Tlalpujahua stones. These rocks have been used during the last decades, but the selection criterion was exclusively limited to their similar color to the original rock and no petrophysical criterion was taken into account. A complete petrographic and petrophysical characterization of each rock was carried out in this paper. This study was focused on porosity, hydric and durability tests (capillarity, water absorption, water desorption, and salt crystallization test). According to the results, the original rock (Piedra Vieja variety) presents the best characteristics to be used as building material due to its relative low porosity (around 26%), its medium capillary coefficient and its low water absorption and desorption coefficients. The Jamaica Stone is revealed as the most suitable replacement rock in the Morelia's Heritage due to its similar petrophysical behaviour. Finally, the use of the Cointzio Stone is not recommended in outdoor areas due to its low durability and its water absorption facility.

Keywords: durability, salt crystallization test, capillarity, porosity, Ignimbrite, replacement stone

[1] J. Martinez-Martinez*
Universidad de Alicante, Facultad de Ciencias, Mexico
Javier.martinez@ua.es

[2] A. Pola Villaseñor, L. García-Sánchez L.S. Osorio Ocampo and J.L. Macías Vazquez
Universidad Nacional Autónoma de México, Instituto de Geofísica, Mexico

[3] G. Reyes-Agustín
Universidad Michoacana de San Nicolás de Hidalgo, Instituto de Investigaciones en Ciencias de la Tierra, Mexico

[4] J. Robles-Camacho
Instituto Nacional de Antropología e Historia, Laboratorio de Arqueometría del Occidente-Centro INAH Michoacán, Mexico

*corresponding author

1. Introduction

Morelia (Michoacán state, México) is a colonial city included in the list of world heritage sites by UNESCO in 1991. One of the most singular aspects of its architectural heritage is the use of a local pink stone. That fact gives a high aesthetical homogeneity to the historic city. Consequently, one of the most restrictive criteria during the restoration works of buildings is the prevalence of its aesthetical homogeneity. That fact limits the possibilities for selecting the replacement rock, being mandatory the use of pink stones. The original rock employed in the architectural heritage of Morelia is a rhyolitic ignimbrite, named "Piedra Vieja" (Fig. 1). These rocks have been recently described as the ~16 Ma Atecuaro Ignimbrite (Gómez-Vasconcelos *et al.*, 2015). Historical quarries of this original stone are located in the vicinity of the old city and nowadays are under the new buildings of the urban expansion area. As a consequence, it is impossible to obtain new rock volume from the old historic quarries for restoration works and therefore, different replacement stones must be chosen.

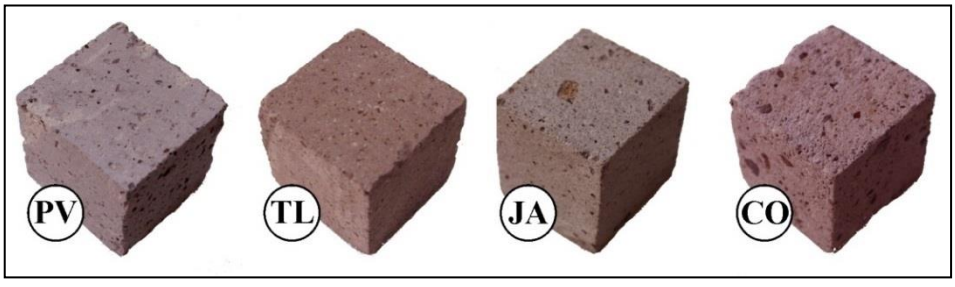

Fig. 1: samples of the four rocks used in the architectural heritage of Morelia. PV: Piedra Vieja; TL: Tlalpujahua; JA: Jamaica; CO: Cointzio.

Three different building rocks have been used during the last decades: Cointzio, Jamaica and Tlalpujahua stones (Fig. 1). Cointzio and Jamaica varieties are quarried in the vicinity of Morelia, whilst the Tlalpujahua quarries are located in the homonym town (Tlalpujahua de Rayón, Michoacán), 140 km far east from Morelia city. These rocks have been used during the last decades, but the selection criterion was exclusively limited to their similarity in colour to the original rock and no to their petrophysical features. This has been a serious mistake because when repairs are being planned for a large building, a special attention must be done for selecting substitution stones with satisfactory aesthetic aspect and properties that enable to expect a satisfactory compatibility with the original stone (Doehne and Price, 2010).

The preservation state of the rocks used in the restoration works in Morelia during the lasts decades has been variable (Fig. 2). On one hand, the original building rock (Piedra Vieja) as well as the Tlalpujahua rock show a good preservation state (in general terms). The most common decay pattern in these varieties is the differential erosion (Vergès-Belmin, 2008) with loss of components (pumice fragments, Fig. 2c), but other different patterns can also be observed (flakes, pitting and scaling). On the other hand, the Cointzio rock variety shows intensive weathering degrees in some places related to alveolization, disintegration, scaling and differential erosion processes (Fig. 2a).

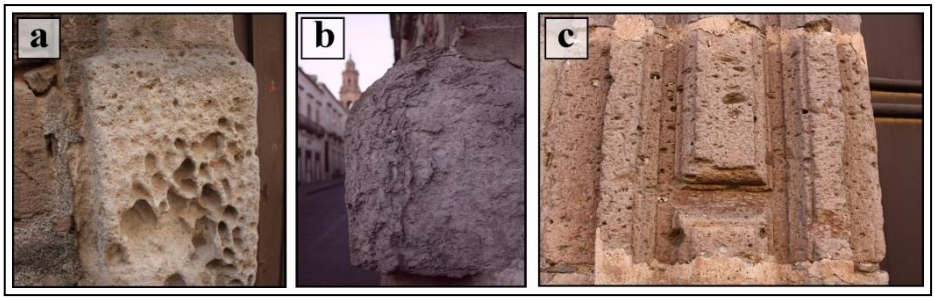

Fig. 2: Decay patterns developed on Cointzio (a), Jamaica (b) and Piedra Vieja (c) varieties.

The aim of this work, therefore, is to carry out a complete petrographic and petrophysic characterization of each rock in order to offer petrophysical criteria for selecting or rejecting a specific rock variety. The petrophysic study was focused on the porous system of the rocks, their hydric properties (capillarity, water absorption and water desorption) and their durability evaluated via salt crystallization test.

2. Methodology

Samples of each rock variety were collected directly from the manufacturing plant of building rocks. At least, two thin sections of each rock variety were obtained for their petrographic characterization. Prismatic blocks (20×20×60 mm) were cut for laboratory tests.

2.1. Petrographic evaluation

Polarised optical (POM) microscope was used in order to study the petrographic features of rocks. Several thin sections (30 μm) of each stone type were examined under an Assioscop Zeiss transmitted light microscope.

2.2. Open porosity

The open porosity (ϕ_O) was calculated using the vacuum water saturation test. Samples were dried at a temperature of 70°C for 48 hours until constant mass. Dried samples were placed in vacuum at 20 ± 7 mbar for three 5-hours cycles (after UNE-EN 1936). Connected porosity is defined as the relationship between the volume of voids (ratio of absorbed water to water density) and the volume of the sample, expressed as a percentage.

2.3. Hydric properties

The capillary absorption test was carried out in accordance with the UNE-EN 1925. Prismatic samples were placed in a container with a thin layer of distilled water. The water must cover only the lower 2 mm of the sample and consequently, water only can access to the rock through the base and rise to the highest part by means of capillary forces. Samples are weight at different time intervals in order to check the water absorption. Results were plotted as absorbed water per area of the sample against the square root of elapsed time. The Capillary Absorption Coefficient, C_c, was calculated from the slop of the first part or the curve obtained. The atmospheric absorption coefficient (C_a) was calculated in a similar way than the capillary absorption coefficient. Difference between both procedures is that, in this case, samples were placed in the container completely filled with distilled water, and

consequently, water access to the inner sample through any surface. The desorption test is also very similar to the two previous ones. In this case, samples are initially saturated with distilled water and they are placed in a desiccator with silica gel. Samples are weighted at different time intervals in order to check the loss of water. Results were plotted as loss weight per area of the sample against the square root of elapsed time. This representation shows two parts: the first part defines fast water evaporation and the second part defines slow water evaporation. Two different parameters were calculated from this curve. On the one hand, the desorption coefficient, C_d, corresponds to the slop of the fast-evaporation part of the obtained curve. On the other hand, W_d quantifies the amount (%) of water evaporated at the end of the test.

2.4. Salt Crystallisation Test

Rock durability was estimated via a salt crystallization test. Five samples of each kind of lithofacies were tested and a 14 % w/w Na_2SO_4 solution was used, in accordance with the EN-12370 recommendations. Firstly, clean and dry samples were introduced vertically into a container and covered with the solution at a temperature of 20ºC for 4 hours. Secondly, the samples were taken out of the container and introduced into the heating cabinet at 60ºC for 16 hours. Finally, the samples were subjected to room conditions (20ºC) for 4 hours. The cycle duration was 24 hours, and 50 cycles were carried out. At the end of the test, samples were dried until they reached a constant weight, which was the point where two serial measures have a difference in weight of less than 0.2 % over a period of 24 hours. The dry weight loss, ΔW [%], was calculated at the end of this stage.

3. Results

3.1. Petrographic characterization

All the studied samples correspond to welded rhyolitic ignimbrites with eutaxitic textures. In general terms, the observed minerals are quartz, plagioclase, orthopyroxene, oxides and biotites. Lithics and pumice fragments are also observed. All these crystals and clasts are surrounded by a groundmass that, in general terms, constitutes around the 90% of the rock. This groundmass is predominately composed by glass. Specific percentages of each variety are shown in Tab. 1.

Tab. 1: petrographic quantification of rock components under Petrographic Microscope. PV: Piedra Vieja; JA: Jamaica; CO: Cointzio; TL: Tlalpujahua. Qtz: quartz; Pl: plagioclase; Opx:orthopyroxene; Ox:oxides; Bt: biotite;Lth:lithics framents; PF:pumice fragments; Gm:groundmass.

	Mineral content [%]					Lth [%]	PF [%]	Gm [%]
	Qtz	Pl	Opx	Ox	Bt			
PV	7.5	1	-	1	0.5	-	*	90
JA	1	8	-	0.5	1.5	-	-	89
CO	-	5	-	0.8	0.2	4	1	94
TL	-	10	2	1.5	0.5	0.5	1.5	87

* Pumice fragments in PV at this magnification are not observed. However, large pumice fragments (>5 cm) are frequent in hand sample.

3.2. Petrophysic characterization

Tab. 2 shows all the parameters obtained from the petrophysic characterization of the studied rocks. Fig. 3 shows the obtained curves during the capillary absorption test, the atmospheric absorption test and the desorption test.

Tab. 2. Petrophysic parameters measured in the studied rocks: Piedra Vieja (PV), Cointzio (CO), Jamaica (JA) and Tlalpujahua (TL). ϕ_O: open porosity; C_c: Capillary absorption coefficient; C_a: atmospheric absorption coefficient; C_d: desorption coefficient; W_d: water evaporated during desorption test; ΔW: dry weight loss during salt crystallization test.

	ϕ_O	C_c	C_a	C_d	W_d	ΔW
	%	kg/(m^{2}h$^{0.5}$)	kg/(m^{2}h$^{0.5}$)	kg/(m^{2}h$^{0.5}$)	%	%
PV	26.52 ±0.80	0.24	1.11	-0.12	95.61	6.53 ±1.46
CO	40.36 ±0.35	0.76	4.24	-0.12	97.36	72.36 ±12.27
JA	28.71 ±2.11	0.05	0.01	-0.05	64.61	23.74 ±27.53
TL	26.79 ±1.47	0.20	0.76	-0.08	94.71	10.06 ±1.43

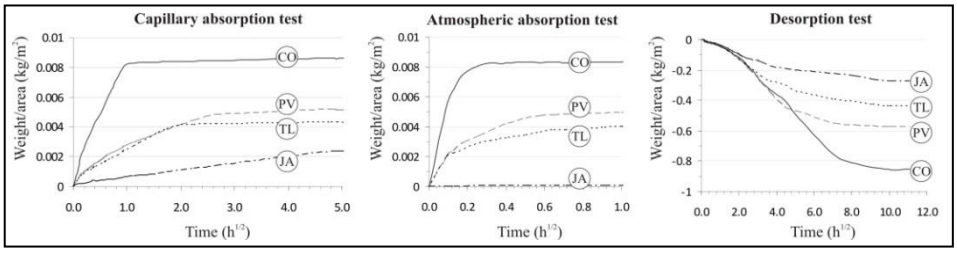

Fig. 3: Hydric behaviour of the four tested rocks (PV: Piedra Vieja; CO: Cointzio; TL: Tlalpujahua; JA: Jamaica).

Cointzio variety results the most porous rock (more than 40%) and its porous system is well connected, offering a rapid and direct water transfer from the inner to the outside part of the rock, and vice versa. As a consequence, this rock presents both the highest Capillary and Atmospheric Absorption coefficients, and this is the rock that allows removing the highest amount of water during the drying processes, after its Desorption coefficient (table 1). On the contrary, despite the fact that the Jamaica variety is not the less porous rock (table 1), its porous system is exactly the worst connected. Water movement through this rock is difficult and needs a lot of time for going out or going into the block. This is reflected in its hydric properties, showing the lowest coefficients in all the three tests carried out. Moreover, the drying process in the Jamaica stone is not efficient, remaining a significant amount of water inside the rock in spite of the dry environment surrounding the rock block.

Tlalpujahua and Piedra Vieja stones present an intermediate behaviour between the two above discussed rocks. Although both rocks have similar porosities (around 26%), the porous system of Piedra Vieja variety is slightly more open than the Tlalpujahua one, giving a little faster response to the capillary absorption and desorption processes.

The obtained results from the salt crystallization test reveals that the most durable rock is Piedra Vieja (table 2) and the softest one is Cointzio. On the one hand, the weight loss by Piedra Vieja stone during the weathering cycles was 6% and it was mainly related to the disintegration of the pumice fragments contained in the rocks (Fig. 4). This type of decay pattern was also observed in this kind of rock in the constructions of the old city of Morelia. On the other hand, Cointzio variety suffers a strong disintegration (weight loss higher than 70%) by means of crumbling and granular disintegration. Weathering signs were observed after a few number of salt crystallization cycles.

Jamaica and Tlalpujahua varieties present a moderate durability but this behaviour is very heterogeneous. Most of the tested blocks of both varieties remain quasi-unweathered at the end of the salt crystallization test (JA1 and TL1 in Fig. 4). However, some of them suffered strong damages such as fractures of scaling (JA2 and TL2 in Fig. 4).

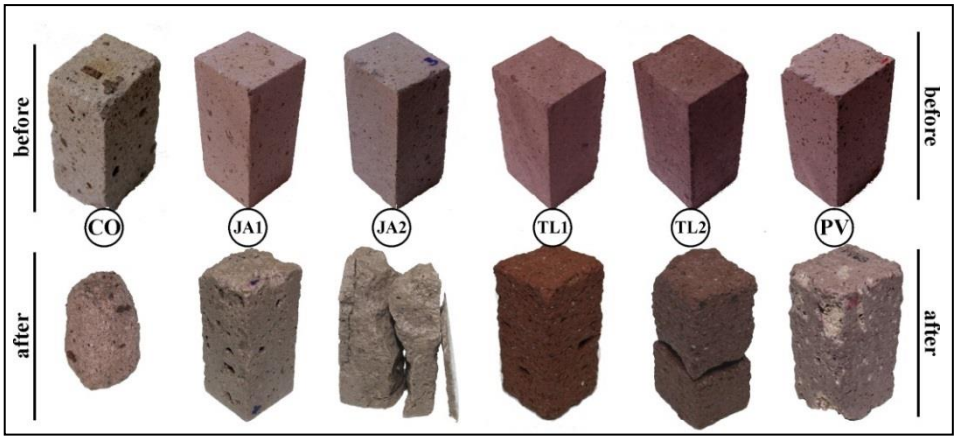

Fig. 4: some examples of different samples before and after the salt crystallization test. CO: Cointzio; JA: Jamaica; TL: Tlalpujahua; and PV: Piedra Vieja.

4. Discussion

The alteration state of the building stones in the city of Morelia, that is extremely strong in some cases, is due to the combination of chemical and physical weathering processes. The chemical and biochemical weathering of the Morelia ignimbrites has been studied previously (Ostrooumov *et al.*, 2003; Alonso and Martínez, 2003; Ostrooumov, 2009). However, the magnitude of these processes was revealed to be very low and the depth of weathered layer does not surpass 3-5 mm (Ostrooumov, 2009). For this reason, chemical weathering can not be the main decay process that affects the architectural heritage. Physical weathering (salt crystallization in pores, for example) is expected to be much more aggressive.

After the salt crystallization test carried out in the laboratory, this process is confirmed as one of the most important processes acting on the building stones of the Morelia's heritage. This is due to the fact that the decay patterns observed in the samples are the same that those described in the monuments. For example: CO samples are intensely disintegrated, most of PV and TL samples show differential erosion with loss of pumice fragments and weak components, and JA suffers pitting and scaling.

Each rock tested in laboratory presents a different durability after the salt crystallization test. The ranking of durability (from strongest to softest) is: PV>TL>JA>CO. Durability shows a direct relationship with porosity: the higher porosity, the lower durability. However, PV and TL show similar porosity values, but their durability is significantly different. This is due to the fact that PV is a heterogeneous rock that presents abundant pumice fragments with high porosity. Consequently, porosity is not homogeneously distributed throughout the rock: there is a massive matrix with very low porosity surrounding several porous pumice fragments. Rocks with this kind of heterogeneous porosity distribution result stronger than those rocks with homogeneous one.

Taking into account the durability results and the hydric behaviour of both the original rock (PV) and the restoration stones (CO, TL and JA), we can assert that the most appropriate variety for restoration works is TL. From a durability point of view, TL is the most resistant rock (after the original rock, PV). Moreover, its behaviour during capillary uptakes and water absorption and desorption is very similar to the original rock. This fact makes TL as the most compatible rock.

On the contrary, the variety CO is revealed as the worst restoration stone. On the one hand, its durability is extraordinarily low (some decay patterns were observed after only 5 cycles of salt crystallization test). This low resistance is also demonstrated by the high degradation degree observed in the monuments restored during the last decades in which this rock was used. On the other hand, the facility in which water can access as well as go out to/from the rock is an inconvenient property. This accessibility allows salty water to fill the porous system and later evaporate causing the salt crystallization.

5. Conclusions

Three different rocks have been used in the restoration works carried out during the last decades in the architectural heritage of Morelia: Jamaica, Tlalpujahua and Cointzio rocks. All of them are welded rhyolitic ignimbrites with porosity values ranging from 26% (Tlalpujahua and Jamaica) to 40% (Cointzio variety). They were initially selected due to their aesthetic similarity to the original building rock used in the ancient monuments of the city. This original building rock is known as Piedra Vieja and it is a pink ignimbrite with a moderate porosity (26%). However, after the results obtained in this study, not all the used restoration rocks are convenient. The most appropriate variety for restoration works is the Tlalpujahua rock. From a durability point of view, this rock is highly resistant and its behaviour during capillary uptakes and water absorption and desorption is very similar to that of the original rock. This fact makes Tlalpujahua as the most compatible rock with Piedra Vieja. On the contrary, the Cointzio variety is revealed as the worst rock for restoring the architectural heritage of Morelia. On the one hand, its durability is extraordinarily low. On the other hand, water can access easily to the inner part of the porous system of this rock (according to its both high capillary and atmospheric absorption coefficients) and also water can evaporate easily. This high mobility is a potential problem because of the fact that favours the salt crystallization process and the subsequent rock degradation.

References

Alonso, E. and Martínez, L. (2003): The role of environmental sulfur in degradation of ignimbrites of the Cathedral in Morelia, Mexico. Building and Environment, 38: 861-867.

Doehne, E. and Price, C.A. (2010): Stone conservation. An overview of Current Research. Getty Conservation Institute (ed). Canada. 158 pp.

Gómez-Vasconcelos, M.G., Garduño-Monroy, V.H., Macías, J.L., Layer, P.W. and Benowitz, J.A. (2015): The Sierra de Mil Cumbres, Michoacán, México: Transitional volcanism between the Sierra Madre Occidental and the Trans-Mexican Volcanic Belt. Journal of Volcanology and Geothermal Research, 301: 128-147.

Ostrooumov, M. (2009): A Raman IR and XRD análisis of the deterioration on historical monuments: case study from Mexico. Spectrochimica Acta Part A, 73: 498-504.

Ostroumov, M., Garduño-Monroy, V.H., Carreón-Nieto, H., Lozano-Santa Cruz, R. (2003): Mineralogía y geoquímica de los procesos de degradación en monumentos históricos: primer acercamiento a un caso mexicano (Morelia, Michoacán). Revista Mexicana de Ciencias Geológicas, 20 (3): 223-232.

UNE-EN 12370. Natural stone test method. Determination of resistance to salt crystallization. European Committee for Standarization.

UNE-EN 1925. Natural stone test method. Determination of water absorption coefficient by capillarity. European Committee for Standarization.

UNE-EN 1936. Natural stone test method. Determination of real Density and Apparent Density and of Total and Open Porosity. European Committee for Standarization.

Vergès-Belmin, V. (ed. 2008): Illustrated Glossary on Stone Deterioration Patterns. ICOMOS (International Council on Monuments and Sites) and ISCS (International Scientific Committee for Stone). Paris.

ASSESMENT OF A NON-DESTRUCTIVE AND PORTABLE MINI PERMEAMETER BASED ON A PULSE DECAY FLOW APPLIED TO HISTORICAL SURFACES OF POROUS MATERIALS

J.-D. Mertz[1*], E. Colas[2], A. Ben Yahmed[3] and R. Lenormand[4]

Abstract

A non-destructive and portable hand-held air mini-permeameter based on a transient air flow created by vacuum pulse decay has been tested on a well-known referenced sandstone type in order to evaluate its applicability and relevance in stone conservation. Measurements were performed first using the manufactured mini-permeameter TinyPerm II and secondly coupled with the original software Cydar™ dedicated to data acquisition and permeability calculation. In laboratory conditions, the real stone volume involved in the measurement has been investigated by gradually reducing the size of the studied stone sample. We assumed a relevant threshold value around 10 mm deep reflecting the investigated volume taken into account in the permeability measurements. Since this size ranged around the penetration depth of consolidation products during treatment, applicability of the method has been tested on-site. Measurements were carried out on the building sandstones of Strasbourg's cathedral in order to assess a significant change of the initial permeability due to superficial modifications. Data indicated a reproducible and sensitive tool being able to discriminate slight change of the surface properties due to a consolidation treatment or a local-scale weathering.

Keywords: air permeability, red sandstone, on-site measurements, diagnostic tool

1. Introduction

In the field of stone conservation, air permeability measurement is a major issue because permeability affects stone breathing, hydric equilibrium with environmental conditions and durability. However, the term "permeability" can be used for two different transfer mechanisms. The first mechanism according to the EN15803 standard destructive testing method is related to diffusion of water vapour under a difference of concentration without any pressure gradient. The second one works on the transfer of dry air flow caused by a pressure gradient generally called "Darcy" permeability. The involved properties within the

[1] J.-D. Mertz*
Laboratoire de Recherche des Monuments Historiques, CRC-LRMH USR3224, France
jean-didier.mertz@culture.gouv.fr

[2] E. Colas
Fondation de l'Œuvre Notre Dame, OND, France

[3] A. Ben Yahmed
Ecole Nationale des Travaux Publiques de l'Etat, ENTPE, France

[4] R. Lenormand
Cydarex Company, France

*corresponding author

two mechanisms are different. Diffusion is related to porosity and tortuosity of the porous network while Darcy's permeability is mainly due to the pores size. In order to study the stone properties change during alteration processes as well as for conservation state diagnosis, current destructive techniques should be avoided to prevent the integrity of cultural heritage materials. Then the development of non-destructive testing (NDT) methods is very important (Paolleti *et al.,* 2010) to perform on-site measurements and to limit sampling and to avoid the damage of valuable building stones.

During the last decades, the usual permeameters for gas-driven measurements use the Hassler cell which requires cylindrical core samples generally tested under a steady-state fluid flow, especially for high pressure experiments (David *et al.*, 1993). Due to petrographic heterogeneity of most rocks, the measured permeability depends on the volume of the tested core sample to clearly differentiate crack permeability and matrix permeability. Recently, several developments (Davis *et al.*, 1994; Tidwell, 2006; Sena da Fonseca *et al.*, 2015) have been performed not only on probe permeameter devices that work on a steady flow but also on a transient regime. The pulse decay is a valuable method for very low permeability or in order to reduce the experiment duration (Gilicz and Bodi, 2012). Major innovation is related to the rate of measurements so that NDT permeameter become an important tool, providing fast permeability data for both laboratory and on-site applications (Davis et al., 1994). Since hand-held mini-permeameters can be used to detect small variations at a centimeter-scale, relevance of measurements has been studied directly by contact with the stone surface. Recent development (Al-Jabari *et al.*, 2012) focuses on new portable permeameters without any contact to stone surfaces but they require high permeability and very smooth surface.

The pulse-decay method is preferred because it is easier to control the fluid transfer by applying a vacuum into the stone rather than injecting a pressurized gas volume in order to minimize air leakage at the stone interface. Permeability is determined by applying a fixed depressurized volume of air against the porous stone surface and by measuring the resulting flux versus time. The manufactured device called TinyPerm II (New England Research Company, USA) has been used in combination with the Cydar™ software (Cydarex Company, F) dedicated to data acquisition, data fitting and the measurement of the absolute or relative permeability. In this paper, we describe measurement of Darcy's permeability in order to (i) assess relevance and accuracy of the method, (ii) characterise the effective stone volume involved in permeability measurements and (iii) identify the sensitivity of the method to highlight small changes in permeability due to a consolidation treatment or a surface weathering.

2. Materials and methods

2.1. Studied sandstones

The studied rock material is a red sandstone so called "grès à meules" (upper Buntsandstein, 245 My) used for the construction and restoration of major monuments in the north-east part of France, especially for the Strasbourg's cathedral. This sandstone is yellow-grey to red-purplish coloured according to the content and nature of iron mineral phases. The selected test samples were two pristine sandstone blocks (12×12×5 cm^3 in size) from the Adamswiller (F) quarry for the in-lab analyses. A large ashlar of similar red sandstone (up to 30 cm in length) has been also selected to perform on-site investigations

on the cathedral. This block is a replacement ashlar located on the cornice of the eastern turret on the south facade of the cathedral.

2.1.1. Mineralogy and porosity

Petrographic characterization has been obtained by coupling optical microscopy (OM) observations on thin sections and mineralogical analysis by X-ray diffraction (XRD) with a Bruker D8 Advance diffractometer. Fluid storage properties are analyzed by mercury intrusion porosimetry (MIP) using the Autopore IV Micromeritics® porosimeter allowing to investigate pore size distribution (PSD) in the range of 200 µm to 0.003 µm in radii.

2.2. Measurement of the permeability

2.2.1. Background

Intrinsic permeability, i.e. independent of the fluid's nature, was defined by Darcy for non-compressible fluids. Unlike water, dry air is not reactive with mineral phases that is an advantage in favor for the use of gas, especially for clay-rich stones subjected to high moisture sensitivity. The Recommended Practice of the American Petroleum Institute (API, 1998) defined a relationship between the pressure difference applied across the material and the flow rate of gas Q measured at atmospheric pressure. Considering a compressible ideal gas, the permeability (K_g) for a given sample-size is determined from the one-directional gas flow equation:

$$K_g = \frac{2 \cdot \mu \cdot Q \cdot Pr \cdot L}{A \cdot (Pin^2 - Pout^2)} \qquad \textit{(Eq. 1)}$$

where µ is the gas viscosity, Pin the inlet pressure, Pout the outlet pressure, Pr the reference (atmospheric) pressure, L the length of the sample, A the cross-sectional area of the sample. For small pores, interactions of gas molecules with the pore wall introduce errors due to the Klinkenberg slippage effect. Corrections on the calculated values must be applied only for low permeability materials (<1 mD) and low pore fluid pressure (Lenormand *et al.*, 2010).

2.2.2. The geometrical factor

Application of equation (1) provides a simple and rapid K_g measurement for a sample with well-defined dimensions like a cylindrical core since the gas flow describes a linear and uniform flow field in the porous medium. On large surfaces and on-site measurements, the "equivalent length" L and the "equivalent surface" A of samples are not known because the lines morphologies of the flow field are divergent. This flow field depends on the transfer properties of the stone, the experimental conditions (gas flow rate, gas pressure, ambient temperature and pressure) and the geometrical size parameters of the sealing tip (Fig. 1a). In order to take into account all these parameters in equation (1), a correction factor G_0 has been provided by Goggin *et al.* (1988) as a function of the parameters of the sealing tip.

$$A/L = G_o \cdot r_i \text{ and } G_0 = f(r_o/r_i) \qquad \textit{(Eq. 2)}$$

where r_i is the internal radius of the sealing tip and r_o the external radius of the sealing tip. Previous researches (Filomena *et al.*, 2014) recommend a minimum sealing-tip size ratio r_o/r_i higher than 1.5.

2.3. The use of TinyPerm II coupled with the Cydar™ software

The air permeability (K_g) has been first measured using the TinyPerm II device. It works as an inverse pomp which operates a vacuum into a 100 cm^3 volume cylinder controlled by a pressure transducer. A microprocessor monitors the transient vacuum pulse created at the surface. After vacuum dissipation, a *T*-value is provided which is linked to air permeability (K_g) according to the calibration equation (3) noted in the operational manual:

$$T = -0.8206\ log_{10}(K_g) + 12.8737 \qquad (Eq.\ 3)$$

where (K_g) is expressed in mD. The original dimensions of the rubber sealing tip geometry show a ratio r_o/r_i=2.42 and r_i=4.8 10^{-3} m. As boundary conditions require a minimum distance d such that $d > 4 \cdot r_i$ where d is the theoritical diameter of the analysed surface, all test zones larger than 2 cm in width satisfy the flow law application.

The second calculation method of permeability uses the Cydar™ software connected to the same device. Extrinsic parameters like sealing-tip size, experimental temperature, pressure and air viscosity as well as porosity are considered. In our case, *L* and *A* values taken into account in order to simulate the "equivalent sample size" were $L = r_i$ and $A = Go \cdot r_i^2 = 1.087 \times 10^{-4}$ m^2. Inertial effects based on the calculation of the Reynolds number ($Re << 1$) were also checked in order to verify the fluid flow regime. In addition, Cydar™ allowed calculating the air permeability by fitting the experimental data due to vacuum dissipation versus time (Fig. 1b) using successive iteration tests and appropriate Spline functions.

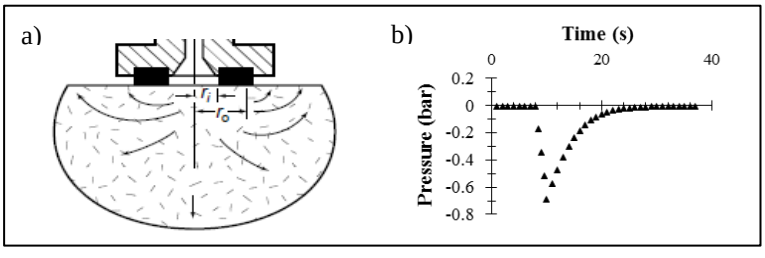

Fig. 1: a) Schematic diagram of the contact device-stone. r_i and r_o are the internal and external radius of the sealing-tip (API, 1998); b) Experimental kinetic curve of vacuum dissipation rate and return to the atmospheric pressure (Pout=0).

2.4. Methodology and selection of relevant tests

All measurements were carried out by the same operator to reduce systematic errors due to air leakage along the stone/seal interface. For both methods, the average value and standard deviation are significant of 10 permeability measurements for reproducibility and representability.

2.4.1. Evaluation of the investigated volume

In order to evaluate the real stone volume taken into account in the permeability values, measurements were performed at a same place in the middle part of a sample in a direction perpendicular to the bedding. Six gradual reductions of the sample thickness from 49 mm to a minimum thickness of 4 mm have been carried out by sawing before the measurement.

2.4.2. Sensitivity to a consolidation treatment

A consolidation treatment using 3 TEOS-based products Motema PKSE®30 (Interacryl), BS®OH100 (Wacker) and Funcosil®500E (Remmers) was performed to evaluate the impact of product amount. Each product has been applied by manual brushing on 3 neighboring small areas of 4×4 cm^2 in size. Quantities for each product are respectively 1.1±0.1, 2.0±0.1 and 3.5±0.1 L/m^2 in good agreement with practice within this sandstone type. Direct comparison of the permeability measurements were carried out before and after treatment in order to evaluate the relevance of the method.

2.4.3. Point out a conservation state

Investigations were performed on a degraded ashlar of the cornice of a turret of the south transept of the Strasbourg's cathedral dated from a XIXth century restoration campaign. Visual observations of the degraded ashlar emphasize a superficial thin dark patina and a visible 2 cm deep crack related to a parallel desquamation of the exposed surface. Permeability profiles were obtained along a cross-sectional direction located outside the cracked zone, 5 cm below. Measurements were carried out from the patinated external surface towards the inner parts of the block with an acquisition frequency of 3 cm.

3. Results and discussion

3.1. Mineralogical and microstructural properties

Optical microscopy reveals a quartzic-feldspar sandstone composed by well sorted fined-grains quartz (70%, particle size about 200 µm in diameter), K-feldspar (15%) and mica. Clay minerals (kaolinite, illite, rare smectite) often mixed with iron (oxihydr)oxides are present in a discontinuous coating around the Q-grains (Colas, 2011). Microscopic analyses indicate that pressure-solution and creation of a secondary porosity can occur during rock compaction and post-diagenetic processes. As a result, large evolutions in the original porous network of sandstone happen at a centimetre-scale causing high dispersion of porosity and permeability values. MIP provided an open porosity of 21%, a bulk density of 2.05 $g{\cdot}cm^{-3}$ and a 1-mode pore size distribution (PSD) associated with a mean pore radius around 5 µm. Calculated permeability based on the Swanson model provided a value of 0.237 $\times 10^{-12}$ m^2 (0.237 D). This value is in good agreement with the literature data (David *et al.*, 1993; Filomena *et al.*, 2014) which indicate an average permeability between 200 to 500 mD showing a low dispersion of measurements (×2.5) by contrast with the permeability of most building stones which is in the range of 1 nD to 10 D (factor 11).

3.2. In-depth investigated volume

Permeability evolution with the decreasing sample thickness is illustrated in Fig. 3. Error bar is equal to the standard deviation calculated for each analyzed area. The absolute difference between values obtained with the two methods is constant and results in a shift toward lowest values with Cydar™. The shift associated to the use of Cydar™ underlines the high impact of geometric parameters of the sealing tip and consequently is in close relation with the used flow models. This is in accordance with others works (Filomena *et al.*, 2014) reporting an average overestimated value around +37% when using only Tinyperm II compared to Hassler cell. However, a similar tendency of permeability values is also related to practical measurement conditions like the applied pressure on the sealing tip and the operator expertise in order to reduce air leakage. Others tests using

reversible material like mastic or velvet added on the sealing-tip allow further reducing leakage.

Regular reduction of the sandstone thickness leads only in a small decrease in permeability until a limit-size of 10 mm which is relevant according to the standard deviations. Otherwise, for the smallest sample thicknesses (i.e. 5.6 mm and 3.7 mm), permeability values increase quickly towards a maximum *K*-value of 653 mD and 345 mD, respectively, for TinyPermII and TinypermII with Cydar™ software. Therefore a threshold-value of 10 mm (Fig. 2) had been highlighted for this specified sealing-tip geometry (r_i=4.8 ×10^{-3} m and r_o/r_i=2.42). We assumed that this small thickness threshold-value is correlated with a faster vacuum breakage in the porous network due to a bigger volume of the divergent vacuum flow field than the analyzed stone volume.

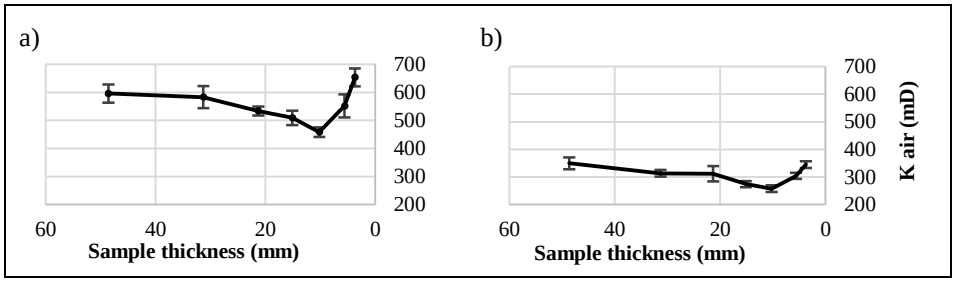

Fig. 2: Permeability versus thickness a) TinyPerm II and b) TinyPerm II with Cydar™.

3.3. Pore blocking characterization

Permeability data about the 9 tested areas are reported in Table1. Mean permeability value before treatment is 375±25 mD in good agreement with the literature data. Standard deviation is similar to the average value of the calculated standard deviations (24 mD) calculated on each of the 9 analyzed areas. As a consequence, permeability related to inter-area and intra-area measurements underlines a homogeneous material volume.

*Tab. 1: Permeability K data (in mD) using TinyPerm II with Cydar™ for the three treatments. Δ*K/K*: decrease of K (in %). Mean values and standard deviation in brackets*

TEOS treatment		**1.1 L/m^2**	**Δ*K/K***	**2.0 L/m^2**	**Δ*K/K***	**3.5 L/m^2**	**Δ*K/K***
Motema PKSE®30	Before	353 *(48)*	42	409 *(29)*	63	348 *(34)*	83
	After	204 *(26)*		152 *(12)*		60 *(4)*	
BS®OH 100	Before	396 *(15)*	37	389 *(16)*	41	356 *(11)*	43
	After	251 *(16)*		231 *(11)*		202 *(11)*	
Funcosil® 500E	Before	367 *(18)*	39	390 *(22)*	54	370 *(26)*	60
	After	224 *(7)*		181 *(7)*		148 *(9)*	

After consolidation treatments, permeability values are always reduced in the range of 37-42% of the initial *K* value for the lowest consumption (1.1 L/m^2) until reaching the highest decreasing in permeability around 83% for the strongest treatments. Such a good correlation between the decreasing in permeability and the applied product quantity

highlights the ability of the air permeability method to detect pore blocking. Moreover considering the strongest treatment (3.5 L/m^2), data comparison between consolidation products provides the lowest permeability reduction ($\Delta K/K$= 43%) using BS®OH100 product which well correlated with its lowest solid content (33%w versus 50%w for Funcosil®500E). The implemented method allows to distinguish treated zones and untreated ones as well as to assess the efficiency of a consolidation treatment.

3.4. Efficient tool for the diagnose of alteration state

Permeability measurement results (Fig. 3) showed good agreement from Tinyperm II with or without using the Cydar™ software. The differences between the two measured profiles are in close relation with the flow model used for the calculation as seen in §.3.2.

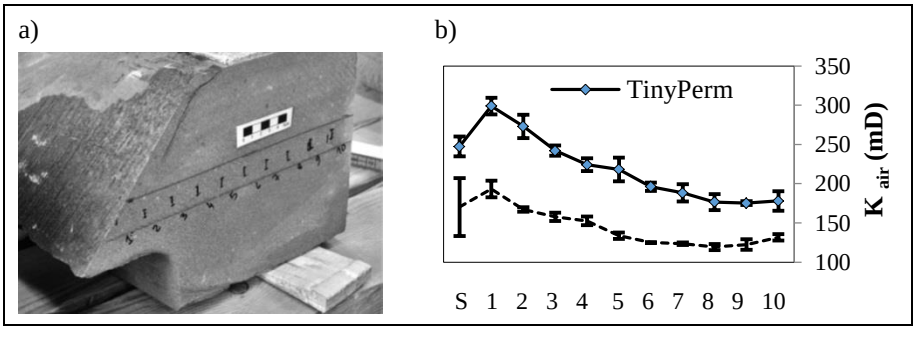

Fig. 3: Results of permeability profiles using two different methods.

According to the low standard-deviations, values are significant of a continuous decreasing in permeability versus depth except the 0-3 cm zone (Zone 1) which presents the highest permeability value (299 mD and 193 mD respectively for TinyPerm II and TinyPerm II with Cydar™). Two different factors can be considered. On one hand, permeability on the external surface (S) is higher than the inside ones that can highlight an active weathering phenomenon inducing superficial changes in porosity and surface roughness. As a result, the external patinated surface presented the highest standard deviation, especially with the TinyPerm II and Cydar™ so that the method which could be used as an indicator of the patina surface properties. On the other hand, permeability strongly increased in the 0-3 cm zone which is consistent with the presence of cracks even if they are not visible with naked eyes. As a result, weathering is not only occurring in the near cracked zone and also affects the stone until 20 cm deep with respect to the regular decrease in permeability.

4. Conclusions

Permeability measurements using the portable NDT TinyPerm II based on a pulse decay flow has been successfully tested for laboratory and on-site measurements. The device enables a simple, quick and highly sensitive measurement providing an accurate diagnostic tool. Nevertheless the method is adapted to dry, clean, smooth and regular surfaces in order to prevent air leakage at the sealing tip/stone interface. Measurements are governed by the quality of the sealing interface with stone surfaces which is highly influenced by the applied pressure and the surface roughness. Main interest of device coupling with the Cydar™ software is the real-time control of pressure dissipation and air leakage. Therefore standard deviations are lower. Measurements showed that the real investigated volume of

stone is ≤10 mm deep using the original tip of the apparatus in good agreement with the (r_o-r_i) thickness of the sealing-tip. It could thus be quite possible to optimize geometry, type and properties of the tip to reach other volumes in depth.

About stone conservation issues, the used method allowed to distinguish a local-scale modification of stone surfaces and to highlight the involved pore blocking effect due to a consolidation treatment as well as to establish weathering profiles. Further adaptations and uses of this new method for relevant diagnose of cultural heritage materials make it a reliable tool to provide quantitative indications on restoration techniques like cleaning. Further outlook could be the comparative analysis with water vapor permeability measurements according to a microstructural and mineralogical control.

References

Al-Jabari, N., Bowen D., Smart B. and Somerville J., 2012, First non-contact mini-permeameter, Inter. Symp. of the Society of Core Analysts (SCA2012), Scotland, presentation SCA2012-45, 6p.

API, 1998, Recommended Practice 40 in Recommended Practices for Core Analysis, section 6: Permeability determination, American Petroleum Institute, STEP (eds), Second edition, API Publications and Distribution, 1-58.

Colas, E., 2011, Impact de l'humidité et des solutions salines sur le comportement dimensionnel de grès du Buntsandstein : contribution à la sélection des faciès de restauration, PhD of Reims University (URCA), 321pp.

David, C., Darot, M. and Jeannette, D., 1993, Pore structures and transport properties of sandstones, Transport in Porous Media, 11, 161-177.

Davis, J.M., Wilson, J.L. and Phillips F.M., 1994, A portable air mini-permeameter for rapid in situ field measurements, Ground Water, 32 (2), 258–266.

Filomena, C.M., Hornung, J. and Stollhofen, H., 2014, Assessing accuracy of air-driven permeability measurements: a comparative study of diverse hassler-cell and probe permeameter devices, Solid Earth, 5, 1-11.

Gilicz, A. and Bodi, T., 2012, Measurement of porosity and gas permeability on tight rocks by the pulse decay method, Geosciences and Engineering, 1, 65–74.

Goggin, D.J., Thrasher, R.L., and Lake, L.W., 1988, A theoretical and experimental analysis of mini-permeameter response including gas slippage and high velocity flow effects, In Situ, 12(1-2), 79–116.

Lenormand, R., Bauget, F. and Ringot, G., 2010, Permeability measurements on small rock samples, Intern. Symp. of the Society of Core Analysts (SCA2010), Canada, presentation SCA2010-73, 12 pp.

Paoletti, D., Ambrosini, D., Sfarra, S. and Bisegna, F., 2013, Preventive thermographic diagnosis of historical buildings for consolidation, Journal of Cultural Heritage, 14, 116-121.

Tidwell, V.C., 2006, Air permeability measurements in porous media, in Gas Transport in Porous Media, Ho, C. and Webb, S. (eds.), Springer, 273-286.

MONITORING OF SALTS CONTENT IN MONUMENTS OF TORUŃ OLD TOWN COMPLEX

W. Oberta[1*] and J.W. Łukaszewicz[1]

Abstract

One of the most important degrading factors destroying brick walls are water soluble salts. The migration of salts across a brick wall may result in significant damage due to salt crystallization, its volume increase due to increase in hydration degree and chemical reaction. Moreover, the water soluble salts exhibit hygroscopic properties, which cause the constant moisture of the wall. Furthermore, some of the salts may stimulate microbial growth, which causes progressive damage to the monument. Thus, an extremely important issue in the brick-made heritage protection is the systematic qualitative and quantitative analysis of salts present in the monuments. The currently applied methods of analysis of salts present in brick walls and other historical objects, are related to the sampling from these objects. Next the samples are ground and water extracted. The obtained solutions are then analysed in terms of qualitative and quantitative content of the salts. The aim of this paper is an evaluation of the applicability of capillary electrophoresis in salts investigation and monitoring in historic brick walls. Further, this rapid qualitative and quantitative method will be applied to the continuous monitoring of the state of preservation of brick monuments. Within the project, rapid in-situ method of salts sampling from an object is under development. For this purpose, specific poultices will be in use. The electrophoretic methods, i.e. capillary zone electrophoresis (CZE) and capillary isotachophoresis (ITP), are used for analysis of salts. The monitoring program covers also qualitative analysis of efflorescences taken from the ramparts of the Old Town and from the ruins of the old Teutonic Order Castle in Toruń.

Keywords: electrophoresis, water soluble salts, brick, efflorescences, monitoring

1. Introduction

The Old Town in Toruń has been put on the UNESCO cultural heritage list and remains a unique group of medieval brick-made buildings, developed in the 13th-15thcenturies under the supervision of the Teutonic Order. Since then, these objects have been exposed to the activity of various deterioration factors, which may have influenced their systematic, step-by-step degradation.

Water-soluble salts are recognized as one of the most dangerous and most common factors causing deterioration to brick monuments (Fig. 1). Water-soluble salts affect those objects by a complex mechanism. Salts may damage surface layers of a brick in a physical way,

[1] W. Oberta* and J.W. Łukaszewicz
Department for Conservation of Architectonic Elements and Details, Faculty of Fine Arts, Nicolaus Copernicus University, Toruń, Poland
woberta@umk.pl

*corresponding author

due to crystallization and the growth of further crystals, which causes the disintegration of layers. The crystal growth causes crystallization pressure, which varies depending on temperature and the salt type. This phenomenon may be even increased by the continuing changes in the crystal volume of the salt remaining in equilibrium with water and water vapour in its surrounding. This concerns especially the salts able to crystallise with various amount of water, e.g. sodium sulphate (Na_2SO_4). The full hydration of sodium sulphate to $Na_2SO_4 \times 10H_2O$ causes 400% crystal volume increase (Domasłowski 2003, p. 114, Charola 2000, p. 327).

Fig. 1: Fragment of Toruń old town ramparts (Vistula river side). The bricks have been damaged by salts. One of the sampling places (photo by W. Oberta).

If the salts present in the object are able to undergo hydrolysis, which causes the *pH* change of capillary water, the chemical deterioration mechanism is activated. Moreover, water soluble salts cause a high increase of hygroscopicity, which may facilitate microbial growth and corrosion (Domasłowski 2003, p. 107). Therefore, the stone object desalination seems an essential step in every conservation action and water-soluble salts monitoring is a key factor in a state of preservation assessment as well as during and after the desalination process. Various methods are applied to monitor the total salt content, however all of them are based on the analysis of the water solution. The aqueous solution is always an extract of salts taken from a stone monument sample. Gravimetric and conductometric methods are commonly applied for quantitative salts analysis. The gravimetric method is relatively time-consuming and requires high extract volumes (min. 50 cm^3 of extract prepared from 1-4 g of the sample and 100 cm^3 of water) (Domasłowski 2003, p. 97). Similar mass/volume ratios are required in the conductometric method, however a minimum of 15-20 cm^3 of the extract is required (Bläuer and Böhm 2005). In both methods the qualitative salt analysis must be applied separately. The identification of salt species is carried out e.g. with microcrystaloscopic or colourimetric methods. The commercially available tests are used commonly for colourimetric analyses which makes them relatively expensive and time-consuming (Borelli 1999). The separation techniques, such as ion chromatography make possible simultaneous qualitative and quantitative salts analysis, which constitutes their advantage over the gravimetric and conductometric methods. Ion~~ic~~ chromatography requires small extract volumes (ca. 1 cm^3) and it is very precise. Unfortunately, this method is extremely expensive in terms of the device and the particular analysis costs (Borelli 1999). Capillary electrophoresis is a good alternative for the methods described above. Generally, the electrophoretic techniques make possible the simultaneous qualitative and quantitative analysis of ions by means of their separation from the mixture. The essence of

electrophoretic ions separation is the differences in their migration velocities. Thus, the separation in capillary electrophoresis occurs along a thin capillary under a constant electric current field. In this paper, the application of capillary electrophoresis in the analysis of salted porous materials was estimated. In this study the Capillary Zone Electrophoresis (CZE) and Capillary Isotachophoresis (ITP), were applied. In the CZE method, the ions separation occurs in a capillary fully filled with a background electrolyte (BGE) of a specific composition, optimized for the best ions separation. The ITP method requires two electrolytes, the first one of a mobility higher than the mobility of the fastest ion in the mixture (leading electrolyte, LE), the second one of a mobility lower than the mobility of the slowest ion in a mixture (terminating electrolyte, TE). The ions separation occurs between these two electrolytes and the ions migrate in the order of their mobility, from the fastest to the slowest (Foret *et al.* 1993, Boček *et al.* 1988). The electrophoretic methods are flexible and sensitive and make possible the analysis of various chemicals or even microbials.

2. Experimental

2.1. Sample preparation

Brick samples of a total absorption of solutions of 18.11 % were used in the experiments. Eleven samples of 5×2.5×1 cm³ were cut from the brick for laboratory studies. One sample was left for a blank analysis. Ten samples were saturated with model salts solutions, i.e. NaCl, KNO_3, $Ca(NO_3)_2$, $Mg(NO_3)_2$, $NaNO_2$, Na_3PO_4, Na_2SO_4 (every solution of 10 % concentration), and NaF (4 %), respectively. Finally, two samples were saturated with mixed salt solutions, i.e. **M1**: NaCl 1.50%, KNO_3 2.00%, Na_2SO_4 0.30%, $Ca(NO_3)_2$ 0.20%, $NaNO_2$ 3.00%, $Mg(NO_3)_2$ 3.00%; **M2**: NaF 2.00%, Na_3PO_4 2.00%, KNO_3 3.00%, Na_2SO_4 2.00%, NaCl 3.00%. The samples were saturated first by capillary rise and next by full immersion in the salt solutions. Immediately after saturation was accomplished, the samples were dried until constant weight in a laboratory dryer at 378 K. All brick samples from the ramparts and the ruins of the Teutonic Order castle in Toruń were collected with traditional methods and were extracted and analysed according to the methodology for the laboratory samples treatment. The salt efflorescences, sampled from the ramparts of Toruń old town, were analysed as follows: 0.1g of each efflorescence (dried in a laboratory oven at 60°C until constant mass) was dissolved in 50 cm^3 of distilled water and left for 24 hours. Then the solution was separated from the residue as extract ready for analysis.

2.2. Salt extraction

Firstly, a quarter of each salt loaded sample was taken (always from the same side). Then the samples were ground with a mortar and sieved through a 0.125 mm mesh sieve. An aliquot of 2.5 g of each sample was treated with water (10 cm^3 per 1 g of sample). The formed suspensions were shaken for one hour by mechanical shaker and then filtered through a hard filter (type 390, mm diameter, 84 g/m^2 weight). The filtrate was always collected in a 100 cm^3 measuring flask and filled up to dash with distilled water. The same procedure was applied simultaneously to the unsalted material as a reference.

The discussion of the results was related to the real salt content in the analysed samples. The real salt content (Z_{rz}) was calculated using the gravimetric method, basing on equation (1), where m_z and m_0 mean the mass of salted and unsalted sample [g], respectively.

$$Z_{rz} = \frac{(m_z - m_0)}{m_z} \times 100\% \qquad \textit{(Eq. 1)}$$

2.3. Conductometric analysis

Conductivity was measured at 298 K using a CPC-551 (Elmetron) multimeasure device. The salt content (Z_k) was estimated with the conductometric method, basing on the equation (2), where κ means the conductivity [mS×cm^{-1}], p is the empirical factor for conductivity to mass conversion (p = 0,0586 [g×cm×mS^{-1}]), m_p means the sample mass [g] (Domasłowski 2003, p. 227-229).

$$Z_k = \frac{\kappa \times p}{m_p} \times 100\% \qquad \textit{(Eq. 2)}$$

2.4. CZE analysis

The CZE analyses of anions were conducted with the EA 102 device (Villa Labeco, Slovakia). The concentration of the following anions was analysed: Cl^-, SO_4^{2-}, NO_3^-, NO_2^-, F^-, PO_4^{3-}. For this purpose the calibration solution of the following anions concentrations were prepared: 0.5 ppm, 1.0 ppm, 2.5 ppm and 5.0 ppm. For the analysis the following background electrolyte (BGE) was used: succinic acid (Sac) 7.5 mmol·dm^{-3} + bistrispropane (BTP) + methylhydroxyethylcellulose (MHEC) 0.1 % + poli(vinylpyrrolidone) (PVP) 7.5 %. The following experimental conditions were found to be optimal (Blatny and Kvasnička 1999, Kaniansky *et al.* 1999):

Step 1: time: 70 s, current: 40 µA;

Step 2: time: 200 s, current: 40 µA.

The conductometric detector was used for anions detection. All water extracts were 100× diluted with distilled water prior to analysis.

2.5. ITP analysis

The ITP analyses of cations were run at the same EA 102 device as used for CZE anion analysis. The following cations were analysed, i.e. K^+, Na^+, Ca^{2+}, Mg^{2+}. Calibration solutions of following concentrations were prepared for each cation: 0.5 ppm, 1.0 ppm, 2.5 ppm and 5.0 ppm. Sulphuric acid of 7.5 mmol×dm^{-3} concentration was used as the leading electrolyte (LE). Lithium citrate of 10 mmol×dm^{-3} concentration was used as the terminating electrolyte (TE). The optimum experimental conditions were found to be as follows (Kvasnička *et al.* 1993):

Step 1: time: 400 s, current: 300 µA; Step 2: time: 1000 s, current: 250 µA, comparator: 10 µA; Step 3: time: 350 s, current: 85 µA; Step 4: time: 1000 s, current: 50 µA.

The total salt content in the samples (Z_e) was determined electrophoretically as a sum of particular ions (cations and anions). The particular ion concentration was calculated with equation (3), where C_J means the ion concentration in ppm [mg×dm^{-3}], m_p is the sample mass [mg], V is the filtrate volume [dm^3].

$$J_{\%} = \frac{C_J \times V}{m_p} \times 100\%, \rightarrow Z_e = \sum J_{\%} \qquad \textit{(Eq. 3)}$$

The total water uptake of a sample was calculated according to equation (4), where m_n means the saturated sample mass [g], m_0 means the dried sample mass [g].

$$N = \frac{m_n - m_0}{m_0} \times 100\% \qquad \textit{(Eq. 4)}$$

3. Results and discussion

As shown in Tab. 1, the total water absorption of all samples was similar, which made allowed for comparative studies of salinities with various salts. All the samples exhibited similar salinities, with the exception of sample 7C, salted with sodium fluoride of lower concentration, as stated in the experimental section.

Tab. 1: Absorption (N) and total salinity of samples, estimated with various methods.

Sample	***N***	***Z_{rz}* (Eq. 1)**	***Z_k* (Eq. 2)**	***Z_e* (Eq. 3)**
	[%]	[%]	[%]	[%]
1C	18.01	1.57	2.58	2.19
2C	19.10	1.85	1.87	1.96
3C	17.32	1.70	1.85	1.97
4C	18.44	2.26	1.88	1.86
5C	19.44	1.92	2.03	2.09
6C	18.53	1.72	1.91	2.07
7C	16.76	0.62	0.76	0.77
8C	18.11	1.99	1.96	2.08
9C	18.55	1.52	1.80	1.83
10C	16.83	2.02	1.81	1.85

Despite some slight differences, all the results are similar. Some minor differences may result from the formation of complex structures, e.g. hydrated salts, which are not recognizable by the conductometric and electrophoretic techniques. Nevertheless, it may be assumed that both methods (conductometric and electrophoretic) were useful to determine salt contents in the analysed samples since they delivered comparable results.

In the further study, the brick samples taken directly from the ramparts were analysed. The particular ions present in the mixture were identified and quantified for better recognition of the salt type. The results are collected in Tab. 2.

Tab. 2: Quantitative ion contents estimated by conductivity and capillary electrophoresis in the samples from the ramparts of the Old Town of Toruń (Ciechanowska, 2012).

	Z_k	Na^+	K^+	Ca^{2+}	Mg^{2+}	Cl^-	SO_4^{2-}	NO_3^-	NO_2^-	F^-	PO_4^{3-}	Z_e
	[%]	[%]	[%]	[%]	[%]	[%]	[%]	[%]	[%]	[%]	[%]	[%]
1	0.08	0.01	0.01	0.04	0.00	0.00	0.01	0.00	0.00	0.00	0.00	0.07
2	0.09	0.00	0.01	0.03	0.00	0.01	0.01	0.01	0.00	0.00	0.00	0.07
3	3.32	0.13	0.12	0.75	0.02	0.13	1.04	0.99	0.00	0.00	0.00	3.19
4	2.56	0.16	0.08	0.47	0.01	0.35	0.81	0.57	0.00	0.00	0.00	2.44
5	1.76	0.16	0.08	0.34	0.01	0.22	0.37	0.46	0.00	0.00	0.00	1.65
6	3.85	0.53	0.29	0.52	0.04	0.72	0.43	1.59	0.00	0.00	0.00	4.12
7	3.52	0.72	0.26	0.37	0.03	0.62	0.14	1.64	0.00	0.00	0.00	3.78
8	4.10	0.74	0.31	0.58	0.03	0.59	0.54	1.69	0.00	0.00	0.00	4.48
9	2.36	0.50	0.18	0.22	0.02	0.43	0.04	0.92	0.00	0.00	0.00	2.31
10	2.27	0.36	0.15	0.24	0.02	0.55	0.14	0.91	0.00	0.00	0.00	2.36

As presented, ten types of commonly present ions were identified and quantified. The total salt content was estimated as the sum of all the ions found in a particular sample. As noticeable and confirmed by the practice in conservation, the most common ions present in the samples are Na^+, K^+, Ca^{2+}, Cl^-, SO_4^{2-}, NO_3^-. None of the unusual anions were found, i.e. NO_2^-, F^-, PO_4^{3-}. It means that no specific factors, e.g. chemical treatment, special industrial pollutants, were affecting the object in the past. The absence of phosphorous(V) anions may result also form very low solubility inorganic phosphates. Thus, further acidic treatment of the post-extraction residues and the consecutive analysis should be performed for full recognition. Finally, the overall salt content, varying from 0.07 % up to 4.48 % remains within the typical values for salt affected monuments.

In the last step, the commonly present salt efflorescences, as depicted in Fig. 1, were analysed by the electrophoretic methods. However, there is no a clear relation between the salt content in bricks and it the efflorescence. The results of quantitative salt analysis present in efflorescences should not be treated as representative for the salt content in bricks. All the samples were taken from the ramparts and the Teutonic Order castle ruins in the Old Town of Toruń, from the Vistula river side. Similarly as in the brick sample analysis, only the common ions were identified and quantified. The results are collected in Tab. 3. As noticeable, the calculated sums do not amount to 100 %. This phenomenon may be explained by the presence of insoluble salts in the efflorescences or by the presence of other insoluble inorganic matter, e.g. brick powder, collected together with efflorescences. This hypothesis is confirmed by the presence of solid residues after sample dissolution. Brick powder as red dots are visible on the microscopic photo of one of the samples (Fig. 2).

Fig. 2: Microscopic photo of efflorescences, sample 4.3 (photo by W. Oberta).

Tab. 3: Quantitative ion contents by capillary electrophoresis in the efflorescences samples from ramparts and Teutonic order castle in Toruń (Vistula river side).

Sample	**Na^+**	**K^+**	**Ca^{2+}**	**Mg^{2+}**	**Cl^-**	**SO_4^{2-}**	**NO_3^-**	**NO_2^-**	**F^-**	**PO_4^{3-}**	***Sum***
	[%]	[%]	[%]	[%]	[%]	[%]	[%]	[%]	[%]	[%]	[%]
1.1	10.23	25.81	1.26	0.18	0.75	16.40	37.38	0.00	0.00	0.00	92.00
1.2	8.11	17.51	1.39	0.18	0.59	15.08	29.06	0.00	0.00	0.00	71.91
2.1	20.70	2.00	1.46	0.18	0.92	45.54	1.88	0.00	0.00	0.00	72.69
3.1	15.83	6.15	1.16	0.16	0.89	24.71	7.49	0.00	0.00	0.00	56.39
3.2	14.60	23.55	1.18	0.17	0.00	24.57	28.04	0.00	0.00	0.00	92.12
3.3	31.01	5.42	1.15	0.12	0.85	39.77	3.77	0.00	0.00	0.00	82.10
4.1	11.41	8.39	1.30	0.20	0.00	13.78	27.72	0.00	0.00	0.00	62.80
4.2	17.84	6.29	4.39	0.30	1.59	43.39	0.,92	0.00	0.00	0.00	74.73
4.3	17.89	5.79	2.14	0.19	1.17	25.66	3.63	0.00	0.00	0.00	56.47
4.4	16.88	8.89	1.54	0.17	0.61	31.65	15.54	0.00	0.00	0.00	75.28
4.5	31.49	5.56	1.17	0.15	0.14	13.02	5.19	0.00	0.00	0.00	56.72
4.6	32.23	3.,41	1.13	0.,15	0.00	60.26	1.66	0.00	0.00	0.00	98.84
5.1	3.32	0.64	8.72	0.26	0.00	14.73	0.54	0.00	0.00	0.00	28.22
5.2	29.31	3.13	1.14	0.15	0.00	26.14	1.83	0.00	0.00	0.00	61.70
6.1	0.98	10.79	1.70	0.21	0.00	1.00	36.40	0.00	0.00	0.00	51.08

4. Conclusions

The laboratory-scale experiments enabled the successful development of a new field of application of electrophoresis, in restoration research. The artificially salt loaded specimens as well as the historical object samples were analysed, and a good correlation of conductometric and electrophoretic results with the real salt content measured gravimetrically was found. Capillary electrophoresis exhibits an advantage over the conductometric analysis by the ion specific nature of analysis. Thus, by the experiments conducted on the historic object samples, the potential of electrophoretic techniques for a rapid and reliable quantitative ion analysis was proved. Bases on the findings of the laboratory tests, it was found that the coupling of the conductometric analysis with electrophoresis constitutes a perfect combination. The conductometric analysis reveals the bulk salt content, so that then electrophoresis can be performed with a known analytical dilution, what shortens the overall test time. The electrophoretic techniques are also applicable for the analysis of the salt efflorescence. The advantage of electrophoresis provides a tool for a completely innovative salinity monitoring programme. This research will be continued by particular investigations to which this paper constitutes the basic research.

References

Blatny, P., Kvasnička, F., (1999), Application of capillary Isotachophoresis and capillary zone electrophoresis to the determination of inorganic ions in food and feed samples, J. Chromatogr. A, 834, 419-431.

Bläuer Böhm, C., (2005), Quantitative salt analysis in conservation of buildings, Restoration of Buildings and Monuments, 11, 409-418.

Boček, P., Deml, M., Gebauer, P., Dolnik, V., (1988), „Analitycal Isotachophoresis", VCH, Weinheim, ISBN 9780895734778, p. 13.

Borelli, E., (1999), „Conservation of architectural heritage, historic structures and materials, ARC laboratory handbook, Salts", ICCROM, Rome, ISBN 9290771577, p. 3.

Charola, A. E. (2000), Salts in the deterioration of porous materials: an overview, Journal of the American Institute for Conservation, 39 (3), 327-343.

Ciechanowska, J., (2012), "Rola bakterii nitryfikacyjnych w procesie niszczenia zabytków ceglanych", MScthesis, Promotor prof. Jadwiga W. Łukaszewicz, Nicolaus Copernicus University, Toruń 2012, 30-34.

ed. Domasłowski, W., (2003), "Preventive conservation of stone objects", Wydawnictwo Naukowe UMK, Toruń 2003, ISBN 83-231-1645-8.

Foret, F., Křivánková, L., Boček, P., (1993), "Capillary Zone Electrophoresis", VCH, Weinheim, ISBN 3527300198, p. 1-5.

Kaniansky, D., Masár, M., Marák, J., Bodor, R., (1999), Capillary electrophoresis of inorganic anions, J. Chromatogr. A, 834, 133-178.

Kvasnička, F., Parkin, G., Harvey, CH., (1993), Capillary Isotachophoresis as a new tool in sugar factory analysis, Int. Sugar J., 95, 451-458.

COMPARABILITY OF NON-DESTRUCTIVE MOISTURE MEASUREMENT TECHNIQUES ON MASONRY DURING SIMULATED WETTING

S.A. Orr[1], H.A. Viles[1*], A.B. Leslie[2] and D. Stelfox[3]

Abstract

Detecting the presence of moisture in historical masonry is essential to understanding how a structure interacts with the environment, and diagnosing the potential for damage from a range of physical, chemical, and biological processes. In-situ, non-invasive diagnostic techniques have been developed in preference to methods that require irreversible modifications to a structure. These techniques include: electrical resistivity, microwaves, and infrared thermography. Independently, these approaches provide limited snapshots of surficial and internal moisture regimes; this project sought to assess the comparability of multiple techniques. Simulated post-rain spell drying was monitored over 48 h on limestone and sandstone monoliths in a controlled laboratory environment and also in ambient conditions on purpose-built masonry located in Oxfordshire, UK. Repeat measurements were taken using electrical resistance tomography (ERT), electrical and microwave moisture meters, and infrared thermography. Three aspects of comparability are discussed: i) data transformations and geological comparability, ii) depth-resolving meter readings, iii) the localised benefits of employing multiple technologies and instruments.

Keywords: moisture mapping, drying processes, non-destructive testing (NDT), instrument comparability, stone masonry

1. Introduction

Water is an important factor in stone deterioration, acting as a primary and secondary agent in a range of chemical, physical, and biological deterioration mechanisms. The role of water in specific mechanisms depends on its spatial and temporal patterning (Mamillan 1981). To this end, it is necessary to be able to detect and monitor local variation of water within stonework and masonry structures.

Non-invasive moisture monitoring techniques have been developed for the historical environment as an alternative to invasive techniques. These include electrical resistance tomography (ERT), which has been employed to successfully monitor short-term moisture

[1] S.A. Orr and H.A. Viles*
School of Geography and the Environment, University of Oxford, United Kingdom
heather.viles@ouce.ox.ac.uk

[2] A.B. Leslie
Historic Environment Scotland, United Kingdom

[3] D. Stelfox
Consarc Design Group, United Kingdom

*corresponding author

regimes in historic masonry (Martinho *et al.* 2010). In contrast, thermography and handheld moisture meters (or 'damp' meters) have been adopted from civil engineering, but are primarily intended for use on twentieth-century materials. Handheld meters have been assessed for relative performance and best practice (Eklund *et al.* 2013) for use on stone but their applicability to masonry with regards to how they compare to more robust analytical equipment is yet to be established. This paper compares two handheld moisture meters and infrared thermography to electrical resistance tomography to investigate moisture dynamics, discussing aspects of technological comparability for complex masonry constructions and information gained by combining multiple devices.

2. Materials and methods

2.1. Materials

Two stone monoliths were used – a sandstone block measuring 55×32×25.5 cm (obtained from a quarry) and a limestone block (from a waste site) measuring 71×38 cm in height and length respectively (see Fig. 1a), with an uneven width varying from 9–20 cm. The limestone block has a discoloration running down the front surface suggesting near-surface physical inconsistencies, and could be indicative of defects at further depths.

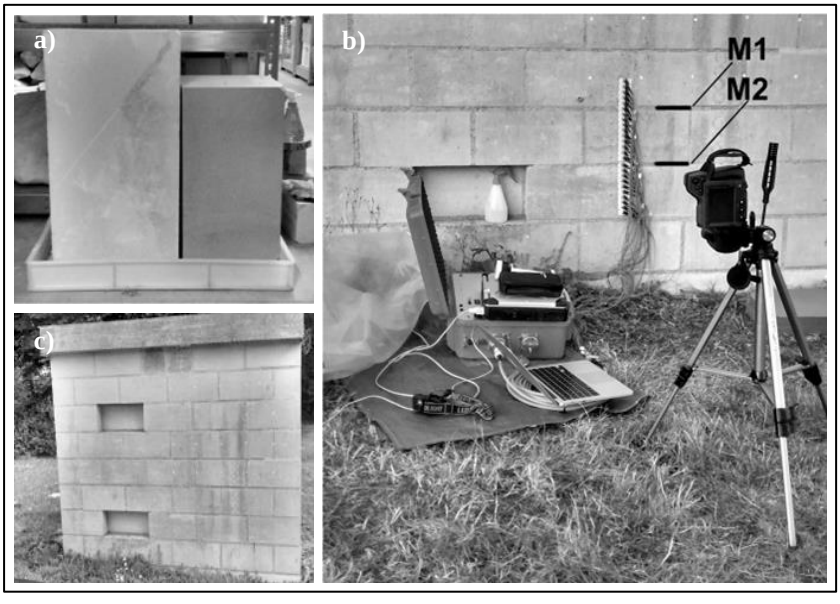

Fig. 1: The monoliths (left, limestone; right, sandstone) (a) and the traditional masonry construction (b). An example of the simultaneous instrument set-up with positions of the mortar joints: M1 and M2 (c).

The masonry construction is 1.8 m high and 2.0 m wide, and comprises a single skin of Elm Park limestone ashlar blocks (20×20×40 cm) with 2 cm lime mortar joints (Fig. 1b). It is located in a field with sparse tree cover in Oxfordshire, England. Measurements were taken in July 2015. The wall has an exposed western façade that receives direct sunlight between 13:00–15:00 h and 17:00–19:00 h daily in summer if not obscured by cloud cover.

2.2. Experimental protocol

This study monitored drying for 48 h after simulated rain events across 48 cm vertical transects of 25 evenly-spaced 2 cm nodes. The ERT apparatus could not be removed from the stone surface for the employed time scales, so handheld meter measurements were taken on a parallel transect separated from the former by 8 cm (Fig. 1c). Preliminary testing on the monoliths demonstrated two ERT transects separated by 15 cm and equally-distanced from the edges were highly correlated, and had similar wetting and drying properties (Orr 2015). Thus, the parallel transects were considered to be comparable representations of drying processes, with error $\leq$ 15%. The monoliths were equilibrated and tested under stable temperature and *RH*.

Moisture instrument readings were taken along the transects at hourly intervals for the initial 12 h of drying, after which measurements were taken at 3, 6, 12 and 24 h; this timescale captures the dynamic nature of surface desorption through evaporation. For unsaturated flow in porous media the cumulative moisture migration i (in this case, i_{drying}) can be defined as $i_{dry} = Rt^{1/2}$,in which R is a material property of desorptivity equal to the Boltzman transformation $\varphi = xt^{1/2}$ integrated over a moisture content θ differential for a vertical distance x in time t (Hall and Hoff 2012, p. 114). This relationship dictates that rates of desorption decrease significantly with time; deviations typically occur in fabricated materials and were unexpected for the selected stones (Hall and Hoff, 2012, p. 129).

A driving rain index was derived to determine the quantity of water that should be applied to emulate driving rain spells based on EN ISO 15927-3:2009 for the Oxfordshire field site. Meteorological data was taken from the UK MIDAS database at a site ~20 km from the site; in predominantly flat regions, indices are applicable up to 100 km away. The following parameters were employed:

- Roughness factor for Tier II terrain for 'farm land with boundary hedges, occasional small farm structures, houses or trees'
- Wall geometry factor = 0.4, reflecting the lower portion of a 'two-story building with flat roof (pitch < 20°)'
- Topography and obstruction factors = 1, i.e. no index reductions

The determined spell index I_S is the 67th percentile of I'_S, representing the maximum value of I'_S likely to occur in a three year period. A wall spell index = 6.5 $L \cdot m^{-2} \cdot h^{-1}$ (calculated for 1985–2014) of distilled water was applied over 1 h with a small pressured spray bottle in roughly rectangular areas surrounding the transects.

2.3. Instrumentation

A GeoTom device (Geolog2000; Augsburg, Germany) was used to collect the two-dimensional resistance profiles in conjunction with crocodile clip shielded cables and self-adhesive electrocardiogram electrodes affixed to the stone surface. Adhesive electrodes were used instead of drilled-in steel electrodes as they are non-invasive, and have been shown to have similar contact resistance to implanted steel electrodes (Sass and Viles 2006). Data were collected with a linear Wenner array and inverted into apparent resistivity models using RES2DINV v. 3.59 (GeoTomo Software; Malaysia).

Electrical resistance is also influenced by material properties, physical characteristics, and salts (Martinho *et al.* 2010) which creates ambiguity leading to misinterpretation of direct-current measurements (Kruschwitz 2007, p. 2). However, ERT has been shown to relate to

moisture contents with gravimetric calibration methods (Sass 1998) through an extension of Archie's Law relating saturation and resistivity with the appropriate assumptions (Sass and Viles 2010). Lime mortar has been shown to have commensurate dielectric properties to limestone (Ball *et al.* 2011). In addition to ERT, the following were used to monitor moisture:

- Surveymaster Protimeter (GE Measurement & Control; Billerica, MA, USA) includes a pin-type resistance meter with a sensor consisting of two 10 mm long stainless steel pins spaced approximately 14 mm apart, a wood moisture equivalent (WME) from 0–100.
- T610 (Trotec; Marchtrenk, Austria) produces a microwave field penetrating 20-30 cm that is subsequently reflected and converted into nominal values from 0-200.
- T460 thermal imaging camera (FLIR; Wilsonville, OR, USA) was used to capture surface temperatures of the monoliths and masonry wall areas surrounding the transects; it has a thermal sensitivity of <0.03°C and an output resolution of 240×320 pixels.

3. Results and discussion

3.1. Data transformations

ERT timeseries were logarithmically transformed and normalised to initial, pre-wetting stage resistivities (ρ_{pw}). These do not represent completely 'dry' states; the pre-wetting measurements represent the stone at a particular phase of hygrothermal transition. The transformed resistivities $\rho'_i = -log_{10}(\rho_i/\rho_{pw})$ enabled comparison between the monoliths and the masonry construction at depths with pseudo-values linearly proportional to moisture contents. Values of ρ'_i theoretically range within $(\infty, 0)$; as $\rho' \to 0$ the resistivity (and thus purported moisture content) are returned to the pre-wetting stage. Practically, values of ρ' did not exceed 2.

Inversion uncertainties were greater for the pre-wetting states, tending to increase over the duration of the drying process: this is likely caused by the software's difficulty with handling the geological realism of inverting very dry stone (Sass and Viles 2010). This complicated obtaining appropriate values of ρ_{pw}; however, the benefit of lognormal transformation is that the pre-wetting denominator induces only a vertical shift of ρ' in the lognormal dimension. While pre-wetting resistivities can be analysed, two parameters independent of this enable valuable discussion: i) the shape of the drying curve, and ii) $\Delta\rho_{f-0}$.

The meter readings ν exhibit linear behaviour similar to the ERT depth ρ' curves (Fig. 2). This suggests that the instrument readings calibrate linearly to moisture contents. This implies that relative meter readings (additive/subtractive from a reference value, i.e. $\Delta\nu_{ref-i}$) can be considered proportional to moisture contents. While the idea of 'relative readings' is not novel in moisture meter best practice, previous guidance has suggested using ν_i/ν_{ref} (Burkinshaw and Parrett 2003); this relationship is not ideal for interpreting the readings of some handheld meters.

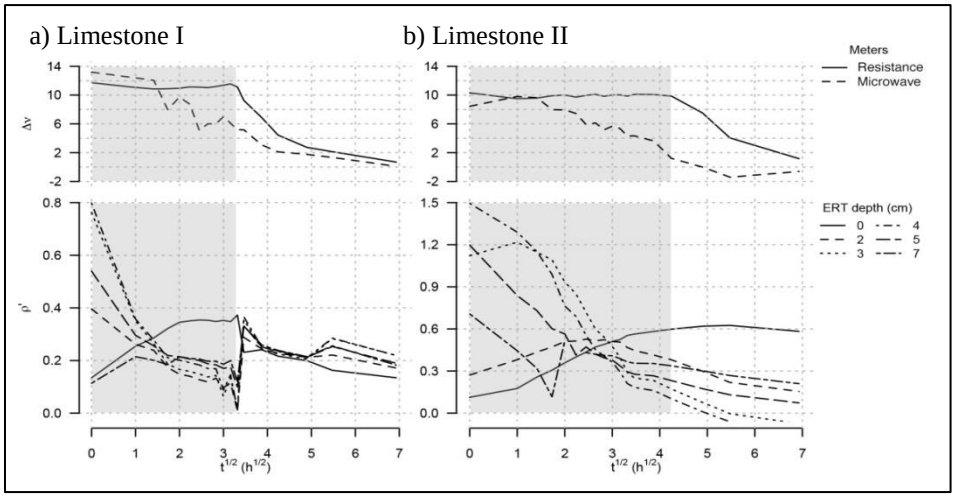

Fig. 2: Transformed meter readings Δν and ERT depth moisture profiles ρ′ for two iterations of the limestone monolith moisture regimes.

The surface resistance meter captured a constant surface value of moisture before decreasing to the pre-wetting conditions, which corresponds to the inversion of the ERT surface measurement. It has been shown that this meter model is able to produce WMEs higher than these values on English limestones (Eklund *et al.* 2013), so it was not suspected to represent moisture contents out of instrumental range.

3.2. Depth-resolved damp meter modelling

No single ERT depth profile was found to characterise the moisture meter readings over the total drying duration in isolation: there were periods when certain depths had Pearson's $R > 0.8$, but negative coefficients indicated relationships to a lack of moisture following a migration to adjacent depth(s). To this end, multiple linear regression models were created using non-negative least squares (NNLS) regression for each of the monolith and stone masonry experimental runs.

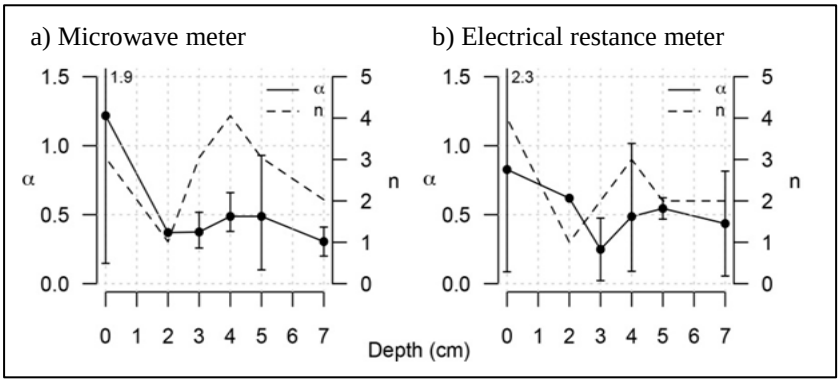

Fig. 3: NNLS regression results for handheld meters: Coefficients α and quantity of regression models incorporating depth. Vertical bars indicate maxima and minima.

NNLS is a least squares regression in which coefficients are restricted to positive values, based on an algorithm developed by Lawson and Hanson (1995). As the residuals of a NNLS regression are not normally distributed, typical evaluation parameters (eg. confidence intervals, p-values) are not applicable, so each predictor column (ERT depths) and the meter reading vectors were normalised between 0 and 1 (Slawski *et al.* 2013): regressions coefficients represent the relative contributions of independent variables. Both handheld meters exhibited decreasing correlation with the ERT as depth increased, an effect that was seen more strongly with the microwave meter (Fig. 3).

3.3. Multi-instrument utility

The surface resistance meter captured distinct mortar behaviour due to the high resolution and localised readings. In contrast, the microwave meter and ERT did not capture distinct moisture movements through the mortar as clearly due to wider detection range and smoothing techniques, respectively.

Passive IR thermography was able to capture early rapid edge-adjacent evaporation transitioning to front surface evaporation in the stone monoliths, in addition to subsequent higher moisture concentrating at the base, adjacent to an impermeable plastic barrier (Fig. 4). These phenomena are difficult to assess or characterise with other non-destructive techniques due to interference from the adjacent air space.

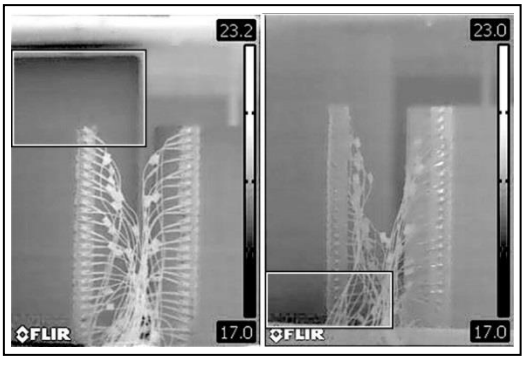

Fig. 4: A distinct transfer of significant moisture migration at monolith edges mid-drying (left) and collected base water at 48 h (right) is highlighted in boxes, where darker zones represent areas of higher moisture content.

Mortar-adjacent behaviour was assessed by comparing the mortar moisture contents to the adjacent ashlar units: positive values represent mortar readings greater than the surrounding areas, as would be expected for a more porous building material designed to aid moisture migration through masonry.

The early electrical mortar readings were commensurate to the surrounding stone representing similar moisture contents during the latent phase of activity, after which mortar moisture contents increase (Fig. 5). Differences in dielectric properties can be discounted as a crucial factor: pre-wetting readings differed by 0.1 WME between the mortar joints and the surrounding stonework, respectively. The microwave meter captures the mortar joint behaviour to a lesser extent: there is significant variation above and below the mortar joint during the latent phase of moisture transport but mortar meter readings are

similar to the electrical resistance meter after $t^{1/2} = 2$. In contrast, ERT does not exhibit any distinct near-mortar behaviour.

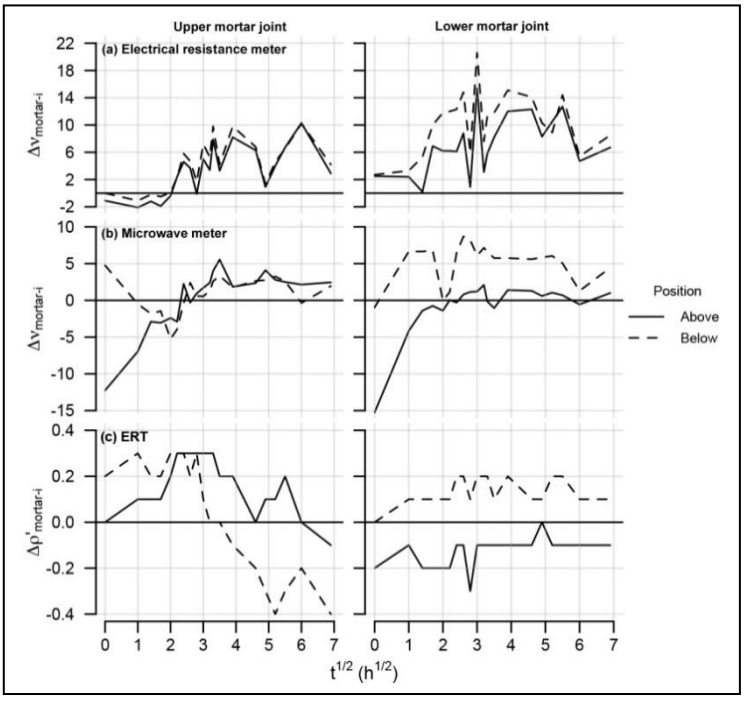

Fig. 5: Differential instrument readings above and below mortar joints within the stone for the electrical resistance meter (a), the microwave meter (b), and ERT (c). Values are presented relative to the upper (M1) and lower (M2) mortar joint values (see Fig. 1c); positive values represent higher moisture than the surrounding areas.

4. Conclusions

Spatial and temporal comparisons of data from handheld moisture meters and infrared thermography with electrical resistance tomography produced valuable information on how instrument measurements interacted with the masonry elements. Distinct mortar joint and near-edge behaviour was distinguished by the handheld meters and infrared thermography, identifying important characteristics of moisture migration that would have otherwise been unnoticed by ERT. Although handheld meter signals may penetrate a certain range, they are less attuned to detecting water at greater depths as their readings are more representative of near-surface moisture regimes. Identifying building elements and conditions for which instrument types are most applicable enables efficient moisture surveys, but interpretation should consider different building materials and, if possible, incorporate laboratory validation.

Acknowledgements

Many thanks to Hong Zhang and Mona Edwards for logistical support. This work was enabled by financial support provided by the EPSRC through the Centre for Doctoral Training in Science and Engineering for Arts, Heritage, and Archaeology.

References

Ball, R. J., Allen, G. C., Starrs, G., and McCarter, W. J., 2011, Impedance spectroscopy measurements to study physio-chemical processes in lime-based composites, Applied Physics A, 105(3), 739–751.

EN ISO 15927-3:2009 –Hygrothermal performance of buildings. Calculation and presentation of climatic data. Calculation of a driving rain index for vertical surfaces from hourly wind and rain data.

Burkinshaw, R. and Parrett, M., 2003, Diagnosing Damp. RICS Books, London, UK.

Eklund, J.A., Zhang, H., Viles, H.A., and Curteis, T., 2013, Using handheld moisture meters on limestone: Factors affecting performance and guidelines for best practice, International Journal of Architectural Heritage, 7(2), 207–224.

Hall, C. and Hoff, W.D., 2012, Water Transport in Brick, Stone and Concrete, 2nd ed., Taylor & Francis Group, London, UK.

Kruschwitz, S.F., 2007, Assessment of the Complex Resistivity Behaviour of Salt Affected Building Materials, Ph.D. thesis, Technischen Universitaet Berlin, Germany.

Lawson, C.L. and Hanson, R.J., 1995, Solving Least Squares Problems, Society for Industrial and Applied Mathematics, Philadelphia, USA.

Mamillan, M., 1981, Alteration et Durabilité des Pierres. In proceedings of Seminaire Alteration et Durabilité des Bétons et des Pierres, St.Remy-Les-Chevreuse, France.

Martinho, E., Alegria, F., Grangeia, C., Dionisio, A., and Almeida, F., 2010, Electrical resistivity imaging: Overview and a case study in stone cultural heritage. In: 3D Imaging: Theory, Technology, and Applications, Duke, E.H. and Aguirre, S.R (eds.).

Orr, S.A., 2015, Comparative synthesis of handheld damp meters and infrared thermography with 2D-resistive tomography, M.Res. thesis, UCL.

Sass, O. and Viles, H.A., 2006, How wet are these walls? Testing a novel technique for measuring moisture in ruined walls, Journal of Cultural Heritage, 7(4), 257–263.

Sass, O. and Viles, H.A., 2010, Wetting and drying of masonry walls: 2D-resistivity monitoring of driving rain experiments on historic stonework in Oxford, UK, Journal of Applied Geophysics, 70(1), 72–83.

Slawski, M., Hein, M., 2013, Non-negative least squares for high-dimensional linear models: Consistency and sparse recovery without regularization, Electronic Journal of Statistics, 7, 3004–3056.

WATER ABSORPTION AND PORE-SIZE DITRIBUTION OF SILICA ACID ESTER CONSOLIDATED POROUS LIMESTONE

Z. Pápay[1*] and Á. Török[1]

Abstract

Miocene porous limestone is an important construction material of Central Europe, since emblematic monuments were constructed in Hungary, Slovakia, Austria, Romania and the Czech Republic from this lithotype. Cylindrical test specimens were made from quarried blocks of Hungarian limestone (Sóskút) and were consolidated by using silica acid ester (SAE). Test specimens were immersed in three consolidants representing different concentration of silica acid. Density and ultrasonic pulse velocity were measured prior and after the conservation. The amount of consolidant and the distribution of silica acid ester in the pore system were documented by using Scanning Electron Microscopy and mercury porosimetry. Water absorption properties were also measured and the results were compared to porosity and pore-size distribution changes of non-consolidated and consolidated samples. A fine-grained porous limestone was tested with connective porosities of 35.4 V%. It has been visualised by the applied techniques that SAE consolidant partly fills the pores and causes the loss in porosity. The loss in porosity is not proportional to the changes detected by ultrasonic pulse velocity measurements.

Keywords: porous limestone, water absorption, porosity, consolidation, silica acid ester

1. Introduction

Porous limestone can be found in emblematic monuments of Central European region (Kertész 1988, Török *et al.* 2004, Bednarik *et al.* 2014). In many cases these historical building show significant deteriorationin its stone material. The main reason for decay of the porous limestone besides air pollution (Török 2003) is its high water absorption ratio. Water is harmful for porous stone in three aspects. It is a fluid medium that softens stone and transports pollution particles and salts inside the rock. On the other hand if water is frozen it expands by about 9.05 % of its volume causing stress on pore walls (Park *et al.* 2014).Numerous studies deal with water absorption phenomena and its effect on physical and mechanical properties of stone. The chemical components of stone however do not have direct effects on water absorption. Vásárhelyi and Ván (2006) study the influence of water content on strength, while Juhász *et al.* 2014 studied the water absorption properties of porous limestone. Our study focuses on the changes in water absorption ratio due to stone consolidation.

[1] Z. Pápay* and Á. Török
Department of Engineering Geology and Geotechnics, Budapest University of Technology and Economics, Hungary
zita.papay@gmail.com

*corresponding author

2. Materials and Methods

Samples were treated with three different types of silica acid ester (SAE) consolidants. These materials are commonly used in monument restoration projects in Europe and also for the consolidation of porous limestone structures in Hungary. All tested agents have the same base, ethyl silicate. All agents made by Remmers GmbH. The SAE are compounds of silicon and ethyl alcohol (C_2H_5OH). KSE 300 E is considered as an "elasticised stone strengthener" according to the manufacturer. It acts as a consolidat but it also increases E-modulus (providing a better stress-strain behaviour) of the consolidtaed stone structure. KSE 300 HV is recommended especially for limestone by the manufacturer because it contains a specific coupling *agent*. The SAE consolidants and their properties are listed in Tab. 1.

Tab. 1: SAE consolidants and their properties.*

Consolidant	**Active ingredient content**	**Kinematic viscosity**	**Density** (liquid form / consolidated silica gel)
	wt.%	s	g/cm³
KSE 100	ca. 20	11	0.79 / 1.74
KSE 300E	ca. 50	11	0.90 / 1.66
KSE 300HV	> 95	12	0.99 / 1.75

*from Remmers technical data sheets except silica gel density

SAE consolidants react with water or water vapour stored in the pores or available in the air (humidity). While the ethanol evaporates amorphous and hydrous silicon dioxide (SiO_2, "silica gel") is formed in pores as an additional bond between the particles. Gel formation rate is approx. 300 g/l for KSE 300E and 300HV, and 100 g/l for KSE 100, respectively. None of these three strengthening agents have a hydrophobic effect. A fine-grained porous limestone from Sóskút was used in tests. It is a white to pale yellow packstonewith an average porosity of over 35 V% (Fig. 1a and Fig. 1b). According to mercury porosimetry its pore-size distribution shows that pores above 0.1 μm and below 10 μm are dominant (Fig. 1c). Cylindrical specimens were drilled from blocks perpendicular to the bedding planes and divided into groups according to the results of non-destructive tests (density, ultrasonic pulse velocity, open porosity according to EN 1936 and EN 14579). The samples were immersed gradually in consolidants and were fully immersed for 10 minutes under atmospheric pressure. Tests samples were stored in climate room for 4 weeks and the drying process of consolidants was observed after consolidation by recording the changes in weight. Density and ultrasonic pulse velocity were measured prior and after the consolidation. Water saturation was performed by EN 13755 on cylindrical specimens of 50 mm in diameter and 20 mm in height. Water saturation lasted 16 days and the results presented in this paper are average values of 6 samples. Open porosity were calculated from water immersion test results. Capillary water absorption was determined on 2 samples from each analytical group according to EN 1925 using cylindrical specimens of 50 mm in diameter and in height. Pore-size distribution was determined by mercury porosimetry

(Brakel et al. 1981). The measurements were made on cylindrical specimens of 10 mm in diameter with a Carlo Erba 2000 porosimeter. The data evaluation was made by a Pascal softver for the measured pores pore radii of 0,001 µm to 100 µm. The limitations of this technique are related to the fact that it detects the largest entrance of the pores and not the inner size of the pores.

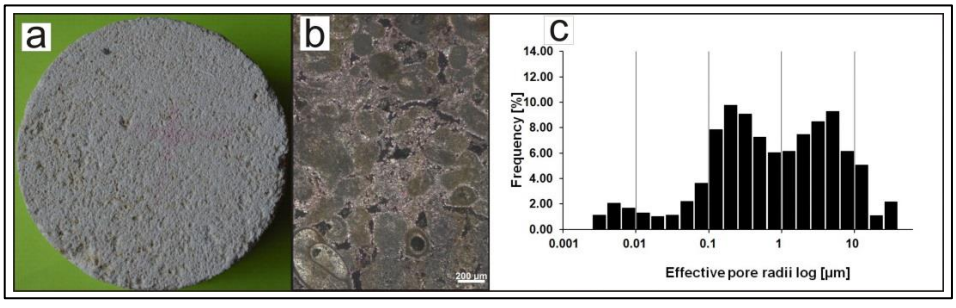

Fig. 1: Fabric (a) and microscopic image (b) and pore-size distribution (c) of fine-grained porous limestone.

3. Results

The average water absorption of non-treated and treated samples under atmospheric pressure shows clear differences (Fig. 2). The water absorption is more rapid in non-treated samples than in consolidated ones. The steeper curve marks faster penetration. When the penetration rates of all the consolidated samples are compared the fastest penetration rate was observed at KSE 300HV, while the slowest at KSE 300E treated samples (Fig. 2).KSE 100 showed high standard deviation in absorption results in the first 3-4 hours. KSE 100 consolidated samples started water absorption slower than KSE 300 HV, but ultimately they took up more water than KSE 300 HV consolidated ones. Change in open porosity of consolidated samples are reported in Tab. 2. Open porosity of KSE 100 treated samples is 33.06 vol% in average, while 19.12 vol.% of KSE 300E and 28.91 vol.% of KSE 300HV. Thus, consolidation with KSE 100 causes the lowest loss in porosity (2.91 vol.%), while consolidation with KSE 300E reduced the porosity the most (17.28 vol.%). The change in porosity at KSE 300HV treated samples is 7.41vol.%.

The water capillary tests were made a year after consolidation. The capillary rise curves in consolidated porous limestones with reference to non-treated samples are markedly different (Fig. 3). SAE100 shows the fastest water absorption rate from all applied agents. The graph illustrates that there are significant differences between the water penetrations of consolidated limestones. Water absorption of SAE 100 treated samples is relatively fast; it nearly approaches the values of the non-treated limestone. On the other hand there is no detectable capillary rise in KSE 300 E treated samples. The water absorption KSE 300 HV consolidated samples is between the two former ones. Changes in porosity, apparent density and ultrasonic pulse velocity in relation to the penetration of consolidants are given in Tab. 2.

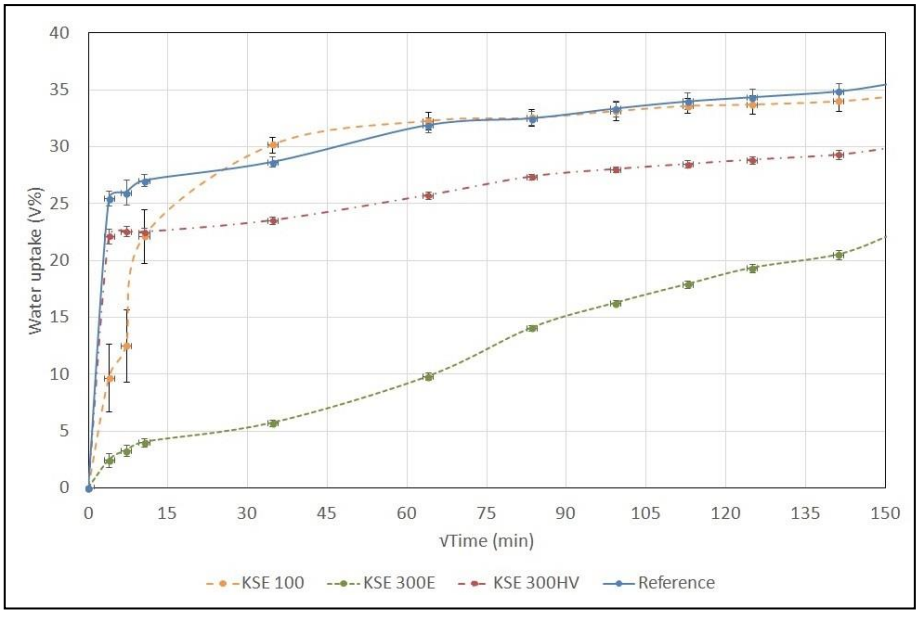

Fig. 2: Average water uptake in V% as a function of root time.

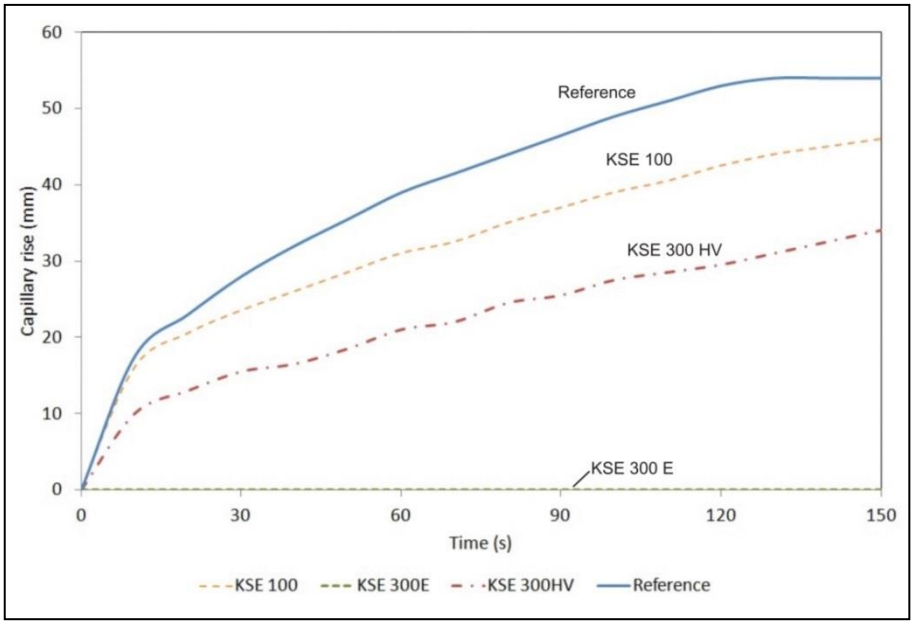

Fig. 3: Water capillary rise in consolidated and non-consolidated porous limestone. Tests were made one year after the consolidation.

Tab. 2: Changes of physical properties due to consolidation.

Consolidant	Change in porosity	Calculated amount of silica gel in pores	Change in ultrasonic pulse velocity
	ΔV%	V %	%
KSE 100	-2.91	2.19	6.6
KSE 300E	-17.28	4.39	8.7
KSE 300HV	-7.41	4.91	4.0

The pore-size distribution of samples also reflects variations in penetration of consolidants. The distribution of pore radii of KSE 100 consolidated samples is nearly the same as non-consolidated limestone (Fig. 4a and Fig. 1c). Treatment with KSE 300HV decreases the amount of pores in the pore-size interval of 1-10 μm (Fig. 4a and Fig. 1c).There is a significant change in pore-size distribution when the porous limestone is treated with KSE 300E. Amount of pores decreases in the 0.1-10 μm interval. Conversely, an increase in percentage of pores is observable, in the pore range smaller than 0.01 μm. All of the tested consolidated samples show a small increase in porosity below the pore radius of 0.01 μm.

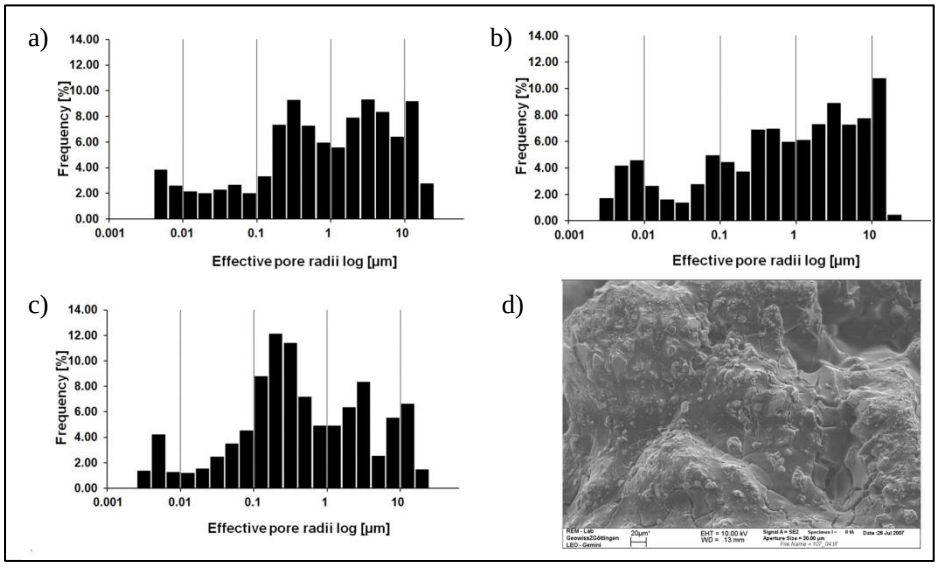

Fig. 4: Pore-size distribution and SEM image of consolidated limestone; a) SAE 1; b) SAE 2; c) SAE 3; d) SEM image of consolidant partly occluding pore space of porous limestone.

4. Conclusions

Small increase in ultrasonic pulse velocity was observed after the consolidation of the porous limestone samples. Accordingly, this non-destructive test method is capable to

detect consolidation. However, it was not possible to detect the amount of consolidant by using this method, since the measured pulse velocities do not show correlation with the apparent densities. One possible explanation to this is that the silica acid gel forms very thin layers on pore walls, and do not entirely occlude pores, thus do not increase proportionally the ultrasonic pulse velocities. A better tool to characterise the pore system is the water absorption. The water absorption curves clearly mark the changes in porosities related to consolidation. This simple method is a good indicator of the rate of consolidation. Open porosity results showed a significant loss in KSE 300E treated samples (17.28 vol.%) while only 4.39 vol.% of silica gel occluded the pores, compared to unconsolidated limestone. KSE 300 E closed off 12.89 vol.% of open pores in medium-grained limestone due to consolidation. The amount of closed pores is 0.79 vol.% and 2.5 vol.% of KSE 100 and of KSE 300HV consolidated limestones, respectively.

Acknowledgements

The financial support provided by the National Research, Development and Innovation (NKFI) Fund (ref. no. K 116532) is appreciated.

References

Bednarik, M, Moshammer, B, Heinrich, M, Holzer, R, Laho, M, Rabeder J, Uhlir C, Unterwurzacher, M., 2014, Engineering geological properties of Leitha Limestone historical quarries in Burgenland and Styria, Austria. Engineering Geology, 176, 66-78.

Brakel, J. van, Modry, S. and Svata, M. 1981, Mercury porosimetry: State of art, Powder technology, 29, 1-12

Juhász, P., Kopecskó, K. and Suhajda, Á.,2014, Analysis of capillary absorption properties of porous limestone material and its relation to the migration depth of bacteria in the absorbed biomineralizing compound, Period. Polytech. Civil Eng., 58,2, 113-120.

Kertész, P., 1988, Decay and conservation of Hungarian building stones,in proceedings of The Engineering Geology of Ancient Works, Monuments and Historical Sites, IEAG Conference,Marinos P.G. & Koukis, G.C. (eds.),Athens,Balkema, Rotterdam, Vol. II, 755-761.

Park, J., Hyun, C-U., and Park, H-D., 2015, Changes in microstructure and physical properties of rocks caused by artificial freeze-thaw action, Bulletin of Engineering Geology and the Environment, 74, 555-565.

Török, Á., Rozgonyi N, Prikryl, R., and Prikrylová, J., 2004, Leithakalk: the ornamental and building stone of Central Europe, an overview, In: Prikryl, R. (ed), Dimension stone. Balkema, Rotterdam, 89-93.

Török, Á., 2003, Surface strength and mineralogy of weathering crusts on limestone buildings in Budapest, Building and Environment, 38, 9-10., 1185-1192.

Vásárhelyi, B. and Ván, P., 2006, Influence of water content on the strength of rock,Engineering Geology, 84, 70-4.

CONSERVATION STATUS AND BEHAVIOUR MONITORING SYSTEM OF GONGSANSEONG FORTRESS WALL IN GONGJU, KOREA

J.H. Park[1], K.K. Yang[1], C.U. Park[1], Y.H. Jo[1] and C.H. Lee[1*]

Abstract

The purpose of the study is to interpret the behaviour characteristics of the Gongsanseong fortress wall in Gongju, Korea. To achieve these purposes, this study performed visual inspection to assess the conservation status of Gongsanseong rampart, selected damaged areas, and established a monitoring system for rampart behaviour. The result obtained from these investigations will be used as the basic data for the structural safety analysis of rampart.

Keywords: Gongsanseong, behaviour monitoring system, electrolytic tilt sensor

1. Introduction

The Gongsanseong is the fortress wall which located in Gongju City, Republic of Korea. It is a Pogok style fortress surrounding Mt. Gongsan of 110m in altitude and a small peak in west. The fortress is made of soil and stone. The length of the fortress wall is 2,660m. It is assessed as valuable relics to figure out the cultural life of Baekje for the history of Ungjin Period (475 to 538 AD). It was excavated through a series of consecutive excavation surveys since 1960s. However, rampart area was partly collapsed on September 14 in 2013, and rain inflow, unstable foundation, projection, dislocation and ground subsidence have been progressed. Because such damages operate intricately, stability of rampart is in great danger. Accordingly, this study performed visual inspection to assess conservation status of Gongsanseong rampart, selected damaged area, and established a monitoring system for rampart behaviour.

[1] J.H. Park, K.K. Yang, C.U. Park, Y.H. Jo and C.H. Lee*
Department of Cultural Heritage Conservation Sciences, Kongju National University, Republic of Korea
chanlee@kongju.ac.kr

*corresponding author

2. Conservation status and monitoring system

2.1. Conservation status

As a result of precision visual inspection, structural deformation was found in 41 spots out of 2.6 km. Among these, 11 spots required monitoring due to severe problem of stability, and 30 spots are deteriorated spots that need continual observation as damage is in early stage. By the type of damage (Fig. 1), inflating phenomenon was the largest with 31.8%, followed by unstable foundation and loss with 25.4% and 19.0%, respectively. And types include projection with 7.9%, crack with 3.2%, subsidence of center with 3.2%, dislocation with 1.6% and sink hole with 1.6%.

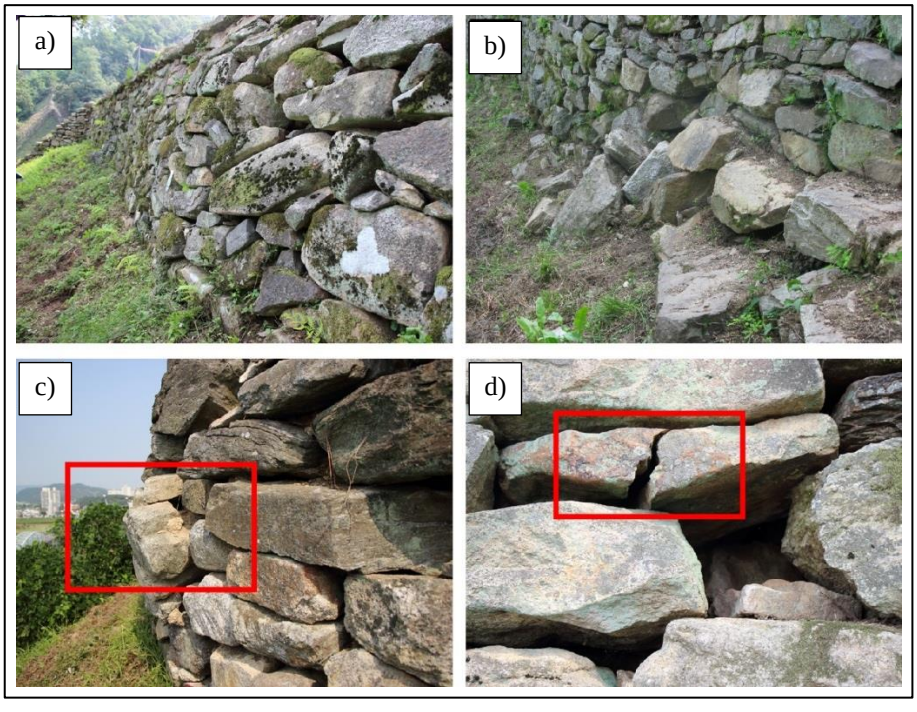

Fig. 1: Occurrences of various deterioration status: a) inflating phenomenon; b) unstable foundations; c) projection; d) crack.

2.2. Monitoring system

To analyse behaviour features of Gongsanseong rampart, automatic precision calibration monitoring were performed. The analysis on the behaviour of Gongsanseong rampart has been performed by an inclinometer. The obtained data is stored in the datalogger, which is connected to a computer for analysis through a modem. The slopes of ground and structure are known to be affected significantly by temperature of atmosphere, pressure, precipitation, quantity of solar radiation and underground water level changes and etc. (Kumpel *et al.*, 1988; Lee, 1993; Suh and Park 1997). In this study, we installed tiltmeters T1 to T11 at 11 spots that required monitoring due to severe problems of stability and carried out monitoring for about 1 year from April 2, 2014 to April 2, 2015 (Fig. 2).

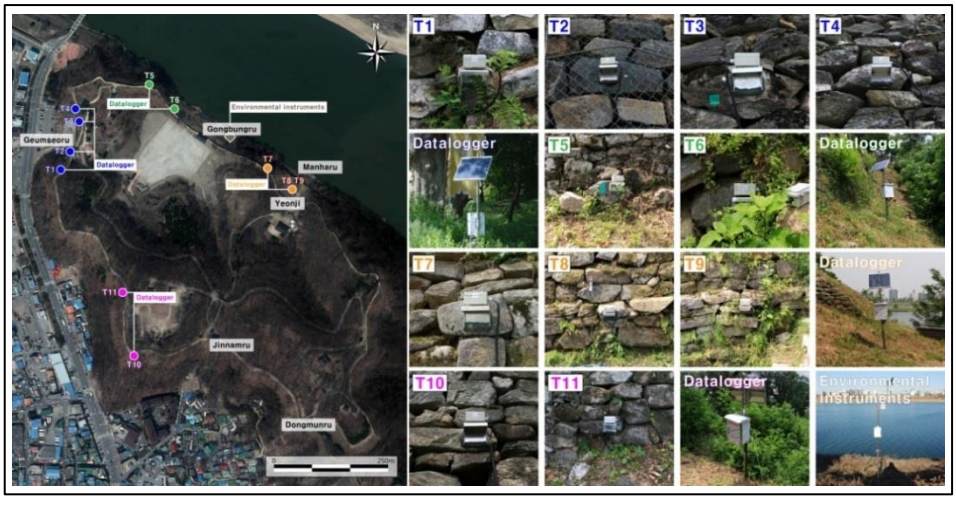

Fig. 2: Occurrences of the automatic monitoring system installed the Gongsanseong.

3. Results and discussions

3.1. Annual characteristics

The largest displacements were measured on X axis and Y axis of tiltometer T4: were 19,668.14μrad and 2,384.75μrad had the largest displacement. In the next place, X axis and Y axis of T7 and T11 were 995.98μrad, 10,135.57μrad, 1,431.94μrad and 8,577.64μrad, respectively. If displacement increases continually as in T4, T7 and T11, stones are moved?, and vertical load is imposed on the lateral face of rampart which may cause swelling or bulging phenomenon of rampart to the outside (Fig. 3). Accordingly, it is urgent to establish safety measurement against rampart collapse and to repair damaged sections as soon as possible.

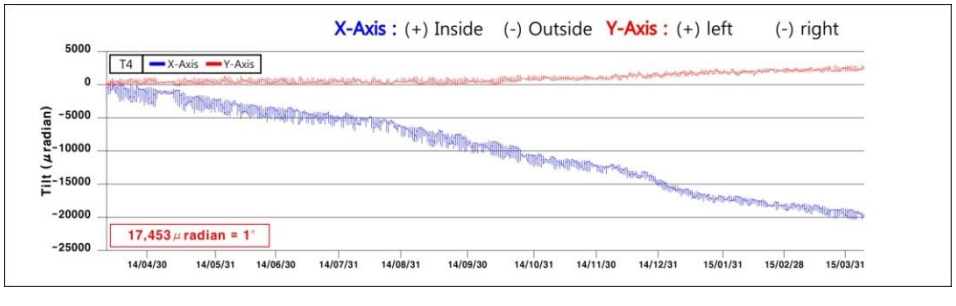

Fig. 3: movement monitoring measured by T4.

3.2. Seasonal and monthly characteristics

To examine behaviour characteristics by season, data measured at 24:00 on the 2nd day of each month was set as base data and monthly behaviour direction and displacement were calculated. Most behaviours are complex due to movement from left to right and from inside to outside without regularity (Fig. 4). The largest displacement was taken in August for T6, November for T10 and T11, December for T1, T3, T4 and T5, January for T7 and T8, February for T9 and March for T2.

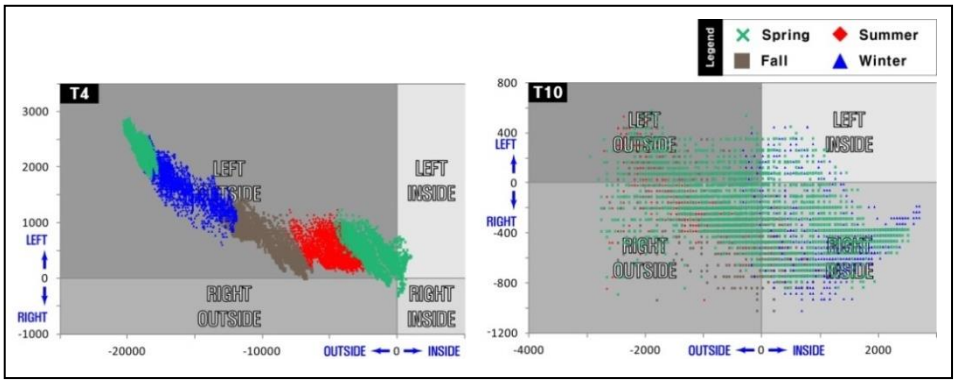

Fig. 4: Distribution diagram of the accumulation movement quantity measured by T4 and T10 at Gongsanseong Fortress.

As for monthly average displacement at each spot, January was the largest with 1,288.78 μrad, followed by December with 1,288.78 μrad. February had relatively large value with 759.13μrad. The month with the largest displacement during the calibration period was January in T8 with 4,045.99 μrad. When average displacement by season was calculated, winter season had the largest displacement followed by fall, summer and spring (Fig. 5).

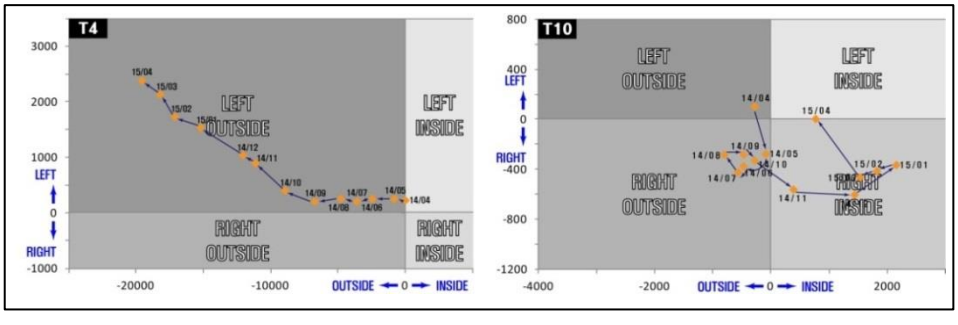

Fig. 5: Monthly movement variation of Gongsanseong measured by T4 and T10 in one year.

3.3. Environmental characteristics

When behaviour characteristics of T1, T2, T8 and T9 were analysed, T1 and T2 were the most affected by temperature variations. In contrast, while air temperature, Humidity and wind velocity had only slightly affected T8 and T9, rain falls caused main changes (Fig. 6). As such, since main causes of rampart behaviour at each part are different, structural status of rampart, atmospheric environment, damaged area site conditions must be considered for accurate analysis.

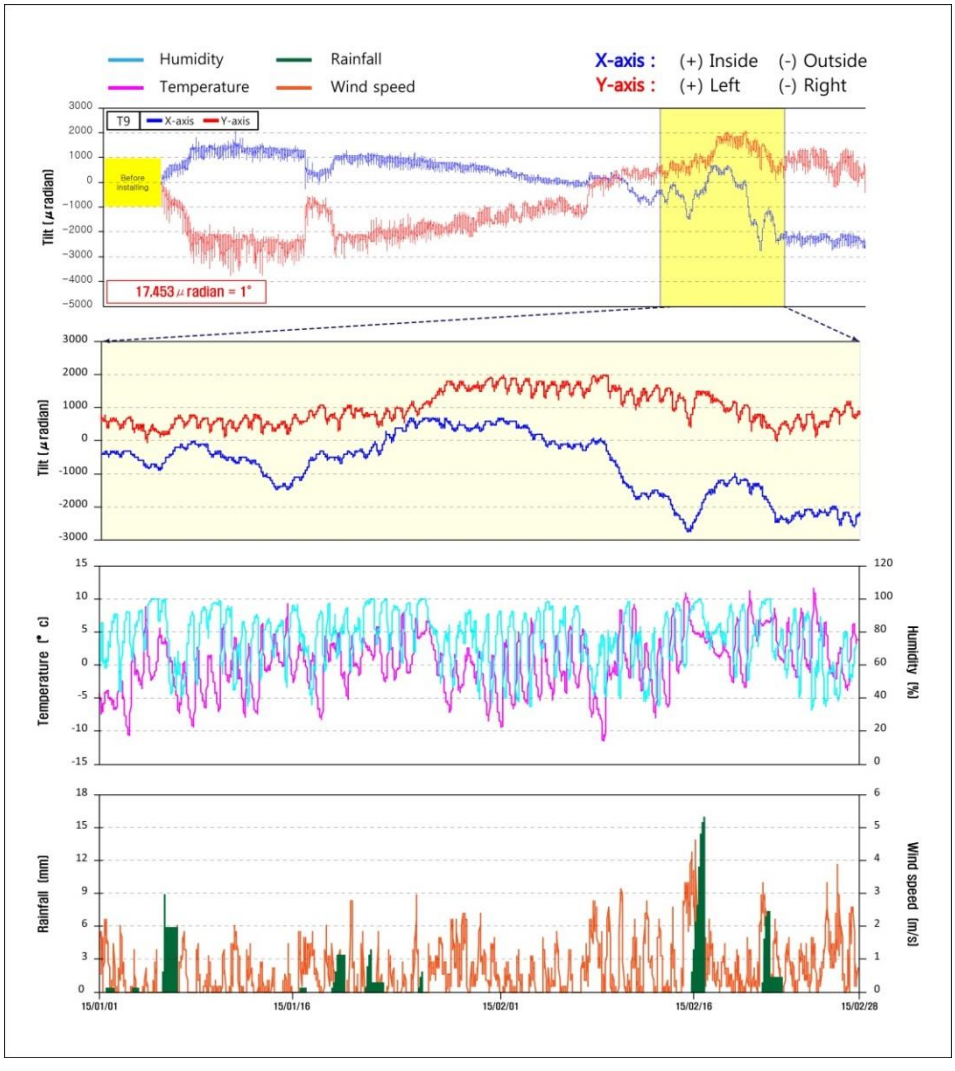

Fig. 6: Environmental and movement variations registered by T9 on Gongsanseong fortress wall from January to February 2015.

4. Conclusion

The Gongsanseong rampart suffered from various damages such as inflating, unstable foundation, projection, dislocation, subsidence of center and sink hole in a complicated way all over the area The damaged area of rampart had difference in urgency by the development of damage and its target area was large. Thus, it is recommended to establish systematic conservation and management plan by developing behaviour monitoring system together with precision calibration to measure minute behaviour on real-time basis as well as simple calibration that can be checked at the site.

References

Kumpel, H-J., Peters, J.A., Bower, D.R., 1988, Nontidal tilt and water table variations in a seismically active region in Quebec, Canada, Tectonophysics, 152, 253-265.

Lee, S.K., 1993, Shallow-depth Tilt Monitoring for Engineering Application, The journal of Engineering Geology, 3, 279-293.

Suh, M.C., Park, E.J., 1997, Characteristics of Subsurface Movement and Safety of the Songsanri Tomb Site of the Baekje Dynasty using Tiltmeter System, The Journal of Engineering Geology, 7, 191-205.

GROUND PENETRATING RADAR AND THE DETECTION OF STRUCTURAL ANOMALIES OF HIGH HISTORICAL VALUE: A CASE STUDY OF A BURGHER HOUSE IN TORUŃ, POLAND

M. Pilarska[1*], J. Rogóż[1], A. Cupa[1], K. Krynicka-Szroeder[1] and P. Szroeder[2]

Abstract

Medieval Town of Toruń, a UNECSO World Heritage, consists of two urban structures: Old and New Town (founded 1233 and 1264, respectively).The historic part of the city is considered one of the Polish architectural gems. However, some of its magnificent buildings are in desperate need of conservators' attention. For that reason, a cross-disciplinary team from the Institute for Conservation Restoration and Study of Cultural Heritage from Toruń's University, has worked for the past year on documentation of one of the finest examples of tenement housing in Toruń: a rare complex consisting of three medieval tenement houses located on Mostowa Street No 6. The aim was to assess its condition, estimate its historical value and point issues of highest priority. The whole complex was fine till 2007, when a severe fire took place. Since then there has been no funding provided for conservation works, what affected in slow destruction of the salvaged remains. This research project will hopefully become an introduction to the complicated process of fundraising for the conservation works required. As the complex had been rebuilt many times in the past, one of the aims of the research was to detect those modifications. To do so, the GPR technology was deployed. Over 800 separate scans were generated, covering over 70 correlated areas and mapping structural abnormalities. This resulted in locating walled up niches, and a discovery of a hypocaust-like heating system. A small room located in the basement was connected to storeys above it, with the aid of the chimney flues aimed to distribute hot air to the chambers above. The following paper is a presentation of the case study aiming to prove the potential that GPR has in structural diagnostics of historic buildings.

Keywords: GPR, non-destructive analyses, architectural analyses, hypocaust system

1. Introduction

Medieval Town of Toruń, (German: Thorn, Latin: Thorunia, Torunium) has gained the status of the UNECSO World Heritage in November 4th 1997. It consists of two urban structures: Old Town (founded 1233) and New Town (founded 1264), both famous for their red brick architecture. The historic part of the city is a famous architectural gem considered

[1] M. Pilarsk*a**, J. Rogóż, A. Cupa and K. Krynicka-Szroeder
Department of Painting Technology and Techniques; Institute for Conservation Restoration and Study of Cultural Heritage; Nicolaus Copernicus University, Toruń, Poland;
mpil@doktorant.umk.pl

[2] P.Szroeder
Institute of Physics; Nicolaus Copernicus University, Toruń, Poland

*corresponding author

one of the Polish national treasures. It owes its origins to the Teutonic Order, which built a castle there in the mid-13th century as a base for the conquest and evangelization of pagan Prussia. Soon after that the city gained a commercial function as part of the Hanseatic League. In the Old and New Town, the imposing public and private buildings from 14th and 15th century (including the house of Nicolaus Copernicus) are striking evidence of Torun's importance. Nevertheless, aside those remarkable buildings, well preserved and looked after, there are some of much worse condition, on which time has left its mark. They became the focus of a multi-disciplinary research team, which worked on a project aiming to develop a coherent strategy for diagnostics, preservation and conservation of such buildings. A team from the Institute for Conservation Restoration and Study of Cultural Heritage from Toruń's University, worked for over a year on the documentation of one of the finest examples of tenement housing in Toruń: a rare complex of three medieval, multi-storey red brick buildings located on Mostowa Street Nr 6. Buildings frames date back to 13th-14th century, however their structure was repeatedly modified (in 14th century, 2nd quarter of 16th century, and in: 1627, 1699, and ca. 1865) which lead to merging of three buildings into one entity (Raczkowski 2015).

Fig. 1: The remaining façade of the Mostowa No. 6; from left: section C, B, A (marked for the purposes of the project).

The entire complex was fine till March 2007, when a severe fire took place. Since that time the building was left with a minimal supervision and no funding granted for any conservation works needed. This research project was aimed to be a first step to obtaining such, through establishing a thorough methodology for a complex diagnostics of architectural objects. In general, the methodology would entail a strict protocol of deployment of non-invasive techniques for artworks analysis followed by sampling. All of that would be preceded by archival survey gathering all information about the object in question.

In this particular case a range of non- invasive analytical techniques was deployed to analyse the condition of the object. Multispectral imaging was used to find traces of long forgotten medieval polychromes, both inside the building and on its facade. As the complex had been rebuilt many times in the past, one of the aims of the project was to detect those modifications (Basiul 2015b).

The focus of this paper is to present the results of the Ground Penetrating Radar (GPR) survey that allowed for identification of structural modifications and hidden elements of construction. Over 800 separate scans were generated to map the inconsistencies in the structure of walls and floors of the building. This resulted in locating walled up niches, passages between buildings, and discovery of a hypocaust-like heating system.

2. GPR Survey Methodology

Ground Penetrating Radar (GPR) is a geophysical method which due to its ability to measure variations in electro-magnetic properties of materials, enables detection of subsurface abnormalities within investigated area (Davis & Annan 1989; Daniels 2004). Over the years its applications have been proved useful in many areas ranging from geology (Chamberlain *et al.* 2000; Kruse *et al.* 2006) geotechnical engineering (Corin *et al.* 1997; Orlando 2003) or material characterization (Nazarian *et al.* 2007; Tosti *et al.* 2013). It was found highly effective in establishing the location of archaeological sites (Shaaban *et al.* 2009; Francese *et al.* 2009), unmarked burial grounds (Fiedler *et al.* 2009) or discovering hidden chambers (National Geographic & Hessler 2016). The non-invasive nature of the method is particularly crucial when dealing with objects or sites of significant historical value. The remaining evidence of for instance settlement could otherwise been lost if traditional excavation commenced with no support from the GPR survey. Because of that, in the case of the Mostowa No 6 merchant house, the GPR technique was identified as essential for mapping historic structure of the building and the changes it has gone through.

The survey was conducted with RIS IDS radar system equipped with 2GHz bipolar antenna and 900 MHz antenna. The first was used to investigate structure of walls, and the latter to investigate the structure of the backyard of the building. The distance between each individual scanning profile in each section was set to 10 cm (Basiul 2015a).The aim of the GPR survey was to visualise abnormalities in subsurface of the areas in question. For the purposes of the project each building of the whole complex was marked with an identification letter: A, B, C (south to north, see Fig. 1).

All datasets were acquired between July 2014 and April 2015. Archival data and previous documentations were a starting point for establishing the areas potentially having the most significant historical value. Based on that, the plan for GPR survey was developed. 5 sections of interest were marked in the backyard, 18 within building A, 15 within building B and 35 within building C. All areas were measured and photographically documented prior to conducting a GPR survey.

Raw GPR scans were processed in Gred3D software, which enables enhancement of the captures of anomalies discovered in particular sections through application of user customised filters and macros. Processed scans were then merged into radar maps associated with particular areas of the building. Final stage resulted in obtaining a tomographic image of the investigated structure, showing abnormalities inside the architectural subsurface. Interactive character of such, that allows smoothly manipulate the

depth of the investigated area along the chosen axis, enabled tracking of the abnormality course change. The most representative depth slices from every single area were then superimposed onto architectural drawings of the building to map the abnormalities distribution.

3. Results and Discussion

During architectural survey conducted prior to GPR testing, a heating system was discovered in the basement of the building. It was not clear though where the chimney flues distributing hot air to the upper chambers were localised and the hope was for GPR survey to determine their location. However preliminary analyses conducted by historians indicated that the heating system discovered had a structure of a hypocaust (Prarat 2015).

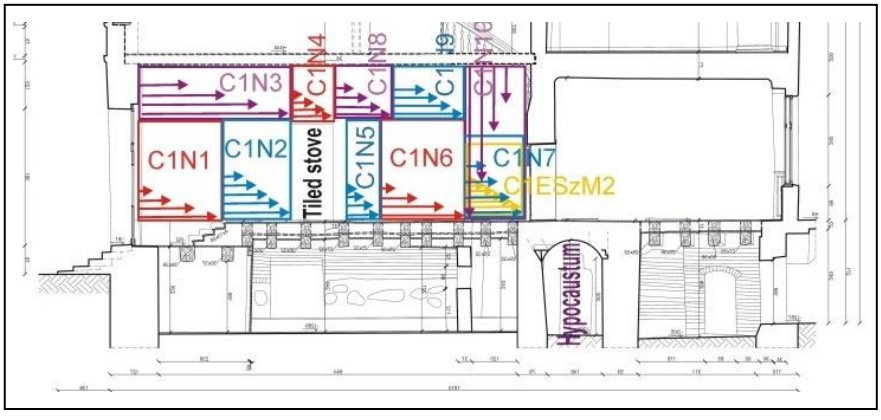

Fig. 2: Section C, longitudinal, ground floor. Markers indicate areas where GPR survey was conducted. Each symbol represents different scanning area. All scans performed on the north wall of the ground floor representative chamber, where the chimney flues from the heating system were detected (marked in the basement section as "hypocaustum"); architectural drawing by M.Prarat and U.Schaff.

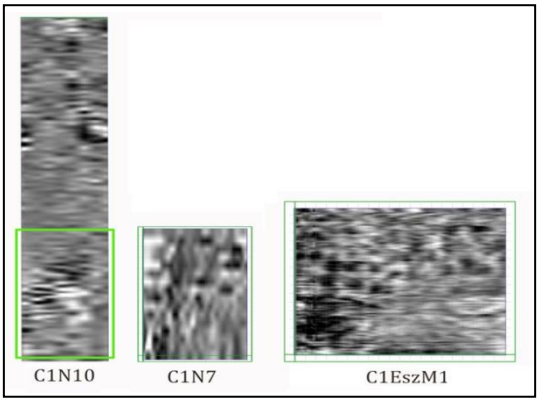

Fig. 3: Detailed GPR spectra of areas in Section A where chimney flue was found. Each spectrum is a result of the scans taken with different parameters; all show that abnormality in this area forms a consistent shape.

Some chimney flues were indeed discovered in the structure of the buildings A and C, however their existence was presumed by the specialists. The survey confirmed that no modifications have been introduced to the structure of the flues. However, it was not determined whether there are some additional ones within the structure. Nevertheless discovering the heating system itself indicates the prestige of the building. To determine all flues within the complex more scans would have to be acquired. As the project had its limitations, especially in terms of accessibility to certain parts of the building, acquisition of additional scans was not possible at this stage. In some cases health and safety standards would not allow for researchers to go into a particular area with heavy equipment, in other cases, the team would face a refusal from few inhabitants to conduct the scans at their flats, as some sections of the complex, even despite the condition of the building, are still inhabitable. In order to conduct the survey in a private property, a different approach would have to be established and community involvement should be considered at the initial stage of the project. Within the given timeframe and the extent of other research to be conducted in the building, unfortunately there was not enough time to establish a relationship with the building community that could potentially lead to higher amount of scans generated. The survey though provided thorough information about the architectural structure of the building and its historic modifications.

In section A, on the first floor, a very strong abnormality in the shape of an arch was discovered that was believed to be a walled up niche. Within the structure of the southern wall of section A, chimney flues were discovered, located closely to eastern corner of the chamber. Within the structure of the same wall many walled up niches were also detected along with remains of architectural structures, which visible traces were lost to modifications (Rogóż et al. 2015c).

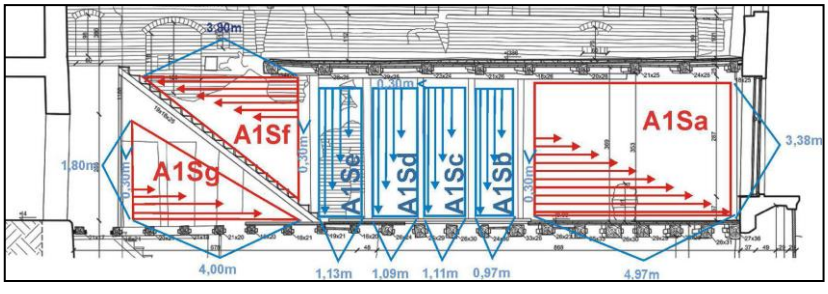

Fig. 3: 'Section A', longitudinal, ground floor, south wall. Markers indicate areas where GPR survey was conducted; architectural drawing by M.Prarat and U.Schaaf.

Fig. 4: 'Section A', longitudinal, ground floor, south wall. Markers merged into a photograph of the area in question.

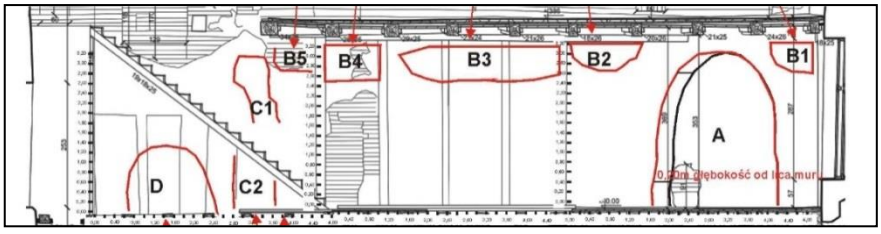

Fig. 4: 'Section A', longitudinal, ground floor, south wall Outlines of abnormalities detected marked in red. Abnormalities C1 and C2 identified as chimney flues, architectural drawing by M.Prarat and U.Schaaf

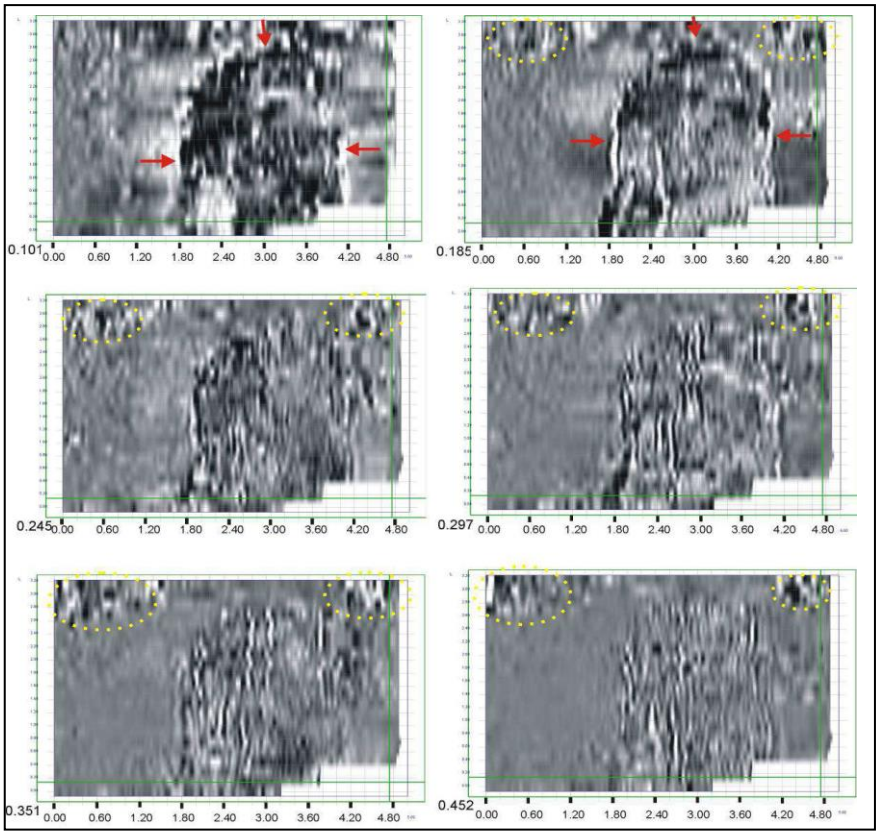

Fig. 6: Selected time slices from the GPR survey area A1Sa. Captures from the depth of: 0.101 m, 0,185 m, 0.245 m, 0.297 m, 0.351 m, 0.452 m. Detected abnormality is 2.80 m high and 2.30 m wide and is believed to be an entryway. Two smaller abnormalities detected above the main one are presumably walled up niches.

Survey conducted on the ground floor in '*Section A*', provided clear information about structural modifications of the building. Walled up niches and a wide opening, (presumably an entryway) were detected. Survey conducted in '*Section B*', on the northern wall in particular, allowed for detection of door openings localised on each storey of the building,

that have not been documented previously (Rogóż *et al.* 2015b). In northern part of section C, numerous walled up niches were identified. Survey also showed passages between the back and the front of the first floor of the building, not visible today. On second floor of the same building, the survey was used to establish the localisation of historic ceiling beams (Rogóż *et al.* 2015a). In some areas of '*Section C*', despite conducting the survey, its results were illegible. Due to faulty piping system within the building, some sections of the whole complex show risen humidity levels. This affects the legibility of spectra acquired during the survey.

4. Conclusions

The GPR survey proved to be an effective tool for investigating the subsurface of the building in question. Historic structural modifications have been detected and identified. Survey results provided new information about entire complex and when combined with the remaining analyses conducted it created a thorough documentation about the object in question. Areas that need further investigation include the localisation of the remaining chimney flues and scanning of the sections inaccessible at the time of the project execution. Further analyses are also needed in sections of high humidity. Risen levels of moisture compromise the results of GPR survey and cause disturbances of radar spectra, even to the point of complete loss of legibility of obtained image. Confirmation of gathered results can be obtained only through invasive research.

Acknowledgements

Ground Penetrating Radar survey was a part of the project "Multimodal interdisciplinary non-invasive techniques of investigating architectural objects, on the example of gothic merchant houses from Toruń", co funded by Polish Government and European Regional Development Fund within Regional Operational Program of Kuyavian-Pomeranian voivodship for years 2007-2013; No RPKP.05.04.00-04-005/13. All project deliverables, including research reports and documentation (written in Polish) containing architectural drawings, GPR time slices of each individual section, multispectral images and results on analytical tests are freely available for download from the project's official website (http://www.projektmostowa6.umk.pl/?badania,13), and the dedicated dropbox folder (https://goo.gl/5x1TQU)

References

Basiul, E., 2015a. Metodyka Konserwatorskich Badań Nieinwazyjnych Kamienic przy Ulicy Mostowa 6. Zadanie 23.1, Toruń.

Basiul, E., 2015b. Opracowanie Całościowe Dokumentacji Nieniszczących i Inwazyjnych Badań Konserwatorskich Kamienic przy ul. Mostowej 6 w Toruniu - Zadanie 22.1, Toruń.

Chamberlain, A.T. *et al.*, 2000. Cave detection in limestone using ground penetrating radar.tle. Journal of Archaeological Science 27, pp.957–964.

Corin, L. *et al.*, 1997. Radar tomography applied to foundation design in a karstic environment. Modern Geophysics and Engineering Geology, Geological Society of London, Special Publication, Engineering Geology, 12, pp.167–173.

Daniels, D.., 2004. Ground Penetrating Radar 2nd ed., London, United Kingdom: Institution of Electrical Engineers, Radar, Sonar, Navigation and Avionics Series.

Davis, J.L. & Annan, A.P., 1989. Ground penetrating radar for high resolution mapping of soil and rock stratigraphy. Geophysical Prospecting, 37, pp.531–551.

Fiedler, S. *et al.*, 2009. The effectiveness of ground-penetrating radar surveys in the location of unmarked burial sites in modern cemeteries. Journal of Applied Geophysics, 68, pp.380–385.

Francese, R.G., Finzi, E. & Morelli, G., 2009. 3-D high-resolution multi-channel radar investigation of a Roman village in Northern Italy. Journal of Applied Geophysics, 67, pp.44–51.

Kruse, S. *et al.*, 2006. Sinkhole structure imaging in covered karst terrain. Geophysical Research Letters, 33 (16).

National Geographic & Hessler, P., 2016. Exclusive Pictures From Inside the Scan of King Tut's Tomb. Available at: http://news.nationalgeographic.com/2016/04/160401-king-tut-tomb-radar-scan-nefertiti-archaeology/ [Accessed April 1, 2016].

Nazarian, S., Xiong, Y. & Rosenblad, B., 2007. Innovative applications of geophysics in civil engineering, American Society of Civil Engineers.

Orlando, L., 2003. Semiquantitative evaluation of massive rock quality using ground penetrating radar. Journal of Applied Geophysics, 52, pp.1–9.

Prarat, M., 2015. Opracowanie Całościowej Dokumentacji Wykorzystanie Tachimetrii i Fotogrametrii w Dokumentacji Zabytków Architektury na Przykładzie Inwentaryzacji Pomiarowo-Rysunkowej Zespołu Kamienic na ul. Mostowej 6 w Toruniu, Toruń.

Raczkowski, J., 2015. Dokumentacja Końcowa - Opracowanie w Zakresie Podsumowania Wiedzy z Zakresu Historii Obiektów i Z Zakresu Analizy Stylistyczno-Porównawczej w Kontekście Wyników Badań Kompleksowych - Zad. 22, Toruń.

Rogóż, J. *et al.*, 2015a. Dokumentacja bada ń radarowych zespołu kamienic mieszcza ń skich na ul . Mostowej 6 w Toruniu Kamienica C, Toruń.

Rogóż, J. *et al.*, 2015b. Dokumentacja badań radarowych zespołu kamienic mieszczań skich na ul . Mostowej 6 w Toruniu Kamienica B, Toruń.

Rogóż, J. *et al.*, 2015c. Dokumentacja badań radarowych zespołu kamienic mieszczańskich na ul . Mostowej 6 w Toruniu Kamienica A, Toruń.

Shaaban, F.A. *et al.*, 2009. Ground-penetrating radar exploration for ancient monuments at the Valley of Mummies-Kilo 6, Bahariya Oasis, Egypt. Journal of Applied Geophysics, 68, pp.194–202.

Tosti, F. *et al.*, 2013. Clay content evaluation in soils through GPR signal processing. Journal of Applied Geophysics, 97, pp.69–80.

STRATEGIES FOR THE CONSERVATION OF BUILT HERITAGE BASED ON THE ANALYSIS OF RARE EVENTS

Y. Praticò[1], F. Girardet[2] and R.J. Flatt[3*]

Abstract

The traditional approach to conservation of built heritage rests on the assumption that the behaviour of materials is governed by a function of degradation versus the intensity of degradation agents. This led to designing accelerated laboratory tests with an exaggerated intensification of the damaging conditions, poorly representing field conditions. This work aims at proposing a new approach that relies on identifying the occurrence of critical events known as "Dragon-Kings". The Dragon-King theory is a recent chaos theory for the prediction and prevention of crises, which belongs to the family of analysis of rare events. In this paper, this approach is applied to study the degradation of the cathedral of Lausanne. More specifically, this work is focused on the degradation of clay bearing sandstones consolidated with ethyl silicates, which is driven by cycles of wetting and drying. Through on-site sensors capable of determining water transport in stones, we intend to identify the critical cycles and reproduce them in the laboratory with a device specifically built for this purpose. Durability testing then becomes a question of multiplying in laboratory the most critical events, without entering the domain of unrealistic conditions. The combination of on-site measurements and laboratory testing in light of the Dragon King theory constitutes the originality of the approach proposed.

Keywords: rare events, Dragon-Kings, on-site monitoring, accelerated testing, water distribution

1. Context and objectives

The degradation of materials exposed to the environment is a slow and irreversible process that can involve various mechanisms. For natural building materials, salt crystallization and freezing damage are the most relevant ones (Siegesmund and Snethlage, 2011); in other cases, the swelling of clays associated to cycles of wetting and drying also plays a major role (Jiménez-González *et al.*, 2008). The speed and extent of these degradation phenomena determines the service life of the materials, as they compromise both their aesthetical and

[1] Y. Praticò
Physical Chemistry of Building Materials, Institute for Building Materials, ETH Zürich, Stefano-Franscini-Platz 3, Zürich 8093, Switzerland

[2] F. Girardet
RINO Sàrl, Ruelle Belle Maison 14, Blonay 1807, Switzerland

[3] R.J. Flatt*
Physical Chemistry of Building Materials, Institute for Building Materials, ETH Zürich, Stefano-Franscini-Platz 3, Zürich 8093, Switzerland
flattr@ethz.ch

*corresponding author

structural functions. In the field of conservation, the desire to preserve the original materials lead practitioners and researchers to put a lot of effort into finding solutions to slow down these processes as much as possible. The research carried out to provide such solutions most often relies on accelerated ageing tests. A critical issue in designing accelerated ageing tests is – however – to define conditions that are aggressive enough to produce degradation, but not so much as to change the nature of the degradation mechanism. The difficulty in finding a reasonable compromise leads many standard laboratory tests to be criticized for their poor ability to represent field conditions. As a consequence, many field practitioners have become very sceptical towards laboratory testing as well as towards innovations. This dispute finds its origin in the fact that one generally considers the behaviour of materials and structures to be most strongly influenced by the most frequently occurring conditions and that the speed of degradation is determined by the intensity of the degradation agents. Therefore, most accelerated laboratory testing is performed by selecting what is considered to be the most relevant degradation agent and reproducing it with an exaggerated intensity, but without much concern with respect to its magnitude as long as the material degrades in a short enough period of time. The aim of this work is to propose a novel approach for the conservation of built heritage based on the idea that the degradation is in fact driven by the occurrence of critical, rare events and is therefore not proportional to the intensity of the degradation agents. The strategy is to observe the on-site conditions (monitoring the micro-climate and the response of the material to it), to identify the critical wetting/drying conditions by means of the Dragon-King theory (Sornette, 2009), and to faithfully reproduce these conditions with a device especially built for this purpose. In light of this, possible consolidation treatments can be reliably tested, hence providing the tools for outlining a targeted conservation strategy.

2. Lausanne Cathedral

Built from 1165 onwards and consecrated in 1275, the Lausanne Cathedral is the largest Gothic monument in Switzerland and is considered to be one of the most important in Europe, along with Notre-Dame in Paris and in Chartres. Due to the vulnerability of its building materials, the Cathedral has always presented problems related to the conservation of its structure and façades (Commission technique de la cathédrale de Lausanne, 2012). Until the 19th century, the material most widely employed was the grey molasse of Lausanne, a soft sandstone quarried in the Lausanne region that is subjected to severe damage associated with the presence of swelling clays (see section 2.1). Only with the restoration of Viollet-le-Duc in 1870 and the following campaigns in the early 20th century, was this molasse partly replaced by stones less susceptible to degradation (mostly calcareous rocks). However, after the publication of the Venice Chart in 1964, the renewed interest in preserving the original materials led back to using local molasses for the following restoration campaigns, from the mid-20th century on. As a consequence, the problem of the degradation of swelling clay-bearing stones became of primary importance for the durability of the cathedral itself. In the context of the upcoming restoration campaign, this work intends to provide a deeper understanding of the circumstances leading to damage and, hence, recommendations on the conservation strategies to be adopted.

Fig. 1: Left. Sketch of the south façade of the Lausanne Cathedral (source: http://www.patrimoine.vd.ch/no_cache/monuments-et-sites/eglises/cathedrale-de-lausanne/); Right. Scaling damage observed on the south façade.

2.1. Swelling damage

Swelling clay-bearing stones can expand and shrink when subjected to cycles of wetting and drying. This phenomenon leads to the formation of stress and strain gradients in the material, which can result in damage such as cracking or buckling. Moreover, the consequences of the presence of swelling clays in building stones are aggravated by the ineffectiveness of ethyl silicate-based consolidation treatments on such materials. Indeed, the dimensional changes of the stone cause the cracking of the consolidant and the loss of most of its benefit already in the first wetting cycle (Félix, 1994). However, swelling inhibitors reduce the swelling strain of clays (Gonzalez and Scherer, 2004; Snethlage and Wendler, 1990; Wangler and Scherer, 2009) and – used as a pre-treatment - enhance the durability of consolidation treatments (Caruso *et al.*, 2012). Yet, questions about the long-term behaviour subsist. With this work, we also intend to explore in what cases the ethyl-silicate treatments can be successfully applied on swelling clays-bearing sandstones, and how these treatments can be potentially optimized with the use of swelling inhibitors.

3. Analysis of rare events and Dragon-King theory

The analysis of rare events has raised the interest of the conservation community, yet without finding a substantial application in the field (Doehne and Price, 2011). One example of the use of this approach can be found in some studies on the monitoring of the structural behaviour of historical buildings (Baraccani *et al.*, 2014). However, a broader application of the analysis of rare events to conservation problems seems to have been discouraged by the idea that rare events are random out-of-distribution events, hence non predictable. Nonetheless, new developments in the field of the statistical analysis of complex systems have recently shown that rare events known as “dragon-Kings” can be predicted and – in some cases – controlled. The Dragon-King theory (Sornette, 2009) is a chaos theory for the prediction and prevention of crises, recently developed in the Chair of

Entrepreneurial Risks at ETH Zurich, which shows how critical events can occur more often and earlier than predicted by the statistical description of the small or medium intensity events. The "dragon-kings" correspond to the so-called meaningful outliers, which reveal the presence of self-organized systems, i.e. a failure regime, which are not apparent otherwise. The presence and importance of dragon-kings was empirically observed in different systems – from economics to materials sciences – using different diagnostic methodologies (Sornette and Ouillon, 2012).

In this work, we explore the possibility to exploit the dragon king theory similarly to (Nechad *et al.*, 2005). In that study dedicated to creep experiments, the material deformation is described as going through three stages: primary, secondary and tertiary. In particular, the secondary phase can last years or decades but, in absence of sufficient healing, it transforms into the tertiary regime of "catastrophic" acceleration towards complete failure. From an external point of view, this means that such material would look indefinitely stable but could unexpectedly undergo damage, due to an unpredicted transition of regime. Nevertheless, it was shown that it is in fact possible to predict such changes once the precursors are identified. Monitoring is therefore crucial to characterise the possible existence and specific origin of these changes of regime that could occur from a roughly stable stationary state to a fast evolving degrading state.

4. *On-site* monitoring

Various sensors for on-site monitoring were developed in collaboration with Rino S.A.R.L, a Swiss SME active in consulting for the preservation of cultural heritage. In particular, these sensors measure the temperature and relative humidity in the atmosphere, at the surface of stones, as well as at various depths (Demoulin *et al.*, 2014). More information can be obtained by impedance measurements, which allow for a quantification of the water content profile in the stone. On-site monitoring also requires weather data in addition to temperature and humidity monitoring at the stone façade. These weather data include precipitation, wind speed, and wind direction, and allow for the estimation of wind driven rain amounts on the façade.

4.1. Temperature and relative humidity

The sensors for temperature and relative humidity (*RH*) are capacitive iButtons Temperature/Humidity loggers DS1923 (Maxim Integrated, San Jose, CA, USA). The sensors applied at the surface of the materials are encapsulated in expanded PVC, and the thermal contact is ensured with a metallic washer surrounded by a filter of PTFE. The sensors measuring the temperature and humidity in the air are positioned a few centimeters from the wall, protected from direct sun radiations by a white screen. Measurements of temperature and relative humidity at different depths were performed by means of a custom set-up consisting of iButtons stacked in a cylindrical shape. More details about the set-up can be found in (Demoulin *et al.*, 2014).

4.2. Wind-driven rain (WDR) and wind speed

The research on the quantification of wind-driven rain on building facades is extensive (Blocken and Carmeliet, 2010). To estimate wind driven rain quantities, there exist several methods, including semi-empirical calculations and direct on-site measurements. In this work, the ISO method (ISO Standard, 2009) and the Straube-Burnett method (Straube and Burnett, 2000) are used in combination with WDR gauges for the quantification of the

WDR at different orientations. The WDR gauges consist of a 40 cm×100 cm vertical panel for the collection of water and a tipping bucket mechanism with continuous data logging to register the WDR quantity. Tipping buckets were provided by DAVIS Instruments Corp., Hayward, California, USA. The data loggers were EL-USB-5 event data loggers, by LASCAR Electronics Ltd., Salisbury, United Kingdom. Wind speed and direction is recorded with a cup anemometer with a WindmasterMark3 for signal acquisition, provided by Schiltknecht Messtechnik AG, Gossau ZH, Switzerland.

4.3. Water distribution in the stone

Water content profiles, as well as measurements of temperature and *RH* at different depths were obtained by means of a SMARTMOTE wireless monitoring system (TTI GmbH - TGU Smartmote, Stuttgart, Germany). The system consists of two basic components: a Smartbase for signal acquisition and network data transmission, and a Smartmote wireless sensor node, which can be equipped with different sensors. In the present study, Smartmotes are equipped with 6 couples of electrodes for impedance measurements at different depths, and 6 sensors for temperature and humidity (SHT25 by SENSIRION, Staefa (ZH), Switzerland) for the correction and calibration of the impedance signals at each depth.

5. Laboratory testing

One of the main goals of this work is to provide more representative laboratory tests for the study of the degradation mechanism and the design of possible conservation strategies. For this reason, a new accelerated test for wetting and drying cycles was developed. This consists in increasing the number of damaging cycles rather than in magnifying their intensity. The critical cycles identified by means of the analysis of rare events (see section 3) are therefore reproduced in the laboratory with an instrument specially built for this purpose. Durability testing then becomes a question of multiplying in laboratory the most critical events, without entering the domain of unrealistic conditions. This allows a high acceleration of the degradation without however changing its nature. The experimental set-up is shown in Fig. 2. Samples with all but one surface sealed off are suspended below a scale, so that their weight evolution may be measured overtime. In front of them, a water spray is set up to deliver a defined amount of water onto the unsealed surface. Flux, drop size and impact angle can be adjusted by regulating distance, inclination and working pressure of the nozzles. A system for masking of the sprayed water is also present to simulate one-sided wetting cycles happening on one side only; the position of the mask can be adjusted to prevent any contact with the sample and to be used with samples of different dimensions. The evolution over time of the mass balance makes it possible to follow the rate of water ingress. Such measurements are complemented by impedance measurements between electrodes inserted in drill holes made on the backside at different depths. Sensors inserted in the samples monitor temperature and humidity changes at different depths. Drying conditions such as temperature, radiation and wind speed are regulated by means of IR lamps and fans. The objective is to establish wetting and drying rates, which will be representative of different on-site exposures.

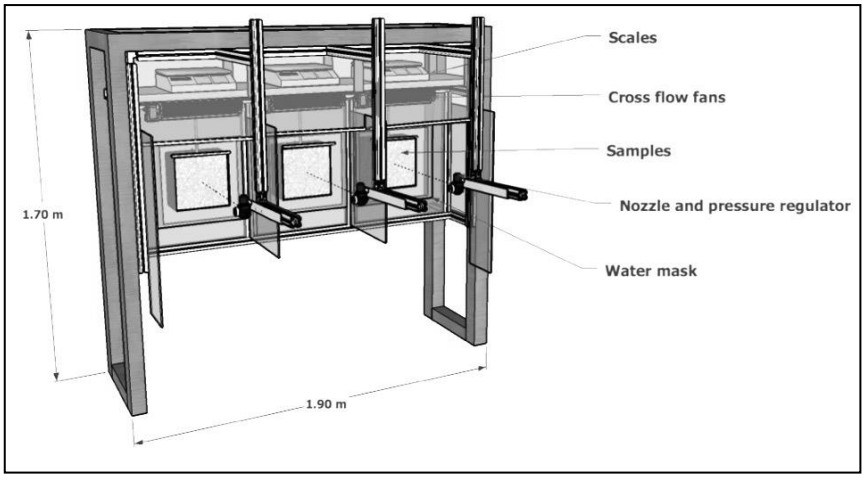

Fig. 2: Sketch of the experimental set up for accelerated laboratory testing.

6. Ongoing work and outlook

In this section, we outline the work in progress and describe the methodology applied in our case study. As illustrated in Fig. 3, this work consists of three different parts: on-site investigation, laboratory testing, and data analysis in light of the dragon king theory. These three stages are interconnected and do not follow a chronological order. However, the work strategy can be described in the following steps.

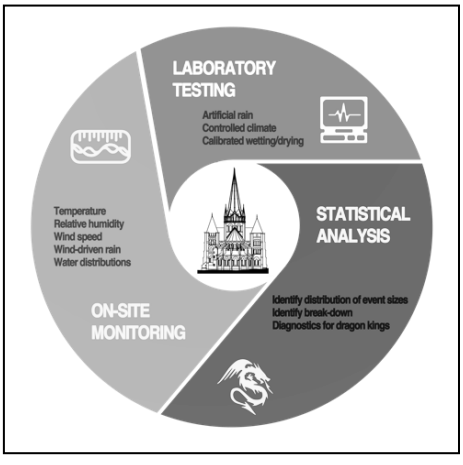

Fig. 3: Scheme of the conservation strategy adopted for the Lausanne Cathedral.

During a pre-diagnostic phase, a first identification of the characteristic degradation of the Lausanne Cathedral was performed. The historical documentation (courtesy of the technical committee of the Lausanne Cathedral) was complemented with the discussion with the practitioners to identify the locations where the degradation occurred in a more evident and

faster way. Following these observations, the micro-climate of these locations was investigated. In particular, through on site measurements and calculations of wind-driven rain (see section 4.2) the characteristic wetting/drying cycles were determined, with the objective of selecting the combination of weathering agents that are potentially leading to most damage. At the same time, the on-site investigations are used to design a targeted laboratory testing, capable of reproducing faithfully the conditions observed on-site.

During laboratory testing, the selected cycles are faithfully reproduced on consolidated and unconsolidated samples. The measurement of impedance profiles allows for checking that the resulting water distribution in the lab samples is comparable to the on-site one at those conditions. During the accelerated testing, the behaviour of the stone at different types of cycles is observed.

From the various cycles tested in the lab, we aim at detecting the possible existence of changes of regimes, of critical transitions that could for example occur, from a roughly stable stationary state to a fast evolving degrading state. The statistical study of both the on-site results of the laboratory testing and the on-site monitoring in light of the dragon-king theory will possibly enable to identify the so-called "oscillators" (combinations of degradation agents) which cause an abrupt acceleration in the failure of the material, hence are responsible of most damage. If this is the case, this would suggest that our dragon kings are combinations of degradation agents.

As stated in introduction, our final step and objective will then be to carry out accelerated test of our potential consolidation treatments, not by magnifying the amplitude of the average weathering agents but by increasing the frequency of the identified dragon kings.

Aknowledgements

The authors would like to thank Mr Christophe Amsler and Ms Olga Kirikovafor for their openness and support in discussing conservation issues in relation to the Cathedral of Lausanne. Also, they would like to thank Prof. Dr. Didier Sornette for the useful insights and the suggestions on the application of the dragon-king approach in our study.

References

Baraccani, S., Trombetti, T., Palermo, M., Gasparini, G., Silvestri, S., Dib, A., 2014. A Methodology of Analysis for a Critique Interpretation of the Data Acquired from Monitoring Systems of Historical Buildings. Presented at the EWSHM - 7th European Workshop on Structural Health Monitoring.

Blocken, B., Carmeliet, J., 2010. Overview of three state-of-the-art wind-driven rain assessment models and comparison based on model theory. Build. Environ. 45, 691–703.

Caruso, F., Wangler, T.P., Aguilar Sanchez, A.M., Richner, H., Melchior, J., Flatt, R.J., 2012. Effect of swelling inhibitors and self restraint on the durability of ethyl-silicates consolidants applied to clay-bearing stones, in: 12th International Congress on the Deterioration and Conservation of Stone Columbia University. New York.

Commission technique de la cathédrale de Lausanne, 2012. Déontologie de la pierre. Stratégies d'intervention pour la cathédrale de Lausanne. Actes Colloq. Pluridiscip. 14 15 Juin 2012 hors-série 1.

Demoulin, T., Girardet, F., Flatt, R.J., 2014. Reprofiling of altered building sandstones : on-site measurement of the environmental conditions and their evolution in the stone. Presented at the 32èmes Rencontres de l'AUGC, Polytech Orléanss, ETH-Zürich, Orléans.

Doehne, E., Price, C.A., 2011. Stone Conservation: An Overview of Current Research, Second edition edition. ed. Getty Conservation Institute, Los Angeles, Calif.

Félix, C., 1994. Déformations de grès consécutives à leur consolidation avec un silicate d'éthyle, in: Proceedigns of the 17th Congress on the Int. Association of Engeneering Geology.

Gonzalez, I.J., Scherer, G.W., 2004. Effect of swelling inhibitors on the swelling and stress relaxation of clay bearing stones. Environ. Geol. 46, 364–377.

ISO Standard, 2009. Hygrothermal performance of buildings - Calculation and presentation of climatic data -- Part 3: Calculation of a driving rain index for vertical surfaces from hourly wind and rain data. Int. Organ. Stand. ISO 15927-3:2009.

Jiménez-González, I., Rodríguez-Navarro, C., Scherer, G.W., 2008. Role of clay minerals in the physicomechanical deterioration of sandstone. J. Geophys. Res. Earth Surf. 113, F02021.

Nechad, H., Helmstetter, A., El Guerjouma, R., Sornette, D., 2005. Andrade and critical time-to-failure laws in fiber-matrix composites: Experiments and model. J. Mech. Phys. Solids 53, 1099–1127.

Siegesmund, S., Snethlage, R. (Eds.), 2011. Stone in Architecture - Properties, Durability, 4th ed. Springer Science & Business Media.

Snethlage, R., Wendler, E., 1990. Surfactants and Adherent Silicon Resins - New Protective Agents for Natural Stone, in: Symposium G – Materials Issues in Art and Archaeology II, MRS Online Proceedings Library.

Sornette, D., 2009. Dragon-Kings, Black Swans and the Prediction of Crises. ArXiv09074290 Phys.

Sornette, D., Ouillon, G., 2012. Dragon-kings: Mechanisms, statistical methods and empirical evidence. Eur. Phys. J. Spec. Top. 205, 1–26.

Straube, J.F., Burnett, E.F.P., 2000. Simplified prediction of driving rain on buildings. Presented at the International Physics Conference, Eindhoven University of Technology, Eindoven, the Netherlands, pp. 375–382.

Wangler, T., Scherer, G.W., 2009. Clay swelling inhibition mechanism of α,ω-diaminoalkanes in Portland Brownstone. J. Mater. Res. 24, 1646–1652.

DIRECT MEASUREMENT OF SALT CRYSTALLISATION PRESSURE AT THE PORE SCALE

N. Shahidzadeh[1*], J. Desarnaud[1] and D. Bonn[1]

Abstract

The devastating action of salts in monuments, rock outcrops and artefacts is a major problem for their preservation. Damage due to salt is commonly attributed to the pressure that a growing crystal from a supersaturated solution exerts on its confining walls. However, its direct measurement at microscale remains a challenging task. Here, we report experimental results obtained with an innovative setup which enables observation of spontaneous nucleation and growth during evaporation of a salt solution while directly measuring the force exerted by a crystal during its growth in confinement. These experiments show the crucial role of wetting films between the growing crystal and the confining walls for the development of the pressure; if the walls are made hydrophobic, no film and no crystallisation pressure are detected. The results obtained for the growth of KCl and NaCl crystals between hydrophilic and hydrophobic glass walls suggests that the pressure originates from a repulsive interaction between charged surfaces separated by a thin liquid film. We also show that the magnitude of this pressure is consequently system-specific depending on the type of salt and the solid materials.

Keywords: crystallisation pressure, porous media, surface charge, confinement, damage, sodium chloride

1. Introduction

The precipitation of salt minerals in confinement (e.g. pores in stones) is known to severely damage buildings, to be responsible for the weathering of rocks and to reduce the permeability in oil reservoirs (Fig. 1). In all of these cases, crystal growth occurs within the pore spaces of the material, inducing mechanical stresses on the scale of the individual grains or pores (Shahidzadeh-Bonn *et al.* 2010, Espinoza-Marzal *et al.* 2013, Flatt *et al.* 2014, Rijners *et al.* 2005). A condition for damage to occur is that the crystal continues to grow even in confinement, so that the resulting stress damages the rock or stone. Arguments explaining that growing crystals can exert a pressure have been given for more than 150 years based on macroscale experiments that reveal that a crystal can grow in a supersaturated solution, overcoming external forces resisting its growth (Becker and Day 1905, Taber 1916, Correns 1949). Thermodynamics allows this when the crystal grows from a supersaturated solution (Correns 1949, Scherer 1999, 2000, Flatt *et al.* 2007, Steiger 2005) but does not explain why the crystal would not simply grow in a direction in which it

[1] N. Shahidzadeh*, J.Desarnaud and D.Bonn
Van der Waals-Zeeman Institute-Institute of Physics-University of Amsterdam, Science Park 904, 1098 XH Amsterdam, The Netherlands
N.Shahidzadeh@uva.nl

*corresponding author

is not confined, especially as according to both Riecke's principle and crystal growth theory, a mechanically constrained crystal, because of its higher solubility, should dissolve rather than exert a pressure. The direct measurement of the force exerted by a growing crystal in confinement is challenging, as illustrated by the small number of experiments reporting results for different salts *(*Correns 1949, Hamilton *et al.* 2010, Sekine *et al.* 2011, Royne and Dysthe 2012, Desarnaud *et al.* 2013). This opens the debate on the mechanism for the development of such a crystallisation pressure.

Fig. 1: Granular disintegration of stone scultpures and historical monuments due to salt crystallisation *(Lecce; Italy).*

Here, we study the primary nucleation and growth of one crystal and measure the force that the growing crystal exerts as it spontaneously precipitates in confinement at microscale (Fig. 2); Our experiment differs from those reported in the literature *(Taber, 1916,* Correns 1949, Hamilton *et al.* 2010, Royne and Dysthe 2012, Desarnaud *et al.* 2013) as we do not impose a certain supersaturation, or impose a given load on a pre-existing crystal in solution. Sodium chloride (NaCl) and potassium chloride (KCl) are used, firstly because of their abundance and their same crystalline structure (i.e. rock-salt structure). Secondly, in recent experiments on evaporation of NaCl solutions it has become clear that, high supersaturations $S=m_c/ms$ =1.6±0.2 can be reached at the onset of crystallisation (Desarnaud *et al.* 2014). These recent findings suggest a scenario in which the force exerted by a growing NaCl crystal should be more easily detected than in the previous reported experiments where the growth of a pre-exisiting crystal in its saturated solution is studied *(*Correns 1949, Hamilton *et al.* 2010, Royne and Dysthe 2012, Desarnaud *et al.* 2013). In the latter case which consists of a secondary nucleation process, only very modest supersaturations can be achieved during crystal growth.

2. Experimental

We use a home-built innovative set-up to directly measure the force induced by a growing crystal. An inverted phase contrast microscope (Zeiss) is coupled to a rheometer (Anton Paar DSR 301) inside a homemade controlled climatic chamber with controlled relative humidity and temperature T = 21±1ºC (Fig. 2). The plate on which the rheometer measures

the torque and normal force is glued to a glass slide, which is either hydrophilic or hydrophobic depending on the experiment. The rheometer records the value of the normal force and the apparent elastic modulus during the duration of the experiment, t = 300 min.

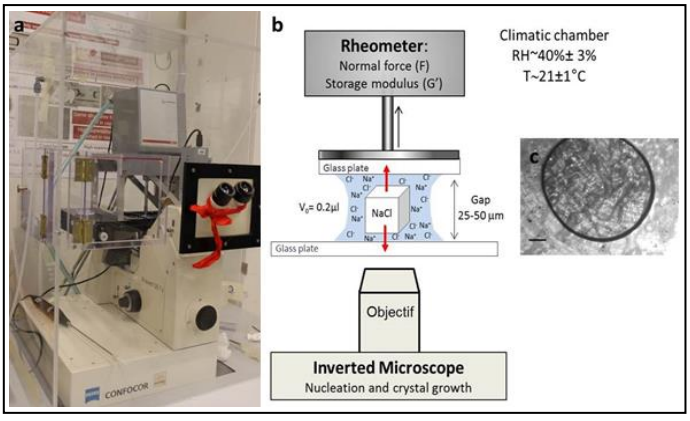

Fig. 2: a and b): The homemade innovative setup for the visualization of the spontaneous crystal precipitation during evaporation and the simultaneous measurement of the induced force during the growth; c) The image obtained with the microscope of the entrapped salt solution between the two glass plates at the beginning of the experiment.

A very small volume of the salt solution (NaCl or KCl) is deposited on a cleaned glass slide on the inverted microscope. The salt solutions are slightly below the saturation $S = c_i/c_0 = 0.9$ with c_i concentration of the solution and c_0 concentration of the solution at saturation (i.e., $c_i = 5.5$ mol.kg^{-1} and $c_i = 4.1$ mol.kg^{-1} for NaCl and KCl, respectively). The second glass slide attached to the rheometer plate confines the drop from above; the rheometer sets the gap between the two confining plates at 50±5 µm. Evaporation is induced under isothermal conditions (T = 21±1°C) at controlled relative humidity of the ambient air in the climatic chamber (Shahidzadeh and Desarnaud 2012). By direct visualization using a CCD camera coupled to the inverted optical microscope, we follow, during the evaporation, the volume change of the entrapped salt solution, the onset of the crystal precipitation, and the crystal growth in the solution. Processing of the data allows us to determine the evaporation rate, the concentration of the solution at the onset of crystallisation and the growth rate of the crystal (Fig. 2).

3. Results and discussion

In general only one crystal is observed to precipitate as the water evaporates. The growing crystal fills the gap between the two plates in the first 5 seconds after nucleation, leaving only a thin liquid film between crystal and glass (Fig. 3). Simultaneously a repulsive (positive) force is detected (Fig. 4, stage 1). The force increases with further evaporation and lateral growth of the crystal until a maximum constant value is reached. This maximum force is achieved when there is no more solution around the lateral sides of the crystal: the remaining salt solution is a liquid film between the glass plates and the crystal (Fig. 3c to Fig. 3f and Fig. 4 stage 2). Its subsequent evaporation is observed to induce the formation of steps on the confined face of the crystal. We find that the crystals can exert forces of

about ~0.035±0.02 N on the glass plates, the force being largest when the film is thinner than the optical resolution (Fig. 4).

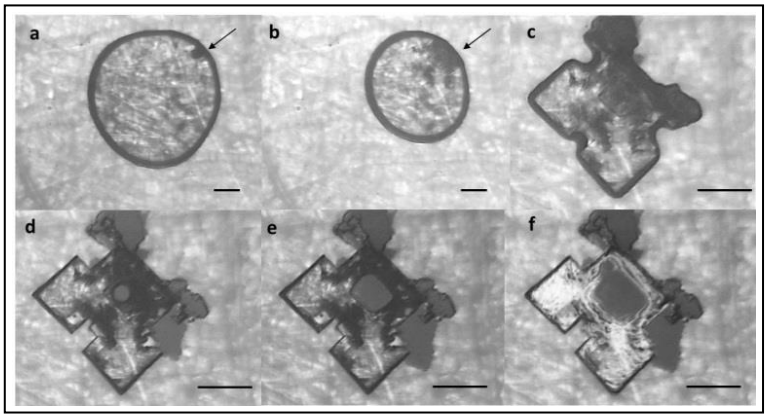

Fig. 3. NaCl crystal precipitation at supersaturation S~1.3 followed by crystal growth and drying of the liquid film between the crystal and the glass plates. (Scale bars: 100 μm)

In order to convert the measured force into a pressure, we need to quantify the contact area between the crystal and the walls. The confined faces of the crystal analysed by SEM reveal very complex microscale surface roughness due to the formation of steps which make it impossible to estimate directly from the imaging process. However, the area of contact can be estimated thanks to the rheometer, as the latter gives the shear modulus of any solid material that occupies the gap between the two plates, by measuring the shear stress necessary for a certain imposed deformation. The growth of the crystal is indeed observed to lead to a strong increase of the apparent shear modulus that increases in a similar fashion as the force with the drying of the film of solution (Fig. 4). The salt solution is liquid and does not resist shear, whereas the salt crystal does. This allows us to obtain the filling degree and hence the real area of contact at the end of the experiment knowing R the radius of the upper plate ($12.5 \cdot 10^{-2}$ m), G_{app} the storage modulus (Fig. 4), G_{real} the shear modulus of NaCl crystal ($12.61 \cdot 10^{9}$ Pa):

$$A_{crystal} = \frac{G_{app} \,.\, \pi . R_{plate}^2}{G_{crystal}} \qquad \textit{(Eq. 1)}$$

In this way we obtain a contact area of 48 μm^2 at the end of the experiment in Fig. 4. Hence, for the experiment shown in Figures 3 and 4, the crystallisation pressure deduced from the measured force and contact area turns out to be $P=F/A$ ~ 590±50 MPa, a very large pressure that is sufficient to damage the stone.

We have also performed the same experiment with glass plates that are made hydrophobic by treatment with silane. In this case, as the formation of a wetting film is prevented, the crystal grows in a way to minimise its contact area with the plates (i.e. on its edges) and no repulsive force is detected during growth within the experimental uncertainty (Fig. 5). This in good agreement with the kinetics of growth and the very low crystallisation pressure measured for the growth of NaCl crystal in contact with hydrophobic PDMS mirochannels (Sekine *et al.*2011).

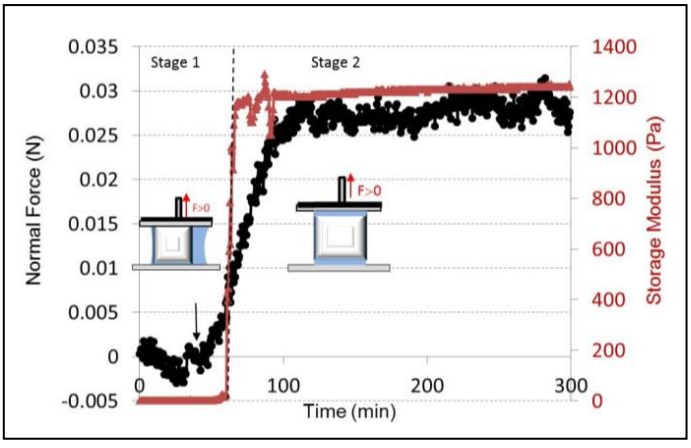

Fig. 4: Evolution of the normal force and the storage modulus with the growth of NaCl between the two glass plates from the solution during evaporation. The arrow shows the moment of crystal precipitation.

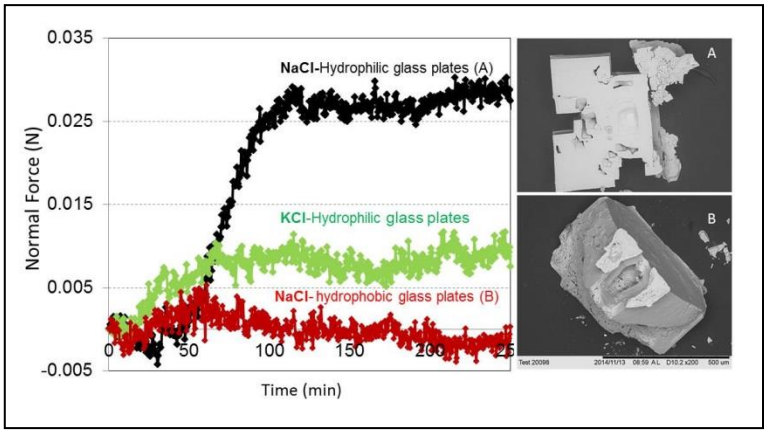

Fig. 5: Evolution of the detected repulsive force during the growth of NaCl crystal between hydrophilic (A) and hydrophobic (B) glass plates; KCl crystal between hydrophilic glass plates; SEM images of the NaCl crystal at the end of experiments (A) and (B).

The importance of a thin film for the crystallisation pressure has been discussed theoretically (Taber, 1916, Correns 1949, Scherer 1999, 2000, Flatt *et al.* 2007, Steiger 2005). Our experimental results show that in order for a crystallisation pressure to develop, one needs to maintain a film of liquid by some repulsive forces between the crystal and the wall as it allows for continued crystal growth by the addition of extra ions to the crystal lattice. Similar repulsive interaction has been also reported between a silica-covered AFM tip and a potassium sulfate crystal separated by a film of salt solution (Hamilton *et al.* 2010). If a growing crystal fully bridges the gap between two confining walls, no crystallisation pressure will be developed and no extra layers of salt can be added to give rise to such a pressure. Consequently, these experimental results make thin-film forces an obvious candidate for the origin of the crystallisation pressure (Israelchvili 1999, Hamilton

2010, Espinoza-Marzal 2012). If this is the case, the *disjoining pressure Π(l)* within a film of thickness *l*, pushing the two surfaces apart, would be of the (simplified) form:

$$\Pi(l) \sim A \exp(-\kappa l) \text{ , with } A = \frac{2\sigma^2}{\varepsilon\varepsilon_0} \qquad \textit{(Eq. 2)}$$

and σ the charge density at the surface, ε and ε_0 the relative permittivity of the bulk and free space, respectively, and the Debye screening length, κ^{-1}:

$$\kappa^{-1} = \frac{0{,}304}{\sqrt{(NaCl)}} \qquad \textit{(Eq. 3)}$$

with (NaCl) the molar sodium chloride concentration (Israelchvili 1999, Scherer 2000). However, the scenario of a repulsive force also requires that the crystal/solution and the solution/glass interfaces carry a charge of identical sign.

Consequently, we have determined the surface charges in highly concentrated salt solutions (i.e. close to saturation) using cationic (methylene blue) and anionic (Eosine-Y) dyes. We first measure the absorption of the dye in salt solution using Vis-Spectrometer, and then add a large amount of salt crystals or glass beads. If the surface is charged, the dye of opposite charge will adsorb onto the glass or salt crystals and the de-coloration of the solution can be noticed. This in turn will mean that the absorption of the solution above the beads or crystals will decrease, due to the lower concentration of dye in solution. The decrease is a measure of the amount of adsorbed dye. For the cationic dye, the experiments show that the addition of glass beads and NaCl or KCl crystals to the reference solutions reduces the absorbance indicating that glass, NaCl and KCl crystals surfaces are indeed negatively charged. Moreover, the difference in the amplitude of absorbance for the two salt solutions highlights the difference in the surface charge density in contact with KCl and NaCl solution. The reduction in the absorbance is about 30% when glass beads are added to NaCl/methylene blue solution and 8% when the beads are added to KCl/methylene blue solution. The lower charge density of the glass beads in the KCl solution is probably due to the larger size of K^+ (ionic radius of 1.33 Å) compared to Na+ (0.96 Å), which results in smaller hydrated radii and subsequently K^+ ions bind more easily to the negatively charged silica surface at high concentrations (Dihson *et al.* 2009). Since the surface charge features directly in the amplitude A of the disjoining pressure, we would anticipate a much smaller crystallisation pressure for KCl compared to NaCl. We have consequently repeated the experiments with KCl solution, and indeed we find indeed much smaller pressures; in a typical experiment P ~ 70 ±15 MPa, roughly an order of magnitude smaller than for NaCl (Fig. 5). Reflecting these lower crystallisation pressures we also find much less damage when we expose pieces of sandstone to multiple dissolution-drying cycles using a KCl solution compared to NaCl (Desarnaud *et al.* 2015).

4. Conclusion

We have performed direct measurements at a microscale of the pressure exerted by the spontaneous precipitation of NaCl and KCl crystals during evaporation in a confinement similar to that found in pore network in stones (Desarnaud *et al.* 2016). The magnitude of the measured pressure is very high, and well in excess of the tensile strength of various stones used in artworks, sculptures and monuments and may account for the damage due to crystal growth in porous materials. Our results constitute a direct experimental confirmation of the assumption that thin liquid films between the crystal and the wall are at the origin of

the crystallisation pressure. The induced pressure during crystal growth originates from a repulsive interaction between charged surfaces separated by a thin liquid film. In contrast, if the walls are made hydrophobic, no film and no crystallisation pressure are detected. These experimental results show why a homogeneous hydrophobic treatment used in conservation (Wheeler 2005) could prevent damage, as has been assumed theoretically (Scherer 1999). Moreover, the dependence on the wetting properties and the surface charge also account for the experimentally observed variability for different salts crystallizing in different materials. Understanding processes that are at the origin of the alteration of porous artworks is of great importance for managing and preserving them for future generations.

References

Becker, G.F. & Day, A.L., 1905. The linear force of growing crystals, Proc. Washington Academy of Sciences, 7, 283-288.

Correns, C.W., 1949. Growth and dissolution of crystals under linear pressure, Discussions of the Faraday Soc. 5, 267-271.

Desarnaud, J., Grauby, O., Bromblet, P., Vallet, J.M. & Baronnet, A., 2013. Growth and Dissolution of Crystal under Load: New Experimental Results on KCl. Cryst. Growth Des., 13, 1067–1074.

Desarnaud, J., Derluyn, H., Carmeliet, J., Bonn, D. & Shahidzadeh. N, 2014. Metastability limit for the nucleation of NaCl crystals in confinement. J. Phys. Chem. Lett., 5, 890-895.

Desarnaud, J.; Derlyun, H., Molari, L.; de Miranda, S. ; Cnudde, V. ; Shahidzadeh, N., 2015. Drying of Salt contaminated porous media ; Effect of primary and secondary nucleation. J.App. Phys. 118, 114901.

Desarnaud, J., Bonn, D., Shahidzadeh, N. 2016 Measurement of the pressure induced by salt crystallization in confinement. Scientific Reports , under review

Dihson, M., Zohar, O. & Sivan, U., 2009. From repulsion to attraction and back to repulsion: the effect of NaCl, KCl, and CsCl on the force between silica surfaces in aqueous solution. Langmuir, 25 (5), 2831-2836.

Espinosa-Marzal, R. & Scherer, G.W., 2013. Advances in understanding damage by salt crystallization. Environ. Earth Sci., 69, 2657−2669.

Espinoza-Marzal, R.M., Drobeck, T.; Balmer, T., Heuberger, M.P., 2012. Hydrated ions ordering in electrical double layers, Phys. Chem. Chem. Phys., 14, 6085–6093.

Flatt, R.J., Caruso, F., Sanchez, A.M.A. & Scherer, G.W., 2014. Chemomechanics of salt damage in stone. Nature communications, 5823.

Flatt, R.J., Steiger, M. & Scherer, G.W. 2007. A commented translation of the paper by C.W. Correns and W. Steinborn on crystallization pressure. Environ. Geol., 52, 187–203.

Hamilton, A., Koutos, V. & Hall, C. , 2010. Direct measurement of salt mineral repulsion using atomic force microscopy. ChemComm. 46, 5235-5327.

Israelchvili, J.1992. Intermolecular and surface forces, Academic Press . second edition.

Rijners, L.A, Huinink, H.P. Pel, L. Kopinga, K. 2005. Experimental Evidence of Crystallization. Pressure inside Porous Media. Phys. Rev. Lett. 94, 75503.

Royne, A. & Dysthe, D.K. , 2012 Rim formation on crystal faces growing in confinement. J. of Crystal Growth. 346, 89-100.

Scherer, G.W.,1999, Crystallization in pores. Cem. Concr. Res., 29, 1347-58.

Scherer, G.W., 2000. Stress from crystallization of salt in pores, Proceedings of 9th international congress on deterioration and conservation of stone, Venice-Italy.

Sekine, K., Okamoto, A. & Hayashi, K., 2011. In situ observation of the crystallization pressure induced by halite crystal growth in a microfluidic channel. American Mineralogist., 96, 1012-1019.

Shahidzadeh-Bonn, N., Desarnaud, J., Bertrand, F., Chateau. X. & Bonn, D., 2010. Damage in porous media due to salt crystallization., Phys. Rev. E . 81, 066110.

Shahidzadeh N., Desarnaud J., 2012. Damage in porous media: role of the kinetics of salt (re) crystallization, EPJAP, 60 , 24205.

Steiger, M. 2005. Crystal growth in porous materials: I The crystallization pressure of large crystals. J. Crys. Growth. 282, 470.

Taber, S., 1916. The growth of crystal under external pressure. Am. J. Sci. 4-41, 532-556

Wheeler, G., 2005 , Alkoxysilane and the consolidation of stones . Getty publications, Los Angeles.

DRILLING RESISTANCE MEASUREMENT IN MASONRY BUILDINGS: A STATISTICAL APPROACH TO CHARACTERISE NON-HOMOGENEOUS MATERIALS

E. Valentini[1*] and A. Benincasa[1]

Abstract

The Drilling Resistance Measurement System (DRMS) is a valuable tool for the determination of the mechanical characteristics of the materials used in historic masonry buildings, which are generally non-homogeneous materials. The paper presents the details of the statistical treatment of test results, implemented in the calculation software of the test device and shows some examples of application for drilling tests on mortars of different resistances.

Keywords: drilling resistance measurement (DRMS), mortar, masonry

1. Introduction

The Drilling Resistance Test Method can be used for the characterization of historic masonry materials, in situ and in laboratory. It makes it possible to obtain information concerning the mechanical properties of materials and to evaluate the performance of consolidation treatments. The test consists in drilling a small hole at a set constant rotational speed and constant penetration rate and measuring the penetration force versus depth. In recent decades, the test method has been successfully applied on various materials including stone, bricks, gypsum plaster, wall paintings, mortars, and so on. (Tiano *et al.*, 2000b; Pamplona *et al.*, 2007). Technical literature reports correlations between the drilling resistance and the mechanical properties of the material (Unconfined Compression Stress - UCS), for example, natural stones (Exadaktylos *et al.*, 2000; Theodoridou *et al.*, 2015), mortars (Tiano *et al.*, 2000c; Del Monte *et al.*, 2008; Nogueira *et al.*, 2014), clay bricks (Fernandes *et al.*, 2007). Some of these materials (e.g. mortars and clay bricks) present high fluctuations in the drilling resistance around the mean value, due to their intrinsic non-homogeneity. These materials need to be characterised not only with average parameters but also through indices that take into account the non-uniformity of the material (Valentini *et al.*, 2008). It is also important to eliminate insignificant data due to the presence of cracks or large aggregates. This paper presents the statistical treatment of test results, implemented in the calculation software of the Drilling Resistance Measurement System (DRMS).

[1] E. Valentini* and A. Benincasa
SINT Technology s.r.l., Italy
emilio.valentini@sintechnology.com

*corresponding author

2. DRMS Cordless Device

The DRMS Cordless device (Fig. 1), developed by SINT Technology, is designed to perform simple and accurate Drilling Resistance tests on natural stones and masonry materials. During the penetration of a drill bit, the system continuously measures the force necessary to drill the hole in the investigated material (Tiano *et al.*, 2000a; Fratini *et al.*, 2005). The portability of the equipment makes it suitable for use in both laboratories and in situ. During testing, the rotation speed and the penetration rate are kept constant. The rotation speed ranges from 50 to 1000 rpm, the penetration rate varies from 1 to 80 mm/min and the measurable force is comprised between 0 and 100 N. It is possible to investigate up to 50 mm inside the specimen, but the usual hole depth that is analysed is between 15 and 35 mm. The position of the drill in relation to the surface of the target (starting point) is always known because it is directly checked by the system through an encoder.

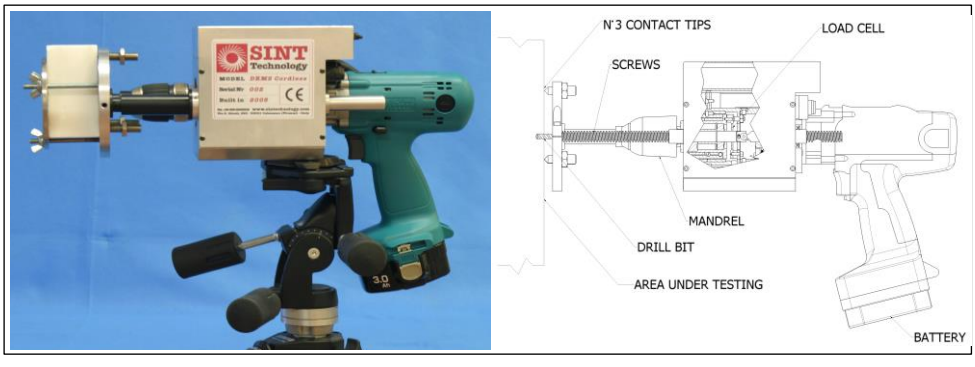

Fig. 1: DRMS Cordless.

The acquired data (force and drill position) are recorded and processed with dedicated software. This application, developed with LabVIEW™ (National Instruments), has many capabilities related to data acquisition, graphic representation and loading / saving data files from the archive. Some important features are the capability to manage a complete test, the real time graph of the force vs. depth, the data filtering and averaging options and the possibility to elaborate and compare different tests simultaneously.

Recently, several improvements have been added. In particular:

- Statistical analysis of the test results
- Database of the tests performed with a customizable repository of materials and drill bits
- Possibility to take into account the wear of the drill bit

The drilling must be done with a drill bit capable of producing a hole with a flat bottom surface, and made of a wear resistant material. We normally use a drill bit made with the application of a polycrystalline diamond plaque (Fig. 2). The Drilling Force is equivalent to the mean value of the Force versus Depth. This parameter is measured by drilling a single hole or by averaging the acquired data of a set of holes in the same restricted area. Another parameter is the Coefficient of Variation (CVOL.%), defined as the ratio of the standard deviation s to the mean Drilling Force.

Fig. 2: Polycrystalline Diamond drill bit.

The principal advantages of the DRMS measuring system are the following.

- Direct measurements of the Drilling Force during the drilling operation.
- Metrological traceability. The internal load cell can be calibrated against an external reference load cell.
- Detailed information about the variation of the material strength with depth.
- Possibility to perform drilling tests in every direction
- Reduction of the wear effect on the tool, with special diamond drills.
- Possibility of correction for wear.
- Light (5.5 kg), easy to use on scaffolding.

3. Statistical processing of data

3.1. Data acquisition and filtering

The data acquisition from the load cell normally takes place with an acquisition frequency of about 30-40 Hz. In the case of non-homogeneous materials an acquisition frequency of around 300 Hz (streaming mode) is used. In the first stage of data processing, you can apply a filter (low pass or band stop filter).

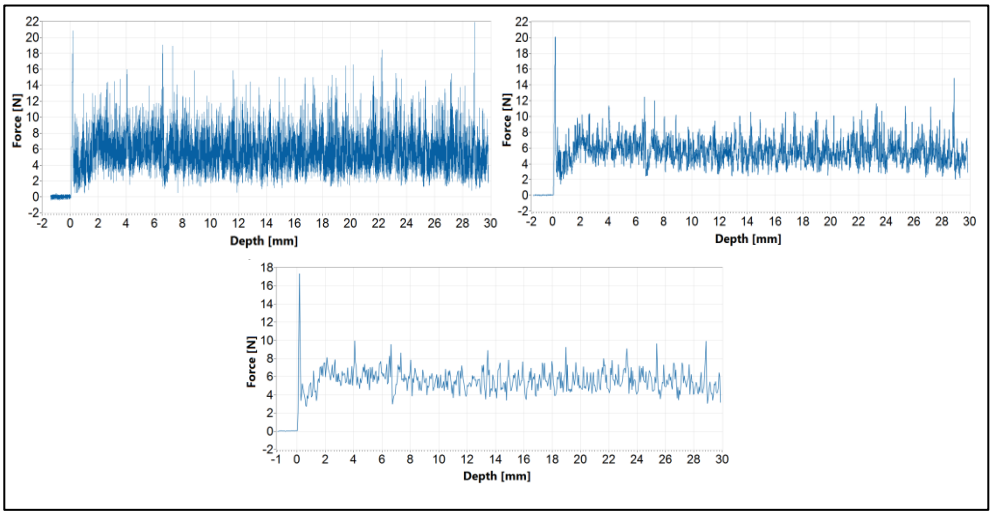

Fig. 3: Force versus depth (to the left as acquired, to the right with filter 3 Hz, below with filter and spatial average).

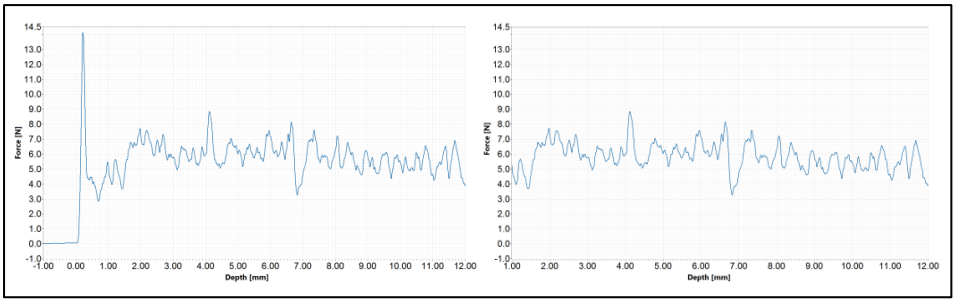

Fig. 4: Force versus depth before (left) and after (right) the elimination of the insignificant data.

The software also allows a spatial average of the data to obtain the desired spatial resolution, for example between 0.001 and 0.1 mm. Fig. 3 shows an example of application of the filters (low pass at 3 Hz) and of the spatial average (0.05 mm).

3.2. Elimination of initial penetration data

The software eliminates the data acquired prior to contact with the surface of the material as well as the data related to the first penetration of the tip that are not significant in the determination of the characteristics of the material (Fig. 4).

3.3. Calculation of statistical parameters

For a number *n* of samples of the filtered data as above, the software calculates the statistical parameters of centrality, dispersion and shape.

3.4. Box plots. Identification of Outliers.

Through the Box plot (or Box and Whiskers) we obtain information on the shape of the statistical distribution. It is obtained by superimposing, on the horizontal line that goes from maximum to minimum of the data, a rectangle (box) that goes from the first quartile Q1 to the third quartile Q3 with a vertical line that divides the level of the second quartile Q2, which corresponds to the sample median M.

It is possible to build modified box plots where outliers are identified. Outlier is a term used in statistics to define, in a set of observations, a value so clearly far from other available observations (Tukey 1977). Through the quartiles it is possible to give a quantitative definition of outliers. The weak outliers are the outliers outside of range:

$$[Q1-1.5\cdot(Q3-Q1),\ Q3+1.5\cdot(Q3-Q1)] \qquad \textit{(Eq. 1)}$$

While the strong outliers are the outliers outside of range

$$[Q1-3.0\cdot(Q3-Q1),\ Q3+3.0\cdot(Q3-Q1)] \qquad \textit{(Eq. 2)}$$

Generally, we eliminate only the strong outliers, thus eliminating the most extreme values.

3.5. Histograms

Once the spatial interval to be analysed is defined, it is possible to construct the histograms relating to the statistical distribution of the experimental data. The software of the DRMS makes it possible to identify with objective criteria the number of classes to be analysed using the method of Sturges or the method of Scott.

According to the method of Sturges (Sturges 1926), where n is the number of observations, the optimal number of classes of the histogram C is given by

$$C = 1 + (3.10) * log10\ (n) \qquad (Eq.\ 3)$$

According to the method of Scott (Scott 1979), where s is the standard deviation, the optimal amplitude of the classes h is given by

$$h = (3.5\ s) / \sqrt{n} \qquad (Eq.\ 4)$$

On each histogram it is possible to overlay the Gaussian distribution with mean $\bar{x}$ and standard deviation s. The histograms can be plotted before and after eliminating outliers.

4. Drilling test results

Below we present the results of the drilling tests carried out on the following three materials: Mortar N2/01, Mortar N2/04 and ARS.

Tab. 2: Measured Statistical Parameters (with and without outliers).

Material	**Mortar N2/01**		**Mortar N2/04**		**ARS**	
Rotation speed (RPM)	300		300		600	
Penetration Rate (mm/min)	40		40		10	
Drill Bit Diameter (mm)	5		5		5	
Minimum calculation depth (mm)	1		1		1	
Maximum calculation depth (mm)	30		30		10	
Number of holes	10		10		15	
	Outliers		**Outliers**		**Outliers**	
	with	without	with	without	with	without
Mean (N)	5.32	5.27	18.48	13.79	6.59	6.59
Median (N)	6.39	6.36	19.86	16.70	6.87	6.87
Mode (N)	4.66	4.60	8.43	8.77	6.45	6.45
Variance (N^2)	4.04	3.58	346.23	79.24	0.17	0.17
Standard Deviation (N)	2.01	1.89	18.61	8.90	0.41	0.41
Coefficient of Variation (CV) %	37.79	35.89	100.67	64.55	6.26	6.26
Min (N)	0.46	0.46	0.46	0.46	5.61	5.61
Max (N)	28.02	12.45	102.88	46.99	7.79	7.79
Range (N)	27.56	12.00	102.42	46.54	2.18	2.18
Kurtosis	6.37	3.55	9.40	5.11	2.69	2.69
Skewness	1.17	0.73	2.49	1.55	0.40	0.40

The mortars N2/01 and N2/04 are composed of the following proportions by weight: one part of binder to three parts of aggregate, and a certain amount of water. The binder is NHL2 Natural Hydraulic Lime of Saint-Astier without the addition of clay or any other material. The aggregate is river sand of a maximum size of 1 mm or 4 mm, respectively. The binder was chosen to reproduce historic mortars (Del Monte *et al.*, 2008)

ARS is an Artificial Reference Stone and it is used to calibrate the DRMS measurement system. It is a ceramic stoneware (porcelain gres) mixture composed of K-and Na-feldspars (30-35 %), sandy feldspar rocks (10- 15 %), Illitic and Kaolinitic clays (30-40 %), Sands (10-15%). It is prepared by wet milling and sieving and is further spray-dried and pressed hydraulically at approx. 300 kg/cm^2, and finally baked at 950°C.

Tab. 2 shows the statistical data of the tests performed on the three materials, with and without outliers. As regards the mortar N2/01, Fig. 5 shows the histograms generated using the method of Scott, before and after the removal of outliers; Fig. 6 shows the variation of the force (the minimum, maximum and average values) as a function of depth before and after the removal of outliers. As regards the mortar N2/04 the histograms and the variation of the force are shown in Fig. 7 and Fig. 8.

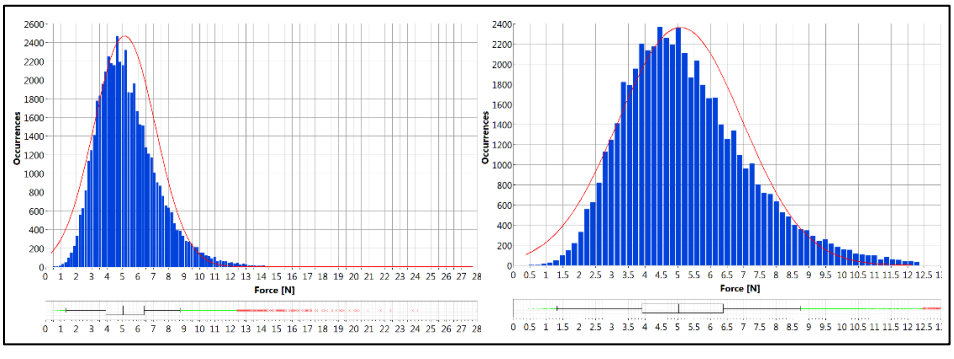

Fig. 5: Mortar N2/01. Histograms with outliers (left) and without outliers (right).

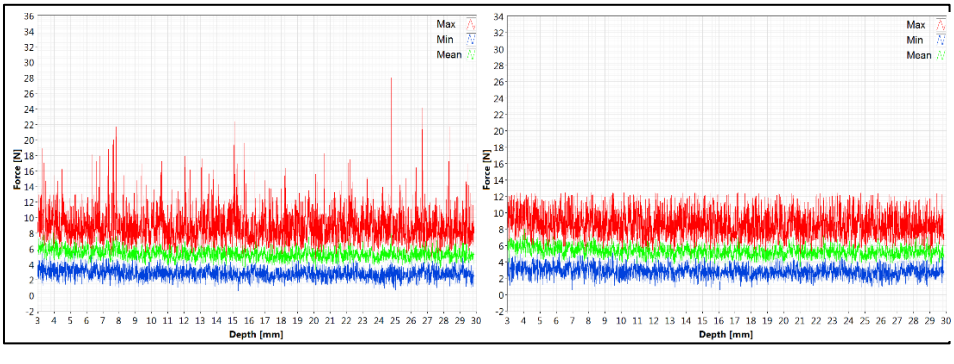

Fig. 6: Mortar N2/01. Force versus depth with outliers (left) and without outliers (right).

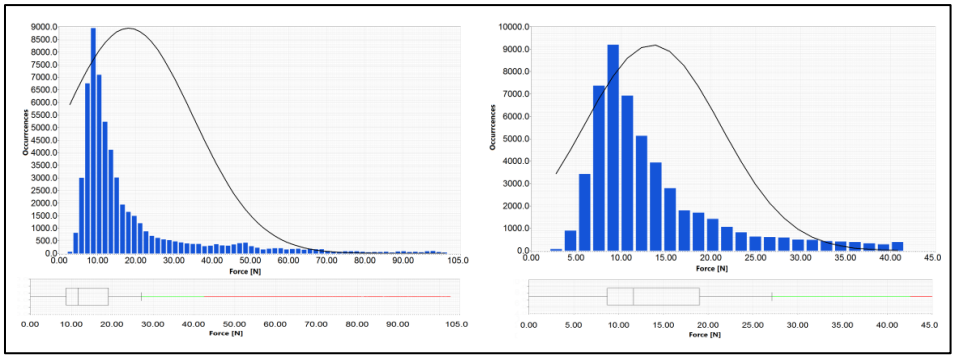

Fig. 7: Mortar N2/04 Histograms with outliers (left) and without outliers (right).

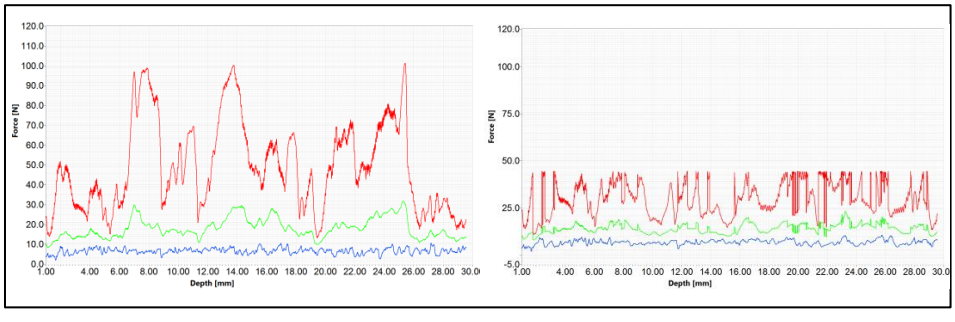

Fig. 8: Mortar N2/04 Force versus depth with outliers (left) and without outliers (right).

It is observed that on the ARS material, because of the greater homogeneity, the experimental results are less dispersed and the coefficient of variation (CVOL.%) is much lower than the 2 mortars. The mortar N2/04 (Fig. 7 and Fig. 8) is less homogeneous because it presents aggregates of larger dimensions. The elimination of outliers leads to an appreciable reduction in the mean value for the mortar N2 / 04 (-25%), while the reduction is much reduced for the mortar N2 / 01 (-1%) and virtually non-existent for the ARS material (0%). The skewness for the mortar N2 / 04 is larger than for the mortar N2 / 01 and for the ARS material.

Acknowledgements

The authors thank M. Aresu, L. Bertelli, S. Caidominici and M. Menichetti of SINT Technology for their valuable contribution to the development of the instrument and the calculation software, and the University of Florence for providing the mortars used in the tests.

References

Del Monte E., Vignoli A. (2008). "In Situ Mechanical Characterization of the Mortars in Masonry Buildings with DRMS". *Proc. of On Site Assessment of Concrete, Masonry and Timber Structures – SACoMaTiS 2008*, 1-2 September 2008, Varenna, Italy, 421-430

Exadaktylos G., Tiano P., Filareto C. (2000) "Validation of a Model of Rotary Drilling of Rocks with the Drilling Force Measurement System". *International Journal for Restoration of Buildings and Monuments*, vol 6, n° 3, 2000, 307-340.

Fernandes, F. and Lourenço, P.B. (2007) "Evaluation of the Compressive Strength of Ancient Clay Bricks Using Microdrilling". *Journal of Material in Civil Engineering* ASCE, September 2007, pp791-800.

Fratini F., Rescic S., Tiano P. (2005) "A New Portable System for Determining the State of Conservation of Monumental Stones" - *Materials and Structures 38* (Dec 2005), 139-147.

Nogueira R., Ferreira Pinto A.P., Gomes A. (2014), "Assessing mechanical behaviour and heterogeneity of low-strength mortars by the drilling resistance method". *Construction and Building Materials* 68 (2014) 757-768.

Pamplona, M., Kocher, M., Snethlage, R. & Aires Barros, L. (2007): "Drilling Resistance: Overview and Outlook". *Z. dt. Ges. Geowiss*, 158: 665–676, Stuttgart.

Scott, David W. (1979). "On Optimal and Data-based Histograms". *Biometrika 66 (3): 605–610*. doi:10.1093/biomet/66.3.605

Sturges, H. A. (1926). "The Choice of a Class Interval". *Journal of the American Statistical Association*: 65–66. doi:10.1080/01621459.1926.10502161.JSTOR2965501

Theodoridou M., Dagrain, F., Ioannou, I. (2015) Micro-destructive cutting techniques for the characterization of natural limestone. *International Journal of Rock Mechanics and Mining Sciences* 76, pp. 98-103.

Tiano P., Filareto C., Ponticelli S., Ferrari M. and Valentini E., (2000a) "Drilling Force Measurement System, a New Standardisable Methodology to Determine the Stone Cohesion: Prototype Design and Validation". *International Journal for Restoration of Buildings and Monuments*, vol 6, n° 2, 133-150.

Tiano P., Delgado Rodrigues J., De Witte E., Verges-Belmin V., Massey S., Snethlage R, Costa D., Cadot-Leroux L., Garrod E., and Singer B. (2000b) "The Conservation of Monuments: a New Method to Evaluate Consolidating Treatments". *International Journal for Restoration of Buildings and Monuments*, vol 6, n° 2, 115-132.

Tiano P., Viggiano A., (2000c) "A New Diagnostic Tool for the Evaluation of the Hardness of Natural and Artificial Stones". *International Journal for Restoration of Buildings and Monuments*, vol. 6, n° 5, 555-566.

Tukey, J.W. (1977). "Exploratory Data Analysis". *Addison-Wesley*. ISBN 0-201-07616-0. OCLC 3058187.

Valentini E., Benincasa A., Tiano P., Fratini F., Rescic S., (2008) "On Site Drilling Resistance Profiles of Natural Stones - In Situ Monitoring of Monumental Surfaces". *Proceeding of the International Workshop SMW08*, 27-29 October 2008 - Convitto della Calza - Florence (Italy), 195-204.

IN SITU ASSESSMENT OF THE STONE CONSERVATION STATE BY ITS WATER ABSORBING BEHAVIOUR: A HANDS-ON METHODOLOGY

D. Vandevoorde[1,2*], T. De Kock[2] and V. Cnudde[2]

Abstract

This paper describes the use of the water absorbing behaviour (WAB) for assessment of the conservation state of stone *in situ*. A test methodology, consisting of a combination of techniques for *in situ* measurement of the WAB, was applied in a case study on Lede stone, a sandy limestone, used in a medieval facade in Ghent, Belgium. The methods used were the contact sponge method (CSM), the Karsten tube (KT) and the droplet method (DM). Additionally, the residual hardness of the stone was measured by Schmidt hammer (SH). After careful selection of representative measuring points, a qualitative analysis of the stone's condition could be made, based on its WAB, residual hardness, reference data from laboratory experiments and thorough visual observations. From this analysis it could be concluded that CSM, KT and SH generated coherent and compatible results; that DM could indicate superficial alterations which were not necessarily representative for the sub-superficial WAB and that this methodology could give an insight on the conservation state, beyond visual observations, when combined with reference data.

Keywords: porous stone materials, water absorbing behaviour, contact sponge method, Karsten tube, droplet method, capillary uptake

1. Introduction

Water absorption of a natural stone is of significant importance for its conservation, as water is a key element in most degradation processes. The water absorbing behaviour (WAB) of a stone material is governed by its pore structure and is constituted of the open porosity, pore size distribution, pore geometry and interconnectivity and chemico-physical properties of the internal pore surface (Hall and Hoff 2002). Consequently alterations in this pore structure will induce differences in the WAB (Kourkoulis 2006). These differences can be caused by variations in the natural state of the stone, such as different stone qualities and weathering degrees, presence of salts, bio colonization, crusts, etc. Additionally, due to treatments such as (old) water repellent treatments or the lack thereof, recent consolidation treatments, anti-graffiti etc. the WAB can be altered. When assessing a stones conservation state *in situ*, the WAB will be governed by a complex combination of these factors.

[1] D. Vandevoorde*
Ghent, Belgium and Rephine Stoneworks, Belgium

[2] D. Vandevoorde*, T. De Kock and V. Cnudde
Pore-scale PROcesses in Geomaterials RESearch Group (PProGRess), Ghent University, Belgium
d.vandevoorde@ugent.be

*corresponding author

In this paper a methodology, consisting of a combination of *in situ* applicable WAB measuring techniques, namely the droplet method (DM), contact sponge (CSM) and Karsten tube (KT) is presented as diagnostic tool or the assessment of a stones conservation state. As these methods are quick, cheap and do provide directly applicable and easily understandable information, this methodology meets the requirements of the practical field and the restrictions of large scale *in situ* investigations. The methodology was tested in a case study regarding the pre-investigation of the condition of Lede stone, used in the medieval facade. Previous to this case study, the WAB methods were extensively tested under laboratory conditions on non-weathered stone samples (Vandevoorde *et al.*, 2009 and 2013) and Lede stone was elaborately studied by De Kock *et al.* (2015). Consequently this case study was the ideal opportunity to test knowledge acquired in laboratory under *in situ* conditions, where weathering, previous treatments and environmental factors could influence the measurements. The aim of the study was twofold: (1) Investigation of the practical applicability and compatibility of the methods under *in situ* conditions and (2) investigation of the sensibility of the methods for indication of structural variations of the stone, degree of weathering and presence of past treatments within the facade.

The case study on WAB was part of a more elaborate study of the condition the medieval facade of the Free Boatmen's Guild House (1531) in the centre of Ghent, Belgium (Fig. 1a). The Lede stone was aged and weathered and was subjected to several restoration campaigns in the past. In order to define an adequate restoration strategy, which would ensure an optimal conservation of the facade, a pre-investigation of the conservation state and study of consolidation treatments was prescribed. The examination of the conservation state consisted of a historical study of the facade, a thorough visual analysis, determination of deterioration patterns, analysis of types of Lede stone, laboratory investigation of samples, measurement of stone strength with a Schmidt hammer, measurement of the WAB, and IR-thermography. This paper will focus on the measurement of the WAB.

2. Materials and methods

2.1. Lithotype: Lede stone

The Lede stone is a sandy limestone with a high historical importance in north eastern Belgium and adjacent parts of the Netherlands. Due to the natural variety within the stones components and fabric, porosities can range from below 5 vol-% to above 10 vol-%. This is mostly related to the amount of macrofossils and concomitant moldic pores. Microscopically, the stone is a packstone to grainstone with a large siliciclastic fraction, mainly quartz and some glauconite. When exposed outside an iron rich patina will form at the surface. Taking into account the geological variability, the stones in the facade were macroscopically divided in a fine grained and a coarse grained type (Fig. 1b and Fig. 1c). The fine grained type was defined by a compact, low porous and homogeneous texture with a low macrofossil content. The coarse grained type is defined by the presence of foraminifera *(Nummulites variolarius)* and serpulids (*Ditrupa strangulate)*, which results in a rougher surface due to differential erosion.

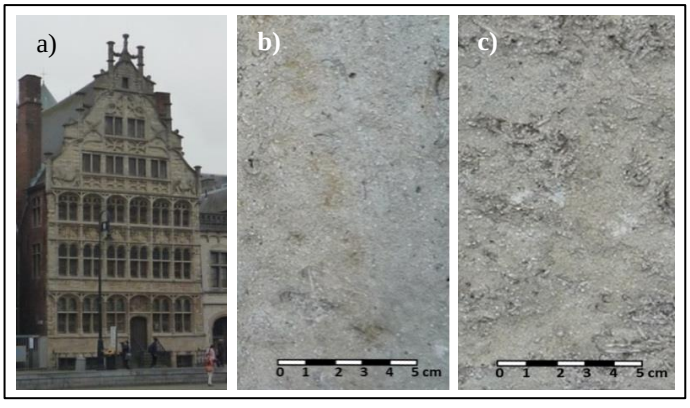

Fig. 1: Facade of the Free Boatsmen's Guild House in the historic centre of Ghent, Belgium (a) and details of the fine grained (b) and coarse grained (c) Lede stone.

2.2. Test methodology

2.2.1. Registration of measuring points and environmental conditions

For an accurate interpretation of the obtained data, one should register all information which could have influenced the measurements. A datasheet was completed for each stone, containing the encoding and location of measuring point, time of measurement, weather conditions and environmental temperature and relative humidity. All measurements were performed in the same period under similar weather conditions to minimize the possible influence of variable environmental conditions. As a liquid, water could be present in the stone due to rain, fog, rising damp, hygroscopic salts, etc. To help indicate the presence of liquid water, the moisture content and temperature of the surface were recorded by using a moisture meter and IR-thermometer. Photographs were taken before and after measurement to register visual anomalies which occurred during the measurements such as absorption in microcracks, hindrance by soiling, leaks, etc.

2.2.2. Measuring techniques

The WAB measuring techniques used in this study were the droplet method (DM), the contact sponge method (CSM) and the Karsten tube (KT). The residual hardness of the surface was tested using a Schmidt hammer (SH). A combination of all data was used for evaluation of the stone quality, together with visual observations. In this paper the methods will be described only briefly. For further information the authors refer to previous publications (Vandevoorde *et al.*, 2009 and 2013).

The DM (Fig. 2a and Fig. 2b) is based on the classical contact-angle method (ASTM D7334-08 2008). *In situ* applicable variations of this method are frequently used in the field by conservators and restorers for e.g. assessment of the residual efficiency of water repellent treatments (Blaüer *et al.*, 2012, Ferreira-Pinto and Delgado-Rodrigues 2000, *pers. comm.* Andrew Thorn and Olivier Rolland). In this case study a calibrated droplet of 100 µl demineralized water was dropped on a vertical surface using an Eppendorf-micropipette. The width and the length of the path of absorption were measured immediately after the droplet had completely been absorbed. The width was measured twice, at the start and end

of the droplets path and the average width was calculated. The degree of hydrophobicity of the surface was calculated by dividing the average width of the path by its length and multiplying the result by 100 for a better readability of the results. Consequently a low value indicated a water repellent surface, and a high value a water absorbing surface.

The CSM (UNI 11432-2011) consists of pressing a wet sponge against the stone surface (Fig. 2c) and measuring the water absorption from the sponge by the difference in mass before and after contact. The WAB is calculated by dividing the amount of water absorbed by the contact surface and the time of contact. In this case 5g of water was added to the sponge and the contact time was 90s.

The KT (RILEM 25-PEM 1980, NEN EN 16302 2013) consists of an open tube with a larger cylindrical body at the end which is attached to the surface of the stone by plastiline and is then filled with water. The amount of water absorbed over a certain period of time can be recorded by the reduction of the water in the graded tube (Fig. 2d). The WAB was calculated by dividing the amount of water absorbed between the 5th and the 15th minute by the contact surface and the time of contact (600 sec). The contact area is variable for each measurement due to the inwards expansion of the plastiline joint when pressing the pipe against the stone. Therefore, the contact area was calculated based on the average diameter, measured from the plastiline after removal of the pipe for each measurement.

The SH (ASTM D5873-14 2014, NEN EN 12504-2 2012) was used to measure the residual hardness of the stones. The test consists of hitting the stone surface with a controlled impact by a spring loaded steel hammer (‘Classic Schmidt hammer, Type ‘N’ with impact of 2.207 Nm, Fig. 2e). The distance of rebound of the piston is measured and gives an indirect indication of the stones hardness, which can be used only for qualitative comparison. This measurement provides information on possible structural disintegration of the stone just below the surface (Bostenaru *et al.*, 2009). For each stone, the average value of ten consecutive measurements divided over de surface was calculated.

For interpretation of the results obtained *in situ*, reference measurements for the different methods were made in laboratory on sound fine and coarse grained dry Lede stones. The reference values are the average values with standard deviation of ten consecutive measurements for each method.

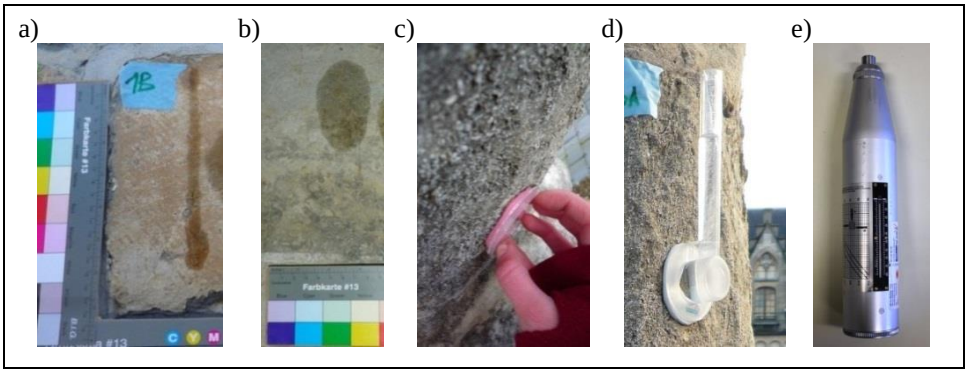

Fig. 2: Illustration of DM for a hydrophobic (a) and hydrophilic (b) surface, CSM (c), KT (d) and SH (e).

Tab. 1: Overview of field of application of WAB methods

Characteristic	DM	CSM	KT
Measured area	surface	subsurface to bulk	subsurface to bulk
Capillary uptake of stone	all	low uptake	elevated uptake
Sensitivity	-	0.01g	0.1g
Contact time	-	30 s up to120 s	5 min up to 1 h or more

3. Results and discussion of the test methodology

The registration of the measured stones included the description of the lithotype (fine/coarse), the observed weathering (using the ICOMOS-ISCS Illustrated glossary on stone deterioration patterns by Vergès-Belmin 2008) and the known treatments. Based on this description the measured stones were classified in 9 categories (Tab. 2).

Tab. 2: Classification of measured stones based on their conservation state

Cat.	Stone type	Condition
1	Fine	Granular disintegration and delamination. Stones used for consolidation tests.
2	Fine	Sound stone with iron rich patina at the surface.
3	Fine	Spalling of iron rich patina. Measurements made on patina, not on spalled parts.
4	Fine	Sound stone, without iron rich patina. Surface is bleached by exposure to rainfall.
5	Fine	Spalling of the iron rich patina and granular disintegration.
6	Fine	Heterogeneous stones with laminated structure. Hair cracks.
7	Fine	No iron rich patina. Surface is bleached by exposure to rainfall. Slight soiling and biological colonization
8	Coarse	Spalling, soiling and biological colonization.
9	Coarse	Differential erosion and roughening of the surface Soiling and biological colonization.

As mentioned above it has to be taken into account that variable factors (such as environmental factors or moist) can influence the measurements *in situ*. Besides, in larger monuments, only a selection of measuring points of the overall surface can be analysed. Therefore, quantitative and statistically solid results will be hard to obtain. Hence, qualitative analysis of the results, in combination with visual observations and results of other diagnoses will be more apt to assess the conservation state of larger structures such as

monuments. In this study a qualitative comparison was made. Therefore the results of each method were visualized in scalebars (Fig. 3). Each scalebar contains the reference values for sound fine (Rf) and coarse (Rc) Ledestone, obtained from measurements in laboratory on dry and non-weathered stones. Below the scalebars the *in situ* obtained values for the nine categories were plotted. For evaluation of the stones condition the *in situ* obtained values were compared to the reference values, and interpreted in combination with the visual observations.

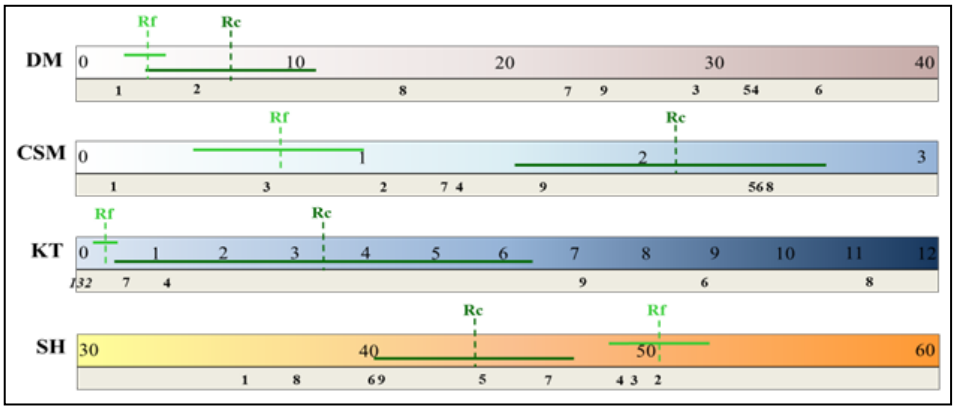

Fig. 3: Scalebars showing the results for DM (mm/mm), CSM (g/m²s), KT (g/m²s) and SH (Schmidt Hammer Rebound Value).Rf and Rc are the average reference values for fine and coarse Ledestone. Their respective standard deviations are indicated with the green lines in the scalebars. Below the scalebars the average results for each of the nine categories (1 to 9) is plotted.

For DM most categories clearly exceed the reference values, meaning that the surface absorbs more water than sound stones. From the visual observations it could be noticed that the surface is weathered and superficially rough compared to non-weathered stones. Therefore it can be assumed that the weathering of the surface causes the higher absorption. Only Cat. 1 and 2 display a remarkably lower absorption compared to the rest of the facade. Cat. 1 showed clear repellence of the droplet, which can be ascribed to the consolidation tests. As ethylorthosilicate consolidant was freshly applied, the solvent was still present in the pores, making the stone temporarily water repellent until evaporation of the solvent. The lower absorption for Cat. 2 could be related to its healthy condition, but remained lower than Cat. 3, which had a similar superficial conservation state. Consequently an additional alteration of the surface was presumed. The conjecture was made of an anti-graffiti treatment, from the fact that this hydrophobicity was only present in the lower part of the facade and that traces of washed off graffiti were present on certain stones.

CSM indicated an acceptable WAB compared to the reference values for Cat. 2, 3, 9. This indicates that these stones show no sub-superficial irregularities in their pore structure. Cat. 4 and 7 show a slightly higher, but still acceptable WAB, probably caused by the absence of the iron rich patina after natural weathering. The higher WAB of Cat. 5, 6, 8 is in accordance with their poor visual condition. Cat. 1 was clearly hydrophobic, also in depth, due to the presence of the solvent of the recent consolidant.

KT could only be used in case of higher WAB. Therefore, no results could be obtained for Cat. 1, 2, 3. The tests also failed for Cat. 5, as excessive leaking occurred, caused by the granular disintegration. For Cat. 4, 6, 7, 8, 9 measurements with KT confirm the visual observations as well as the results of CSM. This illustrates the coherence of CSM and KT for the analysis of Lede stone. Also their limitations were highlighted. KT was not able to measure the less absorbing stones of Cat. 1, 2, 3, while CSM reached its limit for testing the more absorbing stones of Cat. 6, 8, 9. It has to be mentioned that practical hindrances of KT noticed in laboratory, were clearly more predominant *in situ*, causing more tests to fail. Moreover, the standard deviation for KT was remarkably higher than for CSM.

SH confirms the visual observations and WAB measurements made by CSM and KT for all categories. Cat. 1, 5, 6, 7, 8 have a lower residual hardness and Cat. 2, 3 and 4 an acceptable hardness compared to the reference values. The inferior structural hardness corresponds to a higher WAB due to the more open structure of the weathered stones.

From the combination of these measurements and visual observations following considerations concerning the different categories could be made:

- *Cat. 1:* Weakened stone with a very low superficial and sub-superficial absorption measured with DM, CSM and KT. Freshly consolidated weakened stone.
- *Cat. 2:* Lower superficial absorption shown by DM, but normal sub-superficial absorption according to CSM. Conjecture of anti-graffiti on sound stone.
- *Cat. 2 and 3:* Stones in a good condition according to CSM and SH.
- *Cat. 4, 7 and 9:* Higher WAB and lower residual hardness compared to sound stones, but generally sound condition without precarious deterioration patterns.
- *Cat. 5, 6 and 8:* Higher superficial and sub-superficial absorption by DM, CSM and KT and low hardness by SH. Stones in a poor conservation state.

Concerning the performance of the methods, the results of CSM, KT and SH turn out to be coherent for all categories, indicating the compatibility of the methods. DM analyses the superficial absorption and demonstrates that this is not always related to the sub-superficial condition of the stone.

4. Conclusions

The WAB measuring techniques DM, CSM, KT and the hardness meter SH showed to be valuable and compatible tools for *in situ* analysis of the stones conservation state, ranging from surface to sub-surface and bulk. As expected, DM illustrated to be capable of indicating superficial alterations, while CSM, KT and SH gave an insight in the sub-superficial condition. Considering the variable factors present *in situ* and the large scale investigation, results could only be assessed qualitatively in relation to reference values of sound stones and in combination with a thorough visual analysis of the stones conservation state.

References

ASTM D5873-14, 2014, Standard Test Method for Determination of Rock Hardness by Rebound Hammer Method, West Conshohocken, PA, USA.

ASTM D7334-08, 2008, Standard Practice for Surface Wettability of Coatings, Substrates and Pigments by Advancing Contact Angle Measurement, 3.

Bläuer, C., Franzen, C., Vergès-Belmin, V., 2012, Simple field tests in stone conservation, in proceedings of the 12th International Congress on Deterioration and Conservation of Stone, Colombia University, New York, USA. *In press*.

Bostenaru, M.D., Prikryl, R., Török, A., 2009, Materials, Technologies and Practice in Historic Heritage Structures, Springer Science & Business Media, ISBN 9048126843, 371.

De Kock, T., Boone, M., Dewanckele, J., De Ceukelaire, M., Cnudde, V., 2015, Lede stone: a potential "Global Heritage Stone Resource" from Belgium, EPISODES, 38(2), 91–96.

Ferreira-Pinto, A.P., Delgado-Rodrigues, J., 2000, Assessment of durability of water repellents by means of exposure tests, in proceedings of the 9th International Congress on Deterioration and Conservation of Stone, Venice, Italy, 273-285.

Hall, C., Hoff, W.D., 2002, Water transport in brick, stone and concrete, Spon Press, ISBN 9780415564670, 374 .

Kourkoulis, S.K., 2006, Fracture and Failure of Natural Building Stones, Applications in the Restoration of Ancient Monuments, Springer Netherlands, ISBN 9781402050770, 592.

NEN EN 12504-2, 2012, Testing concrete in structures - Part 2: Non-destructive testing - Determination of rebound number, 8.

NEN EN 16302, 2013, Conservation of cultural heritage – Test methods – Measurement of water absorption by pipe method, 15.

RILEM 25-PEM, 1980, Recommended tests to measure the deterioration of stone and to assess the effectiveness of treatment methods, Materials and structures, 75, Paris, France, 175-253.

UNI 11432-2011, 2011, Beni culturali, Natural and artificial stone – Determination of the water absorption by contact sponge, Milano, Italy.

Vandevoorde, D., Cnudde, V., Dewanckele, J., Brabant, L., de Bouw, M., Meynen, V., Verhaeven, E., 2013, Validation of in situ applicable measuring techniques for analysis of the water adsorption by stone, in proceedings of Yococu 2012, Antwerp, Belgium, Procedia Chemistry, online paper, 317-327.

Vandevoorde, D., Pamplona, M., Schalm, O., Vanhellemont, Y., Cnudde, V., Verhaeven, E., 2009, Contact sponge method: Performance of a promising tool for measuring the initial water absorption, Journal of Cultural Heritage, 10(1), 41-47.

Vergès-Belmin, V., 2008, Illustrated glossary on stone deterioration patterns, ISBN 9782918068000, 78.

SURFACE HARDNESS TESTING FOR THE EVALUATION OF CONSOLIDATION OF POROUS STONES

W. Wedekind[1*], C. Pötzl[2], R.A. López Doncel[3], T.V. Platz[4] and S. Siegesmund[1]

Abstract

In the present study a commercial hardness tester was used to evaluate the effectiveness of consolidation on two monumental tombs composed of different sandstones. Furthermore different stone types were also repeatedly treated in a stepwise fashion and retested. The main goal was to determine whether it would be possible to detect even a small increase of consolidation by reloaded treatments. The results of the surface hardness tests on the stone samples correlated to their compressive strength. Tests were also conducted to determine whether a correlation between the increase of hardening of the surface in relation to the increase of the uniaxial compressive strength and ultrasonic velocity measurements exist. In an applied case study the consolidation effect has been verified after the consolidation of sandy stone parts with the same consolidant.

Keywords: consolidation, surface hardness, ultrasonic velocity, porosity

1. Introduction

To evaluate the state of weathering and the effectiveness of consolidation on-site only a few methods are available. The most common non- or low destructive technique is the ultrasonic wave measurement and the drilling resistance test, which has been applied for around 20 years in the field of stone conservation. The drilling resistance test is a useful method for detecting scales and exfoliations especially in sandstones (Cnudde *et al.* 2009, Siedel *et al.* 2010). However, the test cannot differentiate exactly between consolidated and untreated areas (Lotzmann and Sasse 1999). Using results from different sources a comparison between drilling resistances and uniaxial compressive strength could be derived (Fratini *et al.* 2006, Pamplona *et al.* 2007). However, the investigations in this study show that there is a clear positive correlation between the surface hardness and the compressive strength (Fig. 1). Testing stone objects with a low impact affect can be performed by using a Schmidt hammer. The method is a well-known portable field test. The testing tool applies an impact force and the rebound of the hammer applying the force is measured. Different

[1] W. Wedekind* and S. Siegesmund
Geoscience Centre of the University Göttingen, Germany
Germany, Applied Conservation Science (ACS), Göttingen, Germany
wwedekind@gmx.de

[2] C. Pötzl
Geoscience Centre of the University Göttingen, Germany

[3] R.A. López-Doncel
Geological Institute, Autonomous University of San Luis Potosí, Mexico

[4] T.V. Platz
Unit for Material Technology, University of Innsbruck, Austria

*corresponding author

types of hammers are in use, but the testing tool in general was developed for the testing of cement and not for weak and soft materials such as weathered building stones. In some cases the hammer will damage the material tested. The rebound hammer used in this study is comparable with a micro-rebound hammer with a low impact force. An overview on surface hardness measurements in geomorphology and heritage science can be found in Viles *et al.* 2010. Booth *et al.* (2012) show that the device used in this study could be used to detect the effect of different consolidation materials on stone.

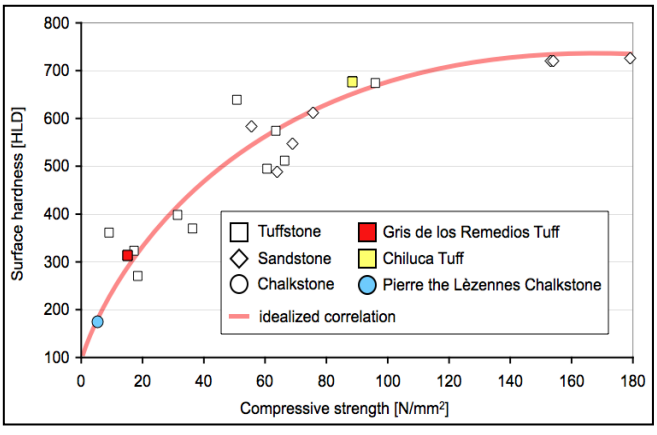

Fig. 1: Surface hardness versus compressive strength for different stone types and the three stone samples investigated in this study.

2. Testing material and case studies

The testing material included two tuffstones (Fig. 2b and Fig. 2c) and one poorly cemented limestone (Fig. 2a). These stone types show different petrophysical properties. Two of them (the chalkstone and the Remedios tuff) can be classified as low or weakly bound building stones. The object tested and treated in this study are two monumental pillar tombs in the historical Bartholomew Cemetery of Goettingen, Germany (Fig. 2d and Fig. 2e). The tested object is constructed from two different types of sandstone. They show different types of weathering as well as different forms of crusts and deposits.

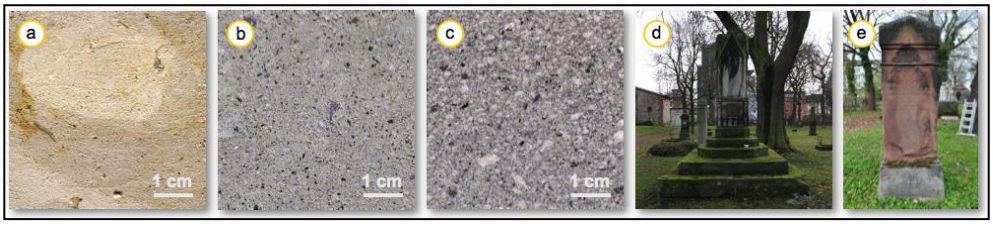

Fig. 2: a) Pierre the Lèzennes Chalkstone; b) The Gris de los Remedios tuff; c) The Chiluca andesitic tuff; d) The Pickardt tomb monument and e) the Schneider pillar tomb.

2.1. Stone material

2.1.1. Pierre the Lèzennes Chalkstone

The chalkstone investigated in this study is a glauconitic, granular calcareous chalk of the Maisières Chalk Formation. The rock is an important building stone and is known in France as "Verts", "Gris des mineurs" (Mons), “Pierre the Lézennes” (Lille), “Craie grise du Cambrésis” or "Bonne Pierre de Valenciennes". This chalk was worked in underground quarries for use as a building stone. The stone contains basal beds yielding phosphate grains or pebbles. Many fossil-like bivalves can be found in the highly porous matrix. The porosity of the stone reaches nearly 43 % and the compressive strength only 5 N/mm^2.

2.1.2. Gris de los Remedios Tuff

The volcanic rock of Remedios is a lapilli tuff, supported by an ash matrix. The color of this tuff is gray to light gray (Fig. 2c). The ash matrix is more or less gray. Within the matrix, dark spots occur that can be traced back to mafic minerals. The mafic minerals often show prismatic crystal shapes and represent mostly idiomorphic developed hornblende crystals. The white lapilli fragments are dominated by pumice. Microscopic examinations revealed the presence of minerals such as crystobalite, clays, sodium plagioclase and hornblende. The porosity of the Gris de los Remedios ranges from 24.5 to 31.5%, whereas their bulk density is around 1.78–1.92 g/cm^3. The Remedios variety has an average compressive strength of 17.3 N/mm^2 and a Youngs modulus of 8.29 kN/mm^2 (Wedekind *et al.* 2011). The investigated material originates from the quarries of Los Remedios located in the mountains northwest of Mexico City.

2.1.3. Chiluca Tuff

The Chiluca tuff is a pyroxene ash tuff with a high proportion of fragmented feldspar single crystals, giving the rock a porphyritic appearance. The tuff is gray in color with dark inclusions of mafic minerals (Fig. 2b). Feldspar single crystals occur in a fine-grained matrix. The Chiluca variety shows a porosity of 8% and a density of 2.58 g/cm^3 and a compressive strength of 90.5 kN/mm^2 (Wedekind *et al.* 2011). Historical quarries of the Chiluca tuff can be found on some islands of the former Lake Texcocco, now modern day Mexico City.

2.2. Case Studies

2.2.1. Tombs of Schneider and Pickardt

The tombs of Schneider and Pickardt are located in the historical Bartholomew Cemetery in Goettingen, Germany (Fig. 2d and Fig. 2e). The construction material predominately used for the tombs is the highly porous Buntsandstein. Here, the rocks of the Solling Formation of the Middle Buntsandstein are especially significant (Kracke *et al.* 2007). The Pickardt tomb is a neo-gothic pillar tomb (1857) made from the light coloured local Reinsberg variety. The Schneider tomb (1850) is a classical pillar tomb made from the Arenshausen variety (Kracke *et al.* 2008).

3. Methods

3.1. Porosity

In order to acquire the matrix and bulk density as well as the porosity, hydrostatic weighing was carried out. Stone samples were measured using hydrostatic weighting (DIN 52 102) for determining the open (effective) porosity as well as the density. The water-saturated mass, the buoyancy mass of the samples measured after water saturation under vacuum, and the dry sample mass were used to calculate the porosity.

3.2. Compressive strength

For the compressive strength tests, standard cylindrical specimens of 50 mm in diameter and 50 mm in length with co-planar end-faces were used. The uniaxial compressive strength in this study was only measured in Z-direction 10 times. The compressive load was applied by a servo-hydraulic testing machine with a very stiff testing frame (3000 kN/mm^2) and a class 1 load range up to 300 kN. The load was applied to the end-faces of the specimen with a strain rate of 10^{-5} s^{-1} until failure. The maximum load is defined as the uniaxial compressive strength.

3.3. Surface hardness

Surface hardness measurements were done in situ as well as on stone samples in the laboratory. The testing instrument works with the rebound method. Like the well-known Schmidt Hammer, it indirectly measures the loss of energy of a so-called impact body. D. Leep, the inventor of this method defined his own hardness value called the Leep hardness value: HL. For the measurements an Equotip 3 (proceq) portable testing device with an impact device D was used. Therefore, the final results are given as HLD. The instrument offers extended capabilities such as measurements on almost all parts with different geometries, with a high accuracy of ± 4 HL (0.5% at 800 HL) and automatic correction for impact direction. For each investigated area 10 individual measurements were done and the average value calculated. In the laboratory the measurements were done on dry and water-saturated samples. To optimise the testing results the tested surface of the cylindrical specimens were polished to reduce the roughness of the material. The specimens were consolidated by total saturation within a commercial silicic acid ester with a gel deposit rate of 10 % (KSE 100). In total 30 specimens of each stone type were treated: 10 samples one time, 10 samples two times and 10 samples three times.

3.4. Ultrasonic velocity

Ultrasonic velocity measurements were carried out the cylindrical specimens. Transient times of ultrasonic pulses (piezoceramic transducers, resonant frequency 1 MHz) were measured in the Z-orthogonal direction using the pulse transmission technique (Birch 1960, 1961).

4. Results

4.1. Laboratory studies

In general, the three different stone types show very different initial values and an increase in strength and hardness after consolidation treatment (Fig. 3).

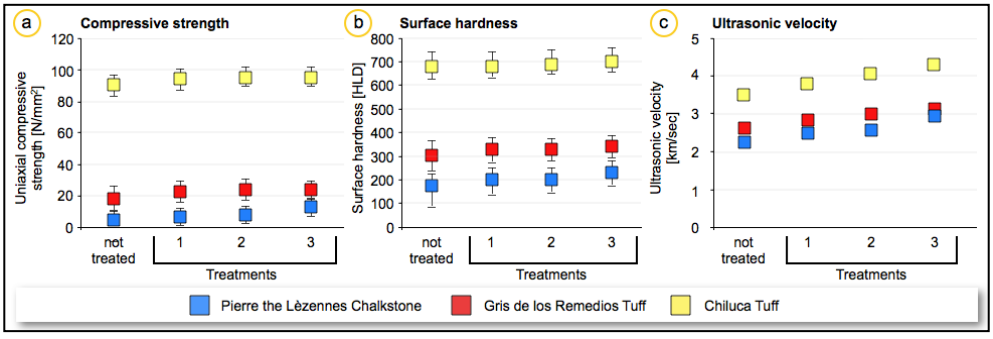

Fig. 3: Results of the different petrophysical measurements before and after stepwise consolidation treatment; a) Compressive strength; b) surface hardness; c) ultrasonic velocity.

4.1.1. Uniaxial compressive strength and porosity

The chalkstone shows the largest increase in compressive strength after consolidation. However, with only 5 N/mm^2 the sample was the one with the lowest strength and the highest porosity (42.5%). After the first treatment an increase of 34 % took place. After the second treatment the compressive strength reaches 10.7 N/mm^2 with an increase of 114% related to the untreated value. After the third treatment 13.2 N/mm^2 was reached, again a significant increase of another 50%. At the same time a decrease in porosity took place: from nearly 5% (1st treatment) to 16.5% (2nd treatment) and finally after the 3rd treatment to nearly 36% (Fig. 4a). The increase in surface hardness of the Remedios tuff only reaches around 30% comparable to the untreated samples. Between the second and third treatment the increase was quite low with a value of only 1.1%. In contrast, the decrease in porosity shows the highest values by reaching 40.5% (Fig. 4b). For the Chiluca tuff the effect of strength increase was the lowest. The stone shows the highest compressive strength with more than 90 N/mm^2, but only an increase of 6% after the third treatment (Fig. 4c). Also the porosity shows the lowest decrease from 7% to 10.5% and finally 21%.

4.1.2. Surface hardness

The percentage increase of surface hardness shows the highest values for the chalkstone congruent to the uniaxial compressive strength. After the first treatment an increase of 15.4% took place, then another 9% after the second treatment and after the last treatment another 8% occurred. Surface hardness ranges between 175.9 to 233.75 HLD (Fig. 3b). Surface hardness of the Remedios tuff shows values between 308 to 342 HLD (Fig. 3b). After the first treatment the percentage increase of the Remedios tuff reaches 7.1% and after the second one only another 1.1% and finally another 3% is attained. In the case of the Chiluca tuff the surface hardness is the highest but the increase after treatment the lowest. The HLD values range between 680 and 701 (Fig. 3b), but the increase after the first treatment only reaches 0.14%, after the second 1.1% and finally another 1.7 %.

4.1.3. Ultrasonic velocity

In general, the highest initial value of ultrasonic velocity is shown by the Chiluca tuff (3.516 km/sec), the second highest is the Remedios tuff (2.65 km/sec) and the lowest is the chalkstone with a value of 2.26 km/sec. The values of ultrasonic velocity of the different samples show closer values of percentage increase after treatment than the destructive mechanical testing procedures. After the first treatment the chalkstone shows an increase of nearly 10% followed by another 4.4% and finally a significant step of 16.8% (Fig. 4a). The Remedios tuff has a comparable increase of 7.1% after the first treatment and a stepwise further increase of another 5.7% followed by another 4.5% after the last treatment (Fig. 5b). The values of the Chiluca tuff range between the ones of the chalkstone and the Remedios tuff. In the first step of consolidation an increase of 8.5% was established. After the second treatment another 7.5% was attained, which is nearly doubled and finally again an increase of 7.2% could be measured (Fig. 4c).

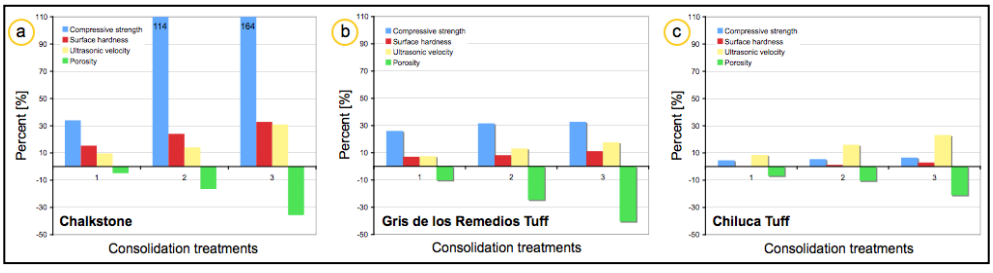

Fig. 4: Percentage increase of the compressive strength, the surface hardness, the ultrasonic velocity and the decrease after stepwise treatments. a) For the chalkstone, b) the Gris de los Remedios tuff and c) the Chiluca tuff.

4.2. Case Studies

During 2014 and 2015 a scientific consolidation treatment project was done on the tomb monuments presented in this study. The weathered areas show sanding and are located mostly in those areas where no water runs down during a rainfall and are visible by dark deposits and microbiology (Fig. 5a and Fig. 5b). Where decorative areas of the Pickardt tomb and the Schneider tomb are exposed to rain, only low weathering or none could be observed. At these areas the surface hardness averaged 481 HLD for the Pickardt tomb and 479 HLD for the Schneider tomb (Fig. 5c). Surface hardness for the pedestal of the Schneider tomb averaged only 331 HLD but is made from another sandstone variety than the pillar. The areas affected by weathering show an average value of 355 HLD for the Pickardt tomb (Fig. 5d) and 332 HLD for the Schneider tomb (Fig. 6d). Some areas of the Schneider tomb that were highly affected by weathering and sanding were not measurable by the equotip device (Fig. 6d). After consolidation of the weathered areas (Fig. 5b, red areas by silicic acid ester (KSE 100)), the surface hardness could be increased to around 445 HLD for the Pickardt tomb and 400 HLD for the Schneider tomb (Fig. 5e and Fig. 6e).

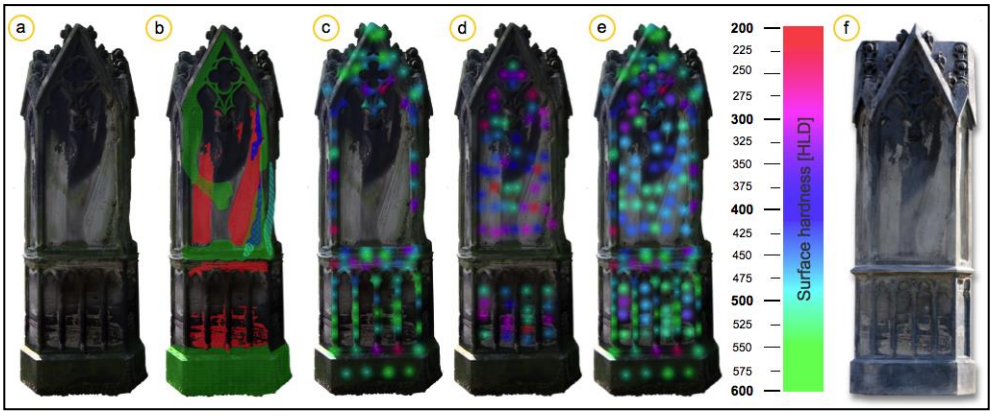

Fig. 5: a) The Pickardt tomb before consolidation and restoration. b) Damage mapping of the monument with indications of microbiology (green), sanding areas (red), gypsum crusts (blue) and delamination (light blue). c) Surface hardness of the exposed decorative parts of the monument. d) Surface hardness of the backside of the monument. e) Surface hardness after the consolidation treatment. f) The monument after conservation and restoration.

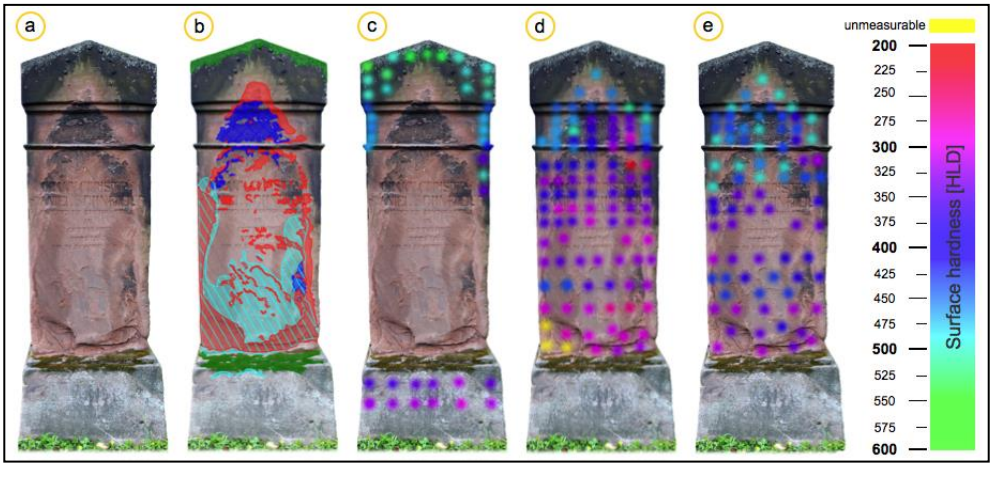

Fig. 6: a) The Schneider tomb before consolidation and restoration. b) Damage mapping of the monument with indications of microbiology (green), sanding areas (red), gypsum crusts (blue) and delamination (light blue). c) Surface hardness of the parts exposed to rain water, viseble due to the dark discoloration. d) Surface hardness of the weathered areas of the monument. e) Surface hardness after the consolidation treatment.

5. Discussion and conclusions

By comparing the compressive strength with the surface hardness it becomes clear, that the highly porous, poorly cemented chalkstone shows no linear relation between the values of the two different methods but a continuous decrease (Fig. 7a). In contrast the two other stones exhibit a nearly linear relation (Fig. 7a). There is probably a direct correlation between the surface hardness and the compressive strength, if the consolidation affect reaches less than 100% in comparison to the non-treated stone. The relation between the porosity and the surface hardness for the Remedios tuff and the chalkstone show a linear relation. The same is also the case for the Chiluca tuff (Fig. 7b). There is a clear relationship between porosity and surface hardness. Ultrasonic velocity and surface hardness show a nearly linear relation for the two low bound stones (chalkstone and Remedios tuff) and a linear regression for the Chiluca tuff (Fig. 7c). That indicates, that for the two low bound (chalkstone and Remedios tuff) stones a linear relation between surface hardness and ultrasonic velocity can be detected.

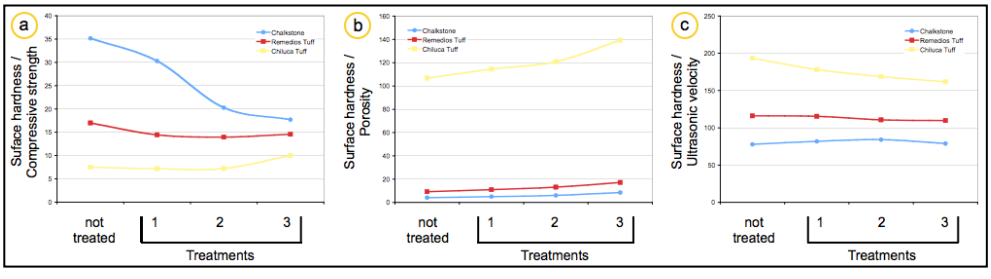

Fig. 7: a) Relation between surface hardness and compressive strength. b) Relation between surface hardness and porosity. c) Relation between surface hardness and ultrasonic velocity.

Our data shows that even a low consolidation affect can be detected by surface hardness measurements, whereas the affect measured by compressive strength is not always clearly comparable. In the case of stone types with a low increase of compressive strength, a clear correlation between the measured surface hardness and compressive strength could be shown. A clear effect could be detected by surface hardness in situ at the two tomb monuments. Thus, surface hardness measurements can be used for understanding the conservation state as well as a means for evaluating the consolidation. Moreover, it can be used as a suitable tool for non-destructive testing in stone conservation.

Acknowledgments

We would like to thank Ms Birgit Busse, who is the city authority responsible for gardens and green areas in Goettingen and for their support and friendly cooperation.

References

Birch, F., 1960, The velocity of compressional waves in rocks up to 10 kilobars. Part I. Journal of Geophysical Research, Volume 65, pp 1083–1102.

Birch, F., 1961, The velocity of compressional waves in rocks up to 10 kilobars. Part 2. Journal of Geophysical Research, Volume 66, pp 2199–2224.

Booth, J., Viles, H., Fletcher, P., 2012 An assessment of three consolidants for use on museums artefacts in comparison to organo silanes. In: Proceedings of the 12th International Conference on the Deterioration and Conservation of Stone (in print).

Cnudde, V., Silversmit, G., Boone, M. Dewanckele, J., De Samber, B., Schoonlans, T., De Witte, Y., Elburg, M. Vincze, L., Van Hoorebeke, L., Jacobs, P., 2009, Multi-disciplinary characterisation of a sandstone surface crust. Science of the Total Environment, Volume 407, Issue 20, pp 5417-5427.

Fratini, F., Rescic, S., Tiano, P., 2006, A new portable system for determining the state of conservation of monumental stones. Materials and Structures, Volume 39, Issue 2, pp 139-147.

Kracke, T., Mueller, C., Krinninger, S., Wedekind, W., Ruedrich, J., Siegesmund S., 2007, Buntsandsteine Goettingens: Verwendung und Verwitterungsverhalten am Beispiel des Bartholomaeus Friedhofs. Z. dt. Ges. Geowiss., Volume 158, Issue 4, pp 957-984.

Kracke, T., Ruedrich, J., Wedekind, W., Müller, C., Siegesmund, S., 2008, Weathering Behaviour and the Effects of Consolidation Approaches on the Buntsandstein: a Case Study from the Bartholomew Cementery in Göttingen. In: Jadwiga W. Lukaszewicz & Piotr Niemcewicz (eds.) 11th International Congress on Deterioration and Conservation of Stone. 15 - 20 September 2008. Torún. Poland. Proceedings Volume I, Torún 2008, pp 677 - 684.

Lotzmann, S., Sasse, HR., 1999, Drilling resistance as an indicator for effectiveness of stone consolidation. In Sickels-Taves, L.B. (ed.) The use and need for Preservation standards in architectural conservation, American Society for testing and materials, West Conshohocken, pp 77-89.

Pamplona, M., Kocher, M., Snethlage, R., Aires Barros, L., 2007, Drilling resistance: overview and outlook. Z. dt. Ges. Geowiss., Volume 158, Issue 3, pp 665–676.

Siedel, H., Pfefferkorn, S., von Plehwe-Leisen, E., Leisen, H. Sandstone weathering in tropical climate: Results of low-destructive investigations at the temple of Angkor Wat, Cambodia. Engineering Geology, Volume 115, Issues 3-4, October 2010, pp 182-192.

Viles, H., Goudie, A., Grab, S., Lalley, J., 2010, The use of the Schmidt Hammer and Equotip for rock hardness assessment in geomophology and heritage science: a comparative analysis. Earth Surf Process Landforms, Volume 36, Issue 3, pp 320-333.

Wedekind, W., Ruedrich, J., Siegesmund, S., 2011, Natural building stones of Mexico–Tenochtitlán: their use, weathering and rock properties at the Templo Mayor, Palace Heras Soto and the Metropolitan Cathedral. Environ Earth Sci, Volume 63, Issue 7/8 pp 1787–1798.

This page has been left intentionally blank.

OTHER MATERIALS

This page has been left intentionally blank.

LONG-TERM MONITORING OF DECAY EVOLUTION IN BRICKS AND LIME MORTAR AFFECTED BY SALT CRYSTALLISATION

C. Colla[1*], E. Gabrielli[1] and F. Grüner[2]

Abstract

The consequences of moisture and dissolved salt capillary rise in porous construction materials are major causes of aesthetic and mechanical decay in masonry. Given the limitations of the present testing standards related with construction materials ageing, work is necessary to reduce some of the gaps. For a better comprehension of the evolution of this complex phenomenon and of its effects, an experimental work was initiated some years back in the Building Science group in Bologna University, Italy, aimed at monitoring environmental degradation in masonry materials typical of historic structures. Of particular interest is natural ageing with low-concentration brines and long-term monitoring. To achieve this aim, a first step is to know the mechanical and hygrothermal properties of masonry's constituent materials, in at least two rather different stages in the structure's lifetime, together with the environmental conditions endured during that timeframe. Knowing in quantitative terms how the physical and load-bearing properties may have decreased, can help in establishing degradation indexes to predict the rate of material decay. The contribution reports on the outcome of capillary water absorption tests conducted in a controlled environment on solid brick units and lime mortar prisms. The materials were tested twice: as-new and after five summer seasons of natural outdoor exposure in southern European climate together with provoked capillary rise either by tap water or by low-concentrated sodium chloride or sodium sulphate brines. The values of the absorption rate determined for the different materials and salts are compared with the pre- and post-experimental ultrasonic signal velocities. By means of thin section analysis, alterations of the different materials during the long term monitoring were observed. The obtained values are of interest from different viewpoints, such as to evaluate possible changes in the masonry material's diffusivity, to create a database or as input for numerical simulations.

Keywords: masonry, damp rise, salt crystallisation, experimental work, brick, monitoring

1. Introduction and aims of the work

Moisture and dissolved salt capillary rise is one of the major causes of aesthetic and mechanical decay in porous construction materials. The existing test standards related with ageing phenomena only focus on testing individual porous materials, such as sandstone, limestone, brick or mortar, in contact with water or brine. There are no test codes which

[1] C. Colla* and E. Gabrielli
DICAM Dept. and CIRI-EC, Engineering Faculty, Univ. of Bologna, Italy
camilla.colla@unibo.it

[2] F. Grüner
MPA, Materials Testing Institute, University of Stuttgart, Germany

* corresponding author

embrace the more complex behaviour of built masonry walls. Moreover, in the case of accelerated ageing test standards, the relation between natural and accelerated ageing procedures and effects is still an open question. Such test standards allow the observation of appearance changes, the susceptibility to damage or the determination of physical parameters, such as the water absorption coefficient. The changes of properties and the effects of salt crystallisation are determined only for single materials with highly concentrated brines (EN 12370, RILEM PEM/25, VDI 3797), but not under long-term monitoring with low-concentrated brines. Consequently, despite the numerous researches conducted at different material and structural scales, work is still necessary to reduce the highlighted gaps in the comprehension of environmental decay evolution in porous materials. For a better understanding of the damp rise and salt crystallisation phenomena and their consequences in masonry walls, an experimental and numerical work was initiated some years back in the Building Science group in Bologna University aimed at monitoring, evaluating and predicting the environmental degradation progress in masonry materials typically found in historic structures. To achieve this aim, a first step is to know the mechanical and hygrothermal properties of both masonry's constituent materials and of masonry as a composite, in at least two rather different stages in the structure's lifetime, together with the environmental conditions. Knowing the microclimatic conditions endured by the structure during that time frame and knowing, in quantitative terms how the physical and load bearing properties may have decreased, can help in establishing degradation indexes to predict the rate of material decay. An experimental work was undertaken on series of bricks and mortar specimens subjected to long-term weathering in natural outdoor exposure while capillary rise was provoked either by water or by brines with the aim of monitoring the evolution of the weathering. Of specific interest was natural ageing with low-concentration brines and long-term monitoring. The initial determination of the two materials' physical and mechanical characteristics and their verification after 5 years was carried out by laboratory analyses and tests and by non-destructive methodologies (water capillary absorption, ultrasound signal propagation and thin-section observations) with the final purpose of obtaining an inside-view in the decay process for each of the two materials as well as quantitative values of property changes that can be of practical use for the evaluation of the decay advancement.

2. Brick and mortar materials and their long-term weathering

Several specimens of low-temperature fired-clay bricks of standard dimensions $25\times12\times5.5$ cm^3 and hydraulic lime mortar prisms of dimensions $4\times4\times16$ cm^3 were considered in the study. Bricks were new, commercial, solid units, whilst the mortar prisms were casted in the laboratory from dry, pre-mixed commercial bags and let mature for many months before starting the experiments. The specimens were subjected to five summer seasons of natural outdoor exposure in the southern European climate of Bologna, Italy. In addition, capillary rise from their base was provoked either by tap water or by sodium chloride or sodium sulphate solutions (0.05 wt.-%). The brine concentrations used were similar to what masonry would experience in realistic situations from groundwater capillary rise through building foundations (Colla 2011). Roughly between May and November each year, an as-constant-as-possible layer of water/brine (few centimetres high) was maintained into the specimens' containers for damp rise. The specimens, which would stand vertically into their tubs, were rotated upside down once in each season. At the end of each ageing period, the sets of bricks and mortar prisms were let dry and stored indoors for winter.

3. Calculation of water absorption rates

Capillary water absorption tests were conducted both on the new bricks and mortar prisms and repeated after five years, in a climatic chamber of the laboratory in Bologna at constant values of air temperature (20°C) and relative humidity (60%). According to EN ISO 15801 and RILEM PEM/25, 1980, previous to the test, samples were dried to constant mass; moreover, they were weighted at the beginning and end of the absorption test for roughly estimate the sucked water amount. Each specimen was prepared by marking a 5-mm graduated scale on one front face. The groups of specimens were placed standing on a mat of hydrophilic material in a basin constantly supplied with a thin layer of distilled water (Fig. 1a) whilst the experiments were monitored via webcam. Later, the water front migration height according to the passing time was visually measured on each specimen by analysing the recorded images thanks to the colour change of the wet material surface. To take into account the porosity variability of the materials, 3 specimens for each water or brine ageing type were tested. The mean value of suction velocity and rate were calculated. The tests on the mortar prisms lasted between 8 and 16 hours according to the brine used for the weathering. Thus, diverse values of suction velocity (cm/h$^{0.5}$) -determined as the slope of each absorption curve- were obtained (Fig. 1b). To estimate the capillary suction

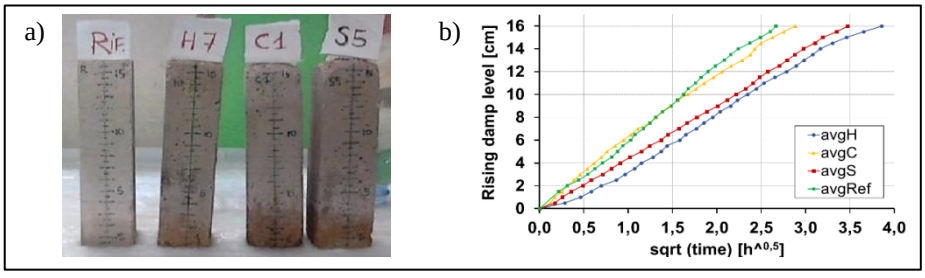

Fig. 1: Mortar prisms: a) phase of capillary rise tests; b) damp rise vs. SQRT of time: average curves for water (H), chloride (C), sulphate (S), reference (R).

rate, which expresses how much water is absorbed in the unit of time by the unit of specimen's area in contact with the water container, the distilled water density and, for all the mortar specimens, the porosity value of 20.6% measured for the new mortars (Gabrielli *et al.* 2012) were used as input, although the latter parameter may have changed during ageing. The undamaged (reference) mortars show the highest velocity and suction rate, followed by the NaCl contaminated prisms and the Na_2SO_4 contaminated prisms, which had respectively 6.5% and 26% lower rates than the reference mortars. Salts would tend to occlude the micro-pores and thus to slow the moisture rise within the material (Gabrielli and Colla 2012) but surprisingly the lowest measured suction rate belong to the water-contaminated mortars (about 31% lower than the undamaged prisms). This is not associated with the least amount of water absorbed, which, instead, pertains to the Na_2SO_4 contaminated prisms (Tab. 1). Note also that, contrary to salt contaminated prisms, water aged prisms show a weight increase compared to reference. On the bricks, each absorption test lasted a minimum of 3 days. The fastest velocity and suction rate were measured for the undamaged bricks. The 3 sets of aged bricks show slightly lower velocity than reference material, with differences ranging between 2.5% for the Na_2SO_4 contamination and 8.5% for the NaCl contaminated samples (Tab. 2). These small entity differences of the 3 groups

of aged units may arise from a lower sensitivity of this material to the ageing procedure. The suction rate values were estimated considering a porosity of 23.2% (upper limit for the water-accessible pore space in the new bricks).

Tab. 1: Mortar prisms, average values from capillary rise tests.

Specimen	**Start weight**	**Weight variation**	**Final weight**	**Absorbed water**	**Suction velocity**	**Capillary suction rate**	**Rate variation**
	g	%	g	%	$cm/h^{0.5}$	$kg/m^2h^{0.5}$	%
Reference	508.8		567.6	11.6	6.24	12.85	
H_2O_mortar (H)	511.9	+0,60	566.0	10.6	4.29	8.84	-31.2
NaCl_mortar (C)	484.8	-4,72	538.5	11.1	5.83	12.01	-6.5
Na_2SO_4 mortar(S)	492.3	-3,25	543.0	10.3	4.61	9.50	-26.1

Tab. 2: Bricks, average values from capillary rise tests.

Specimen	**Start weight**	**Weight variation**	**Final weight**	**Absorbed water**	**Suction velocity**	**Suction rate**	**Rate variation**
	g	%	g	%	$cm/h^{0.5}$	$Kg/m^2h^{0.5}$	%
Reference	2899.3		3340.4	15.2	3.03	7.04	
H_2O_brick (H)	2934.9	1,23	3289.0	12.1	2.90	6.73	-4.4
NaCl_brick (C)	2938.3	1,35	3299.5	12.3	2.78	6.44	-8.5
Na_2SO_4 brick (S)	2920.0	0,71	3293.2	12.8	2.96	6.86	-2.5

4. Ultrasound measurements

High-frequency ultrasound (US) signal propagation velocity measures at the two time periods were undertaken in Bologna on a representative number of mortar prisms and bricks. The wave velocity parameter is of great interest because related to the material density and mechanical properties (modulus of elasticity). Placed the transducers in contact with the specimen, the waves emitted by the sender are recorded by the receiver after travelling inside the material. Knowing the path length (in m), the signal travel time along the measurement path (time of flight, in μs) is used to calculate the signal velocity in the material (m/s). In addition, the signal attenuation (in dB), which is more sensitive than velocity to the material decay status is recorded. The US tests were carried out via a commercial, portable Olympus EPOCH 1000 system with signal amplifier. The probes (1 MHz in frequency, 13mm in diameter), were chosen because of the obtainable very high resolution. After conditioning the samples in a room at defined temperature and humidity, the US measures were collected in direct transmission of the signal along two directions of the samples: longitudinal and transversal. The longitudinal measures would cross areas with different degradation level. Hence, they should provide an average estimation of the decay in the entire sample. Instead, the 3 transversal measures (1 and 3 near the specimen's heads; 2: central) should allow obtaining information on the damage spread along each specimen. For the three sets of aged mortars, after 5 years the average longitudinal signal velocity is greater than the value obtained on undamaged samples (equal to 1915 m/s) (Fig. 2a). The highest values were recorded for the samples subjected to water rise (10% greater than the reference), whilst the lowest values for the Na_2SO_4 contaminated mortars (2% greater than reference). Attenuation values in longitudinal direction had an opposite trend: all the aged

mortars show a greater attenuation than the undamaged prisms. The highest attenuation value was obtained for Na_2SO_4 contaminated samples (~ 3dB) and the lowest (~ 1.8dB) for the mortar subjected to water rise (Fig. 2a). Similar results were obtained along the 3 transversal paths: the velocity and attenuation measured were greater than the respective values from the reference mortars (Fig. 2b). The greatest velocity and least attenuation belong to the water-contaminated prisms, whilst the other 2 types show comparable values of velocity but greater attenuation. A little difference is noticed among the 3 signal paths for all the aged prisms: the two paths near the specimen's heads, which is near or above the supposed salt-crystallisation areas, indicate slightly lower velocity than the central path. For the aged bricks, the US longitudinal values show higher velocity and unexpectedly lower attenuation than the undamaged samples (Fig. 3a): velocity varies of very small entity between the groups (about 10 m/s on average) but attenuation is distinct for the different contaminations (approx. 0.5dB relative changes). Along the transversal paths (Fig. 3b) both the velocity and attenuation for the 3 sets of aged bricks are comparable and slightly greater than the reference values.

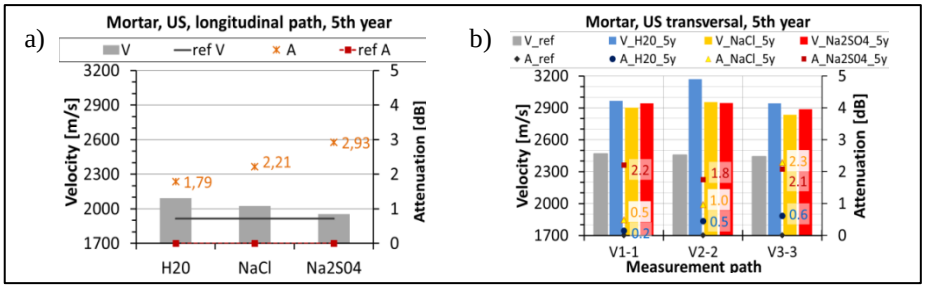

Fig. 2: US velocity and attenuation on mortar prisms: a) longitudinal measurements; b) transversal measurements

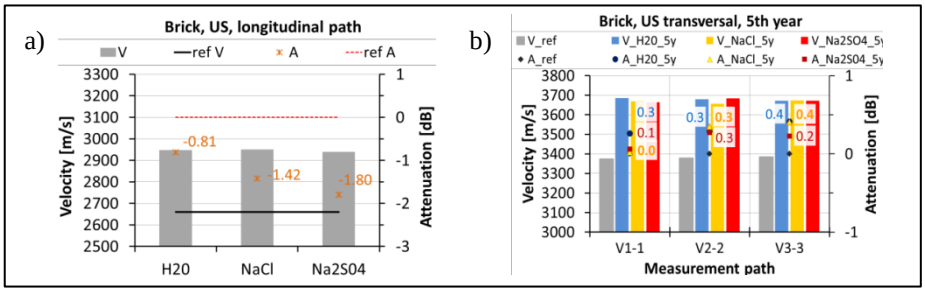

Fig. 3: US velocity and attenuation on bricks: a) longitudinal measurements; b) transversal measurements

5. Thin section analysis

By means of thin section analysis, the alteration of the different materials during the long-term ageing could be observed. Microscopic investigations on thin sections of the aged bricks and lime mortar specimens were carried out at the MPA of the University of Stuttgart to detect material structural changes at microscopic level. One thin section was

prepared per each brick and mortar ageing type. For a better visibility of the porosity the samples were vacuum-impregnated with a blue coloured resin. A Leitz Orthoplan-pol microscope was used in this study. The binder of the mortar prisms consists of a mixture of natural hydraulic lime and burnt lime. The microstructure of the unaged, carbonated reference sample shows pores and relict grains of dicalcium silicate (belite) (Fig. 4, left). Instead, non-hydraulic limes have very few (if any) belite grains in their texture. The carbonated (hardened) lime binder appears very dark to black under the microscope; with increasing hydraulic hardening the fine-grained binder matrix becomes more transparent and light (Fig. 4, left). The microscopic examination of the mortar after 5 years of ageing with provoked tap water capillary rise did not show significant changes in the texture and porosity of the hardened NHL-lime binder. On top of the surface only a very thin and slightly brown coloured layer of carbonate had developed as a result of the ageing process (Fig. 4, centre). At this stage of ageing, first cracks were developed close to the surface.

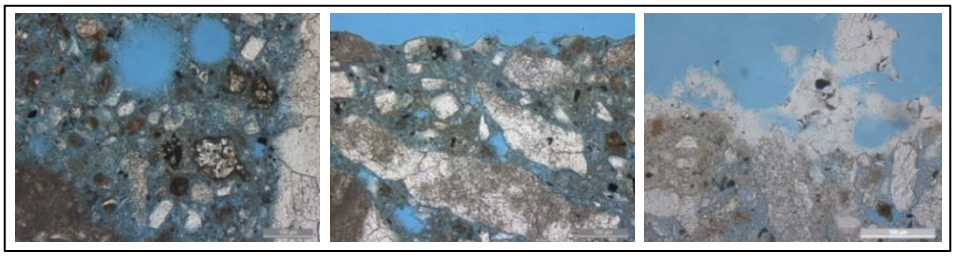

Fig. 4: Carbonated NHL-lime binder: unaged reference sample (left); hardened NHL-lime mortar treated with tap water (center) and subjected to ageing with NaCl rise (right).

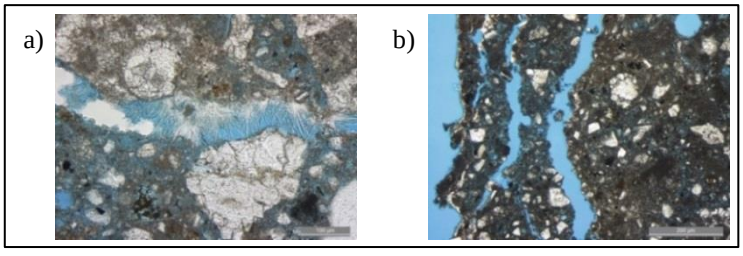

Fig. 5: NHL lime mortar, subjected to Na_2SO_4ageing: a) evolution of thenardite needles in the cracks; b) appearance of multiple crack system and spalling of the surface.

On the surface of the samples subjected to diluted NaCl capillary rise, now there is a crust of well-crystallized NaCl, whose crystals appear in light white colour (Fig. 4, right). Due to the high mobility and solubility of NaCl in the pore solution, the sodium chloride was enriched in the evaporation zone. Here again, there are single cracks parallel to the surface, similarly to the tap water contaminated sample. Instead, in contrast to NaCl ageing, the ageing process using diluted Na_2SO_4 brine forms multiple cracks inside the mortar fabric and some of them are now filled with distinct needles of thenardite as shown in Fig. 5a. The formation of a well-developed, multiple crack system after only 5 seasons of ageing with Na_2SO_4 capillary rise leads to intense spalling off the surface and rapid loss of mortar material (Fig. 5b). The low-fired clay bricks after 5 seasons of ageing showed fewer changes in texture than the NHL–mortar prisms under the optical microscope. In the case of treatment with tap water only some minor salt efflorescences (probably sulphates) appeared

at the surface in the evaporation zone (Fig. 6, left) together with some green accumulations indicating microbiological growth. Beneath the surface single cracks are formed, presumably caused by hydric swelling and shrinkage of relict clay minerals (e.g. illite, kaolinite). The breakdown of clay minerals and evolution of a mainly glassy matrix during firing process of bricks generates at higher temperatures, greater than approx. 900°C. Instead, low-fired bricks as used in this study still have a higher amount of clay minerals in the brick texture and a higher potential in hydric dilatation. The blue coloured resin of the impregnation procedure did not penetrate the bricks, therefore the cracks look white in thin section (Fig. 6, left). A slightly higher decay in the outer zone emerged after 5 ageing seasons with NaCl. The surface shows evidence of slight material loss (sanding) and lifted particles in the evaporation zone. Furthermore the formation of cracks increased (Fig. 6, centre). In case of Na_2SO_4 rise some visible salt efflorescence of thenardite ccurred in the evaporation zone and an initial indication of thin layers spalling of brick material is visible (Fig. 6, right).

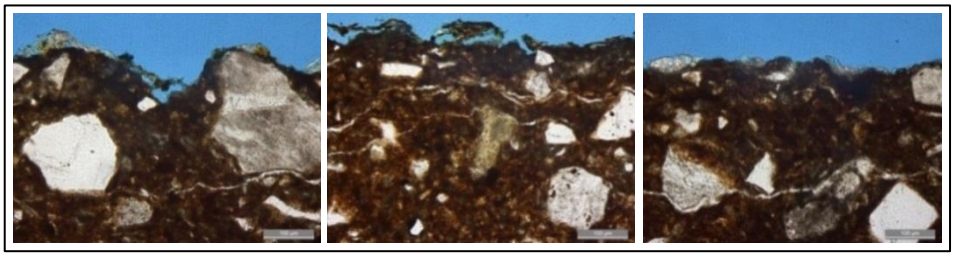

Fig. 6: Brick subjected to tap water rise (left), NaCl rise(centre) and Na_2SO_4 rise (right).

6. Discussion of results

The lime mortar prisms after 5 years of ageing show lower absorption rate than the same material in new conditions but surprisingly the lowest value belongs to water-contaminated mortars (-31%) and it is associated with a dry weight increase of these specimens compared to reference ones, whilst salt-contaminated prisms show a dry weight decrease, sign of material loss. Hence it appears that in the mortars, two factors are in competition: the weight increase due to carbonation progress in the "new" mortars together with the uptake and enrichment of salts on one side and the weight decrease due to solution processes of carbonate (and calcium hydroxide) in the binder during ageing on the other side. US tests confirmed this aspect: the aged mortars show slightly higher longitudinal velocity than the reference ones thus appearing denser (Na_2SO_4 prisms showing the least increase) but also remarkably high attenuation values, clear sign of decay. The 3 groups of mortars appear differently decayed in this order: mortars subjected to Na_2SO_4 rise, NaCl rise and water rise from most to least degraded, thus confirming the more damaging effect of Na_2SO_4 contamination compared to water or NaCl. Similar results were obtained in transversal direction. The combination of US velocity and attenuation values provides a good indication of the decay level. The presence of decay at microscopic scale is demonstrated by the thin section investigations of the aged mortar prisms. The evolution of a multiple crack system in the mortar subjected to Na_2SO_4 rise indicates a higher potential for damage than NaCl or water. Thus, at the microscopic scale, the greatest level of damage appears for the Na_2SO_4 contaminated prisms, followed by mortar prims subjected to NaCl rise and finally to water rise samples which show the least degradation. The aged bricks show

slightly lower suction rates than the reference material, thus appearing less affected by the conducted weathering than the mortar, but here the NaCl contaminated samples exhibit the lowest rate value, contrary to observations in mortars. All 3 sets of aged bricks show higher dry weight than reference (the weight increase is controlled by the uptake of salts and their accumulation) with the sulphate contaminated bricks showing the smallest weight increase (probably because of a greater loss of material due to damage). The US longitudinal values on aged bricks show higher velocity (confirming denser material) and lower attenuation than for undamaged ones: small velocity variations between the groups but distinct attenuation for the different contaminations (bricks subjected to Na_2SO_4 more damaged than others). This issue is confirmed by the thin section analysis as, at the microscope, the bricks showed less degradation than mortars subjected to the same ageing procedure. Anyhow, similarly to the results obtained for mortars, the least degradation appeared in the bricks subjected to water rise, followed by NaCl and finally Na_2SO_4 rise. In this brick series a slightly greater loss of material was evident by brick flakening.

7. Conclusions

Outcome from long-term monitoring of decay evolution in fired-clay bricks and lime mortar prisms affected by salt crystallisation is leading to novel observations as the values obtained by lab analyses and non-destructive tests are in agreement. At least in the initial phases (after 5 years of ageing) of the phenomenon, a clear increase in material density is associated with already detectable damage. Recorded changes in physical and mechanical parameters are of interest from different viewpoints: to evaluate changes in the masonry materials diffusivity, to create a database which does not exist in these terms, as input for numerical simulations aimed at properly modelling the diffusion processes in porous materials, at establishing degradation indexes to predict the decay rate in masonry structures. This latter aspect is of primary importance for architects/engineers dealing with historic structures preservation.

References

Colla, C., 2011, Comparative testing for improved diagnosis of historic structures, Proc. EWCHP-2011, Krüger M. (Ed.), Fraunhofer Verlag, Berlin, 140-147.

EN 12370, 2001, Natural stone test methods – Det. of resistance to salt crystallization.

Gabrielli, E., Colla, C., 2012, Laboratory investigation of damp rise in porous masonry construction materials, Proc. of SAHC 2012, Jasieńko J. (Ed.), Dolnośląskie Wydawnictwo Edukacyjne, Wroclaw, Poland, 659 – 667.

Gabrielli, E., Colla, C., Gruener, F., 2012, Evaluation of damage evolution in masonry due to environmental parameters and salt capillary rise, Proc. 15th IB2MaC, Roman H.R., Parsekian G.A. (Eds.), Florianopolis, Brazil, 10 pp.

RILEM PEM/25, 1980, V. Durability tests. Test No.V.1a, Crystallisation test by total immersion; V.2 Cryst. test by partial immersion; II.6 Water absorption coefficient.

UNI EN ISO 15801, 2010, Conservation of cultural property. Test methods: determination of water absorption by capillarity.

VDI 3797, 1980, Testing of the presumable resistance of preserved and not preserved natural stone against air pollutants-Sodium sulphate crystallization test.

ASSESSMENT OF THE PHYSICAL BEHAVIOUR OF HISTORIC BRICKS AND THEIR MECHANICAL CHARACTERISTICS VIA ABSORPTION AND ULTRASOUND TESTS

C. Colla[1*] and E. Gabrielli[1]

Abstract

Capillary suction rate in construction materials is probably the main parameter controlling decay phenomena related to water together with environmental conditions and it is directly related to porosity. On site, when performing non-destructive tests on masonry such as acoustic tests the moisture content distribution or other building material physical properties, i.e. density or porosity, are generally unknown. These affect the acoustic signal propagation and attenuation and, in historic brick masonry, it is expected to find high variability of them. Guidance in this sense cannot be found in test standards because of the almost infinite number of masonries. The paper reports laboratory work conducted on several fired clay bricks sampled from historic buildings, of diverse dimensions, age and health-state conditions. Capillary rise tests were carried out and suction velocities were determined. Moreover, hydrostatic and saturated weights were measured. In addition, the bricks were mechanically characterised via high-frequency ultrasonic tests, repeated in dry and saturated material conditions. The results are useful for a better insight into the hygro-physical variations and behaviour of historic masonry and for a more accurate mechanical characterisation of structural elements in historic constructions.

Keywords: historic bricks, damp rise, open porosity, ultrasound test, physical properties

1. Introduction and aim of the work

Capillary suction rate in construction materials is probably the main parameter controlling decay phenomena related to water together with environmental conditions. This is directly related to porosity, i.e. pore size, pore distribution and open porosity (Cultrone *et al.*, 2005; Hall and Hoff, 2007). On-site, when performing non-destructive tests on masonry – such as acoustic investigations with the aim of assessing masonry wall quality, health state and presence of heterogeneities (Colla and Pascale, 2010) - the operator generally knows neither the moisture content distribution nor other physical properties of the building materials (i.e. density or porosity). Nonetheless, these parameters together with the path lengths and material heterogeneity affect the acoustic signal propagation and attenuation. Some studies clearly showed that, in the case of stone, moisture content highly influences the ultrasonic pulse velocity and that saturation increases the compressional velocities (Vasconcelos *et al.*, 2008). In historic brick masonry, due to variability of age, geographical area and manufacture as well as of material degradation, it is expected to find high

[1] C. Colla* and E. Gabrielli
Engineering Faculty, University of Bologna, Italy
camilla.colla@unibo.it

*corresponding author

variability of those parameters (Colla *et al.*, 2014). Guidance in this sense cannot be found in standards because of the almost infinite number of masonries. Similarly, in the literature only little and very sparse information is found, sometimes contradictory. As an example, in (Lopez-Arce *et al.*, 2003) it was found, for ancient - apparently sound- bricks of Toledo, a water absorption ranging between 19% and 22%, whilst (Stefanidou *et al.*, 2015) stated that water absorption of old sound bricks is typically around 15%. In the present, on-going lab experimental work, several laboratory tests were carried out on bricks sampled from existing or historic masonry buildings to non-destructively characterise their main physical and mechanical properties. The overall aim is to obtain a better understanding of the hygro-physical properties, variations and behaviour of bricks, which are the main constituent material of masonry structures. The results are intended to be of aid for obtaining a better characterization of historic masonry behaviour.

2. Brief description of the sampled brick units

The 19 fired-clay brick units or portions considered had different origins, composition, texture, size, age and health-state conditions. Some of them were handmade, others industrially produced (Table. 1).

Tab. 1: Studied specimens.

Specimen code	Type and origin
M_...	Portions of handmade historic bricks collected in Mirandola, Italy
TOR	Portion of historic brick from “Clock tower” in Mirandola, Italy
V1 and V2	Handmade brick, sampled from Palazzina della Viola (Bologna, Italy)
GHR1 & GHR2	Not original and handmade bricks from Ghirlandina tower (Modena, IT);
VIC F1	Portion of handmade frogged brick, from a historic English building
VIC 1	Portion of handmade brick, pink, sampled from a historic English building
FE1	Handmade brick unit from a historic building in Finale Emilia (Italy)
CPOP	Portion of industrial brick from “Casa Popolare via Carracci, Bologna"(I)
SF1 and SF2	Portion and full industrial brick unit sampled from a school in Forlì (Italy)
IBL	New low-fired clay bricks and portions (producer: “IBL”, Bologna, IT)
NB	New fired-clay brick units (producer: “Brioni”, Mantua, Italy)

Most of the specimens were from historical buildings located in Bologna (North Italy) or in the surroundings. For example, 9 specimens (coded with "M_..."and TOR) were taken from ancient structures situated in Mirandola (Modena province) following the 2012 earthquake. Instead, V1 and V2 are full-units of handmade clay-bricks, both sampled in the 15th C. building of Palazzina della Viola, in Bologna, whilst both the full-bricks GHR1 and GHR2 the first industrially produced, probably for restoration, and the second handmade, were collected inside the 13th C. Ghirlandina bell-tower of Modena. Only two specimens were from outside Italy: VIC F1 and VIC1 are from historic buildings in England, both handmade: the first is a frog brick, presenting a cavity in one of the bedding faces. New industrial fired-clay bricks from two Italian manufacturers were considered for comparison. Colours ranged from a light-red/pink of V1, VIC 1 and SF1 to the yellowish of GHR1, to the purple red of VIC F1 (Fig. 1a). Macropores and large heterogeneities were visible both on the handmade brick portions collected in Mirandola (Colla *et al.*, 2014) and in the frog-brick from England (Fig. 1b). Decay and manufacturing defects, such as longitudinal or transversal cracks, were detected, i.e. in VIC F1 and CPOP.

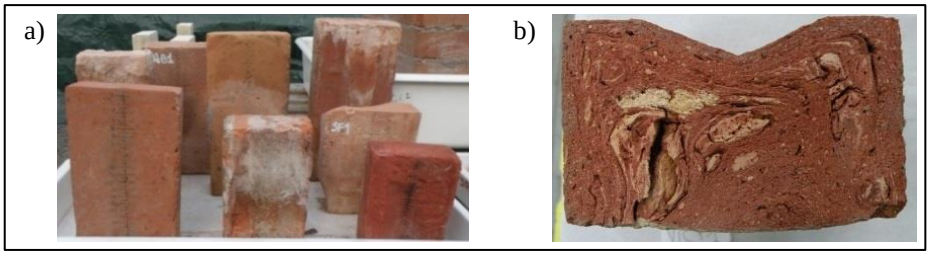

Fig. 1: a) some of the tested brick units and portions; b) close-up view of brick VIC F1.

3. Physical characterization

Among the several different laboratory tests undertaken to evaluate the characteristic physical properties of the bricks, to determine the apparent density and open porosity, first the values of dry, saturated and hydrostatic weights of the specimens were measured, according to EN 1936: 2007. Due to the limited dimensions of part of the testing equipment available for such tests at the mineralogical laboratory of the DICAM dept., these measures could be carried out only on the smaller historic brick units. Two portions of new bricks underwent the same test for comparison purposes. The testing procedure consisted in: drying the specimens to constant mass in oven at 70ºC; placing them for 2h into a vacuum vessel at pressure lower than the atmospheric one to eliminate the air contained into the open pores; inserting demineralized water into the vessel at the same pressure (thus causing forced water absorption) and finally, leaving the immersed specimens under water for 24h at atmospheric pressure (Fig. 2, left). The specimens' hydrostatic and saturated weights were measured and, as they were irregular in dimension, the volumes were calculated too. The apparent density, ρ_A (kg/m^3) and open porosity, p_0 (%) were estimated according to:

$$\rho_A = \left(\frac{m_d}{m_s - m_h}\right) \cdot \rho_w \qquad \textit{(Eq. 1)}$$

$$p_o = \left(\frac{m_s - m_d}{m_s - m_h}\right) \cdot 100 \qquad \textit{(Eq. 2)}$$

where: m_d is the mass of dry specimen; m_s is the saturated mass; m_h is the mass in water; ρ_w is the density of water (in our case: 997.565 kg/m^3).

On average, historic bricks show lower values of apparent density and higher open porosity than the new ones, which is in line with the findings of other authors (Stefanidou *et al.*, 2015). Their mean value of ρ_A is about 11.7% lower than for new units. Accordingly, open porosity is, on average, about 26.5% greater than for new bricks (Tab. 2). A strong linear relationship between apparent density and open porosity values was found for all the units (Fig. 2, center). The density values, ρ, of the 10 remaining sampled brick units (with volumes greater than 0.7 dm^3) were determined according to the basic relationship: $\rho = m/V$ where m (kg) is the mass of the specimen and V (m^3) the volume. The weighting was repeated twice, considering both dry and saturated specimens. In the first case, the measures were carried out after drying the units in oven at 60°C up to constant mass whilst in the second case specimens weighting was after total immersion in water for at least 72 h and up to constant mass. As these units were regular, the volumes were calculated from the average dimensions by recording at least three measures for each side. Overall, the dry density of these sampled brick units varies between 1449.8 (FE1) and 1789.4 kg/m^3 (SF1), whilst for new bricks between 1540.1 and 1797.6 kg/m^3 (Fig. 2, right). In the graph, the vertical dotted line separates the specimens which did not undergo to the treatment in vacuum vessel (to the left of the line) from the others (to the right side). These values were later used to non-destructively estimate the elastic modulus from ultrasound velocity.

Tab. 1: Apparent density and open porosity for new and historic brick portions.

Specimen	m_d	m_h	m_s	**Volume**	ρ_A	P_o
	g	g	g	dm^3	kg/m^3	%
IBL1-rif	724.46	454.91	856.95	0.40	1797.57	32.95
IBL2-rif	691.25	434.5	820.83	0.39	1784.92	33.54
Average values	*707.85*	*444.70*	*838.89*	*0.395*	*1791.25*	*33.25*
TOR	1022.29	648.5	1322.23	0.68	1513.66	44.52
M_MZ0	323	204.95	404.41	0.20	1615.43	40.82
M_MZ0_2D	323.91	205.7	406.10	0.20	1612.38	41.01
M_MZ0_1C	307.61	194.83	372.62	0.18	1725.97	36.57
M_MZ3_4	349.05	220.64	451.30	0.23	1509.58	44.33
M_D2_A	600.68	380.73	756.61	0.38	1594.17	41.48
M_D2_B	543.19	344.59	684.77	0.34	1592.88	41.62
M_D7	303.01	191.96	384.62	0.19	1568.94	42.36
M_U4_D	509.13	324.81	664.59	0.34	1494.76	45.75
Average values	*475.76*	*301.86*	*605.25*	*0.30*	*1580.86*	*42.05*

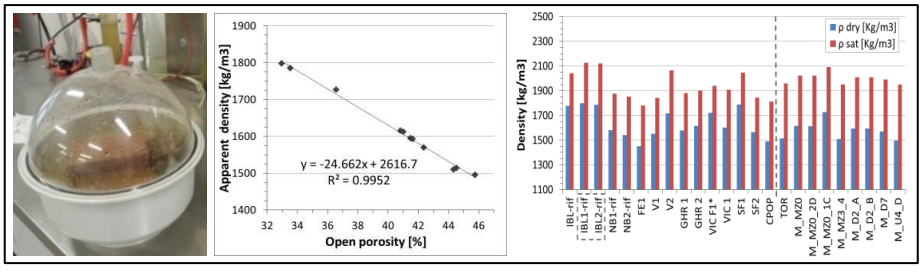

Fig. 2: Water absorption in vacuum (lf.); measured open porosity vs apparent density values (center); dry and saturated brick densities (right).

In addition, capillary water absorption tests were carried out to evaluate the hydric behaviour of all the 19 historic brick units (Tab. 4). For comparison purposes, new brick units of the two manufacturers were also tested in the same conditions (Tab. 3), that is were carried out in a climatic chamber of the LISG lab of Bologna University. The procedure at constant values of air temperature (20°C) and relative humidity (60%) is also described in (Colla *et al.*, 2016). In brief, after drying the specimens to constant mass, these were placed standing into a basin with constant height of demineralized water. The water front migration height was monitored over the time and the suction velocity values (cm/h$^{0.5}$) were calculated as the slope of each absorption curve (Fig. 3). Finally, it was estimated the capillary suction rate which is the amount of water absorbed in the unit of time by the unit of specimen's area in contact with the water container. Note that it was not possible to determine the suction rate for all the tested units because it is a function of the porosity, which was available only for the specimens tested according to the vacuum procedure. Thus, the suction rate was calculated only for 9 historic brick portions – porosity values of Tab. 2- and for the new units. In this latter case, the porosity values were obtained in a different test by mercury intrusion porosimetry (MIP): 23.2% for IBL, 30.77% for NB bricks (Colla *et al.*, 2014). Porosity of the reference new bricks (they show similar suction velocity but quite different rates, Tab. 3) were obtained from water absorption tests repeated, respectively, on three and two units. Results on sampled bricks are more scattered than for new bricks (Tab. 4); tests lasted between 3 hours and 6 days for different specimens. Old bricks show wide variability of suction velocity values which reflects their diverse characteristics and origins, however, Fig. 3 right shows that most absorption curves are concentrated in a narrow zone, with suction velocities between 3.01 and 6.85 cm/h$^{0.5}$. Note that for handmade bricks, hygric behaviour is not clearly distinct from industrially produced bricks. However, considering all specimens, the average suction velocity of sampled units is approx. 30% greater than for new bricks. The absorbed water amount does not appear directly related with suction velocity: the slowest unit, SF1, shows the least amount of absorbed water, but the fastest unit, VIC F1 has not the greatest value, which instead is shown by TOR. This trend is probably to be attributed to the diverse dimensions and distribution of pores. On average, the amount of absorbed water for sampled units is about 8% greater than for new bricks. Much more pronounced differences are found in capillary suction rate values: on average, the "old" specimens show a rate approximately double than new ones (Tab. 3 and Tab. 4).

Tab. 3: New bricks: results of capillary rise tests.

Specimen	Start weight	Final weight	Absorbed water	Suction velocity	Capillary suction rate
	g	g	%	$cm/h^{0.5}$	$kg/m^2h^{0.5}$
IBL	2899.3	3340.4	15.2	3.03	7.04
NB	2467.1	2946.9	19.4	3.78	11.63
Average	*2683.2*	*3143.6*	*17.3*	*3.40*	*9.33*
CoV (%)	*9*	*7*	*14*	*20*	*32*

Tab. 4: Historic brick units: results of capillary rise tests

Specimen	Start weight	Final weight	Absorbed water	Suction velocity	Capillary suction rate
	g	g	%	$cm/h^{0.5}$	$kg/m^2h^{0.5}$
TOR	1025.40	1280.80	24.91	3.97	17.67
M_MZ0	381.00	452.80	18.85	4.10	16.75
M_MZ0_2D	395.10	467.40	18.30	4.16	17.07
M_MZ0_1C	398.80	453.10	13.62	4.91	17.96
M_MZ3_4	350.20	408.50	16.65	3.01	13.34
M_D2_A	603.60	725.40	20.18	5.38	22.32
M_D2_B	544.40	659.00	21.05	5.55	23.11
M_D7	303.20	369.00	21.70	4.01	16.97
M_U4_D	508.90	631.20	24.03	6.85	31.34
FE1	2420.40	2941.50	21.53	5.29	/
V1	3982.60	4728.90	18.74	3.85	/
V2 *	3562.50	4382.20	23.01	4.21	/
GHR 1	3519.80	4156.70	18.09	4.44	/
GHR 2 *	5109.60	5940.20	16.26	4.23	/
VIC F1	1797.90	2010.30	11.81	10.65	/
VIC 1	2207.50	2672.20	21.05	3.48	/
SF 1	2355.90	2506.20	6.38	0.81	/
SF 2 *	3713.80	4372.90	17.75	0.87	/
CPOP	2685	3259.60	21.40	4.08	/
Average	*1887.66*	*2232.52*	*18.70*	*4.41*	*19.61*
CoV (%)	*81*	*81*	*24*	*47*	*27*

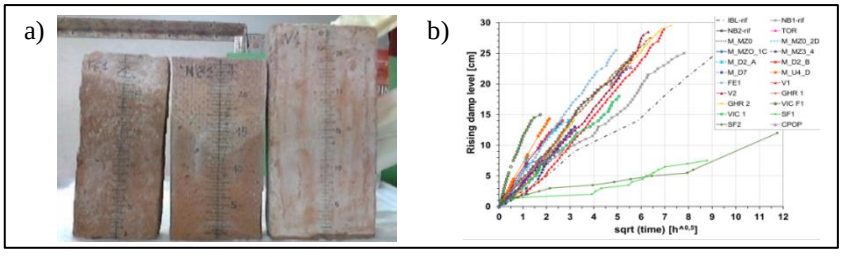

Fig. 3: Capillary rise test in different bricks (a); brick absorption curves (b).

4. Non-destructive testing for mechanical characterization

Ultrasound tests were undertaken on bricks to non-destructively evaluate the elastic-mechanical characteristic. Signals were propagated in two perpendicular directions of the units, longitudinal and transversal (bedding direction), via a portable Olympus EPOCH 1000 system with two probes of 1 MHz frequency and 13mm diameter. The tests were carried out in direct transmission mode, being the transmitter and receiver located directly opposite each other on parallel faces. Once the transducers are in contact with the specimen, the receiver records the arriving waves after these have crossed the material. Knowing the path length (in m), the signal travel time along the measure path (in μs) is used to calculate the signal velocity (m/s). The difference in velocity is an index of the diverse mechanical material properties. Then, the velocity values, *V*, are used to estimate the dynamic elastic modulus, E_d (GPa):

$$E_d = \rho \cdot V^2 \cdot \sqrt{\frac{(1+\nu)\cdot(1-2\cdot\nu)}{(1-\nu)}} \qquad \textit{(Eq. 3)}$$

where ρ is the specimen density and ν is the Poisson coefficient (herein set to 0.2). The dynamic modulus may be used to estimate the static elastic modulus by corrective factors (Colla, Pascale, 2010). To check the influence of water content on the ultrasonic velocity, the tests were repeated twice, in dry (oven dried at 60°) and saturated materials conditions (vacuum assisted method or by total immersion). It is known that in stones, the presence of water into the pores may increase the velocity up to 50% of the dry value (EN 14579:2004), thus it would apparently increase the estimated value of elastic modulus. Historic units show quite variable average longitudinal velocities (V_{long}) in both material conditions (Tab. 5, Fig. 4a): 0.5% lower and 10.5% greater than for new bricks in dry and in saturated conditions, respectively. No values were recorded for VIC F1 because the signal could not cross the large heterogeneities. Specimens CPOP, SF2 and FE1 showed in both materials conditions lower velocity (about 60%) than new units: CPOP and SF2 were visibly cracked; FE1 instead appeared sound. Instead, on average, the elastic dynamic modulus value, $E_{d,long}$ for dry sampled bricks is about 4% greater than for new bricks and in saturated conditions, the difference is much more accentuated (33%; Fig. 4b). Note that only units subjected to vacuum assisted water absorption show saturated velocity values always higher than dry ones: it is likely that the absorption procedure by simple total immersion of the larger units was unable to fill in all the pores. Similar considerations arise from results of ultrasound testing in transversal direction (bedding direction of the bricks). In the sampled specimens, most dry velocities are lower than saturated velocities (Fig. 4c).

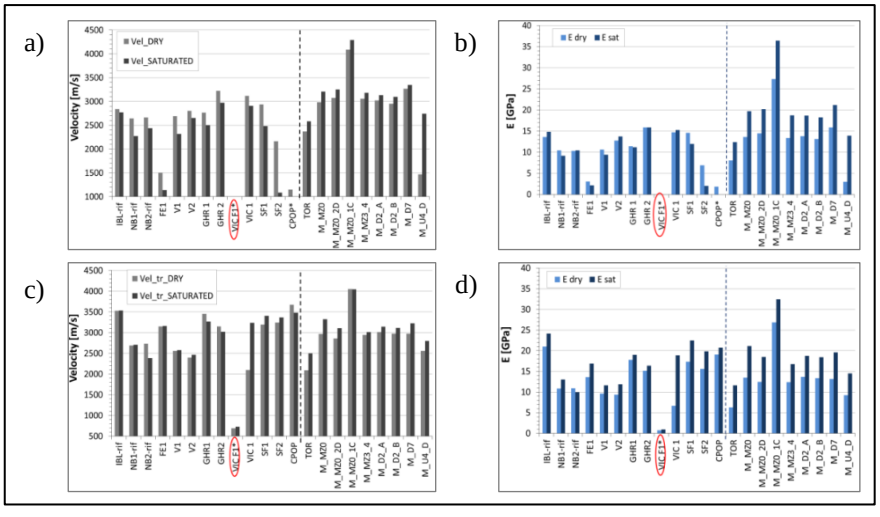

Fig. 4: Historic and new bricks: a and c) longitudinal US velocity; b and d) dynamic elastic modulus.

Tab. 5: New and historic brick units: US results in longitudinal and transversal directions.

Parameter		New		Old	
		Dry	**Sat.**	**Dry (specimen code)**	**Sat. (specimen code)**
$V_{long.}$ (m/s)	min	2640.4	2274.5	1145 (CPOP)	1083.2 (SF2)
	max	2841.1	2771.9	4086 (M_MZO_1C)	4288.2 (M_MZO_1C)
	average	**2714**	**2495**	**2700**	**2758**
	CoV (%)	*4.07*	*10.1*	*27.02*	*27.8*
$E_{d, long.}$ (GPa)	min	10.34	9.21	1.85 (CPOP)	2.05 (SF2)
	max	13.62	14.88	27.34 (M_MZO_1C)	36.47 (M_MZO_1C)
	average	**11.47**	**11.51**	**11.93**	**15.38**
	CoV (%)	*16.2*	*25.8*	*49.9*	*51*
$V_{transv.}$ (m/s)	min	2687.4	2381.7	2086.6 (TOR)	2461 (V2)
	max	3529.9	3534.7	4048.6 (M_MZO_1C)	(M_MZO_1C)
	average	**2984**	**2874**	**2843**	**2997**
	CoV (%)	*15.8*	*20.7*	*25.12*	*22*
$E_{d, transv.}$ (GPa)	min	10.8	9.97	0.8 (VIC F1)	0.97 (VIC F1)
	max	21.02	24.2	26.8 (M_MZO_1C)	32.4 (M_MZO_1C)
	average	**14.3**	**15.7**	**12.9**	**17.4**
	CoV (%)	*41*	*47*	*43*	*35*

US transversal value was measured also for VICF1, although very low velocity was detected (dry: 691.3; saturated: 727.0 m/s) clearly indicating presence of voids or cracks inside the material. On average, old bricks exhibited lower dry velocity and higher saturated velocity than new ones. The same trend was found for transversal dynamic elastic modulus (Fig. 4d), but variability is too wide to clearly extrapolate a tendency (Tab. 5 bottom).

5. Conclusions

In this on-going experimental work, the physical-mechanical behaviour of bricks sampled from ancient masonry structures was non-destructively assessed. Bricks had different ages, colours, textures and health-state conditions. This variability is clearly reflected on the measured properties, both in the hydric and mechanical behaviours. Despite these peculiarities which enforce the idea of considering each historic building uniqueness, general considerations may be extrapolated. On average, the sampled bricks show greater open porosity, lower apparent density, higher suction velocities and absorption rates than new bricks. The "old" specimens show higher velocity and dynamic modulus than new units. Moreover, fully-saturated bricks show higher velocity than in the dry case.

References

Colla, C., Gabrielli, E., Grüner, F., 2016, Long-term monitoring of decay evolution in bricks and lime mortar affected by salt crystallisation, 13th Int. Congress on the Deterioration and Conservation of Stone, Peislay, (submitted).

Colla, C., Gabrielli, E., Savoia, M., 2014, Laboratory experience of flood effects monitoring in fired-clay bricks and adobe, Proc. of 9IMC, 7-9 July, Guimarães, PT, 12 pp.

Colla, C., Pascale, G., 2010, Non-destructive and semi-destructive tests for the characterisation of the masonries of the Ghirlandina tower in Modena, in La torre Ghirlandina – storia e restauro, R. Cadignani (Ed.), Rome, 218-227.

Cultrone G., Sidrabab, I., Sebastian, E., 2005, Mineralogical and physical characterization of the bricks used in the construction of the "Triangul Bastion", Riga (Latvia), Applied Clay Science 28: 297– 308.

EN 1936, 2007 Natural stone test methods. Determination of real density and apparent density, and of total and open porosity. EN 14579, 2004 Natural stone test methods. Determination of sound speed propagation.

Hall, C., Hoff, W.D., 2007 Rising damp: capillary rise dynamics in walls, In: Proc. *R. Soc. A*, 463, 1871-1884.

Lopez-Arce, P., Garcia-Guinea, J., Gracia, M., Obis, J., 2003, Bricks in historical buildings of Toledo City, Materials Characterization 50: 59– 68.

Stefanidou, M., Papayianni, I., Pachta, V., 2015, Analysis and characterization of Roman and Byzantine fired bricks from Greece, Materials and Structures 48: 2251-2260.

Vasconcelos, G., Lourenco, P.B., Alves, C.A.S., Pamplona J., 2008, Ultrasonic evaluation of the physical and mechanical properties of granites, Ultrasonics 48: 453-466.

This page has been left intentionally blank.

ACRYLIC-BASED MORTAR FOR STONE REPAIR: A VISCOELASTIC ANALYSIS OF THE THERMAL STRESSES

T. Demoulin [1], G.W. Scherer [2], F. Girardet [3] and R.J. Flatt [1*]

Abstract

In this study we analyse the magnitude of the thermal stresses that originate in an acrylic-based repair mortar used for the reprofiling of natural sandstone. This kind of mortar displays the interesting property of reversibility in an appropriate solvent, but also possesses a high thermal expansion that might expose the stone that it aims to repair to high thermal stresses. However, due to its polymeric nature, it also has time- and temperature-dependent mechanical properties that could relieve the stresses, depending on the temperature of the material and on the heating or cooling rate. To evaluate the risk of thermal stresses we propose an analytical solution that considers the viscoelasticity of the repair layer. The viscoelastic behaviour of the artificial stone has been characterised by stress relaxation experiments at different temperatures in the laboratory. The numerical analysis is based on two situations that could be of potential danger: a high heating during summer time, and a very fast cooling as could happen during an extreme weather event. The analysis shows that the relaxation time of the repair mortar allows relaxation of most of the stresses that develop due to the mismatch of thermal expansion coefficients. In conclusion, we show that viscoelastic relaxation accounts for the durability of this particular repair material, as observed by the practitioners.

Keywords: repair mortar, acrylic resin, thermal stress, viscoelasticity, compatibility

1. Introduction

In historical buildings, repair of altered stone using a "plastic" mortar is an attractive strategy, since it avoids the full replacement of the original stone and extends its lifetime. The term "plastic" refers to the workability of the mortar in its fresh state rather than to a polymer component. The action of filling lost parts of stone with plastic mortar is called "reprofiling" or "filling", and is regarded as a minimal intervention that complies with modern building conservation philosophy (Forster 2010). It is one of the reasons that explains the increased use of plastic mortar in the repair of historical stone masonry, as pointed out by Torney in Scotland (Torney *et al.* 2012). However, the stresses that could arise due to a mismatch of dimensional changes (thermal expansion or hygric/hydric swelling) between the repair layer and the stone substrate might significantly reduce the

[1] T. Demoulin and R.J. Flatt*
Institute of Building Materials, ETH Zurich, Zurich, Switzerland
flattr@ethz.ch

[2] G.W. Scherer
Civil and Environmental Engineering Department, Princeton University, United States of America

[3] F. Girardet
RINO Sarl, Blonay, Switzerland

*corresponding author

durability of the repair and affect the historical material. A more comprehensive understanding of the material properties and the materials interactions would provide the foundation to decide in which situations repair mortars could be beneficial or not. Here we focus on a particular repair mortar that had been developed in the late seventies by Prof. Furlan's team in the Ecole Polytechnique Fédérale de Lausanne (EPFL). The binder of the mortar (hereafter also called artificial stone) is an acrylic polymer, which gives interesting properties of reversibility to the mortar. By applying an appropriate solvent, it can be removed without breaking the original stone substrate when, or if, time has come for another repair. Indeed, reversibility was proven to be effective after more than thirty years of use in the townhall of Lausanne. Another interesting feature lies in its ability, after hardening, to be worked like the sandstone due to its similar stiffness, thus making the integration of the repair possible by the normal tools of a stone carver. However the two materials display very different physical properties. The sandstone is a soft elastic material, while the mortar has the properties of the acrylic resin, including viscoelasticity, namely time and temperature-dependent mechanical properties, and a thermal expansion coefficient more than twice that of the molasse sandstone. The aim of this work is to assess whether thermal stresses can be a threat for the integrity of the repair and the historical stone. We present the general approach for this and illustrate its use with two situations that could represent a risk for the repair. The physical properties of the materials, namely the thermal expansion coefficient, the tensile strength and the viscoelastic modulus of the artificial stone have been measured in the laboratory. The numerical evaluation is achieved through the development of an analytical solution presented below.

2. Mechanical analysis of the repair

The analysis follows the steps and the notation developed in the analysis of the sandwich seal (Scherer 1986) and of which a detailed application to repair mortars can be found elsewhere (Demoulin *et al.* 2016,). The simplest case of reprofiling can be seen as a bilayer composite material made of a thin mortar layer ("patch") on a thick stone substrate. If we extract a part of the composite from the wall, it would look like the scheme of Fig. 1a. The two materials being bound together, if they have dissimilar expansion properties, mismatch forces arise at the interface and internal stresses built-up. That is the case for thermal expansion mismatch, as illustrated in Fig. 1b.

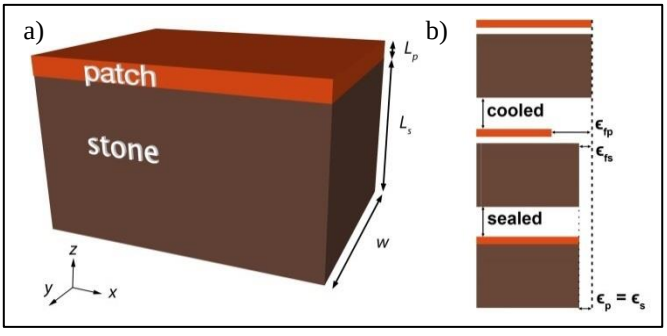

Fig. 1: a) Schematic of the patch layer on top of the stone substrate; b) Illustration of the thermal expansion mismatch between the two materials.

Consider two plates of repair mortar and natural stone of equal width, but of different thicknesses, L_p for the patch and L_s for the stone substrate; after cooling, the patch contracts by $\epsilon_{f,p}$ and the stone by $\epsilon_{f,s}$, respectively the free strain of the patch and the stone. However, if they were connected, they are constrained to contract by an amount $\epsilon_p = \epsilon_s$ intermediate between $\epsilon_{f,p}$ and $\epsilon_{f,s}$. In a typical reprofiling, the thickness of the patch is very small compared to the thickness of the stone substrate, on the order of 1/20, thus $L_s >> L_p$; moreover, the elastic modulus of the patch is lower than that of the stone, so the natural stone imposes its deformation on the repair mortar. The stress induced in the repair layer is

$$\sigma_p = (\frac{E_p}{1-\nu_p})(\epsilon_{f,s} - \epsilon_{f,p}) \qquad \textit{(Eq. 1)}$$

where E_p is the instantaneous elastic modulus of the patch and ν_p the Poisson's ratio of the patch. This equation describes a situation where the stress is maximal in the repair layer. The stress induced in the stone, σ_s, can be obtained by considering the edge of the composite, where the net force in the isolated sample must be zero, thus giving:

$$\sigma_s = -\frac{L_p}{L_s}\sigma_p \qquad \textit{(Eq. 2)}$$

But, since the repair material has a polymeric nature and exhibits a viscoelastic behaviour, the stresses developed in the mortar might be relaxed, depending on the temperature of the material and on the heating or cooling rate. The relaxation function that describes the viscoelasticity of the repair material, has the form of a stretched exponential:

$$\psi[t] = \psi_0 + (1-\psi_0)\exp(-(t/\tau)^\beta) \qquad \textit{(Eq. 3)}$$

where ψ is the dimensionless relaxation function, ψ_0 the residual fraction of the stress that does not relax, τ the relaxation time and β an exponent ($0 < \beta < 1$).

The viscoelastic solution of Eq. 1, according to the correspondence principle, is found by substituting the elastic quantities by their appropriate transformed quantities in the Laplace domain (Scherer 1986; Flügge 1975). After inversion in the time domain, and substantial mathematical development, we find that the stress in the patch is expressed as

$$\sigma_p = \frac{E_p}{1-\upsilon_p}(\psi_0(\epsilon_{f,s} - \epsilon_{f,p}) + (1-\psi_0)(\alpha_s\Delta_s - \alpha_p\Delta_p)) \qquad \textit{(Eq. 4)}$$

where α_s and α_p are the coefficients of thermal expansion of the stone and the patch, respectively, and

$$\Delta_s = \int_0^t \exp(-(\int_{t'}^t \frac{dt''}{\tau_0 \exp(\frac{Q}{T_p[t'']})})^\beta)\frac{dT_s}{dt'}dt' \qquad \textit{(Eq. 5)}$$

and

$$\Delta_p = \int_0^t \exp(-(\int_{t'}^t \frac{dt''}{\tau_0 \exp(\frac{Q}{T_p[t'']})})^\beta)\frac{dT_p}{dt'}dt' \qquad \textit{(Eq. 6)}$$

are the integrals that consider the difference of temperature between the two materials (as the massive wall responds more slowly to environmental changes than the thin patch). Equation 4 can be used to calculate the stresses induced by a thick elastic substrate in a thin viscoelastic layer on the central region of the composite, with the two materials having different inner temperatures. In turn, this makes it possible to calculate the stresses affecting the thick elastic layer (the stone), simply by using Eq. 2.

3. Materials and methods

3.1. Thermal expansion

The thermal expansion was measured on cubes of 1 cm^3 using a Dynamic Mechanical Analyser from Perkin Elmer (DMA 7e). The dynamic mode is not used in this experiment, which is thus equivalent to using the device as a dilatometer. The temperature range went from -20 to +60°C with a heating rate of 0.5°C/min under nitrogen flow.

3.2. Tensile strength

The direct tensile strength tests were performed on a universal testing machine Zwick 1454 with a 10 kN load cell, on six specimens of natural stone and five of artificial stone. The cylindrical samples had diameters of 20 mm and lengths of 50 mm on average. The natural stone was an Ostermundigen blue sandstone, widely spread in the historical buildings in Switzerland. The bedding has been chosen perpendicular to the strain. The artificial stone was prepared with ground Ostermundigen blue mixed with 20 wt% of Plextol D512. Since the T_g of the polymer is around 20°C, and consequently the relaxation of the stresses at room temperature is very fast, the samples were conditioned in a climatic chamber and wrapped in rockwool before the test to ensure an inner temperature lower than 15°C, as measured by a thermocouple embedded in a sample. The strain rate adopted was 0.5 mm/min.

3.3. Stress relaxation

The viscoelasticity of the artificial stone is studied through the measurement of the relaxation of a load at a constant strain. The relaxation tests are three-point bending tests performed with a homemade device consisting of a mechanical loading stage and a computer-assisted control unit. A thorough description of the device is given in (Cai 2012). The specimens are in the form of rectangular beams with thickness of 4 mm, width of 12 mm and length of 50 mm, while the length of the support span is 48 mm, allowing an aspect ratio of 1:3:12. The strain rate adopted was 0.045 mm/min. The dependence of the relaxation on temperature is studied by repeating the measurement in a climatic chamber at temperatures from -5 to 25°C. Higher temperatures, even though often reached during summer at the surface of the building, are not relevant because they are higher than the glass transition temperature of the polymer (T_g = 20°C), where the relaxation is quasi-instantaneous.

4. Results

4.1. Thermal expansion

The thermal expansion coefficient of the artificial stone, before the glass transition temperature T_g, is 2.5 times higher than that of the natural stone. The values are reported in Tab. 1 below.

Tab. 1: Tensile strength and thermal expansion of the materials.

Specimen	Tensile strength	Coefficient of thermal expansion
	MPa	10^{-6} K^{-1}
Artificial stone	2.7	32.7
Natural stone (dry)	1.0	12.9
Natural stone (wet)	0.3	-

4.2. Tensile strength

The two materials have a relatively low tensile strength, as reported in Tab. 1. The natural stone loses $2/3$ of its strength when wet.

4.3. Stress relaxation

The decay of the stress in the relaxation experiments can be described by a stretched exponential function (Eq. 5). The fit of the stress relaxation curves provides thus E_0, τ, β and ψ_0. The relaxation time τ shows an Arrhenius-type dependence. These parameters are summarized in Tab. 2.

Tab. 2: Parameters describing the viscoelasticity of the artificial stone.

E_0	τ	β	ψ_0
GPa	s	-	-
2.03	$4.87 \cdot 10^{-59} \exp(3.94 \cdot 10^4/T$	0.206	$6.95 \cdot 10^{-3}$

5. Calculation of the thermal stresses

Situations that might induce high thermal stresses involve a fast temperature variation and, due to the time-dependent mechanical properties of the mortar, this variation should take place at a high rate. Two situations are considered below: heating during a warm summer day, and very fast cooling during winter time. A comparison between the stresses that do not consider the viscoelasticity of the repair material and the stresses that do include it is very useful to grasp the importance of this relaxation phenomenon and the magnitude of the stresses it relaxes.

5.1. Heating situation

High temperature variations and high heating rates are associated with the summer season, when the repair material is directly exposed to the warm sun. The temperature of the repair layer and of the natural stone have been recorded in Notre-Dame de Vevey, Switzerland, a church where the artificial stone has been used. The experimental equipment and the data are described in (Demoulin *et al.* 2014). A particularly high temperature variation and heating rate were recorded on July 31st, 2014. This day the temperature of the patch went over the T_g of the repair material (20°C) and reached 37.2°C. The temperature profile and the stress it induced in the patch are shown in Fig. 3. If the viscoelasticity of the repair

patch were ignored in the calculation, the patch would have felt a compressive stress of 0.8 MPa (positive stress refers to tensile stress while negative refers to compressive) . However, since the relaxation time above the T_g is fast, all the stresses are relaxed and the stresses induced in the patch, and thus in the natural stone, are nonexistent. This means that all the temperatures above the T_g of the repair layer are not conducive to damaging either the repair material or the stone. The most dangerous period for the materials is thus when the temperature becomes lower than the T_g of the repair material, a situation that is examined in the next section.

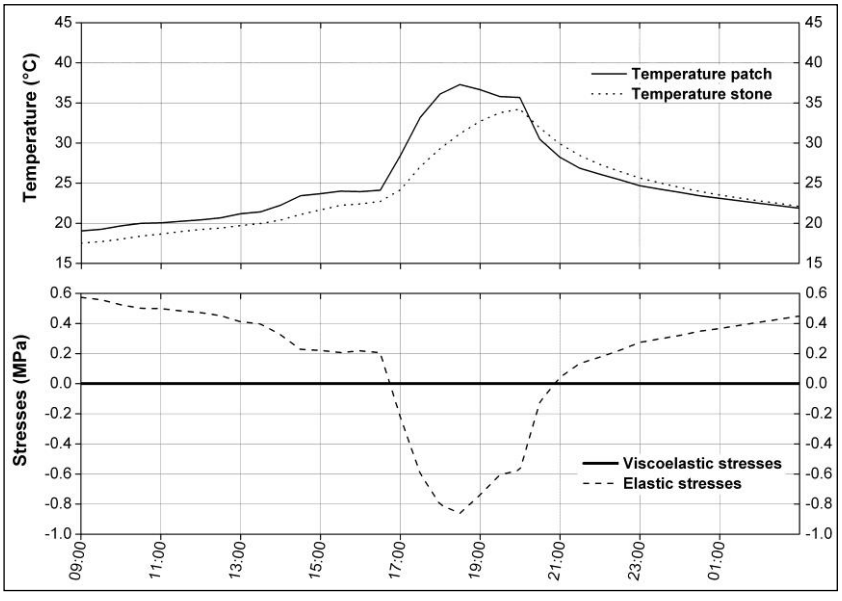

Fig. 2: On top, the temperature profile of the patch and of the stone, as measured in Vevey on July 31st, 2013. Below, the induced viscoelastic stresses, compared with the stresses calculated without considering the viscoelasticity of the mortar (elastic stresses).

5.2. Cooling situation: case of Amarillo, USA, Dec. 12th 1919

Since the data gathered in Notre-Dame de Vevey did not include a very cold winter, the evaluation of the stresses due to cold temperatures has to be done with external data. One of the most extreme cooling events within a single day in a populated area was recorded in Amarillo, Texas, on December 12th, 1919 (USA National Weather Service 2009). On that day, a fast-moving cold front known as a Blue Norther caused air temperature to drop from 19.4 to -17.2°C in seven hours, and at some points at a rate of 24.4°C/h. Here, we only have at our disposal the air temperature, and thus we will assume what could have been the worst situation for the materials in this exceptional event. This would be that the temperature of the stone is the temperature of the air at the beginning of the cold front, while the temperature of the mortar follows the variation of the temperature of the air. The temperature profile and the stresses in the repair layer are shown in Fig. 4. If the mortar had not relaxed any stress (elastic case), there would have been a tensile stress of 4 MPa, higher than its tensile strength; the mortar would have been damaged. However, by considering the

viscoelasticity of the repair layer, we find that the maximum stress induced in the mortar is lower than 2 MPa, and thus lower than its tensile strength (2.7 MPa). The stress induced in the stone is a small fraction of the stress in the mortar, according to Eq. 2. Even in this extreme weather event, the stress in the stone would only have been 0.1 MPa, three times lower than its tensile strength, even in the wet state.

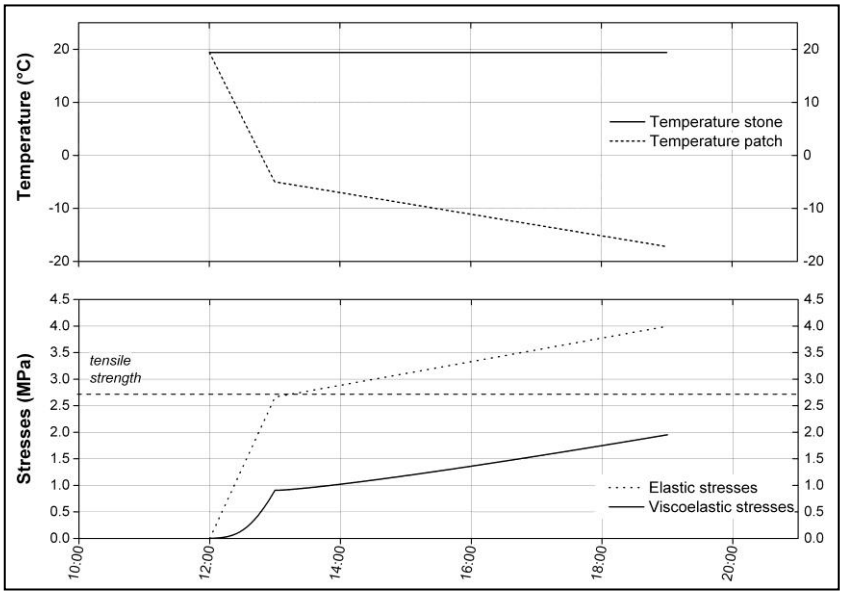

Fig. 3: On top, the temperature profile of the materials that could have been recorded after the extreme weather event of December 12th, 1919. On the bottom, the viscoelastic stresses that could have appeared in the repair layer, compared with the tensile strength of the mortar and with the stresses calculated without considering the viscoelasticity of the mortar (elastic stresses).

6. Conclusion

We have examined the question of thermo-mechanical compatibility of an acrylic-based repair mortar and a sandstone. Given the large thermal expansion coefficient mismatch between the acrylic-based mortar and the sandstone it aims to repair, the question of the magnitude of the thermal stresses that could be induced in the two materials is legitimate. Indeed, a calculation that would treat the repair mortar as a purely elastic material would deliver a result of stress higher than its tensile strength. But since the acrylic-based mortar displays viscoelastic properties associated with a relatively low T_g (20°C), the relaxation processes specific to this type of material have to be considered. The amplitude of the temperature variations, the value of the coldest temperature reached and the rate at which the temperature variations occur all play a role in the magnitude of the thermal stresses. The analysis shows that thermal stresses develop particularly during the cold season, a period where the temperature amplitude and the heating or cooling rate are low. Even by considering the worst-case scenario, it also shows that the thermal stresses are not high

enough to harm the repair material, and more importantly are insignificant for the integrity of the historical substrate. The study points out that choosing an acrylic polymer with a T_g in the range of temperatures found on-site exploits an interesting property of the polymer, its reversibility, without having to suffer from one of its drawback, a high thermal expansion coefficient. The thermal stresses are of course only a part of the compatibility issue between a repair layer and the stone it aims to protect. However, we demonstrate here that the viscoelasticity of the acrylic-based mortar is a property that should be considered, because it allows relief of stresses that are related to expansion mismatch, whether from thermal expansion or hygric and hydric swelling.

Acknowledgements

The authors acknowledge the contribution of Mr Pierre Lachat and Mr Daniel Lachat for helpful discussions and access to job sites. They also would like to thank Jakob Scherer, Heinz Richner and Francesco Caruso for their technical support during the mechanical tests, and Joanna C.H. Wong for giving access to the DMA instrument.

References

Cai, W., 2012, Subcritical crack growth in hardened cement paste, PhD thesis, ETH Zurich. Available at: http://e-collection.library.ethz.ch/view/eth:6304.

Demoulin, T., Scherer, G.W., Girardet, F. and Flatt, R.J., 2016, Thermo-Mechanical Compatibility of Viscoelastic Mortars for Stone Repair, Materials, 9(1), 61.

Demoulin, T., Girardet, F. and Flatt, R.J., 2014, Reprofiling of altered building sandstones : on-site measurement of the environmental conditions and their evolution in the stone. In 32èmes Rencontres Universitaires de Génie Civil, Orléans, France, 4-6 June 2014.

Flügge, W., 1975. Viscoelasticity - 2nd revised edition, Berlin Heidelberg: Springer Verlag. Available at: http://www.springer.com/book/978-3-662-02276-4.

Forster, A.M., 2010. Building conservation philosophy for masonry repair: part 1 - ethics. Structural Survey, 28(3), pp.165–188.

Scherer, G.W., 1986. Relaxation in glass and composites, New York: Wiley.

Torney, C. *et al.*, 2012. "Plastic" repair of natural stone in Scotland: perceptions and practice. Structural Survey, 30(4), pp.297–311.

USA National Weather Service, 2009. Extreme Temperature Ranges. Available at: http://www.srh.noaa.gov/ama/?n=50ranges [Accessed November 25, 2015].

CHARACTERIZATION AND TEST TREATMENTS OF CAST-STONE MEDALLIONS AT THE SMITHSONIAN

C.A. Grissom[1*], E. Aloiz[2], E.P. Vicenzi[1], N.C. Little[1] and A.E. Charola[1]

Abstract

The Smithsonian Institution's Arts and Industries Building (1879-1881) is decorated with 48 medallions and 24 spandrels molded in cast stone. Their gray coloration mimics more costly Euclid bluestone otherwise used for the brick building's trim. The fabricator of the medallions and spandrels, Saxon immigrant Charles Seltman, is newly identified, and their fabrication is placed within the history of American decorative concrete. The cast-stone material and its deterioration were characterised primarily using light microscopy and scanning electron microscopy accompanied by hyperspectral energy dispersive analysis (SEM-EDS). Cross-sections showed that each casting was made in two layers: a fine-grained, well-bound surface layer measuring 2-3 mm in thickness above a more porous layer with large quartz aggregate and smaller ilmenite and hematite particles; the binder in both layers was a mixture of lime and pre-rotary kiln Portland cement. Loss of the more durable surface layer has exposed the weaker lower layer on at least a third of medallion surfaces, invariably those higher in relief, and dissolution of these higher-relief surfaces appears to be ongoing. SEM-EDS showed that uptake of atmospheric sulfur oxides has resulted in conversion of calcite to more soluble gypsum to a depth of ~50 μm in a well-preserved area and to a much greater depth where the surface layer has been lost. With the goal of selecting the best treatment for potential conservation in future, tests were performed on eight west facade medallions, including pre-treatment with ammonium carbonate, consolidation with Prosoco's Conservare OH 100 (an ethyl silicate solution) or barium hydroxide, and application of ammonium oxalate as a protective coating. Photography, colorimetry, water absorption, and adhesive tape testing were performed before and after test treatments. The best method for determining the success of treatment appears to be assessment of surface-layer loss based on comparison of photographs over the long term.

Keywords: cast stone, ethyl silicate, barium hydroxide, ammonium carbonate, ammonium oxalate

[1] C. Grissom*, E. Vicenzi, N.C. Little and A.E. Charola
Museum Conservation Institute (MCI), Smithsonian Institution, United States of Amirca, grissomc@si.edu

[2] E. Aloiz
John Milner Associates Preservation, United States of America

*corresponding author

1. Introduction

The Smithsonian Institution's Arts and Industries Building (1879-1881) in Washington, DC, was designed by the architects Adolf Cluss and Paul Schulze to house the U.S. National Museum and is sometimes said to be the least expensive federal building per square meter ever erected. It was almost certainly to minimize costs that 48 decorative medallions and 24 spandrels were molded in gray-coloured cast stone to mimic more costly Euclid bluestone otherwise used for the red brick building's trim. The building's exterior elevation is identical on all four facades (Fig. 1): six medallions are installed between window arches on a pair of ranges on either side of a tower and six spandrels in corners above three window arches on the tower itself. Each medallion is identified here by the cardinal direction of the façade (N, S, E, or W) followed by a number from 1 to 12, left to right. Two flower designs alternate on the building, distinguished by rounded or pointed petals and leaves. The condition of the medallions was chosen for further study from 2011 to 2013, when they were accessible from scaffolding erected for the building's restoration. The material and its deterioration were analysed, and conservation test treatments were applied and evaluated.

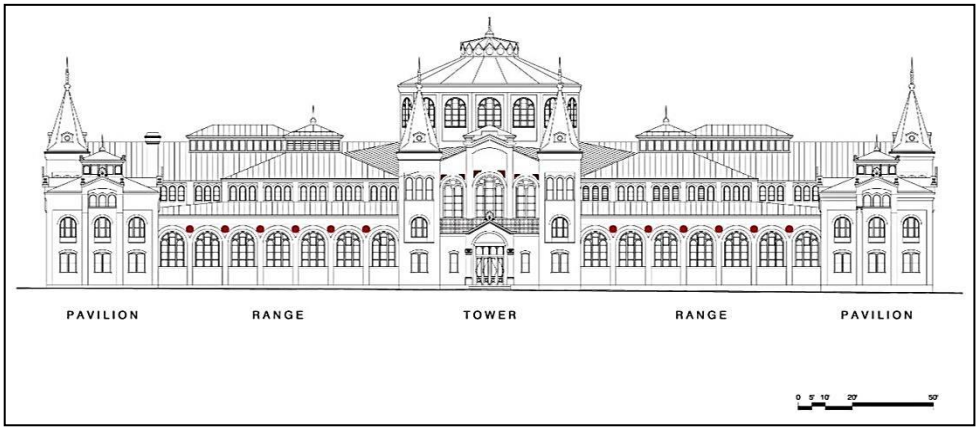

Fig. 1: Exterior elevation of the Smithsonian Institution's Arts and Industries Building (1879-1881). Medallions and spandrels are indicated in solid red.

2. Characterization of the cast stone

2.1. Description

The medallions measure 61 cm in diameter; perimeter rims are recessed 2 cm from the brick wall, but areas of highest relief (on leaves) project slightly from the brick. The medallions were cast face down, confirmed by smooth finishes on well-preserved areas and settlement of silt-sized silica particles (<50 μm) at surfaces. A thin section made from a well-preserved, smooth-surfaced area of medallion N5 shows that two layers were used to mold each casting (Fig. 2): a fine-grained, well-bound surface layer 2-3 mm thick above a much more porous, poorly bound layer containing large silica (quartz) aggregate and small opaque particles of black ilmenite ($FeTiO_3$) and iron oxide, probably hematite (Fe_2O_3). In both layers the binder was identified microscopically as lime mixed with pre-rotary kiln

Portland cement (John Walsh, pers. comm.). Hydrochloric-acid digestion of a sample from the lower layer found (by weight) 42% effervescing acid-soluble material; 50% aggregate, dominated by rounded to angular quartz as large as 1.5 mm in the longest dimension and smaller amounts of ilmenite (a component of some sands) and iron oxide measuring up to about 0.2 mm in largest dimension; and 8% fines consisting mainly of very finely divided gray quartz. The cast stone is porous. Surface water absorption using vertical RILEM tubes is rapid compared to stone, measuring 5 minutes for 5 ml of water in a well-preserved area.

Fig. 2: Thin section from a well-preserved, smooth-surfaced area on N5 in transmitted light; calcite is stained yellow and the epoxy medium, blue. The cross-section shows two layers: a dense surface layer and a more porous lower layer with large quartz aggregate (white in this image) and small black ilmenite particles. Width of sample is 11 mm. Photo by Mel Wachowiak.

The fabricator of the medallions and spandrels, hitherto unknown, is now identified as the Washington-based Saxon immigrant Charles Seltman (1827-1907), "Modeler & Pattern-maker." Seltman was paid the first $80 of a total of $355 for "Modelling 2 rosets [the medallions] and 2 corner ornaments [the spandrels] for the four Main Walls, making casts of same and making and furnishing the boxes for molding the same in Portland cement" (Invoice 1879). This use of cast stone was relatively early in the United States (Prudhon 1989). Just ten years before, the French inventor François Coignet had applied for nine American patents for artificial stone and monolithic concrete. In 1870, rights to Coignet's patents were sold to John C. Goodridge, Jr., superintendent of the Brooklyn-based New York and Long Island Coignet Stone Company (Goodridge 187-, Gillmore 1871, Chamberlin 1983). The company's polychromed Cleft-Ridge Span (1871-1872) by Calvert Vaux in Brooklyn's Prospect Park demonstrated the ornamental potential of molded concrete, and its products may have served as an impetus for use of cast stone on the new museum building.

2.2. Deterioration

All 48 medallions were surveyed and photographed. They were found to be in remarkably good condition given 135 years of weathering. None was found to have major cracks, and it proved a challenge to find damaged areas for minimally invasive sampling. Of concern, however, is the loss on all medallions of at least a third of the smooth, dense surface layer, invariably from areas of higher relief (Fig. 3 and Fig. 4). Evaluation of the porosity of the two layers was hampered by the inaccessibility of intact surface layers in recessed areas. However, RILEM tube tests consistently showed that rims with partial surface retention absorbed water at half the rate of higher-relief leaves on which the surface layer has been lost.

Fig. 3: Medallion W10, before treatment (January 30, 2013).

Fig. 4: Drawing after the previous, with areas retaining the surface layer marked in black; such areas are invariably lower in relief.

The cause of surface loss was investigated in cross-sections. Deterioration in the form of conversion of calcite to gypsum following uptake of atmospheric sulfur oxides was found even where the surface layer is still present, as in Fig. 2. An SEM image of that sample shows sulfur to a depth of ~50 µms from the surface (Fig. 5). On a sample from medallion S9 taken from an area that has lost most of the surface layer, in contrast, calcite was found to have converted to gypsum to a depth of ~250 µm (Fig. 6); below that, an even thicker zone of mixed gypsum and calcite was present. Thus, it appears that loss of the surface layer has increased the depth of conversion to gypsum, probably in part because of the porosity of the lower layer. A major source of sulfur was almost certainly coal, used to heat the Arts and Industries building until around 1910. The amount of airborne sulfur in the vicinity of the building has been limited since then, and the current rate of sulfation of the medallions should be minimal. Deterioration, however, is likely ongoing because gypsum is approximately one hundred times more soluble than calcite. Several observations underline the key role that rainwater plays in deterioration. Greater water absorption during rainfall and slower drying afterward were observed on high-relief areas, in contrast to low-relief areas (cf. Fig. 7 and Fig. 8). Moreover, high-relief areas invariably appear clean and light,

almost certainly from ongoing dissolution of gypsum by rainwater; while recessed areas are dark and smooth, with soiling retained by relatively intact surface layers (Fig. 3). Visual comparison also indicated that predominant rain directions play a role in greater surface-layer loss on west and north façade medallions compared to those on east and south façades. An unexpected finding was that both thin sections showed thin surface layers (~5-7 µm thick) enriched in fluorine (Fig. 5). This is attributed to past hydrofluoric acid or ammonium bifluoride cleaning of the building.

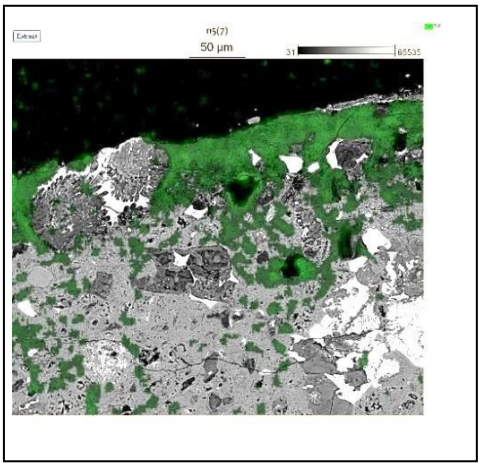

Fig. 5: SEM backscatter electron image of the fine-grained upper layer of thin section N5 (cf. Fig. 3) shows raw sulfur x-ray counts at the surface in green false colors to a depth of ~50 µm. The thin bright line at the upper right surface is enriched in calcium fluoride.

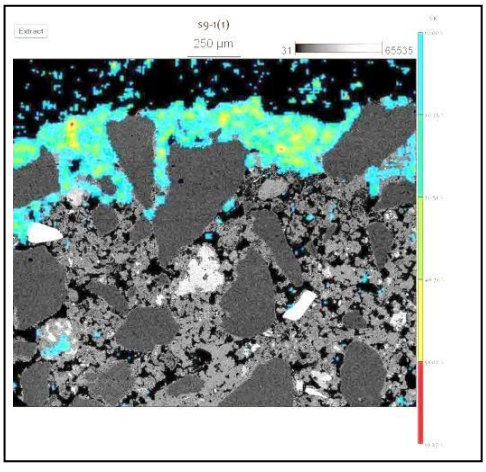

Fig. 6: SEM backscatter electron image of thin section S9, which has lost nearly all of the fine-grained upper layer, shows sul-fur to a depth of ~250 µm in false colors. Only sulfur above 10 atom per cent (blue on the bar at right) is displayed, ranging up to 61% (red on the bar). Large dark gray particles are quartz.

3. Testing

Concern about deterioration of the medallions has been limited, because they remain readable from a sculptural standpoint on account of relief areas being light in value and background areas dark (Fig. 3). Substantial loss of surface layers and conversion of calcite to gypsum, however, led to a proposal for test treatments. The relatively good condition of the cast stone and limited experience and literature in treating similar problems also rendered test treatments a sensible option.

Fig. 7: Medallion W9 after rainfall, before treatment (September 28, 2012). Low-relief areas are dry, indicated by their relative lightness; in contrast, when the entire medallion is dry, low-relief areas are darker than high-relief areas (cf. Fig. 8).

Fig. 8: Medallion W9 two-and-a-half years after treatment with ammonium carbonate, $Ba(OH)_2 \cdot 8H_2O$, and ammonium oxalate (July 16, 2015).

Tab. 1 lists test combinations of a pretreatment solution, two consolidants, and a coating applied to eight medallions on the west façade. These treatments were selected based on successful use on stone (Bracci 2008), modified for potential use on the building by a contractor. Pretreatment with ammonium carbonate is mainly intended to convert gypsum to more soluble ammonium sulfate. Poultice application produces optimal results because of prolonged exposure, and the method of Botticelli *et al.* (1984) for frescoes was employed on the first medallion treated, using Arbocel 1000 paper pulp. The cast stone appeared cleaner after removal of the poultice, but fragile black surface particles were also lost, and the process proved time consuming. Thereafter, saturated solutions of ammonium carbonate were applied by spray or brush. An ethyl silicate stone consolidant (Prosoco's Conservare OH 100 based on Wacker OH 100) was applied to deposit silica in the cast stone. On W1 it was spray applied at intervals of 5-15 minutes in three cycles of three applications each, per specifications for stone. On W4 twice the amount (~1 liter) was applied without refusal, and it seemed that absorption could continue *ad infinitum*. Barium hydroxide was applied to convert gypsum or remaining ammonium sulfate into highly insoluble barium sulfate, as well as to deposit insoluble barium carbonate. Although optimally applied by poultice, it was brush applied to avoid losses that occurred with the ammonium carbonate poultice, as well as because it would be a simpler method for use by a contractor. A saturated solution of ammonium oxalate is usually applied by poultice as a protective coating on stone sculpture, but again brush application was substituted.

Tab. 1: Test treatments.

#	Pretreatment	Consolidant	Coating
W1		Conservare OH by spray	
W4		Conservare OH (2x amt.) by spray	
W10	Ammonium carbonate by spray	6% $Ba(OH)_2 \cdot 8H_2O$, by brush	
W2	Ammonium carbonate poultice	6% $Ba(OH)_2 \cdot 8H_2O$, by brush	Ammonium oxalate by brush
W9	Ammonium carbonate by brush	6% $Ba(OH)_2 \cdot 8H_2O$, by brush	Ammonium oxalate by brush
W12		6% $Ba(OH)_2 \cdot 8H_2O$, by brush	Ammonium oxalate by brush
W11		6% $Ba(OH)_2 \cdot 8H_2O$, by brush	
W8			Ammonium oxalate by brush
W7			Siloxane PD

Each of the eight medallions was photographed in detail, and three types of testing were done before and after treatment. A ninth medallion treated before this study using a water repellent (Prosoco's Sure Klean Weather Seal Siloxane PD) was also tested. Water absorption rates were similar after treatment to those before treatment on both rims and leaves of medallions to which the mineral-based solutions had been applied; this was considered a favorable result, because it indicates that no undesirable alteration in porosity occurred. Exceptions were medallions that could not be properly tested because of water repellency: those treated with the water repellent (Siloxane PD) and Conservare OH 100, which remained hydrophobic even nine months after treatment. Colorimetric measurements made with a Konica-Minolta CR-300 colorimeter were limited to leaves because of the size of the instrument's head. They showed only small changes after treatment: slight yellowing of medallions treated with Conservare OH 100 and lightening of those treated with barium hydroxide, such as W9 (Fig. 8). These changes are not noticeable from ground level, however, and are expected to disappear with time. Tape tests were done with clear adhesive tape (Scotch tape). The tape was applied on both rough and smooth areas, rubbed gently several times, and removed. Since the medallions are symmetrical, mirror-image areas were tested before and after treatment. The tapes were photographed through a Wild microscope using a Leica camera, and negative images were compared by inverting them using Adobe Photoshop for easier assessment. However, consistent differences in the amount or size of particles removed before and after treatment could not be discerned. For assessing the

effectiveness of the test treatments over the longer term, comparison of photographs appears to represent the best option, since loss of the surface layer can be seen. Four years after the medallions were first photographed and nearly three years after treatment, no further loss of the upper layer can be discerned on all twelve west façade medallions, both treated and untreated.

4. Conclusion

Light microscopy and SEM EDS of thin sections of early decorative cast-stone medallions on the Smithsonian's Arts and Industries Building show that deterioration has occurred even on apparently intact surfaces, but to a far greater depth where the surface layer has been lost on areas of highest relief and a coarser lower layer is now exposed. Conservation treatments were tested; however, this project illustrates the challenges of treatment evaluation in the short term. Future examination of the medallions by comparison to photographs taken in the course of the present project is expected to determine the best method for treatment among those applied to eight medallions on the west façade.

Acknowledgements

Staff time for research and testing of the Arts and Industries Building's cast stone was underwritten by the Smithsonian's Museum Conservation Institute (MCI# 6477.5). The authors would also like to thank Sharon Park for initiating the project at the Smithsonian.

References

Botticelli, G., Danti, C., and Giovannoni, S., 1984, Twenty years of barium application on mural painting: Methodology of application, Preprints for the ICOM Committee for Conservation 7th Triennial Meeting, Copenhagen, 84.15.6-11.

Bracci, S., Sacchi, B., Ferreira Pinto, A.P., and Delgado Rodrigues, J., 2008, Inorganic consolidants on stone artefacts: Optimization of application procedures for marble and limestones, International Symposium on Stone Consolidation in Cultural Heritage – Research and Practice, J. Delgado Rodrigues and J.M. Mimoso (eds.), Lisbon, 81-90.

Chamberlin, W.P., 1983, The Cleft-Ridge Span: America's first concrete arch, The Journal of the Society for Industrial Archaeology, 9 (1) 29-44.

Gillmore, Q.A., 1871, Practical Treatise on Coignet-Béton and other Artificial Stone, Van Nostrand, 108 p.

Goodridge, J.C. 187-, Beton-Coignet: Description of the Material and its Uses in France and America, Sutton, 16 p.

Invoice, 1879 (August 26), Smithsonian Institution Archives, Models of Rosettes, Box 12, RU 71.

Prudhon, T.H.M., 1989, Simulating stone, 1860-1940: Artificial marble, artificial stone, and cast stone, APT Bulletin, 21 (3-4), 79-91.

COMPOSITION OF STONE PLASTERS AND PIGMENTED PLASTERS APPLIED IN THE 1920s AND 1930s IN BERLIN, GERMANY

S. Laue[1*]

Abstract

In the end of the 19th and in the beginning of the 20th century new dry mortars were developed and applied to imitate stone surfaces (stone plasters) or to decorate building surfaces with pigmented plasters (coloured mortars). Stone plasters and pigmented plasters are finished products manufactured as dry mortars and were marketed by companies, e.g. "Terranova-Industrie" or "Terrasit-Industrie" in Europe. During a research project 19 plasters of 7 different housing estates or monuments were investigated and analyzed to understand the composition of the plasters leading to an appropriate conservation concept. Samples were taken even from monuments of the so called "Hufeisensiedlung" and "Weiße Stadt" which are part of the UNESCO World Heritage Housing Estates in Berlin. Hydraulic lime and aggregates together with pigments including zinc white, barite, red ochre (iron oxide), yellow ochre, ultramarine, chrome oxide green were used to create pigmented plasters. In contrast, stone plasters are mixed with cement as a binder together with stone aggregates including quartz, feldspar, calcite, dolomite, mica and pyroxene. The investigations led to the creation of suitable repair mortars using similar binders, aggregate and pigments as analysed.

Keywords: Berlin, stone plaster, coloured plaster, decorative plaster, housing estates, hydraulic lime

1. Introduction

In the first decades of the 20th century in central Europe, the use of colour and designed surfaces in architecture was trendy. The criticism of the bloc developments of the 19th century with their social and hygienic injustices was a criticism against the cheer- and colourless city. The demand on moral, social and artistic regeneration generated new concepts of urban design and architecture especially in the 1920s (Brenne 2013). One of the best-known papers promoting colour in architecture was written by Bruno Taut and published in "Bauwelt" (Taut 1919) titled "Proclamation of coloured construction". The proclamation was a demonstration of public self-awareness for coloured architecture and was signed by many prominent architects. The architects worked theoretically and practically on the topic creating characteristic qualities in mass house building like housing estates, commercial buildings, schools, kindergartens etc. These qualities in the mass house

[1] S. Laue*
Department of Conservation and Restoration, University of Applied Sciences Potsdam, Germany
st.laue@fh-potsdam.de

*corresponding author

building of the 1920s received its appreciation in recent times when six estates in Berlin were listed as examples in the UNESCO World Heritage in 2008.

In the same period of the 19th and early 20th centuries, new dry mortars were developed and applied following the visions of the architects. The new dry mortars were colourful enough to decorate building surfaces with pigmented plasters (coloured mortars). Other plasters imitated stone surfaces (stone plasters). Both coloured and stone plasters were finished products manufactured as dry mortars and marketed by companies like "Terranova-Industrie" or "Terrasit-Industrie" in Europe (Rettig 1912, Lietz *et al.* 2016). "Terranova" stood for "new plaster". These new products consisted of hydraulic lime or cement as a binder and were modified by different aggregates and pigments resulting in rather colourful and decorative house facades. Stone plasters are intended to imitate stone facades whereas coloured plasters should change dull facades into modern facades with charisma (light and colourful). The new mortars were very successful: In the end of the 1920s, 77% of the new buildings in Berlin contained the new materials (Kapferer 1928). Further details of the history and development of the decorative plasters are to be found in Lietz *et al.* (2016).

During a research project – financed by the German Federal Environmental Foundation (Az 26503-45) – 19 plasters of 7 different housing estates and buildings respectively were investigated and analysed to document and better understand the composition of the plasters leading to an appropriate conservation concept. Here results of the composition of the plasters are presented showing the high variety of applied aggregates and pigments which are responsible for the decorative plasters.

Fig. 1: Example of a coloured plaster (yellow ochre) at the housing estate "Hufeisensiedlung" in Berlin-Britz.

Fig. 2: Example of a coloured plaster (blue) at the housing estate "Hufeisensiedlung" in Berlin-Britz.

2. Samples and analytical methods

2.1. Samples

19 plaster samples from the following 7 housing estates and buildings were analyzed:

- Hufeisensiedlung (architects: Bruno Taut and Martin Wagner, construction period: 1925-1932)
- Weiße Stadt (Otto-Rudolf Salvisberg, 1929-1931)
- Großsiedlung Siemensstadt (Hans Scharoun, Fred Forbat, 1930-1931)
- Kissingenviertel (Goettel, Mebes & Emmerich, 1929-1931)
- Academy of Arts (Werner Düttmann, Sabine Schumann, 1960)
- Paediatric Clinic in Berlin-Weißensee (Carl James Behring, 1911)
- Titania Palace in Berlin-Steglitz (Schöffler, Schlönbach & Jacobi (1927-1928)

All housing estates and buildings were renovated and the plasters were renewed during the last decades. Some samples of the original plasters had been put aside, so that they could be analysed during this study. The samples are described in Tab. 1.

2.2. Analytical methods

The combination of different analytical methods gives evidence to the composition and structure of the plasters. Before any other analytical procedure was executed, all plaster surfaces were analysed with a portable XRF-analyzer (Nitron XL3t/Thermo Electron) measuring typical elements and producing information about the pigments and/or aggregates. The structure and aggregates of the plasters were analysed by polarising microscopy (PLM) (BX51 Olympus) of thin sections which had been impregnated with coloured resins (red resin for blue plasters, blue resin for all other samples). To identify the crystalline and mineralogical phases of the binders and aggregates, XRD was carried out with a Siemens D5005 using CuKα-radiation. Analysis of the sieve curve was executed by dissolving the binder and sieving the washed aggregates through gradually finer sieves. Additional chemical analyses were performed on some samples to analyse the amount of CSH-phases following the chemical procedure:

- Drying the samples at 50°C
- Dissolution of carbonates and sulphates by cold and hot HCl
- Residue was mixed up with a saturated Na_2CO_3-solution determining soluble SiO_2-content, which can be interpretated as soluble CSH-phases
- Sieve curve (grain size distribution of the aggregates)

Fig. 3: Example of a blue-coloured plaster from the housing estate "Hufeisensiedlung" in Berlin-Britz, on the surface where the colour turned to grey (grey crust contains gypsum).

Tab. 1: Locations, samples and colourants (cp = coloured plaster, sp = stone plaster, quartz and feldspars are not mentioned).

Housing estate / builiding	Sample	Discription	XRF-significant elements	Pigments / aggregates
Hufeisensiedlung	Huf 01	red cp	Fe	red ochre
Hufeisensiedlung (see Fig. 1)	Huf 02	yellow cp	Fe	yellow ochre
Hufeisensiedlung	Huf 03	dark red cp on light cp	Fe, Ba	red ochre, barite
Hufeisensiedlung	Huf 04	white cp	Ca	calcite
Hufeisensiedlung	Huf 05	light white cp	Ca, Zn	calcite, zinc white
Hufeisensiedlung (see Fig. 2)	Huf 06	blue cp	Al, Si	ultramarine (Fig. 4 and Fig. 6)
Siemensstadt	Siem	white cp with white paint	Ca, Zn	calcite, zinc white
Weiße Stadt	WS 01	white sp	Ca, Mg	calcite, dolomite
Weiße Stadt	WS 02	grey reddish sp	K, Al, Si	potassium feldspar, some pyroxen
Weiße Stadt	WS 03	light ochre sp	Fe, Ca	ochre coloured calcite, yellow ochre
Weiße Stadt	WS 04	dark ochre sp	Fe, Ca	ochre coloured calcite, yellow ochre
Weiße Stadt	WS 05	grey sp with white and dark aggregates	Ca, Mg	white: calcite (marble) dark: dolomite
Kissingenviertel	Kiv 01	light red cp	Fe, Ca, Mg	red ochre, dolomite
Kissingenviertel	Kiv 02	brown cp	Fe, Mn, Ca, Mg	brown ochre, dolomite
Kissingenviertel	Kiv 03	light yellow cp	Fe	yellow ochre
Kissingenviertel	Kiv 04	brown cp	Fe, Mn, Ca	brown ochre, calcite
Academy of Arts	Aca	dark blue cp	Al, Si Cr	ultramarine, chrome oxide green
Infant Hospital	InfH	white cp	Ca	calcite (marble)
Titania Palace	TiP	ochre cp with ochre paint	Fe	yellow ochre

3. Results and discussion

The results of the analyses are summarized in Tab. 1 and Tab. 2. In Tab. 1 the sample identification, the results by using XRF, and the pigments and aggregates which coloured the plasters are described. In Tab. 2 the binders, the binder/aggregate ratio and the aggregates except the pigments are represented.

Nearly all coloured plasters contain hydraulic lime as a binder (see Tab. 2) which was mixed with different kinds of aggregates and pigments to create different types of decorative plasters. Aggregates could be determined by PLM and XRD; they consist of quartz, feldspar, calcite, dolomite, mica, and pyroxene. As calcite and dolomite dissolve as well as parts of the binder, in some samples the binder/aggregate ratio is too high and imprecise. Regarding the binder/aggregate ratio, the fact has been taken into account that pigments can react with calcium hydroxide during the curing process creating additional phases, which can result in incorrect binder/ratio contents. Despite these uncertainties, in the coloured plasters the binder/aggregate ratio varies between 1:4 and 1:6, which is quite typical in hydraulic lime mortars (Gödicke-Dettmering 1997).

Due to the fact that parts of the binder and of the aggregates dissolve in acid during the chemical analysis, no binder/aggregate ratio can be stated for samples, which contain calcite (limestone, marble) and dolomite (Tab. 2).

Pigments that coloured the plasters consist of zinc white, barite, red ochre (iron oxide), yellow ochre, ultramarine (see Fig. 3) and chrome oxide green. All pigments are stable in alkaline systems, even if they are exposed to weak acid industrial atmosphere like in Berlin in the last decades. Darker surfaces of the pigmented plaster (Fig. 3) resulted from dust and the formation of gypsum as is well known due to numerous publications (e.g. Arnold and Zehnder 1990). The stone plaster applied at the *"Weiße Stadt"* contains cement as a binder and different aggregates like calcite (lime stone, marble), dolomite and only a few quartz.

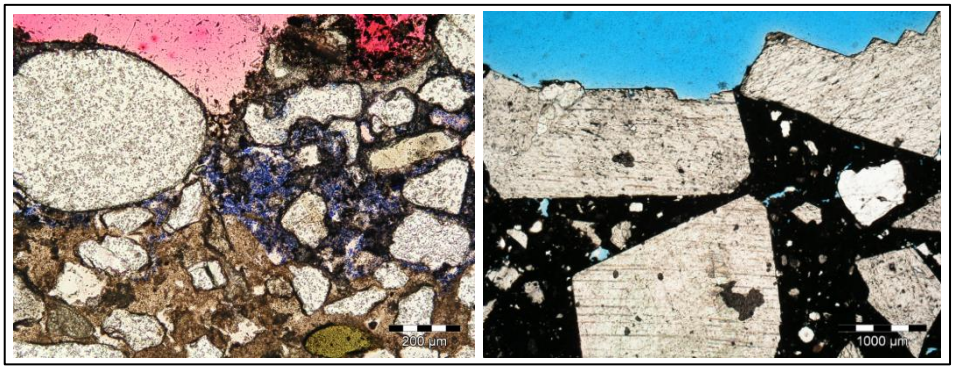

Fig. 4: PLM of thin sections, II-pol, left: Huf 06, blue plaster coloured by ultramarine, right: W05, huge marble aggregates and small dolomite in cement.

Tab. 2: Binder, binder/aggregate ratio and aggregates (except pigments) of the plasters (qtz = quartz, fsp = feldspar, pfsp = potassium feldspar, cc = calcite (lime stone), do = dolomite, pyx = pyroxen, rp = rock particles, n.d. = not determinable).

Sample	Binder	Binder to aggregate ratio	Aggregates
Huf 01	hydraulic lime	1:5	qtz, some fsp, cc
Huf 02	hydraulic lime	1:5	qtz, some rp, cc
Huf 03	hydraulic lime	1:4	qtz, some fsp, cc
Huf 04	hydraulic lime	1:4	qtz, some fsp
Huf 05	hydraulic lime	1:3	qtz, some fsp
Huf 06	hydraulic lime	1:4	qtz, some fsp
Siem	hydraulic lime	1:6	qtz
WS 01	cement	n.d.	cc, do, some qtz
WS 02	cement	n.d.	pfsp, qtz, rp, cc, pyx
WS 03	cement	n.d.	cc, qtz
WS 04	cement	n.d.	cc, some qtz
WS 05	cement	n.d.	cc (marble), do
Kiv 01	hydraulic lime	n.d.	do, qtz, rp, fsp
Kiv 02	hydraulic lime	n.d.	do, qtz, rp, fsp
Kiv 03	hydraulic lime	1:5	qtz
Kiv 04	hydraulic lime	n.d.	qtz, fsp, rp, cc
Aca	cement	n.d.	qtz, cc
InfH	hydraulic lime	n.d.	qtz, cc (marble), fsp
TiP	hydraulic lime	n.d.	cc, qtz,

4. Conclusion

Due to the fact that today no original plasters exist at the investigated housing estates, the research is a fundamental contribution to the survey and documentation of coloured and stone plasters of the 1920s in Berlin. Although there are some uncertainties in the quantitative analyses of the binders and aggregates as discussed in section 3, the investigations showed which binders, aggregates, and pigments were applied creating diversified surfaces used in mass architecture in the 1920s to enhance the quality of life for ordinary people.

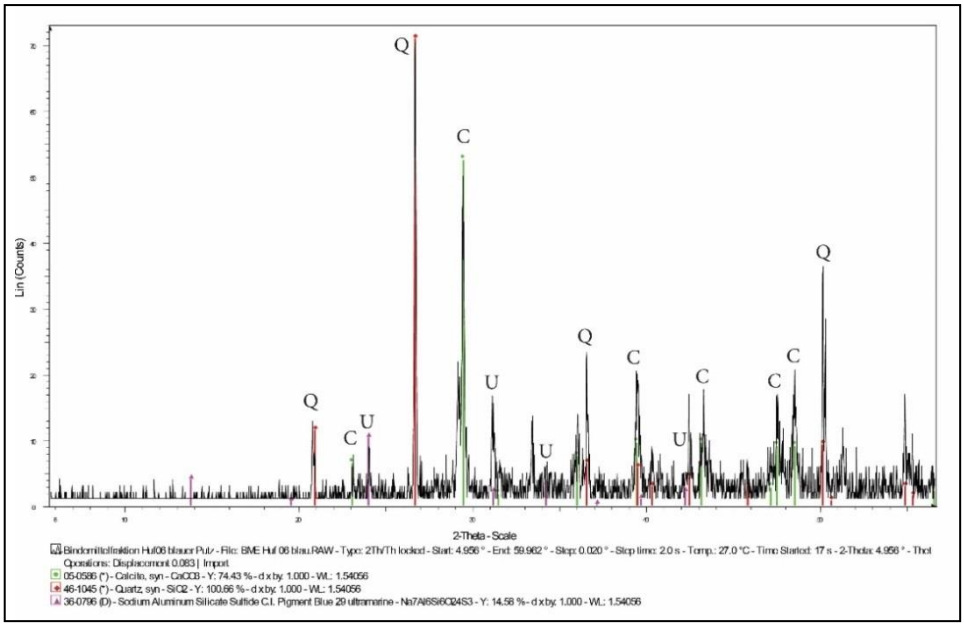

Fig. 5: XRD-pattern of sample Huf 06 demonstrating ultramarine as blue pigment (Q = quartz, C = calcite, U = ultramarine).

Acknowledgements

This study was developed within the project "Edelputze und Steinputze" financed by the German Federal Environmental Foundation (Az 26503-45). The author wishes to thank Bettina Lietz, Werner Koch and Sven Wallasch for very good collaborations and helpful discussions.

References

Arnold, A. and Zehnder, K., 1990, Salt weathering on monuments in proceedings of the Advanced workshop of Analytical Methodologies for the Investigation of Damaged Stones, 14.-21.09.1990, Pavia (Italy), 31-59.

Brenne, W., 2013, Die Konservierung und Restaurierung der Polychromie in der Stadt. Die Siedlungen in Deutschland in La conservazione delle policromie nell'architectura der XX secolo, Jean, G. (ed.), Scuola universitaria professionale delle Svizzera italiana, Lugano, 122-139.

Lietz, B, Wallasch, S. and Koch, W., 2015, Edelputze und Steinputze in Potsdamer Beiträge zur Konservierung und Restaurierung, Band 4, ISBN 978-3-00-049282-2, 148pp.

Kapferer, H., 1928, Der deutsche Putzbau unter der besonderen Berücksichtigung und Darlegung des Marktes der farbigen Trockenmörtel, Dissertation, University of Munich.

Taut, B., 1919, Aufruf zum farbigen Bauen in Bauwelt 10, Nr. 39, 11.

RECOVERING THE ARCHITECTURAL HERITAGE OF THE NUEVA TABARCA ISLAND (SPAIN) BY STUDYING THE DURABILITY OF ORIGINAL AND REPAIR MORTARS

J. Martinez-Martinez[1*] and A. Arizzi[2]

Abstract

Nueva Tabarca is a small island located in the Mediterranean Sea, close to the city of Alicante (SE of Spain). Although the island is mainly known for its marine reserve, its fortified village is an exceptional example of Baroque architectural heritage, mainly built with stone and lime mortars. However, in spite of the singularity of its monuments, the majority of walls and buildings of the old town of Tabarca are in an alarming state of conservation. Airborne salt, Aeolian erosion and anthropic activity are the main causes of decay. Although several restoration works were carried out during the 70's and in the first decade of the present century, all of them have shown to be ineffective, due to the low durability of the repair materials used. To investigate the causes of such an intense decay of both original and repair mortars, a complete characterisation of these materials has been carried out, by means of both field and laboratory studies that included: diagnosis of the conservation state of buildings, mineralogical and textural analyses of mortars, and determination of mortar strength. Our investigations have demonstrated that the decay patterns found in the repaired buildings cannot be related only to the weathering conditions of the island, but also to the choice of inappropriate repair materials. Laboratory results have shown, indeed, that the original mortars are more resistant to decay processes compared to the repair mortars used, mainly because of their lower porosity and higher mechanical strength.

Keywords: lime mortar, Mediterranean climate, durability, salt crystallisation

1. Introduction

This study is focused in the old town of the Nueva Tabarca island (Alicante province, SE of Spain) (Fig. 1). This fortified village represents an exceptional example of homogeneous baroque architectural heritage. The singularity of the monuments was recognized by means of several local and national projects. The initial plans for this fortified city were focused on the construction of a thick wall around part of the island as well as of several buildings with military, religious and civil functions (Canales Martínez and Romero Carrasco, 2014). The reason for this important intervention was to offer a stronger resistance against the Barbary pirates. The construction works began in the middle of 18th century, but they were

[1] J. Martínez-Martínez
Universidad de Alicante, Facultad de Ciencias, Spain
javier.martinez@ua.es

2 A. Arizzi
School of Geography and the Environment. Oxford University, United Kingdom

*corresponding author

interrupted in 1770 due to economical, political and logistic problems. This resulted in the construction of most parts of the wall, the church, the government building and a complex hydraulic system in order to supply the population with fresh water (Fig. 1).

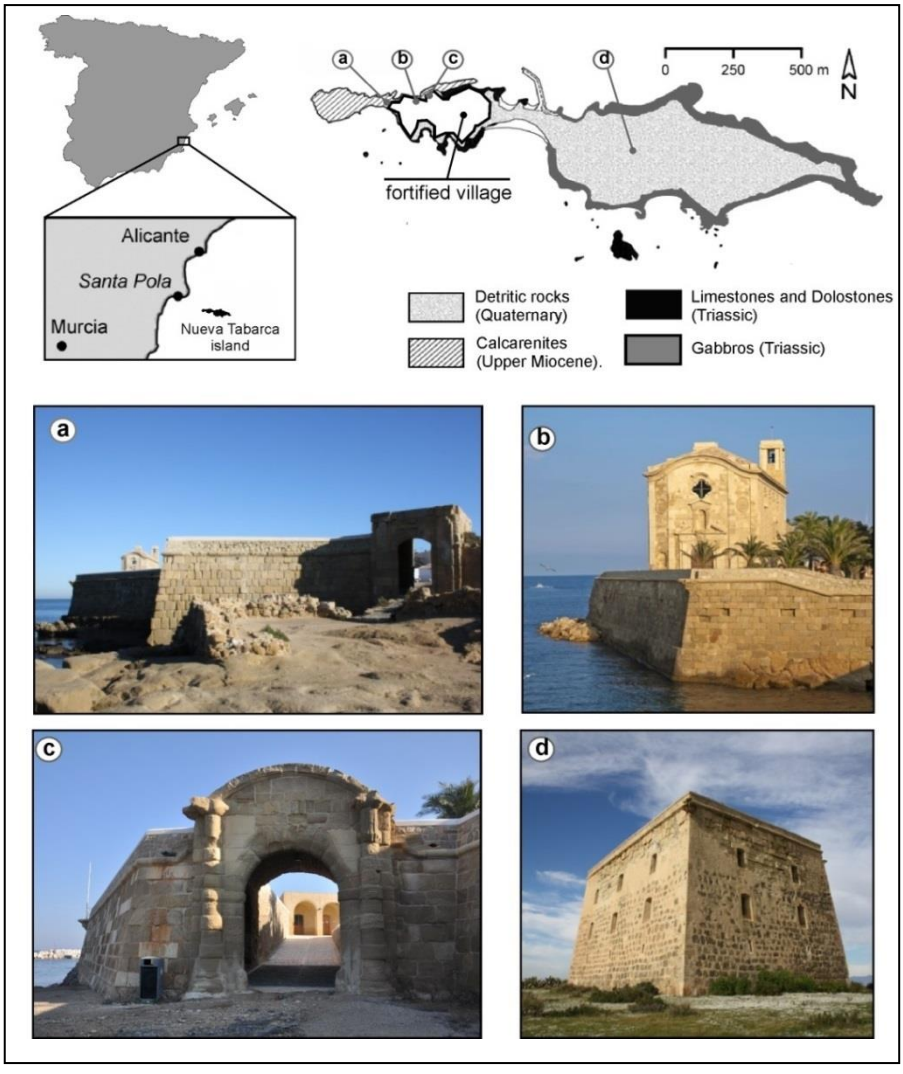

Fig. 1: Above left: Nueva Tabarca island location; above right: map of the island showing the main lithologies and the location of the fortified village; down: some elements of the architectural heritage of the Nueva Tabarca village (a: San Gabriel door, b: San Pedro and San Pablo church, c: San Miguel door, d: San José tower).

Nowadays, the weathering state of walls and buildings is alarming. The proximity to the sea and salt water, the effect of the aeolian abrasion, and the anthropic damage are the most significant decay causes of the original building materials. Several restoration works were carried out in the local heritage focused mainly on the walls and the church. Two of the

most important works were executed during the 70's and the first decade of the present century. All the interventions are now being seriously discussed due to their low efficacy and the use of foreign reintegration rocks aesthetically different from the original materials.

One of the weakest aspects of the last restoration work regards the repair mortar chosen. Fig. 2 shows the current situation of a non-restored city wall (a) and a rebuilt section during the 70's (b). In the original masonry (a) it is possible to appreciate how the original lime-mortar remains well preserved whilst the ashlars are completely eroded. The rebuilt part, instead, presents the opposite behaviour: the rock ashlars show a slight to moderate weathering, whilst the new lime-mortar is strongly deteriorated.

Fig. 2: examples of two parts of the city walls of Nueva Tabarca: original (a and a') and rebuilt masonry (b and b').

With the purpose to understand the reasons for the different durability of both the original and the repair lime mortars, a complete petrographic and petrophysical characterization of these materials has been carried out in the present work.

2. Methodology

Four types of lime-mortars were collected from the original and restored city walls. Firstly, each sample was cut in two pieces and the obtained flat surfaces were scanned for their textural analysis and description. Secondly, one piece was powdered for the chemical and mineralogical analysis, while the other one was cut in a regular shape for the study of its pore system. Owing to the small size of the samples, their mechanical properties were not studied by means of laboratory tests (e.g. uniaxial compression test), but using the Schmidt Hammer *in situ*.

2.1. Textural and mineralogical characterisation

For the textural study, 48-bits colour images were obtained for each mortar type with a resolution of 600 ppp. An Epson Perfection 2480 PHOTO scan was used. In order to improve the quality of the obtained image, the surfaces of the sample were priory moistened. A semi-quantitative mineralogical analysis was carried out by X-Ray Diffraction using a Phillips PW-1710 powder diffractometer with CuKα radiation and a PHILIPS PW-1404 calibrated with standards from CNRS.

2.2. Pore system characterisation

The connected open porosity (ϕ_O), defined as the relationship between the volume of voids (ratio of absorbed water to water density) and the volume of the sample and expressed as a percentage, was found using the vacuum water saturation test. Samples were dried at a

temperature of 70°C for 48 hours until constant mass. Dried samples were placed under vacuum at 20 ± 7 mbar for three cycles of 5 hours each (after UNE-EN 1936). The gases trapped in the pores were eliminated during the first cycle. During the second cycle, samples were gently immersed under distilled water, where they were left for 5 hours. Atmospheric pressure was re-established and maintained throughout the last cycle. The pore size distribution of samples was measured by means of Mercury Intrusion Porosimetry (MIP), using an Autopore IV 9500 Micrometics mercury porosimeter. The pore size interval investigated by MIP ranges from 0.002 to 200 μm, which corresponds respectively to highest and lowest head pressures. Finally, the real density (ρ_r) of samples was obtained using an AccuPyc 1330 Helium pycnometer.

2.3. Mechanical characterisation

The Schmidt hammer, also named Sclerometer or Rebound Hammer, is a non-destructive test for assessing the uniaxial compressive strength and the Young's modulus of materials. The used sclerometer is a L-type instrument. This apparatus measures the distance of rebound of a controlled impact on a rock surface. When the Schmidt Hammer is pressed against a surface, its piston is automatically released onto the plunger. The distance travelled by the piston after it rebounds is called the rebound (*R*) value. Harder materials have higher R values. If sclerometer measurements are done in an inclined way, the R values must be normalized with reference to the horizontal direction. A minimum of 15 rebound values were carried out in each tested sample in order to obtain a representative value. Highest and lowest values were discarded (Viles *et al.*, 2011). Uniaxial compressive strength (UCS) and Young's modulus (*E*) were indirectly determined with the Schmidt hammer test using empirical relations proposed by Yagiz (2009):

$$UCS = 0.0028 \cdot R^{2.584} \qquad \textit{(Eq. 1)}$$

$$E = 0.0987 \cdot R^{1.55454} \qquad \textit{(Eq. 2)}$$

These equations were adopted because they were considered the most suitable for carbonate rocks according to Andriani and Germinario (2014).

3. Results and discussion

Figures 3a and 3b shows the aspect of both original (XVIII century) and new (XX century) lime-mortars used in Nueva Tabarca fortified village. Tab. 1 and Fig. 3c includes the obtained data from the different tests carried out in this work.

A mortar system is characterised by the presence of aggregate grains surrounded by a matrix in continuous mineralogical and textural transformation. Non-hydraulic lime-based mortars, in particular, are characterised by a hardening process (carbonation) that is much slower over time with respect to the hydration reactions that occur in cement mortars and concrete. Initially, the lime-based mortar matrix is mainly composed by portlandite ($Ca(OH)_2$), which slowly reacts with the atmospheric CO_2 present in the pores to form calcite (CaCO3) (Moorehead, 1986). In the case of the Tabarca's mortars, the matrix mineralogy is expected to be mostly calcite, due to the materials age and the chemical aggressiveness of the marine environment where these mortars are placed, which causes the dissolution and removal of the unreacted portlandite. Indeed, portlandite was not detected by XRD (table 1), confirming a completed carbonation process in both types of mortars. From the XRD data we can estimate that both types of mortars present a similar binder-to-

aggregate ratio (approximately 1:1.5 by weight), and that the matrix constitutes around 40% of the sample. However, there are significant differences between the two types of mortars in terms of mineralogy and size of their aggregates. On the one hand, the original lime mortar presents a broad and continuous grading, showing particles with diameters ranging between 1 mm and 4 cm. The clasts nature corresponds to dolostones and gabbros, which were probably collected from the local beach deposits. On the other hand, the aggregate of the repair mortars, mainly proceeding from dolostones, has grains of bigger sizes and with a discontinuous grading (between 5 and 10 mm) (Fig. 3).

Tab. 1: Data obtained from both original (NT-org) and repair lime-mortars (NT-rest) used during the 70's restauration works. Parameters included in this table: Mineralogical composition (Cc: calcite; Dol: dolomite; Px: pyroxene; Pl: plagioclase); Open porosity (ϕO); Real density (ρr), Rebound value after Schmidt Hammer (R) and uniaxial compressive strength (UCS) and Young's modulus (E) estimated from R value.

	Mineralogical Composition, %					ϕ_O	ρ_r	***R***	**UCS**	***E***
	Cc	Dol	Q	Px	Pl	(%)	(g/cm^3)	(-)	(MPa)	(GPa)
NT-org	39.85	14.58	4.97	18.82	21.87	17.20 ±2.75	2.77 ± 0.01	19.65 ±5.47	7.13 ±4.34	10.43 ±4.59
NT-rest	41.85	55.81	2.42	-	-	23.33 ±5.41	2.64 ±0.01	13.76 ±2.39	2.60 ±1.16	5.89 ±1.59

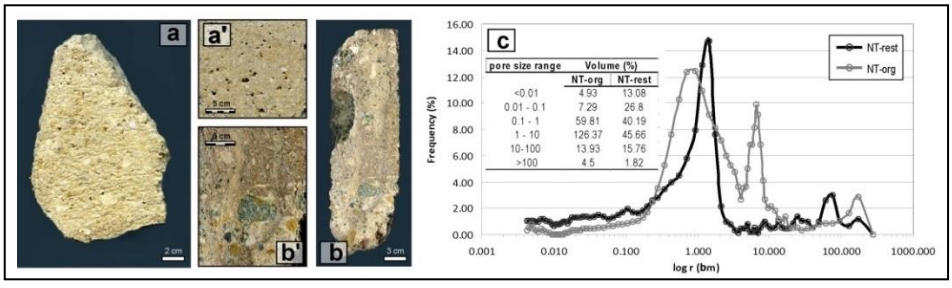

Fig. 3: Images a and b: original (a and a') and repair (b and b') lime mortars of the walls. Graph c: pore size distribution of both original and restoration mortar (NT-org and NT-rest, respectively).

The pore system of original and repair mortars is also different. The open porosity of the original mortar (around 17%) is lower than that of the repair one (~23%). However, the open porosity in both cases is not too high if we compare them with similar materials (porosity values ranging between 30% and 40% for other lime-based mortars with similar binder-to-aggregate ratio, Arizzi *et al.*, 2013). Pore size distribution is also different (Fig. 3c): the original mortar presents a main size of pores of 0.8 µm and the 60% of the pores are comprised between 0.3 and 10 µm. On the contrary, the pore size distribution of the repair mortar is much more homogeneous (unimodal distribution), being the majority of the pore radii centred between 0.5 and 2 µm. The most frequent pore size in this mortar is slightly higher (1.5 µm). Moreover, the repair mortar presents close rounded pores (in the form of bubbles, Fig. 3) likely to be formed during evaporation of the kneading water.

Finally, the mortar used in the original masonry presents higher mechanical properties (strength and stiffness) than that used during restoration works. This fact can be observed in table 1, where the uniaxial compression strength value (estimated after the R value) is nearly three times higher in the original mortar than in the repair one. This fact is mainly due to the higher porosity and the presence of rounded pores in the latter.

4. Conclusions

The repair mortar collected from the wall of the Nueva Tabarca Island has shown a lower durability compared to the original mortar (XVIII century), as demonstrated by the worse conservation state of the former after only 40 years since the last intervention. This is due to two complementary factors: 1) mortars are exposed to an arid and maritime environment, with the main decay caused by salts (both from the capillary water and the sea spray), aeolian erosion (especially during frequent storms) and sun radiation; 2) the repair mortar shows a worse quality due to its higher porosity (with the majority of pores with size of 1 μm) and its lower mechanical resistance and cohesion, which make it more vulnerable to salt crystallisation and wind erosion. According to this study the repair mortar needs to be replaced with a new one with improved textural and mechanical characteristics. With this purpose, a new repair mortar is being designed for this particular location and environment. As an added value, sustainable materials from the Tabarca Island are being used in the new formulation.

Acknowledgements

This research was supported by project GRE12-03 (University of Alicante). The authors are grateful to José Manuel Pérez, Felio Lozano and Antonio Ruso for their help and assistance during the field works; as well as to the *Excmo. Ayto. of Alicante* (*Concejalía de Medio Ambiente*) and to the *Reserva Marina de Tabarca* who allowed us using their available means.

References

Andriani, G.F. and Germinario, L. (2014): Thermal decay of carbonate dimension stones: fabric, physical and mechanical changes. Environment Earth Sciences, 72: 2523-2539.

Arizzi, A., Martínez-Martínez, J. and Cultrone, G. (2013): Ultrasonic wave propagation through lime mortars: an alternative and non-destructive tool for textural characterization. Materials and Structures, 46:1321-1335.

Canales Martínez, G. and Romero Carrasco, O. (2014): La población de Nueva Tabarca, un proyecto ilustrado de fortificación insular. In: Nueva Tabarca, un desafío multidisciplinar. Canales, G., Pérez, J.M. and Lozano, F. (Coords.). Ed: Diputación de Alicante and Instituto Alicantino de Cultura Juan Gil Albert. 204 pp.

Moorehead D.R. (1986): Cementation by the carbonation of hydrated lime, Cement and Concrete Research, 16 (5):700-708

UNE-EN 1936. Natural stone test method. Determination of real Density and Apparent Density and of Total and Open Porosity. European Committee for Standarization.

Viles, H., Goudie, A., Grab, S. and Lalley, J. (2011): The use of the Schmidt Hammer and Equotip for rock hardness assessment in geomorphology and heritage science : a comparative analysis. Earth Surface Processes and Landforms, 36: 320-333.

Yagiz, S. (2009): Predicting uniaxial compressive strength modulus of elasticity and index properties of rocks using the Schmidt hammer. Bulletin of Engineering Geology and the Environment, 68: 55-63.

This page has been left intentionally blank.

STONE-MORTAR INTERACTION OF SIMILAR WEATHERED STONE REPAIR MORTARS USED IN HISTORIC BUILDINGS

B. Menendez[1*], P. Lopez-Arce[1,2,3], J.-D. Mertz[2], M. Tagnit-Hamou[1,3], S. Aggoun[3], A. Kaci[3], M. Guiavarch[2] and A. Cousture[3]

Abstract

Many basements of historic buildings from the city of Paris (France) have been constructed with Euville stone. Salt crystallization weathering processes related to urban pollution have induced the decay on these buildings where stone repair mortars have been used to reconstruct the surface of this limestone in the last few decades. Three different commercial natural-hydraulic lime mortars used during the last 2008/2010 campaign of restoration works have been selected in order to compare the interaction between these surface repairing mortars and the Euville natural stone. Physico-chemical results obtained by several non-destructive techniques (NDT) applied on Parisian historic buildings to measure moisture, temperature, permeability, ultrasonic velocity, colorimetry and salt content distribution show the behaviour and the stone-mortar interaction on-site. The characterisation of stone and mortar specimens, manufactured at the laboratory and exposed to different temperature, relative humidity and CO_2 concentration environmental curing conditions, together with stone-mortar specimens, was also performed at the laboratory using the same NDT together with complementary micro-destructive analytical techniques. The durability of these stone-mortar specimens was assessed after two types of accelerated salt crystallisation ageing tests. Laboratory tests together with on-site measurements allow predicting (i) the behaviour and durability of these restoration mortars (ii) the differential compatibility of each mortar type, and (iii) their interactions with the Euville limestone submitted to the future environment change.

Keywords: stone repair mortar, historic buildings, salt crystallisation, petrophysics, durability

[1] B. Menendez*, P. Lopez-Arce and M. Tagnit-Hamou
Géosciences et Environnement Cergy, GEC (EA 4506), Université de Cergy Pontoise, France
beatriz.menendez@u-cergy.fr

[2] P. Lopez-Arce, J.-D. Mertz and M. Guiavarch
Laboratoire de Recherche des Monuments Historiques (CRC-LRMH USR3224),
29 rue de Paris F-77420 Champs sur Marne France

[3] P. Lopez-Arce, M. Tagnit-Hamou, S. Aggoun, A. Kaci and A. Cousture
Laboratoire de Mécanique et Matériaux du Génie Civil, L2MGC (EA 4114), Institut des Matériaux (FD 4122), Université de Cergy Pontoise, F-95000 Cergy Pontoise, France

*corresponding author

1. Introduction

This paper presents the DIMPPA project ("Durabilité de l'Interaction Mortier-Pierre dans le Patrimoine Architectural", durability of the interaction mortar-stone in the architectural heritage) partially funded by "Fondation des Sciences du Patrimoine". In restoration works repair mortars with similar appearance and properties as the original stone, are used in order to substitute the weathered parts or to reconstruct the lost parts (Isebaert *et al.*, 2014). These mortar reconstructions allow for keeping in place the original stones without a complete substitution. This aspect is especially important in the restoration of the sculptured parts and statues. DIMPPA project deals with a problem that will have an increasing importance in the next years, which will be the behaviour of mortars used in the restoration of built cultural heritage as a function of the environmental conditions and the stone support.

The project has different objectives: a) to review the different stone-repair mortars used in France. We only study pre-formulated mortars in order to assure reproducible results; b) to characterise the "in situ" behaviour of couple stone-mortar repairs; c) to identify the compatibility and possible mortar-stone interactions and their influence on the conservation of stone compatibility, (Schueremans, *et al.*, 2011); d) to study the durability of the mortar-stone under different environmental conditions; e) finally, to propose suitable mortars as a function of the environmental conditions and the stone to be restored. All the goals of this project have not been reached and more research should be done. This paper presents some results related to the durability of mortars comparing "in situ" results, laboratory simulations and future conservation models.

2. Materials and methods

2.1. Methodology of the project

The first step was to do an inventory of the "ready to use" stone-repair mortars currently applied on stone cultural heritage restoration and their conservation degree on some selected monuments. We have selected three mortars and three buildings where the mortars have been applied on the same stone. The selected stone is Euville limestone that is mainly used on the basements of historic buildings in Paris. The buildings are: Grand Palais, where Lithomex (*Chaux de Saint Astier*) mortar has been used to restore the façade, Palais de la Decouverte where some sculpted parts have been restored with Artopierre mortar (*Parexlanko*) and the building of the police "prefecture" restored with Altar Pierre mortar (*ECP*) (Fig. 1). The three buildings are close to one another and to the Seine River. In all cases the restoration has been done between 2008 and 2010.

A second part of the research was to characterise the mortars (raw and cured materials), the Euville stone and the interactions between mortars and stone. On anhydrous raw materials we measured their grain size distribution, chemistry (energy dispersive X-ray analysis), mineralogical composition (X-ray diffraction, differential thermal analysis and thermogravimetry). The content of soluble salts from mortar samples collected in the buildings has been obtained by ion chromatography on water extractions. Two different kinds of specimens have been made in laboratory, 4×4×16cm mortar and stone-mortar specimens. On these specimens several physical properties have been measured: porosity, capillarity water absorption, evaporation, gas permeability, vapour permeability, mechanical strengths (compressional and flexural), P-wave velocity, colour and adhesion mortars-stone. Euville and couples mortar-stone samples have been petrographically characterised on thin sections under an optical polarized microscope.

To investigate the influence of curing environmental conditions (CO_2 concentration, temperature and relative humidity) on the physico-chemical behaviours of restoration mortars, four sets of specimens have been prepared under four different conditions of CO_2 content, temperature and relative humidity. The first set of samples corresponds to the most frequent Paris environmental conditions (11°C, relative humidity 65% and 400 ppm CO_2) and is the one we will present here.

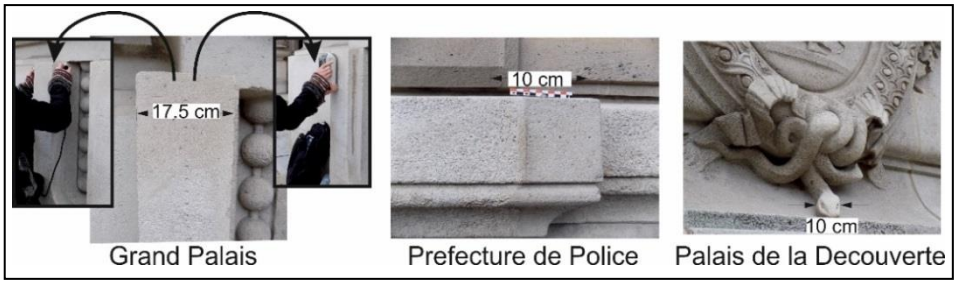

Fig. 1: Selected studied areas from the historic buildings.

Durability of mortars has been estimated in to different ways. First, some physical properties were measured "in situ" on stone-mortar repaired areas (measuring the surface of stone, mortar and their interface) that have been exposed during five years to Paris environmental conditions. When possible a small sample of mortar and stone has been collected. A second way, was in the laboratory by accelerated ageing tests. Two types of tests have been carried out: salt crystallisation tests (imbibition by capillarity/drying) and exposition to polluted atmosphere (based on UNE-EN 13919:2003). In all cases control specimens have followed the same tests but only using deionized water. The choice of the solution composition (0.1% $CaSO_4$, 3% Na_2SO_4, 1% KNO_3 and 1% NaCl) and gases (NOx and SO_2 obtained from evaporation of sulfurous acid (6%), and nitric acid (78%) solutions) has been done as a function of the salt found on the monuments and pollution data obtained from Airparif database. After the ageing tests materials have been characterised using different methods. A detailed description of the accelerated ageing tests can be found in Lopez-Arce *et al.*, 2015b.

2.2. Materials

The studied stone come from the Euville (Meuse department, France) quarry of Rocamat. Euville limestone is an Oxfordian crinoïdal grainstone with a coarse-grained texture and syntaxial calcitic cement. It is composed almost only of calcite (98%). The Euville quarry in Commercy shows a reef complex characterised by a crinoidal limestone (Humbert 1971, Fronteau 2000). Euville limestone has been employed from the XVI century, in 1574 a document mentioned for the first time one quarry of this stone (www.pierredeuville.org, www4.ac-nancy-metz.fr). Even if at the beginning its use is mainly regional, after the XVII century it has been employed in many buildings of France and Belgium and in other countries. We can also find it in different civil monuments of Francfort, Essen, Anvers, in the cathedrals of New-York and Baltimore and on the plinth of the statue of liberty.

A detailed characterization of the three mortars can be found in Lopez-Arce *et al.* (2015a). All are mixtures of natural and hydraulic lime mortars, with or without aerial lime. Lithomex mortar is defined as a natural hydraulic lime, with hydraulic binders, sand and

specific additives (water repellent), and has been used in the Grand Palais; Artopierre mortar is an aerial lime with hydraulic minerals and some additives and has been used on the Palais de la Decouverte; Altar Pierre is composed of hydraulic binder with mineral grains, and additives. It has been used in the restoration of the Prefecture de Police.

3. Results and discussion

In this paper we will discuss some of the obtained results concerning durability. In particular the monitoring of the conservation stage of mortars and stone by "in situ" measurements of P-wave velocity and colour in mortars exposed during 5 years to the Paris environment. These results will be compared to stone-mortars specimens artificially weathered in laboratory by salt crystallisation tests.

3.1. Physico-chemical characterization of stone and mortars

We will briefly present the results of the physical characterization of mortars and Euville stone. A more detailed description can be found in Lopez-Arce et al. (2015a). Most of the measurements have been done after 28 days of curing in order to compare all the samples in the same conditions (Lanas et al 2004).

Porosity is generally higher in mortars than in Euville, between 30% and 37% for Lithomex, 40% and 43% for Artopierre and 22% and 25% for Altarpierre, whereas Euville porosity is around 14% to 16%. No significant trend can be observed on the variation of porosity of the mortars with CO_2 concentration.

Capillary properties do not depend on the CO_2 concentration during the curing period, but some differences can be observed between 400 ppm and 1000 ppm. Capillarity coefficient (C) is highly variable from one set to another. In general, for Lithomex mortar C is much lower than for the others, for Artopierre it is similar to Euville C, and for Altar Pierre it is slightly lower. Euville limestone has the largest evaporation coefficient, followed by Artopierre mortar and then Altar Pierre and Lithomex mortars. This can be explained by the different mineralogical compositions between limestone and mortars. Mechanical properties and P-wave velocity have also been measured in mortars cured at different environmental conditions. In Tab. 1 we show the values of P-wave velocity (V_p) and colour measured in laboratory on "intact" samples.

3.2. Mortar's durability

Durability has been first estimated by "in situ" studies on "natural" exposed mortars from the historic buildings, and in laboratory by means of accelerated ageing tests.

3.2.1. "In situ" measurements

In Tab. 2 we present the V_p values of mortars and stone obtained in each building and the difference to the laboratory measurements. Colour measurements and variations between laboratory measurements and "in situ" measurements are compiled in Tab. 3. Systematically V_p "in situ" is higher than Vp in laboratory, especially for Altar mortar. Two different factors can explain this observation: in monuments materials are not dry and this humidity can increase V_p (V_p of saturated samples in laboratory is 4725 m/s) and the mortars can have a higher V_p due to hydrolysis and carbonation processes after 5 years.

Tab. 1: P-wave velocities (V_p) and colour parameters for the three mortars and Euville limestone. Mean values and standard deviation in brackets.

Material	V_p, m/s	*L**	*a**	*b**	*C**	Hue	*ΔE**
Lithomex	2560 (90)	78.44 (0.10)	2.35 (0.02)	11.32 (0.04)	11.56 (0.04)	78.30 (0.06)	3.22
Artopierre	2025 (75)	88.05 (0.11)	0.93 (0.03)	6.34 (0.08)	6.47 (0.08)	81.72 (0.13)	7.8
Altar Pierre	3000 (160)	76.36 (0.06)	1.60 (0.01)	9.56 (0.03)	9.70 (0.04)	80.50 (0.06)	5.16
Euville limestone	3550 (140)	81.38 (1.09)	2.68 (0.28)	10.06 (1.44)	10.41 (1.45)	74.98 (1.46°	--

Tab. 2: "in situ" P-wave velocities for the three monuments. Mean values and standard deviation in brackets.

Building	**Material**	V_p, m/s	□ V_p
Palais Decouverte	Artopierre	2315 (258)	+290
	Euville	3680 (678)	+130
Grand Palais	Lithomex	2700 (72)	+140
	Euville	4100 (270)	+550
Prefecture Police	Altar Pierre	3585 (117)	+700
	Euville	3700 (136)	+150

Tab. 3 shows that colour parameters are not very different between mortars and stone. However, total colour difference (ΔE^*) calculations between both materials shows higher differences at the Palais Decouverte, followed by Grand Palais and Prefecture Police. Only the latter fulfils the suitability criteria used to assess conservation treatments. The most significant observation is the low L value of Euville stone on the Palais de la Decouverte. This may be due to an experimental bias due to the more irregular shape of surface or just to the natural variability of the stone.

In the Grand Palais and Prefecture de Police we have collected small samples of mortar, and of stone in the Prefecture. In Fig. 2 we can observe the microstructure of these samples compared to the intact mortar and quarry samples. The soluble salt composition obtained from building samples have been used to model the mineralogical precipitations from this solution by ECOS model (Price 2000). In all the samples from buildings we found Cl^-, SO_4^{2-}, NO_3^-, Na^+, K^+, Mg^{2+} and Ca^{2+}. The most important result is that SO_4^{2-} in Euville samples is very high. We can observe that Euville texture is very different from mortars and that mineral grains in Altar mortar from Prefecture de Police present more cracks than the laboratory samples.

Tab. 3: "in situ" mean colour parameters values and standard deviation in brackets.

Building	Material	*L**	*a**	*b**	*C** (D65)	Hue (D65)	Δ*C**	Δ*E**
Palais de la Decouverte	Arto	71,27 (2.85)	3.14 (0.43)	12,51 (0.43)	12.91 (0.51)	75.97 (1.50)	0.34	10.34
	Euville	60,91 (0.72)	2.88 (0.62)	12.00 (0.42)	12,35 (0.30)	76,47 (3.16)		
Grand Palais	Lithomex	70.89 (0.77)	2.50 (0.09)	11.49 (0.30)	11.76 (0.31)	77.72 (0.22)	4.84	6.00
	Euville	74.44 (1.77)	1.40 (0.20)	6.78 (0.48)	6.92 (0.49)	78.30 (1.42)		
Prefecture Police	Altar	69.72 (1.11)	2.76 (0.17)	10.91 (0.58)	11.25 (0.61)	75.81 (0.24)	0.82	3.91
	Euville	73.53 (2.28)	2.04 (0.48)	10.52 (0.68)	10.03 (1.37)	79.03 (1.37)		

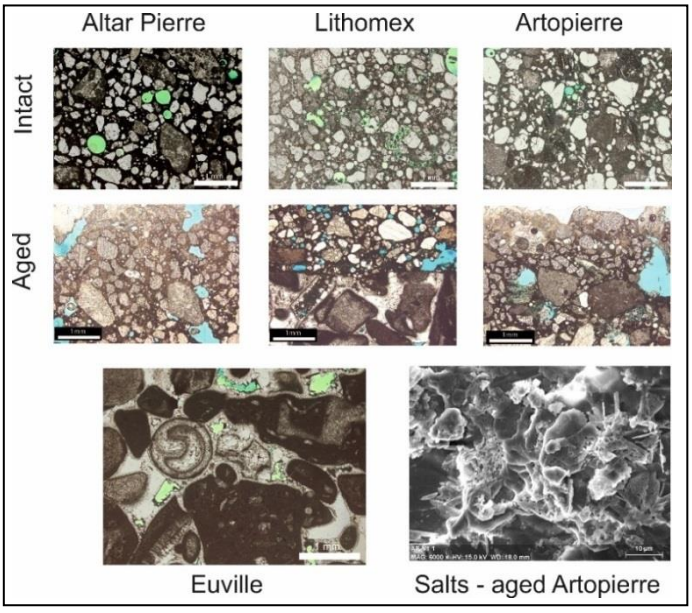

Fig. 2: Microscopy images of intact and artificial aged samples; and Euville quarry sample. Blue and green: open porosity. Sodium sulphate from aged Artopierre sample surface.

3.2.2. Laboratory ageing tests

Before and after the ageing tests a complete characterization has been done: mineralogy and chemical composition and physical properties, on weathered and control samples. Samples have been observed using optical and scanning electronic microscopes, with mineralogical and chemical determinations. Soluble ions have also been analysed and the physical properties were measured as well. All the results can be seen in Lopez-Arce et a*l* (2015b).

After the ageing tests, mortars are more affected by salt crystallisation and acid exposure tests compared to the stone. Artopierre mortar develops salt efflorescences.Altar Pierre shows efflorescence as well however to a lower degree. Lithomex mortar does not show salt efflorescences, but powdering of the surface took place after the acid exposure test. We assume that such behaviour with salt crystallisation is related to water-repellent product as additive in Lithomex. At the surface of Artopierre mortar crusts and cracks can also be observed. Specimens exposed to the acid atmosphere show important colour changes.

V_p and colour have been measured on control and artificial weathered mortar-stone samples. Results are shown in Tab. 4. As no V_p measure has been done on intact mortar-samples, we consider the mean of V_p on mortar and Euville limestone. In all cases V_p increases with salt crystallisation. At this point of the test not much material has been lost and salt precipitates on the pores facilitating wave transmission. If we calculate the average velocity between 'in situ" V_p for mortars and V_p of Euville in laboratory we obtain 3125m/s for Lithomex, 3570 m/s for Altar and 3125 m/s for Artopierre. These values are comparable to the V_p values of the artificially aged samples.

Tab. 4: P-wave velocity (salt crystallisation test) and colour parameters (vapour exposition tests); Mortar-stone samples: I = intact; A = aged sample.

Samples		**Lithomex**		**Altar Pierre**		**Artopierre**		**Euville**	
		I	**A**	**I**	**A**	**I**	**A**	**I**	**A**
Colour	*L**	78.44	72.72	76.36	73.63	88.05	85.66	81.38	80.18
	*a**	2.35	3.5	1.6	2.15	0.93	1.41	2.68	2.95
	*b**	11.32	17.58	9.56	11.81	6.34	8.98	10.06	12.08
V_p(m/s)		3060	3150	3275	4250	2790	3235		

4. Conclusions

We have developed a comprehensive study about the durability of stone-repair mortars used in many monuments in France. In order to compare the behaviour of some mortars exposed to different environmental conditions we wanted to limit the number of variables as much as possible. For this reason we have chosen mortars that have been applied on the same stone, at the same time and under the same (as much as possible) environmental conditions. We have studied three monuments in Paris, close to the Seine River, less than 2km away one from the other, and in which Euville limestone has been used, in combination to other limestones. The selected areas located on the lower part of the monuments (less than 2m high) have been restored with three different "pre-formulated" mortars between 2008 and 2010.

Mortars have been characterised physically, mineralogically and chemically. The interaction between mortars and Euville stone and the durability of the couple, has been determined "in situ" by non-destructive techniques and in laboratory by the study of specimens artificially weathered by salt crystallisation and acid exposure tests. In order to estimate future durability we did some preliminary tests using ECOS model and Aladin climatic model (Meteofrance). We can conclude that in future, more degradation (~15%) could be expected compare to past time.

After all these preliminary studies no clear final conclusion can be drawn. Some mortars have close mechanical properties to the Euville stone while others show a better hydric compatibility with the stone. More research is needed to better understand the physical and chemical interaction between mortar and stone and how these interactions act on their future durability.

References

AENOR UNE-EN 13919 (2003) Natural stone test methods - Determination of resistance to ageing by SO_2 action in the presence of humidity.

Fronteau, G, 2000, Comportement telogenetiques des principaux calcaires de Champagne-Ardenne, en relation avec leur facies de dépôt et leur séquence diagénetique. PhD Université de Reims Champagne-Ardenne, 296 p.

Humbert L, 1971, Recherche méthodologique pour l'histoire biosédimentaire d'un bassin. L'ensemble carbonaté oxfordien de la partie orientale du Bassin de Paris. Thèse d'Etat Univ. Nancy.

Isebaert, A. V Parys, L. and Cnudde, V., 2014, Composition and compatibility requirements of mineral repair mortars. Construction and Building Materials 59, 39–50.

Lanas J, Perez Bernal JL, Bello MA, Alvarez Galindo JI, 2004, Mechanical properties of natural hydraulic lime-based mortars. Cem Concr Res 34:2191–2201.

Lopez-Arce, P. Tagnit-Hammou, M. Menendez,B. Mertz, J.D. and Kaci, A., 2015a, Physico-chemical stone-mortar compatibility of commercial stone-repair mortars of historic buildings from Paris. Submitted to Construction & Building Materials.

Lopez-Arce, P. Tagnit-Hammou, M, Menendez, B, Mertz J.D and Kaci, A., 2015b, Durability of stone-repair mortars used 1 in historic buildings from Paris. Submitted to Materials and Structures.

Price, C, 2000, An Expert Chemical Model for Determining the Environmental Conditions Needed to Prevent Salt Damage in Porous Materials. Archetype Publications. ISBN 1873132522, 136p.

Schueremans, L. Cizer, O. Janssens, E. Serré, G. and Van Balen, K., 2011, Characterization of repair mortars for the assessment of their compatibility in restoration projects: Research and practice. Construction and Building Materials 25 (12) 4338–4350.

RESTORATION OF WEATHERED LOAD BEARING MASONRY WITH OPTIMISED GYPSUM BASED MORTARS

B. Middendorf[1*] and U. Huster[2]

Abstract

In the past gypsum had a wide distribution as building material and was used in some specific areas as masonry mortar. Gypsum mortars have a high water solubility and a significant loss of strength by moisture saturation. Nevertheless, still intact long-term weathered masonry exists constructed with gypsum mortars. Commercially available gypsum based mortars are not suitable for restoration and cement based mortars are not compatible. For this reason, compatible and weathering resistant gypsum lime mortars for the restoration of historic masonry, originally built with gypsum mortar, were developed in a German research project. These were successfully monitored and tested as masonry mortars for more than 10 years in outdoor weathered brick masonry walls. For the first time in 2015 these water resistant gypsum lime mortars were used for the restoration of weathered load-bearing masonry. A restoration of the St. Urbani Church in Munster, Germany was realised at the fieldstone masonry of the bell tower, which was partially dismantled and next rebuilt with the optimised and for this particular case separately approved gypsum lime mortar. In addition to the development and the properties of the gypsum based mortar, the restoration project of the St. Urbani Church and its implementation will be described.

Keywords: restoration, historic masonry, gypsum mortar, water resistant, compatibility

1. Introduction

The use of calcium sulphate based mortar has a long tradition. A difficulty for the restoration and the conservation of monuments is the missing information about the composition of the historic mortars. After the first half of the 19th century, knowledge of the production, preparation and properties of different gypsum based materials ran out of fashion when hydraulic binders like Portland cement were introduced (Steinbrecher 1992). Modern gypsum based building materials are always designed for interior use, due to the special properties of this material. General advantages of calcium sulphate based building materials are low production costs, quick and controllable setting behaviour, good adhesion to stone as well as the simplicity of application. However, its high solubility in water (2.14 g l^{-1}), the low compressive strength as well as the creeping under water saturated conditions restrict its use to the interior of buildings (Twelmeier 2011; WTA 2008). Nevertheless,

[1] B. Middendorf*
Department of Structural Materials and Construction Chemistry, University of Kassel, Germany
middendorf@uni-kassel.de

[2] U. Huster
HAZ Engineers, Kassel, Germany

*corresponding author

mineralogical investigations of historic joint mortars from different brick buildings in northern Germany and Italy have shown that gypsum anhydrite mortars with a small amount of lime have also been used on the outside of sacred buildings (Cioni 1991; Middendorf and Knoefel 1998). A great part of these joints and of the masonry is still well preserved. Also, in central Germany some monuments were built with natural stone or brick and gypsum based mortars, like the St. Urbani Church in Munster. According to Steinbrecher (1992) this durability is due to its composition as well as to its preparation with extremely small quantities of water which effects a dense micro structure with low porosity. A water/binder value of less than 0.4 and a bulk density of 2.0 g cm^{-3} are mentioned for historic gypsum mortars. Results of the studies of historic calcium sulphate based mortars (Werner 1986, Lucas 1992; Middendorf 1994) formed the basis to the development of gypsum based mortars for restoration purposes. The focus is on the improvement of the water resistance of calcium sulphate based restoration mortars and on the establishment of guidelines for the development and industrial production of these mortars.

2. Water resistant gypsum mortar

2.1. Composition

There are numerous publications and patents dealing with the increase of water resistance of calcium sulphate based building materials (*e.g.* Balzer 1991; Gerhardinger *et al.,* 1994: Middendorf 2002, Tesch 2007). There are several different approaches; one of them makes use of additives in order to increase the resistance to the dissolving effect of water. Another approach to increase the water resistance of calcium sulphate based building materials turns to hydraulic, latent hydraulic and pozzolanic admixtures. Apart from reactive microsilica, cement rich in alumina and low in aluminate content, fly ash (Singh and Garg 1992) and granulated blast furnace slag sand (Koschany *et al.;* 1969) are also used. The strength of the micro structure is caused by the crystallisation of calcium silicate hydrate (CSH)- and calciumaluminate hydrate (CAH) phases and partly by ettringite. The most promising approach is the inherent passivation of surfaces through recrystallisation processes. From preservation of brick monuments it is known that masonry made of gypsum mortar with small amount of lime has shown resistance to weather attack, although dihydrate can be highly soluble in water. As the reproduction of historic building material is nearly impossible, because normally the recipes are not sufficiently known, nor are the places of origin available. It has been attempted to develop water resistant calcium sulphate based mortar for exterior masonry based on industrial building materials. Mortars from α-hemihydrate, *β*-hemihydrate and/or anhydrite and hydrated white lime (CL 90, acc. EN 459) as binders and limestone powder and fine quartz sand as aggregates correspond fairly well to demands, as has been confirmed by building investigations over many decades (Middendorf 1994; Tesch 2007). The formulation of the mortar is listed in Tab. 1.

2.2. Inherent passivation of mortar surface - results

Water resistance is developed because gypsum lime mortar can close pores and cracks by moisture through recrystallisation processes. This can be called autogenous healing or as inherent passivation of the surface. As outlined in Fig. 1 the gypsum lime mortar is partly dissolved by water but owing to the amount of lime and aggregate. They are not considerably worn out. The biggest part of the gypsum having been dissolved partly by water is absorbed via capillary pores into the micro structure and precipitates there again.

This process causes a reduction of both the amount of capillary pores and the total porosity resulting in decreasing water absorption capacity. Both calcite and aggregate have been enriched on the weathered joint surface because they are less soluble than gypsum. In this way, the joint mortar shelters the gypsum rich part of the inner joint. Furthermore during time the lime hydrate will carbonate at the surface and will dense it too. In this case gypsum lime mortars are no longer susceptible to moisture reduction of mechanical strength. The formulation of the optimized and for the restoration of the bell tower of the St. Urbani Church used mortar is listed in Tab. 1.

Tab. 1: Composition of used gypsum lime mortar.

Binder	**Content wt.%**
α-hemihydrate	80
lime hydrate (CL 90 acc. EN 459)	20
Aggregate	**Content wt.%**
silica sand < 0.6 mm	15.75
silica sand < 4 mm	5.00
limestone powder coarse	60.00
	19.25
tartaric acid	1 ‰ applied to the content of α-hemihydrate
binder/aggregate-ratio:	1/4 by mass

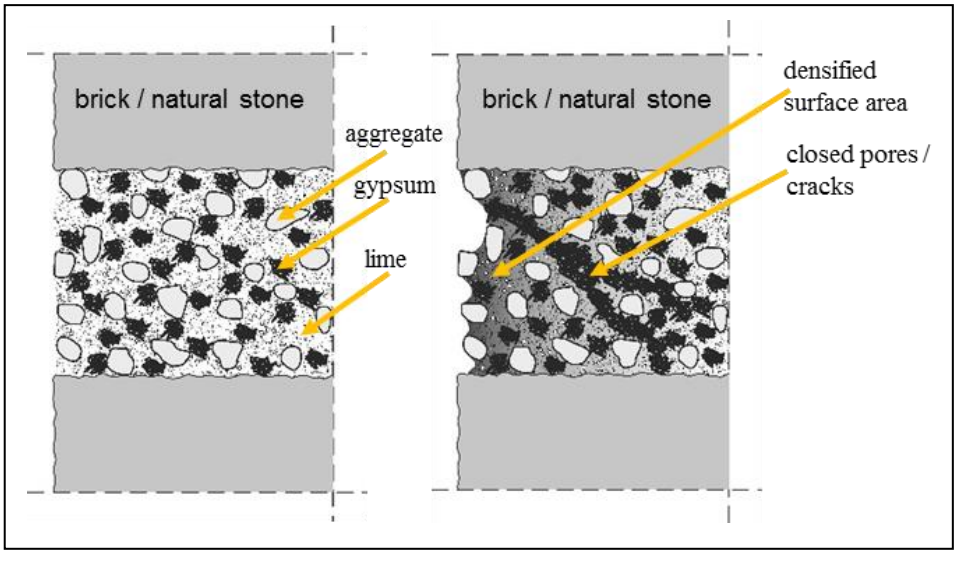

Fig. 1: Principle of inherent passivation; left: before weathering; right: after weathering with closed pores and densified surface.

Freely weathered brick masonry mortar joints were tested by microscopic methods after 10 years of external weather exposure. Light microscopic pictures of polished sections show that the weathered mortar surface appears to be more dense than the mortar inside the joint (Fig. 2a).The results of scanning electron microscopy confirm this study (Fig. 2b). In energy dispersive X-ray scans a decrease in sulfur can be detected on the surface which also confirms the thesis of the inherent passivation of gypsum and/or gypsum lime mortars (Fig. 3). By using mercury intrusion porosimetry it can also be seen that the outer surface is more dense (total porosity: 13.9 vol.%) than the inner part (total porosity: 18.9 vol.%) of the mortars. The difference in porosity is due to the reduced capillary pores; the difference in air voids and gel pores of both mortar parts is small which can be seen in Fig. 4.

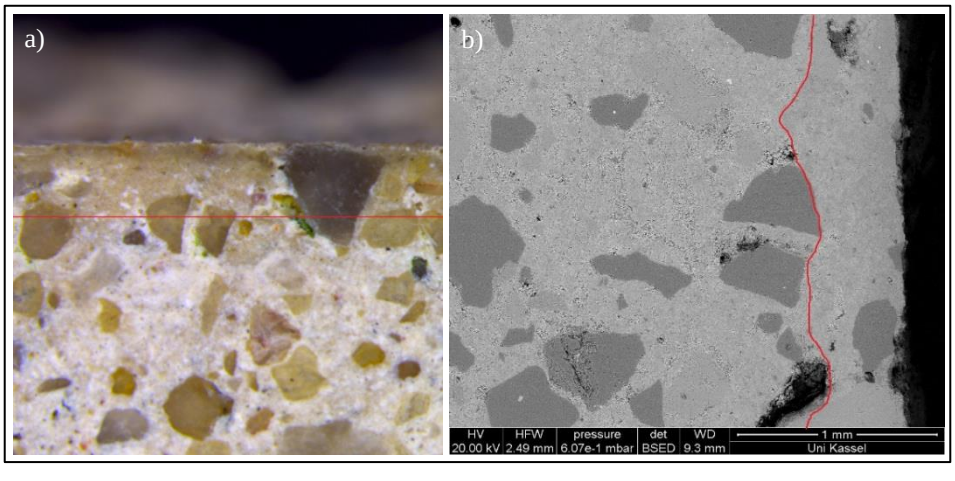

Fig. 2: a) Light microscopic picture with dense surface (above); b) SEM-picture taken with BSE-detector; right the dense surface can be seen.

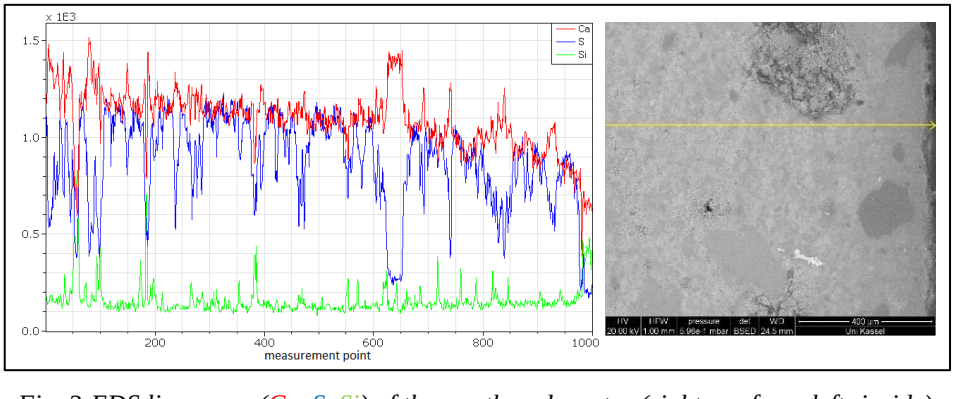

Fig. 3:EDS line scans (Ca, S, Si) of the weathered mortar (right: surface; left: inside).

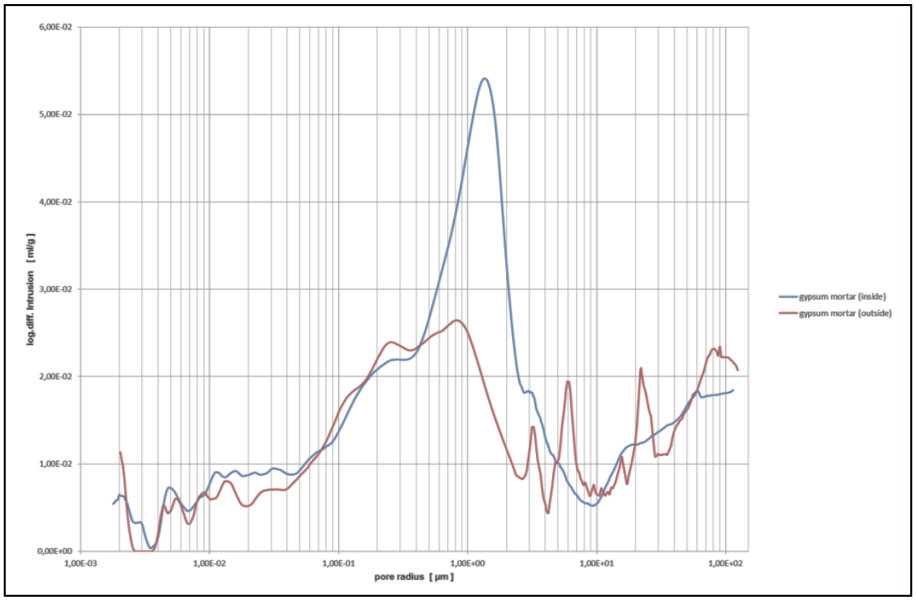

Fig. 4: Mercury intrusion porosimetry results; less capillary pores in outer mortar part.

3. Application

3.1. History of restauration of St. Urbani Church, Munster

The St. Urbani church in Munster is approximately 450 years old and the bell tower made of brick and natural stone masonry was extensively restored in 2003 (Fig. 5a). The refurbishing work that also included masonry injections was completed in 2004. One year later already, numerous cracks appeared in the brickwork of the bell tower which could be traced to material incompatibilities and creeping based on high moisture entry (Fig. 5b). In response, the tower was scaffolded again in 2006 (Fig. 5a). Based on various experts' reports a requirement for the second restoration was developed. The new restoration has to be sustainable and historically authentic. The masonry is to be maintained in situ and not to be entirely reconstructed. Damaged and cracked sections of the brick and stone masonry need to be raised and filled with water resistant gypsum based mortar in order to avoid incompatibilities. An approval for the individual case was filed for, because gypsum based building materials must not be applied in statically load-bearing masonry or in weathered exterior areas. After the approval the restoration work started and the masonry was gradually removed and reconstructed by using the gypsum lime mortar described in section 2. This mortar was chosen due to existing long-term experiences with this material.

3.2. Mortar composition

For the reconstruction of the masonry parts of the bell tower the mortar listed in Tab. 1 was used for bricking and jointing. As the historic masonry partly contained gypsum mortar it was only possible to restore the tower by using gypsum mortar. The gypsum mortar chosen and described in Tab. 1 had a compressive strength in dry condition of approximately 15 MPa and in moist condition still approximately 5 MPa. By adding of 8 wt% support grain

in the aggregate the creeping value in moist conditions could be drastically reduced. The work was exclusively performed by specialized companies and in addition monitored externally. Fig. 6 shows the masonry work during the refurbishing period. Fig. 7 shows St. Urbani Church after the completion of the restoration. Hence, it is the only church in Germany where gypsum mortar was applied in the weathered exterior area in statically load-bearing masonry.

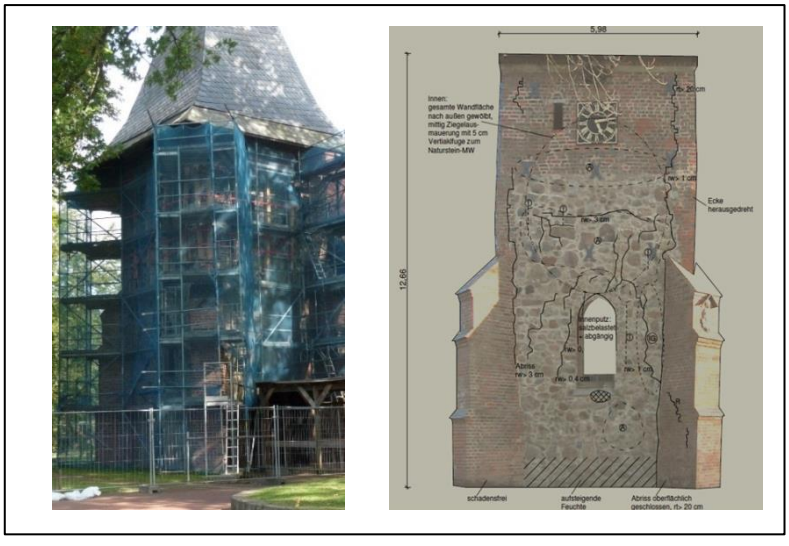

Fig. 5: St. Urbani Church in Munster, Germany, a) mixed masonry of bell tower of the church; natural stones and bricks, during restoration, b) damaged masonry of tower after the first restoration in 2003.

Fig. 6: Masonry of the bell tower during restoration.

Fig. 7: Restorated St. Urbani Church in 2015: a) Total view of the St. Urbani; b) Restorated field stone and brick masonry with gypsum lime mortar.

4. Summary

Buildings containing gypsum mortar require special attention as they may only be restored with compatible construction materials. On the one hand, the construction materials have to be chemically-mineralogically compatible with the original gypsum mortar and on the other hand also the mechanical properties have to be adapted. But as gypsum materials are soluble in water and their strength considerably decreases when soaked by moisture, their appliance in exterior areas is forbidden. The gypsum lime mortar developed here disposes of adjusted strengths and an inherent passivation of the surface, so that is may be applied outside. Due to the approval in the individual case, after 10 years of extensive testing, it could successfully be used in statically load-bearing masonry in exterior areas.

References

Balzer, M., 1991, Untersuchungen zur Steigerung der Wasserfestigkeit von Gipsbindern, Ph.D. thesis, Technical University Clausthal, Germany.

Cioni, P., 1991, Small thickness brick vaults in Tuscany: theirs characteristics and consolidation, Proceedings of the 9th International Brick/Block Masonry Conference, Berlin, Germany, Vol. 3, 1523-1530.

Gerhardinger, D. and Mayer, H. and Mittermeier, J., 1994, Verfahren zur wasserabweisenden Imprägnierung von Gips, patent DE-44 19257 A1, Germany.

Koschany, R. and Fietsch, G. und Vogt, H., 1969. Verfahren zur Herstellung von Erzeugnissen aus $CaSO_4$-Bindemitteln, alkalisch reagierenden Bindemitteln und Industrieanfallstoffen, patent DE 79 948.

Lucas, H. G., 1992. Gips als historischer Außenbaustoff in der Windsheimer Bucht - Verbreitung, Gewinnung und Beständigkeit im Vergleich zu anderen Natursteinwerken, Ph.D, thesis, RWTH Aachen, Germany.

Middendorf, B., 1994, Charakterisierung historischer Mörtel aus Ziegelmauerwerk und Entwicklung von wasserresistenten Fugenmörteln auf Gipsbasis, Ph.D. thesis, University Siegen, Germany.

Middendorf, B. and Knoefel, D., 1998, Gypsum and lime mortars of historic German brick buildings: analytical results as well as requirements for adapted restoration material, In: Baer, N.S. *et al.* (eds) Conservation of Historic Brick Structures: Case Studies and Reports of Research. Donhead Publishing, Dorset, England, 197-208.

Middendorf, B., 2002, Physico-mechanical and microstructural characteristics of historic and restoration mortars based on gypsum: current knowledge and perspective, Geological Society London, Special Publications 205, pp. 165-176.

Singh, N.B. and Garg, M., 1992, Investigation of a durable gypsum binder for building materials, Construction & Building Materials, 6, 52-56.

Steinbrecher, M., 1992, Gipsestrich und -mörtel: Alte Techniken wiederbeleben. Bausubstanz, 10, 59-61.

Tesch, V., 2007, Gefügeoptimierte Instandsetzunsmörtel auf Calciumsulfat-Basis für die Anwendung im Außenbereich, Ph.D. thesis, Kassel University Press GmbH, Kassel, ISBN 978-3-89958-333-5.

Twelmeier, H., 2011, Dauerhaftigkeitsprognose der Verfugung von gipshaltigem historischem Mauerwerk, Ph.D. thesis TU Braunschweig, Germany, ISBN 978-3-389288-197-1.

WTA-Merkblatt 2-11, 2008, Gipsmörtel im historischen Mauerwerksbau und an Fassaden, WTA-Publications Munich, ISBN 978-3-8167-7593-5.

Werner, A., 1986, Sanierung von Kirchenbauten an der Elbe, Bausubstanz, 5, 36-40.

ACQUISITION AND ANALYSIS OF PETROPHYSICAL PROPERTIES OF THE ROCK OF THE MASONRY OF THE CATHEDRAL OF AGUASCALIENTES, MEXICO

R. Padilla Ceniceros[1*], J. Pacheco Martínez[1] and R.A. López Doncel[2]

Abstract

The Basilica Cathedral of "Nuestra Señora de la Asuncion" is the principal catholic building in the city of Aguascalientes and one of the most emblematic. It was built through the period of 1704-1738, in sober Solomonic Baroque style. Presently, it shows signs of deterioration and instability in some elements, principally in the outer walls of the temple due to weathering and exposure to a high humidity. The lithological material used in most of the walls of the Cathedral of Aguascalientes is a volcanic rock known as tuff, this material is characteristic for its low mechanical and petrophysical properties. With the goal of characterising the resistance of the rock in the masonry to the outdoor environment, tests related to the physical properties were performed, such as: the capillary water absorption, the distribution of pore sizes and the density as well as the resistance to salt crystallisation cycles. The results show that the rock in the temple walls has a high porosity, which contributes to its degradation principally due to the effects of rising damp. The realised tests allow for the characterisation of the susceptibility of the constitutive stone to weathering. The data obtained allow an estimation of the susceptibility of the entire building to weathering.

Keywords: Aguascalientes, tuff, rock characterisation, rising dampness, porosity

1. Introduction

Since ancient times**,** a recurrent use of stone in monumental constructions around the world was registered, principally for the construction of walls and structural elements. The easy extraction of rock as a construction material contributed to its wide use during civilisation periods for the construction of buildings and monuments. However, through most of their life these constructions underwent changes, modifications, and even collapses, due to anthropic processes and extreme natural phenomena (earthquakes, intense rainfalls, volcanic eruptions, etc.), or the simple effect of gradual weathering. Weathering phenomena are perhaps the most recurring, as they depend on the intrinsic quality of the stone and past conservation measures, in a way that the level of degradation in the stone is an indication of the health of the entire heritage built. However, the heterogeneity of the

[1] R. Padilla Ceniceros and J. Pacheco Martínez
Autonomous University of Aguascalientes, Science Center of Design and Construction, Aguascalientes, Mexico
raudelpc@gmail.com

[2] R.A. López Doncel
Autonomous University of San Luis Potosí, San Luis Potosí, Mexico

*corresponding author

stone type used for the construction of the building provokes changes of different intensities in physical, chemical and mechanical properties. Both construction techniques and conservation measures of historic buildings require a profound knowledge of the constitutive stone material. Hence, the deterioration characteristics of the stone are crucial for the selection of preservation and conservation interventions (Siegesmund *et al.*, 2002). Studies related to the changes in the properties of rock enable an evaluation of the susceptibility of stone material to deterioration, i.e. its durability when exposed to weathering agents (Ahmad, 2012). However, the interaction between the properties of stone and the processes of weathering that affect it are very complex in such a way that there is no unique parameter capable to measure the process of weathering, but rather a series of involved factors (Nicholson, 2001). In this work, research findings related to the characterisation of the susceptibility to degradation of four stone types from the wall masonry of the Cathedral of Aguascalientes are presented. The characterisation consists of laboratory tests that aim to understand the effects that water, sun, wind, environmental pollution, etc. have on the stone materials. Finally, the test results are related to the level of deterioration on the walls of masonry.

2. Materials and methods

The most used stone in the historic constructions of the state of Aguascalientes is a moderately welded tuff, due to its ease of extraction and low volumetric weight (less than 2000 kg/m^3), as well as its thermic and acoustic isolation properties (Fitzner and Basten, 1994). However, tuff rock is known for its low mechanical properties (resistance to compression and tension) and deterioration patterns such as flaking, scaling, alveolization, discolouration, detachment of the black crust, soiling and scratch. The principal deterioration factor is generated by the migration of water through capillary rising damp, generally till a height op 1.5 m in the walls. Petrographic tests were realised in laboratory on samples with dimensions of 6.5×6.5×6.5 cm of rock extracted from the masonry of the Cathedral of Aguascalientes. The rocks used in this investigation are: rock R1 has an intense pink colour and a moderately welded matrix, contains 20% of semi-round intrusive lithic fragments having a size from 0.2 to 0.8 cm and has a medium hardness; rock R2 is pink coloured and has a medium consolidated matrix, has a small percentage of lengthened pumice, contains about 10% round lithic fragments of a size ranging from 0.1 to 0.4 cm, and has a medium hardness; rock RR is light pink coloured, often used in the restauration interventions, has a few percentage of round lithic fragments of 0.1 to 0.3 cm size, a well consolidated matrix, and a medium hardness; rock B is whitish-purple coloured, contains some small round lithic fragments of 0.1 to 0.3 cm size, has a medium consolidated matrix and a medium hardness; and finally, rock M which is a light purple coloured rock type having similar characteristics as rock B.

The following tests were performed:

a) Mercury intrusion test to determine the pore size distribution and the porosity of the rock. The test was applied in accordance with the norm DIN 66133.
b) Capillary water absorption. This test was performed to obtain water absorption values and the time to reach water saturation, according to the norm DIN ISO 15148.

c) Hydrostatic weighing test to determine matrix density (ρmatrix) and Bulk density (ρBulk), and data about the open porosity in the rock. The test was applied in accordance with the norm DIN EN 772-4, using a KERN PCB 6000-0 digital scale with a maximum capacity of 200 g and a fastening system to hold the sample.

d) Salt crystallisation test to evaluate the behaviour of the stone in the presence of sulphates. The procedure was realised in accordance with the norm DIN EN 12370. The test consists of cycles of 4 hours for the immersion of the stone in a 10% sodium sulphate solution followed by drying at 75° during 4 hours. By means of a semi-professional camera (Canon model SX 400 IS) visual changes caused by deterioration are registered at the end of each cycle.

3. Results

3.1. Mercury intrusion test

The samples analysed in this test were: rock R2, R1 and RR. Fig. 1 presents the total porosity and the effective pore radii characteristics. For rock R1 and RR, the main pore size ranges from 1 and 10 µm, while that of R2 from 0.001 and 0.01 µm.

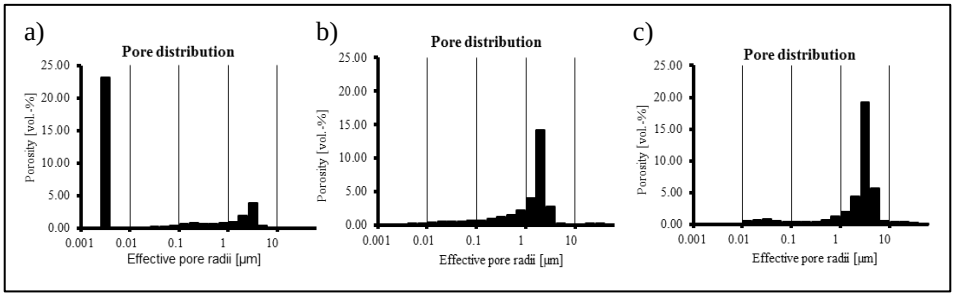

Fig. 1: Pore size distribution and total porosity of rocks R2 (a), R1 (b) and RR (c).

3.2. Capillary water absortion

Figure 2 presents the evolution of the water uptake performed according to the X, Y and Z axes, identified in correlation to the orientation of the lithic fragments aiming to determine whether anisotropy exists in terms of water absorption properties. The blue coloured curves are representative for rock B, the saturated value of 99.19 kg/m^2 is reached in 70 min. The curves of rock RR, localized at the bottom, show a saturated water content of 63.84 kg/m^2 that is reached after 170 min.

3.3. Salt crystallisation test

Fig. 3 illustrates the evolution of the mass change as a function of salt crystallisation cycle number. The resisted cycles range from 16 to 18 cycles, and the weight loss reaches values up to 83%. In the first 10 cycles samples show an increase in weight due to the presence of sulphates reaching up to 111% of the total weight. The R2 tuff shows a good behaviour until the disintegration after 16 cycles, sample M disintegrates after 17 cycles, while the B and RR tuff disintegrate after 18 cycles.

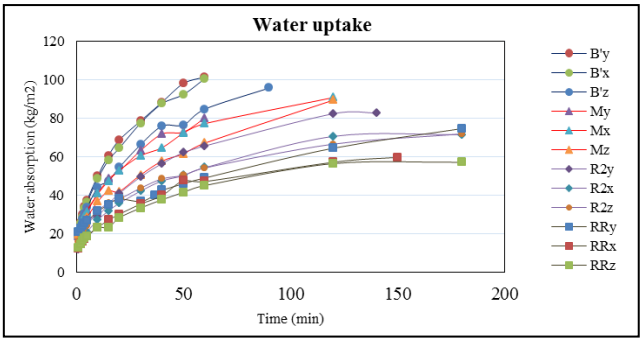

Fig. 2: Capillary water uptake curves of rocks RR, R2, B and M.

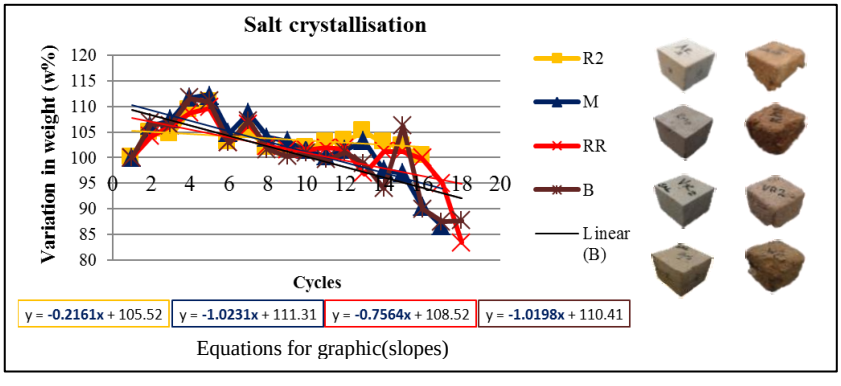

Fig. 3. Evolution of the mass change as a function of salt crystallisation cycle number of R2, M, RR and B. The samples before and after the salt crystallisation cycles are presented in the right part.

3.4. Hydrostatic weighing test

Tab. 1 presents the matrix density, bulk density and porosity obtained from the hydrostatic weight data. The stones with the lowest bulk density are R2 and M (1.63 g/cm^3) while the rock with highest one is RR (1.73 g/cm^3). Concerning the porosity M and RR stand out with 33.32 and 28.65% respectively.

Tab. 1: weight of the samples in dry and wet condition, porosity and density obtained from the hydrostatic weighing test.

Sample	Dry weight	Submerged weight	Wet weight	Porosity	Bulk density	Matrix density
R2	434.99 g	253.17 g	520.09 g	31.88%	1.63 %	2.39 %
M	457.13 g	269.83 g	550.74 g	33.32%	1.63 %	2.44 %
B	434.92	256.5 g	519.63 g	32.19%	1.65 %	2.44 %
RR	496.36 g	290.57 g	578.98 g	28.65%	1.72 %	2.41 %

4. Discussion

There are three kinds of pores: micropores (less than 0.1 μm), capillary pores (1 mm – 0.1 μm) and macropores (greater than 1 mm) (Siegesmund and Snethlage, 2011). The analysed tuff in the three rocks have a medium-high effective porosity. In two of the studied samples (R1 and RR) capillary pores predominates with pore measurements between 1 and 10 μm. Rock R2 mainly consists of micropores having a size < 0.1 μm. According to Lucia (1983, 1995, 1999) an increase in porosity is considered a negative factor in the behaviour of the rock, in a sense that it becomes more fragile in outdoor conditions. In the case of the developed experiments M and B tuff show a lower resistance and high porosity. The stone of light colours (B and M) reached water saturation rapidly; on the contrary, in the samples of pink tones (RR and R1) the process of water saturation is slow. The former means that the wet-dry cycles in stones B and M are faster, which can result in a greater deterioration of the stone. According to Siegesmund and Snethlage (2011), the capillarity mechanism principally depends on the size of pore and the geometry of the pore system. In the case of the samples, R2 with micropores at 31.88% of porosity reaches its saturation in less time that the sample RR with macropores at 28.65% (Tab. 1), which means that micropores geometry and hight percentaje contributes to a rapid saturation. In the salt crystallisation test, the quantity of cycles that the samples resist and the quantity of material loss per cycle are indicative of the rock's resistance to sodium sulphate crystallisation. The slopes of the graphs in Fig. 3 are indicative of salt resistance in a sense that small slopes show a greater resistance. According to the obtained slopes, the samples M and B show a low resistance to sulphates with a slope of 1.02. RR and R2 samples improve the resistance to sulphates with a lower slope -0.76 and -0.22 respectively. When considering the resistance to salt crystallisation, one should taking into account two parameters, the number of cycles and the slope of material loss. In that sense, R2 resists less cycles and shows a smaller slope. The sample showed no significant weight loss until cycle 16, after that, it began to lose a high percentage of weight whereas sample RR resisted well during 18 cycles and presented a considerably smaller slope of -0.76 (Fig. 3). Samples M and B show similar results of porosity and matrix density. The parameter for the greater weight is the bulk density, as it reflects the density of the sample's mass, without taking into account its porosity. An ample variation in the considered parameters does not exist; however, the rock with the best characteristics is RR both in terms of porosity and bulk density.

5. Conclusions

According to the capillary water absorption tests, the light-coloured samples (B and M) present a greater absorption rate. On the contrary, the dark-coloured samples (R2 and RR) showed a rather slow saturation process and less quantity of water was absorbed. This could represent the variation of deterioration that different rocks show in the cathedral. Within the water absorption tests, the anisotropic characteristics of the rock were revised, concluding that there are no significant variations, therefore the rock can be considered isotropic in terms of capillary water absorption. In the mercury intrusion test, the analysis of only three types of rock (B and M) was possible. Two of the tried samples (R2 and RR) resulted with a macroporous structure ranging from 1 to 10 μm of pore radius. On the other hand, sample R was clasified, according to the results, as having high microporosity.

Porosity is considered the most important parameter in rock, and an increase in porosity has a negative influence in its resistance to the outdoors (Siegesmund and Snethlage, 2011). Consequently, sample M with a 31.88% porosity, is the sample with the least resistance to weathering, while the rock RR, resulting with 28.65% porosity, is the rock that should be characterised by the highest resistance. Based on the porosity data, it can be concluded that the light-coloured samples are more susceptible to weathering factors. From the salt crystallisation test, sample RR stood out, as it resisted more cycles and presented a smaller degradation slope compared to the other sample. The rock M and B shows a lower resistance to the crystallisation of sodium sulphate. This rock is found in minimum quantity in the first meters of wall, therefore the damages to the masonry due to salt crystallisation in these zones are significant. Aguascalientes Cathedral has small areas with presence of sodium sulphate in the wall of the main facade.

References

Ahmad, A., 2012, Characterization of natural and consolidated stones from Jordan with non-destructive ultrasonic technique and physico-mechanical methods (Doctoral dissertation).

Fitzner B. and Basten D., 1994, Gesteinsporosität—Klassifizierung, meßtechnische Erfassung und Bewertung ihrer Verwitterungsrelevanz—Jahresberichte aus dem Forschungsprogramm ‘‘Steinzerfall-Steinkonservierung’’ 1992, Förderprojekt des Bundesministers für Forschung und Technologie. Verlag Ernst & Sohn, Berlin

Lucia F.J., 1983, Petrophysical parameters estimated from visual description of carbonate rocks: a field classification of carbonate pore space. J Petrol Tech 35:626–637.

Lucia F.J., 1995, Rock fabric/petrophysical classification of carbonate pore space for reservoir characterization. Am Assoc Petrol Geol Bull 79:1275–1300.

Lucia F.J., 1999, Carbonate reservoir characterization. Springer, Berlin.

Nicholson, D.T., 2001. ‘Pore properties as indicators of breakdown mechanisms in experimentally weathered limestones’. Earth Surface Processes and Landforms, 26: 819-838.

Siegesmund, S., and Snethlage, R., 2011, Stone in architecture. Springer, 4th ed. doi, 10, 978-3.

Siegesmund, S., Weiss, T., and Vollbrecht, A., 2002, ‘Natural stone, weathering phenomena, conservation strategies and case studies: introduction’. In Natural stone, weathering phenomena, conservation strategies and case studies, Siegesmund, S., Weiss, T., and Vollbrecht, A. (ed.) 1-7. Geological Society, London.

THE ASSESSMENT AND TREATMENT OF TWO CAST STONE FOUNTAINS FROM THE 1920'S IN PALM BEACH, FLORIDA, USA: TECHNICAL AND THEORETICAL ISSUES IN THE PRESERVATION OF AGED CAST STONE

M. Rabinowitz[1*], J. Sembrat[1] and P. Miller[2]

Abstract

Palm Beach, Florida developed into one of the premier winter playground for America's elite early in the 20th century when grand mansions, hotels, public buildings and, particularly, fountains were built in the Mediterranean Revival style along its pristine barrier island beaches. These were primarily constructed of reinforced concrete and cast stone to resemble the stone Spanish and Italian design sources. As these structures are approaching their centennial, the inherent vulnerability of the material: erosion of the soft concrete; carbonation of the paste and resulting deterioration of embedded iron; exposure to aerosol salts from the marine environment; bio-growth fostered by the tropical climate, damages from impact, wear and the occasional hurricane; and poor quality of previous interventions, has left many requiring substantial reconstruction. These conditions are particularly acute in fountains, where the constant exposure to chemically treated water exacerbates the issues. Conservation Solutions, Inc has recently completed the assessment, analysis, and overseen treatment of two public fountains there; the Main Fountain at the Breakers Hotel and the Town Hall Fountain by Addison Mizner, architect of many of Palm Beach's finest structures. After extensive study and review, both fountains were restored in 2015. This paper will present the testing that was performed, the plans that were developed, and the resulting treatments, including overcoming the technical challenges of preserving the original material. One particular point of interest that will be covered is the ethical question of replication versus restoration of original materials and design and how this was addressed differently on each fountain.

Keywords: cast stone, concrete, fountains, tropical conditions

1. Introduction

Palm Beach is one of the string of resorts developed in the late 19th century by Henry Morrison Flagler on Florida's east coast running south from Saint Augustine to Miami, tied together by his railroad line. Palm Beach remains one of the premier winter playgrounds for America's elite which blossomed with buildings and structures in the Mediterranean Revival style. Grand houses, hotels, public buildings and, particularly, fountains were built

[1] M. Rabinowitz* and J. Sembrat
Conservation Solutions, Inc., United States of America
mark@conservationsolutionsinc.com

[2] P. Miller
Preservation Society of Newport County, United States of America

*corresponding author

of reinforced cast stone and concrete to resemble stone Spanish and Italian design sources. As these structures are approaching their centennial, the inherent vulnerability of the material has become evident. These include erosion of the soft concrete; carbonation of the paste and resulting deterioration of embedded iron; exposure to aerosol salts from the marine environment; bio-growth fostered by the tropical climate, damages from impact, wear and the occasional hurricane; and poor quality of previous interventions. These conditions are particularly acute in fountains, where the constant exposure to chemically treated water exacerbates the issues. Conservation Solutions, Inc (CSI) has recently completed the assessment, analysis and overseen treatment of two public fountains there; the Main Fountain at the Breakers Hotel and the Town Hall Fountain. After extensive study and review, both fountains were restored in 2015. This paper will present the testing that was performed, the plans that were developed from them, and the resulting treatments, including overcoming the technical challenges of preserving the original material. One particular point of interest that will be covered is the ethical question of replication versus restoration of original materials and design and how this was addressed differently on each fountain.

2. Fountain Conditions

2.1. The Breakers Hotel Main Fountain

2.1.1. History & Conditions

Fig. 1: Breakers Hotel Main Fountain before restoration.

The fountain consists of a central sculptural feature of four nymphs supporting two tiers of basins, spindles and a finial within an octagonal pool. There are eight putti holding either alligators or herons alternating around the fountain atop the corners of the pool copings. The pool is raised within a stepped plaza that is centrally sited at the terminus of the main entrance drive just west of the hotel entrance. The fountain was built during the construction of the current hotel in 1926. The Breakers fountain was created from designs by Leo Lentelli, a sculptor who contributed extensively to the decoration of the Panama - Pacific Exhibition in San Francisco in 1915, including the design for a fountain similar to The Breakers fountain. Both are based on a Renaissance original at the entrance to the Boboli Gardens in Florence, Italy.

Conservation Solutions, Inc. was engaged to study the fountain, determine the causes of deterioration, and recommend a course of action for restoration. The fountain was surveyed in 2007 and found to be in poor condition. The mechanical systems had all failed and been replaced with unsatisfactory stopgap equipment. The original cast stone suffered from spalls due to deteriorating rebar near the surface and repeated parges and paint layers to hide those losses. Erosion from exposure to running water, previous repairs and stopgap fixes to plumbing had also compromised the original design.

2.1.2. Cast Stone Analysis

Analysis was performed on cores that were taken from the sculptures and walls of the fountain and the pointing mortar.

Tab. 1: Laboratory Analysis of Breakers Fountain Cast Stone and Mortar[1].

	Core 2	**Core 3**	**Mortar 1**
Aggregate (Average Volume, %)			
Coarse Aggregate (4.7-2mm)	5 %	5 %	0 %
Sand (<2mm)	95 %	95 %	100 %
Paste/Aggregate Ratio	0.15/ 0.85	0.15/ 0.85	0.12/ 0.88
Depth of Carbonation (Mass Percentage, %)	~5mm	~5mm	N/A
Quartz	75	74	90
Calcite	23	24	2
Portlandite	ND	ND	6
Other (unidentified)	~2	~2	~1

The high sand content, low depth of carbonation and high *pH* of the core samples indicated that the rebar throughout was not immediately threatened. Losses due to deteriorating rebar were confined to the arms of the nymphs and the putti where there was minimal cover of the iron that was placed close to the skin of the forms. This and other deterioration of rebar and subsequent spalling was tied to the high level of water soluble salts from both water treatment and aerosol exposure. As the quality of the cast stone mixture was determined to be inherently good, and deterioration was localized, stabilization and preservation of the majority of the elements was recommended with only selective replication required where details were either lost from erosion, obscured by parges, or where severe corrosion of the rebar had occurred. The best surviving examples were to be used as models for replication in new cast stone, while other elements were recommended to be retained.

[1] EMSL Analytical, Inc, Westmont, NJ, USA, 4/19/2007. Tests included: Polarized Light Microscopy, epi-Reflected Light Microscopy, Scanning Electron Microscopy, Energy-dispersive X-Ray Spectrometry, X-Ray Diffraction Spectrometry, X-Ray Fluorescence Spectrometry. CSI performed wet chemical analysis.

Fig. 2: Detail of a nymph showing rusting rebar, spalls and over-paint.

2.2. Town Hall Square (Mizner Fountain)

2.2.1. History & Conditions

The main fountain of the Town Hall Square was designed by Addison Mizner and dedicated in 1929. The Square includes the fountain, which sits on a raised deck surrounded by balustrades accessed by a set of steps to the north, a rill that cascades down below the steps to a basin, and a reflecting pool. The designer, a former boxer and subject of a musical by Steven Sondheim, was responsible for many of Palm Beach's most iconic buildings, including the stores and offices on Worth Avenue which successfully create the artifice of a warren of European streets and remain the high end commercial center of the island.

Fig. 3: Overall view of Town Hall fountain before restoration.

The fountain consists of a circular basin or pool approximately 16' in diameter. Within it there are a set of bowls and stems of diminishing size resting on four hippocamps or mythological sea horses. The design is based on the *Fontana dei Cavalli Marini* in the Borghese Gardens in Rome. All elements of the fountain are composed of cast stone intended to look like coral stone. The design drawings state that the stone is called 'Keyite', most likely a trade name for cast stone that mimics coral stone of the Florida Keys. It has a variegated color and intentionally pitted to resemble the porous stone. The fountain was surveyed by CSI in 2012 and found to be in poor condition. The cast stone suffered from heavy erosion from running water as well as direct spray that had removed extensive amounts of the sculptural detailing at the basin, stem, finial, and legs and heads of the hippocamps. Additional losses from deteriorating re-bar had substantially compromised the sculptural forms and structural integrity of the hippocamp legs and elsewhere.

2.2.2. Cast Stone Analysis

Tests were performed on samples of the cast stone from one of the hippocamps and from a section of the pool wall. The material was found to be composed of a high percentage of calcium carbonate paste and aggregate with very little sand.

Tab. 2: Summary of XRD Analysis Town Hall Fountain[1].

Mineral Constituents	Hippocamp	Pool Wall
Quartz	7%	1%
Calcite	84%	80%
Aragonite	5%	6%
Portlandite	~	3%
Amorphous	4%	10%

The binder was softer and had resisted the erosion of flowing water with much less success than that used at the Breakers. Although no cores were taken, the same conditions of high salt content and, possibly here, carbonation of the paste and lower pH, had lead to rust jacking that was particularly egregious on the hippocamp's legs and heads. Due to the higher level of erosion and loss, as well as the existence of original drawings and early photographic documentation to support the replication of the missing elements, we recommended that only the hippocamp bodies be retained while other elements be recreated to return the original design and display.

3. Treatments

3.1. Oversight & Approvals

Both fountains are listed as local or national landmarks. Oversight for treatment rests with the local Preservation Board, the State Historic Preservation Office, and the National Park Service. The Town of Palm Beach owns the Town Hall Fountain while The Breakers Hotel

[1] Mineralogy, Inc. Tulsa, OK, USA, 11/15/2012. Tests include: Polarized Light Microscopy, Energy-dispersive X-Ray Spectrometry, X-Ray Diffraction Spectrometry. CSI performed wet chemical analysis.

is privately controlled. Both owners initially favoured 100% replication, contending preservation of the original material was less important than the longevity achieved by recreation and replacement with new materials without the inherent vices of the originals. The owners doubted that repairs could be done in a way that were visually and structurally viable. However, treatment paths diverged, and not because of differences in material conditions per se. Public resistance and the desire to retain authenticity mitigated the choice for longevity by replication on the Town Hall Fountain. There was a strong public objection to the notion that the original cast stone could be replicated without loss of authenticity. Letters to oversight agencies and repeated public hearings occurred before a plan was approved that followed the assessment recommendations to retain the hippocamps' bodies. This same resistance did not trouble the plans for the Breakers Fountain, where the owner's goal of 100% replication was approved without objection. Although Lentelli is a prominent and collected sculptor with a recognizable style, the importance of preserving the Breakers fountain as an original work created by his own hand carried far less weight than Mizner, whose Town Hall fountain design was carried out by others. Whether it was the importance that the architect represents for Palm Beach, or the desire to retain some original historic fabric in a place that is frequently being renewed and remade is unclear. Ownership may also have factored heavily in the choice, with a higher level of scrutiny and burden of proof being applied to a publicly owned work than a private one.

3.2. Restorations

After documentation each fountain was disassembled and reconstructed. Work ran concurrently but under different contractors and artisans. In both cases, the detailed sculptural elements were salvaged and used as models for replication except for the hippocamps, which were restored and re-installed. Architectural elements such as the basins, stems, copings, walls, steps, etc, were profiled and measured before being demolished and entirely re-created from new models.

Fig. 4: Breakers Hotel fountain after restoration.

3.2.1. Breakers Main Fountain Re-Creation

The putti were removed and the best existing examples of each type were cleaned of parges and paint by carefully executed wet sand blasting. Working from the evidence revealed after the cleaning, along with historic photographs of the fountain and other examples of Lentelli's work, each was rebuilt with clay over the weathered cast stone. Restoration campaigns that had altered the designs, such as changes in the configuration of the herons' beaks, the alligators' fore claws and heads, as well as closing of the sprayers that once exited the animal's mouths, were all reversed in the process. There was a tension in getting the sculptor performing the work to follow the style of Lentelli, one that was based on the play of light over the relatively un-articulated surface with occasional deep shadowed cuts, and his contemporary tendency to fully articulate all forms. In the end, however, this tension produced an acceptable result that is sympathetic with the originals without being mistaken for them. Other elements that had been heavily eroded were recreated after salvage in a similar fashion with less difficulty. The nymphs, which had remained protected under the large basin and which were largely intact, were generally left alone with repairs limited to rebuilding the arms and patching areas where the rebar had spalled before molds were taken. The replicas retain the tool marks and flaws of the originals to a remarkable degree.

New castings were created in a high strength concrete with the addition of a plastizer and densifier that was color-matched to the original paste and aggregate. The fountain structure was re-engineered and elements originally designed as separate castings assembled on site were instead cast in place as a single unit with extensive stainless steel reinforcing. While this presented logistical difficulties, the resulting structure is substantially stronger than the original. New water and electrical feeds were run within the structure from a new supply chamber to the side of the fountain. Feeds included programmable lighting that could add additional decorative features to the water display.

3.2.2. Town Hall Fountain Restoration

The hippocamps were stabilized, excavated, and removed to a studio for treatment. The rest of the fountain elements were demolished after careful documentation. During demolition it was possible to observe the original pointing mortar and pool lining colors which had been hidden under multiple repair campaigns. Each was sampled and matched to Munsell color standards which were used in specifying replacements. The engineering that supported the cantilevered hippocamps was also revealed during the disassembly and used to guide re-installation plans.

Much work went into recreating the finial and basins to match the long-lost original detailing and re-create the intended bridal veil water display. Unlike at the Breakers, where the originals were mostly still intact and modelling occurred atop existing examples, these were newly re-created. This was done through direct modelling in clay, casting in resin, and water tests to confirm the display. Once a model was prepared that both matched the appearance of the drawings, historic photographs, weathered original detailing, and produced an appropriate display, it was reproduced on a full scale model to match the dimensions of the original. All were then recast in color-matched concrete without modifying the design of the units so that, unlike at the Breakers, re-assembly would follow the same plan as the original.

The hippocamps were cleaned of coatings and soiling and the legs were removed once the original mounting system was understood. These were re-created in new castings with stainless steel armatures. Mild steel rebar that could be accessed from the backs or areas of damage of the bodies was core drilled and removed. Rebar that could not be removed was cleaned and coated with a corrosion inhibitor-modified epoxy paint. A migrating corrosion inhibitor (MCI) was applied to the cast stone around the remaining embedded rebar. Losses were then reconstructed with a color-matched, naturally hydraulic lime mortar patching and the entire restored element was coated with a potassium silicate-based paint to blend with the new castings. Restored and new elements were then re-assembled at the site in a re-constructed pool.

Fig. 5: Restored Town Hall Fountain.

4. Conclusion

Both treatments have been well received and are considered successful restorations by the owners. Although only the hippocamps were retained, each is considered to be the original, in so far as the designs remained unchanged. The inherent vice of embedded iron rebar in cast stone, and the vulnerabilities of in-situ repairs in fountains, where constant erosion will shorten the life of even well engineered repair materials, supports the argument that replication is generally preferable to repair. On the other hand, the concern about loss of authenticity is not unfounded. None of the replications attempted to match the original paste formulae, for example, and even careful replication entails some degree of change. While the design and operation of the fountains is retained, the original material mostly exists now in our reports. This supports the value of thorough analysis and documentation prior to treatment, even if ultimately the treatment results in complete replication.

DATING THE PRE-ROMANESQUE CHURCH OF SAN MIGUEL DE LILLO, SPAIN: NEW METHODS FOR HISTORIC BUILDINGS

A. Rojo[1], L.L.Cabo[2], C.M. Grossi[3*] and F.J. Alonso[4]

Abstract

This article presents a methodology for dating historic buildings that combines absolute and relative dating of lime mortars. This methodology combines petrophysical examination with methods of radiocarbon dating using accelerator mass spectrometry (AMS). For the absolute dating we propose a protocol for pre-treatment of mortar samples to detect and reduce dating error sources derived from fossil or recrystallized calcite. This protocol pools existing procedures and involves thermal shock, sieving and isolation of two CO_2 fractions released during hydrolysis with phosphoric acid. Lime lumps were also analysed with this sequential capture of CO_2, without any previous physical pre-treatment. Lime mortar samples from the Heritage Site of San Miguel de Lillo (Asturias-Spain) church have been examined and compared to radiocarbon analysis of vegetal charcoal from mortar joints. The treated carbonate matrix and lime lumps rendered internally consistent radiocarbon dates, which are also consistent with the historiographical attribution dates. Consequently, the dates obtained met all the established criteria for the validation of radiocarbon dates from sequenced CO_2. The dates also agreed with those obtained from radiocarbon analysis of vegetal charcoal.

Keywords: heritage conservation, radiocarbon dating, petrophysics, lime mortar, Asturian pre-Romanesque

1. Introduction

Radiocarbon (^{14}C) dating is the most widely employed dating technique in archaeological contexts. When organisms die or stop exchanging carbon with the atmosphere their ^{14}C content starts to decrease at predictable rates, so that the age of the organism at the time of its death can be reliably estimated from the relative content of ^{14}C (Walter 2005). Consequently, vegetal charcoals or animal exoskeletons, frequently used for radiocarbon dating, provide only ages referring to the growth or death of the organisms, rather than their

[1] A. Rojo
Gea asesoría geológica, Oviedo, Spain

[2] L.L. Cabo
Mercyhurst Archaelogical Institute, Mercyhurst University, Erie, PA, United States of America

[3] C.M. Grossi*
School of Health Sciences, University of East Anglia, United Kingdom
c.grossi-sampedro@uea.ac.uk

[4] F.J. Alonso
Área de Petrología y Geoquímica, Facultad de Geología, Universidad de Oviedo, Spain

*corresponding author

utilization in the archaeological structure, which bias the ^{14}C ages towards older dates (Waterbolk 1983).

In contrast, lime mortars are manufactured onsite during construction, and not reutilised. The atmospheric carbon dioxide (CO_2) is fixed in the carbonate during the setting of the mortar, and thus the ^{14}C proportion in the matrix and lime lumps would theoretically refer to the exact construction dates. However, these types of mortars are also particularly sensitive to contaminations from fossil calcites, such as those derived from incompletely burnt limestone and fossil remains (Pesce and Ball 2012), which would push the radiocarbon dates downward, and from calcite dissolution and recrystallisation in the presence of water, which would artificially rejuvenate the sample.

The use of accelerator mass spectrometry (AMS), which allows analysing much smaller samples, has made possible to assess not only the overall radiocarbon composition of mortar samples, but of each of their different carbonate sources and components, provided they are identified and separated before analysis, through techniques such as acid hydrolysis (Lindroos *et al.* 2007). Pure lumps are also free of contaminants, thus reducing contamination biases (Vecchiattini *et al.* 2012).

1.1. Mortar radiocarbon dating methods

The Centre for Isotopic Research on Cultural and Enviroment heritage (CIRCLE) developed a technique (Marzioli *et al.* 2011), which is a modification of the protocol described by Nawrocka *et al.* (2005), based in the assumption that binder carbonates are characterised by a more easily breakable structure. This protocol targets the efficient suppression of C from unburned primary limestone, through the isolation of different suspensions of carbonaceous materials by means of strong ultrasonic attacks. The technique involves six major steps: cryobraking, ultrasonication of sieved fragments, suspension centrifugation, overnight drying, acid digestion, and isotopic measurements on isolated suspensions. Ringbom *et al.* (2014) proposed a technique based on anthropogenic binder carbonate grains being irregular, poorly crystalline, and rapidly soluble, while inorganic carbonate grains tend to be dense and crystalline, and dissolve more slowly. Samples of binder or lime lumps without aggregate inclusions are first separated by sieving and identified through microscopic examination (Lindroos *et al.* 2014), and subjected to acid digestion with 85% phosphoric acid. Once the hydrolysis has started, the CO_2 fractions are isolated and sequentially collected from the gas flow based of reaction time.

1.2. Goals

We propose a modified methodology for dating historic buildings that combines petrophysical examination with absolute dating of lime mortars. Our main goals were assessing the validity of mortar ^{14}C dating methods and improving sample pre-treatment protocols to aid in the detection and, whenever possible, control or removal of error sources from samples destined for AMS radiocarbon dating.

2. Methods

The proposed method integrates relative and absolute dating. Relative dating was established from petrophysical characterisation: textural determination, mineralogical, chemical and physical characterisation, and strata superposition. In addition, aggregates and pigments were also used to establish chronological analogies between mortars or paint layers, since they can be used as coating guide sequences. This characterisation allowed us

to determine the nature of binder and aggregate, and assess possible contaminations from fossil or newly-formed materials. Absolute dating was provided by AMS from samples of carbonates of the binder, lime lumps and vegetal charcoal.

2.1. Site

The lime mortar samples were extracted from San Miguel de Lillo (Asturias-Spain), a pre-Romanesque church listed among the UNESCO World Heritage Sites (Fig. 1). Well-established historiographical sources attribute the church to King Ramiro I of Asturias (842-850), resulting in a date of construction around the second half of the 9th century (García de Castro 1995). The original church structure was modified several times during to the Middle Ages (García de Castro 1995; Caballero *et al.* 2010), with the different construction phases providing an additional, reliable baseline for relative dating.

Fig. 1: The pre-Romanesque church of San Miguel de Lillo and location.

2.2. Sampling

Mortar samples from both interior and exterior areas were collected during a restoration in 2011 and a characterisation study in 2014. Calcite matrix and lime lumps were extracted from interior mortars, and the vegetal charcoal fragments from exterior ones, both from the original, initial building.

2.3. Relative dating: petrophysical characterisation of mortars

Macro and microscopical examination (polarised stereoscopic, petrographic optical and electronic scanning microscopy) served to infer mortar texture, and the composition of aggregates and binder. The chemical and mineralogical composition was further corroborated by x-ray fluorescence, x-ray dispersive energy and x-ray diffraction. The ratio aggregate/binder was estimated after dissolution with hydrochloric acid of the carbonate binder fraction. The insoluble residue was studied microscopically to identify fragments of charcoal present in mortars. Lime lumps, were separated mechanically under stereoscopic microscopy.

2.4. Absolute dating: new protocol for sampling preparation and analysis

The proposed method combines those in Marzioli *et al.* (2011) and Ringbom *et al.* (2014). After the petrophysical analyses, bulk mortar samples of 65 g were immersed in liquid

nitrogen for 5 minutes, and then heated in an oven at 80°C for 10 minutes. This thermal shock, taken from the Marzioli *et al.* method, produces the disaggregation of the mortar, and was repeated for 10 cycles. The sample was not crushed to avoid breaking the mineral grains under pressure. The resulting mortar samples were dry sieved through a 60 µm mesh size filter. Two particle size fractions were retained for further analysis: <60 µm and 60-120 µm. The grain size differs from those in Ringbom *et al.* (2014) and Marzioli *et al.* (2011). Following Ringbom *et al.* (2014), 1 g of the sample from each grain size portion was treated with 50 ml of phosphoric acid at 85%, with magnetic stirring in a Schlenk's flask. The system was previously vacuum treated, recording the pressure to ensure correct capture of CO_2 and avoid the addition of atmospheric CO_2. The released CO_2 was collected during the initial 8-10 seconds and after 60 seconds of hydrolysis. Unlike in Ringbom *et al.* (2014), the CO_2 was not collected cryogenically. Vials with the CO_2 generated in the process were subsequently sent to the DirectAMS laboratory, where samples were converted into solid graphite before AMS dating (www.directams.net). The sequential capture of CO_2, was also applied to untreated lime lumps.

2.5. Absolute dating: additional analysis of charcoal fragments

The charcoal fragments were extracted from the mortar through chemical attack with a 15% solution of hydrochloric acid, identified and isolated microscopically, and submitted to Beta Analytic INC for AMS dating. Beta Analytic uses an acid/alkali/acid pre-treatment (see www.radiocarbon.com).

3. Results and discussion

3.1. Relative dating

Seven different types of mortars were identified and chronologically sequenced. Two of them correspond to the initial, primitive church: the construction mortar (mortar joints), and the base plaster of the wall paintings. Both are lime and quartz-sand mortars, with similar composition but different colour, texture, aggregate, grain size and aggregate/binder ratios. The indoors construction mortar was used for AMS dating, as it contained a higher amount of lime lumps, whereas charcoal aggregates were only found outdoors.

3.2. Absolute dating

Tables 1 to 3 summarise the radiocarbon calibrated (conventional) dates from the AMS analysis: Bulk mortar (six samples) and lime lumps (two samples) results are shown in Tab. 1 and Tab. 2, and vegetal charcoal (three samples) in Tab. 3. Ages were calibrated using Calib 6.1.0 for Mac and Calib REV7.1.0 for PC (Stuiver and Reimer, Copyright 1986-2015). Bulk mortar and lime lumps ages vary from 772 to 995 AC and were validated using the four criteria established by Ringbom *et al.* (2014; pp. 623-624):

> *Criterion I*: The ^{14}C ages of the first and second CO_2 fractions are not significantly different. If this is the case, a single sample per building unit is enough for a conclusive result. Samples MRM1 A (χ^2= 0,569, 1 df; p= 0,451) and MRMN (χ^2= 2.531, 1 df; p= 0.112) met this criterion.

Criterion II: Mutual agreement between the dates of the first CO_2 fractions in a series of three of more samples per building unit. This criterion is met by samples MRM1 A, MRM1 B and MRMN, which agreed not only in their first CO_2 fractions, but also on the second ones (χ^2= 0.173, 2 df; p= 0.917), thus coming to satisfy the next criterion:

Criterion III: Mutual agreement between the dates of the first CO_2 fractions in two samples.

Criterion IV: The first CO_2 fractions from one sample in a building unit yields a date that fits into a relative chronology. Samples MRM1 A, MRM1 B and MRMN met this criterion, as they rendered internally consistent dates that also agree with the historiographical attribution to mid 9th Century Asturian king Ramiro I as the key promoter of the project.

Vegetal charcoal ages vary from 660 to 779 AC. The resulting ages of three samples do not show any significant difference (χ^2= 0.405, 2 df; p= 0.817).

Tab. 1: Calibrated ^{14}C radiocarbon ages from AMS analysis from CO_2 released from carbonate hydrolysis with 85% H_3PO_4

Reference	CO_2 fractions isolated	Grain-size	cal AD age ranges (2σ)
MRM1 A	1st fraction	< 60 µm	892-995
MRM1 A	2nd fraction	< 60 µm	772-894
MRM1 B	1st fraction	< 60 µm	888-990
MRM1 B	2nd fraction	< 60 µm	768-892
MRMN	1st fraction	Lime lumps	893-990
MRMN	2nd fraction	Lime lumps	765-975
MRM4	1st fraction	>60<120 µm	773-894
MRM4	2nd fraction	>60<120 µm	676-777

The lack of significant differences between the first and second CO_2 fractions of several samples allows us to increase the precision of the age ranges by combining the results of five mortar samples (both fractions of MRM1 A and MRMN and the first fraction of MRM1 B) and the three vegetal charcoal samples to calculate the confidence intervals (Tab. 2 and Tab. 3). The treated carbonate matrix and/or lime lumps rendered internally consistent radiocarbon dates, placing the early phases of construction of the building between the ends of the 9th and 10th centuries. These dates are also consistent with the historiographical attribution to mid 9th Century Asturian king Ramiro I as the key promoter of the project, although it would have been completed by later monarchs. In this manner, the treated samples and obtained dates met all the established criteria for the validation of radiocarbon dates from sequenced CO_2 released during carbonate hydrolysis. The new dates also agreed with those obtained from radiocarbon analysis of traditional organic

materials, and fell into the expected loci along the construction phase sequence. As would be expected from their additional inbuilt age, the vegetable charcoal samples dated to a period immediately preceding and not overlapping that defined by the mortar dates.

Tab. 2: Results of the radiocarbon dating (raw age BP and calibrated age AD) of the matrix and lime lumps combined (χ^2= 3.172, 4 df; p= 0.529)

Samples	Radiocarbon age BP	cal AD age ranges	Confidence interval 95.4 (2σ)
MRM1 A + MRM1 B_1 + MRMN	1109 ± 11	894 – 930	0.473
		937 – 980	0.527

Tab. 3: Results of the radiocarbon dating (raw age BP and calibrated age AD) of vegetal charcoals from outdoors mortar joints

Samples	Radiocarbonage BP	cal AD age ranges	Confidence interval 95.4 (2σ)
SML43	1250±30	677-779	0.785
SML45	1300±30	660-730	0.677
SML39	1260±30	669-778	0.899
SML43 + SML45 + SML39	1270±30	663-777	0.968

4. Concluding remarks

The proposed pre-treatment protocols were successful in detecting, characterising and removing contaminants, coming to provide accurate and more precise dates. These results also illustrate the advantages of integrating the petrophysical analyses linked to conservation efforts, with the usually concurrent archaeological and geochronological protocols aimed at understanding the building's history and characteristics. If the lime mortar does not present high contamination or fire-damage, the collection of two CO_2 fractions seems sufficient and appropriate; although additional fractions, as in Ringbom *et al.* (2014), are likely necessary in more altered samples. Lime lumps and carbonate matrix <60 μm are very suitable for radiocarbon dating. Both give similar age profiles in the first and second CO_2 fractions. Carbonate grains ≥ 60 μm do not appear appropriate, and most probably derive from incompletely burnt limestone.

Acknowledgements

This work was partially funded for the Consejería de Educación, Cultura y Deporte del Gobierno Principado de Asturias. Especial thanks to Conchi Ania and J.B. Parra for their help with the CO_2 collection.

References

Caballero Zoreda L., Rodríguez Trobajo, E., Murillo Fragero, J. I. y Martín Talaverano, R., 2010, Las iglesias de San Juan Evangelista de Santianes de Pravia y Santo Adriano de Tuñón (Asturias), Arqueología de la Arquitectura, Anejos de AEspA, LIV, p. 27-28.

García de Castro, C., 1995: Arqueología Cristiana de la Alta Edad Media en Asturias, RIDEA, Oviedo, p. 417-418.

Lindroos A., Heienemeier J., Ringbom A., Braskèn M., Sveinnbjörnsdóttir ÁE., 2007, Mortar dating using AMS ^{14}C and sequential dissolution: examples from medieval, non-hydraulic lime mortars from Aland Islands, SW Finland. Radiocarbon 49(1): 47-67.

Lindroos A., Ranta H., Heinemeier J. and Lill JO., 2014, ^{14}C chronology of the oldest Scandinavian church use. An AMS/PIXE study of lime lump carbonate in the mortar. Nuclear Instruments and Methods in Physics Research B 331, 220-224.

Marzaioli F., Lubritto C., Nonni S., Passariello I., Capano M. and Terrasi F., 2011, Mortar Radioarbone Dating: Preliminary Accuracy Evaluation of Novel Methodology. Analytical Chemistry, ACS Publications, pubs.acs.org/ac.

Nawrocka D., Michniewicz J., Pawlyta J., Padzur A., 2005, Geochronometria , 24, 109-115.

Pesce, G. L. A. and Ball, R. J., 2012, Dating of Old Lime Based Mixtures with the "Pure Lime Lumps" Technique. In: Nawrocka *et al.* 2005.

Ringbom A., Lindroos A., Hienemeier J. and Sonck-Koota P., 2014, 19 years of mortar dating: Learning from experience. Radiocarbon, Vol 56, Nr, 2014, p 619-635.

Vecchiattini R. , Pesce G.L., Quarta G. and Calcagnile L., 2013, Sampling problems in the radiocarbon dating of old mortars and plasters with the “pure lime lumps” technique. Built Heritage 2013 Monitoring Conservation Management, 1066-1074 http://hdl.handle.net/11567/644367.

Stuiver, M. and Reimer, P.J., 1993, Extended 14C data base and revised CALIB 3.014 C age calibration program, Radiocarbon, 35, 215-230

Walter M., 2005, Quaternary dating methods. John Wiley & Sons p. 19.

Waterbolk HT., 1983, Ten guidelines for the archaeological interpretation of radiocarbon dates. PACT 8:57-70.

This page has been left intentionally blank.

SWELLING INHIBITION OF CLAY-BEARING BUILDING MATERIALS USED IN ARCHITECTURAL MONUMENTS

A. Stefanis[1*] and P. Theoulakis[1]

Abstract

The presence of clay minerals in natural stones and adobes used in monuments produces a series of problems, which relate to the internal stresses developed during the absorption of moisture and the consequential swelling and shrinkage cycles. The phenomenon evolves gradually by trapping water molecules in between the crystalline structure of the clay-mineral platelets, which present different water absorption rates. Long exposure of the building materials to this mechanism, leads to the total decay and crumbling, threatening the stability of the whole monument. In these cases, treatment of the building materials with a consolidation agent combined with a swelling inhibitor is the objective, since the restoration of the internal cohesion and the reduction of the weathering rate can be achieved. Thus, the aim of the present project is the study of the performance efficiency of the action of different types of consolidation materials such as silanes and calcium hydroxide nano-dispersions in alcohols. The originality of the present project lies on the fact that it studies and evaluates the relation between the lithological characteristics of the building materials, the swelling mechanism and alteration of clay minerals in correlation to the particular characteristics of the direct environment of the monument, and the effect of the abovementioned parameters to the efficiency and durability that different types of treatments provide. The evaluation of the system stone-environment-treatment is based on the development of a multiparemeter model - algorithm - that accepts and processes objectively measurable properties. This combination is particularly important for the protection and conservation of historic buildings that are constructed of clay-bearing building materials. Especially today, the issue is significant, since climate change is affecting the microclimatic conditions of the monuments and consequently the weathering rates of the materials.

Keywords: building material, swelling clays, stone, inhibition

1. Introduction

The objective of the present work is the study of the use of clays as building materials and of their pathology as a function of their composition and the specific characteristics of the immediate environment of monuments. The research focuses on the role of the swelling phases of clays, which is proved to create a number of issues, which are associated both with the internal shear and tensile stresses developing during the absorption/desorption of moisture and swelling/shrinkage, and secondly to the fatigue of the building materials

[1] A. Stefanis* and P. Theoulakis
Department of Conservation of Antiquities and Works of Art,
Technological Educational Institute of Athens, Greece
astefanis@teiath.gr

*corresponding author

(plasters or mud-bricks) during the successive wetting-drying cycles. The above-mentioned phenomena are interpreted by two mechanisms: the initial intergranular/bilayer swelling due to the hydration of the balance cations and due to the long-term swelling by electrostatic osmosis. As a direct result of the mechanical stress caused by the swelling of clays in natural stones and mud-bricks, and in combination to the chemical and mechanical damage that may be caused by the presence of water on sites, building materials present surface weathering and loss of internal cohesion. Long-term exposure of clays to this weathering factor leads to total deterioration.

As representative case studies, two significant archaeological sites are examined. The excavation of the prehistoric settlement of Toumba in Thessaloniki and the prehistoric settlement of Dispilio in Kastoria, both in Greece. The first traces of habitation at Toumba date from the early Bronze Age continuing to the Archaic and Hellenistic periods (from 3000 BC to 200 BC). The materials used for the construction of buildings were mainly mud-bricks. The second site at Dispilio, was discovered in 1932 and systematically excavated in 1992. The remains of a large lakeside settlement of the Late Neolithic period were revealed, one the most important and oldest of its kind in Europe. The findings are dated between the middle and late Neolithic period (5500-3000 BC).

A large number of samples from these two sites was studied and categorised according to the mineralogical, petrographic and chemical composition in order to link the preservation state and the damage typology of clays to their intrinsic characteristics. Furthermore, widely used consolidation agents were applied and tested for their efficacy in inhibiting the weathering phenomena.

2. Pathology of the material

The weathering of the clay findings from the two prehistoric settlements, appears in the form of extensive and irregular disintegration, leading to a significant loss of material and gradually to a serious deterioration of their form. This type of damage is generally associated to the behaviour of aluminous materials in atmospheric conditions, to the composition and the microstructure of the material and to the fluctuations of the relative humidity and temperature of the atmosphere. During the absorption of water, clay-bearing materials tend to hydrate and increase their volume. This swelling results in the development of strong stresses within the material that ultimately leads to their collapse. During the drying phase clays shrink and gradually disaggregate (thixotropic behaviour), (Scherer and González 2008). Another important weathering factor is the presence of soluble salts whose crystallisation cycles cause disintegration of the clay material (Scherer and González, 2008). Laboratory measurements on fragments and soil samples which were obtained from both sites, showed high conductivity of the desalination's solutions and the existence of chlorides, sulphates and nitrates. Finally, the environmental conditions of the areas with low winter temperatures cause freeze-thaw cycles, which lead to further decay of the material.

3. Characterisation of the material

3.1. Macroscopic and microscopic observations

The macroscopic and microscopic examination of the samples from the settlement of Toumba shows that the clay is generally light coloured with low concentration in natural inclusions (aggregates) whereas plant fibres were used to reinforce the mud bricks.

Regarding the clay samples from the site of Dispilio, they present a variety in colour and texture. The clays were classified according to their macroscopic characteristics as: a) pale (whitish), porous with several impurities, b) dark (brown or ash), compact without any impurities and c) clay with intense orange or red colour shade, which is quite dense and contains aggregates in various grain sizes, small clay pieces of secondary origin, organic material such as straw while traces of firing can be observed on the surface.

3.2. Mineralogical and chemical analysis

Samples were mineralogically characterised by X-ray diffraction (XRD) before and after treatment with a diluted acetic (CH_3COOH) and hydrochloric acid (HCl) (5%w/w and 3%w/w respectively) in order to remove carbonates and acquire a rich spectrum of clay minerals. Analysis of the samples before the acid treatment was performed on powdered material <63 μm. A small quantity of the samples was powdered (<125 μm) and analysed by an Energy Dispersive X-ray (EDS) microanalysis system.

Selected samples were subjected to water absorption tests in order to record the behaviour and durability of the samples in sorption and desorption moisture cycles (Baroghel-Bouny 2007). Wetting and drying cycles were performed on samples with sufficient quantity, following the methodology described in the literature (González and Scherer 2006). Finally, the cation exchange capacity (CEC) was determined in selected clays samples, according to ASTM D7503-10. XRD analysis identified the presence of smectites in almost all of the samples from the excavation of Toumba. The peaks of swelling minerals such as illite, montmorillonite, and kaolinite (abundant to very abundant) are higher compared to in the samples from Dispilio (abundant). This suggests that they are raw clays, as it can be deduced by the macroscopic and microscopic observation of the samples. Hygric swelling of Toumba specimens was between 0.980 and 1.540 $mm \cdot m^{-1}$ whereas for the Dispilio specimens it ranged between 0.760 and 0.840 $mm \cdot m^{-1}$. The samples from Dispilio indicate, in their majority, that they have been exposed to fire deliberately or accidentally. Based on the literature (Grim and Bradley 1940), incomplete destruction of the illite lattice and failure to identify minerals such as spinel, indicate that the materials that have had a thermal past should not have been exposed to temperatures above 600-650°C.

From the results of the elemental analysis by means of EDS, the samples were classified into two major categories: in calcareous (%Ca>6%) and non-calcareous (%Ca<6%). The percentage of calcium-containing samples from the settlement of Toumba is 80%, whilst from Dispilio is 57%. The calcium levels in the calcareous samples from the settlement of Toumba is ranging between 8% and 22.6%, whilst in the samples from Dispilio is ranging between 9% and 32.6%.

4. Experimental

4.1. Experimental methodology

The scope of the experiment was to conclude to the best available treatment to preserve the clay findings in situ. Both sites were thoroughly examined macroscopically in order to obtain information on the conditions that the clays are found. Then the sampling procedure was designed and applied. The samples were used in order to study the physical, chemical and mineralogical properties of the material. Then five widely used consolidation agents were selected to treat the clay samples. The selection of the consolidation agents was based not only on their ability to restore the internal cohesion of the clays but also on their

hydrophobic properties that would reduce the absorption of water by the clays. After the clay samples were treated with the consolidation agents, treatments were qualitatively evaluated by comparing the physical properties of the clays before and after treatment.

The aim of the consolidation treatment is the rehabilitation of the coherence of the decayed material that presents loose structure, as well as the reinforcement of its durability on the excavation environment, fact that corresponds to the restriction of the ability to absorb and circulate water in the capillarity network. The effectiveness of the treatment is evaluated by supporting the broader demand to implement safer and more effective interventions for the artefacts. The most common evaluation approach of conservation treatments is the measurement of specific properties, which have been selected as critical for the effectiveness of the treatment. The drawback of this approach is the interpretation of the results and therefore, the difficulties caused in decision-making. In this study physical and mechanical properties were measured before and after treatment (Theoulakis *et al.* 2008)

4.2. Consolidation materials and treatments

Five consolidating agents were selected to treat the clay specimens: Two colloidal dispersions **(**nano-particles) of calcium hydroxide $Ca(OH)_2$ in alcohol: Calosil E25, (25g $Ca(OH)_2$/l in ethyl alcohol) and CalosiL IP25 (25g $Ca(OH)_2$/l in isopropanol). Consolidation is achieved by the epitaxial deposition of calcium carbonate ($CaCO_3$) produced from the reaction of $Ca(OH)_2$ with the atmospheric carbon dioxide (CO_2). The disadvantage of the traditional alkaline earth hydroxides treatments is the limited penetration and consolidation ability, which has been surpassed by the nano-scale particle size of the dispersions applied in this study (Dei and Salvadori 2006, Karatasios *et al.* 2007). An acrylic emulsion, Lascaux Hydrogrund 5%w/w in deionised water. The polymer is dispersed in water and it is deposited after the evaporation of the medium. The acrylic resin increases the durability of the clay and reduces water absorption (Price 1996). Two types of alcoxysilanes: Funcosil Steinfestiger 100 and Funcosil SL, with the latter presenting hydrophobic properties, were applied. Silane-based materials have been widely used as consolidants over the past decades with successful performance in both siliceous and calcareous materials. They exhibit very high penetration ability, while they can provide significant strength improvements without completely filling the pores of the material to be consolidated. The consolidation effect is achieved by the formation and deposition of both, the amorphous and hydrous silicon dioxide (SiO_{2aq}, "silica gel") end-products, through polymerisation. These reactions take place inside the pores space after the material has been absorbed by the porous medium. The deposited material is very stable to UV radiation or when exposed to acid rain. Different types of silane products include tetraalkoxysilanes, alkyl trialkoxysilanes, polysiloxanes, silicon hydrides and halogen bearing silanes. Some types (e.g. alkyl trialkoxysilanes) have a degree of water repellence, which can be controlled by altering the properties of starting material (Wheeler *et al.* 1992, Price 1996, Gozalez *et al.* 2000, Young *et al.* 2003). All consolidation materials were applied by physical sorption and by spraying the clay specimens. In both cases consolidating agents impregnated the clay material by capillarity. After the impregnation with the consolidants, clay specimens were left to dry in room conditions to achieve the evaporation of the solvent and the polymerisation of the agents.

5. Results

5.1. Porosity

The applied agents altered the porosity of the specimens both from Dispilio and Toumba. Porosity of the untreated specimens from Dispilio originally ranged between 33.4% and 36.6% with a mean value for three samples at 35,7% whereas for Toumba porosity ranged between 32.1% and 35.1% with a mean value of 33.6% for three samples. Overall, porosity's alteration percentage of the clay specimens after treatment is reduced between 24.22% and 72.94%. The samples mostly affected were the ones that had been treated with Funcosil SL (decrease from 40.5% to 72.94%). Secondly, specimens treated with Hydrogrund presented a decrease in porosity from 31.8% to 47.44%, and those treated with Funcosil 100 a decrease in porosity from 30.3% to 36.41%. Finally the porosity of those treated with Calosil IP 25 or Calosil E 25, was reduced between 24.22 % and 35.9% and between 29.27 % and 36.36%, respectively. As a result, porosity's reduction was achieved by Funcosil SL, then by Hydrogrund, followed by Funcosil 100.

5.2. Capillary rise

Many of the deterioration processes are associated with the presence and movement of aqueous solutions through the mass of the clay. The most common route for the ingress of water in porous materials is by capillarity. One of the main properties related to the absorption of water and the deterioration phenomena is the water absorption coefficient by capillarity (*C*) (Theoulakis *et al.* 2004). Capillary rise coefficient for Dispilio samples is in average 513 $g/m^2s^{0.5}$ for three samples, whereas for Toumba is 643 $g/m^2s^{0.5}$. In general, capillary rise coefficient was reduced between 6.25% and 98.65%. Funcosil SL, Funcosil 100 and Hydrogrund reduced it more than the other agents, that is between 62.07% and 98.65%, 62.16% and 98.33%, 6.45% and 93.75% respectively. Hydrogrund, presented a surprisingly low decrease of 6.45%. Finally, the reduction of capillary rise coefficients was from 32.32% to 83.48% for the specimens which were treated with Calosil IP 25 and from 6.25% to 57.81% for those which were treated with Calosil E 25. As a final point, the samples which were treated with Funcosil SL or Funcosil 100 were mostly affected.

5.3. Water absorption

Water absorption of the untreated samples of Dispilio was in average 28.27% for three specimens, whereas for the samples from Toumba was 30.87%. After treatment water absorption was reduced between 7.29% and 91.04%. Funcosil SL reduced water absorption between 77.14% and 91.04%, presenting the highest values. Consequently, Hydrogrund reduced water absorption between 13.22% and 43.18%, Calosil IP 25 between 18.61% and 34.37%, Calosil E25 between 7.29% and 17.42%, and Funcosil 100 between 11.37% and 31.76%. It is worth pointing out that the samples treated by Funcosil SL showed the greatest alteration of water absorption property.

5.4. Mechanical properties

Considering that the main goal of consolidation is to strengthen the total structure and to reinstate the lost cohesion of the weathered areas, a number of properties should be selected, in order to provide sufficient quantitative data on the internal cohesion of the treated material. Compressive strength of treated and untreated clay specimens was measured according to EN 196-1:1995. Specimens were treated with each of the consolidation agents and then tested to measure their mechanical characteristics that were

then compared to those of the untreated specimens. The mean compressive strength three untreated specimens from Dipsilio was 2.76 MPa whereas for Toumba specimens was 2.71 MPa. Calosil E25 increased the compressive strength of the specimens to 6.57 MPa, Calosil IP25 to 5.55 MPa, Funcosil 100 to 6.27 MPa, Funcosil SL to 3.25 MPa and Hydroground to 5.23 MPa.

5.5. Resistance to the action of water

Water absorption tests classified clay materials into three categories: low absorption (<6%), medium absorption (6-9%) and high absorption (12.9%). The higher water retention occurs in samples in which, based on the mineralogical analysis, the quantity of illite along with smectite minerals appears to be higher. The values of CEC in selected samples are very low. To test and calibrate the measurement procedure, a sample of commercial clay was used. The resulting value from the measurement (0.09 mol/kg) is within the expected values for clays where kaolinite and illite are dominant. Soils presenting values within the range of 0 to 0.03 mol/kg are sandy with a lack of organic material. It is possible that the archaeological samples tested, have lost their cations due to leaching suffered both during the period of use of the settlements as well as during burial. However, the comparison of the results indicates that the samples originating from the settlement of Toumba show higher values of CEC than those of Dispilio. During wetting-drying cycles it was observed that samples of raw clays (Toumba samples) collapsed at the first cycle, while Dispilio samples, which present both in their microstructure and on the mineralogical composition indications of firing, exhibited better behaviour.

6. Evaluation of treatments

In this study the performance criteria of the consolidation agents were set and then the physical and mechanical properties of clays were compared before and after treatment in order to qualitatively evaluate the results. Besides qualitative methods, a preliminary attempt towards a methodology for assessing the consolidation treatments based on the quantitative interpretation of a set of evaluation parameters was published in our previous work (Theoulakis *et al.* 2008). The evaluation of the above results could be based on the determination of an Efficiency Index (EI), which can be calculated through the algorithm. This algorithm incorporates a function of selected performance parameters, applicable to all types of stone and consolidants. For the interpretation of the results, the properties of untreated weathered specimen are used as reference. The values of the above properties can be modified according to the dominant deterioration mechanism or any other specific requirement ($P_{i(\min)}$). Considering that the main performance requirements for consolidation are strengthening, durability and compatibility, the properties associated to those requirements could be used in the proposed algorithm.

7. Conclusions

Macroscopic and microscopic examination of the samples from Toumba showed that the clay is typically a light coloured, with a low concentration in natural inclusions and traces of fibre. Samples from Dispilio present variability in terms of their colour and texture. Mineralogical analysis indicates the presence of smectites in almost all of the samples from Toumba. The peaks of illite, montmorillonite, and kaolinite are more prominent than in the samples from Dispilio and indicate that they are raw clays. On the contrary, the majority of samples from Dispilio show evidence that they have been exposed to fire, deliberately or

accidentally. The values of CEC in all samples are quite low, probably due to leaching the material has suffered both during the period of use as well as during burial. However, samples from the settlement of Toumba present comparatively increased values. Samples that showed durability in the action of water are in their majority the samples from Dispilio which presented signs of firing and have a reduced content of smectite minerals. Toumba's samples with higher values of CEC disintegrated faster. Results indicate that the diffusion and deposition of the solids of the consolidating agents in the clay matrix, was not achieved by all tested agents. It is clear that silanes surpass the other two categories of agents which as suspensions do not present significant absorption. Furthermore, the deposited solids of the acrylic resin and the $Ca(OH)_2$ dispersions are located on the external surfaces of the clay. Silanes, having low viscosity can deeply penetrate the clay and deposit SiO_2. In the case of silanes though, the control of the treatment is necessary in order to avoid fast and intense evaporation of the solvent, otherwise the consolidating agent will be transferred and deposited on the surface during the evaporation state. As far as the issue of compatibility is concerned, the agents which deposit inorganic material within the pores of the clay, are positively evaluated. These are the colloidal dispersions of $Ca(OH)_2$ and silanes which deposit amorphous SiO_2. The less compatible is the acrylic resin. The coherence of the clays is significantly increased in the clay specimens treated with the dispersions of $Ca(OH)_2$ and with silanes. The acrylic resin did give satisfactory results which are consistent with the aim of the project. In conclusion, the project proposes the use of silanes for the particular problem. Silanes consolidate the clays and buffer the phenomena of water diffusion without any crucial alteration in the appearance of clays. It is important to apply adequate treatments on clays and adobe structures that not only reinstate the coherence of the original material but also provide sufficient swelling inhibition.

References

ASTM D7503-10, Standard Test Method for Measuring the Exchange Complex and Cation Exchange Capacity of Inorganic Fine-Grained Soils.

Baroghel-Bouny, V., 2007 Water vapour sorption experiments on hardened cementitious materials Part I: Essential tool for analysis of hygral behaviour and its relation to pore structure, Cement and Concrete Research, 37, 414-437.

Dei, L. and Salvadori, B., 2006, Nanotechnology in Cultural Heritage Conservation: Nanometric Slaked Lime Saves Architectonic and Artistic Surfaces from Decay, Journal of Cultural Heritage, 7, 110-115.

EN 196-1:1995, Methods of testing cement, Part 1: Determination of strength.

González, I.J. and Scherer, G.W., 2006, Evaluating the potential damage to stones from wetting and drying cycles, Konsta-Gdoutos, M.S, (ed.), Measuring, Monitoring and Modeling Concrete Properties, Springer, 685–693.

Grim, R.E. and Bradley W.F., 1940, Investigation of the effect of heat on the clay minerals illite and montmorillonite, Journal of the American Ceramic Society, 23, 242-248.

Karatasios, I., Kilikoglou, V., Colston, B., Theoulakis, P., Watt, D., 2007, Setting Process of Lime-Based Conservation Mortars With Barium Hydroxide, Cement and Concrete Research, 37, 886-893.

Price, C.A., 1996, Stone Conservation: An Overview of Current Research, The Getty Conservation Institute, USA.

Scherer, G.W., González J.I., 2008, Swelling Clays and Salt Crystallisation: Damage Mechanisms and the Role of Consolidants, in proceedings of the International Symposium on Stone Consolidation in Cultural Heritage – research and Practice, Lisbon, 6-7 May 2008.

Theoulakis, P., Karatasios, I., Sotiropoulos, A., Kilikoglou, V., 2004, The Selection of Stone for Historic Buildings Repair: The Use of Cypriot Stone in the Medieval City of Rhodes, in proceedings 6th International Symposium on the Conservation of Monuments in the Mediterranean Basin, Lisbon, 352-360.

Theoulakis, P., Karatasios, I., Stefanis N.A., 2008, Performance Criteria and Evaluation Parameters for the Consolidation of Stone, in proceedings of the International Symposium on Stone Consolidation in Cultural Heritage – Research and Practice, Lisbon, 6-7 May 2008, 279-288.

Wheeler, G.S. Fleming, S.A., Ebersole, S., 1992, Comparative Strengthening Effect of Several Consolidants on Wallace Sandstone and Indiana Limestone, in proceedings Deterioration and Conservation of Stone, Lisbon, 1033-1041.

Young, M., Cordiner, P., Murray, M., 2003, Chemical Consolidants and Water Repellents for Sandstones in Scotland. Historic Scotland, Edinburgh.

LONG-TERM MECHANICAL CHANGES OF REPAIR MORTAR USED IN RESTORATION OF POROUS LIMESTONE HERITAGE

B. Szemerey-Kiss[1*] and Á. Török[1]

Abstract

The present paper studies the long-term 180 and 360 days changes in strength of different ready-made repair mortars and some newly designed mortars with different binder/aggregate ratio. The tests results of uniaxial compressive strength, density of specimens were measured 3, 7, 14, 28, 90, 180 and 360 days of casting, respectively. 250 samples were made and three curing conditions were analysed: the samples were kept in a climate chamber (air temperature 20±2°C, relative humidity of 50-55%), under dry (T = 60°C, RH = 30-40%) and under humid conditions (T ~20°C, RH < 75%). According to the results the highest compressive strength were measured on mortars with Portland cement binder. Compared to 14 days after the casting the mean compressive strength showed a slight increase 180 days after casting. Mortars with trass cement binder did not show a clear trend in strength. The mortars with a combined binder of trass cement and slaked lime had low compressive strength values. The utilisation of trass binder with the combination of Portland cement resulted in a relatively high compressive strength. Curing conditions also influenced significantly the strength of tested repair mortars, since mortars kept under very humid environment show a slight decrease in strength. Higher temperature and dry conditions resulted in a rapid loss in strength in time. Our tests have demonstrated that long-term changes in strength of repair mortars do occur and besides the standardised strength tests after 28 or 90 days of curing further long-term tests are required to understand the behaviour of repair mortars.

Keywords: repair mortar, compressive strength, curing conditions

1. Introduction

Restoration of natural stone objects with repair mortars bring several open questions. Previous studies dealt with the analysis and testing of historic mortars, lime grouts, lime and cement bonded mortars (Arizzi *et al.* 2012, Arizzi and Cultrone 2012, Lindqvist 2009, Hanley and Pavia 2008, Karatasios *et al.* 2007, Lanas *et al.* 2006, Mosquera *et al.* 2006, Lanas *et al.* 2004, Lanas and Alvarez 2003, Montoya *et al.* 2003, Degryse *et al.* 2002, Elert *et al.* 2002), but only limited data are available of comprehensive analysis of commercially available products for stone repair mortars (Torney *et al.* 2014, Szemerey 2013, Torney *et al.* 2012, Szemerey and Török 2011). However the compatibility requirements of the stone and the restoration material are well known (Isebaert *et al.* 2014, Schueremans *et al.* 2011, Rodrigues and Grossi 2007, van Balen *et al.* 2004). Lime have been becoming more and more popular, however binders such as Portland cement are still

[1] B. Szemerey-Kiss* and Á. Török
Engineering Geology and Geotechnics, Budapest Technical University, Hungary
szemerey@mke.hu

*corresponding author

commonly used in the restoration of deteriorated stone and heritage structures. The incompatibility problems related to the use of portland cement is clearly documenetd (Callebaut 2001). The use of different kinds of lime such as quicklime, natural hydraulic lime. in repair mortars has proved to be better in terms of compatibility (Schueremans *et al.* 2011, Rizzo and Megna 2008, Pavia *et al.* 2006, Lanas *et al.* 2004). This work aims to determine the long-term behaviour of manufactured restoration mortars made using lime and Portland cement containing, that are available in Hungary and also used in other countries worldwide.

2. Research

2.1. Materials and Methods

Two types of mortars were prepared in the laboratory with commercial hydrated lime (CL-90S) and Portland cement (Cem I, DDC) and pozzolanic cement (Cem IV). Another three types of basic and analogous restoration mortar were selected for the tests. All of these are available in Hungary but manufactured in Germany (the commercial mortars are abbreviated by R, K and T in this paper). The commercially available materials have not been formulated with any additional pigments, aggregates or additives. According to earlier laboratory test results (Szemerey 2013, Szemerey *et al.* 2013) the mortars contain Portland cement (~100-250 kg/m^3), hydrated lime and one of them contains pozzolanic cement. All the tested mortars also contain well sorted quartz sand aggregates. A limestone aggregate was also used, obtained from the Sóskút quarry, Hungary, where highly porous Miocene age limestone are found. Two hundred and fifty mortar specimens were prepared using demountable steel moulds. The specimens were compacted mechanically to produce 30×30×30 mm cubes and 40×40×160 mm rectangular prisms (during the laboratory tests thousands of 30×30×30 mm were made) for compressive strength and flexural strength tests, respectively. The abbreviation for and contents of the mortars are given in Tab. 1.

The commercially available products were prepared in accordance with the guidelines provided by the manufacturer (e.g. with different water-cement ratio). The sample preparation was performed under laboratory conditions (air temperature 20±2°C, relative humidity of 50-55%). Before the samples were removed from the moulds, the initial curing environment was the same for all samples. Three different test conditions were utilised. The first set of the samples were kept in laboratory condition (T ~20°C, RH ~ 50-55%), the second set of the samples were kept in humid environment with (T ~20°C, RH < 75%), and the last set of the specimens were stored in a dry climate chamber at elevated temperature (T = 60°C, RH = 30-40%).

Uniaxial compressive strength tests and flexural strength tests were made according to the methodology described in EN 1015-11 by using a DigiMess M-10 equipment with a maximum load capacity of 200 kN and loading velocity of 0.2 kN/s. Strength tests were performed 3, 7, 14, 28, 90, 180 and 360 days after casting, respectively.

Tab. 1: Constituents of each of the tested mortars.

Name	Binder -		Aggregate			Units
	Cement (C)	Lime (L)	Quartz sand (Q)	Limestone sand (LA)	Quartz sand (Q)	C:L:Q:LA
A	Portland cement	Hydrated lime	Ø 0.25-0.5	Ø 1-2	Ø 0.25-0.5	1:1:1:3
B	Trass cement (Portland pozzolanic cement)	Hydrated lime	-	Ø 1-2	-	1:0.25:4
T	Portland cement	Hydrated lime	Ø 0.2-0.4	-	Ø 0.2-0.4	1:0.25:4
R	Portland cement	Hydrated lime	Ø 0.3-0.5	-	Ø 0.3-0.5	1:0.3:3
K	Portland pozzolanic cement	Hydrated lime	Ø 0.3-0.5	-	Ø 0.3-0.5	1:0.3:3.5

3. Results and discussion

Compressive strength values of the mortars as a function of time are given in Figures 2, 3 and Fig. 4, respectively. The Flexural strength of the tested mortars are presented in Fig. 4. Compressive strength values of the mortars kept in laboratory conditions ($T \sim 20°C$, $RH \sim 50–55\%$) increased gradually until 14-28 days while no increase was recorded after 28 days (Fig. 1). The average value of the compressive strength of the mortars kept in the damp environment decreased slightly (Fig. 3.). Samples kept in high temperature show the lowest strength. After 14 days a rapid decrease was detected in compressive strength and the one fourth of the laboratory values were detected after the 360 days. The loss in strength was the highest at 'K' mortars which has a trass cement binder. The uniaxial compressive strength reduced from 4.0 MPa to 0.9 MPa. Flexural strength values of the mortars cured in laboratory temperature increased gradually until 28 days with the exception of 'A' mortar. After the 28 days no considerable increase was recorded (Fig. 5). The average density of the tested mortars is given in Tab. 2 and Fig. 1. The density of tested mortar show fairly rapid decrease in the first two weeks except mortar 'A' and mortar 'B', which represent the opposite trend - significant increase in the first 28 days. On long term in, one year four of the tested mortars have lower densities than the initial one, while mortar 'B'show an increase in density. The different trends are related to the loss of water content (short-term), or probably the dehydration of binders.

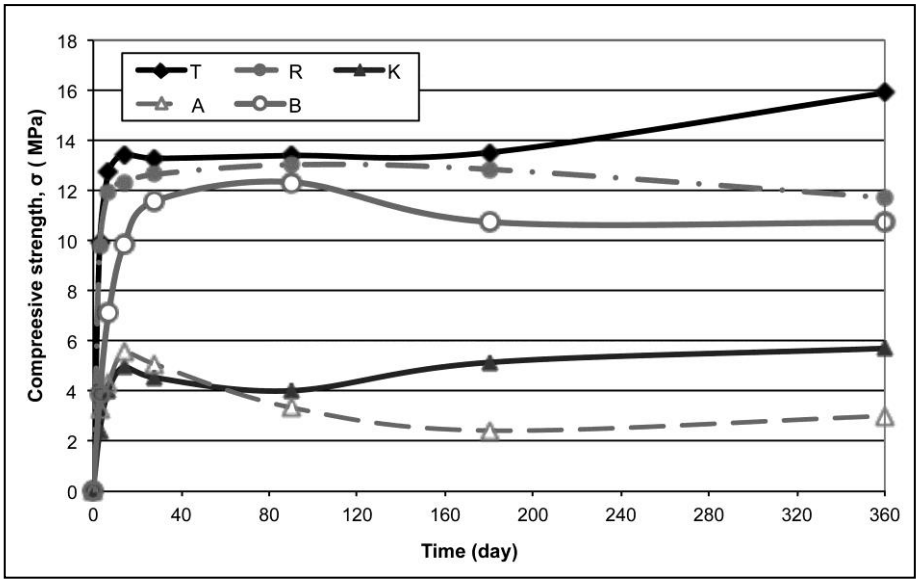

Fig. 1: Density of the tested mortars
(based onmeasurements on more than 2000 samples earlier).

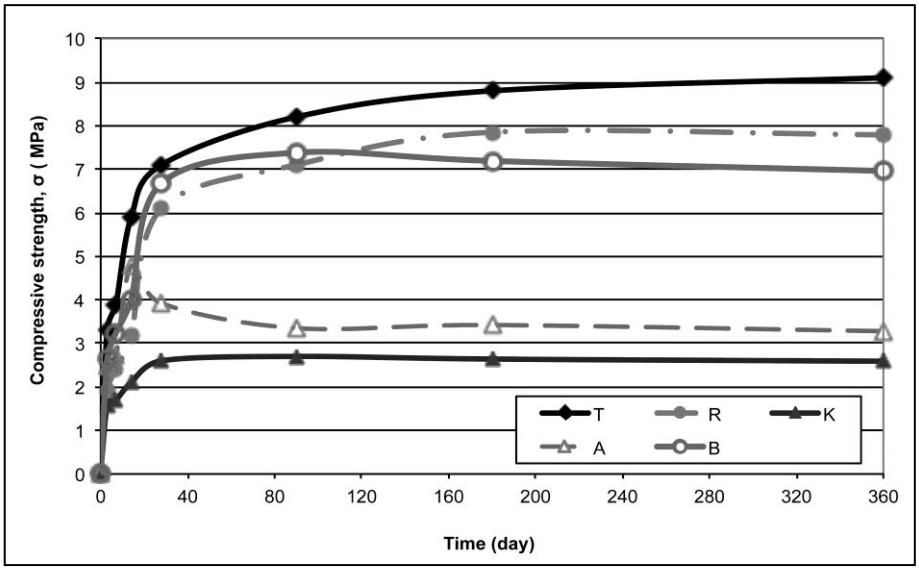

Fig. 2: Uniaxial compressive strength of the tested mortars
kept in damp environment.

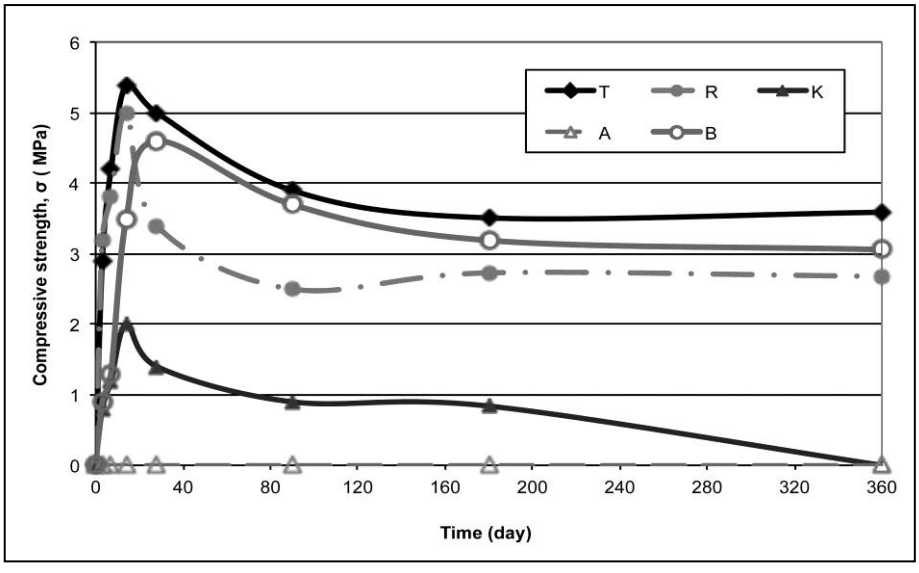

Fig. 4: Uniaxial compressive strength of the tested mortars kept in high temperature climate chamber.

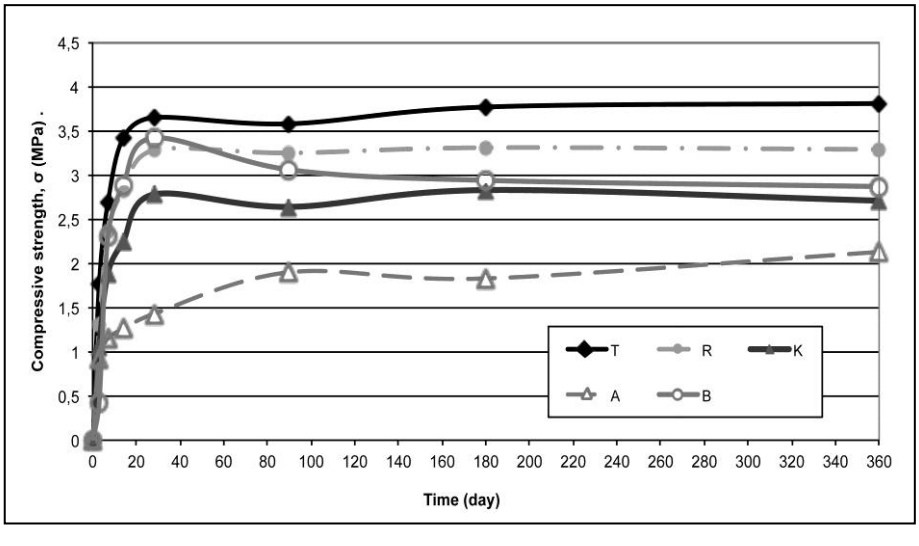

Figure5: Flexural strength of the tested mortars kept in laboratory condition.

Tab. 1: Average density of the tested mortars.

	Density in kg/m³				
Mortars	**A**	**B**	**T**	**R**	**K**
3-day	1673 ±18	1781±32	1869±83	1663±39	1632±34
7-day	1651±23	1735±21	1938±83	1628±18	1564±17
14-day	1643±19	1741±28	1824±41	1643±53	1577±40
28-day	1639±26	1745±28	1800±10	1584±49	1630±64
90-day	1645±16	1760±37	1817±22	1602±17	1675±19
180-day	1649±16	1768±29	1798±20	1620±9	1660±26
360-day	1653± 7	1761±20	1796±53	1628±29	1674±33

4. Conclusions

The strength estimation of heterogeneous, porous materials such as mortars is a difficult task. The long-term assessment of the performance of the restoration mortars under different environmental conditions was simulated under laboratory conditions. The exposure to harsh conditions were modelled in the laboratory and tried to simulate the most common problems that occur during the applications of stone repair mortars (the high temperature or the high relative humidity). Besides the heterogeneity of the porous materials, the w/c, the aggregate type and curing conditions influence the strength. The final strength of the mortar highly depends on the environment, but the binding process continues after 28 days. The environmental conditions had a significant effect on the strength parameters of all tested mortars. Flexural strength is more sensitive to curing conditions especially to relative humidity than compressive strength. Uniaxial compressive strength of tested mortars showed a relative high deviation when the environmental conditions are considered. Mortars kept at higher temperatures than standard laboratory condition (60°C) demonstrated a high degree of strength reduction in time. The compressive strength was one-third, or one-fourth than that of the mortars kept under normal laboratory conditions, indicating the importance of available moisture in the curing and strengthening of mortars.

Acknowledgement

The financial support of OTKA post-doctoral grant to BSZK (reference number is: PD 112-955) and National Research, Development and Innovation (NKFI) Fund to ÁT (ref. no. K 116532) are appreciated.

References

Arizzi, A., Cultrone, G., 2012, Aerial lime-based mortars blended with a pozzolanic additive and different admixtures: A mineralogical, textural and physical-mechanical study, Construction and Building Materials, 31, 135-143.

Arizzi, A., Viles, H., Cultrone, G., 2012, Experimental testing of the durability of lime-based mortars used for rendering historic buildings, Construction and Building Materials, 28, 807–818.

Callebaut, K., Elsen, J., Balen, K.V., Viaene, W., 2001, Nineteenth century hydraulic resaturation mortars in the Saint Michael's Church (Leuven, Belgium), Natural hydraulic lime or cement, Cement and Concrete Research, 31, 397–403.

Degryse, P., Elsen, J., Waelkens, M., 2002, Study of ancient mortars from Sagalassos (Turkey) in view of their conservation, Cement and Concrete Research, 32, 1457-1463.

Elert, K., Rodriguez-Navarro, C., Pardo, E.S., Hansen, E., Cazalla, O., 2002, Lime mortars for the conservation of historic buildings, Studies in Conservation, 47, 67-75.

Hanley, R., Pavia, S., 2008, A study of the workability of natural hydraulic lime mortars and its influence on strength, Materials and Structures, 41, 373-381.

Isebaert, A., Van Parys, L., Cnudde, V., 2014, Composition and compatibility requirements of mineral repair mortars for stone – A review, Construction and Building Materials, 59, 39–50.

Karatasios, I., Kilikoglou, V., Colston, B., Theoulakis, P., Watt, D., 2007, Setting process of lime- based conservation mortars with barium hydroxide, Cement and Concrete Research, 37, 886-893.

Lanas, J., Alvarez, J.I., 2003, Masonry repair lime-based mortars: Factors affecting the mechanical behaviour, Cement and Concrete Researc, 33, 1867-1876.

Lanas, J., Pérez Bernal, J.L., Bello, M.A., Alvarez, J.I., 2004, Mechanical properties of natural hydraulic lime-based mortars, Cement and Concrete Research, 34, 2191–2201.

Lanas, J., Pérez Bernal, J.L., Bello, M.A., Alvarez, J.I., 2006, Mechanical properties of masonry repair dolomitic lime-based mortars, Cement and Concrete Research, 36, 951-960.

Lindqvist, J.E., Sandström, M., 2000, Quantitative analysis of historical mortars using optical microscopy, Materials and Structures, 33, 612–617.

Lindqvist, J.E., 2009, Repair mortars for historic masonry: Testing of hardened mortars, a process of questioning and interpreting, Materials and Structures, 42, 853-865.

Montoya, C., Lanas, J., Aradigoyen, M., Navarro, I., Casado, P.J.G., Alvarez, J.I., 2003, Study of ancient dolomitic mortars of church of Santa María de Zamarce in Navarra (Spain): comparison with simulated standards, Thermochimica Acta, 398, 107-122.

Mosquera, M.J., Silva, B., Prieto, B., Ruiz-Herrera, E., 2006, Addition of cement to lime-based mortars: Effect on pore structure and vapor transport, Cement and Concrete Research, 36, 1635-1642.

Pavia, S., Fitzgerald, B., Treacy, E., 2006, An assessment of lime mortars for masonry repair, Concrete Research in Ireland Colloquium, University College Dublin, Dublin, 101-108.

Rizzo, G., Megna, B., 2008, Characterization of hydraulic mortars by means of simultaneous thermal analysis, Journal of Thermal Analysis and Calorimetry, 92, 173-178.

Rodrigues, J.D., Grossi, A., 2007, Indicators and ratings for the compatibility assessment of conservation actions, Journal of Cultural Heritage, 8, 32-43.

Schueremans, L., Cizer, Ö., Janssens, E., Serré, G., Van Balen, K., 2011, Characterization of repair mortars for the assessment of their compatibility in restoration projects: Research and practice, Construction and Materials, 25, 4338-4350.

Szemerey-Kiss, B., Török, Á., Siegesmund, S., 2013 The influence of binder/aggregate ratio on the properties and strength of repair mortars, Environmental Earth Sciences, 69, 1439-1449.

Szemerey-Kiss, B., 2013, Compatibility of monumental stone repair mortars and Hungarian, Miocene limestones, Ph.D. thesis, Budapest Technical University Hungary.

Szemerey-Kiss, B., Török, Á., 2011 Time-dependent changes in the strength of repair mortar used in loss compensation of stone, Environmental Earth Sciences, 63, 1613-1621.

Torney, C., Forster A.M., Szadurski E.M., 2014, Specialist 'restoration mortar' for stone elements: a comparison of the physical properties of two stone repair materials, Heritage Science, 2:1.

Torney, C., Forster A.M., Kennedy, C.J., Hyslop E.K., 2012, Plastic' repair of natural stone in Scotland: perceptions and practice, Struct Surv, 30, 297-311.

Van Balen, K., Papayianni, I., Van Hees, R., Binda, L., Waldum, A., 2005, Introduction to requirements for and functions and properties of repair mortars, RILEM TC 167-COM: "Characterisation of Old Mortars with Respect to their Repair", In: Materials and Structures, 38, 781-785.

PROPRIETARY MORTARS FOR MASONRY REPAIR: DEVELOPING A PREDICTIVE FRAMEWORK FOR ASSESSING COMPATIBILITY

C. Torney[1*]

Abstract

Proprietary restoration mortars are fast becoming the 'go-to' material for masonry repair work. The convenient 'mix and go' approach of these products makes them attractive to specifiers and end users, obviating the multi-faceted specification procedures traditionally followed and aiming to minimise the risks of failure associated with inaccurate batching of materials. The multi-substrate suitability of some products is perhaps a cause for concern as it assumes universal compatibility with a compositionally and texturally diverse range of substrates – in some cases this includes a range of stone types as well as concrete block and brick. Before new products can be used with confidence, a comparison with potential substrates must be made to give an indication of compatibility. In the case of historic buildings, philosophical considerations often add a layer of complexity and due to the preferred (or enforced) non-destructive approach it is often difficult to access the quantities of stone required to provide reliable results on material properties. The current research aims to develop a model for predicting substrate properties based on the moisture diffusion analysis of historic and currently available building stone samples. Results will enable the assessment of compatibility of proprietary repair products with their substrates, whilst adopting a minimal or non-destructive testing regime.

Keywords: stone repair, historic buildings, compatibility, mortar

1. Introduction

Proprietary restoration mortars are pre-mixed 'convenience' mortars designed specifically for the repair of natural stone. These materials fall within the general category of 'plastic repairs' (Fig. 1) and are sometimes referred to as 'surface repair mortars' but are different from the bespoke lime mortars traditionally used for repair to stone work (Torney, 2015) and the pre-mixed mortars used for repointing (Gulotta *et al.*, 2013). A number of products are commercially available, the composition of which can differ significantly. Restoration mortars typically consist of aggregate and a binder (which may be lime, cement, a combination of these, or a resin (typically epoxy) but may also contain inert fillers (which effectively act as aggregate) and additives that impact specific performance characteristics on the fresh and/or hardened mortar (Torney *et al.*, 2015).

[1] C. Torney*
Historic Environment Scotland, United Kindom
clare.torney@hes.scot

*corresponding author

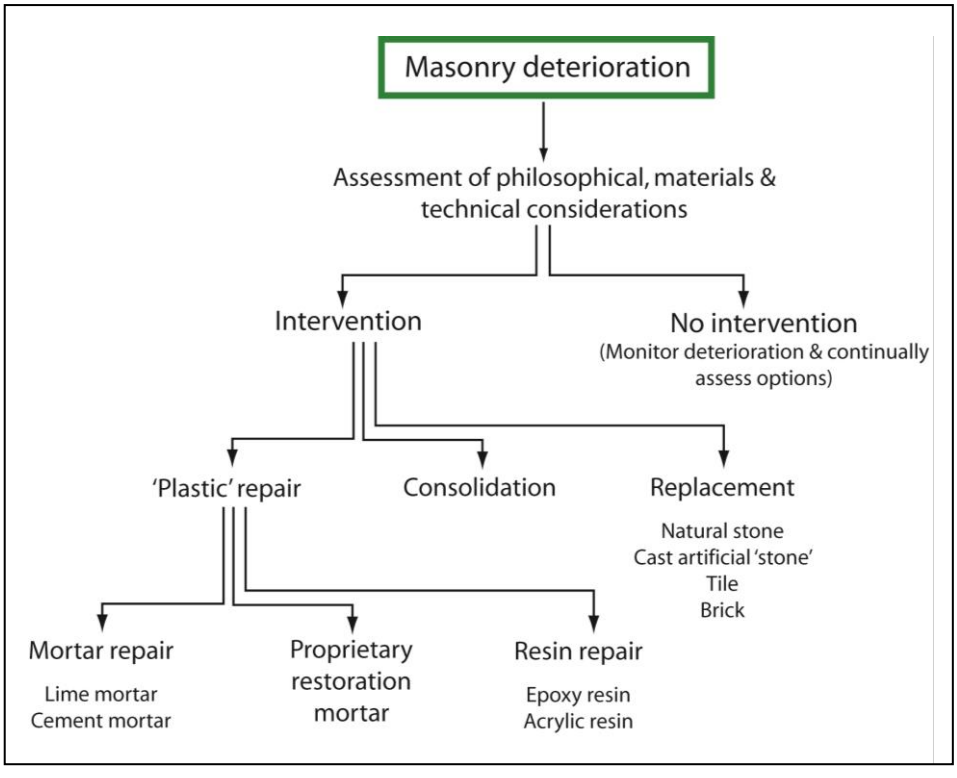

Fig. 1: Classification of proprietary restoration mortars in the context of intervention methods for building stone repair (image from Torney et al., 2015).

The intricacies of specifying lime mortar repairs are well publicised (Forster and Carter, 2011; Allen *et al.*, 2003) and it is perhaps the perceived complexity of the specification procedure that makes proprietary repair materials attractive to specifiers. Although there is significant variation in the composition of restoration mortar products, many of these claim to be suitable on the same wide range of substrates with little explanation of how this 'universal compatibility' is achieved, nor quantification of compatibility-related properties. The technical information provided by most manufacturers focuses on compressive strength data, the 'standard' property by which lime binders are typically classified. In some cases, information on vapour or liquid permeability is also provided, however, without the context of substrate properties, data provided on mortar properties is effectively meaningless.

Analysis of the moisture diffusion properties of stone can be fairly easily established through basic experimentation to assess properties including vapour permeability and capillarity. Depending on availability of test equipment, these tests can be done in-situ, or in the laboratory, the latter requiring sampling of stone. In-situ testing can require the use of expensive equipment, and although such approaches may be employed in research studies, they are rarely considered to be financially viable for commercial projects. Additionally, more basic tests which can be carried out in the laboratory are not always possible as, when dealing with conservation of traditional and/or historic buildings especially those of cultural significance, sampling of stone for destructive analysis is rarely acceptable.

Here, a regime for assessing the compatibility between restoration mortars and building stone substrates is outlined. Assessment is based on the availability of stone (both new and old) for laboratory testing and the work aims to use these samples to develop a predictive framework for assessing material's compatibility that can be used in instances where sampling of original stone is not permitted. Over time, the availability of supporting evidence from site trails of restoration mortars would allow for refining of the model, and an increase in confidence in decisions drawn from it. The availability of compatibility data will allow for more informed decisions to be made regarding the use of proprietary repair materials, and will lead to more rapid decision making on commercial projects, saving both time and money.

2. Methodology

2.1. Selection of stone for testing

Twenty-three different sandstone samples were obtained for laboratory analysis; 7 of these were historic building stones, obtained during building repair and/or building stone analysis, and the remaining 16 were freshly quarried commercially available UK sandstones. Historic Sandstone samples were sourced from the British Geological Survey (BGS) Building Stone Collection and represent a number of different buildings on both the East and West of Scotland. Additionally, a single specimen of sandstone was obtained from the Main Building at the University of Glasgow during conservation works in Summer 2011. The commercially available sandstones were provided by the Hutton Stone Company.

Petrographic analysis was carried out on samples to enable classification of rock types (Fig. 2); composition and porosity were determined by point counting, a minimum of 600 points at 600 µm intervals were taken for each sample. The stone samples selected cover a range of sandstone types; quartz arenite, subarkosic arenite, arkosic arenite, lithic arenite, lithic greywacke as illustrated in Fig. 3.

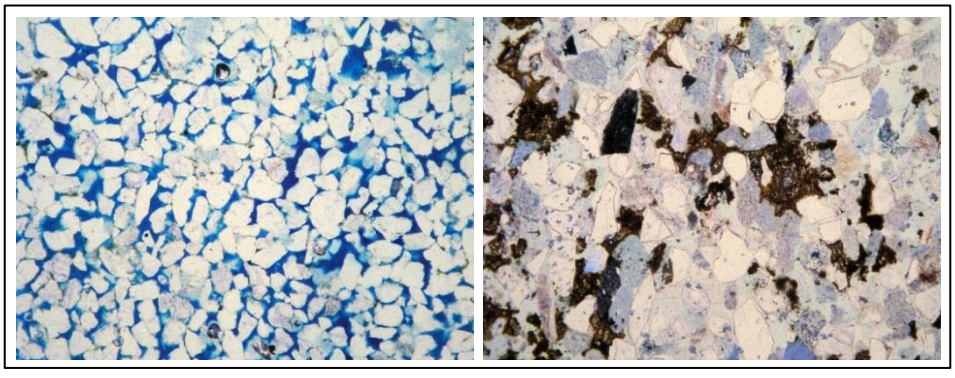

Fig. 2: Petrographic thin section images of two of the historic building stone samples viewed in plane polarised light. L-R, a quartz arenite from an ecclesiastical structure in Midlothian, Scotland; a lithic greywacke from a privately owned castle, Ayrshire, Scotland. FOV = 3.3 mm.

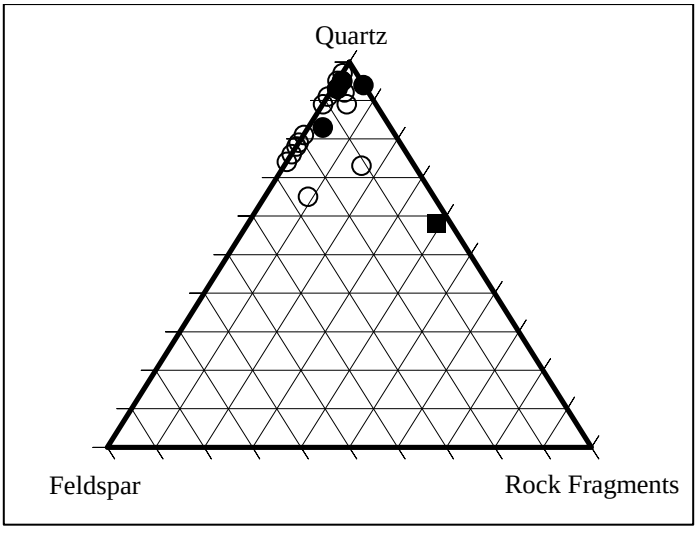

Fig. 3: Classification of test sample sandstones based on the Dott (1965) classification method. Image produced using Tri-plot (Graham and Midgley, 2000). Solid markers indicate historic building stone samples, and unshaded markers indicate freshly quarried building stone samples. Note: due to the 2-dimensional nature of this diagram, the elevated matrix clay content of the lithic greywacke sample (square marker) is not evident.

2.2. Testing procedures

2.2.1. Water absorption testing

Water absorption of stone samples was conducted by two methods. (1) Sorptivity testing following Hall and Hoff's (2010) direct gravitational method to determine the flow of moisture through unsaturated porous media, and (2) full immersion water absorption calculated by measuring weight gain in samples immersed in water for 72 hours. The reason for using both methods, is to enable as close comparison as possible with existing data on restoration mortar moisture diffusion data (Torney *et al.*, 2014; 2015).

2.2.2. Vapour Permeability Testing

Vapour permeability testing was carried out on sandstone samples using the wet-cup method; the procedure adopted follows the same general principles as BS EN 1015-19:1999. Thin slices of sandstone (8-10 mm) were cut from stone cores/samples. Discs/samples were placed on the mouth of a cup containing a saturated potassium nitrate solution and sealed in place using silicone sealant. Sample cups were placed in an TAS Series 3 MTCL environmental test chamber with constant conditions of 20°C and 65% *RH*. Weight was recorded at the beginning of the experiment and periodically over a period of 21 days. Permeance and vapour permeability were calculated using the equations in BS EN 1015-19:1999.

3. Preliminary results

Preliminary results from an experimental sub-set of samples shows that, as expected, sandstone samples have a range of water transmission values, with significant variation in water absorption and some variation in vapour permeability. Comparison of permeance values with point counting results (and therefore sandstone classification), is expected to highlight correlations between moisture diffusion and porosity and additionally, moisture diffusion and composition (Fig. 4).

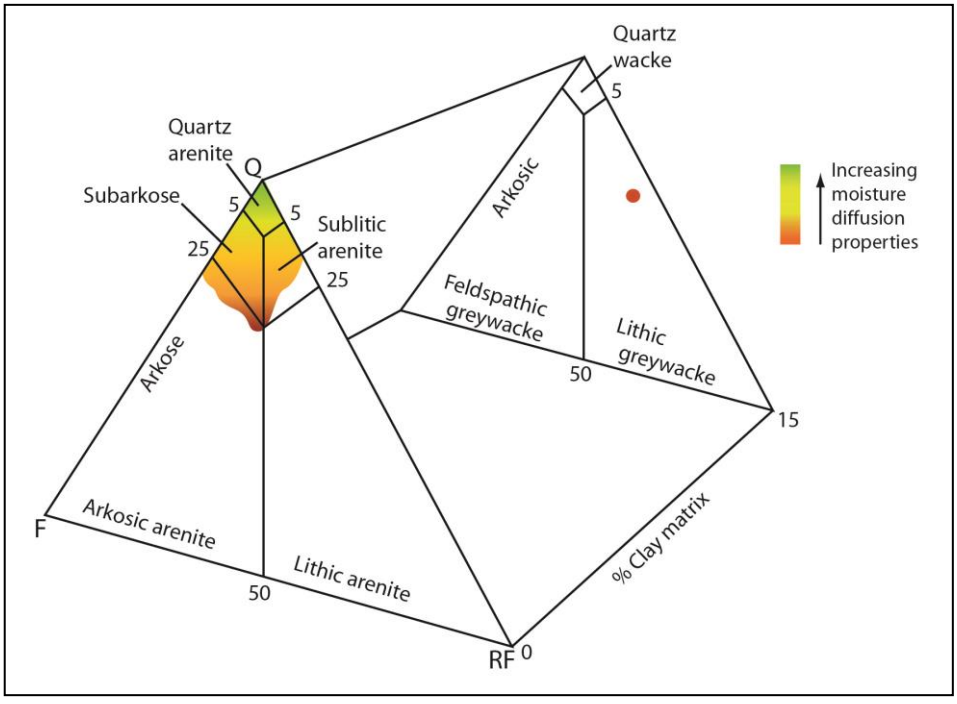

Fig. 4: Schematic illustration of how moisture diffusion data might be overlain on compositional data to enable prediction of properties based on stone type.

Compatibility of plastic stone repair materials is largely determined by comparison of their moisture diffusion characteristics with those of their intended substrates, as well as an assessment of their durability and reversibility. Overlaying repair material's moisture diffusion data with that of stone, will allow an assessment of compatibility to be made. Data from Torney *et al.* (2015) shows that in the case of one particular stone repair mortar, vapour permeance and water absorption of the mortar falls largely within the same region as two arkosic arenites tested. As results from the present study become available, it will be possible to directly assess the compatibility of repair materials with all 23 different sandstone types, and by using sandstone classification as a guide, to infer the compatibility of repair materials with a much wider range of stone simply through visual analysis of the stone in-situ. Continued observation of material performance on-site will be required to verify the findings of laboratory tests and to strengthen decisions based on predictive modelling.

Acknowledgements

The authors thank the British Geological Survey, Building Stones North Team for providing historic sandstone samples and thin sections. Marcus Paine (Hutton Stone Co.), Beverly Hill (Stancliffe Stone Ltd) are thanked for provision of freshly quarried sandstone samples, and Prof. Martin Lee (University of Glasgow) for providing an historic sandstone sample from the University of Glasgow.

References

Allen, G., Allen, J., Elton, N., Farey, N., Holmes, S., Livesey, P. and Radonjic, M., 2003, Hydraulic lime mortar for stone, brick and block masonry, Donhead, 1-873394-64-0, 84.

British Standards Institution, 1999, BS EN 1015–19:1999, Methods of test for mortar for masonry – determination of water vapour permeability of hardened rendering and plastering mortars, BSI, 0-580-30750-6, 8.

Dott, R.H., 1964, Wackes, greywacke and matrix: what approach to immature sandstone classification. Journal of Sedimentary Research, 34, 625–632.

Hall, C. and Hoff, W.D., 2012, Water transport in brick, stone and concrete, Taylor & Francis, 978-0-415-56467-0, 370.

Graham, D.J. and Midgley, N.G., 2000, Graphical representation of particle shape using triangular diagrams: an Excel spreadsheet method, Earth Surface Processes and Landforms, 25(13), 1473-1477.

Forster, A.M. and Carter, K., 2011, A framework for specifying natural hydraulic lime mortars for masonry construction, Structural Survey, 29, 373-396.

Gulotta, D., Goidanich, S., Tedeschi, C., Nijland, T.G. and Toniolo, L., 2013, Commercial NHL-containing mortars for the preservation of historical architecture. Part 1: Compositional and mechanical characterisation, Construction and Building materials, 38, 31-42.

Torney, C., 2015, Modern Restoration Mortar: The Future of Lime in Masonry Repair? The Journal of the Building Limes Forum, 22, 7-14.

Torney, C., Forster, A.M., Kennedy, C. J. and Hyslop, E.K., 2012, 'Plastic' repair of Natural Stone in Scotland: Perceptions and Practice. Structural Survey, 30 (4), 297-211.

Torney, C., Szadurski E., Forster, A.M., 2014, Specialist 'Restoration Mortars': A Comparison of the Physical Properties of Two Stone Repair Materials, Heritage Science, 2 (1), 12.

Torney, C., Forster, A.M., Banfill, P.F.G. and Szadurski, E., 2015, The Effects of Site Practice on the Physical Properties of Proprietary Stone Restoration Mortar, Construction and Building Materials, 75, 359-367.

STUDY OF EFFICIENCY AND COMPATIBILITY ON SUCCESSIVE APPLICATIONS OF TREATMENTS FOR ISLAMIC GYPSUM AND PLASTER FROM THE ALHAMBRA

R. Villegas Sanchez[1*], F. Arroyo Torralvo[1], R. Rubio Domene[2] and E. Correa Gomez[2]

Abstract

The restoration of Islamic gypsum plaster decoration of the Alhambra has to be carried out considering the environmental factors affecting the material. A continuous program of restoration works is developed, and it could be necessary to reapply treatments when the former ones lose efficacy. The present work has been developed to test the compatibility of this second treatment with weathered, previously treated gypsum samples. Gypsum samples were treated with consolidants: organosilicic, silica and lime nanoparticles. Changes in surface hardness, ultrasonic velocity, colour and capillary water absorption were measured before and after the application of treatments and after two accelerated weathering tests, simulating freezing-thawing and thermal stress. Altered samples were treated again with the same conservation products and the weathering tests were repeated. Treatments were less effective than in the first application. The samples properties after weathering changed very negatively, with hardness and ultrasonic velocity decreased. The morphology of the surfaces shown the deterioration of both gypsum crystals and treatment films; in some cases, the treatment remains showing the voids where the gypsum crystals have fallen. In conclusion, the application of treatments usually used for stone does not protect correctly the gypsum plaster, nor the first neither the second time. The thermal stress affects the gypsum decoration of the Alhambra, and produces severe deterioration, so it is one of the most important weathering factors to be considered in this monument.

Keywords: gypsum plaster, consolidation treatment, SEM, thermal weathering, freezing-thawing

1. Introduction

Gypsum was a rather common building and decorative material in the Mediterranean countries, especially during the Middle Ages (Rubio 2010, Elsen 2006, Blasco-Lopez and Alejandre 2013). Plasterworks are decorative elements typical of Islamic or Islamic-based art ("mudejar"), applied on walls, arches, and vaults. Gypsum, is abundant in nature and easy to work. However, it is a fragile material with poor mechanical and structural strength. Therefore, the plaster decoration would have required continual maintenance (Lopez Borges *et al.* 2005). There are numerous examples of medieval Islamic architecture, such as

[1] R. Villegas Sanchez* and F. Arroyo Torralvo
Chemical and Engineering Department, University of Seville, Spain
rvillegas@etsi.us.es

[2] R. Rubio Domene and E. Correa Gomez
Patronato de la Alhambra y el Generalife, Spain

*corresponding author

the Alhambra in Granada (12th-15th centuries) (Fig. 1a) or the Alcazar in Seville (13th-16th centuries) (Fig. 1b), both in Spain.

This paper focused in the study of the main Islamic plasterwork ("yeserías") from the Alhambra of Granada, unique in the world. The specialized workers ("alarifes") that made these plasters combined two techniques, casting and carving (Rubio 2010, Garcia Bueno and Medina Florez 2004). As finishing a preparation layer to protect against water and to polychrome with red, blue, black and gold colours (Fig. 2) (Blasco-López *et al.* 2015).

Fig. 1: Alhambra, Granada (left) and Alcázar, Seville (right)

Due to the continental climate of Granada and the exposition of the plasterworks (many of them outdoor), daily changes in temperature that can arise 30ºC, humidity, direct solar irradiation, rain or rising damp water or freezing episodes affect the material. So, maintenance and restoration works are carried out continuously by the restoration team of the monument. The most frequent treatments are the fixing of the polychrome and the consolidation of gypsum support, needed to limit deterioration. However, consolidation of historical gypsum plaster is not well studied, contrary to stone. Consolidation could be achieved applying organic or inorganic consolidants commonly used in stone conservation. This is the case of acrylic polymers, alkoxysilanes and their copolymers (Cotrim *et al.* 2008, Rubio 2010). Alkoxysilanes have also been applied for consolidation, especially on silicate substrates such as sandstones (Rubio 2010, Wheeler 2005). Recently, nanolimes have been proposed as a consolidant for gypsum stucco (Daehne and Herm 2013), yet little is known about its effectiveness.

To restore gypsum plaster decorations on the Alhambra, ethyl silicate is being used up to now with good results. Foreseeing the necessity of reapplication of treatments when pieces reach a high degree of deterioration, the *Patronato de la Alhambra* has promoted the present study, complemented with on site tests that are being carried out since 2013.

2. Materials and methods

2.1. Materials

Cubic samples (5 cm approx.) of plaster have been prepared using a commercial gypsum normally employed on the Alhambra as joining or filling material to restore the gypsum plasterworks (Fig. 2). The gypsum has been mixed with water in a proportion 210 g gypsum/162 g water.

Fig. 2: Restoration of plasterwork in the Alhambra

Samples were treated with commercial consolidants (six replicates), by immersion of the upper half part of the cubes during 8 seconds and repeating the procedure after 30 seconds. The drying period has been monitored by weighing the samples daily until constant weight and, after that, samples properties have been measured. The consolidants used appear on table 1, as well as the dilutions employed. All of them are supplied by CTS. Estel 1100 is also water repellent due to the presence of polysiloxane. Treatments were applied twice: to unaltered samples and after the weathering tests (altered samples). Each sample has been impregnated with the same treatment both times, except for the case of Nanoestel; this product does not impregnate correctly the samples, so in the second phase these groups of samples have been treated with Estel 1000 diluted with ethanol.

Tab. 1: Consolidants applied

Product	**Composition**	**Dilution**	**Denomination**
Estel 1000	Tetraethoxysilane	8:2 ethanol	G1
		as received	G2
Estel 1100	Tetraethoxysilane + oligomeric polysiloxane	as received	G3
Nanoestel	Colloidal nanoparticles of silica	1:1 water	G4
		1:2 water	G5
Nanorestore	Nanoparticles of calcium hydroxide	as received	G6
		8:2 i-propanol	G7

2.2. Experimental techniques

Different techniques were performed to characterise the physical properties of the samples and to evaluate the effectiveness and compatibility of each treatment. In order to evaluate the effect of treatments on the compactness of the gypsum, ultrasonic velocity and surface hardness were measured. Ultrasound was measured using a Steimkamp BP-5 equipment

provided with transducers of 50 kHz. Surface hardness was measured on the Shore C scale with a portable meter model Bareiss HPE, following UNE 102.039-85.

The variations in colour between untreated and treated samples and after the weathering tests were determined with a Minolta CR-210 colorimeter. The global colour variations (ΔE) due to the treatments are calculated as follows:

$$\Delta E = \sqrt{(L_0 - L_t)^2 + (a_0 - a_t)^2 + (b_0 - b_t)^2} \qquad \textit{(Eq. 1)}$$

Where L_0, a_0, b_0 and L_t, a_t, b_t are the original chromatic coordinates of untreated gypsum and treated samples (average in this case), respectively. Capillarity water absorption was determined to assess the hydric behaviour of samples. Accelerated weathering tests were carried out to simulate the action of the two main deterioration agents on the Alhambra (freezing-thawing test and thermal stress test). 20 freezing-thawing cycles were performed to water-saturated samples. On the thermal test the samples were heated 6 hours a day on the upper face while the lower face was maintained on contact with wet sand; in this way, the water flows upward the samples and evaporates during the heating phase. This test was performed also 20 cycles. Properties of samples were measured again in order to evaluate the response. Morphology and texture of the treatments on the samples surface before and after the weathering tests were studied by SEM, using a JEOL 6460LV equipment provided with SEI, BSE and EDS detectors.

3. Results and discussion

3.1. Degree of compactness

The application of treatments causes a slight increment on the ultrasonic velocity, similar on both phases (Tab. 2). But the effect of weathering tests is much greater on the second phase, with a diminution from 30-35% on the freezing-thawing test or 38-45% on the thermal test.

Tab. 2: Ultrasonic velocity (m/s)/Surface hardness (Shore C units).

	First phase			**Second phase**			
	After tr.	Th. Test	F-Z test	Before tr.	After tr.	Th. Test	F-Z test
Untr	2148/80	2153/57	2119/73	2136/73		1456/40	1614/65
G1	2334/80	2137/52	2304/86	2220/69	2345/89	1323/55	1521/79
G2	2277/80	1855/60	2318/85	2087/73	2354/88	1315/55	1514/83
G3	2302/79	2114/55	2286/84	2200/69	2314/85	1255/67	1508/83
G4	2221/83	1957/51	2233/83	2095/67	2292/89	1312/56	1458/81
G5	2328/83	2075/51	2303/84	2189/67	2346/88	1298/60	1511/83
G6	2244/74	1924/35	2250/77	2087/56	2219/79	1310/34	1524/67
G7	2116/76	2109/45	2206/78	2158/61	2116/79	1296/35	1475/67

Surface hardness (Tab. 2) does not change noticeably with the first application of treatments, while experiments increments of 20-40% in the second application (altered samples). After the thermal test the values are much lower, while the freeze test affects in a lesser extent. Hardness of Nanorestore treated samples (G6-G7) is more affected by weathering on all cases, probably due to a lack of adherence between the lime layer formed by the treatment to the gypsum substrate.

3.2. Colour

After the application of treatments (on the first phase) colour does not change significantly, (Tab. 3) with the exception of Nanorestore (G6-G7) which causes a lightening in the plaster colour, mainly due to increments in *L** (because lime is whiter than gypsum). On the contrary, the second impregnation causes very high changes for all the tested products, all of them visible to the naked eye (> 3).

Treated samples showed less colour changes after F-Z tests compared with untreated ones. Same behaviour can be seen after second thermal test, but not after the second thermal test, because some treatments caused higher colour changes when they are compared with untreated samples.

Tab. 3: Colour differences (ΔE).

	Treatment app.		**Weathering tests**			
	First	Second	1st Thermal	2nd Thermal	1st F-Z	2nd F-Z
Untr			2,73	2,94	8,78	9,04
G1	0,64	10,61	4,40	0,62	1,75	1,30
G2	0,87	10,20	4,35	1,45	1,29	0,88
G3	0,48	10,86	4,61	1,08	1,41	1,80
G4	0,70	10,08	4,47	0,63	1,78	1,36
G5	0,51	9,86	4,22	0,84	2,77	2,10
G6	3,17	7,15	2,25	4,21	2,80	2,97
G7	4,92	8,01	1,38	5,22	2,75	3,23

3.3. Hydric properties

The capillary absorption has been measured after both applications of treatments, given similar results to those showed on Fig. 3. The hydrophobic effect of Estel 1100 is clearly seen, while Estel 1000, with both dilutions, reduces slightly the rate and quantity of water absorbed. After all the weathering tests the results are similar to those on Fig. 4, having disappeared the water repellency of these three treatments.

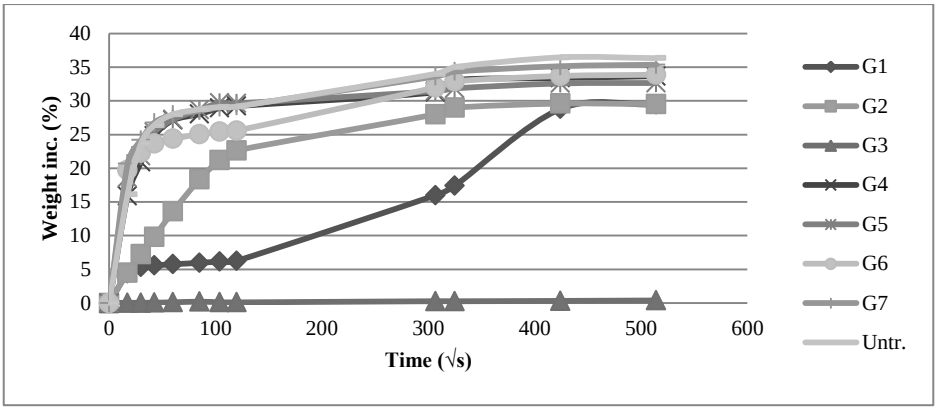

Fig. 3: Capillary absorption. First application of treatments.

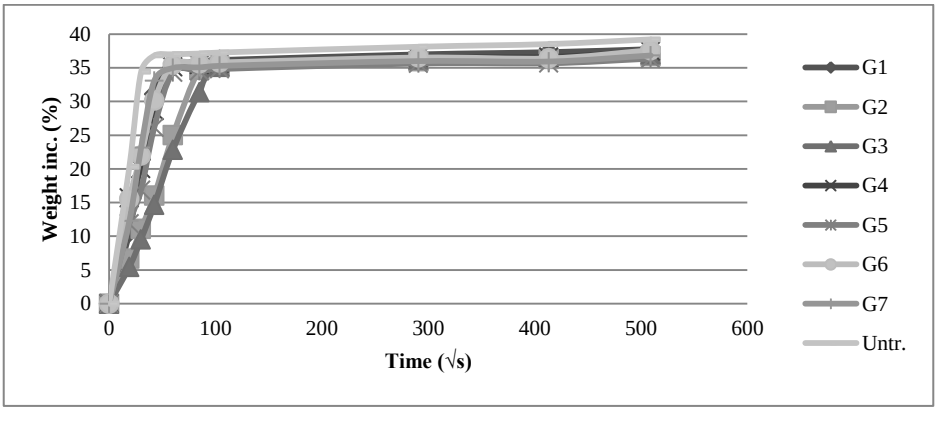

Fig. 4: Capillary absorption after thermal weathering test.

3.4. Weathering tests. Visual indicators

On both phases, the alteration is higher on the samples submitted to the thermal test (Fig. 5, up and down). On the first test the samples suffered losses of material from the surface, while on the second one almost all of them showed cracks and fissures besides surface erosion. The treatments did not protect the material, the weathering indicators were similar on all the samples. The first freezing-thawing test did not cause macroscopic alterations (Fig. 5, middle) and the second time cracks appeared on only two of the samples treated with Estel 1000, while the rest of them maintained a good state of conservation.

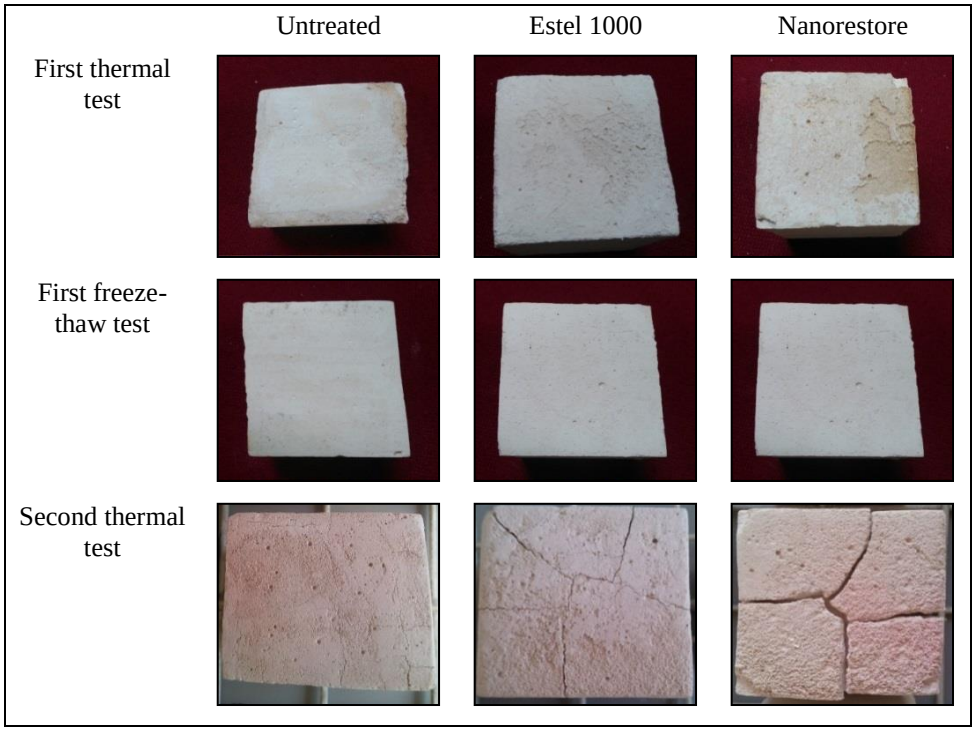

Fig. 5: Aspect of samples after weathering tests.

3.5. SEM

SEM observation of the samples before and after the thermal weathering test has been carried out. In general, the treatment film is not clearly seen; only with high magnification the detection is possible thanks to the fissures formed on this surface layer (Fig. 6 left). After the alteration several changes take place: modification in the morphology of gypsum crystals, new and wider fissures on the treatment layer, and detachment of gypsum crystals leaving holes on the treatment film (Fig. 6 right).

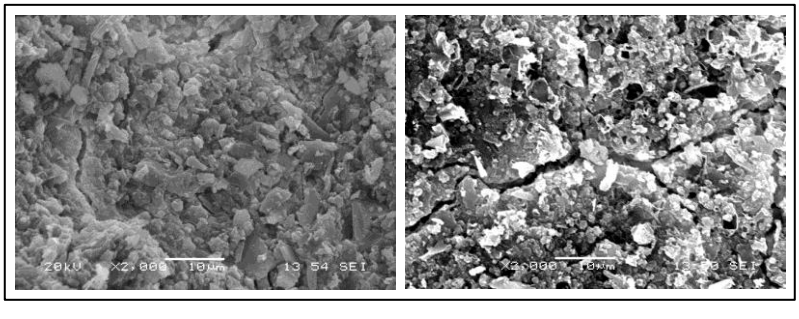

Fig. 6: SEM image of sample treated with Estel 1000 before (left) and after (right) thermal weathering test.

4. Conclusions

The treatments studied do not improve significantly the characteristics and weathering resistance of the gypsum in any of the two phases and, in the second application, the results after the weathering tests are quite worse than in the first phase. It is necessary to research about different treatments with the aim of consolidating the gypsum plasterwork properly. The results can be used also on other monuments with similar ornamental motifs, abundant on the South of Spain.

References

Blasco-López, F.J., Alejandre Sánchez, F.J., 2013, Porosity and surface hardness as indicators of the state of conservation of Mudéjar plasterwork in the Real Alcázar in Seville, J Cult Heritage, 14,169–73.

Blasco-Lopez, F.J., Alejandre, F.J., Flores-Ales, V., 2015, Methodology for characterising microlayers in historical plasterwork, Construction and Building Materials, 93, 463–470.

Cotrim, H.,Veiga, M.R., de Brito, J., 2008, Freixo palace: Rehabilitation of decorative gypsum plasters, Construction and Building Materials, 22, 41–49.

Elsen, J. Microscopy of historic mortars—a review, 2006, Cem Concr Res,36,1416–24.

Daehne A, Herm C., 2013, Calcium hydroxide nanosols for the consolidation of porous building materials – results from EU-STONECORE, Heritage Sci,1-11.

Doehne, E., Price, C., (2010), Stone conservation: an overview of current research. 2nd ed. Los Angeles, CA: The Getty Conservation Institute, ISBN 978-1-60606-046-9, 158pp.

García Bueno, A., Medina Flórez, V.J., 2004, The Nasrid plasterwork at "qubba Dar al-Manjara l-kubra" in Granada: characterisation of materials and techniques, Journal of Cultural Heritage, 5, 75–89.

Jroundi, F., Gonzalez-Muñoz,M.T., Garcia-Bueno, A., Rodriguez-Navarro, C., 2014, Consolidation of archaeological gypsum plaster by bacterial biomineralization of calcium carbonate, Acta Biomaterialia, 10,3844–3854.

Lazzarini L, Tabasso ML. Il Restauro della Pietra. Padova: Cedam; 1986.

López Borges, V.H., Burgio, L., Clark, R.J.H., 2005, Documentación y autentificación de yeserías nazaríes a través del tratamiento de conservación y el análisis científico. Preprints GE-IIC conference Investigación en conservación y restauración, Spain, 109–17.

Rubio Domene, R., 2010, Yeserías de la Alhambra: Historia, Técnica y Conservación. Patronato de la Alhambra y Generalife. Universidad de Granada.

COMPARATIVE STUDIES ON MASONRY BRICKS AND BEDDING MORTARS OF THE FORTRESS MASONRY OF THE TEUTONIC ORDER STATE IN PRUSSIA: MALBORK, TORUŃ, AND RADZYŃ CHEŁMIŃSKI CASTLES

K. Witkowska[1*] and J.W. Łukaszewicz[1]

Abstract

The paper presents part of the results of ongoing studies aimed at examining historic masonry bricks and bedding mortars originating from the fortress masonry of the Teutonic Order State. The comparative research concerns technological aspects of the chosen historic materials: masonry bricks and bedding mortars. The samples of materials mentioned above come from the following Teutonic castles: Malbork, Toruń, and Radzyń Chełmiński. The following properties of bricks and mortars were determined: composition, physical properties, structure, texture, and technological faults. The above-mentioned characterisation is the result of examinations carried out in accordance with the following methodology: determination of composition of masonry materials by thermal analysis (DSC-TG) and petrographic analysis. To properly recognise the materials, a quantitative analysis of mortars and an analysis of the physical properties of bricks and mortars was carried out. It was found that in spite of many similarities in the examined materials' composition, there are differences in the proportions of components. Research results can be a contribution to complex studies of similar groups of architectonic objects and facilitate the comparison of Polish and European medieval masonry workshops. The above mentioned data will also make it possible to find better methods of conservation and restoration.

Keywords: medieval fortress masonry, masonry brick, bedding mortar

1. Introduction

The paper presents part of the research on the characterisation of historic masonry bricks and bedding mortars originating from the fortress masonry of the Teutonic Order State focused on their constitution and properties. The technology and conservation aspects of the masonry of the Teutonic Order State has so far been an unsolved problem. Some research literature relevant to brick work conservation is available. There are publications which are the results of the research carried out by the members of ZKEiDA (NCU in Toruń): Skibiński (1993), Domasłowski *et al.* (2004), Domasłowski (ed.) (2011). It is possible to find in the works presented above brief information about medieval bricks and mortars and their constitution and properties. This kind of data, concerning individual monuments, can

[1] K. Witkowska* and J.W. Łukaszewicz
Department of Conservation and Restoration of Architectonic Elements and Details,
Faculty of Fine Arts, Nicolaus Copernicus University in Toruń (NCU), Poland
karolina.witkowska@umk.pl

*corresponding author

be obtained from conservation reports.

Unfortunately, conservation reports are not published so they do not add anything to the public perception of the problem. To sum up, the current scope of the exploration of the subject is not enough to provide a detailed description and to solve the problems of this group of monuments in its technological and conservation aspects. Therefore it is necessary to begin regular research including especially that part of the enormous heritage represented by Teutonic fortress masonry. Moreover, the reason for taking on these tasks is the fact that for a very long time only the architectural details made of brick were considered as a subject of legal protection and deserving of respect. Not long ago deteriorated historical bricks, which were mass-product articles, were replaced by new ones. The same situation occurred with masonry mortars. The situation has fortunately changed and brick walls are within the field of interests of both conservators-restorers and conservation scientists. The ICOMOS colloquium in 1992 devoted to the brick heritage constituted a turning point in the attitude to discussed problem (Colloque ICOMOS, Le patrimoine en brique, Albi, France, 17-18.09.1992). Characterisation of these masonry materials is an important contribution to finding the ways of preserving architectural surfaces as a part of the material heritage.

2. Materials and methods

2.1. Materials

The research concerns the technology aspects of chosen historic materials: masonry bricks and bedding mortars. Samples of the above mentioned materials come from the following Teutonic Castles: Malbork, Toruń, and Radzyń Chełmiński. The criteria for the choice of the analyzed monuments were: all the objects are representative examples of Teutonic fortress architecture, and all of the chosen monuments have sufficiently well preserved medieval parts. These were imperatives for a proper collection of samples. Considering the need for limiting research material, it was decided to start the research from the examples of castles of varied size and significance. Representative of an architectural layout of great scale and significance is, of course, Malbork castle. In comparison to the above, the conventional castles of Toruń and Radzyń Chełmiński are medium scale examples, although of great significance. Taking samples from all the buildings mentioned above made it possible to analyse historic material coming from the following period: from the 2nd half of the 13th century to the middle of the 14th century. The time of construction of the elements of particular castles, where investigated masonry materials were sampled, was determined on the bases of a historical and architectural survey. The gathered information was compared with available data on mortars and bricks. As the presented results of investigations are the initial part of the research project, it has not resolved the issue yet.

2.2. Methods

Several types of analysis were undertaken in order to characterise and compare chosen masonry materials. To determine the structure and texture of the materials a stereomicroscope Nikon SMZ800 with a zoom range of ×1 to ×6.3 equipped with a digital camera, was used. The petrographic analysis of the selected samples of both bricks and mortars was carried out on thin sections using a Zeiss petrographic microscope operating in transmitted and incident light. For bedding mortars thermal analysis (differential scanning calorimetry–thermogravimetry (DSC-TG)) was performed. DSC-TG curves were recorded with PerkinElmer STA 6000 system. The temperature range was 30–950°C and a heating

rate of 10°C/min. Simultaneously, an acid treatment of the mortars was carried out (2M solution of hydrochloric acid). Finally for chosen bricks, an examination of the rate of capillary water suction was carried out and its water absorption capacity (after 24 hours) was determined. The test was performed in accordance with the methodology defined by Polish Norm PN-85/B-04101 on the samples from 12 to 14 cm high (Domasłowski, 2011).

3. Results and discussion

3.1. Masonry bricks

The research focused particularly on determining the constitution and properties of chosen bricks. Ceramic had different colours: from orange-red (Mja, Mjb, MW2c, RdzC1, RdzC2) through red (McC1, M7.1, M8.1, MW1c), reddish-brown (TzGd4) to purple-grey (MW3).

3.1.1. Research on constitution

The petrographic study of thin section of 8 brick samples from Malbork Castle made it possible to determine approximately their constitution (Tab. 1).

Tab. 1: Volumetric ratio of components of brick samples (without pores).

Location within Malbork Castle:	**Date ***	**Matrix + opaque minerals**	**Feldspars + quartz**	**Rock fragments**	**Other components**	**Code**
		[%]	**[%]**	**[%]**	**[%]**	
Middle Castle, west wing, cellars	1280-1290	48.5	45.0	2.0	4.5	McC1
	1330-1335	48.0	46.0	3.0	3.0	MjaC1
	1330-1335	50.5	42.5	4.0	3.0	MjbC1
High Castle, south wall of the cellars under the first chapel	after 1330 (transformation)	59.5	35.5	4.0	1.0	M7.1
	before 1280	58.0	37.5	4.0	0.5	M8.1
Spot footing of the bridge connecting the Voit gate and Heinrich von Plauen rampart	1320 - 1340	66.0	31.5	2.0	0.5	MW1c
	1320 - 1340	62.0	34.0	3.5	0.5	MW2c
	1320 - 1340	65.0	33.0	1.5	0.5	MW3c

Dating based on: *Torbus (2014, pp. 109-126, 320-334), Jesionowski, B. (2012, *pers. comm.*)

The examination revealed that despite the overall similarity of the samples (matrix structure, texture), some of them differ in terms of matrix/aggregate ratio, composition of aggregate, particle size distribution and colour. All the bricks but one exhibit cryptocrystalline structure. The exception is the M7.1 sample, which has a microcrystalline structure. The aggregates have particles of fine and coarse fraction (their size is mainly in

the range from 1.0 mm to 0.1 mm, exceptionally 2 – 2.5 mm, only in M8.1 to 0.05 mm). In all the samples the grains are mainly isometric, rarely elongated and those of smaller size are very angular to angular, while a big fraction is rounded or well-rounded. The matrix (volume indicated with opaque minerals) ranges between 48% to 66%. It is noticeable that there are similarities in the matrix/aggregate ratio in groups of bricks coming from the same part of the Castle. However, in the light of further results, materials from the Middle Castle (besides MjaC1 and MjbC1) and the High Castle cannot be considered as the same group. The aggregate of all the samples is dominated by quartz accompanied by feldspars and rock fragments. As an accessory component several types of minerals can be found: oxyhornblende (McC1, MjaC1, MjbC1, M7.1, MW1c, MW2c), glauconite (McC1, MjaC1, MjbC1, M8.1, MW1c, MW2c), muscovite (McC1, MjaC1, MjbC1, M7.1, MW2c), zircon (McC1, MjaC1, MjbC1, M7.1), garnet (McC1, MjbC1, M7.1) and rutile (only M7.1). For the MW3c sample, accessory compound are rock fragments and no minerals listed above are present. Moreover, in MjaC1 and MjbC1 matrix dark mica lamellae and also in M7.1clay minerals remains were noticed. The performed analysis revealed that there are small amounts of crazing in some samples' matrix (McC1, M8.1) and the matrix of one sample is heavily cracked (MW3c). Finally among all the bricks one has a different particle size distribution. For most samples there is correlation: the size of grains is inversely proportional to their quantity while in the M7.1 sample the number of particles of different size (apart from coarse grain and very coarse grain) is approximately equal.

3.1.2. Research on the capillary properties of chosen bricks

The investigation was carried out on 5 bricks from Malbork, Radzyń Chełmiński and Toruń castles. Materials were obtained during conservation and archaeological works. The test samples could have big size (from whole-brick to at least half-brick), which resulted in achieving average results (Tab. 2). The brick samples of comparable colour (Mja, RdzC1, RdzC2), which is mainly the result of firing conditions, but also their raw components, have very similar capillary properties. Reddish-brown and purple-grey ceramic examples of materials fired in a high temperature share a similar water absorption capacity. Since they have bigger, less diverse pores and lower porosity their water absorption capacity is definitely lower, but the time of capillary rise is very short.

There are also available the results of tests concerning the capillary properties of bricks from Toruń Castle. For material identified by the author as coming from the 14th century (Skibiński 1993), water absorption capacity [A_W] was determined. For six samples, after 24 hours it is in the range from 10.4% to 11.1%. For two samples, most probably coming from overburnt ceramic, it is 5.2% and 2.2%. Furthermore, similar information for brick taken from the castle's bergfried (ruin of free-standing fighting tower dating back to the years 1300-1330 (Torbus 2015) can be found. The test carried out showed that for this material, the time needed for capillary rise of water to 4 cm is about 5 minutes and water absorption capacity, A_W, is 10,89% (Smagłowicz 2012). Considering the time of capillary rise, the result is approximately the same for the samples from Malbork Middle Castle (west wing, cellars under the Great Refectory, the end of 13th c. or the beginning of 14th c.) and their water absorption capacity is close: 9.46% - 9.70% (Łukaszewicz, *et al.* 2009).The results of the measurements are relatively homogenous when taking into consideration the different methodology of the research (mainly the different sizes of the samples). As the research project is ongoing, the collection of data will be carried out to characterise more widely the properties of the masonry bricks.

Tab. 2: Capillary properties of chosen bricks.

Location	Date	Time of capillary rise of water to 4 cm	Water absorption capacity, A_W	Colour	Code
Malbork Castle					
Middle Castle, west wing, cellars	1330-1335	22 min	12.32%	orange--red	Mja
Spot footing of the bridge connecting the Voit gate and Heinrich von Plauen rampart	1320-1340	15 min	6.14%	purple--grey	MW3
Radzyń, Chełmiński Castle**					
	1310-1340	27 min	12.27%	orange- -red	RdzC1
		29 min	11.19%	orange- -red	RdzC2
Toruń Castle,dansker***					
	1300-1330	23 min	8.87%	reddish--brown	TzGd4

Dating based on: **Wasik (2015, p. 17), Torbus (2014, p. 185), ***Torbus (2014, pp. 62-65)

3.2. Bedding mortars

The analysis was performed for 18 samples of bedding mortars from Malbork, Radzyń Chełmiński, and Toruń castles. They were examined first with the naked eye to determine their colour, hardness, and coherence. All the mortars have cream-grey to beige-grey colour, and they are relatively hard and semicoherent. Moreover, the investigation has evidenced that accumulations of lime binder (lime lumps) appear in all the samples. In almost all the mortars lime lumps are evenly distributed, and the biggest particles in individual samples are in the range from 3 to 5 mm. The exception are 3 samples where bigger lime accumulations were found (MWz1 up to 20 mm, MjbZ and MW1z1 up to 10 mm). A significantly lower amount of lime lumps (of size up to 3 mm) is noticeable in the mortars collected from Toruń Castle's dansker. On the basis of thermal analysis and the acid treatment there have been shown to be some differences in the binder compounds, binder/aggregate ratio (Tab. 3) and aggregate composition. With the exception of the Rdz8 sample, all the mortars have only lime binder. For Rdz8 the appearance of gypsum was identified (about 3.5%). It is probably an accidental addition or effect of a secondary gypsum crystallisation in deposits. As a result of petrographic investigation performed for two samples (McZ, MjbZ) it was established that the binder of these mortars is composed of almost pure micrite. Considering the binder/aggregate ratio it is possible to conclude that mortars of the same origin have similar proportions (in the case of the samples from Malbork Middle Castle even regardless their age). It is different when taking into account samples from Malbork High Castle: older mortar has a significantly higher content of binder. A higher concentration of lime in the MW1z1and TzGd1.1 samples in comparison

to other samples of the same origin may be caused by the insufficient mixing of the components. Furthermore the group of mortars from Radzyń Chełmiński Castle is relatively homogenous and rich in lime binder. The identification of the mortar's filler (beside McZ and MjbZ) was based on macroscopic and microscopic analysis. Therefore to describe them precisely more research is needed. The optical study of a thin section of the aforementioned mortars shows that the main component of the filler is quartz (45-47%), which is accompanied by feldspars (3-4%), opaque minerals, and rock fragments (2.5-3%) with different types of accessory minerals: glauconite, garnet, amphibole, zircon (McZ), and epidote (MjbZ). Aggregate grains have mainly isometric, rarely elongated shape, and they are rounded or well-rounded which indicates the river origin of the sand.

Moreover in the MjbZ sample, vegetable fibres and ceramic particles were found. Ceramic particles, most probably as an accidental additive, were also identified in other samples. They can reach a large size (7mm in M8z, 3 mm in Rdz8), but usually are smaller (up to 1mm in MW1z, MW2z and 0.5 mm in MjbZ). Beside the appearance of the large brick particles, the M8z sample is characterised by the presence of charcoal, which is probably a residue of the fuel used during the burning of limestone. Furthermore, the size of the biggest grains of the mortars aggregate makes it possible to distinguish groups of samples collected from Radzyń Chełmiński Castle and Toruń Castle. The mortars from Radzyń Chełmiński are characterised by a content of medium gravel (8-11mm) and from Toruń of very coarse sand (up to 1.5 mm) while the maximum fraction of aggregate from Malbork castle corresponds to different grain sizes.

Comparative data on mortars from Malbork Castle {are?} provided {in?} research and conservation reports. Several medieval bedding mortars were analysed to identify binder/aggregate ratio and aggregate composition. For mortars in the Middle Castle cellars (the end of 13th c. or the beginning of 14th c.) the binder/aggregate ratio is as follows: from 1:2.4 to 1:2.9 and the binder is composed only of calcium carbonate (Łukaszewicz *et al.* 2008, pp. 22-24). A significantly higher content of lime binder with lime lumps (1:1.4) is shown in the result of an analysis of a mortar from The Great Master's Wardrobe (2nd half of 14th c; Kozarzewski *et al.* 2007). An interesting case is a mortar sampled from the High Castle entrance gate (after 1280). Its binder/aggregate ratio is 1:2.3 and the binder is composed, apart from lime, of a quarter part of clay (Juźków 2003). Another modification of the binder composition is a group of early mortars dated to about 1280 from the High Castle church of Our Lady (Rogóż *et al.* 2002). Apart from calcium carbonate their binder is composed of magnesium carbonate and the binder/aggregate ratio is in the range from 1.4 to 3.0. The presence of the magnesium carbonate indicates that the binder is dolomitic lime deriving from the decomposition of dolomite limestone.

Tab. 3: Summary of the analytical procedure (DSC-TG and the acid treatment) carried out on the chosen mortars samples.

Location/	Date	Adsorbed water + water of crystallisation [30-560°C]	Calcium carbonate [above560°C]	Solid residues	Solid residues (after treatment with acid)	Binder to aggregate ratio by weight	Code
Malbork Castle							
Middle	1280-1290	1.82%	21.35%	76.83%	77.67%	ca. 1:3.5	McZ
Castle,west wing, cellars	1330-1335	1.82%	18.61%	79.57%	77.73%	ca. 1:3.5	MjbZ
High Castle, south wall of the cellars under the first chapel	after trans-formation in 1330	7.29%	16.86%	76.03%	no data	ca. 1:3.5	M7z
	before 1280	6.10%	19.94%	73.96%	no data	ca. 1:2.5	M8z
Spot footing of the bridge connecting the Voit gate and Heinrich von Plauen rampart	1320-1340	1.72%	19.12%	79.17%	76.34%	ca. 1:3.1	MWz1
		2.08%	28.87%	69.06%	62.58%	ca. 1:1.7	MW1z1
		2.27%	22.28%	75.45%	74.41%	ca. 1:2.9	MW2z1
Radzyń Chełmiński Castle							
	1310-1340	1.88%	33.54%	64.58%	62.62%	ca. 1:1.7	Rdz1
		2.15%	27.70%	70.15%	62.47%	ca. 1:1.8	Rdz2
		1.81%	31.08%	67.11%%	64.97%	ca. 1:1.8	Rdz2’
		2.27%	32.01%	65.72	59.01%	ca. 1:1.5	Rdz6
		3.22%	25.58%	67.72%	63.12%	ca. 1:1.7	Rdz8****
		3.41%	23.20%	73.39%	60.06%	ca. 1:1.7	Rdz10
		2.67%	27.98%	69.36%	60.05%	ca. 1:1.5	Rdz11
		4.06%	26.61%	69.33%	64.39%	ca. 1:1.8	Rdz12
Toruń Castle, dansker							
	1300-1330	2.64%	22.66%	74.70%	no data	ca. 1:3.0	TzGd1c
		2.81%	27.58%	69.61%	no data	ca. 1:1.7	TzGd1.1
		2.85%	23.08%	74.04%	no data	ca. 1:3.0	TzGd5
		2.47%	21.94%	75.59%	no data	ca. 1:3.1	TzGd6

**** Gypsum [95-245°C] = 3.48%

4. Conclusions

The results of initial research on capillary properties of bricks may lead to the conclusions that they are not dependent on their origin. A high similarity was noted despite the fact that the clay used in its production came from different sources. The investigation showed the evidences for a wide range of firing temperatures. Moreover, the appearance of a large amount of sharp shaped grains for all the samples of bricks may indicate that the material used for their manufacturing was boulder clay (Pavia, Caro 2007, p.8). It was found that in spite of many similarities in the composition of the examined materials there are differences in the proportions of components. Among the samples of mortars there can be distinguished a group from Radzyń Chełmiński, which is characterised by a high content of lime binder and the appearance of the filler up to medium gravel size. Although several analyses were carried out and the results were compared with those available in the literature and reports, drawing conclusions is difficult because of the great inhomogeneity of the brick wall structure and the different methodology of investigation. As the research project is ongoing, the presented outcome of the studies does not make it possible to characterise masonry materials coming from all the phases and stages of construction of the studied castles. However, the presented paper offers a sampling that can represent a useful point of reference for further analysis. Since the available research results are preliminary, the study will continue to provide more data which it is hoped will make it possible to solve problems of this group of monuments in its technological and conservation aspects.

Acknowledgements

The investigation was partially funded by the Polish National Science Centre (UMO-2014/ 13/N/HS2/02879). The authors wish to thank Dr W. Bartz (Institute of Geological Sciences, University of Wrocław) for performing petrographic analyses, W. Topolska, M.Sc. M. Chylińska, M.Sc. (ZKEiDA, NCU in Toruń) for measurement and evaluation of thermal analyses. We would also like to thank Senior Curator B. Jesionowski (the Department of Malbork Castle Conservation) for useful indications during research in Malbork.

References

Domasłowski, W., Kęsy-Lewandowska, M., Łukaszewicz, J. W., 2004, Badania nad konserwacją murów ceglanych, Wydawnictwo UMK, Toruń, ISBN 8323117187, 189pp.

Domasłowski, W. (ed.), 2011, Zabytki kamienne i metalowe, ich niszczenie i konserwacja profilaktyczna, Wydawnictwo UMK, Toruń, ISBN 9788323126812, 565pp.

Juźków, Sz. R., 2003, Dokumentacja konserwatorska XIII w. portalu zamku wysokiego w Malborku, Toruń, conservation report, 1-20.

Kozarzewski, M., Wielocha, A., Zalewska, K., 2007, Garderoba Wielkiego Mistrza -- Badania materiałowe, Malbork, research report, 1-16.

Łukaszewicz, J. W., Bartz, W., Oberta, W., Topolska, W., Kraska, B., Lisek, K., 2008, Malbork. Badania konserwatorskie pomieszczeń piwnicznych pod skrzydłem zachodnim na Zamku Średnim, Malbork – Toruń, research report, 1-27.

Pavia, S., Caro, S., 2007, Petrographic microscope investigation of mortar and ceramic Technologies for conservation of the building heritage, Proc. SPIE Vol. 6618, Optics for Arts, Architecture, and Archaeology , Munich, Germany.

Rogóż, J., Gryczewski, J., Stachera, J., 2002, Badania polichromii, zapraw, kamieni naturalnych i sztucznych oraz glazur ceramicznych z Kościoła NMP na zamku w Malborku, Toruń, research report, 213-303.

Skibiński, S., 1993, Przyczyny niszczenia cegieł zabytkowych murów obronnych Torunia oraz zamku krzyżackiego w Toruniu, Naukowe podstawy ochrony i konserwacji dzieł sztuki oraz zabytków kultury materialnej, Strzelczyk A., Skibiński S. (eds.), Wydawnictwo UMK, Toruń, ISBN 8323104115, 187-199.

Smagłowicz, S., 2012, Możliwość wykorzystania młotka Schmidta (sklerometru) do wykonania pomiarów wytrzymałości mechanicznej materiałów budowlanych w obiektach zabytkowych, MSc thesis conducted under supervision of Łukaszewicz, J. W., Nicolaus Copernicus University in Toruń, Toruń, 55.

Torbus, T., 2014, Zamki konwentualne Państwa krzyżackiego w Prusach, Wydawnictwo słowo/obraz terytoria, Gdańsk, ISBN 9788374531344, 472pp.

Wasik, B., 2015, Zamek w Radzyniu Chełmińskim. Technika i etapy budowy siedziby krzyżackich komturów i konwentu, Ochrona Zabytków, LXVIII (1), 167-181.

This page has been left intentionally blank.

ORGANIC ADDITIVES IN MORTARS: AN HISTORICAL TRADITION THROUGH A CRITICAL ANALYSIS OF RECENT LITERATURE

K. Zhang[1], L. Rampazzi[2], A. Sansonetti[3*] and A. Grimoldi[1]

Abstract

There has been a long history of applying organic additives (OA) in mortars, and an understanding of both their historical uses and the scientific study on them is fundamental to produce restoration materials which are compatible with historical mortars. In this paper, a critical analysis of literature is given, on both characterisation studies of historical mortar samples as well as studies of laboratory-made mortar specimens. By doing so, we hope to provide more insight to future work in the field of architectural conservation.

Keywords: mortar, organic additive, conservation, literature critical analysis, characterisation study, mechanism study

1. Introduction

Mortars as one of the important components of architecture possess many functions including to bond masonry units together, to coat external and internal façades and to decorate. Since the performance of mortars is crucial to the longevity of constructions, organic additives (OA) were added in ancient times to improve the plastic properties of fresh mortar and/or to enhance the hardened mortar's performances. The scientific community has devoted increasing interest in the topic of organic additives (OA) into mortars, and this issue could be approached by different points of views: 1. the critical examination of historical sources; 2. the study of real samples in the attempt to detect residues of OA into mortars. It is a challenge for modern analytical techniques, but the only possibility to put in evidence the real additions used in the building practice; 3. The set of model samples containing different OA, in the attempt to link a real addition to a specific measured performance. Unfortunately the existing bibliography is spread over a vast set of references, so that the first problem in leading a study on OA consists in understanding and connecting new data with the previous ones. The present paper proposes a critical and synthetic review on 49 modern scientific papers from the time span of 1983-2015, including 25 papers regarding characterisation study on historical mortar samples and 24

[1] K. Zhang and A. Grimoldi
Dipartimento di Architettura e Studi Urbani, Politecnico di Milano, Italy

[2] L. Rampazzi
Dipartimento di Scienza e Alta Tecnologia, Università dell'Insubria, Italy

[3] A. Sansonetti*
Institute for Conservation and Valorisation of Cultural Heritage, Italy
sansonetti@icvbc.cnr.it

*corresponding author

papers regarding mechanism study on laboratory-made mortar specimens. This work on bibliographic research will also take part of a wider research in the next years.

2. Analysis of characterisation study on historical mortar samples

A selection of 25 papers of characterisation study on historical mortar samples (1994-2015) are investigated in this section; the majority of samples are from Europe, and there are also some examples in Asia (Fig. 1). The historical constructions or architectural elements (e.g. sculptures), from which the mortar samples were taken, date back to as early as 6th (Ellora caves, India) or 7th century (Vadakumnathan temple, India), and as late as 19th and 20th century (Estoi Palace, Portugal). However, it is difficult to deduce the age of the mortar samples, since many buildings were restored, sometimes even reconstructed, and these samples can come from any period of the process.

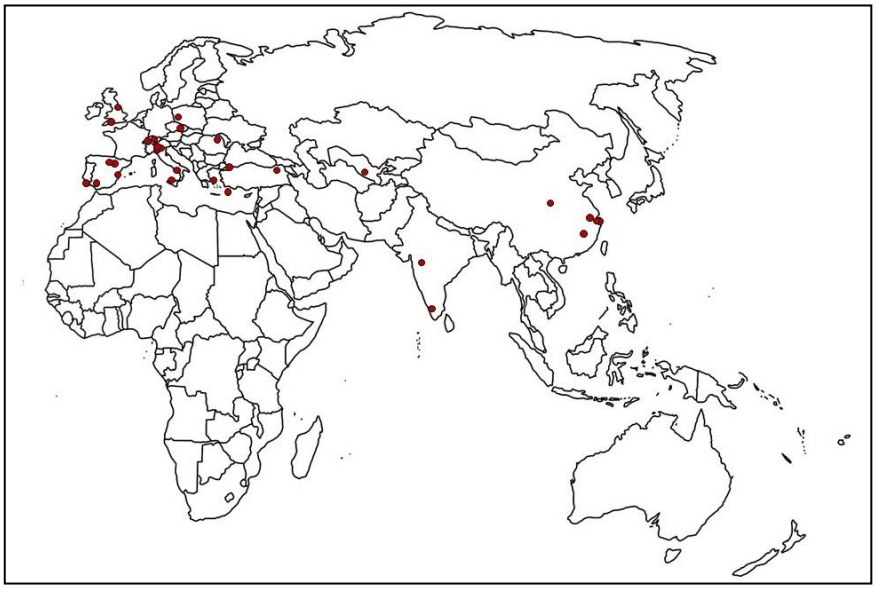

Fig. 1: Geographic locations of historic mortar samples.

A total of 52 mortar "recipes" were summarized from 25 papers of characterisation study on historical mortar samples. Here the "recipe" is defined as different mortar compositions with different mortar functions (e.g. masonry mortar, plaster, stucco, repairing mortar), different binders (e.g. lime, gypsum, lime+ gypsum), different OA (e.g. saccharides, proteins, lipids), and from different historical constructions (e.g. churches, statues, and other architectural constructions). The relationship between binder compositions and mortar functions is shown in Fig. 2a. The masonry mortar discussed in this section includes jointing mortars and bedding mortars; plaster includes internal and external plasters, renders, and wall painting plasters; stucco includes bulk and finishing layers. It is shown in Fig. 2a that 40% or 21 of the mortar recipes apply lime as binder, and it is mostly applied in plasters. What's interesting to note from the pie chart is that 27% or 13 of the recipes apply a combination of lime and gypsum as the binder, and this binder composition is used for a variety of mortar functions (masonry mortar, plaster, stucco and repairing mortar).

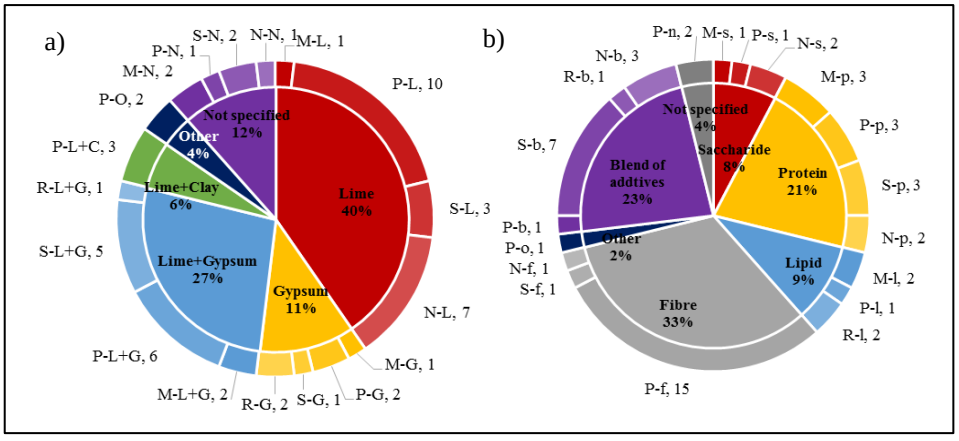

Fig. 2: Pie chart of 52 mortar "recipes" from 25 papers of characterisation study on historical mortar samples, classified first by binder compositions (Fig. 2a) or by organic additives (Fig. 2b), then sub-classified by mortar functions. M: masonry mortar; P: plaster; S: stucco; R: repairing mortar; N: not specified.

The relationship between organic additives and mortar functions is shown in Fig. 2b. There does not seem to be a particular pattern to use a certain organic additive for a certain mortar function, in other words, for saccharides, proteins and lipids, they all appear in a variety of mortars. As for fibres, however, they show a clear trend of being mostly applied in plasters (15 out of 17 recipes). Half (9 out of 17) of the recipes contain vegetal fibres (2 hay, 2 wood, and the others are not specified), and the remaining half (8 out of 17) contain animal fibres (1 ox hair, and the others are not specified). Among saccharides, proteins and lipids, proteins seem to be mostly applied, which account for 21% of all recipes, of which 3 contain collagen, 4 contain milk, 3 contain egg protein, and 1 needs further investigation. Lipids is applied in 5 out of 52 recipes, 1 contains drying oil, 1 contains egg yolk, 2 contain mixture of wax and drying oil, and 1 contains mixture of oil and animal fat. The 8% or 4 recipes containing saccharides, 1 contains natural gum, 1 contains starch, 1 contains sugar, and the other 1 not specified. It is worth noting that some of the recipes contain a blend of different types of OA, which is nearly one-fourth (23%) of all recipes. 4 of them contain both lipids and saccharides, 2 contain eggs, 1 contains both egg and animal glue, 2 contain lipids, proteins and saccharides, and in the remaining 3 recipes a mixture of fibres and other OA are present.

Regarding the OA amount, different recipes seem to include various additive quantities. The natural gum (possibly) in bedding mortar of a medieval military shipyard in Amalfi, Italy is around 0.01%-w (Rampazzi *et al.*, 2015). The egg protein in stuccoes from the Church of Santa Maria dei Ghirli in Campione d'Italia (Como, Italy) is around 1 ppm (Rampazzi *et al.*, 2012). The collagen in stuccoes used to seal sculptures in the Cathedral of S. Martino (Lucca, Italia) is around 0.5% (Ronca 1994). The stuccoes of sculptures in two churches from Palermo, Italy contain around 1% lipid and 1% sugar, and a statue finishing contains 2.5% lipid, 0.5% sugar and 6.1% protein (Montana and Ronca 2002). The plaster used in Vadakumnathan temple (Tirussur, India) contained around 10% fermented herbs, 5% proteins, and 3% fats (Thirumalini *et al.*, 2015). The accuracy of the provenance of the OA sometimes depends on the method used, for example, study of (Kuckova *et al.*, 2009)

used a peptide mass mapping method, which could conclude that the collagen in Romanesque rotunda of Saint Catherine in Znojmo (Moravia, Czech Republic) was probably made from bovine materials. The study of (Montana and Ronca 2002) showed that different characterisation methods could also lead to different quantification results. For instance, by applying different extraction methods (n-pentane extraction and chloroform-methanol extraction), the amount of lipids detected by the latter is approximately twice of that by the former.

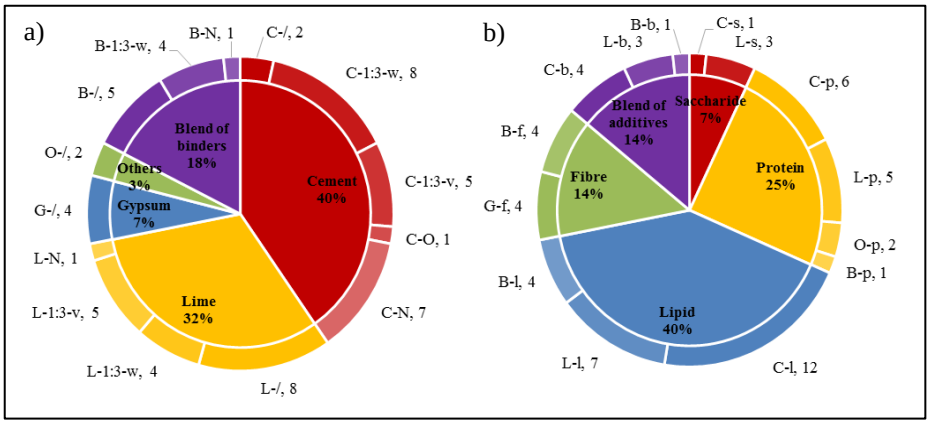

Fig. 3: Pie chart of 57 mortar "recipes" from 24 papers of mechanism study on laboratory-made mortar specimens. Fig. 3a: Pie chart classified first by binder compositions, then sub-classified by binder/aggregate ratio. /: no aggregate; -w: binder/aggregate ratio by weight; -v: binder/aggregate ratio by volume; O: others; N: not specified. Fig. 3b: Pie chart classified first by organic additives, then sub-classified by binder compositions. C: cement; L: lime; G: gypsum; O: others; B: blend of binders.

3. Analysis of mechanism study on laboratory-made mortar specimens

Similar to section 2, 57 mortar "recipes" were summarized from 24 papers of mechanism study on laboratory-made mortar specimens (1983-2015). Here the "recipe" is defined as different mortar compositions with different binders (e.g. cement, lime, gypsum) and different OA (e.g. saccharides, proteins, lipids). A part of the studies are performed on cement, with the primary goal of re-using waste materials as additives to cement. Although these studies do not share the same goal as ours, their results of effect of OA on mortars could provide very useful information, so they are also included in the literature investigation.

The relationship between binder compositions and binder/aggregate ratio is shown in Fig. 3a. As stated above, 40% of the recipes use cement as binder, and most of the rest 60% are restoration-related. Recipes with lime as binder occupy half of them (32%), and most of the lime used was air lime. There are also recipes with a blend of binder compositions (18%), most of which are composed of lime and pozzolanic materials such as natural pozzolan, metakaolin and blast-furnace slag. Regarding binder/aggregate ratio, the proportion of 1:3 seem to be the most popular, while in some recipes it is by weight, in others it is by volume. It should be noted that some recipes do not specify the B/A ratio,

and this has 2 folds of meanings: 1st, the ratio is not given; and 2nd, the ratio is given but whether it is by weight or by volume is not clarified. There are also a number of recipes without aggregate (2 for cement, 8 for lime, 4 for gypsum, 2 for others, and 5 for blend of binders), and they constitute around 37% (21/57) of all recipes.

The relationship between organic additives and binder compositions is shown in Fig. 3b. Lipids seem to be the mostly applied, which account for 40%, followed by proteins (25%), and saccharides occupy 7% of all recipes. 10 out of the 40% or 23 recipes with lipids contain linseed oil, 2 contain olive oil, 2 contain sunflower oil, 2 contain tung oil, and the other 7 contain other oils and fatty acids. 5 of the 40% or 14 recipes with proteins contain pig blood, 3 commercialized blood proteins, 2 casein, and the remaining 4 contain gluten, egg albumen, animal glue and a acidified protein. Out of the 7% or 4 recipes with saccharides, 2 of them contained sticky rice, and the rest 2 contained a monosaccharide and a potato starch. Fibres and blend of additives both take up 14% of all recipes. For recipes with fibres, 4 contain an industrial hemp shiv, and the other 4 contain lamb's wool, straw, cork, etc. The blend of additives here is also defined as a mixture of different types of OA, and 5 of the 8 recipes contain cactus (saccharides and proteins), 1 contains gram (saccharides and proteins), 1 contains gram+ oil, and the other 1 contains egg albumen+ coconut fibre.

As for effects of organic additives on mortar properties, different studies may give different results, which is affected by various factors. Lipid additives improve hydrophobicity, which is basically reflected in all related studies, and the study of (Justnes *et al.*, 2004) indicated that oils with high content of monounsaturated fatty acids seem to be the most effective. What's more, lipids tend to decrease proportion of pores and improve durability. The main difference among the results is the effect on mechanical strengths, with some studies claiming that lipids decrease it, and others showing the contrary. According to the papers investigated, the decrease or increase of mechanical strengths could depend on which type of lipid is used (Albayrak *et al.*, 2005), on the amount of lipid added (Cechova 2009), and on the composition of the binder (Nunes *et al.*, 2012). Protein additions in mortars generally entrain more air, increase hydrophobicity, increase durability and decrease bulk density. However, in some studies protein additions seem to decrease mechanical strengths (Jasiczak and Zielinski 2006, Remadnia *et al.*, 2009), while in some others they seem to increase them (Ventolà *et al.*, 2011, Chandra and Aavik 1987). Two studies on cement show that proteins retarded the setting (Jasiczak and Zielinski 2006, Chandra and Aavik 1987), while another two studies on lime show that they accelerate the process (Fang *et al.*, 2015, Zhao *et al.*, 2014). The addition of fibres show improved mechanical strengths (Vegas *et al.*, 2013, Walker *et al.*, 2014). For saccharides and blend of additives, they don't seem to provide enough information to be summarized as a pattern here.

4. Discussions

Comparing the binder compositions of historical samples and mortar specimens, we can see that lime-based mortars are indeed the most frequently applied and studied mortars in the field of architectural conservation. Also, the mixture of lime and gypsum, which takes up 27% of the historical sample recipes, doesn't seem to have been studied on the lab-made mortar specimens.

In both historical samples and lab-made specimens there exists the blend of OA in mortars. Also in the relatively scarce historical literature in english language the use of multiple

additives in one recipe was frequently recorded. For example, "confectio maltae", a late antique recipe for plaster preparation is composed of lime, oil, cheese, egg yolk, egg white and flax (for the most recent literature on its transmission through the Middle Age see (Brun 2015)). Accounts for the repairs of the steeple of Newark Church in 1571 described a mortar composed of lime, malt and eggs (Unknown 1891). In (Neve 1703), it is described that the cold cement is composed of quicklime, old Cheshire cheese, cow's milk, and egg whites. In 18th century India, mortars were recorded to be prepared by mixing same volumes of pit-sand and stone-lime, together with jiggery, gram and myrabolan; and the second coat of plastering could be made by adding egg whites, ghee and butter-milk to lime and sand, and beat all well together (Unknown 1819). However, some of these recipes were not real mortars, but they could be considered as mastics for adhesion purposes.

Regarding binder/aggregate ratio, as stated in section 3, apart from the mortars without aggregate, the most commonly applied ratio is 1:3, both by weight and by volume. For characterisation studies on historical mortar samples, however, most papers investigated don't give binder/aggregate ratio, and those who give them, generally show high B/A ratio, in some cases the binder takes up more than half of the inorganic material in mortar (Duran *et al.*, 2008, Montana and Ronca 2002), and in other cases the B/A ratio is 1:1 (Bartz and Filar 2010, Luxan *et al.*, 1995) or 1:2 (Thirumalini *et al.*, 2015, Kurugöl and Güleç 2012).

As stated in section 2, the OA amount detected in historical samples ranges from 1ppm to 6%, and there was also a 10% of addition for plant fibres. For lab-made mortar specimens, the amount generally ranges from 0.05% to 5% to the weight of the binder, and in some cases they can go beyond 15% (Fang *et al.*, 2014, Fang *et al.*, 2015). Certainly we would hope to get some information on OA amount from the historical samples, so as to help our mechanism study on them. However, it is barely possible to compare these results. For one thing, organic matters degrade, so generally the amount detected would be lower than the actual content. Also as stated above, accuracy on the detection values may depend on the method applied. It should be also noted that the detected amount in historical samples sometimes does not equal to the OA amount in lab-made mortar specimens. For example, protein content in egg white is around or less than 10%, therefore if 1% of egg white protein is detected in an historical sample (suppose that this result is accurate), the organic amount of egg white should be around or more than 10%.

5. Future work

This paper serves as a part of the basis of a future work of mechanism study on organic additives (OA) in mortars, however this is still a preliminary step, and more questions should be considered and answered before making and carrying out the experimental plan.

Acknowledgement

The financial support by China Scholarship Council under the Grant No. 201406320210 is acknowledged.

References

Albayrak, A.T., Yasar, M., Gurkaynak, M.A., *et al.*, 2005, Investigation of the effects of fatty acids on the compressive strength of the concrete and the grindability of the cement, Cem. Concr. Res., 35, 400-404.

Bartz, W. and Filar, T., 2010, Mineralogical characterization of rendering mortars from decorative details of a baroque building in Kożuchów (SW Poland), Mater. Charact., 61, 105-115.

Brun, G., 2015, The transmission and circulation of practical knowledge on art and architecture in the Middle Ages, Ph.D. thesis, Politecnico di Milano, Italy.

Cechova, E., 2009, The effect of linseed oil on the properties of lime-based restoration mortars, Ph.D. thesis, Universita di Bologna, Italy.

Chandra, S. and Aavik, J., 1987, Influence of proteins on some properties of Portland cement mortar, Int. J. Cem. Compos. Lightweight Concr., 9, 91-94.

Duran, A., Robador, M., Jimenez de Haro, M., *et al.*, 2008, Study by thermal analysis of mortars belonging to wall paintings corresponding to some historical buildings of Sevillian art, J. Therm. Anal. Calorim., 92, 353-359.

Fang, S., Zhang, H., Zhang, B., *et al.*, 2014, A study of Tung-oil-lime putty - a traditional lime based mortar, Int. J. of Adhes. Adhes., 48, 224-230.

Fang, S., Zhang, K., Zhang, H., *et al.*, 2015, A study of traditional blood lime mortar for restoration of ancient buildings, Cem. Concr. Res., 76, 232-241.

Jasiczak, J. and Zielinski, K., 2006, Effect of protein additive on properties of mortar, Cem. Concr. Compos., 28, 451-457.

Justnes, H., Østnor, T. and Barnils Vila, N., 2004, Vegetable oils as water repellents for mortars, Proceedings of the 1st International Conference of Asian Concrete Federation, Chiang Mai, 28-29.

Kuckova, S., Hynek, R. and Kodicek, M., 2009, Application of peptide mass mapping on proteins in historical mortars, J. Cult. Herit., 10, 244-247.

Kurugöl, S. and Güleç, A., 2012, Physico-chemical, petrographic, and mechanical characteristics of lime mortars in historic Yoros Castle (Turkey), Int. J. Archit. Herit., 6, 322-341.

Luxan, M.P., Dorrego, F. and Laborde, A., 1995, Ancient gypsum mortars from St. Engracia (Zaragoza, Spain): characterization, identification of additives and treatments, Cem. Concr. Res., 25, 1755-1765.

Montana, G. and Ronca, F., 2002, The "recipe" of the stucco sculptures of Giacomo Serpotta, J. Cult. Herit., 3, 133-144.

Neve, R., 1703, The City and Country Purchasers, & Builder's Dictionary, London, J. Sprint, G. Conyers, and T. Ballard.

Nunes, C., Slížková, Z., Křivánková, D., *et al.*, 2012, Effect of linseed oil on the mechanical properties of lime mortars, 18th International Conference Engineering mechanics, Svratka, 955-967.

Rampazzi, L., Colombini, M., Conti, C., *et al.*, 2015, Technology of Medieval Mortars: An Investigation into the Use of Organic Additives [Online], Archaeometry.

Rampazzi, L., Rizzo, B., Colombo, C., *et al.*, 2012, The Stucco Technique of the Magistri Comacini: The Case Study of Santa Maria Dei Ghirli in Campione D'italia (Como, Italy), Archaeometry, 54, 926-939.

Remadnia, A., Dheilly, R., Laidoudi, B., *et al.*, 2009, Use of animal proteins as foaming agent in cementitious concrete composites manufactured with recycled PET aggregates, Constr. Build. Mater., 23, 3118-3123.

Ronca, F., 1994, Protein determination in polychromed stone sculptures, stuccoes and gesso grounds, Stud. Conserv., 39, 107-120.

Thirumalini, S., Ravi, R., Sekar, S., *et al.*, 2015, Knowing from the past - ingredients and technology of ancient mortar used in Vadakumnathan temple, Tirussur, Kerala, India, J. Build. Eng., 4, 101-112.

Unknown, 1819, Encyclopaedia Londinensis, London, Encyclopedia Office.

Unknown, 1891, Journal of the Royal Society of Arts, London, G. Bell and Sons.

Vegas, F., Mileto, C., Cristini, V., *et al.*, 2013, Parameterisation of gypsum mortar for alternative structural consolidation of traditional floors, Adv. Mater., 2, 48-52.

Ventolà, L., Vendrell, M., Giraldez, P., *et al.*, 2011, Traditional organic additives improve lime mortars: new old materials for restoration and building natural stone fabrics, Constr. Build. Mater., 25, 3313-3318.

Walker, R., Pavia, S. and Mitchell, R., 2014. Mechanical properties and durability of hemp-lime concretes, Constr. Build. Mater., 61, 340-348.

Zhao, P., Li, G.Y. and Zhang, Y.S., 2014. Understanding and assessment of ancient Chinese pig blood-lime mortar, Adv. Mat. Res., 997, 446-449.

ABSTRACTS

This page has been left intentionally blank.

DAMAGE:

IMPACT OF HEAT EXPOSURE (FIRE DAMAGE) ON THE PROPERTIES OF SANDSTONE

T. Howind[1*], W. Zhu[1] and J.J. Hughes[1]

Abstract:

The present study was conducted in support of damage examination as part of the reconstruction efforts currently undertaken on the Charles Rennie Mackintosh - Glasgow School of Art after the building suffered severe fire damage in 2014. In this study, compared to most of similar nature, attention was paid to the minimisation of the effects caused by the apparent heterogeneity within sandstone (even when sourced from the same quarry) to understand the consequences of heat for the structural stability of the building. Mechanical property values related to mechanical strength such as compressive strength, ultrasound pulse velocity (UPV) and surface hardness, as well as petrophysical properties (bulk density, water sorptivity and porosity) were measured on sandstone specimens burnt at temperatures of 300°C, 450°C, 600°C, 750°C and 900°C. In conjunction with investigations of mineralogical and textural changes, a correlation was attempted between attributes that were analysed/determined non-destructively with the mechanical strength and structural damage level, to allow for a better on-site judgement on the degree of damage. The results showed that even minor mineralogical and textural variation within the stone specimens of a test series lead to very significant differences in the observable effects after burning. Nonetheless it became clear that the performance of the burnt stone specimens started to deteriorate significantly beyond temperatures of 450°C. As expected, from a material science's point of view, a discrepancy between UPV, compressive strength results and Leeb rebound values (surface hardness) was observed. Evaluating the mechanical performance of materials, such as sandstone, based on surface hardness may be misleading if one is unaware of the physics behind the testing technique and the materials to be tested.

Keywords: sandstone, fire damage

[1] T. Howind*, W. Zhu and J.J. Hughes
School of Engineering and Computing, University of the West of Scotland, Paisley, Scotland, United Kingdom
torsten.howind@uws.ac.uk

*corresponding author

INVESTIGATION METHODS:

SANDSTONE WEATHERING: NEW APPROACHES TO ASSESS BUILDING STONE DECAY

J. Dassow[1*], M. Lee[1], P. Harkness[2], S. Hild[3] and A.B. Leslie[4]

Abstract

New approaches to assess masonry decay are required to help in the preservation of built heritage, including maintenance costs, especially in Scotland. Consistent methods of measurement and empirical data analysis to evaluate the progress of weathering have to be defined to substantiate the classification of stone decay. Our project aims to identify the exact length scale (nanometre to centimetre) and timescale (seconds to years) of weathering processes. Developing two new non-/minimally invasive tools will improve our assessment of the state of decay and help to determine which stone(s) need to be replaced. The project focusses on assessing sandstone masonry with a drilling tool to estimate the structural properties and a laser interferometer to measure dilatation over time to nanometre precision. The ultrasonic drilling tool allows the identification of changes in the structure of a sample while drilling a hole to a depth of some millimetres. By measuring the force or power required to drill, porosity changes and/or the presence of salt at depth within the sample can be mapped. The use of ultrasonic tools enables penetration of the rock with less damage to vulnerable stone. With the laser interferometer we aim to observe precisely weathering processes like swelling of clay minerals or salt crystallisation, because of the high spatial and temporal resolutions of the device. The laser interferometer allows measurement of very small (nanometre) scale expansion of a sample and can identify the effects of hourly or daily changes in stone condition. The developed techniques allow for better prediction of the decay processes, including upscaling from the lab to the field, and can potentially be used in situ on historical buildings under site conditions.

Keywords: building stone decay, drilling resistance measurement (DRMS), laser interferometer

[1] J. Dassow* and M. Lee
School of Geographical and Earth Sciences, University of Glasgow, United Kingdom
j.dassow.1@research.gla.ac.uk

[2] P. Harkness
School of Engineering, University of Glasgow, United Kingdom

[3] S. Hild
School of Physics and Astronomy, University of Glasgow, United Kingdom

[4] A. Leslie
Historic Scotland, United Kingdom

*corresponding author

INVESTIGATION METHODS:

PORE-SCALE FREEZE-THAW EXPERIMENTS WITH ENVIRONMENTAL MICRO-CT

T. De Kock[1*], H. Derluyn[1], T. De Schryver[2], M.A. Boone[1,3] and V. Cnudde[1]

This abstract presents a laboratory study on the pore-scale processes involved in freeze-thaw experiments. Micro-CT has proven to be a useful tool in the analysis of (geo-)materials. Creating 3D images, it provides spatial information on materials' structure. As such, it is applied on building stones to characterise the pore network or to evaluate decay phenomena on the pore scale (typical from 1 µm to > 100 µm). At the Centre for X-ray Tomography of the Ghent University (UGCT; www.ugct.be), an Environmental Micro-CT (EMCT) was developed to study dynamic processes in materials. This gantry-based system allows stationary samples to be scanned at very high speed (i.e. scans < 1 minute). In addition, it easily configures with add-on modules designed for specific applications. For this research, a cooling stage was designed to perform freeze-thaw cycling on rock samples of 10 mm diameter. Samples from an miliolid limestone from the Paris Basin, with 35 vol.-% porosity, were subjected to freeze-thaw cycles between +20°C and -15°C. The samples were scanned at the end of each freezing and thawing stage, and continuous scanning was performed during each cooling stage. It can be seen that a fracture develops in function of the amount of freeze-thaw cycle. Subsequent scans illustrate that the fracture opens during freezing and closes during subsequent thawing. In addition, continuous scanning during the cooling stage allowed for visualising the sample at the moment just before and just after the occurrence of an exotherm, measured by a temperature sensor and interpreted as a proxy for ice crystallisation. This illustrates that the fracture opening coincides with the exotherm. Fracturing is thus a result of ice crystallisation. Furthermore, the location of the fracture could be linked to the stone's texture and water uptake. Altogether, the spatial and temporal information provided by micro-CT provides valuable information on the process of freeze-thaw decay and it's relation to the stone's intrinsic properties.

Keywords: limestone, freeze-thaw decay, environmental micro-CT, dynamic imaging

[1] T. De Kock*, H. Derluyn, M.A. Boone and V. Cnudde
UGCT – PProGRess, Department of Geology & Soil Science, Ghent University, Belgium

[2] T. De Schryver
UGCT, Department of Physics and Astronomy, Ghent University, Belgium

[3] M.A. Boone
X-ray Engineering BVBA (XRE), Ghent, Belgium

*corresponding author

INVESTIGATION METHODS:

CONSERVATION STUDY OF STONE MASONRIES USING IRT: DISCOVER HIDDEN INFORMATION BY THERMAL PROPERTIES

C. Franzen[1] and J.-M. Vallet[2]

Abstract

In increasing numbers IRT investigations are regularly performed also on heritage objects. While the main focus is most often the detection of energy losses or localisation of damages, the images frequently show additional information easily overseen or neglected for further interpretation. In building inspection, investigations of the differences in thermal conductivity are the basis for a successful IRT study. That counts for damaged areas as well as for the intact parts. By making visible the underlying structures of e g a plastered masonry important data for building history and on the construction in general is provided. An improved interpretation of all that data, which is already there, is promoted. The paper shows several examples of IRT damage investigations and energy related inspections where interesting findings on the carrying masonry were made. In the case of the Waaghaus in Bozen the aim of the study was to detect thermal losses in the construction. By the thermal investigation more constructive details became obvious. Thermal images show clearly the arc constructions bracing the load above the windows in the cobble stone masonry of the building. Damage investigations were carried out on mural painting in the church in Kühren, on an façade part in Jena and on a plaster in the crypt on Freiberg cathedral in Germany and in Sigale in France. By active IRT, inspection gaps and voids, and crack extensions beneath the plaster are detected. But moreover also the masonry structure of the rubbleworks or the ashlar blocks is exhibited. Here the correlation between details of the construction and the damage become obvious: most of the gaps and voids are referred to course of the masonry joints.

Keywords: IRT, thermal imaging

[1] C. Franzen*
Institut für Diagnostik und Konservierung an Denkmalen in Sachsen und Sachsen Anhalt e.V., Dresden, Germany
franzen@idk-denkmal.de

[2] J.-M. Vallet
CICRP, Marseille, France

*corresponding author

INVESTIGATION METHODS:

ACTIVE IRT AND THEORETICAL SIMULATION INPUTS FOR THE VOIDS DETERMINATION IN BUILDING MATERIAL

K. Mouhoubi[1], C. Franzen[2], J.-M. Vallet[3*], V. Detalle[4], O. Guillon[3] and L. Bodnar[1]

Abstract

The sufficient space resolved localisation of gaps and voids in building parts like masonry or plaster is a major problem. Especially on heritage material preferentially non-destructive methods are desirable. A promising technique for that kind of investigation is active IRT. Compared to the still most widely used percussion investigation thermography yields precise images and works even contactless on the surface. On a well-defined test specimen experimental investigations were carried out with different activation systems and different IR cameras. The light dense concrete test specimen hides 10 voids in different depths from 5 to 30 mm. There are voids with identical geometrical size and enlargement laying in different depth positions or show different volumes in terms of height size. 8 voids are parallel to the surface with a variable distance from the surface (0.5 to 30 mm) and 2 others have a ramp form and plunged towards the depth. 4 of them simulate cracks parallel to the surface, 4 other are laminar voids which are 0.5mm in thickness. The ramps have a triangle form with a peak (ramp 1) or a face (ramp 2) nearest the surface. Stimulated IRT has been performed with different halogen sources covering the activation phase and the subsequent cooling recorded by different IR cameras. Several post treatments have been applied on the experimental heating/cooling curve. Depending of the applied post treatment, the artificial defects can be detected or not. The results clearly show the time related detection of voids referring to depth and thermal conduction. In conclusion, the comparison of the excitation techniques and IRT cameras show that the experimental protocol to detect voids must be chosen carefully and has to be adapted to the item of concern. The results coming from the use of active IRT is highly increased thanks to the development of mathematical treatments that can be applied on the experimental data.

Keywords: IRT, thermal imaging

[1] K. Mouhoubi
Université de Reims Champagne Ardenne /GRESPI, Reims, France

[2] C. Franzen
Institut für Diagnostik und Konservierung an Denkmalen in Sachsen und Sachsen Anhalt e.V., Dresden, Germany

[3] J.-M. Vallet* and O.Guillon
CICRP, Marseille, France
Jean-Marc.Vallet@cicrp.fr

[4] V. Detalle
LRMH, Champs sur Marne, France

*corresponding author

INVESTIGATION METHODS:

EVALUATION OF HARMFULNESS OF TRADITIONAL CLEANING TECHNIQUES OF STONE WITH 3D OPTICAL MICROSCOPY PROFILOMETRY

C. Tedeschi [1], M.P. Riccardi [2], S. Perego[1] and M. Taccia[1]

Abstract:

In Cultural Heritage cleaning techniques used on stone removes materials in an irreversible way. The degree of cleaning achieved with each technique is a balance of benefit and potential damage. This paper investigates the effectiveness of 3D optical microscopy profilometry on monitoring natural stones (Angera Stone, Carrara Marble, Noto Calcarenite and Pietra Serena) before and after mild cleaning of surface deposits. We focus on the evaluation of the surface effects, 3D mapping and roughness profile, of cleaning of encrusted stones. Treated samples were analysed with Optical Profilometer Alicona IF-Portable before and after cleaning to monitor eventual morphological changes induced on the marble substrate. Also physical characterisation including bulk density, capillary absorption, mercury intrusion porosimetry and B.E.T, cross and thin section analysis were performed.

Keywords: stone cleaning, harmfulness, 3D profilometry

[1] C. Tedeschi *
Department of Civil and Environmental Engeneering, Politecnico di Milano, Italy
cristina.tedeschi@polimi.it

[2] M.P. Riccardi
Department of Heart and Environmental Sciences, University of Pavia, Italy

*corresponding author

OTHER MATERIALS:

MULTIFUNCTIONAL POLYMERS FOR THE RESTORATION OF THE DETERIORATED MINERAL GYPSUM (SELENITE) OF THE MINOAN PALATIAL MONUMENTS OF KNOSSOS

I.E. Grammatikakis[1*], K.D. Demadis[1] and K. Papathanasiou[1]

Abstract

Palatial Minoan architecture is uniquely characterised by the utilization of mineral gypsum (selenite) used for both building as well as for ornamental purposes. Despite the susceptibility of gypsum to weathering, it has been used extensively in the Minoan palatial architecture. The catalogue with the building and ornamental elements that are part of the monumental complex of the Knossos Palace which consists of 2,185 entries (S. Hood and D. Smyth, *Archaeological Survey of the Knossos Area*, 2nd edition; London: Thames and Hudson, 1981]. One of the main issues concerning the state of preservation of gypsum (selenite) of the palatial monuments of Knossos is its solubility. Gypsum is a rather soft and water-soluble mineral. The dissolution of gypsum, leads to loss of cohesion of the crystal aggregates and eventually to loss of original material. The parameters that define the decay mechanisms and results of gypsum are related, but not limited to its physical and chemical properties. They are involved in a function in which the other important factor is the nature of the solvent, which is consequently highly related to the natural environment of the Knossos site. During the past few decades, extensive research has appeared concerning stabilizers based on Silicon (Si), mainly regarding additives based on silicate esters. The polymerization of these species (*via* hydrolysis) leads to the generation of amorphous silica, which penetrates through the discontinuities of deteriorated stone and acts as a stabilizer. In short, amorphous silica that is produced *in situ* acts as a consolidant and binds the microcrystals and/or crystal aggregates of the inorganic compound together, restoring the structural integrity of the stone element. Although such materials have been used with partial success, there are some important disadvantages which include:

a) Limited stabilizing efficiency due to their low affinity for the rock surface;

b) Hydrolysis is not quantitative;

c) The (limited) stabilizing efficiency is irreversible;

d) The stone porosity is eliminated, which results in inhibition of water permeability.

[1] I.E. Grammatikakis*, K.D. Demadis and K. Papathanasiou
Department of Chemistry, University of Crete, Heraklion, Crete, GR-71003, Greece
ggrammat@chemistry.uoc.gr

*corresponding author

In this work we focus on silicon-based polymer design, free of the disadvantages mentioned before. Thus, we more specifically focus on the design, physicochemical characterisation, and evaluation of "dual-functionality" monomers. Such monomers have a silicon-based skeleton, which is necessary for the polymerisation after the hydrolysis process, but also with functional moieties with enhanced chemical affinity for calcium bearing minerals (G.M. Van Rosmalen *et al.*, *The adsorption of additives onto the gypsum surface*, *J. Cryst. Growth* 1987, *82*, 528-542). According to this approach, the bridging groups will be attached on the gypsum surface, creating a more stable connection between the consolidant and the restored surfaces, through the creation of chemical bonds.

Keywords: multifunctional polymers

OTHER MATERIALS:

CONSOLIDANT EFFICIENCY OF NEWLY DEVELOPED CONSOLIDANT BASED ON THE SOLUBLE CALCIUM COMPOUNDS

A. Pondelak[1], L. Škrlep[1], T. Howind[2], J.J. Hughes[2] and A. Sever Škapin[1]

Abstract

This paper reports on the examination of consolidant efficiency of a newly developed consolidant that is based on calcium carbonate compounds. The main advantages of the new consolidant [L. Škrlep, A. Pondelak, A. Sever Škapin. *Method for reinforcing porous construction materials and use of calcium acetoacetate solution to this aim*: international application no. PCT/SI2014/000028. [S. l.]: Europen Patent Office (EPO) (ISA/EP), 2014] are (a) deep consolidation, where re-cohesion between the particles of deteriorated historic materials is established, (b) its compatibility with carbonate based substrates and (c) good appearance with no whitening effect and minimal colour change on the surface of the historic material. Consolidation efficiency of the newly developed consolidant was studied on especially laboratory prepared lime based render samples. The specimens obtained were then consolidated using the new consolidant solution and exposed to different conditions in order to study the influence of temperature and relative humidity on the increase in hardness of the sample material. On the consolidated lime specimens a combination of non-destructive testing (surface hardness method) and destructive test methods (drill resistance measurements - DRMS, X-ray diffraction – XRD and FT-IR spectroscopy) was conducted to determine the effectiveness of the consolidation. This work has been supported by the 7th Framework Programme [FP7/2007-2013] of the European Union under grant agreement n° 282992.

Keywords: consolidation, drilling resistance measurement (DRMS), surface hardness, lime render

[1] A. Pondelak*, L. Škrlep and A. Sever Škapin
Slovenian National Building and Civil Engineering Institute, Ljubljana, Slovenia
andreja.pondelak@zag.si

[2] T. Howind and, J.J. Hughes
School of Engineering and Computing, University of the West Scotland, Paisley, Scotland, United Kingdom

*corresponding author

This page has been left intentionally blank.

LIST OF AUTHORS

E

F

G

H

I

J

K

L

M

N

O

P

R

S

T

V

W

Y

Z

LIST OF KEYWORDS

D

E

F

G

H

I

K

L

M

N

O

P

Q

R

S

T

U

V

W

X

Conference sponsor and partners

UWS UNIVERSITY OF THE WEST of SCOTLAND